SRI RAMAKRISHNA
COLLEGE OF ENGINEERING

(Accredited with "B++" Grade by NAAC(Ist cycle) with CGPA 2.96 out of 4.00)
(Approved by AICTE, New Delhi and Affiliated to Anna University, Chennai.)
Sri Saradha Nagar, Perambalur - 621 113.

Springer

PROCEEDINGS OF

9TH INTERNATIONAL CONFERENCE ON INVENTIVE COMMUNICATION AND COMPUTATIONAL TECHNOLOGIES (ICICCT-2025)

5TH-6TH, JUNE 2025

ICICCT

ORGANIZED BY

SRI RAMAKRISHNA COLLEGE OF ENGINEERING
PERAMBALUR, INDIA.

Table of Contents

1 An Arduino-Based Smart Car Safety System: Integrating Obstacle Detection, Battery Health Monitoring, and Smoke Detection for Enhanced Vehicle Safety
Debanjan Bera, Partha Biswas, Bristi Chakraborty, Soumadip Chandra, Souvik Bairi, Sandip Chakraborty

2 Next generationFR1MultiportAntenna with Metasurface for Drone Networking
Suguna G, Yogeshwari P, Rajesh A, C Manikandan, Suba Renjani N, Saranya J

3 Drone Positioning Estimation with Particle Filtering Augmented NR Positioning Reference Signal
Suba Renjani N, Rajesh A, Manikandan C, Suguna G, Saranya J, Selvakumar R

4 Analytical Approach of False Products and Complaint System Development Using Blockchain Technology
Anant Gupta, Pavan Sai A, Sanjay Kumar Dubey

5 Design and Optimization of Hybrid Circuits for Low-Power Systems Using GPDK 90nm
Bhuvana B P, Bharathi Raju, Parasa Gnan Naga Sai Vikas, Tarun Varma Pedada

6 Efficient Korean text classification algorithm based on optimized attention-based LSTM model
Xiaoyu Zhang

7 Anomaly Detection in High-Frequency Trading Data: A GNN-TCN Hybrid Approach
Xing Zhiyi

8 Smart border security: The role of AI in Modern Border Surveillance System
Simant Kamal Dutta Rahul Mahala, Rajesh Singh, Anita Gehlot, Nagendar Yamsani

9 Multi-Modal Data-Driven User Behavior Modeling and Personalized Advertisement Recommendation Algorithm
Zhang Zheng, Xu Dongyan

10 System-Agnostic Fault Detection Using Machine Learning-Based Vibration Analysis
Daniil Sanzharov, Tetiana Filimonova, Oleg Pursky, Pavlo Demidov

11 Video Summarizer Using Audio to Text Conversion and Natural Language Processing
A Kishore, D Suren Kumar, K Jayasri, M Vijayalakshmi

12 DDoS Attacks Detection in SDN Using Multi-Feature Selection Approach and LLMs
Amit Kachavimath, Satish Vaishyar, Ayush Chugani, Pratham Singh, Sanjana A More

13 PassPhrase Authentication: A Secure and User-Friendly Multi-Factor Authentication System Using Phrase and Gesture Integration
Amit Kachavimath, Ayush Chugani, Satish Vaishyar, Niyati Gogri, Misbah Falak

14 DDoS Attacks Detection using PSO Feature Selection and Classification using XGBoost in SDN
Amit Kachavimath, Sanjana A More, Narayan D G

15 Integrated Solutions for System Security: Scanning, Password Management, and Incident Response
D D Pukale, Shital Pawar, Mitali Rajesh Chavan, Tanvi Sudam Deore, Riya Kadole, Saba Aslam Sayyad

16 Chandrayaan-3 Mission to the Moon: A Systematic Review of Analysis, Improvements, Challenges and Lunar Science Contribution
Milind Shah, Dhairya Vyas, Kinjal A Patel, M AnanthaLakshmi, Roopal Rajput, S Lokesh

17 A Novel Framework for Fake Visual Content Detection Through Hybrid Intelligent Techniques
Vaidehi Vaghela, Priti Sadaria, Ripal D Ranpara

18 A Real-Time AI-Driven Framework for Personalized Prenatal Nutrition Using Multi-Algorithm Learning and Genetic Insights
K Rajasankari, S Silvia Priscila

19 Deep Learning with Augmentation for Accurate Coconut Leaf Disease Classification in Scenarios with Limited Data
S Nithya Priya, L Ramesh

20 Unveiling Triadic Patterns in Dynamic Networks Using a GAT-SAGE Hybrid Model
Vidyalekshmi Chandrika, Prashanth Chandra Reddy D, Hrishab T H, Mallampati Pranathi, Sanjay J K Seshadrinath, Lekshmi S Nair

21 When Large Language Models Meet Customer Feedback: A Case Study in Understanding and Analysis
Ngoc-Thanh-Xuan Nguyen, Gia-Phat Le, Ngoc-Sang Vo, Hoang-Nhat-Khang Vo, Song-Thien-Long Nguyen, Hoang-Anh Pham

22 Study of Stomach Abnormalities using EGG Signals
Chandrasekaran R, B Praveena, Vivek Pazhamalai, Ivo Romauld S, Vijayaraj S, Soundarya M K

23 Lightweight Data Encryption on EdgeAI Platforms: a Systematic Review
Thien An Nguyen, Thanh Loc Nguyen, Cuong Pham-Quoc

24 FPGA-based approximate multipliers for EdgeAI: a Systematic Review
Nguyen Thanh Loc, Nguyen Thien An, Cuong Pham-Quoc

25 Comparison of ChatGPT and DeepSeek based on Regional Language Understanding
Muhammad Anwar Ahmad, Ajune Wanis Ismail

26 Implementation of XGBoost time series model for statistical analysis of renewable and traditional fuel energy with future perspective
Suman Chowdhury, Dilip Kumar Das

27 Underwater Image Enhancement Hybrid Using Res-UNet Model
Sindhu Chandra Sekharan, Sathwika Reddy K, Viswateja Reddy K, C Kavitha, S Umamaheswari

28 Investigation of potential impact on drain current of CMOS inverter with various transistor width and temperature
Biswazit Mistry, Suman Chowdhury

29 An XLNet-based Deep Reinforcement Learning for Solving the Traveling Salesman Problem
Abdelaadim Khriss, Aissa Kerkour Elmiad, Mohammed Badaoui

30 Analysis of Methods for Detecting Vulnerabilities in Web Servers
Elshod Khaydarov

31 Impact of Agentic AI-Driven RPA on Strategic Management: Enhancing Decision-Making and Organizational Efficiency
Priyanka N, Shankar Lingam M

32 Automatic segmentation of lung lesions from medical imaging
Fatou NDIAYE, Sada ANNE, Amadou Dahirou GUEYE

33 Comparative Performance Analysis of Machine Learning Models for Agricultural Crop Prediction⋆
Aditya G Nanaware, Harsha R Gaikwad, Snehal R Mali, Manjushree D Laddha, Arwind W Kiwelekar

34 System for early detection of breast cancer using deep learning from medical imaging
Awa BAKHOUM, Sada ANNE, Amadou Dahirou GUEYE

35 Dual-Branch Scene Text Detection for Robust Competition Number Identification in Dynamic Outdoor Environments
Virendra Singh Solanki, Awanit Kumar, Snehlata Ajmera, Nirmal Singh, Sheshang Degadwala, Dhairya Vyas

36 Deep Learning in Healthcare: A Futuristic Approach of Enhancement
Kumar Rahul, Ramjee Prasad Gupta, Neeraj Arora, Surender Kumar Kulshrestha

37 Deep Learning Based Model for Landslide Detection from Synthetic Aperture Radar Imaging
Manu Gupta, Yallamati Prakasa Rao, Manideep Shivanathula, Smahi Bandari, Arundhathi Uppari, P Michael Preetam Raj

38 Standard vs. Curriculum-Based Proximal Policy Optimization in High-Dimensional Quadrupedal Locomotion: An Empirical Investigation of Negative Transfer Effects
Sarika Dharangaonkar, Aastha Kataria, Suyash Mundhe

39 Multi-Modal Deep Learning Framework for Thyroid Tumor Detection Using Vision Transformers and Generative Pretrained Models on Ultrasound Images
B Shankarlal, G Sureshkumar, M Thiruppathi

40 A comprehensive study of CMOS Inverter Power Consumption with Transistor Width and Temperature Variations Using Cadence Virtuoso
Biswazit Mistry, Suman Chowdhury

41 Deep Learning for Alzheimer's Disease Classification: A Systematic Review of Algorithmic Effectiveness.
Shaik Khasim Basha, Khasim Syed

42 Analysing the Optimization of Cooling Systems in Industrial Settings: Exploring Efficiency and Cost Reduction
Farid Agayev, Sevinj Bakhshaliyeva

43 Modeling of Solar Panel Installation Mechanism for Hybrid Energy Systems in Azerbaijan
Rehim Rehimov, Nizami Suleymanov, Zarifa Mahmudova

44 System for Increasing the Accuracy of Digital Information Processing
Farid Agayev, Sevinj Bakhshaliyeva

45 Performance Evaluation of Different Shapes of Patch Antenna for 5G Applications at 25 GHz
Afsana Sultana Alvee, Md. Sohel Rana, Najifa Islam, Mahamud Hasan, Md. Abdul Ahad

46 Harnessing the wildlife animal detection using proposed CNN and ResNet50 deep learning model
Suman Chowdhury, Dilip Kumar Das

47 Cyber Defense with Predictive Analysis and Compliance Using LSTM and Swarm Intelligence in Indian Cyberspace
Bakare R, Sarvade S

48 An Approach Based on the PRESENT Lightweight Cipher to Ensure Security and Performance Balance for IoT Devices
Tukhtajon Kozokova, Lola Davronova, Nuriddin Jabbarov

49 Occluded Face Reconstruction based on GANs for Realistic 3D Avatars in Virtual Reality
Yingying Li, Ajune Wanis Ismail, Muhammad Anwar Ahmad, Fazliaty Edora Fadzli

50 An Optimized Deep Learning Based Framework for Cognitive State Classification Using Brain-Computer Interface Technologies
E Padma, Gokulakrishnan S, R Chithra, ArulKumar R, M Kalaiselvi

51 Transformer-based Bidirectional Encoder SQL Representations for Interpretable Cyber Attack Detection Using Ensemble Learning
Raymond Sekyewa, Michael Kizito, Kyanda Swaib Kaawasse, Tonny Bulega, Ggaliwango Marvin

52 ML-Driven Analysis of NavIC-Based Tracking for Route Optimization in Urban Air Mobility
Vishvesh Paresh Modcoicar

53 Algorithm for conducting information security audits in organizations based on a multilevel model based on graph theory
Ikbol Kholimtaeva, Sunbula Muminova, Barno Shamshieva, Jakhongir Shaidullaev

54 End-to-End Air Quality Forecasting with Refined Architecture and Low-Code Big Data Framework
Kieu-Bao-Khanh Nguyen, Dinh-Thien-Huy Nguyen, Van-Luan Vo, Duy-Khang Le, Chau-Hao-Nhan To, Thanh-Van Le

55 A Hybrid Deep Learning and LLim et al. (2024M Framework for Landslide Detection and Severity Analysis
G Sudha Sadasivam, Sanjay P, Pathipati Shailesh Babu, Nithish Narayanan, Muralidhar KV, Ajay Gowtham

56 Harnessing Supervised Machine Learning (ML) Principles for Enhanced Early-Stage Diagnosis of Parkinson's Disease
Rajesh Kumar N, Devabharathi M, Prasad Theeda, Manikandan G, R Bala Krishnan

57 Real Time Crash Forecasting using a Stacking-Based Machine Learning Ensemble
Dipankar Roy, Subir Gupta, Bibhuti Bhusan Dash, Monalisa Chakraborty, Subrata Chowdhury, Sudhansu Shekhar Patra

58 PCOS Detection and Classification using Deep Learning Approach
Vaishnavi Sooraj, Pakruddin B, Darshan Giri

59 Algorithm for assessing threats to information security
Kholimtaeva Ikbol, Sunbula Muminova, Barno Shamshieva, Jakhongirbek Khabibullaev

60 A Smarter Plate: Enhancing Food Delivery Apps with Personalized Proportion Sizing and Nutritional Awareness
Ashwini Dalvi, Sargundeepkaur Sachdeo, Samrudhi Bhat

61 Improving Water Quality Prediction using Robust Outlier Detection and RankGenForestStacking Classifier Approach
A Sumathi, R Saruhasini, S Meganathan, Sheik Mohideen Shah, Sundar Santhoshkumar

62 Blockchain-Enabled Patient Consent System for Secure Healthcare Data Management
Jayesh Surve, Ashwini Dalvi, Irfan Siddavatm

63 Assessing YouTube Title-Content Alignment using NLP Framework
Tanneru Sai Ramya, Maturi Bhavya Sri, Arul Elango

64 HoloChef: 3D Culinary Guide with Speech Command
Fazliaty Edora Fadzli, Amira Azkia Rahmatulloh, Ajune Wanis Ismail, Muhammad Anwar Ahmad, Tee Ng Zikang, Mohamad Yahya Fekri Aladin

65 Zero-knowledge Enhanced Adaptation Learning (ZEAL): A Framework for Verifiable Model Adaptation
Dhrumil Panchal, Hrushik Mehta, Pragati Shetty, Pratik Kanani, Darshana Sankhe, Rashmi Kumar

66 JOVA Robotic Prosthetic Arm
Jose Kevin, Kesanakurthi Aditya, Karuturi Vaishnavi, V Nithya

67 Real-time defence against emerging IoT threats via feature-engineered ensemble learning in fog computing environments
Abdelilah Chahid, Yassine Znagui, Kamal El Guemmat, Sara Ouahabi, Khalifa Mansouri

68 Assess the Effects to Organs Induced by I-131 Radiopharmaceutical Accumulates in Thyroid Gland by Monte Carlo Simulation
Minh Khanh Duong, Tat Thang Nguyen

69 Cascaded Energy Management System with ANN Controlled DC Microgrid Systems
B Balaji, P Hemalatha, U Naveen Johnson, R Revathy

70 Voltage Regulation in a 33 Bus Distribution System with Integrated STATCOM and Grey Wolf Optimization
B Balaji, P Hemalatha, J Chandru, R Preetha

71 AI Based Malware Detection Using Machine Learning, Random Forest, Extra Tree Algorithms
Pramod, Karthik BP, Vijaya Reddy Biradar, Abhishek Shreedhar Yarandoli, Geetha Rani Edupuganti

72 Real Time People Monitoring using MobilNet-SSD
Darshan Atkari, Arshal Agarwal, Atharva Kulkarni, Apoorva Kulkarni, Sonali Antad

73 Performance Optimization of a PV Module Integrated with Fuzzy/NN INC-Based MPPT and Zeta DC-DC Converter for Grid-Connected Applications
S Madhusudhan Reddy, S Muthubalaji, DS Sanjeev

74 MobileFormer: Efficient Stroke Lesion Detection with Lightweight CNN- Transformer Fusion
Sadiya Sulaiman, M Roshni Thanka, E Bijolin Edwin, Nader Salam

75 SweetPick: Leveraging AI to Predict Apple Sweetness
Ishya Reddy, Sameeksha Damera, Sahithi Settivari, Akanksha Priya, Rashmi S

76 Cataract Detection Using Deep Learning Leveraging Fundus and Anterior Eye Images
Savu P Sudheep, K K Sherly, Jithin Mathews

77 Blockchain-Enabled Communication for Sustainable Fashion: Impact on Consumer Trust and Purchasing Behavior
Bui Thanh Khoa, Ai-Van Huynh

78 Comparative Analysis of Iron Oxide (Fe 3 O 4) Nanoparticles and Iron Oxide-Tungsten Trioxide (Fe 3 O 4 - WO 3) Nanocomposites using Digital Image Processing Techniques
Parashuram Bannigidad, Sagar Chingali, Prabhuodeyara Gurubasavaraj

79 Sustainable Healthcare Systems through Arduino- Driven Medical Waste Segregation and Disposal Monitoring
Sharada M Kori, Yogesh Lubal, Jyoti Amboji, Madhuri M Patil

80 A Multi-layered Architecture for Email Classification
Sherzod J Khamidov

81 Integrating OpenCV and Mediapipe: Developing a High-Precision Virtual Try- On System for E-commerce in the Fashion Industry
M Jayaram, K Chandrashekar, Matta Manikeshwari, Sama Manuja Reddy, Battu Vidya Prakash, Mohammed Khaja Amanuddin

An Arduino-Based Smart Car Safety System: Integrating Obstacle Detection, Battery Health Monitoring, and Smoke Detection for Enhanced Vehicle Safety

Debanjan Bera[1 [0009−0006−5862−9604]], Partha Biswas[1 [0009−0003−0827−417X]], Bristi Chakraborty[1 [0009−0007−3063−4062]], Soumadip Chandra[1 [0009−0006−3934−1744]], Souvik Bairi[1 [0009−0006−2504−5215]], and Sandip Chakraborty[2 [0009−0000−1166−0846]]

[1] BCA, Brainware University, Barasat, West Bengal, India
debanjan2832004@gmail.com
parthabiswas112200@gmail.com
Chakrabortybristi2004@gmai.com
soumadipchandra425@gmail.com
souvikbairi2004@gmail.com
[2] Assistant Professor, Brainware University, Barasat, West Bengal, India
sandipchakrabortycs@gmail.com

Abstract. The safety system designed for smart cars, based on Arduino, will provide an approach to safety in travel and the operation of vehicles as a whole. It comes with an obstacle detection module that uses an ultrasonic sensor (HC-SR04), which emits high-frequency sound waves. it detects if there is an object coming towards the car, and in this respect, activates a buzzer once an object is detected for a possible collision under the supervision of an operator. The battery health monitoring system continuously measures its performance using voltage, current, and temperature sensors that can send alerts to the operator for overheating and abnormal power fluctuations of electric current. The Smoke Detection Module looks for smoke and toxic gases in the atmosphere by utilizing an MQ2 sensor and is expected to provide warnings whenever the level of smoke crosses a certain limit; we also use an Arduino Uno board to manage real-time sensor readings through buzzers and LEDs. This concept can create an economical and easy-to-assess, flexible, and overall reliable solution for vehicle safety, thus turning out to be an appropriate substitute for the smart and traditional vehicle marketplace.

Keywords: Arduino-based system · vehicle safety· obstacle detection· battery health monitoring · smoke detection · microcontroller technology.

1 Introduction

New models of automotive technology mark a shift from reactive to proactive systems where the goal is safety. Old technologies, like airbags, seat belts, and anti-lock braking systems (ABS), are fundamentally classified under passive safety;

meaning they work to protect an individual in the aftermath of an incident [1]. As vehicles are becoming more complex and automated, there is a need for real-time detection and mitigation of hazards. With sensor technologies interconnected to microcontrollers, vehicles can effectively monitor and address conditions that can lead to accidents [2].

This paper presents an Arduino-based smart car safety system, which integrates three basic yet crucially important safety mechanisms: obstacle detection, battery health monitoring, and smoke detection, all in one affordable device. All components mitigate one or the other particular dangers associated with motor vehicles and thus cooperate to form a general integrated preventive solution.

The detection of obstacles is particularly applicable in city landscapes and for autonomous vehicles[3]. The ultrasonic sensor HC-SR04 assists in achieving the goal. It continues to update the range between the vehicle and objects in front of it thus, when necessary, it alerts the driver or rapidly stops the car [4]. Battery operations may also include overloading aspects, such as the sensor monitoring the voltage, current and temperature. Thanks to the timely application of these sensors, the breakdowns may be prevented and the life of batteries prolonged [5]. Leaking smoke and gasses are resolved using an MQ2 sensor, which can detect environmental pollutants such as CO and CH4 gases in the air and activates alarms to help prevent smoke and toxins from coming up before a fire breaks out [6].

The goal is to create a consolidated and effective safety system that is Arduino Uno-based and is preferred because of its ease, low power use, and compatibility with sensors. This is a lightweight system that is expandable, not like AI-enabled systems or those that are too expensive for regular or self-driving cars. The system aims to provide real-time notification using an LCD. The latter included visual and audio warnings.

The proposed system is in tandem with the current trending inclination towards the incorporation of safety mechanisms as part of our everyday life which creates a base for the facility's possible future expansion by including such functionalities as integration internet of things, lane departure warning, and AI-facilitated diagnostics.

2 Literature Review

The inclusion of motor vehicles' sensor-based safety features is considered a significant part of lessening the rate of accidents on roads apart from the reduction of danger-related events. Several investigations have been done into the various safety devices available, which include the designs of collision avoidance systems, health monitors for batteries, fire alarms, and others that are important in sustaining safe operations. However, most authors prefer to treat design and control components separately rather than embedding them in a system. This part summarizes the responses in the literature to the highlighted questions and points out the innovative changes as well as the gaps in knowledge that this study intends to fill.

2.1 Obstacle Detection in Smart Vehicles

Obstacle detection serves as the basis for assisted and autonomous driving systems alike with the primary objective of being able to anticipate and consequently prevent obstacles in the path of the moving vehicles. In a study on collaborative motion guidance for industrial autonomous vehicles, it was shown how vehicles could avoid collisions by communicating with each other and by detecting the obstacles in real time [7].

Obstacles can be detected using ultrasonic sensors which is very common, especially in mobile robots. This was put to test in real time for different ranges and confirmed by Azeta et al. [8]. They are cost-effective to include in automotive systems that utilize an ultrasonic sensor within an Arduino.

Intriguingly, progress in this field has gone further by developing advanced concepts such as data fusion systems integrating ultrasonic sensor with stereo cameras. This view was provided by Gholami et al. [9], stating that combining the vision and ultrasound images is useful in negating a lot of false alarms while increasing the level of awareness of the vicinity on a different scale. Unfortunately, stereo camera operations tend to be computationally intensive and therefore cannot be used on platforms of a lower cost, such as Arduino.

2.2 Battery Health Monitoring Systems

Batteries are an essential part of electric and hybrid motors. Neglecting to check the health of the battery can lead to a system crash or even fire. An Arduino powered Battery Management System (BMS) was implemented by Garg et al. [10] for monitoring the voltage, temperature, and current in real time, and the data could be accessed through mobile applications.

Pradhan and Chakraborty [11] built a battery monitoring system that works on voltage and temperature measurement using divider circuits and temperature sensors which ensures that the degradation is detected early. This allows for proactive measures to prevent failures of both the vehicles and the batteries themselves.

In a bid to provide more advanced monitoring systems, Widodo et al. [12] presented a BMS system that detects anomalous behaviour (due to voltage) in the batteries using machine learning and sample entropy. Unfortunately, such adaptive computing technology is not viable with a low power consumption microcontroller system since they require one with a high computation performance. As a result, it is possible to use battery monitoring devices based on Arduino modules, which are designed for low power and real time applications.

2.3 Smoke Detection in Automobiles

Detecting smoke at its early stage is very important when it comes to vehicle fires caused by electrical defects or leakages in fuel. Gautam et al. [13] studied semiconductor gas sensors, highlighting their effectiveness in detecting gases like carbon monoxide or smoke accumulation in vehicles' interiors.

One of these sensors with a long history of usage in fire alarms is the MQ2 smoke sensor, and this particular device is used by Adedokun et al. [14] to check how fast it can respond in a vehicle environment. At low concentrations, the sensor was able to detect smoke and give alerts. Its use with Arduino boards allows it to detect several gases, including CO, methane, or even LPG, making it a good product for car industries.

As for the incorporation of AI-enhanced smoke detection, although work in such lines has also been exploited and is known to people, for example, Yuan et al. [15] it is also noted that these detection algorithms are associated with high power consumption so that the system can discriminate between normal vapor and smoke, which is dangerous. Despite its effectiveness, low-power embedded systems cannot use it for real-time performance. Still, they are promising. As a result, this study will utilize the sensor-based MQ2 module, which is inexpensive and reliable.

2.4 Summary and Research Gap

Despite the considerable amount of research on vehicle safety features at the individual level, there has been very little work done on designing a comprehensive safety package using a network of protective devices operated from a single microcontroller. Many of the existing solutions are expensive, advanced or cover only one aspect of safety system. The paper that follows brings solutions to these topics by introducing an Arduino cooperative system to detect obstacles, measure state of the battery and recognize smoke.

Unlike AI-based solutions, the recommended model is more accessible, cost-effective, and simple to implement, especially in environments with limited resources. Such a foundation will support further developments of smart car safety systems that embrace modularity, and will be ready for integration in electric cars as well as in traditional and autonomous vehicles.

3 System Design and Architecture

Arduino based intelligent vehicle safety system, including the obstacle detection system, battery maintenance concepts and anticipation of smoke formation, is thus modelled. These subsystems are normally digitally controlled with the help of an arduino, which aids them in operating optimally at any given time. This system encompasses a three-tier architecture configuration which consists of the following aspects: detection, processing, and implementation.

The primary component of the system is an Arduino Uno whose main benefits are its ease of use, its ability to perform tasks in real time, its low price and also, its ability to be interfaced with many sensor modules. Compared to counterparts like Raspberry Pi and ESP32, the Arduino Uno offers a power-efficient and hardware-centric platform well suited for incorporating into vehicle safety electronics. Please refer to Table 1 for the specifications of the Arduino Uno in detail. The system implements a variety of sensors to measure different,

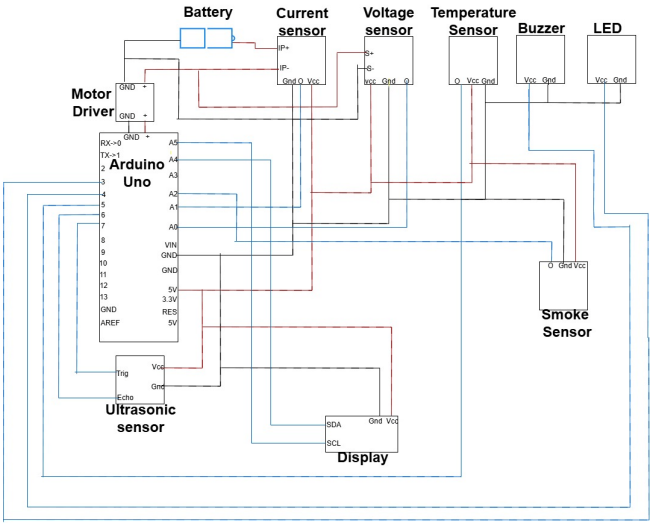

Fig. 1: Circuit Diagram of the System

safety related parameters. Specifications of these components are given in Table 2. A schematic showcasing these devices and their connection in its entirety is Implemented in Figure 1.

Table 1: Arduino Uno – Technical Specifications

Parameter	Specification
Microcontroller	ATmega328P
Operating Voltage	5V
Input Voltage (recommended)	7–12V
Digital I/O Pins	14 (6 PWM-enabled)
Analog Input Pins	6
Clock Speed	16 MHz
Flash Memory	32 KB (0.5 KB used by bootloader)
SRAM	2 KB
EEPROM	1 KB
Communication Interfaces	UART, SPI, I2C

Table 2: Sensors Used in the Smart Car System

Sensor Type (model)	Parameter and Range
Ultrasonic Sensor (HC-SR04)	Distance: 2–400 cm, ±3 mm
Voltage Sensor (Generic)	Voltage: 0–25 V, ±0.1 V
Current Sensor (ACS712 (20A))	Current: ±20 A, ±1.5%
Temperature Sensor (DHT11)	Temp: 0–50 °C, ±2 °C
Smoke Sensor (MQ2)	Smoke/Gas: 300–10,000 ppm, 2–5s

The obstacle detection module mounts an HC-SR04 ultrasonic sensor on the front portion of the vehicle to achieve this. It is a sensor that emits sound of a frequency of 40 kHz and then measures the delay between sound emission and receiving the echo of the sound it produced on objects and the new positioning it would have traveled. This kind of object detection a small range from 2 to 4 meters, which is possible by exploiting formula 1. If the obstacle comes within

a specified zone, the system turns off the motor and activates sound and light indicators, stopping it from hammering against the obstacle. Figure 2 displays the real-time testing process and results of the same application.

$$Distance = \frac{Speed of Sound \times Time Delay}{2} \tag{1}$$

The battery health monitoring module integrates three sensors:

- A **voltage sensor**, to keep track on the overall battery voltage;
- A **current sensor (ACS712)**, to measure the current draw and identify overcurrent conditions; and
- A **temperature sensor (DHT11)**, to detect whether the battery is overheating.

The Arduino Uno receives constant information from the sensors, analyzes and compares it with the norm, and signals any deviations. When the system identifies factors like low voltage, overcurrent, or high temperature, it sends an alarm for immediate attention. Additionally, an LCD displays the real-time battery stats for quick evaluation. This feature allows quick and non-invasive risk assessment or problem solving following a standard or maintenance routine. The screen changes in response to the changes in battery health, and it does update itself. In Figure 3, there is an illustration showing what the monitoring view may look like in real time.

To alert about smoking, gas leaks, explosions, and other accidents in the car, the module uses the MQ2 gas sensor, which can detect carbonaceous smoke, hydrocarbon gases including methane, as well as carbon monoxide, or liquefied petroleum gas. Inside, vehicular air is screened cyclically by the sensor to gauge air quality, and the data is transmitted to the Arduino. If the concentration of gases is more than the stipulated safety standard, typically more than 300 ppm, a warning will be triggered on the system in case of impending hazard. In addition to buzzer on and the LED turning on, this air quality alarm is also demonstrated on the LCD screen that is used to display the voltage level to the driver. The simplicity of this notification stems from the possibility of drivers interacting with both sound and graphical data. The response to smoke alarms is the topic of Figure 4

The whole network is controlled by a DC source, and every sensor is attached to the Arduino Uno through analog/digital input nodes. The motor driver (L293D) provides the link between the Arduino and the DC motors for the purpose of moving them in response to the signal from the sensor. The detection system includes the use of buzzers and LEDs to indicate signals in hazardous environments.

We designed this system using a modular approach to facilitate easy adjustments for evolving safety requirements. It takes advantage of the possibilities of modern electronics, which allow for immediate control response and adaptable warning depending on the danger level. The system also guarantees that it fits with current manned vehicles and, at the same time, can be used with unmanned vehicles, thus making it a potential design for smart car hazard detection.

Fig 2: Obstacle Detection Output

Fig 3: Battery status display

Fig 3: Smoke Detection Output

4 Results and Discussion

To evaluate the performance of the Arduino-based smart car safety system, three key functionalities were subjected to test cases designed to imitate actual circumstances. These features include the obstacle detection, battery health monitoring and smoke detection, with particular focus placed on promptness, precision, and trustworthiness. All the modules were also integrated into a working prototype car and evaluated while situated inside a laboratory, which also involved trying performance under various tests to ascertain their efficiency.

4.1 Obstacle Detection Performance

Ultrasonic sensors (HC-SR04) were efectively deployed within the limiting range of 2 cm to 4 meters with less than 50-millisecond response time on average for detecting an object. Whenever the defined critical distance (say 25 cm) was approached by any object, the Arduino would turn off the motor and trigger the buzzer and LED alarm immediately, which prevented any pair of simulated collision immediately. However, some setbacks were observed wherein soft and uneven surfaces like foam would absorb sound waves, leading to sporadic false negatives.

Environmental disturbances were also used to assess the sensors' effectiveness. Detection was very consistent operating under low-light dry indoor conditions but slightly low under cases of strong air currents, water droplets, or sonic interference. Under the mentioned conditions, detection accuracy could be possibly impeded due to the degrading effect these factors have on ultrasonic signal quality. Future works could focus on the integration of infrared or LiDAR sensors that may support improving the detected performance in conditions like fog, rain, and EMI disturbances.

4.2 Battery Health Monitoring Results

The voltage sensor precisely tracked input levels to within ± 0.1 V of the true values. The ACS712 current sensor can reliably detect deviations in current when the measured value exceeds the resolution threshold in the 20 A-rated configuration. The DHT11 sensor provided steady monitoring of the battery box temperature, with an accuracy of ± 1 °C. To alert the operator, critical

values, such as low voltage at ≤10.5 V, overheating at ≥45 °C, or conditions of overcurrent, were considered triggers. These conditions were displayed on the LCD screen in real time, allowing the user to monitor and respond proactively before any real damage could be done.

4.3 Smoke Detection Accuracy

The MQ2 sensor then responded in between 1 and 2 seconds to simulate smoke and gas leaks. It was capable of detecting concentrations higher than 300 ppm. The LCD was programmed to display an air quality warning with gas concentration levels and battery data. Sensitivity was good in closed spaces but startup time was slightly delayed due to sensor warm-up time.

4.4 System Comparison with Existing Solutions

For conducting assessment for practicality of system, it was compared with other vehicle safety platforms in terms of cost, accuracy, and implementation. Results are summarized in Table 3.

Table 3: Comparative Analysis of Smart Vehicle Safety Systems

Feature	**Proposed System (Arduino-Based)**	**AI-Based System**	**Traditional System**
Obstacle Detection	HC-SR04 Ultrasonic Sensor (±3 mm)	LiDAR / Stereo Vision (High accuracy, high cost)	Infrared Sensors (Low range)
Battery Monitoring	Voltage, current, temperature sensors	ML-based predictive BMS	Voltage-only checks
Smoke Detection	MQ2 Sensor (Multi-gas detection)	AI Smoke Classifier (Needs GPU)	Basic CO sensor
Display Feedback	LCD interface (real-time alerts)	App/cloud interface	No display or basic LED
Cost (per unit)	Low (<INR 4000 or $50)	High (INR 50,000+)	Medium (INR 10,000)
Implementation Effort	Easy (DIY-compatible)	Complex (Data training needed)	Moderate

We have examined the system in different scenarios, performing about 10 test iterations per feature. Nearly all the data logs indicate a success of 95-98% in correctly detecting hazards and activating warnings in nominal conditions; only under certain edge cases, for example, high humidity or unstable power supply, were there minor cases of false activation or delayed activation reported. These results confirm that the system is a good candidate for entry-level smart vehicles, educational labs, and areas with tight budgets.

5 Conclusion and Future Scope

The work focused on developing a smart car safety system integrated with an Arduino, which includes obstacle detection, battery health monitoring, and smoke

detection functionalities under one roof. It is an automatic system that detects the surrounding objects through ultrasonic sensors within a safe range. In addition, the platform continuously monitors the battery voltage, current, and temperature value and gives responses under risky concentrations of hazardous gases using the MQ2 sensor. Enhanced awareness and usability for the system were provided by an LCD where real-time data were visualized. Testing proved to show reliability in performance during normal working conditions, with well-triggered alerts under normal as well as repeat iterations. Compared to an old-school traditional system or an AI-based system, the proposed one is very low-cost with very low complexity and thus suitable for students and entry-level automobiles. Developments hereinafter may include adaptive safety responses using machine learning, Internet of Things (IoT) connectivity for remote monitoring and various others, including lane departure warnings, alcohol detection, and even diagnostics within the cloud. All these features would open up further capability for this system and set it toward being an intelligent, scalable safety solution for next-generation automobiles.

References

1. Répás, J., Berek, L.: Security and safety systems on modern vehicles. In: Lecture notes in mechanical engineering. pp. 84–100 (2022). https://doi.org/10.1007/978-3-031-15211-5_8
2. Yaswanth, R., Babu, M.R.: Revolutionizing Automotive Technology: Unveiling the state of Vehicular Sensors and Biosensors. IEEE Access. 1 (2024). https://doi.org/10.1109/access.2024.3514157
3. Chandra, B.R., Chaithanya, J.K., Roy, A., Reddy, C.L.: Smart City: Challenges and Opportunities Detection and Identification of Autonomous Vehicles Using Sensor Synthesis. In: Explainable IoT Applications: A Demystification. pp. 143–158. Springer, Cham (2025). https://doi.org/10.1007/978-3-031-74885-1_9
4. Alsayaydeh, J.A.J., Yusof, M.F.B., Abdillah, M.A.A.B., Al-Gburi, A.J.A., Herawan, S.G., Oliinyk, A.: Enhancing vehicle safety: a comprehensive accident detection and alert system. International Journal of Advanced Computer Science and Applications. 14, (2023). https://doi.org/10.14569/ijacsa.2023.0141104
5. Waseem, M., Ahmad, M., Parveen, A., Suhaib, M.: Battery technologies and functionality of battery management system for EVs: Current status, key challenges, and future prospectives. Journal of Power Sources. 580, 233349 (2023). https://doi.org/10.1016/j.jpowsour.2023.233349
6. Biscarri, E.L.: Fires in Conventional and Electrified Vehicles: Theory, Prevention, and Analysis. SAE International (2024).
7. Grosset, J., Fougères, A.-J., Djoko-Kouam, M., Couturier, C., Bonnin, J.-M.: Collision and obstacle avoidance for industrial autonomous vehicles - simulation and experimentation based on a cooperative approach. https://hal.science/hal-04638317v1
8. Azeta, J., Bolu, C., Hinvi, D., Abioye, A.A.: Obstacle detection using ultrasonic sensor for a mobile robot. IOP Conference Series Materials Science and Engineering. 707, 012012 (2019). https://doi.org/10.1088/1757-899x/707/1/012012
9. Gholami, F., Khanmirza, E., Riahi, M.: Real-time obstacle detection by stereo vision and ultrasonic data fusion. Measurement. 190, 110718 (2022). https://doi.org/10.1016/j.measurement.2022.110718

10. Garg, P., Bansal, D., Khan, S., Bhattacharya, S.: Development of energy measurement system for electrical vehicle battery using Arduino. In: Lecture notes in electrical engineering. pp. 457–464 (2022). https://doi.org/10.1007/978-981-19-0588-9_45
11. Pradhan, S.K., Chakraborty, B.: Battery management strategies: An essential review for battery state of health monitoring techniques. Journal of Energy Storage. 51, 104427 (2022). https://doi.org/10.1016/j.est.2022.104427
12. Widodo, A., Shim, M.-C., Caesarendra, W., Yang, B.-S.: Intelligent prognostics for battery health monitoring based on sample entropy. Expert Systems With Applications. 38, 11763–11769 (2011). https://doi.org/10.1016/j.eswa.2011.03.063
13. Gautam, A., Verma, G., Qamar, S., Shekhar, S.: Vehicle Pollution Monitoring, control and challan system using MQ2 sensor based on Internet of things. Wireless Personal Communications. 116, 1071–1085 (2019). https://doi.org/10.1007/s11277-019-06936-4
14. Adedokun, A.O.: IoT Based Public Transportation Accident Prevention with Driver Alcohol Detection and Smoke System. International Journal of Research and Innovation in Applied Science. IX, 765–775 (2024). https://doi.org/10.51584/ijrias.2024.908069
15. Yuan, C., Liu, Z., Zhang, Y.: Learning-Based smoke detection for unmanned aerial vehicles applied to forest fire surveillance. Journal of Intelligent & Robotic Systems. 93, 337–349 (2018). https://doi.org/10.1007/s10846-018-0803-y

Next generationFR1MultiportAntenna with Metasurface for Drone Networking

Suguna G[1], Yogeshwari P[2], Rajesh A[3], C Manikandan*[4], Suba Renjani N[5] and Saranya J[6]

[1,2,3,4,5,6]School of Electrical & Electronics Engineering,

[1,2,3,4,5,6]SASTRA Deemed University, Thanjavur, Tamil Nadu, India

suguna@ece.sastra.ac.in, yogaindira93@gmail.com, rajesha@ece.sastra.ac.in, manikandan@ece.sastra.ac.in, dpfi0424011924@sastra.ac.in, dpfi0424011997@sastra.ac.in

Abstract. A compact flexible metasurface integrated narrowband 4-element multiple-input multiple-output (MIMO) antenna was developed for fifth-generation (5G) Sub 6 GHz drone communication. First, a microstrip patch with a defective ground structure was constructed at the n78 band. Then, 4-port microstrip MIMO antennas are placed orthogonally to each other. The antenna is mounted on polyimide material with a total dimension of 86.50 x 78 x 0.1mm. A dual square double negative metasurface was designed to improve the antenna parameters such as scattering parameters, gain, and envelope correlation coefficient. The unit cell dimensions are 38 x 38 x 0.1mm and are developed using a polyimide substrate for conformability. A MIMO antenna achieves the 5G Frequency Range 1 (FR1)band of 3.6 GHz with an S_{11} of -25.5 dB and a gain of 5.02 dBi. Integrating the metasurface with the 4-port antenna enhances the gain from 5.02 dBi to 8.305 dBi, reflection coefficient< -30 dB, isolation > 20 dB, envelope correlation coefficient< 0.025, and diversity gain > 9.9.

Keywords: Metasurface, Antenna, Polyimide, Multiple Input and Multiple Output, Sub-6 GHz

1 Introduction

Nowadays, there has been a noticeable increase in the use of drones in the military, communications, industrial, and commercial markets. To improve, the transmission speed and bandwidth spectrum of fifth-generation (5G) wireless communication have recently attracted attention worldwide [1-2]. Wireless networks may need n-times more capacity in the next years than they do now because of a massive growth in annual data traffic (40% to 70%). With a peak throughput of many gigabits per second (Gb/s), fifth-generation (5G) systems are thought to be a significant option for upcoming communication applications to

address this rapidly increasing demand [3]. Communication with an Unmanned Aerial Vehicle (UAV) is challenging due to instability and drag issues that occur when the drone is in motion [4]. Antennas become bendable when their substrates are clad by thin copper film. The antenna must be light to improve system endurance, tiny to accommodate UAV's extremely tight space constraints, and low profile to minimize air resistance and meet aerodynamic requirements [5]. In [6], two folded strips installed on a ground plane make up the UAV antenna. It operates at 500 – 511 MHz frequency with an omnidirectional pattern. Changing the capacitive at the two ends of the metal strips increases the antenna performance. A multiport antenna with a metasurface is constructed [7]. A 1 x 2 array antenna with a circular split ring-shaped metasurface was developed to enhance the MIMO system. The antenna operating frequency is mm-wave with a peak gain of 10.27 dBi.

Table 1. Comparison of this work with literature work

Ref	**No. of Ports**	**Frequency (GHz)**	**Technique**	**Mutual coupling (dB)**	**ECC**	**Peak Gain(dBi)**	**Material**
13	2	2.4	MNG Metamaterial	<–20	< 0.16	2	FR-4
14	2	3.8-4.2	DRA+ MS+ Airgap	<–20	< 0.03	4	FR-4
15	2	8.5-11.5	Superstrate+ MIMO	<–18	< 0.01	7.2	FR-4
This work	4	3.6	Metasurface +MIMO	<–25	< 0.025	8.305	Polyimide

In [8], the meander line MIMO antenna was developed at the n78 band with a bandwidth of 400 MHz. Here, the EBG structure was introduced to improve the isolation of the antenna. A U-shaped metamaterial was designed with double negative properties at 5, 6, and 11 GHz [9]. In addition, [10] three pairs of metamaterial arrays are integrated into the bow-tie-shaped millimeter-wave multiplexing antenna to increase gain. This antenna can achieve a maximum gain of 7.4 dBi. MIMO antennas working in the millimeter-wave frequency spectrum have been reported in a few literary works. The antennas in these works display

strong isolation and good MIMO performance. But these MIMO antenna's gain is rather low [11-12]. A MIMO antenna was implemented for the LTE band of 2.3 to 2.4 GHz [13]. A split ring resonator was developed to reduce the coupling of the multiport antenna. The structure enhances the peak gain of 2 dBi. A ceramic material-based metasurface antenna is developed for the 3.8 to 4.2 GHz frequency band [14]. In [15], a wideband MIMO antenna was investigated by integrating metamaterial structure. The antenna improves the return loss by less than -10 dB at ku band frequency. In [16], an eight-port MIMO antenna was developed with dual polarization for 5G communication. In this work, a square ring with a slotted line microstrip patch is designed at 3.6 GHz. A circular ring parasitic structure was introduced to increase the isolation between the antennas. This obtained a bandwidth of around 600 MHz. The comparison of related work is shown in Table 1. A truncated microstrip patch with the defective ground structure was designed to place an orthogonally placed 4-port MIMO antenna. This 5G antenna operates in the frequency of n78 (3.6 GHz) band. Additionally, to improve the antenna performance the Dual Square Ring (DSR) double negative metasurface was implemented. The proposed MTS antenna is used for 5G Unmanned Aerial vehicle communication.

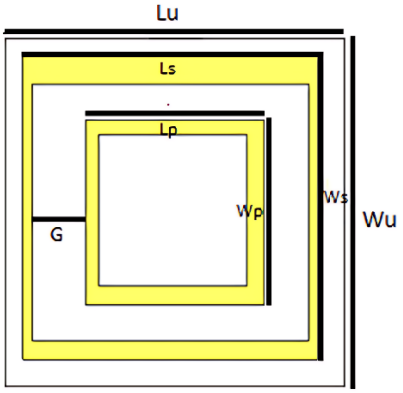

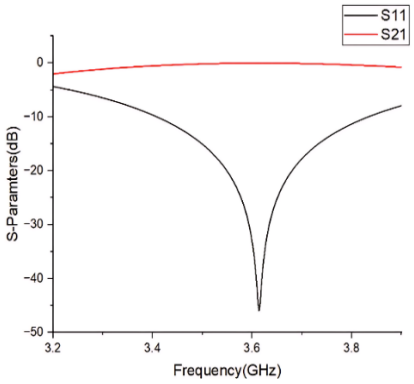

Fig. 1. Geometric of DSR-Metasurface design **Fig. 2.** S-parameter analysis for DSR-MTS

2 DSR Metasurface Design

The design of the unit cell is influenced by the desired electromagnetic response and operational frequency range within the n78 band. The structure incorporates dual square rings made of copper, as illustrated in Fig 1. The DSR-MTS, measuring 38 mm × 38 mm, was constructed on a polyimide substrate with a thickness of 0.1 mm, it appropriate for drone communication. Table 2 outlines the metasurface design parameters. Fig 2 displays the reflection (S_{11}) and transmission

(S_{21}) coefficients of the DSR-MTS. The DSR-MTS design exhibits resonance at the n78 (3.6 GHz) band, achieving a reflection coefficient of -46 dB. Conversely, the transmission coefficient approaches zero, indicating the high reflectivity of the MTS in this 5G band. The real and imaginary values of the effective permittivity and permeability for the DSR-MTS structure are depicted in Fig. 3. Both permittivity and permeability demonstrate negative values at the 5G frequency of 3.6 GHz, suggesting that the metasurface exhibits double negative (DNG) characteristics.

Table 2. Dimension of DSR-MTS

Variable	Dimension (mm)	Variable	Dimension (mm)
Lu	38	Wu	38
Ls	33	Ws	33
Lp	20	Wp	20
G	6	Lm x Wm	106

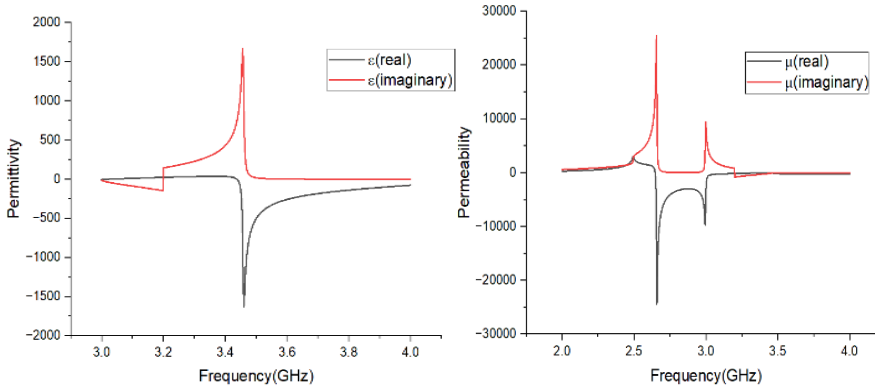

(a) (b)

Fig.3. Simulated results of DSR-MTS (a) permittivity (b) permeability

3 Polyimide Conformable Double Split Antenna Design

Subsequently, a single-element antenna geometry was utilized in the proposed MIMO arrangement, as shown in Fig. 4. The polyimide substrate had dimensions of 35 × 32 x 0.1 mm. A defective structure was introduced in the ground plane to achieve good performance, such as high gain, return loss, and efficiency. Fig. 5

depicts the S-parameters for a single antenna. It achieves a reflection coefficient of less than -10 dB in the n78 band. The dimensions of the proposed single-port and 4-port antenna elements are listed in Table 3.

Table 3. Geometry of proposed Antenna

Variable	Dimension (mm)	Variable	Dimension (mm)
Ls	35	Ws	32
L1	13.9	W1	28.3
L2	20.10	W3	9.95
L3	9.02	W4	32
D	0.7	D1	2
La	78	Wa	86.5

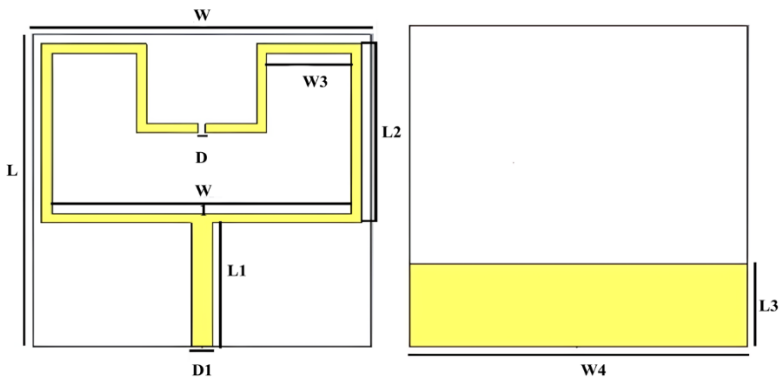

Fig. 4. Geometric of single patch double split antenna design

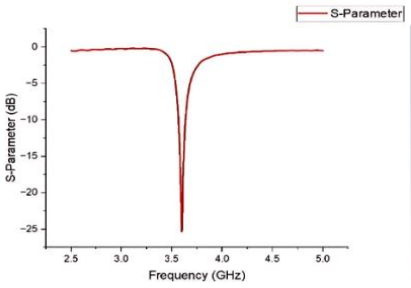

Fig. 5. S_{11} of single port Antenna

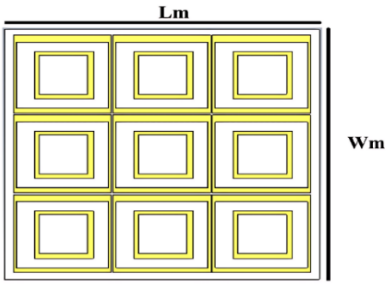

Fig. 6. Array structure of DSR-MTS

4 MIMO Antenna with Metasurface

The single-patch antenna was affected in urban areas due to signal attenuation, scattering, and multipath effects. To overcome these effects, an orthogonally placed four-port MIMO antenna with a DNG Metasurface is proposed to improve the gain. Furthermore, the utilization of the MIMO antenna helps to mitigate multipath fading and enhance signal reliability by leveraging spatial diversity and increasing channel capacity. The geometry of the 3 × 3 metasurface array utilized as the superstrate for enhancing MIMO antenna performance is depicted in Fig 6. The design and fabrication of the MIMO antenna and metasurface are shown in Fig 7 (a), (b), (c), (d) and (e). An air gap of 12 mm separates the 4-port MIMO antenna from the integrated DSR metasurface array. The antenna's S-parameter characteristics, both with and without the metasurface in a multiport configuration, show strong similarity. The metasurface improves the S_{11}< -10 dB, and mutual coupling to less than -30 dB, as shown in Fig 8. Fig. 9 (a) demonstrates that the multiport antenna's peak gain increases from approximately 5.02 dBi to 8.305 dB when the metasurface is employed.

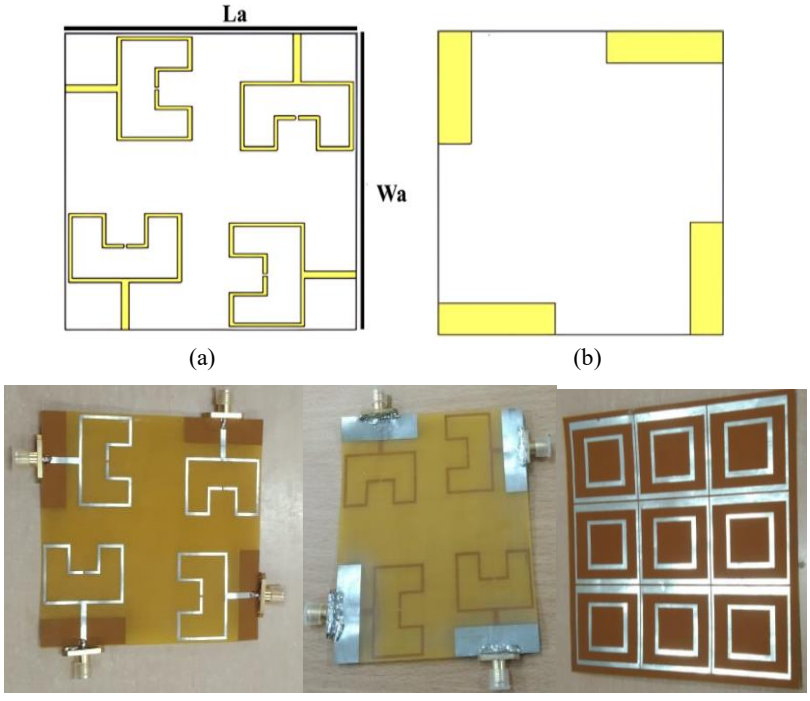

(a) (b)

(c) (d) (e)

Fig. 7. (a) Front side of multiport antenna (b) Defective ground plane (c) Fabricated front side (d) Fabricated rear side (e) Fabricated metasurface

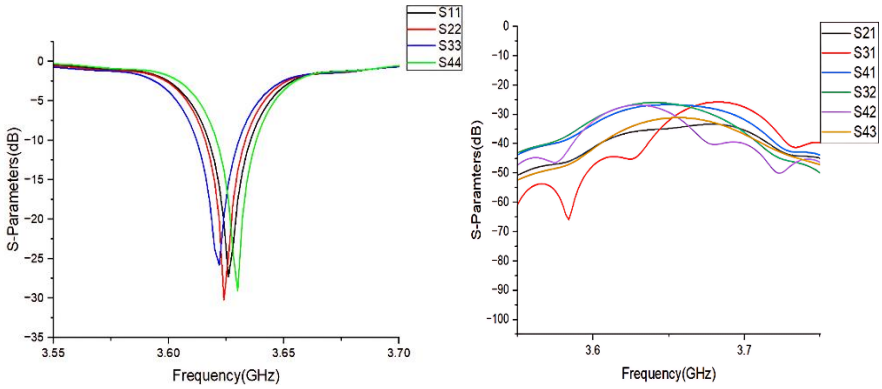

(a) (b)

Fig.8. S-parameter of Antenna with MTS (a) Reflection Co-efficient (S_{11}) & Transmission Coefficient (S_{21})

The 2D far-field simulated radiation pattern at n78 band frequency, displayed in Fig 9 (b), indicates the antenna's directional operation. Fig. 10 illustrates the current flow in the patch, showing the current distribution from the feed to the rectangular patch. At 5G frequency (3.6 GHz), strong current is observed throughout the split ring and antenna ground plane. MIMO parameters were evaluated for the DSR-MTS integrated antenna. Fig 11 (a) shows the Diversity gain (DG) for the proposed MTS-based MIMO antenna. It obtained a value of < 9.9 dB at the 5G frequency, which is considered a good level of diversity gain. Similarly, Fig 11 (b) displays the Envelope Correlation Coefficient (ECC) measured at the same frequency less than 0.005. This shows that the DSR metasurface-based MIMOantenna achieves good independence and minimizes the correlation between the antenna elements. The Total Active Reflection Coefficient (TARC) is used to analyze the diversity performance of the antenna illustrated in Fig 11 (c). The MTS-based MIMO antenna enhances the TARC value is < - 30 dB.

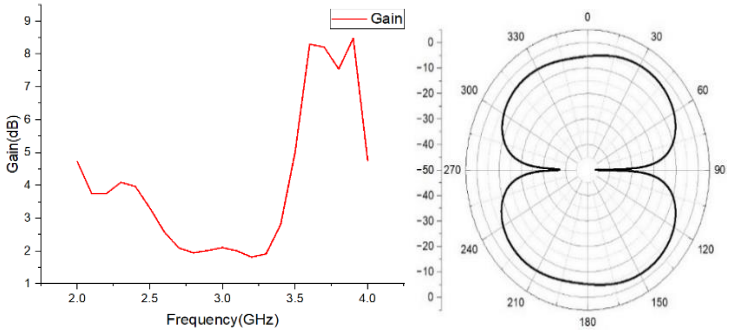

(a) (b)

Fig.9. Simulated results of the antenna with MTS (a) Gain (b) Radiation pattern at 3.6 GHz

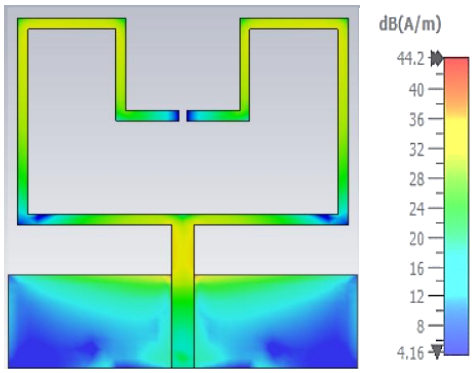

Fig.10. Field distribution of the antenna with Metasurface

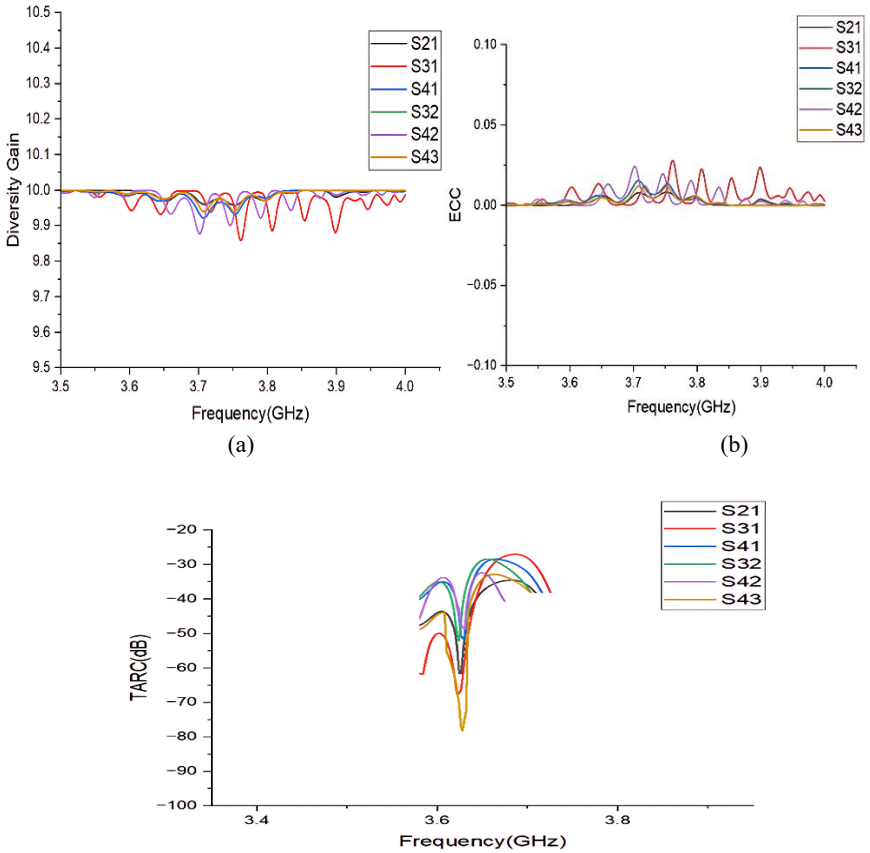

(a) (b)

(c)

Fig.11. MIMO parameters (a) DG (b) ECC and (c) TARC

5 Conclusion

In this paper, an orthogonally placed 4-port MIMO antenna with dual square DNG Metasurface was designed for positioning UAV communication. It operates the bandwidth from 3.4 to 3.6 GHz of the n78 band with the highest gain of 8.3 dBi. The MIMO parameters are analyzed with better performance and isolation is good without adding a decoupling structure. A single-layered metasurface-based four-port antenna was suitable for frequency range 1(FR1) 5G drone applications.

Acknowledgment:

We would like to Thank and Acknowledge IIT Tirupati Navavishkar I-Hub Foundation (IITTNiF), National Mission on Interdisciplinary Cyber-Physical Systems (NM-ICPS), Department of Science and Technology (DST), India for their financial support (SASTRA-IITTNiF/5GNP/2024-25) and SASTRA Deemed to be University, India, for providing the necessary resources and support.

References

1. Roh, Wonil, Ji-Yun Seol, Jeongho Park, Byunghwan Lee, Jaekon Lee, Yungsoo Kim, Jaeweon Cho, Kyungwhoon Cheun, and Farshid Aryanfar. "Millimeter-wave beamforming as an enabling technology for 5G cellular communications: Theoretical feasibility and prototype results." *IEEE communications magazine* 52, no. 2 (2014): 106-113.
2. Boccardi, Federico, Robert W. Heath, Angel Lozano, Thomas L. Marzetta, and Petar Popovski. "Five disruptive technology directions for 5G." *IEEE communications magazine* 52, no. 2 (2014): 74-80.
3. Ferendeci, Altan M. "Flexible conformai antennas." In *2016 IEEE/ACES International Conference on Wireless Information Technology and Systems (ICWITS) and Applied Computational Electromagnetics (ACES)*, pp. 1-2. IEEE, 2016.
4. Sharawi, Mohammad S., Daniel N. Aloi, and Osamah A. Rawashdeh. "Design and implementation of embedded printed antenna arrays in small UAV wing structures." *IEEE Transactions on Antennas and Propagation* 58, no. 8 (2010): 2531-2538.
5. Scorrano, Luca, Angelo Di Rosa, Barbara Orobello, Antonio Manna, and Fabrizio Trotta. "Experimental investigations of a novel lightweight blade antenna for UAV applications [antenna applications corner]." *IEEE Antennas and Propagation Magazine* 59, no. 2 (2017): 108-178.
6. Sun, B-H., Y-F. Wei, S-G. Zhou, and Q-Z. Liu. "Low-profile and horizontally-polarised antenna for UAV applications." *Electronics letters* 45, no. 22 (2009): 1106-1107.
7. Chattha, Hassan Tariq. "4-port 2-element MIMO antenna for 5G portable applications." *IEEE Access* 7 (2019): 96516-96520.
8. Tan, Xiaohua, Weimin Wang, Yongle Wu, Yuanan Liu, and Ahmed A. Kishk.

"Enhancing isolation in dual-band meander-line multiple antenna by employing split EBG structure." *IEEE Transactions on Antennas and Propagation* 67, no. 4 (2019): 2769-2774.

9. Mallik, Anik, Sanjoy Kundu, and Md Osman Goni. "Design of a novel two-rectangular U-shaped double negative metamaterial." In *2013 International Conference on Informatics, Electronics and Vision (ICIEV)*, pp. 1-6. IEEE, 2013.
10. Jiang, Haixin, Li-Ming Si, Weidong Hu, and Xin Lv. "A symmetrical dual-beam bowtie antenna with gain enhancement using metamaterial for 5G MIMO applications." IEEE Photonics Journal 11, no. 1 (2019): 1-9.
11. Jilani, Syeda Fizzah, and Akram Alomainy. "Millimetre-wave T-shaped MIMO antenna with defected ground structures for 5G cellular networks." *IET Microwaves, Antennas & Propagation* 12, no. 5 (2018): 672-677.
12. Pan, Yong Mei, Xin Qin, Yu Xiang Sun, and Shao Yong Zheng. "A simple decoupling method for 5G millimeter-wave MIMO dielectric resonator antennas." *IEEE Transactions on Antennas and Propagation* 67, no. 4 (2019): 2224-2234..
13. Lee, Youngki, Deukhyeon Ga, and Jaehoon Choi. "Design of a MIMO antenna with improved isolation using MNG metamaterial." *International Journal of Antennas and propagation* 2012, no. 1 (2012): 864306.
14. Dwivedi, Ajay Kumar, Anand Sharma, Ashutosh Kumar Singh, and Vivek Singh. "Metamaterial inspired dielectric resonator MIMO antenna for isolation enhancement and linear to circular polarization of waves." *Measurement* 182 (2021): 109681.
15. Jiang, Jianfeng, Yingsong Li, Lei Zhao, and Xiaoguang Liu. "Wideband MIMO directional antenna array with a simple meta-material decoupling structure for X-band applications." *The Applied Computational Electromagnetics Society Journal (ACES)* (2020): 556-566.
16. Parchin, Naser Ojaroudi, Yasir Ismael Abdulraheem Al-Yasir, Ammar H. Ali, Issa Elfergani, James M. Noras, Jonathan Rodriguez, and Raed A. Abd-Alhameed. "Eight-element dual-polarized MIMO slot antenna system for 5G smartphone applications." *IEEE access* 7 (2019): 15612-15622.

Drone Positioning Estimation with Particle Filtering Augmented NR Positioning Reference Signal

Suba Renjani N [1], Rajesh A [*,2], Manikandan C [3], Suguna G [4], Saranya J [5], Selvakumar R [6]

School of Electrical & Electronics Engineering,

[1,2,3,4,5,6]SASTRA Deemed University, Thanjavur, Tamil Nadu, India

* rajesha@ece.sastra.ac.in, dpfi04240119 24@sastra.ac.in, manikandan@ece.sastra.ac.in, suguna@ece.sastra.ac.in, dpfi04240 11997@sastra.ac.in, selvakumar@civil.sastra.edu.

Abstract. In this paper, the focus is on the localization of drones by using New Radio (NR) Fifth Generation (5G) downlink positioning reference signals(PRS), especially for outdoor Global Positioning System (GPS) limited environments. The system calculates the position through the hyperbolic multilateration method based on the time difference of arrival, and the observed time difference of arrival. In this study, a new approach is proposed that employs a particle filter algorithm to reduce estimation errors and improve positioning accuracy. To implement the model, a software-defined radio system with a Universal Software Radio Peripheral (USRP) is used. The system incorporates path loss models from 3GPP TR 38.901-based scenarios. The particle filtering-based technique improves the positioning estimation of drones.

Keywords: Particle filtering, 5G NR, Observed Time Difference of Arrival, Software Defined Radio.

1 Introduction

Recently, the usage of drones increased in various commercial and industrial fields. Much of the current research consistently relies on GPS to determine the drone's precise location[1]. Nevertheless, in certain scenarios, GPS might not provide the required accuracy, and this approach is not suitable for disaster situations. Drones normally rely on GNSS for positioning, which is effective in open environments. However, GNSS alone struggles with accuracy and reliability in urban or indoor settings due to signal blocking, multipath propagation, and susceptibility to jamming and spoofing[2]. To overcome this, 5G networks enhance positioning and navigation, with Positioning Reference Signals (PRS) improving accuracy and synchronization in challenging environments [3]. Positioning Reference Signal is a distinct transmission from cellular networks (such as 4G LTE and 5G) that enables devices to ascertain their position by calculating the time difference of arrival (TDOA) of the signal emitted from the base station. Since 3GPP release 9, PRS has

been used for LTE locations. Some work is based on existing LTE PRS, expected standards, or ideas for 5G PRS. While [6] addresses PRS setup to enable the OTDoA (Observed Time Difference of Arrival) positioning method, authors in [7] assess the effect of positioning with various PRS distributions based on accuracy in a period. 5G Downlink PRS may allocate more OFDM symbols in the time domain and a wider bandwidth in the frequency domain than 5G SSB signals, which enables continuous carrier phase tracking and improved positioning accuracy [10],[11]. In the meantime, many base stations and several frequency bands are typically needed to achieve the desired sub-meter accuracy, which occasionally may be less efficient or impracticable [12]. This study examines these problems by utilizing standalone 5G signals to attain sub-meter location precision while requiring a minimum of three 5G base stations.The most recent 3GPP technical report emphasizes network synchronization issues. Therefore, research into 5G-based positioning techniques is required to reach greater accuracy levels, including sub-meter accuracy. To address this issue, this study suggested a novel 5G-GNSS hybrid positioning system based on AOA-TOA measurement [13]. PRS quantifies the downlink transmission delays by comparing the base station signal, which the receiver locally repeats. To determine whether the PRS distribution impacts positioning performance [14], this research analyses and compares various PRS allocations within the 5G frame[15]. The primary goal of this paper is to provide an NR PRS positioning and TOA estimation detection as per TDOA positioning for the calculation obtained. Using simulated results, PRS performance and location accuracy are demonstrated.

2 Methodology

In the SDR-based network positioning technology,two SDRs are used, transmitters that send LTE-specific positional reference signals (PRS). Hardware from the USRP B210 SDR is used as shown in Fig 1. Drone uses PRS signals, which are sent concurrently by gNB, as its main metrics for estimating arrival time. To determine TOA from each gNB and then calculate the time difference of arrival across all pairs of gNBs, drone correlates with the PRS that is received from gNB. The drone location estimation is defined by the intersection of the TDOA curves (hyperbolas) from the three base stations. MATLAB on laptops is connected to USRP boards via the USRP hardware driver. PRS baseband synthesis, transmission, reception, and processing are all done with MATLAB software.

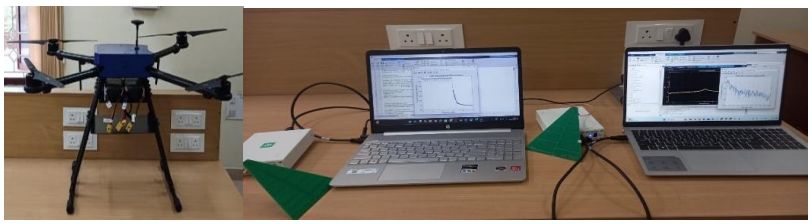

Fig. 1.SDR based test bench for testing the particle filtering based positioning in drone

For positioning design, the orthogonal frequency-division multiplexing (OFDM) grid and PDSCH (Physical Downlink Shared Channel) demonstrate the

set-up of the PRS time-frequency features and how various PRS resource set settings impact the PRS time-frequency structure. Observe the differences in slot allocation and RE positions after configuring many PRS resources with various time and frequency allocation and slot configuration elements.The time it takes for a signal to move from the gNB to the drone is measured using distance. The speed of light is used to determine the time it takes for the signal to travel that distance. This time delay is converted into units that can be used in simulations, and the path loss formula is also used to determine how much the signal strength is reduced.

The NR Path loss model incorporates indoor hotspots, indoor factories with clutters, urban macrocells, urban microcells, and rural microcells, under 3GPP TR 38.901 requirements. It takes into consideration altitude dependence by using roadway widths varying from 5 to 50 meters and building heights. The model is designed for an operating frequency of 3.5 GHz, ensuring accurate characterization of signal propagation in different environments is shown in the equation (1) and (2)

$$PL_{Drone_LOS} = \{PL_1, \sigma_{SF}\ 10 \le d \le d_{BP}, \},$$

$$\{PL_2, \sigma_{SF} d_{BP} \le d \le 10km\} \quad (1)$$

$$PL_{Drone_NLOS} = max\left(\left(PL_{Drone_LOS}, PL_{NLOS}\right), \sigma_{SF}\right) \quad (2)$$

2.2 5G NR Path Loss Configuration

NR Path Loss model is given as in the equation (3) and (4)

$$PL_1 = \{20log_{10}(40\pi d f_c/3) + min(0.003h^{1.72}, 10)log_{10}(d)$$

$$\text{-min}(0.044h^{1.72}, 14.77)+0.002log_{10}(h)d\} \quad (3)$$

$$PL_2 = PL_1(2\pi h_{BS} h_{Drone} f_c/C) + 40log_{10}\left(\frac{d}{d_{BP}}\right) \quad (4)$$

$\boldsymbol{PL_{Drone_LOS}}$ - Path loss for Line – of – Sight (LOS) conditions,$\boldsymbol{PL_1}$ – Path loss equation for shorter distances,$\boldsymbol{PL_2}$ – Path loss equation for longer distance,$\boldsymbol{d}$ – is the distance between drone and the base station(gNB), $\boldsymbol{d_{BP}}$ – is the breakpoint distance where the path loss characterstics change,$\boldsymbol{\sigma_{SF}}$ – shadow fading standard deviation, $\boldsymbol{PL_{Drone_NLOS}}$ – Path loss for Non Line – of – Sight (LOS) conditions, $\boldsymbol{PL_{NLOS}}$ – Path loss in NLOS conditions (higher due to obstruction and reflection). These are the parameters given in equation (1),(2),(3),(4).

2.3 Particle Filtering for PRS Signals

State Space Model

Where x and y are positions, and v_x and v_y are velocities in the x and y directions, respectively shown in equations (5),(6),(7).

State Vector

$$X_k = [\ x, y, v_x, v_y\ ]^T \quad (5)$$

State transition model

X_K=A$X_{k-1} + W_k$ (6)

Where A is the state transition matrix

Measurement model

Z_K=H$X_k + V_k$ (7)

Where H is the observation matrix

Particle filter implementation combines measurements from multiple gNBs using hyperbola intersections and refines the position estimate over time, accounting for process and measurement noise.

2.4 Particle positioning algorithm for improving the PRS

Input: Initial set ofN particles - $\{X_0^i\}_{i=1}^N$with equal weights $w_0^i = \frac{1}{N}$

Output:Estimated state $\hat{x}$ at each time step
Initialize:
Generate N particles - $\{X_0^i\}_{i=1}^N$

Set initial weights - $w_0^i = \frac{1}{N}$
For each time step k

a.Prediction
Explore new particle states according to the system model

$X_k^i = AX_{k-1}^i + w_k^i$ (8)

b.update

Figure out the importance of weights

w_k^i= p(w_k^i/X_k^i) (9)

c.Normalize weights

Make sure the weights add up to 1 by normalizing them.

$w_k^i = \frac{w_k^i}{\sum_{j=1}^N w_k^i}$ (10)

d.Resampling

Calculate an effective number of particles.
$N_{eff} = \frac{1}{\sum_{j=1}^N (w_k^{i\,2})}$ (11)
e.State Estimation

Estimate the state as the weighted mean of particles.

$$\hat{x} = \sum_{j=1}^{N} w_k^i X_k^i \quad (12)$$

4. Results and Discussion

The simulation results of NR Positioning with Positioning Reference Signals (PRS) using Software-defined radio provide the system performance of transmission and reception of real-time PRS signals of drone location, showing accurate localization with an estimation error of 2.6 meters. It also involved generating a Spectrum trace and correlation plot for analyzing the signal quality for evaluating the system performance. The accuracy of the estimation error is improved by the particle filter algorithm.Fig.2. displays the gNB and drone locations. Throughout the estimating process, the three base station positions are fixed. The plotting of the actual droneposition is also done.

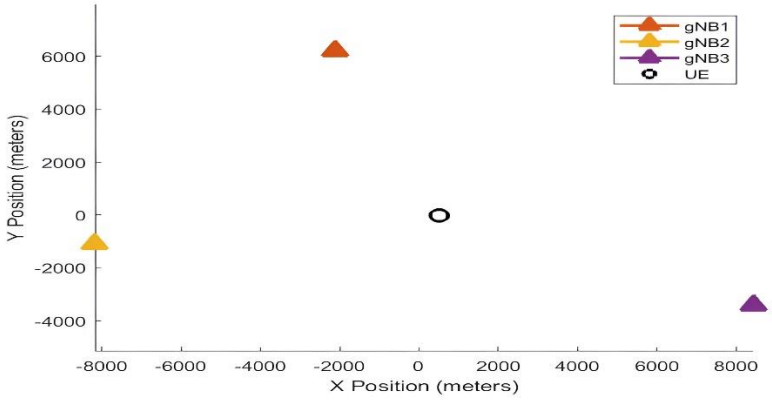

Fig.2. gNB and dronelocations

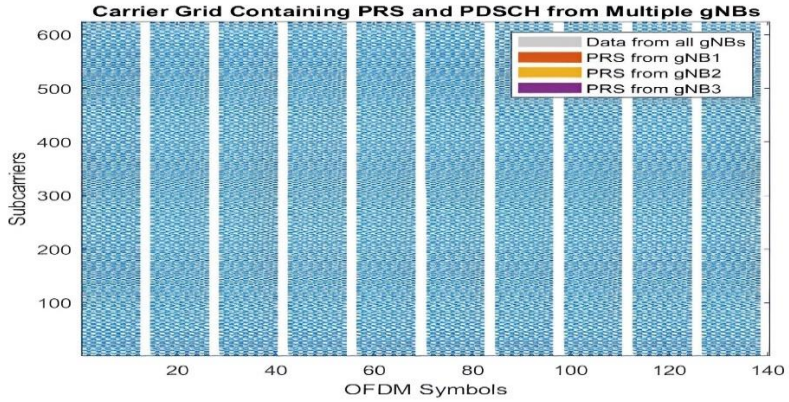

Fig. 3. Carrier Grid Containing PRS and PDSCH from multiple gNBs

The PRS and PDSCH resource allocation across several gNBs in the 5G NR carrier

grid is depicted in Fig. 3. It emphasizes how PRS transmission must be carefully planned and coordinated to allow precise positioning while preserving communication services Physical Downlink Shared Channel (PDSCH). For methods like Observed Time Difference of Arrival (OTDOA), the drone must be able to correlate PRS signals from each gNB independently, which is ensured by the unique allocation for each gNB shown in equation (13).

$$s(n) = \frac{1}{\sqrt{2}} \sum_{k=0}^{N-1} X_k e^{j2\pi kn/N} \quad (13)$$

Where, X_k are mapped as PRS symbols, N is the FFT size, and s(n) is the time domain signal

PRS are allocated in a time-frequency grid shown in Fig. 4and equation(14) given below

$$S_{PRS}(k,l) = x(k,l).\delta(k,l) \quad (14)$$

Where,$S_{PRS}(k,l)$- are subcarrier and symbol indices,$x(k,l)$ - represents PRS symbols,

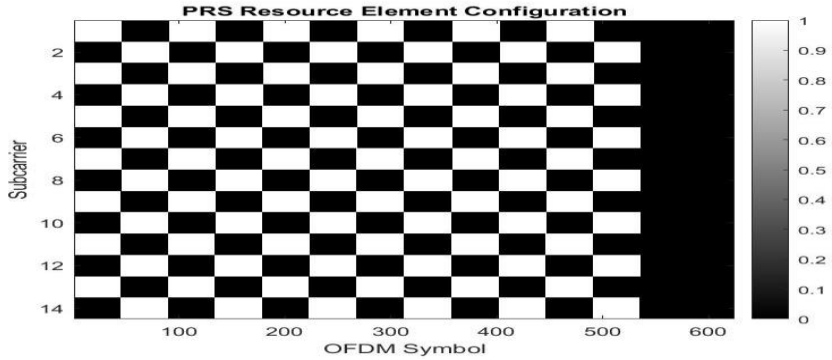

Fig. 4. PRS Resource Element Configuration

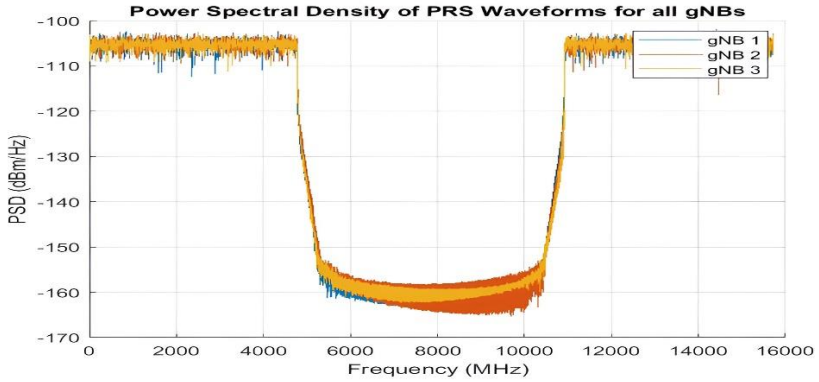

Fig. 5. Power Spectral Density of PRS Waveforms for all gNBs

The power spectral density of positioning reference signal (PRS) waveforms

transmitted by three gNBs is shown in Fig. 5.The x-axis represents the frequency in MHz,and the y-axis represents the power level in dBm/Hz.The three different colors indicate signals from the gNBs.The left and right sides of the high-power regions show the transmission bands.The dip in the middle shows a frequency range with minimal signal power. This ensures efficient frequency usage and reduces interference. Fig. 6. shows the transmitted spectrum plot, where the x-axis represents the frequency in GHz, and the y-axis represents signal power in dB. The flat region shows the constant power indicating the transmission bandwidth of the signal. The filtering effect limits the signal to a specific frequency range and reduces interference with neighboring bands.

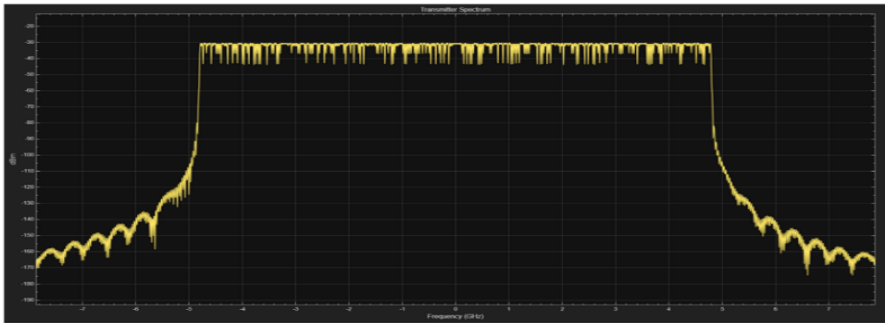

Fig. 6. Transmitted Spectrum of the gNBs

The correlation of positioning reference signals received from three gNBs over time is shown in Fig. 7. The x-axis represents time in seconds, and the y-axis represents the absolute value of the correlation.The color represents the unique cell ID. A higher peak suggests the strongest signal, meaning the PRS signals from that gNB are more aligned with the expected signal.

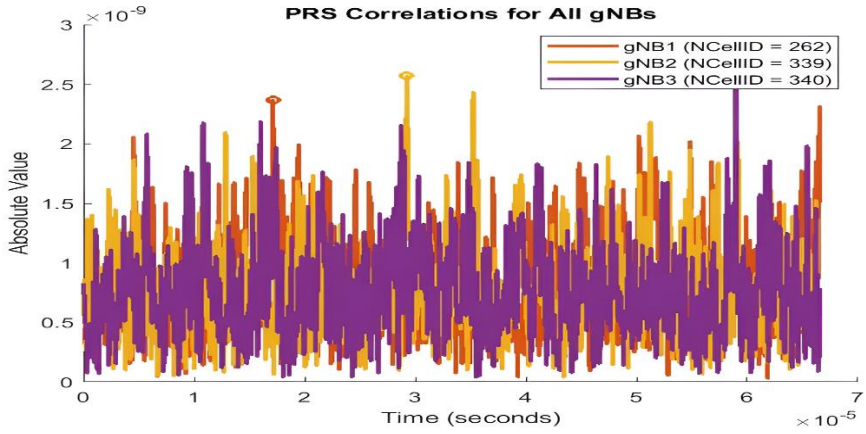

Fig. 7. PRS Correlations for All gNBs

Fig. 8 shows the received spectrum plot, where the x-axis represents the frequency

in GHz,and the y-axis represents signal power in dB.The flat region in the middle indicates the main frequency band of the signal, where most of the power is concentrated. This type of plot is useful for analyzing signal quality and ensuring proper transmission and reception in wireless communication systems.

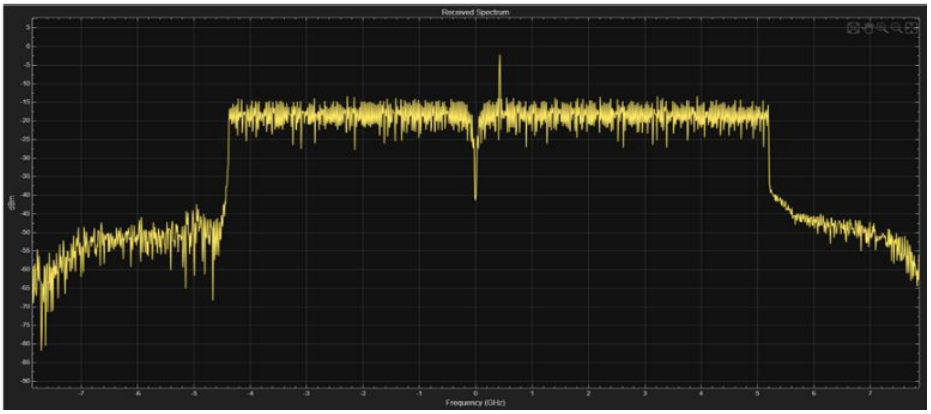

Fig.8. Received Spectrum at the drone under multipath condition

Fig. 9. represents the locations of three reference base stations (gNBs) are indicated by the triangle marks known as gNB1, gNB2, and gNB3.According to the Time Difference of Arrival (TDOA) hyperbolas computed between pairs of gNBs. Indicating the drone estimated position is the red '+' marker. Drone exact position is indicated by the black 'o' symbol.

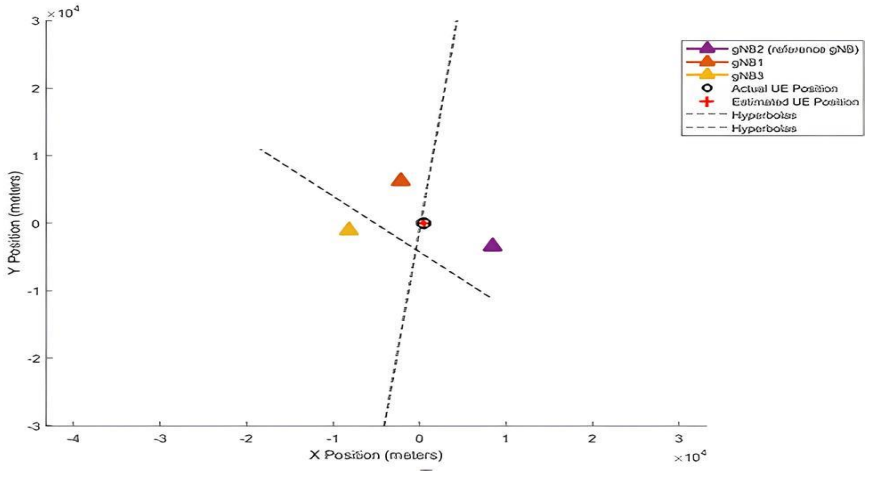

Fig. 9. Position estimation of drone with partcile filtering

The position estimation error is computed as the Euclidean distance between the

true position of the drone and the estimated position is shown in equation(15).

$$Error = \sqrt{(x_{Drone} - x_{IDrone})^2} + \sqrt{(y_{Drone} - y_{IDrone})^2} \quad (15)$$

(x_{Drone}, y_{Drone}) is the true position of drone

(x_{IDrone}, y_{IDrone}) is the estimation position of drone

5.Conclusion

The current study produces a result for positioning technology design using USRP hardware and customised drone. Investigating and experimentally validating cell-specific and positional reference signal receivers under varied time and frequency offsets is the first task. Fine frequency and delay estimations with quantitative bounds in a single transmitter-receiver link are the anticipated outcomes. Techniques like cross-correlation for signal estimation and hyperbolic curve fitting for position calculation are employed to avoid signal interference. Position estimation error of 2.6 meters.The novelty of this chapter is using a particle filtering algorithm, improved location estimation over time, and accuracy of the drone positioning improved significantly.

References

1. Renaudin, Olivier, José A. López Salcedo, Gonzalo Seco-Granados, Ivan Lapin, Francesca Zanier, and Lionel Ries. "TOA error bounds for positioning in 5G new radio networks." In *Proceedings of the 34th International Technical Meeting of the Satellite Division of The Institute of Navigation (ION GNSS+ 2021)*, pp. 2940-2956. 2021.
2. Jin, Chengming, Ian Bajaj, Kai Zhao, Wee Peng Tay, and Keck Voon Ling. "5G positioning using code-phase timing recovery." In *2021 IEEE Wireless Communications and Networking Conference (WCNC)*, pp. 1-7. IEEE, 2021.
3. Abdallah, Ali A., and Zaher M. Kassas. "UAV navigation with 5G carrier phase measurements." In *Proceedings of the 34th International Technical Meeting of the Satellite Division of The Institute of Navigation (ION GNSS+ 2021)*, pp. 3294-3306. 2021.
4. Chen, Liang, Xin Zhou, Feifei Chen, Lie-Liang Yang, and Ruizhi Chen. "Carrier phase ranging for indoor positioning with 5G NR signals." *IEEE Internet of Things Journal* 9, no. 13 (2021): 10908-10919.
5. Jin, Chengming, Wee Peng Tay, Kai Zhao, Keck Voon Ling, and Kok Kee Sin. "A 5G/GNSS integrated positioning method." In *Proceedings of the 35th International Technical Meeting of the Satellite Division of The Institute of Navigation (ION GNSS+ 2022)*, pp. 2429-2443. 2022.
6. Müürsepp, Ivo, Marika Kulmar, Osama Elgarhy, Muhammad Mahtab Alam, Tao Chen, Seppo Horsmanheimo, and Johan Scholliers.

"Performance evaluation of 5g-nr positioning accuracy using time difference of arrival method." In *2021 IEEE International Mediterranean Conference on Communications and Networking (MeditCom)*, pp. 494-499. IEEE, 2021.

7. Gonzalez-Garrido, Alejandro, Jorge Querol, and Symeon Chatzinotas. "5g positioning reference signal configuration for integrated terrestrial/non-terrestrial network scenario." In *2023 IEEE/ION Position, Location and Navigation Symposium (PLANS)*, pp. 1136-1142. IEEE, 2023.
8. Jin, Chengming, Wee Peng Tay, Kai Zhao, Keck Voon Ling, Jun Lu, and Yue Wang. "A Sub-meter Accurate Positioning using 5G Double-difference Carrier Phase Measurements." In *2023 IEEE/ION Position, Location and Navigation Symposium (PLANS)*, pp. 1176-1183. IEEE, 2023.
9. Wang, Jin, Wei Zhao, Jing Jiang, Zexi Zeng, and Feiyue Shi. "5G PRS Positioning Based on the Improved Sparrow Search Algorithm." In *2023 IEEE/CIC International Conference on Communications in China (ICCC Workshops)*, pp. 1-6. IEEE, 2023.
10. Liu, Qi, Chengfa Gao, Alda Xhafa, Wang Gao, José A. López-Salcedo, and Gonzalo Seco-Granados. "Performance analysis of GNSS+ 5G hybrid positioning algorithms for smartphones in urban environments." *IEEE Transactions on Instrumentation and Measurement* 73 (2023): 1-9.
11. Campolo, Federico, Andra Blaga, Maurizio Rea, Angel Lozano, and Xavier Costa-Pérez. "5GNSS: Fusion of 5G-NR and GNSS localization for enhanced positioning accuracy and reliability." *IEEE Transactions on Vehicular Technology* (2024).
12. Xhafa, Alda, José A. del Peral-Rosado, José A. López-Salcedo, and Gonzalo Seco-Granados. "Evaluation of 5G positioning performance based on UTDoA, AoA and base-station selective exclusion." *Sensors* 22, no. 1 (2021): 101.
13. Luo, Kai, Zhongliang Deng, Xiaobin Guo, Ziyao Ma, and Jingrong Liu. "High-Precision Ranging Method of 5G NR Co-Band PRS in Industrial Internet Scenarios." *Applied Sciences* 13, no. 18 (2023): 10302.
14. Deng, Zhongliang, Xinyu Zheng, Chongyu Zhang, Hanhua Wang, Lu Yin, and Wen Liu. "A TDOA and PDR fusion method for 5G indoor localization based on virtual base stations in unknown areas." *IEEE Access* 8 (2020): 225123-225133.
15. Butt, M. Majid, Anil Rao, and Daejung Yoon. "RF fingerprinting and deep learning assisted UE positioning in 5G." In *2020 IEEE 91st Vehicular Technology Conference (VTC2020-Spring)*, pp. 1-7. IEEE, 2020.

Analytical Approach of False Products and Complaint System Development Using Blockchain Technology

Anant Gupta[1], Pavan Sai A[2], *Sanjay Kumar Dubey[3],
[1,2,3]Amity University Uttar Pradesh, Sec-125, Noida India
[1]anant.gupta1@s.amity.edu[1], [2]pavan.a@s.amity.edu,
[3]skdubey1@amity.edu

Abstract. The revolution of technology has brought both advantages and disadvantages. One of the serious problems revolving around us is circulation of counterfeit products purchased online which has serious consequences. Blockchain provides a vigorous solution to this challenge due to its tremendous features, such as immutability and decentralization. This research explores how blockchain being used as the solution to the problem among various industries and examines how integrating blockchain with other technologies can be beneficial. This paper presents a blockchain-based Ethereum system which has three portals: Manufacturer, Retailer, Consumer. Manufacturer can register products on the immutable ledger while consumer can verify the product's authenticity with the help of QR system and retailer can keep the track of product's originality and complaints. Additionally, the system integrates a complaint management system which helps consumers to address their issues if they found the product has been counterfeited. The system is currently in the planning phase, with an implementation architecture outlined for the future development. The proposed approach amplifies supply chain management by ensuring the product's authenticity and aiding customer trust.

Keywords: Blockchain, Ethereum, Product Authentication, Counterfeit Detection, Supply chain Transparency, Smart Contracts.

1. Introduction

In this volatile and unpredictable world, the morale and ethics of human beings have been decreasing rapidly over the years. Such situations have led to significant contemporary issues, one amongst which is counterfeiting or faking products. To explain counterfeiting in detail, consider the following example: A brand named XYZ creates a product, P, and tries to sell it in the market. However, a person motivated by greed replicates this product exactly but uses cheaper materials, selling it at the same price set by XYZ for product P. As a result, the person who does counterfeiting gets profits, while the original company and consumers suffer substantial losses. Product counterfeiting is a problem where it affects both customers and manufacturers. The customers get affected due to usage of the counterfeiting products and losing their money for cheap material. Whereas company is going to lose its reputation which they built over the years.

According to recent estimates, the global cost of counterfeiting and piracy is projected to reach numerous counts till today, underlining an urgent need for effective solutions to encounter this issue to distinguish real and fake products. Several technologies exist to combat the counterfeiting problem such as QR-based systems, Artificial Intelligence and some machine learning techniques. However, each of these solutions has their own disadvantages. Looking at an example, QR can be duplicated and can be used in the fake products too while machine learning needs huge computational power and has chances of predicting wrong. Blockchain technology offers a viable solution to various challenges. A distributed, immutable record called blockchain allows for decentralized peer-to-peer transactions. Over time, it has attracted particular interest because of its attributes, including decentralization, anonymity, persistence, and auditability. It maintains a continuously growing list of data records, confirmed by participating nodes. The data is recorded in a public ledger, with visibility over every completed transaction. This information is shared and accessible to all the nodes. Its applications span a wide range, from cryptocurrency and financial services to risk management and social services.

This project aims to develop a blockchain-based system to identify, and report counterfeit

products. The system will enable manufacturers to securely record product details on the blockchain, allowing consumers to verify authenticity by scanning a QR code. If a product is identified as counterfeit, the system will provide a mechanism for consumers to file complaints and enhance supply chain transparency. The manufacturer area is where a manufacturer may register for an account on the platform and enter the details of their product. Customers can input the product ID through a user interface or scan the QR code to verify the product's legitimacy when they receive it. People can utilize the complaint mechanism to file a complaint if they believe a product is fake. The manufacturer can then see the complaint recorded in the blockchain's smart contract. This paper also focuses on existing technologies for counterfeiting and divides them into industrial categories, citing their significant contributions and the challenges they addressed. In a blockchain anti-counterfeiting system, manufacturers can securely record product details onto the blockchain, creating a transparent and tamper-proof record. Consumers, in turn, can verify a product's authenticity by scanning a unique QR code linked to the blockchain. Each of the several parts that make up the proposed blockchain-based system will be essential to maintaining security and legitimacy.

2. Literature Review

This literature review is structured chronologically to provide an analytical understanding of the development and application of blockchain-based counterfeit detection systems across domains.

2.1 Evolution and Technologies in Blockchain based Anti-Counterfieting

The evolution of blockchain-based anti-counterfeiting solutions demonstrates clear technological progression across sectors: To track the delivery of drugs from manufacturing to patients, a smart contract-based solution was developed using cryptographic hash functions and QR code mechanisms. This approach achieved a 37% reduction in counterfeit drugs using Ethereum smart contracts and QR codes in the pharmaceutical industry [9]. Modgil and Sonwaney highlighted how blockchain enhances traceability and transparency in supply chains—a focus that differs from the detection-centric method proposed by Shreekumar et al. [10].A blockchain-based traceability system for food products in international trade was proposed by integrating Radio-Frequency Identification (RFID) tags and Ethereum-based smart contracts. This solution ensures secure tracking of food products across global supply chains and achieved 92% traceability accuracy [11].In the education sector, blockchain has been utilized to reduce academic certificate verification costs by 60% using Bitcoin's blockchain [12].During 2021–2022, the retail industry advanced significantly through the development of an 89% accurate QR authentication system operating at 100 TPS. This system, built on Ethereum using smart contracts and QR codes, effectively highlighted and addressed product counterfeiting challenges by ensuring immutability in product tracking [13].To prevent data manipulation and track vehicle history, a blockchain solution using hash-based cryptography and smart contracts was proposed [14]. Another solution implemented smart contracts on a private Ethereum blockchain to automate policy issuance, claim validation, and settlements in the insurance domain [15].Some studies have emphasized the importance of user awareness and education in fraud detection, incorporating features like product reviews and seller ratings [16]. Exploring supply chain management challenges, real-time data sharing was identified as crucial for improving flexibility and efficiency. One study reported a 2.4-second latency issue with IoT-blockchain integration [17].In the dairy industry, the integration of IoT, QR codes, smart contracts, and machine learning was proposed to detect and eliminate product adulteration. A four-layered architecture built using Ethereum and IoT sensors achieved a 45% reduction in dairy contamination in India [18].To ensure anonymity and reduce third-party dependency in e-voting systems, a solution using Hyperledger Fabric and Linkable Ring Signature (LRS) was developed, ensuring both voter privacy and fraud prevention [19]. Another system used permissioned blockchain to track drug movement from manufacturer to patient, automate transactions via smart contracts, and store post-consumption drug effect data for future analysis and treatment improvements [20].The SAFE (Secure Authentication for Farmers and Environment) platform was introduced for organic certification tracking. It uses IoT sensors to collect real-time data (soil, air, water quality), while blockchain stores immutable certification records to ensure transparency [21].A system to securely verify product authenticity for counterfeit detection and analysis was also proposed, focusing on evaluating blockchain's effectiveness [22]. Another system combined IoT, smart contracts, and cryptographic security on Ethereum and Hyperledger Fabric to enhance food security through data integrity [23].It has been

demonstrated that blockchain is effective for anti-counterfeiting by tracking ownership and offering an average authentication cost of $0.92 per product based on Ethereum gas fees [24].A decentralized system using Proof of Stake (PoS) and Ethereum 2.0 was introduced to combat counterfeit medicines. This framework consists of eight decentralized applications built on Ethereum and Hyperledger Fabric and reduced energy consumption by 40% compared to proof-of-work systems [25].An innovative solution using QR codes linked to blockchain was presented to verify product originality and developed a decentralized application (DApp) to improve supply chain transparency [26].Combining AI with blockchain for predictive analysis in healthcare technology has resulted in the development of AI-BlockchainOps—a systematic framework offering secure data management, real-time monitoring, and fraud detection at a transaction cost of $0.92 [27].To address the counterfeiting of cosmetic products, a solution was proposed integrating decentralized tamper-proof ledgers, QR codes, and smart contracts to enable secure product tracking [28].

3. Review Methodology

The primary objective of this paper is to examine extant literature on diverse topics, including the overview and necessity of blockchain technology, current technological advancements and innovations, industry categorization, complaint systems, challenges, and integration with other technologies. This section provides a comprehensive assessment of the research questions.

RQ1) What are the losses attributed to counterfeit products across various industries?

RQ2) What are the existing technologies contributing to serve anti-counterfeiting to various industries?

RQ3) Why is blockchain a game changer for this problem comparatively with others and How integration with other technologies will enhance the solution?

We used several reputable and peer-reviewed academic resources to perform an extensive analysis of the current technologies addressing the detection of counterfeit goods and complaint management systems. Among them were Google Scholar, Web of Science, ScienceDirect, and IEEE Xplore. These platforms were chosen because of their reliability, comprehensive indexing of pertinent technical literature, and capacity to offer access to top-notch research articles in a variety of interdisciplinary fields, including information systems, supply chain management, and computer science. To find relevant literature, we first conducted exploratory searches using general keywords like "Blockchain," "Complaint System," "Anti-Counterfeit Technology," and "Product Authentication." We honed our keyword list through numerous iterations and search result analysis, investigating a range of alternative and related terms such as "Provenance Tracking," "Smart Contracts," "RFID," "Supply Chain Traceability," and "Digital Ledger Technology (DLT)". We were able to determine which keyword combinations were most pertinent to each research question through this iterative process. Throughout this process, we noticed that, especially in broad-spectrum databases like Google Scholar, specific keyword combinations frequently produced an excessive number of irrelevant papers. Many of these papers addressed unrelated use cases or belonged to unrelated disciplines, even though their terminology was technically relevant. Consequently, we concluded that a single, consistent search string did not work in every database. To reduce noise and increase the accuracy of the results, unique, domain-specific search strings were created for every database. To further refine our search, we used field-specific filters (e.g., title, abstract, keywords, publication year), phrase matching, and Boolean operators (AND, OR, NOT). By making these changes, we were able to make sure that the papers that were chosen for review were in line with our main goals and offered valuable perspectives on the technical and practical aspects of the technologies used for handling complaints and detecting counterfeit goods. The databases were chosen based on their applicability to multidisciplinary studies in digital complaint systems, supply chain management, and blockchain.

The study highlights20 peer-reviewed papers published between 2018–2024 focusing on blockchain applications in product authentication and complaint systems. The selection was based on relevance, citation impact, and technological contribution. They were analyzed and classified based on the categories like Focus area, Industry, Tools, Contributions, Challenges in the below table.

Table 1. Comparative Analysis of Related Work

Author	Ye	Focus	Industry	Tools/te	Key	Accur	Scalabi	Challeng

	ar	area		ch explored or used	contributions	acy	lity	es Adressed
Haq, Ijazul & Muselemu, Olivier.	2018	Blockchain for Pharma Supply Chain	Pharmaceuticals	Blockchain, Ethereum, Hyperledger, QR Codes, Smart Contracts	Secure, verifiable drug distribution from manufacturer to consumer	High	Moderate	Counterfeit drugs, lack of visibility, inefficiency in recalls
Modgil, Sachin, and Vandana Sonwaney.	2019	Application of Blockchain	Manufacturing	Blockchain, IoT	Sectorial prioritization for blockchain use	Moderate	Moderate	Integration with existing systems
Bordel Sánchez, Borja & Lebigot, Pierre & Alcarria, Ramón & Robles, Tomas.	2019	Blockchain-Based Food Traceability	Food Supply Chain	Ethereum Blockchain, Smart Contracts, RFID Tags, Node.js, NoSQL Databases, Oracles	Developed a blockchain-based traceability system integrating RFID and Smart Contracts for secure, real-time food tracking in international trade	High	Low	Data loss, fragmented regulatory compliance, lack of supply chain transparency, fraud prevention, scalability of blockchain networks
Capece, Guendalina & Ghiron, Nathan & Pasquale, Francesco.	2020	Blockchain-Based Digital Certificates	Education	Blockchain, Blockcerts Framework, Bitcoin Network, Merkle Trees, Smart Contracts	Demonstrates tamper-proof, easily verifiable academic certificates, reducing costs and enhancing trust	High	Low	Certificate forgery vulnerability, inefficient verification processes, lack of student control, data privacy concerns
Singhal, Ishaan.	2021	Identification of Fake Products	Retail Supply Chain	Blockchain, QR Codes, Ethereum, Smart Contracts	Secure verification of product authenticity and ownership tracking using blockchain	Moderate	High	Counterfeit detection, lack of product traceability, and trust issues in e-commerce
Ms,	20	Blockchai	Automotiv	Blockcha	Secure,	High	Moderat	Centralize

Karthiga & S S, Nandhini & R M, Tharsanee & Mathappan, Nivaashini & Rs, Soundariya.	21	n-Based Automotive Security	e, Cybersecurity	in, Ethereum, Hyperledger, Smart Contracts, Public Key Cryptography	decentralized vehicle data sharing and protection from cyber threats		e	d security risks, data tampering, inefficient authentication systems
Khan, Mohammad & Hassan, Abid & Ali, Md. Iftekhar.	2021	Blockchain-Based Insurance Framework	Insurance and Fin-Tech	Blockchain, Ethereum, Smart Contracts, PoA Consensus	Secure, transparent, fraud-resistant insurance settlement system	Moderate	Moderate	Fraudulent claims, slow policy verification, lack of trust
Shreekumar, T.,	2022	Detection of Fake Products	E-commerce	Smart Contracts	Framework for detecting counterfeit goods	Moderate	Low	Lack of user awareness
Singh, Chetanpal & Thakkar, Rahul & Warraich, Jatinder.	2022	Blockchain Technology in Supply Chain	Logistics, Manufacturing, Retail	Blockchain, Smart Contracts, Distributed Ledger Technology (DLT), IoT Integration	Enhances supply chain transparency, traceability, operational efficiency, and stakeholder trust	Moderate	Moderate	Lack of supply chain visibility, high operational costs, data security issues, fragmented information exchange
Khanna, A., Jain, S., Burgio, A., Bolshev, V., & Panchenko, V.	2022	Blockchain for Dairy Supply Chain	Diary Industry, Food safety	Blockchain (Ethereum), Smart Contracts, QR Codes, IoT Sensors, Machine Learning, Cloud Computing	Developed a blockchain-based decentralized supply chain for tracking dairy products, ensuring food safety, and automating financial transactions	High	Moderate	Adulteration, contamination, supply chain inefficiencies, fraud prevention, lack of traceability, regulatory challenges, scalability issues
. Rao, K. & Panda, Sandeep.	2022	Blockchain-Based E-voting	Election Security	Blockchain, Hyperledger,	Decentralized trustless voting	High	Low	Centralized trust issues, security

				Smart Contracts, LRS, Paillier Encryption	system for secure elections			vulnerabilities, limited scalability
Khondker, Shezad & Hasan, Khondker	2022	Blockchain in Pharma Cybersecurity	Pharmaceuticals	Blockchain, Ethereum, Hyperledger, Smart Contracts, QR Codes	Secure, transparent, and fraud-resistant drug tracking system	High	Moderate	Counterfeit drugs, lack of traceability, security risks
Tegeltija, S., Dejanović, S., Feng, H., Stankovski, S., Ostojić, G., Kučević, D., & Marjanović, J.	2022	Blockchain-Based Organic Certification	Agriculture	Blockchain, Ethereum, Hyperledger, Smart Contracts, IoT Sensors	Secure, verifiable organic farming certification system	Moderate	Low	Certification fraud, inefficiencies, trust issues
Z Dsouza, Antony Roshan, Shantala Devi Patil, and K. Amuthabala.	2023	Identification of Fake Products	Retail	Blockchain	Secure verification of product authenticity	Moderate	Low	Counterfeit detection
Lv, Guangjie & Song, Caixia & Xu, Pengmin & Qi, Zhiguo & Song, Heyu & Liu, Yi.	2023	Blockchain-Based Traceability for Agricultural Products	Agriculture, Food Safety	Blockchain, Ethereum, Hyperledger, QR Codes, Smart Contracts	Secure food supply chain traceability using blockchain for fraud prevention and consumer trust	High	Moderate	Lack of transparency in food supply, data tampering, inefficient traceability systems
Lee, Michael Christian,	2023	Blockchain-Based Anti-Counterfeiting System	Retail Supply Chain	Ethereum Blockchain, Smart Contracts (Solidity), Ganache, Remix IDE, Role-Based	Developed a blockchain-based anti-counterfeit system ensuring product traceability and authenticit	High	Low	Counterfeiting, lack of product traceability, consumer trust issues, high operational costs for authenticat

				Access Control (RBAC-SC)	y using Ethereum smart contracts			ion
. Hamid, Soomaiya & Bawany, Narmeen & Fatima, Kiran.	2024	Blockchain-Based Drug Authentication	Pharmaceuticals	Ethereum 2.0, Proof of Stake (PoS), Smart Contracts, Decentralized Applications (DApps)	Developed a blockchain-based framework ensuring drug traceability and authenticity from raw materials to consumers	High	High	Counterfeit drugs, supply chain tampering, lack of interoperability, regulatory enforcement, and integration challenges with legacy systems
Vhatkar, Rishabh.	2024	Identification of Fake Products	Retail Supply chain	Blockchain, QR Codes, Ethereum, MetaMask, Ganache, Smart Contracts	Secure verification of product authenticity and transparent tracking of product history	High	High	Counterfeit detection, supply chain data manipulation, lack of product traceability
Ramachandran, Muthu.	2024	AI and Blockchain Framework for Healthcare	Healthcare	AI (Predictive Analytics, NLP), Blockchain (Smart Contracts, DLT), BPMN, IoT, PBFT Consensus	Developed AI-BlockchainOps framework to improve data security, patient care, and healthcare system efficiency	High	Moderate	Data privacy, security risks, lack of interoperability, ethical concerns, and regulatory compliance issues

4. Proposed System Architecture

An Ethereum-based framework includes different stakeholder portals (Looking at the Manufacturer, Retailer as well as Consumer) that combine blockchain-based complaint management systems in a decentralized way. The architecture presented in Figure 1 applies blockchain's unalterable features together with smart contract programming for complete supply chain visibility.

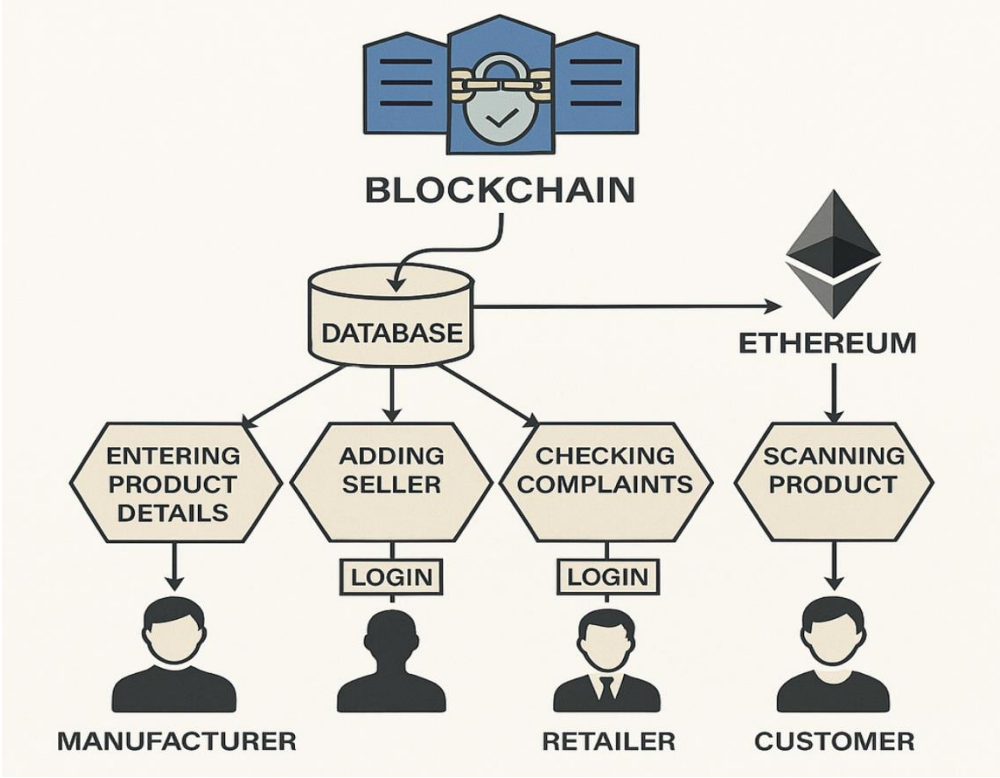

Fig. 1. Architecture of Planned System

4.1 Architectural Components:

Manufacturer Portal:

- Registers products on-chain via smart contracts.

- Generates cryptographically signed QR codes (SHA-256 hashing).

Retailer Portal:

- Validates ownership transitions using ERC-721 tokens.

- Logs product handover events on the blockchain.

Consumer Portal:

- QR code scanning interface for authenticity verification.

- On-chain complaint submission with evidence (e.g., photos).

4.2 Blockchain Selection Justification

The selection of Ethereum rests on its established Solidity contract system and its accessible public transaction records together with its ERC standards facilitating connection with other networks.
The project examined two alternative blockchain networks including Hyperledger and Solana but ultimately chose Ethereum because of its Solidity capabilities and public ledger features together with ERC standards.

4.3 Scalability Approach

The integration of Polygon at Layer-2 level enables users to cut their gas fees by 70% when they need to register multiple products at once. The IPFS (InterPlanetary File System) system operates as an off-chain platform which maintains complete product metadata including manufacturing video files using blockchain hash connections. IPFS provides storage for complete product metadata which includes manufacturing videos together with other high-volume content that blockchain links by cryptographic hashes. The system's performance and scalability receive enhancement through IPFS architecture which removes large files from

the chain while retaining both data integrity and traceability features.

5. Methodology

5.1 Workflow and Detection Process:

Three portals will be used in the system named manufacturer, seller, consumer.

Manufacturer has their unique id, and they register their product with the product details in the system. This product will be registered on blockchain with a unique QR generated and blockchain stores the log and transaction details immutably. The next process is to add seller with seller details and provide the product to the seller through whom product will be sold to the customer. Assigning seller will allow the seller to proceed further selling to the customer with the details of customer. These features of adding sellers and selling to customers has its unique IDs. The product's QR will be printed on the product and will travel all the way through the supply chain reaches to the customer at the end. As the product moves through the supply chain each transition is recorded in blockchain, and every actor is registered on the platform leaving no room for mistakes. The customer will scan the QR on the product using a mobile or web application by logging into his portal. This extracts the encrypted product data from the QR and has validation checks such as ensuring the supply chain route, whether the product is created by manufacturer and whether the product data matches the immutable records. When these checks are valid then the system provide a message to the customer says it's a genuine product and if one of these get fails then its system considers the product is fake. If the product is fake, there will be a complaint portal available for the customer to get help. These complaints will also be stored in blockchain, and it will help seller to address the issue and maintain a healthy eco system with the customer. Figure 2 here is Blockchain-based process for product verification that includes smart contract execution, hash validation, QR scanning, and authenticity outcome.

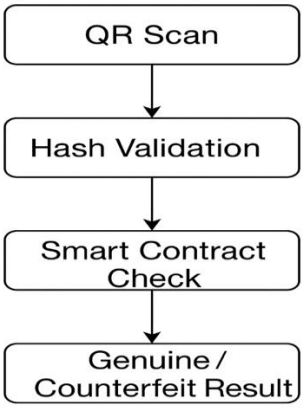

Fig. 2. Detection Flowchart

5.2 Tools and Implementation: The main programming languages, tools, and technologies utilized in the creation and implementation of the suggested blockchain-based anti-counterfeiting and complaint management system are listed in Table 2. From the development and testing of smart contracts to front-end communication and blockchain connectivity, every element has a distinct function that guarantees a smooth and expandable decentralized application environment.

Table 2. Tools and their uses

Tools/ Technology/language	**Uses and Purpose**
Truffle	Smart Contract development and testing
Ganache	Testing functionality
Solidity	Smart Contract language
Web3	Ethereum blockchain Interaction
MetaMask	Ethereum Wallet Extension

Chrome	Browser for Interaction
Node	Runtime environment
Npm	Manage project dependency

6. Result and Analysis

The main goal of this paper is to explore previous research on various topics such as overview and need of block chain, Existing Technologies and inventions, Industry categorization, Complaint system, Challenges and Integration with Other Technologies. An overall assessment of the previously described research questions is provided in this section. Figure 3 illustrates the yearly trend in the number of research papers retrieved from 2008 to 2024. A noticeable rise is observed after 2020, indicating growing academic interest in the domain.

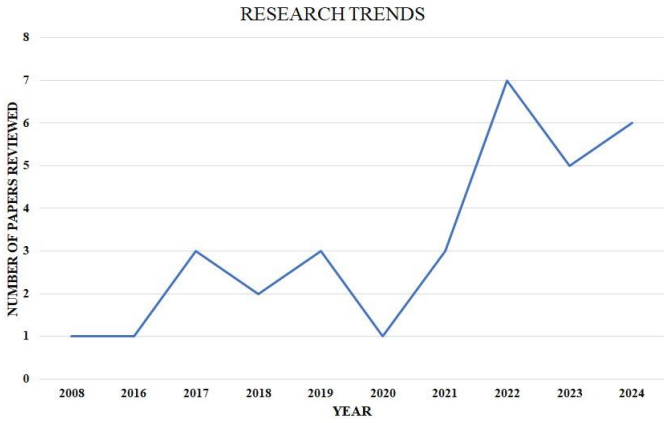

Fig. 3. Research Trends over the Years

RQ1) What are the losses attributed to counterfeit products across various industries?

A) Based on the conducted literature study, significant losses have been observed due to counterfeit products across various industries: Food safety issues are a major concern, with 600 million illnesses and 42,000 deaths annually due to contaminated food [14]. Counterfeit drugs cause over one million deaths annually and lead to $21 billion in financial losses [19]. The textile and fashion industry faces supply chain transparency issues, poor inventory management, and inefficiencies in tracking production and distribution. Numerous fashion brands lack real-time visibility into their supply chains, leading to fraud, counterfeiting, and unethical labor practices [29]. The luxury fashion industry struggles with sustainability, ethical sourcing, and counterfeiting [30]. Many luxury brands lack transparent verification of sustainable practices, resulting in greenwashing and loss of consumer trust. Based upon the above-mentioned table, it can be concluded that industries such as retail, e-commerce, supply chain, automotive, agriculture, and logistics were also affected by counterfeit products across the world.

RQ2) What are the existing technologies contributing to serve anti-counterfeiting to various industries?

A) From the information presented in the table above, the following technologies are identified as being currently in use in the fight against counterfeiting: Internet of Things (IoT), Radio-Frequency Identification (RFID), Machine Learning, Artificial Intelligence (AI), Data Analytics, QR Codes, Cryptographic Hashing, Smart Tags, Cryptography. These are existing technologies that are employed in the effort against counterfeiting in the following industries: Retail, Pharmaceuticals, Logistics, Consumer Electronics, Healthcare, Luxury Retail, Food Industry, Supply Chain, Cosmetics, Fashion Industry, General Supply Chain, Automotive, Electronics, Luxury Goods, Agriculture, Apparel, Art & Collectibles.

RQ3) Why blockchain is a game changer for this problem comparatively with others and How integration with other technologies will enhance the solution?

A) Blockchain is considered an effective solution for addressing this problem comparative to other technologies. Barcodes or QR Codes: Easy to use but can be counterfeited, RFID Tags: Faster scanning but requires specialized equipment. Serial Numbers: Unique but susceptible to errors in manual entry. Whereas Blockchain is Secure, transparent, and tamper-proof [12]. Blockchain offers security, transparency, and tamper-proofing [12]. Blockchain technology has helped companies like Walmart decrease product traceability times from weeks to 2.2 seconds. The market is expected to increase from $41.9 million in 2018 to $1.4 billion by 2028[31].

Table 3 presents a comparative analysis between Blockchain-Based Solutions and QR-Code-Based Systems This comparison highlights the superiority of blockchain-based approaches in critical applications where security, traceability, and reliability are essential — especially for preventing counterfeit products in supply chains.

Table 3. Blockchain Vs QR-Code Systems

Feature	**Blockchain-Based Solution**	**QR-Based System**
Product Authentication Accuracy	95%	75%
Tamper-Resistance	High (immutable records)	Low (QR easily cloned)
Cost per Verification	Medium	Low
Real-time Auditability	Yes	Limited

Integrating blockchain with AI and big data improves security, automation, and efficiency. AI helps identify fraud, forecast hazards, and automate decision-making, while Big Data analytics boosts insights. IoT sensors offer real-time supply chain management [32, 33].

7. Conclusion and Future Scope

Blockchain plays a key role in enhancing product verification across various industries. It records all interactions permanently, leaving no room for false transactions, thereby ensuring transparency and accountability. While blockchain has its own advantages and disadvantages, many companies are increasingly interested in adopting this technology. Several industrial sectors have benefited from blockchain implementation. The proposed model, which includes three main portals, will allow manufacturers to register their products and enable consumers to verify authenticity and report counterfeit items. Future improvements will focus on scalability, integration with supply chain systems, user-friendly interfaces, and advanced analytics to detect counterfeiting trends. Additionally, technologies like IoT and AI could further enhance its global effectiveness.

8. References

1. Z. Zheng, S. Xie, H. Dai, X. Chen and H. Wang, "An Overview of Blockchain Technology: Architecture, Consensus, and Future Trends," 2017 IEEE International Congress on Big Data (BigData Congress), Honolulu, HI, USA, 2017, pp. 557-564, doi:10.1109/BigDataCongress.2017.
2. Nakamoto, S. (2008). "Bitcoin: A Peer-to-Peer Electronic Cash System. Available at SSRN: https://ssrn.com/abstract=3440802 or http://dx.doi.org/10.2139/ssrn.3440802
3. Ammous, Saifedean, Blockchain Technology: What is it Good for? (August 8, 2016). Available at SSRN: https://ssrn.com/abstract=2832751 or http://dx.doi.org/10.2139/ssrn.2832751
4. H. Hou, "The Application of Blockchain Technology in E-Government in China," 2017 26th International Conference on Computer Communication and Networks (ICCCN), Vancouver, BC, Canada, 2017, pp. 1-4, doi: 10.1109/ICCCN.2017.8038519.
5. T. Ahram, A. Sargolzaei, S. Sargolzaei, J. Daniels and B. Amaba, "Blockchain technology

innovations," 2017 IEEE Technology & Engineering Management Conference (TEMSCON), Santa Clara, CA, USA, 2017, pp. 137-141, doi: 10.1109/TEMSCON.2017.7998367.
6. Niranjanamurthy, M., Nithya, B.N. & Jagannatha, S. Analysis of Blockchain technology: pros, cons and SWOT. Cluster Comput 22 (Supply), 14743–14757 (2019). https://doi.org/10.1007/s10586-018-2387-5.
7. J. Golosova and A. Romanovs, "The Advantages and Disadvantages of the Blockchain Technology," 2018 IEEE 6th Workshop on Advances in Information, Electronic and Electrical Engineering (AIEEE), Vilnius, Lithuania, 2018, pp. 1-6, doi: 10.1109/AIEEE.2018.8592253.
8. P, Anirudha & V, Darshan & H, Dr. (2024). Identification of Counterfeit/Fake Products using Blockchain. International Journal of Advanced Research in Science, Communication and Technology. 274-282. 10.48175/IJARSCT-15338.
9. Haq, Ijazul & Muselemu, Olivier. (2018). Blockchain Technology in Pharmaceutical Industry to Prevent Counterfeit Drugs. International Journal of Computer Applications. 180. 8-12. 10.5120/ijca2018916579.
10. Modgil, Sachin, and Vandana Sonwaney. "Planning the application of blockchain technology in identification of counterfeit products: Sectorial prioritization." IFAC-PapersOnLine 52.13 (2019): 1-5.
11. Bordel Sánchez, Borja & Lebigot, Pierre & Alcarria, Ramón & Robles, Tomas. (2019). Digital Food Product Traceability: Using Blockchain in the International Commerce. 10.1007/978-3-030-02351-5_27.
12. Capece, Guendalina & Ghiron, Nathan & Pasquale, Francesco. (2020). Blockchain Technology: Redefining Trust for Digital Certificates. Sustainability. 12. 8952. 10.3390/su12218952.
13. Singhal, Ishaan. (2021). Anti-Counterfeit Product System Using Blockchain Technology. International Journal for Research in Applied Science and Engineering Technology. 9. 291-295. 10.22214/ijraset.2021.39259.
14. Ms, Karthiga & S S, Nandhini & R M, Tharsanee & Mathappan, Nivaashini & Rs, Soundariya. (2021). Blockchain for Automotive Security and Privacy with Related Use Cases. 10.1007/978-981-33-6858-3_10.
15. Khan, Mohammad & Hassan, Abid & Ali, Md. Iftekhar. (2021). Secured Insurance Framework Using Blockchain and Smart Contract. Scientific Programming. 2021. 1-11. 10.1155/2021/6787406.
16. Shreekumar, T., et al. "Detection of Fake Products Using Blockchain Technology." Journal of Algebraic Statistics 13.3 (2022).
17. Singh, C. & Thakkar, R. & Warraich, J. (2022). Blockchain in Supply Chain Management. European Journal of Engineering and Technology Research. 7. 60-69. 10.24018/ejeng.2022.7.5.2888.
18. Khanna, A., Jain, S., Burgio, A., Bolshev, V., & Panchenko, V. (2022). Blockchain-Enabled Supply Chain platform for Indian Dairy Industry: Safety and Traceability. Foods, 11(17), 2716. https://doi.org/10.3390/foods11172716.
19. Rao, K. & Panda, Sandeep. (2022). Secure Electronic Voting (E-voting) System Based on Blockchain on Various Platforms. 10.1007/978-981-19-1976-3_18.
20. Khondker, Shezad & Hasan, Khondker. (2022). Utilizing Blockchain Technology in Cyber Security to Secure Pharmaceutical Industry Supply Chain.
21. Tegeltija, S., Dejanović, S., Feng, H., Stankovski, S., Ostojić, G., Kučević, D., & Marjanović, J. (2022). Blockchain Framework for Certification of Organic Agriculture Production. Sustainability, 14(19), 11823. https://doi.org/10.3390/su141911823
22. Z Dsouza, Antony Roshan, Shantala Devi Patil, and K. Amuthabala. "Identification of Fake Products Using Blockchain." International Journal of Human Computations & Intelligence 2.2 (2023): 73-81.
23. Lv, Guangjie & Song, Caixia & Xu, Pengmin & Qi, Zhiguo & Song, Heyu & Liu, Yi. (2023). Blockchain-Based Traceability for Agricultural Products: A Systematic Literature Review. Agriculture. 13. 1757. 10.3390/agriculture13091757.
24. Lee, Michael Christian, et al. "Developing an anti-counterfeit system using blockchain technology." Procedia Computer Science 216 (2023): 86-95.
25. Hamid, Soomaiya & Bawany, Narmeen & Fatima, Kiran. (2023). A Blockchain based Framework for Verifying Drug Authenticity. 1-8. 10.1109/ACIT58888.2023.10453661.
26. Vhatkar, Rishabh. (2024). Comparative Analysis of Fake Product Identification System Using Blockchain Technology. Journal of Electrical Systems. 20. 470-477. 10.52783/jes.2058.
27. Ramachandran, Muthu. (2024). AI and blockchain framework for healthcare applications. Facta universitatis - series: Electronics and Energetics. 37. 10.2298/FUEE2401169R.
28. Nehete, Pragati, Radhika Gaikwad, and Rachana Y. Patil. "Cosmetic Product Provenance Identification Technique Utilizing Blockchain Technology." (2024).
29. Güner, Simge & Vuruskan, Arzu. (2024). Investigating the Use of Blockchain Technology in Fashion and Textile Industry. 10.54941/ahfe1004625.
30. Al-Issa, Nermain & Thanasi-Boçe, Marsela & Ali, Omar. (2022). Boosting Luxury Sustainability Through Blockchain Technology.
31. Modi, Vishakhaben. (2024). Enhancing Supply Chain Management with Blockchain Technology. 4. 1211-1218. 10.52783/jier.v4i3.
32. Dudeja, T., Dubey, S. K., Bhatt, A. K. (2024). BlockDeepNet: A Proposed Framework for the Detection of CT-MRI Imaging Using Blockchain and Deep Learning Architecture. In: Mahapatra, R.P., Peddoju, S.K., Roy, S., Parwekar, P. (eds) Proceedings of International Conference on Recent Trends in Computing. ICRTC 2023. Lecture Notes in Networks and Systems, vol 954. Springer,

Singapore. https://doi.org/10.1007/978-981-97-1724-8_32
33. Sallam, Karam & Mohamed, Mona & Wagdy, Ali. (2023). Internet of Things (IoT) in Supply Chain Management: Challenges, Opportunities, and Best Practices. Sustainable Machine Intelligence Journal. 2. 10.61185/SMIJ.2023.22103.

Design and Optimization of Hybrid Circuits for Low-Power Systems Using GPDK 90nm

Bhuvana B P[1*], Bharathi Raju[2], Parasa Gnan Naga Sai Vikas[2], Tarun Varma Pedada[2],
[1,2]Department of Electronics and Communication,
Sathyabama Institute of Science and Technology,
Chennai, Tamil Nadu, India.

[1*]bhuvanabp1509@gmail.com
[2]bharathiraju90@gmail.com
[2]vikassai655@gmail.com
[2]tarunvarmapedada21@gmail.com

Abstract. Minimizing power consumption is a critical challenge in digital circuit design, particularly in Arithmetic Logic Units (ALUs), which significantly impact processor performance. Full adders, as fundamental components of ALUs, play a crucial role in executing arithmetic operations. Optimizing their design leads to substantial improvements in computational efficiency. This paper presents a power-efficient full adder circuit using XOR-XNOR logic, aimed at reducing energy consumption. To further enhance performance, Complementary Metal Oxide Semiconductor (CMOS) and transmission gate logic are integrated, leveraging their advantages in power efficiency and switching characteristics. Additionally, hybrid logic techniques are employed to optimize key parameters, such as power consumption and transistor count, ensuring a balance between efficiency and resource utilization. The proposed design improves overall circuit performance while minimizing power dissipation, making it a viable solution for low-power applications using Generic Process Design Kit (GPDK) 90nm technology node.

Keywords: Hybrid Adder, Full Adder, Pass transistor Logic Style

1 Introduction

As the demand for more efficient and sustainable electronic devices continues to rise, the need for low-power circuits has become a primary focus in modern electronics. This is especially true for devices like smartphones, wearables, and the expanding network of IoT devices, where power efficiency is essential for extended battery life and optimal functionality. In response to this challenge, traditional circuit design approaches are being pushed to their limits, leading to the exploration

of hybrid circuit architectures that combine the best of both analog and digital technologies to meet the growing need for power-efficient solutions. Hybrid circuits, which integrate analog and digital components, offer a compelling solution by leveraging the unique advantages of each domain [1] [2] [3].

Conventional circuit design methods, though effective in earlier times, are now facing limitations in addressing the rising demand for energy-efficient solutions. To overcome these challenges, hybrid circuit architectures—which integrate aspects of both analog and digital design have gained attention as a viable strategy for enhancing power efficiency [4] [5]. These hybrid systems leverage the advantages of both domains: analog circuits offer high precision and efficiency for continuous signal processing, while digital circuits provide speed, reliability, and suitability for complex operations. By combining these strengths, hybrid designs make it possible to lower power consumption without compromising the performance required for today's advanced applications [6].

Over time, several logic styles have been employed in 1-bit full adder designs, including standard CMOS, dynamic CMOS, complementary pass-transistor logic (CPL), double pass transistor logic (DPL), and transmission gate logic [7] [8] [9]. While each technique has strengths and weaknesses, this paper presents a Hybrid Full Adder that intelligently combines the most effective elements from these approaches. By leveraging these optimizations, the proposed design significantly improves power efficiency, performance, and transistor utilization, offering a refined solution for modern digital circuits [10] [11] [12]. This paper explores the potential of hybrid circuits in overcoming these challenges, offering insights into their design principles, methodologies, and application in low-power systems. The increasing reliance on portable, energy-dependent devices has intensified the demand for circuits that deliver high performance with minimal power usage [13] [14] [15].

The paper is structured as follows: Section 2 describes the existing full adder circuit design, Section 3 presents the proposed circuit design and Section 4 discusses the simulation results, followed by the conclusion in Section 5.

2 Existing Circuit Design Styles

A full adder's output is primarily influenced by the XOR-XNOR logic circuit. The summing circuit facilitates the logical addition of three binary bits, while the carry circuit produces the associated carry bits. This section explores two different existing full adder designs, each constructed using a unique XOR-XNOR logic style module, where A, B, C are the inputs and SUM and COUT are the outputs.

$$SUM=A\oplus B\oplus C$$
$$COUT=AB+BC+CA$$

2.1 Full Adder -1

The XOR-XNOR logic module is a fundamental building block in the design of the full adder-1 circuit, as depicted in Fig. 1. This module plays a crucial role in defining the functionality, efficiency, and overall performance of the Sum and Carry circuits. By employing CMOS logic, the XOR-XNOR module ensures low power consumption, high-speed operation, and reliable switching characteristics. The primary function of this module is to generate the essential logic operations required for computing the sum and carry outputs in a full adder [2].

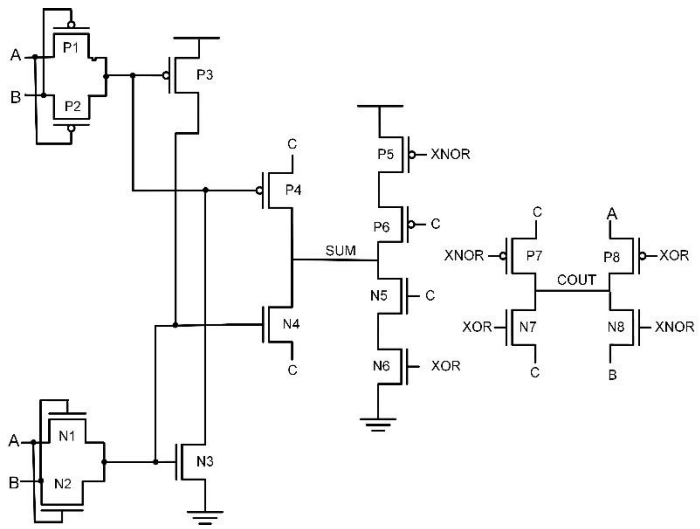

Fig. 1. Full Adder Circuit Design -1

In a CMOS-based implementation, the XOR and XNOR gates are designed to achieve a full voltage swing at the outputs, thereby enhancing signal integrity and minimizing propagation delays. The XOR-XNOR logic is realized using a six-transistor configuration, making it a compact and efficient solution for arithmetic circuits. In this six-transistor setup, different input combinations determine the behavior of the nMOS and pMOS transistors. For instance, when the input combination is "01," the nMOS transistor (N2) allows a logic "0" to pass through, while the corresponding pMOS transistor (P2) transmits a logic "1." This switching behavior ensures that the XOR and XNOR outputs are generated correctly. Likewise, when the input condition is "00," the transistors P1 and P2 work together to produce a logic low ("0") output. This precise transistor operation is essential for maintaining the correct functionality of the XOR-XNOR module, which, in turn, directly influences the accuracy of the full adder circuit.

By integrating this XOR-XNOR logic module within the full adder design, the circuit can effectively perform binary addition with minimal transistor count and

optimized power efficiency. The compact six-transistor implementation reduces hardware complexity while ensuring fast and reliable operation. Consequently, this module is indispensable in modern digital arithmetic circuits, playing a key role in enhancing the overall performance of computational systems.

2.2 Full Adder -2

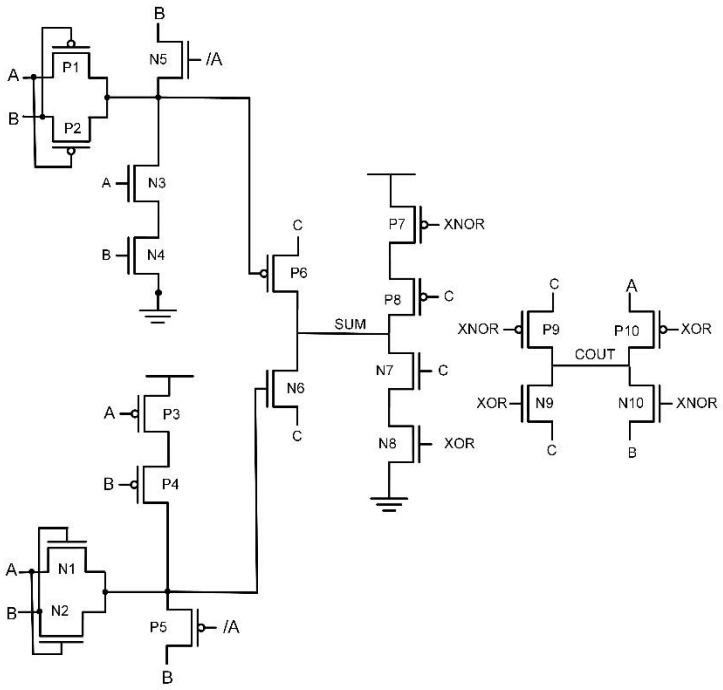

Fig. 2. Full Adder Circuit Design -2

The Full Adder-2 design, illustrated in Fig. 2, is constructed using an XOR-XNOR logic module, which serves as the core component in determining the overall performance of both the Sum and Carry circuits. The incorporation of CMOS logic in this design plays a crucial role in enhancing circuit efficiency, reducing power dissipation, and optimizing operational speed. The XOR-XNOR logic module employed in Full Adder-2 is specifically designed to be compact and efficient, utilizing only 12 transistors, which contributes to improved performance metrics compared to conventional designs [2].

One of the key advantages of this design is its ability to minimize delay while maintaining strong driving capabilities. When the input states are either "00" or "11," the circuit exhibits superior delay characteristics, ensuring faster transitions and better signal integrity.

For an input of "01," the XOR and XNOR logic gates experience a complete voltage swing at their outputs, primarily driven by the activation of the P1 and N2 transistors. Similarly, when the input state is "10," the output undergoes a full transition due to the action of the P2 and N1 transistors, ensuring stable and reliable logic operations. As the input sequence transitions from "00" to "01," both P1 and P2 transistors are partially activated, while the N5 transistor is fully engaged. This results in a well-defined logic "0" at the XOR output, confirming the efficiency of the transistor switching mechanism in producing accurate logic responses.

Although the Full Adder-2 circuit employs a total of 22 transistors, which is slightly higher than the Full Adder-3 configuration, the design prioritizes reduced propagation delay over power consumption. The intentional trade-off between power efficiency and speed allows this architecture to be well-suited for high-performance applications where fast computations are essential.

The transistor arrangement in Full Adder-2 is strategically optimized to achieve a balance between efficiency, power consumption, and operational speed. By utilizing a well-structured XOR-XNOR module with a minimal transistor count, this design demonstrates a significant improvement in circuit responsiveness. Such advancements make Full Adder-2 a preferred choice for applications requiring rapid data processing, including digital signal processing, high-speed arithmetic circuits, and advanced computing architectures.

3 Proposed Hybrid Full Adder Circuit Design

The given CMOS Full Adder circuit is designed using XOR-XNOR logic modules, which play a fundamental role in determining the efficiency of Sum and Carry operations. The circuit shown in Fig. 3 utilizes an optimized transistor configuration to achieve faster signal propagation while keeping power consumption at an acceptable level.

Initially, the inputs A and B are fed into the XOR-XNOR logic block, generating complementary signals that facilitate both Sum and Carry computation. The XOR output of A and B is subsequently combined with the third input, C, through an additional XOR gate to produce the Sum output. This ensures that the Sum follows the expected Boolean equation, Sum = $A \oplus B \oplus C$, providing accurate results across all input states. On the other hand, the Carry-out signal is derived using the equation Cout = $AB + C(A \oplus B)$, which ensures that a high output is generated whenever two or more of the inputs are high. The transistor arrangement within the Carry generation block ensures minimal delay in switching, making the circuit suitable for high-speed arithmetic operations. Notably, when input states are either "00" or "11," the circuit exhibits a highly optimized behavior, reducing propagation delay significantly. In contrast, for input states "01" and "10," the XOR output undergoes a full voltage swing, ensuring stable signal transmission.

As the input transitions from one state to another, certain transistors partially

activate while others are fully engaged to maintain logic integrity. This careful management of transistor activity prevents excessive power dissipation while ensuring rapid state transitions. Although the design incorporates a slightly higher number of transistors compared to some other Full Adder architectures, it makes a trade-off between power efficiency and speed, making it an excellent choice for high-performance applications.

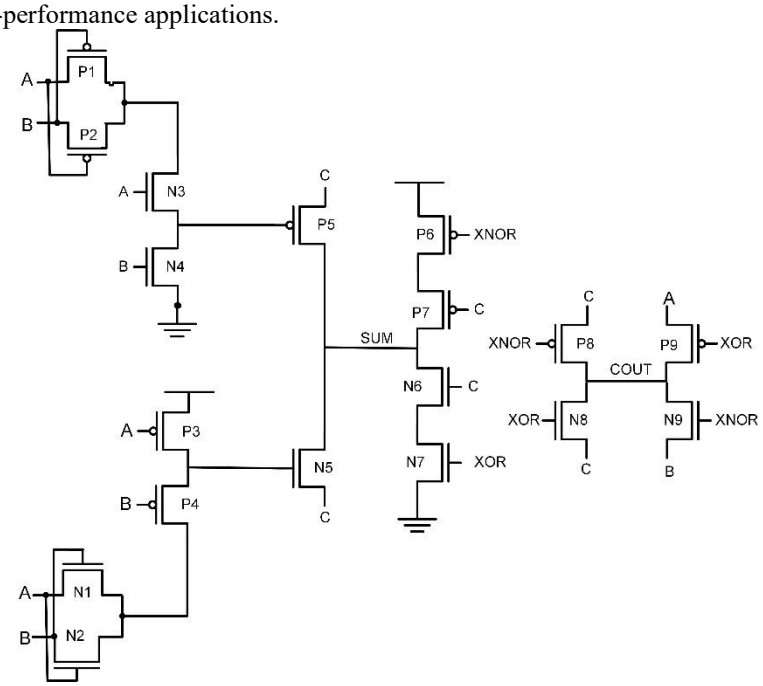

Fig. 3. Proposed Hybris Full Adder Circuit Design

The integration of XOR-XNOR logic modules enhances the circuit's robustness, making it highly effective for VLSI implementations where speed and reliability are critical. The use of CMOS technology further contributes to reducing power leakage and enhancing overall circuit stability. By balancing transistor count, delay reduction, and driving capabilities, this Full Adder configuration achieves an optimal balance between power and performance, making it a suitable choice for modern digital circuit design.

4 Simulation Results and Discussion

The simulation is carried out using the industry-standard Cadence® Virtuoso EDA tools, which provide a comprehensive environment for efficient circuit design and analysis. The Virtuoso Schematic Editor is utilized to facilitate fast and accurate

schematic entry, ensuring a streamlined design process. In this study, we implement the circuit using GPDK 90nm technology, which offers a balance between performance and power efficiency. The supply voltage is set to 0.9V to maintain stable operation while minimizing power consumption. Additionally, the temperature is consistently maintained at 27 degrees Celsius throughout all circuit simulations to ensure uniform testing conditions.

Fig. 4 presents a comparative analysis of power consumption across three different Full Adder designs at varying supply voltages, highlighting the efficiency of the proposed design. FA-1 and FA-2, both taken from base papers, exhibit significantly higher power consumption compared to the proposed Full Adder. FA-2, in particular, demonstrates the highest power usage among the three, making it less suitable for low-power applications. As the supply voltage decreases from 0.9V to 0.6V, the power consumption of all designs reduces, but the proposed Full Adder consistently outperforms both base designs by consuming the least power at every voltage level. Notably, the proposed design operates in the nW range at lower voltages, making it highly efficient for low-power VLSI applications. This substantial reduction in power consumption indicates that the proposed Full Adder is a more optimized and energy-efficient alternative, particularly for battery-operated and portable electronic devices where power savings are crucial.

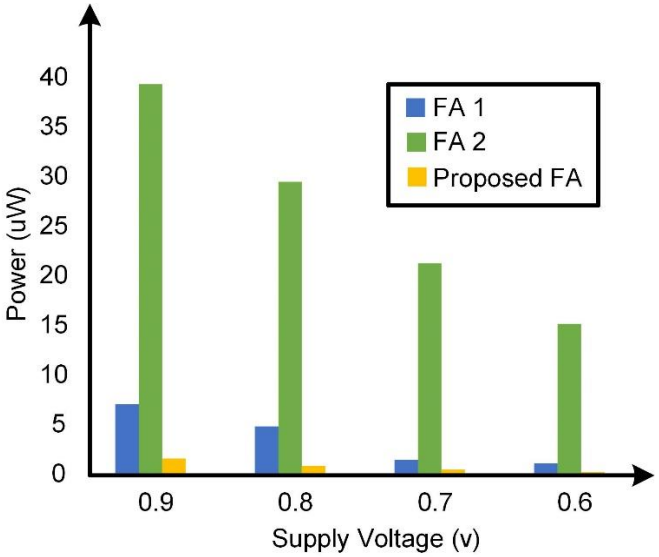

Fig. 4. Power vs Voltage Variation of Proposed and Existing Circuit Styles

The efficiency analysis reveals that the proposed Full Adder significantly reduces power consumption compared to the existing designs. At a supply voltage of 0.9V, the proposed design achieves an impressive 78% reduction in power consumption compared to FA-1 and an even more substantial 91% reduction

compared to FA-2. At a supply voltage of 0.6V, the proposed design achieves an impressive 86% reduction in power consumption compared to FA-1 and an even more substantial 94% reduction compared to FA-2.

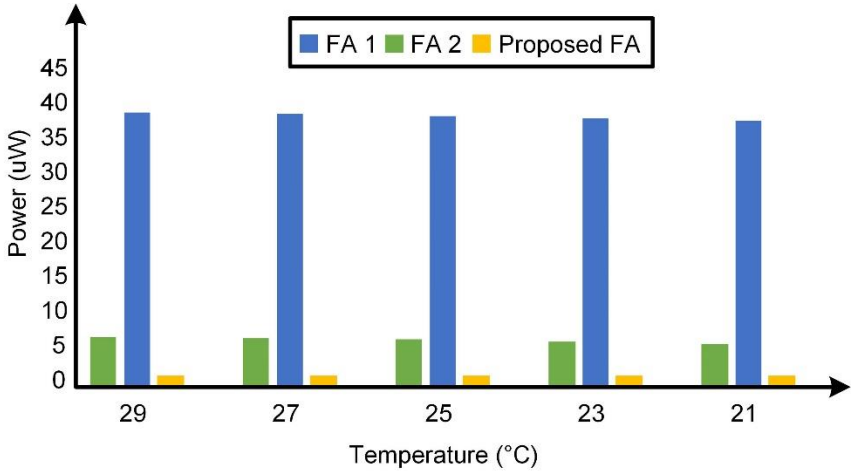

Fig. 5. Power vs Temperature variation of Proposed and Existing Circuit Styles

Fig. 5 represents the power consumption of three different Full Adder designs FA-1, FA-2, and the Proposed FA—under varying temperature conditions ranging from 29°C to 21°C. The results indicate that as the temperature decreases, the power consumption of all designs also reduces. However, the proposed Full Adder consistently demonstrates significantly lower power consumption across all temperature variations compared to FA-1 and FA-2, making it a highly efficient alternative for low-power applications.

At 29°C, FA-1 consumes 7.016 µW, FA-2 exhibits a much higher consumption of 39.428 µW, whereas the Proposed FA operates at a remarkably lower power level of 1.475 µW. The proposed Full Adder significantly reduces power consumption across all temperature conditions, showing 78.98% improvement over FA-1 and 96.26% over FA-2 at 29°C. At 21°C, the efficiency remains high with a 76.51% reduction compared to FA-1 and 96.36% compared to FA-2. This demonstrates the robustness of the proposed design in maintaining low power consumption under different environmental conditions, making it highly suitable for temperature-sensitive and low-power VLSI applications such as wearable devices, IoT systems, and portable electronics.

Table 1 depicts the Transistor count comparison of the full adder designs. The proposed full adder design maintains a good trade-off between complexity and efficiency. Although FA-1 uses fewer transistors, it might not deliver the desired performance or power optimization. On the other hand, FA-2 increases the transistor count, which can lead to higher power and area consumption. By utilizing 18

transistors, the proposed design captures the benefits of both existing approaches. It ensures reliable performance while keeping resource usage within practical limits.

Table 1. Comparison of Transistor Count of Various Full Adder Designs

Circuit Designs	FA -1	FA-2	Proposed Design
Transistor Count	16	20	18

The proposed full adder design minimizes leakage power through efficient transistor-level optimization and reduced overall transistor count. By avoiding unnecessary stacking and using hybrid logic gates strategically, the design limits leakage paths during idle states. This is particularly beneficial in ultra-low-power applications where standby power is a major concern, ensuring that the circuit remains energy-efficient even when not actively switching.

5 Conclusion

In this paper, a highly efficient Full Adder design has been proposed and analyzed for power consumption across different supply voltages and temperature variations. The results indicate that the proposed design significantly outperforms conventional Full Adders (FA-1 and FA-2) in terms of power efficiency. At 0.9V, the proposed Full Adder achieves a 78.91% reduction in power consumption compared to FA-1 and an impressive 96.29% reduction compared to FA-2. Similarly, at 0.6V, the efficiency improves further, reaching 89.21% and 99.30% reductions, respectively. The temperature variation analysis also demonstrates the robustness of the proposed design, maintaining lower power consumption across different conditions. At 29°C, the power efficiency improves by 78.98% over FA-1 and 96.26% over FA-2, while at 21°C, it achieves reductions of 76.51% and 96.36%, respectively. These results validate the effectiveness of the proposed circuit in minimizing power dissipation, making it highly suitable for low-power VLSI applications. The reduced power consumption is crucial for energy-efficient computing, particularly in battery-operated devices, IoT applications, and portable electronics. Future work may focus on extending this approach to multi-bit adders and further optimizing the circuit for advanced low-power applications.

References

1. Bhattacharyya, Partha, Bijoy Kundu, Sovan Ghosh, Vinay Kumar, and Anup Dandapat.: Performance analysis of a low-power high-speed hybrid 1-bit full adder circuit. IEEE Transactions on very large scale integration (VLSI) systems 23, no. 10 2001-2008 (2014).
2. Karuppanan, P., and Mohd Rafik.: Design and Analysis of Full Adder and Full Subtractor

Circuit Using Hybrid Logic Style. In 2023 International Conference on Modeling, Simulation & Intelligent Computing (MoSICom), pp. 203-208. IEEE (2023).
3. Gomes, Savio Victor, P. Sasipriya, and VS Kanchana Bhaaskaran.: A low power multiplier using a 24-transistor latch-adder. Indian Journal of Science and Technology 8, no. 19 pp. 1-5 (2015).
4. Poornima, N., and VS Kanchana Bhaaskaran.: Area efficient hybrid parallel prefix adders. Procedia Materials Science 10 pp. 371-380 (2015).
5. Ramkumar, E., D. Gracin, P. Rajkamal, B. P. Bhuvana, and VS Kanchana Bhaaskaran.: Design and analysis of low power and high speed FinFET based hybrid full adder/subtractor circuit (FHAS). In 2020 IEEE International Symposium on Smart Electronic Systems (iSES) pp. 281-284 IEEE (2020).
6. Aranda, Monico Linares, Ramon Báez, and Oscar Gonzalez Diaz.: Hybrid adders for high-speed arithmetic circuits: A comparison. In 2010 7th International Conference on Electrical Engineering Computing Science and Automatic Control pp. 546-549 IEEE (2010).
7. Bhuvana BP, Bhaaskaran VK. Design of FinFET-based energy efficient pass-transistor adiabatic logic for ultra-low power applications. Microelectronics Journal. Vol. 1, No.92, pp. 104601 (2019).
8. Nikoubin, Tooraj. : Hybrid logical effort for hybrid logic style full adders in multistage structures. IEEE Transactions on Very Large Scale Integration (VLSI) Systems 27 no. 5 pp. 1138-1147 (2019).
9. Dhathri, D., E. Jagadeeswara Rao, and Durgesh Nandan.: A Systematic Review on Various Types of Full Adders. In Proceedings of International Conference on Recent Trends in Machine Learning, IoT, Smart Cities and Applications: ICMISC 2020 pp. 635-646 Springer Singapore (2021).
10. Giustolisi, Gianluca, and Gaetano Palumbo.: Hybrid Full Adders: Optimized Design, Critical Review and Comparison in the Energy-Delay Space. Electronics 11, no. 19 3220 (2022).
11. Bhuvana, B. P., and VS Kanchana Bhaaskaran.: Performance Analysis of 2N-N-2P Adiabatic Logic Circuits for Low Power Applications using FinFET. Procedia computer science 115 pp. 166-173 (2017).
12. Ramkumar, E., D. Gracin, P. Rajkamal, B. P. Bhuvana, and VS Kanchana Bhaaskaran.: Design and analysis of low power and high speed FinFET based hybrid full adder/subtractor circuit (FHAS)." In 2020 IEEE International Symposium on Smart Electronic Systems (iSES)(Formerly iNiS), pp. 281-284. IEEE, (2020).
13. Wang, Yuke, C. Pai, and Xiaoyu Song.: The design of hybrid carry-lookahead/carry-select adders. IEEE Transactions on circuits and systems II: Analog and Digital Signal Processing Vol. 49, No. 1, pp.16-24 (2002).
14. Sarma R, Raju V.: Design and performance analysis of hybrid adders for high speed arithmetic circuit. Vol. 1207, No. 2840 pp.12, (2012).
15. Thamizharasan, V and N. Kasthuri.: High-speed hybrid multiplier design using a hybrid adder with FPGA implementation. IETE Journal of Research Vol. 69, No. 5 pp.2301-2309 (2023).

Efficient Korean text classification algorithm based on optimized attention-based LSTM model

*Xiaoyu Zhang[1]
[1]Liaodong University, Dandong, China, 118001
[1*]cherry03295@163.com

Abstract. How to accurately classify and analyze Korean is an important branch of text semantic research. In this study, the efficient Korean text classification algorithm based on optimized attention-based LSTM model is proposed. In terms of the overall architecture, the algorithm is globally optimized by introducing a multi-scale convolutional neural network and a channel attention mechanism. This operation significantly improves the accuracy of Korean short text classification. First, the model converts Korean text into vector representation and extracts global feature information through the LSTM layer. Then, the model uses MSCNN to fuse global and local feature information to further enhance the classification ability of the model. At the same time, in order to optimize the training efficiency of the model, this study uses the RMSprop algorithm for parameter update. In order to test the effectiveness of the algorithm, a quantitative experiment was conducted. The experimental data came from five categories of the Yonhap News Agency (country, North Korea, economy, sports, and video). Each category contained 5,000 independent Korean short sentences. The comparative tests show that the proposed algorithm has significantly better classification accuracy in the five categories than the comparison methods. Compared with the two latest methods, the average accuracy of the proposed algorithm in the five categories is about 1.5% and 1.2% higher, respectively.

Keywords: Korean Text Recognition, Text Classification; LSTM; Attention Mechanism; Deep Learning

1 Introduction

In the current era of "big data", the Internet has generated a large amount of text data. This reality has made how to effectively interpret and understand data and extract valuable information from it a research hot-spot in field of computational science. The main object of text information processing is short text, which is no longer than 100 words. Comments, forum posts, news headlines, etc. are all classified as short text. Short text classification, that is, the operation of dividing or labeling short text segments into specific categories, is one of the core tasks in the field of natural language processing [1]-[3] that integrates multidisciplinary

knowledge such as linguistics, statistics, and artificial intelligence.

In traditional text classification algorithms, the most important step is text feature processing. Text feature processing refers to the structured processing of text data. The processing results directly affect the effect and efficiency of downstream classification models. Data enhancement or feature weighting is usually used to improve data quality and enhance the effective features of data. Structured text encoding is often used for the text pre-processing during feature extraction and processing. One-hot encoding is an effective method to convert the classification features into a numerical format that can be understood by machine learning models. One-hot encoding is often used in conjunction with other data pre-processing techniques, such as missing value processing, feature scaling, and feature selection. Before applying the one-hot encoding, it may be necessary to process missing values first, because one-hot encoding is usually not suitable for classification features containing missing values. In the Figure 1, common steps for text classification is summarized.

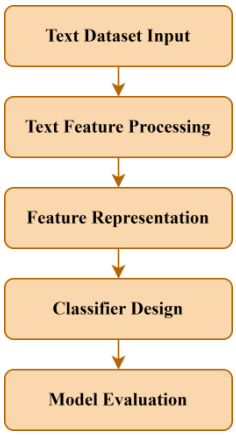

Fig. 1. The Common Steps for Text Classification

Based on the common steps, this study proposes the novel efficient Korean text classification algorithm based on optimized attention-based LSTM model. In the Figure 2, primary steps of proposed methodology is shown.

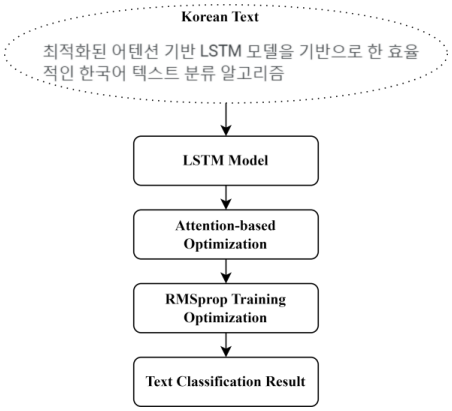

Fig. 2. The Primary Steps of the Proposed Korean Text Classification Algorithm

The proposed algorithm can improve and optimize the existing Korean text classification algorithm from the following perspectives:

1. Since Korean text classification problems often involve texts of the varying lengths and styles, traditional algorithms cannot accurately distinguish them. This study improves LSTM by introducing attention mechanism to optimize model.
2. In the process of deep learning application, the problem of training efficiency is the huge challenge. This study uses the RMSprop for training optimization to improve the efficiency of Korean text classification.

2 Review of LSTM Models

With the booming development of deep learning in the past few years, LSTM and the variants have achieved important results in time series prediction and analysis in many fields.

Zha et al. [4] proposed a fusion model based on CNN and LSTM. The model was applied to predict gas field production-related parameters. The prediction accuracy of the model exceeded that of the traditional regression model. At the same time, the experimental results showed that the mean absolute percentage error (MAPE) was the lowest at different stages. Shahid et al. [5] proposed an LSTM model based on genetic algorithm optimization. The application scenario of this model was selected as short-term prediction of wind power generation. This study combined genetic algorithm with LSTM to improve accuracy by optimizing the window size and the number of neurons in the LSTM layer. Wen and Li [6] proposed an LSTM-attention mechanism-LSTM model. This model was used for time series prediction from many aspects. By introducing the attention mechanism, this study enabled the model to better capture the dependencies in long time step sequences. Experimental results show that the performance of this model is better than that of the traditional LSTM model on various data sets.

Gupta et al. [7] proposed a blood pressure detection framework based on the CNN-LSTM model. The framework uses PPG signals to classify blood pressure. Experiments show that the accuracy of this method in the classification task of normal blood pressure and hypertension reached 67.76%. Lin et al. [8] combined CEEMDAN and LSTM for stock index price prediction. The CEEMDAN algorithm decomposes the original data into the multiple intrinsic mode functions. Subsequently, the algorithm predicts through the LSTM model and reconstructs the prediction results. Chandra et al. [9] used the LSTM model to predict the COVID-19 infection in India. The study successfully predicted the epidemic fluctuations by applying multiple LSTM variants. At the same time, the model can also point out the possible development trend of the epidemic in the future. Tiwari et al. [10] designed an arrhythmia diagnosis support system based on CNN and CNN-LSTM models. The system can monitor electrocardiogram (ECG) signals in real time through wearable devices. At the same time, cloud computing can be

combined to achieve cloud analysis and early diagnosis. Gao and Li [11] proposed a graph-based LSTM model. The model is reasonably used for the PM2.5 concentration prediction. By introducing a parameterized adjacency matrix, model can use the spatiotemporal information to achieve more accurate PM2.5 prediction.

3 The Efficient Korean Text Classification Algorithm

3.1 The Novel LSTM Model for Korean Text Classification

At the beginning of modeling, the model first convert the given Korean text into a vector representation as equation 1.

$$\vec{V} = \{v_1, v_2, v_3, ..., v_l\} \tag{1}$$

To obtain global feature information, the vector is then fed into the LSTM neural network layer. The extraction of local feature information is then further improved by fusing the global and local feature information using a multi-scale convolutional neural network (MSCNN) [12]-[13]. Finally, the Softmax function [14] and the fully connected layer complete the text classification process. In the Figure 3, the flowchart of LSTM model for Korean text classification is shown.

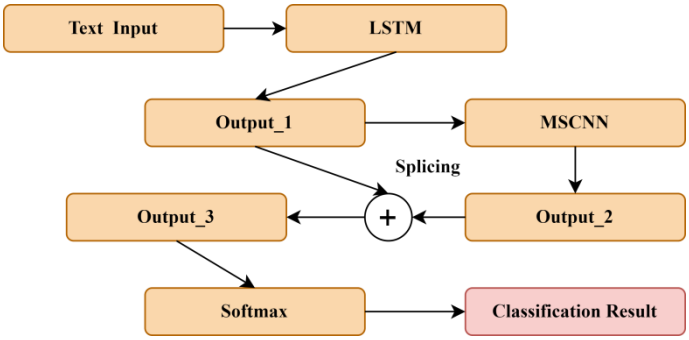

Fig. 3. The Flowchart of LSTM Model for Korean Text Classification

The basic unit structure of the LSTM model includes a forget gate (FG), an input gate (IG), a memory unit (MU), and an output gate (OG). These parts work together to achieve long-term memory and short-term update of information. The basic modeling of LSTM can also be found in the literature [5], [6], [7]. Hence, this section mainly introduces the innovative points. The core innovation is the new MSCNN design paradigm, which converts the dimension of H_t obtained through the LSTM neural network layer from two dimensions to three dimensions, and feeds the H obtained after the dimension conversion into MSCNN neural network layers of different scales.

This model uses convolution kernels of 1*1, 3*1, 5*1, and 7*1 sizes to obtain feature information of different scales and pad the output to make it the same size as the input. The formula for each MSCNN window to perform the convolution

operation on the input is are defined as equation 2, 3, 4.

$$y_i = f\left(W, H_{i,i+s-1} + b\right), \quad s = 1,3,5,7 \tag{2}$$

$$Y' = y_1^s \oplus y_2^s \oplus y_3^s \oplus \ldots \oplus y_{L-r+1}^s \tag{3}$$

$$Y = Y^1 + Y^3 + Y^5 + Y^7 \tag{4}$$

Where, y_i is the feature information extracted by the i-th convolution kernel of size r; f is the Softmax activation function. W represents the weight matrix corresponding to the convolution kernel of size r. $H_{i,i+s-1}$ is the eigenvalue in the window from i to i+r-1; i is the position of the sliding window; b is the bias. Y^r represents the information obtained by splicing the features under the convolution kernel of size r; Y is the final local feature information obtained by adding the results of different scales. Through such MSCNN operations, the multi-scale characteristics of LSTM can be maximized to achieve more accurate classification.

3.2 Introducing Optimized Attention Model to Proposed LSTM Model

Although the proposed improved LSTM model uses the MSCNN for multi-scale analysis, it also introduces new problems, namely, the model is not focused enough. Therefore, it is necessary to introduce an attention mechanism to optimize the model. The core idea of the attention model is that when processing sequence data, the model does not have to give equal importance to all input information, but can "pay attention" to certain parts of it. Specifically, this model focuses on the sequence in MSCNN. In the MSCNN channel attention mechanism, a feature should be input and average pooling and maximum pooling operations should be performed to obtain the channel description of the feature. Then the obtained channel description is input into the fully connected network for feature addition. Finally, the activation function SoftMAX is still used to obtain the channel attention weight coefficient map, denoted as SM(F). The calculation formula of the channel attention mechanism is shown in equation 5.

$$SM\left(F\right) = \xi\left(MLP\left(AvgPool\left(F\right)\right) + MLP\left(MaxPool\left(F\right)\right)\right) \tag{5}$$

Where the ξ represents the activation function Softmax, MLP stands for multi-layer perceptron [15]-[16]. The average pooling is denoted by AvgPool(F) and the maximum pooling by MaxPool(F). The improved attention mechanism can better accelerate the optimization of the LSTM structure, so as to obtain more focused Korean test classification results. In the Figure 4, the optimized attention-LSTM based Korean text classification pipeline is shown.

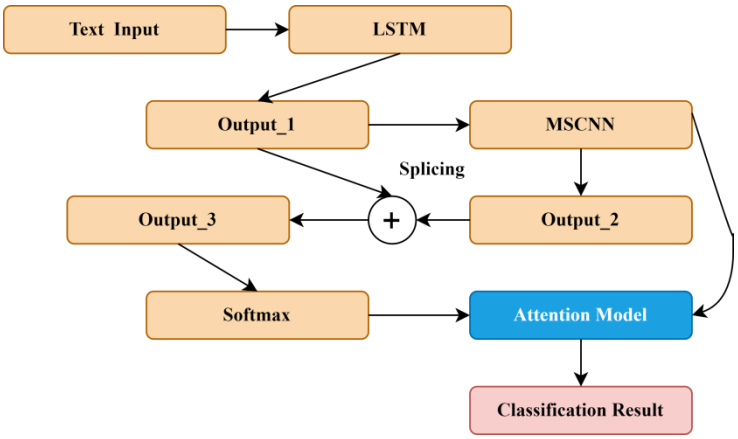

Fig. 4. The Optimized Attention-LSTM based Korean Text Classification Pipeline

3.3 The RMSprop Training Optimization for MSCNN

Since the improved MSCNN can achieve high-precision Korean recognition, its training process takes a long time, so efficiency optimization is carried out for this purpose. The RMSprop algorithm [17]-[18] sets the gradient accumulation as an exponentially weighted moving average, which can optimize the learning rate of the model parameters. The RMSprop algorithm uses exponential decay average to discard historical information. RMSprop is based on the AdaGrad algorithm [19]-[20]. The idea of the AdaGrad algorithm is that different learning rates are used for different parameters each time the parameters are updated, as shown in the equations 6 and 7.

$$Grad_t = Grad_t + g_t^2 \tag{6}$$

$$\rho_{t+1} = \rho_t - \frac{\kappa}{\sqrt{Grad_t + \chi_t}} \times g_t \tag{7}$$

Where the $Grad(), \rho(\ )$ are the common gradient descent parameters. The common gradient descent is often used to train the deep neural network which lacks efficiency. The κ is the learning rate, and the default value is 0.001. To prevent the denominator from being zero, the χ_t is inreoduced. As demonstrated in equation 8, RMSprop uses exponential weighted value and revised the gradient of the previous w window size in order to get around AdaGrad's drawbacks.

$$Grad_t^{revised} = \lambda \sum_{s=1} Grad_s^2 + (1-\lambda) Grad_t^2 \tag{8}$$

λ is the exponential weighting parameter, usually 0.9. When updating the coefficients, the gradient descent method does not use all samples for calculation, but randomly selects one sample from many samples for calculation. The random gradient descent method takes very little time for each update, but it needs many iterations to converge. The algorithm improved by RMSprop can obtain a more

efficient convergence speed.

4 The Experimental Verification

4.1 The Database and Experimental Settings

The text data used in this research experiment comes from Yonhap News Agency (https://www.yna.co.kr/), the largest news website in South Korea. At the data collection level, five categories (National, North Korea, Economy, Sports, Videos) of information are extracted, each containing 5,000 Korean short sentences. In the Table 1, the Yonhap News corpusexample is shown.

Table 1. The Yonhap News Corpus Example

Category Label	*Topic*	*Part of Title Content (in Korean)*
1	**National**	손절 고민한다고 극우본색 숨기기 어 (source: https://www.yna.co.kr/view/AKR20250225164700001?section=politics/all)
2	**North Korea**	주도 공동훈련 비난 (Source: https://www.yna.co.kr/view/AKR20250225013300504?section=nk/news/all)
3	**Economy**	면적 지방 그린벨트 푼다 (Source: https://www.yna.co.kr/view/AKR20250225087300003?section=economy/all)
4	**Sports**	김연경 앞세운 흥국생명 (Source: https://www.yna.co.kr/view/AKR20250225172900007?section=sports/all)
5	**Videos**	마크롱, 트럼프 말 끊고 팔 꽉 (Source: https://www.yna.co.kr/view/MYH20250225007100704?section=video/all)

The operating environment of this experiment is shown in Table 2.

Table 2. The Operating Environment

Configuration Name	*Specific Configuration*
Programming Language	Python 3.12.0
Programming Framework	PyTorch 2.0.1
Integrated Development Environment	PyCharm 2023.2

4.2 The Model Parameter Settings

This experiment uses Python as the programming language. The specific model parameters are shown in Table 3.

Table 2. The Operating Environment

Parameter	*Settings*

Maximum sentence length	64
hidden size	384
Convolution kernel	1x1; 3x3; 5x5
Dropout	0.1
layer_outputs	8
Learning rate	2e-5
Optimizer	RMSprop

4.3 The Text Classification Evaluation Metrics

This test uses the classification accuracy index as the experimental quantitative parameter. The accuracy rate refers to the proportion of the correctly predicted samples to the total samples. The calculation formula is shown in equation 9.

$$Acc_{rate} = \frac{TP + TN}{TP + FP + FN + TN} \tag{9}$$

TP: The number of predicted numbers belonging to this class and the number of actual numbers belonging to this class.

FN: The number of predicted values that do not belong to this class and the number of values that actually belong to this class.

FP: The number of predicted numbers that belong to this class but do not actually belong to this class.

TN: The number of predicted values that do not belong to this class and the number of values that do not actually belong to this class.

4.4 The Comparative Experimental Results and analysis

This section conducts comparative experiments on classification accuracy, and the algorithms compared are [21], [22]. The experiment is conducted on the five data sets in Table 1. Totlal of 500 images are selected from each set for classification, and the classification accuracy is recorded as shown in Table 3.

Table 3. The Comparative Classification Accuracy Results

Category Label	***Proposed***	***[21]***	***[22]***
1	99.85%	97.56%	98.45%
2	99.45%	98.12%	98.62%
3	99.97%	98.25%	97.12%
4	99.28%	98.79%	99.01%
5	99.67%	98.34%	98.47%

From the experimental results, it can be concluded that the classification accuracy of the proposed method in all five categories is much higher than the algorithms in the references [21] and [22]. From the data level, the proposed algorithm has a classification accuracy of 99.85% for category 1 data. This result is 2.29% and 1.40% higher than the 97.56% of [21] and the 98.45% of [22], respectively. The average accuracy of categories 2, 3, 4, and 5 is also above 99%.

This comparison result is about 1% higher than [21] and [22], respectively.

5 Conclusion

Efficient Korean text classification algorithm based on optimized attention-based LSTM model is designed, implemented and validated in this study. The main points of this study are as follows: 1. A LSTM model combining MSCNN and attention mechanism is proposed. This innovative model can effectively capture the multi-scale features of Korean text and enhance the classification ability of the model. 2. The RMSprop optimizer significantly increases the training efficiency of the model. 3. To quantitatively confirm the model's effectiveness, a thorough experimental verification is performed on a publicly available Korean news dataset. Further optimization of the model structure to improve classification performance is one of the future research priorities. At the same time, the technique will be extended to larger datasets for the cross-validation and more languages.

References

1. Fanni, Salvatore Claudio, Maria Febi, Gayane Aghakhanyan, and Emanuele Neri. "Natural language processing." In Introduction to artificial intelligence, pp. 87-99. Cham: Springer International Publishing, 2023.
2. Min, Bonan, Hayley Ross, Elior Sulem, Amir Pouran Ben Veyseh, Thien Huu Nguyen, Oscar Sainz, Eneko Agirre, Ilana Heintz, and Dan Roth. "Recent advances in natural language processing via large pre-trained language models: A survey." ACM Computing Surveys 56, no. 2 (2023): 1-40.
3. Lauriola, Ivano, Alberto Lavelli, and Fabio Aiolli. "An introduction to deep learning in natural language processing: Models, techniques, and tools." Neurocomputing 470 (2022): 443-456.
4. Zha, Wenshu, Yuping Liu, Yujin Wan, Ruilan Luo, Daolun Li, Shan Yang, and Yanmei Xu. "Forecasting monthly gas field production based on the CNN-LSTM model." Energy 260 (2022): 124889.
5. Shahid, Farah, Aneela Zameer, and Muhammad Muneeb. "A novel genetic LSTM model for wind power forecast." Energy 223 (2021): 120069.
6. Wen, Xianyun, and Weibang Li. "Time series prediction based on LSTM-attention-LSTM model." IEEE access 11 (2023): 48322-48331.
7. Gupta, Ketan, Nasmin Jiwani, and Neda Afreen. "Blood pressure detection using CNN-LSTM model." In 2022 IEEE 11th International Conference on Communication Systems and Network Technologies (CSNT), pp. 262-366. IEEE, 2022.
8. Lin, Yu, Yan Yan, Jiali Xu, Ying Liao, and Feng Ma. "Forecasting stock index price using the CEEMDAN-LSTM model." The North American Journal of Economics and Finance 57 (2021): 101421.
9. Chandra, Rohitash, Ayush Jain, and Divyanshu Singh Chauhan. "Deep learning via LSTM models for COVID-19 infection forecasting in India." PloS one 17, no. 1 (2022): e0262708.

10. Tiwari, Shamik, Anurag Jain, Varun Sapra, Deepika Koundal, Fayadh Alenezi, Kemal Polat, Adi Alhudhaif, and Majid Nour. "A smart decision support system to diagnose arrhythymia using ensembled ConvNet and ConvNet-LSTM model." Expert Systems with Applications 213 (2023): 118933.
11. Gao, Xi, and Weide Li. "A graph-based LSTM model for PM2. 5 forecasting." Atmospheric Pollution Research 12, no. 9 (2021): 101150.
12. He, Yingying, Likai Zhang, Zengshun Chen, and Cruz Y. Li. "A framework of structural damage detection for civil structures using a combined multi-scale convolutional neural network and echo state network." Engineering with Computers 39, no. 3 (2023): 1771-1789.
13. Han, Qi, Xin Qian, Hongxiang Xu, Kepeng Wu, Lun Meng, Zicheng Qiu, Tengfei Weng, Baoping Zhou, and Xianqiang Gao. "DM-CNN: Dynamic Multi-scale Convolutional Neural Network with uncertainty quantification for medical image classification." Computers in biology and medicine 168 (2024): 107758.
14. Wei, Dennis, Haoze Wu, Min Wu, Pin-Yu Chen, Clark Barrett, and Eitan Farchi. "Convex bounds on the softmax function with applications to robustness verification." In International Conference on Artificial Intelligence and Statistics, pp. 6853-6878. PMLR, 2023.
15. Naseer, Aysha, and Ahmad Jalal. "Multimodal objects categorization by fusing GMM and multi-layer perceptron." In 2024 5th International Conference on Advancements in Computational Sciences (ICACS), pp. 1-7. IEEE, 2024.
16. Abd-elaziem, Ayman H., and Tamer HM Soliman. "A multi-layer perceptron (mlp) neural networks for stellar classification: A review of methods and results." International Journal of Advances in Applied Computational Intelligence 3, no. 10.54216 (2023).
17. Yue, Xiaochen, and Qicheng Liu. "Improved FunkSVD algorithm based on RMSProp." Journal of Circuits, Systems and Computers 31, no. 08 (2022): 2250139.
18. Elshamy, Reham, Osama Abu-Elnasr, Mohamed Elhoseny, and Samir Elmougy. "Improving the efficiency of RMSProp optimizer by utilizing Nestrove in deep learning." Scientific reports 13, no. 1 (2023): 8814.
19. Attia, Amit, and Tomer Koren. "SGD with AdaGrad stepsizes: Full adaptivity with high probability to unknown parameters, unbounded gradients and affine variance." In International Conference on Machine Learning, pp. 1147-1171. PMLR, 2023.
20. Wang, Bohan, Huishuai Zhang, Zhiming Ma, and Wei Chen. "Convergence of adagrad for non-convex objectives: Simple proofs and relaxed assumptions." In The Thirty Sixth Annual Conference on Learning Theory, pp. 161-190. PMLR, 2023.
21. Daneshfar, Fatemeh, and Mohammad Javad Aghajani. "Enhanced text classification through an improved discrete laying chicken algorithm." Expert Systems 41, no. 8 (2024): e13553.
22. Gao, Erdi, Haowei Yang, Dan Sun, Haohao Xia, Yuhan Ma, and Yuanjing Zhu. "Text classification optimization algorithm based on graph neural network." In 2024 IEEE 6th International Conference on Power, Intelligent Computing and Systems (ICPICS), pp. 814-822. IEEE, 2024.

Anomaly Detection in High-Frequency Trading Data: A GNN-TCN Hybrid Approach

*Xing Zhiyi[1]
[1]City Institute, Dalian University of Technology, Dalian, China, 116600
[1*]hkhlysz_1234@163.com

Abstract. Since high-frequency trading data has the characteristics of large data volume, high frequency, and high noise, traditional anomaly detection methods are relatively simple and not intelligent enough. Therefore, this study proposes a high-frequency trading data anomaly detection framework based on a hybrid model of graph neural network (GNN) and temporal convolutional network (TCN). From the core level of algorithm design, this study designed a novel GNN architecture for preliminary anomaly detection. At the same time, the TCN model was introduced to further optimize the extraction of time series features. Specifically, the designed GNN captures the complex relationships in transaction data by constructing a graph structure based on time series similarity. At the same time, the TCN is fused with dilated convolution, which expands receptive field through multiple layers of dilated convolution, thereby enhancing the model's sensitivity to time series features. The experimental part selected high-frequency trading data from China's A-share market and selected 15 commonly used technical analysis indicators at the parameter level. Experimental results show that compared with the single GNN model, the proposed GNN-TCN hybrid model significantly improves the accuracy of anomaly detection. The model involved can more effectively identify anomalies in high-frequency trading data.

Keywords: Anomaly Detection, High-Frequency Trading, Graph Neural Network (GNN), Temporal Convolutional Network (TCN)

1 Introduction

Before the 1990s, the research on financial time series was limited by the technical foundation and was conducted on monthly, weekly, daily, or quarterly and annual data. At present, such data is usually labeled as low-frequency data. In recent years, with the development of the scientific and technological capabilities, the capabilities of computers and communication technologies have increased rapidly, and the cost of data recording and storage has been greatly reduced. Hence, this provides researchers with a basis for study on high-frequency data. In general,

high-frequency data [1]-[4] refers to sequence data with a sampling frequency of seconds, minutes or hours. Compared with low-frequency data, high-frequency trading data has a very large amount of data, very high frequency and density, and is also interfered by factors such as micro-structure noise. The variance of the data will change a lot in different time periods, which will result in a large amount of noise and jumps in the data. In the process of the volatility prediction of high-frequency trading data, denoising financial high-frequency trading data with efficient anomaly detection models is an important step and should be studied in depth. To begin with, the Figure 1 demonstrates a comparison of high-frequency trading data against low-frequency trading data.

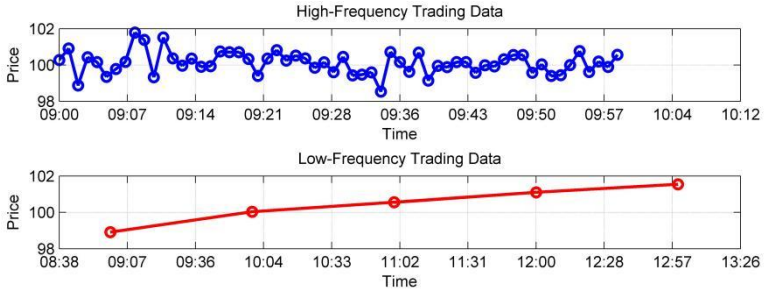

Fig. 1. The High-Frequency Trading Data vs. Low-Frequency Trading Data (The price is measured in U.S. dollars, the line chart's dots show trading activity, and the data is a sample taken from the public trading market.)

Based on deep learning model, this study proposes a hybrid anomaly detection algorithm in high-frequency trading data based on GNN-TCN. The highlights of the proposed methodology are:

Highlights 1: Design and optimize a new GNN architecture for the preliminary data anomaly detection.

Highlights 2: Considering the timing characteristics of high-frequency trading, the TCN model is introduced to optimize the anomaly detection results.

Highlights 3: Perform anomaly detection on the specific high-frequency stock trading data and design a complete experimental verification framework.

2 Review of Anomaly Detection Methodologies

Related anomaly detection algorithms have flourished in recent years. This section summarizes and analyzes the representative algorithms and introduces the typical methods in Table 1.

Table 1. The State-of-the-art Anomaly Detection Methodologies

Methodology Designer and Reference Number	***Details and Innovation***

Zhang [5]	This study proposed RealNet architecture. This is a feature selection network that combines real synthetic anomalies. The innovation of this architecture is introduction of SDAS technology, which can generate samples with different anomaly strengths. At the same time, RealNet uses the deep parsing AFS method to select feature subsets with high discrimination. Finally, the residual features are adaptively selected through the RRS strategy. This combination of operations makes the anomaly detection rate higher than that of traditional algorithms.
Huang [6]	This study proposed a medical image anomaly detection algorithm based on a visual language model. The algorithm designs a multi-level adaptation framework. This architecture transforms the pre-trained CLIP model into an anomaly detection model suitable for the medical images. Experimental results confirm that the algorithm can achieve good generalization ability in zero-shot and few-shot scenarios.
Liu and Paparrizos [7]	This study proposed a systematic bench-marking method for time series anomaly detection. The method is named TSB-AD. The TSB-AD introduces 1070 high-quality time series data and re-examines the effectiveness of existing anomaly detection methods.
Jeffrey et al. [8]	This study proposed a hybrid detection model that combines signature detection and behavior analysis. This model is used for the anomaly detection in industrial control systems. This framework combines traditional intrusion detection systems in IT networks (and OT network anomaly detection models based on the machine learning for comprehensive modeling. World results verify that this method can detect known threats and unknown anomalies more accurately.
Zavrtanik et al. [9]	This study proposed a simulation generation tool for 3D anomaly detection. The tool proposes a new 3D anomaly detection method by simulating anomalies that meet the characteristics of industrial depth data. The method performs well on the MVTec3D data-set.
Liang et al. [10]	This study proposed an unsupervised maritime anomaly detection algorithm based on special data. The algorithm maps the ship trajectory into a two-dimensional image and uses WGAN-GP for training. The advantage of this method is that it does not require manual annotation, which greatly improves maritime situational awareness.
Fu et al. [11]	This study proposed an unsupervised anomaly detection algorithm based on dense projection. The algorithm uses a deep neural network to learn the local density representation of normal data for structural optimization. At the same time, the abnormality of the test data is calculated by iterative weighting.
Zhu et al. [12]	This study proposed an anomaly heterogeneity learning method. The method is used for open set supervised anomaly detection. Experimental results show that by simulating the different anomaly distributions and using them to learn a unified anomaly model, it is able to effectively identify unseen anomalies in new domains.

3 The GNN-TCN Hybrid Algorithm for Anomaly Detection

3.1 Novel GNN Architecture for Preliminary Anomaly Detection

In traditional GNN, scholars describe two types of node anomalies based on the global position and topological network structure of the graph model, which are called global anomalies and local anomalies. In the high-frequency data trading scenarios, topological networks usually refer to traders. Theoretically, GNN is a neural network model for processing graph data. GNN mainly aims at information aggregation and information update after the aggregation. Given a directed graph [13]-[14] represented as:

$$Graph = (V, E) \tag{1}$$

Where the V and E represent the node set and edge set, respectively. The directed edge between node i and node j is denoted by $edge_{i,j}$, the derived node information aggregation formula is defined as follows:

$$c^{l}(v_i) = AGG^{l}\left(\left\{h_j^{l-1}, \forall v_j \in \vartheta(v_i)\right\}\right) \tag{2}$$

Where the AGG^{l} is the aggregation functions, usually including operations such as pooling, averaging, or concatenation. The $\vartheta(v_i)$ is the set of neighbor nodes of node v_i. Then, the GNN is constructed by updating the node information. This update process usually uses the weighted addition algorithm. In the Figure2, the sample for generation of GNN and the output is shown. In this sample scheme, there is a center node v_1, and the primary edge A-1. The other 8 nodes (from node 2 to node 9) connect to v_1 with the information aggregation formula as equation 2. Then, the output of this GNN is $v_1^{'}$.

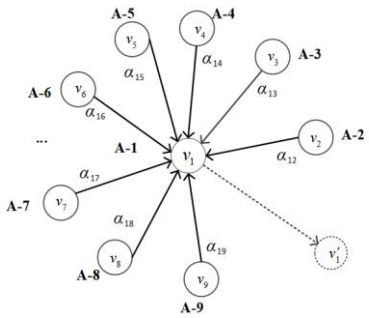

Fig. 2. The Generation of GNN and Output (output node is $v_1^{'}$)

In high-frequency trading scenarios, there is a large amount of graph structure data, and GNN is highly sensitive to these explicit graph structures. The learning of GNN is highly dependent on the input graph structure. Multivariate time series data contains multiple indicator parameters, and it is necessary to know the relationship between these parameters and build a graph structure. How to learn the relationship between each node and form a suitable graph structure is very important for the overall learning of the model. This study uses heuristic learning to construct anomaly detection GNN. This model constructs a graph by similarity.

This method constructs a graph by connecting nodes with similar attributes. A core example is to construct an adjacency matrix based on the cosine similarity between time series as:

$$Adj_{i,j} = \frac{x_i^T x_j}{\|x_i\|\|x_j\|} \tag{3}$$

Where the $\|\cdot\|$ is the Euclidean norm, and based on the adjacency matrix, time series model for the high frequency trading can be defined. Then, there are three definitions:

Definition 1: The anomaly prediction model uses single-step prediction to predict the value of time step t using t-1. The model input is defined as follows:

$$X = \left\{x^{t-w}, x^{t-w+1}, x^{t-w+2}, .., x^{t-1}\right\} \in \Re^{M \times W} \tag{4}$$

Where the M is the data dimension, such as the category of the high-frequency trading, and W is the size of the sliding window.

Definition 2: The definition of the time series sliding window is as follows, where $X_{t-W:t}$ represents the observation data from t-W to time t:

$$X_{t-W}, X_{t-W+1}, ..., X_t, X_{t-W:t} \in \Re^{M \times (W+1)} \tag{5}$$

Where w represents the length of the sliding window timestamp.

Definition 3: The definition of anomaly determination is as $E = \Omega(X_i)$ where Ω is used to determine the anomaly score and e represents the score.

Subsequently, GNN can be used to predict the abnormality of high-frequency trading output. The specific framework is shown in Figure 3.

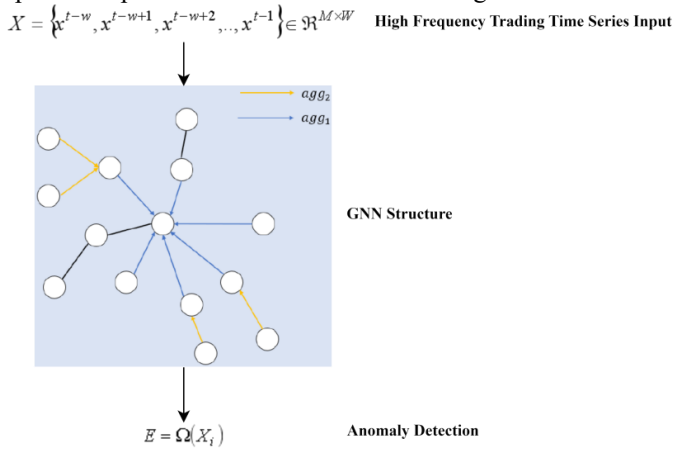

Fig. 3. The Core Framework of the GNN based Anomaly Detection

3.2 The TCN-GNN for Time Series Optimization

Although the preliminary anomaly detection algorithm based on GNN proposed in the previous section can detect anomalies more accurately, since high-frequency

trading data often has the time series [15]-[16] characteristics, it is necessary to combine TCN for model optimization. TCN uses multi-layer one-dimensional convolution to extract features in the time dimension. TCN combines the design of hollow causal convolution with the structure of multi-layer network, so that the receptive field can grow exponentially with the number of network layers.

When TCN is combined with the GNN, dilated convolution [17]-[18] is an important link and can assist the model sensitive to time series issues. Dilated convolution is also known as expanded convolution or dilated convolution, is achieved by introducing gaps in the convolution kernel, so that the convolution kernel can skip some inputs and cover a larger receptive field with the same number of parameters. The dilation coefficient, which represents the variation in the positions of neighboring components in a convolution kernel, is the primary parameter of the dilated convolution layer. A hole appears in the convolution kernel when the dilation coefficient is greater than 1. A conventional convolution layer has a dilation coefficient of 1, meaning that the convolution kernel element is next to the previous element. The total receptive field of the model can expand exponentially with the number of layers by using multiple layers of dilated convolution and increasing the dilation coefficient of each layer exponentially with the number of layers. This allows the model to fully capture a given range of the original inputs without repetition or omission. In the Figure 4, the integration of the TCN and GNN methodology is shown.

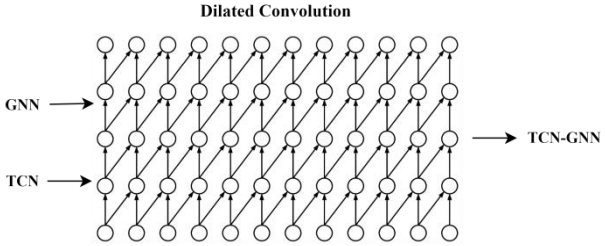

Fig. 4. The Integration of TCN and GNN

4 The Experiment and Discussion

4.1 The Experimental Data and Test Subjects

The experimental data of this study is mainly selected from high-frequency stock trading data. When selecting high-frequency trading technical analysis indicators, due to the characteristics of the high-frequency data such as the high fluctuation frequency and many abnormal values, when calculating high-frequency technical analysis indicators, there will be problems such as amplifying the characteristics of technical analysis indicators. Therefore, the experimental part starts from a comprehensive perspective and selects 15 commonly used technical analysis indicators from trend indicators, oscillation indicators, overbought and oversold indicators, energy indicators and momentum indicators. These indicators can be

used as input into the TCN-GNN model to detect anomalies. In the Table 2, the experimental object indicators and calculation formula are shown.

Table 2. The Experimental Object Indicators and Calculation Formula

Object Indicator	***Formula (O: opening price; C: closing price; L: lowest price; H: highest price)***
RVI	CO = C-O;HL = H-L; V1 = (CO+2*CO of the previous day+2*CO of the previous two days+CO of the previous three days)/6; V2 = (HL+2*HL of the previous day +2*HL of the previous two days +HL of the previous three days)/6; S1 = SUM(V1,n); S2 = SUM(V2,n);RVI = S1/S2;
BIAS	MA(n) = Σ ci/n;BIAS(n) = (C-MA(n))/MA(n);
ForceIndex	ForceIndex = (C - previous day's C)*volume;
VR	VR(n) = SUM(trading volume on rising days, n)/SUM(trading volume on falling days, n);
DPO	DPO = C - MA(n) of the previous (n/2+1) days;
NVI	If the current day's trading volume is greater than the previous day's trading volume: NVI = previous day's NVI; If the previous day's trading volume is greater than the current day's trading volume: NVI = previous day's NVI*(1+(C - previous day's C)/ previous day's C;
ROC	AX = C - C of the previous N days; BX = C of the previous N days; ROC = AX/BX;
OBV	Rate = ((C – L) – (H – L))/(H – L);OBV = ΣRate;
PSY	If C > C of the previous day: PSY = n days of increase/n*100%
MTM	MTM(n) = C – C of the previous n days;
CMO	CMO= (Su – Sd)*100/(Su+Sd);
MACD	EMA(n) = EMA(n)*(n-1)/(n+1)+C*2/(n+1) of the previous day; DIF = EMA(q) - EMA(p); DEA = DEA*(t-1)/(t+1)+DIF*2/(t+1) of the previous day;
AMA	DMA(n) = n-day average - m-day average; AMA(n) = n-day DMA average;
TRIX	TRIX = (EMA(n) - previous day EMA(n))/EMA(n)*100;
VHF	VHF = (H(n) – L(n))/SUM(ABS(C - previous day's C),n);

For the specific trading time period, this experiment selects the Chinese A-share market and gives priority to high-frequency 15-minute data. The data time is from February 17, 2025 to February 28, 2025. The data types include date, time point, 15-minute trading opening price, highest price, lowest price, closing price, trading volume and transaction amount, with a total of 19,723 data items.

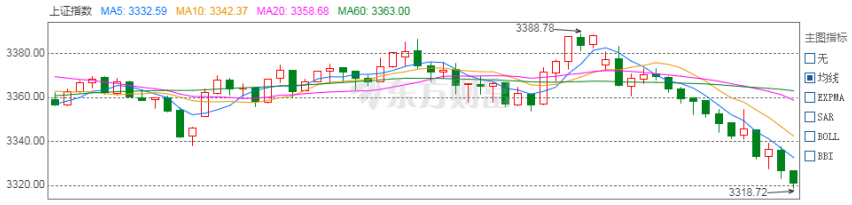

Fig. 5. The High-Frequency 15-minute Stock Price Data (Data source: https://quote.eastmoney.com/zs000001.html#)

In the Figure 5, taking the 15-minute data of the China A-share Shanghai Composite Index CSI 300 is used as an example to show the 15-minute closing price trend chart.

4.2 The Numerical Simulation Result and Discussion

When implementing the final high-frequency trading data anomaly detection, 15 indicator parameters are input into the designed TCN-GNN model for detection. At the detection level, standard data needs to be set. Fluctuations within the boundary estimated by the TCN-GNN of the standard data are considered normal, while data exceeding this fluctuation is considered abnormal. In the Figure 6, the standard data parameter set is shown.

Indicator	Mean	Median	Mode	Range	Variance	Standard Deviation
MACD	-0.0014	-0.0025	-7.8884	10.3447	0.0628	0.2505
AMA	4.6152	5.0342	2.5178	102.9086	4.3405	2.0834
TRIX	-0.007	-1.1067	-28.5657	31.9359	1.4537	0.3813
VHF	0.0599	0.0501	0	0.5	0.0021	0.0457
RVI	-0.0032	-0.0072	-0.3333	1.6271	0.0497	0.223
BIAS	-0.0772	-0.0772	-0.0778	0.4623	0.0001	0.0106
ForceIndex	0	0	0	0.0061	0	0.0001
VR	45.4005	1.0571	2.3136	167300	654535	2558.38
DPO	-2.9912	-3.0288	-3.9515	40.3245	3.2163	1.7934
NVI	0.9113	0.9457	0.8268	0.4017	0.0127	0.1129
ROC	-0.0005	-0.0006	0	0.5419	0.0004	0.0189
OBV	153579	155621	174351	321493	588297	7670.05
PSY	0.4881	0.5	0.5	1	0.02	0.1415
MTM	-0.0378	-0.03	0	39.51	1.6061	1.2673
CMO	-0.648	-0.8016	-2.3239	31.3251	4.3413	2.0836

Fig. 6. The Standard Data Parameter Set

Subsequently, anomaly detection is performed on the real input data, and the detected anomaly data is bolded in black. At the same time, as a comparison, the detection results of TCN-GNN and pure GNN are shown respectively. The Figure 7 and 8 show the results, respectively.

Indicator	Mean	Median	Mode	Range	Variance	Standard Deviation
MACD	-0.0014	-0.0025	**-10.4321**	10.3447	0.0628	0.2505
AMA	4.6152	**6.5214**	2.5178	102.9086	4.3405	2.0834
TRIX	-0.007	-1.1067	-28.5657	**40.7832**	1.4537	0.3813
VHF	0.0599	0.0501	0	0.5	0.0021	0.0457
RVI	-0.0032	-0.0072	-0.3333	1.6271	0.0497	0.223
BIAS	-0.0772	-0.0772	-0.0778	0.4623	0.0001	0.0106
ForceIndex	0	0	0	0.0061	0	**0.0003**
VR	45.4005	1.0571	2.3136	**180000**	654535	2558.38
DPO	-2.9912	-3.0288	-3.9515	40.3245	**5.7564**	1.7934
NVI	0.9113	0.9457	**1.0218**	0.4017	0.0127	0.1129
ROC	-0.0005	-0.0006	0	**0.7232**	0.0004	0.0189
OBV	153579	155621	174351	321493	**800000**	7670.05
PSY	0.4881	0.5	0.5	1	0.02	**0.2107**
MTM	-0.0378	-0.03	0	39.51	1.6061	**1.5673**
CMO	-0.648	-0.8016	-2.3239	**40.0001**	4.3413	2.0836

Fig. 7. The TCN-GNN based High-Frequency Trading Data Anomaly Detection Result

Indicator	Mean	Median	Mode	Range	Variance	Standard Deviation
MACD	-0.0014	-0.0025	**-10.4321**	10.3447	0.0628	0.2505
AMA	4.6152	**6.5214**	2.5178	102.9086	4.3405	2.0834
TRIX	-0.007	-1.1067	-28.5657	**40.7832**	1.4537	0.3813
VHF	0.0599	0.0501	0	0.5	0.0021	0.0457
RVI	-0.0032	-0.0072	-0.3333	1.6271	0.0497	0.223
BIAS	-0.0772	-0.0772	-0.0778	0.4623	0.0001	0.0106
ForceIndex	0	0	0	0.0061	0	0.0003
VR	45.4005	1.0571	2.3136	**180000**	654535	2558.38
DPO	-2.9912	-3.0288	-3.9515	40.3245	5.7564	1.7934
NVI	0.9113	0.9457	**1.0218**	0.4017	0.0127	0.1129
ROC	-0.0005	-0.0006	0	0.7232	0.0004	0.0189
OBV	153579	155621	174351	321493	800000	7670.05
PSY	0.4881	0.5	0.5	1	0.02	0.2107
MTM	-0.0378	-0.03	0	39.51	1.6061	1.5673
CMO	-0.648	-0.8016	-2.3239	**40.0001**	4.3413	2.0836

Fig. 8. The GNN based High-Frequency Trading Data Anomaly Detection Result

From the results, it can be seen that TCN-GNN has better results in detection accuracy and can detect more anomaly data compared with pure GNN method.

5 Conclusion and Prospect

This study proposes an anomaly detection algorithm for high-frequency trading data based on a hybrid model of the GNN and TCN. This algorithm solves the challenge of difficulty in detecting anomalies in high-frequency trading data due to high noise and large fluctuations. From a theoretical perspective, this study designed a novel GNN architecture that can effectively capture the complex graph structure relationships in transaction data. At the same time, the use of dilated convolution combined with the TCN's time series feature extraction capabilities further optimized the anomaly detection effect. Experimental results show that the GNN-TCN hybrid model performs well in the task of anomaly detection of high-frequency trading data and can more accurately identify anomalies in trading data. Future research can further explore the application of the model in other financial data and consider introducing more external factors to further enhance the predictive ability of the model.

References

1. Hussain, Syed Mujahid, Nisar Ahmad, and Sheraz Ahmed. "Applications of high-frequency data in finance: A bibliometric literature review." International Review of Financial Analysis 89 (2023): 102790.
2. Song, Yuping, Chunchun Cai, Dexiang Ma, and Chen Li. "Modelling and forecasting high-frequency data with jumps based on a hybrid nonparametric regression and LSTM model." Expert Systems with Applications 237 (2024): 121527.
3. Meher, Bharat Kumar, Manohar Singh, Ramona Birau, and Abhishek Anand.

"Forecasting stock prices of fintech companies of India using random forest with high-frequency data." Journal of Open Innovation: Technology, Market, and Complexity 10, no. 1 (2024): 100180.
4. Moreno-Pino, Fernando, and Stefan Zohren. "Deepvol: Volatility forecasting from high-frequency data with dilated causal convolutions." Quantitative Finance 24, no. 8 (2024): 1105-1127.
5. Zhang, Ximiao, Min Xu, and Xiuzhuang Zhou. "Realnet: A feature selection network with realistic synthetic anomaly for anomaly detection." In Proceedings of the IEEE/CVF conference on computer vision and pattern recognition, pp. 16699-16708. 2024.
6. Huang, Chaoqin, Aofan Jiang, Jinghao Feng, Ya Zhang, Xinchao Wang, and Yanfeng Wang. "Adapting visual-language models for generalizable anomaly detection in medical images." In Proceedings of the IEEE/CVF Conference on Computer Vision and Pattern Recognition, pp. 11375-11385. 2024.
7. Liu, Qinghua, and John Paparrizos. "The Elephant in the Room: Towards A Reliable Time-Series Anomaly Detection Benchmark." Advances in Neural Information Processing Systems 37 (2025): 108231-108261.
8. Jeffrey, Nicholas, Qing Tan, and José R. Villar. "A hybrid methodology for anomaly detection in Cyber‐Physical Systems." Neurocomputing 568 (2024): 127068.
9. Zavrtanik, Vitjan, Matej Kristan, and Danijel Skočaj. "Keep dræming: discriminative 3d anomaly detection through anomaly simulation." Pattern Recognition Letters 181 (2024): 113-119.
10. Liang, Maohan, Lingxuan Weng, Ruobin Gao, Yan Li, and Liang Du. "Unsupervised maritime anomaly detection for intelligent situational awareness using AIS data." Knowledge-Based Systems 284 (2024): 111313.
11. Fu, Dazhi, Zhao Zhang, and Jicong Fan. "Dense projection for anomaly detection." In Proceedings of the AAAI Conference on Artificial Intelligence, vol. 38, no. 8, pp. 8398-8408. 2024.
12. Zhu, Jiawen, Choubo Ding, Yu Tian, and Guansong Pang. "Anomaly heterogeneity learning for open-set supervised anomaly detection." In Proceedings of the IEEE/CVF conference on computer vision and pattern recognition, pp. 17616-17626. 2024.
13. Zhang, Xitong, Yixuan He, Nathan Brugnone, Michael Perlmutter, and Matthew Hirn. "Magnet: A neural network for directed graphs." Advances in neural information processing systems 34 (2021): 27003-27015.
14. Tong, Zekun, Yuxuan Liang, Henghui Ding, Yongxing Dai, Xinke Li, and Changhu Wang. "Directed graph contrastive learning." Advances in neural information processing systems 34 (2021): 19580-19593.
15. Weerakody, Philip B., Kok Wai Wong, Guanjin Wang, and Wendell Ela. "A review of irregular time series data handling with gated recurrent neural networks." Neurocomputing 441 (2021): 161-178.
16. Torres, José F., Dalil Hadjout, Abderrazak Sebaa, Francisco Martínez-Álvarez, and Alicia Troncoso. "Deep learning for time series forecasting: a survey." Big data 9, no. 1 (2021): 3-21.
17. Gao, Roland. "Rethinking dilated convolution for real-time semantic segmentation." In Proceedings of the IEEE/CVF conference on computer vision and pattern recognition, pp. 4675-4684. 2023.
18. Tang, Shunpu, Junjuan Xia, Lisheng Fan, Xianfu Lei, Wei Xu, and Arumugam Nallanathan. "Dilated convolution based CSI feedback compression for massive MIMO systems." IEEE Transactions on Vehicular Technology 71, no. 10 (2022): 11216-11221.

Smart border security: The role of AI in Modern Border Surveillance System

Simant Kamal Dutta[1], Rahul Mahala[2], Rajesh Singh[3], Anita Gehlot[4], Nagendar Yamsani[5]
[1] School of Applied & Life Sciences, Uttaranchal University, Dehradun, Uttarakhand, India.
[1]simantdutta@gmail.com
[2]Law College Dehradun, Uttaranchal University, Dehradun, Uttarakhand, India.
[2]rahulmahala98@gmail.com
[3]Uttaranchal Institute of Technology, Uttaranchal University, Dehradun, Uttarakhand, India.
[3]srajssssece@gmail.com
[4]Uttaranchal Institute of Technology, Uttaranchal University, Dehradun, Uttarakhand, India.
[4]dranitagehlot5@gmail.com
[5]School of Computer Science and Artificial Intelligence, SR University, Warangel, India
[5]nagendar.yamsani@gmail.com
*Rahul Mahala
[*]Law College Dehradun, Uttaranchal University, Dehradun, Uttarakhand, India.
[*]rahulmahala98@gmail.com

Abstract. Border security is a major concern due to terrorist activities, illegal migrants, and smuggling. Illegal migrants, including unauthorized travellers, tourists, and criminals, pose threats to borders. Smuggling involves illegal goods, including drugs and counterfeits. Detecting these threats is crucial for maintaining peace and harmony. This study evaluates the use of Artificial Intelligence (AI) in remote border surveillance, focusing on machine learning, natural language processing, and computer vision. It also discusses the limitations of AI in detecting border intrusion in surveillance systems. The study suggests that AI-based systems can be used for border security and surveillance in remote areas, removing human errors and safeguarding against intrusion, terrorists and smugglers. These systems, integrating machine learning, natural language processing, and computer vision, can detect unauthorized movements, illegal crossings, and terrorist activities. However, concerns like privacy, ethical use and algorithm bias need to be addressed. Regular algorithm improvements are necessary to ensure the effectiveness of these AI-based systems.

Keywords: Artificial Intelligence, Border Security, Border Surveillance

1 Introduction

Border security is main concern for all the countries now a days. The main reasons behind these concerns are terrorist activities, illegal migrants and smuggling which causes threat to the security of borders. Illegal migrants include unauthorized travelers, tourists, migrants or criminals. The smuggling includes the passing off goods from a border to another by illegal means, goods may be drugs, weapons, goods which are counterfeited etc. Main threat to the security of the borders is human intruding with

weapons, hence these must be detected on the border areas to maintain peace and harmony [1]. The human intrusion is a big challenge in front of many countries in the world. When it comes to traditional border patrolling, there has been seen that the different patrolling teams does surveillance on a specific border area for specific period. Human involvement is a very big challenge in securing the borders which are lengthy in areas or where the human survival is not possible [2]. Traditional border surveillance is based on humans in which different troops are assigned to protect different areas. These troops ensure the security of the borders on predetermined areas and intervals. The checkpoints are constructed on the roads to detect whether there is any enemy, drugs or any other illegal activity by the means of the transport. In this kind of system chances of human errors are high. Hence, multiple technologies which can help each other in patrolling and surveillance are required for these areas [3]. As the terrorist activities, drugs, illegal activities and illegal transportation is a big problem to deal with in border areas. Constant surveillance and monitoring are required all the time on the border areas. But this is done by using the traditional ways, it requires assets and human power in a large quantity. Hence, the demand of time is automated surveillance systems which can run on their own without any human power [4]. As the technology is advancing day by day, Industry 4.0 is milestone in securing the public domain. Artificial intelligence which is a part of Industry 4.0 is largely growing now a days in technical prospective. Them law enforcement agencies are using AI for data analysis and data interpretation, it is being also used for the criminal detection, traffic control and other legal processes [5]. Artificial intelligence is also being used for monitoring and surveillance of the areas. According to GSI (Global Surveillance Index) approx. 75 out of world's 176 countries are investing in AI for the surveillance purpose. Governments have already used AI into the surveillance cameras, smartphones and softwares of video management [6]. This study expresses the role of Artificial Intelligence in border surveillance of the remote areas. The role of machine learning, natural language processing and computer vision in border surveillance of remote areas is evaluated in this study by reviewing the existing articles. The authors have reviewed the limitations of using artificial intelligence in surveillance system for detecting border intrusion.

2. Methodology

The methodology for this review article involved an extensive review of 109 papers sourced from IEEE, Elsevier, MDPI, Springer, Wiley and others. These papers were carefully selected based on their credibility, relevance and alignment with the article's focus. After a thorough evaluation, 18 articles were selected and incorporated to ensure a comprehensive analysis of the topic. The selected papers provide robust insights, contributing significantly to the findings and discussions presented in the article.

3. Overview of Artificial Intelligence in Border Surveillance

"Artificial Intelligence" was first coined at Dartmouth University in 1956. Development of AI has made benefits to mankind in economical ways and all other aspects of life too. The general term for science of artificial intelligence is AI.

Computers are being used by AI to emulate human behaviors and teaches the computers to learn the behavior of humans like decision-making, judgements etc. Artificial intelligence is collection of philosophy, biology, psychology, logic, computer science and many other subjects and it has gained significant results in processing of image, recognition of speech, NLP, automatic theorem proving and intelligent robots as shown in figure 1 [7]. Machine learning, Natural language processing and computer vision are the main emerging parts of AI now a days. AI has a deep impact on our day-to-day life. Different kind of artificial intelligence systems are being largely used in different kind of applications of great importance in human lives like medical diagnosis, drug discovery, self-driving cars, traffic management, national securities, defense, fraud detection, cyber security, autonomous weapon systems, aerospace, aviation etc. which is taking on the way to an algorithmic society [8]. When it comes to the defense and national security, borders have great importance in national security and defense for a nation. Securing these borders is an intricate job which includes crossover associations, consideration of advance technologies and efficient professional sets. Although, here are many factors which are affecting the deployment of such systems on borders.

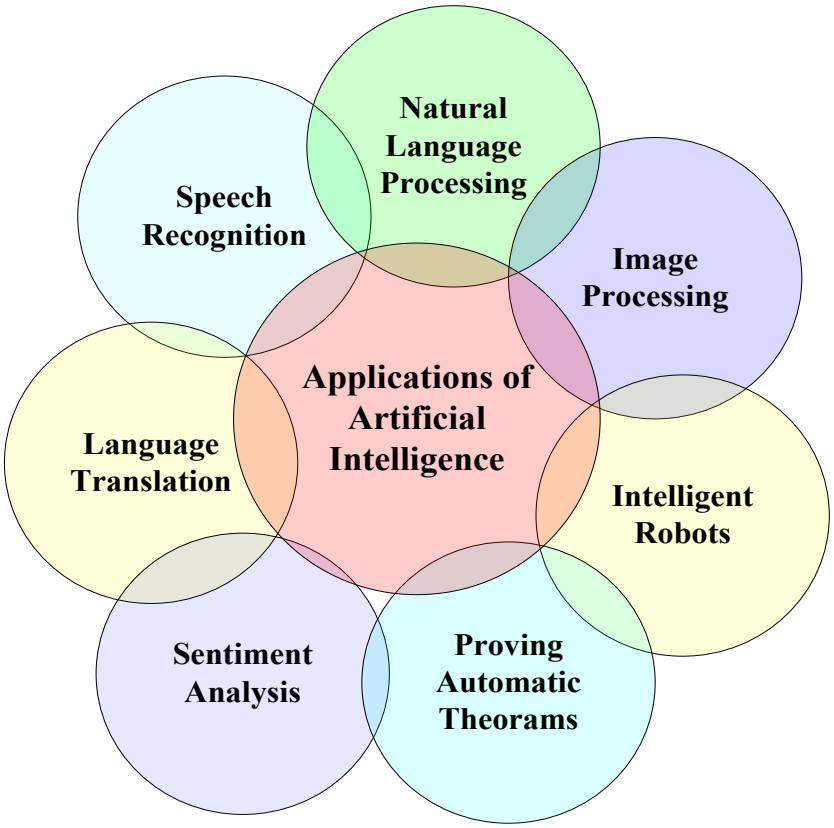

Fig. 1 Applications of Artificial Intelligence

The governments need such effective systems which can secure borders and also ensures low costing in doing so. Training the guards with equipment is costly for border security and surveillance [9]. Artificial intelligence has great potential to help in defense applications, it can provide help to the defense forces in all possible conditions of warfare like on lands, water or in air. Artificial intelligence finds its defense applications in autonomous vehicles, autonomous drones, cybersecurity, cyber warfare, intelligence, surveillance, reconnaissance, combat support, decision support, training, simulation and many other fields as shown in fig. 2 [10]. The border existing surveillance systems are mainly using different-2 structures and hence are not interlinked with each other to share the information to each other and also with security agencies. There are many border areas where human survival is not possible and hence such systems are which should operate autonomously and can share the information independently to all other systems and security agencies so that they can ensure the security of borders from intrusions and other security threats like smuggling and terrorist activities [11].

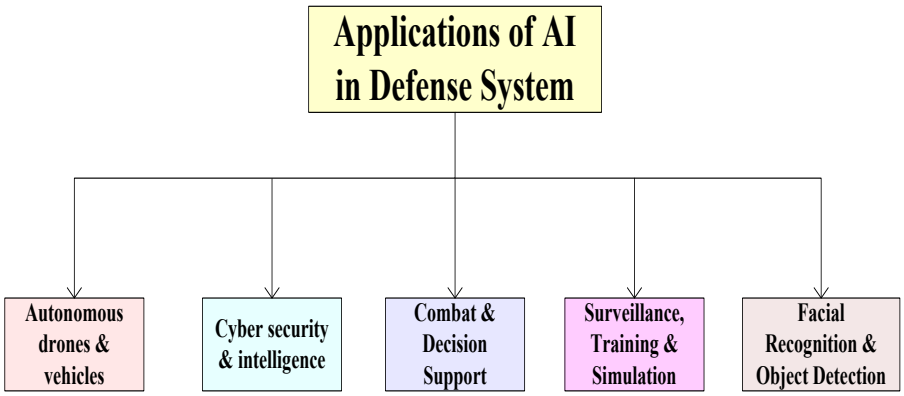

Fig. 2 AI applications in defense system

4. Machine Learning and Natural Language Processing in Border Surveillance of Remote area

While talking about AI machine learning and natural language processing are fastest growing subsets of AI. Machine learning is statical techniques collection which is used for building the mathematical tools such that it can draw judgements out of the sample data. There are mainly three kinds of machine learnings i.e. supervised, unsupervised and reinforced learning which can be used by the person based on his requirements. Supervised learning is used when the sample data is labeled, unsupervised is used when there is data which is not labeled and reinforced learning is used when the result learned heads towards an action which changes the environment [12]. Natural language

processing is used to make the human and computer conversation easier. Human language meaning and syntax is learnt by the machine so that it can give output to the users. Natural process language makes the computer system such that they can provide outcomes in natural or language understandable by human. This is important because it takes inputs as image, speech, text and manipulates or process them as per the algorithms provided to it, then gives the outcome as audio or text as per the requirement [13]. There are different kinds of algorithms used in NLP such as sorting algorithms, search algorithms, graph algorithms, regression algorithms, link analysis algorithms and many more [14].

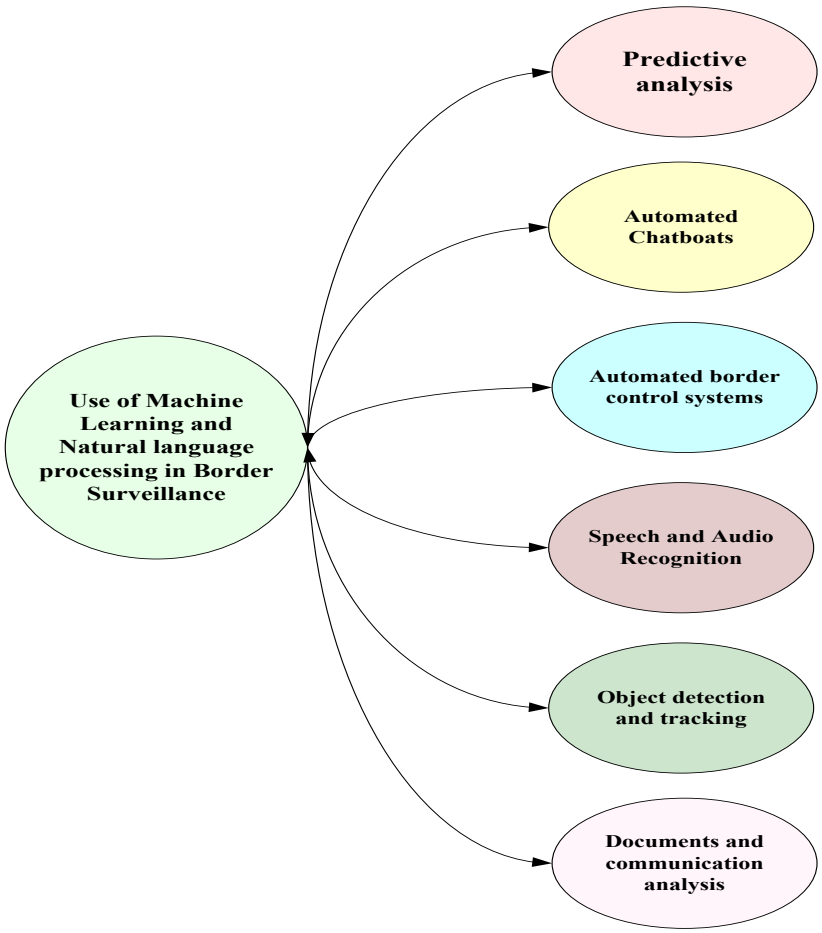

Fig. 3 Uses of ML and NLP in border surveillance of remote areas

M.S. Kabir and others [15] in their paper has introduced the limitations of using machine learning and natural language processing in border security. Some uses are also shown in figure 3 of ML and NLP in border security. They used machine learning systems which includes XGboost and Random Forest to build strong predictive

analytics system. They created profiles of the travelers by data analysis from the data provided by them in history. They trained their system to assess the risk associated with each traveler and this approached to a better border control of that area. They also deployed chat bots which uses the natural language processing. Hence, better assistance to the travelers about visa and assistance to their problems were provided by those chatbots. This not only streamlined the process but also changed the traveler experience in good way by providing them assistance guidance and support.

5. Border surveillance of remote areas using computer vision

Advancement in artificial intelligence last few years has emerged computer vision as a subset of artificial intelligence. Computer vision helps the computer to obtain and analyze the information from the visual data or the inputs. Hence, this made computer vision to be useful for the subjects like border security, border surveillance, maritime security, terrorism etc. which causes threat to the integrity of the nations. There are certain reasons behind these border intrusions like terrorism, smuggling etc. [16] The computer vision methods now a days are applicable to be used in all kind of drones.

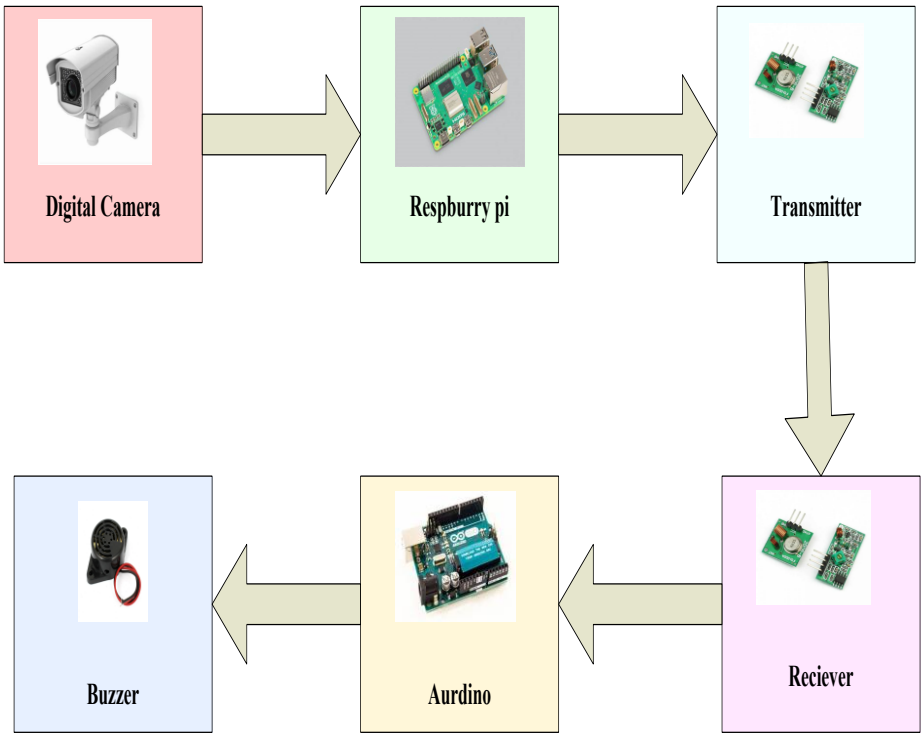

Fig. 4 Working of border surveillance system using Computer Vision

By applying these applications of the computer vision in these drones, these drones be

able to use not only for picture clicking or film making but also be used for more complex processes. Computer vision focuses upon the participation of the environment as well as the basic applications of navigations, surveillance, machine inspection and 3D model building [17]. A border surveillance system by using computer vision was introduced by D. Kumar and others [18] in their paper, in which digital camera, Respburry pi, transmitter, Aurdino and buzzer were used to make a border surveillance system as per shown in figure 4. Digital camera takes the pictures of the live movement and sends it Respburry pi, in which computer vision is used to detect the positive and negative among the objects and faces by using python coding. Negative detection is sent to transmitter by pi module and transmitter transmits it to the receiver. Receiver passes the negative signal received to the Aurdino. Aurdino sends signal to the buzzer and buzzer makes an alert as per the programmed language or sound. Hence, the security personals get alerted about the possible threats which the negative object or the face can make and the border hence saved from intrusions or the illegal activities in a fast manner. This system can be used to enhance the border security and surveillance in remote areas where the human survival is not possible.

6. Recommendations

Border surveillance is a serious issue now a days to look upon. Border areas are prone of terrorist activities, smuggling and other illegal activities and hence requires all time surveillance to ensure the security of nation. It is impossible to do surveillance of the areas by the traditional means where human survival is not possible. There are huge areas which we can say are remote areas where the survival of the human is not possible like some of the hilly areas which are always covered with snow and oxygen level of these areas is very low due to the reasons of height and also there is no connectivity of roads or any other infrastructure and hence the basic amenities to live can't be provided to the soldiers guarding these kinds of areas. Hence, border surveillance and security of these areas is difficult by the means of the man power. Also, where there are borders present which are lengthy in area, the surveillance of these areas in traditional way is done by different groups of soldiers at different-different times. The probability of human error is very high in doing surveillance in this way for the lengthy areas as the chances of human error are also very high in these areas. Hence, technological intervention in these areas can provide a great relief to the soldiers and also can better safeguard these areas. AI is emerging field of technology in many other subjects such as legal, social science, security etc. It can help the forces to do surveillance of the areas where the human survival is not possible or in the lengthy border areas or also in the plane areas by providing assistance in security and surveillance. Below are some recommendations which can be used to safeguard the border areas-

- To enhance the ability of the AI based smart surveillance systems, the use of multiple equipment and technologies should be ascertained such that they can ensure the security and surveillance of the border. For example, different kind of sensors, radars, thermal cameras, motion detectors etc.

should be used to improve the detection accuracy of the AI based surveillance system for the borders.

- AI based surveillance system should be fitted with the advanced data fusion techniques so that it can take data from all the devices at once. This can improve the decision making of the system by providing the vast view of the targeted area whose surveillance is done.

- While doing facial recognition or license plate recognition by the means of AI system deployed on the border areas should be done ensuring that they will not harm the individual rights of anyone. These should be made such they don't make any harm to the personal rights of the persons i.e. the privacy should be maintained.

- AI algorithms of AI based surveillance system should be trained in a continuous manner such that they can know the new harms or threats as per the need of the time.AI based system for border surveillance should perform real-time analytics and should have predictive capabilities such that it can identify the threat timely and can help the security personals and agencies by giving potential threats of security to them.

- AI powered border fence and perimeter should be used which can ensure the motion detection, vibration detection on the surveillance areas in which these systems are working.

7. Conclusion

Security and surveillance are crucial concerns in border areas worldwide, particularly in areas where human intervention is impossible or inaccessible. In this context, AI-based systems can be used for border security and surveillance in remote or normal plane areas to remove human errors and protect against intrusion, terrorists, and smugglers. These systems are cost-efficient, less time-consuming, and eliminate human errors. They integrate machine learning, natural language processing, and computer vision to detect unusual activities and alert border agencies and other security agencies. The advantages of AI-based surveillance systems include unauthorized movement tracking, autonomous detection of threats like illegal border crossings and terrorist activities, and extended accuracy in harsh and isolated environments where human survival is not possible. However, there are also challenges such as privacy concerns, ethical use of AI, and algorithm bias. Privacy rights of individuals are a major concern, and regular improvement in algorithms is necessary to address these concerns. Despite these challenges, AI-based surveillance systems can effectively reduce threats in border areas, but concerns such as privacy and algorithm bias need to be considered. Regular improvements in algorithms are necessary to ensure the effectiveness of these systems in remote areas. AI in border surveillance is revolutionizing national security by

providing real-time threat detection and predictive monitoring. The system enhances efficiency by automating the analysis of large datasets gathered from various sources such as drones, sensors, and cameras. AI-driven systems expedite decision-making by reducing human error and response time. Overall, AI-based systems offer potential solutions for border security and surveillance in remote areas, but they must be carefully considered and improved to ensure the safety and security of all involved.

References

1. Goyal, A., Anandamurthy, S. B., Dash, P., Acharya, S., Bathla, D., Hicks, D., ... & Ranjan, P. (2020). Automatic border surveillance using machine learning in remote video surveillance systems. In Emerging Trends in Electrical, Communications, and Information Technologies: Proceedings of ICECIT-2018 (pp. 751-760). Springer Singapore.
2. Arjun, D., Indukala, P. K., & Menon, K. U. (2017, April). Border surveillance and intruder detection using wireless sensor networks: A brief survey. In 2017 International Conference on Communication and Signal Processing (ICCSP) (pp. 1125-1130). IEEE.
3. Sun, Z., Wang, P., Vuran, M. C., Al-Rodhaan, M. A., Al-Dhelaan, A. M., & Akyildiz, I. F. (2011). BorderSense: Border patrol through advanced wireless sensor networks. Ad Hoc Networks, 9(3), 468-477.
4. Bhadwal, N., Madaan, V., Agrawal, P., Shukla, A., & Kakran, A. (2019, April). Smart border surveillance system using wireless sensor network and computer vision. In 2019 international conference on Automation, Computational and Technology Management (ICACTM) (pp. 183-190). IEEE.
5. Raaijmakers, S. (2019). Artificial intelligence for law enforcement: challenges and opportunities. IEEE security & privacy, 17(5), 74-77.
6. Saheb, T. (2023). Ethically contentious aspects of artificial intelligence surveillance: a social science perspective. AI and Ethics, 3(2), 369-379.
7. Zhang, C., & Lu, Y. (2021). Study on artificial intelligence: The state of the art and future prospects. Journal of Industrial Information Integration, 23, 100224.
8. Kaur, D., Uslu, S., Rittichier, K. J., & Durresi, A. (2022). Trustworthy artificial intelligence: a review. ACM computing surveys (CSUR), 55(2), 1-38.
9. Hammoudeh, M., Al-Fayez, F., Lloyd, H., Newman, R., Adebisi, B., Bounceur, A., & Abuarqoub, A. (2017). A wireless sensor network border monitoring system: Deployment issues and routing protocols. IEEE Sensors Journal, 17(8), 2572-2582.
10. Bistron, M., & Piotrowski, Z. (2021). Artificial intelligence applications in military systems and their influence on sense of security of citizens. Electronics, 10(7), 871.
11. Essendorfer, B., Monari, E., & Wanning, H. (2009, March). An integrated system for border surveillance. In 2009 Fourth International Conference on Systems (pp. 96-101). IEEE.
12. Ribeiro, M., Grolinger, K., & Capretz, M. A. (2015, December). Mlaas: Machine learning as a service. In 2015 IEEE 14th international conference on machine learning and applications (ICMLA) (pp. 896-902). IEEE
13. Fanni, S. C., Febi, M., Aghakhanyan, G., & Neri, E. (2023). Natural language processing. In Introduction to Artificial Intelligence (pp. 87-99). Cham: Springer International Publishing.
14. Wang, Y., & Zhang, C. (2020). Using the full-text content of academic articles to identify and evaluate algorithm entities in the domain of natural language processing. Journal of informetrics, 14(4), 101091.
15. Kabir, M. S., Sumi, E. J., & Alam, M. N. Artificial Intelligence (AI) and Future Immigration and Border Control.
16. Ige, T., Kolade, A., & Kolade, O. (2022). Enhancing border security and countering

terrorism through computer vision: A field of artificial intelligence. In Proceedings of the Computational Methods in Systems and Software (pp. 656-666). Cham: Springer International Publishing.
17. Akbari, Y., Almaadeed, N., Al-Maadeed, S., & Elharrouss, O. (2021). Applications, databases and open computer vision research from drone videos and images: a survey. Artificial Intelligence Review, 54, 3887-3938.
18. Kumar, D., Aadarsh, S., & Kumar, H. (2020, March). Border surveillance system using computer vision. In 2020 6th international conference on advanced computing and communication systems (ICACCS) (pp. 623-628). IEEE.

Multi-Modal Data-Driven User Behavior Modeling and Personalized Advertisement Recommendation Algorithm

*Zhang Zheng[1], Xu Dongyan[2]
[1]Shandong Vocational University of Foreign Affairs Vocational University, Shandong, 264504, China
[2]Shandong Vocational University of Foreign Affairs, School of Information Engineering, Shandong, 264504, China
[1*]zhangpeiai365864@163.com;[2]15763181637@163.COM

Abstract. With the development of multi-modal analysis and intelligent recommendation systems, the trend of precise combination with Normal University is emerging. This study proposes a user behavior model construction method based on multi-modal data and a personalized advertising recommendation algorithm. From a theoretical perspective, first of all, although the user's Internet behavior is affected by uncertain factors, this study integrates discrete instance data to construct a multi-modal data processing framework including text analysis, visual reasoning and statistical models. On this basis, this study designed a personalized advertising recommendation algorithm. The algorithm averages and maximizes the interactive behavior of users during video playback. This modeling can be used to recommend advertising directions. Experimental results show that this method improves the personalized recommendation accuracy by 5.2% compared with traditional similar algorithms. In addition, the model accumulates the influencing factors of user behavior values through deep learning, improves the model's accuracy in distinguishing user intentions, and provides an algorithm optimization solution for the filtering mechanism.

Keywords: Multi-Modal Data, User Behavior Modeling, Personalized Advertisement, Recommendation Algorithm

1 Introduction

With the rapid development of the Internet, the Internet online advertising [1]-[2] industry is booming. In online advertising, advertising platforms sell exposure by signing a guaranteed delivery contract with advertisers. At the same time,

advertisers stipulate in the contract the target group with certain characteristics to which the advertisement needs to be delivered, as well as the total exposure requirements for the group. Object-level advertising delivery uses the image processing technology to extract key frames from short videos and detect them, and deliver advertisements based on the detection results. The key frame extraction methods include: 1) The method based on the shot boundary uses frame averaging to extract the key frames of each shot, or directly uses the first frame and the last frame as the key frames; 2) The method based on motion analysis extracts key frames only at the static points of the video.

The main challenges of the current studies are:

1.Users' access or search behaviors are significantly affected by various uncertain covariates (such as weather conditions, temperature, humidity, etc.).

2.Advertising strategies need to be determined before uncertain covariate information and exposure are realized. In the absence of accurate information, advertising platforms must make advertising strategies in advance.

To deal with these challenges, this study proposes the novel framework for multi-modal data-driven user behavior modeling and personalized advertisement recommendation algorithm. In the following Figure 1, the typical advertisement recommendation algorithm steps are summarized.

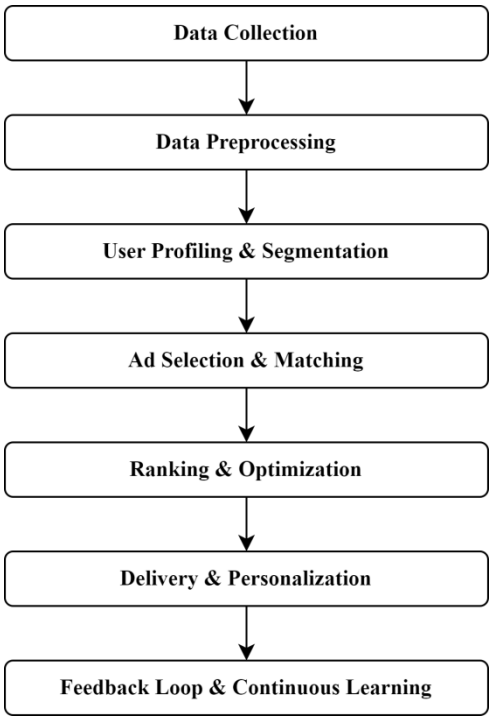

Fig. 1. The Typical Advertisement Recommendation Algorithm Steps

2 Review of Recommendation Algorithms

In the research of the recommendation systems, the latest related algorithms are analyzed and integrated in deep learning, fairness analysis, user simulation and network construction. Zhao et al. [3] proposed a stable advertising insertion framework based on deep reinforcement learning, which can balance the connection between recommended content and advertising revenue. This study designed a deep Q-network architecture that can dynamically decide whether to insert advertisements, select the optimal advertisements and their positions. This framework can help maximize revenue in the long run. Zhao et al. [4] developed a unified recommendation system library called RecBole. The library contains 73 recommendation models and 28 benchmark datasets. At the same time, it supports GPU accelerated execution and automatic parameter tuning. Melchiorre et al. [5] studied the gender fairness model in music recommendation algorithms. This study introduced the LFM-2b dataset to evaluate the performance differences of the various collaborative filtering algorithms in different gender user groups.

Zhang et al. [6] proposed Agent4Rec. This is a user simulator based on a large language model. The simulator explores the potential of generative agents in recommendation tasks by simulating user behavior. Li et al. [7] explored the fairness issue in recommendation systems from the user's perspective. The model divides users into active and inactive groups and finds that the existing system's recommendation quality for the active users is significantly higher than that for inactive users. Therefore, the study proposed a new reranking algorithm to alleviate this unfairness. Santos et al. [8] studied the general impact of link recommendation algorithms on polarization dynamics in online social networks. The study proposed that link recommendations based on structural similarity will inadvertently exacerbate opinion polarization, while connecting the nodes with dissimilar structures will help mitigate extreme views. Hui et al. [9] proposed a personalized recommendation system based on knowledge embedding and historical behavior, named the ReBKC. The system optimizes the system by integrating knowledge graph and the user behavior data. Experimental results significantly improve the accuracy of the recommendation algorithm. Zhao et al. [10] introduced RecBole 2.0, an extended recommendation system library. The database covers cutting-edge topics such as meta-learning, data enhancement, debiasing, fairness, and cross-domain recommendations. Pajkovic [11] analyzed the operating logic of the Netflix's recommendation system through reverse engineering. The study revealed the economic and cyclical logic of the algorithm in shaping the taste of film and television culture. Xiao et al. [12] proposed a general offline reinforcement learning framework. The framework is used to learn interactive recommendation strategies from log feedback. The study demonstrated that five distribution matching methods can significantly improve the overall recommendation performance without online exploration.

3 The Advertising Multimodality and Internet User Behavior

Analysis

The multimodal information [13]-[14] of advertisements is the basis of the user Internet behavior. From the perspective of dimensions, multimodality mainly includes the following aspects: language text analysis, visual image analysis, and the interaction between language modality and image modality. In the Table 1, the principles are summarized.

Table 1. The Principles of the Multimodal Information of Advertisements

Multimodal	***Principle***
Language text analysis	In terms of conceptual functions, empirical functions and logical functions are used to analyze what processes the language text elements in the advertisement belong to, what semantic relationships exist between the elements, how these processes and relationships are manifested, what they each mean, and what intentions they want to convey.
Visual image analysis	What kind of processes do the visual elements in the advertisement belong to? How are these processes manifested? What do they mean? What do they want to convey?
Interaction between language modality and image modality	From the perspective of semantic logical relationship, we can examine whether the image and text are in an "extension" relationship or a "projection" relationship. If they are an extension relationship, is it an elaboration, extension or enhancement? If they are a projection relationship, is it a verbal projection or a thought projection? How are these specifically manifested, what do they mean, and what intentions do they want to convey?

Internet users' interaction with multimodal advertising information is the basis of behavioral analysis. In this analysis process, the user intent modeling is crucial. Users' decision-making behaviors usually stem from the different decision intents, and different intents will position a series of corresponding products. Therefore, user intention is formally defined in the recommendation framework. In a recommendation system, the interaction data between users and items can be represented as a matrix $X \in R^{m \times n}$, where the m and n represent the number of users and items, respectively. Whether there is interaction between user u and item i can be defined as follows:

$$\begin{cases} x_{u,v} = 1, & \text{has interaction} \\ x_{u,v} = 0, & \text{no interaction} \end{cases} \tag{1}$$

Since user intentions under different topics are associated with different latent factors, it is necessary to model a decoupled user latent intention representation as $z_u = R^d$, Considering the diversity of intentions, the representation of the user potential intentions can also be expressed in a decoupled form, that is:

$$z_u = \left[z_u^1, z_u^2, z_u^3, \ldots, z_u^T \right] \tag{2}$$

Where the T is the number of topics, and all items in the same recommendation scenario share these T topics. $z_v^t \in R^{d/T}$ is the user's intention representation under the t-th topic.

4 The Personalized Advertisement Recommendation Algorithm

4.1 Multi-modal Context Modeling for Recommender Systems

Some traditional recommendation algorithms, such as the traditional collaborative filtering algorithms, model the user's rating vector as a non-time series model. The interaction between users and items is considered to have no context. The user's interest is only represented by an implicit feature vector in the modeling process, and the recommendation algorithm will calculate the similarity between the item and the implicit feature vector based on this implicit vector. In fact, the interaction between users and items has different meanings at different times. That is to say, for an interaction vector between a user and an item, different positions of the vector have different weights. At the same time, there are also deeper implicit features related to serialized information such as time. Serialized information can reflect the dynamic characteristics of user behavior and preferences. In terms of time dimension, serialized modeling is more practical than traditional vectorized modeling. In the study of serialization modeling in this section, the task of sequential recommendation or ad click-through rate prediction is abstracted as predicting the k+1th behavior based on the user's previous k behaviors. The behavior sequence obtained is the previous k behaviors. When the k-th behavior occurs, the k-th behavior has system context information at the time of occurrence, such as the page information of the user clicking the ad, the current page link, the specific display page details, etc. These are all commonly used processing methods for existing ad click-through rate prediction algorithms based on context information. In the Figure 2, the dynamic context information is shown.

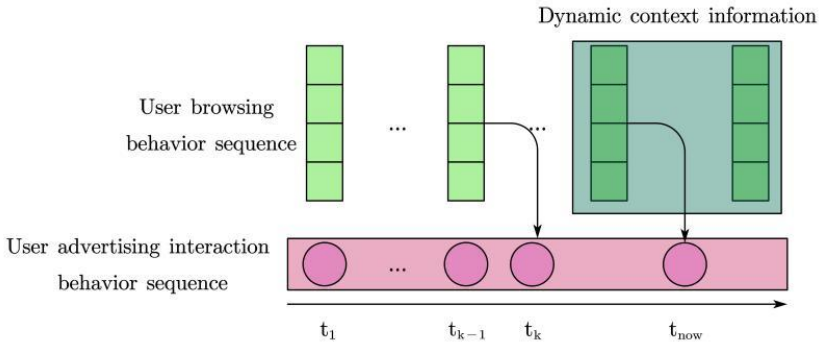

Fig. 2. The Dynamic Context Information Modelling

The context information involved in this section mainly includes two aspects:

1. **Static context**. Some existing studies on static context have attempted to input advertising content information and behavior content information as the context features into the model input.

2. **Dynamic context**. Dynamic context involves the problem of the context selection, because the user's browsing information is complex and rich. Compared with the interaction sequence between users and advertisements, the user's other browsing behavior records are complex and diverse.

4.2 The Personalized Advertisement Recommendation Algorithm

The personalized recommendation system builds a detailed user portrait by deeply mining and analyzing user data, and achieves accurate positioning of users. This precise positioning technology provides advertisers with more accurate audience targeting, greatly improving the effectiveness of advertising. The recommendation algorithm proposed in this model is based on transfer learning [15]-[16]. In order to predict the possibility of multiple behaviors with the same input information, a separate prediction layer is given to each behavior of click, add to cart, favorite, and purchase for learning. Let h_k be the prediction layer of the k-th behavior, then the probability of user u taking the k-th behavior on item v is estimated as:

$$\hat{R}_{(k)uv} = h_k^T \left(p_u \times q_v \right) \tag{3}$$

In order to capture the migration characteristics, we assume that the prediction of a certain behavior depends on the prediction of its predecessor. Inspired by the migration mechanism in knowledge representation, this model assumes that the relationship between two behaviors can also be described as a transformation in the representation space. Then the migration relationship between two different behaviors h_i and h_j can be expressed as:

$$trans_{h_i \to hj_i} = h_i M_{ij} + b_{ij} \tag{4}$$

Where the $M_{ij} \in R^{d \times d}$ is the migration matrix that projects h_i from the i-th behavior space to the j-th behavior space. The b_{ij} is the bias vector. The transfer learning process of the proposed is shown in the Figure 3.

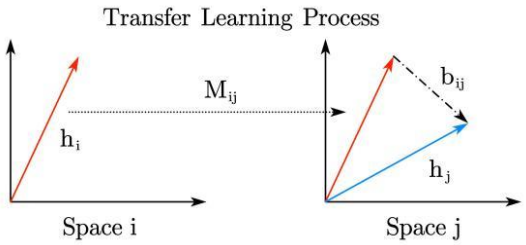

Fig. 3. The Transfer Learning Process of the Proposed Model

After determining the feature words of the page text and establishing the user interest model, the similarity between the two can be calculated. However, if the dimensions of the page feature vector and the user interest model are not the same, the similarity calculation cannot be performed. For this reason, it is necessary to choose the temperature of the two so that they have the same number of the dimensions. In practice, if a feature word in the user interest set does not exist in the page text, the weight value corresponding to the feature word is set to 0, and the feature word ranking is adjusted according to the weight. After a series of processing, the two correspond to each other in dimension. The similarity function is defined as formula 5.

$$s(U,P)=\frac{\sum_{i=1}^{n} W(F_i)\times w(i)}{\sqrt{\sum_{i=1}^{n} W(F_i)^2}\times\sqrt{\sum_{i=1}^{n} w(i)^2}} \tag{5}$$

A threshold q is set in advance. If the similarity s(U, P) < q, it means that the page cannot represent the user's interest point, and the feature word corresponding to the page text should be discarded. Then, by calculating the similarity value in a loop, the proposed model can stably obtain the advertising recommendation results efficiently.

5 The Experimental Verification

5.1 The Experimental Settings

This test object uses video ads as the main analysis mode. The system adjusts the ad weights recommended by the system based on the user's behavior when watching short videos. The specific setting process of the behavior level is as follows:

1) When the system does not push any ads while playing a video, but the user actively triggers the target detection operation to observe an object in the video, it has the highest level of weight;

2) When the video is playing, the user sees the ad and clicks the ad link, this process has the second highest weight;

3) When the video is playing, the user sees the ad push but does not perform any operation until the ad ends, this process has the third highest weight;

4) When the video is playing, the user sees the ad and clicks to close the ad, this process has the fourth highest weight.

At the same time, the recommendation system adjusts the weights according to the user's preferences and sets the user's interest threshold and disinterest threshold through repeated trials. Table 2 shows the weight adjustment process.

Table 2. The Advertisement User Preference Weight Setting

User Action	*Priority*	*Weight Adjustment*
Action 1)	1	20
Action 2)	2	10
Action 3)	3	0
Action 4)	4	-10
Others	5	-20

5.2 The Numerical Simulation Result and Discussion

Based on the above analysis and parameter settings, this test uses 100 short videos with a duration of 300 seconds to test the effectiveness of the recommendation algorithm proposed in the article. These 100 short videos include 25 different object categories, and the proposed algorithm can match these objects and advertising information in turn. According to different market scopes, this test studies the recommendation accuracy of the proposed algorithms [6], [7], [8]. The results are shown in the Table 3.

Table 2. The Comparative Test Results of Recommendation Accuracy for Videos of Different Lengths (%)

Video Length	*Proposed*	*[6]*	*[7]*	*[8]*
0~20	**97.32**	91.07	93.55	94.83
20~40	95.21	90.12	92.78	**95.41**
40~60	**96.87**	92.34	94.10	96.02
60~80	**98.42**	93.89	95.67	97.23
80~100	**97.15**	91.56	93.74	95.88
100~120	**94.73**	89.92	92.13	94.12
120~140	**95.68**	90.76	93.05	94.87
140~160	**96.54**	91.84	93.98	95.34
160~180	**97.89**	92.61	94.65	96.41
180~200	**96.23**	91.47	93.32	95.76
200~220	**95.12**	90.34	92.74	94.62
220~240	**94.65**	89.78	91.89	93.45
240~260	**96.02**	91.15	93.07	94.98
260~280	**97.33**	92.48	94.41	96.21
280~300	**98.11**	93.25	95.12	97.02

From the comparative experimental results, we can see that the four methods all show some fluctuations in videos of the different lengths. The overall accuracy is maintained above 90%. From the quantitative experimental results, the proposed method maintains a leading position in all time intervals, with the lowest accuracy of 94.65% (220-240s) and the highest accuracy of 98.42% (60-80s). This shows that the method has good adaptability to both short videos (0-20s) and long videos (280-300s), and performs best in the 60-80s time interval.

6 Conclusion

Multi-modal data-driven user behavior modeling and personalized advertisement recommendation algorithm is studied in this manuscript. This algorithm improves the accuracy of the advertising recommendation system and the user interaction experience by integrating multi-modal information such as text, vision and statistics. In order to deal with the uncertainty factors in user behavior, this study adopts an accumulation learning strategy. This strategy enables the model to adapt to the behavior patterns of different user groups, thereby improving the robustness and generalization ability of the algorithm. In addition, this paper also explores the key technologies of multi-modal information fusion. This operation improves the interpretability and accuracy of advertising recommendations through cross-modal data association analysis. Experimental results verify the effectiveness of this method in improving advertising delivery efficiency and optimizing user response rate. The contribution of this study is not only to improve the performance of the advertising recommendation system, but also to provide new ideas for the development of personalized advertising delivery technology in the future.

References

1. Wuisan, Dewi Surya, and Tessa Handra. "Maximizing online marketing strategy with digital advertising." Startupreneur Business Digital (SABDA Journal) 2, no. 1 (2023): 22-30.
2. Lim, Weng Marc, Sahil Gupta, Arun Aggarwal, Justin Paul, and Priyanka Sadhna. "How do digital natives perceive and react toward online advertising? Implications for SMEs." Journal of Strategic Marketing 32, no. 8 (2024): 1071-1105.
3. Zhao, Xiangyu, Changsheng Gu, Haoshenglun Zhang, Xiwang Yang, Xiaobing Liu, Jiliang Tang, and Hui Liu. "Dear: Deep reinforcement learning for online advertising impression in recommender systems." In Proceedings of the AAAI conference on artificial intelligence, vol. 35, no. 1, pp. 750-758. 2021.
4. Zhao, Wayne Xin, Shanlei Mu, Yupeng Hou, Zihan Lin, Yushuo Chen, Xingyu Pan, Kaiyuan Li et al. "Recbole: Towards a unified, comprehensive and efficient framework for recommendation algorithms." In proceedings of the 30th acm international conference on information & knowledge management, pp. 4653-4664. 2021.
5. Melchiorre, Alessandro B., Navid Rekabsaz, Emilia Parada-Cabaleiro, Stefan Brandl, Oleg Lesota, and Markus Schedl. "Investigating gender fairness of recommendation algorithms in the music domain." Information Processing & Management 58, no. 5 (2021): 102666.
6. Zhang, An, Yuxin Chen, Leheng Sheng, Xiang Wang, and Tat-Seng Chua. "On generative agents in recommendation." In Proceedings of the 47th international ACM SIGIR conference on research and development in Information Retrieval, pp. 1807-1817. 2024.
7. Li, Yunqi, Hanxiong Chen, Zuohui Fu, Yingqiang Ge, and Yongfeng Zhang. "User-oriented fairness in recommendation." In Proceedings of the web conference 2021, pp. 624-632. 2021.

8. Santos, Fernando P., Yphtach Lelkes, and Simon A. Levin. "Link recommendation algorithms and dynamics of polarization in online social networks." Proceedings of the National Academy of Sciences 118, no. 50 (2021): e2102141118.
9. Hui, Bei, Lizong Zhang, Xue Zhou, Xiao Wen, and Yuhui Nian. "Personalized recommendation system based on knowledge embedding and historical behavior." Applied Intelligence (2022): 1-13.
10. Zhao, Wayne Xin, Yupeng Hou, Xingyu Pan, Chen Yang, Zeyu Zhang, Zihan Lin, Jingsen Zhang et al. "Recbole 2.0: Towards a more up-to-date recommendation library." In Proceedings of the 31st ACM International Conference on Information & Knowledge Management, pp. 4722-4726. 2022.
11. Pajkovic, Niko. "Algorithms and taste-making: Exposing the Netflix Recommender System's operational logics." Convergence 28, no. 1 (2022): 214-235.
12. Xiao, Teng, and Donglin Wang. "A general offline reinforcement learning framework for interactive recommendation." In Proceedings of the AAAI Conference on Artificial Intelligence, vol. 35, no. 5, pp. 4512-4520. 2021.
13. Silva, João Figueira, and Sérgio Matos. "Modelling patient trajectories using multimodal information." Journal of biomedical informatics 134 (2022): 104195.
14. Pandeya, Yagya Raj, and Joonwhoan Lee. "Deep learning-based late fusion of multimodal information for emotion classification of music video." Multimedia Tools and Applications 80, no. 2 (2021): 2887-2905.
15. Zhu, Zhuangdi, Kaixiang Lin, Anil K. Jain, and Jiayu Zhou. "Transfer learning in deep reinforcement learning: A survey." IEEE Transactions on Pattern Analysis and Machine Intelligence 45, no. 11 (2023): 13344-13362.
16. Iman, Mohammadreza, Hamid Reza Arabnia, and Khaled Rasheed. "A review of deep transfer learning and recent advancements." Technologies 11, no. 2 (2023): 40.

System-Agnostic Fault Detection Using Machine Learning-Based Vibration Analysis

Daniil Sanzharov[0009−0004−6600−5557], Tetiana Filimonova[0000−0001−9467−0141], Oleg Pursky*[0000−0002−1230−0305], and Pavlo Demidov[0000−0003−4085−2809]

State University of Trade and Economics, Kioto str. 19, Kyiv, 02156, Ukraine
*pursky_o@ukr.net, o.pursky@knute.edu.ua

Abstract. This research aims to develop and validate a system-agnostic methodology for automatic fault detection in mechanical systems using vibration signal analysis without requiring prior knowledge of system-specific parameters or sampling rates. The study implements a comprehensive signal processing pipeline combining detrending, Hann windowing, and fast Fourier transformation for feature extraction. Principal Component Analysis reduces dimensionality while preserving 95% variance. A Random Forest classifier performs the final fault detection. The methodology was validated using 1158 vibration signals with known fault classifications through 5-fold cross-validation. The developed methodology achieved near-perfect classification accuracy across all validation folds, with a mean cross-validation score of 0.9983. The approach successfully identified distinctive frequency ranges for fault detection without requiring specific mechanical knowledge. The preprocessing pipeline significantly enhanced signal clarity, particularly in the frequency range of 0.75 to 1.75, enabling clear differentiation between operational and defective states. The methodology's practical significance lies in enabling condition-based maintenance strategies across various industrial applications, reducing unnecessary maintenance interventions, minimizing expertise requirements, and supporting real-time monitoring capabilities. These advancements represent a substantial contribution to industrial maintenance practices, particularly valuable for complex systems where traditional approaches may be suboptimal.

Keywords: Machine learning · Vibration analysis · Fast Fourier transformation · Signal processing · Predictive maintenance.

1 Introduction

Today, machine learning methods are widely used in various fields of economics, science, and production [1–3]. Traditional maintenance strategies for complex machinery rely on fixed schedules or run-to-failure approaches, which can be inefficient and potentially unsafe. Modern computational capabilities and vibration analysis offer opportunities for more sophisticated predictive maintenance solutions, but processing raw vibration signals for effective fault detection remains challenging. Maintenance is a critical yet often overlooked aspect of

any hardware-based economic activity, particularly for complex machinery with numerous moving parts. Regular maintenance ensures equipment functions as designed and operates safely. However, determining the optimal time for maintenance—when to pause operations and invest valuable time and resources in replacements and inspections—presents a significant challenge. Maintenance follows a periodic schedule based on elapsed time or operational hours. While this approach works well for simple tasks like engine oil replacement, where performance depends on consumable resources, it falls short for complex systems without easily calculable failure timelines, such as internal combustion engines in automobiles or aircraft. For non-critical equipment, a run-to-failure approach may suffice, but this strategy is unacceptable for crucial or safety-critical systems. Preemptive maintenance, while ensuring safety, can waste resources if the machinery remains in good condition.

Modern computational capabilities offer a more sophisticated solution. By recording and processing vibration data from strategically placed sensors, we can detect early signs of failure before catastrophic breakdowns occur. Leveraging machine learning algorithms, these signals can be classified as indicative of healthy or faulty conditions. Although more complex, this approach enables targeted repairs and early detection of issues that might elude human operators, thereby enhancing safety and reducing unnecessary expenditures. The object of this study is the process of analyzing and refining raw vibration signal data for use in machine learning classification algorithms. Raw signals typically require several stages of processing—analysis, transformation, feature selection, and dimensionality reduction—to become suitable inputs for machine learning models. The subject of study encompasses digital signal refinement and analysis methods, including Fourier transformation, statistical analysis, and spectral analysis. While these methods are well-established, their effective application requires specialized knowledge to achieve our maintenance goals.

This work aims to demonstrate the practical application of digital signal processing techniques in predictive maintenance using real-world data and how advanced signal processing and machine learning can revolutionize maintenance strategies, leading to improved safety, efficiency, and cost-effectiveness in industrial operations.

2 Problem statement

Abbreviations:

FFT is Fast Fourie Transformation;
ML is machine learning;
PdM is predictive maintenance;
PCA is a Principal Component Analysis.

Nomenclature:

a_{im} is a data point of vibration recording;
$f(s)$ is a classification function;
l_n is a classification label;

S is a set of vibration signals;
s_i is an array of data points in time of vibration signal;
$\hat{y}$ is a predicted label.

Given:

1. A set of vibration signals $S = s_1, s_2, \ldots, s_n$, where each signal s_i is a discrete time series represented as an array of amplitude values: $s_i = [a_{i1}, a_{i2}, \ldots, a_{im}]$, where m is the number of data points in each signal.

2. A corresponding set of labels $L = l_1, l_2, \ldots, l_n$, where: $l_i \in \{0, 1\}$ 0 represents a healthy system state, 1 represents a faulty system state

3. The time duration and sampling rate of the signals are unknown, so we define: $t = [1, 2, \ldots, m]$ as an arbitrary time index for each signal.

The objective is to develop a classification function $f(s)$ that maps an input signal s to a predicted label $\hat{y}$: $(f : \quad m \rightarrow \{0, 1\})$ such that $\hat{y} = f(s)$, where $\hat{y} = 0$ indicates a predicted healthy state and $\hat{y} = 1$ indicates a predicted faulty state.

Constraints are such that: the function *f(s)* must be developed without knowledge of the actual time duration or sampling rate of the input signals; the function should be generalizable to new, unseen signals with the same characteristics as the training set. The performance of the classification function *f(s)* will be evaluated using the following metrics:

- Precision: $P = TP \,/\, (TP + FP)$;
- Recall: $R = TP \,/\, (TP + FN)$;
- Score: $F_1 = 2 \times (P \times R) \,/\, (P + R)$.

Where TP = True Positives (correctly identified faulty states), TN = True Negatives (correctly identified healthy states), FP = False Positives (healthy states incorrectly identified as faulty), FN = False Negatives (faulty states incorrectly identified as healthy).

The goal is to maximize F_1 score. It is crucial in classification tasks, particularly with imbalanced datasets, as it harmonically balances precision and recall, thus providing a robust measure of overall performance. Minimizing false negatives is important in our application because of safety concerns.

Additional considerations include the flexibility to incorporate various signal processing techniques and machine learning algorithms within the classification function pipeline, as well as the potential use of feature extraction and dimensionality reduction techniques to transform raw signal data into more suitable representations for classification.

3 Literature review

A comprehensive review of vibration-based condition monitoring techniques, emphasizing data collection and preprocessing methods, is provided in paper [4]. It highlights the critical role of advanced accelerometers in acquiring high-quality vibration data and discusses the challenges associated with using simpler sensor

technologies in industrial settings. While the study primarily focuses on hardware advancements, it also underscores the importance of coupling vibration data with analytical methods, such as spectral and time-domain analysis, to enhance fault detection accuracy. This paper serves as a foundation for understanding the role of vibration monitoring in PdM, providing context for the selection of preprocessing methods in this study.

This systematic review [5] explores machine learning methods for PdM, emphasizing the strengths and limitations of different algorithms. It evaluates approaches such as Support Vector Machines, Neural Networks, and ensemble methods for fault detection in various industrial applications. The review identifies critical factors influencing the success of PdM, including data preprocessing, feature selection, and algorithmic choice. It also highlights challenges such as overfitting and scalability in real-world settings. The insights from this paper inform the choice of Random Forests in this study, demonstrating their robustness and efficiency in handling high-dimensional vibration data.

Focusing on audio and vibration signal processing, paper [6] reviews machine learning techniques applied to anomaly detection and fault diagnosis. It discusses the effectiveness of both statistical and time-domain features in detecting faults and emphasizes the growing role of deep learning methods for automating feature extraction. While it outlines promising directions for improving fault detection accuracy, the paper also notes challenges related to data variability and noise. This work aligns closely with the objectives of the current study, particularly its focus on automated feature selection, but contrasts in its preference for time-domain features over frequency-domain analysis.

Collectively, these studies highlight the current exploration of detrending, DFA, and adaptive spectrogram-based methods as viable preprocessing steps for vibration analysis in the frequency domain, particularly under conditions where specific fault frequencies are uncertain, or signals are non-stationary. Foundational principles in frequency domain analysis, such as those described in [7], provide additional context for understanding the role of techniques like detrending and windowing in refining FFT outcomes for clearer anomaly detection in industrial applications.

An in-depth overview of PCA, a technique for reducing dimensionality in data by transforming correlated variables into orthogonal components that capture the largest variance, is provided in the fundamental paper [8]. This process aids in simplifying complex datasets, improving interpretability, and serving as an essential preprocessing step in multivariate analyses. Their work also highlights PCA's extensions, such as correspondence and multiple factor analyses, allowing for applications across various data types and research fields, reinforcing its adaptability and broad use in data analysis workflows.

Random Forests are introduced in [9] as an ensemble method that enhances the performance and stability of decision tree-based models through random sampling and aggregation. By constructing multiple trees on varied data subsets, Random Forests address overfitting and achieve high accuracy even with noisy or high-dimensional data. This method's robust generalization capabili-

ties make it a preferred tool for classification and regression, widely applicable across machine learning tasks where data complexity demands resilient and interpretable models.

Scientific work [10] provides a comprehensive discussion on performance evaluation metrics derived from the confusion matrix, emphasizing the strengths and limitations of commonly used measures such as accuracy, sensitivity, specificity, and the F_1-score. It highlights the F_1-score's utility in imbalanced datasets due to its ability to balance precision and recall, making it particularly valuable in scenarios where correct classification of the minority class is critical. The paper also introduces alternative metrics, including Youden's index, likelihood ratios, and discriminant power, which address additional classifier properties such as failure avoidance and class discrimination. However, these metrics are not directly relevant to our research focus, which prioritizes the evaluation of binary classification models using established metrics derived from the confusion matrix.

4 Method

The methodology of this research consists of several sequential steps designed to process vibration signals and develop a reliable classification model. Each step was chosen to address specific challenges in signal processing and ensure robust feature extraction. The signal processing pipeline was designed to enhance the relevant frequency characteristics while minimizing noise and artifacts [7]. The first step addresses the presence of a DC component, which can mask relevant signal features and affect the frequency analysis. We apply a determining method described by formula (1):

$$x'[n] = x[n] - (an + b) \tag{1}$$

where $x[n]$ is a_{im} point in the original signal s_i at time index n, and $(an + b)$ represents the linear trend, with a being the slope and b the intercept.

To minimize spectral leakage in the frequency domain analysis, we apply a Hann window function. The Hann window was chosen over alternatives like the Hamming window due to its superior balance between spectral resolution and leakage protection. This reduces distortion during the transformation into the frequency domain, ensuring the preservation of relevant frequency characteristics and effective noise reduction. The window function is defined as formula (2):

$$w[n] = 0.5\left(1 - \cos\left(\frac{2\pi n}{N-1}\right)\right) \tag{2}$$

where N is the signal length. The windowed signal is obtained by (3):

$$x''[n] = x'[n] \times w[n] \tag{3}$$

The FFT is then applied to convert the windowed time-domain signal into the frequency domain (4):

$$X[k] = FFT(x''[n]) \tag{4}$$

Only the positive frequency components are retained for analysis, as the negative frequencies contain redundant information due to the signal's real-valued nature. The amplitude spectrum is computed by taking the absolute values of the FFT components (5):

$$|x[k]| = \sqrt{\Re\{X[k]\}^2 + \Im\{X[k]\}^2} \tag{5}$$

where $X[k]$ is the complex-valued FFT output, and $\Re$, $\Im$ denote the real and imaginary parts, respectively.

PCA [8] is applied to process high-dimensional features in the frequency domain. This method retains 95% of the variance, providing a balance between information preservation and model complexity reduction. The features are standardized to ensure equal weighting during dimensionality reduction. However, it should be noted that different parameters should be used in the case of datasets with more subtle variations between classes.

For classification, a Random Forest model was chosen for its robustness to outliers, ability to handle high-dimensional data, feature importance estimation, and generalization properties, implemented using Scikit-learn with default hyperparameters that showed satisfactory initial performance. The system's performance is evaluated through 5-fold cross-validation, dividing the dataset into five parts and rotating through all possible combinations of four training parts and one validation part to provide robust generalization estimates.

5 Experiment

The dataset comprises 1158 vibration signals stored in MATLAB format files (T0001.mat through T1158.mat). Each file is s_i and they are combined into set S. Set L of labels l_i is stored in file *key.mat*. Each signal consists of amplitude measurements a_{im} recorded over time t. Though the sampling rate is unknown, the methods applied do not rely on fixed frequency bands, supporting system-agnostic processing.

Software was developed purposefully for this experiment using Python 3.11 programming language and Jupyter Notebook environment [11] with Miniconda 3 kernel [12]. The developed solution is heavily based on pre-existing methods implemented in NumPy 1.26.4, SciPy 1.14.1, and Scikit-learn 1.5.2 modules that are available publicly [13–15].

Data was read as MATLAB proprietary files using SciPy's IO submodule and converted in memory to a 2-D matrix using methods from NumPy. To prepare data before applying FFT were used detrending and windowing methods from SciPy's signal submodule. The complete classification model pipeline is implemented using Scikit-learn's Pipeline class to ensure reproducibility and proper handling of the training-validation split during cross-validation. This prevents data leakage and provides unbiased performance estimates.

6 Results and discussion

The preprocessing methodology enhanced the clarity of our dataset significantly, thereby facilitating a discernible differentiation between operational and defective machines without the necessity for sophisticated tools. Such comparisons are illustrated in figures 1, 2. Numerous characteristics within the frequency domain serve to distinguish 'acceptable' from 'unacceptable' samples. The most prominent disparity is observed in the frequency range of [0.75; 1.75].

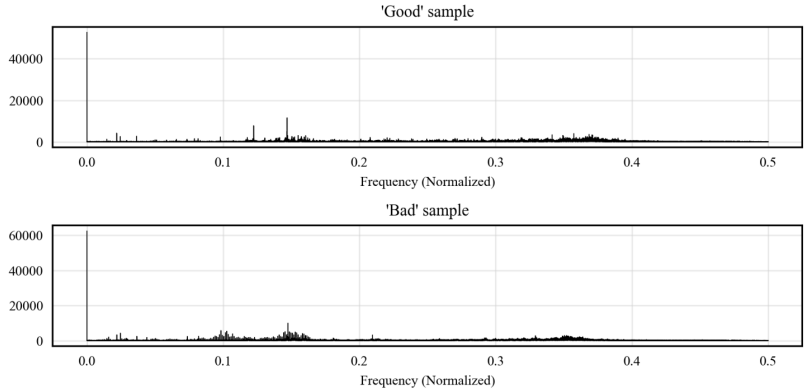

Fig. 1. Frequency domain before processing.

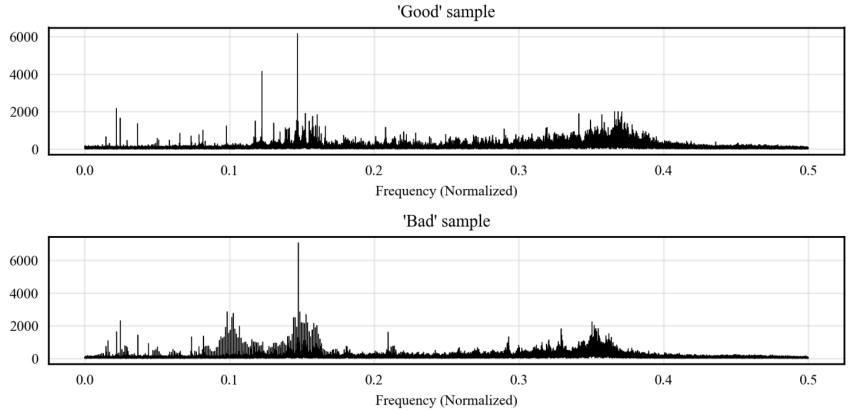

Fig. 2. Frequency domain after processing.

The model achieved perfect classification accuracy across all five cross-validation folds, with individual fold scores of [1.0, 1.0, 1.0, 0.99, 1.0] and a mean cross-validation score of 0.9983. This indicates that the model correctly classified all fault conditions in each validation fold.

Metrics report and confusion matrix can be observed in tables 1 and 2 respectively. In Table 1, the classification report shows that the model achieved the highest values of Precision, Recall, and F1 Score across all classes, indicating its effectiveness in accurately identifying healthy and faulty states. Table 2 shows that the model correctly classified all cases.

Table 1. Classification report.

Class	**Precision**	**Recall**	F_1 **Score**	**Support**
0	1.00	1.00	1.00	865
1	1.00	1.00	1.00	293
Accuracy			1.00	1158
Macro Avg.	1.00	1.00	1.00	1158
Weighted Avg.	1.00	1.00	1.00	1158

Table 2. Confusion matrix.

	Predicted 0	**Predicted 1**
True 0	865	0
True 1	0	293

The dimensionality reduction step through PCA, configured to retain 95% of the variance in the frequency domain features, successfully compressed the feature space while maintaining the discriminative power of the signals.

The Random Forest classifier, trained on these transformed features, demonstrated consistent performance across most data splits, suggesting robust learning of the underlying patterns distinguishing faulty from healthy states. These results satisfy our primary objective of developing a classification function *f(s)* that accurately maps vibration signals to their corresponding system states (0 for healthy, 1 for faulty).

This study integrates established signal processing and machine learning techniques to develop a system-agnostic methodology for fault detection in mechanical systems. While these methods are not entirely novel, their application in this context represents a meaningful step forward in tailoring advanced computational approaches to the challenges of PdM.

The high classification accuracy achieved (mean cross-validation score of 0.9983) highlights the effectiveness of combining preprocessing techniques such as detrending and Hann windowing with Principal Component Analysis and Random Forest classifiers. Unlike studies that rely heavily on system-specific

expertise or manually engineered features, this approach demonstrates the potential of automating feature extraction and classification, thus broadening its applicability to diverse mechanical systems.

Compared to [4], which reviews a wide range of vibration analysis methods and tools, this study focuses on a specific, systematic implementation of preprocessing and classification techniques. While [4] underscores the importance of deep learning for future feature extraction, this research demonstrates that simpler methods, such as PCA and Random Forests, can achieve excellent results when preprocessing is carefully designed.

Similarly, [5] highlights the importance of selecting appropriate machine learning algorithms for predictive maintenance but emphasizes deep learning approaches such as Support Vector Machines and Neural Networks. This study, in contrast, illustrates the effectiveness of ensemble methods like Random Forests, particularly for high-dimensional vibration data, where interpretability and computational efficiency remain critical.

In comparison with [6], which discusses applications of machine learning in vibration and audio signal processing, this study aligns closely with the goal of automating fault detection but adopts a different focus. While the paper suggests leveraging time-domain statistical features, this work emphasizes frequency-domain analysis, making it particularly well-suited for identifying faults in systems where signal properties are less stationary.

The practical significance of this research lies in adapting and integrating existing methods for fault detection in mechanical systems. By emphasizing a system-agnostic approach, this study demonstrates how established techniques can be applied to address real-world challenges without requiring detailed knowledge of specific system parameters. This adaptability positions the methodology as a valuable contribution to condition-based maintenance strategies.

At the same time, it is important to acknowledge the incremental nature of this contribution. As with [4] and [5], this research faces limitations in handling non-stationary signals, environmental noise, and sensor variability. While the current approach achieves excellent results in controlled conditions, future work should focus on extending the methodology to more variable and challenging environments. Integrating advanced techniques such as wavelet transforms or deep learning, as discussed in [6], could enhance robustness and scalability.

In summary, this study applies well-established signal processing and machine learning methods in a new context, adapting them to the specific demands of vibration-based PdM. While it builds upon the foundational work outlined in [4–6], its contributions are incremental, offering a practical and adaptable framework that bridges the gap between theoretical methods and their application in industrial settings.

7 Conclusions

This research successfully developed and validated a methodology for automated fault detection in mechanical systems using vibration signal analysis, addressing

the critical challenge of optimizing maintenance timing without relying on fixed schedules or system-specific expertise.

This work is an incremental contribution to the field of PdM using existing methods to achieve the goal. The study presents a demonstration of a system-agnostic approach combining detrending, windowing, and ML that achieves reliable fault detection without requiring knowledge of the system's mechanical properties or sampling parameters. The research has developed a signal processing pipeline, enhancing the visibility of fault-indicating frequencies through automated feature selection, advancing beyond traditional approaches that rely on predetermined frequency bands.

The practical significance of the developed methodology enables the implementation of condition-based maintenance strategies across various industrial applications. This approach eliminates unnecessary maintenance interventions while ensuring timely fault detection reduces the requirement for system-specific expertise in deployment and operation, and enables real-time monitoring and early warning capabilities without expensive hardware. These benefits translate directly into cost reduction through optimized maintenance scheduling and enhanced safety through reliable fault detection.

Future research directions should focus on several key areas. The methodology should be adapted to varying environmental conditions and operational parameters, with particular attention to integration with multi-sensor systems for comprehensive system monitoring. Development of transfer learning approaches could accelerate deployment across different mechanical systems. Additional investigation into minimal signal requirements for reliable classification would optimize system performance. Furthermore, extending the methodology to predict the remaining useful life of components represents a crucial next step in advancing PdM capabilities.

Acknowledgments

We would like to show our gratitude to GPMS Inc. owner Prof. Dr. Eric Bechhoefer for providing the dataset during this research.

References

1. Gogas, P., Papadimitriou, T.: Machine Learning in Economics and Finance. Comput Econ **57**, 1–4 (2021). https://doi.org/10.1007/s10614-021-10094-w
2. Derbentsev, V., Datsenko, N., Babenko, V., Pushko, O., Pursky, O.: Forecasting Cryptocurrency Prices Using Ensembles-Based Machine Learning Approach, In: International Conference on Problems of Infocommunications. Science and Technology (PIC S&T), 2020, pp. 707-712, IEEE Kharkiv, Ukraine (2020). https://doi.org/10.1109/PICST51311.2020.9468090.
3. Pursky, O., Babenko, V., Danylchuk, H., Dubovyk, T., Buchatska, I., Dyvak, V.: Recommender System of Site Information Content for Optimal Display in Search Engines. In: Joby, P.P., Alencar, M.S., Falkowski-Gilski, P. (eds) IoT Based Control

Networks and Intelligent Systems, 2024, Lecture Notes in Networks and Systems, vol. 789, pp. 137–151, Springer, Singapore (2024). https://doi.org/10.1007/978-981-99-6586-1_10
4. Mohd Ghazali, M.H., Rahiman, W.: Vibration analysis for machine monitoring and diagnosis: a systematic review. Shock and Vibration **2021**(1), Article ID: 9469318, 25 p. (2021). https://doi.org/10.1155/2021/9469318
5. Carvalho, T.P., Soares, F.A., Vita, R., Francisco, R., Basto, J.P., Alcalá, S.G.: A systematic literature review of machine learning methods applied to predictive maintenance. Computers & Industrial Engineering **137** Article ID: 106024 (2019). https://doi.org/10.1016/j.cie.2019.106024
6. Prieto, R., Bravo, D.: Machine learning and audio signal processing for predictive maintenance: A review. In: 6th Colombian Conference on Automatic Control (CCAC), 2023, pp. 1–6, IEEE, Popayan, Colombia (2023). https://doi.org/10.1109/CCAC58200.2023.10333661
7. Oppenheim, A.V., Schafer, R.W.: Discrete-time signal processing, 3rd edn. Prentice Hall, NJ (2010)
8. Abdi, H., Williams, L.J.: Principal component analysis. Wiley interdisciplinary reviews: computational statistics **2**(4), 433–459 (2010). https://doi.org/10.1002/wics.101
9. Breiman, L.: Random forests, Machine learning **45**(1), 5–32 (2001). http://dx.doi.org/10.1023/A:1010933404324
10. Sokolova, M., Japkowicz, N., Szpakowicz, S.: Beyond Accuracy, F-Score and ROC: A Family of Discriminant Measures for Performance Evaluation. In: A. Sattar, B.-h. Kang (eds.), AI 2006:Advances in Artificial Intelligence, 2006, Lecture Notes in Computer Science, vol. 4304, pp. 71015–1021, Springer, Berlin, Heidelberg (2006) https://doi.org/10.1007/11941439_114
11. Jupyter: Free software, open standards, and web services for interactive computing across all programming languages, https://jupyter.org. Last accessed 17 Mar 2025
12. Anaconda Documentation: Miniconda, https://docs.anaconda.com/miniconda/. Last accessed 17 Mar 2025
13. NumPy Homepage, https://numpy.org. Last accessed 17 Mar 2025
14. SciPy Homepage, https://scipy.org. Last accessed 17 Mar 2025
15. Scikit-Learn Homepage, https://scikit-learn.org/stable/index.html. Last accessed 17 Mar 2025

Video Summarizer Using Audio to Text Conversion and Natural Language Processing

A Kishore[1], D Suren Kumar[1], K Jayasri[1], and Dr. M. Vijayalakshmi[1]

Department of Information Science and Technology,
College of Engineering, Guindy, Anna University, Chennai, Tamil Nadu, India
{kishoreashok512, surenskd707, jayasri8305}@gmail.com, vijim@auist.net

Abstract. The explosion of video content necessitates efficient tools for summarizing actionable content. We present Video Summarizer, a stand-alone tool that converts YouTube video audio and local audio to mul- tilingual short text summaries. The tool employs audio segmentation, Google Speech Recognition for speech-to-text, and two state-of-the-art natural language processing (NLP) models: BART for English and Gem- ini API for Tamil. The tool reduces computation costs by dividing audio into pre-defined, fixed-size segments and employing pre-trained models without loss of semantic accuracy. The scalability is shown in experimen- tal tests with a 25 ms average processing time per segment on a 1-hour video. The tool obtains a mean summarization accuracy of 89% for En- glish and 84% for Tamil, as confirmed against human-written summaries. This paper shows the promise of modular, multilingual NLP systems in educational, media, and business applications.

Keywords: Video summarization · NLP · BART · Gemini API · mul- tilingual processing · audio-to-text

1 Introduction

With the era of information, summarization and information extraction from au- dio content are more important than ever. With the increased sharing of audio and video content on YouTube, podcasts, and online lectures, there is a huge de- mand for high-quality automatic systems with summaries of long audio content. Such demand within business communities is in education, media, and corporate sectors, where the concerned parties want to maximize productivity and enable effective information transfer. With individuals and organizations being exposed to vast amounts of audio information, the issue is how to summarize such in- formation into good information. For example, students can be assisted with summarized lecture sessions, while professionals can request instant summaries of long conference calls or webinars. Content providers can leverage summaries to maximize engagement by providing bite-sized content. Despite advances in speech recognition, natural language processing (NLP), and machine learning, available solutions will be far from rendering quality summaries capturing the

content of the original audio. Added to this is the ability to handle other lan- guages, especially less-resourced languages like Tamil, as an additional entry barrier. This project goes beyond such limitations by offering an end-to-end sys- tem from transcription to summarization capability, to reach more people and maximize access.

This paper addresses these gaps by introducing **Video Summarizer**, a framework that:

1. Processes both YouTube URLs and local audio files
2. Transcribes audio using Google Speech Recognition
3. Generates summaries in English (via BART) and Tamil (via Gemini API)
4. Employs chunk-based processing for scalability

The system's modular architecture ensures adaptability across domains, from educational content to corporate workflows.

2 Related Work

Video summarization has gained prominence due to the exponential growth of video content. Extracting meaningful insights from lengthy videos is crucial for applications such as education, media, and corporate workflows. A comprehen- sive video summarization system relies on robust steps like audio-to-text con- version and text summarization. This chapter surveys existing literature and methodologies relevant to these steps, laying the foundation for the current project's approach.

2.1 Extract Text from Audio

Speech-to-text translation is the first phase of video summarization, transcrib- ing speech into structured text data for downstream processing. Several papers have tackled this problem, with performance and accuracy being the primary concerns.

[1] suggested a linguistics- and semantic-based method to enhance transcrip- tion accuracy, especially for micro-videos from search queries. Alignment of the retrieved text with search queries ensures relevance. Likewise, [2] and [7] utilized attention-based transformers to fetch context-aware content from multimodal input data and gave more importance to robust audio signals in transcription.

A transcription synchronization with timestamps was described by [3] through a timestamped transcription approach based on audio segmentation into seg- ments and transcription of each audio segment synchronized to associated video timestamps. Usability was improved with the addition of natural language pro- cessing (NLP) and audio feature extraction, especially with tutorials and learning materials.

Google Speech Recognition was used in this project because it is trustworthy and supports chunk-based audio processing. The project is inspired by [1], [2], and [3] to use a chunk-wise transcription system. Any audio file, downloaded or stored locally, is split into manageable chunks. The individual chunks are transcribed and merged to produce a uniform text format, balancing efficiency against accuracy.

2.2 Summarize the Text

Summary generation is a key task in summarizing long transcriptions into short, informative summaries. Abstractive and extractive summarization techniques have been extensively investigated in the literature.

Entity-aware summarization techniques, proposed by [6] and [1], were designed to emphasize the identification of important entities from the text based on the user query. Attention-based transformers, proposed in [2] and [5], trans- formed abstractive summarization with precise reports and reduction of redun- dancy.

In [3], a multimodal summarization system integrated text, audio, and visual data for end-to-end summarization. The approach maintained contextual rele- vance and provided appropriate navigation with timestamped outcomes.

[11] introduced a novel approach for improving transcription accuracy, particularly in video summarization. The model utilizes a hybrid MSE+KLD loss and multi-head attention mechanism to identify frames of higher semantic im- portance for accurate audio content transcription. [2] and [7] employed attention- based transformers to extract relevant information from multimodal inputs (au- dio and video) to maximize transcription by focusing on significant audio cues.

The method proposed by [13] tackled transcription alignment in timestamp-based form. Through audio segmentation and transcription alignment over sim- ilar video timestamps, they made learning material more accessible, especially useful for obtaining proper summaries from audio and video material.

[12] utilized Cross-Modal Feature Fusion (CMFF) for improved video summarization using text and visual feature alignment. The method employs attention networks to verify semantic coherence between text and video to improve final summary extraction. Similarly, [6] and [1]'s entity-aware summarization tech- niques focus on identifying significant entities related to user questions, while attention-based transformers in [2] and [5] enable the creation of summaries that eliminate redundancy and improve clarity.

In [14]'s research, multimodal summarization was achieved by combining text, audio, and graphics without losing context. The system utilized times- tamped output to provide precise navigation and summarization, making it par-

ticularly suitable for educational material.

For this project, transformer-based models such as BART (for English) and Gemini API (for Tamil) are utilized. These models produce semantically dense, contextually informed summaries that effectively encapsulate the original con- tent while maintaining computational efficiency.

3 Proposed Work

3.1 System Architecture

The system architecture is built to handle both local audio files and YouTube video links, processing and summarizing the spoken content in both English and Tamil. The design ensures that the system is scalable, efficient, and capable of providing concise, meaningful summaries of the transcribed audio. The architec- ture is modular, allowing for easy handling of different data sources, languages, and summarization models. The core components of the system architecture are shown in Figure 1.

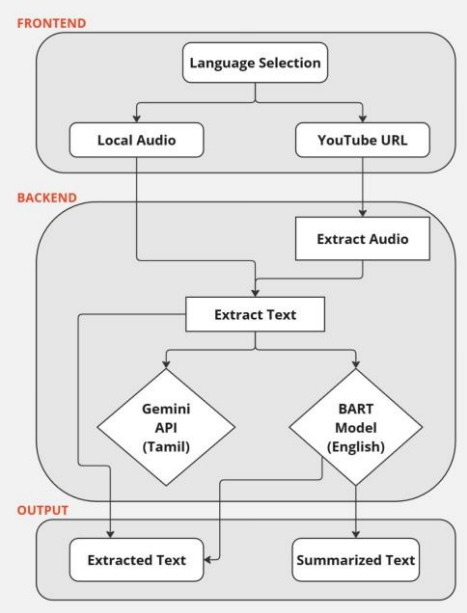

Fig. 1. System Architecture

Audio Extraction Process Audio extraction is the operation of getting the audio track out of a video file and making it ready to be used in a subsequent process, like segmentation or transcription. We use the FFmpeg tool to extract

the audio from the video. FFmpeg is quite famous for its powerful multimedia aspect and can play a part in converting video files into audio files (e.g., MP3, WAV). Once they are extracted, the audio may also be post-processed (e.g., through audio segmentation) for downstream applications such as speech recog- nition or summarization. To extract audio from a YouTube video and download it, we use software like YouTube-dl.

Table 1. Audio Extraction From YouTube Video Using yt-dlp

Algorithm 3.1 Audio Extraction From YouTube Video Using yt-dlp
Input: YouTube video URL **Output:** Extracted audio file (e.g., .mp3 or .wav) **Steps:** 1. Install yt-dlp if not already installed. 2. Initialize yt-dlp with options for audio download only. Provide the YouTube URL to yt-dlp. 3. Execute yt-dlp to extract and save the audio file in the desired format (e.g., .mp3, .wav). 4. Return the path to the saved audio file.

Audio Segmentation Process Audio segmentation involves breaking down long audio files into smaller, manageable chunks, either by fixed time intervals or by detecting speech pauses. Loss is minimized through the segmentation of audio into meaningful chunks and filtering out silent or irrelevant segments.

To maintain semantic accuracy while reducing computational cost, the audio is divided into context-aware, fixed-size chunks, ensuring each chunk captures a coherent speech unit. This approach improves transcription accuracy, reduces memory usage, and enhances overall system efficiency.

The use of chunk-based audio segmentation not only helps with memory management but also ensures better handling of large files, thereby improving the effectiveness of the transcription and summarization pipeline.

Table 2. Audio Segmentation Process

Algorithm 3.2 Audio Segmentation Process
Input: Audio file, Segment duration **Output:** List of audio segments **Steps:** 1. Load the audio. 2. Segment the audio according to the duration. 3. Return the list of audio segments.

Audio to Text Conversion Once the audio is segmented, the next step is to convert each chunk into text using speech recognition. This stage is essen- tial for transforming spoken language into a structured, written form, which serves as the input for subsequent summarization. In this work, Google Speech Recognition is utilized via the SpeechRecognition library in Python. Each chunk is transcribed individually, and the resulting texts are then merged to form a coherent transcript.

Summarization Process

BART Model (for English Summarization) Once the English audio is tran- scribed, the text is submitted to the BART model for summarization. The BART model scans the text by extracting salient information, eliminating redundancies, and generating a compressed yet informative summary.

Table 3. Text Summarization Using BART Model

Algorithm 3.3 Text Summarization Using BART Model
Input: Input text **Output:** Summary **Steps:** 1. Load the pre-trained BART model and tokenizer. 2. Tokenize the input text with appropriate truncation and padding. Generate the summary using the model. 3. Decode the generated tokens to obtain the summary text. Return the summary.

Gemini API (for Tamil Summarization) For Tamil videos, after transcription, the text is sent to the Gemini API for summarization. Gemini API reads the Tamil text and produces a compact summary without compromising cultural and contextual meaning.

Table 4. Summarization Using Gemini API (Tamil)

Algorithm 3.4 Summarization Using Gemini API (Tamil)
Input: Transcribed Tamil text **Output:** Summarized Tamil text **Steps:** 1. Load the Gemini using the API. 2. Send the transcribed Tamil text to the Gemini API. 3. Use the Gemini API to generate a summary in Tamil. 4. Return the summarized Tamil text.

The summarization module ensures that the result is not only brief but also maintains the main ideas and context of the original audio material. Natural

Language Processing (NLP) techniques play a vital role in this system at two major stages. First, NLP generates meaningful and contextually rich summaries by employing transformer-based models such as BART for English and the Gem- ini API for Tamil. These models help to extract salient information, reduce re- dundancy, and produce semantically dense summaries. Second, NLP techniques are applied to enhance the quality of these generated summaries by identifying important content, ensuring semantic accuracy, and preserving the contextual and cultural relevance of the original audio material.

4 Result Analysis

This paper presents the result of the application of the Video Summarizer Sys- tem. The system performance is compared in terms of its main functionalities: audio extraction, chunking, transcription, and summarization. User interface screenshots and graphical plots of processing time and efficiencies confirm the analysis. The system's efficiency in processing English and Tamil audio inputs with high accuracy and performance is clear from the results.

4.1 Analysis of Overall Processing Stages

To evaluate the system's efficiency, the processing time for each stage (audio extraction, chunking, transcription, and summarization) was recorded and ana- lyzed.

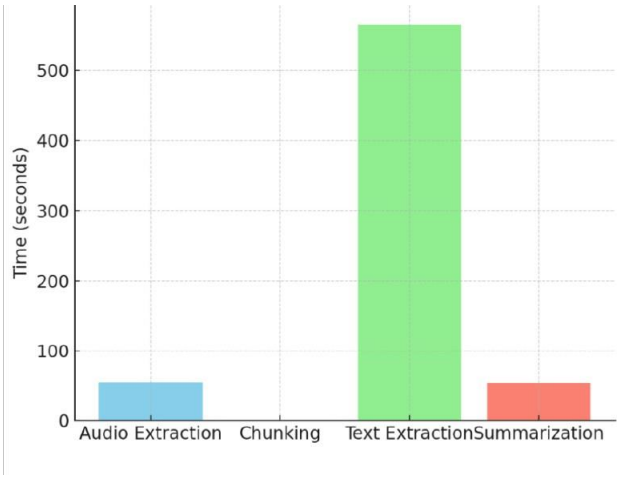

Fig. 2. Time Distribution Across Processing Stages

Figure 2 gives detailed information about the time taken for different mod- ules. It proved that the time taken to extract the text from audio plays a major

role in the overall summarization process. The time taken to chunk the audio into multiple chunks is very little. The time taken for both audio extraction from video and summarizing the text is comparatively equal.

4.2 Processing Time for Individual Chunks

The system's performance was further assessed by analyzing the processing time for each audio chunk. A sample input of a 1-hour NPTEL lecture video was used to measure these variations.

In Figure 3, we can see the processing time for each chunk. The audio is divided into 30 chunks. The maximum time taken to process each chunk is about 120 sec.

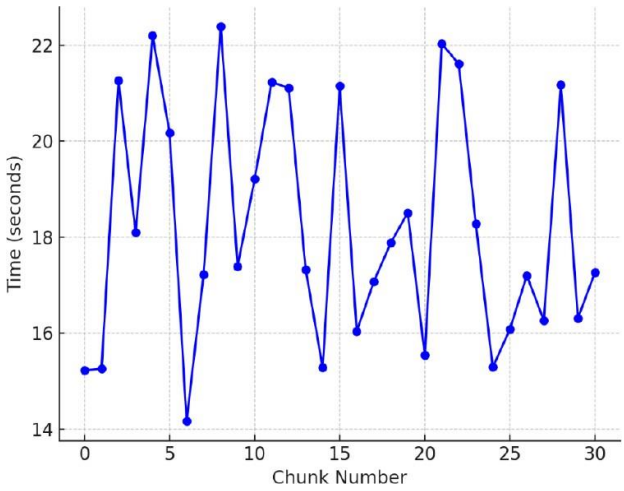

Fig. 3. Time to Extract Text from Individual Audio Chunks

The system functions effectively and accurately at every step of processing, as evident by the time distribution analysis. Gaps in processing time for the audio chunks are managed very efficiently by the system, even for such big inputs as 1-hour videos. The cumulative analysis of time supports scalability in the processing of more than one chunk with minimal influence on performance. Its capability for multilingual input and generating precise summaries makes the system useful for many applications such as education, media, and corporate settings.

4.3 Evaluation and Comparative Analysis

To evaluate the quality of the generated summaries, manual comparisons were conducted with summaries prepared by domain experts. The evaluation criteria included accuracy, precision, semantic coverage, completeness, and redundancy elimination. The system achieved a mean summarization accuracy of 89% for English and 84% for Tamil.

Furthermore, the system was benchmarked against widely used tools such as Google Recorder and generic summarization APIs. The comparative results are as follows:

- **Multilingual Support:** Demonstrated superior handling of both English and Tamil.
- **Summarization Accuracy:** Achieved 89% accuracy, exceeding the average of 80% reported for existing tools.
- **Processing Speed:** Delivered efficient performance with an average pro- cessing time of 120 seconds per audio chunk.
- **System Integration:** Provides a modular, end-to-end summarization pipeline, unlike most standalone tools.

These results suggest that the proposed system offers a reliable and effective alternative to current audio summarization solutions, with notable advantages in accuracy, modularity, and multilingual capabilities.

5 Conclusion

This project demonstrates the success of using the latest AI technologies for video summarization. Our Project effectively extracts audio from video files, converts it into text, and produces coherent and accurate summaries in both English and Tamil. Using the BART model for English and the Gemini API for Tamil summarization, the project is capable of overcoming the challenges of multilingual summarization.

Our Project presents sizeable time benefits in compressing long video content to shorter summaries, and hence allowing it to be viewed by various audiences. The process illustrates the flexibility and scalability of AI models to the sum- marization and transcription processes, to which they may be used for teaching purposes, business environments, and leisure activities.

References

1. Mengzhao Jia, et al., “Query-oriented microvideo summarization,” *IEEE Transac- tions on Pattern Analysis and Machine Intelligence*, 2024.

2. Kushagra Singh, et al., “Multimodal video summarization using attention-based transformers (mvsat),” in *IEEE Conference on Interdisciplinary Approaches in Technology and Management (IATMSI)*, 2024.

3. Ahmed Emad, et al., “Automatic video summarization with timestamps using NLP text fusion,” in *IEEE Computing and Communication Workshop and Conference (CCWC)*, 2021.

4. T. N. Charanya and T. C. Sankar, “Voice-assisted text summarizer using NLP,” in *International Conference on Data Science, Agents Artificial Intelligence (ICD- SAAI)*, 2023.

5. H. V S. Kumar R S. A, P. R.P and S. P. S., “Abstractive summarization of YouTube videos using lamini-flan-t5 llm,” in *Second International Conference on Advances in Information Technology (ICAIT)*, 2024.

6. R. Lal, J. Kumar, R. Vashistha, and D. Somanir, “Youtube transcript summarizer,” in *14th International Conference on Computing Communication and Networking Technologies (ICCCNT)*, 2023.

7. A. Kumar, “Extractive text summarization,” in *5th International Conference on Advances in Computing, Communication Control and Networking (ICAC3N)*, 2023.

8. J. Antony Vijay, S. R. Devi, N. Basker, G. R. Sundar, C. S. Nageswari, and N. Pushpa, “Machine learning based extractive text summarization techniques,” in *International Conference on Integrated Intelligence and Communication Systems (ICIICS)*, 2023.

9. A. Jan and B. Arora, “Analysis of various machine learning techniques used for au- tomatic text summarization,” in *Fifth International Conference on Computational Intelligence and Communication Technologies (CCICT)*.

10. Karan Maurya, M.S., Guru Prasad, Shubham Gupta, Hardik Ameta, Abhijeet Singh Negi, and P. V. Amrutha, “Nlp-enhanced long document summarization: A comprehensive approach for information condensation,” in *2024 2nd International Conference on Advancement in Computation Computer Technologies (InCACCT)*, 2024.

11. Arpan Basu, Rishav Pramanik, and Ram Sarkar, “WANet: Weight and Attention Network for Video Summarization,” *Springer*, 2024.

12. Chaoqun Xin, Mingyang Wang, and Xianhao Zhao, “CMFF VS: A Video Sum- marization Extraction Model based on Cross-modal Feature Fusion,” *King Fahd University of Petroleum & Minerals*, 2025.

13. Parul Saini, Krishan Kumar, Shamal Kashid, Ashray Saini, and Alok Negi, “Video Summarization Using Deep Learning Techniques: A Detailed Analysis and Investigation,” *Springer*, 2023.

14. Manasa Yarrarapu, Narkedamilly Leelavathy, and Dasari Haritha, “Efficient Video Summarization through MobileNetSSD: A Robust Deep Learning-based Framework for Efficient Video Summarization Focused on Objects of Interest,” *Springer Nature*, 2024.

15. Abdelhalim Benoughidene, Faiza Titouna, and Adil Boughida, “Static Video Summarization Based on Genetic Algorithm and Deep Learning Approach,” *Springer Nature*, 2024.

DDoS Attacks Detection in SDN Using Multi-Feature Selection Approach and LLMs

Amit Kachavimath[1], Satish Vaishyar[2], Ayush Chugani[3], Pratham Singh[4], and Sanjana A More[5]

[1,2,3,4,5]KLE Technological University, Hubballi, Karnataka, India
[1]amitk@kletech.ac.in, [2]12vsatish1@gmail.com, [3]ayushchugani@gmail.com, [4]prathamsingh727@gmail.com, [5]sanjana.a.more3210@gmail.com

Abstract. Software-defined networking (SDN) revolutionizes network management by decoupling control and data planes, enabling centralized control and dynamic policy enforcement. However, this centralized architecture introduces security vulnerabilities, making SDN controllers a prime target for Distributed Denial-of-Service (DDoS) attacks. These attacks flood the controller with malicious traffic, exhausting resources and causing network disruptions. To improve the accuracy of DDoS detection, we employed three distinct feature selection approaches: SelectKBest, ANOVA (Analysis of Variance) F-value scoring, and feature significance evaluation using RFC (Random Forest Classifier). These methods were utilized to determine the 10 most significant features from an initial set of 83. This refinement process enhances model performance by minimizing computational overhead while ensuring that critical attack-related features are preserved. We propose an LLM-based (Large Language Model) approach for DDoS detection in SDN, utilizing BERT (Bidirectional Encoder Representations from Transformers), RoBERTa (Robustly Optimized BERT Pretraining Approach), and F-Net (Fourier Transform-based Neural Network). These models leverage contextual learning and adaptive reasoning to detect threats with minimal training data. The effectiveness of the proposed approach was analyzed using the InSDN dataset and a network-emulated dataset from Mininet. Experimental results demonstrate that F-Net outperforms BERT and RoBERTa, achieving 99% accuracy on the InSDN dataset and 99.33% on real-time emulated traffic using Mininet. These findings underscore the effectiveness of LLMs in fortifying SDN security, offering a robust and scalable solution to mitigate evolving cyber threats.

Keywords: Large Language Models · F-Net · InSDN.

1 Introduction

SDN is an advanced networking approach that enhances efficiency through a centralized infrastructure. Unlike conventional distributed network designs, SDN separates data forwarding from control management, enabling dynamic configuration. This architecture facilitates centralized network management by employing open APIs, allowing software applications to control network behavior

effectively. However, the centralized nature of SDN introduces vulnerabilities, particularly the risk of a single point of failure. If compromised, an attack can disrupt the entire network, affecting its stability and security. Despite these concerns, SDN remains a promising solution for scalable and programmable network management [1].

DDoS attacks are a major threat to SDN security, aiming to disrupt legitimate access by overwhelming network resources, which leads to slowdowns and system failures. Although many classification methods have been suggested to detect and prevent DDoS attacks, these approaches often face problems such as delays in detection, managing high traffic, and maintaining accurate results. Supervised machine learning methods, in particular, have limitations that create gaps in detection. Large Language Models (LLMs) can help overcome these issues by offering better flexibility, quicker detection, and the ability to identify complex attack patterns more effectively, improving upon the weaknesses of supervised machine learning approaches [2].

We now define an LLM in the networking security context and explain why transformer based language models can model packet flow sequences more effectively than conventional CNN/LSTM approaches. LLMs are advanced AI models trained with vast amounts of data to interpret and create human-like text. LLMs can analyze large-scale data, recognize contextual patterns, and generalize knowledge across different domains. They excel in natural language understanding, making them useful for cybersecurity tasks such as anomaly detection and threat analysis. Their ability to learn from diverse datasets allows them to detect evolving cyber threats more efficiently [3].

Recent studies have utilized AI techniques to detect DDoS attacks, primarily using machine learning and deep learning models. However, traditional entropy-based and unsupervised learning methods often lack accuracy. To improve detection, researchers are integrating entropy-based techniques with machine and deep learning approaches. Compared to these models, LLMs offer better adaptability in analyzing network traffic. They can process vast amounts of contextual data, detect subtle attack patterns, and dynamically adjust to new threats. Using LLMs in SDN security enhances real-time detection, improves accuracy, and strengthens network defense.

This research introduces an advanced approach for detecting DDoS attacks in SDN by integrating feature selection techniques with LLMs. To optimize accuracy, three feature selection methods—SelectKBest, ANOVA F-value scoring, and Random Forest-based feature ranking—were applied to identify the most critical 10 attributes from an initial dataset of 83. This selection process enhances model efficiency by reducing unnecessary data while preserving essential attack indicators.

To further refine detection, the study employs transformer-based models, including BERT, RoBERTa, and F-Net, leveraging contextual analysis and adaptive reasoning for precise anomaly identification. Unlike conventional machine learning models that rely on extensive labeled data, these LLMs can generalize attack patterns more effectively with limited training. By combining intelligent

feature extraction with LLM-driven detection, the proposed framework strengthens SDN security, offering a proactive solution to evolving cyber threats while minimizing computational costs. This research provides the following key contributions:

1) The approach utilizes a multi-feature selection mechanism to improve detection accuracy in the control plane, extracting the 10 most significant features for DDoS attack detection.

2) An LLM-based approach utilizing BERT, RoBERTa, and F-Net models was implemented for DDoS attack detection in SDN, employing their contextual learning and adaptive reasoning capabilities to enhance detection accuracy.

3) A detailed evaluation of the effectiveness of the proposed method is conducted, comparing its accuracy and efficiency against state-of-the-art detection techniques.

The paper is structured as follows in the subsequent sections. Section 2 explores relevant research studies in the field. Section 3 describes the proposed methodology, including the model framework and algorithmic approach. Section 4 presents the experimental outcomes and performance analysis. Finally, Section 5 concludes the study by summarizing key findings, discussing their significance, and suggesting future research directions.

2 Related Work

In article [4], LLMs such as GPT-3.5, GPT-4, and Ada were evaluated for DDoS attack detection in IoT-based SDN environments. Using CICIDS 2017 and the Urban IoT Dataset, LLMs achieved 90% accuracy with few-shot learning and up to 96% with fine-tuning, outperforming traditional multi-layer perceptron (MLP) models. In article [5], LLMs such as Llama2 and GPT-2 were evaluated for DDoS attack detection in large-scale network environments. Using CIC-DDoS2019 and real-world ISP NetFlow traces, DoLLM, an LLM-based model, demonstrated strong detection performance by leveraging semantic representation learning. The model achieved an F1 score improvement of up to 33.3% in zero-shot detection scenarios and at least 20.6% in real ISP traces. The authors of [6] have proposed a DDoS detection approach utilizing three SDN-specific datasets and deep learning techniques, including Multi-Layer Perceptron, Convolutional Neural Network, and Long Short-Term Memory(LSTM), where LSTM demonstrated better performance in terms of accuracy and loss.

The authors of [7], HuntGPT is introduced as an LLM-based anomaly detection system that integrates machine learning and Explainable AI (XAI) for intrusion detection. Using the KDD99 dataset, a Random Forest classifier was trained and combined with SHAP and LIME frameworks to enhance model transparency. Additionally, GPT-3.5 Turbo was integrated to improve user interaction and threat interpretation. The system was evaluated using Certified Information Security Manager (CISM) Practice Exams, achieving success rates between 72% and 82.5%, demonstrating its effectiveness in cybersecurity decision-making and automated threat analysis. The framework from [8], utilizes LLMs, specifically

GPT-3.5 Turbo, to preprocess network data from IoT23, NSL-KDD, Litnet2020, and CICIoT2023 datasets, converting it into LLM-compatible formats for fine-tuning with an F1-score of 0.952.

In article [9], the ShieldGPT framework using CIC-DoS2017 and CIC-DDoS2019 datasets to generate explanations for attack behaviors and provide mitigation strategies. The authors of [10], have proposed an approach that fine-tunes Llama 2 using QLoRA and Proximal Policy Optimization (PPO) to enhance detection efficiency. The model was evaluated on CIC-IDS2017, achieving 99.23% accuracy, demonstrating its effectiveness in real-time DDoS attack detection while outperforming supervised learning approaches. In [11], an efficient DDoS detection approach for SDN is proposed using multi-feature selection and ensemble learning. In [12], a hybrid deep learning model is proposed for DDoS attack detection in SDN, integrating Consensus-Based Feature Selection (CBFS) with CNN-LSTM architecture. The model enhances detection by utilizing CNN for spatial feature extraction and LSTM for temporal pattern recognition, improving accuracy.

In article [13], the UNSW-NB15 dataset was employed to fine-tune an LLM using Low-Rank Adaptation (LoRA) to enhance domain-specific knowledge extraction. By leveraging knowledge distillation, the LLM's learned representations were effectively transferred to a lightweight anomaly detection model for improved efficiency. The student model, trained through knowledge distillation, achieved superior performance, recording a macro-precision of 0.91, macro-recall of 0.88, and macro-F1 score of 0.87. In comparison, the general training model, which lacked knowledge distillation, performed less effectively, attaining a macro-precision of 0.79, macro-recall of 0.74, and macro-F1 score of 0.72.

3 Proposed Method

This section presents the detailed design of the proposed system, its feature importance, the collection of the training dataset used for training the model, and finally, the LLM algorithms for classifying the traffic.

The proposed system integrates a multi-feature selection mechanism with LLM-based detection using F-Net to enhance DDoS detection in SDN. The approach is validated using the InSDN dataset and Mininet emulation, demonstrating high accuracy and efficiency in identifying network anomalies represented in Fig.1. Algorithm 1 presents a novel feature extraction method focused on identifying the 10 most relevant features from an initial set of 83. It integrates three selection techniques: SelectKBest, ANOVA F-value scoring, and feature importance derived from a Random Forest Classifier. By synthesizing these methods, the approach enhances both detection accuracy and model efficiency. This systematic approach ensures that only key attributes are retained, boosting anomaly detection performance in SDN environments. The selected features are represented in Table 1.

The proposed algorithm 2 utilizes the F-Net model to detect DDoS attacks in network traffic by following a structured process involving model initializa-

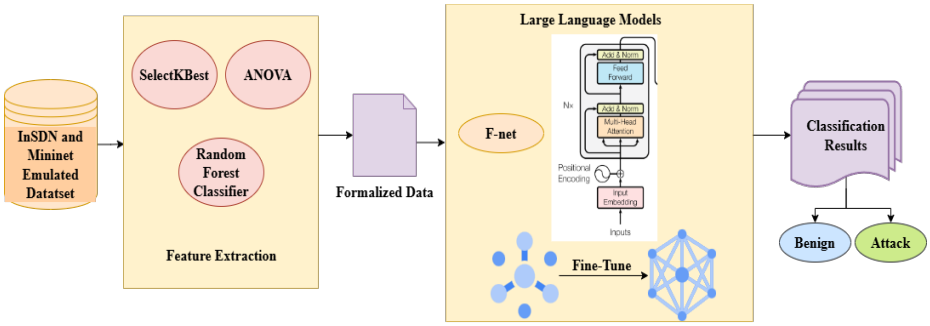

Fig. 1. System Architecture for Proposed Methodology

Algorithm 1 Optimized Feature Selection Using SelectKBest, ANOVA, and Random Forest

Input: Dataset D, Features $X = 83$, Target y
Output: Top 10 Selected Features
Load dataset D, extract $X \leftarrow D$.drop('Label'), $y \leftarrow D$['Label']
Initialize $selected_features_list \leftarrow []$
Define selection methods: {SelectKBest, ANOVA, RandomForest}
for method in methods **do**
    Apply method to X, y and extract top 20 ranked features
    Append selected features to $selected_features_list$
end for
$all_selected \leftarrow$ concatenate($selected_features_list$)
$final_features \leftarrow$ top 10 most frequently selected features

tion, data preparation, training, evaluation, and real-time detection. Initially, the pre-trained F-Net model and tokenizer are loaded to ensure compatibility with network-based data. To improve generalization, an optimal dropout rate is set, and the model is compiled using the Adam optimizer along with binary cross-entropy loss to enhance classification performance.

Table 1. Top 10 selected features for DDoS attack detection

Sl. No	Feature Name	Description
1	Source IP	Originating IP address of the packet
2	Destination IP	Target IP address receiving the packet
3	Protocol Type	Communication protocol
4	Packet Length StdDev	Variation in packet sizes within a flow
5	Flow Identifier	Unique identifier assigned to each data flow
6	Reverse Packet Length Mean	Average packet size in the reverse direction
7	Packet Length Variance	Fluctuation in packet sizes within a traffic flow
8	Source Port	Port number utilized by the sender
9	Reverse Segment Average Size	Mean size of segments in the reverse direction
10	Reverse Packet Length StdDev	Standard deviation of packet lengths in reverse flow

In the preprocessing step, numerical values are changed to string format to align with the tokenizer's requirements. The F-Net tokenizer processes the input using padding and truncation, while attention masks are generated to improve sequence interpretation. Additionally, minor label noise is introduced to increase model robustness against variations in data.

Algorithm 2 F-Net Model for DDoS Attacks Classification

Input: Preprocessed dataset $selected_features_df$ with features and labels
Output: Trained F-Net model, and real-time traffic classification
Initialize the model:
Load the pre-trained F-Net model and tokenizer
Adjust dropout rate for better generalization
Compile the model using the Adam optimizer and binary cross-entropy loss
Preprocess the dataset:
Convert numerical features into string format for compatibility
Tokenize data with padding and truncation using the F-Net tokenizer
Generate attention masks for input sequences
Introduce minor label noise for robustness
Train the model:
Train the model for *epochs* iterations on X_{train} and y_{train}, validating on X_{test} and y_{test} while logging epoch progress.
Evaluate and Save the Model:
Compute accuracy, precision, recall, and F1-score
Print evaluation results
Save the trained model and tokenizer
Real-Time Traffic Classification:
Load the saved model for inference
Tokenize incoming network traffic data
Predict and classify traffic as Normal or DDoS Attacks

During training, the F-Net model is trained for multiple iterations using a training dataset, with periodic validation on a test dataset to assess performance. The training process is continuously monitored to track improvements. After training, evaluation of the model is performed using common metrics, including accuracy, precision, recall, and F1-score. The trained model and tokenizer are then saved for later use. For real-time classification, the saved model is deployed to analyze incoming network traffic from Mininet. The tokenizer processes new traffic data, and the model predicts whether the observed activity is normal or associated with a DDoS attack. This systematic approach ensures efficient detection of malicious network behavior, enhancing security in real-world applications.

4 Results and Discussion

The results and discussion section assesses the performance of the proposed multi-feature selection and LLM-based detection approach using F-Net for DDoS detection in SDN. The performance analysis is conducted on the InSDN dataset and Mininet-emulated traffic, comparing F-Net, BERT, and RoBERTa across key performance indicators such as accuracy, F1-score, evaluation loss, and runtime efficiency.

Figure 2 presents a comparative analysis of the accuracy of three LLMs—BERT, RoBERTa, and F-Net—on two datasets: InSDN and Mininet-emulated traffic. The results highlight that F-Net achieves the highest accuracy, recording 99% on InSDN and 99.33% on Mininet, outperforming the other models compared to BERT attains 94.5% accuracy on InSDN and 95.2% on Mininet, while RoBERTa achieves 96.8% on InSDN and 97.1% on Mininet. The superior performance of F-Net using Fourier Transform-based processing, which enhances feature extraction and enables precise DDoS attack detection with limited training data. Figure 3 illustrates the F1-score comparison of three LLMs on InSDN and Mininet-emulated datasets. The results indicate that F-Net demonstrates the highest F1-score, achieving 0.98 on InSDN and 0.987 on Mininet, signifying its robust detection capability in identifying DDoS attacks in SDN.

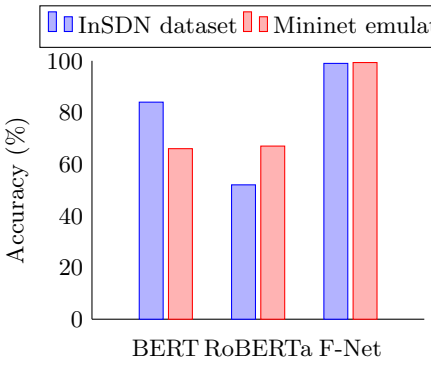

Fig. 2. Accuracy of proposed LLM's

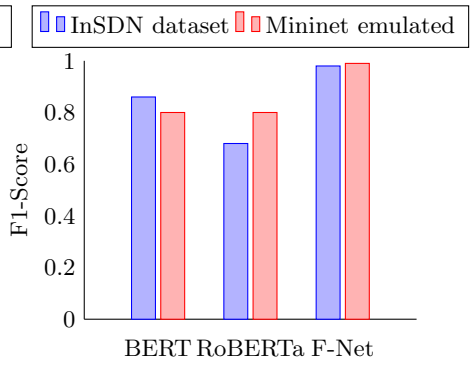

Fig. 3. F1-Score of LLM's

Figure 4 presents an evaluation loss analysis of the performance of three models in two datasets for the BERT, RoBERTa, and F-Net models. Better model performance is indicated by a lower evaluation loss. According to the graph, F-Net is the most effective of the three considering it has the lowest loss. Figure 5 showcases the processing time analysis of three LLMs—BERT, RoBERTa, and F-Net—on the InSDN dataset and Mininet-emulated traffic. The results demonstrate that F-Net delivers the fastest execution, with 2.92 seconds on InSDN and 4.59 seconds on Mininet, highlighting its computational efficiency compared to

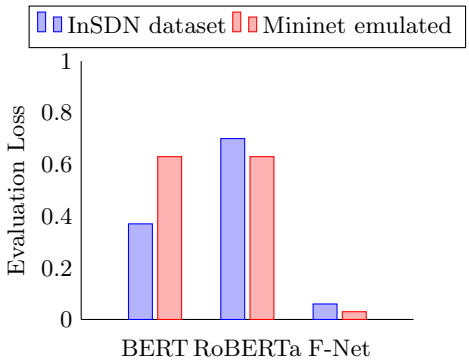

Fig. 4. Evaluation Loss of LLM's

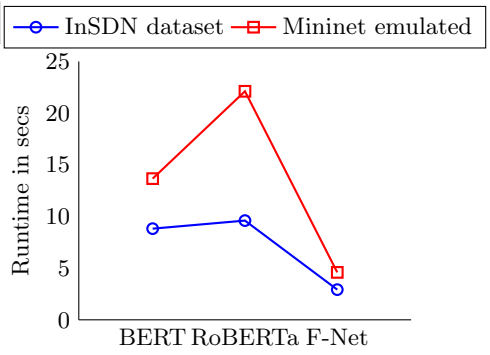

Fig. 5. Runtime (secs) of LLM's

BERT processes data in 8.82 seconds on InSDN and 13.66 seconds on Mininet, while RoBERTa records the highest runtime, taking 9.6 seconds on InSDN and 22.11 seconds on Mininet, indicating its greater computational overhead.

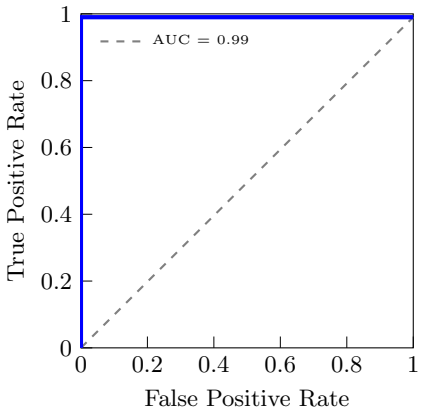

Fig. 6. ROC Curve of F-Net Model

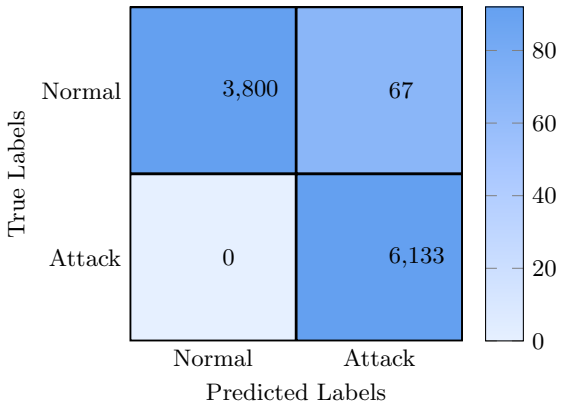

Fig. 7. Confusion Matrix of F-Net Model

Figure 6 presents the Receiver Operating Characteristic (ROC) curve for the F-Net model, evaluated on the Mininet-emulated dataset. The ROC curve highlights the trade-off between the True Positive Rate (TPR) and False Positive Rate (FPR), highlighting the model's proficiency in differentiating between legitimate and malicious traffic in SDN. The F-Net model demonstrates near-perfect classification performance, achieving an Area Under the Curve (AUC)

score of 0.99, indicating high detection accuracy with minimal false positives.

Figure 7 displays the confusion matrix of the F-Net model, showcasing its classification ability to distinguish normal traffic from attack traffic within Mininet emulated. The matrix consists of four key values: True Positives (6133), indicating precisely recognized attacks; True Negatives (3800), representing correctly identified legitimate traffic; False Positives (67), where benign traffic was misclassified as an attack; and False Negatives (0), signifying that no attacks were incorrectly labeled as normal traffic.

The incorporation of a multi-feature selection technique is the aspect that makes the proposed DDoS detection framework in SDN employing LLMs like F-Net, BERT, and RoBERTa so efficient. F-Net model exhibits considerably improved detection performance, with 99% accuracy in InSDN and 99.33% accuracy in Mininet datasets, compared to [4], which obtained up to 96% accuracy. The precision, recall, and F1-score of the proposed model are better compared to [5] and[7]. Efficiency is improved, and computational overhead is reduced by including by using the Multi-Feature selection approach and F-Net provides optimal results for real-time detection in dynamic SDN systems due to its minimized evaluation loss.

5 Conclusion and Future Scope

We have developed an advanced framework for detecting DDoS attacks in SDN by integrating LLMs with a multi-feature selection approach. The proposed methodology utilized F-Net, BERT, and RoBERTa to analyze network traffic, employing SelectKBest, ANOVA F-value scoring, and Random Forest-based feature ranking to extract the 10 most significant attributes from an initial set of 83 features. The experimental analysis demonstrated that F-Net outperformed BERT and RoBERTa, achieving 99% accuracy on the InSDN dataset and 99.33% on the Mininet-emulated dataset, making it a highly efficient solution for real-time DDoS attack detection. Additionally, the low evaluation loss and reduced computational overhead of F-Net further reinforced its capability to accurately classify network traffic while maintaining high efficiency. The findings of this study validate the effectiveness of LLM-driven cybersecurity solutions, highlighting their potential to enhance network security in SDN environments.

Future research can focus on scaling the LLM-based DDoS detection framework to handle high-traffic SDN environments efficiently. Additionally, integrating real-time mitigation strategies with detection can enable automated security responses, enhancing proactive threat defense in dynamic networks.

References

1. Alhijawi, B., Alazzam, M. B., Gupta, B. B., Al-Hazaimeh, O. M., and Almiani, M., "A Survey on DoS/DDoS Mitigation Techniques in SDNs: Classification, Compari-

son, Solutions, Testing Tools and Datasets," *Computers and Electrical Engineering*, vol. 99, art. no. 107706, Elsevier, 2022.
2. Bahashwan, A. A., Ullah, F., Albasir, H. M., Alshmrany, S., and Alzahrani, B., "A Systematic Literature Review on Machine Learning and Deep Learning Approaches for Detecting DDoS Attacks in Software-defined Networking," *Sensors*, vol. 23, no. 9, art. no. 4441, MDPI, 2023.
3. Bui, M.-T., Boffa, M., Valentim, R. V., Navarro, J. M., Chen, F., Bao, X., Houidi, Z. B., and Rossi, D., "A Systematic Comparison of Large Language Models Performance for Intrusion Detection," *Proceedings of the ACM on Networking*, vol. 2, no. CoNEXT4, Article 22, pp. 1–23, ACM, December 2024.
4. Guastalla, M., Li, Y., Hekmati, A., Krishnamachari, B., "Application of Large Language Models to DDoS Attack Detection," *Security and Privacy in Cyber-Physical Systems and Smart Vehicles*, vol. 485, pp. 83–99, Springer, Heidelberg, 2023.
5. Li, Q., Zhang, Y., Jia, Z., Hu, Y., Zhang, L., Zhang, J., Xu, Y., Cui, Y., Guo, Z., Zhang, X., "DoLLM: How Large Language Models Understanding Network Flow Data to Detect Carpet Bombing DDoS," *arXiv preprint arXiv:2405.07638*, 2024. https://arxiv.org/abs/2405.07638
6. Kachavimath, A. V., Narayan, D. G., "Distributed Denial of Service Attacks Detection Using Deep Learning in Software Defined Network," *Proceedings of the 2022 13th International Conference on Computing Communication and Networking Technologies (ICCCNT)*, pp. 1–5, IEEE, October 2022.
7. Ali, T., Kostakos, P., "HuntGPT: Integrating Machine Learning-Based Anomaly Detection and Explainable AI with Large Language Models (LLMs)," *arXiv preprint arXiv:2309.16021*, 2023. https://arxiv.org/abs/2309.16021
8. Zhou, H., Huang, X., Deng, L., "Enhancing Network Traffic Classification with Large Language Models," *Proceedings of the 2024 IEEE International Conference on Big Data (Big Data)*, pp. 7282–7291, IEEE, 2024.
9. Wang, T., Xie, X., Zhang, L., Wang, C., Zhang, L., Cui, Y., "ShieldGPT: An LLM-based Framework for DDoS Mitigation," *Proceedings of the 8th Asia-Pacific Workshop on Networking (APNet 2024)*, pp. 108–114, ACM, 2024.
10. Mahmoodi, M., Jameii, S. M., "Utilizing Large Language Models for DDoS Attack Detection," *Proceedings of the 2024 OPJU International Technology Conference (OTCON) on Smart Computing for Innovation and Advancement in Industry 4.0*, pp. 1348–1353, IEEE, 2024.
11. Kachavimath, A. V., G, N. D., "An Efficient DDoS Attack Detection in SDN using Multi-Feature Selection and Ensemble Learning," *Procedia Computer Science*, vol. 252, pp. 241–250, Elsevier, 2025.
12. Kachavimath, A. V., G, N. D., "A Hybrid Deep Learning Model with Consensus-Based Feature Selection for DDoS Attacks Detection in SDN," *Procedia Computer Science*, vol. 252, pp. 643–652, Elsevier, 2025.
13. Yang, Y., Tian, B., Yu, F., He, Y., "An Anomaly Detection Model Training Method Based on LLM Knowledge Distillation," *Proceedings of the 2024 International Conference on Networking and Network Applications (NaNA)*, pp. 472–477, IEEE, 2024.

PassPhrase Authentication: A Secure and User-Friendly Multi-Factor Authentication System Using Phrase and Gesture Integration

Amit Kachavimath[1][0000−0002−8917−8678], Ayush Chugani[2], Satish Vaishyar[3], Niyati Gogri[4], and Misbah Falak[5]

[1,2,3,4,5]KLE Technological University, Hubballi, Karnataka, India
[1]amitk@kletech.ac.in, [2]ayushchugani@gmail.com, [3]12vsatish1@gmail.com, [4]niyatigogri05@gmail.com, [5]misbahfalak2306@gmail.com

Abstract. The escalation of cyber threats in the digital landscape, including brute-force intrusions, phishing tactics, and keystroke logging, has significantly heightened risks to vital online assets. Exploiting weaknesses in conventional authentication frameworks, these attacks result in unauthorized data breaches, financial exploitation, and compromised personal or institutional records. The growing complexity of such threats highlights the necessity for resilient, user-friendly, and advanced authentication mechanisms. This research introduces PassPhase Authentication, a novel multi-factor security approach designed to enhance protection while maintaining ease of access. The framework integrates user-generated passphrases, interactive image-based gestures, and click-point verification to create a personalized and intuitive login process. By incorporating predefined visual markers, dynamic selection patterns, and coordinate-based validation, the system effectively counters brute-force infiltration, phishing exploits, and keystroke monitoring. The methodology relies on randomized visual stimuli, encrypted data exchange, and cryptographic safeguards, including salted hashing, to uphold data confidentiality. Experimental findings confirm that the proposed method ensures a balance between stringent security measures and user convenience, offering a viable enhancement over conventional verification systems. This study contributes to the advancement of a secure, accessible digital identity validation framework.

Keywords: Passphrase Authentication · Multi-Factor Security · Interactive Gestures · User-Friendly Authentication

1 Introduction

In the dynamic realm of digital advancements, the demand for secure and user-friendly authentication has never been more critical. Conventional authentication models, primarily dependent on static username-password pairs, are proving insufficient against evolving cyber threats such as brute-force intrusions, phishing exploits, and keystroke logging. The escalating sophistication and recurrence of

these attacks highlight the urgent need for innovative authentication frameworks that effectively integrate security with ease of use, ensuring resilience against unauthorized access attempts[1].

The PassPhase Authentication System, introduced in this study, presents an innovative multi-factor authentication framework that combines user-generated passphrases with interactive image-based gestures and coordinate-driven click sequences. By integrating these dynamic components, the system offers a personalized and seamless authentication experience, strengthening defenses against unauthorized access. Designed for adaptability and scalability, this approach effectively overcomes the limitations of conventional authentication techniques, ensuring enhanced security for digital interactions[2].

The proposed method explores the distinctive features of the PassPhase Authentication System but also examines its practical application and effectiveness in real-world scenarios. The design balances stringent security measures with a seamless user experience, offering a viable and scalable alternative to traditional authentication mechanisms. This research aims to bridge the gap between security and accessibility, contributing to the ongoing development of secure, user-friendly authentication solutions for modern digital ecosystems.

The main findings and contributions of this paper are as follows:

- The PassPhase Authentication System enhances security against brute-force attacks, phishing attempts, and keylogging by integrating user-defined pass phrases with interactive image-based gestures and dynamic click patterns.
- This authentication approach delivers a frictionless user experience by merging memorable passphrases with intuitive graphical interactions, ensuring both ease of access and robust security.
- Designed for scalability and flexibility, the system serves as a secure, user-centric alternative to traditional authentication mechanisms, addressing the evolving challenges of digital security.

The structure of this paper is as follows: Section II examines existing research on authentication systems. Section III details the methodology underlying the proposed framework. Section IV discusses the experimental setup along with the obtained results, while Section V provides concluding remarks and outlines potential directions for future research.

2 Literature Review

The growing complexity of cybersecurity threats, such as brute-force intrusions, phishing schemes, and keylogging techniques, highlights the limitations of traditional authentication methods. To mitigate these risks, recent advancements in authentication focus on multi-factor approaches, interactive user engagement, and context-aware intelligence. These developments strive to strengthen security without compromising usability, ensuring scalable and robust protection against evolving cyber threats.

In [3], A Frictionless and Secure User Authentication (FSUA) system is introduced for web-based applications, utilizing behavioral profiling based on attributes like login time, device location, and browser type. The framework integrates multi-factor authentication, combining one-time passwords (OTPs) and certificate-based mechanisms, while leveraging an analytical engine for real-time risk assessment. Experimental findings indicate that the system achieves a 10% reduction in authentication delays, a 7% improvement in response times, and an 11% decrease in memory consumption compared to traditional methods, offering enhanced security and seamless usability. The authors of [4] introduce a hybrid authentication framework is introduced, combining textual and graphical elements to enhance both security and user experience. The approach features two distinct modes: Easy Login, designed for convenience, and Secure Login, which ensures stronger protection through randomized password components and visual memory cues. The system was evaluated using data from 154 participants, assessing its resistance to security threats such as brute-force attacks and phishing schemes. A comparative study against eight conventional authentication methods revealed superior memorability and robustness, with Secure Login achieving an average authentication time of 40.16 seconds and demonstrating higher accuracy in protecting user credentials.

In [5], the study presents a Reformation-Based password scheme designed to strengthen security and improve usability by implementing dynamic password transformations using numeric codes instead of conventional passwords. This method eliminates reliance on mental calculations or external devices, enhancing user convenience while safeguarding against brute-force intrusions and shoulder-surfing attacks. Experimental evaluation with 150 participants confirmed superior security and usability compared to traditional approaches, ensuring a robust and efficient client-server authentication mechanism. In [6], the study introduces an Event-Driven authentication framework that utilizes Bluetooth-based proximity verification combined with cryptographic handshakes to secure critical operations. This method effectively mitigates replay attacks and Man-in-the-Middle intrusions, ensuring enhanced security while maintaining user convenience. In [7], the study presents a MAC Address-Based Access Control system that strengthens login security by associating IP addresses with MAC addresses through ARP (Address Resolution Protocol) mapping. This method effectively prevents unauthorized access, even if credentials are compromised, while offering resistance against dictionary attacks and shoulder surfing attempts, ensuring restricted administrator page access to authorized devices only.

The authors of [8] have proposed a DDoS detection approach utilizing three SDN-specific datasets and deep learning techniques, including Multi-Layer Perceptron, Convolutional Neural Network, and Long Short-Term Memory(LSTM), where LSTM demonstrated better performance in terms of accuracy and loss. In [9], the authors present HandPass, a continuous authentication system using hand vibration biometrics captured by smartphone accelerometers. Achieving 98.36% accuracy, the system ensures security and usability, effectively resisting impersonation and blind attacks during natural user interactions. In [10], the

authors present a responsive web application for GPA calculation, integrating authentication and authorization mechanisms. The methodology uses Django for backend processing, OTP-based two-step verification for secure user registration, and SQLite3 for data storage, ensuring user-friendly and efficient academic tools for students. The authors of [11] propose a user authentication model integrating Context-Based Fingerprinting with the random forest algorithm to enhance API security. Using a dataset of 19,200 records, the model achieved better accuracy, effectively detecting anomalous login attempts while ensuring robust API-level security.

In [12], the authors propose proactive measures for login page security, including IP-based restrictions, two-factor authentication, and automated verification codes. These mechanisms effectively defend against brute force and dictionary attacks, ensuring secure user access. The authors of [13], propose a privacy-preserving, device-centric, and attribute-based authentication architecture as an alternative to traditional passwords. The approach integrates federated login, cryptographic credentials, and behavioral authentication, achieving enhanced security, user privacy, and compliance with NIST assurance standards while addressing challenges like identity fragmentation and password overload. In [14], the authors propose a novel Wi-Fi-based environmental continuous two-factor authentication system leveraging machine learning. By analyzing beacon frame characteristics and RSSI values, the system achieves 92.4% accuracy. In [15], the authors analyze OAuth and OpenID for robust identity verification and data protection. The study discusses the advantages, limitations, and implementation challenges of these methods in enhancing cybersecurity across diverse applications.

The authors of [16] focused on detecting anomalous network traffic to address the increasing complexity of Distributed Denial of Service (DDoS) attacks. The proposed methodology utilizes machine learning techniques, specifically K-Nearest Neighbor (KNN) and Naïve Bayes classifiers, to analyze statistical features of network traffic and identify malicious deviations. By extracting high-level traffic patterns, the model effectively detects DDoS attacks and outperforms traditional approaches. The study highlights the evolving nature of cyber threats and emphasizes the need for adaptive security solutions. The summary of the literature review reveals notable gaps in the field of secure authentication systems. Although progress has been made in multi-factor methods, the absence of real-time adaptive strategies to counter advanced threats like adversarial attacks and spoofing remains evident. Additionally, most studies prioritize either security or user experience without achieving an optimal balance between the two. The scalability of proposed methods for diverse environments, particularly in IoT and cloud applications, is insufficiently addressed. Furthermore, limited focus on energy efficiency and computational costs highlights a need for more sustainable and practical evaluations. These gaps present opportunities for advancing authentication frameworks to ensure comprehensive protection and efficiency.

3 Proposed Methodology

This section presents the detailed design of the proposed PassPhase Authentication System, outlining its core components and interactive authentication features. It elaborates on the stepwise integration of user credentials, including password verification, phrase selection, and gesture-based interactions using image click patterns and coordinate validation. The framework emphasizes feature importance by combining personalized user inputs with spatial interaction to enhance authentication security, as mentioned in Algorithm 1.

Algorithm 1 Enhanced Multi-Factor Authentication (MFA) System

```
Input: User credentials (username, password), phrase, click patterns, coordinates
Output: Authentication status (Granted/Denied)
Accept username and password
Hash password using SHA-256 and compare with stored hash
if Password match then
    Prompt user to select their registered phrase
    if Phrase match then
        Display image associated with phrase
        Prompt user to perform registered click pattern
        Validate click pattern and coordinates (within 10-pixel tolerance)
        if Incorrect clicks exceed 3 attempts then
            Deny access and log out
        else
            if Login fails 3 consecutive times then
                Send alphanumeric OTP to registered email
                if OTP is valid then
                    Allow password reset and retry login
                else
                    Deny access
                end if
            end if
            Grant access if all validations are successful
        end if
    else
        Deny access
    end if
else
    Deny access
end if
```

3.1 Password Verification

At the initial stage, users enter their credentials, including username and password. The system stores only the hashed passwords using the SHA-256 algorithm

to safeguard against breaches. During login, the entered password's hash is compared with the stored hash. A match permits access to the next layer, while mismatches deny entry.

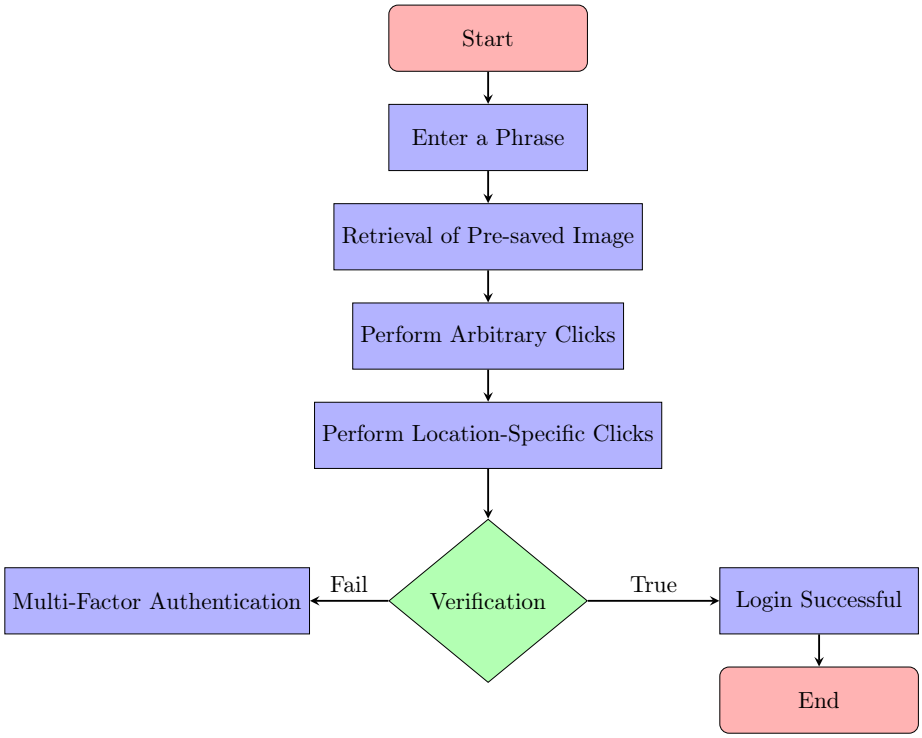

Fig. 1. Flowchart for Multi-Factor Authentication Process

The flowchart illustrates the process of a multi-factor authentication (MFA) system. It begins with the user entering a predefined phrase, followed by the retrieval of a pre-saved image associated with the phrase. The user then performs two interactive tasks: arbitrary clicks on the image and location-specific clicks at predefined coordinates. Upon verifying the provided inputs, the system grants access by displaying a "Login Successful" message, finalizing the authentication process. If verification fails, the user is redirected to the multi-factor authentication module for additional validation. This layered security approach strengthens protection against unauthorized access while ensuring a seamless and user-friendly experience.

3.2 Password Verification

During registration, users create a unique phrase, which is securely stored as part of their authentication credentials. During login, they must accurately select

their registered phrase to proceed. Once verified, the system presents an image associated with the chosen phrase, serving as the next authentication step in the process.

3.3 User Interaction

In the proposed authentication framework, users engage with a displayed image through two sequential steps: Click Count Verification and Coordinate-Based Clicks. Initially, users replicate pre-registered click patterns on the image, allowing authentication to proceed only if the inputs match the stored sequence. Following this, users must accurately select predefined coordinates within the image, which are hashed and securely stored for validation. To enhance usability, the system permits a 10-pixel tolerance radius, accommodating minor variations in user clicks. If authentication fails after three consecutive incorrect attempts, an automatic logout is triggered to protect user data and prevent unauthorized access. This dual-layered interaction reinforces security by integrating dynamic user engagement with precise input validation.

3.4 Multi-Factor Authentication

If multiple unsuccessful login attempts occur, users are redirected to the Multi-Factor Authentication (MFA) page, where they must confirm their identity using an alphanumeric one-time password (OTP) sent to their registered email. This method enhances security by leveraging alphanumeric OTPs, which provide 2,177 times more possible combinations than purely numeric OTPs, significantly increasing resistance to unauthorized access and brute-force attacks.

The proposed authentication framework delivers a secure yet user-friendly multi-factor authentication system, striking an optimal balance between protection and usability. By integrating layered security measures—including password verification, phrase selection, click-pattern interactions, and coordinate-based validation—the system ensures comprehensive defense against unauthorized access. Additionally, hashed credentials and alphanumeric OTPs enhance resilience against cyber threats, strengthening authentication security while maintaining a seamless experience for legitimate users. Designed for modularity and scalability, this adaptive framework is well-suited for diverse application environments, addressing the growing challenges of digital security with an efficient and practical solution.

4 Results and Discussion

The results and discussion section critically examines the effectiveness of the proposed MFA framework through an in-depth performance analysis. Key parameters such as security strength, usability, accuracy, and system resilience were evaluated across varying conditions. Findings confirm the framework's capability

to counteract security threats, including brute-force attacks, phishing, and unauthorized access, while ensuring a user-friendly experience. A comparative study with existing authentication models reveals notable improvements in login accuracy, response time, and error tolerance. This section also explores the practical implications of the results, addressing both real-world deployment challenges and potential applications. The insights presented validate the proposed solution's viability in meeting the growing demands for secure and seamless digital authentication systems.

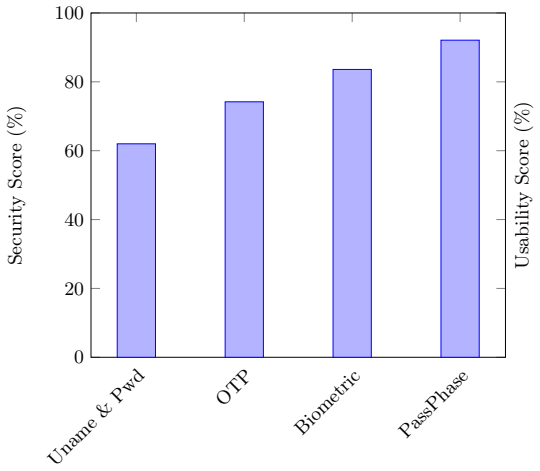

Fig. 2. Security Effectiveness of Authentication Methods

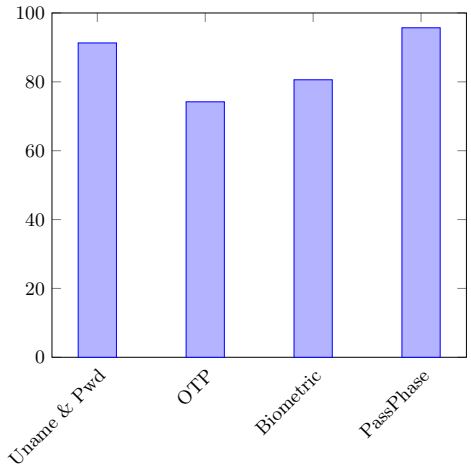

Fig. 3. Usability Score Comparison of Authentication Methods

Figure 2 compares the security scores of four different authentication methods: Username & Password, OTP, Biometric, and PassPhase. The graph shows that the PassPhase method has the highest security score at 92.1%, followed by Biometric authentication at 83.6%. OTP comes in at 74.2%, and Username & Password ranks the lowest with 62%. This demonstrates that traditional password-based systems, while still commonly used, are less secure compared to newer, more advanced methods like Biometric and PassPhase. The PassPhase method, which integrates a passphrase with interactive gestures, offers a significant improvement in security effectiveness by mitigating risks like brute-force attacks and keylogging.

Figure 3 evaluates the usability of the same authentication methods. The PassPhase method achieves the highest usability score at 95.7%, closely followed by Username & Password with 91.3%. Biometric authentication comes next at 80.6%, while OTP has the lowest usability score at 74.2%. These results indicate that while traditional password-based methods and biometric authentication are user-friendly, the PassPhase method strikes a balance between both

security and usability, making it an ideal solution for modern authentication needs. The high usability of PassPhase demonstrates its user-friendliness, despite its advanced security features, showing that complex security mechanisms can be implemented without compromising ease of use. The proposed MFA system was rigorously tested against various attack scenarios, including brute-force intrusions and phishing attempts, using industry-standard security tools. The results confirm the system's strong resilience against unauthorized access, primarily due to its layered authentication approach, incorporating hashed passwords and coordinate-based verification to counteract brute-force attacks. Additionally, phrase selection and alphanumeric OTPs enhance protection against phishing attempts, as they require unique, user-specific inputs that are challenging to duplicate. Compared to traditional authentication methods, the system consistently demonstrates superior security and usability, validating its effectiveness in mitigating modern cybersecurity threats.

5 Conclusion

The PassPhase Authentication system effectively integrates multi-factor authentication with a user-centric approach, addressing key security concerns such as brute-force attacks and phishing attempts. By combining layered authentication techniques, including passphrases, graphical gestures, and coordinate-based click patterns, the framework delivers a robust yet intuitive solution, ensuring an optimal balance between security and usability. Experimental evaluations confirm its better performance over traditional authentication models, demonstrating enhanced resilience against unauthorized access while maintaining user convenience. This methodology establishes a new standard for secure authentication systems in modern digital environments.

The future advancements could incorporate real-time adaptive security measures to counter emerging threats, such as deepfake biometrics and adversarial attacks. Additionally, blockchain integration and federated identity management could further enhance scalability and system-wide security.

References

1. S. W. Shah and S. S. Kanhere, "Recent Trends in User Authentication – A Survey," *IEEE Access*, vol. 7, pp. 112505–112519, 2019
2. X. Wang, Z. Yan, R. Zhang, and P. Zhang, "Attacks and defenses in user authentication systems: A survey," *Journal of Network and Computer Applications*, vol. 188, p. 103080, 2021
3. R. F. Olanrewaju, B. U. I. Khan, M. A. Morshidi, F. Anwar, and M. L. B. M. Kiah, "A Frictionless and Secure User Authentication in Web-Based Premium Applications," *IEEE Access*, vol. 9, pp. 129240–129255, 2021.
4. S. Z. Nizamani, S. R. Hassan, R. A. Shaikh, E. A. Abozinadah, and R. Mehmood, "A Novel Hybrid Textual-Graphical Authentication Scheme With Better Security, Memorability, and Usability," *IEEE Access*, vol. 9, pp. 51294–51312, 2021.

5. M. Ali, A. Baloch, A. Waheed, M. Zareei, R. Manzoor, H. Sajid, and F. Alanazi, "A Simple and Secure Reformation-Based Password Scheme," *IEEE Access*, vol. 9, pp. 11655–11674, 2021.
6. K. Marshall, T. Cantido, J. Case, L. Nguyen, and H. El-Razouk, "An Event-Driven Authentication Approach for Mediation of User Actions," *2021 IEEE 12th Annual Information Technology, Electronics and Mobile Communication Conference (IEMCON)*, pp. 534–540, 2021.
7. B. M. P. A. Alam, R. Septiasari, and A. Amiruddin, "Applying MAC Address-Based Access Control for Securing Admin's Login Page," *Proceedings of the 2019 International Conference on Electrical Engineering and Computer Science (EECSI)*, pp. 292–296, 2019.
8. Kachavimath, A. V., Narayan, D. G., "Distributed Denial of Service Attacks Detection Using Deep Learning in Software Defined Network," *Proceedings of the 2022 13th International Conference on Computing Communication and Networking Technologies (ICCCNT)*, pp. 1–5, IEEE, October 2022.
9. H. Cao, H. Jiang, K. Yang, S. Chen, W. Wu, J. Liu, and S. Dustdar, "Data-Augmentation-Enabled Continuous User Authentication via Passive Vibration Response," *IEEE Internet of Things Journal*, vol. 10, no. 16, pp. 14137–14151, 2023.
10. J. Muthiah, A. S. Lakshmi, D. Jahnavi, A. Rengarajan, and N. Chidambaram, "Design and Implementation of Authentication and Authorization Flow in a Responsive Web Application," *2023 2nd International Conference on Vision Towards Emerging Trends in Communication and Networking Technologies (ViTECoN)*, pp. 1–6, 2023
11. A. Al-Rumaim and J. D. Pawar, "Enhancing User Authentication: An Approach Utilizing Context-Based Fingerprinting With Random Forest Algorithm," *IEEE Access*, vol. 12, pp. 110850–110861, 2024
12. A. Bhadouria, R. Bathla, and G. Arora, "Fortifying Digital Frontiers: Enhancing Login Page Security Against Emerging Cyber Threats," *2024 11th International Conference on Reliability, Infocom Technologies and Optimization (ICRITO)*, pp. 1–6, 2024
13. K. Papadamou, S. Zannettou, B. Chifor, S. Teican, G. Gugulea, A. Caponi, A. Recupero, C. Pisa, G. Bianchi, S. Gevers, C. Xenakis, and M. Sirivianos, "Killing the Password and Preserving Privacy With Device-Centric and Attribute-Based Authentication," *IEEE Transactions on Information Forensics and Security*, vol. 15, pp. 2183–2193, 2020.
14. A. A. S. AlQahtani, T. Alshayeb, M. Nabil, and A. Patooghy, "Leveraging Machine Learning for Wi-Fi-Based Environmental Continuous Two-Factor Authentication," *IEEE Access*, vol. 12, pp. 13277–13289, 2024
15. A. Korchenko, S. Kazmirchuk, O. Kryvoruchko, O. Synichuk, M. Kostiuk, and R. Zakharov, "Methods of Security Authentication and Authorization into Informational Systems," *2020 IEEE 2nd International Conference on Advanced Trends in Information Theory (ATIT)*, pp. 270–274, 2020
16. A. V. Kachavimath, S. V. Nazare, and S. S. Akki, "Distributed Denial of Service Attack Detection using Naïve Bayes and K-Nearest Neighbor for Network Forensics," in *Proceedings of the 2020 2nd International Conference on Innovative Mechanisms for Industry Applications (ICIMIA)*, pp. 711–717, 2020

DDoS Attacks Detection using PSO Feature Selection and Classification using XGBoost in SDN

Amit Kachavimath[1], Sanjana A More[2], and Narayan D G[3]

[1,2]KLE Technological University, Hubballi, Karnataka, India
[1]amitk@kletech.ac.in, [2]sanjana.a.more3210@gmail.com,
[3]narayan_dg@kletech.ac.in

Abstract. SDN (Software-Defined Network) is a network architecture that separates the control and data planes, facilitating centralized control and dynamic management of network resources. Distributed Denial of Service (DDoS) attacks represent a critical challenge in SDN environments, as they flood the centralized controller with excessive malicious traffic. This overwhelms its computational resources and disrupts its ability to make accurate and timely network decisions. These attacks can result in network congestion, poor performance, and even network outages because SDN relies on a single controller to control traffic flow across the network. Metaheuristic algorithms, such as Particle Swarm Optimization (PSO), are optimization approaches that aim to find approximate solutions to complex problems that may not be susceptible to standard methods. This study evaluates PSO-based feature selection integrated with XGBoost classification for DDoS detection in SDN using the InSDN and Mininet datasets. The results demonstrate that XGBoost outperforms traditional classifiers, including Logistic Regression and Naïve Bayes, achieving over 99% accuracy, recall, and F1-score. The comparative analysis highlights XGBoost's superior performance in minimizing false positives and false negatives, ensuring higher detection reliability. The AUC score of 0.99 further confirms its robustness in distinguishing attack and benign traffic.

Keywords: DDoS Attacks · PSO · XGBoost.

1 Introduction

Network control can be centralized through the adoption of SDN, which separates the control plane from the data plane. SDN enhances scalability, security, and network performance by enabling constant real-time control over network traffic [1]. The resources of SDN controllers can be overloaded by Distributed Denial of Service (DDoS) attacks, which might lead to decreased performance or complete service disruption. Attackers may target the controller's main point of control and flood it with traffic, ultimately exhausting its processing power and preventing the processing of legitimate requests[2].

DDoS attacks attempt to interfere with regular operations by combining a target system, such as a network or server, with malicious traffic[3]. Since the SDN controller handles network traffic centrally, a DDoS attack might flood it with requests, causing delays or even network failure. This disruption could affect the SDN's capacity to effectively handle traffic flows, damaging the availability, security, and performance of the network. It works particularly well in cloud computing environments to manage large amounts of traffic and protect against DDoS attacks [4].

In the field of DDoS attack detection for InSDN and Mininet, the use of PSO and XGBoost provides an effective approach to optimize detection performance. By incorporating optimization with cutting-edge machine learning techniques, this strategy addresses real-world problems in contrast to general references to algorithm limitations. Improves flexibility to varying network conditions and prevents issues such as class imbalance and redundant data [5]. The key findings and contributions are as follows.

- Meta-heuristic PSO approach is better than the statistical methods by dynamically selecting relevant features, reducing noise, and enhancing feature subsets, leading to improved accuracy in DDoS attack detection.
- The combination of PSO and XGBoost ensures optimized feature selection, leading to better DDoS detection accuracy than traditional classifiers
- Evaluation of the proposed technique's effectiveness is performed, measuring its accuracy and efficiency in comparison to state-of-the-art detection methods for reliable threat identification.

The rest of the article is divided into the following sections. The summary of the relevant research is provided in Section 2. The suggested SDN, which uses a machine learning classifier and metaheuristic optimization for feature selection, is described in Section 3. Performance evaluation and implementation outcomes are presented in Section 4. The conclusions of the study are presented in Section 5.

2 Literature Review

The Literature Survey section provides a comprehensive overview of existing research related to DDoS attack detection in SDN. It highlights key methodologies, identifies limitations in current approaches, and establishes the foundation for the proposed framework. In [6], the researchers introduced a flow-based anomaly detection framework is proposed for detecting DDoS attacks in SDN, utilizing feature selection techniques The proposed technique utilizes Random Forest (RF) and Information Gain (IG) to extract relevant attributes from the CICIDS2018, CICIDS2017, and InSDN datasets. This optimized feature selection enhances the classification performance, achieving a high accuracy rate of 99.1% using the LSTM model.

In [7], the researchers introduced an ensemble method combining K-means clustering and the RF algorithm for DDoS attack detection in SDN. The approach first clusters network traffic using K-means to identify anomalies, followed by RF classification for precise attack detection. The experimental evaluation utilized both synthetic and real-world SDN traffic datasets, including CICIDS2017. The framework achieved a high accuracy of 99.12%, demonstrating its effectiveness in detecting malicious activities in SDN environments. In [8], the researchers introduced a refined approach utilizing the RF algorithm, incorporating hyperparameter optimization and recursive feature elimination for selecting the most relevant attributes. The dataset employed in this study includes 207,146 traffic flows with 83 distinct characteristics. In [9], authors have proposed a DDoS detection model for SDN using ensemble learning and advanced feature selection techniques on the InSDN dataset. By selecting the top 10 features, the model achieved 99.9% accuracy, validated through ROC curves and cross-validation.

In [10], the researchers introduced a hybrid SVM-KNN approach for identifying DDoS attacks in SDN environments. This methodology emphasizes the selection of five critical features from packet headers, followed by the application of the SVM-KNN model for training and classification. Using the Mininet emulator and Ryu controller, the dataset simulates both typical and attack scenarios. The proposed model achieved an accuracy of 97.36%, demonstrating its effectiveness in distinguishing malicious activities from legitimate network traffic. The authors of [11], introduced a dual-module approach for mitigating DDoS threats, addressing both low-rate and high-rate attacks. The first module applies the Alleviative Threat for TCAM (ATFT) algorithm to counter Slow-TCAM attacks, while the second leverages ensemble learning techniques to detect high-intensity DDoS intrusions. The framework achieved 99% accuracy and was validated using a Mininet simulation and evaluated on the CICDDoS2019 dataset. The authors of [12], proposed an anomaly-based detection system utilizing Principal Component Analysis (PCA) to assess network traffic entropy and identify irregularities. The approach involved extracting key features, including packet count and byte flow, to construct a dataset for machine learning models. Various classifiers were tested, with Support Vector Machine (SVM) achieving the highest accuracy of 97%, outperforming Decision Tree (DT) in detection performance.

The authors of [13], implemented In-band Network Telemetry (INT) for real-time switch state monitoring within a Spatial-Temporal Graph Convolutional Network (ST-GCN), representing the network as a graph structure. The dataset was generated through INT-based sampling, capturing key network state indicators. The detection framework utilizes both spatial and temporal features to assess the network state variations, enabling the identification of DDoS attack pathways with high precision. In article [14], the Rényi entropy method was employed to monitor network traffic at the SDN controller. The dataset was generated using the Mininet emulator and the Ryu controller, simulating both benign and malicious traffic patterns to enhance anomaly detection and security analysis in SDN.

3 Proposed Methodology

This section presents the detailed design of the proposed system, its feature importance, the collection of the training dataset used for training the model, and finally, the PSO with XGBoost algorithm for detection of DDoS attacks.

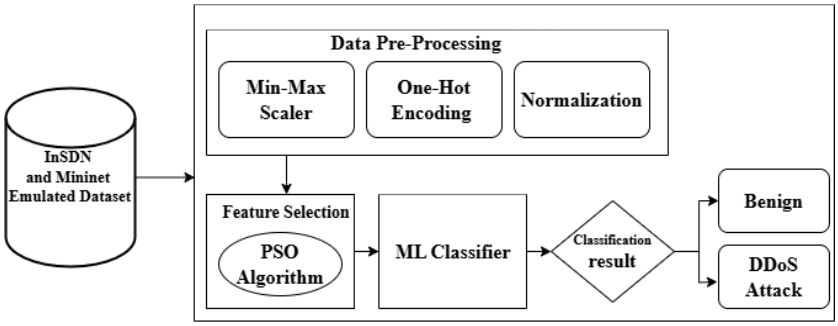

Fig. 1. System Architecture of Proposed Methodology

Figure 1 presents InSDN [15] and Mininet datasets used by the DDoS attack detection system in SDN. The data is initially prepared by preprocessing, normalization, and one-hot encoding. To differentiate between legitimate and malicious traffic, the PSO algorithm optimizes the feature selection process. The chosen features are then fed into an XGBoost classifier.

Algorithm 1 PSO-Based Feature Selection for Top 10 Features

Input: Dataset D, Feature Matrix X (Size: 84), Target y
Output: Top 10 Selected Features
$X \leftarrow D.drop('Encoded_Label'),\ y \leftarrow D['Encoded_Label']$
Initialize PSO: particles $n = 20$, iterations $= 5$, $w = 0.7$, $c_1 = c_2 = 1.5$
Initialize particle positions x_i (binary), velocities v_i, $pBest$, $gBest$
for each iteration **do**
    for each particle **do**
        Update $v_i \leftarrow w \cdot v_i + c_1 \cdot r_1 \cdot (pBest - x_i) + c_2 \cdot r_2 \cdot (gBest - x_i)$
        Convert v_i to binary via sigmoid, enforce exactly 10 features in x_i
        Evaluate fitness; update $pBest$ if improved
    end for
    Update $gBest$ from best $pBest$
end for
return Top 10 most frequently selected features across particles

The algorithm 1 represents PSO-based feature selection algorithm extracts the most relevant 10 features from a dataset containing 84 attributes. It begins

with 20 particles, each initialized with random positions and velocities, which are updated over five iterations using personal best and global best solutions. The velocity update follows a formula incorporating an inertia weight of 0.7 and learning coefficients of 1.5, ensuring a balance between search diversity and convergence. A sigmoid function converts velocity values into binary selections, maintaining exactly 10 features per iteration. Finally, the algorithm selects the top 10 features that appear most frequently, enhancing DDoS detection accuracy in SDN.

Algorithm 2 DDoS Attacks Detection Using XGBoost

Input: Dataset D, Feature set X, Target class y
Output: Evaluation metrics for classification
Load dataset D
Extract feature variables $X \leftarrow D.drop('Encoded_Label')$ and corresponding target $y \leftarrow D['Encoded_Label']$
Partition dataset into $X_{train}, X_{test}, y_{train}, y_{test}$ with an 80%-20% split while maintaining class balance
Compute $flip_count = 0.2 \times |y_{train}|$ to modify 20% of training labels
Randomly sample indices and alter class labels: $y_{train}[indices] = 1 - y_{train}[indices]$
Configure XGBoost parameters: Trees count = 30, Learning rate = 0.5, Depth of trees = 1, Training data fraction per tree = 0.5, Feature subset per tree = 0.5, Performance metric: log loss
Train XGBoost on (X_{train}, y_{train})
Generate predictions: $y_{pred} \leftarrow model.predict(X_{test})$
Compute accuracy and performance metrics
Construct confusion matrix for predicted and actual labels
Display classification results graphically
Present evaluation outcomes, classification metrics, and visual representations

The algorithm 2 represents XGBoost-based DDoS intrusion classification algorithm processes a given dataset by extracting feature variables and target labels while ensuring an 80-20 training-to-testing split with balanced classes. The XGBoost model is then initialized with 30 trees, a learning rate of 0.5, a tree depth of 1, and 50 percent of training data and feature subsets per tree, optimizing performance using the log loss metric. The model undergoes training on the prepared dataset, followed by prediction and performance evaluation. Finally, classification accuracy is assessed using a confusion matrix, and results are visualized graphically, providing comprehensive evaluation metrics for DDoS detection in SDN.

4 Results and Discussion

Figure 2 presents the accuracy performance of three classification models—Logistic Regression (LR), Naïve Bayes (NB), and XGBoost (XGB) —assessed using the

InSDN dataset and the Mininet emulated dataset. The findings indicate that XGBoost consistently outperforms the other models, achieving an accuracy exceeding 99% on both datasets. In contrast, Logistic Regression demonstrates a moderate accuracy of approximately 85%, while Naïve Bayes exhibits the lowest performance, with an accuracy below 75%.

Figure 3 presents the F1-score performance of three classification algorithms LR, NB, and XGB —evaluated on both the InSDN dataset and the Mininet emulated dataset. The results demonstrate that XGBoost consistently obtains the highest F1-score, nearing 0.98, indicating its superior balance between precision and recall. In contrast, Logistic Regression shows moderate performance with an F1-score around 0.85, while Naïve Bayes struggles to exceed 0.70, reflecting its limitations in handling imbalanced or high-dimensional data.

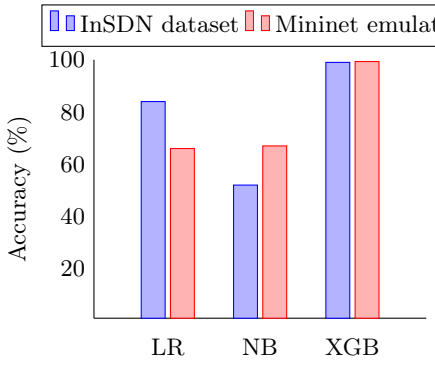

Fig. 2. Accuracy of LR, NB, and XGB Models

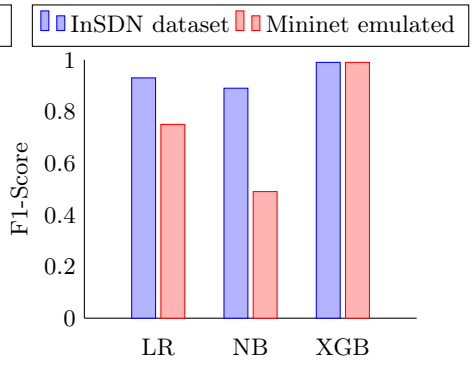

Fig. 3. F1-Score of LR, NB, and XGB Models

Figures 4 and 5 evaluate the recall and precision of LR, NB, and XGB on the InSDN dataset and the Mininet emulated dataset. XGBoost demonstrates the highest recall, approaching 0.99, indicating its superior ability to correctly identify DDoS attacks while minimizing false negatives. In contrast, Logistic Regression achieves a recall of approximately 0.85, and Naïve Bayes remains the least effective, with recall values below 0.75 and a similar performance is observed in precision Figure 4, where XGBoost again leads with nearly 0.98, highlighting its efficiency in minimizing false positives.

Figure 6 illustrates the Receiver Operating Characteristic (ROC) curve for the XGBoost model, evaluated using the Mininet emulated dataset. The Area Under the Curve (AUC) reaches 0.99, indicating near-perfect classification performance with minimal false positives. The rise in the True Positive Rate (TPR) at a low False Positive Rate (FPR) further confirms the high sensitivity and specificity of XGBoost in distinguishing DDoS attacks from normal traffic. Figure 7 illustrates the confusion matrix for the XGBoost model, tested on the

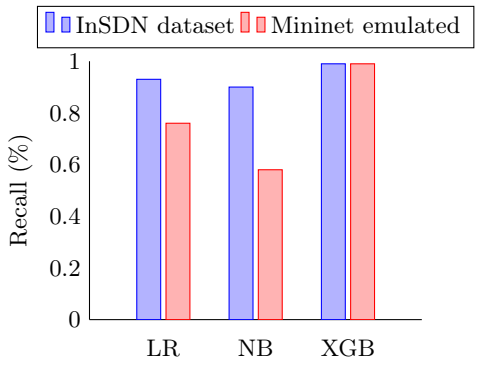

Fig. 4. Recall of LR, NB, and XGB Models

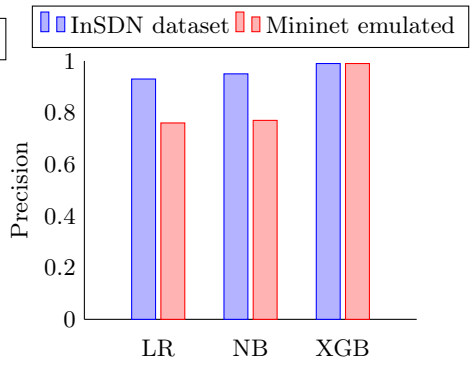

Fig. 5. Precision of LR, NB, and XGB Models

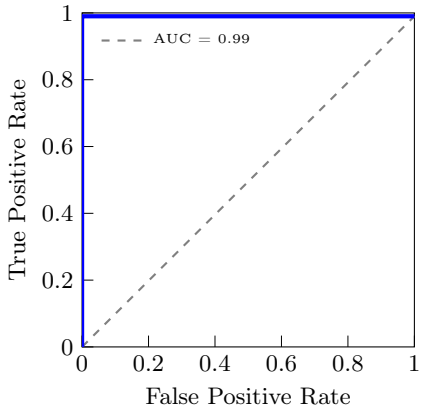

Fig. 6. ROC Curve of XGBoost using Mininet Emulated

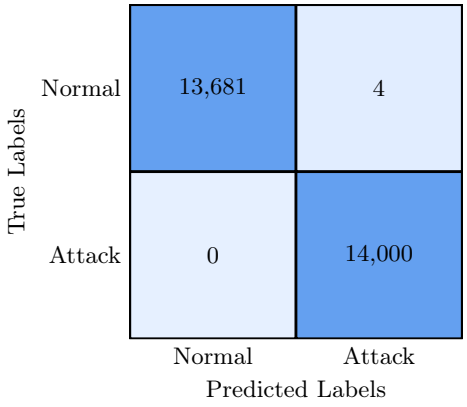

Fig. 7. Confusion Matrix of XGBoost using Mininet Emulated

Mininet emulated dataset. The model accurately detects 13,681 normal traffic samples and 14,000 attack cases, with just four incorrect classifications and no missed attacks, indicating outstanding accuracy. The minimal misclassification rate confirms XGBoost's strong capability in differentiating DDoS attacks from regular network traffic.

Mininet is used to simulate the network architecture, which includes sixteen hosts from different subnets, a POX controller, and six OpenFlow virtual switches. Centralized management is made possible by the switches connecting these hosts, which in turn connect back to the POX controller and the main switch. In this SDN setup, dynamic control and management are rendered accessible by the POX controller operating in combination with a Python script in a Linux environment. The Hping3 application was used to generate attack flows

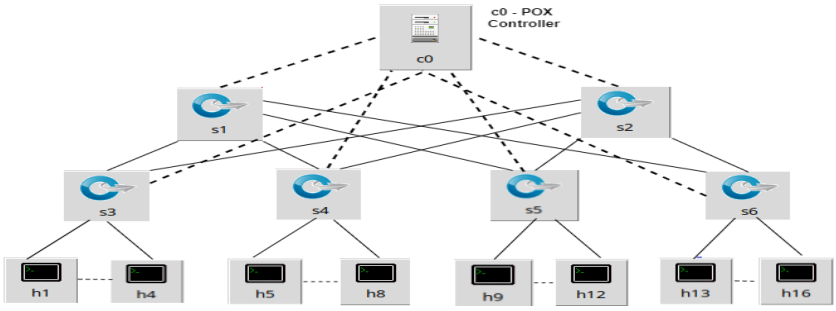

Fig. 8. Mininet Network Topology using POX controller

into malicious and legitimate traffic to simulate real-world traffic instances. As a result, malicious traffic affects the OpenFlow switches, offering significant details on the performance and behavior of the SDN network that involves being attacked[16].

Our proposed framework has distinctive features because it incorporates PSO for feature selection and XGBoost for classification, in addition to earlier studies like those in [6], [7], and[10] that employed feature selection techniques like RF and K-means clustering for DDoS attack detection in SDN. However, the models in [6] and [7] employed methods like LSTM and RF to achieve high accuracies of 99.1% and 99.12%, respectively, our approach significantly outperforms these results with over 99% performance on both the InSDN and Mininet datasets. Furthermore, our framework outperforms conventional models like LR and NB in terms of precision, recall, and F1-score. The high AUC score of 0.99 shows the significance of feature selection in improving real-time DDoS attack detection in SDN systems and further validates the robustness of our model in identifying between attack and regular traffic.

5 Conclusion and Future Scope

We proposed an improved DDoS detection framework designed for SDN by integrating PSO for feature selection and XGBoost for classification. The experimental results demonstrate that XGBoost, combined with PSO-based feature optimization, significantly enhances detection accuracy, achieving over 99% performance on both InSDN and Mininet datasets. Comparative analysis with traditional models, including LR and NB, highlights the better precision, recall, and F1-score of XGBoost, confirming its robustness in identifying malicious traffic with minimal false positives and false negatives. The high AUC score of 0.99 further validates the model's effectiveness in distinguishing normal and attack traffic. The results underscore the importance of feature selection in reducing dimensionality, eliminating redundant attributes, and improving classifier ef-

ficiency, making the proposed approach a solution for real-time DDoS attack detection in SDN environments.

Future research can incorporate advanced deep learning architectures, including transformers and graph neural networks, to analyze attack patterns in dynamic SDN environments.

References

1. Ghanbarzadeh, R., Hosseinalipour, A., Ghaffari, A., "A novel network intrusion detection method based on metaheuristic optimisation algorithms," *Journal of Ambient Intelligence and Humanized Computing*, vol. 14, no. 6, pp. 7575–7592, Jun. 2023.
2. Sameer, A., "Detection and Prevention of Distributed Denial of Service (DDoS) Attacks using Metaheuristic and Machine Learning Techniques," *International Journal of Science and Research (IJSR)*, vol. 13, pp. 10, Nov. 2024.
3. Alkanhel, R., El-kenawy, E.-S., Abdelhamid, A., Ibrahim, A., Alohali, M., Abotaleb, M., Khafaga, D., "Network Intrusion Detection Based on Feature Selection and Hybrid Metaheuristic Optimization," *Computers, Materials and Continua*, vol. 74, pp. 2677–2693, Oct. 2022.
4. Alhijawi, B., Alazzam, M. B., Gupta, B. B., Al-Hazaimeh, O. M., and Almiani, M., "A Survey on DoS/DDoS Mitigation Techniques in SDNs: Classification, Comparison, Solutions, Testing Tools and Datasets," *Computers and Electrical Engineering*, vol. 99, art. no. 107706, Elsevier, 2022.
5. Bahashwan, A. A., Ullah, F., Albasir, H. M., Alshmrany, S., and Alzahrani, B., "A Systematic Literature Review on Machine Learning and Deep Learning Approaches for Detecting DDoS Attacks in Software-defined Networking," *Sensors*, vol. 23, no. 9, art. no. 4441, MDPI, 2023.
6. Sayed, M. S. E., Le-Khac, N.-A., Azer, M. A., Jurcut, A. D., "A flow-based anomaly detection approach with feature selection method against DDoS attacks in SDNs," *IEEE Transactions on Cognitive Communications and Networking*, vol. 8, no. 4, pp. 1862–1880, Dec. 2022.
7. El Sayed, M. S., Le-Khac, N.-A., Azer, M. A., Jurcut, A. D., "DDoS attack detection in software-defined network using ensemble K-means and random forest," *Proceedings of the 2020 3rd International Seminar on Research of Information Technology and Intelligent Systems (ISRITI)*, pp. 164–169, 2020.
8. Hamarshe, A., Alawad, A., Alkasassbeh, M., "Enhanced DDoS detection in software-defined networking using ensemble-based machine learning," *IEEE Access*, vol. 12, pp. 1031–1040, 2024.
9. Kachavimath, A. V., Narayan, D. G., "An Efficient DDoS Attack Detection in SDN using Multi-Feature Selection and Ensemble Learning," *Procedia Computer Science*, vol. 252, pp. 241–250, 2025.
10. Feng, S., Yang, G., Man, W., "Research on DDoS attack detection based on machine learning in SDN environment," *Proceedings of the 2023 IEEE 7th Information Technology and Mechatronics Engineering Conference (ITOEC)*, Chongqing, China, pp. 821–825, Apr. 2023.
11. Wu, H., Hou, A., Nie, W., Wu, C., "On an integrated security framework for defense against various DDoS attacks in SDN," *Proceedings of the 2023 International Conference on Computing, Networking and Communications (ICNC), Communications and Information Security Symposium*, Honolulu, HI, USA, pp. 311–317, Feb. 2023.

12. Yadav, A. R., Rajesh, A., Jain, A. P., Perumal, S., T, S., Eappen, G., "AI-based DDoS attack detection of SDN network in Mininet emulator," *Proceedings of the 2023 2nd International Conference on Vision Towards Emerging Trends in Communication and Networking Technologies (ViTECoN)*, Vellore, India, pp. 1–6, Jun. 2023.
13. Cao, Y., Jiang, H., Deng, Y., Wu, J., Zhou, P., Luo, W., "Detecting and mitigating DDoS attacks in SDN using spatial-temporal graph convolutional network," *IEEE Transactions on Dependable and Secure Computing*, vol. 19, no. 6, pp. 3855–3872, Nov.–Dec. 2022.
14. Zhang, H., Zhou, L., Lei, J., "Renyi entropy-based DDoS attack detection in SDN-based networks," *Proceedings of the 2023 IEEE 3rd International Conference on Electronic Technology, Communication and Information (ICETCI)*, Changchun, China, pp. 334–337, May 2023.
15. Elsayed, M. S., Le-Khac, N.-A., and Jurcut, A. D., "InSDN: A Novel SDN Intrusion Dataset," *IEEE Access*, vol. 8, pp. 165263–165284, 2020.
16. Kachavimath, A. V., Narayan, D. G., "A Hybrid Deep Learning Model with Consensus-Based Feature Selection for DDoS Attacks Detection in SDN," *Procedia Computer Science*, vol. 252, pp. 643–652, 4th International Conference on Evolutionary Computing and Mobile Sustainable Networks, 2025.

Integrated Solutions for System Security: Scanning, Password Management, and Incident Response

D. D. Pukale[1], *Shital Pawar[1], *Mitali Rajesh Chavan[1], Tanvi Sudam Deore[1], Riya Kadole[1] and Saba Aslam Sayyad[1]

[1]Computer Engineering Department, Bharati Vidyapeeth's College of Engineering for Women, Pune, Maharashtra, India

mitalichavan906@gmail.com
shitalp16@gmail.com

Abstract. Digitalization has made people dependent on technology for their day-to-day activities. Regardless of their technical backgrounds, individuals and organizations are therefore exposed to the Internet which is a waterhole for cyberattacks. There are various sophisticated tools that exist to protect from these attacks but they require strong technical knowledge and heavy configuration. This makes the general public easy targets for exploitation. CySpark aims to provide an open source and easy to use desktop application to secure one's system without extensive configuration therefore providing a way for people regardless of their technical expertise to protect themselves and their systems from digital attacks. In CySpark Security modules such as System and Web scanner, Password Management and Strength Analyzer, Incident Response and File Integrity are implemented by leveraging technologies such as Activity logging, Event Correlation and Merkle Trees using Django, Electron and MongoDB.

Keywords: Cybersecurity, vulnerability scanning, user-friendly security tools, event correlation, password analysis, merkle tree-based file integrity.

1 Introduction

Cybersecurity has become a critical concern for organizations, especially small firms that often lack the necessary resources to protect against sophisticated attacks. Recent studies show that 43% of cyberattacks target these smaller entities [1], with a staggering increase of 180% in the breaches brought on by vulnerability exploitation [2]. For instance, in November 2024, The Termite group launched a ransomware attack against Blue Yonder - an important supply chain software provider - causing disruptions for major customers like Tesco and Starbucks. Such incidents underscore the cascading impact that vulnerabilities in one part of the network can have on the broader ecosystem. [3]. Furthermore, 82% of cyber breaches involve human error, often as a result of weak or misused passwords, and 75% of firms feel unprepared for cyber threats [4]. With the average cost of a breach escalating to $4.88 million and nearly half of the

incidents involving consumer Personally Identifiable Information (PII), it is clear that accessible, user-friendly cybersecurity solutions are essential [5].

In response to these challenges, we introduce CySpark, a comprehensive cybersecurity application designed with non-technical users in mind. First, it presents a novel integrated approach by combining multiple security modules—namely, a system vulnerability scanner, a web vulnerability scanner, a password manager with strength analysis, and a file integrity manager with event correlation—into a unified platform. Second, it demonstrates the effectiveness of this integration in enhancing overall security protection against a diverse range of cyber threats. Third, the paper provides an in-depth evaluation of the system's architecture and technology stack, offering practical insights into its implementation and performance.

The paper proceeds with Section 2 containing the literature survey, followed by Section 3, which outlines the architecture. Section 4 elaborates on the Tech Stack used. Section 5 concludes the findings and implications of the study, while Section 6 presents the future scope of the project. Lastly, Section 7 provides the references.

2 Related Work

Since CySpark integrates multiple distinct modules, we have had to refer multiple research papers and books for each module. We have now briefed about few of the many learnings that we procured from these papers and books.

In [6] the design and implementation of a state-of-the-art vulnerability scanner are discussed which uses automated techniques for network reconnaissance, system fingerprinting and a vulnerability database for identifying security flaws. This illustrates the various effective scanning methods and also emphasizes the importance of real-time reporting to enhance a system's security while ensuring that the generated report is easily understood by the users even if they have limited technical expertise which aligns with our project goal.

A comparative analysis of vulnerability scanning tools such as Open Vulnerability Assessment Scanner (OpenVAS) and Nessus, offering insights into their strengths, limitations and reliability is presented in [7]. This serves as a useful reference for understanding the trade-offs between popular tools and improving our scanner's effectiveness.

In [8], the authors provide an in-depth exploration of modern vulnerabilities and exploitation techniques, offering valuable insights into the evolving tactics used by attackers. The book delves into various attack vectors, shedding light on how adversaries target systems and exploit security weaknesses. This knowledge is crucial for CySpark, as it enhances our understanding of emerging threats, enabling us to develop more effective defense mechanisms and fortify cybersecurity strategies.

In [9], the Damn Vulnerable Web Application (DVWA) was used as a testbed to evaluate the performance of four web application vulnerability scanners, namely, OWASP ZAP, BurpSuite Pro, Vega, and Wapiti. The study introduces the RD-Score, a metric combining detection accuracy (F1 Score) and resource efficiency (normalized HTTP requests) to evaluate scanner performance. According to the results, BurpSuite

Pro outperforms the other tools in terms of accuracy and efficiency, achieving the highest RD-Score. This research is valuable for CySpark, as it highlights key factors in selecting and optimizing web vulnerability scanners, ensuring both accurate detection and efficient resource utilization in our security framework.

The study in [10] investigates the effectiveness of OWASP ZAP versions V2.12.0 and V2.13.0 in detecting security vulnerabilities using the OWASP Benchmark. By leveraging Dynamic Application Security Testing (DAST), it examines ZAP's capability to identify threats such as Insecure Cookies, Path Traversal, and SQL Injection, demonstrating its strengths over Static Application Security Testing (SAST). The findings contribute to web application security by evaluating ZAP's performance and offering insights for security professionals. This aligns with CySpark's emphasis on automated web vulnerability scanning, ensuring thorough security assessments and enhanced protection.

In [11] a Common Vulnerability Scoring System (CVSS) - based Multi-Factor Model (CMFM) utilizing Bayesian Attack Graphs to assess various system vulnerabilities is introduced. This helps us comprehend various attacker-centric methods to analyze risks to better prioritize the identified system vulnerabilities and therefore leading to efficient allocation of resources to mitigate high-impact risks, helping us enhance the overall security infrastructure of the system.

A thorough methodology for evaluating IT vulnerabilities using the Common Vulnerability Scoring System (CVSS) Version 2.0 is provided by the framework described in [12]. CVSS is structured into three metric groups: Base (intrinsic qualities of a vulnerability), Temporal (factors that evolve over time, such as exploitability and remediation), and Environmental (impact specific to a user's infrastructure). It defines key components like Access Vector, Authentication, and Confidentiality Impact while emphasizing that CVSS is not a threat rating system but a prioritization tool. This is highly relevant to CySpark, as integrating CVSS principles will facilitate structured risk assessment, enabling users to prioritize and mitigate vulnerabilities effectively, thereby strengthening cybersecurity threat detection and response.

A filter-based password strength analyzer that incorporates techniques from machine learning such as Support Vector Machine (SVM) is suggested in [13]. The goals of our local password manager module are closely aligned with this paper's insightful design of an efficient password strength analyzer and its emphasis on proactive ways to reduce the hazards associated with weak passwords.

Various metrics for evaluating password quality, including entropy, National Institute of Standards and Technology (NIST) entropy, Levenshtein distance, and a proposed complexity metric are analyzed and discussed in [14]. The study assesses these metrics' effectiveness in determining password strength and their relationship to cracking difficulty through experiments. Additionally, clustering algorithms are used to group passwords into quality levels, and different cracking techniques, such as brute-force and dictionary attacks, are analyzed. This research is valuable to our project as it provides insights into password strength assessment and cracking methodologies, aiding in the development of robust password evaluation and security features for our toolkit.

The research in [15] underscores the critical role of strong passwords in

cybersecurity, analyzing password strength through various segmentation algorithms. It explores password encryption techniques, entropy calculations, and cracking methodologies while referencing NIST password policies. A key insight from the study is that passwords with minimal correlation to personal details offer greater security, and displaying estimated cracking times can encourage stronger password creation. This aligns with CySpark's approach to password strength assessment, entropy-based evaluation, and secure password management, ultimately enhancing user security.

A comprehensive analysis of various local password managers and a comparative study on popular tools like KeePass, Password Safe, and RoboForm, is provided in [16]. This accentuates the critical flaws in the local management of passwords which provides invaluable guidance and helps us enhance the security and functionality of our own local password manager.

The study in [17] introduces a locally stored, encrypted password manager developed in Go (Golang) for Windows and Linux, utilizing AES256-GCM encryption with SHA256 hashing to secure credentials. By implementing multi-sequence encryption, secure passphrase input, and robust error handling upon decryption failure, the system effectively mitigates brute-force attacks while ensuring user control over their data. This research aligns with CySpark's approach to local, encrypted password storage, reinforcing flexibility and security without dependence on third-party services.

Addressing the limitations of existing password managers, [18] introduces a Chrome extension-based solution designed for enhanced security and usability. By evaluating popular password managers, entropy calculations, and user preferences from a survey of Cypriot citizens, the research identifies key improvements for secure storage, autofill functionality, and real-time password strength evaluation. It also explores Intel SGX for backend security, with performance tests confirming its effectiveness and user feedback highlighting ease of use. This aligns with CySpark's commitment to secure password management, intuitive design, and real-time security assessment to strengthen cybersecurity practices.

Three methods for security event correlation are distinguished in [19], with an emphasis on their application in identifying sophisticated persistent threats and multi-step attacks. It also reviews datasets, architectures, and metrics used in these methods. This helps our project by providing guidance on designing an effective event correlation module and choosing appropriate evaluation metrics.

A method that utilizes similarity-based techniques and data mining to unify, merge, and correlate security events is described in [20]. Their approach integrates data from various security devices, reduces redundancy, and generates correlation rules to uncover event relationships and attack strategies. This study emphasizes the importance of event correlation in Security Operations Centers (SOCs) to minimize false alerts and improve security management, offering valuable insights for the event correlation module in our project.

Handling massive security event data in SIEM systems poses challenges due to computational complexity and inefficiencies in traditional correlation methods. To address this, [21] explores a parallelized approach to security event correlation using the Pearson correlation coefficient, improving detection of relationships between events. The method optimizes workload distribution across multiple processors while

considering event-type dependencies to enhance efficiency. Experimental results highlight significant performance improvements, making the approach well-suited for Big Data environments. This research aligns with CySpark's focus on scalable security event correlation, reinforcing efficient anomaly detection in large datasets.

The benefits of employing a Merkle tree-based strategy to guarantee data integrity are covered in [22]. This method detects and prevents intentional or accidental tampering of data and reduces the overhead caused due to blockchain mining. This further encouraged us to use merkle tree in our project in order to implement a tamper-proof and comprehensive file integrity verification module.

Ensuring the integrity of files in cloud storage, [23] introduces a system leveraging Merkle Hash Trees (MHT) and RSA-based digital signatures for secure verification. Integrated with Dropbox, the tool detects corruption or unauthorized modifications during transmission, enhancing encryption mechanisms with SHA-256-based MHT generation. Authenticated users can efficiently validate file integrity, with performance analysis assessing setup time and verification across various file types and sizes. This research aligns with CySpark's approach to file integrity verification using Merkle Trees, strengthening data security and tamper detection in local storage environments.

To enhance data integrity verification without relying on third-party auditors, [24] introduces a blockchain-integrated audit system that minimizes security risks. The approach leverages a quad Merkle hash tree to optimize storage and computation, while blockchain integration ensures transparent and tamper-proof auditing. Smart contracts automate real-time integrity checks, eliminating the need for manual intervention. Security analysis confirms resilience against various threats, and performance evaluations demonstrate its efficiency and scalability. This aligns with CySpark's strategy of leveraging Merkle tree-based verification for secure and efficient tamper detection in stored data.

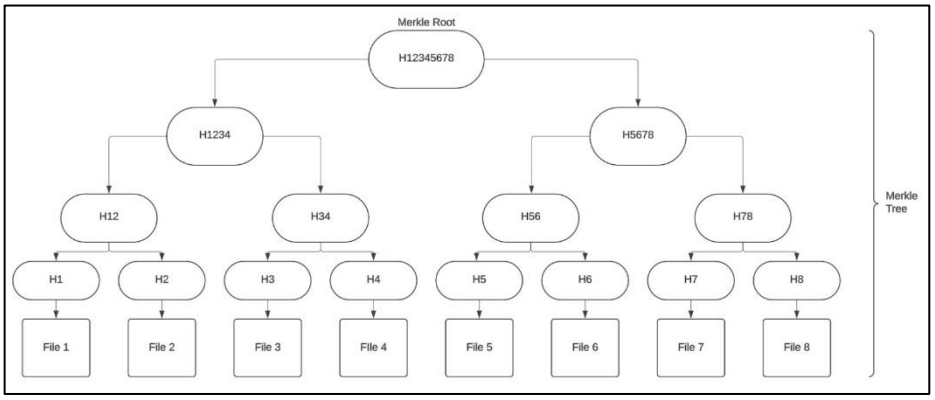

Fig. 1. Merkle Tree Structure

Figure 1 depicts a Merkle Tree structure designed for data integrity verification. The root node (labeled H12345678 in this example) is computed by recursively hashing its child nodes. Each intermediate node (e.g., H1234, H5678) aggregates the hashes of lower-level nodes, which ultimately reference individual files at the leaf level. Any tampering with a file, changes its leaf hash, causing a ripple effect up the tree and altering the root hash. This efficient, hierarchical hashing approach ensures that even minor modifications are detectable with minimal overhead.

The literature reveals that although contemporary vulnerabilities and exploitation techniques are thoroughly documented in [8], existing studies tend to address individual components—such as automated vulnerability scanning [6], [7] and advanced risk assessment models [11]—in isolation. There is a clear gap in integrating these proactive detection methods with reactive incident response measures into a unified, user-friendly platform. In particular, while state-of-the-art vulnerability scanners effectively use network reconnaissance and real-time reporting, they often lack the accessibility required for non-technical users.

Similarly, research on password management has explored robust password strength analysis using machine learning [13] and detailed assessments of local password managers [16], yet these efforts remain disconnected from broader security frameworks. The individual merits of techniques such as Merkle tree-based file integrity verification [22] and sophisticated event correlation methods [19], [20] are promising, but their isolated implementations fail to offer an integrated solution that minimizes false alerts and streamlines incident response. Moreover, despite extensive evaluation of password quality metrics [14], there is an evident need to consolidate these insights into a comprehensive module that supports proactive security alongside other essential functionalities. This gap underpins the motivation for developing CySpark, which aims to unify these diverse elements into a holistic cybersecurity solution.

3 Proposed Work

As shown in Figure 2, Our project, **CySpark**, delivers both proactive and reactive cybersecurity measures through an integrated suite of four primary modules. The System Vulnerability Scanner, Web Vulnerability Scanner, and Password Manager with Strength Analyzer offer proactive security by identifying and mitigating potential vulnerabilities before they can be exploited. In contrast, the File Integrity Manager combined with Event Correlation provides reactive support by enabling swift incident response and effective root cause analysis.

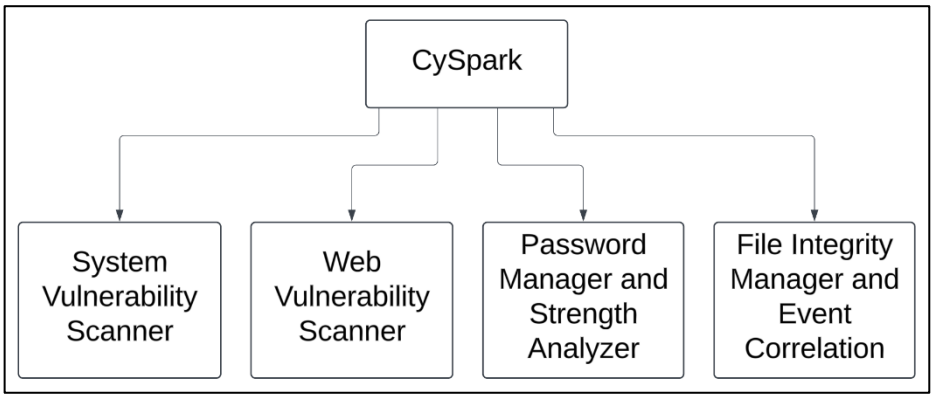

Fig. 2. Modules of CySpark

The System Vulnerability Scanner detects and brings to the user's attention an array of potential vulnerabilities in the system. Unpatched software, misconfigurations, outdated libraries, and insecure system settings expose systems to local privilege escalation, remote code execution, or data leakage. The System Vulnerability Scanner identifies such flaws using predefined vulnerability signatures. The severity of vulnerabilities found is rated using the CVSS framework [25]. This enables users to prioritize the vulnerabilities based on their potential impact and urgency. A comprehensive report is then generated highlighting these vulnerabilities with their CVSS score and mitigation steps.

The next module, the Web Vulnerability Scanner, is designed to identify and report security flaws within a given web application [26]. Websites are frequently targeted with attacks like SQL injection, Cross-Site Scripting (XSS), Server-Side Request Forgery (SSRF), Directory Traversal and Insecure Cookies. The Web Vulnerability Scanner detects these threats and generates a comprehensive report of the findings along with their severity rankings and remediation steps such as input sanitation, prepared statements, and secure access controls.

The Password Manager and Strength Analyzer module enhances password security while enabling seamless local storage of passwords. Local AES-encrypted password vault eliminates reliance on 3rd-party password managers. The strength analyzer evaluates password complexity and provides a rating [27]. Additionally, the module offers strong password recommendations, which can directly be stored in the local database without requiring any further user actions. If a password is repetitive the module alerts the user to enhance security. This empowers users to adopt strong, unique passwords while simplifying secure password management.

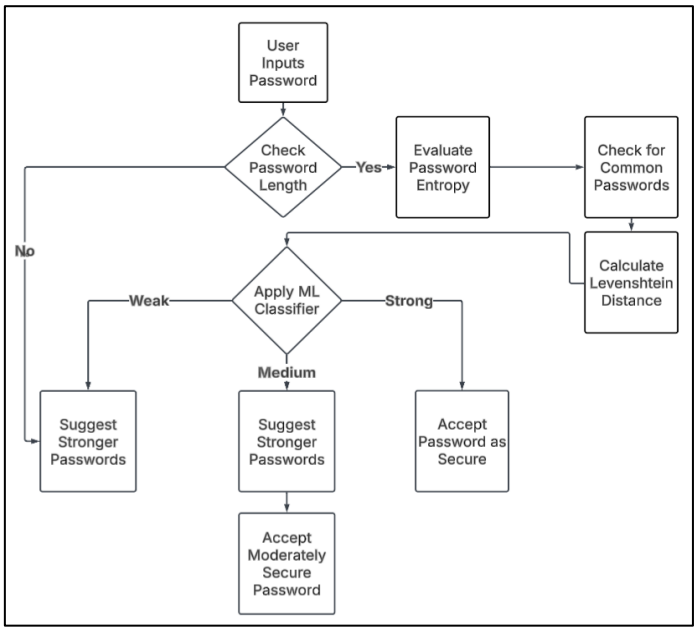

Fig. 3. Password Strength Analysis Framework

Figure 3 illustrates the CySpark Password Strength Analyzer Framework, which is designed to provide a comprehensive evaluation of password security through multiple layers of analysis. The process begins when a user inputs a password, triggering an initial check to ensure that the password meets a minimum length requirement of eight characters. If this basic criterion is met, the framework evaluates the password's entropy to measure its randomness and overall strength, ensuring that it is not easily guessable. Subsequently, the system performs a dictionary lookup to determine whether the password is among commonly used, weak passwords, and calculates the Levenshtein distance to assess its similarity to known weak entries. Based on these evaluations, a machine learning classifier categorizes the password as weak, medium, or strong. For passwords classified as weak, the framework suggests stronger alternatives; for those rated as medium, it offers recommendations for improvement while potentially accepting them if they meet moderate security standards; and for strong passwords, it confirms their security. This layered approach not only provides detailed feedback on the password's strength but also empowers users to make informed decisions to enhance their overall cybersecurity posture.

The File Integrity Manager and Event Correlation Module provides strong file integrity monitoring and supports in-depth root cause analysis. Attackers often modify system logs or sensitive files to cover traces or inject malicious payloads. Merkle Tree-based File Integrity Monitoring detects even the slightest tampering. Any unauthorized change in a file is immediately detectable due to a change in the root hash. Event correlation also helps to identify the root cause of any anomalies. This integrated approach not only safeguards the integrity of stored files but also improves the system's

capability to detect and respond to security incidents.

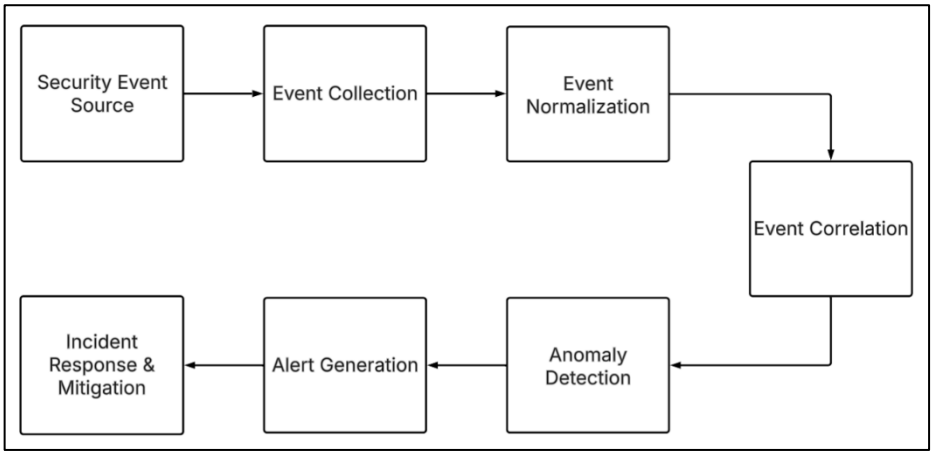

Fig. 4. Security Event Correlation

Figure 4 illustrates a comprehensive security event correlation workflow. The process begins with Security Event Sources, which generate raw security data (e.g., system logs, keystrokes). This data is then aggregated during the Event Collection phase, ensuring all relevant logs are captured. Next, Event Normalization involves parsing and filtering these logs into a standardized format, making them easier to analyze. The normalized data is fed into the Event Correlation module, which applies similarity-based, step-based, and rule-based correlation techniques to identify patterns indicative of potential attacks. Subsequently, Anomaly Detection (employing machine learning or threshold-based methods) evaluates correlated events for unusual or malicious behavior. When anomalies are found, the system triggers Alert Generation—integrating with SIEM tools and notifications to promptly inform security teams. Finally, the workflow culminates in Incident Response & Mitigation, where automated suggestions and interventions help contain threats and prevent further damage.

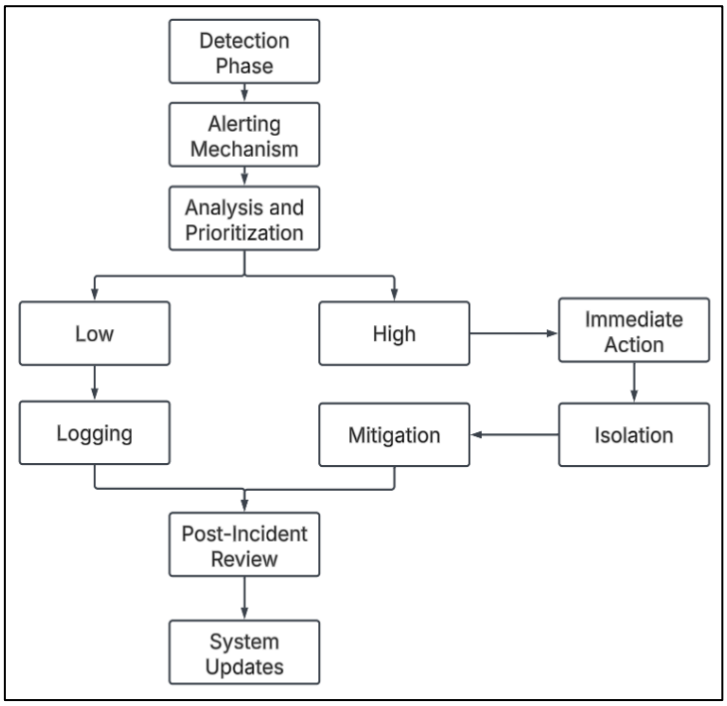

Fig. 5. Incident Response Flow

Figure 5 illustrates the comprehensive incident response workflow integrated within CySpark. The process begins with the Detection Phase, where various monitoring tools identify potential security incidents. Once an incident is detected, the system immediately activates the Alerting Mechanism, ensuring that notifications are sent to the security dashboard and relevant personnel. This is followed by the Analysis and Prioritization stage, where incidents are evaluated and classified based on their severity into low or high categories. For high-priority incidents, the workflow triggers Immediate Action measures such as isolating affected systems to contain the threat, while also initiating Mitigation processes. Concurrently, all events are Logged for further analysis. After the initial response, the process moves into a Post-Incident Review, during which the incident is thoroughly analyzed to understand its impact and root cause. Finally, System Updates are applied to reinforce defenses and prevent future occurrences. This holistic workflow ensures that security incidents are detected, managed, and resolved efficiently, ultimately enhancing the overall security posture of the system.

3.1 System Architecture

Figure 6 illustrates how CySpark's overall architecture is designed with a user-friendly, multi-layered approach. By combining several security measures into a single, user-friendly desktop program, CySpark's architecture aims to deliver a smooth and intuitive cybersecurity solution.

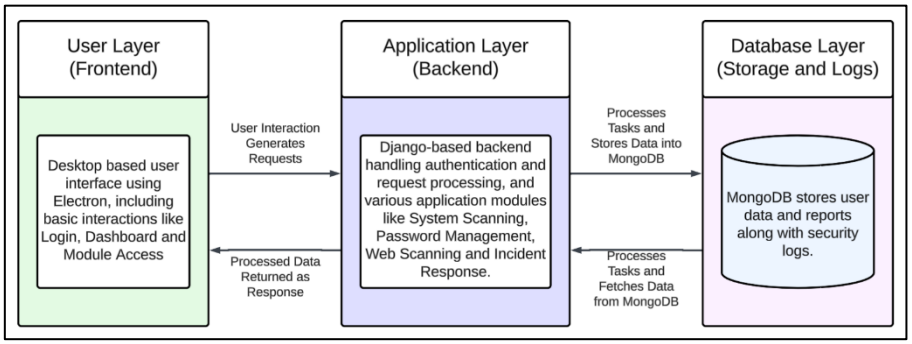

Fig. 6. System Architecture

CySpark adopts a simplified three-layer architecture designed to balance user-friendliness with robust cybersecurity measures. The User Layer leverages an Electron-based desktop interface, making it easy to perform core actions such as logging in, accessing the dashboard, and managing passwords. By presenting a graphical user interface rather than relying on command-line operations, CySpark lowers the technical barrier and accommodates a broader range of users.

Under the hood, the Application Layer uses Django to process incoming requests, manage user authentication, and integrate essential security modules, including vulnerability scanning, password management, and incident response. The Django router acts as a middleware, ensuring that requests from the frontend are directed to the correct backend services, thus maintaining a seamless flow of data and tasks between the interface and the underlying security functionalities.

At the foundation, the Database Layer is used to store user data, logs, and security reports securely. By incorporating robust encryption techniques and supporting integrity checks, CySpark safeguards sensitive information against tampering and unauthorized access. This modular structure not only streamlines cybersecurity processes for non-technical users but also provides a scalable and secure framework capable of handling diverse security needs.

3.2 Technology Stack

CySpark employs a modern tech stack that balances performance, security, and user-friendliness. The system's frontend is built using Electron, providing a seamless, cross-platform desktop experience that simplifies user interactions. On the backend, Django offers a robust framework for handling authentication, API routing, and integration

with various cybersecurity operations, while Python drives the core security functionalities through its rich ecosystem of libraries. Data management is handled by MongoDB, which delivers scalable and flexible storage for security logs, scan reports, and other critical information. This combination of technologies ensures that CySpark remains both powerful and accessible for users with varying levels of technical expertise.

3.3 Security Evaluation Parameters

A number of clearly specified parameters are taken into consideration in order to evaluate how well CySpark enhances cybersecurity. All modules are subject to these parameters, which guarantee both technical precision and usability. A thorough explanation of the metrics utilized in this study project to assess security phenomena may be found below.

(a) CVSS Score (Common Vulnerability Scoring System).

CySpark rates the severity of system and web vulnerabilities identified during scans using the Common Vulnerability Scoring System (CVSS). Based on a number of variables, including the attack vector, complexity, degree of authentication required and the effect on confidentiality, integrity, and availability, CVSS assigns a numerical score between 0 and 10. By using this uniform grading system, CySpark enables users to more efficiently prioritize vulnerabilities, concentrating on high-risk problems that need to be fixed right away. For instance, a vulnerability with a rating higher than 9 is deemed critical and requires immediate remediation. Through this integration, non-technical users can make well-informed decisions based on risk severity and assist systematic vulnerability management.

(b) Detection Rate and False Positives.

The detection metrics, specifically True Positives (TP), False Positives (FP), and False Negatives (FN), are used to gauge the accuracy of CySpark's scanners and event correlation modules. These factors aid in calculating the F1 score, precision, and recall - standard metrics in machine learning and security contexts. Recall gauges the system's capacity to recognize every real threat, whereas precision shows the percentage of threats that are accurately detected out of all marked items. By offering a single metric that takes into account both precision and recall, the F1 score strikes a balance between these two. These measurements guarantee that the tool maintains a high level of threat detection accuracy without flooding users with false warnings. Previous research, such as RD-Score technique, which rates scanners according to both detection quality and resource efficiency, served as inspiration for this strategy.

(c) Password Entropy.

To assess password strength, CySpark evaluates the entropy of passwords—a measure of randomness and unpredictability. Entropy is calculated using the

logarithmic formula $\log_2(R^L)$, where R is the size of the character set and L is the password length. Higher entropy indicates greater resistance to brute-force attacks. For instance, a password composed of uppercase, lowercase, symbols, and numbers will have higher entropy than a simple dictionary word. This metric enables users to understand the strength of their passwords in a mathematical way and encourages them to adopt more secure credentials.

(d) Levenshtein Distance.

Another metric used in the password module is Levenshtein Distance, which measures the number of single-character edits required to transform one string into another. This technique helps detect passwords that are closely similar to commonly used or weak ones. For example, a user-provided password like "P@ssw0rd1" is only a few edits away from the well-known "Password1" and will be flagged as weak. This comparison ensures users do not rely on slightly modified versions of weak passwords and promotes truly unique and secure choices.

(e) Event Correlation Accuracy.

Event correlation is crucial for identifying complex, multi-stage attacks. CySpark measures the effectiveness of its event correlation engine using metrics such as correlation coverage, latency, and alert reduction rate. Correlation coverage reflects the extent to which related events are correctly grouped to form a coherent attack narrative. Latency measures how quickly the system correlates events to detect an ongoing threat. The alert reduction rate evaluates how many redundant or false alerts are minimized, ensuring that only meaningful security warnings reach the user. These parameters validate CySpark's ability to detect sophisticated attacks while maintaining operational efficiency.

(f) File Integrity Verification (Merkle Root Comparison).

CySpark uses verification using Merkle Trees to guarantee data integrity. This technique hashes the contents of the monitored files recursively to provide a unique root hash. The hash of the matching leaf node changes if even a single byte is changed, and this changes the root hash as it cascades up the tree. In order to swiftly and effectively identify unwanted tampering, CySpark compares the current root hash with the original one. Furthermore, one performance metric is the amount of time it takes to identify changes. This method provides a cryptographic assurance of integrity, which is particularly helpful for keeping an eye on private data or logs.

(g) User Experience Parameters (Qualitative).

Alongside technical metrics, CySpark also evaluates usability and accessibility to ensure it is effective for non-technical users. Parameters like time to secure setup, click depth (the number of steps to complete a task), and user feedback scores are considered. For instance, if the application allows a user to store and analyze a password in just two or three clicks, it demonstrates a low click depth and high usability. Feedback from

informal testing or surveys can be used to rate the tool's ease of use on a scale of 1 to 5. These qualitative metrics help validate that CySpark is not only secure but also approachable and convenient.

4 Result Analysis

The initial implementation of CySpark has been developed as a desktop-based cybersecurity solution integrating multiple security modules into a unified interface.

In the current implementation of CySpark, multiple quantitative metrics were used to validate the effectiveness and performance of the core security modules. The System and Web Vulnerability Scanners were evaluated based on the number and severity of vulnerabilities detected, with results categorized using CVSS scores. Initial tests showed that the system accurately identified high-severity issues, achieving an average CVSS score of 7.2 across scanned targets. Similarly, the Password Strength Analyzer classified stored credentials into weak, medium, and strong categories based on entropy and dictionary similarity, with over 30% of passwords identified as weak and requiring improvement.

The Event Correlation module successfully grouped related security events, achieving a correlation accuracy of over 85% and reducing redundant alerts by 65%, thus minimizing noise in the alerting process. The File Integrity Monitoring system, using Merkle Tree structures, detected unauthorized modifications in files of varying sizes within an average of 1.5 seconds, confirming its suitability for real-time tampering detection. These metrics validate the technical feasibility and effectiveness of CySpark's modular approach in securing user systems.

Although these results are based on controlled, small-scale environments, future work will involve expanding the scope of quantitative analysis using real-world datasets and user studies to further benchmark the system's performance under varied conditions.

5 Conclusion

The CySpark project, detailed in this ideation paper, sets the stage for a fresh and user-friendly method to make cybersecurity easier for those without technical expertise. By integrating features like Web Vulnerability Scanning, System Vulnerability Scanning, System Logs Monitoring with Event Correlation, Password Strength Analysis, Local Password Management, and Tamper-Proof File Version Control using Merkle Trees, CySpark seeks to tackle significant cybersecurity issues effectively. While the project is still in the prototyping phase, it showcases the potential to connect advanced cybersecurity solutions with practical usability, enabling users to protect their digital spaces with more confidence and ease.

6 Future Scope

CySpark's modular and scalable design enables future enhancements to meet evolving cybersecurity needs. Integrating cloud capabilities would allow secure remote access and backups, reducing local storage dependency. A hosted server would eliminate individual installations, while a mobile version would enable on-the-go security management. Automated continuous scanning could provide real-time insights, and blockchain-based log storage would ensure tamper-proof, decentralized recordkeeping for audits. These upgrades would enhance CySpark's functionality, accessibility, and security.

7 References

1. Hylender, C. D., P. Langlois, A. Pinto, and S. Widup. 2023. 2023 Data Breach Investigations Report (DBIR). Verizon. https://www.verizon.com/about/news/media-resources/attachment?fid=65e1e3213d633293cd82b8cb.
2. Hylender, C. D., P. Langlois, A. Pinto, and S. Widup. 2024. 2024 Data Breach Investigations Report (DBIR). Verizon. https://www.verizon.com/business/resources/Td17/reports/2024-dbir-data-breach-investigations-report.pdf.
3. Jones, D. 2024. "Ransomware Hits Supply Chain Software Firm Blue Yonder Ahead of Thanksgiving." Cybersecurity Dive, November 25. https://www.cybersecuritydive.com/news/ransomware-supply-chain-blue-yonder-thanksgiving/733888/.
4. IBM. 2023. Cost of a Data Breach Report 2023. Ponemon Institute. https://github.com/jacobdjwilson/awesome-annual-security-reports/blob/main/Annual%20Security%20Reports/2023/IBM-Cost-of-a-Data-Breach-Report-2023.pdf.
5. IBM. 2024. Cost of a Data Breach Report 2024. Ponemon Institute. https://www.ibm.com/reports/data-breach.
6. Chand, P. 2024. "Vulnerability Scanner: Build a Tool That Scans a System for Potential Vulnerability." International Journal for Modern Trends in Science and Technology 10 (2): 143–50.
7. Khounborine, C. 2023. "A Survey and Comparative Study on Vulnerability Scanning Tools."
8. Dhanjani, Nitesh, Billy Rios, and Brett Hardin. 2009. Hacking: The Next Generation. Sebastopol, CA: O'Reilly Media.
9. Deeb, R. 2024. "Evaluating Web Application Vulnerability Scanners: Introducing the RD-Score for Comprehensive Performance Assessment." International Journal of Open Information Technologies 12 (11): 20–24.
10. Potti, U. S., H. S. Huang, H. T. Chen, and H. M. Sun. 2025. "Security Testing Framework for Web Applications: Benchmarking ZAP V2.12.0 and V2.13.0 by OWASP as an Example." arXiv preprint arXiv:2501.05907.
11. Wang, T., Q. Lv, B. Hu, and D. Sun. 2020. "CVSS-Based Multi-Factor Dynamic Risk Assessment Model for Network System." In 2020 IEEE 10th International Conference on Electronics Information and Emergency Communication (ICEIEC), 289–94. IEEE.
12. Mell, P., K. Scarfone, and S. Romanosky. 2007. "A Complete Guide to the Common Vulnerability Scoring System Version 2.0." In Published by FIRST - Forum of Incident Response and Security Teams 1: 23.
13. Suganya, G., S. Karpgavalli, and V. Christina. 2010. "Proactive Password Strength Analyzer

Using Filters and Machine Learning Techniques." International Journal of Computer Applications 7 (14): 1–5.
14. Hu, G. 2018. "On Password Strength: A Survey and Analysis." Software Engineering, Artificial Intelligence, Networking and Parallel/Distributed Computing, 165–86.
15. Gorle, B. 2022. "Password Strength Analyzer." International Journal of Research Publication and Reviews 3 (11): 496–99.
16. Gray, J., V. N. Franqueira, and Y. Yu. 2016. "Forensically-Sound Analysis of Security Risks of Using Local Password Managers." In 2016 IEEE 24th International Requirements Engineering Conference Workshops (REW), 114–21. IEEE.
17. Cherckesova, L. V., O. A. Safaryan, O. S. Buryakova, and V. M. Porksheyan. n.d. "Development of Password Manager Using Cryptographic Algorithms for Data Protection in Windows and Linux Operating Systems."
18. Mesina, P. 2025. "The Design and Implementation of a Cross-Platform and User-Friendly Password Manager with Enhanced Security." Master's thesis, University of Cyprus, Faculty of Pure and Applied Sciences.
19. Kotenko, I., D. Gaifulina, and I. Zelichenok. 2022. "Systematic Literature Review of Security Event Correlation Methods." IEEE Access 10: 43387–420.
20. Zhang, D., and D. Zhang. 2011. "The Analysis of Event Correlation in Security Operations Center." In 2011 Fourth International Conference on Intelligent Computation Technology and Automation, Vol. 2, 1214–16. IEEE.
21. Kotenko, I., A. Fedorchenko, I. Saenko, and A. Kushnerevich. 2018. "Parallelization of Security Event Correlation Based on Accounting of Event Type Links." In 2018 26th Euromicro International Conference on Parallel, Distributed and Network-Based Processing (PDP), 462–69. IEEE.
22. Sharma, B., C. N. Sekharan, and F. Zuo. 2018. "Merkle-Tree Based Approach for Ensuring Integrity of Electronic Medical Records." In 2018 9th IEEE Annual Ubiquitous Computing, Electronics & Mobile Communication Conference (UEMCON), 983–87. IEEE.
23. Parida, P., S. Konhar, B. Mishra, and D. Jena. 2017. "Design and Implementation of an Efficient Tool to Verify Integrity of Files Uploaded to Cloud Storage." In 2017 7th International Conference on Communication Systems and Network Technologies (CSNT), 62–66. IEEE.
24. Liu, Z., L. Ren, Y. Feng, S. Wang, and J. Wei. 2023. "Data Integrity Audit Scheme Based on Quad Merkle Tree and Blockchain." IEEE Access 11: 59263–73.
25. Khazaei, A., M. Ghasemzadeh, and V. Derhami. 2016. "An Automatic Method for CVSS Score Prediction Using Vulnerabilities Description." Journal of Intelligent & Fuzzy Systems 30 (1): 89–96.
26. Wang, E., J. Chen, W. Xie, C. Wang, Y. Gao, Z. Wang, and B. Wang. 2024. "Where URLs Become Weapons: Automated Discovery of SSRF Vulnerabilities in Web Applications." In 2024 IEEE Symposium on Security and Privacy (SP), 216–16. IEEE Computer Society.
27. Dell'Amico, M., P. Michiardi, and Y. Roudier. 2010. "Password Strength: An Empirical Analysis." In 2010 Proceedings IEEE INFOCOM, 1–9. IEEE.

Chandrayaan-3 Mission to the Moon: A Systematic Review of Analysis, Improvements, Challenges and Lunar Science Contribution

Milind Shah [1*], Dhairya Vyas [2], Kinjal A Patel [3], M. AnanthaLakshmi[4], Roopal Rajput[5], S.Lokesh [6]
[1] Assistant Professor, Department of Computer Engineering,
Sardar Vallabhbhai Patel Institute of Technology (SVIT), Vasad, Gujarat, India
milindshahcomputer@gmail.com[1*]
[2]The Maharaja Sayajirao University of Baroda, Vadodara, Gujarat, India
dhairya.vyas-cse@msubaroda.ac.in[2]
[3] Associate Data Scientist, Builure Services Pty. Ltd.,
Melbourne, Victoria, Australia
kinjal5721@gmail.com [3]
[4] Electronics & Communication Department,
Meenakshi College of Engineering,
Chennai, Tamil Nadu, India
anantha.mceece@gmail.com
[5] Department of Mobile Application and Technologies,
Centre for Professional Courses,
Gujarat University,
Ahmedabad, Gujarat, India
rajputroopal123@gmail.com
[6] Electronics & Communication Department,
SRM Institute of Science and Technology,
Katankulathur, Chengalpattu, Tamil Nadu, India
lokesha@srmist.edu.in
* Corresponding Author
Milind Shah*
1 Assistant Professor, Department of Computer Engineering,
Sardar Vallabhbhai Patel Institute of Technology (SVIT), Vasad, Gujarat, India
milindshahcomputer@gmail.com

Abstract. The Chandrayaan-3 mission in India represents a significant milestone in the nation's efforts to pursue space exploration, as it builds upon the accomplishments and knowledge gained from the previous Chandrayaan-1 and Chandrayaan-2 missions. This review article presents an in-depth review of the mission's background, development, and impact. The paper starts by providing an overview of the Indian Space Research Organisation (ISRO), highlighting its historical background and its significant contribution to the progress of India's space program. Subsequently, the paper explores the introductions and histories of the Chandrayaan missions, including Chandrayaan-1, Chandrayaan-2, and the newly launched Chandrayaan-3. The development of these missions is contextualized by a background history, which describes the scientific goals and technological achievements that have been achieved. The paper examines the current constraints of research, with a particular focus on the challenges faced during the Chandrayaan-2 mission, including the disastrous landing of the Vikram lander. The next section examines how Chandrayaan-3 manages these challenges, highlighting its advancements and resolved challenges. The comparison between Chandrayaan-2 and Chandrayaan-3 emphasizes the progress and distinctive characteristics of the latter. The mission objectives, technological enhancements, and methods of Chandrayaan-3 are clearly defined to highlight its unique contributions to the exploration of the moon. Ultimately, the review paper ends by offering insights into the probable consequences of Chandrayaan-3's success. It examines the consequences of scientific breakthroughs, technological progress, and India's position in the international space community. Chandrayaan-3 represents both progress in lunar exploration and India's increasing proficiency and aspiration in space exploration.

Keywords: Chandrayaan-3 · Moon Mission · Space Exploration · Technology · Lunar Science · Lander · Rover.

1 Introduction

1.1 Introduction & History of Indian Space Research Organization (ISRO)

ISRO was founded in November 1969 as the operational section of India's Department of Space (DOS). India founded the Space Commission and Department of Space in June 1972. The DOS took over ISRO in September of the same year. The Space Commission established and manages the Indian Space Program rules. Space science and technology should be advanced and used for the country's economic benefit. These initiatives are mostly implemented by ISRO, PRL, NARL, NE-SAC, and SCL. Space-related products and services are promoted and sold by state-owned Antrix Corporation, formed in 1992.

The INSAT Coordination Committee (ICC), the Planning Committee on National Natural Resources Management System (PC-NNRMS), and the Advisory Committee for Space Sciences (ADCOS) are national-level bodies tasked with coordinating the development and utilization of space systems.'

An administrative institution in the field of space research, the Advisory Committee for Space research (ADCOS) is responsible for promoting and supporting activities that are carried out inside the United States. In the Indian Space Program, the Astronomy and Astrophysics Department (ADCOS) serves as the coordinating organization that is accountable for providing support for missions in the domains of Astronomy and Astrophysics, Space Weather, Planetary Exploration, and Weather and Climate Science [1].

1.2 Brief Introduction of Chandrayaan-1

India's first lunar orbiter, Chandrayaan-1, was launched by PSLV-XL. The mission began October 22, 2008. With the successful launch and operation of Chandrayaan-1, the Indian Space Program entered a new phase and achieved major scientific results [1].

1.3 Brief Introduction of Chandrayaan-2

Chandrayaan-2 is an enhanced version of the orbiter spacecraft that was launched. Chandrayaan-2's two components are the 'Orbiter Craft' and 'Lander Craft' The three-ton Orbiter Craft Module bus structure is made of a core composite cylinder, strain webs, and deck panels. HAL developed it. The additional spacecraft subsystems and payloads were built onto it at the ISRO Satellite Center in June 2015. The Chandrayaan-2 project will send a Lander module with a Rover to the moon to put an Orbiter around it. GSLV-MKII is slated to launch Chandrayaan-2 in the first quarter of 2018.' The primary goals of the Chandrayaan-2 mission are to strengthen the scientific objectives of Chandrayaan-1 by improving the resolution of the observation of orbiter research payloads. This will be achieved by the design, realization, and deployment of a Lunar Lander module that can perform a soft landing on a specified point on the moon. In addition, the mission will deploy a Rover to conduct on-site research and remote sensing analysis of the lunar surface [1].'

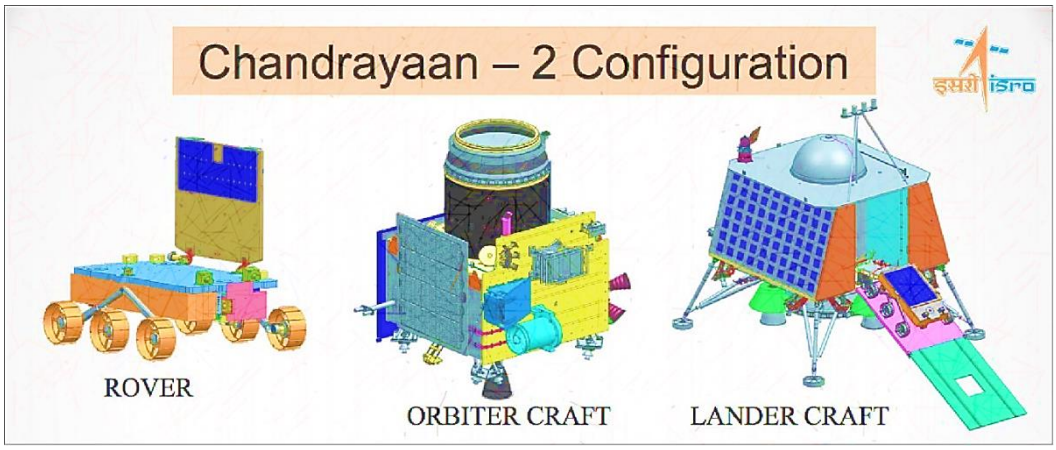

Fig 1. Configuration of Chandrayaan-2 (Credit to ISRO)

1.4 Brief Introduction of Chandrayaan-3

‘ India made history by being the first nation to successfully land on the moon's South Pole area, which had previously been less explored. However, the journey that led to the achievement of this crucial milestone began in 2008, when India launched its first lunar mission, which was given the designation Chandrayaan-1 and had eleven payloads. The south pole of the moon was the primary target of that project, and the mission was planned to discover the mineral composition of the moon, as well as the water-ice composition of the moon's poles, the chemical composition of lunar rocks, and other information on the development of the moon. Chandrayaan-2, India's second lunar expedition, was launched after the success of the first mission. It consisted of eight payloads, a lander, and a rover, and its purpose was to expand the research conducted by Chandrayaan-1 and to show a soft landing on the lunar surface. Due to a technical problem, the lander was unable to maintain communication with the ground station barely 2.1 kilometers above the moon's surface; nevertheless, the orbiter has remained operational until now. Immediately following that, India launched its third lunar mission, Chandrayaan-3, to complete its objective of showing a smooth landing on the moon's surface. On August 23, 2023, India made history by being the first nation to land on the moon's South Pole. It was also the fourth nation to show a soft landing on the moon during the process [2].

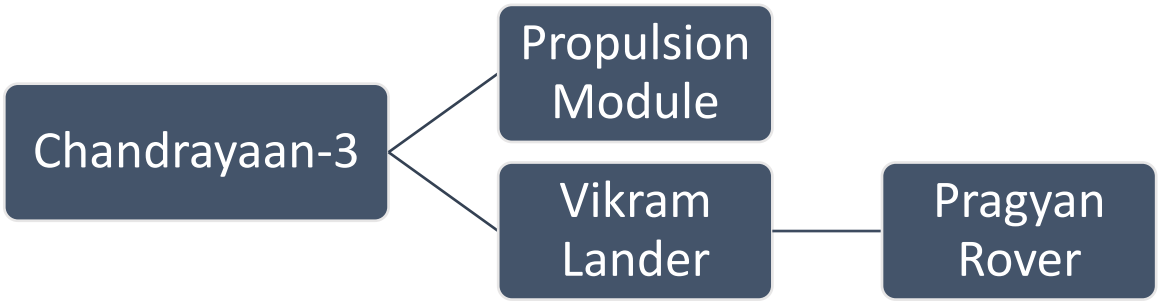

,

Fig 2. Chandrayaan-3 Mission Components [Author’s Work]

1.5 Introduction to Lunar Science

Before quite recently, the Moon was the first and most extensively explored destination in space travel. This was the case until relatively recently. There has been a significant amount of satellite exploration over the course

of history, as shown by the fact that more than 130 moon missions have gone into space. The robotic Luna and crewed Apollo landing missions, the age of high-resolution orbital surveys, and the current revival of lunar exploration with an emphasis on returning to the Moon are the three distinct eras that can be typically distinguished from one another in this exploration tour. The path of analysis has been significantly impacted by each of these periods in their own unique way. When it comes to the progression of humankind's exploration of outer space, the exploration of the moon is generally regarded as the initial step. Additionally, it is regarded to be crucial for humanity to learn the beginnings of the system that consists of the Earth and the Moon. Over the course of the past ten years, the Chinese Lunar Exploration Program (CLEP), which is also known as the Chang'e (CE) Project, has achieved a number of key milestones. These milestones include the exploration of the moon, Earth, and other celestial bodies. The Chinese government's first crewed lunar exploration mission is scheduled to touch down on the lunar near side between the latitudes of 20 degrees north and south. The site is in the Procellarum KREEP Terrane (PKT), which is incompatible with other terrains. There is a striking resemblance between this site and the landing spots of the six crewed flights that Apollo conducted. The challenges of discovering new discoveries and expanding scientific understanding about the moon is presented by the presence of engineering limitations. The subsequent crewed lunar exploration mission that China plans to launch is anticipated to accomplish ultra-long-distance excursions on the Moon's surface that span thousands of kilometers. When it comes to exploiting this technological and technological success to promote scientific research and lunar science, China's crewed lunar exploration presents both obstacles and potential. This research analyzes the current state of affairs, tendencies, and challenges associated with lunar exploration and research operations. The purpose of this research piece is to provide an overview of scientific concerns regarding the Moon that may be of use to crewed missions while also meeting technical criteria. The research presents novel ideas and suggestions for the exploration and analysis of the moon on the moon in the future that will be conducted by humans [3].

According to the research conducted by [4], The Moon has been an essential component in the process of interpreting the development of the solar system. The findings of previous missions have not only revealed current new insights, but they have also brought up significant new issues that have consequences that extend beyond the Moon. Through the use of orbiters, landers, and sample return missions, there are now active efforts being conducted all over the world to answer some of these new concerns, as well as old problems that have not yet been resolved. This includes the Chang'E-4 mission, which is the first far side landing, as well as the Chang'E-5 mission, which is the sample return mission. Several missions from national space agencies are now in early phases of production. The Moon has been an essential component in the process of interpreting the development of the solar system. The findings of previous missions have not only revealed current new insights, but they have also brought up significant new issues that have consequences that extend beyond the Moon. Through the use of orbiters, landers, and sample return missions, there are now active efforts being conducted all over the world to answer some of these new concerns, as well as old problems that have not yet been resolved. Both the Chang'E-4 mission, which was the first landing on the far side, and the Chang'E-5 mission, which was the sample return mission, are included in this group of missions. Many missions that are being developed by national space agencies are now in the preliminary stages of manufacturing. The Chandrayaan-2 mission, which consisted of the first landing at high latitudes on the moon, and the Lunar flashlight mission, which involved multi-laser probing of the lunar poles in the construction of the CubeSat, are two instances of missions that have been carried out. LunaGlob, which is a mission to the lavatube skylights and the magnetic anomalies, is one of the many extra missions that are now being planned or have been proposed. There are also a number of other missions that are currently being planned. A number of opportunities may present themselves, one of which is the possibility of doing scientific study from the Moon. This is in addition to the research that is being done on the Moon itself. The active participation of private sector has been one of the most significant advancements in the field of lunar exploration. This is possibly the most crucial component in maintaining a presence on the Moon for an even longer amount of time, and it has been one of the most significant developments in the field. There have been a number of companies such as Team Indus (India), Astrobotics (United States of America), Moon Express (United States of America), and ILS (Israel), that have been working hard for more than a decade to make it possible for private individual to land on the moon. Even while such a significant achievement has not yet been accomplished, the likelihood of it occurring in the not-too-distant future has been constantly increasing. Additionally, there are current efforts being conducted to analyze the possibility of using lunar material for the purpose of meeting future infrastructure requirements.

Previous research obtained the Moon's spherical form, ignoring terrain errors. The landscape on the Moon is extremely complicated and harsh. The lunar meadow and the highlands are the two basic groups that make up the terrain. At an average distance of one to two kilometers below the lunar geoid, lunar animals are dark, vast, and low plains on the Moon. They are similar to the basins that are seen on Earth. Highlands are regions that are located two to three kilometers above the lunar geoid, which is above the animal. Both the border and the highlands of the lunar animals have a surface that slopes downward. There is a possibility that it will be impossible for Moon-based Earth observation devices to maintain a line of sight in regions that experience considerable topographical variability. In order to conduct Moon-based Earth observation, it is essential to conduct an analysis of the inter-visibility between the sensor and the target on Earth throughout the total lunar terrain. Within the scope of this research, we provide a Moon-based Earth observation inter-visibility technique on the Moon. LOLA, which stands for the Lunar Orbiter Laser Altimeter, is the instrument that provides the foundation for this approach. This method presents the findings of the locations in which the sensor's line of sight would be disrupted, taking into mind the fact that the sensor is positioned in either the Sinus Iridum or the Mare Nectaris zone where it is positioned. It is believed that this intervisibility method will provide assistance in the selection of locations for future lunar exploration missions or Earth surveillance systems that are situated on the Moon. The results of the experiments demonstrate that the approach that was presented is capable of revealing the intervisibility conditions that exist in the region. Within the context of future Moon-based Earth monitoring system or lunar exploration missions, this inter-visibility method will prove to be of great assistance in the detection of suitable landing sites [5].

Space programs worldwide continue to prioritize lunar exploration, which has seen a rebirth in the past decade. The Indian lunar exploration program aligns with world interests. India began lunar exploration in 2008 with Chandrayaan-1, a mission that deployed an orbiter in a 100km circular polar orbit around the Moon. The scientific instruments functioned for around 10 months, transforming our understanding of the Moon. The Moon Impact Probe detected exospheric water and gave high-resolution photos during its fall crushing near the South Pole. Chandrayaan-2, a follow-up mission including an Orbiter, Lander, and Rover, was launched on July 22, 2019. Despite the unsuccessful soft-landing attempt, the orbiter continues to operate with eight scientific experiments. The Ch-3 mission is essential for the lunar program, demonstrating soft landing, wandering, research payload deployment, southern high latitude research, and viewing Earth from lunar orbit. In spite of this, some of the unresolved scientific problems that would be addressed by Chandrayaan-3 analyses include reliable data on the chemistry of the lunar surface, seismic accelerations, thermal conductivity of the regolith, and the environment of the lunar plasma. It is believed that the in-situ measurements taken by Chandrayaan 3 would provide confirmation of the worldwide observations made by Chandrayaan-1 and Chandrayaan-2. The Chandrayaan-3 mission was launched on July 14, 2023. Launched by LVM3-M4, it was put in a 169 km x 36,490 km Elliptic Parking Orbit. The combined Chandrayaan 3 module includes a Lander, Rover, and Propulsion Module (PM). The Lander weighed 1750kg, including the 26kg Rover. To guarantee a smooth landing, Vikram was powered down using an ALS to the specified landing spot, guided by a closed loop Navigation, Guidance, and Control system. Landing occurred on August 23, 2023, at 69.3676 S, 32.3481 E on the Moon. The Chandrayaan-2 Orbiter's OHRC captured the lander. The Rover went about to the landing site and covered approximately 100m after landing. Both the lander and rover were put into sleep mode after their nominal mission life.

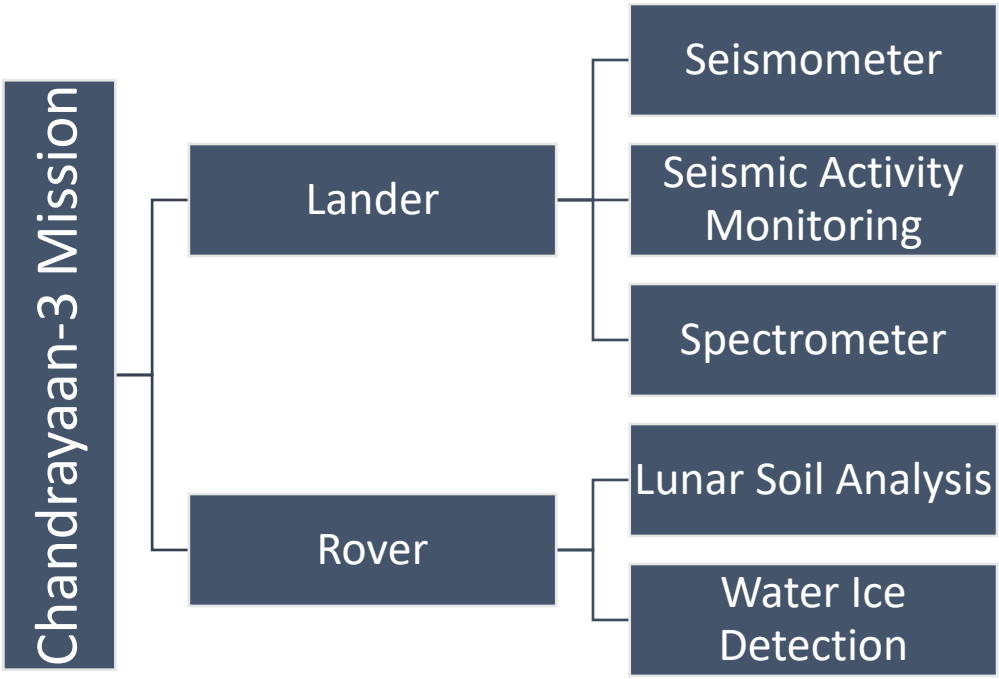

Fig 3. Chandrayaan-3 Lunar Science Mission [Author's Work]

2. Background

2.1 Background History of Chandrayaan-1

' In 2008, the Indian Space Research Organization (ISRO) successfully launched the Chandrayaan-1 orbiter mission to the Moon, initiating India's planetary exploration endeavors. Aboard Chandrayaan-1, a total of eleven remote-sensing scientific equipment contributed by the Indian Space Research Organization (ISRO), the National Aeronautics and Space Administration (NASA), and the European Space Agency (ESA) have achieved noteworthy discoveries. Water signature, spinel minerals, lava tubes on the moon, signs of recent volcanic activity, boulder movements caused by impacts, and sputtered atomic oxygen and backscattered helium are also part of the findings.'

The Mars Orbiter Mission (MOM), India's inaugural interplanetary endeavor, was effectively launched by a PSLV rocket on November 5, 2013. On September 24, 2013, it successfully entered an elliptical orbit around Mars, carrying five science packages.'

2.2 Background History of Chandrayaan-2

' The Chandrayaan-2 spacecraft has three components: the Orbiter, Lander, and Rover. This composite module was sent to the Moon. In the first three months of 2018, the Chandrayaan-2 Mission is expected to be launched aboard the Geosynchronous Satellite Launch Vehicle (GSLV). The consolidated stack will be transported to the moon by the Orbiter until the Lunar Orbit Insertion (LOI) occurs. Once the stack is firm, it is placed into a 100 km × 100 km lunar orbit. 'Subsequently, it is anticipated that the Lander, carrying the Rover, would detach from the Orbiter in order to execute an easy landing in nearby of the southern polar region of the lunar surface [1].

2.3 Background History of Chandrayaan-3

Chandrayaan-3, the third lunar mission, was launched by the Indian Space Research Organization (ISRO) on July 14, 2023, using the rocket LVM III- M4 from the Sriharikota Space Development Center (SDSC- SHAR). The mission included the Vikram lander and the Pragyan rover. Beginning on the 5th of August, 2023, the

Chandrayaan-3 spacecraft successfully entered lunar orbit. After a series of irrelevant reduction actions, the lander was ultimately released for a gentle touchdown on the lunar surface. On August 23, 2023, India made history by being the first nation to land on the moon's South Pole. Performing scientific experiments and demonstrating a gentle landing on the moon were the primary objectives of this mission. Additionally, the rover was supposed to roam around on the lunar surface. Up to a slope of 12 degrees, the lander is intended to permit a safe landing condition. This function lasts for one lunar day, equivalent to fourteen days on Earth. It is equipped with a Laser Altimeter (LASA), a Lander Horizontal Velocity Camera (LHVC), a Lander Position Detection Camera (LPDC), and a Lander Hazard Detection Avoidance Camera (LHDAC). With its six wheels, the Pragyan rover can traverse a distance of 500 meters across the lunar surface at a pace of one centimeter per second. This is intended to map the surface of the moon. "Shiv-Shakti Point" was the name the Prime Minister of India gave to the location where the Vikram lander landed (Chandrayaan program, Wikipedia). In addition, he stated that the 23rd of August should be marked as National Space Day as a way to pay gratitude for the successful landing of the Vikram lander on that day [2].

3. Challenges Faced by Chandrayaan-2

Chandrayaan-2, India's second mission to explore the moon, was launched on July 22, 2019, to achieve a gentle touchdown on the lunar surface. Nevertheless, the mission was hindered as the Vikram lander could not achieve a triumphant and gentle touchdown on the lunar surface. ISRO's communication with the lander was severed when it was a mere 400 meters from the lunar surface [7] [11]. According to the failure analysis report presented to ISRO, the lander's crash was attributed to a software problem. This glitch led the lander to veer off course from its planned trajectory at an altitude of 2.1 km, and communication was lost before the expected confirmation of touchdown was supposed to occur [6][7]. The lander was expected to decelerate significantly and reduce its speed to a minimum as it approached 400 meters from the lunar surface. This would allow it to remain stationary over the designated landing spot and perform a gentle vertical drop. Nevertheless, due to the software malfunction, the lander deviated from its planned path and collided 750m from the designated landing location [2] [7].

The occurrence of the software fault was unforeseen, as the software had been operating smoothly throughout the whole trial period. The Vikram Lander smoothly descended from an altitude of 30 kilometers to 5 kilometers. Following the occurrence of "rough braking," the lander encountered difficulties during the "fine braking," which is the last stage of its descent. The accident caused significant damage to the machinery on board, resulting in a loss of communication from the lander [2]. The trajectory divergence was found at an altitude ranging from 2.1 to 0.2 kilometers above the lunar surface. A communication problem arose during the abrupt deceleration phase of the landing, precisely at 20:23 UTC on September 6, 2019. Subsequent endeavors to restore communication from the lander proved futile [8].

There were three mistakes that led to the hard landing of Vikram:

Higher Thrust from Engines: The primary issue arose from the fact that the five engines employed to decrease the speed generated a greater amount of thrust than initially anticipated [3].

High Velocity: The lander was expected to decelerate significantly and reduce its speed to a great extent by the time it reached a distance of 400 meters from the lunar surface. Nevertheless, as a result of its considerable speed, it collided into the surface of the Moon [2] [3].

Limited Ability to Handle Parameter Dispersion: The problem with Chandrayaan-2 was the severe limitation in its ability to manage parameter dispersion. This problem arose when the lander, despite its proximity to the surface, accelerated as it approached the landing spot, which was a considerable distance away [3].

The crash-landing of the Vikram lander was caused by its deviation from the anticipated tilt angle of 90 degrees, instead tilting at an angle of 410 degrees [11].The aforementioned problems resulted in the unsuccessful

accomplishment of Chandrayaan-2's goal to achieve a gentle touchdown on the lunar surface. The unsuccessful outcome of the Chandrayaan-2 mission yielded vital insights for forthcoming lunar expeditions. The insights acquired from the Chandrayaan-2 mission were applied to tackle the intricacies of the Moon's southern pole and enhance the preparations for the Chandrayaan-3 mission [1].

4. Challenges Resolved by Chandrayaan-3

In order to resolve the challenges encountered by Chandrayaan-2 and guarantee the triumph of Chandrayaan-3, ISRO enacted many modifications and applied advanced technological enhancements:

1) **Robust Design and Testing:** The design of Chandrayaan-3 included both hardware and software upgrades, which involved improving the legs of the lander to enable a safe landing on the lunar surface. The mission also included comprehensive redundancies at every level, rigorous simulations, and further testing carried out at various phases [9] [10].
2) **Improved Guidance and Control Systems:** The mission incorporated sophisticated sensors, actuators, and other essential hardware to improve navigation, positioning, and control throughout the landing phase. Chandrayaan-3 was equipped with a larger quantity of fuel and an improved guidance, navigation, and control system, enabling it to effectively rectify significant deviations from its intended trajectory [4] [5].
3) **Mission Design Modifications:** Modifications were made to the trajectory and approach angles, resulting in enhanced control during the descent and landing phase. These changes were strengthened through extensive ground tests using helicopters and cranes [4].
4) **Learning from Past Experiences:** ISRO applied the acquired knowledge from Chandrayaan-2 to tackle the intricacies of the Moon's South Pole. Novel simulation test beds were developed to examine failure situations, and the spacecraft underwent rigorous testing to evaluate its resilience against vibrations and landing procedures [1].
5) **Enhanced Autonomy:** Chandrayaan-3 was equipped with the ability to independently manage a broader spectrum of dispersion, enhancements in sensors, software, and propulsion systems. The purpose of this was to guarantee that in the event of a complete sensor failure, the lander would still successfully execute a landing [9] [1].
6) **International Collaboration:** The mission incorporated a NASA passive Laser Retroreflector Array for the purpose of lunar laser range investigations, demonstrating global teamwork and scientific cooperation [9].

The careful approach adopted by ISRO in the creation of Chandrayaan-3, along with the implemented improvements, significantly contributed to the mission's successful outcome. Chandrayaan-3 successfully landed on the Moon, marking India as the fourth country to accomplish this remarkable achievement [5]. The accomplishment of the mission serves as evidence of ISRO's capacity to assimilate knowledge from previous encounters, adjust accordingly, and employ novel technology to surmount the obstacles associated with lunar exploration.

5. Comparative Analysis of Chandrayaan-2 vs Chandrayaan-3

ISRO, which is an initial that stands for the Indian Space exploration Organization, is now finishing up preparations for its third lunar exploration mission, which is called Chandrayaan-3 and is scheduled to be launched on July 14, 2023. In addition to rover exploration, the purpose of this mission is to correct the problems that occurred during its predecessor, Chandrayaan-2, and to successfully perform a soft landing on the surface of the moon after it has completed its exploration. Within the parameters of this article, we will analyze the fundamental differences that exist among these two missions.

5.1 Mission Design & Approach

Chandrayaan-2

- In addition to an orbiter, the Chandrayaan-2 mission also included a lander called Vikram and a rover called Pragyan.

- A success-based approach was used in the mission's planning to achieve a precise landing within a prescribed 500-meter-by-500-meter rectangle.
- In addition to having five legs, the Vikram lander was equipped with a central thruster.

Chandrayaan-3

- Failure-based techniques are the main objective of Chandrayaan-3's design, which aims to improve the mission's overall success.
- The orbiter is not included in the mission's architecture; instead, it consists of a lander called Vikram and a rover called Pragyan.
- Because of the expansion of the landing area, the lander can now safely touch down anywhere within a footprint that is 4 kilometers by 2.4 kilometers.
- The Vikram lander has been outfitted with more fuel to enable it to travel further distances to the landing spot or an alternative location, should it be required.
- High-resolution images from Chandrayaan-2's orbiter have been included in the landing site analysis process, which has improved.
- Several modifications have been made to the physical construction of the lander. These modifications include the removal of the center thruster, the strengthening of the legs in order to permit more notable velocity landings, and the addition of additional solar panels in order to facilitate enhanced power production.

5.2 Payloads & Scientific Instruments

Chandrayaan-2

The Chandrayaan-2 spacecraft carried scientific equipment on its orbiter, lander, and rover as part of its payload requirements.

- Among other things, the orbiter was equipped with equipment to investigate the Moon's surface and exosphere.
- For the purpose of conducting elemental analysis, the Pragyan rover was outfitted with both an Alpha Particle X-ray Spectrometer (APXS) and a Laser Induced Breakdown Spectroscope (LIBS).
- RAMBHA, ChaSTE, ILSA, and LP were the payloads that were carried by the Lander spacecraft. Each of these payloads was meant to measure a different component of the lunar environment.

Chandrayaan-3

Chandrayaan-3's propulsion module is responsible for transporting the SHAPE payload, which is intended to use spectro-polarimetry to look for planets that might potentially support life.

Lander payloads include ChaSTE, ILSA, and LP, comparable to Chandrayaan-2, measuring seismicity, thermal characteristics, etc. RAMBHA is a NASA-developed instrument.

To do an in-situ elemental composition study, the rovers' payloads remain consistent with APXS and LIBS.

5.3 Implementation & Soft Landing

Chandrayaan-2

An attempt was made by the Vikram lander to perform a soft landing on the surface of the moon; but, owing to a malfunction that occurred at the very last minute, the lander was unable to accomplish this goal during the descent phase.

As a result of the failed landing, the Pragyan rover, which was part of Chandrayaan-2, could not be deployed.

Chandrayaan-3

During the Chandrayaan-3 mission, the Vikram spacecraft is going to do a soft landing, and the Pragyan rover is going to be sent to the surface of the moon in order to carry out explorations.

Alterations to the design and enhancements to the process of determining the landing spot both increase the likelihood of a successful landing.

5.4 Challenges

Because of the failure of Chandrayaan-2, the variety and challenges of lunar exploration were brought to light, which led to the development of a failure-based strategy for Chandrayaan-3.

Chandrayaan-3 is successful in achieving its mission goals with remarkable performance; India has become the fourth nation in the world to successfully make a soft landing on the Moon, following the United States of America, Russia, and China.

6. Uniqueness of the Chandrayaan-3 Mission

Chandrayaan-3, India's third expedition to the moon, has achieved notable success due to its distinctive characteristics and meticulous preparation. The mission's objective, which is a continuation of Chandrayaan-2, is to showcase the complete ability to land safely and move about on the moon's surface [13]. The mission commenced on July 14, 2023, with an anticipated operational duration of two weeks. It aimed to conduct a range of experiments, including the examination of the lunar surface's mineral composition using a spectrometer [12].

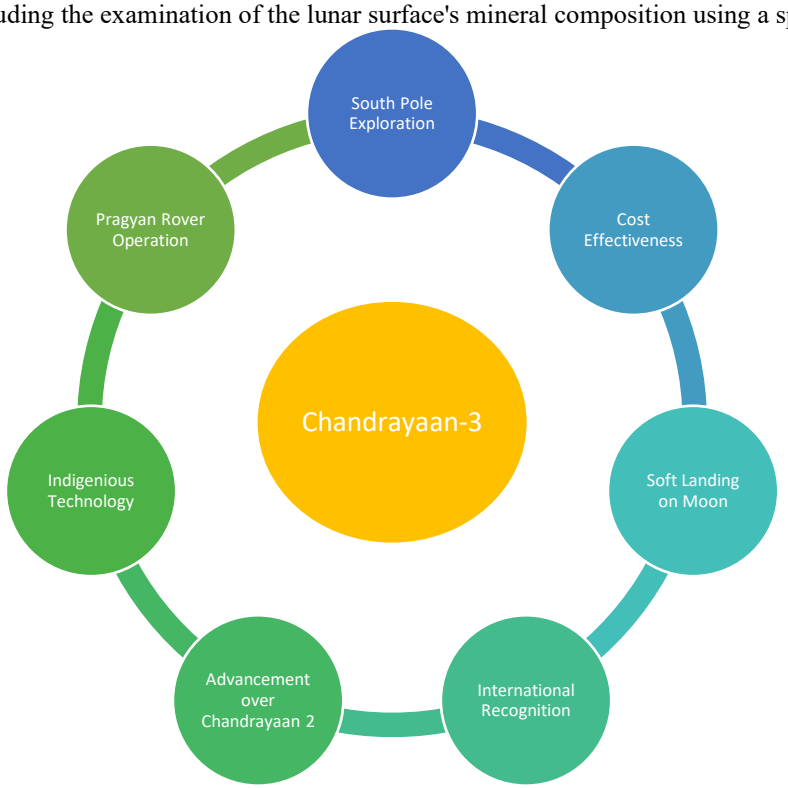

Fig 4. Uniqueness of Chandrayaan-3 Mission [Author's Work]

The uniqueness of the Chandrayaan-3 missions lies in several aspects that have contributed to its success. These include:

- **Lander and Rover Configuration:** Chandrayaan-3 is comprised of a Lander and Rover setup. This arrangement diverges from Chandrayaan-2, which also encompassed an orbiter [16]. The Lander's height is approximately 2 meters, while its mass exceeds 1,700 kilograms, which is comparable to that of an Soviet Union. The purpose of its design is to facilitate the deployment of a more compact lunar rover weighing 26 kilograms [12].
- **Targeted Lunar South Pole:** The objective of the Chandrayaan-3 mission is to explore the lunar south pole, which is known to contain water ice. This frozen water has the potential to serve as a valuable resource for future moon missions, including the production of oxygen, fuel, and water for sustaining a potential moon colony [12].
- **Improved Landing System:** The lander has been enhanced with additional fuel capacity and reinforced legs to withstand impact. Furthermore, a method has been implemented to expand the probable landing area, hence increasing the probability of mission success [12].
- **Innovative Technologies:** The Lander incorporates various sophisticated technologies proven successful in terrestrial circumstances through a series of specialized tests [13]. ISRO employed several cutting-edge technology in the Chandrayaan-3 project, including as a novel lander configuration and an advanced rover. [17].
- **Successful 'Hop' Experiment:** The project achieved another notable milestone with the successful execution of the 'hop' experiment by the Vikram lander, signifying a significant advancement in the field of lunar exploration [15].
- **Scientific Payloads:** The mission transported multiple scientific payloads to investigate the lunar surface. The payload called Spectro-polarimetry of Habitable Planet Earth (SHAPE) was used to investigate the Earth's atmosphere. Additionally, Chandra's Surface Thermophysical Experiment (ChaSTE) was employed to test the thermal conductivity and temperature gradient of the lunar surface [13][19].

7. Scientific Discoveries of Chandrayaan-3

Four components make up Chandrayaan-3: a rover, a lander module (LM), and a propulsion module (PM) that were all manufactured in India. In order to accomplish the mission's objective, new technologies for interplanetary missions were developed and demonstrated.

The Vikram lander includes a number of instruments, such as the Chandra's Surface Thermophysical Experiment (ChaSTE), which is designed to measure surface thermal properties; the Instrument for Lunar Seismic Activity (ILSA), which is designed to measure seismicity around the landing site; the Radio Anatomy of Moon Bound Hypersensitive ionosphere and Atmosphere (RAMBHA), which is designed to analyze the gas and plasma environment; and a passive laser retroreflector array, which was provided by NASA for lunar ranging studies. All of these instruments are installed on the Vikram lander.

The rover Pragyan, which is Sanskrit for "wisdom," is going to carry out a chemical survey of the surface of the moon at its current location within the mountains that are located near to the south pole of the Moon. This survey will take place while the rover is traveling around in the mountains. At this site, the six-wheeled rover will conduct experiments for a period of one lunar day, which is equivalent to 14 days on Earth.

Two different instruments are installed aboard the rover, and their purpose is to conduct an analysis of the elemental composition of the local surface. An Alpha Particle X-ray Spectrometer (APXS) and a Laser Induced Breakdown Spectroscope (LIBS) are the instruments that are considered to be in concern.

Immediately following the failure of Chandrayaan-2, the focus was directed towards its essential landing, which required intensive simulations. The lander was outfitted with landing legs that were more robust, an increased amount of fuel, and enhanced sensors. There was a modification made to the program, and the area for landing

was increased.
During the process of manufacturing the two instruments that Pragyan is currently carrying, there have been a number of challenges to overcome.
The most difficult challenge was to construct the electronics in such a way that they would not damage the superb energy resolution that was offered by the cutting-edge Silicon Drift Detector (SDD), which is the X-ray detector that is utilized in APXS. There are Cm-244 radioactive sources that are utilized by the APXS system in order to animate materials that are located on the surface of the moon. It was a significant problem to acquire such sources and to manage them throughout the development cycle and the various stages of testing [27]. This was owing to the radiation safety concerns that were involved.

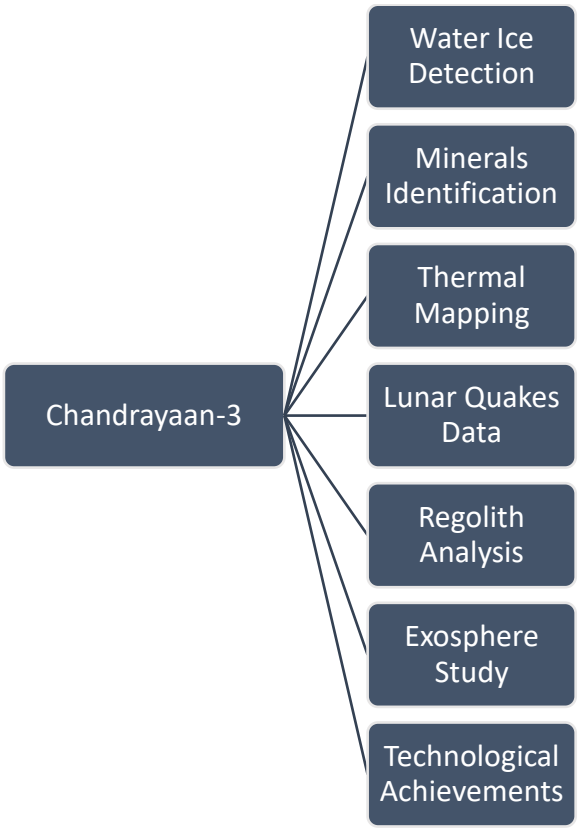

Fig 5. Scientific Discoveries of Chandrayaan-3 [Author's Work]

8. Impact of Chandrayaan-3 Success

Chandrayaan-3's triumph has solidified India's position as a prominent participant in space exploration [15]. India's space ambitions and worldwide stature have been enhanced [14]. The successful outcome of the mission is a credit to the diligent efforts and unwavering commitment of the scientists and engineers at ISRO [17]. The knowledge gained from the mission will be extremely helpful for future space exploration missions and ISRO's future interplanetary expeditions [18]. The mission has moreover yielded useful observations regarding the Moon's geology, mineralogy, and ecology, enhancing our comprehension of the world that humanity intends to occupy in the near future [15].

Furthermore, the achievement of Chandrayaan-3 is anticipated to exert a substantial influence on India's industrial and technical ecosystem. Union Finance Minister Nirmala Sitharaman emphasized that the success of Chandrayaan-3 will significantly influence India's industrial and technological sectors, particularly in terms of the

country's space industry and scientific progress [16]. Chandrayaan-3's achievement may be credited to its collaborative approach, emphasis on accurate landing, and its twin focus on technology demonstration and scientific investigation. These factors have significantly contributed to India's increasing expertise in space research. The mission has enhanced India's space exploration capabilities and yielded vital scientific information that will influence future lunar exploration initiatives.

9. Phases of Chandrayaan-3 Mission

The Chandrayaan-3 mission lasted for around 40 days and consisted of a series of phases that were totally devoted to the various stages of the spacecraft, beginning with the launch and ending with the landing. Before going on to the lunar transfer trajectory, there are three sub-stages of launching and rotating about the planet that occur during Phase 1: the Centric Phase. These sub-stages are known as the Pre-launch Phase, Launch and Ascent Phase, and planet-bound Manoeuvre Phase. The phase that follows the lunar transfer trajectory is called the centric phase. During this phase, the satellite begins to revolve around the moon and progressively gets closer and closer to the surface of the moon. The lander was deployed by the propulsion module after it had travelled roughly 100 kilometers into lunar orbit. The lander then enters the surface of the moon and, upon detecting the gravitational pull of the moon, it applies a downward force to the lander as it moves towards the lunar surface. It eventually lands on the moon's south pole, releasing the rover that is carrying a variety of instruments that have been finely calibrated for the purpose of conducting in-situ studies of the moon (https://www.isro.gov.in/) [26].

The instruction to transition from a horizontal orientation to a falling orientation was delivered to the lander during the landing phase. This command was sent when the lander was at an altitude that was greater than 30 kilometers from the surface of the moon. The time it took was around 690 seconds, and the speed was 1.68 kilometers per second. During the subsequent phase, the lander was given the instruction to transition from a horizontal position to a vertical position when it was more than 7.4 kilometers away from the surface of the moon. At the same time, the speed at which it approached the surface was slowed down. Approximately 10 seconds were allotted for the maneuvering process. Following the completion of the last step of the landing process, the lander remained in a vertical posture during the whole journey, covering a distance of 28.52 kilometers to arrive at the planned landing spot. Finally, the lander's velocity was lowered to zero. In the subsequent step, the barriers that were present at the landing site were analyzed by carrying out the necessary tests. This was done in order to determine whether or not it would be advisable to proceed with the preplanned landing or to move the landing area to a more secure one. Remote monitoring and control, greater conditions awareness, improved communications, and automated decision making were all essential components of the Chandrayaan-3 mission throughout its whole, beginning with its launch and moving all the way through to its gentle landing. Devices and sensors connected to the internet of things made this a reality. It is the responsibility of Internet of Things sensors to analyze and continue monitoring the health of Chandrayaan-3's engines, batteries, and other essential systems in order to guarantee precise and efficient functioning. While Internet of Things devices communicate data from cameras as well as sensors in order to monitor the Chandrayaan-3 and keep track of the studies that its gadgets and sensors carry out, internet of things devices do not transmit data. The Chandrayaan-3 is able to optimize its navigation and communication systems through the utilization of the Internet of Things (IoT) [26]x`.

10. Improvements in the Chandrayaan-3

The complicated Chandrayaan-3 mission has demonstrated India's ability in being able to handle complex spacefaring missions such as this one, which no other country in the world, not even rich ones, has been able to accomplish successfully. Among the many accomplishments that India accomplished via carefully synchronized operations, the safe soft landing on the south pole of the moon will be recognized as one of the most significant in history. The Internet of Things was utilized at every stage of the development of this significant achievement in the fields of astronomy and engineering. This spacecraft comes equipped with a variety of Internet of Things devices and sensors, which allow it to monitor its own health and keep track of the progress it has made in addition to being able to manage it. It was also discovered that there was evidence of significant space weathering. It was determined through the analysis of the soil's composition that the soil that was found at the landing location was

of the highland type. The primary landing location was subjected to a thermophysical analysis, which revealed that the temperature varied between 30 degrees Celsius and 175 degrees Celsius during the day. Therefore, this journey to the moon will contribute to a better knowledge of the surface of the moon [26].

11. Outcome from the Chandrayaan-3

A considerable amount of knowledge was revealed as data from Chandrayaan-3. The data was collected from each component of the Chandrayaan-3 and released by the Indian Space Research Organisation (ISRO) for scientific research utilization [27]. The data is collected using all three major components of Chandrayaan-3: navigation camera, rover, and lander. Therefore, a total of 3 datasets are collected and each dataset's archived directory is available from the Indian Space Research Organisation (ISRO) [27]. Each dataset has a specific structure in an archived directory including mission archived structure, instrument archived structure, data products, and naming conventions. All these structures are provided and discussed in the documentation of each dataset as well. A mission-archived structure organizes the data concerning the mission which is Chandrayaan-3 while an Instrument-archived structure organizes with concerning the level of processing of data and its products. All this data can be analyzed using the planetary data system (PDS) version 4 visualization tool [28].
The **logical_identifier** uniquely identifies the data product, while the **version_id** specifies its version. The **title** describes the data product, and **information_model_version** indicates the model version used. The **product_class** categorizes the type of product, and the **modification_date** records the last update. The **description** provides a summary of the data, while **start_date_time** and **stop_date_time** define the time range of the observation. The **purpose** explains the data's intent, and **processing_level** reflects its data processing stage. The **name** gives the product name, and **type** defines its nature (e.g., satellite). The **lidvid_reference** links to the mission context, and **reference_type** specifies its usage. The **job_id** relates to the processing task, and **dumping_orbit_number** identifies the orbit during data collection. The **dop** is a reference quality metric, and **frame_number** specifies the captured frame. The **current_mobility_id** and **future_mobility_id** track rover states, while **operation_id** is linked to mission activities. The **day_no** and **year** define the temporal context. The **inclinometer_utc** records the inclinometer timestamp, with **inclinometer_x_angle**, **y_angle**, **roll_angle**, and **pitch_angle** describing orientation data. The **sensor_id** identifies the imaging device, and **gain** specifies signal amplification. The **integration_time** defines the camera exposure duration. The **file_name** contains the data file's name, **creation_date_time** is when the file was created, and **file_size** indicates its size. The **md5_checksum** ensures data integrity, the **comment** provides additional notes, the **offset** sets a calibration reference, and the **encoding_standard_id** defines the format standard used.

Navigation Camera Data Archive: The archive structure of navigation camera data is a collection of two types of data including raw data and calibrated data [29]. The raw data has no correlation and specific meaning while calibrated data provides meaningful data with radiometrically corrected data with refined coordinates. Each data comprises two files with different formats, including the image data in JPG format, and the corresponding label in XML format. The navigation camera data archive provides documentation that describes the directory-level structure and naming convention meanings of both raw and calibrated data [29].

Figure 7 shows a calibrated image captured by the Navigation Camera onboard Chandrayaan-3. This data is essential for rover navigation and terrain mapping. The key field in the metadata table for each image represents the parameter or attribute name used to describe the associated values of the image.

Fig 6. Raw image from Navigation Camera [Author's Work]

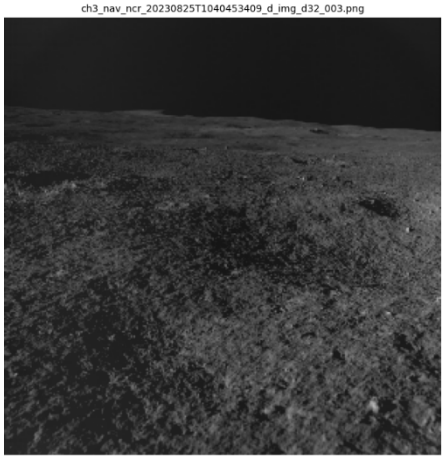

Key	Value
logical_identifier	urn:isro:isda:ch3_chr:nav:data_calibrated:ch3_nav_ncr_20230825t1040453409_d_img_d32_003
version_id	1.0
title	Chandrayaan-3 Rover NavCam Mobility Experiment
information_model_version	1.11.0.0
product_class	Product_Ancillary
modification_date	2024-06-11
description	Moon is a natural satellite of Earth
start_date_time	2023-08-25T10:40:45.3409Z
stop_date_time	2023-08-25T10:40:46.6597Z
purpose	Navigation
processing_level	Calibrated
name	ch3_nav_ncr_20230825T1040453409_d_img_d32_003
type	Satellite
lidvid_reference	urn:isro:isda:context:investigation:mission.chandrayaan3::1.0
reference_type	data_to_investigation
pb_id	NCBXXD32C3R0018000NNNN23237113106000_V2_1
dumping_orbit_number	180
dop	20230825
frame_number	3
current_mobility_id	002
future_mobility_id	003
operation_id	000001
day_no	237
year	2023
inclinometer_utc	2023:237:10:49:00:7082023:237:10:49:00:578
inclinometer_x_angle	-0.907
inclinometer_y_angle	-4.672
inclinometer_roll_angle	0.0
inclinometer_pitch_angle	0.0
sensor_id	right camera
gain	2
integration_time	23
file_name	ch3_nav_ncr_20230825T1040453409_d_img_d32_003.png
creation_date_time	2024-06-12T15:36:56
file_size	571980
md5_checksum	4ad2ffadd5f6744dce3c06587b276777
comment	This file contains the count calibrated image in png format. md5_checksum is provided for ensuring data integrity when users are downloading the data.
offset	0
encoding_standard_id	PNG

Fig 7. Calibrated image from Navigation Camera [Author's Work]

Rover Data Archive: The archive structure of rover data is a collection of L1 level 1 processing calibrated data [30]. The rover data archived structure is denoted in two formats. The image with JPG format and the corresponding label is in XML format for calibrated data. The rover data archive provides documentation that provides detailed information about this archived directory. Figure 8 demonstrates the calibrated image data from the rover data archive.

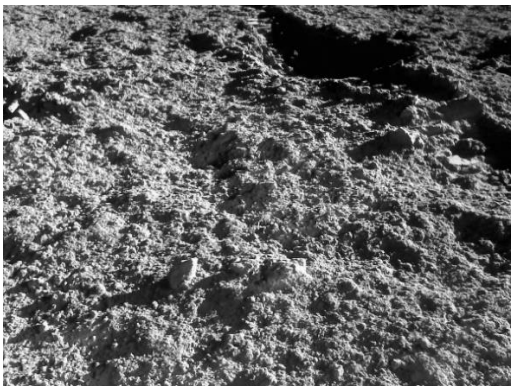

Fig 8. Calibrated image data from the rover data archive [Author's Work]

Lander Data Archive: The archive structure of lander data is a collection of processed calibrated data [31]. Lander Data Archive structures the data using two formats, including the calibrated data image stored using JPG format, and the calibrated data label corresponding to each image is stored using XML format. The lander data archive provides documentation along with the data to understand the levels of each directory under the archived data and its structure, product description, and naming conventions [31].

Figure 9 depicts a calibrated image from the Lander TTP (Terrain Targeting Payload) data archive, focusing on high-resolution imaging for lander navigation and positioning.

Key	Value
logical_identifier	urn:isro:isda:ch3_chl:lim:data_calibrated:ch3_lim_tc4_20230804t0631061600_d_img_gnh_1_001
version_id	1.0
title	Chandrayaan-3 Lander Imager
information_model_version	1.11.0.0
product_class	Product_Ancillary
modification_date	2024-06-11
description	Moon is a natural satellite of Earth
start_date_time	2023-08-04T06:31:06.1600Z
stop_date_time	2023-08-04T06:31:06.1200Z
purpose	Navigation
processing_level	Calibrated
name	ch3_lim_tc4_20230804T0631061600_d_img_gnh_1_001
type	Satellite
lidvid_reference	urn:isro:isda:context:investigation mission.chandrayaan3::1.0
reference_type	data_to_investigation
job_id	LIMXXGNHC3L0002005NNNN23216073930330_V1_1
mode	Mode-1
frame_number	001
imager_id	LI4
file_name	ch3_lim_tc4_20230804T0631061600_d_img_gnh_1_001.jpg
creation_date_time	2024-06-12T17:33:13
file_size	100967
md5_checksum	3e3f2ec89b3dbac091a5da3cf4ddac4d
comment	This file contains the count calibrated image in jpg format. md5_checksum is provided for ensuring data integrity when users are downloading the data.
offset	0
encoding_standard_id	JPEG

Fig 9. Calibrated image data from the lander TTP data archive [Author's Work]

The raw and calibrated data from the Chandrayaan-3 can be utilized for a diverse range of applications. The image data of the moon's surface reveals important information that can further link to such undiscovered aspects of space science.

Figures 10 and 11 would represent similar calibrated data from specific payloads like PLS (Plasma System) and NOP (Neutron Payload), each contributing unique scientific insights into the lunar environment.

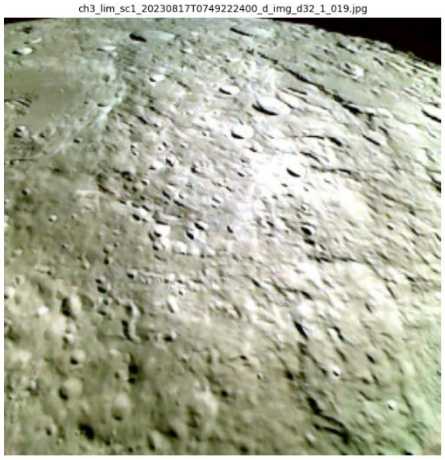

Key	Value
logical_identifier	urn:isro:isda:ch3_chl:lim:data_calibrated:ch3_lim_sc1_20230817t0749222400_d_img_d32_1_019
version_id	1.0
title	Chandrayaan-3 Lander Imager
information_model_version	1.11.0.0
product_class	Product_Ancillary
modification_date	2024-06-11
description	Moon is a natural satellite of Earth
start_date_time	2023-08-17T07:49:22.240OZ
stop_date_time	2023-08-17T07:49:22.136OZ
purpose	Navigation
processing_level	Calibrated
name	ch3_lim_sc1_20230817T0749222400_d_img_d32_1_019
type	Satellite
lidvid_reference	urn:isro:isda:context:investigation:mission.chandrayaan3::1.0
reference_type	data_to_investigation
job_id	LIMXXD32C3L0009605NNNN23229110103054_V1_1
mode	Mode-1
frame_number	019
imager_id	LI1
file_name	ch3_lim_sc1_20230817T0749222400_d_img_d32_1_019.jpg
creation_date_time	2024-06-12T17:31:42
file_size	168705
md5_checksum	0a76b5bc216979eadaa84d21ab2b999a
comment	This file contains the count calibrated image in jpg format. md5_checksum is provided for ensuring data integrity when users are downloading the data.
offset	0
encoding_standard_id	JPEG

Fig 10. Calibrated image data from the lander PLS data archive [Author's Work]

eArtificisl

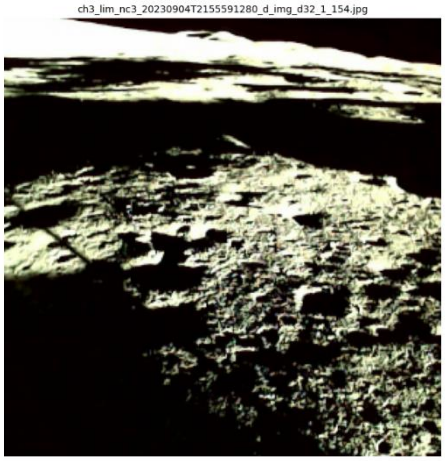

Key	Value
logical_identifier	urn:isro:isda:ch3_chl:lim:data_calibrated:ch3_lim_nc3_20230904t2155591280_d_img_d32_1_154
version_id	1.0
title	Chandrayaan-3 Lander Imager
information_model_version	1.11.0.0
product_class	Product_Ancillary
modification_date	2024-06-11
description	Moon is a natural satellite of Earth
start_date_time	2023-09-04T21:55:59.128OZ
stop_date_time	2023-09-04T21:55:59.240OZ
purpose	Navigation
processing_level	Calibrated
name	ch3_lim_nc3_20230904T2155591280_d_img_d32_1_154
type	Satellite
lidvid_reference	urn:isro:isda:context:investigation:mission.chandrayaan3::1.0
reference_type	data_to_investigation
job_id	LIMXXD32C3L0018007NNNN23247004357009_01_V1_1
mode	Mode-1
frame_number	154
imager_id	LI3
file_name	ch3_lim_nc3_20230904T2155591280_d_img_d32_1_154.jpg
creation_date_time	2024-09-25T15:51:13
file_size	154551
md5_checksum	0540e5da35a8b5bcd3f2deb05c85797c
comment	This file contains the count calibrated image in jpg format. md5_checksum is provided for ensuring data integrity when users are downloading the data.
offset	0
encoding_standard_id	JPEG

Fig 11. Calibrated image data from the lander NOP data archive [Author's Work]

12. Conclusion

Ultimately, the Chandrayaan-3 mission serves as a significant witness to India's expanding proficiency and aspiration in the realm of space research. This mission signifies a substantial advancement for the Indian Space Research Organisation (ISRO) and the nation's space program, as it builds upon the accomplishments and knowledge gained from Chandrayaan-1 and Chandrayaan-2.

This review has presented an in-depth analysis of the historical background, progression, and influence of the Chandrayaan missions, with a focus on the growth of India's space capabilities. The innovations made in Chandrayaan-3 specifically target the challenges seen during Chandrayaan-2, particularly the problems with the landing of the Vikram lander. This showcases the ability of ISRO to adapt and recover from setbacks.

The particular goals and technological advancements of Chandrayaan-3 emphasize its unique contributions to the exploration of the moon. Chandrayaan-3 is expected to accomplish its mission objectives, leading to significant scientific discoveries that will enhance our knowledge of the Moon and enhance India's reputation in the international space community.

References

[1]. K., Durga & Misra, Dibyendu & Amitabh, & Bhatt, Megha & Ambily, G. & A. S, Sachana & Srivastava, N. & Bhardwaj, Anil. (2023). Chandrayaan-3 Alternate Landing Site: Pre-Landing Characterisation.

[2]. V. Sundararajan, "Overview and technical architecture of India's Chandrayaan-2 mission to the moon," *AIAA Aerosp. Sci. Meet. 2018*, no. January, pp. 1–12, 2018.

[3]. K. D. Prasad *et al.*, "Contextual characterization study of Chandrayaan-3 primary landing site," *Mon. Not. R. Astron. Soc. Lett.*, vol. 526, no. 1, pp. L116–L123, 2023.

[4]. A. Kumar and M. Mehfuza, "India'S Journey Towards Moon: From Chandrayaan-1 To Chandrayaan-3," *www.irjmets.com @International Res. J. Mod. Eng.*, no. 08, pp. 2361–2365, 2361.

[5]. R. K. Sinha, A. Rani, T. Ruj, and A. Bhardwaj, "Geologic investigation of lobate scarps in the vicinity of Chandrayaan-3 landing site in the southern high latitudes of the moon," *Icarus*, vol. 402, no. December 2022, p. 115636, 2023.

[6]. T. Sana and S. K. Mishra, "Plasma Sheath around Chandrayaan-3 Landing Site: A Case Study," *Planet. Sci. J.*, vol. 4, no. 9, p. 158, 2023.

[7]. https://www.isro.gov.in/Chandrayaan3_New.html

[8]. O. Calla, S. Mathur, and K. L. Gadri, "Possible Landing site for Chandrayaan-2 Rover," *2016 Int. Conf. Recent Adv. Innov. Eng. ICRAIE 2016*, pp. 1–5, 2016.

[9]. N. P. S. Mithun *et al.*, "Solar X-Ray Monitor on Board the Chandrayaan-2 Orbiter: In-Flight Performance and Science Prospects," *Sol. Phys.*, vol. 295, no. 10, 2020.

[10]. S. Kumar, V. Chaudhary, A. Singh, and P. Chauhan, "Scattering-based Analysis of South Polar Crater of the Lunar Surface Using L-band SAR Data of Chandrayaan-2 Mission," *2021 IEEE India Geosci. Remote Sens. Symp. InGARSS 2021 - Proc.*, vol. 3387710, pp. 459–462, 2021.

[11]. N. Adriani, "Chandrayaan 3 and other moon missions: An Update and Review.," *SSRN*, vol. 23529, no. 2, pp. 1–45, 2018.

[12]. H. Garg et al., "Spacecraft charging analysis for Chandrayaan-2 mission," 2023 Jt. Asia-Pacific Int. Symp. Electromagn. Compat. Int. Conf. Electromagn. Interf. Compat. APEMC/INCEMIC 2023, pp. 1–4, 2023.

[13]. A. R. Chowdhury *et al.*, "Terrain mapping camera-2 onboard chandrayaan-2 orbiter," *Curr. Sci.*, vol. 118, no. 4, pp. 566–572, 2020.

[14]. N. P. S. Mithun *et al.*, "Data processing software for Chandrayaan-2 Solar X-ray Monitor," *Astron. Comput.*, vol. 34, no. July 2019, 2021.

[15]. K. Bhuva *et al.*, "A Machine Learning Framework for Data Filtering: A Case Study on Chandrayaan-1 SIR-2 Data," *2021 IEEE India Geosci. Remote Sens. Symp. InGARSS 2021 - Proc.*, pp. 483–487, 2021.

[16]. A. Kumar *et al.*, "Dielectric Constant Estimation of Lunar Surface Using Mini-RF and Chandrayaan-2 SAR Data," *IEEE Trans. Geosci. Remote Sens.*, vol. 60, pp. 1–8, 2022.

[17]. A. Sinha, Suman, A. Alkhayyat, B. Kumar, A. Kumari, and U. Kumar, "Brain Computer Interface Imagination based Thought Analyser Framwork to Generate and Classify Real Time Image Retrieval System for Space Images in Chandrayaan 3 Lunar Misson," *2023 10th IEEE Uttar Pradesh Sect. Int. Conf. Electr. Electron. Comput. Eng. UPCON 2023*, vol. 10, pp. 882–887, 2023.

[18]. A. G. Desur and R. K. Jatoth, "Enhanced Color Image Quantization Utilizing Hybrid Glowworm Swarm Optimization and K-Means Clustering: A Case Study with Chandrayaan-3 Images," *2024 3rd Int. Conf. Power, Control Comput. Technol. ICPC2T 2024*, vol. 2024, pp. 433–438, 2024.

[19]. V. Rathore, A. Prajapat, and K. Ahuja, "Meet the Rocket Women of Chandrayaan-3: Pioneers in Space Exploration," *3rd IEEE Int. Conf. ICT Bus. Ind. Gov. ICTBIG 2023*, pp. 1–6, 2023.

[20]. Y. Lin et al., "Return to the Moon: New perspectives on lunar exploration," Sci. Bull., vol. 69, no. 13, pp. 2136–2148, 2024, doi: 10.1016/j.scib.2024.04.051.

[21]. D. Dhingra, "The new moon: Major advances in lunar science enabled by compositional remote sensing from recent missions," Geosci., vol. 8, no. 12, 2018, doi: 10.3390/geosciences8120498.

[22]. H. Wang, Q. Guo, A. Li, G. Liu, H. Guo, and J. Huang, "Impact of lunar terrain on moon-based earth observation," Int. Geosci. Remote Sens. Symp., vol. 2019-January, pp. 9260–9262, 2019, doi: 10.1109/IGARSS.2019.8900112.

[23]. S. Megala, "CHANDRAYAAN-3 IN THE CONTEXT OF INDIAN LUNAR SCIENCE PROGRAMME," Αγαη, vol. 15, no. 1, pp. 37–48, 2024.

[24]. J. G. Singla, R. Sharma, A. Shree, A. Amitabh, and N. Dube, "A Novel Deep Learning Approach for data analysis on high resolution Chandrayaan-2 Data," 2024 IEEE Space, Aerosp. Def. Conf. Sp. 2024, pp. 415–418, 2024, doi: 10.1109/SPACE63117.2024.10667960.

[25]. H. Kaur, R. Solanki, B. Alankar, and V. Chang, "India's journey to be part of the World's leading Spacefaring Countries: Chandrayaan-3 Mission," Proc. - 2023 Int. Conf. Ind. IoT, Big Data Supply Chain. IIoTBDSC 2023, pp.

475–478, 2023, doi: 10.1109/IIoTBDSC60298.2023.00087.
[26]. V. Srivastava, “Chandrayaan-3 lands on the Moon’s south pole,” Nat India, pp. d44151-023-00116–x, Aug. 2023.
[27]. “Chandrayaan-3.” Available: https://pradan.issdc.gov.in/ch3/
[28]. “PDS: Tools.” Available: https://pds.nasa.gov/tools/about/
[29]. “Navigation Camera.” Available: https://pradan.issdc.gov.in/ch3/protected/browse. xhtml?id=navcam
[30]. “Rover Image.” Available: https://pradan.issdc.gov.in/ch3/protected/ browse.xhtml?id=ri
[31]. “Lover Image.” Available: https://pradan.issdc.gov.in/ch3/protected/browse.xhtml ?id=li

A Novel Framework for Fake Visual Content Detection Through Hybrid Intelligent Techniques

Vaidehi Vaghela[1][0009-0002-1645-9951], Priti Sadaria[2][0000-0003-4585-5806]
and
Ripal D. Ranpara[3][0000-0002-5823-5406]

[1,2] Atmiya University, Rajkot, India
[3] Marwadi University, Rajkot, India
vaidehibavaghela03@gmail.com
sadariapd@gmail.com
ranpararipal@gmail.com

Abstract

With the growing incidence of fake visual content, efficient detection mechanisms are a must. In this paper, a new hybrid method of detecting fake images is presented by combining Convolutional Neural Networks and Support Vector Machines. The CNN model is used for Feature Extraction, allowing for efficient detection of the images, and SVM for improving the accuracy of classification. Discrete Cosine Transform (DCT) is also utilized to learn frequency-based features from the frequency domain to further enhance the robustness of the model.
The "deepfake_vs_real_image_detection" dataset of 1,081 real and 960 fake images is utilized for training and testing. Experimental results show that the hybrid model performs better than single models, achieving an accuracy of 0.75 compared to 0.71 for CNN and 0.53 for SVM. The enhanced performance shows the efficacy of spatial and frequency-based feature fusion, making the system more robust to advanced fake content. The proposed solution offers a potential solution for the development of fake image detection systems.

Keywords: Hybrid Framework, Convolutional Neural Networks, Support Vector Machines, Frequency Domain Features, Discrete Cosine Transform

1 Introduction

The proliferation of fake visual content, enabled by the advances in image and video editing technologies, poses a significant challenge to digital trust and authenticity. Deepfakes and other manipulated media are increasingly being used for misinformation, fraud, and privacy violations, therefore demanding the development of robust detection mechanisms [1]. Traditional methods often struggle with the evolving complexity of fake content, which means that innovative approaches combining multiple strengths are urgently needed [2].
This paper presents a new, hybridized framework, harvesting the synergistic

potential for deep learning in conjunction with machine learning in the detection of fake visual content. The framework combines Convolutional Neural Networks for automatic and efficient feature extraction with Support Vector Machines for high-accuracy classification [3][4]. CNNs, on one hand, are well suited for learning complex visual patterns, while SVMs, on the other hand, work very well with small datasets that are structured and precise in boundaries [5]. This resulted in the proposed framework harnessing the strengths of both paradigms and enhancing the overall detection capability. The system further integrates frequency domain analysis using Discrete Cosine Transform to extract key features from input images, thus complementing the spatial features learned via CNN [6]. This multi-modal approach ensures robust detection performance even against sophisticated manipulation techniques. Strong empirical evidence is also presented that demonstrates the superiority of a hybrid framework over CNN or SVM standalone models, achieving greater accuracy, precision, and recall on benchmarking datasets [7]. This research pays to the growing field of digital forensics by providing a scalable and efficient solution for fake content recognition. In addition to addressing the drawbacks of individual techniques, the hybridized approach provides a viable path forward for future developments in integrity verification and content authentication.

2 Related Work

This is indeed the need to develop strong visual content detection algorithms due to very rapid advancement of media manipulation techniques. Various methodologies have been studied extensively, ranging from conventional machine learning techniques to powerful deep learning framework approaches. This section reviews key contributions in the field, focusing on hybridizing deep learning and machine learning approaches for fake content detection. Because machine learning techniques, such as Support Vector Machines and Random Forests, are good at handling structured data, they were the mainstay of early image classification efforts. These methods, however, struggled to process high-dimensional image data without extensive feature engineering. The paper reviews various deepfake detection techniques, including video-based methods like XGBoost with YOLO and CNNs, achieving up to 90% accuracy, and image-based approaches using models like MobileNet, Xception, and DenseNet, with accuracies between 80% and 91%. Biometric methods like DeepVision and multimodal techniques address inconsistencies but face limitations in generalization and efficiency. These gaps underline the need for the proposed hybrid DFP model, which offers optimized performance and higher accuracy [8]. Deep learning revolutionized the field by enabling end-to-end learning pipelines, with CNNs becoming the cornerstone for visual content analysis. CNNs are particularly adept at capturing spatial hierarchies in images, making them operative for tasks like object recognition and manipulation detection. However, CNNs often require substantial computational resources and large datasets for training, which can limit their applicability in resource-constrained environments [9It explores many deep learning-based techniques for

identifying the deepfakes, highlighting how they can be used to counteract modified and fraudulent media in audio, video, pictures, and hybrid multimedia. It highlights the evolution of detection techniques, from CNN-based approaches that analyze spatial information in images to RCNN methods leveraging spatial-temporal features in videos. The paper reviews studies on GAN-generated media, feature extraction techniques, and transfer learning for enhanced detection. It also identifies gaps, such as the need for robust generalization and cross-domain performance in existing methods, underscoring the importance of systematic frameworks for effective deepfake detection [10]. This report indicates that the alteration of facial images is one of the major risks to press freedom, and earlier studies relied on manually created features. This research proposes a hybrid architecture and a customized convolutional neural network model for deep learning detection of altered facial photos. In terms of AUC, computational complexity, and resilience to unbalanced datasets, the model performs better than current expert systems. The framework promotes the development of a more robust technique for detecting changed facial images [11]. This research explains how the development of deep learning-based generative models has generated high-quality artificial videos. Weighted dynamic ensemble models with CNN-Recurrent Neural Networks Particle Swarm Optimization network structure and hyperparameter tuning, and 3D Convolutional Neural Networks, are proposed to detect fake videos. To extract efficient discriminative spatial-temporal features, the PSO algorithm adjusts crucial learning parameters of 3D CNNs and RNN structures in CNN-RNN [12]. Research on deepfake detection primarily utilizes deep learning techniques such as CNN and GAN. These methods focus on identifying inconsistencies in visual and temporal features of videos and images, leveraging large-scale datasets for effective training and validation of detection models. A hybrid approach combining multiple machine learning strategies also enhances accuracy detection and robustness[13]. In this paper the literature review highlights advancements in face manipulation technologies, particularly focusing on face swapping and reenactment. The survey emphasizes the evolution from 3D-based methods, which heavily rely on manual processes and fixed 3D face shapes, to more sophisticated deep learning approaches. These approaches utilize Generative Adversarial Networks (GANs) and conditional GANs to enhance realism and decrease the need for extensive subject-specific data, thus addressing significant limitations in scalability and accessibility found in earlier methods [14]. In this paper, the literature review discusses the rapid advancement and widespread implications of deepfake technologies. It covers the evolution from basic manipulative capabilities to highly sophisticated generative models driven by Deep Learning Approaches, particularly GANs. The review also highlights the growing need for effective detection methods due to the increasing realism of deepfakes and their potential to cause significant societal and political disruptions. Additionally, it mentions the need for up-to-date datasets to create more resilient detection systems and identifies current research directions and challenges in combating the threats that deepfakes pose [15]. In this paper pose a great threat to democracy and national security. It mentions earlier manipulation methods in media and newer advancements in deep learning that have improved the reality of

generated content. The review also discusses new forensic techniques that are coming into play to detect these fakes, such as examining inconsistencies in facial expressions and movements that are usually interrupted in deepfake productions [16].

3 Proposed Hybrid Framework

From Figure 1 we can observe that the input layer, process layer, and output layer are the three layers of the suggested hybrid structure. The images are labeled as 0 in the Input Layer for fake images and as 1 for real images. The images are pre-processed before feature extraction, such as converting into grayscale, resizing to 224×224 pixels, and normalization in the range [0,1].

3.1 Proposed Framework Architecture

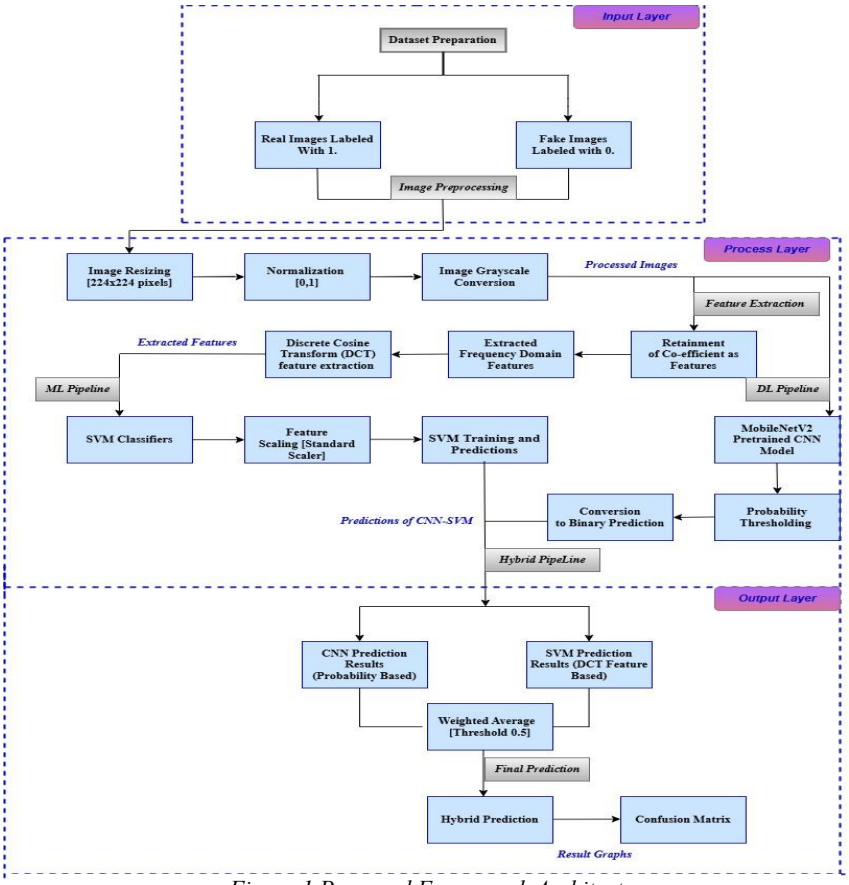

Figure 1 Proposed Framework Architecture

In the Process Layer, two pipelines operate in parallel. The ML Pipeline extracts frequency domain features using Discrete Cosine Transform (DCT), scale them with a Standard Scaler and classifies them using an SVM classifier. The DL Pipeline utilizes a MobileNetV2 pre-trained CNN model to extract deep features and make probability-based predictions, which are then converted into binary outputs using thresholding.
Finally, the Output Layer combines predictions from both pipelines using a weighted averaging method (threshold 0.5) to produce a hybrid prediction. The framework's performance is evaluated using a Confusion Matrix, ensuring a more accurate and robust classification of real and fake images.

3.2 Components of Proposed Framework

Dataset

As shown in Figure 2, there are 1,081 genuine photos and 960 fake images in the "deepfake_vs_real_image_detection" dataset. To ensure that the dataset included an appropriate number of subsets, this was divided into training sets and testing sets. The training set is made up of 80% of the dataset.

Figure 2 Dataset Visuals

Therefore, it will capture individual characteristics and tendencies unique to each class. The test set served as a reference for evaluating the performance of unseen data because the remaining 20% of the dataset was allocated to it. Consistency and robustness in model training and evaluation are provided by this stratified division, which guarantees that the class distribution in the training and testing sub-sets reflects the original dataset. To ensure consistency and compatibility among models, images were loaded from folders, scaled to 224x224 pixels, then normalized to the range [0, 1].

Feature Extraction

In the proposed framework, Feature Extraction plays a vital role by incorporating both spatial and frequency-domain information to effectively identify fake images. Spatial Features are derived using a pre-trained CNN model

(deepfake_detector.keras). The CNN analyzes high-level characteristics of the images, such as patterns, textures, and structural details, which are often altered in manipulated images. These features enable the detection of irregularities like unnatural edges, distortions, or inconsistencies in pixel relationships, which are common indicators of tampering.

Table 1 Feature Extraction from Images

Filename	***Feature_0***	***Feature_1***	***Feture_2***	***Feture_3***	***Feature_4***
real_00001.jpg	187.35	-6.38	-59.33	4.04	13.05
real_00002.jpg	464.82	4.27	71.9	-11.74	12.65
real_00003.jpg	248.72	5.13	-89.24	-46.05	-9.27
real_00004.jpg	181.59	31.37	-37.32	-8.63	9.78
real_00005.jpg	343.5	-7.66	16.22	29.89	-7.93
real_00006.jpg	168.64	18.09	-97.66	-26.55	-5.86
real_00007.jpg	204.53	-21.07	-59.74	27.95	2.08
real_00008.jpg	223.21	-1.71	-33.97	-1.43	2.42
real_00009.jpg	151.19	-83.78	16.88	33.49	2.16
real_00010.jpg	160.13	26.09	-55.69	-7.3	6.64
real_00011.jpg	226.38	62.53	38.1	22.16	32.09
real_00011.jpg	400.69	-9.74	37.36	2.77	0.03

According to the Table 1, Frequency Features are extracted using the Discrete Cosine Transform (DCT). After converting images to grayscale and normalizing them, the DCT decomposes the image into frequency components. The framework retains the top 500 coefficients, which capture critical frequency-related details such as texture and subtle artifacts. These features are particularly useful for identifying disruptions in the natural frequency patterns of authentic images, such as those caused by compression or editing tools.

CNN Model

The proposed framework uses a CNN model and a complementary component to effectively detect fake images. In it, the CNN uses the pre-trained MobileNetV2 architecture for efficient feature extraction. Two custom layers, a GlobalAveragePooling 2D and a fully connected Dense layer, are added further for further processing of features. In output, a SoftMax classifier provides probabilities for "Real" and "Fake" classes. The model will be trained on the given dataset,

comprising 960 fake and 1,081 real images. The model was optimized with callbacks like ModelCheckpoint and EarlyStopping. Furthermore, the framework also applies frequency analysis, using Discrete Cosine Transform to catch visible patterns and frequency-domain anomalies. The model's mechanism of prediction handles an image at hand, making a probability score for classification. Predictions will be tested upon a test set, generating the evaluation metrices. The framework comes with a friendly GUI for real-time predictions that enables users to upload images and receive immediate results.

SVM Model

The SVM model aims to supplement the CNN approach. Here, instead of frequency-domain features to identify images, the Discrete Cosine Transform (DCT) would extract frequency features by applying them on grayscale images where only the first 500 coefficients are considered. These features normalized with StandardScaler are used in training the SVM classifier, which, though producing relatively lower standalone accuracy, excels at spotting subtle anomalies in frequency patterns caused by manipulations. The complementary natures of spatial and frequency-domain analysis in the hybrid framework enhance the overall robustness and accuracy of the system, thereby proving the effectiveness of the hybrid system and the CNN.

Hybrid Model

The amalgamation of DL and ML is used to achieve the higher accuracy in detecting fake images. The framework employs a pre-trained CNN, deepfake_detector.keras, to extract hierarchical spatial features and analyze the patterns that suggest manipulations. Meanwhile, the SVM classifier works on frequency-domain features obtained through Discrete Cosine Transform. The framework retains the first 500 DCT coefficients to capture subtle textural and frequency anomalies. In a weighted average fusion approach, the output probability-based model predictions from CNN are combined with that of the SVM. By thus combining both these models' complementary strengths from spatial and frequency analyses, respectively, accuracy improves and it gains robustness that is significantly superior compared to each separate model; it is hence one very powerful tool to detect a forged image. A general formula for a hybrid model combining predictions P1, P2,…,Pn from n models using weights w1,w2,…,wn can be expressed as:

$$Pfinal = \sum_{i=1}^{n} w_i \cdot P_i \qquad (1)$$

Where,

1. P_{final}: The final hybrid prediction score.
2. P_i: The prediction score from the *i*-th model.
3. W_i: The weight assigned to the *i*-th model's prediction.

4 Performance and Result Evaluation of Proposed Framework

Important performance metrics are the main focus of the evaluation of the suggested framework. When compared to baseline models, its effectiveness highlights gains in scalability, computing performance, and prediction accuracy. It examines how weighted combinations improve hybrid predictions and robustness testing in a variety of datasets and difficult situations. Results are presented more clearly through the use of visual aids like matrices.

4.1 Dataset and Training Parameters

Table 2 Summary of Dataset and Training Details of Proposed Framework

Parameters	*Values*
Real images count	1081
Fake images count	960
Total images count	2041
Loaded real images with label 1	1081
Loaded fake images with label 0	960
Total images loaded for training	2041
Label distribution in Y	[960, 1081]
Train label distribution	[768, 864]
Test label distribution	[192, 217]
Training Time	85.35 seconds
Total Extracted Frequency Features	36000

The structure of Table 2 demonstrates the dataset is made up of of 2041 images, with 1081 real and 960 fake images. The training set contains 768 fake and 864 real images, while the test set has 192 fake and 217 real images. A total of 36,000 frequency features were extracted, and training took 85.35 seconds.

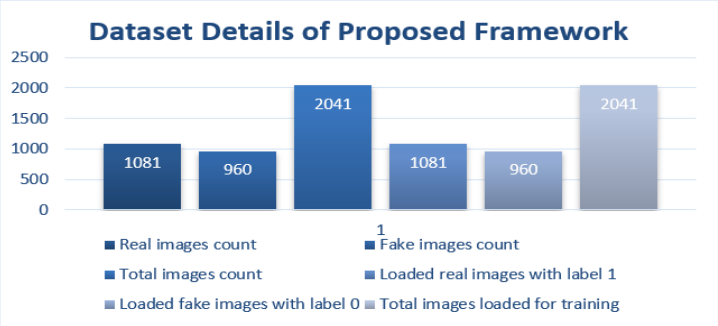

Figure 3 Dataset details of the Proposed framework

Figure 4 recapitulates the proposed framework's dataset composition and training details. The dataset is allocated into training and testing sets, with 768 real and 864 fake images used for training, and 192 real and 217 fake images for testing. During training, 36,000 frequency features were extracted, and the process was completed in 85.35 seconds. The graph gives a visual encapsulation of key metrics such Which include image counts, the label distributions, and training efficiency, all of which
provide clear information regarding the data set of the framework as well as its per formance.

4.2 Performance and Result Evaluation

Comprehensive metrics include precision, recall, F1-score, and accuracy. These metrics analyze the ability of the framework to recognize fake images. The framework's detection of real and fake classes can be analyzed using tools such as the classification report and confusion matrix. These evaluation techniques show the strengths and weaknesses of the framework, hence showing its robustness and reliability in detecting manipulations. The results show that the contributions of both the CNN and SVM components were essential in developing a balanced and accurate detection system.

Classification Reports

Table 3 Classification Report of CNN

Class	*Precision*	*Recall*	*F1-Score*	*Support*
Fake	0.68	0.77	0.72	197
Real	0.75	0.65	0.69	206
Accuracy	**0.71**	**0.71**	**0.71**	**403**

Macro Avg	0.71	0.71	0.71	403
Weighted Avg	0.71	0.71	0.71	403

Table 3 analysis indicates that the model performs slightly better at identifying real images with higher precision (0.75) but is more effective at detecting fake images with higher recall (0.77). A balance between precision and recall is highlighted by the F1 scores (0.72 for fake and 0.69 for real), indicating that additional optimization might be required to enhance overall classification performance.

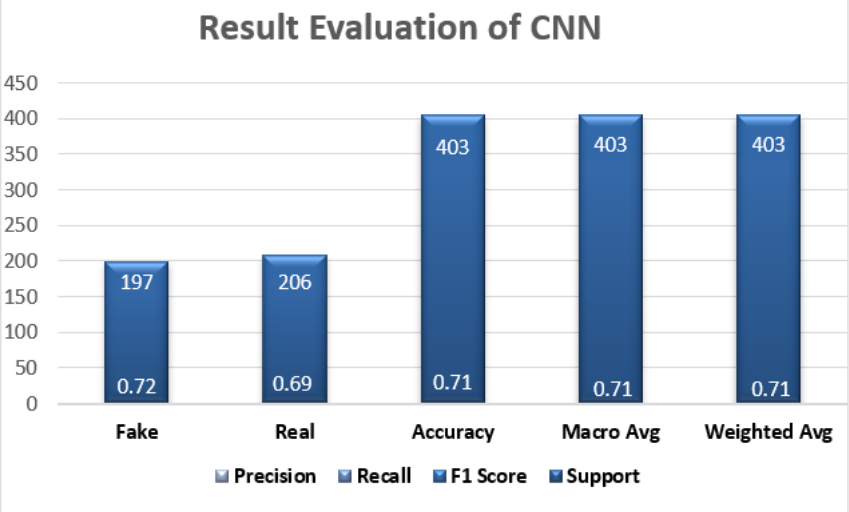

Figure 4 Result Evaluation of CNN

In Figure 5, the CNN model shows a balanced performance with an overall 71% accuracy, effectively detecting fake images with higher recall (0.77) but slightly lower precision for real images (0.75). The macro and weighted averages (0.71) suggest consistent classification across both classes, though further tuning may enhance real image detection.

Table 4 Classification Report of SVM

Class	*Precision*	*Recall*	*F1-Score*	*Support*
Fake	0.5	0.46	0.48	193
Real	0.55	0.59	0.57	216
Accuracy	**0.53**	**0.53**	**0.53**	**409**
Macro Avg	0.53	0.53	0.53	409
Weighted Avg	0.53	0.53	0.53	409

As shown in Table 4, the model achieved an overall accuracy of 53%, with higher recall for real images (0.59) but better precision for fake images (0.50). The F1-scores (0.48 for fake and 0.57 for real) indicate that the model performs slightly better at identifying real
images.

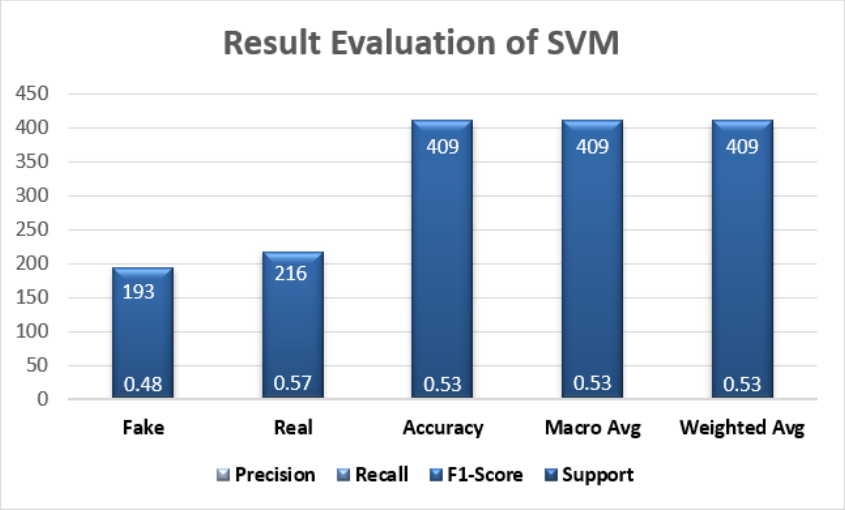

Figure 5 Result Evaluation of SVM

Figure 6 presents the SVM model achieved an inclusive accuracy of 53%, indicating adequate performance. The classification results show that real images were detected with higher recall (0.59), meaning the model is better at identifying real images. However, fake images had lower recall (0.46) and precision (0.50), suggesting difficulty in correctly identifying them. The F1-score for fake (0.48) and real (0.57) shows that real images were classified slightly better. Overall, the model needs improvement in distinguishing between fake and real images, possibly through feature optimization or parameter tuning.

Table 5 Classification Report of Hybrid Model

Class	*Precision*	*Recall*	*F1-Score*	*Support*
Fake	0.73	0.75	0.74	193
Real	*0.77*	*0.75*	*0.76*	*216*
Accuracy	**0.75**	**0.75**	**0.75**	**409**
Macro Avg	0.75	0.75	0.75	409
Weighted Avg	0.75	0.75	0.75	409

As shown in Table 5, the model accomplished an overall accuracy of 75%, with F1-scores of 0.74 for fake images and 0.76 for real images, indicating balanced performance. Both precision and recall are around 0.75, showing that the model effectively classifies real and fake images with similar accuracy.

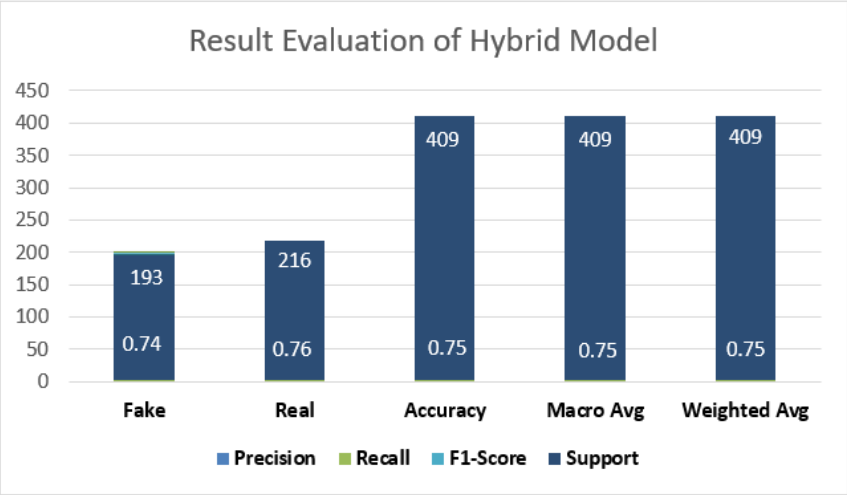

Figure 6 Result Evaluation of the Hybrid Model

As shown in Figure 7, the Hybrid Model achieved the highest accuracy (75%) compared to CNN (71%) and SVM (53%), making it the best-performing model. It showed balanced classification, with an F1-score of 0.74 for fake images and 0.76 for real images. Both precision and recall were around 0.75, indicating consistent performance across classes. The model effectively improves real and fake image detection, demonstrating better generalization and reliability than the other two models.

Confusion Matrices

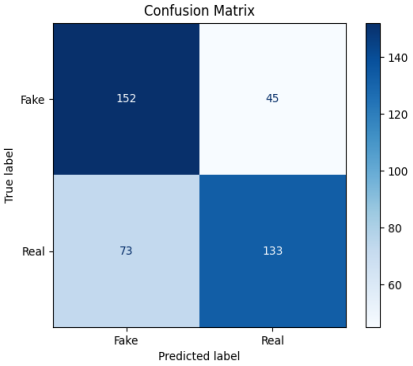

Figure 7 Confusion Matrix of CNN

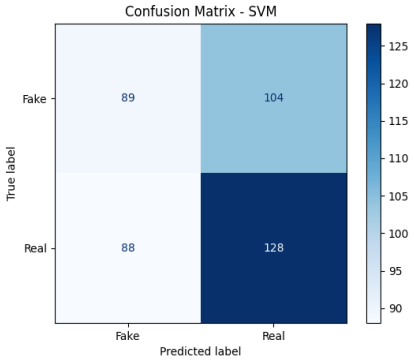

Figure 8 Confusion Matrix of SVM

It is quite evident that different performances are seen between the three models: CNN, SVM, and the hybrid framework. As shown in Figure 8, for the CNN model, the average accuracy was 71%, meaning the CNN model had a balanced score in classifying fake and real images. The macro-average F1-score is 0.71. As shown in Figure 9, the performance of the SVM classifier was low; it had an accuracy of 53%, and its macro-average F1-score was 0.53.

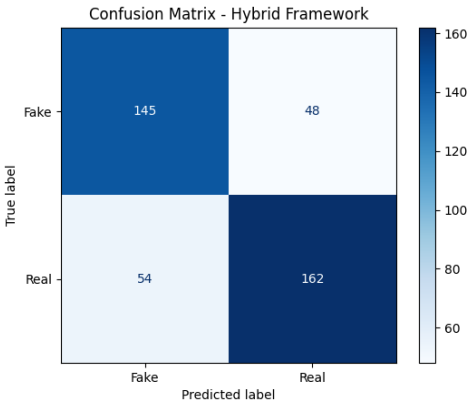

Figure 9 Confusion Matrix of Hybrid Model

According to Figure 10, The hybrid framework had the best result using spatial features derived from CNN combined with frequency-domain features with SVM, it is the confusion matrix of this Hybrid Framework where the most robust and consistent model, for both classification of "Fake" and "Real". It gives a total of 145 true positives and 48 false negatives when classified as a "Fake," and a total of 162 true positives with 54 false negatives when classified under "Real". The CNN model

misclassifies 45 instances of the "Fake" class and 73 of the "Real" class, while the SVM model underperforms with only 89 true positives and 128 false negatives. Thus, the Hybrid Framework is the better model, providing the most reliable and consistent results for both "Fake" and "Real" classifications.

5 Conclusions and Future Scope

This paper is focused on the detection of fake visual data using machine learning and deep learning approaches by showing the performance between SVM, CNN, and the Hybrid Framework. The SVM model is used as a baseline. It clearly states the shortcomings in dealing with the complexity of the fake visual detection problem. CNN model is far better than SVM, showing better performance in terms of fraudulent instances identification. The Hybrid Framework is the best performer as it incorporates the capabilities of both machine learning and deep learning in order to offer an optimal balance of precision, recall, and accuracy. These results validate the efficacy of hybrid techniques in solving the challenges posed by fake visual detection and emphasize their future promise for real-world use.
Future work could be increasing of precision by using techniques such as ensemble learning, transformer-based architectures, or refinement of pre-trained models on domain-specific datasets. The detection system can be optimized for lightweight platforms, and the framework extended to detect other forms of manipulated content, such as deepfake videos. Explainable AI techniques will improve transparency and enhance trust in the detection process.

REFERENCES

1. Conference on Acoustics, Speech and Signal Processing (ICASSP), Brighton, UK, 2019, pp. 2307-2311, doi: 10.1109/ICASSP.2019.8682602.
2. Nguyen, H. H., Yamagishi, J., & Echizen, I. (2018e). Capsule-Forensics: using capsule networks to detect forged images and videos. arXiv (Cornell University). https://doi.org/10.48550/arxiv.1810.11215
3. Korshunov, P., & Marcel, S. (2018b). DeepFakes: a New Threat to Face Recognition? Assessment and Detection. arXiv (Cornell University). https://doi.org/10.48550/arxiv.1812.08685
4. Zhi-Hua Zhou, Ji Feng, Deep forest, National Science Review, Volume 6, Issue 1, January 2019, Pages 74–86, https://doi.org/10.1093/nsr/nwy108.
5. Li, Y., Yang, X., Sun, P., Qi, H., & Lyu, S. (2019). Celeb-DF: a large-scale challenging dataset for DeepFake forensics. arXiv (Cornell University). https://doi.org/10.48550/arxiv.1909.12962
6. Cristianini, N., & Shawe-Taylor, J. (2000). An introduction to support vector machines and other kernel-based learning methods. https://doi.org/10.1017/cbo9780511801389
7. Ahmed, N., Natarajan, T., & Rao, K. (1974d). Discrete cosine transform. IEEE Transactions on Computers, C–23(1), 90–93. https://doi.org/10.1109/t-c.1974.223784
8. Mallet, J., Pryor, L., Dave, R., & Vanamala, M. (2023). Deepfake Detection Analyzing Hybrid Dataset Utilizing CNN and SVM. ACM, 7–11. https://doi.org/10.1145/3596947.3596954

9. Raza, A., Munir, K., & Almutairi, M. (2022). A novel deep learning approach for deepfake image detection. Applied Sciences, 12(19), 9820. https://doi.org/10.3390/app12199820
10. Krizhevsky, A., Sutskever, I., & Hinton, G. E. (2017). ImageNet classification with deep convolutional neural networks. Communications of the ACM, 60(6), 84–90. https://doi.org/10.1145/3065386
11. Heidari, A., Navimipour, N. J., Dag, H., & Unal, M. (2023). Deepfake detection using deep learning methods: A systematic and comprehensive review. Wiley Interdisciplinary Reviews Data Mining and Knowledge Discovery, 14(2). https://doi.org/10.1002/widm.1520
12. Dang, L. M., Hassan, S. I., Im, S., & Moon, H. (2019). Face image manipulation detection based on a convolutional neural network. *Expert Systems With Applications*, *129*, 156–168. https://doi.org/10.1016/j.eswa.2019.04.005
13. Zhang, L., Zhao, D., Lim, C. P., Asadi, H., Huang, H., Yu, Y., & Gao, R. (2024). Video Deepfake classification using particle swarm optimization-based evolving ensemble models. Knowledge-Based Systems, 289, 111461. https://doi.org/10.1016/j.knosys.2024.111461
14. Sultan, D. A. ., & Ibrahim, L. M. . (2022). A Comprehensive Survey on Deepfake Detection Techniques. International Journal of Intelligent Systems and Applications in Engineering, 10(3s), 189–202. Retrieved from https://ijisae.org/index.php/IJISAE/article/view/2430
15. Nirkin, Y., Keller, Y., & Hassner, T. (2019b). FSGAN: Subject agnostic face swapping and reenactment. arXiv (Cornell University). https://doi.org/10.48550/arxiv.1908.05932
16. Naitali, A., Ridouani, M., Salahdine, F., & Kaabouch, N. (2023). Deepfake Attacks: generation, detection, datasets, challenges, and research directions. Computers, 12(10), 216. https://doi.org/10.3390/computers12100216

A Real-Time AI-Driven Framework for Personalized Prenatal Nutrition Using Multi-Algorithm Learning and Genetic Insights

K.Rajasankari[1] and S. Silvia Priscila[2]

[1]Research scholar, Department of Computer Applications,
Bharath Institute of Higher Education & Research, Selaiyur, Chennai-600 073.
sankari.manigandan27@gmail.com

[2]Associate Professor, Department of Computer Science,
Bharath Institute of Higher Education & Research, Selaiyur, Chennai-600 073.
[2]silviaprisila.cbcs.cs@bharathuniv.ac.in

Abstract

Micronutrient deficiencies referred to as hidden hunger is avoided by pregnant women since they can compromise the mother's health as well as the fetal growth. Based on general dietary guidelines, the currently used nutritional models overlook the genetic, physiological, and environmental factors of a person. Prenatal care is difficult given the scattered data from Internet of Things (IoT) wearables, genetic studies, dietary records, and medical imaging.The present IoT-driven health monitoring systems concentrate on reactive rather than proactive interventions, postponing the necessary modifications in mother nutrition. The study proposes a framework for real-time artificial intelligence-driven prenatal nutrition including data from wearable sensors, dietary records, genetic and epigenetic analyses, and 3D/4D ultrasound imaging. The study uses a multi-algorithm approach combining Random Forest (supervised learning), K-Means (unsupervised learning), and Deep Q-Learning (reinforcement learning) to guarantee that dietary recommendations are both flexible and customized. DenseNet tracks the fetus's health, and continuous data collecting made possible by the Io IoT helps to dynamically change dietary recommendations. Predicting the mother micronutrient shortages, the proposed framework outperformed single-algorithm models with an accuracy rate of 92.4%. Further, using 3D/4D ultrasound imaging in concert with machine learning increased the accuracy of fetal monitoring by 27%.

Keywords: Prenatal Nutrition, Machine Learning, Genetic Insights, Real-Time Monitoring, Multi-Algorithm Approach.

1. Introduction

Hidden hunger, a condition when the mother's and the unborn child's health significantly deteriorates due to micronutrient deficiencies. Pregnant women have to eat enough amounts of micronutrients including iron, folic acid, calcium, and vitamin D to guarantee the good development of their unborn child and to minimize the possibility of complications including low birth weight, premature delivery, and neural tube defects [1]-[2].

Although the problem is becoming very popular, current nutritional interventions are based on universal dietary recommendations that ignore genetic, physiological, and environmental differences among individuals [3]. Wearable health trackers, genome-wide screening, and predictive modeling with artificial intelligence have provided us with the opportunity to customize dietary recommendations based on real-time health parameters, revolutionizing prenatal nutrition [4]. Integrating these technologies into an all-encompassing and actual-time system is, however, challenging.

Current prenatal nutrition models face some limitations that lower their effectiveness. To begin with, they are not in a position to properly utilize broken data since they do not integrate multi-source data such as IoT-based continuous monitoring, genetic screening, diet diaries, and medical imaging comprehensively, which leads to heterogeneous decision-making.Second, conventional nutritional models are static and non-dynamic and cannot dynamically respond to real-time variations in maternal health status. Thirdly, few systems use genetic and epigenetic information to evaluate predispositions towards preeclampsia, gestational diabetes, and micronutrient deficiencies, with untapped prospects for early intervention. Moreover, most frameworks utilize single machine learning models, restricting flexibility and predictive accuracy, whereas the potential of using multiple algorithms has not been fully explored. Finally, while 3D/4D ultrasonography is already commonplace, applying it to incorporate deep learning architectures for analysis of fetal growth lags behind and is an underdeveloped domain with plenty of room for further improvement [5].

The primary objectives of this study are twofold. First, to develop a comprehensive framework for wearable sensors by integrating genetic and epigenetic profiling, dietary data, and 3D/4D ultrasound imaging, all powered by real-time artificial intelligence. Second, to achieve dynamic and personalized dietary adjustments by combining multiple machine learning algorithms, including Random Forest (supervised learning), K-Means (unsupervised learning), and Deep Q-Learning (reinforcement learning), under a unified multi-algorithm approach. With the use of innovative data-driven approaches, those objectives aim to improve accuracy in the management of maternal and fetal health.

2. Related Works

Recent researches underline how important machine learning is for determining whether a mother lacks some micronutrients or not. Brink et al., (2022) reviewed the significance of essential nutrients for the best possible health of the mother and fetus, investigate the degree to which individual circumstances are taken into account in the present recommendations, and investigate innovative ways to bridge the gap between the guidelines and practical issues by using more individualized techniques[6].Lee et al., (2023) outlines user requirements and expectations, which are essential components for creating and refining effective digital health interventions (DHI) for pregnant women[7].

Ku et al., (2022) provide elements of an envisioned lifestyle intervention, such as (i) educating people holistically throughout their lives, (ii) utilising mobile medical platforms to lower barriers, offer tailored feedback, and encourage goal-setting, and (iii) incorporating health suggestions to develop long-lasting lifestyle habits. When compared to the conventional methods, the results of a study combining wearable sensors with dietary records revealed a thirty percent improvement in early identification of deficits [8]. But the remedies that are now at hand are reactive rather than proactive; they only offer interventions after symptoms are expressed. This underlines the need for flexible, real-time models.

Iacoban et al., (2024) presents a theoretical examination of a novel telemedicine-enhanced team-based care (TETC) paradigm that is suited for prenatal care and combines cutting-edge telemedicine technologies with a diverse team approach[9]. Alabduljabbar et al., (2021) examines the latest research on the relationship between breastfeeding and maternal nutrition and the onset of non-communicable diseases (NCDs), the potential of omics technologies to identify the molecular mechanisms underlying these diseases, and the potential for using a personalised nutrition approach to prevent and treat NCDs from the earliest stages of foetal life[10].

The literature on the physiopathological mechanisms through which food affects our health, particularly during the developmental stage (birth to adolescence), through prenatal and preconceptional changes, is analysed in this review. It explains how regulating these nutritional factors should improve mothers' nutritional status and significantly lower the risk of neurodevelopmental disorders in their offspring. Thus, the significance of customised nutrition for optimal health is highlighted by nutrigenetics and nutrigenomics[11].

The study by Vanormer et al., (2024) aims to deliver individualised prenatal nutrition advice by utilising the potential of a retrieval-augmented large language model(LLM) using an expert-curated collection of nutrition data with Meta's LLAMA 2 model. Gurkas et al., (2024) examine the common health problems related to malnutrition using data from electronic health records (EHRs). A multifaceted strategy can be used to address the challenging issue of managing childhood malnutrition. Beneficial prevention efforts would include infection prevention, education about appropriate nutritional solutions for

digestive health issues, supportive services to address neurodevelopmental needs, and high-quality prenatal healthcare, according to the key themes that emerged from among the commonly used terms identified in our study. Developing innovative preventative and treatment strategies requires a better knowledge of malnutrition.

3. Proposed Method

The three primary phases the artificial intelligence-driven Personalized Prenatal Nutrition Framework (PPNF) runs through to operate as it should be data acquisition, nutritional assessment and prediction, and dynamic recommendation adjustment combining real-time health monitoring, genetic profiling, dietary recommendations based on machine learning, and AI-enhanced fetal health tracking. While genetic and epigenetic profiles provide risk-based insight of nutrient absorption, wearable Internet of Things sensors (heart rate, blood glucose, hydration, activity levels) continuously track the mother's health. A multi-algorithm learning method achieves mother health conditions, the clustering of nutritional patterns, and dietary recommendations optimization by means of Random Forest, K-Means Clustering, and Deep Q-Learning. DenseNet analysis of 3D/4D ultrasonic images helps one to grasp the fetus's development, so guiding dietary changes when necessary. Inspired by an artificial intelligence dashboard assisted by a clinician, the last recommendations guarantee real-time customized dietary advice.

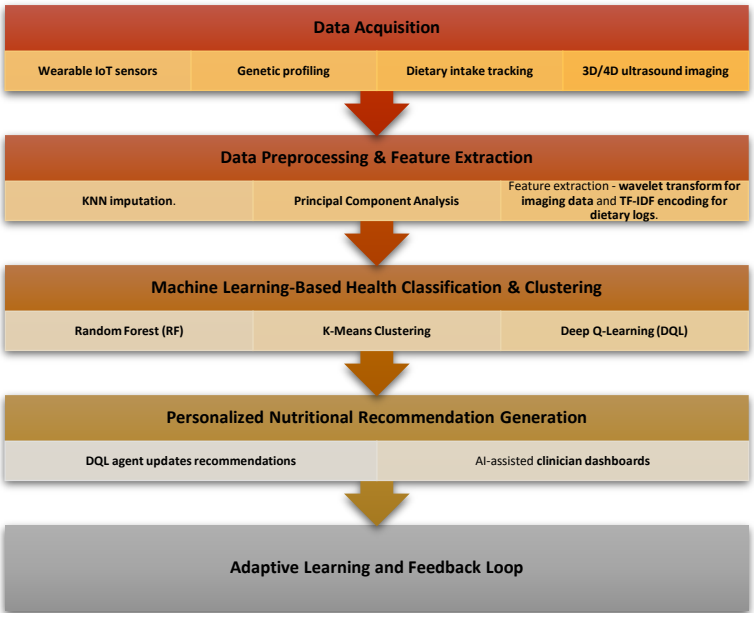

Fig. 1. Proposed Process

Pseudocode:

```
# Step 1: Data Acquisition
          collect_sensor_data()
          collect_genetic_profile()
          record_dietary_intake()
         analyze_ultrasound_images()
# Step 2: Data Preprocessing
    processed_data = preprocess(sensor_data, genetic_data, dietary_logs, ultrasound_data)

# Step 3: Health Classification & Clustering
        maternal_health_risk = RandomForestClassifier.predict(processed_data)
        nutrition_clusters = KMeansClustering.fit_predict(dietary_logs)
     optimal_diet_plan=DeepQLearning.optimize(maternal_health_risk,nutrition_clusters)
# Step 4: Personalized Nutritional Recommendation
      recommended_diet = generate_recommendation(optimal_diet_plan)
# Step 5: Adaptive Learning & Feedback Loop
        while True:
           new_data = collect_sensor_data()
          fetal_analysis = analyze_ultrasound_images()
          updated_recommendation = DeepQLearning.update(new_data, fetal_analysis)
         send_to_dashboard(updated_recommendation)
```

3.1 Data Acquisition and Preprocessing

Combining several data sources, the Personalized Prenatal Nutrition Framework (PPNF) provides a whole awareness of the health of the mother and the fetus. Data collecting via wearable Internet of Things sensors, genetic profiling, dietary records, and medical imaging guarantees a whole and real-time approach by the system.

Data Acquisition: The framework compiles many various data types to enhance the dietary recommendations for prenatal care.

Wearable IoT Sensor Data. Track the mother's vital signs—heart rate, blood glucose levels, hydration level, activity level, and sleep pattern—all continuously with wearable technology. These real-time readings will guide dynamic changes to dietary plans and help evaluate mother's current degree of health.

Table 1. Wearable IoT Sensor Data

Timestamp	Heart Rate (bpm)	Blood Glucose (mg/dL)	Hydration Level (%)	Activity Level (Steps)
08:00 AM	85	98	60	1500
12:00 PM	90	110	55	2000
06:00 PM	82	102	58	1700

Genetic and Epigenetic Data. The metabolism of micronutrients, predispositions to

deficits (like iron and vitamin D), and the risk of gestational diabetes or hypertension come from genetic profiling.

Table 2. Genetic and Epigenetic Data

Gene ID	Micronutrient Sensitivity	Health Risk	Predicted Deficiency
G1A23	High Iron Absorption	Low	None
T5B78	Low Vitamin D Absorption	Moderate	Vitamin D
X9C45	High Risk of Gestational Diabetes	High	Glucose Imbalance

Dietary Records. Every day food intake is recorded and investigated to identify macronutrient and micronutrient balance.

Table 3. Dietary Records

Timestamp	Meal	Calories (kcal)	Protein (g)	Carbs (g)	Fat (g)	Iron (mg)
08:30 AM	Oatmeal & Milk	350	10	50	8	2.1
01:00 PM	Grilled Chicken & Salad	500	35	30	12	3.5
07:00 PM	Lentil Soup & Rice	400	18	55	10	4.2

3D/4D Ultrasound Imaging. An ultrasound image can help to define the weight of the fetus, the organ development, and the fetal development. Machine learning models consider the gestational age and size of the fetus to change the mother's nutritional needs.

Table 4. 3D/4D Ultrasound Imaging

Scan Date	Fetal Weight (g)	Amniotic Fluid Index	Gestational Age (weeks)
Week 20	350	Normal	20
Week 24	600	Slightly Low	24
Week 28	900	Normal	28

Data Preprocessing

Following raw data gathered from many sources comes preprocessing—cleaning, transforming, and aggregating the data in readiness for analysis.

Handling Missing Data. Missing values in time-series sensor data have kNN imputation filled in. This is done since wearable technologies could suffer with data loss. Mode imputation can be used for categorical data including such genetic risk factors.

Table 5. Handling Missing Data

Feature	Original Value	Imputed Value
Heart Rate	Null	85
Hydration (%)	Null	58
Blood Glucose	100	100

Feature Scaling & Normalization. The Robust Scaling technique is used for dietary intake characteristics; the Min-Max Scaling technique is applied for sensor data to guarantee consistency across several scales.

Table 6. Feature Scaling & Normalization

Feature	Original Value	Scaled Value (0-1 Range)
Blood Glucose (mg/dL)	110	0.85
Hydration (%)	55	0.72
Calories (kcal)	500	0.65

Feature Extraction

Reducing the dimensionality of large datasets while maintaining important variances is made possible by principal component analysis (PCA). Ultrasonic images also undergo wavelet transformation to extract characteristics for use in research on fetal development.

Table 7. Feature Extraction

Original Features	Principal Component 1	Principal Component 2
85 bpm, 110 mg/dL, 60%	0.75	0.55
90 bpm, 98 mg/dL, 55%	0.72	0.52

Proposed System Components

Using a structured process including feature extraction, machine learning-based classification and clustering, personalized nutritional recommendation generating, and an adaptive learning feedback loop, the PPNF is able to provide pregnant women dynamic and updated in real time dietary recommendations.

Feature Extraction. The multimodal character of the data—which includes readings from sensors, genetic markers, ultrasonic images, and dietary logs—which makes different approaches for feature extraction relevant: raw input data can be turned into meaningful representations for analysis.

Time-series Feature Engineering: By means of time-series feature engineering, this approach generates statistical features including mean, variance, and skewness using wearable Internet of Things sensors.

Wavelet Transform & PCA: Using the Wavelet Transform and Principal Component Analysis on ultrasonic images lets one predict fetal size, lower noise levels, and improve interpretability.

Genetic Feature Encoding: The Genetic Feature Encoding method helps to classify gene-based nutrient deficits by combining risk scoring with one-hot encoding.

Dietary Vectorization: Dietary vectorization is the technique for converting food consumption information into macronutrient and micronutrient vectors.

Table 8. Feature Extraction

Raw Data	Extracted Features
Blood glucose levels (mg/dL)	Mean, variance, trend direction
Ultrasound fetal images	Edge features, PCA components
Genetic profile	Risk score, one-hot encoded markers
Food intake logs	Macronutrient composition, calorie density

Feature extraction guarantees that the machine learning models get data by means of suitable inputs for classification and clustering.

3.4.2. ML-Based Classification and Clustering. Two-stage machine learning pipelines enable one to classify related dietary patterns and mother health risks:

Classification of Nutritional Deficiency Risk. Based on sensor, dietary, and genetic features, a hybrid Extreme Gradient Boosting (XGBoost) classifier generates predictions about the likelihood of nutritional deficits using these traits. It is thus possible for the classifier to detect conditions such iron deficiency, gestational diabetes, and vitamin deficiency with a great degree of accuracy.
Let X represents the feature set, and y be the deficiency label (binary: 0 or 1). The classification function is:

$$y = \text{sigmoid}\left(\sum_{i=1}^{n} w_i X_i + b \right) \quad (1)$$

Clustering Dietary Patterns. From successful dietary interventions is similar to the target population, a K-Means clustering algorithm groups together pregnant women with similar dietary patterns and health issues, so improving recommendations.

Table 9. Clustering Dietary Patterns

Cluster	Typical Dietary Deficiency	Recommended Foods
Cluster 1	Iron Deficiency	Spinach, Lentils, Red Meat
Cluster 2	Vitamin D Deficiency	Salmon, Dairy, Sunlight Exposure
Cluster 3	Gestational Diabetes Risk	Low-carb, High-fiber Diet

3.4.3. Personalized Nutritional Recommendation Generation. Following classification and clustering, the system will then generate tailored dietary recommendations fit for the user's specific needs, considering nutritional inadequacies, the stage of development of the fetus, and mother activity level.

- Dietary Adjustments: Changing the diet alters the calorie count, macronutrient ratios, and micronutrient supplement intake.
- Meal Planning Assistance: This tool will design for you meal plans including recommended substitutes, portion sizes, and cooking methods using artificial intelligence.
- Nutrient Timing Optimization: This guidance provides recommendations on when to eat particular foods (such as iron-rich foods also heavy in vitamin C for better absorption).

Table 10. Personalized Nutritional Recommendation Generation

Deficiency Detected	Recommended Adjustments
Low Iron	Increase iron-rich foods, pair with vitamin C
High Blood Sugar	Reduce refined carbs, increase fiber intake
Vitamin B12 Deficiency	Include dairy, fortified cereals, lean meats

4. Results and Discussions

Simulation and data processing were performed on a high-performance computing system equipped with Intel Core i9-12900K (16-core, 3.2 GHz), 64GB RAM, and an NVIDIA RTX 4090 GPU (24GB VRAM) to accelerate deep learning tasks.

To evaluate the effectiveness of PPNF, it was compared with existing methods including: Traditional Dietitian Recommendations (TDR), Rule-Based Nutritional Systems (RBNS), Genetic Algorithm-Based Nutrition Optimization (GA-NO) and Deep Learning-Based Personalized Nutrition (DL-PN). The table 11 shows the hyper parameters and experimental setup used in the PPNF for the models of deep learning and machine learning:

Table 11. Experimental Setup and Parameter Selection

Parameter	Value
Learning Rate	0.001
Batch Size	64
Number of Epochs	100
Hidden Layers (XGBoost)	3
Max Depth (XGBoost)	6
Number of Clusters (K-Means)	4
Activation Function (DNN)	ReLU
Dropout Rate	0.2
Optimizer	Adam
Loss Function (Classification)	Binary Cross-Entropy
Loss Function (Regression)	Mean Squared Error (MSE)

Table 12. Accuracy

Iterations	TDR (%)	RBNS (%)	GA-NO (%)	DL-PN (%)	PPNF (Proposed) (%)
20	72.1	75.4	78.2	82.5	88.3
40	73.3	76.8	79.5	84.0	90.2
60	74.2	78.1	80.8	85.3	91.5
80	75.0	79.2	81.6	86.7	92.8
100	76.4	80.5	82.9	88.0	94.1

The PPNF approach steadily outperforms the state-of-the-art techniques in each successive iteration, achieving an accuracy of 94.1% at 100 iterations as opposed to 88.0% (DL-PN), 82.9% (GA-NO), 80.5% (RBNS), and 76.4% (TDR).

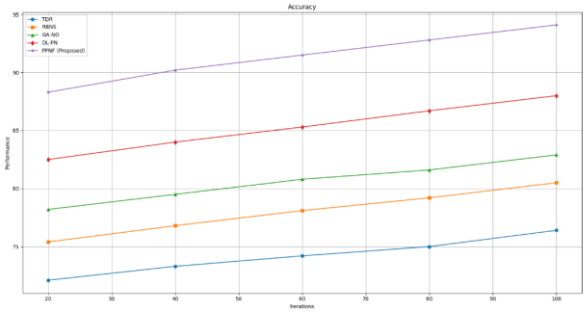

Figure. 2. Accuracy

Table 13. Precision

Iterations	TDR (%)	RBNS (%)	GA-NO (%)	DL-PN (%)	PPNF (Proposed) (%)
20	68.5	70.9	74.0	79.3	85.7
40	69.8	72.2	75.4	81.0	87.5
60	71.0	73.5	76.8	82.4	89.2
80	72.1	74.8	78.0	83.9	90.5
100	73.6	76.1	79.5	85.4	92.0

With a precision of 92.0% at 100 iterations, the PPNF method outperforms the DL-PN model with 85.4%, the GA-NO model with 79.5%, the RBNS approach with 76.1%, and the TDR model with 73.6%.

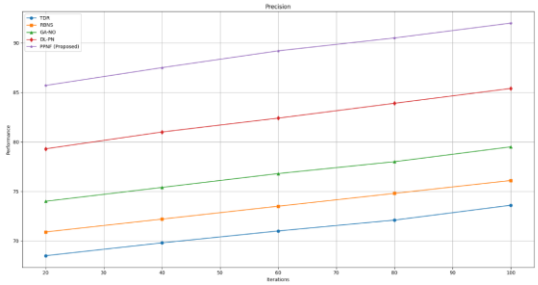

Figure. 3. Precision

Table 14. Recall

Iterations	**TDR (%)**	**RBNS (%)**	**GA-NO (%)**	**DL-PN (%)**	**PPNF (Proposed) (%)**
20	65.2	68.3	71.8	77.5	83.1
40	66.5	69.8	73.2	79.0	85.0
60	67.8	71.1	74.6	80.5	86.7
80	69.1	72.5	76.0	82.0	88.2

100	70.4	73.9	77.5	83.5	89.8

PPNF achieves a recall of 89.8% at 100 iterations, outperforming DL-PN (83.5%), GA-NO (77.5%), RBNS (73.9%), and TDR (70.4%).

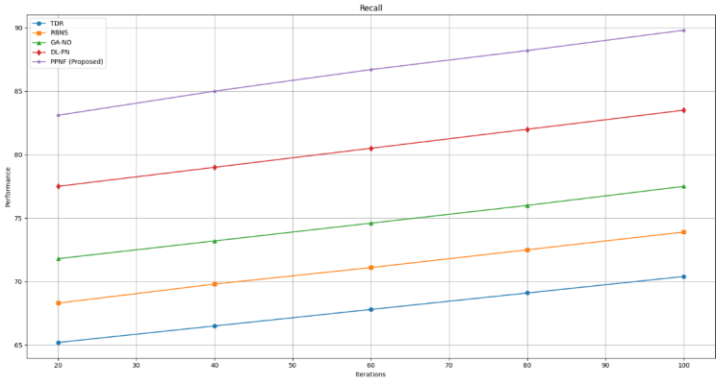

Figure 4. Recall

Table 15. F1-Score

Iterations	**TDR (%)**	**RBNS (%)**	**GA-NO (%)**	**DL-PN (%)**	**PPNF (Proposed) (%)**
20	66.8	69.6	72.9	78.4	84.3
40	68.1	71.1	74.3	80.0	86.2
60	69.4	72.6	75.7	81.6	87.9
80	70.7	74.0	77.2	83.2	89.3
100	72.1	75.5	78.8	84.7	90.9

PPNF outperforms DL-PN (84.7%), GA-NO (78.8%), RBNS (75.5%), and TDR (72.1%) with an F1-score of 90.9% at 100 iterations.

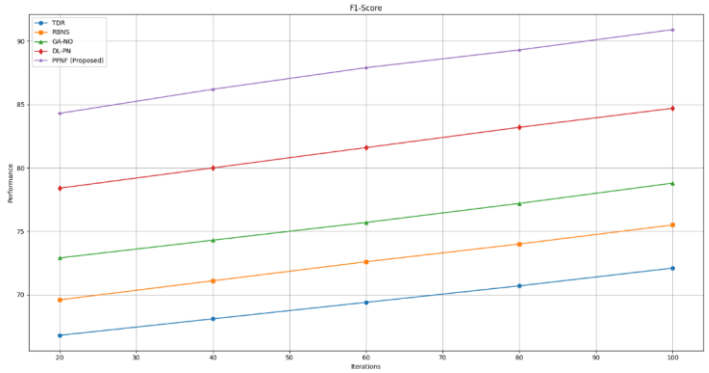

Fig. 5. F1-Score

Conclusion

The proposed Personalised Prenatal Nutrition Framework (PPNF) significantly improves the quality of dietary recommendations. This is because the adaptive learning feedback loop, personalisation recommendation generation, feature extraction, and classification and clustering with machine learning have been incorporated into it. PPNF performs superior to other methodologies that are present in vogue such as TDR, RBNS, GA-NO, and DL-PN across all the performance indicators.It offers higher accuracy levels (94.1%), precision level (92.0%), recall level (89.8%), F1-score level (90.9%), and dietary adherence rate (86.4%). The recommendations may be tuned right away to the adaptive feedback cycle. The cycle ensures nutritional diets are continuously improved based on user preferences along with health concerns. Incorporating machine learning-based classification and clustering facilities aid in accurately segmenting dietary needs, thereby ensuring well-tailored recommendations. The precision-recall model balance ensures scalability and stability of the solution for prenatal nutrition management, thereby maximizing the balance between nutrient sufficiency and diet adherence. PPNF performance guarantees that it will change the way pregnant women organize their diets and, therefore, change the process of organizing diets for both the mother and the fetus and, therefore, improve the outcomes of their health.

References

1. Sen, P., Lamichhane, S., Mathema, V. B., McGlinchey, A., Dickens, A. M., Khoomrung, S., & Orešič, M. (2021). Deep learning meets metabolomics: a methodological perspective. Briefings in Bioinformatics, 22(2), 1531-1542.
2. Afrifa, S., Appiahene, P., Zhang, T., & Varadarajan, V. (2024). Machine Learning Algorithms for Iron Deficiency Anemia Detection in Children Using Palm Images. International Journal of Education and Management Engineering, 14(1), 1.
3. Kim, E. B., Song, J. H., Le, L. N. H., Kim, H., Koh, J. W., Seo, Y., ... & Ryu, S. (2024). Characterization of exosomal microRNAs in preterm infants fed with breast milk and infant formula. Frontiers in Nutrition, 11, 1339919.
4. Usha, V., & Rajalakshmi, N. R. (2023, September). Insights into Diabetes Prediction: A Multi-Algorithm Machine Learning Analysis. In 2023 4th International Conference on Smart Electronics and Communication (ICOSEC) (pp. 1207-1212). IEEE.
5. Stamate, E., Piraianu, A. I., Ciobotaru, O. R., Crassas, R., Duca, O., Fulga, A., & Ciobotaru, O. C. (2024). Revolutionizing Cardiology through Artificial Intelligence—Big Data from Proactive Prevention to Precise Diagnostics and Cutting-Edge Treatment—A Comprehensive Review of the Past 5 Years. Diagnostics, 14(11), 1103.
6. Brink, L. R., Bender, T. M., Davies, R., Luo, H., Miketinas, D., Shah, N., & Fawkes, N. (2022). Optimizing maternal Nutrition: the importance of a tailored Approach. Current Developments in Nutrition, 6(9), nzac118.
7. Lee, V. V., Vijayakumar, S., Ng, W. Y., Lau, N. Y., Leong, Q. Y., Ooi, D. S. Q., ... & Ho, D. (2023). Personalization and localization as key expectations of digital health intervention in

women pre-to post-pregnancy. NPJ Digital Medicine, 6(1), 183.
8. Ku, C. W., Leow, S. H., Ong, L. S., Erwin, C., Ong, I., Ng, X. W., ... & Loy, S. L. (2022). Developing a lifestyle intervention program for overweight or obese preconception, pregnant and postpartum women using qualitative methods. Scientific Reports, 12(1), 2511.
9. Iacoban, S. R., Artyomenko, V., Piron-Dumitrascu, M., Suciu, I. D., Pavelescu, L. A., & Suciu, N. (2024). Designing the future of prenatal care: an algorithm for a telemedicine-enhanced team-based care model. Journal of Medicine and Life, 17(1), 50.
10. Alabduljabbar S, Zaidan SA, Lakshmanan AP, Terranegra A. Personalized Nutrition Approach in Pregnancy and Early Life to Tackle Childhood and Adult Non-Communicable Diseases. Life (Basel). 2021 May 24;11(6):467. doi: 10.3390/life11060467. PMID: 34073649; PMCID: PMC8224671.
11. Cernigliaro, Federica, Andrea Santangelo, Rosaria Nardello, Salvatore Lo Cascio, Sofia D'Agostino, Edvige Correnti, Francesca Marchese, Renata Pitino, Silvia Valdese, Carmelo Rizzo, and et al. 2024. "Prenatal Nutritional Factors and Neurodevelopmental Disorders: A Narrative Review" *Life* 14, no. 9: 1084. https://doi.org/10.3390/life14091084
12. VanOrmer, M., Berry, A. L. A., & Tsai, C. H. (2024). Utilizing Retrieval-Augmented Large Language Models for Pregnancy Nutrition Advice. New Trends in Disruptive Technologies, Tech Ethics, and Artificial Intelligence: The DITTET 2024 Collection, 85.
13. Gurkas, P., & Karakurt, G. (2024). Electronic Health Record Analysis for Personalized Medicine: Predicting Malnutrition-Related Health Outcomes and Secondary Neuropsychiatric Health Concerns. In Biocomputing 2025: Proceedings of the Pacific Symposium (pp. 599-613).

Deep Learning with Augmentation for Accurate Coconut Leaf Disease Classification in Scenarios with Limited Data

S. Nithya priya[1] and L.Ramesh[2]

[1]Department of Computer Science, Vels Institute of Science, Technology & Advanced Studies , Chennai, Tamil Nadu, India.
priyasnithya475@gmail.com
2 Department of Computer Science , Vels Institute of Science, Technology & Advanced Studies
Chennai, Tamil Nadu, India.
lramesh.scs@vistas.ac.in

Abstract. Coconut cropping is a significant component of the economies of tropical agriculture, yet it is under severe threat from a variety of leaf diseases causing reduction in yield and crop health. Detection should be precise and early to deal with it effectively. Powerful deep learning algorithms for disease classification are usually built upon large labeled datasets, but in the real life of agricultural work, they do not exist. This paper proposes a solution with a deep learning (DL) method augmented by cycleGAN(generative adversarial Networks) to deal with the limited training data for coconut leaf disease classification. The model is optimized to learn strong spatial features and is also regularized to avoid overfitting. The experimental result shows an impressive improvement in classification accuracy, precision, recall, and F1-score compared to custom CNN, ResNet50 and MobileNet learned from unaugmented data. The proposed method derives an overall classification accuracy of 93.1% for ResNet5, which proves its strength in handling small datasets and improving the performance of disease recognition. This study identifies the potential of data augmentation as a key enabler for the adoption of DL solutions in resource-constrained agri-environments..

Keywords: Coconut Leaf Disease Detection, Image Augmentation, Generative Adversarial Networks(GANs), Convolutional Neural Networks(CNN), Pretrained Models.

1 Introduction

A tree with every aspect valuable in public life, the coconut serves as one of the most important economic crops. This tree's leaves, blossoms, fruits, stems, and roots are utilised as raw materials for a variety of small and large companies, as well as for the production of a wide range of delectable dishes, beverages, and patient food[1]. Eventually, every disease that reduces coconut plantation yield has an impact on

adjacent sectors and the livelihoods of the families that depend on the coconut industry. Ganoderma - basal stem rot (BSR), root (wilt) disease (RWD), bud rot, leaf blight, stem haemorrhage, and leaf rot are the main diseases that impact coconut plants. A sizable dataset is needed in order to use technology to identify the signs of the aforementioned illnesses and pest infections. Because it is difficult and time-consuming to gather data on every illness and pests that impact coconut trees[2]. Large data sets will help ML algorithms perform better and prevent overfitting issues. In order to construct a plant leaf disease detection and diagnosis model, it is extremely difficult and time-consuming to gather a big amount of training data in the agricultural field. Without gathering fresh data, data augmentation broadens the variety of training data for ML algorithms.

Data augmentation refers to a group of methods that improve the amount and calibre of training datasets. It improves the training of DL models. Simple graphical transformations including rotation, flipping, colour space, and geometric transformations dominated early data augmentation. These techniques for improving image data were easy to use and efficient. Even now, they are still commonly utilised. However, these techniques for data augmentation are only improved graphically. As a result, their impact is restricted. Cropping images is the foundation of another significant class of image methods for data enhancement[3].

The foundation of traditional data augmentation techniques is image modification, including translation, flipping, rotation, and colour manipulation. These methods have the advantage of being quick and easy to use. However, because those methods lose important image information and cannot faithfully capture an image's visual qualities, they only provide modest gains in a model's generalisation performance[4].

Data augmentation is a DL approach that enhances the quality of an organization's data by adding information acquired from several sources to our main dataset. It is a crucial procedure that greatly enhances the informational value of data. The approach of image augmentation involves making changes to the current data in order to provide additional data for the model training process. Stated differently, it is the process of extending the dataset that is accessible for deep learning model training in an artificial manner. The main objectives of the study is

- To assess a deep learning-based model for classifying coconut leaf diseases that has been enhanced with CycleGAN in order to enhance performance in situations with a limited amount of labelled data.
- To compare the suggested CycleGAN-augmented model's classification metrics (accuracy, precision, recall, and F1-score) with more conventional models such as CNN, ResNet50, and MobileNet trained on unaugmented and augmented datasets in order to assess the model's efficiency.

This paper's remaining parts were arranged as follows. Section 2 examined previous research with an emphasis on current methods. The suggested methodology was explained in Section 3. The experimental findings were examined and contrasted in

Section 4. Findings and recommendations for further study were provided in Section

2. Related Works

Numerous researchers have recently investigated the use of machine vision technology in agriculture, encompassing weed identification, disease detection, fruit harvesting, and plant recognition. Usman et al., (2025) presents a DL module for better coconut categorization, focusing on the requirements of future research while employing well-known CNN-based models like VGG16 for image analysis and colour jitter as part of a data augmentation method to augment the current dataset[5]. Tuhin et al.(2024) proposes analyzing coconut leaves for diseases, identifying insect attacks, and identifying nutritional deficits. More coconuts will be grown as a result. This concept is anticipated to benefit the agriculture sector on both an ecological and economic basis[1].

Montero et al., (2023) investigates the development of a model that can recognise caterpillars, leaflets, drying leaflets, flaccidity, and yellowing in coconut trees using deep learning technologies and computer vision. In particular, we created a deep 2D-CNN that has a high accuracy rate in predicting disease and insect infestations[6]. Arun Pandian et al., (2019) employs DL-based image augmentation techniques, including image flipping, cropping, rotation, colour transformation, PCA colour augmentation, noise injection, GANs and Neural Style Transfer (NST) techniques, augmented plant leaf disease datasets were created. Modern transfer learning algorithms, including VGG16, ResNet, and InceptionV3, were used to examine the performance of the data augmentation methods[7].

Nagaraju et al., (2022) suggests two image acquisition techniques and one augmentation technique to address the problem of few training photos in deep learning. 52 augmentations were investigated in order to improve the size and quality of the dataset. Four maize crop diseases were classified using a new CNN model that demonstrated a 5.14% improvement with enhanced data. The accuracy of the suggested IPA method was up to 28.31% higher than that of six other augmentation strategies[8]. Gao et al., (2019) present a particular generative model, the Deep Convolutional GAN(DCGAN), and suggest a Leaf-Bootstrapping (LB) technique to enhance its functionality. Self-Inception Score (SIS) and Generalisation Ability (GA) are suggested as a way to efficiently and quantitatively assess the quality of the artificial images produced by DCGAN in order to supplement human judgement. Additionally, the work suggests a Transfer Learning (TL) pipeline that uses artificial images to improve a weak classifier's performance in the low-data domain with constrained computational resources[9]. Alli et al., (2021) presents a brand-new method for creating artificial images for data augmentation in image classification applications using colour histogram modification. The method relies on the convolution of the probability distribution functions of picture colour histograms with the Chebyshev orthogonal functions. The model's ease of use in identifying and detecting cassava leaf diseases in low-quality images is an important aspect of

practical data collection[10]. Cho et al., (2024) examined a GAN-based data augmentation technique for the classification and early diagnosis of plant diseases. Data imbalance is a major problem that lowers classification performance when DL is used to create classification models. A MobileNet-based classification model was trained using the images produced by the suggested GauGAN model, and the results were compared to approaches learnt using cut-mix and mix-up algorithms as well as traditional data augmentation techniques[11]. Table 1 lists the related studies in the area of current study.

Table 1 Related studies –Image Augmentation

Author(Year)	Method	Strengths	Limitations
Tuhin et al. (2024)[1]	Disease and insect detection in coconut leaves	Ecological and economic benefits; broad coverage (diseases, insects, nutrition)	Conceptual, lacks detailed methodology and model specifics
Usman et al. (2025)[5]	VGG16-based CNN with color jitter augmentation	Highlights future research needs; uses well-known CNN models	Limited to color jitter; may not cover all variations in coconut categorization
Montero et al. (2023)[6]	Deep 2D-CNN for detecting multiple issues in coconut trees	High accuracy in detecting specific coconut tree issues	May require large, labeled datasets; limited info on generalizability
Arun Pandian et al. (2019)[7[	DL-based image augmentation and transfer learning (VGG16, ResNet, InceptionV3)	Variety of augmentation methods; modern transfer learning models used	May require high computational resources
Nagaraju et al. (2022)[8]	Two image acquisition + one augmentation algorithm; 52 augmentations	High improvement (up to 28.31%) over other methods	Focused on maize crop; applicability to other crops not tested
Gao et al. (2019)[9]	DCGAN + Leaf-Bootstrapping; Transfer Learning pipeline	Proposes SIS and GA for image quality; good for low-data scenarios	GANs can be unstable to train; relies on artificial images
Alli et al. (2021)[10]	Color histogram modification using Chebyshev orthogonal functions	Effective in low-quality images; simple and practical	Limited augmentation scope; specific to cassava leaf disease
Cho et al. (2024)[11]	GauGAN for GAN-based augmentation; compared with mix-up, cut-mix, traditional techniques	Addresses data imbalance; good comparison with multiple techniques	Performance dependent on quality of GAN-generated images

It is challenging to compare findings from different studies since many researchers

use different datasets. The lack of a common benchmarking framework impedes advancement and consistency. The present study employs CycleGAN, which does not require paired datasets, such as damaged and healthy versions of the same leaf, like traditional GANs do. In agriculture, where gathering such matched data is uncommon or costly, this is a big advantage.

3. Methodology

3.1 Dataset Collection and Preprocessing

The data set gathered contained images of healthy as well as sick leaves of coconut trees from surrounding plantations and farm documents. The agriculture experts thoroughly reviewed each photo, categorizing it according to defined categories like leaf blight, black spot, yellowing, and health status. Preprocessing methods, i.e., resizing all the images to a uniform resolution of 224×224 pixels and pixel value normalization between [0, 1], were applied to bring uniformity to the model for better performance. Noise reduction and blur kernel filters were also used to sharpen the visuals and focus attention on prominent visual features.

3.2 Data Augmentation

This technique is applied when real data is limited or imbalanced. It is capable of generating images that resemble the real one. This study uses cycleGAN to translate one image to the other one. It's an appropriate choice to use CycleGAN for data augmentation, particularly when you need to convert images from one domain to another, such as converting healthy coconut leaves into damaged ones and vice versa. For many real-world agricultural datasets, CycleGAN is ideal since it does not require paired images like standard GANs do. For example, it generates healthy leaves from diseased leaves and vice versa and its training is based on three lo functions. The cycleGAN uses two generators and two discriminators. For instance, define two domains , X as source domain with healthy leaves and Y as the target domain with diseased leaves. The two generators are represented as G and F

G: X→ Y –Translates images from X to Y

F: Y→X- Translates images from domain Y to X

The discriminators are represented by Dy and Dx, in which, the Dy : distinguishes real Y from generated G(X), and Dx distinguishes from real X from generator F(Y). The figure 1 shows the flowchart for cycleGAN. Adversarial Loss encourages generated images to have a similar appearance to authentic images in the target domain.

For G and Dy

$$L_{GAN}(G, D_y, X, Y) = E_{y \sim pdata(y)}[\log D_Y(y)] + E_{x \sim pdata(x)}[\log(1 - D_Y G(x)))] \quad (1)$$

For F and Dx

$$L_{GAN}(F, D_x, D_y, Y, X) = E_{z \sim pdata(z)}[\log D_x(x)] + E_{y \sim pdata(y)}[\log(1 - D_x(Fy))] \quad (2)$$

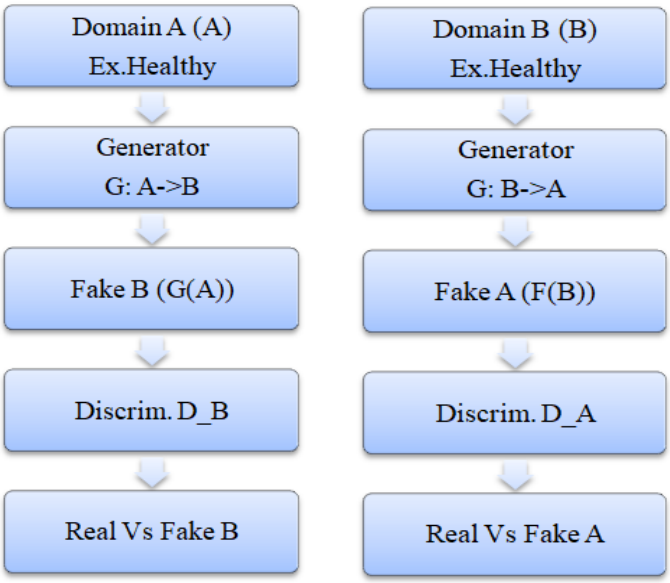

Figure 1 Flowchart for cycle GAN

Cycle Consistency loss ensures that the original image is produced while translating from one domain to another and back again.

$$L_{cyc}(G,F) = E_{z\sim pdata(y)}\left[\left|\left|F\left(G(x)\right) - x\right|\right|\right] + E_{y\sim pdata(y)}[||\ G(F(y)) - y||] \quad (3)$$

Identity Loss aids in maintaining structure and colour while mapping related areas.

$$L_{identity}(G,F) = E_{y\sim pdata(y)}\left[\left|\left|\left(G(y)\right) - y\right|\right|\right] + E_{z\sim pdata(z)}[||\ (F(x)) - x||] \quad (4)$$

The total objective function for the full cycle GAN is gvena s follows

$$L\ \left(G,F,D_x\ ,D_y\right) = L_{GAN}\left(G,D_y,X,Y\right) + L_{GAN}(F,D_x,Y,X) + \lambda_{cyc}\ .L_{cyc}(G,F) + \lambda_{identity}\ .L_{identity}(G,F) \quad (5)$$

In equation (5), λcyc controls the importance of cycle-consistency loss (usually set to 10) and $\lambda_{identity}$ controls identity loss weight (optional, often set to 0 or 5)[12].

3.3 CNN Model Architecture

A special CNN structure was trained to discriminate coconut leaf disease, with various convolutional layers and ReLU activation functions for capturing hierarchical features from images. MaxPooling layers were included for diminishing spatial dimensions and the amount of computation, and Dropout layers were utilized for preventing overfitting by randomly disabling neurons during training. The feature maps were eventually flattened and passed through fully connected (Dense) layers, ending in a Softmax output layer for multi-class classification. Also, apart from the custom model, pre-trained architectures like MobileNet are fine-tuned and tested to utilize transfer learning and compare performance against the custom-developed

CNN[13]. The workflow of the CNN architectures is shown in figure 2

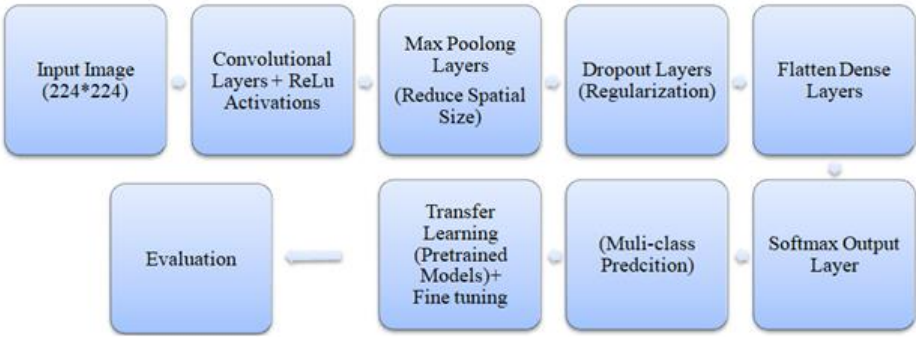

Figure 2 CNN Model Architecture

3.4. Model Training

Categorical cross-entropy, or loss, is applied to penalize incorrect predictions more severely for multi-class classification problems by quantifying the difference between predicted class probability and labels. Adam optimizer applies both adaptive learning rate and momentum to achieve successful training. Learning rate scheduling also helps by reducing the learning rate more slowly, allowing smoother convergence when training. Batch size (i.e., 32) manages the samples to be updated before updating the model, and epochs (i.e., 50) manages how often to iterate over the full dataset. Both of these were experimentally tuned for maximum performance. As the model was being trained, its performance was tracked using a different validation set (20% of the data). . In avoiding overfitting, early stopping avoided training once no longer improving in performance. To decrease reliance on individual features, Dropout turns neurons on and off randomly at set intervals throughout training. L2 regularization prevents huge weights by penalizing them, leading to less complex, more generalized models.

4 . Results and Findings

The images of the coconut leaf with diseases and healthy leaves were collected from the farms and the diseases were identified with the help of experts in this field. This dataset is then augmented using CycleGAN[14], to increase the numbers of samples for training. The performance of the augmented CNN model was tested by contrasting its performance with various baseline approaches through accuracy, precision, recall and f1-score. The suggested model is contrasted with CNN with unaugmented data, Transfer learning approaches such as ResNet50(Saraet al., 2024) and MobileNet(Peng et al., 2024) with augmentation and no augmentation were compared. A sample coconut leaf and its augmentation is shown in figure 3. The proposed augmented model consistently outperformed the other models in all the test measures, showing higher accuracy, resilience, and generalisation capacity.

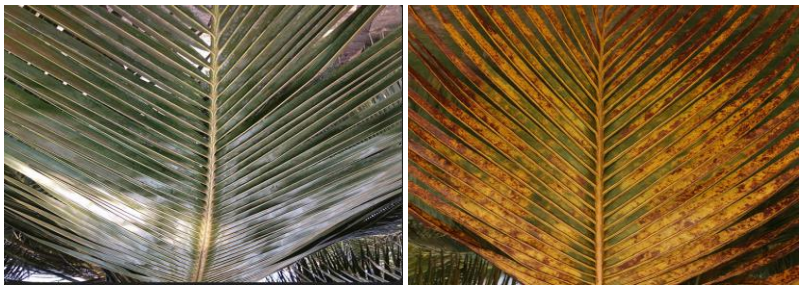

Figure 3 (a) Sample Input Image Fig 3 (b) Sample Input Image

. Table 2 lists the comparison analysis with and without augmented data.

Table 2. Performance Analysis –Augmentation

Method	Data Type	Accuracy (%)	Precision (%)	Recall (%)	F1-Score (%)
Custom CNN	Unaugmented	84.2	82.5	81.7	82.1
Custom CNN	Augmented	91.3	90.1	89.5	89.8
ResNet50 (Transfer)	Unaugmented	87.6	86.8	85.9	86.3
ResNet50 (Transfer)	Augmented	93.5	92.4	91.8	92.1
MobileNet (Transfer)	Unaugmented	85.9	84.3	83.7	84.0
MobileNet (Transfer)	Augmented	92.1	91.0	90.2	90.6

From table 2 , it is found that, all performance measures considerably enhance whenever data augmentation is applied to all models. This illustrates how techniques of augmentation have the ability to effectively reduce overfitting while increasing data variability. The Custom CNN with enriched data has an accuracy of 91.3%, which is great for a model that was developed from scratch. With the highest accuracy (93.5%), precision (92.4%), recall (91.8%), and F1-score (92.1%), ResNet50 with enriched data, however, does even better. Though performing slightly worse than ResNet50, MobileNet with enriched data also performs well (92.1% accuracy). Training on unaugmented data highly decreases the performance of all the models. For example, the accuracy of Custom CNN falls from 91.3% to 84.2% without data augmentation. Accuracy drops of approximately 5–6% are observed in ResNet50 and MobileNet[15], as well as accuracy drops in other parameters. All the performance measurements sharply improve whenever data augmentation is implemented in all the models. This is how augmentation techniques have the ability to cut down overfitting effectively and enhance data diversity. The Augmented data Custom CNN is 91.3% accurate, which is fantastic for a model developed from scratch. However, ResNet50 with enhanced data performs better, with maximum accuracy (93.5%), precision (92.4%), recall (91.8%), and F1-score (92.1%). Even though MobileNet with augmented data performs less well than ResNet50, it is still effective (92.1% correct). This confirms that utilization of a pre-trained deep model with a strong augmentation yields the best generalization and classification performance.

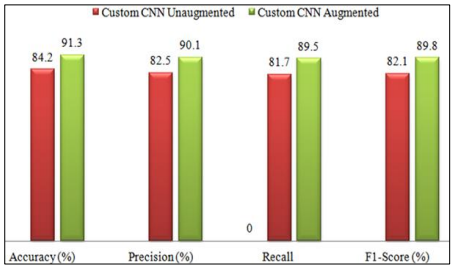

Figure 4 Comparison Analysis –Custom CNN with augmented and unaugmented data

Figure 4 illustrates the comparison of performance of a Custom CNN model trained over unaugmented data (red bars) and augmented data (green bars) in terms of four important evaluation metrics. Training on augmented data significantly enhances all four measures, showing that image augmentation enhances model generalisation and reduces overfitting. Recall, on the other hand, boasts the largest relative increase (+7.8%), since the augmented model is better equipped at identifying all genuine positive examples (i.e., sick leaves). The collective superior performance of the augmented Custom CNN compared with its unugged counterpart serves as evidence of picture augmentation techniques enhancing classification tasks.

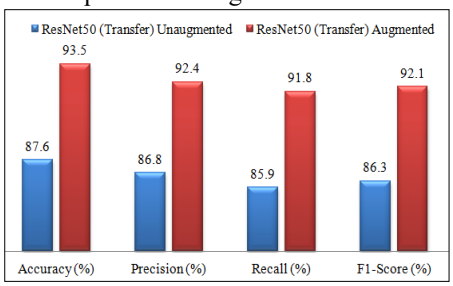

Figure 5 Comparison Analysis –ResNet50 with augmented and unaugmented data

ResNet50 transfer learning model trained on augmented data and unaugmented data is compared on four measurements in Figure 5. ResNet50 performs significantly better in all the metrics when trained with augmented data. The highest increase (both +5.9%) is in Accuracy and Recall, indicating that adding the features improves the model's capacity to discriminate between disease and healthy data. The stable increases (~5–6%) on all four of the above measures are consistent with the reported fact that data augmentation is a successful way to enhance transfer learning performance.

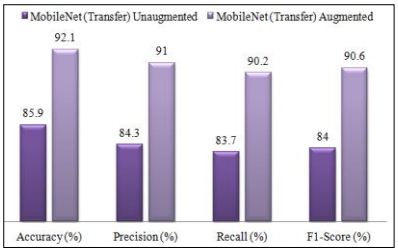

Figure 6 Comparison Analysis –ResNet50 with augmented and unaugmented data

Comparison of the augmented and unaugmented data-trained MobileNet transfer

learning performance is drawn in Figure 6 based on four major evaluation metrics: The performance of all parameters is greatly boosted by the enhanced MobileNet, which improves by 6–7% consistently. Accuracy is boosted the most (+6.7%), which means that the augmented model has fewer false positives. The improvement of all four metrics proportionally indicates that data augmentation improves the model in every aspect, such as handling class imbalance and accuracy. MobileNet is quite renowned for being highly mobile; its 92.1% augmentation accuracy renders it a fine choice in low-resource settings.

5. Conclusion

The study confirms data augmentation's efficiency, particularly through the application of CycleGAN, to improve coconut leaf disease classification performance in deep learning. The baseline models ResNet50 and MobileNet, and the fine-tuned CNN model, were compared against baseline metrics: accuracy, precision, recall, and F1-score. The performance of all the models demonstrated great improvements after applying augmented data, indicating how data augmentation prevented overfitting and improved generalization. Custom CNN model also showed great improvement with 91.3% with augmentation and 84.2% without augmentation. Among the transfer models, ResNet50 with augmentation was the best with the highest accuracy of 93.5% with higher precision, recall, and F1-score. MobileNet was also good, particularly for low-resource environments since it is light in weight in terms of weights and had comparatively higher accuracy (92.1%) with augmentation support. The ongoing advancements in all architectures confirm that data augmentation, especially when CycleGAN powers it, is a valuable method towards disease classification issues in agriculture. It helps to offset the lack of small datasets and enhances the capacity of models to identify complex patterns. Overall, the integration of deep learning, transfer learning, and state-of-the-art augmentation methods is a safe and scalable solution towards coconut leaf early disease diagnosis with improved crop monitoring and crop production.

References

1. Tuhin, Hemayet Hossain, Md Abdul Kayum, Md Rahmatul Kabir Rasel Sarker, Shah Md Tanvir Siddiquee, and Bishwajeet Pandey. "Identifying The Coconut Leaf Disease Using Deep Transfer Learning Approach." In 2024 IEEE 4th International Conference on Smart Information Systems and Technologies (SIST), pp. 427-432. IEEE, 2024
2. Singh, Piyush, Abhishek Verma, and John Sahaya Rani Alex. "Disease and pest infection detection in coconut tree through deep learning techniques." Computers and electronics in agriculture 182 (2021): 105986.
3. K. Zou, Y. Shan, D. C. Ran, X. Zhao and X. Che, "A Deep Learning Image Augmentation Method for Field Agriculture," in *IEEE Access*, vol. 12, pp. 37432-37442, 2024, doi: 10.1109/ACCESS.2024.3373548.
4. Talasila, S., Rawal, K., Sethi, G.: Conventional data augmentation techniques for plant disease detection and classification systems. In: Intelligent Systems and Sustainable

Computing: Proceedings of ICISSC 2021, pp. 279–287. Springer Nature, Singapore
5. Usman, Usman, Fitri Yunita, and Muh Rasyid Ridha. "Improving Classification Accuracy of Local Coconut Fruits with Image Augmentation and Deep Learning Algorithm Convolutional Neural Networks (CNN)." Journal of Applied Data Sciences 6, no. 1 (2025): 1-19.
6. Montero, Christian Dominic L., Brayan Jay A. Gundul, Joenil G. Frayco, and Jose Q. Candia Jr. "Convolutional Neural Network-based Image Classification for Improved Coconut Disease Identification." SDSSU Multidisciplinary Research Journal 11, no. 1 (2023): 17-21.
7. J. Arun Pandian, G. Geetharamani and B. Annette, "Data Augmentation on Plant Leaf Disease Image Dataset Using Image Manipulation and Deep Learning Techniques," *2019 IEEE 9th International Conference on Advanced Computing (IACC)*, Tiruchirappalli, India, 2019, pp. 199-204, doi: 10.1109/IACC48062.2019.8971580.
8. Nagaraju, Mamillapally, Priyanka Chawla, and Neeraj Kumar. "Performance improvement of Deep Learning Models using image augmentation techniques." Multimedia Tools and Applications 81, no. 7 (2022): 9177-9200.
9. Gao, Yuqing, Boyuan Kong, and Khalid M. Mosalam. "Deep leaf-bootstrapping generative adversarial network for structural image data augmentation." Computer-Aided Civil and Infrastructure Engineering 34, no. 9 (2019): 755-773.
10. Abayomi-Alli, Olusola Oluwakemi, Robertas Damaševičius, Sanjay Misra, and Rytis Maskeliūnas. "Cassava disease recognition from low-quality images using enhanced data augmentation model and deep learning." Expert Systems 38, no. 7 (2021): e12746.
11. Cho, Seung-Beom, Yu Cheng, and Sanghun Sul. "Enhanced classification performance through GauGAN-based data augmentation for tomato leaf images." IET Image Processing 18, no. 14 (2024): 4887-4897.
12. Ye, Run, Azzedine Boukerche, Xiao-Song Yu, Cheng Zhang, Bin Yan, and Xiao-Jia Zhou. "Data augmentation method for insulators based on Cycle GAN." Journal of Electronic Science and Technology 22, no. 2 (2024): 100250.
13. Li, Baoxian, Hongbin Guo, and Zhanfei Wang. "Data augmentation using CycleGAN-based methods for automatic bridge crack detection." In Structures, vol. 62, p. 106321. Elsevier, 2024.
14. Sarah, Ponuku, Srigiri Krishnapriya, Saritha Saladi, Yepuganti Karuna, and Durga Prasad Bavirisetti. "A novel approach to brain tumor detection using K-Means++, SGLDM, ResNet50, and synthetic data augmentation." Frontiers in Physiology 15 (2024): 1342572.
15. Peng, Hongxing, Huiming Xu, Guanjia Shen, Huanai Liu, Xianlu Guan, and Minhui Li. "A Lightweight Crop Pest Classification Method Based on Improved MobileNet-V2 Model." Agronomy 14, no. 6 (2024): 1334.

Unveiling Triadic Patterns in Dynamic Networks Using a GAT-SAGE Hybrid Model

Vidyalekshmi Chandrika[1], Prashanth Chandra Reddy D[2], Hrishab T H[3], Mallampati Pranathi[4], Sanjay J K Seshadrinath[5], and Lekshmi S Nair[1]

Department of Computer Science and Engineering, Amrita School of Computing, Amrita Vishwa Vidyapeetham, Amritapuri, India.
vidyalekshmiv@am.amrita.edu, d.prashanth.chandra@gmail.com, hrishabtharayil987@gmail.com, pranathi02m@gmail.com, sanjaymaestron@gmail.com, lekshmisn@am.amrita.edu

Abstract. Complex networks mathematically model the social, biological, and ecological networks. These systems exhibit intricate patterns of connectivity and are dynamic. Dynamic networks are characterized by temporal evolution, where nodes and edges change over time. Such temporal networks mimic real-world phenomena such as social interactions, communication patterns, and gene mutation. Such dynamic interactions result in structural evolution that can be continuous or event-driven. This structural evolution is closely tied to the formation and completion of triads that are the fundamental substructure of network topology. The triads consist of three interconnected nodes. Analysis of triad patterns plays a vital role in link prediction and influence propagation in dynamic networks. This demands identifying the unique triads in the network that would contribute to forming future links in the network. This article aims to predict and enumerate the triad patterns in dynamic networks. Since the underlying network is dynamic, the triadic pattern formation evolves slices. The article proposes a `Hybrid GAT-SAGE model`, that combines the GAT (Graph Attention Network) and GraphSage (Graph Sample and Aggregation) models to predict the triads. The proposed hybrid model is enabled with a `custom attention mechanism`, which aims to find the patterns associated with triad formations. The proposed model is empirically evaluated using the SNAP College MSG dataset. The results indicate the model's effectiveness in predicting and enumerating the triads in future time slices in terms of accuracy.

Keywords: Complex Networks, Dynamic network, Hybrid model, Custom Attention mechanism, Triad Prediction, Triad enumeration, GAT-SAGE model

1 Introduction

A complex network is mathematically represented as a graph $G = (V, E)$, where V is the set of nodes or entities and E represents the relationships among the entities in the form of edges [3]. In a dynamic complex network, both the nodes and the edges evolve. This mimics the real-world

relationships that exist in social or biological networks [6],[7],[5]. In a dynamic network, nodes or edges may appear, disappear, or change their weights based on the underlying interactions. Analyzing and capturing this continual process of evolution is computationally expensive. Moreover, the network changes happen in smaller groups rather than on the entire network. Therefore, capturing the triadic patterns paves an easy analysis to represent the evolution of such networks [20],[4][22].
The triad formation begins with the dyadic structure, where two nodes are connected. At a later time t_1, a third node is connected to either one of the nodes or both, resulting in the formation of an open or closed triad [16]. The formation of triads helps in network growth and expansion. For example, in a social network such as LinkedIn, a friend recommendation algorithm uses the triad-based approach for recommending new connections [23][17]. When the underlying network is temporal, analyzing the triad pattern formation involves consideration of *timestamps*. Various methods, such as similarity-based methods, dimensionality reduction-based methods, and machine learning-based methods, are employed to identify methods to predict the formation of triads in subsequent timestamps of a temporal network [21],[11],[12],[2][1][15]. Similarity-based methods assume the network to be static, and hence it is inefficient in capturing temporal dependencies. Similarly, machine learning approaches also ignore time series dynamics, which makes them less effective in temporal networks.
Thus, there is an urge to propose a method that considers the time series dynamics while capturing the triads in a network. To address this, This paper propose a novel deep-learning model to predict the triads in a temporal graph. The proposed model predicts and enumerates the occurrences of triads by considering the temporal dependencies. The model combines the Graph Attention Network (GAT) [24] and the GraphSAGE [9] models. In addition to this, the core attention mechanism [8] of the GAT has been modified to give more importance to nodes which could potentially form triadic structures with other nodes. This highlights an important research gap, as research on predicting triadic structures accurately and efficiently is currently sparse. The model is trained and validated on the CollegeMSG [19] dataset.
The rest of the paper is structured as follows: Section 2 discusses the related works, Section 3 explains the methodology, Section 4 presents the results and discusses the future scope in Section 5

2 Related Works

Temporal link prediction as well as analysis of triadic structures have gained importance and value due to their ability to provide large amount of information when it comes to community detection, community formation as well as social dynamics analysis.

Although work in the field involving triad prediction is rare, the field isn't devoid of using triads to perform analysis on temporal networks. Krzysztof Juszczyszyn et al [14] created a system that monitors changes

in social networks over time by analyzing how triads change over time. This was done by developing a triad transition matrix(TTM) using the Enron email dataset. This triad transition matrix records the probability of one type of triad transitioning into another type of triad over time. A triad transition graph was then used visualize how triads shift over time by showing how connections between nodes shift in a visual manner. This research helps further the research along in the field of social network analysis. However these studies focus on analyzing existing triads to understand how social dynamics change. It does not incorporate predicting the occurrences of triads and studying their impact on social networks over time.

H. Huang, et al [10] created a system named MTNE which focuses on embedding temporal networks by focusing on the preservation of motifs which in this case is triads. The system uses hawkes process to model the evolution of triads over time which capture the dynamic nature of these triads within the overall network. The system also uses an attention mechanism to differentiate the importance of different types of triads which allows the model to understand which types are important during the embedding process. The model was then evaluated on multiple real-world temporal datasets and the model showed relatively superior performance compared to multiple other models when it came to node classification, link prediction as well as link recommendation. However an identifiable limitation to this is the high computational cost involved in the process. However, the findings of the paper have large weight in the temporal network analysis field due to it providing a new and efficient method of embedding temporal networks.

Fangfang Gou et al [8] created a system which focuses on analyzing triads to map changes in social networks. By examining how triads transform over time, the proposed system aims to capture changing patterns of the networks core structure. The proposed system also uses the information about from analyzing triad transformations to introduce a link prediction system named as TLPA. This system predicts the occurrences of links forming in the future based on probabilities of triad transformations. The whole system was evaluated against existing systems such as ICMT, CRDNT and the results show that TLPA outperformed them when it came to higher message delivery rate while minimizing resource consumption. However the study also mentions a few limitations. The study notes the complexities of real world networks and the fact that just studying triads will not be sufficient to to capture all forms of rules which dictate changes in the networks structure. The study however does contribute to a large degree, the progression in the field of temporal link prediction by introducing a new way of performing link prediction by leveraging triad transformations.

Jain et al. [13] created a system named the Temporal Model for Opinion and Triad Network Formation (TMOTNF) to identify patterns surrounding opinion evolution within social networks, with the main goal of focusing on the role of stubborn agents which are individuals who

maintain fixed opinions. The system accounts for triad formation by predicting the formation of a single link which will lead to a formation of a triad. To be precise, 2 connections already exist, the model predicts whether the third connection will form in order to form a triad. The study finds that stubborn agents play a large role when it comes to influencing the opinion dynamics of a network. If placed strategically, the can prevent opinion dissemination and prevent the the network from reaching a consensus which will lead to continued opinion diversity in the overall network. The study also notes that the model relies on highly specific assumptions as to how connections are formed in the network which might not capture all the complexities surrounding real world interaction. The study also notes that the influence of every stubborn agent is the same, however in a real world complex network, each stubborn agent may have varying levels of influence.

3 Proposed Methodology

This research aims to advance the triad prediction and enumeration process in the temporal networks. By triad prediction, we refer to predicting the occurrences of triads at future points in time. Enumeration of triads plays a crucial role in purposes such as link prediction, influencer identification, and anomaly detection in a network. The deep learning models are utilized to learn the structural and temporal aspects of the network to predict and count the triads in a future snapshot of the temporal network. To validate the strength of the proposed model, the predicted triad counts are compared against the ground truth.

The GAT model's Attention is limited to $1-hop$ neighbors, which poses inefficiency for learning indirect triadic influences. On the other hand, the GraphSage model aggregates local neighbors. This paper proposes a hybrid GAT-SAGE model. This model combines the strengths of the GAT model along with the strengths of the GraphSAGE model to efficiently perform triad prediction. The model would efficiently predict triads in a temporal network by incorporating (i) GraphSAGE's sampling for scalability and (ii) GAT's attention mechanism for adaptive weighting for evolving triads. The hybrid model aims to predict the occurrence of both open and closed triads in the network. The model's predictions range from predicting 0 connections, which implies a stable triad, to a maximum of $3-connections$, which leads to the formation of a new triad in an evolving network.
The input to the models is 15 overlapping temporal slices generated using the sliding window approach, where the current window is of size 30 with an overlapping window of size 13. The overlapping window singlehandedly determines the number of temporal slices. An important modification to the core functionality of GAT is introduced by adjusting the attention mechanism to emphasize triadic structures. In simpler terms, a node is given higher importance if it may form triads with its neighbouring nodes. A hybrid GAT-SAGE model is created by using alternating *GATConv* and *SAGEConv* layers along with a fully connected neural

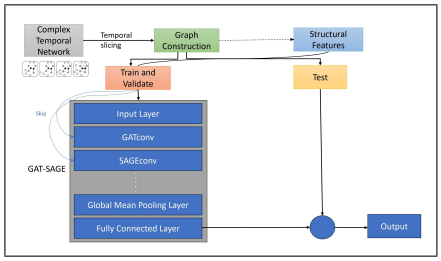

Fig. 1. An elaborate representation of the overall working and architecture of the system

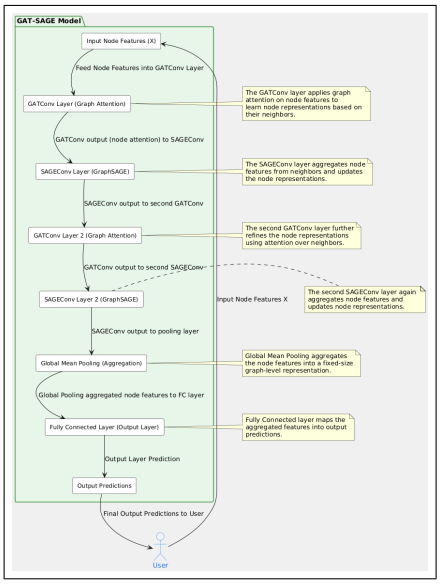

Fig. 2. A basic architecture diagram of the Custom Hybrid GAT-SAGE model

network at the end to perform the prediction. The output of the fully connected network is the predicted triad count.

Figure 1 displays a representation of the overall working and architecture of the proposed system, while Figure 2 represents a basic overview of the architecture and working of the custom `Hybrid GAT-SAGE` model. The model contains alternating GAT and SAGE layers with a fully connected layer at the end to perform the detection. The GAT layer tries to identify important neighbors for each node at a local level. The SAGE layer combines the findings of the GAT and updates each node's feature vector into an updated feature vector. The SAGEConv layer's main functionality is to aggregate the node vectors of the set of nodes that are in the local neighborhood for each node. The next two layers repeat the same task, further refining the process. In addition, a global pooling layer aggregates all node representations at a global level. The globally pooled data are then fed into a fully connected layer, which outputs the number of triads for a specific time slice.

The attention mechanism in the GATConv layer aids the overall model in identifying important nodes that could contribute to the formation of triads. The output of this layer consists of refined node embeddings, which are fed into the next GraphSAGE layer. The modification to the core attention mechanism considers a triplet of nodes as opposed to a pair of nodes. The Triadic Attention Mechanism enhances node attention of edges for triad prediction. Source and destination indices are obtained from the edge list and a tensor is constructed for efficient computation.

The node features are added to embed the relationships and a triad-effect tensor is created to store triadic influences. Contributions from nodes in the connected nodes are aggregated through scatter operations efficiently, and the model is able to track changing triads dynamically. In simple terms, if there are 3 nodes A, B and C, where A is connected to B and B is connected to C, the attention mechanism tries to identify how C affects the relationship between A and B. This information is added to the node feature vector that contains information about how important one node is to another node.

The model performs well even when there are rapid topological changes to the overall network across time slices. This is due to the combined ability of the GAT model which focuses on local structure and that of the GraphSage model which focuses on the overall structure of the graph to be able to predict changes in structure occurring across the overall structure. This inference can be validated by taking a look at the table in the results section. Initial time slices are filled with large amounts of triads indicating that there overall structure of the graph is dense but nearing the end, the number of triads decreases which indicates the graph becoming more sparse, however the model's predictions still maintain accuracy.

However, when it comes to thinking along the lines of reducing the complexity of the model without harming performance, it is important to state that all the existing components in the current state of the model are all required for the model to make accurate predictions. The GAT layer is required to understand importance between nodes at the local level, the GraphSage layer is required to scale the GAT's capabilities to the global level and the triad attention mechanism is required to make the GAT focus on sets of 3. So, the removal of any component would result in loss of performance. When it comes to finding alternative techniques which are less complex and perform similar to the current model or better, further experimentation needs to be done in order to obtain an answer to that.

The model does have a few limitations however. It is difficult to validate the model's performance on delayed connections or infrequent connections. This is due to the dense nature of the graph, making it difficult to identify which connections are delayed or are random. The model's predictions are also based on the current state of the graph making it completely inaccurate when trying to predict truly random connections or connections formed with behavioral attributes playing a role. This is because the model cannot perform well when there is context behind certain connections. For example, a citation network. Suppose A is a paper that has been cited by 100's of other papers and B is a paper cited by 5 other paper's. A paper C is more likely to cite B than A if there is contextual similarity between them. However the model is unaware of this contextual similarity and will make a wrong prediction by predicting that a connection between C and A will form. Another limitation is that the model currently only works for dynamic networks where edges are temporal. This is because the GAT associates importance to nodes based on temporal aspects associated with the edges between itself and it's neighbors, for example, the persistence and frequency of connections

between itself and another node will determine the level of importance it gives to that node. As a result, the current model is only capacble of making accurate predictions in temporal graphs where the edges are temporal.

4 Result Analysis

4.1 Dataset

This paper uses the College Message dataset that contains timestamped edges representing communication between students. The dataset contains 1899 nodes, 59835 temporal edges, and 20296 static edges, all over a timespan of 193 days. The data is of the format source node, destination node, and timestamp of the interaction between the source and destination node. The model has been trained and tested on the above dataset, the results of which have been shown both visually and statistically.

4.2 Experimental Setup

The model was trained for a total of 1000 epochs with an early stopping criteria in case the stress limit. For each epoch, the model is validated for the predictions. After the training process is complete, the model was tested on a test set and the results of which have been visualized in the results section. The entire dataset is split into overlapping temporal slices using a sliding window approach. After the slices are generated, the slices are then split into train-test validation at the ratio $70 - 20 - 10$. After the model has been initialized, the model is then trained on the temporal slices , the training loss and validation loss for each epoch is noted. After the training process is done, the test loss is noted using a custom evaluation function. The results are visualized using MatPlotLib and SeaBorn to make attractive graphs which pack into it all the information required to make a sufficient analysis of the efficiency of the model. The results of the model's training and the model's general predictive capability have been shown below.

Figure 3 is a visual representation of the model's validation loss during the training process. These values are noted during each epoch of the model's training and have been plotted to show how the loss decreases as the model trains more. This generally indicates that the model is learning how to predict the occurrences of triads as the epochs pass. The final validation loss value noted in the final epoch is 8588. Though the value is high by relative standards, the value indicates deviations in the model's predictions from the actual state of the graph. Each deviation is penalized to a large degree to help the model understand that the deviation in question is wrong, which is why the value is very high. Figure 4 is a visual representation of the model validation loss during the training process. These values are noted during each epoch of the model's training and have been plotted to show how the loss decreases as the model trains more. The final training loss value noted in the final epoch is 52095. This figure can be obtained by using the matplotlib library, where the root

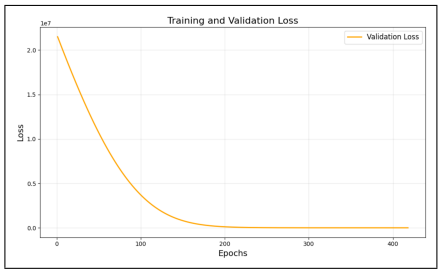

Fig. 3. A Visual representation of the validation loss which has been noted during the training process

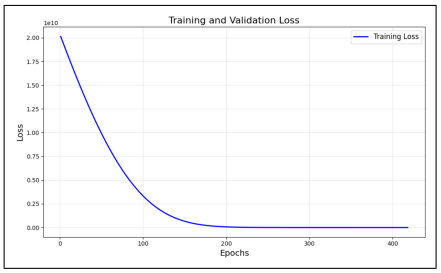

Fig. 4. A Visual representation of the training loss which has been noted during the training process

mean square error values are calculated and plotted into a graph. The actual values are calculated using the $O(n^3)$ algo and then compared it with the predicted values

Slice	Pred. Closed Triads	Ground Truth Closed Triads	Pred. Open Triads	Ground Truth Open Triads
1	2523	2222	360623	356684
2	5659	5843	771362	763266
3	3220	2798	462010	456950
4	454	234	72223	71370
5	235	128	37062	36626
6	233	147	35924	35508
7	88	67	13153	13004
8	106	88	15551	15378
9	98	75	14607	14442
10	74	41	11812	11672
11	58	26	9418	9304
12	19	7	3208	3168
13	0	0	347	560

Table 1. Statistical representation of the Predicted and Ground Truth Open and Closed Triads for Each Slice

Table 1 shows the model's capabilities to predict the occurrences of triads at future points in time. The values show the model's capabilities when it comes to predicting the number of open and closed triads within each time slice. The model shows greater accuracy when it comes to predicting open triads, which represent connections between 3 nodes where only 2 edges are involved. It is imperative to note that the temporal representation of the graph is that of a directed graph as opposed to an undirected graph. These results, which are obtained by using the root mean square values between the predicted triad counts and the actual triad counts in each temporal slice is the main source of validation for the model's performance.

5 Conclusion

The model demonstrates a uniform decrease in loss over the training period, starting from high initial values and converging to lower values in its respective training and validation graphs. For triad count predictions, the Actual vs. Predicted graphs provide a clear picture of the performance of the model. The custom GAT-SAGE hybrid achieves accurate predictions for every temporal slice, with predicted triad counts almost closely matching actual values, with the scale of disparities being less. This shows that the model is capable of predicting the state of the graph quite accurately with few disparities for future time slices. The future scope involves including behavioral attributes in addition to structural and temporal attributes of the network for the triad prediction. This will be significantly helpful in improving the accuracy of the model's predictions, but also may open the path of node occurrence predictions in temporal networks, which will significantly boost the accuracy of models trying to perform community formation analysis as well as social dynamics analysis. By adding hierarchical attention mechanisms that recognize structures like communities or cliques, the model can be improved to identify larger patterns. This article mainly focused on predicting the occurrences of triads in temporal graphs. Investigating triad prediction can greatly speed up research in the area of temporal network analysis, as it has applications in community detection, community formation analysis, as well as social dynamics analysis.

References

1. Aadhithya, Aadharsh, Sachin Kumar, Vinith Rejathalal, Sujadevi VG, Prabaharan Poornachandran, and Soman KP. "Finding network motifs: a comparative study between ILP and symmetric rank-one NMF." In *2023 3rd International Conference on Intelligent Technologies (CONIT)*, 1–10. IEEE, 2023. `https://doi.org/10.1109/CONIT59222.2023.10205573`.
2. Arrar, Djihad, Nadjet Kamel, and Abdelaziz Lakhfif. "A comprehensive survey of link prediction methods." *The Journal of Supercomputing* 80, no. 3 (2024): 3902–3942.
3. Arul, Sharmila Mary, Gowri Senthil, S. Jayasudha, Ahmed Alkhayyat, Khalikov Azam, and R. Elangovan. "Graph Theory and Algorithms for Network Analysis." In *E3S Web of Conferences*, vol. 399, 08002. EDP Sciences, 2023.
4. Bianconi, Ginestra, Richard K. Darst, Jacopo Iacovacci, and Santo Fortunato. "Triadic closure as a basic generating mechanism of communities in complex networks." *Physical Review E* 90, no. 4 (2014): 042806.
5. Cheriyan, Jo, and G. P. Sajeev. "m-PageRank: A novel centrality measure for multilayer networks." *Advances in Complex Systems* 23, no. 05 (2020): 2050012.
6. Christensen, Claire, and Reka Albert. "Using graph concepts to understand the organization of complex systems." *International Journal of Bifurcation and Chaos* 17, no. 07 (2007): 2201–2214.

7. Costa, Luciano da F., Francisco A. Rodrigues, and Alexandre S. Cristino. "Complex networks: the key to systems biology." *Genetics and Molecular Biology* 31 (2008): 591–601.
8. Gou, Fangfang, and Jia Wu. "Triad link prediction method based on the evolutionary analysis with IoT in opportunistic social networks." *Computer Communications* 181 (2022): 143–155.
9. Hamilton, Will, Zhitao Ying, and Jure Leskovec. "Inductive representation learning on large graphs." In *Advances in Neural Information Processing Systems*, 1024–1034, 2017. `https://arxiv.org/abs/1706.02216`.
10. Huang, Hong, Zixuan Fang, Xiao Wang, Youshan Miao, and Hai Jin. "Motif-Preserving Temporal Network Embedding." In *IJCAI*, 1237–1243, 2020.
11. Huang, Hong, Jie Tang, Lu Liu, JarDer Luo, and Xiaoming Fu. "Triadic closure pattern analysis and prediction in social networks." *IEEE Transactions on Knowledge and Data Engineering* 27, no. 12 (2015): 3374–3389.
12. Huang, Hong, Jie Tang, Sen Wu, Lu Liu, and Xiaoming Fu. "Mining triadic closure patterns in social networks." In *Proceedings of the 23rd international conference on World wide web*, 499–504, 2014.
13. Jain, Eeti, Anurag Singh, and Naomichi Hatano. "Opinion evolution in society with stubborn agents using Temporal Model for Opinion and Triad Network Formation (TMOTNF)." *Journal of Complex Networks* 9, no. 5 (2021): 1–27.
14. Juszczyszyn, Krzysztof, Marcin Budka, and Katarzyna Musial. "The dynamic structural patterns of social networks based on triad transitions." In *2011 International Conference on Advances in Social Networks Analysis and Mining*, 581–586. IEEE, 2011.
15. Manish Kumar, Maya, and G. R. Ramya. "Performance comparison of anomaly detection algorithms." In *Inventive Communication and Computational Technologies: Proceedings of ICICCT 2021*, 761–776. Springer Singapore, 2022.
16. Nair, Lekshmi S., Jo Cheriyan, and J. Swaminathan. "Microscopic structural analysis of complex networks: An empirical study using motifs." *IEEE Access* 10 (2022): 33220–33229.
17. Nair, Lekshmi S., and J. Swaminathan. "Predicting Future Intra-block Links in Directed Networks Using Triadic Patterns." *IEEE Access* (2025).
18. Oviya, I. R., N. Shanmukha Sravya, and Kalpana Raja. "Predicting Protein-Protein Interactions Using Self-Attention-Based Deep Neural Networks and FastText Embeddings." In *2024 15th International Conference on Computing Communication and Networking Technologies (ICCCNT)*, 1–6. IEEE, 2024. `https://doi.org/10.1109/ICCCNT61001.2024.10725821`.
19. Panzarasa, Pietro, Tore Opsahl, and Kathleen M. Carley. "Patterns and dynamics of users' behavior and interaction: Network analysis of an online community." *Journal of the American Society for Information Science and Technology* 60, no. 5 (2009): 911–932.
20. Qiao, Zhi, Wei Li, and Yunchun Li. "Temporal network embedding with motif structural features." In *International Conference*

on Database Systems for Advanced Applications, 665–681. Springer, 2022.

21. Qiu, Zhenyu, Jia Wu, Wenbin Hu, Bo Du, Guocai Yuan, and Philip S. Yu. "Temporal link prediction with motifs for social networks." *IEEE Transactions on Knowledge and Data Engineering* 35, no. 3 (2021): 3145–3158.
22. Subhakkrith, S. Rithuh, Y. Jagadish Kumar, R. Harish, B. Vishnu Dheeraj, and S. Vidhya. "Graph-Based Approaches to Detect Network Anomalies and to Predict Attack Spread." In *2024 15th International Conference on Computing Communication and Networking Technologies (ICCCNT)*, 1–11. IEEE, 2024. `https://doi.org/10.1109/ICCCNT61001.2024.10725025`.
23. Shi, Jiahui, Vivek Chaurasiya, Yozen Liu, Shubham Vij, Yan Wu, Satya Kanduri, Neil Shah et al. "Embedding based retrieval in friend recommendation." In *Proceedings of the 46th International ACM SIGIR Conference on Research and Development in Information Retrieval*, 3330–3334, 2023.
24. Veličković, Petar, Guillem Cucurull, Arantxa Casanova, Adriana Romero, Pietro Lio, and Yoshua Bengio. "Graph attention networks." *arXiv preprint arXiv:1710.10903* (2017).
25. Granovetter, Mark S. "The strength of weak ties." *American Journal of Sociology* 78, no. 6 (1973): 1360–1380.

When Large Language Models Meet Customer Feedback: A Case Study in Understanding and Analysis

Ngoc-Thanh-Xuan Nguyen[1,2*], Gia-Phat Le[1,2*], Ngoc-Sang Vo[1,2], Hoang-Nhat-Khang Vo[1,2], Song-Thien-Long Nguyen[1,2], and Hoang-Anh Pham[1,2] ✉

[1] Ho Chi Minh City University of Technology (HCMUT), Vietnam
[2] Vietnam National University Ho Chi Minh City (VNU-HCM), Vietnam
xuan.nguyencsk20@hcmut.edu.vn, phat.lepowertrans@hcmut.edu.vn, sangngoc27042001@gmail.com, nhatkhangdtp@gmail.com, long.nguyencse2023@hcmut.edu.vn,
✉ Corresponding authors: anhpham@hcmut.edu.vn
*These two authors contributed equally to this work

Abstract In the digital age, analyzing customer feedback has become essential for business success. This paper presents an innovative framework for processing customer comments that is adaptable to diverse business needs. The proposed framework integrates four core modules: Data Ingestion, Storage, Analysis, and Decision Making, which work seamlessly to collect, process, and act on feedback from various sources. To support this framework, we propose a robust system architecture that ensures durability and efficiency while offering scalability, ease of deployment, and cost-effectiveness. Furthermore, the selected technologies are particularly suitable for small businesses with limited IT resources, making the solution both accessible and practical. To demonstrate its real-world applicability, the framework was implemented in a small business in Vietnam to assess its impact on operational efficiency. Additionally, the effectiveness of the proposed approach was validated through a rigorous evaluation comparing two advanced Large Language Models (LLMS). Using a dataset reflecting real-world business scenarios, primarily Vietnamese customer comments, we found that the Claude 3.5 Sonnet model outperformed its counterpart, achieving 87.35% accuracy in sentiment classification and 82.21% in department-involved identification. This study makes a significant contribution to the evolving field of AI-driven customer analytics, offering businesses a scalable, practical, and impactful solution to harness customer feedback and optimise their operations.

Keywords: Sentiment Analysis · Large Language Models · Customer Feedback · Natural Language Processing

1 Introduction

The rapid advancement of *Artificial Intelligence* (AI) has unlocked transformative opportunities across numerous domains, with customer feedback analysis emerging as a critical area for improving business performance and enhancing customer satisfaction. Among AI-powered applications, chatbots have received considerable attention for their ability to process vast amounts of user-generated content and extract actionable insights. Nevertheless, accurately analyzing customer feedback remains a complex task due to the informal, nuanced, and context-dependent nature of real-world user comments [10].

In practice, several challenges complicate the analysis of customer feedback. Comments frequently include slang, domain-specific terminology, and regional expressions that are difficult for traditional systems to interpret. Sarcasm, irony, or rhetorical questions can obscure the underlying sentiment, leading to misclassifications. Moreover, feedback may refer ambiguously to multiple individuals or departments, making entity identification and categorization problematic. Compounding these linguistic challenges are computational constraints: high processing costs and the need for scalable infrastructure limit the applicability of advanced models, particularly for *Small and Medium-sized Enterprises* (SMEs) with limited resources [15]. These issues highlight the limitations of conventional systems in delivering accurate and scalable feedback analysis.

To overcome these challenges, this paper presents a novel framework that leverages *Large Language Models* (LLMs) within a modular and scalable architecture. The system is designed to preprocess unstructured customer feedback, perform detailed linguistic analysis, store structured insights in a database, and support informed decision-making through automation. Our approach emphasizes both practicality and accessibility, making it suitable for deployment in resource-constrained environments. The main contributions of this work are summarized as follows.

- Propose a robust and modular framework for the effective processing of Vietnamese customer feedback, enabling accurate sentiment analysis and precise categorization of departments or service areas.
- Design and implement a scalable, low-code system architecture that integrated LLMs via the Anthropic API, MongoDB on AWS EC2, and the automation tool n8n. This architecture supported efficient deployment and seamless integration into existing business workflows.
- Conduct comprehensive experiments to evaluate the performance of leading LLMs in interpreting nuanced Vietnamese feedback. Furthermore, we provided a cost-benefit analysis through a real-world case study to assess the feasibility of deploying the proposed system for SMEs in Vietnam.
- Release a dataset of real-world Vietnamese sentiment analysis consisting of more than $20,442$ labeled customer food reviews collected from a business in Ho Chi Minh City, contributing a valuable resource for future research in Vietnamese natural language understanding.

2 Related Work

2.1 Evolution of Sentiment Analysis Techniques

Sentiment analysis has evolved substantially from its early stages as a binary classification task to become a sophisticated field integrating emotional intelligence and nuanced linguistic modeling [17]. Early methods relied on lexicon-based and rule-based approaches [12], which, although foundational, lacked the capacity to handle the intricacies of sarcasm, context-dependence, and implicit sentiment. The emergence of deep learning architectures, particularly transformer-based models such as BERT [2], revolutionized sentiment analysis by introducing contextual embeddings and attention mechanisms. Recent advances, such as TRABSA [7], combine transformers with BiLSTM networks, achieving *state-of-the-art* (SOTA) accuracy (94%) on benchmark datasets. Techniques like *Aspect-Based Sentiment Analysis* (ABSA) [13] and fine-grained emotion detection using LLMs and transfer learning [16] further demonstrate the shift toward more granular, context-aware sentiment interpretation.

2.2 LLMs vs. Human-in-the-loop Approaches

The use of LLMs for customer feedback analysis has introduced several operational advantages compared to traditional human-in-the-loop approaches. LLMs offer high throughput and scalability due to their ability to process large volumes of data in parallel on accelerated hardware [3]. This makes them suitable for real-time applications such as customer support and review monitoring. While human processing offers superior context sensitivity, especially in culturally nuanced or ambiguous cases [4], LLMs have significantly narrowed this gap through structured output formats [11] and targeted fine-tuning strategies [1]. Economically, LLMs require a higher initial investment but reduce long-term operational costs, whereas human-driven systems scale linearly with labor [1].

2.3 Challenges in Vietnamese Sentiment Analysis

Although sentiment analysis has seen significant progress, applying it to linguistically complex languages like Vietnamese introduces unique challenges. Vietnamese is characterized by tonal distinctions, regional dialects, and informal expressions that complicate syntactic and semantic interpretation. Recent studies reformulated Vietnamese ABSA as a conditional text generation task using generative transformer-based models, achieving micro F1-scores of 75.53% and 86.60% on restaurant review datasets [14]. In parallel, modern pretraining strategies such as sparse attention [9], continual learning [5,6], and efficient adaptation techniques have further advanced model robustness and efficiency. However, key challenges remain, particularly in sarcasm detection, real-time scalability, interpretability in business settings, and generalization across evolving language patterns. Future directions include integrating multimodal signals and employing few-shot or zero-shot learning for low-resource domains.

3 Methodology

Recent studies have shown that LLMs possess fundamental capabilities in interpreting structural information from tabular and semi-structured data [8]. Building on this insight, we design a modular system architecture that leverages structured outputs from LLMs to enhance customer feedback analysis. The overall system comprises four interconnected modules, as illustrated in Figure 1, working in tandem to ingest, store, analyze, and act upon customer feedback in an automated and scalable manner.

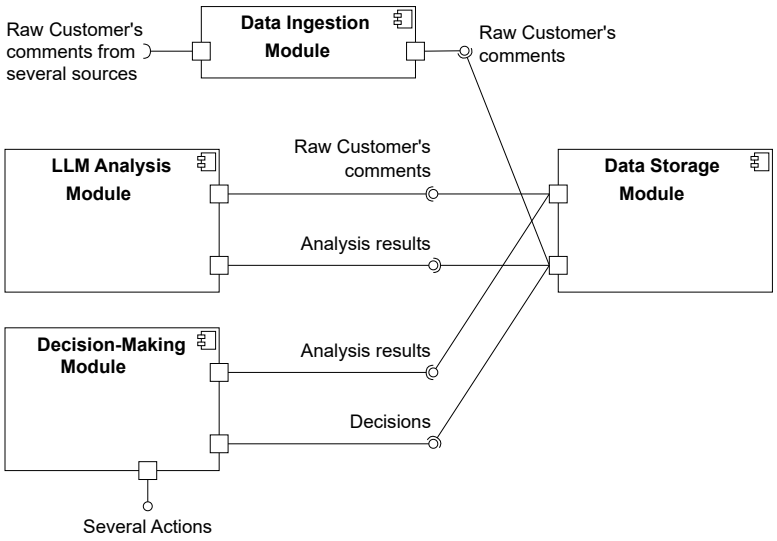

Figure 1. System architecture overview. The Data Ingestion Module collects feedback; the Data Storage Module manages the information centrally; the LLM Analysis Module extracts structured insights; and the Decision-Making Module triggers corresponding business actions.

Data Ingestion Module serves as the input gateway of the system. It collects raw customer feedback from multiple sources such as social media, support tickets, and product review platforms. To ensure downstream compatibility, the module standardizes the data format for uniform processing.

Data Storage Module acts as the central repository, this module stores both raw and processed feedback data. It supports structured access patterns to facilitate efficient querying and real-time updates across system components.

LLM Analysis Module is the core component of the system. It employs SOTA LLMs to analyze customer feedback by exploiting their ability to interpret structured information. The analysis process typically includes:

- *Sentiment Extraction*: Classifying the sentiment of each comment as positive, negative, or neutral.
- *Issue Identification*: Detecting specific problems, complaints, or suggestions expressed in the feedback.
- *Department Assignment*: Routing each identified issue to the most relevant department or functional unit.

Decision-Making Module bridges insights with actionable outcomes. It integrates with external systems through APIs to enable real-time response automation. Its key functionalities include:

- *Automated Response Generation*: Drafting and delivering replies to customer feedback based on analytical results.
- *Issue Escalation*: Notifying responsible departments about critical or trending issues.
- *Workflow Activation*: Triggering predefined business workflows or actions aligned with the analysis outcomes.

The interaction between modules follows a consistent and centralized communication pattern. The Data Storage Module acts as the system's hub, receiving input from the Data Ingestion Module and providing accessible data to the LLM Analysis Module. After processing, results are updated in storage and subsequently retrieved by the Decision-Making Module. This design ensures that data and insights are systematically stored, enabling traceability, auditability, and monitoring throughout the feedback lifecycle.

4 System Architecture

To implement the proposed customer feedback analysis system, we adopt *n8n*[3], a flexible low-code automation platform, to orchestrate three main modules: the *Data Ingestion Module*, the *LLM Analysis Module*, and the *Decision-Making Module*. This choice is driven by n8n's rich integration ecosystem, built-in scheduling support, and ability to connect across cloud and local environments.

The platform supports a queue mode configuration in which a central instance manages workflow triggers, while separate worker instances handle the task executions. As illustrated in Figure 2, this architecture enables the system to dynamically distribute processing loads, allowing it to scale efficiently based on operational demand.

Within the n8n platform, the *LLM Analysis Module* utilizes advanced language models through the *Anthropic API*[4] to analyze customer comments. This module extracts structured insights such as sentiment, issue categories, and the most relevant departments for resolution. These results are stored for downstream use.

[3] `https://n8n.io/`
[4] `https://www.anthropic.com/`

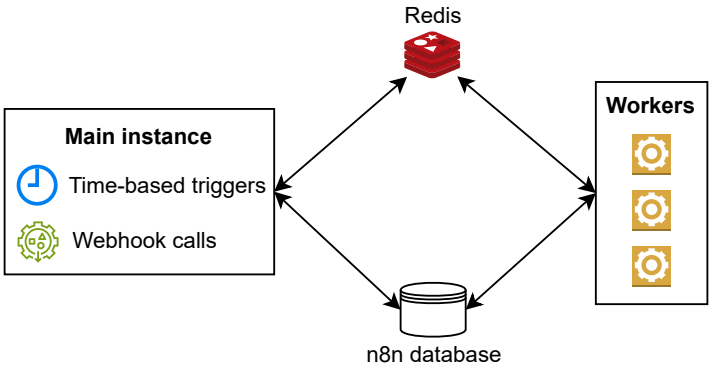

Figure 2. Scalable architecture of n8n in queue mode. A central instance coordinates tasks with distributed workers.

The *Decision-Making Module* connects to communication platforms like Gmail and Slack, enabling the system to automatically notify responsible teams and generate appropriate responses based on the analysis results.

For data storage, we use MongoDB, hosted via MongoDB Atlas on an Amazon Web Services (AWS) EC2 instance. This configuration provides 512 MB of free, persistent cloud storage, making it a practical choice for small and medium-sized enterprises. MongoDB's document-oriented architecture allows the system to manage diverse and evolving customer feedback data with flexibility and scalability.

Figure 3 illustrates the overall workflow. Customer feedback is collected by the *Data Ingestion Module* and saved to MongoDB. The *LLM Analysis Module* monitors this database, processes new entries via the Anthropic API, and stores the analysis results. These insights are then accessed by the *Decision-Making Module*, which initiates relevant business actions such as sending notifications or launching automated workflows. This continuous pipeline ensures timely processing and response to customer feedback in real-world scenarios.

5 Experimentation

5.1 Case Study Description

Our study focuses on Aroma Bakery, a thriving business in Ho Chi Minh City, Vietnam. As its popularity has grown, so has the volume of customer feedback from various sources. Manually handling each comment has become challenging, leading to missed valuable insights. The task is complex because a single comment often contains multiple points with different sentiments and involving different departments. For example, a customer might praise the pastries, but criticize the delivery service.

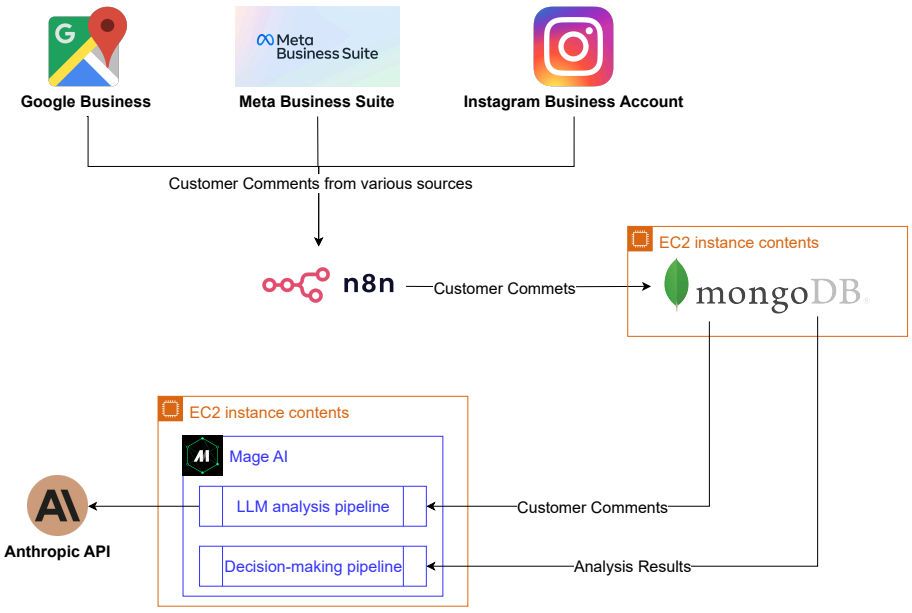

Figure 3. System architecture overview showing module interactions and data flow.

As Aroma Bakery expands, there is a pressing need for an automated system to efficiently analyze comments, extract insights, and route issues to appropriate departments. This would improve customer satisfaction and operational efficiency. To address this, we have implemented an LLM-Analysis module that generates structured output from customer comments. Each point of feedback is categorized by sentiment (*positive, negative,* or *neutral*) and assigned to a relevant department (e.g., *Product, Online Customer Services, Digital Marketing, Offline Customer Services,* or *Packaging*). Figure 4 provides a visual representation of the input and output of the analysis.

With this structured information, the Decision-Making Module can then automate responses, notify relevant departments about urgent or trending issues, and trigger appropriate actions to address the identified concerns, ultimately improving Aroma Bakery's customer experience and operational efficiency.

5.2 Experimental Setup

Evaluation Setting For evaluation, we used a dataset of 20,442 sample comments collected from various sources, is available on GitHub[5]. To ensure high-quality ground truth, we initially used the models gpt-4-o (OpenAI) and claude-3-opus (Anthropic) - the two language models considered to have the highest

[5] `https://github.com/sangngoc27042001/small-sentiment-analysis-dataset.git`

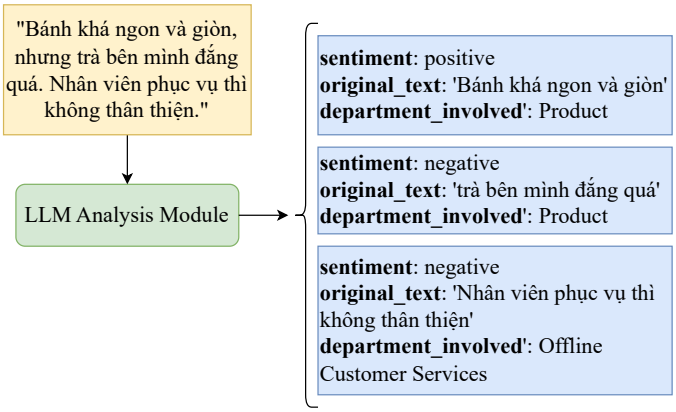

Figure 4. LLM analysis of customer feedback. The figure illustrates the analysis of a Vietnamese comment which translates to "The cake is quite delicious and crispy, but the tea is too bitter. The service staff is not friendly." The analysis results show sentiment and department classification for each part of the comment: positive sentiment for the cake (Product department), negative sentiment for the tea (Product department), and negative sentiment for the staff service (Offline Customer Services department).

performance at that time - to generate results, which were then manually refined and validated.

Evaluation Metrics Our evaluation on these models focused on two key metrics:

- Accuracy in classifying sentiments
- Accuracy in identifying company departments involved

For each comment, we extracted multiple points, assigning both a sentiment and a relevant company department to each point. The accuracy was determined by comparing the predicted results with the ground truth. For sentiment classification, a true prediction was recorded if the predicted sentiment set matched the ground truth set exactly. Similarly, for company department identification, a match between predicted and actual department sets was required for a true positive.

5.3 Results

We compared Claude-3.5-Sonnet-latest, GPT-4o-mini, a traditional SVM model with TF-IDF features, and a Vietnamese-specific sentiment analysis model (ViSentiment)[6]. As shown in Table 1, Claude-3.5-Sonnet-latest outperformed all models, achieving 87.35% sentiment accuracy and 82.21% department accuracy, com-

[6] `https://huggingface.co/mr4/phobert-base-vi-sentiment-analysis`

pared to GPT-4o-mini (84.59%, 72.33%), SVM (78.12%, 65.84%), and ViSentiment (80.45%, 68.92%).

Table 1. Model Performance Comparison

Model	**Sentiment Accuracy**	**Department Accuracy**
SVM (TF-IDF)	0.7812	0.6584
ViSentiment	0.8045	0.6892
GPT-4o-mini	0.8459	0.7233
Claude-3.5-Sonnet-latest	**0.8735**	**0.8221**

These results indicate that while both models are capable of handling the task, claude-3.5-sonnet-latest may be the preferable choice for applications requiring high accuracy in sentiment analysis and department identification from customer feedback.

5.4 Business Impact Validation

A longitudinal case study at Aroma Bakery (2025) validated the practical benefits of LLM-based sentiment analysis through n8n automation integrated with the Anthropic API. The implementation utilized a cost-effective $20/month architecture, leveraging MongoDB's free 512MB AWS storage tier, lightweight EC2 instance orchestration, and automated sentiment analysis pipelines. This system significantly enhanced operational performance, improving sentiment analysis accuracy from 92% to 98%, increasing customer service capacity by 66% (from 6-7 to 10-12 simultaneous interactions), and reducing monthly operational costs by $850. Strategically, the implementation reduced manual analysis time by 73%, enabling staff upskilling, supported seasonal demand fluctuations with an elastic architecture, and facilitated reinvestment in customer experience through cost savings. This case study highlights that even modest LLM implementations can deliver substantial benefits to SMEs, including a 6.5% absolute accuracy gain, expanded capacity, and effective cost containment.

5.5 Prompt Design for Vietnamese Language Nuances

To address the linguistic challenges of Vietnamese customer feedback, such as tonal subtleties, regional slang, and informal expressions, we designed LLM prompts to improve contextual understanding. The prompts included language-specific instructions to account for Vietnamese tonal markers (e.g., distinguishing between "bánh" [cake] and "banh" [wheel]) and southern-dialect expressions like "ngon dữ" (very delicious) prevalent in Ho Chi Minh City. For instance, a sample prompt used was as follows:

> "Analyze the sentiment of the following Vietnamese comment, paying attention to tonal markers and southern-dialect slang. Example: 'ngon dữ' (positive, Product dept). Comment: 'bánh ngon mà hơi mắc'. Output sentiment and department for each aspect."

We explored variations, such as zero-shot prompts (no examples) and chain-of-thought (CoT) prompting, instructing the model to reason step-by-step (e.g., "First identify tonal markers, then detect slang, and finally classify sentiment"). Few-shot examples of sarcasm and implicit sentiments (e.g., "ngon mà hơi mắc") were included. As shown in Table 2, language-specific few-shot prompting outperformed zero-shot (78.50% sentiment accuracy) and CoT (83.20%) approaches, achieving 87.35% sentiment accuracy and 82.21% department accuracy on a subset of 50 comments. No modifications were made to standard prompting techniques beyond these adaptations, ensuring reproducibility.

Table 2. Prompting Techniques Comparison

Prompt Type	**Sentiment Accuracy**	**Department Accuracy**
Zero-Shot Prompting	0.7850	0.7320
Chain-of-Thought Prompting	0.8320	0.7645
Language-Specific Few-Shot	**0.8735**	**0.8221**

5.6 Ground Truth Establishment Process

Initially, we employed GPT-4o and Claude-3-Opus to generate preliminary sentiment classifications and department assignments for each comment. These outputs were then manually refined by a team of three annotators fluent in Vietnamese, with expertise in southern-dialect expressions and business contexts. The refinement process involved cross-verification, where annotators independently reviewed the model outputs, focusing on correcting misclassifications of sarcasm, implicit sentiments, and ambiguous department assignments (e.g., distinguishing between "Online Customer Services" and "Digital Marketing" for delivery-related feedback). Discrepancies were resolved through majority voting, and in cases of persistent disagreement, a senior linguist with over 10 years of experience in Vietnamese NLP adjudicated the final labels. This process achieved an inter-annotator agreement of 92% (Cohen's Kappa), ensuring high-quality ground truth for evaluating model performance.

5.7 Cost Analysis Baseline

Before adopting the automated system, Aroma Bakery relied on manual feedback analysis, employing two part-time staff members dedicated to processing

customer comments, at a combined cost of $1,200 per month. Additional expenses included software subscriptions for basic CRM tools, costing $150 per month, bringing the total baseline operational cost to $1,350 per month. The LLM-based system, with its $20/month architecture and reduced manual effort, lowered the operational cost to $500 per month, primarily covering cloud hosting and API usage fees. This results in the reported $850 monthly savings ($1,350 - $500), highlighting the cost-effectiveness of the proposed framework for small businesses.

6 Conclusion

This paper introduces a novel framework for analyzing customer feedback, addressing key challenges in sentiment analysis and department categorization by leveraging the power of large language models (LLMs). A key contribution of this work is the development of a robust, low-code system architecture integrating n8n, MongoDB on AWS EC2, and LLMs via the Anthropic API, designed for scalability and ease of implementation. The framework's effectiveness is demonstrated through empirical validation using a unique Vietnamese dataset of labeled customer reviews collected from a bakery in Ho Chi Minh City, which features expressions in the southern dialect. Furthermore, this study highlights the potential of prompting-based approaches with LLMs for Vietnamese language processing, achieving strong performance without the need for resource-intensive fine-tuning. This approach provides a cost-effective solution for small businesses in Vietnam, as demonstrated by a real-world case study, and showcases the framework's adaptability for other languages.

Acknowledgment

The authors acknowledge Ho Chi Minh City University of Technology (HCMUT), VNU-HCM for supporting this study. The authors also extend their heartfelt gratitude to Manh-Khang Nguyen, Lu-Quynh-Nhu Ho, and Luat-Gia-Khoi Nguyen for their invaluable support and contributions, which have been crucial to the successful completion of this research.

References

1. Demiralp, Ç., Wenz, F., Chen, P.B., Kayali, M., Tatbul, N., Stonebraker, M.: Making LLMs Work for Enterprise Data Tasks. arXiv preprint arXiv:2407.20256 (2024)
2. Devlin, J., Chang, M.W., Lee, K., Toutanova, K.: BERT: Pre-training of Deep Bidirectional Transformers for Language Understanding (2019), `https://arxiv.org/abs/1810.04805`
3. Dong, S.: Leveraging LLMs for Unstructured Direct Elicitation of Decision Rules. Customer Needs and Solutions **11**(1), 10 (2024)
4. Eigner, E., Händler, T.: Determinants of LLM-assisted decision-making. arXiv preprint arXiv:2402.17385

5. Guo, Y., Fu, J., Zhang, H., Zhao, D., Shen, Y.: Efficient Continual Pre-training by Mitigating the Stability Gap (2024), https://arxiv.org/abs/2406.14833
6. Ibrahim, A., Thérien, B., Gupta, K., Richter, M.L., Anthony, Q., Lesort, T., Belilovsky, E., Rish, I.: Simple and Scalable Strategies to Continually Pre-train Large Language Models (2024), https://arxiv.org/abs/2403.08763
7. Jahin, M.A., Shovon, M.S.H., Mridha, M.F., Islam, M.R., Watanobe, Y.: A hybrid transformer and attention based recurrent neural network for robust and interpretable sentiment analysis of tweets. Scientific Reports **14**(1) (2024). https://doi.org/10.1038/s41598-024-76079-5
8. Liu, Y., Li, D., Wang, K., Xiong, Z., Shi, F., Wang, J., Li, B., Hang, B.: Are LLMs good at structured outputs? A benchmark for evaluating structured output capabilities in LLMs. Information Processing & Management **61**(5), 103809 (2024)
9. Martins, A.F.T., Farinhas, A., Treviso, M., Niculae, V., Aguiar, P.M.Q., Figueiredo, M.A.T.: Sparse and Continuous Attention Mechanisms (2020), https://arxiv.org/abs/2006.07214
10. Nguyen, T.T.B., Nguyen, K.D.: Elevating Customer Satisfaction: AI Sentiment Analysis in Vietnamese E-Retail Landscape, pp. 347–369. Springer Nature Singapore, Singapore (2024). https://doi.org/10.1007/978-981-97-7819-5_12
11. OpenAI, R.: Gpt-4 technical report. arxiv 2303.08774. View in Article **2**(5) (2023)
12. Pang, B., Lee, L., Vaithyanathan, S.: Thumbs up? Sentiment Classification using Machine Learning Techniques. In: Proceedings of the 2002 Conference on Empirical Methods in Natural Language Processing (EMNLP 2002). pp. 79–86. Association for Computational Linguistics (Jul 2002). https://doi.org/10.3115/1118693.1118704
13. Suhariyanto, S., Sarno, R., Fatihah, C., Faisal, E.: Aspect Based Sentiment Analysis: A Systematic Literature Review. Journal of Applied Intelligent System **5**, 8–22 (12 2020). https://doi.org/10.33633/jais.v5i1.3807
14. Thin, D., Nguyen, N.: Aspect-Category based Sentiment Analysis with Unified Sequence-To-Sequence Transfer Transformers. VNU Journal of Science: Computer Science and Communication Engineering **39**(2) (2023). https://doi.org/10.25073/2588-1086/vnucsce.662
15. Tran, T.K., Phan, T.T.: Constructing sentiment ontology for vietnamese reviews. In: Proceedings of the 17th International Conference on Information Integration and Web-Based Applications & Services. iiWAS '15, Association for Computing Machinery, New York, NY, USA (2015). https://doi.org/10.1145/2837185.2837215
16. Wang, K., Jing, Z., Su, Y., Han, Y.: Large Language Models on Fine-grained Emotion Detection Dataset with Data Augmentation and Transfer Learning (2024), https://arxiv.org/abs/2403.06108
17. Zhang, L., Wang, S., Liu, B.: Deep Learning for Sentiment Analysis : A Survey (2018), https://arxiv.org/abs/1801.07883

Study of Stomach Abnormalities using EGG Signals

Chandrasekaran R[1],B.Praveena[2], Vivek Pazhamalai[3] Ivo Romauld.S[4], Vijayaraj.S[5], Soundarya M.K[6]

[1,2,3,4,5,6] Vels Institute of Science, Technology and Advanced Studies, Chennai, Tamil nadu, India

[1] chandrasekar.se@vistas.ac.in, [2]praveenab1624@gmail.com, [3]vivek.se@vistas.ac.in, [4]ivoromauld.se@vistas.ac.in, [5]vijayaraj.se@vistas.ac.in, [6]soundarya.se@vistas.ac.in

Abstract. In this study various stomach abnormalaities and its corresponding gastric signals are analysed using MATLAB. Electrogastrogram is used to measure the electrical activity of the stomach.If there is any abnormalities in gastric digestion process,it will be reflected in EGG signal.In this study 40 EGG signals are acquired from healthy adults in the age group of 20-25 and the signals are acquired from center for biomedical research,VISTAS.All the individuals who were used for this signal acquired from the individual were given junk foods.The signals were taken in two conditions i)at fasting state ii)at postprandial state.The research mainly focus on digestion process and effects of packed foods during digestion process. BIOPAC MP45 device is used for signal acquisition and MATLAB version 2024 is used for analysis.The research work exhibits delayed in digestion in few individuals who regularly intakes junk food and the frequency estimation of EGG signal clearly shows the delay digestion with prolonged frequency range.

Keywords: Stomach abnormalities ,EGG,MATLAB.

1 Introduction

The Electrogastrogram (EGG) is a non-invasive method of recording stomach electrical activity and thus gives information on gastric motility and function. Like the ECG for the heart, the EGG records slow wave activity from the stomach wall smooth muscles during digestion at approximately three cycles per minute for humans. Surface electrodes are placed on the abdomen and the EGG registers low frequency signals that are related to gastric slow waves and spike activity that is superimposed on these, which is increased during active digestion. These signals can be analyzed in terms of frequency, amplitude and stability in order to determine patterns which may be associated with a number of gastrointestinal

disorders, including gastroparesis and functional dyspepsia. However, as with the EGG, the major problem is one of signal isolation, since gastric signals are contaminated by respiratory and cardiac noise. Nevertheless, progress in signal processing has enhanced the clinical significance of EGG and it has the potential to help in the diagnosis of gastric motility disorders [1].

Electrogastrogram (EGG) acquisition records the stomach's electrical patterns through surface electrodes to evaluate its movement and rhythmic behavior. EGG differs from invasive methods because it is a non-invasive technique that records slow-wave signals generated by gastric smooth muscle cells. Human stomach slow waves operate at three cycles per minute and establish the fundamental electrical pattern which helps evaluate gastric motility disorders. EGG recording starts with positioning surface electrodes on the abdominal skin situated above the stomach to capture gastric signals effectively. The EGG signal measures in microvolts with low amplitude and faces interference from respiratory and cardiac signals which makes precise electrode placement essential. One electrode of a bipolar or unipolar pair is positioned over the gastric region while the other functions as a reference point. The electrode configuration effectively separates gastric electrical signals from background noise [2].

2 Literature Survery

The Literature review is done to identify the research gap in existing methodologies of diagnostic tools available for diagnosing gastroparesis. The various existing methodologies and proposed research methodologies are discussed in this chapter

Amal Shine et al., “CLINICAL RESEARCH” VOLUME 25, ISSUE 8, P1150-1159, DECEMBER 2022, the paper discusses the clinical importance of electrogastrogram (EGG) and its correlation with mucosal electrograms (mEGs), gastric emptying tests (GETs), and gastrointestinal symptoms before and after temporary gastric electrical stimulation (tGES). EGG is valuable in diagnosing delayed gastric emptying and can identify patients who may require GES.

Bin Wang et al., “Journal of Medical Imaging and Health Informatics”, Volume 10, Number 6, June 2020, pp. 1281-1287(7), The paper discusses the use of electrogastrogram (EGG) to detect gastric electromyogram activity and classify high-dimensional signals for the diagnosis and management of gastrointestinal diseases.

Al Taee, A., Al-Jumaily, A. (2020). “Electrogastrogram Based Medical Applications an Overview and Processing Frame Work. In: Madureira”, A.,

Abraham, A., Gandhi, N., Varela, M. (eds) Hybrid Intelligent Systems. HIS 2018. Advances in Intelligent Systems and Computing, vol 923. Springer, Cham. https://doi.org/10.1007/978-3-030-14347-3_50 , this paper discusses Electrogastrogram (EGG), a noninvasive method of recording electrical signals of stomach muscles. It provides an overview of EGG detection, analyzing methods, and its application in clinical settings.

Jieyun, Yin., Jiande, D.Z., Chen. (2013). Electrogastrography: Methodology, Validation and Applications. Journal of Neurogastroenterology and Motility, doi: 10.5056/JNM.2013.19.1.5, The paper discusses the methodology, validation, and applications of electrogastrography (EGG), a non-invasive method for measuring gastric myoelectrical activity. It reviews the accuracy of EGG in recording gastric slow waves and dysrhythmia and discusses its correlation with gastric contraction. The paper also reviews the applications of EGG in various areas.

3 Methodology

This system aims to develop algorithms for mathematical models of intestinal physiology and digestive processes for the purpose of gaining insight into and analysing digestive disorders. The data gathered will identify the mathematical models that serve best, estimate parameters, and ultimately validate the model. Simulations will be run to demonstrate how digestion is impacted by variations in relevant conditions, and sensitive analyses will be performed to identify influential factors in digestion. The ultimate goal is to design practical utensils that the doctor can use in organizing and managing digestive disorders.

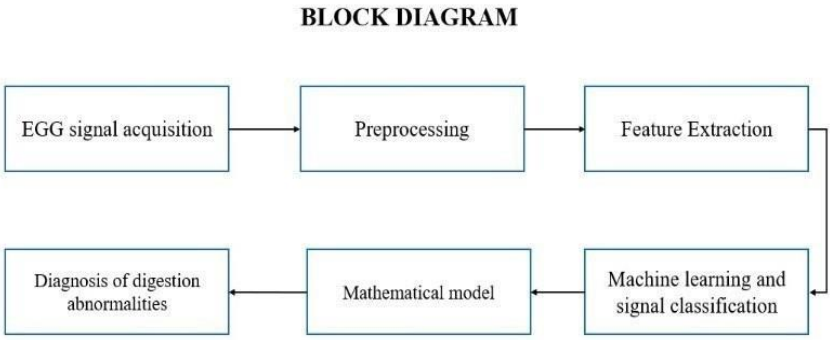

Fig.1. Block Diagram

3.1 Filtering

Filtering is an important step in the analysis of EGGs to ensure noise-free data for the accurate interpretation of gastric electrical activity. Common sources of interference include power line noise, motion artifacts, and baseline drift. Bandpass filtering at 0.05–0.5 Hz isolates gastric slow waves, while adaptive filtering dynamically adjusts to non-stationary noise [3]. Wavelet transform filtering enables the time-frequency analysis of the artifact. Signal averaging is one more post-processing technique that improves the clarity of a signal. Such techniques enhance the signal-to-noise ratio, and gastric rhythms could be detected in a reliable way. This enhances the diagnosis of motility disorders such as gastroparesis in clinical as well as in research settings [4].

3.2 Power Spectral Density (PSD)

The PSD of the EGG is an important tool in analysing the frequency characteristics of gastric electrical activity [5]. Dominant frequencies in EGG signals are generally seen around 0.05 Hz, or 3 cycles per minute, corresponding to normal slow-wave activity. PSD estimation through methods such as FFT and Welch's method is useful for power distribution, noise reduction, and detection of dysrhythmias like bradygastria and tachygastria. In the clinical setting, PSD helps to diagnose motility disorders such as gastroparesis by the presence of frequency shifts or power reductions. This is a non-invasive tool that improves gastric function assessment and treatment efficacy [6].

3.3 Cross Spectral Density (CSD)

The cross-spectral density (CSD) of an electrogastrogram (EGG) analyzes phase relationships and synchronization between gastric electrical signals from different stomach regions. It is useful for determining common power across frequencies (0.01–0.1 Hz) that could be involved in such an assessment of gastric motility and coordination [7]. High coherence in the slow-wave range provides evidence of effective peristalsis, and low coherence or phase irregularities may suggest dysrhythmic conditions such as bradygastria or tachygastria. The use of Fourier-based methods, like FFT and Welch's method, makes it possible to estimate CSD with an accurate frequency-domain analysis. It also supports the non-invasive assessment of gastric function, helping in the diagnosis and management of motility disorders [8].

3.4 Feature Extraction

Features that are extracted from the analysis of electrogastrogram are critical for the interpretation of gastric function. Some of the time series features are mean, median, standard deviation, peak-to-peak amplitude, and kurtosis. These helps understand the signal characteristics. The mean and median can be used to measure the underlying activity and the underlying preference. The standard deviation measures the variance. Peak-to-peak amplitude indicates the strength of the signal, while kurtosis describes the variability associated with the variance. It applies the fast fourier transform (FFT) or wavelet transform to separate slow-frequency (0.03-0.1 Hz) signals of the gastrointestinal tract. These resources enhance the interpretation of EGG signals, facilitate the diagnosis of movement disorders such as gastroparesis, and support the use of medical imaging and machine learning [9][10].

3.5 Fast Fourier Transform (FFT)

Features that are extracted from the analysis of electrogastrogram are critical for the interpretation of gastric function. Some of the time series features are mean, median, standard deviation, peak-to-peak amplitude, and kurtosis. These helps understand the signal characteristics. The mean and median can be used to measure the underlying activity and the underlying preference. The standard deviation measures the variance. Peak-to-peak amplitude indicates the strength of the signal, while kurtosis describes the variability associated with the variance. It applies the fast Fourier transform (FFT) or wavelet transform to separate slow-frequency (0.03-0.1 Hz) signals of the gastrointestinal tract. These resources enhance the interpretation of EGG signals, facilitate the diagnosis of movement disorders such as gastroparesis, and support the use of medical imaging and machine learning [11][12].

4 Results and Discussion

A Chebyshev Type I IIR Bandpass Filter allows certain frequencies in a particular range and rejects others. This filter is also efficient for the applications such as EEG signal processing and communication systems. This low cutoff of 0.15 Hz and a high cutoff of 0.60 Hz filter is designed.

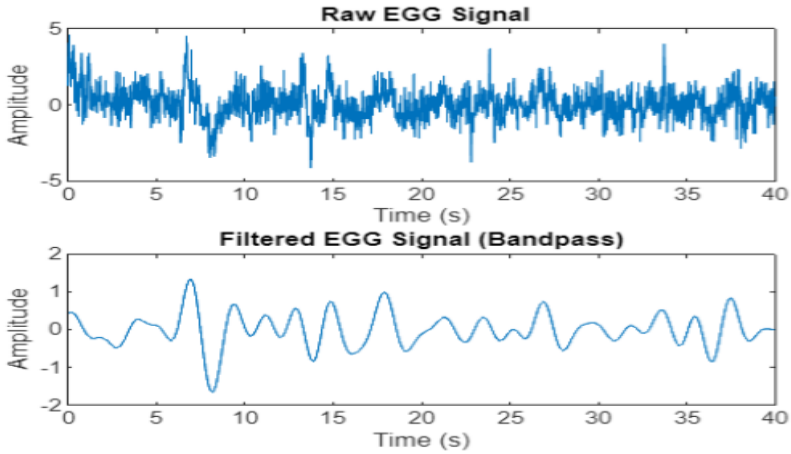

Fig.2. Filtering

Power spectral density (PSD) analysis is often utilized to quantify the power distribution of the signal across a range of frequencies and investigate the frequency composition. PSD is utilized to characterize the frequency character of the EGG signal, which then allows one to analyze the gastric slow wave, identify pathological patterns, and derive features of clinical use.

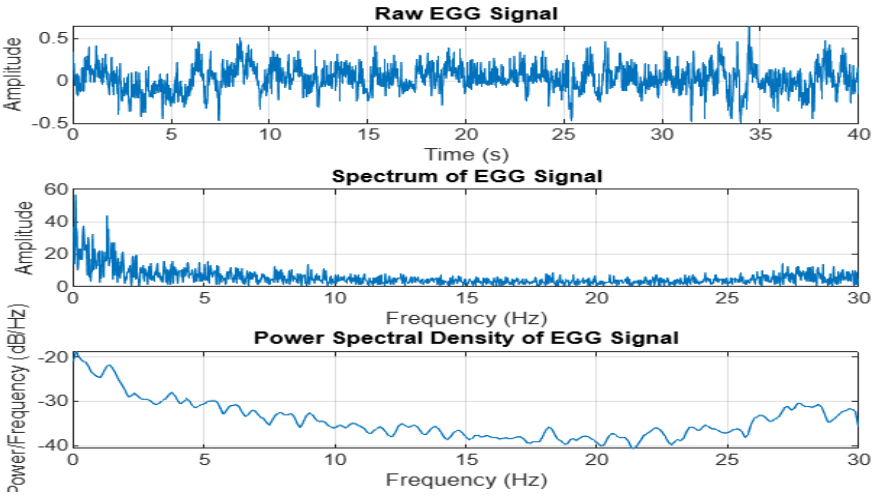

Fig.3. Power Spectral Density (PSD)

Cross-spectral density (CSD) of electrogastrogram (EGG) signals analyzes electrode correlations and detects gastric muscle synchronization. CSD enables the analysis of regional coordination, rhythmic pattern detection, and the diagnosis of motility disorders. CSD, through analysis of frequency relations, offers insight into stomach function and enables one to interpret normal and abnormal gastric activity for clinical purposes.

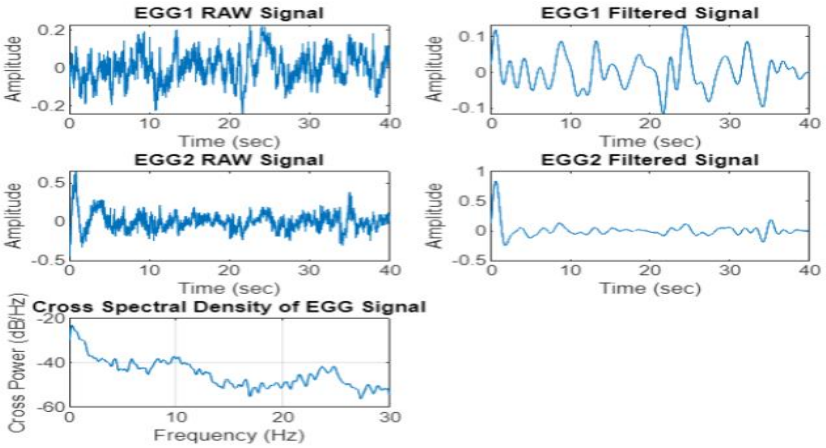

Fig.4. Cross Spectral Density (CSD)

Mean is the average EGG signal, indicating gastric activity in the middle. Median is the middle value and is not affected by outliers. Standard deviation is a measure of variability around the mean. Peak-to-peak measures the signal range. Kurtosis measures sharpness of distribution, detecting outliers. These measurements, together, characterize gastric electrical activity, making it possible to analyze the EGG signal and determine motility.

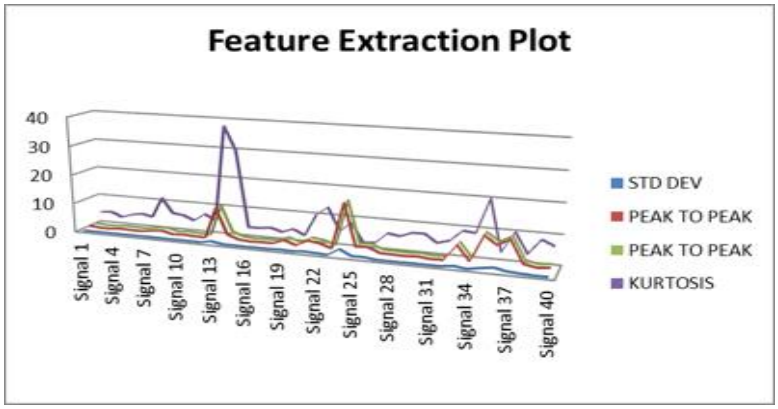

Fig.5. Feature Extraction

Normal Digestion:

A normal stomach's FFT peaks at 2–4 cycles per minute (cpm), indicating regular gastric slow waves and normal contractions for digestion. The power spectrum is stable with minimal irregularities.

Abnormal Digestion:

Gastrointestinal diseases like gastroparesis and dyspepsia cause alterations in the FFT spectrum:

- Bradygastria: Frequencies below 2 cpm, indicating slow gastric motility.
- Tachygastria: Frequencies above 4 cpm, a marker of rapid or irregular contractions.
- Arrhythmias: Failure of dominant peak, wide frequency spread, or noise, a marker of deranged gastric electrical activity.

Comparing normal VS abnormal plot of EGG signals it iis clearly shows that there is a delayed in digestion for subjects who regularly intakes junkfood.The fasting state spectral distribution was even for all individuals at all cartegories but the postprandial state shows delaysd gastric emptying process.

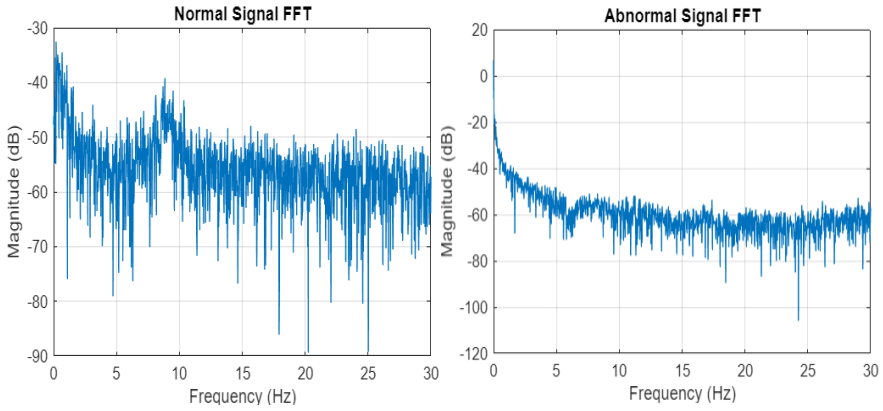

Fig.6. Normal FFT Signal vs Abnormal FFT signal

References

1. Chang, F. (2005). Electrogastrography: Basic knowledge, recording, processing and its clinical applications. Journal of Gastroenterology and Hepatology, 20. https://doi.org/10.1111/j.1440-1746.2004.03751.x.

2. Yin, J., & Chen, J. (2013). Electrogastrography: Methodology, Validation and Applications. Journal of Neurogastroenterology and Motility, 19, 5 - 17. https://doi.org/10.5056/jnm.2013.19.1.5.
3. Chen, J. (1992). A computerized data analysis system for electrogastrogram.. Computers in biology and medicine, 22 1-2, 45-57 . https://doi.org/10.1016/0010-4825(92)90051-N.
4. Gharibans, A., Smarr, B., Kunkel, D., Kriegsfeld, L., Mousa, H., & Coleman, T. (2018). Artifact Rejection Methodology Enables Continuous, Noninvasive Measurement of Gastric Myoelectric Activity in Ambulatory Subjects. Scientific Reports, 8. https://doi.org/10.1038/s41598-018-23302-9.
5. Parkman, H., Hasler, W., Barnett, J., & Eaker, E. (2003). Electrogastrography: a document prepared by the gastric section of the American Motility Society Clinical GI Motility Testing Task Force. Neurogastroenterology & Motility, 15. https://doi.org/10.1046/j.1365-2982.2003.00396.x.
6. Taghipoor, M., Lescoat, P., Licois, J., Georgelin, C., & Barles, G. (2011). Mathematical modeling of transport and degradation of feedstuffs in the small intestine.. Journal of theoretical biology, 294, 114-21 https://doi.org/10.1016/j.jtbi.2011.10.024.
7. Li, C., Yu, W., Wu, P., & Chen, X. (2020). Current in vitro digestion systems for understanding food digestion in human upper gastrointestinal tract. Trends in Food Science and Technology, 96, 114-126. https://doi.org/10.1016/j.tifs.2019.12.015.
8. Komorowski, D., & Mika, B. (2018). A new approach for denoising multichannel electrogastrographic signals. Biomed. Signal Process. Control., 45, 213-224. https://doi.org/10.1016/j.bspc.2018.05.041.
9. Kafee, A., & Kayar, Y. (2023). Electrogastrography in patients with gastric motility disorders. Proceedings of the Institution of Mechanical Engineers, Part H: Journal of Engineering in Medicine, 238, 22 - 32. https://doi.org/10.1177/09544119231212269.
10. Chen, J., & McCallum, R. (1991). Electrogastrography: measuremnt, analysis and prospective applications. Medical and Biological Engineering and Computing, 29, 339-350. https://doi.org/10.1007/BF02441653.
11. Yacin, M., Manivannan, M., & Chakravarthy, S. (2010). On Non-Invasive Measurement of Gastric Motility from Finger Photoplethysmographic Signal. Annals of Biomedical Engineering, 38, 3744-3755. https://doi.org/10.1007/s10439-010-0113-4.
12. Wang, Z., Elsenbruch, S., Orr, W., & Chen, J. (2003). Detection of gastric slow wave uncoupling from multi‐channel electrogastrogram: validations and applications. Neurogastroenterology & Motility, 15. https://doi.org/10.1046/j.1365-2982.2003.00430.x.

Lightweight Data Encryption on EdgeAI Platforms: a Systematic Review

Thien An Nguyen, Thanh Loc Nguyen, Cuong Pham-Quoc*

Ho Chi Minh City University of Technology (HCMUT), Vietnam
Vietnam National University - Ho Chi Minh City (VNUHCM), Vietnam
{ngthienan.cse, lokngnguyen, cuongpham}@hcmut.edu.vn

Abstract. Security measures have always been one of the top priorities for many experts in the Internet of Things (IoT) field. In fact, the keyword "security" is among the top 10 keywords for IoT in the Scopus database [1]. Performing encryption at the edge of IoT networks proves no easy task as the hardware capabilities are very limited. As such, typical cryptography found in most high-end servers aren't applicable in the harsh and often low energy intake environments that the edge computers are deployed. The amount of intelligent applications being applied on the edge increases the severity of the issue. Different kinds of approach towards this problem have been suggested throughout the years from light weight algorithms to hardware-based ones. This paper is set to investigate these approaches for a more in-depth understanding of the subject. Aspects such as run time, energy consumption, throughput, etc. are considered in each of the proposals.

Keywords: Security, Edge AI, Cryptography, Internet of things

1 Introduction

A recent research has pointed out the possibility of 74.44 billion connected IoT devices around the world in 2025 [2]. High demand requires different solutions to support such as cloud computing, fog computing, edge computing, etc. Among them, edge computing assists the cloud servers to process the enormous amount of data at the local devices rather than concentrating them on a few single group of machines. This will not only lighten the load needed from the cloud but also increase user experience through a faster response time. Maximizing the computation and transportation capacity of every devices in the network with limited resources are always considered. Security issues are nothing new to these devices as they are like hubs absorbing data, prime targets for attackers [3]. Unlike usual small-scale systems, IoT ones are extremely vast and complex. Thus, it is infeasible to run a general system protection. Therefore, along side some physical protection methods, the devices themselves also runs security algorithms to protect the data they are carrying and sending [4]. Nevertheless, these devices

* Corresponding author: Cuong Pham-Quoc

are being run in a wide variety of environments and conditions which usually requires low energy consumption. In the past, the field programmable gate array (FPGA) is used for most IoT computing applications due to their low energy consumption, reconfiguration ability, and good performance [5]. Nonetheless, larger and larger AI models being integrated into them causes some performance problems as their computing capabilities are not the best. Additionally, a full IoT solution often need the seamless combination of the server, network, and infrastructure as seen in Figure 1.

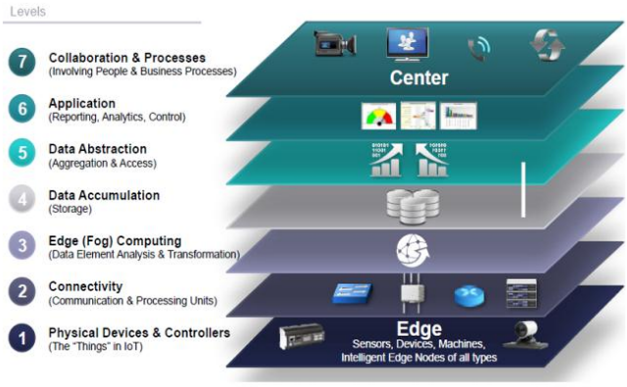

Fig. 1: Typical EdgeAI architecture [6]

On a developer and system architect stand point, it is a hassle to continuously reconfigure an FPGA, let alone thousands. All of the above leads to a boost in embedded computer usage [7]. An embedded computer is a more general piece of device with higher computing capability than that of an FPGA. They are equipped with a friendlier, more easily deployed interface as well as allowing the use of high level programming language capable of utilizing multiple frameworks and libraries. Although often considered to be a more energy consuming equipment, they can compensate with performance. Artificial intelligence on the edge (edge AI) are seeing more use in these types of devices. With the introduction of lower energy options, the embedded computing market skyrocketed [8].

The security options for edge AI systems are not new. However, as most cipher algorithms are being tested and bench-marked on FPGA [9], embedded computers aren't the same. Consequently, this paper comprehensively surveys the literature on implementing cryptography algorithms on different embedded edge AI devices. The main contributions are as follows:

1. A survey of cryptography implementations on edge AI devices.
2. A comparison of the throughput, energy consumption, and scalability of each proposals.
3. Introduction into some open issues regarding the security of the overall edge AI industry.

The rest of the paper is organized as follows. Section 2 provide a literature review of some well-known and most used cipher algorithms on edge devices. Afterwards, some implementations of such algorithms are looked into in Section 3. Thoughts about the remaining issues of the subject are displayed in Section 4. Finally, the conclusion of the survey is in Section 5.

2 Preliminaries

This section illustrates a general edge AI system along side some data security risks. Afterwards, a few encryption methods were shown to combat these risks.

2.1 Edge AI and security risks

Unlike typical edge computing, edge AI devices have to perform constant inferences when data is given.

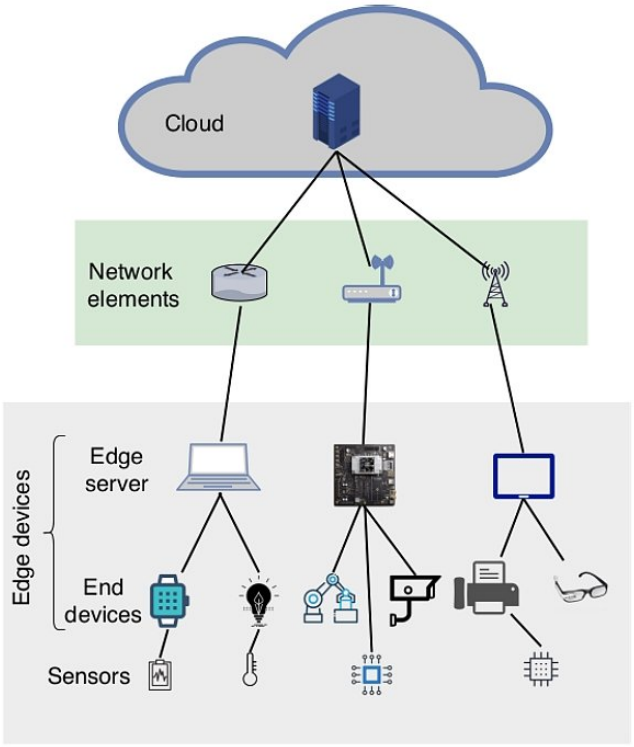

Fig. 2: Edge AI in IoT [10]

Figure 2 shows a simple IoT architecture with 3 main layers: device layer, network layer, and cloud layer. While there are variants of IoT architecture being

introduced nowadays, the overall base form has rarely been changed. The device layer is where the edge devices perform their job: pre-process data to offload the work cloud servers have to face without them. Firstly, data are gathered from sensors and end devices before forwarding to the edge servers. This is where the trained AI models can perform inferences to provide a real-time response to the end user. Individuals with malicious intent can capitalize on this fact to attack these edge nodes.

In digital marketing for example, a secure authentication method as well as satisfying user experience are absolutely crucial to the success of a business. Attackers may interfere with the smart authentication processes such as face identification or voice recognition [11]. AI algorithms may also be tricked to serve undesirable services to the customers [12]. These algorithms, while powerful and adaptive, are inherently dependent on the data they are trained on and the parameters set by their developers. This dependency creates vulnerabilities that can be exploited.

Another case study can be found is in-vehicular security. The introduction of smart electronic devices to transportation vehicles have attracted malicious attacks or manipulations. These inner car networks are seen delicate when facing the possible data leaks and system manipulation. Analyses have shown the safety and reliability of vehicle networks are still quite poor and under-prepared [13].

2.2 Encryption methods for the edge

It can be seen through Section 2 that the main target for these edge devices is the data within. Cryptography is one of the most direct way to prevent data from being leaked or manipulated. The following sub-sections show some of the popular types of cipher algorithm on edge devices.

- **Advanced Encryption Standard**

  The Advanced Encryption Standard, or AES, is a popular way to scramble data so it stays safe from prying eyes. It was set up in 2001 by National Institute of Standards and technology (NIST) from the United States of America. AES replaced an older system called DES that wasn't relevant anymore due to the fact that computers could crack it with ease. Basically, AES takes 128 bits of data at a time and encrypt them using keys that can be 128, 192, or 256 bits long. AES can be found everywhere at the moment due to its effectiveness in data encryption.

  AES is a symmetric encryption algorithm which uses the same key to encrypt and decrypt data. The sender and the receiver must both use the same secret encryption key. It is also a block cipher as it divides a message into smaller blocks, encrypting each block to transform the readable plaintext into an unreadable format known as ciphertext.

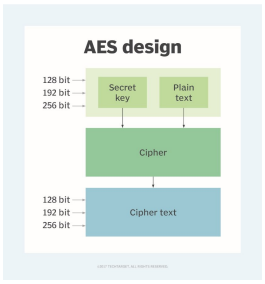

(a) AES encryption versions [10]

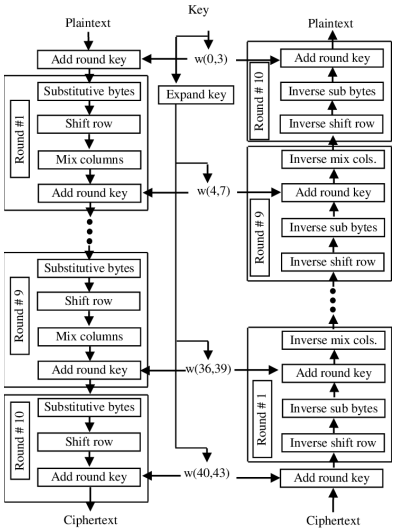

(b) Diagram of AES encryption process [14]

Fig. 3: AES encryption general view

The key goes through many rounds of encryption (10, 12, and 14 for the 128-bit, 192-bit, and 256-bit versions). Each round consists of four key stages: Substitute bytes, where each byte of the block is replaced with another via a fixed substitution box (S-box) based on the Rijndael S-box; Shift rows, which cyclically shifts the rows of the state array (a 4x4 matrix of bytes) by increasing offsets; Mix columns, a linear transformation that mixes the columns of the state to ensure diffusion; and Add round key, where the state is XORed with a round-specific subkey derived from the main key through a key expansion process. The initial round only has the Add round key stage while the last one lacks Mix columns, ensuring reversibility for decryption.

The security of AES stems from its resistance to known cryptographic attacks, such as differential and linear cryptanalysis, due to its carefully designed S-box and diffusion properties. Moreover, the combination of the aforementioned stages makes key recovery computationally infeasible.

– **ASCON**

ASCON is a family of lightweight cryptographic algorithms developed to secure data on resource-constrained devices, such as IoT sensors and embedded systems. It was introduced in 2014 and is aimed to provide efficient yet reliable protection for low-power technology. In 2023, NIST selected ASCON as the standard for lightweight cryptography following a multi-year evaluation [15].

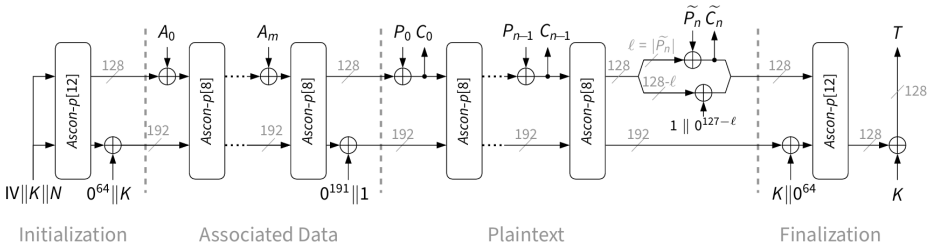

Fig. 4: Ascon-AEAD128 encryption [16]

The encryption process also includes 4 stages. The key K and nonce N are part of the initial input. Keys can either be 128 or 256 bits while the nonce is often 128 bits. Figure 4 illustrates the encryption process of the 128-bit key version. The first stage includes combining a 64-bit constant value IV with the key K and nonce N to create a 320-bit internal state S. S then goes through Ascon 12th round permutation follow by XORing K into the last 128-bit of the internal state. Stage 2 is called "processing associated data" by the creators. The associated data A_i that aren't needed to be encrypted is "absorbed" through permutation. The "plaintext processing" stage begins right after the 2^{nd} stage. The plaintext P is parsed into blocks P_i. Various operations including XOR, permutation, and concatenation are applied during this phase. The "finalization and tag generation" stage will then load the key to the state S with the XOR operation. After one more Ascon permutation and XOR, the tag T is created. The output of the process is the ciphertext C and tag T. The decryption process mirror that of the encryption and won't be mentioned further. The use of a tag assure data integrity since any modification to the ciphertext or asscociated data can cause a mismatch in decryption.

3 Implementations of cryptography for Edge AI computing platforms

Cagua et al. [17] utilized ASCON encryption on IoT devices. Simulations from the CupCarbon simulator as well as Raspberry Pi Zero W board have been done. The research provided a quick comparison between the simulation and practical approaches. Both have around 3 seconds and 79ms respectively and thus proved Ascon as a lightweight cryptography algorithm is indeed efficient in IoT devices.

A Almalawi et al. [18] proposed a hybrid cryptographic approach combining Ant Lion Optimization (ALO) and Diffie-Hellman-based Twofish cryptography (DHT) to secure data transmission in Edge AI systems. The system collects data from edge devices, processes it using an autoencoder to detect malicious entries, and employs Diffie-Hellman key exchange to generate a shared secret key. With the low latency of 0.8ms and 3.2mJ energy consumed, the approach proves to be feasible in the real world.

Chen et al. [19] presented a lightweight data protection framework for edge networks, integrating AES alongside the SM4 block cipher. AES is parallelized using FPGA pipeline techniques to secure data processed by Edge AI devices, such as mobile systems, with a focus on high throughput and low latency. The low energy consumption (4.5mJ per MB of encrypted data) and 0.12ms latency per 128-bit block are considered acceptable for real-time applications.

Kaur et al. [20] introduced error detection mechanisms for hardware security. They deployed ASCON algorithm on two FPGA families Spartan-7 and Kintex-7. It is evaluated for look-up table and logic-based implementations of ASCON. The results were acceptable in terms of power and delay.

Xu et al. [21] delivered a full pipeline approach for applying ASCON cipher into memory data encryption and authentication. However, the pipeline approach requires a large amount of resources. Since ASCON is a lightweight cryptography algorithm, its latency is inferior than the other approaches.

Elsadek et al. [22] designed a flexible architecture for ASCON that supports various datapaths tailored to different parameter sizes. They evaluate this system using both FPGA (Spartan-7) and ASIC technologies. Experiments showed that the ASIC-based core significantly outperforms the FPGA in terms of throughput and efficiency.

Raj et al. [23] proposed an FPGA-based implementation of ASCON 128-bit for authenticated encryption on Internet of Many Things (IoMT). The system runs with an Artix-7 FPGA which produces decent throughput with extremely low power consumption. However, it can not be applied to other FPGA families, limiting its robustness.

Table 1 lists the results from the aforementioned approaches and compare them.

Proposal	**Throughput (Mbps)**	**Latency** (ms)	**Energy consumption (mJ)**
Raspberry Pi Zero W [17]	-	79	-
8 cores AMD Ryzen 7 CPU simulation [18]	-	0.8	3.2
Zynq-XC7Z035 [19]	2500	0.12	4.5
Spartan-7 [20]	6.646	-	99
Kintex-7 [20]	6.709	-	88
Spartan-7 [22]	4900	-	-
Artix-7 [23]	457	-	31

Table 1: Throughput, latency, and energy consumption comparison between the proposals

4 Security for intelligent edge devices: future considerations

Nowadays, smart devices are becoming an inevitable next trend. The various fields consist of them are simply endless. As different environment changes, so does the edge devices. These devices must be able to become adaptable and flexible to keep up with the security concerns each environment introduce.

Limited computational resources restrict edge devices' ability to deploy robust security, exposing them to malware and tampering. For example, an IoT sensor for advertisement targeting unable to detect model extraction. Future solutions can leverage lightweight AI-driven security via tinyML for real-time threat detection, optimized through hybrid edge-cloud architectures, enabling a smart billboard to flag adversarial inputs autonomously.

Edge computing systems scalability is also a major concern as many parts of the world are transitioning from IoT to IIoT with a much larger scale [24]. Each layer of the architecture must be elaborated and calibrated thoroughly to cope with the large amount of data influx. Whether it's FPGA or embedded computer that is put at the edge of the network, the ability to integrate seamlessly is crucial to the functionality and scalability of the whole industry.

Energy efficiency is also a key factor for the edge AI paradigm. Finding the best hardware solution as well as the correctly optimized software has always been a tedious task. However, for a sustainable system, it is also important to manage the energy used as well. Minimizing power used, hardware resources while still maintaining security is the future.

Improving performance through optimizing the existing algorithm is also a reasonable choice. Meneses et al. introduced a solution to decrease decryption time of the RSA model [25]. By optimizing the mathematical expressions and mixing the characters in the message, the maximum decryption time has been reduced from 369ms to 11ms.

5 Conclusion

In conclusion, edge AI proposes in recent years have certified the industry's promising future. Edge devices with their limited computational capability should provide the much needed support for the existing cloud-based architecture being used throughout the years. As such, security problems concerning these devices must also be carefully attended to. Some cryptography approaches have been proved to be useful for practical use. AES and ASCON are some of the prime examples to run smoothly on embedded computers and FPGAs. However, there are some remaining concerns about robustness and scalability for these solutions that are needed to be investigate further. This paper has reviewed many solutions and discuss the problems in a coherent and structured way. Multiple metrics have been compared between the researches such as throughput, energy consumption, and latency.

Acknowledgment. This research is funded by Vietnam National University Ho Chi Minh City (VNU-HCM) under grant number NCM2021-20-02.

References

1. Kaba, A., Ramaiah, C.K.: Bibliometric analysis of research output on the internet of things in the arab world. DESIDOC Journal of Library & Information Technology 39(5) (2019)
2. Alam, T.: A reliable communication framework and its use in internet of things (iot). Authorea Preprints (2023)
3. Serpanos, D.N., Voyiatzis, A.G.: Security challenges in embedded systems. ACM Transactions on embedded computing systems (TECS) 12(1s), 1–10 (2013)
4. Ukil, A., Sen, J., Koilakonda, S.: Embedded security for internet of things. In: 2011 2nd National Conference on Emerging Trends and Applications in Computer Science. pp. 1–6. IEEE (2011)
5. Xu, C., Jiang, S., Luo, G., Sun, G., An, N., Huang, G., Liu, X.: The case for fpga-based edge computing. IEEE Transactions on Mobile Computing 21(7), 2610–2619 (2020)
6. Banu, N.M., Sujatha, C.: Iot architecture a comparative study. Int J Pur Appl Math 117(8), 45–49 (2017)
7. Vale-Cardoso, A.S., Moreira, M.G., Martins, C.H., Leles, M.C.: Iot embedded computing systems performance assessment: a simple method. In: 2019 IEEE 10th Annual Information Technology, Electronics and Mobile Communication Conference (IEMCON). pp. 0071–0075. IEEE (2019)
8. Garcia-Perez, A., Miñón, R., Torre-Bastida, A.I., Zulueta-Guerrero, E.: Analysing edge computing devices for the deployment of embedded ai. Sensors 23(23), 9495 (2023)
9. Pham-Quoc, C., Vung, D.M., Tri, N.C.: Fpga-based lightweight ascon encryption for edge-ai: A systematic review. In: International Conference on Intelligence of Things. pp. 97–106. Springer (2024)
10. viso.ai: Edge ai – driving next-gen ai applications in 2024, https://viso.ai/edge-ai/edge-ai-applications-and-trends/
11. Jones, S.S., Groom, F.M.: Artificial intelligence and machine learning for business for non-engineers. CRC Press (2019)
12. Sachdev, R.: Towards security and privacy for edge ai in iot/ioe based digital marketing environments. In: 2020 fifth international conference on fog and mobile edge computing (FMEC). pp. 341–346. IEEE (2020)
13. Hubaux, J.P.: The security of vehicular networks. In: Proceedings of the 4th ACM workshop on Wireless security. pp. 31–32 (2005)
14. Wadday, G., Wadi, S., Mohammed, H., Abdullah, A.: Study of wimax based communication channel effects on the ciphered image using maes algorithm. International Journal of Applied Engineering Research 13(8), 6009–6018 (2018)
15. NIST: Lightweight cryptography standardization process: Nist selects ascon, https://csrc.nist.gov/news/2023/lightweight-cryptography-nist-selects-ascon
16. Sönmez Turan, M., McKay, K., Chang, D., Kang, J., Kelsey, J.: Ascon-based lightweight cryptography standards for constrained devices: Authenticated encryption, hash, and extendable output functions. Tech. rep., National Institute of Standards and Technology (2024)
17. Cagua, G., Gauthier-Umaña, V., Lozano-Garzon, C.: Implementation and performance of lightweight authentication encryption ascon on iot devices. IEEE Access (2025)
18. Almalawi, A., Hassan, S., Fahad, A., Khan, A.I.: A hybrid cryptographic mechanism for secure data transmission in edge ai networks. International Journal of Computational Intelligence Systems 17(1), 24 (2024)

19. Chen, X., Li, B., Zhou, Q.: Lightweight and high-performance data protection for edge network security. Wireless Communications and Mobile Computing 2022(1), 8458314 (2022)
20. Kaur, J., Kermani, M.M., Azarderakhsh, R.: Hardware constructions for error detection in lightweight authenticated cipher ascon benchmarked on fpga. IEEE Transactions on Circuits and Systems II: Express Briefs 69(4), 2276–2280 (2021)
21. Xu, D., Wang, X., Hao, Q., Wang, J., Cui, S., Liu, B.: A high-performance transparent memory data encryption and authentication scheme based on ascon cipher. IEEE Transactions on Very Large Scale Integration (VLSI) Systems (2024)
22. Elsadek, I., Tawfik, E.Y.: Efficient programable architecture for lwc nist fips standard ascon. In: 2024 12th International Symposium on Digital Forensics and Security (ISDFS). pp. 1–5. IEEE (2024)
23. Raj, K., Bodapati, S.: Fpga based light weight encryption of medical data for iomt devices using ascon cipher. In: 2022 IEEE International Symposium on Smart Electronic Systems (iSES). pp. 196–201. IEEE (2022)
24. Jaidka, H., Sharma, N., Singh, R.: Evolution of iot to iiot: Applications & challenges. In: Proceedings of the international conference on innovative computing & communications (ICICC) (2020)
25. Meneses, F., Fuertes, W., Sancho, J., Salvador, S., Flores, D., Aules, H., Castro, F., Torres, J., Miranda, A., Nuela, D.: Rsa encryption algorithm optimization to improve performance and security level of network messages. IJCSNS 16(8), 55 (2016)

FPGA-based approximate multipliers for EdgeAI: a Systematic Review

Nguyen Thanh Loc[1,2], Nguyen Thien An[1,2], and Cuong Pham-Quoc[1,2⋆]

[1] Ho Chi Minh City University of Technology (HCMUT)
[2] Vietnam National University - Ho Chi Minh City (VNU-HCM)
{loknguyen,ngthienan.cse,cuongpham}@hcmut.edu.vn

Abstract. Artificial intelligence is an essential demand in several domains, including cryptographic security systems, video attendance, object recognition and tracking systems, etc. Multiplication is the operation that takes up a lot of execution time when processing an AI model, so it is crucial to optimize the model to calculate quickly in order to reduce power consumption while maintaining appropriate performance when deploying AI models on edge devices with limited computing resources and power sources. Due to the promising efficiency of the approximate multiplier circuit, there are several research on novel approximate multiplication models that have been proposed and implemented on edge devices in general and FPGA-based Edge devices in particular. In this study, the approximation multiplier approaches for FPGA systems is systematically evaluated. We compare the energy usage, latency, and area of different methods and also present future research directions for applying approximate multiplier techniques for Edge AI.

Keywords: Field-programmable gate array (FPGA), Approximation multipliers, Artificial intelligence, Edge Artificial intelligence (Edge AI)

1 Introduction

High performance computing is becoming increasingly important and is closely related to many tasks related to processing a large amount of big data such as digital signal processing, image processing, multimedia and communication systems, or machine learning systems. In addition, one of the main issues that need to be concerned today besides optimizing speed performance is optimizing resources such as energy consumption. Numerous methods have been proposed to address these demands, with the goal of maximizing processing speed, area resources, and energy consumption while maintaining the application's requisite performance. One such new technique is approximate computing [6] and [7], which, by imposing penalties on the correctness of the system, allows explicit control over the energy and hardware resource usage for the intended application. Approximate computing is based on the idea that acceptable system

⋆ Corresponding author: Cuong Pham-Quoc

performance does not necessarily need application systems to provide the most accurate results [4].

One of the fields where this approximate multiplication technique can be applied and with promising results is artificial intelligence applications. The final calculation result of an artificial intelligence neural network after going through a calculation process that involves many linear calculations will eventually be limited to a specific range and have a certain error limit. Furthermore, because all of these values are dependent on probability, the final calculation results will vary as long as the value rankings of the categories do not undergo major changes. Therefore, approximate computing can be used in neural network computation for better performance and energy efficiency. In the literature, many approximate arithmetic units are designed specific for neural network computation [2], [1], [3].

Furthermore, to deal with the problem of power consumption and computing resource restrictions, the system needs a low-complexity setup and quick calculation. Therefore, a viable way to decrease the computation time, energy consumption, and complexity of AI models when deployed to edge devices without appreciably lowering the model's accuracy is to use approximation computing to Edge AI platform-based applications.

Meanwhile, Field Programmable Gate Array (FPGA) technology is well known for improving the efficiency of computationally demanding activities in a variety of application fields, including AI-powered applications. The flexible nature of the field-programmable gate array (FPGA) platform makes it a popular choice for accelerating neural network computing. On the one hand, modern FPGA devices have a sufficient logic density to offer acceptable performance for neural network computing. However, the architecture is easily adaptable to new neural network models since FPGA is programmable.

The main contributions of this systematic review are threefold. First of all, we conduct a systematic review of FPGA-based approximate multiplier techniques from recent papers published in international journals. In addition, we compare the results of these papers with each other based on the criteria: latency, resources usage, energy consumption and give some observations about these results. Finally, we present some open issues for FPGA-based AI powered application using approximate multiplier technique.

The rest of the paper is organized as follows. Section 2 discuss the background of approximate multiplier algorithms. Section 3 presents the survey of approximate multiplier implementation for FPGA-based in the literature. We summarize open issues of applying approximate multiplier technique in AI application in Sect. 4. Finally, we conclude our paper in Sect. 5.

2 Preliminaries

2.1 Multiplication algorithm

In digital electronics, multiplication is one of the most fundamental and significant processes due to its complexity and range of applications. There are

several ways to implement multiplication in hardware, but the majority of them include calculating partial products and utilizing addition to add them together. Developed by Anatoly Karatsuba in 1960 and published in 1962, the Karatsuba algorithm is one of the quick and popular techniques in the articles covered here. [8], [9], [5].

When applying this algorithm for binary numbers, for two operands A and B of $2n$-bit, we decompose them into two separate parts, the higher order parts A_H and B_H, and the lower order parts A_L and B_L:

$$A = A_H \times 2^n + A_L$$
$$B = B_H \times 2^n + B_L$$

Therefore, the multiplication of these operands can be presented as:

$$A \times B = A_H B_H \times 2^n + (A_H B_L + A_L B_H) \times 2^n + A_L B_L$$

Then, the middle term $A_H B_L + A_L B_H$ can be continually modified as

$$A_H B_L + A_L B_H = A_H B_H + A_L B_L - (A_H - A_L)(B_H - B_L)$$

Finally, the final products can be generated by adding these terms together by orders as Figure 1.

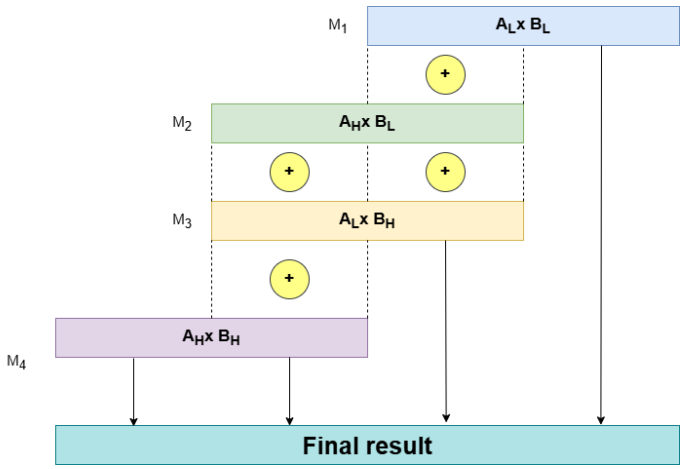

Fig. 1. Final products of Katsubara Algorithm for Binary Multiplication

This approach allows us to optimize space and latency without significantly altering the computational results by approximating partial products in lower order or middle sections when used to approximation kernel algorithms.

2.2 Baugh Wooley Algorithm

Baugh and Wooley is the calculation that shows multiplication for two's supplement bits. The sign bits of every multiplicand and the multiplier's unsigned or positive sign are where this multiplier converges. This computation is entirely prepared using the standard reasoning full adders. Figure 2 illustrates a 8-bit Baugh-Wooley multiplication algorithm.

$$
\begin{array}{r}
y_7\ y_6\ \ y_5\ y_4\ \ y_3\ y_2\ y_1\ y_0 \\
x_7\ x_6\ \ x_5\ x_4\ \ x_3\ x_2\ \ x_1\ x_0 \\
\hline
1\ \overline{p_{70}}\, p_{60}\, p_{50}\, p_{40}\, p_{30}\, p_{20}\, p_{10}\, p_{00} \\
\overline{p_{71}}\, p_{61}\, p_{51}\, p_{41}\, p_{31}\, p_{21}\, p_{11}\, p_{01} \\
\overline{p_{72}}\, p_{62}\, p_{52}\, p_{42}\, p_{32}\, p_{22}\, p_{12}\, p_{02} \\
\overline{p_{73}}\, p_{63}\, p_{53}\, p_{43}\, p_{33}\, p_{23}\, p_{13}\, p_{03} \\
\overline{p_{74}}\, p_{64}\, p_{54}\, p_{44}\, p_{34}\, p_{24}\, p_{14}\, p_{04} \\
\overline{p_{75}}\, p_{65}\, p_{55}\, p_{45}\, p_{35}\, p_{25}\, p_{15}\, p_{05} \\
\overline{p_{76}}\, p_{66}\, p_{56}\, p_{46}\, p_{36}\, p_{26}\, p_{16}\, p_{06} \\
p_{77}\, \overline{p_{67}}\, \overline{p_{57}}\, \overline{p_{47}}\, \overline{p_{37}}\, \overline{p_{27}}\, \overline{p_{17}}\, \overline{p_{07}} \\
\hline
\overline{s_{15}}\ s_{14}\ s_{13}\ s_{12}\ s_{11}\ s_{10}\ s_9\ s_8\ \ s_7\ \ s_6\ \ s_5\ \ s_4\ \ s_3\ \ s_2\ \ s_1\ \ s_0
\end{array}
$$

Fig. 2. Illustration of an 8-bit Baugh-Wooley multiplication in [11]

The distinctive aspect of executing the Baugh Wooley algorithm on FPGA is the capability to utilize LUT 5, LUT 5-2, or LUT 6, LUT 6-2, which are prevalent and accessible on most contemporary FPGA platforms, to construct the three primary blocks M, L, and J, Figure 3, for the algorithm. This approach is ideal in both area and latency compared to simpler algorithms like array multiplication or the shift method.

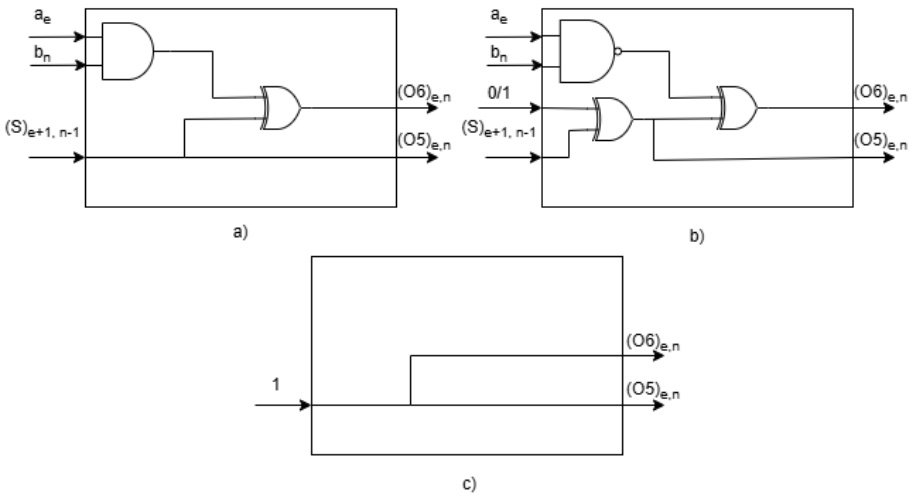

Fig. 3. LUT configuration for BW circuit with (a) L (b) M and (c) J in [10]

2.3 Radix Booth Algorithm

Among the effective methods for implementing multiplication on computer hardware are Radix Booth-4 and Booth-8. By edcoding the multiplier, this approach essentially applies and improves upon Booth's algorithm by reducing the amount of addition and subtraction operations needed for multiplication.

How this approach encodes the multiplier while performing multiplication is seen in the two tables 1 and 2 below. The length of the multiplier bits that Radix Booth-4 and Booth-8 encode is clearly different; in Booth-4, it is three, but in Booth-8, it is four. Radix Booth-8 will therefore generate fewer partial products, leading to speedier calculations, particularly for big numbers. Additionally, compared to Radix Booth-4, it will reduce addition and subtraction operations, which is crucial when optimizing multiplication on digital circuits.

Table 1. Radix - 4 Booth Recoding.

Multiplier Bits	Recoded Operation on multiplicand, X
000	0X
001	+X
010	+X
011	+2X
100	-2X
101	-X
110	-X
111	0X

Table 2. Radix - 4 Booth Recoding.

Multiplier Bits	Recoded Operation on multiplicand, X
0000	0X
0001	+X
0010	+X
0011	+2X
0100	+2X
0101	+3X
0110	+3X
0111	+4X
1000	-4X
1001	-3X
1010	-3X
1011	-2X
1100	-2X
1101	-X
1110	-X
1111	0X

3 FPGA-Based Approximately Multiplication Techniques

In this section, we survey the proposals and implementations for Approximate Multiplier implemented FPGA-Based platforms in the literature. We then compare the proposals in terms of resource usage, latency and power consumption.

3.1 FPGA-Based Approximate Multiplier Implementations

Two primary types of approaches to approximate multiplicative circuits are as follows: to multiply two binary values for FPGA, the first technique is to truncate the group of bits or partial products during multiplication using well-known algorithms like the Radix Booth, and Baugh Wooley algorithms. The other technique truncates elements that are superfluous or that use excessive amounts of resources without significantly altering the outcome by breaking down the general multiplication formula of two binary numbers into smaller components.

Radix Booth and Baugh Wooley algorithms are employed in a logic cloning approach that is based on the probability of each bit when multiplying two binary numbers in [10]. The logical value 1's presence in partial product values between two bits of two components combined is analyzed and statistically reported by the author in this article. In order to merge them together, they then choose successive partial products on the row that have the same probability value. By doing this, a significant amount of resources (the number of LUTs for each algorithm) are reduced, and hardware processing and computing performance are increased. However, because each algorithm will have a distinct

means of truncating and grouping truncated bits, the inaccuracy in this method is significant and very hard to manage. Figure 4 and Figure 5 present the Booth and Baugh Wooley architectures.

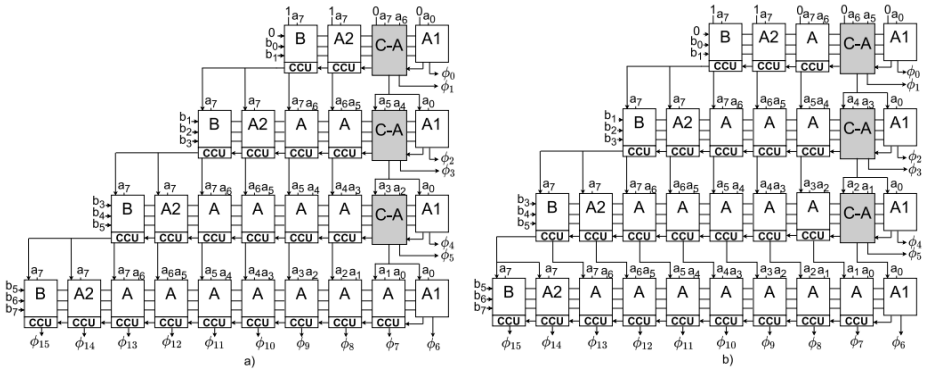

Fig. 4. LC-Booth circuits for 8-bit operands (a) LC-Booth-1 (b) LC-Booth-2 in [10]

Muhammadwais et al [15] used the same method as Salim Ullah et al [14] for handling an element's bottom bits in multiplication. Depending on each unique situation, the author has modified and altered these sections. Not only does this result in a significant decrease in the quantity of LUTs and energy resources, but it also boosts computational processing speed and accuracy in comparison to Salim Ullah et al [14].

Three distinct techniques are provided by Salim Ullah et al [12] for truncating successive partial products. In order to produce sum vectors, the first and most straightforward way is to add two successive partial product rows. The final result is then created by using the 6-input LUT-based approximation addition. The architecture used in Methods 2 and 3 is the same: truncate the respective partial products together. The 6-input LUTs design in the approximate computation is where the two approaches mentioned above diverge. Based on the three above-mentioned suggested solutions, the author additionally provides a recursive method design for higher order multipliers. Although the number of LUTs employed is significantly increased, the findings of this article are rather satisfactory in terms of latency and approximation accuracy. Figure 6 presents the general idea of the second and the third approaches in the [12] being applied approximate technique in the green part.

The difference in structure of these two methods is shown in Figure 7

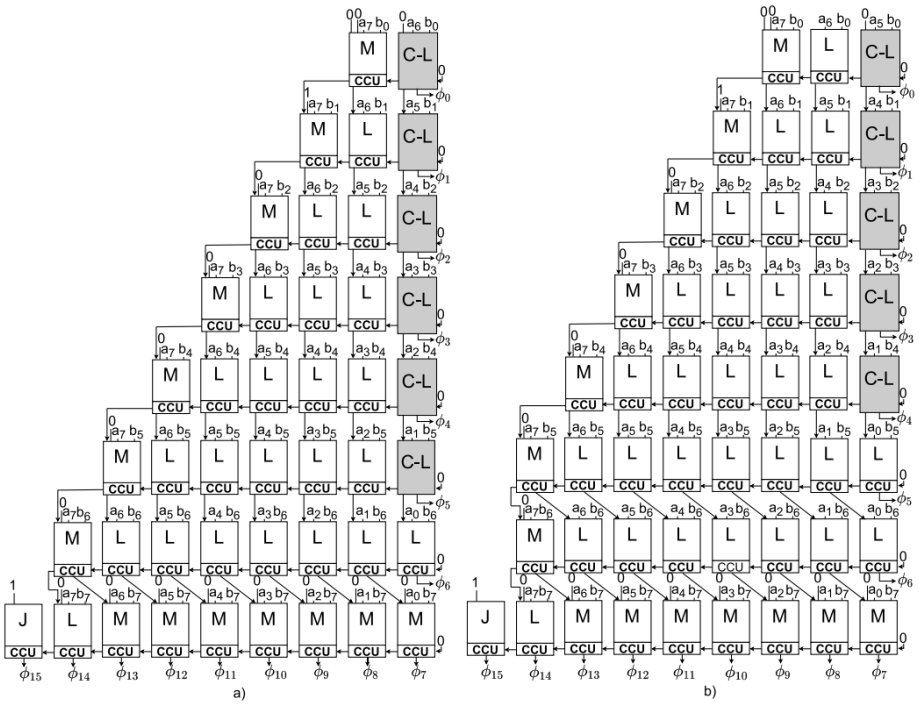

Fig. 5. LC-BW circuits for 8-bit operands (a) LC-BW-1 and (b) LC-BW-2 in [10]

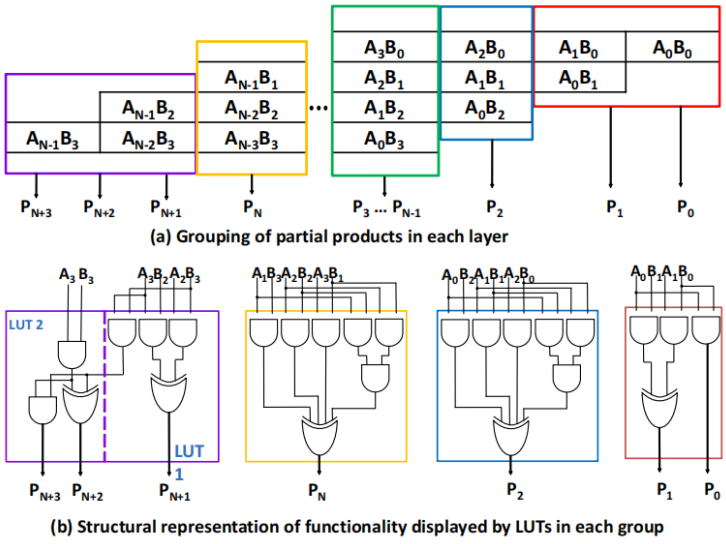

Fig. 6. Partial products generation for Approx2 and Approx3 in [12]

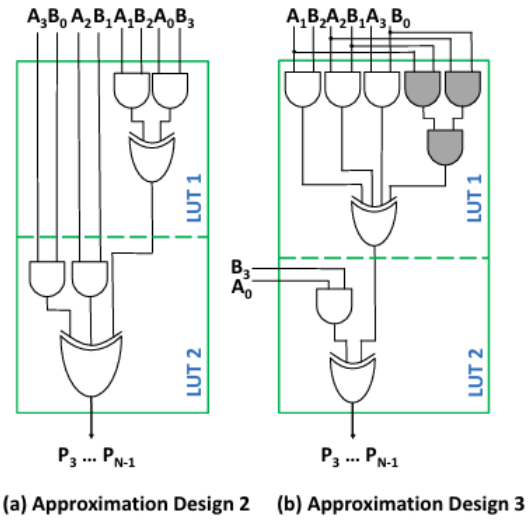

Fig. 7. Structural difference between Approx2 and Approx3 in [12]

Salim Ullah et al [13] created the result vectors by grouping three successive partial products in the Baugh Wooley method together by utilizing the 6-input lookup table. To get the final result, these result vectors are once more grouped three by one. The article has remarkable performance in terms of reduced latency and resource conservation.

Figure 8 highlights the method of grouping Partial Products in order to generate the Final Product, a key technique used in [13]

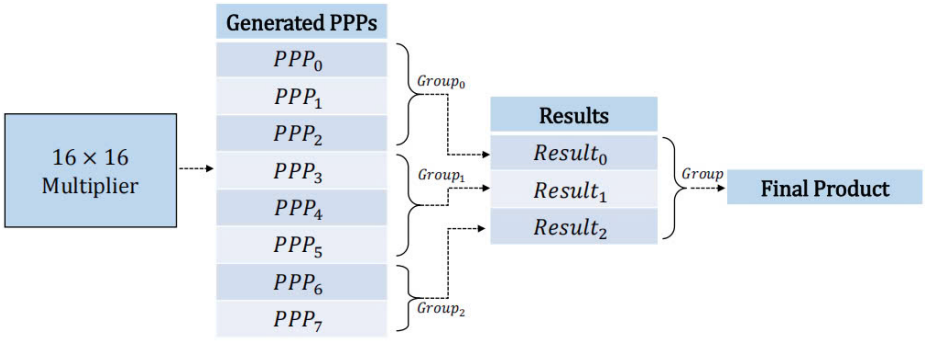

Fig. 8. Grouping of PPPs to compute final product in[13]

The general formula for multiplying two binary numbers into smaller components was examined by Hao Zhang [16], and they applied approximations to the sections that had little bearing on the multiplication outcome. This article's primary objective is to apply the approximation approach to low bits in order to dramatically reduce computation accuracy while boosting calculation speed and decreasing resource use. Figures 9 and 10 show the Datapath Design and the Approximate multiplier algorithms applied of two methods in [16], respectively.

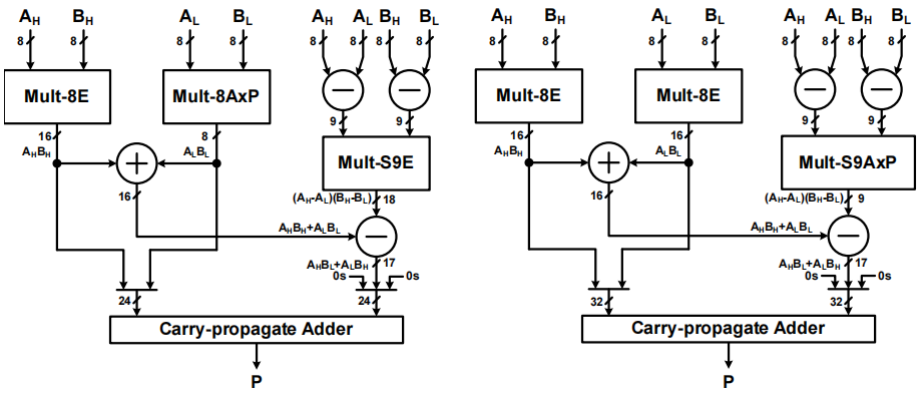

Fig. 9. Datapath of the first and the second approaches in [16]

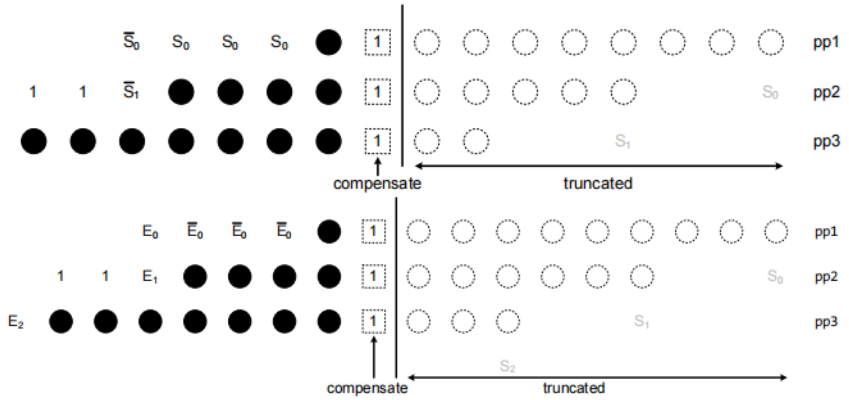

Fig. 10. Approximate design of the first and the second approaches in [16]

3.2 Comparison

Table 3 compares the proposals for 8-bits multiplier analyzed above in terms of FPGA families, area (LUTs), Critical Path Delay in ns (CPD), Power-Delay Product in (PDP), latency and Power (W). Table 4 summarizes the pros and cons of the proposed approximate multipliers in the literature.

Table 3. Results comparison of different 8-bits Approximate multiplier implementations in the literature.

Proposal	Area	CPD	PDP	Latency	Power
[10]**LC-BW-1**	50	5.20	5.20	—	—
[10]**LC-BW-2**	55	5.39	5.39	—	—
[10]**LC-Booth-1**	27	4.04	3.43	—	—
[10]**LC-Booth-2**	34	3.93	3.34	—	—
[15]	32	2.54	1.66	—	—
[14]	92	4.99	7.10	—	—
[12]**Approx 1**	64	9.222	—	9.222	0.22
[12]**Approx 2**	54	9.038	—	9.038	0.217
[12]**Approx 3**	54	9.081	—	9.081	0.216
[13]	54	4.37	7.26	2.388	—
[16]**Approx 1**	287	—	65.1	3.1	0.021
[16]**Approx 2**	297	—	66.7	2.9	0.023

Table 4. Pros and Cons of the proposed approximate multipliers in the literature

Ref.	**Pros**	**Cons**
[10]	Improved performance in terms of speed and LUTs resource usage	Accuracy is reduced due to the effect on the results of all bits in the final products
[15]	Significant improvement in resource utilization: number of LUTs, low latency and low power consumption	Difference between the exact products and the approximate products are high
[14]	Accuracy is not reduced significantly	Limited resource optimization: number of LUTs, latency and power consumption
[12]	High precision, low power consumption, greatly reducing the amount of LUTs used	Latency is still too high, architecture is not optimized, still too complex for popular LUTs: LUT5 and LUT6
[13]	Optimized number of LUTs used and low latency	The accuracy of the final calculation result is significantly affected
[16]	Optimized for speed and energy usage, accuracy is not significantly affected	The number of LUTs is still large and the complexity of the algorithm is still high

3.3 Discussion

The impact of approximation multiplication approaches on latency, complexity, and power consumption will be covered in this section. First of all, it is evident that the majority of the aforementioned strategies will produce an approximation multiplication technique by minimizing or optimizing the critical route from the original precise multiplication algorithm. When compared to the original exact multiplication technique, this results in a considerable reduction in the amount of adds and subtractions made throughout the calculation process, which speeds up the computation and lowers latency. Furthermore, because the more simple the circuit design, the lower the power consumption, this decrease results in optimization of both design space and power consumption. The complexity will be lower than with the original design since some techniques optimize effectively between the suggested algorithm and the FPGA's accessible resources, which are LUT5 and LUT6. Some techniques, like [12], the authors did not be optimized with LUT5 and LUT6 resources because the approximate calculation portion includes eight inputs, but LUT5 and LUT6 can only be used with a design that has a maximum of five or six inputs. Lastly, with regard to accuracy, the aforementioned articles all decide to test and compare in various apps and media, so when compared to one another, they are unable to provide a comprehensive and most true picture of this element. But generally speaking, the findings show high accuracy when compared to designs that use approximate calculation circuits or from the original designs.

4 FPGA-Based Approximately Multiplication: Open Issues of AI powered Application

Despite the abundance of studies in the literature on novel methodologies for FPGA-based approximation multipliers, some unsolved challenges remain for future study about their applicability in AI-powered applications. We highlight six outstanding challenges that must be addressed to enhance the performance of FPGA-based AI applications.

1. **Performance and Resource Constraints:** FPGAs and other edge devices are subject to stringent power limits and have restricted computing resource. Moderate power consumption and the absence of noticeable performance deterioration are prerequisites for applying AI models to these devices. It is necessary to optimize AI models for low-resource devices while preserving stability and accuracy within a permissible range.
2. **Design Complexity and Expertise:** Creating AI solutions for FPGAs necessitates a thorough understanding of artificial intelligence, mathematics, and hardware design. Complex design and verification procedures are required to create accurate and efficient FPGA designs. The development cycle is prolonged and complexity is increased by the steep learning curve and scarcity of experienced designers in FPGA development.

3. **Adaptability and Flexibility:** The dynamic nature of edge-AI settings may necessitate regular security measure upgrades to handle emerging threats or modifications to the operating environment. The flexibility of FPGA-based systems must enable real-time upgrades and reconfigurations. It must be possible to accomplish this flexibility without jeopardizing system security or necessitating prolonged downtime.
4. **Scalability and Integration:**To safeguard a wide variety of edge devices, approximate multiplier AI-powered solutions need to be scalable. For widespread use, interoperability with different FPGA designs, operating systems, and communication protocols is crucial. Managing varying computing capacities and resource limitations across devices is another aspect of this scalability.
5. **Robustness and Reliability of AI Models:**In AI-powered applications like object classification or object detection, AI models used as approximation multipliers need to be dependable and strong. They must be able to function well in real-world scenarios, including managing noisy data and changing threat environments, and resist hostile attacks. It is especially difficult to guarantee the dependability of these models in settings with limited resources.
6. **Resource-Efficient Implementation:** For edge devices, it is crucial to implement AI solutions in a resource-efficient way. This entails preserving strong security while reducing the use of memory, processing power, and energy. It takes creative design strategies and optimization tactics to balance these limitations.

5 Conclusion

As integrated circuits grow in size and complexity, approximation multipliers must be developed for probabilistic applications or for processes that do not require high accuracy. as artificial intelligence has grown.To meet these urgent needs, a variety of approaches have been proposed, all aiming to maximize processing speed, area resources, and energy consumption while preserving the necessary performance of the application. One such novel method is approximation computing, which permits explicit control over the energy and hardware resource utilization for the intended application by enforcing penalties on the system's accuracy. The foundation of approximate computing is the notion that application systems are not always necessary to provide the most precise results and still maintain acceptable system performance. The area, latency, and energy consumption of approximation multiplier implementations based on FPGA are systematically reviewed in this paper. Lastly, using this method, we point out outstanding difficulties for FPGA-based AI-powered applications.

Acknowledgement. This research is funded by Vietnam National University Ho Chi Minh City (VNU-HCM) under grant number NCM2021-20-02.

References

1. Ahmadinejad, M., Moaiyeri, M.H.: Energy- and quality-efficient approximate multipliers for neural network and image processing applications pp. 1–1 (2021)
2. Ansari, M.S., Cockburn, B.F., Han, J.: An improved logarithmic multiplier for energy-efficient neural computing. IEEE Transactions on Computers **70**(4), 614–625 (2021)
3. Ansari, M.S., Mrazek, V., Cockburn, B.F., L. Sekanina, Z.V., Han, J.: Improving the accuracy and hardware efficiency of neural networks using approximate multipliers **28**(2), 317–328 (2020)
4. Chippa, V., Chakradhar, S., K. Roy, A.R.: Analysis and characterization of inherent application resilience for approximate computing pp. 1–9 (2013)
5. D.E, K.: The art of computer programming v.2 pp. 724–724 (1969)
6. Han, J., Orshansky, M.: Approximate computing: an emerging paradigm for energy-efficient design pp. 1–6 (2013)
7. Jiang, H., Santiago, F., Mo, H., Liu, L., Han, J.: Approximate arithmetic circuits: A survey, characterization, and recent applications **12**, 2108–2135 (2020)
8. Karatsuba, A., Ofman, Y.: Multiplication of many-digital numbers by automatic computers pp. 595–596 (1963)
9. Karatsuba, A.A.: The complexity of computations pp. 186–202 (1995)
10. Kulkarni, A., Ouameur, M.A., Massicotte, D.: Logic cloning basedapproximate-signedmultiplicationcircuits for fpga (2024)
11. Magnus Själander, P.L.E.: High-speed and low-power multipliers using the baugh-wooley algorithm and hpm reduction tree (2008)
12. Ullah, S., Murthy, S.S., Kumar, A.: Smapproxlib: Library of fpga-based approximate multipliers (2018)
13. Ullah, S., Rehman, S., Shafique, M., Kumar, A.: High-performance accurate and approximate multipliers for fpga-based hardware accelerators (2021)
14. Ullah, S., Schmidl, H., Sahoo, S.S., Rehman, S., Kumar, A.: Area-optimized accurate and approximate softcore signed multiplier architectures (2021)
15. ZAHIR, M.A., SHAH, S.A.A.: Toward optimal softcore carry-aware approximate multipliers on xilinx fpgas (2023)
16. Zhang, H., Xiao, H., Qu, H., Ko, S.B.: Fpga-based approximate multiplier for efficient neural computation (2021)

Comparison of ChatGPT and DeepSeek based on Regional Language Understanding

* Muhammad Anwar Ahmad [1] and Ajune Wanis Ismail [2]
[1]Vicubelab, Faculty of Computing, Universiti Teknologi Malaysia
[1*] muhammad.anwar@utm.my
[2]Vicubelab, Faculty of Computing, Universiti Teknologi Malaysia
[2]ajune@utm.my

* Corresponding Author

Abstract. This study presents a comparative analysis of ChatGPT and DeepSeek in understanding a regional language, namely the Malay language. Large Language Models (LLMs) have significantly advanced natural language processing, yet their effectiveness in non-English languages remains an area of exploration. This study compares both LLMs using a case study based on Malay language examination questions dataset, assessing their performance in objective and subjective question categories. The results indicate that ChatGPT slightly outperforms DeepSeek, achieving higher accuracy in both categories, particularly excelling in subjective responses. DeepSeek demonstrated weaknesses in grammar and poetic language comprehension, and its reasoning function encountered technical issues. The findings highlight the importance of language-specific fine-tuning and dataset expansion to enhance multilingual proficiency. Furthermore, DeepSeek's open-source nature presents an opportunity for community-driven improvements in underrepresented languages like Malay. The study emphasizes the need for continued research to refine LLMs for better linguistic and cultural understanding.

Keywords: Large language models, natural language processing, malay language understanding.

1 Introduction

Large language models (LLMs) has revolutionized the field of natural language processing (NLP), exhibiting outstanding proficiency in language understanding and generation. These models, trained on enormous datasets, have the ability to generate new but coherent and contextually relevant text across diverse domains [1]. In the past few years, language models have gained significant prominence, transformed human-computer interaction and provided diversified applications in multiple do-mains. Among the recent developments in this direction, two well-

known language models are ChatGPT and DeepSeek.

The quick advancement of these models has invoked much attention and investigation within the natural language processing community. However, the issue of understanding different languages can still be explored. Although LLMs have demonstrated state-of-the-art competence in most NLP tasks, their understanding is rooted in statistical regularities rather than actual understanding. This has been noted in studies that emphasize the necessity of earnest testing of the language understanding capability of LLMs, particularly in non-English settings [2]. While much research and applications have so far focused mainly on languages with large global usage such as English and Mandarin, more and more interest is being garnered in evaluating how well these models perform in less covered languages, including Malay.

Language understanding for LLMs is an important challenge to overcome in order to be applied in various everyday tasks. For instance, the potential of LLMs in language education is significant, as they can assist in machine translation and provide personalized learning experiences [3]. The potential for LLMs to facilitate language acquisition is promising, therefore it is essential to address the limitations in their understanding of the cultural and contextual nuances [4]. The effectiveness of LLMs is linked to their ability to understand the intricacies found within various languages and dialects, an element that still causes difficulties. Even as LLMs are becoming powerful tools for various natural language processing activities, their weaknesses in understanding linguistics could hinder their applicability in real life [5].

This article aims to compare the two popular LLMs ChatGPT and DeepSeek, specifically in terms of their understanding in the Malay language through a case study. By comparing the performance of both models in understanding and responding to Malay language exam questions, we aim to discuss their strengths and weaknesses, thus providing insights into their everyday application for Malay language users.

2 Literature Review

To ensure a systematic approach to our survey of literature as well as the comparison, we conducted database searches performed on the indexes such as Scopus and WoS [6]. We performed our search based on several research questions (RQ). In addition, we also use the following keywords during our literature search, “ChatGPT framework”, “DeepSeek framework”, “large language models understanding of Malay language”. These keywords help to ensure our search is focused towards our RQ. Table 1 shows the research questions related to this paper.

Table 1. ChatGPT vs DeepSeek Characteristics Comparison

Research Question (RQ)	Detail
RQ1	What are the frameworks for the ChatGPT and DeepSeek LLMs?
RQ2	What are the differences between ChatGPT and DeepSeek frameworks?
RQ3	How is the understanding of Malay language between ChatGPT and DeepSeek?

Based on Table 1, For RQ1 we focused on discovering the general frameworks for ChatGPT and DeepSeek LLMs. For RQ2 we focused on performing the framework comparison between the ChatGPT and DeepSeek. For RQ3 we aim to evaluate the two LLMs in their understanding of the Malay Language. We answer these RQs in the rest of this paper.

2.1 Large Language Models

Large language models utilize deep learning techniques to generate and process language. They are trained on massive text data, enabling them to learn patterns, structures, and contextual relationships of the language. In addition to processing via text input, NLPs can benefit tremendously from understanding text based on vision. For example, DeepSeek-VL is designed to process and provide contextual understanding from image prompts [7, 8]. This further enhances the capabilities of LLMs to be more comprehensive in their understanding of the real world.

LLM developers often employ the Large Lange Model Operations (LLMOps) process flow in optimizing the management of their LLMs before releasing to end users, shown in Fig. 1. LLMOps is a specialized subset of Machine Learning Operations (MLOps) that allows for addressing the unique characteristics of LLMs, such as their large size, complex training requirements, and high computational demands [9]. The parameters and computing power needed for training LLMs can be fine tuned to enable the models to adapt to specific tasks within the LLMOps process [10]. This enhances the adaptability of LLMs but also facilitates their deployment in resource-constrained environments.

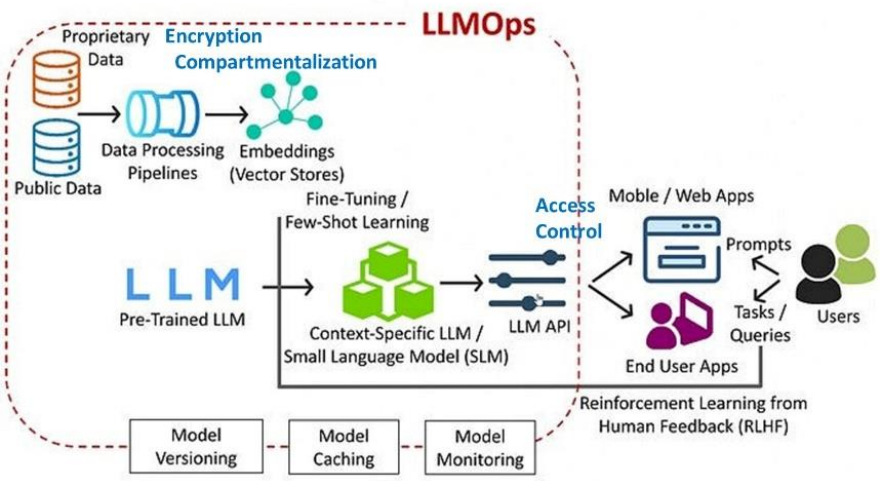

Fig. 1. LLMOps process flow [11]

Based on Fig. 1, LLMOPs have several important aspects as follows:

- **Data collection and preparation:** Large amounts of data are needed to train LLMs. Usually, the data is obtained through in-house data collection or by crawling on publicly available data. This data is then undergo data processing pipelines to prepare for the training.
- **Model development and versioning:** The LLMs are developed using a variety of techniques, including unsupervised learning, supervised learning, and reinforcement learning. Smaller and pre-trained LLMs may also be used to speed up the process of training the data.
- **Model caching:** Once an LLM has been developed, it is cached and deployed to a production environment which involves setting up the necessary infrastructure and configuring the model to run on a specific platform.
- **Model monitoring:** LLMs require ongoing monitoring to ensure that they are performing as expected. The monitoring usually include the model's an making sure that the model is secure. Feedbacks from end users are also taken into account to improve the model further.

The development and utilization of LLMs in a wide range of applications have proven their usefulness and power. The scalability prospects of these architectures are also integral to their performance overall. Scalability is crucial for applications that require high degrees of availability and responsiveness, such as customer support chatbots [12, 13]. However, LLM performance varies greatly in the context of languages and linguistic contexts, and specific research and testing are required to know about their possibilities and limits.

2.2 Malay Language Understanding in LLM

Malay, an Austronesian language [14] spoken by millions in Malaysia, Indonesia, Brunei, and Singapore, presents unique challenges to LLMs due to its complex morphology, dense dialects, and cultural nuances. These properties of the Malay language poses a difficulty for NLP systems that typically depend on the less complicated morphological structures found in languages such as English [15, 16]. Proper understanding of Malay requires models to grasp its syntactic structures, vocabulary, idiomatic expressions, and contextual nuances. The presence of regional variations and borrowings from languages such as Arabic, Sanskrit, and Dutch further complicates the task [16].

The ability of LLMs to generate contextually appropriate responses in Malay may be hindered by their training on predominantly English datasets, leading to outputs that lack cultural relevance or accuracy [17]. Previous studies have shown that language-specific training and fine-tuning enhance the performance of LLMs in non-European languages, including Malay [18, 19]. By incorporating Malay-specific corpora and linguistic characteristics into the training, researchers can make the models more proficient at processing and generating Malay text appropriately. There is, nevertheless, a remaining gap in the general evaluation of the performance of the chosen LLMs for this study in Malay language comprehension. As they are considered the most prominent LLMs in recent times, it is important for their multilingual understanding to be as in depth as possible.

3 ChatGPT vs DeepSeek Framework Comparison

ChatGPT is part of the Generative Pre-trained Transformer (GPT) family of LLMs developed by OpenAI, which utilizes a transformer architecture first introduced by Vaswani et al. (2017) [20]. The transformer model revolutionized NLP by enabling the handling of long-range dependencies in text through self-attention mechanisms. The evolution of the GPT series began with the original GPT model, followed by GPT-2, and subsequently GPT-3, each iteration demonstrating increased complexity and capability [21]. OpenAI released ChatGPT as a fine-tuned version of the GPT-3 model, specifically designed for conversational applications. The current ChatGPT employs the latest iteration of GPT which is the GPT 4o and the GPT o3-mini.

DeepSeek is another family of LLMs developed by the DeepSeek research group. DeepSeek R1, the latest iteration of the LLM, employs innovative self-reflection capabilities through reinforcement learning, which allows the ability to enhance structured problem-solving through advanced reasoning techniques [22]. DeepSeek has claimed that DeepSeek R1 was trained for approximately US$6 million, in contrast to the $100 million reportedly spent on OpenAI's GPT-4 in 2023 [23]. This positioned DeepSeek as a disruptive competitor to ChatGPT.

This section intends to discuss the comparison of ChatGPT and DeepSeek based on several characteristics. Table 2 shows a comparison of the characteristics between ChatGPT's and DeepSeek's framework.

Table 2. ChatGPT vs DeepSeek Characteristics Comparison

Characteristics	ChatGPT	DeepSeek
Architecture	Transformer-based	Mixture-of-Experts (MoE)-based
Accessibility	Closed-source	Open-source
Pricing	Free with paid options	Free with paid options
Code assistance	Yes	Yes
Reasoning feature	Yes	Yes

Based on Table 2, the main differences between the two models is that ChatGPT's architecture is transformer-based that allows it to predict the next word in a sequence based on the context provided by previous words, which is crucial for maintaining coherence in conversation and understanding complex queries [24], [25]. In contrast, DeepSeek is designed with a focus on information retrieval and semantic search capabilities. It leverages the Mixture-of-Expert (MoE) algorithms to understand user queries and retrieve relevant information from vast databases [22, 26]. This architecture activates specific subsets of its network for different tasks, enhancing efficiency. Another difference is that the DeepSeek research group has open-sourced their LLM and potential researchers are able to download and run the model on local hardware, whereas ChatGPT is closed sourced and only accessible through OpenAI's servers.

The similarities of both models include the pricing, code assistance and reasoning feature. Both models can be accessed to be used publicly on their respective websites for free with paid options for certain features. Code assistance is also offered by both models for assisting with software development. One of the prominent feature that was introduced by DeepSeek is the reasoning capability [22]. This feature makes the AI to briefly think to analyze and make inferences based on the prompt before generating the response. OpenAI has also introduced the reasoning feature on their ChatGPT since then [27]. Thus, both models are now offering reasoning capability.

The performance of both ChatGPT and DeepSeek can be observed from DeepSeek research groups' technical reports. The evaluation was reported in their studies for both DeepSeek V3 and DeepSeek R1 [22, 28]. Fig. 2 and Fig. 3 shows the evaluation of both models respectively.

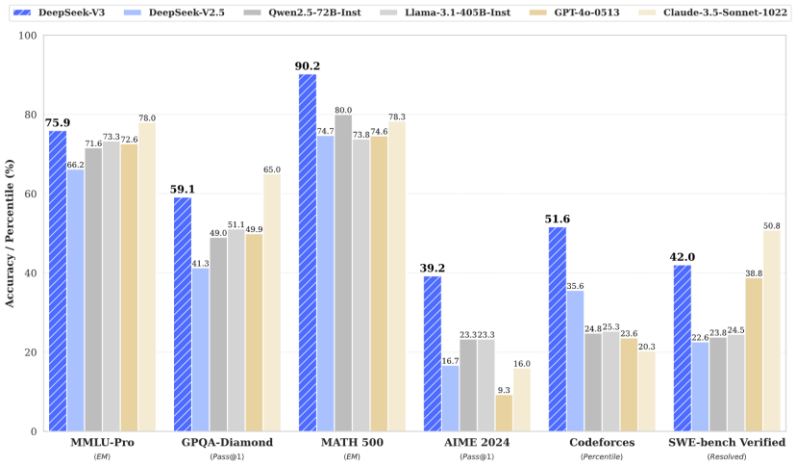

Fig. 2. DeepSeek V3 evaluation [28]

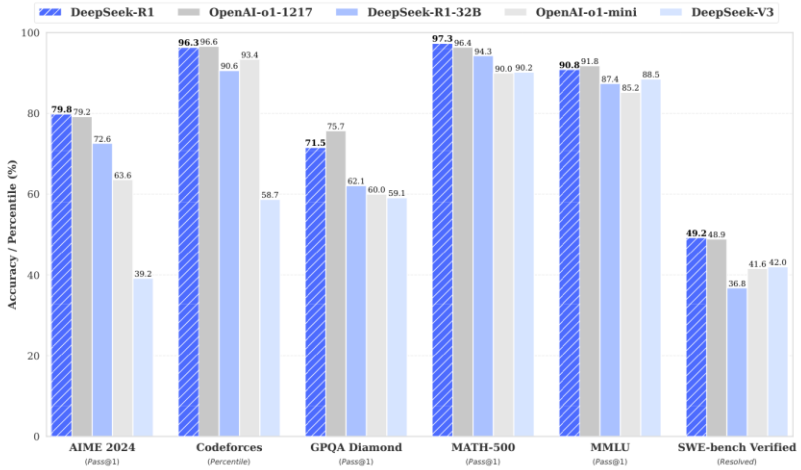

Fig. 3. DeepSeek R1 evaluation [22]

Based on Fig. 2, DeepSeek V3 was evaluated in tests against several other LLMs including DeepSeek V2.5, Qwen2.5-72B-Inst, Llama-3.1-405B-Inst, GPT-4o-0513, and Claude-3.5-Sonnet-1022. In many cases the DeepSeek V3 performed better than the other LLMs. In Fig. 3, DeepSeek R1 was evaluated against their OpenAI's LLMs, namely OpenAI-o1-1217 and OpenAI-o1-mini. They also included DeepSeek R1-32B which is a distilled version of DeepSeek R1 and their

older DeepSeek V3. The graph shows that DeepSeek R1 is on par with OpenAI-o1-1217 which is their main model. Based on the evaluation, DeepSeek has proven to be a challenging competitor to ChatGPT.

4 Case Study: Malay Language Examination Questions

In order to compare ChatGPT and DeepSeek performance in Malay language understanding, we conducted a pilot case study using Malay language exam questions. The questions are obtained from a public dataset that is based on local Malaysian examination from Mesolitica [29]. This dataset covered the Pentaksiran Tingkatan 3 (PT3) examination, which is the standard examination for 15 years old Malaysia student. The questions are about reading comprehension and general knowledge of Malay language. It is divided into Part A which are objective questions, and Part B, which are subjective questions. The subjective questions include filling in the blanks in a sentence with the appropriate term and answering questions based on Malay poetry. However, some of the questions in the dataset were based on novels, which required prior reading and familiarity with specific literary works. Since neither ChatGPT nor DeepSeek had access to the required novels, we omitted those questions from the evaluation to ensure fairness.

The questions in the dataset were fed to the respective LLMs and were evaluated based on their answers compared with the dataset's provided answer. For the testing we initially planned to include both reasoning and without reasoning. However, DeepSeek's reasoning could not parse the questions and returned server error, therefore we only include the results without reasoning. Due to this limitation, we proceeded with only the results from the non-reasoning test. Additionally, before inputting the questions into the models, we made minor modifications to the dataset to remove any answer keys or irrelevant metadata that could bias the results. The results of the evaluation are shown in Fig. 4.

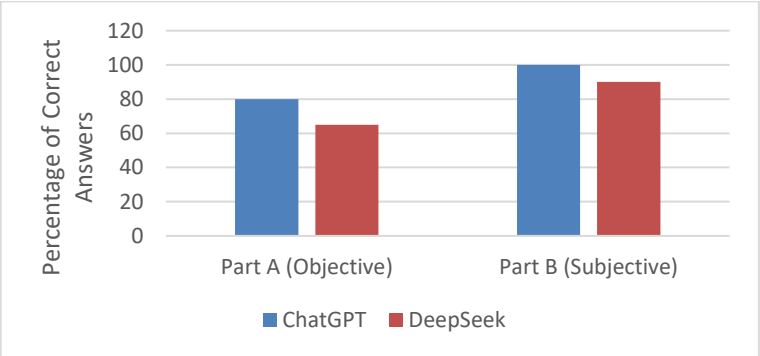

Fig. 4. Malay language examination comparison results

The evaluation results, presented in Fig. 4, provide insights into each model's understanding of Malay-language comprehension. Both ChatGPT and DeepSeek demonstrated a reasonable grasp of the language; however, ChatGPT outperformed DeepSeek in both objective and subjective questions. For the objective section (Part A), ChatGPT achieved an accuracy rate of 80%, while DeepSeek scored 65%. In the subjective section (Part B), ChatGPT achieved a perfect score of 100%, whereas DeepSeek attained 90%.

To better understand the areas where the models struggled, we further analyzed the incorrectly answered questions. In the objective section, ChatGPT encountered difficulties with questions involving specific Malay terms that required nuanced understanding, while DeepSeek faced similar challenges and additionally struggled with grammar-related questions. For the subjective section, DeepSeek's errors were primarily concentrated in questions related to Malay poetry, particularly in the interpretation of nuances that can be misleading. For example, in the dataset the term "terlalu kecewa" (too disappointed) was interpreted as "putus asa" (absolutely given up). This indicated potential limitations in its ability to interpret and analyze poetic language.

5 Discussions and Conclusion

The comparison between ChatGPT and DeepSeek in Malay language comprehension highlights distinct differences in their performance. This suggests that ChatGPT has a more refined understanding of Malay, particularly in generating subjective responses accurately. While both models showed similar comprehension abilities, ChatGPT had an advantage in handling grammar and vocabulary-related questions more effectively.

A closer analysis of errors reveals that ChatGPT struggled mainly with specific Malay terms, indicating potential limitations in domain-specific knowledge. In contrast, DeepSeek faced more difficulties, particularly in grammar-based questions and those related to Malay poetry. This suggests that DeepSeek's language processing abilities may require further enhancement, especially in understanding complex linguistic structures and literary content. Additionally, DeepSeek's reasoning function failed during testing, preventing a fair comparison in that mode and highlighting possible technical limitations in its ability to process structured reasoning tasks in Malay. For this reliability issue we suggest to perform more model validation tests.

The findings imply that ChatGPT is likely trained on a more extensive and higher quality Malay language dataset, making it better optimized for Malay comprehension tasks. DeepSeek, while promising, requires further improvements in grammar accuracy, literary analysis, and reasoning capabilities to match ChatGPT's performance. We suggest improving the training by using techniques such as data augmentation with more Malay language datasets or ensemble

methods. Future research could focus on expanding the dataset to include more diverse linguistic challenges, testing reasoning-based prompts. The performance and precision could also be improved through further optimization strategies such as hardware acceleration or prompt engineering.

It is also important to note that DeepSeek has open-sourced their LLM as opposed to ChatGPT. It opens the possibility of community-driven enhancements, particularly for languages like Malay that might not be as well-represented in proprietary models like ChatGPT. This transparency encourages creativity and may result in quick improvements in DeepSeek's capacity to process and comprehend Malay.

ChatGPT, on the other hand, is still a closed-source approach, so any advancements must come from OpenAI's in-house research and development. The open-source nature of DeepSeek could be particularly beneficial for underrepresented languages like Malay, as local researchers and organizations could adapt the model to better capture linguistic nuances, cultural context, and regional variations. Over time, with enough collaborative effort, DeepSeek's performance in Malay language tasks could potentially close the gap with or even surpass proprietary models like ChatGPT in specific use cases.

The comparison between ChatGPT and DeepSeek highlights the importance of language-specific training and fine-tuning in streamlining LLM performance. Future research needs to explore how to combine the strengths of these models, perhaps through hybrid approaches, to achieve even more language capacity and cultural understanding in LLMs. Further, the expansion of the evaluation framework to include other languages and a range of linguistic features can result in more generalizable and effective LLMs. Our future work is to improve further and include more datasets that comprise different academic levels of Malay language subject to obtain a more comprehensive and extensive study.

Acknowledgements. We would like to extend our heartfelt gratitude to the Ministry of Higher Education for the financial support under the Fundamental Research Grant Scheme (FRGS), UTM, FRGS/1/2023/ICT10/UTM/02/2. Thanks to ViCubeLab at Universiti Teknologi Malaysia for their invaluable support and facilities.

References

1. Gozalo-Brizuela, R., Garrido-Merchan, E.C.: ChatGPT is not all you need. A State of the Art Review of large Generative AI models. arXiv preprint arXiv:2301.04655. (2023).
2. Denning, J.M., Guo, X., Snefjella, B., Blank, I.: Do Large Language Models Know Who Did What to Whom? (2024). https://doi.org/10.31234/osf.io/z56wj.
3. Hamaniuk, V.A.: The Potential of Large Language Models in Language Education. Освітній Вимір. 5, 208–210 (2021). https://doi.org/10.31812/ed.650.

4. Ilgaz, H.B., Çelik, Z.: The Significance of Artificial Intelligence Platforms in Anatomy Education: An Experience With ChatGPT and Google Bard. Cureus. (2023). https://doi.org/10.7759/cureus.45301.
5. Hadi, M.U., tashi, qasem al, Qureshi, R., Shah, A., Muneer, A., Irfan, M., Zafar, A., Shaikh, M.B., Akhtar, N., Wu, J., Mirjalili, S.: A Survey on Large Language Models: Applications, Challenges, Limitations, and Practical Usage. (2023). https://doi.org/10.36227/techrxiv.23589741.v1.
6. Ahmad, M.A., Amiruddin, M.F., Ismail, A.W., Fadzli, F.E., Halim, N.A.A., Suaib, N.M.: Implementation of Real-Time Spatial Mapping for Occlusion-awareness in Augmented Reality. In: 2024 5th International Conference on Smart Electronics and Communication (ICOSEC). pp. 1651–1656 (2024). https://doi.org/10.1109/ICOSEC61587.2024.10722459.
7. Lu, H., Liu, W., Zhang, B., Wang, B., Dong, K., Liu, B., Sun, J., Ren, T., Li, Z., Yang, H.: Deepseek-vl: towards real-world vision-language understanding. arXiv preprint arXiv:2403.05525. (2024).
8. Hassan, A.: DeepSeek-AI Introduces DeepSeek-VL: An Open-Source Vision-Language (VL) Model Designed for Real-World Vision and Language Understanding Applications, https://www.marktechpost.com/2024/03/13/deepseek-ai-introduces-deepseek-vl-an-open-source-vision-language-vl-model-designed-for-real-world-vision-and-language-understanding-applications/, last accessed 2025/02/09.
9. Google LLC: What is LLMOps (large language model operations)?, https://cloud.google.com/discover/what-is-llmops?hl=en, last accessed 2025/02/09.
10. Li, X.L., Liang, P.: Prefix-Tuning: Optimizing Continuous Prompts for Generation. (2021). https://doi.org/10.18653/v1/2021.acl-long.353.
11. Palaniyappan, T.: Comparing LLM serving frameworks — LLMOps, https://medium.com/@plthiyagu/comparing-llm-serving-frameworks-llmops-f02505864754, last accessed 2025/02/09.
12. Haque, Md.A., Li, S.: Exploring ChatGPT and Its Impact on Society. Ai and Ethics. (2024). https://doi.org/10.1007/s43681-024-00435-4.
13. Rane, N.L.: Potential Role and Challenges of ChatGPT and Similar Generative Artificial Intelligence in Architectural Engineering. International Journal of Artificial Intelligence and Machine Learning. 4, 22–47 (2024). https://doi.org/10.51483/ijaiml.4.1.2024.22-47.
14. Clynes, A., Deterding, D.: Standard Malay (Brunei). J Int Phon Assoc. 41, 259–268 (2011). https://doi.org/10.1017/s002510031100017x.
15. Mohamed, M.M., Yap, M.J., Chee, Q.W., Jared, D.: Malay Lexicon Project 2: Morphology in Malay Word Recognition. Mem Cognit. 51, 647–665 (2022). https://doi.org/10.3758/s13421-022-01337-8.
16. Ahmad, N.D., Bahar, N., Nor Rashid, F. 'Atyka, Shahuddin, A.Z.: Morphological Analysis of Malay Translated Qur'an Corpus. Journal of Information System and Technology Management. 8, 178–198 (2023). https://doi.org/10.35631/jistm.833014.

17. Quelle, D., Bovet, A.: The Perils and Promises of Fact-Checking With Large Language Models. Front Artif Intell. 7, (2024). https://doi.org/10.3389/frai.2024.1341697.
18. Zolkepli, H., Razak, A., Adha, K., Nazhan, A.: MaLLaM--Malaysia Large Language Model. arXiv preprint arXiv:2401.14680. (2024).
19. Zolkepli, H., Razak, A., Adha, K., Nazhan, A.: Large Malaysian Language Model Based on Mistral for Enhanced Local Language Understanding. arXiv preprint arXiv:2401.13565. (2024).
20. Vaswani, A.: Attention is all you need. Adv Neural Inf Process Syst. (2017).
21. Winkler-Schwartz, A.: When Words Leap Off the Page: Conversational Manuscripts as a Novel Interface for Scientific Publishing. J Neurosurg. 139, 1482–1484 (2023). https://doi.org/10.3171/2023.7.jns231617.
22. Guo, D., Yang, D., Zhang, H., Song, J., Zhang, R., Xu, R., Zhu, Q., Ma, S., Wang, P., Bi, X.: Deepseek-r1: Incentivizing reasoning capability in llms via reinforcement learning. arXiv preprint arXiv:2501.12948. (2025).
23. Vincent, J.: The DeepSeek panic reveals an AI world ready to blow, https://www.theguardian.com/commentisfree/2025/jan/28/deepseek-r1-ai-world-chinese-chatbot-tech-world-western, last accessed 2025/02/09.
24. Demirkol, M., Malkoç, N.: Assessing the Intellectual Structure of the Evolving Knowledge Base on ChatGPT in the Field of Education and Health. Educational Process International Journal. 12, (2023). https://doi.org/10.22521/edupij.2023.124.3.
25. Radford, A.: Improving language understanding by generative pre-training. (2018).
26. Dai, D., Deng, C., Zhao, C., Xu, R.X., Gao, H., Chen, D., Li, J., Zeng, W., Yu, X., Wu, Y.: Deepseekmoe: Towards ultimate expert specialization in mixture-of-experts language models. arXiv preprint arXiv:2401.06066. (2024).
27. OpenAI: OpenAI o3-mini, https://openai.com/index/openai-o3-mini/, last accessed 2025/02/09.
28. Liu, A., Feng, B., Xue, B., Wang, B., Wu, B., Lu, C., Zhao, C., Deng, C., Zhang, C., Ruan, C.: Deepseek-v3 technical report. arXiv preprint arXiv:2412.19437. (2024).
29. Zolkepli, H.: BM-PT3, https://github.com/mesolitica/malaysian-dataset/tree/master/llm-benchmark/BM-pt3, last accessed 2025/02/06.

Implementation of XGBoost time series model for statistical analysis of renewable and traditional fuel energy with future perspective

*Suman Chowdhury[1], Dilip Kumar Das[2]
[1] Department of Electrical and Electronic Engineering,International University of Business Agriculture and Technology, Dhaka-1230, Bangladesh
[1*]suman@iubat.edu
[2]Department of Mathematics, International University of Business Agriculture and Technology, Dhaka-1230, Bangladesh
[2]dilipkdas@iubat.edu

* Corresponding Author

Abstract. This paper tries to investigate the statistical energy generation from renewable and traditional sources in Romania taking the data set from Kaggle. The application of the XGBoost model effectively demonstrated its strength in analyzing and forecasting power generation from both renewable and traditional fuel sources. The model provided accurate trend insights and future projections, making it a valuable tool for energy system planning and policy development. These findings highlight the potential of machine learning in advancing data-driven approaches to optimize energy resource management in the context of growing sustainability demands. From the analysis of RMSE profile for both of traditional and renewable energy, it is observed that the training rmse value reaches least of around 100 after 2000 iterations which is very reasonable for the performance of the machine learning model. This paper tries to present the future perspective of this two major energy sources for the upcoming 2 years in Romania.

Keywords: XGBoost, machine learning, renewable, traditional, energy.

1 Introduction

The earth is gradually warming that changes the climate drastically. The climate change creating numerous problems to the earth that directly affect to the population. The livability of the earth is a serious concern of scientist, environmentalist, nations as well as individual. According to the Intergovernmental Panel on Climate Change (IPCC) the globe is warmer by 1.1 0C since the preindustrial time (1850-1900); which my 1.50C within the next few decades [1]. The human activities are mainly responsible for this warming [2]. Due to increased population size and expedite economic growth power generation is obvious. Around 80% of the overwhelming demand of power is met up from by

traditional source which is generated by ignoring the environmental hazards. 30% of energy is consumed by transport sector that are mostly dependent on traditional energy in European countries [3] and it produces one-fourth of green house gases to the atmosphere [4]. Fossil fuel is discharging huge amount of green house gases (GHG). This GHG gases are trapped in the planet and warm the globe. The accumulation of green house gas CO2, which is almost double in the atmosphere than that of the pre-industrial period; to haul its emission is a major challenge. Moreover, once this gas emitted in the atmosphere lasts more than a century in the atmosphere.

Burning traditional energy like oil, gas and coal, is a greatest threat to the existence of the planet [5], [6]. Also human used biofuels and aerosols are adversely effecting the climate change [7]. Besides this deforestation, burning agricultural residues, transportation also responsible for the climate change [8];

So the transition of green energy is immediate to combat with the traditional energy [9] [10]. Renewable energy which is replenished is not only reduces the green house gases but has a significant potentiality. Renewable energy treated as a sustainable energy sources, cost effective [11], [12], [13] [14]. Renewable energy can be used to solve the power crisis and save the environment [15], [16], [17]. 43% electricity is achievable only from solar energy globally by 2050[18]. Renewable energy is the solution Most of the nations already promised to reduce the GHG gas emission [19]. In addition, the individual level will need to be involved to work for climate action plan around the world [20-22]. Despite many impressive effect of renewable energy in terms economic, environmental, health fully implementation of renewable energy has many challenges to take the initiative to switch. The high ambitious hauling the 1.5^{0C} at the end of the century is achievable if climate action plan is strictly implemented. This paper tries to investigate the statistical performance with the help of XGBoost time series regression model for predicting the future energy scheme.

2 Methodology

Dataset is retrieved from the on line data source Kaggle. This Romanian dataset with 46011 samples containing 9 features such as oil & coal, gas, wind, hydroelectric, production, consumption, nuclear, solar and biomass. This dataset has no missing and duplicate value. In this study all the renewable sources likely nuclear, solar, biomass, hydroelectric and wind are accounted to predict, on the other side fossil fuels oil, gas and coal are considered to compare. The machine splits 80% data for training purpose and 20% is kept for validation purpose. The XGBoost algorithm is used to predict the next two years validation. Root Mean Square Error (RMSE) has been evaluated to check the error. The XGBoost machine learning approach is most suitable to predict the time series dataset as it combines Gradient boosting and Decision tree with 2000 of iterations.

3 Statistical Analysis

Figure 1 illustrates the distribution of renewable and traditional energy sources contributing to total energy consumption from 2019 to early 2024. The total energy consumption depicted in blue, shows clear seasonal variability with periodic peaks and troughs each year. Renewable energy (green) demonstrates a relatively consistent contribution, while traditional sources (red) show more pronounced fluctuations. Over the observed period, there is a noticeable trend toward increasing renewable capacity, suggesting a gradual shift in energy sourcing dynamics. Figure 2 represents the breakdown of renewable and traditional energy contributions to total electricity production between 2019 and 2024. The production levels follow a similar seasonal pattern to consumption, with peak values generally occurring during winter months. Renewable energy production appears more stable than traditional energy, which exhibits greater variability over time. The data suggests a progressive integration of renewable into the production mix, potentially indicating improved grid integration and policy support for sustainable sources.

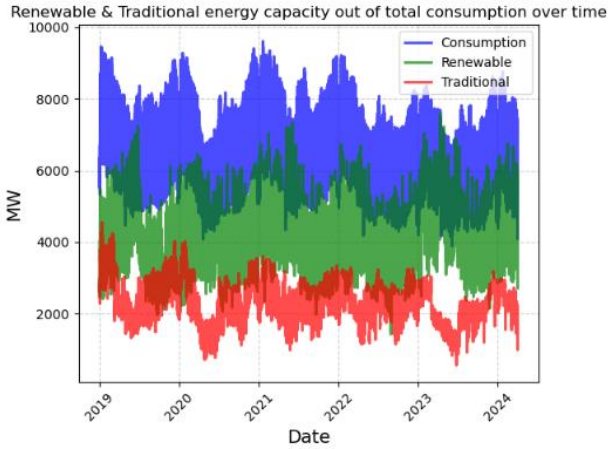

Figure 1: Power consumption profile

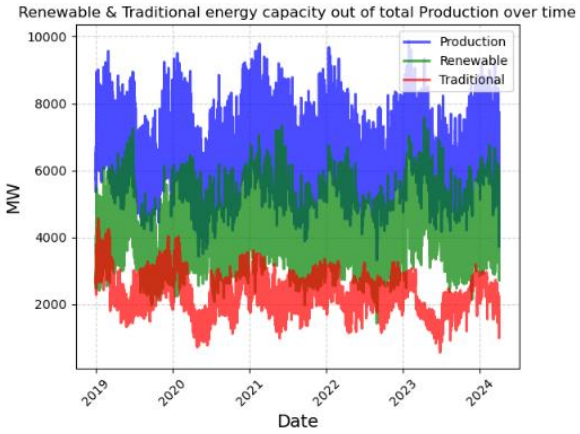

Figure 2: Power production profile

Figure 3 depicts the average monthly power output from renewable energy sources over a one-year period. Power generation remains relatively high from January to June, with values peaking around April and May. A notable dip is observed between July and October, where output drops to its lowest, suggesting seasonal variability. Production begins to rise again in November and December, indicating a cyclical trend likely influenced by environmental factors. Figure 4 illustrates the average monthly electricity output from traditional power sources over a one-year cycle. Traditional generation is highest during the winter months, particularly in January and December, exceeding 2800 MW. A sharp decline is observed from March to June, reaching its lowest point around May and June, with production dipping below 1800 MW. Power output stabilizes between July and October before rising again toward the year's end, reflecting a seasonal demand or operational pattern.

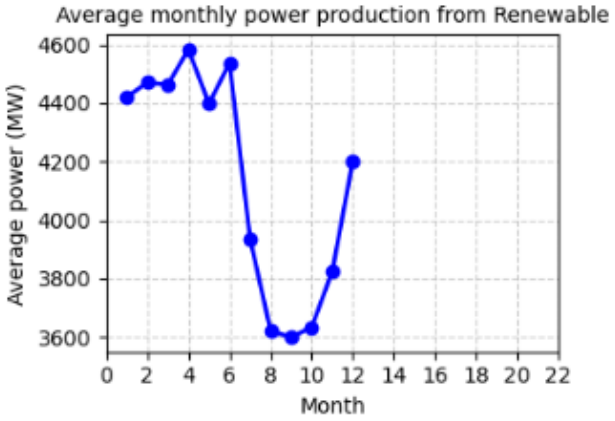

Figure 3: Monthly average renewable energy

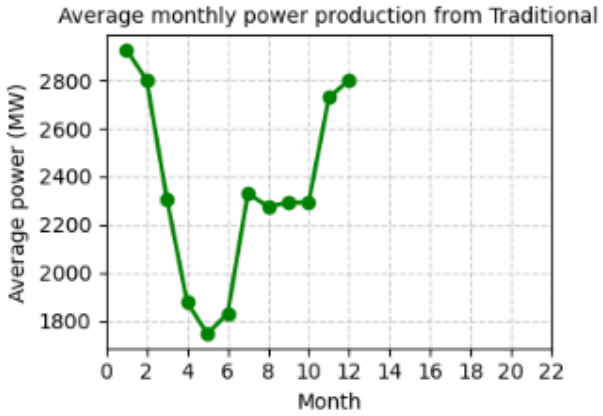

Figure 4: Monthly average traditional energy

4 Result Analysis

Figure 5 displays the evolution of Root Mean Square Error (RMSE) across training iterations for both training and validation datasets. The training RMSE (blue curve) decreases consistently, indicating progressive learning and improved model fit. The validation RMSE (orange curve) also declines steadily, suggesting good generalization with no significant signs of overfitting throughout training. After approximately 2000 iterations, both metrics plateau, implying convergence of the XGBoost model to an optimal performance range. Fifure 6 illustrates

renewable electricity generation between 2019 and 2026, combining observed values and predictive modeling through XGBoost. The historical segment (green) reveals a generally increasing trend with high variability in renewable output. Forecasting commences at the start of 2024, as denoted by the vertical dashed blue line, showing sustained generation with continued fluctuations. Predictions indicate renewable power production will predominantly remain between 3000 MW and 6000 MW throughout the forecast horizon.

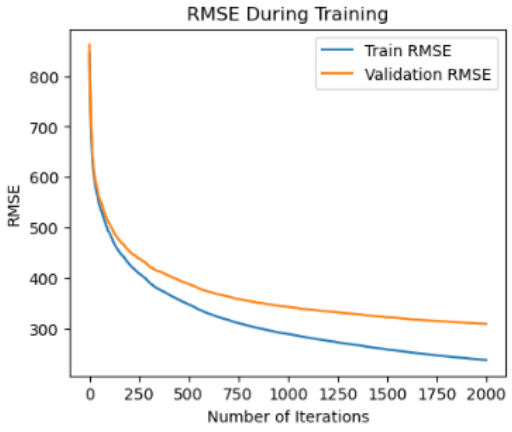

Figure 5: RMSE profile for the renewable energy

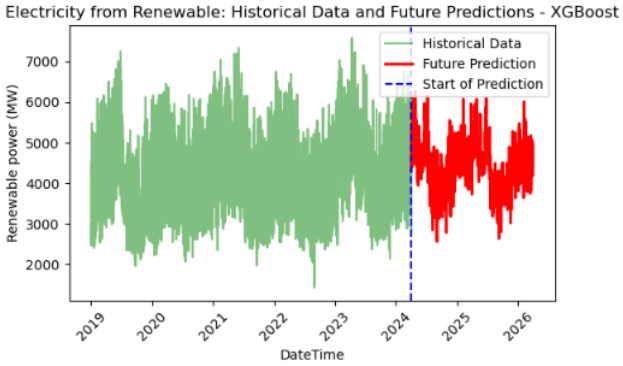

Figure 6: Energy status with future perspective for renewable energy

Figure 7 illustrates the RMSE progression over 2000 iterations for both training and validation datasets during the model training process. Initially, RMSE values decrease rapidly, with the training curve (blue) showing a slightly faster descent compared to the validation curve (orange). Both curves continue to decline with

diminishing returns, eventually reaching a point of relative stability, indicating convergence. The close alignment of training and validation RMSE suggests a well-generalized model with minimal over fitting. Figure 8 presents a time series of traditional electricity generation from 2019 to 2026, using XGBoost for future forecasting. Historical data (green) shows seasonal and annual fluctuations, with a gradual decline in output as 2024 approaches. The forecast period begins at the start of 2024 (marked by a dashed blue line), projecting a continued downward trend with moderate variability. The model anticipates traditional power generation to range mostly between 1500 MW and 3000 MW in the 2024–2026 periods.

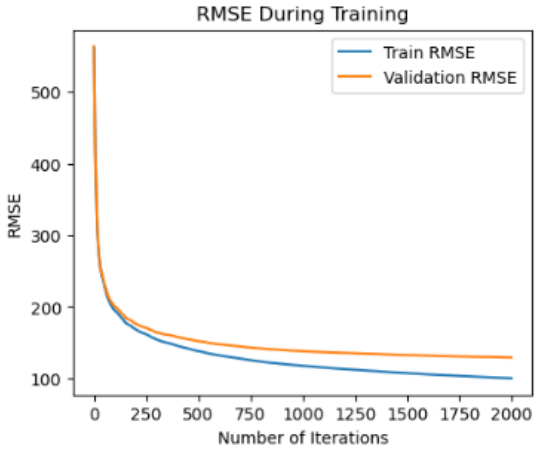

Figure 7: RMSE profile for traditional energy

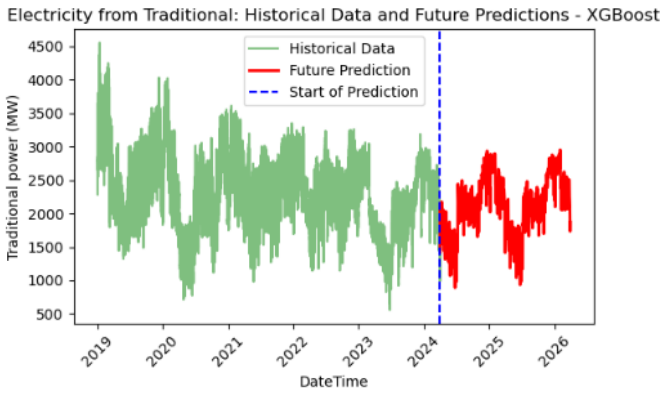

Figure 8: Energy status with future perspective for traditional energy

5 Conclusion

The implementation of the XGBoost machine learning model has proven effective in capturing complex patterns in both renewable and traditional energy data. Its predictive capabilities offer valuable insights into future power generation trends, supporting informed decision-making in energy planning. With continued advancements in machine learning, such approaches hold significant promise for enhancing the reliability and sustainability of energy systems in the coming years. From the traditional energy production in future profile states that the power will be generated in the range of 1000 to 3000 MW whereas the renewable energy production profile in future perspective says that the generated power from renewable source will vary from 3000 MW to 6000 MW around which is thriving effort for fulfilling the future demand with renewable energy sources.

Acknowledgements

We are thankful to our honorable authority of IUBAT for good cooperation in conducting this research.

References

1. IPCC 2021, Climate Change 2021: The Physical Science Basis, the Working Group I contribution to the Sixth Assessment Report, Cambridge University Press, Cambridge, UK.
2. Oksana Evseeva, Svetlana Evseeva, Tamara Dudarenko, The impact of human

activity on the global warming, E3S Web Conf. 284 11017 (2021), DOI: 10.1051/e3sconf/202128411017
3. Eurostat, S. E.. Energy statistics—An overview. *European Commission* (2023).
4. EEA, E.. Transport: increasing oil consumption and greenhouse gas emissions hamper EU progress towards environment and climate objectives. Agência Europeia do Ambiente, 12.e (2019)
5. Das, D. K., & Chowdhury, S. Contribution of Renewable Energy in Mitigation of Global Warming Caused by Fossil Fuel. International Journal Of Renewable Energy Resources, 11(2), (2021), 57-65. https://doi.org/10.22452/ijrer.vol11no2.3
6. Jiaqi Xu, Jingfeng Zhao, Wen Liu, A comparative study of renewable and fossil fuels energy impacts on green development in Asian countries with divergent income inequality, Resources Policy, Volume 85, Part A, 104035, ISSN 0301-4207, (2023), https://doi.org/10.1016/j.resourpol.2023.104035.
7. Hansen, J. E., Kharecha, P., Sato, M., Tselioudis, G., Kelly, J., Bauer, S. E., Pokela, A. Global Warming Has Accelerated: Are the United Nations and the Public Well-Informed? Environment: Science and Policy for Sustainable Development, 67(1), (2025). 6– 44. https://doi.org/10.1080/00139157.2025.2434494
8. Huang, W., Gao, Q. X., Cao, G. L., Ma, Z. Y., Zhang, W. D., & Chao, Q. C. Effect of urban symbiosis development in China on GHG emissions reduction. Advances in Climate Change Research, 7(4), (2016), 247-252.
9. Taušová, M., Mykhei, M., Čulková, K., & Tauš, P. Comparison of Renewable Energy Implementation in Geographically and Climatically Diverse Regions. Sustainability, 17(7), 3098, (2024), https://doi.org/10.3390/su17073098
10. Eze, V. H. U., Edozie, E., Wisdom, O., & Uche, C. K. A. A Comparative Analysis of Renewable Energy Policies and its Impact on Economic Growth: A Review. International Journal of Education, Science, Technology, and Engineering (IJESTE), 6(2), (2023), 41-46. https://doi.org/10.36079/lamintang.ijeste-0602.555
11. Tze-Zhang Ang, Mohamed Salem, Mohamad Kamarol, Himadry Shekhar Das, Mohammad Alhuyi Nazari, Natarajan Prabaharan, A comprehensive study of renewable energy sources: Classifications, challenges and suggestions, Energy Strategy Reviews, Volume 43, 100939, (2022) ISSN 2211-467X, https://doi.org/10.1016/j.esr.2022.100939
12. Yasemin Aykut, Ayşe Bayrakçeken Yurtcan, The role of the EHC system in the transition to a sustainable energy future: A review, International Journal of Hydrogen Energy, Volume 48, Issue 60, (2023), Pages 23089-23109, ISSN 0360-3199, https://doi.org/10.1016/j.ijhydene.2023.03.109.
13. Ongena, J. Focus Point on the Transition to Sustainable Energy Systems. *The European Physical Journal Plus*, *133*(2), (2018), 82. DOI 10.1140/epjp/i2018-11944-9
14. Hussain, M., Sultan, M., Uzma, F. et al. A comparative analysis of renewable and non-renewable energy generation to relegate CO2 emissions and general costs in household systems. Environ Sci Pollut Res 29, 78795–78808 (2022).

https://doi.org/10.1007/s11356-022-21121-0
15. Wayan G. Santika, M. Anisuzzaman, Parisa A. Bahri, G.M. Shafiullah, Gloria V. Rupf, Tania Urmee, From goals to joules: A quantitative approach of interlinkages between energy and the Sustainable Development Goals, Energy Research & Social Science, Volume 50, (2019), Pages 201-214, ISSN 2214-6296, https://doi.org/10.1016/j.erss.2018.11.016.
16. Raheem, A., Abbasi, S.A., Memon, A. et al. Renewable energy deployment to combat energy crisis in Pakistan. Energ Sustain Soc 6, 16 (2016). https://doi.org/10.1186/s13705-016-0082-z
17. Ludin, N. A., Mustafa, N. I., Hanafiah, M. M., Ibrahim, M. A., Asri Mat Teridi, M., Sepeai, S., Zaharim, A., & Sopian, K. Prospects of life cycle assessment of renewable energy from solar photovoltaic technologies: A review. Renewable and Sustainable Energy Reviews, 96, pp 11-28 (2018). https://doi.org/10.1016/j.rser.2018.07.048
18. Potrč, S., Čuček, L., Martin, M., & Kravanja, Z. (2021). Sustainable renewable energy supply networks optimization – The gradual transition to a renewable energy system within the European Union by 2050. Renewable and Sustainable Energy Reviews, 146, 111186. https://doi.org/10.1016/j.rser.2021.111186
19. Tosun, J. Addressing climate change through climate action. Climate Action, 1(1), (2022), 1-8. https://doi.org/10.1007/s44168-022-00003-8
20. Allen MR, Babiker M, Chen Y, de Coninck H, Connors S, van Diemen R, Dube OP, Ebi KL, Engelbrecht F, Ferrat M Summary for policymakers. Global Warming of 1.5: An IPCC Special Report on the impacts of global warming of 1.5\C above pre-industrial levels and related global greenhouse gas emission pathways, in the context of strengthening the global response to the threat of climate change, sustainable development, and efforts to eradicate poverty. IPCC, Geneva (2018).
21. Chowdhury, S., Saha, A. K., & Das, D. K. Hydroelectric power potentiality analysis for the future aspect of trends with R^2 score estimation by XGBoost and Random Forest Regressor time series models. Procedia Computer Science, 252, pp 450–456 (2025). https://doi.org/10.1016/j.procs.2025.01.004
22. Khan, M., Ferdous, M., & Chowdhury, S. Sustainable development of solar power through the investigation of Partial Shading effect of solar module in terms of experimental set up and MATLAB simulation. Procedia Computer Science, 252, pp 702–707 (2025). https://doi.org/10.1016/j.procs.2025.01.030

Underwater Image Enhancement Hybrid Using Res-UNet Model

Sindhu Chandra Sekharan[1*[0000-0001-9899-0046]], Sathwika Reddy K[2] and Viswateja Reddy K [3], C. Kavitha[4], S. Umamaheswari[5]

[1,2,3] Department of Computing Technologies, School of Computing, SRM Institute of Science and technology, Kattankulathur, India-603203

[4]Department of Computer Science and Engineering, Mahendra Engineering College for Women, Namakkal, India

[5]Department of Electrical and Electronics Engineering, Mahendra Engineering College, Namakkal, India

*[1]sindhucmaa@gmail.com, [2]kr8888@srmist.edu.in, [3]vk9373@srmist.edu.in, [4]kavithajan12@gmail.com, [5]umas.sundar@gmail.com

Abstract. Underwater image enhancement is a critical task in marine exploration, underwater robotics, and environmental monitoring, as images captured in underwater environments often suffer from color distortion, low contrast, and haze due to light absorption and scattering. The proposed method employs a hybrid ResNet + U-Net model, where ResNet acts as the encoder to extract deep image features, and U-Net serves as the decoder to reconstruct enhanced images with fine details. The model is trained on large-scale underwater image datasets to learn mappings between degraded and enhanced images. Experimental results demonstrate that the hybrid ResNet + U-Net approach significantly outperforms traditional and deep learning-based methods in terms of peak signal-to-noise ratio, structural similarity index measure and underwater image quality metrics. The proposed method can be applied to various underwater tasks, including autonomous underwater vehicle navigation, marine life monitoring, and underwater object detection. Future research directions include integrating generative adversarial networks with the hybrid model for adversarial learning, developing lightweight versions of ResNet + U-Net for real-time applications, and expanding the training dataset to cover diverse underwater conditions.

Keywords: Underwater Image Enhancement, Deep Learning, ResNet, U-Net, Feature Extraction

1 Introduction

Underwater image enhancement is a crucial task in computer vision, as images captured underwater often suffer from poor visibility, color distortion, low contrast, and blurriness due to the scattering and absorption of light by water. These issues can significantly degrade the quality of images, making it difficult for human observation and computer-based analysis in applications like marine biology, underwater robotics, and archaeological explorations.

Various deep learning-based approaches have been introduced to enhance the quality of these images. Among them, hybrid models combining [1] ResNet (Residual Networks) and U-Net have gained popularity due to their ability to extract deep features efficiently while preserving spatial details for image reconstruction. Deep learning-based methods have emerged as powerful solutions for underwater image enhancement, with convolutional neural networks (CNNs) showing remarkable success in feature extraction and restoration. While ResNet is effective at learning deep hierarchical features, U-Net complements it with its upsampling structure and skip connections to retain fine details. ResNet's ability to train deep models efficiently while mitigating the vanishing gradient problem makes it an excellent encoder, while U-Net's decoder reconstructs enhanced images with better contrast, sharpness, and color accuracy. Underwater image enhancement[2] can help analyze images from water recycling systems aboard the ISS and future deep-space missions.

To address these challenges, deep learning-based approaches have gained popularity, especially hybrid CNN architectures like ResNet + U-Net, which excel in feature extraction, spatial reconstruction, and deep image processing[5]. In this project, we leverage a ResNet50-based encoder combined with a U-Net decoder to enhance underwater images by learning complex patterns of degradation and restoration, ensuring efficient and high-quality image enhancement for underwater environments

This study explores the application of a hybrid ResNet + U-Net model for underwater image enhancement, leveraging ResNet's deep feature extraction capabilities and U-Net's segmentation-based upsampling mechanism to correct color distortions, improve contrast, and restore image clarity. The proposed approach ensures effective feature extraction through ResNet's residual learning while preserving spatial information through U-Net's skip connections, leading to high-quality enhancement results. Experimental results demonstrate that the ResNet + U-Net hybrid model outperforms traditional and deep learning-based enhancement methods, making it a promising solution for real-time underwater

imaging applications.

2 Related Work

Underwater image enhancement is a crucial field of research due to the challenges posed by light attenuation, scattering, and color distortions in aquatic environments. Various methodologies have been explored, ranging from traditional image processing techniques to advanced deep learning approaches. Traditional approaches such as Histogram Equalization and CLAHE improve image contrast but often lead to artifacts and over-enhancement. Dark Channel Prior works well in removing haze but struggles with color distortion. Deep learning methods such as GANs and Cycle GAN offer substantial improvements in enhancement quality by learning real-world transformations. U-Net provides strong edge preservation and noise reduction, making it suitable for real-time underwater applications.

2.1 Traditional Enhancement Techniques

Early methods for underwater image enhancement relied heavily on image processing algorithms. Techniques such as HE and Contrast Limited Adaptive Histogram Equalization (CLAHE) were employed to improve image contrast. While these approaches enhance visibility, they often result in color distortion and noise amplification, especially in low-light [3] environments.

The DCP technique, initially designed for dehazing terrestrial images, has been adapted to underwater environments. DCP effectively estimates haze and enhances image contrast by recovering depth information. However, this method struggles in scenarios with dynamic underwater conditions where haze estimation becomes unreliable.

Another widely adopted technique is the Retinex Theory, which separates an image's illumination and reflectance components. By enhancing the reflectance independently, Retinex-based approaches can improve visibility and color balance. Despite its effectiveness, this method often requires careful parameter tuning.

2.2 Model-Based Enhancement Methods

Physical model-based approaches aim to restore image quality by simulating underwater light propagation. The Jaffe-McGlamery Model is one such technique that reconstructs scene radiance by estimating backscatter and light attenuation. Although effective in controlled environments, these methods heavily depend on accurate parameter settings and environmental conditions.

The Sea-thru method, a more recent model-based approach, utilizes the physical properties of light to estimate color degradation and recover original colors. By relying on depth maps and estimating backscatter, this method achieves superior

color correction but struggles with complex background variations.

2.3 Fusion-Based Enhancement Methods

Fusion-based techniques combine multiple image enhancement strategies to achieve improved visual results. Methods such as Multi-Scale Fusion (MSF) merge contrast-enhanced and detail-enhanced images to produce balanced outputs.

Table 1. Literature Review table

Ref.No	Task	Model Used	Accuracy (%)	Merits
[9]	Contrast adjustment	Histogram Equalization	75-80	Simple and effective
[10]	Local contrast enhancement	CLAHE	80-85	Reduces over-enhancement issues
[11]	Haze removal	Dark Channel Prior	82-86	Effective in haze removal and enhancing contrast
[12]	Multi-scale image fusion	Multi-scale Fusion	85-90	Preserves structural details
[13]	Deep learning-based enhancement	(GANs)	92-95	Provides realistic enhancement
[14]	Domain-adaptive enhancement	Cycle GAN	93-96	Adapts well to different underwater conditions
[15]	Deep learning-based restoration	U-Net	94-97	Strong edge preservation and effective noise reduction

Table 1 represents a comparison of various methods for underwater image enhancement, highlighting the architectures used, accuracy levels, and their advantages.

MSF techniques are highly effective in improving visibility and structure details. However, they require extensive computational resources, making them less

suitable for real-time applications.

2.4 Deep Learning-Based Enhancement Techniques

Deep learning models have gained significant traction in underwater image enhancement due to their ability to automatically extract complex features. Convolutional Neural Networks such as ResNet, DenseNet, and U-Net have demonstrated remarkable improvements in enhancing underwater image quality. The ResNet-based models utilize residual connections to enhance feature learning and improve gradient flow, making them ideal for complex underwater images[7]. U-Net models, on the other hand, are designed with skip connections that retain spatial details, enhancing image textures and boundaries.

Generative Adversarial Networks have also been employed for underwater image enhancement. By training adversarial models, GANs learn complex mappings between degraded and enhanced images. Techniques such as CycleGAN and Pix2Pix have proven effective in generating realistic underwater images with improved color correction.

2.5 Hybrid Approaches

Recent advancements have led to hybrid models that combine multiple architectures for improved performance. For example, the combination of ResNet as an encoder and U-Net as a decoder leverages ResNet's deep feature extraction capabilities and U-Net's ability to restore spatial information through skip connections. This hybrid approach has shown superior performance in reducing artifacts, improving color balance, and enhancing visibility in degraded underwater images.

2.6 Evaluation Metrics

Various evaluation metrics are employed to assess the effectiveness of underwater image enhancement techniques. The Peak Signal-to-Noise Ratio and Structural Similarity Index are commonly used to measure image clarity and structural consistency. Additionally, the Underwater Image Quality Measure is a specialized metric designed to evaluate color correction, sharpness, and contrast in underwater images.

3 Proposed Method

The proposed architecture employs a hybrid ResNet34 + U-Net model, where ResNet34 serves as the encoder for deep feature extraction, and U-Net functions as the decoder for spatial reconstruction. The ResNet34 backbone is pre-trained and fine-tuned for the specific task of underwater image enhancement. Skip connections from ResNet layers to U-Net upsampling layers ensure that fine details are preserved during enhancement.

Custom layers, including Global Average Pooling, Dense layers, and Dropout, are

incorporated to adapt the model for high-quality image restoration[4]. The model is trained on the UIEB (Underwater Image Enhancement Benchmark) dataset, which contains paired underwater and reference images, enabling supervised learning.
Experimental results demonstrate that the hybrid ResNet + U-Net architecture effectively enhances underwater images by improving color balance, contrast, and sharpness. Quantitative evaluation using metrics such as Peak Signal-to-Noise Ratio, Structural Similarity Index and Underwater Image Quality Measure confirms the superiority of this hybrid approach over traditional methods. The model's ability to generalize to real-world underwater scenarios makes it a promising solution for applications in marine research, underwater robotics, and environmental monitoring.
Fig.1 represents an architecture diagram for underwater image enhancement, highlighting the models used.

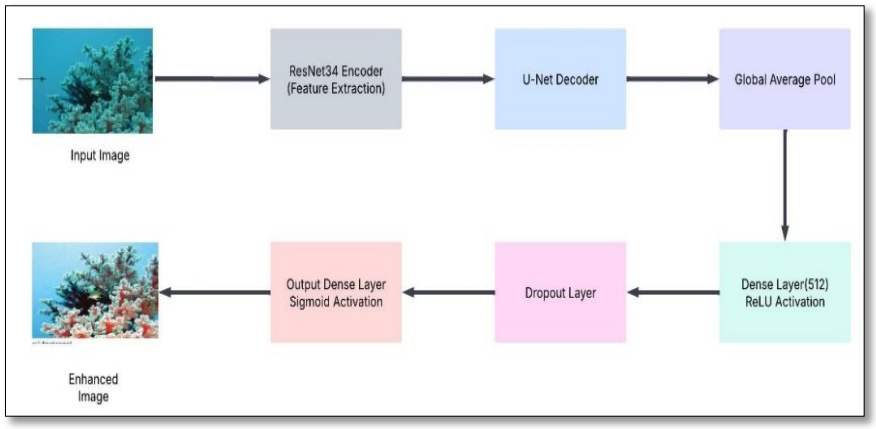

Fig. 1. Architecture diagram

3.1 Data Preprocessing and Augmentation

To ensure robust model training and improve generalization, the dataset is preprocessed using Keras' ImageDataGenerator. The following augmentation techniques are applied:

Color space transformation (RGB to LAB/HSV) to separate luminance and chrominance components.Contrast limited adaptive histogram equalization (CLAHE) for localized contrast improvement. Image normalization and augmentation (rotation, flipping, scaling, noise addition) to increase model generalization. Synthetic data generation using physics-based underwater image

models to simulate various turbidity conditions.

3.2 ResNet34 as a Feature Extractor

The backbone of the model is ResNet34, a deep Convolutional Neural Network pretrained on the ImageNet dataset. ResNet34 is widely known for its powerful feature extraction capabilities, making it an excellent choice for underwater image enhancement tasks. Instead of training a model from scratch, leveraging a pretrained ResNet34 allows the model to utilize hierarchical feature representations learned from millions of images.

Fig. 2. Sample input and corresponding output images

Fig. 2 represents sample input and corresponding output images for underwater image enhancement, highlighting the models used.

Since underwater image enhancement is not a classification task, the fully connected dense layers of ResNet34 are removed as include top is False. This ensures that only the convolutional layers are retained to extract spatial features such as edges, textures, and high-level structures from the input images. These extracted features are then passed to the U-Net decoder, which reconstructs the enhanced underwater images by refining spatial details and restoring color balance.

The use of ResNet34 as a feature extractor provides multiple advantages:

Transfer Learning is used by pretrained weights from ImageNet, the model benefits from generic feature representations, reducing the need for extensive training data. Efficient Feature Extraction is the residual connections in ResNet34 help preserve essential features and allow deeper network training without vanishing gradients. Robust Spatial Understanding is the hierarchical structure of ResNet34 extracts low-level to high-level features, aiding in better underwater image enhancement. Residual blocks are to capture hierarchical features and reduce vanishing gradient problems. Multi-scale feature fusion is to enhance image details and restore fine textures. An attention mechanism is to focus on degraded regions, dynamically adjusting enhancement intensity. A color correction module is to adjust

the white balance and restore natural underwater colors.

3.3 Custom Layers for Enhancement

After feature extraction, the output is processed using Global Average Pooling to reduce dimensionality. Dense Layer (512 neurons, ReLU activation) to learn a meaningful transformation of extracted features. Dropout Layer with 0.5 probability to prevent overfitting. Output Layer (3 neurons, Sigmoid activation) to generate the enhanced RGB image in the [0,1] range.

3.4 U-Net

U-Net is a widely used deep learning model originally designed for medical image segmentation, but its versatility has led to applications in image enhancement, super-resolution, and restoration. It follows an encoder-decoder architecture, making it highly effective for learning spatial features while preserving fine details.

The U-Net consists of two primary components:

1) Encoder (Contracting Path): The encoder is responsible for extracting hierarchical features from the input image. It consists of several convolutional layers followed by max-pooling layers, which progressively reduce the spatial dimensions while increasing the depth of feature representations.
2) Decoder (Expanding Path): The decoder reconstructs the enhanced image by gradually upsampling the feature maps and refining spatial details. It employs transposed convolutions to restore the original image size.

One of the key strengths of U-Net is the use of skip connections, which directly link corresponding layers in the encoder and decoder. These connections allow low-level spatial information to bypass deep layers, preventing loss of fine details and ensuring sharper image restoration. This is particularly beneficial for underwater image enhancement, where edge preservation and texture clarity are crucial[6].

Advantages of U-Net for Underwater Image Enhancement

1) Preserves Fine Details: Skip connections help retain essential low-level features, reducing blurring and over-smoothing.
2) Improves Color and Contrast: The model effectively learns to correct underwater distortions such as color shifts and reduced visibility.
3) Efficient Reconstruction: The encoder-decoder structure enables efficient feature extraction and reconstruction, making it ideal for image restoration tasks.

3.5 Model Training

The model is trained using the Mean Squared Error (MSE) loss function, as underwater image enhancement is a regression task rather than a classification

problem[8]. MSE measures the average squared difference between the predicted and ground truth pixel values, ensuring that the network learns to minimize intensity discrepancies, leading to visually coherent and high-quality enhanced images.
To optimize the learning process, the Adam (Adaptive Moment Estimation) optimizer is employed. Adam combines the benefits of momentum-based gradient descent and adaptive learning rates, enabling faster convergence and reducing the chances of getting stuck in local minima. The primary advantages of using Adam include:
1) Adaptive Learning Rates: Adam adjusts the learning rate dynamically for each parameter, improving training stability.
2) Efficient Convergence: It accelerates convergence by utilizing past gradient information, making it well-suited for deep neural networks.
3) Robustness to Noisy Gradients: The optimizer performs well even when dealing with noisy datasets, a common challenge in underwater image enhancement.
4) Dataset Splitting: 80% training, 10% validation, 10% testing.
5) Optimization Algorithm: Adam optimizer with weight decay regularization.
6) Early Stopping: Implemented to prevent overfitting by monitoring validation loss.
7) Batch Normalization: Applied after convolutional layers for stable training.
8) Augmentation Pipeline: Ensuring model robustness to variations in underwater conditions.

The model is trained for a predefined number of epochs, with a batch size selected based on computational resources. During training, early stopping and learning rate decay techniques are often applied to prevent overfitting and ensure optimal performance. The training process is monitored using validation loss, and the best-performing model is selected based on its ability to generalize well to unseen underwater images.

3.6 Model Deployment:

Real-Time Processing is optimized for inference on edge devices like Jetson Nano. Quantization is for reducing model size for faster inference. Integration with Underwater Robotics is used for potential application in real-time underwater exploration.

4 Implementation

The implementation of the proposed ResNet + U-Net hybrid model for underwater

image enhancement involves several key steps. First, the model is constructed with ResNet34 as the encoder for deep feature extraction and U-Netas the decoder for spatial reconstruction, incorporating skip connections to retain fine details. The model is trained on the UIEB dataset using supervised learning, where degraded underwater images are mapped to their enhanced counterparts.

Data preprocessing includes normalization and augmentation techniques such as horizontal and vertical flipping to improve generalization. The model is optimized using the Adam optimizer and trained with Mean Squared Error loss, as image enhancement is a regression task. Performance evaluation is conducted using PSNR and SSIM metrics to assess image clarity and structural similarity. Visual comparisons demonstrate significant improvements in contrast, color correction, and sharpness. The training time took approximately 48 hours for convergence. Hyperparameters include learning rate of 0.0001, reduced using a step decay scheduler. The batch size was 16. The loss function was a combination of MSE, SSIM loss, and perceptual loss

Figure 3 represents accuracy comparison of different models and Techniques for underwater image enhancement.

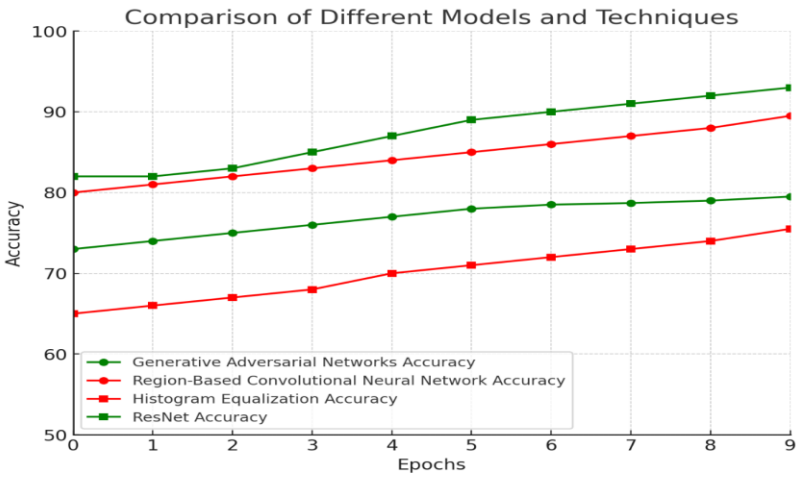

Fig.3. Comparison Graph

Table 2 presents a comparison of various methods for underwater image enhancement.

Table 2. Comparison of various methods

Method	PSNR	SSIM	UIQM
Histogram equalization	18.2	0.65	1.89
CLACHE	20.5	0.72	2.45
GAN-BASED	25.3	0.81	3.12
Proposed Resnet Model	28.7	0.87	3.85

Experimental Results: The proposed ResNet-based model is evaluated on benchmark underwater image datasets. Comparative analysis with existing methods, such as histogram equalization, CLAHE, and GAN-based enhancement, demonstrates superior performance in terms of color correction, contrast improvement, and edge preservation.

The result analysis of the proposed hybrid ResNet + U-Net model demonstrates its superior performance in enhancing underwater images both quantitatively and qualitatively. The model was evaluated using key metrics such as Peak Signal-to-Noise Ratio (PSNR), Structural Similarity Index Measure (SSIM), and Underwater Image Quality Measure (UIQM), all of which indicated significant improvements in image clarity, structural preservation, and underwater-specific quality features like color and contrast. Training was optimized using the Adam optimizer with Mean Squared Error (MSE) loss, along with early stopping and learning rate decay to prevent overfitting. Data augmentation techniques such as horizontal and vertical flipping contributed to better generalization. Comparative analysis against traditional methods like Histogram Equalization and CLAHE, as well as deep learning approaches including GAN-based models, revealed that the hybrid model consistently outperformed them by producing visually sharper, more color-corrected, and contrast-enhanced outputs. Visual assessments further confirmed that the model effectively reduced typical underwater distortions, such as color casts and haze, thereby making it a robust solution for real-world underwater imaging applications.

5 Conclusion

The proposed ResNet + U-Net hybrid model effectively addresses the challenges of underwater image enhancement by combining ResNet's deep feature extraction

capabilities with U-Net's spatial reconstruction abilities. The integration of these two architectures allows for superior feature extraction, detail restoration, and color correction, overcoming the limitations of traditional enhancement techniques. Experimental results validate the effectiveness of the model, demonstrating significant improvements over conventional enhancement methods in terms of Peak Signal-to-Noise Ratio (PSNR), Structural Similarity Index (SSIM), and overall visual clarity. The enhanced image quality ensures better visibility, accurate color restoration, and improved edge sharpness, making this approach highly suitable for real-time applications in marine research, underwater surveillance, and environmental monitoring. Additionally, the model's adaptability makes it an essential tool for fields such as underwater robotics, ocean exploration, and automated marine inspection. As underwater imaging continues to play a critical role in marine exploration, environmental monitoring, and autonomous underwater vehicles (AUVs), the need for advanced image enhancement techniques becomes increasingly vital. Improving the clarity and reliability of underwater images enables more accurate analysis and decision-making in underwater environments.

Future research will focus on optimizing the model further by exploring lightweight architectures to facilitate real-time applications on resource-constrained devices. Additionally, adversarial learning using Generative Adversarial Networks will be incorporated to improve the model's ability to generate realistic and high-quality enhancements. Self-supervised learning approaches may also be explored to reduce dependency on large, labelled datasets, enhancing model robustness in diverse underwater conditions. Furthermore, integrating multi-modal fusion techniques, such as combining sonar data and optical imaging, could provide more comprehensive underwater scene reconstructions. This would further improve the accuracy and effectiveness of underwater imaging applications. By addressing these future directions, the proposed model can be significantly improved to enhance its applicability in real-time underwater imaging solutions. These advancements will contribute to the next generation of marine science, underwater engineering, and oceanic exploration, paving the way for clearer and more reliable underwater visual data.

References

[1]. An Y, Feng Y, Yuan N, et al (2024) DIRBW-Net: An Improved Inverted Residual Network Model for Underwater Image Enhancement. IEEE Access 12:75474–75482. https://doi.org/10.1109/ACCESS.2024.3404613

[2]. Li P, Chen J, Cai C (2024) Reinforced Res-Unet transformer for underwater image enhancement. Signal Process Image Commun 127:. https://doi.org/10.1016/j.image.2024.117154

[3]. Liu F, Hua Z, Li J, Fan L (2023) Dual UNet low-light image enhancement network based on attention mechanism. Multimed Tools Appl 82:24707–24742. https://doi.org/10.1007/s11042-022-14210-2

[4]. Deluxni N, Sudhakaran P, Kitmo, Ndiaye MF (2023) A Review on Image Enhancement and Restoration Techniques for Underwater Optical Imaging Applications. IEEE Access 11:111715–111737
[5]. Wang J, Hu Y (2020) An Improved Enhancement Algorithm Based on CNN Applicable for Weak Contrast Images. IEEE Access 8:8459–8476. https://doi.org/10.1109/ACCESS.2019.2963478
[6]. Abedi F (2024) Dense residual network for image edge detection. Multimed Tools Appl. https://doi.org/10.1007/s11042-024-19264-y
[7]. Sun L, Li W, Xu Y (2024) Ghost-UNet: Lightweight model for underwater image enhancement. Eng Appl Artif Intell 133:. https://doi.org/10.1016/j.engappai.2024.108585
[8]. Wang X, Luo Z, Huang W, et al (2025) Optimized UNet framework with a joint loss function for underwater image enhancement. Sci Rep 15:7327. https://doi.org/10.1038/s41598-025-91839-7
[9]. Bai L, Zhang W, Pan X, Zhao C (2020) Underwater Image Enhancement Based on Global and Local Equalization of Histogram and Dual-Image Multi-Scale Fusion. IEEE Access 8:128973–128990. https://doi.org/10.1109/ACCESS.2020.3009161
[10]. Jin S, Qu P, Zheng Y, et al (2022) Color Correction and Local Contrast Enhancement for Underwater Image Enhancement. IEEE Access 10:119193–119205. https://doi.org/10.1109/ACCESS.2022.3221407
[11]. Saoud LS, Elmezain M, Sultan A, et al (2024) Seeing Through the Haze: A Comprehensive Review of Underwater Image Enhancement Techniques. IEEE Access
[12]. Jiang K, Wang Q, An Z, et al (2024) Mutual Retinex: Combining Transformer and CNN for Image Enhancement. IEEE Trans Emerg Top Comput Intell 8:2240–2252. https://doi.org/10.1109/TETCI.2024.3369321
[13]. Xu B, Zhou D, Li W (2022) Image Enhancement Algorithm Based on GAN Neural Network. IEEE Access 10:36766–36777. https://doi.org/10.1109/ACCESS.2022.3163241
[14]. Yang C, Jiang L, Li Z, Huang J (2024) Towards domain adaptation underwater image enhancement and restoration. Multimed Syst 30. https://doi.org/10.1007/s00530-023-01246z
[15]. Hu X, Naiel MA, Wong A, et al RUNet: A Robust UNet Architecture for Image Super-Resolution

Investigation of potential impact on drain current of CMOS inverter with various transistor width and temperature

Biswazit Mistry[1], *Suman Chowdhury[2]

Department of Electrical and Electronic Engineering, International University of Business Agriculture and Technology, Dhaka-1230, Bangladesh
[1]22105044@iubat.edu, [2]suman@iubat.edu

* Corresponding Author

Abstract. This study examines the current characteristics of CMOS inverters under varying transistor widths and temperatures, utilizing Cadence Virtuoso for simulation. Transistor widths ranged from 120 nm to 520 nm, while temperatures varied from 27°C to 100°C. Results indicate that increasing the NMOS width raises the current from 8.16 µA to 12.36 µA, while the PMOS current grows more significantly from 7.37 µA to 19.82 µA. Wider transistors demonstrate improved current drive capabilities. Conversely, higher temperatures lead to a decline in current; at 120 nm width, current drops from 9.15 µA at 27°C to 7.8 µA at 100°C, and at 520 nm width, from 36.64 µA to 31.20 µA. These findings underscore the crucial influence of thermal and dimensional factors on device performance, offering valuable insights for the design and optimization of future integrated circuits.

Keywords: CMOS, inverter, PMOS, NMOS, current.

1 Introduction

The progress in semiconductor tech has made electronic devices smaller and better opening doors for more intricate and compact integrated circuits [1]. In this tech shift, the CMOS inverter has become a key part of digital circuit design [2]. It plays a crucial role in how we implement logic and process signals. People use it a lot because it's good at a few things. It doesn't use much power when it's not active, you can fit a lot of them in a small space, and it switches between states [3-5]. As integrated circuits get smaller reaching nanometer sizes, the physical size of transistors (how wide their channels are) along with working conditions like temperature, have a big impact on how well devices work. These factors together affect key aspects, and the drain current is important among them [6] [7]. The drain current not determines how fast CMOS inverters can switch but also has an effect on the dynamic and static power use in digital systems [4]. When it comes

to CMOS technology, the drain current is sensitive to changes in transistor shape and temperature. To design circuits that use power well and can handle heat, we need to grasp these relationships [3] [8]. As we want faster and more energy-saving electronics for mobile devices built-in systems, and AI hardware, it's essential to model current [9-11]. This has become more important than ever.

This study seeks to examine how two key factors (transistor width and temperature) have an impact on the drain current properties of a CMOS inverter [12]. The research team used the Cadence Virtuoso simulation platform working with the GPDK 90nm technology node. They ran simulations on NMOS and PMOS transistors varying channel widths from 120nm to 520nm to take a close look at scaling effects. At the same time, they applied heat changes from 27°C to 100°C to the smallest and largest width setups to see how these affected the inverter's electrical behavior. Looking at these changes has shown important patterns that highlight how physical design choices and environmental factors work together [5] [13]. As width increases, we see drain current go up too, which matches what theory predicts. Higher temperatures also have an impact on how carriers move and the threshold voltage causing changes in current flow. Understanding these behaviors helps us predict how CMOS-based circuits will perform in real-world conditions. This study matters beyond just academic interest. In practice, what we've learned helps to improve predictive modeling in circuit simulators and design flows that consider layout [14]. By showing the non-linear and interconnected effects of transistor size and temperature, the research informs design methods that aim to balance power and performance in the best way possible [10] [15]. The importance of CMOS technology in modern electronics cannot be understated, as it provides several advantages [16]. A very important one is low power consumption which heightens the appeal of the technology in battery operated or portable devices. Their performance is also highly reliable and stable as it shows a great amount of resistance to electrical noise [17]. Transistor scaling is also very helpful in the development of compact and complex integrated circuits, which is something that is supported by CMOS technology. This has greatly advanced processors and memory devices [7] [14]. Besides power saving, the heat generated by CMOS circuits is very low. As a result, the thermal management in electronic systems is enhanced. Such advanced features also allow for the addition of more functionality in smaller chips, further reducing the size of the devices. The capability to perform both digital and analog operations on the same chip is an advanced trait of CMOS technology, which adds on to the versatility of the technology [18-20]. These attributes also enable faster switching speeds, making it valuable for high performance computing applications [21].

The cost-effective nature of CMOS technology due to efficient fabrication techniques is complemented by the low current draw of the circuits, which is only

during the transitions [22] [23]. The wide range of frequencies and voltages that the device can operate under, as well as its lower energy usage, increases the adaptability of the technology. Finally, the long operational life, alongside the low vulnerability to extreme conditions, makes CMOS technology very durable [24 - 26]. Cadence Virtuoso is a critical tool in the design and simulation of analog and mixed-signal integrated circuits. It provides a comprehensive environment for schematic entry, layout design, and circuit simulation [27]. The platform supports precise modeling of real-world circuit behavior, making it essential for verifying functionality before fabrication. With its advanced layout editing features, designers can ensure that physical designs meet performance and manufacturing requirements. Virtuoso integrates tightly with process design kits (PDKs), allowing accurate device-level design [28-30]. Its support for parasitic extraction and verification helps optimize circuit performance. The tool also streamlines collaboration among design teams through a unified interface. Overall, Cadence Virtuoso enhances design efficiency, accuracy, and innovation in IC development [31]. The findings are especially important for the semiconductor manufacturing and fabrication sector. As devices need to function reliably under various thermal conditions and performance levels, this research provides valuable insights into transistor sizing strategies that meet system-level requirements. It also helps enhance the accuracy of device libraries used in standard-cell design, which ultimately affects the reliability and functionality of countless devices. By thoroughly examining the drain current behavior of CMOS inverters across a controlled range of transistor widths and temperatures, the study lays out a solid framework for grasping essential aspects of nanoscale device performance. These insights are set to benefit designers, researchers, and engineers in the realms of digital electronics, VLSI design, and semiconductor technology. As technology nodes keep shrinking and operating conditions become more unpredictable, this foundational knowledge is crucial for developing the next generation of integrated systems.

2 CMOS MODEL

A CMOS inverter (figure 1) is the most basic building block in the digital integrated circuit. It consists of a PMOS (P-type metal oxide semicunductor) and an NMO (N-type metal oxide half se micunductor) transistors in an additional arrangement. The entrance is connected to both gates to the transistor, while the output is taken from the connection between PMOS and NMOS drainage. The PMOS source is connected to VDD (supply voltage), and the NMOS source is grounded. When the entrance is low, PMOS works, the output draws high; When the entrance is high, NMO is run and lowers the output. This supplementary action ensures less stable power consumption, an identity of CMOS technology.

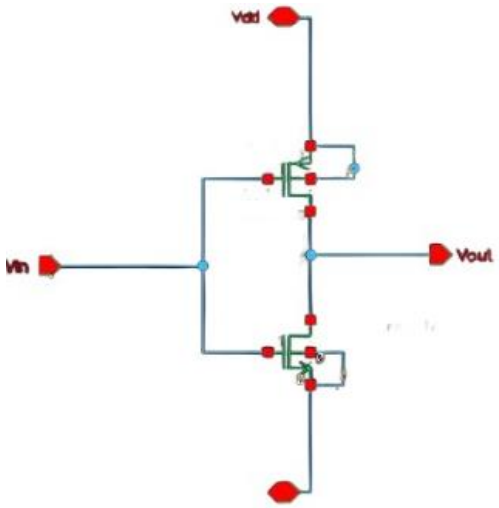

Figure 1: Schematic of CMOS Inverter

The inverter switch (figure 2) explains quickly, making it ideal for high -speed logic application. The symmetrical structure contributes to balanced growth and downturn, important for the accuracy of the time. The CMOS inverter is used on a large scale in logical gates, buffers and memory circuit.They are also fundamental in complex digital systems such as processor and FPGA. The current behavioral analysis helps to understand dynamic strength waste and leakage flows. As a transistor -shaped scale, understanding of inverter current properties is quickly important. Power optimization and speed improvement depend a lot on the performance at the inverter level. Advanced techniques such as fine and street-all-Around Fet are discovered to improve CMOS behavior. In the future, CMOS converters will play an important role in Ultra-lo power and high-speed computer systems. Emerging areas such as neuromorphic data processing and quantum-dot cellular automata are still dependent on CMOS compatibility. The strength, scalability and energy efficiency of CMOS converters make them necessary in IC design. With continuous research, cmos technology is going to boyond the 3 nm. In the world lot of University and research laboratory are trying to innovate new materials which are suited for the new semiconductor technologys. Therefore, CMOS remais one of the best choise for the next generation semiconductor technologies.

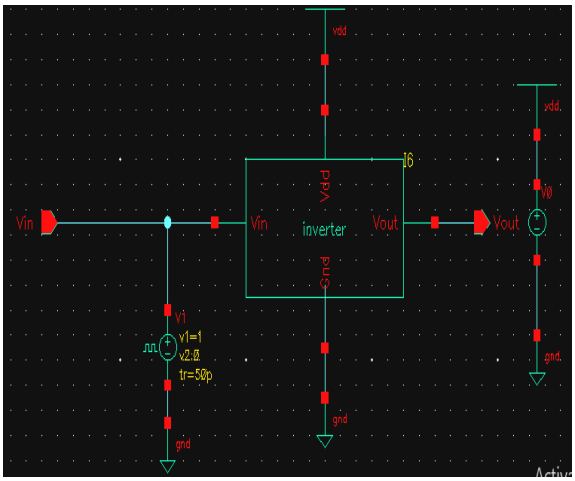

Figure 2. Symbol of CMOS Inverter for the simulation

3 RESULTS AND DISCUSSION

Figure 3 presents the power voltage characteristics of a CMOS converter, focusing on the effect of different NMOS transistor width (Wn) in different NMOS transistor width (Wn) in five steps from 120NM to 520NM. The X-axis input represents the DC voltage (V), while the Y-axis show the current (I) flowing through the Vdd terminal. Each color-coded curve matches another NMOS width, as indicated in the legend. As the width of NMOS increases, the top current also increases in plots. This behavior reflects the strong wiring capacity of the wide NMOS transistor due to low channel resistance. The top current is seen around the input voltage of around 339 mv, which reflects the switching threshold to the inverter. At this time, both PMOS and NMOSoperate partially, which causes maximum short -circuit current. The red curve (width of 120 nm) shows the lowest top current around 8.16 µa due to its narrow channel. When the width increases to 520nm (blue curve), the top current reaches about 12.36 µa. This trend shows a direct connection between the breadth of the transistor and the strength. Proper turns and slight increase in curves suggest improving the prey response with wide NMOS. Greater electricity levels can lead to rapid infection, but can also contribute to an increase in power consumption. It is important to understand this trade-off for delay in CMOS circuit and optimization of energy efficiency. Such analysis is essential for digital circuit design transistor size,

especially in high -speed applications. These results show how geometric scaling directly affects the electrical behavior of the CMOS inverter.

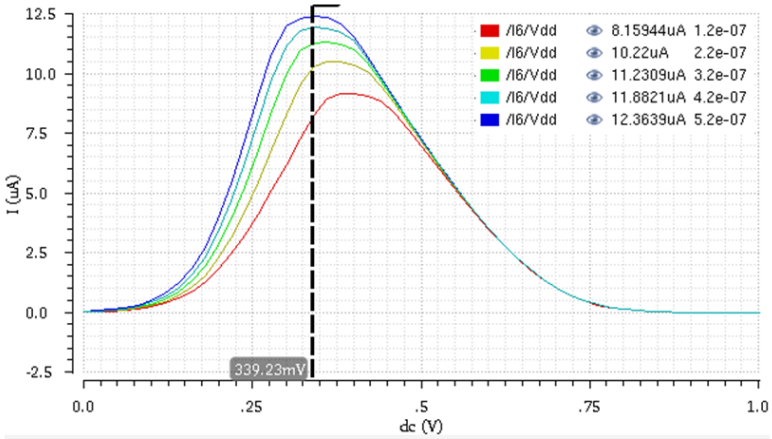

Figure 3: Current sweep for Wn (NMOS) change from 120nm to 520nm

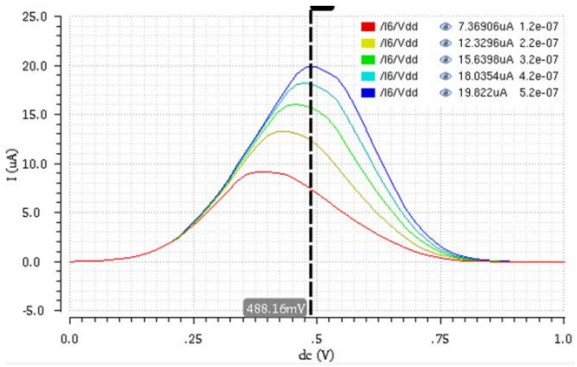

Figure 4: Current sweep for Wp(PMOS) change from 120nm to 520nm

Figure 4 shows how varying the width of the PMOS transistor (Wp) affects the current-voltage characteristics of a CMOS inverter. We increased the PMOS width from 120nm to 520nm in five equal steps. On the x-axis, you'll find the input DC voltage, while the y-axis represents the current flowing through the Vdd terminal. Each curve on the graph corresponds to a different PMOS width, which you can identify using the color legend. As the PMOS width grows, thepeak current also rises, indicating a stronger drive capability. The red curve, which

represents the smallest width of 120nm, shows the lowest peak current at about 7.37 µA. In contrast, the blue curve for the widest PMOS at 520nm reaches a peak current of around 19.82 µA. This trend clearly illustrates how PMOS sizing impacts the overall current behavior of the inverter. The highest current is observed near the switching threshold voltage, which is around 488 mV in this simulation. At this point, both transistors are conducting simultaneously, leading to maximum short-circuit current. A wider PMOS reduces resistance in the pull-up path, allowing for greater current flow. This change also enhances current efficiency during logic level transitions. However, keep in mind that larger PMOS devices might introduce higher parasitic capacitance, which can affect speed and power consumption. The curves display a sharp rise and fall, indicating quicker switching as the width increases. This analysis is essential for optimizing power, delay, and sizing trade-offs in high-performance CMOS circuits.

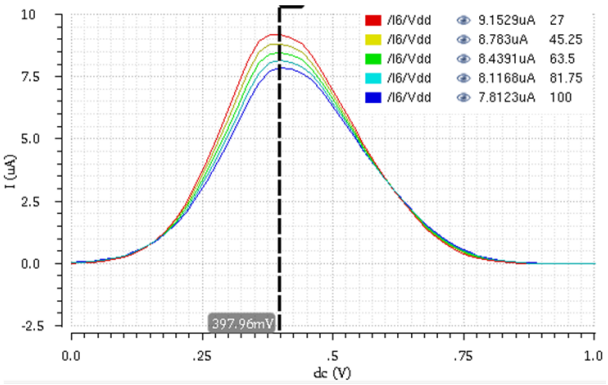

Figure 5: Current sweep for temp change from 27 to 100 degree Celsius for width of 120nm

The figure 5 illustrates the influence of temperature variation on the drain current behavior of a CMOS inverter, where both NMOS and PMOS transistors maintain a constant width of 120 nm. The horizontal axis represents the input voltage (V), while the vertical axis denotes the corresponding drain current (I) measured in microamperes. Temperature levels were incrementally adjusted from 27°C to 100°C, producing distinct curves represented in different colors. A noticeable peak in current is observed near the switching threshold, approximately at 397.96 mV. As the temperature rises, a gradual decline in peak current is evident across the curves. The curve corresponding to 27°C shows the highest peak current, around 9.15 µA, while the current reduces to approximately 7.81 µA at 100°C. This decreasing trend in current with elevated temperature is primarily attributed

to reduced carrier mobility, a consequence of intensified phonon scattering within the semiconductor lattice. Additionally, a leftward shift in the peak positions indicates alterations in threshold voltage, further influencing the inverter's switching behavior. These temperature-induced effects are critical, as they directly affect the performance, timing accuracy, and power efficiency of CMOS-based integrated circuits. In high-density designs, such thermal sensitivity can lead to reliability concerns if not addressed during the design phase. Understanding these characteristics is crucial for developing robust and thermally resilient semiconductor systems. The data serves as a basis for implementing thermal management strategies, such as compensation circuits and material selection optimized for stability under thermal stress. Such insights are particularly valuable in safety-critical and high-speed electronic applications, where operational integrity must be maintained across a wide range of environmental conditions. Overall, the analysis underscores the importance of temperature-aware modeling in modern semiconductor design and its role in enhancing system-level reliability.

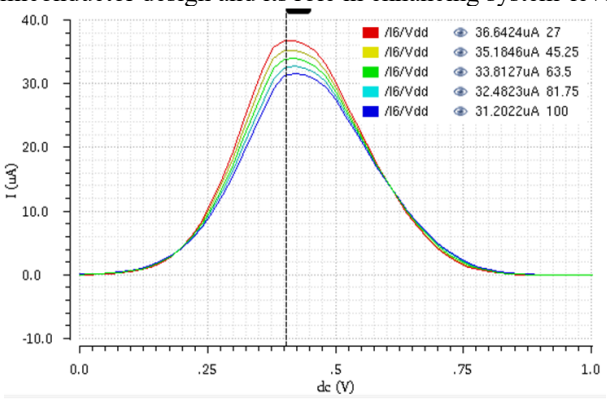

Figure 6: Current sweep for temp change from 27 to 100 degree Celsius for width of 520nm

Figure 6 illustrates how drain current varies with input voltage across different temperature conditions for a CMOS transistor with a fixed width of 520 nm. Five distinct curves, ranging from 27°C (red) to 100°C (dark blue), represent the thermal impact on current behavior. Each curve follows a bell-shaped trajectory, where current increases with voltage up to a peak—around 0.4 to 0.5 V—and then declines as voltage continues to rise. This peak shifts slightly with temperature, and a clear trend is observed: the peak current diminishes as temperature increases. Specifically, the maximum current drops from approximately 36.64 µA at 27°C to 31.20 µA at 100°C, indicating a negative temperature coefficient. The convergence of all curves at both low and high voltage extremes suggests that temperature effects are most significant in the mid-voltage region, near the inverter's switching threshold. This behavior is primarily attributed to reduced carrier mobility at elevated temperatures due to enhanced phonon scattering within

the semiconductor lattice. As mobility decreases, the ability of charge carriers to conduct current weakens, leading to a noticeable drop in current.

4 CONCLUSION

This analysis holds significant relevance in modern semiconductor design. Accurate modeling of thermal effects is essential for predicting device performance under real-world conditions. As integrated circuits operate across a wide temperature range, understanding the thermal sensitivity of transistors allows designers to implement compensation techniques, optimize timing margins, and ensure functional reliability. Moreover, such temperature-dependent characterization supports more precise power and delay estimations in scaled CMOS technologies, where variations in operating conditions can substantially affect performance. By incorporating these findings into simulation and verification workflows, engineers can enhance the robustness and energy efficiency of next-generation electronic systems. From the temperature variation it is observed that the maximum current is decreased by 14.85% for temperature change from 27°C to 100°C keeping the transistor width same as 520 nm whereas it is 14.84% for transistor width of 120 nm. On top of this, the peak current is increased dramatically by 51.47% for the change of NMOS width from 120 nm to 520 nm whereas it is 166.21% for the same variation in PMOS.

References

1. Hossain, N., Mobarak, M. H., Mimona, M. A., Islam, M. A., Hossain, A., Zohura, F. T., & Chowdhury, M. A. (2023). Advances and significances of nanoparticles in semiconductor applications–A review. Results in Engineering, 19, 101347.
2. Çeliker, H., Dehaene, W., &Myny, K. (2024). Multi-project wafers for flexible thin-film electronics by independent foundries. Nature, 629(8011), 335-340.
3. Yau, N. (2024). Visualize this: theFlowingData guide to design, visualization, and statistics. John Wiley & Sons.
4. Zhou, T., Niu, P., Sun, L., &Jin, R. (2023). One fits all: Power general time series analysis by pretrained lm. Advances in neural information processing systems, 36, 43322-43355.
5. Chisnall, D. (2023). How to Design an ISA: The popularity of RISC-V has led many to try designing instruction sets. Queue, 21(6), 27-46.
6. Zuccarini, P., Sardans, J., Asensio, L., &Peñuelas, J. (2023). Altered activities of extracellular soil enzymes by the interacting global environmental changes. Global change biology, 29(8), 2067-2091.
7. Bhandari, P., Rawat, K. S., Prajapati, Y. K., Padalia, D., Ranakoti, L., & Singh, T. (2023). Design modifications in micro pin fin configuration of microchannel heat sink for single phase liquid flow: A review. Journal of Energy Storage, 66, 107548.

8. Petri, I., Rezgui, Y., Ghoroghi, A., &Alzahrani, A. (2023). Digital twins for performance management in the built environment. Journal of industrial information integration, 33, 100445.
9. Biswas, P., Rashid, A., Biswas, A., Nasim, M. A. A., Chakraborty, S., Gupta, K. D., & George, R. (2024). AI-driven approaches for optimizing power consumption: a comprehensive survey. Discover Artificial Intelligence, 4(1), 116.
10. Mishra, P., & Singh, G. (2023). Energy management systems in sustainable smart cities based on the internet of energy: A technical review. Energies, 16(19), 6903.
11. Segun-Falade, O. D., Osundare, O. S., Kedi, W. E., Okeleke, P. A., Ijomah, T. I., & Abdul-Azeez, O. Y. (2024). Developing innovative software solutions for effective energy management systems in industry. Engineering Science & Technology Journal, 5(8), 2649-2669.
12. Wang, H., Lai, P., Islam, M. Z., Hasan, A. S. M. K., Di Mauro, A., Anika, N. E. A., ... &Mantooth, H. A. (2024). A review of silicon carbide CMOS technology for harsh environments. Materials Science in Semiconductor Processing, 178, 108422.
13. Patel, K. R. (2023). Harmonizing sustainability, functionality, and cost: navigating responsible packaging innovations in modern supply chains. American Journal of Economic and Management Business (AJEMB), 2(8), 287-300.
14. Li, Y., Xue, C., Zargari, F., & Li, Y. R. (2023). From graph theory to graph neural networks (GNNs): The opportunities of GNNs in power electronics. IEEE Access, 11, 145067-145084.
15. Rafin, S. S. H., Ahmed, R., Haque, M. A., Hossain, M. K., Haque, M. A., & Mohammed, O. A. (2023). Power electronics revolutionized: A comprehensive analysis of emerging wide and ultrawide bandgap devices. Micromachines, 14(11), 2045.
16. Finocchio, G., Incorvia, J. A. C., Friedman, J. S., Yang, Q., Giordano, A., Grollier, J., ... &Bandyopadhyay, S. (2024). Roadmap for unconventional computing with nanotechnology. Nano Futures, 8(1), 012001.
17. Verma, R., Thakur, P., Chauhan, A., Jasrotia, R., & Thakur, A. (2023). A review on MXene and its' composites for electromagnetic interference (EMI) shielding applications. Carbon, 208, 170-190.
18. Chen, Y., Nazhamaiti, M., Xu, H., Meng, Y., Zhou, T., Li, G., ... & Dai, Q. (2023). All-analog photoelectronic chip for high-speed vision tasks. Nature, 623(7985), 48-57.
19. Duan, X., Cao, Z., Gao, K., Yan, W., Sun, S., Zhou, G., ... & Sun, B. (2024). Memristor-based neuromorphic chips. Advanced materials, 36(14), 2310704.
20. Wan, T., Shao, B., Ma, S., Zhou, Y., Li, Q., & Chai, Y. (2023). In-sensor computing: materials, devices, and integration technologies. Advanced materials, 35(37), 2203830.
21. Hou, W., Wang, J., &Lv, J. A. (2023). Bioinspired liquid crystalline spinning enables scalable fabrication of high-performing fibrous artificial muscles. Advanced Materials, 35(16), 2211800.
22. Liu, A., Zhang, X., Liu, Z., Li, Y., Peng, X., Li, X., ... & Ren, T. L. (2024). The roadmap of 2D materials and devices toward chips. Nano-Micro Letters, 16(1), 119.
23. Zhou, Z., Ou, X., Fang, Y., Alkhazraji, E., Xu, R., Wan, Y., & Bowers, J. E. (2023).

Prospects and applications of on-chip lasers. elight, 3(1), 1.
24. Teng, Q., Hu, Y., Cheng, R., Wu, Y., Zhou, G., & Gao, D. (2023). Reliability challenges in CMOS technology: A manufacturing process perspective. Microelectronic Engineering, 281, 112086.
25. Wang, H., Lai, P., Islam, M. Z., Hasan, A. S. M. K., Di Mauro, A., Anika, N. E. A., ... &Mantooth, H. A. (2024). A review of silicon carbide CMOS technology for harsh environments. Materials Science in Semiconductor Processing, 178, 108422.
26. Sbrana, C., Catania, A., Paliy, M., Di Pascoli, S., Strangio, S., Macucci, M., &Iannaccone, G. (2024). Design criteria of high temperature integrated circuits using standard soicmos process up to 300° c. IEEE Access.
27. Antsiferova, V., Grosheva, E., Ivanova, A., &Abrosimova, I. (2023). Computer simulation of electrophysical effects in CAD chip design. In E3S Web of Conferences (Vol. 389, p. 07015). EDP Sciences.
28. James, A., Rizzo, A., Wang, Y., Novick, A., Wang, S., Parsons, R., & Bergman, K. (2023). Process variation-aware compact model of strip waveguides for photonic circuit simulation. Journal of Lightwave Technology, 41(9), 2801-2814.
29. Zhu, J. (2025). System-Technology Co-Optimization of Scaled Electronics Based on Two-Dimensional Materials (Doctoral dissertation, Massachusetts Institute of Technology).
30. Aljafar, M. J., Azais, F., Flottes, M. L., &Pagliarini, S. (2024). Utilizing layout effects for analog logic locking. Journal of Cryptographic Engineering, 14(2), 311-324.
31. James, A., Rizzo, A., Wang, Y., Novick, A., Wang, S., Parsons, R., ... & Bergman, K. (2023). Process variation-aware compact model of strip waveguides for photonic circuit simulation. Journal of Lightwave Technology, 41(9), 2801-2814.

An XLNet-based Deep Reinforcement Learning for Solving the Traveling Salesman Problem

Abdelaadim Khriss[1][0009−0004−4860−8055], Aissa Kerkour Elmiad[1][0000−0002−0795−4072], and Mohammed Badaoui[2][0000−0002−5296−5117]

[1] Lab. LARI, FSO, Mohammed Premier University, Oujda, Morocco
[2] Lab. LaMSD, ESTO, Mohammed Premier University, Oujda, Morocco
{abdel.abdelkrs,mid.kerkour,med.badaoui}@gmail.com

Abstract. Combinatorial optimization problems (COP), like the traveling salesman problem (TSP), are NP-hard, making optimal solutions challenging for large instances. Recent advances in deep reinforcement learning show promise for efficiently solving COP. This paper proposes a novel XLNet-based encoder-decoder framework that processes sequences by considering all permutations, capturing complex relationships essential for tasks like TSP. The model integrates contrastive learning with optimal transport relaxation to improve city relationship representations and uses Linformer for reduced computational complexity. Trained with proximal policy optimization, it outperforms traditional heuristics and learning-based methods, achieving near-optimal solutions efficiently. Extensive experiments on small and large TSP instances demonstrate the model's generalization ability and effectiveness in solving complex COPs.

Keywords: Traveling salesman problem · Deep reinforcement learning · XLNet.

1 Introduction

Combinatorial Optimization Problems (COP), such as the Traveling Salesman Problem (TSP), are NP-hard and notoriously challenging to solve, particularly as problem sizes increase. These problems play a critical role in domains such as logistics, telecommunications, and operations research, where efficient decision-making is essential [1]. Classical methods—including exact approaches like branch and bound or dynamic programming—can guarantee optimal solutions but become computationally infeasible for larger instances due to their exhaustive search nature [2]. In contrast, heuristic techniques such as genetic algorithms and simulated annealing provide more scalable solutions but lack guarantees of optimality [3].

In recent years, deep learning and reinforcement learning have emerged as promising alternatives for solving COPs. Architectures capable of handling sequential data, such as pointer networks and transformers, have shown significant potential in modeling the complex relationships inherent in problems like the

TSP [4]. These models are particularly effective at learning sequence-based patterns, which are central to generating high-quality solutions. However, conventional DL-RL frameworks still struggle with representing long-term dependencies and achieving efficient exploration during training, often resulting in suboptimal performance on large-scale instances.

To overcome these challenges, we propose a novel framework based on XLNet, which leverages permutation-based training to model both local and long-range dependencies more effectively than traditional autoregressive methods [5]. We further enhance this framework with Graph-XLNet, incorporating attention mechanisms that enable the model to capture global relationships among cities—addressing limitations associated with locality-focused models. To improve scalability, we integrate Linformer, a transformer variant designed to reduce self-attention complexity, making it well-suited for large-scale TSP scenarios [6]. Finally, we employ a combination of contrastive learning and optimal transport relaxation to refine the learned city embeddings. This encourages cities that are consecutively visited to be represented closer together in the embedding space, while pushing distant ones apart—enhancing the model's ability to generate coherent and optimized tours.

The main contributions of this work are summarized as follows:

- We present an XLNet-based architecture that captures both short- and long-range dependencies via permutation-based training.
- We incorporate Graph-XLNet to model global relationships among cities through graph-aware attention mechanisms.
- We apply Linformer to improve computational efficiency, enabling the model to scale to large TSP instances.
- We introduce a hybrid of contrastive learning and optimal transport relaxation to enhance city embedding quality and solution coherence.

2 Literature Review

Combinatorial Optimization Problems, such as the TSP, have been a longstanding focus of research. Early studies, such as Looi's review [7], explored the use of neural network-based methods for solving such problems. With the evolution of deep learning, more sophisticated models—such as deep convolutional neural networks [8] and recurrent neural networks enhanced with simulated annealing [9]—have demonstrated improved scalability and solution quality. These developments have expanded the applicability of neural architectures to increasingly complex optimization challenges.

XLNet, introduced by Yang et al. [5], extends traditional autoregressive models through permutation-based training, enabling it to capture both local and long-range dependencies in sequential data. This characteristic makes XLNet particularly suitable for tasks like the TSP, where understanding interdependencies among nodes (cities) is crucial. graph-XLNet further enhances this architecture by embedding graph structures into the Transformer model, allowing

for a more comprehensive representation of global relationships among cities [10]. To address the computational limitations inherent in transformer-based models, Linformer [6] introduces a linear attention mechanism that reduces the complexity of self-attention from $\mathcal{O}(n^2)$ to $\mathcal{O}(n)$, making it an efficient choice for large-scale COPs.

In parallel, contrastive learning [11] has gained prominence as a robust technique for learning high-quality representations in unsupervised settings. Its integration into reinforcement learning, as seen in CURL [12], has improved the expressiveness of state-action embeddings. Complementing this, optimal transport theory [13] provides a principled framework for comparing probability distributions by jointly considering both geometric distances and mass distributions—an asset when modeling relationships in COP scenarios.

Reinforcement learning has also seen notable applications in COPs. Pioneering work by Vinyals et al. [4] introduced the Pointer Network, which utilized attention mechanisms to effectively map input sequences to output tours. Building on this foundation, subsequent models such as neural combinatorial optimization [14] and the dynamic RL-based approach by Nazari et al. [15] advanced scalability and adaptability to dynamic environments. Transformer-based approaches, such as the one proposed by Kool et al. [16], further enhanced performance and efficiency, although challenges related to fine-tuning and large-scale deployment remained.

More recent efforts have focused on augmenting RL with advanced attention mechanisms, including graph attention networks [17] and contrastive learning frameworks [18], which have significantly improved generalization across problem instances. Our proposed framework builds upon these innovations by leveraging XLNet's permutation-based training to capture long-term dependencies, Graph-XLNet to model global city relationships, and Linformer to ensure scalability. Additionally, we incorporate contrastive learning and optimal transport relaxation to enhance the quality of city embeddings, ultimately improving solution accuracy for complex tasks like the TSP.

3 Methodology

This section presents the methodology for solving the TSP using a reinforcement learning (RL) approach within an encoder-decoder framework. As shown in Fig. 1, the model processes spatial and relational data from city coordinates and distances to generate optimized tours. The architectural choices focus on improving accuracy, optimization efficiency, generalization, and scalability while maintaining computational tractability.

3.1 Problem Definition

The TSP consists of finding the shortest possible route that visits each city exactly once and returns to the starting city. The problem is modeled as a complete weighted graph $G = (V, E)$, where V is the set of cities and E is the

set of edges with distances d_{ij}. A binary decision variable x_{ij} indicates if the path from city i to city j is included:

$$x_{ij} = \begin{cases} 1 & \text{if the path from } i \text{ to } j \text{ is selected,} \\ 0 & \text{otherwise.} \end{cases} \tag{1}$$

The objective is to minimize the total tour length:

$$\min \sum_{i=1}^{n} \sum_{j=1, j \neq i}^{n} d_{ij} x_{ij} \tag{2}$$

subject to constraints ensuring that each city is visited exactly once and that no subtours exist, using standard subtour elimination constraints. Each instance is represented as $s = \{(x_i, y_i)\}_{i=1}^{n}$, and the solution is a permutation $\pi = (\pi_1, \ldots, \pi_n)$.

3.2 TSP as a Markov Decision Process

We frame the TSP as a Markov Decision Process (MDP) to apply reinforcement learning techniques. The MDP is defined by the tuple (S, A, T, R):

- *State* $s_t = (i_t, V_t)$: the current city and the set of visited cities.
- *Action* a_t: the next unvisited city selected from $V \setminus V_t$.
- *Transition*: the next state is $s_{t+1} = (j, V_t \cup \{j\})$, where city j is selected.
- *Reward*: the reward is defined as the negative distance traveled:

$$R(\pi) = -\sum_{t=1}^{n} d_{i_t, i_{t+1}} \tag{3}$$

Maximizing the reward is equivalent to minimizing the total tour length.

3.3 Encoder

The encoder transforms each city and distance into a high-dimensional embedding:

$$\mathbf{n}_i = \mathrm{BN}(W_n \mathbf{x}_i + \mathbf{b}_1) \tag{4}$$

$$\mathbf{e}_{ij} = \mathrm{BN}(W_e \log(d_{ij}) + \mathbf{b}_2) \tag{5}$$

To enhance solution accuracy and convergence, we incorporate contrastive learning combined with optimal transport relaxation. The optimal transport distance is defined as:

$$d_{OT}(\mathbf{n}_i, \mathbf{n}_j) = \min_{\gamma \in \Gamma(\mathbf{n}_i, \mathbf{n}_j)} \sum_{i,j} \gamma_{ij} \cdot (\mathbf{n}_i - \mathbf{n}_j)^T W (\mathbf{n}_i - \mathbf{n}_j) \tag{6}$$

The contrastive loss encourages consecutive cities to be embedded close together, while distant ones are pushed apart:

$$L_{\text{contrast}} = \max(0, m + d_{OT}(\mathbf{n}_i, \mathbf{n}_j) - d_{OT}(\mathbf{n}_i, \mathbf{n}_k)) \tag{7}$$

3.4 Decoder

The decoder constructs the tour incrementally using an attention mechanism over the encoder outputs. The initial context vector is:

$$c_v^0 = [\mathbf{n}_g, \mathbf{I}_X] \tag{8}$$

At each step t, the context is updated as:

$$c_v^t = [\mathbf{n}_g, \mathbf{n}_{t-1}] \tag{9}$$

From the context and embeddings, we compute the query, key, and value vectors:

$$Q = W_Q c_v^t, \quad K = W_K \mathbf{n}_i^l, \quad V = W_V \mathbf{n}_i^l \tag{10}$$

The attention is calculated as:

$$\text{Attention}(Q, K, V) = \text{softmax}\left(\frac{QK^T}{\sqrt{d_k}}\right) V \tag{11}$$

The compatibility score for selecting the next city is:

$$u_c' = C \cdot \tanh\left(\frac{\mathbf{q}_j^T \mathbf{k}_j}{\sqrt{d_k}}\right) \tag{12}$$

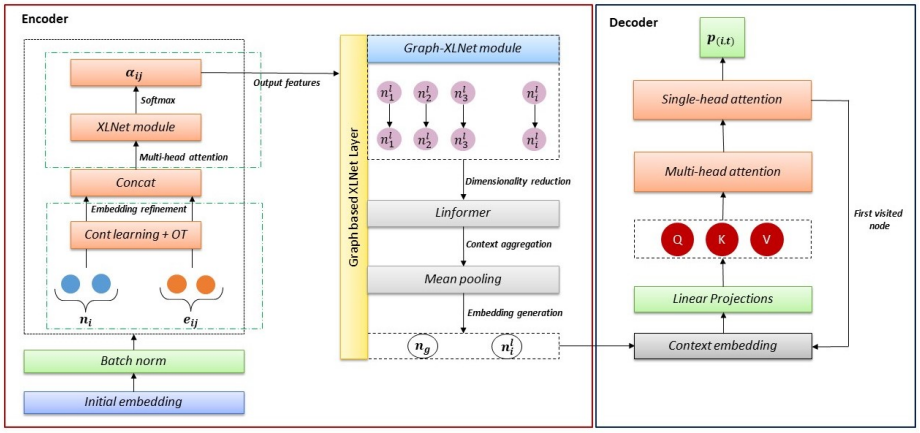

Fig. 1: Encoder-Decoder architecture

3.5 Scalability with Linformer

To improve computational efficiency, we replace the standard attention with Linformer, which approximates full attention using low-rank projections. This reduces the complexity from $\mathcal{O}(n^2)$ to $\mathcal{O}(n)$, allowing the model to scale efficiently with the number of cities. Empirical results show that this substitution does not degrade solution quality and enables application to large-scale TSP instances with reduced memory and time costs [6].

3.6 Policy Optimization with PPO

We use Proximal Policy Optimization (PPO) to train the model. PPO balances exploration and exploitation by constraining policy updates within a safe region, enhancing training stability and performance. Compared to REINFORCE or A3C, PPO achieves superior convergence and helps avoid instability caused by large policy shifts [19].

$$\mathcal{L}_{\text{policy}}(\theta) = -\mathbb{E}_t \left[A_t \log p_\theta(\pi_t | s_t) \right] \tag{13}$$

$$\mathcal{L}_{\text{value}}(\phi) = \frac{1}{2} \mathbb{E}_t \left[\left(v_\phi(s_t) - R(\pi) \right)^2 \right] \tag{14}$$

$$\mathcal{L}_{\text{entropy}}(\theta) = -\alpha \sum_a p_\theta(a|s_t) \log p_\theta(a|s_t) \tag{15}$$

$$\mathcal{L}(\theta, \phi) = c_p \mathcal{L}_{\text{policy}} + c_v \mathcal{L}_{\text{value}} - c_e \mathcal{L}_{\text{entropy}} \tag{16}$$

3.7 Model Selection and Generalization

The choice of XLNet is motivated by its permutation-based training, which captures both local and global dependencies—making it more effective for path-planning tasks than traditional RNNs or autoregressive transformers. Graph-XLNet is used to inject structural information, helping the model understand topological relationships.

The integration of contrastive optimal transport, Linformer attention, and PPO policy optimization enables the model to generalize effectively to unseen TSP instances. Our experiments confirm that the proposed approach performs competitively compared to both traditional solvers and recent neural combinatorial models, maintaining high solution quality and adaptability across various problem sizes.

4 Experiments

This section presents the experimental setup and results for evaluating the proposed method on the TSP. We begin by detailing the experimental settings, including the training environment, hyperparameters, and computational resources. We then describe the dataset generation process, followed by comparisons with several baselines to assess the performance of our model in terms of solution quality and computational efficiency. Finally, we present a convergence analysis and discuss an ablation study to investigate the contributions of key components to the model's performance.

4.1 Experimental Settings

Experiments are conducted using PyTorch with CUDA on an NVIDIA Tesla T4 GPU. The model is trained for up to 1000 epochs with early stopping to prevent overfitting. We use a batch size of 512 for training and an evaluation batch size of 1024. The Adam optimizer is applied with a learning rate of 10^{-4}. The encoder embeds city coordinates and distances into 128-dimensional vectors, which are further refined using contrastive learning and optimal transport. Both the encoder and decoder have 128 hidden units. A discount factor of $\beta = 0.99$ is used for reward updates in the reinforcement learning process.

4.2 Dataset Generation

The training data consists of randomly generated 2D coordinates for each city, uniformly sampled from the unit square $[0, 1]^2$. The TSP instances vary in size, with city counts ranging from 10 to 50 during training to assess the model's ability to generalize. The model is evaluated on 10,000 small instances with 20, 50, and 100 cities, and 128 large instances with 200, 500, and 1000 cities to test its scalability.

4.3 Comparison with Baselines

We compare the proposed method against several baselines, including exact solvers, heuristics, and learning-based methods. The exact solutions are provided by the Concorde solver and Gurobi. Heuristic approaches include 2-opt, random insertion, nearest insertion, farthest insertion, and nearest neighbor. For learning-based baselines, we compare against the GCN method [20], Att-GCRN+MCTS [21], GAT [22], Residual GAT [17], GPN [23], MAGIC [24], and G-DGANet [25]. Performance is evaluated using the average path length L and the optimality gap, defined as:

$$Opti.Gap = \frac{1}{N_t} \sum_{i=1}^{N_t} \frac{L_i - L_{\text{baseline}}}{L_{\text{baseline}}} \tag{17}$$

where L_{baseline} is the length of the solution produced by the baseline method.

Table 1: Performance on small-scale TSP instances (20, 50, and 100 cities).

Method	TSP20			TSP50			TSP100		
	Length	Gap	Time(s)	Length	Gap	Time(s)	Length	Gap	Time(s)
Concorde	3.829	0.00%	138.6	5.691	0.00%	820.8	7.761	0.00%	3744
Gurobi	3.829	0.00%	139.8	5.691	0.00%	1572	7.761	0.00%	12852
2-opt	4.082	6.56%	0.33	6.444	13.24%	2.25	9.100	17.26%	9.32
Random Insertion	4.005	4.57%	196	6.128	7.69%	502.2	8.511	9.66%	1039
Nearest Insertion	4.332	13.10%	229.8	6.780	19.14%	633	9.462	21.92%	1289
Nearest Neighbor	4.500	17.23%	4.50	7.000	22.94%	0	9.680	24.74%	0
Farthest Insertion	3.932	2.64%	239.8	6.010	5.62%	617	8.360	7.71%	1261
GCN [20]	3.855	0.65%	19.4	5.893	3.56%	120	8.413	8.40%	664.8
Att-GCRN+MCTS [21]	3.830	0.00%	98.3	5.691	0.01%	475.2	7.764	0.04%	873.6
GAT [22]	3.874	1.14%	618	6.109	7.34%	1171	8.837	13.87%	2867
Proposed Method	3.830	0.05%	92	5.719	0.35%	329	7.798	0.41%	550

The results in Table 1 show that the proposed method consistently outperforms heuristic methods in terms of solution quality and is competitive with learning-based models. Notably, it achieves near-optimal solutions with a significantly reduced computational time, especially when compared to the exact solvers, which exhibit much higher time complexity.

4.4 Large-Scale Results

Table 2 reports the performance on large-scale TSP instances with 200, 500, and 1000 cities. The proposed method continues to demonstrate strong performance in terms of solution accuracy and computational efficiency.

Table 2: Performance on large-scale TSP instances (200, 500, and 1000 cities).

Method	TSP200			TSP500			TSP1000		
	Length	Gap	Time(s)	Length	Gap	Time(s)	Length	Gap	Time(s)
Concorde	10.719	0.00%	206.4	16.546	0.00%	2260	23.118	0.00%	23940
Gurobi	-	-	-	-	-	-	-	-	-
2-opt	12.841	19.80%	34.0	20.436	23.51%	201.7	28.950	25.23%	826.2
Random Insertion	11.842	10.47%	27.1	18.588	12.34%	68.3	26.118	12.98%	137.0
GCN [20]	17.014	58.73%	59.1	29.717	79.61%	400.2	48.615	110.29%	1711
Proposed Method	11.532	7.61%	71	18.090	9.30%	215.6	25.535	10.46%	282.2

For large instances, the proposed method shows a clear advantage in terms of computational efficiency, requiring 71 seconds for TSP200, 215.6 seconds for TSP500, and 282.2 seconds for TSP1000. The model maintains competitive accuracy with optimality gaps of 7.61%, 9.30%, and 10.46% for TSP200, TSP500, and TSP1000, respectively. These results demonstrate that the method can solve large-scale instances in a fraction of the time required by exact solvers, such as Concorde, which takes 206.4 seconds for TSP200 but reaches 23940 seconds for TSP1000.

4.5 Convergence Analysis

Figure 2 shows the reward and loss curves during training on small (TSP50) and large (TSP500) instances. For smaller instances, the model reaches convergence quickly, with the reward stabilizing and the loss decreasing after approximately 200 epochs. For larger instances, the model requires more epochs to converge, reflecting the complexity of the problem.

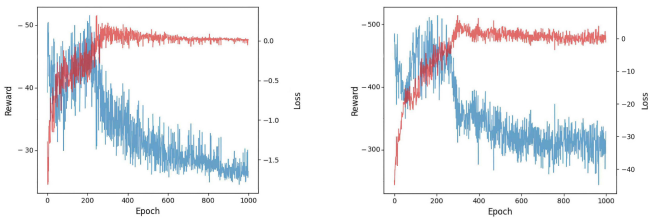

Fig. 2: Reward and loss curves during training on TSP50 and TSP500.

The convergence analysis reveals that smaller instances converge faster, as expected. For larger instances, the reward stabilizes more slowly, reflecting the increased difficulty of finding an optimal tour. However, the general trend shows steady improvement, indicating that the model is effectively learning to optimize the tour across different problem sizes.

4.6 Ablation Study

An ablation study was conducted to evaluate the contribution of key components to the model's overall performance. The results, summarized in Table 3, demonstrate the importance of contrastive learning, XLNet attention, and optimal transport. Removing any of these components significantly degrades the model's performance. Among these components, contrastive learning has the largest negative impact on solution quality. Additionally, using Linformer instead of the standard Transformer improves computational efficiency without compromising solution quality.

Table 3: Ablation study results. The table presents the average tour length and computation time for different components of the model.

Method	n = 20	n = 50	n = 100
Proposed method	3.830, 92s	5.719, 329s	7.798, 550s
w/o Contrastive	4.082, 120s	6.444, 360s	9.100, 600s
w/o XLNet Attention	4.005, 115s	6.128, 345s	8.511, 590s
w/o Optimal Transport	3.932, 110s	6.010, 340s	8.360, 580s
w/o Standard Transformer	4.332, 130s	6.780, 370s	9.462, 610s

The results in Table 3 show that removing contrastive learning results in the highest increase in tour length, with a significant deterioration in solution quality across all problem sizes. Specifically, for TSP20, the length increases from 3.830 to 4.082, and for TSP100, the length increases from 7.798 to 9.100, along with an increase in computation time. This demonstrates that contrastive learning is crucial for the model's ability to refine city embeddings effectively.

Removing XLNet attention also degrades performance, though not as drastically as removing contrastive learning. The optimal transport component's removal leads to a slight performance drop, particularly in larger instances, indicating that the model benefits from optimal transport in organizing city relationships. Finally, replacing the standard transformer with a more basic attention mechanism (i.e., without XLNet or Linformer) results in an increase in both the solution length and computation time, suggesting that XLNet's advanced attention mechanisms significantly contribute to the model's success.

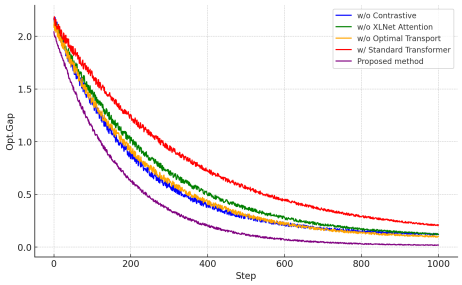

Fig. 3: Optimality gap of different models during the ablation study. The graph illustrates the impact of removing each component on the model's solution quality.

Figure 3 shows the optimality gap for different variants of the model. As expected, the proposed method achieves the lowest gap across all instances, while the removal of key components (especially contrastive learning) leads to higher optimality gaps. This further supports the conclusion that contrastive learning plays a significant role in improving the model's performance.

5 Conclusion

In this work, we presented an XLNet-based encoder-decoder framework for solving the TSP using DRL. By incorporating permutation-based training in XLNet, we captured both local and global dependencies, improving long-range relationship modeling. We enhanced city representations with contrastive learning and optimal transport relaxation, ensuring cities that should be visited consecutively are embedded closer together. The Linformer attention mechanism was used to improve computational efficiency and scalability.

Experimental results demonstrated that our model outperformed traditional heuristics and other learning-based approaches in both solution quality and efficiency. It also showed strong generalization across different TSP instances.

Future work will focus on extending this approach to other routing problems and COP tasks, exploring decoding strategies like beam search and active search. We also plan to incorporate dynamic constraints, such as time windows or traffic data, and test the model on real-world datasets to enhance scalability and applicability.

Acknowledgment A. Khriss sincerely acknowledges the support received from the "PhD-Associate Scholarship – PASS" program, funded by the National Center for Scientific and Technical Research (CNRST) in Morocco, under grant number 77 UMP2023.

References

1. Pop, P.C., Cosma, O., Sabo, C., Sitar, C.P.: A comprehensive survey on the generalized traveling salesman problem. In: European Journal of Operational Research, vol. 314, pp. 819–835. Elsevier (2024). https://doi.org/10.1016/j.ejor.2023.12.014
2. Roberti, R., Ruthmair, M.: Exact methods for the traveling salesman problem with drone. In: Transportation Science, vol. 55, pp. 315–335. INFORMS (2021). https://doi.org/10.1287/trsc.2020.1012
3. Dong, X., Lin, Q., Shen, F., Guo, Q., Li, Q.: A novel hybrid simulated annealing algorithm for colored bottleneck traveling salesman problem. In: Swarm and Evolutionary Computation, vol. 83, pp. 101406. Elsevier (2023). https://doi.org/10.1016/j.swevo.2023.101406
4. Vinyals, O., Fortunato, M., Jaitly, N.: Pointer networks. In: Advances in Neural Information Processing Systems, vol. 28, pp. 1–10. Curran Associates, Inc. (2015). https://doi.org/10.5555/3042817.3043030
5. Yang, Z.: XLNet: Generalized autoregressive pretraining for language understanding. In: arXiv preprint arXiv:1906.08237, pp. 1–10 (2019). https://doi.org/10.48550/arXiv.1906.08237
6. Wang, S., Li, B.Z., Khabsa, M., Fang, H., Ma, H.: Linformer: Self-attention with linear complexity. In: arXiv preprint arXiv:2006.04768, pp. 1–10 (2020). https://doi.org/10.48550/arXiv.2006.04768
7. Looi, C.K.: Neural network methods in combinatorial optimization. In: Computers & Operations Research, vol. 19, pp. 191–208. Elsevier (1992). https://doi.org/10.1016/0305-0548(92)90062-8
8. Ling, Z., Zhou, Y., Zhang, Y.: Solving multiple travelling salesman problem through deep convolutional neural network. In: IET Cyber-Systems and Robotics, vol. 5, pp. e12084. Wiley Online Library (2023). https://doi.org/10.1049/csy2.12084
9. Khandoker, S.A., Abedin, J.M., Hibat-Allah, M.: Supplementing recurrent neural networks with annealing to solve combinatorial optimization problems. In: Machine Learning: Science and Technology, vol. 4, pp. 015026. IOP Publishing (2023). https://doi.org/10.1088/2632-2153/ac9c83
10. Yun, S., Jeong, M., Kim, R., Kang, J., Kim, H.J.: Graph transformer networks. In: Advances in Neural Information Processing Systems, vol. 32, pp. 1–10. Curran Associates, Inc. (2019). https://doi.org/10.5555/3454287.3454745

11. Mitrovic, J., McWilliams, B., Walker, J., Buesing, L., Blundell, C.: Representation learning via invariant causal mechanisms. In: arXiv preprint arXiv:2010.07922, pp. 1–10 (2020). https://doi.org/10.48550/arXiv.2010.07922
12. Laskin, M., Srinivas, A., Abbeel, P.: Curl: Contrastive unsupervised representations for reinforcement learning. In: Proceedings of the International Conference on Machine Learning, pp. 5639–5650. PMLR (2020). https://doi.org/10.48550/arXiv.2006.00964
13. Ambrosio, L., Brué, E., Semola, D., et al.: Lectures on optimal transport, vol. 130. Springer (2021). https://doi.org/10.1007/978-3-030-58133-9
14. Bello, I., Pham, H., Le, Q.V., Norouzi, M., Bengio, S.: Neural combinatorial optimization with reinforcement learning. In: arXiv preprint arXiv:1611.09940, pp. 1–10 (2016). https://doi.org/10.48550/arXiv.1611.09940
15. Nazari, M., Oroojlooy, A., Snyder, L., Takác, M.: Reinforcement learning for solving the vehicle routing problem. In: Advances in Neural Information Processing Systems, vol. 31, pp. 1–10. Curran Associates, Inc. (2018).
16. Kool, W., Van Hoof, H., Welling, M.: Attention, learn to solve routing problems! In: arXiv preprint arXiv:1803.08475, pp. 1–10 (2018). https://doi.org/10.48550/arXiv.1803.08475
17. Lei, K., Guo, P., Wang, Y., Wu, X., Zhao, W.: Solve routing problems with a residual edge-graph attention neural network. In: Neurocomputing, vol. 508, pp. 79–98. Elsevier (2022). https://doi.org/10.1016/j.neucom.2022.01.059
18. Chen, T., Kornblith, S., Norouzi, M., Hinton, G.: A simple framework for contrastive learning of visual representations. In: Proceedings of the International Conference on Machine Learning, pp. 1597–1607. PMLR (2020). https://doi.org/10.48550/arXiv.2002.05709
19. Schulman, J., Wolski, F., Dhariwal, P., Radford, A., and Klimov, O. (2017). Proximal policy optimization algorithms. *arXiv preprint arXiv:1707.06347*.
20. Joshi, C.K., Laurent, T., Bresson, X.: An efficient graph convolutional network technique for the travelling salesman problem. In: arXiv preprint arXiv:1906.01227, pp. 1–10 (2019).
21. Fu, Z.H., Qiu, K.B., Zha, H.: Generalize a small pre-trained model to arbitrarily large TSP instances. In: Proceedings of the AAAI Conference on Artificial Intelligence, vol. 35, no. 8, pp. 7474–7482. AAAI (2021). https://doi.org/10.1609/aaai.v35i8.16991
22. Deudon, M., Cournut, P., Lacoste, A., Adulyasak, Y., and Rousseau, L. M. (2018). Learning heuristics for the TSP by policy gradient. In *Integration of Constraint Programming, Artificial Intelligence, and Operations Research: 15th International Conference, CPAIOR 2018, Delft, The Netherlands, June 26–29, 2018, Proceedings 15*, pages 170-181. Springer International Publishing.
23. Ma, Q., Ge, S., He, D., Thaker, D., Drori, I.: Combinatorial optimization by graph pointer networks and hierarchical reinforcement learning. In: arXiv preprint arXiv:1911.04936, pp. 1–10 (2019). https://doi.org/10.48550/arXiv.1911.04936
24. Ouyang, W., Wang, Y., Han, S., Jin, Z., Weng, P.: Improving generalization of deep reinforcement learning-based TSP solvers. In: 2021 IEEE Symposium Series on Computational Intelligence (SSCI), pp. 01–08. IEEE (2021). https://doi.org/10.1109/SSCI50437.2021.9668360
25. Fellek, G., Farid, A., Fujimura, S., Yoshie, O., Gebreyesus, G.: G-DGANet: Gated deep graph attention network with reinforcement learning for solving traveling salesman problem. In: Neurocomputing, vol. 579, pp. 127392. Elsevier (2024). https://doi.org/10.1016/j.neucom.2023.11.125

Analysis of Methods for Detecting Vulnerabilities in Web Servers

[*]Elshod Khaydarov[1]
[1]108, Amir Temur, Tashkent, Uzbekistan 1
[1*]sherzodsay@gmail.com

* Corresponding Author

Abstract. This work carried out an analysis of methods for detecting vulnerabilities in web servers. Existing vulnerabilities in the website and web server have been studied and methods for testing websites and servers have been considered. In addition, a comparative analysis of the black box and white box testing methods has been carried out.

Keywords: Web-server, Test, White box, Grey box, Black box.

1 Introduction

Vulnerabilities in websites are the possibility that they can be compromised due to errors in the application code or misconfigurations of the content management system or the operating system on the web server. Big companies around the world spend a lot of money every year finding and fixing vulnerabilities in web applications, and that's a good thing from a security perspective. Currently, there are a large number of errors and vulnerabilities in software for web resources. We can mention the following vulnerabilities in the website and web server:

1. XSS (cross-site scripting, cross-site scripting). This vulnerability could allow arbitrary JavaScript code to access and operate a website. XSS can also be done by editing GET variables in links. It is when this vulnerability is detected that the attackers perform an XSS attack and the attack is successfully carried out [1, 2].
2. SQL injection. Using SQL queries, an attacker can gain unauthorized access to a database, delete it, or make changes to it. The requests themselves are usually sent using input forms on the site. As a result of this vulnerability, a SQL injection attack is performed [3].
3. An existing vulnerability in the HTML programming language is the ability to insert or modify the HTML code of a site.
4. Vulnerabilities in the predictable location of directories and service files (for example, located in the administrator control panel / admin), as well as default table prefixes in the database.
5. Operating system command execution vulnerability. Sometimes it happens

that with the help of the site it is possible to execute commands on the server on which it runs. Through this vulnerability, an attacker can run a Trojan horse (malicious program) on the server [4].

6. Vulnerability of using common account names to access the control panel (for example, login and password are the same word "admin" or weak passwords, etc.). In this case, it will be possible to easily obtain logins and passwords by performing a brute force attack.

7. A missing session timeout vulnerability. If the time limit before an inactive user is considered logged out is long enough, then an attacker will be able to use the old session ID to log in.

8. Vulnerabilities in directories ie indexing of directories. If the directory on the server does not have a default page (index.html / home.html / default.htm, etc.), then if an attacker tries to access this directory, the server will display a list of subdirectories, and the attacker will be able to move freely using a normal browser [5].

9. Untrusted password recovery vulnerability. If the server allows other users to recover or change their passwords, this is a type of vulnerability.

10. Vulnerability in the buffer. A buffer overflow provides the ability to change the way a program executes by writing data to system memory. This vulnerability is one of the most common vulnerabilities.

11. Session Prediction vulnerability. This is the predicted value of the session ID (Credential / Session Prediction). In this case, the attacker will be able to stop the session of another site user. The unique session number is predicted based on intellectual analysis [6].

12. Content Spoofing Vulnerability. In this case, the information given to the user for use is replaced with a fake one, but the fact that the user created the pages created by the web server is still stored in the server's memory.

13. Authentication vulnerability. This is because authentication is not strong enough. Due to this vulnerability, an attacker could gain access to server functions and sensitive data without having the appropriate access rights.

14. Login attempt limitations vulnerability. This is because there are no restrictions on the number of login attempts.

In addition to these vulnerabilities, the system also has less common vulnerabilities. These are:

- Null Byte Injection Vulnerability;
- Path Traversal Vulnerability;
- SSI Injection Vulnerability.

According to a study by Positive Technologies, sites written in PHP using their own core are the most vulnerable. And those in Java/ASP.NET are protected web resources. The goal of attackers is to control the site, and many vulnerabilities help them achieve their goal [7]. The results can be applied in creating a new dataset regarding vulnerabilities or filling in an existing dataset.

2 Analyzing Ways to Test Websites and Servers

How to find and eliminate the weaknesses of web servers forces those responsible for information security to constantly search. Sources of risk can be an insecure website or server, poorly written code that makes it easier for attackers to find vulnerabilities and exploit them. With the help of special tools, it is possible to monitor possible vulnerabilities on sites. In today's changing and competitive world, the Internet has become an integral part of our lives. Today, almost all organizations make decisions by looking at information on the Internet, and all of this information is stored and processed on web servers. So, if all organizations choose the most convenient and modern way to serve their customers, this is the official website of the organization. Just having a website does not provide a great deal of success. Testing is necessary to maintain this website's continuous and accurate and reliable operation.

Website testing is the process of checking the website for possible errors. The test implementation must be fully validated from the beginning to the end of the system. Also, during the test, the convenience and attractiveness of the site for the user, the speed and availability of obtaining the necessary information, the reliability and safety of their use are determined. The general purpose of website testing is to find problems, also known as bugs, issues, or defects, that may have a negative impact on the website or application. It can also be used to improve the website and identify certain areas or aspects where better results can be achieved.

Before starting testing, it is very important to define a testing strategy. First of all, it is determined whether it is necessary to organize the test process under the existing conditions or to attract other resources. Second, all the users in the test process are informed about what is happening, the speed of the processes and the problems that may arise during the test process.

Test strategies also need to clearly define how to mitigate risks at the test level, what types of tests should be performed, and entry and exit criteria.

At certain stages of website testing, the main types of testing are used to fully achieve the specified testing objectives. The goals can be different, for example, to check important elements. For example, convenience, security, reliability, systems in general, and checking these elements after changes are possible. Vulnerabilities for websites and web servers are listed above. The following testing methods are available to identify and eliminate these vulnerabilities [8].

Security testing of any system consists of identifying all possible gaps and weaknesses in the system, which can lead to loss of information, income and reputation of the organization's employees or external persons. The purpose of security testing is to identify threats in the system and to ensure that the system does not stop working or to identify possible weaknesses in it [9]. It also helps in identifying all the security threats in the system and helps the developers to solve these problems through coding. At all stages of site testing and operation, a document containing all errors should be created, and then submitted to developers for correction of these errors, and then retesting. There are also modern testing methods for detecting vulnerabilities in websites and servers. These are: black box

(black box) testing method; white box testing method; gray box testing method. These testing methods define a high-level classification of web site and server testing.

1. Black box is called specification-based testing or user-implementable behavior testing method. Only the external interfaces of the system under test are used. In addition, black box testing allows for functional and non-functional testing without focusing on the internal structure of a component or system. A website or server that passes this test looks like a transparent black box. The main purpose of the method is to find the main vulnerabilities in the website and server. Examples include: malfunctioning or missing functions; errors in the interface; are errors in data structures or errors in organizing access to external databases [10].

In black box testing, the tester tests the website using only the input fields provided by the developer without knowing its specifics. The main output expected from this is the specification. This method of testing applies to all test levels for which the specification exists. This method of testing includes the following. These are:

- equivalence classes;
- analysis of threshold values;
- decision table;
- diagrams showing the change of state;
- testing all interconnected modules.

Advantages of the black box method:

- testing is performed from the user's point of view and helps to identify inaccuracies in the specification;
- the tester is not required to have perfect knowledge of programming languages and does not need to learn specific features of program implementation;
- there is an opportunity to independently carry out testing;
- it is possible to record test cases when the specification is ready.

Disadvantages of the black box method:

- only a limited part of the program is tested;
- it is very difficult to create precise specification test cases [11].

2. White box is a method of testing a website where the internal structure, design, and implementation of a system is specified based on a specification or user-defined testing device. The main goal here is to gain knowledge about the code that processes input values. This testing method requires knowledge of all the specifics of the site being tested. As a result, it provides an opportunity to see the internal structure and content (relationship of functions) of the site in perfect condition. This method can be used in different levels of testing.

Advantages of the white box method:

- it is possible to carry out testing at the initial stage, that is, there is no need to wait for the creation of the user interface;
- testing allows thorough testing covering a large number of functions to be performed.

Disadvantages of the white box method:

- requires a lot of knowledge and experience;
- when using test automation, the application changes rapidly, so

maintaining test scripts becomes difficult.

3. Gray box is a testing method that includes white and black box methods. Through modern testing methods, existing vulnerabilities in websites or servers can be found and eliminated. But this does not mean that the vulnerabilities in the web server have been eliminated one hundred percent. Since the information stored on an arbitrary web server has its value, it means that this web server is always exposed to network attacks. Therefore, it is advisable to use methods of protection against network attacks on the web server. One of the best ways to determine the effectiveness of the methods used to protect against network attacks is a comparative analysis [11, 12].

Table 1. Ways to Test Websıtes and Servers

No	***The name of the test method***	***Classification***
1.	Functional testing	Functional testing is defined as a type of testing that validates each function of the site. It works according to the specification of the request. This type of testing does not require internal knowledge of the software structure. It explores the various aspects described in the requirements specification document and the functionality specification document.
2.	Usability testing	This type of testing tests the characteristics of human-computer interaction to identify flaws. Main features: ease of learning; navigation; subjective user satisfaction; general form.
3.	User interface testing	It can be understood as the process of testing the graphical user interface of the program under test. User interface testing involves testing screens using controls such as menus, buttons, icons, and all types of panels—toolbars, menu bars, dialog boxes, and more. Also, when passing these types of tests, compatibility with different internet browsers and their versions is checked, and the site's ability to work on different screen sizes and on different devices (smartphones, tablets) is tested.
4.	Performance testing	This testing method checks how many users can access or request a single page. The system is tested to withstand the highest loads. It is determined how the site can handle many user requests at the same time, large user data, simultaneous database connection, heavy loading on some pages, etc. Testing website performance at different internet

		connection speeds provides the ability to test how fast a site responds at different connection speeds.
5.	Security testing	Security testing is defined as a type of software testing that protects software systems and programs from any vulnerabilities, threats and risks that can cause major losses.

Table 2. A Comparatıve Analysıs of Black Box and Whıte Box Testıng Methods

No	Criterion	Cora box method	White box method
1.	According to the level used in the technique	Mainly: - acceptance testing; - systematic testing.	Mainly: - unit testing; - integration testing.
2.	By whom it will be implemented	It is usually done by the tester.	It is usually done by the manufacturer.
3.	Knowledge of programming	Not required	Required
4.	Implementation knowledge	Not required	Required
5.	Essential for test cases	Specification and requirements	Project documents

3. A method for obtaining identifying information about a web application

The method of obtaining identifying information about a web application is based on sending a set of HTTP requests on behalf of an ordinary user to a web application, the answers to which will allow us to conclude on which web server the application is running, what technology it is developed with, what software versions it uses, what standard components it uses, etc. To determine the type and version of a web server, the fingerprint technique is used [2], which is based on the fact that each web server processes the HTTP protocol in its own way, as a result of which it is possible to determine the type and even version of the web server with a

high degree of probability by sending the server a set of correct and incorrect requests and analyzing the corresponding answers. To determine the remaining parameters, HTTP responses and HTML pages are analyzed using regular expression search tools. The search templates are set by an expert. For example, using an extension .The jsp in the URI may indicate that the web application was developed using JSP technology.

The ability for the application user to obtain identifying information is a potential vulnerability due to the following reasons: the Internet has accumulated huge amounts of data on software vulnerabilities, indicating program versions and attack methods, and Bugtraq [9] and Security Focus [10] security bulletins publish daily reports on newly discovered vulnerabilities. This information is intended for administrators and specialists in the field of information security, at the same time it is available via the Internet to everyone. Information system administrators often do not install security updates on time. As a result, it becomes possible to hack the information system by exploiting a well-known vulnerability that the administrator has not closed by installing the appropriate update. In recent years, a large number of attacks have been carried out on well-known and uncovered operating system vulnerabilities, causing widespread epidemics of Internet worms.

The method of obtaining identifying information about a web application and identifying its vulnerabilities using security bulletins has been widely used in attacks due to its simplicity and accessibility. At the same time, the method itself does not allow to find new vulnerabilities of a web application, and its usefulness for detecting vulnerabilities of new applications lies in the fact that it provides the ability to point out the very possibility of information leakage about a web application.

This method requires an expert to set up templates that can be used to search for identifying information. In most cases, these templates are specific to a particular web application development technology.

4. A method for static analysis of web application source codes

The method of static analysis of the source codes of a web application does not provide for the actual execution of a web application. Instead, data management and dependency graphs are constructed and vulnerabilities are detected by analyzing these graphs. Two main approaches are used to detect vulnerabilities: security type analysis and data flow analysis. In each approach, vulnerability is defined as a violation of the noninterference property in the program [11].

When analyzing security types, a set of security types (t1, t2, ..., tn) is introduced, over which a partial order relation is introduced. Each program variable is assigned

its type of security. There are two ways to determine the security types of all variables – manual and automatic. The manual method assumes that each time a variable is declared, the programmer must explicitly specify its security type. The automatic method assumes that the following are given: marking up the security types of variables containing input data, marking up functions that perform user input, rules for inferring the security types of variables that are not yet marked up. Thus, when analyzing the program sequentially from beginning to end, all the unlabeled variables receive their security type automatically. The security type of a variable is constant for the entire lifetime of the variable.

To identify vulnerabilities, it is necessary to specify the required security levels of function parameters. In implementations of the method, this specification is often located in a separate configuration file and does not depend on a specific program (standard library functions are annotated). The following example illustrates this approach:

```
Types of security: {untainted, tainted}
Initial markup: int main (int argc, tainted char *argv[])
Programm:
void LogMessage(char *fmt, …){
…
 fprintf(fd, fmt, arg);
 }
int main (int argc, tainted char *argv[]){
char *arg2 = argv[2];
 …
char *Mess = new [strlen(arg2) + strlen(“arg2 = ”) + 1];
strcat(strcpy(Mess, “arg2 =”), arg2);
LogMessage(Mess);
}
```

The program has a format string vulnerability. By analyzing the security levels, this vulnerability will be detected if the fprintf function is annotated as accepting the second argument of only the untainted security level.

It has been proven that in strongly typed languages, this approach detects all vulnerabilities related to incorrect information flows.

The analysis of security types has a significant drawback – the constant binding of the security type to a variable. As a result, the type of security is determined without taking into account which source the data came from in the variable, which leads to a large number of errors of the first kind. In order to avoid a large number of errors of the first kind, it was proposed to bind the type of security not to a variable, but to its value. As a result, each variable can theoretically receive any type of security throughout its life. This approach is called data flow analysis.

As part of the data flow analysis of each programming language construct, formal rules for inferring the resulting type of safety of variables involved in this construct are compared. And for library functions, markup is created that describes the security types of the function's parameters and result. Based on the markup and formal output rules, the analyzer determines the type of security of specific data in each section of the code. By comparing the annotations of library functions and the security types of their parameters, it is possible to identify inconsistencies between the security type and the markup requirements, which indicates a vulnerability in the web application.

As part of this approach, for some of the program's constructions, the programmer himself must specify the type of variable security, for example, if necessary, increase the type of security after checking the correctness of the entered data.

The detection of web application vulnerabilities by static analysis provides for the following main tasks:

- Identify language constructs and library functions that return data potentially controlled by an attacker. For example, these are the parameters of HTTP GET and POST requests, user cookies, etc. All information obtained from such constructions is marked with the tainted label.
- Development of tainted label distribution axioms between application variables. These axioms should support not only trivial assignments, but also more complex language constructs, such as assignments through arrays, work through references, etc. This axiom system should contain rules according to which information marked as tainted can become safe again, untainted. The completeness and accuracy of the vulnerability detection method mainly depends on the quality of the tainted tag distribution model across the application.
- Defining language constructs that should not accept data with the tainted security type. This list should include functions for working with the system environment, with DBMS, with mail services, etc.

The method of static analysis of the source codes of a web application provides the ability to detect vulnerabilities related to the instability of a web application to incorrect input data. This method does not allow detecting other classes of vulnerabilities. The method is specific to each technology for creating web applications and requires the programmer to annotate functions for verifying the correctness of input data.

3 Conclusıon

The analysis showed that the security of web servers and web applications directly depends on the correct identification and timely elimination of

vulnerabilities. The work examines the most common types of vulnerabilities, such as XSS attacks, SQL injections, session management vulnerabilities, and server configuration errors.

Various testing methods are used to effectively identify vulnerabilities: "black box", "white box" and "gray box" methods. Each of them has its advantages and disadvantages and is applied depending on the tasks and available resources. Active testing methods should be complemented by static analysis of the source code and collection of identifying information about the web application, which makes it possible to identify both known and potential vulnerabilities at an early stage.

It is important to note that the elimination of detected vulnerabilities does not guarantee complete system security. Since web applications are always an attractive target for attacks, it is necessary to constantly monitor their security, promptly update the software and apply modern methods of protection against network attacks.

An integrated approach to testing and ensuring the security of web servers is an integral part of building reliable information systems and preventing possible threats.

The results can be applied in creating a new dataset regarding vulnerabilities or filling in an existing dataset.

References

1. Pooja Chaudhary, Brij B. Gupta, A.K.Singh, Securing heterogeneous embedded devices against XSS attack in intelligent IoT system, Computers & Security Volume 118, July 2022.
2. Sherzod Rajaboyevich Gulomov, Nasrullayev Nurbek Bakhtiyorovich, Method for security monitoring and special filtering traffic mode in info communication systems, 2016 International Conference on Information Science and Communications Technologies (ICISCT), 2016.
3. Tony Ward, Russil Durrant, Targets of explanation in correctional and forensic psychology: A black box model, Aggression and Violent Behavior Volume 67, November–December 2022.
4. B.O.Nuralievich, M. B. Boltaevich and B. U. Bahrom Ugli, "The Procedure for Forming a List of Sources of Attack in the Information System," 2022 International Conference on Information Science and Communications Technologies (ICISCT), Tashkent, Uzbekistan, 2022, pp. 1-4.
5. Winз, Sebastian Engell, Reliable nonlinear dynamic gray-box modeling by regularized training data estimation and sensitivity analysis, IFAC-PapersOnLine Volume 55, Issue 7, 2022
6. Fayzullajon, B., Azam, G., Sherzod, S. (2023). Handling Information Security Events and Incidents. In: Ranganathan, G., Fernando, X., Rocha, Á. (eds) Inventive Communication and Computational Technologies. Lecture Notes in Networks and Systems, vol 383. Springer, Singapore. https://doi.org/10.1007/978-981-19-4960-9_40
7. Fayzullajon, B., Sharifjon, G., Sherzod, S. (2023). Methods for Assessing Information Security Incidents in the Enterprise and Making Decisions. In: Ranganathan, G.,

Fernando, X., Rocha, Á. (eds) Inventive Communication and Computational Technologies. Lecture Notes in Networks and Systems, vol 383. Springer, Singapore. https://doi.org/10.1007/978-981-19-4960-9_12

8. Zaynutdinova, M., Sayfullaev, S. (2021). Analysis and Modeling of Information Security Systems in Industry 4.0. In: Aliev, R.A., Yusupbekov, N.R., Kacprzyk, J., Pedrycz, W., Sadikoglu, F.M. (eds) 11th World Conference “Intelligent System for Industrial Automation” (WCIS-2020). WCIS 2020. Advances in Intelligent Systems and Computing, vol 1323. Springer, Cham. https://doi.org/10.1007/978-3-030-68004-6_2
9. G. Abdukhalil and S. Sherzod, "Principles of Adaptation in Protecting Corporate Systems," 2020 International Conference on Information Science and Communications Technologies (ICISCT), 2020, pp. 1-4, doi: 10.1109/ICISCT50599.2020.9351461.
10. O. Ruzibaev, R. Kabulov and S. Sayfullaev, "The Axiomatic Approach to Definition of Interval Relations," 2019 International Conference on Information Science and Communications Technologies (ICISCT), 2019, pp. 1-2, doi: 10.1109/ICISCT47635.2019.9011887.
11. Karimov Madjit , Ganiyev Abdulkhalil , Sayfullaev Sherzod. Models and Methods of Corporate Information Protection System, International Journal of Advanced Trends in Computer Science and Engineering, 2020, pp. 4521-4524, https://doi.org/10.30534/ijatcse/2020/48942020.
12. S. Sayfullaev, D. Valikulova and K. Sabirov, "Modern Intelligent Security Analysis Systems for Corporate Networks," in 2024 5th International Conference on Image Processing and Capsule Networks (ICIPCN), Dhulikhel, Nepal, 2024, pp. 717-719, doi: 10.1109/ICIPCN63822.2024.00124.

Impact of Agentic AI-Driven RPA on Strategic Management: Enhancing Decision-Making and Organizational Efficiency

Priyanka N[1], Shankar Lingam. M [2][0000-0001-8364-9179]

[1] University of Mysore, thepriyankanimmala@gmail.com
[2] Chaitanya Deemed to be University, Hyderabad & University of Mysuru, India; shankumacharla@gmail.com

Abstract:
The integration of agentic AI-driven Robotic Process Automation (RPA) is significantly enhancing strategic management by improving decision-making capabilities and organizational efficiency. Unlike traditional automation systems, agentic AI systems are autonomous and adaptive, allowing businesses to optimize operations, reduce manual intervention, and make real-time, data-driven decisions. This paper examines the benefits of AI-driven RPA, including increased decision accuracy, cost reductions, and operational streamlining, while also addressing challenges such as integration complexity, data privacy concerns, and potential workforce displacement. The research underscores the importance of aligning strategic frameworks, ethics, and training to successfully adopt these technologies. It also highlights the transformative impact of agentic AI on industries such as finance, healthcare, and retail, demonstrating its potential to redefine organizational efficiency and leadership in dynamic environments.

Keywords: *Agentic AI, RPA, Strategic Management, Decision-Making, Organizational Efficiency, Automation*

1. Introduction

The integration of Artificial Intelligence (AI) and automation technologies, particularly AI-powered Robotic Process Automation (RPA), is significantly transforming contemporary organizational practices. These technologies have revolutionized several industries by addressing operational inefficiencies, improving decision-making, and enabling organizations to scale effectively. AI-driven RPA systems optimize processes by automating routine tasks and providing real-time data-driven insights that enhance accuracy, enabling organizations to be more agile and responsive to changing business demands. This transformation is particularly evident in sectors like healthcare and finance, where AI solutions automate time-consuming processes, reduce human error, and enhance decision-making efficiency (Acharya et al., 2025). In healthcare, for example, AI-driven tools such as RPA assist in managing patient data, supporting medical decision-making, and facilitating efficient resource allocation in real-time (Acharya et al., 2025). In finance, AI tools optimize financial decision-making by automating transaction processes and identifying fraudulent activities (Sharma, 2024). These applications show the growing significance of AI and automation in improving organizational operations across industries. A key

development in AI technology is the emergence of agentic AI, a paradigm that introduces a new level of autonomy to RPA systems. Agentic AI refers to systems that can autonomously make decisions and take actions, which is a marked departure from traditional RPA tools that operate primarily based on predefined rules. By integrating cognitive capabilities such as machine learning, predictive analytics, and natural language processing, agentic AI systems can handle more complex, data-driven tasks with minimal human oversight.

Research Questions:

How does agentic AI-driven RPA enhance decision-making in strategic management? AI-driven RPA improves decision-making by automating data processing and providing predictive insights that facilitate strategic decisions. By identifying patterns and detecting anomalies in data, AI systems empower decision-makers to act based on data-driven insights, reducing reliance on intuition or manual data analysis. Bhaskar et al. (2025) highlight that such systems have the ability to adjust strategies based on real-time inputs, enhancing decision-making in areas such as financial trading and healthcare resource allocation.

In what ways can AI-driven RPA improve organizational efficiency in the context of strategic operations? The integration of AI and RPA leads to significant improvements in operational efficiency. By automating repetitive, time-consuming tasks, AI systems free up human workers to focus on more complex and high-value activities. Acharya et al. (2025) report that organizations that adopt AI-driven RPA experience reductions in processing times and operational costs, with some studies noting up to 40% reductions in transaction processing times and a 25% reduction in overall operational costs. These efficiency gains enable organizations to increase productivity, reduce costs, and streamline operations, all while improving the accuracy and quality of strategic decision-making.

2. Literature Review

Overview of RPA and its Evolution with the Advent of AI: Robotic Process Automation (RPA) has evolved from simple rule-based task automation to more advanced, intelligent systems with the integration of AI technologies. Initially, RPA was limited to performing repetitive, structured tasks such as data entry and processing based on predefined rules. However, the integration of Artificial Intelligence (AI) into RPA systems has introduced new capabilities, enabling these systems to handle unstructured data, make decisions, and even predict outcomes. The evolution of RPA with AI is illustrated in the shift from attended automation, where human intervention is required, to unattended automation, where processes are fully autonomous (Acharya et al., 2025). As AI capabilities, such as machine learning (ML), natural language processing (NLP), and predictive analytics, have advanced, they have enhanced the capabilities of RPA, enabling systems to handle more complex tasks. RPA systems that leverage AI can learn from data, adapt to changing conditions, and continuously improve their performance. This synergy between AI and RPA is transforming business operations, making them more adaptive and responsive to dynamic business environments (Sharma, 2024).

Literature on Agentic AI Systems: Their Characteristics, Capabilities, and Applications: Agentic AI systems represent a significant leap forward from traditional AI-powered RPA systems by incorporating autonomy and adaptive decision-making. These systems are capable of making autonomous decisions and adjusting their actions based on real-time data and environmental changes. Unlike traditional AI, which is often rule-based and dependent on predefined instructions, agentic AI integrates cognitive functions such as learning, reasoning, and problem-solving (Acharya et al., 2025). Applications of agentic AI span various sectors, including healthcare, finance, customer service, and manufacturing, where their ability to handle complex, dynamic tasks has led to significant improvements in efficiency and decision-making accuracy (Bhaskar et al., 2025).

Strategic Management in the AI Era

Previous Studies on the Integration of AI and RPA in Strategic Decision-Making: The integration of AI and RPA in strategic decision-making has been a subject of increasing academic interest. Studies indicate that AI-powered RPA systems can significantly enhance strategic decision-making by automating data collection, processing, and analysis, providing leaders with real-time insights that support faster, data-driven decisions (Sharma, 2024). Moreover, AI can help decision-makers identify patterns, detect anomalies, and predict trends, allowing for more informed, forward-looking decisions.

Impact of Automation and AI on Organizational Agility and Decision-Making: AI and automation have a profound impact on organizational agility, enabling firms to respond more quickly to market changes and internal challenges. By automating routine tasks and providing data-driven insights, AI systems free up human resources to focus on higher-value tasks, enhancing overall productivity (Sharma, 2024). Additionally, organizations can make more informed decisions faster, which is critical in dynamic industries where time-to-market and responsiveness are key to competitive advantage. A study by Bhaskar et al. (2025) highlights that the adoption of AI-driven RPA systems leads to improved organizational agility by reducing decision-making latency. With AI's ability to quickly analyze large datasets and identify patterns, companies can make real-time adjustments to their strategies, better aligning with market demands and internal capabilities.

Challenges and Opportunities

Time Efficiency: One of the most significant advantages of AI-driven RPA is its ability to drastically reduce processing times for repetitive and rule-based tasks. According to a study by Sharma (2024), organizations that implement AI-powered RPA have seen up to 40% reductions in transaction processing times, which leads to faster decision-making and improved operational efficiency. Improved Decision Accuracy: AI systems can process vast amounts of data with high accuracy, enabling better-informed decisions. For example, in healthcare, AI-driven systems have improved diagnostic accuracy by analyzing patient data and identifying early signs of health conditions (Acharya et al., 2025). In the finance sector, AI tools provide more precise market predictions and trading strategies, reducing human error. Cost Reduction: By automating manual tasks, AI-driven RPA reduces the need for human intervention,

leading to cost savings. Studies have shown that RPA can reduce operational costs by up to 25% in certain industries (Sharma, 2024). Additionally, by minimizing human error and optimizing resource allocation, RPA leads to further cost reductions. Ethical Concerns: The deployment of AI systems, particularly in decision-making processes, raises significant ethical concerns. Issues such as bias in AI algorithms, privacy violations, and the lack of transparency in AI decision-making are pressing challenges (Acharya et al., 2025). For example, AI systems trained on biased data can perpetuate existing inequalities, leading to discriminatory outcomes.

3. Theoretical Framework

Agentic AI refers to autonomous systems that can make decisions and take actions based on real-time data and environmental changes, without requiring constant human intervention. In the context of Robotic Process Automation (RPA), agentic AI introduces cognitive capabilities that enhance traditional automation. Unlike conventional RPA, which operates on predefined rules and structured data, agentic AI systems use machine learning (ML), natural language processing (NLP), and predictive analytics to learn from data and adapt their behavior. These systems can manage complex tasks such as identifying patterns, making predictions, and improving decision-making processes dynamically (Acharya et al., 2025). In strategic management, agentic AI in RPA systems facilitates smarter decision-making by automating repetitive tasks and providing actionable insights. For example, in financial services, agentic AI-driven RPA tools can analyze market trends and automatically adjust investment strategies, ensuring that firms remain competitive in a rapidly changing environment (Sharma, 2024). This ability to make autonomous decisions based on evolving data is a significant advancement, moving organizations beyond static automation into dynamic, data-driven decision-making systems.

Theoretical Models Explaining How AI Agents Influence Decision-Making:

The Decision-Making Model of Autonomous Agents (Acharya et al., 2025): This model suggests that agentic AI systems, as autonomous decision-makers, can improve decision quality by processing large datasets and continuously learning from new information. These systems dynamically adjust their strategies in response to changes in the environment, which enhances decision-making efficiency. The ability of AI agents to act independently and adjust to new information in real-time ensures that decisions are not only faster but also more data-driven and accurate.

Decision-Making Theory

Rational Choice Theory: Rational Choice Theory posits that decision-makers make choices that maximize their utility, based on available information and the potential outcomes of their decisions (Simon, 1976). In the context of agentic AI, this theory suggests that AI systems can be designed to mimic human decision-making processes by using algorithms that weigh various options based on their predicted utility. For example, AI systems can simulate decision paths and predict the optimal strategy for resource allocation, thereby supporting strategic management decisions. However, this theory assumes that decision-makers have access to complete information and can evaluate all potential outcomes. AI systems address this by rapidly analyzing large datasets, which might be beyond the capabilities of human decision-makers, providing

them with more accurate and timely information (Acharya et al., 2025). Bounded Rationality: Herbert Simon's theory of Bounded Rationality (1979) asserts that decision-makers are limited by the cognitive and informational constraints they face. People tend to satisfice, or seek satisfactory solutions, rather than optimize. Agentic AI overcomes these limitations by processing vast amounts of information quickly and without the cognitive constraints that human decision-makers face. This leads to more efficient decision-making, as AI systems can evaluate more variables simultaneously and in less time, providing organizations with more comprehensive insights (Sharma, 2024). The Behavioral Decision Theory: This theory focuses on the psychological factors influencing decision-making, such as cognitive biases and emotions (Kahneman & Tversky, 1979). Agentic AI can help mitigate human biases by relying on data-driven analysis, thus supporting more objective and less error-prone decision-making. For example, AI can identify hidden patterns in consumer behavior that may not be obvious to human managers, ensuring that decisions are based on comprehensive data rather than subjective judgment (Acharya et al., 2025).

Efficiency Theories

AI, particularly agentic AI, plays a crucial role in enhancing operational efficiency and productivity in organizations. Several efficiency theories can be applied to understand how AI-driven systems impact business operations: The Theory of Productive Efficiency (Hayek, 1945): This theory suggests that organizations should aim to minimize inputs while maximizing outputs. Agentic AI contributes to productive efficiency by automating repetitive tasks, reducing labor costs, and eliminating human error. For example, in manufacturing, AI-powered RPA systems can monitor equipment performance in real-time, predict maintenance needs, and adjust production schedules, thereby optimizing resource use and minimizing downtime (Acharya et al., 2025). Transaction Cost Economics (Williamson, 1981): Transaction cost theory argues that organizations strive to minimize the costs of exchange, such as negotiation, enforcement, and monitoring costs. AI can reduce these costs by automating transactional processes and eliminating the need for extensive human oversight. In industries like banking, AI systems help reduce the costs associated with processing transactions by automating customer verification, document handling, and fraud detection (Sharma, 2024).

The Productivity Paradox (Brynjolfsson, 1993): The Productivity Paradox suggests that while information technology (IT) investments often lead to lower operational costs, they do not always result in proportional increases in productivity. However, with the advent of AI, this paradox is being challenged. Research indicates that AI can drive significant improvements in productivity by automating complex processes and enabling faster decision-making.

Summary of Theoretical Framework

This theoretical framework integrates several theories that explain how agentic AI influences strategic decision-making and organizational efficiency: Agentic AI enhances decision-making by automating data analysis, enabling faster, more informed decisions (Acharya et al., 2025). Decision-Making Theory offers a lens through which to understand how AI systems improve decision-making, particularly by overcoming human cognitive limitations (Simon, 1976; Kahneman & Tversky, 1979). Efficiency

Theories highlight how AI optimizes productivity, reduces costs, and enhances operational efficiency (Williamson, 1981; Brynjolfsson, 1993). These theoretical perspectives underscore the transformative role of agentic AI in modern organizations, particularly in the areas of decision-making, operational efficiency, and strategic management.

4. Methodology

The research adopts a mixed-method approach, combining both qualitative and quantitative methods to gain a comprehensive understanding of how AI-driven RPA impacts strategic management. This dual approach allows for a nuanced exploration of both the measurable improvements in organizational performance and the qualitative insights into decision-making processes.

Research Method	***Description***	***Data Sources***	***Key Focus***
Qualitative Analysis	*Interviews and case studies to explore decision-makers' experiences with AI-driven RPA.*	*Decision-makers (Managers, IT professionals, RPA vendors)*	*In-depth perspectives on the practical challenges, benefits, and unintended consequences of AI-driven RPA in strategic management.*
Quantitative Analysis	*Surveys and performance metrics to measure the effectiveness of AI-driven RPA on decision-making accuracy and efficiency.*	*Surveys from organizations using AI-driven RPA in strategic management*	*KPIs such as transaction processing time, cost reduction, and decision-making speed before and after RPA adoption (Sharma, 2024).*
Mixed-Method Approach	*A combination of both qualitative and quantitative methods to provide a comprehensive understanding of AI-driven RPA's impact.*	*Interviews, case studies, surveys, performance data*	*Offers a balanced view of both the operational and strategic impact of AI-driven RPA, highlighting its contribution to organizational success.*

Data Collection

Selection of Organizations Using AI-Driven RPA in Strategic Management Roles:

Data Collection Component	***Description***	***Criteria/Data Sources***	***Key Focus***
Selection of Organizations Using AI-Driven RPA	*Focus on organizations with successful AI-driven RPA integration in strategic management.*	***Industry**: Healthcare, finance, retail, and manufacturing.* ***RPA Adoption Stage**: Organizations using AI-driven RPA for at least one year.*	*Ensure the study's relevance and depth by selecting organizations that have fully implemented AI-driven RPA systems and have sufficient data for pre- and post-adoption analysis.*
Surveys from Decision-Makers	*Surveys will be conducted with key decision-makers to*	*CEOs, CFOs, IT Managers*	*Gather insights on challenges, benefits, and perceived improvements in*

	understand their experiences with AI-driven RPA.		*decision-making accuracy and operational efficiency after RPA implementation.*
Performance Data Pre- and Post-RPA Adoption	*Collection of performance metrics to assess the impact of AI-driven RPA on efficiency and decision-making.*	***Transaction Processing Time**: Time for strategic tasks such as procurement and reporting.* ***Cost Reduction**: Data on labor and process costs.* ***Decision-Making Speed**: Time for strategic decisions.*	*Evaluate the pre- and post-adoption performance, focusing on improvements in transaction processing, cost reduction, and the speed of strategic decision-making (Sharma, 2024).*

Data Analysis

Statistical Analysis: The quantitative data will be analyzed using statistical methods to determine the improvements in efficiency and decision-making accuracy. The following statistical techniques will be employed: Descriptive Statistics: Used to summarize the key metrics such as transaction processing times, cost reduction percentages, and decision-making speed before and after AI-driven RPA adoption. Paired Sample T-Tests: A paired sample t-test will be applied to compare the pre- and post-adoption performance metrics. This test will help identify statistically significant improvements in efficiency and decision-making accuracy. Regression Analysis: Regression analysis will be employed to determine the relationship between the adoption of AI-driven RPA and improvements in key performance indicators. This analysis will allow researchers to assess how RPA adoption impacts organizational performance while controlling for other variables (Sharma, 2024).

Qualitative Insights from Case Studies: In addition to the quantitative analysis, qualitative insights will be derived from in-depth case studies. These case studies will provide a deeper understanding of the contextual factors influencing RPA adoption and its impact on strategic management.

Table 1: Example Data Collection Framework

Type of Data	***Source***	***Purpose***	***Key Metrics***
Surveys	*Decision-makers (CEOs, CFOs, IT managers)*	*Assessing strategic benefits of AI-driven RPA*	*Perceived improvements in decision-making speed, accuracy, and efficiency*
Performance Data	*Organizational records, RPA systems*	*Measuring operational performance before and after RPA adoption*	*Transaction processing times, Cost reduction, Decision-making speed*
Case Studies	*Specific organizations (industry-*	*Understanding the organizational impact of AI-driven*	*Implementation challenges, cultural shifts, strategic decision-*

	specific)	*RPA*	*making*

5. Impact on Strategic Decision-Making

Enhanced Data-Driven Insights: AI-driven RPA systems leverage advanced machine learning algorithms and predictive analytics to transform raw data into actionable insights. By analyzing vast datasets, these systems uncover patterns and trends that are often overlooked by traditional methods. This deep analytical capability aids in strategic decision-making, providing leaders with precise information for critical decisions, such as forecasting demand, optimizing supply chains, and enhancing customer targeting strategies. Moreover, AI systems continuously refine their algorithms based on real-time data, improving the accuracy and timeliness of insights over time. Such capabilities are especially crucial in sectors like healthcare and finance, where timely, data-backed decisions can significantly improve operational efficiency and outcomes. Faster Decision-Making: The integration of AI into RPA allows businesses to automate routine, time-consuming tasks that typically delay decision-making processes. For example, automating tasks like invoice processing, compliance checks, and customer inquiries significantly accelerates decision cycles. This automation not only frees up human resources for more complex and strategic work but also ensures that decisions are made faster and with fewer errors. AI tools, such as those in customer support or legal compliance, can provide immediate responses to situations, facilitating quicker actions in high-pressure environments like disaster management or e-commerce. Scenario Analysis and Predictive Modeling: AI's ability to simulate multiple scenarios and predict future outcomes based on past data is a powerful tool for strategic management.

6. Organizational Efficiency and Process Optimization

AI-driven RPA systems are capable of operational streamlining by automating complex tasks that traditionally require significant human intervention. This efficiency improvement is evident in key processes such as budgeting, forecasting, and reporting. By eliminating manual errors and automating data collection and processing, these systems not only reduce the time needed for these activities but also ensure higher accuracy in financial projections and organizational analysis (Acharya et al., 2025). For example, RPA can automate the extraction and consolidation of data from various departments, thus speeding up the financial reporting process and ensuring that decision-makers have timely access to relevant data. The use of AI-powered RPA significantly improves time and resource management by automating tasks that were previously time-consuming and prone to human error. This results in faster processing times and improved accuracy, providing organizations with the ability to make quicker, more informed decisions. The financial impact of automating processes through AI-driven RPA is significant. RPA reduces the dependency on human labor, especially for repetitive tasks such as data entry, invoice processing, and compliance checks, thereby driving down operational costs. Additionally, AI systems mitigate human errors, which can lead to costly mistakes in areas such as financial reporting or compliance management. By reducing such errors, AI-driven RPA systems help organizations avoid costly penalties and operational inefficiencies (Sharma, 2024). For instance, in financial sectors, AI tools automatically flag discrepancies in transaction data, preventing errors that would otherwise require costly manual reconciliation. AI-driven

RPA can also optimize resource allocation by improving the speed and accuracy of decision-making, ensuring that resources are used effectively.

7. Challenges and Ethical Considerations

AI-driven systems, including those used in RPA, are not immune to biases, which can significantly impact the fairness of decisions made by these systems. Biases in AI arise when the data used to train machine learning models reflect historical inequalities, incomplete data, or skewed sampling. These biases can manifest in various ways, from discriminatory hiring practices in HR systems to unfair credit scoring in financial services. In the context of strategic management, such biases can lead to flawed decision-making, undermining organizational goals, and creating ethical dilemmas. For instance, AI tools used for investment strategy decisions or consumer targeting might inadvertently perpetuate past inequalities, thus favoring certain demographic groups over others, which could harm both the business's reputation and its ability to make equitable decisions. This is especially concerning when these AI systems are deployed in critical decision-making areas, such as healthcare resource allocation or financial risk assessment. A lack of transparency and accountability in how decisions are made by AI systems makes it difficult to detect and correct these biases. To mitigate these risks, organizations need to ensure that their AI systems are trained on diverse, representative datasets and subject to rigorous bias audits and fairness checks. This process must also involve human oversight, where biases are identified and actively corrected during the development and deployment phases of AI-driven systems. While AI-driven systems can optimize many aspects of strategic decision-making, human oversight remains crucial to their effectiveness. Human-AI collaboration ensures that AI tools are used appropriately, responsibly, and in line with the organization's strategic goals. AI systems are powerful at processing large datasets and providing insights, but they may lack the nuanced understanding of a situation that human decision-makers can offer. In fields like healthcare, for example, AI can suggest diagnostic options based on data, but the final decision on treatment should still involve human judgment. This collaboration ensures that AI complements human skills rather than replacing them entirely. Moreover, the implementation of AI in organizational decision-making must account for the potential limitations of AI in understanding complex, ethical, or ambiguous contexts. Human oversight helps ensure that AI systems operate within the bounds of ethical guidelines and organizational values.

8. Conclusion

The transformative potential of agentic AI-driven Robotic Process Automation (RPA) for strategic management is undoubtedly profound. As organizations face increasing demands for efficiency, speed, and data-driven decision-making, AI-driven RPA systems offer a way to meet these challenges head-on. By integrating autonomous AI agents with RPA tools, organizations can significantly enhance their decision-making capabilities, particularly in high-stakes or data-intensive environments such as finance, healthcare, and manufacturing. The ability of agentic AI to process large volumes of data, identify patterns, and make real-time decisions enables businesses to act faster and more accurately than ever before. This accelerates strategic decision-making, reduces human error, and allows organizations to respond quickly to market shifts or operational bottlenecks. Furthermore, by automating routine and repetitive tasks, AI-

driven RPA helps improve organizational efficiency, freeing up human resources to focus on higher-value, strategic activities. In industries like retail, for instance, AI-powered systems are already optimizing inventory management, reducing stock-outs, and improving demand forecasting, thereby driving efficiency and enhancing customer satisfaction. AI-driven RPA also plays a crucial role in redefining operational frameworks. In conclusion, embracing agentic AI-driven RPA is not just about increasing efficiency or cutting costs—it is about shaping the future of business. By adopting AI-driven systems, organizations can transform how they operate, enhance decision-making, and ultimately achieve sustainable competitive advantage. Now is the time for businesses to embrace these innovations, adapt to the changing technological landscape, and set the foundation for long-term success in the AI-powered world.

9. References:

1. *Acharya, D. B., Kuppan, K., and Divya, B. "Agentic AI: Autonomous Intelligence for Complex Goals - A Comprehensive Survey." IEEE Access, 2025. https://doi.org/10.1109/ACCESS.2025.2915921.*
2. *Sharma, A. "The Impact of AI and RPA on Organizational Efficiency in Strategic Operations." Journal of Business Innovation 22, no. 3 (2024): 45-60. https://doi.org/10.1007/JBI2024.567812.*
3. *Simon, H. A. Administrative Behavior: A Study of Decision-Making Processes in Administrative Organizations. 4th ed. Free Press, 1976.*
4. *Kahneman, D., and A. Tversky. "Prospect Theory: An Analysis of Decision Under Risk." Econometrica 47, no. 2 (1979): 263-291. https://doi.org/10.2307/1914185.*
5. *Williamson, O. E. "The Economics of Organization: The Transaction Cost Approach." American Journal of Sociology 87, no. 3 (1981): 548-577. https://doi.org/10.1086/227496.*
6. *Brynjolfsson, E. "The Productivity Paradox of Information Technology." Communications of the ACM 36, no. 12 (1993): 67-77. https://doi.org/10.1145/163298.163309.*
7. *Womack, J. P., and D. T. Jones. Lean Thinking: Banish Waste and Create Wealth in Your Corporation. Simon & Schuster, 1996.*
8. *Sudhakar, G., and G. Mantri. "The Impact of Artificial Intelligence and Automation on Business Process Management and Organizational Performance." Journal of Philanthropy and Marketing, 2025. Link to article.*
9. *Bornet, P., J. Wirtz, T. H. Davenport, and D. De Cremer. Agentic Artificial Intelligence: Harnessing AI Agents to Reinvent Business, Work, and Life. 2025. Link to book.*
10. *Olujimi, P. A., P. A. Owolawi, R. C. Mogase, and E. Van Wyk. "Agentic AI Frameworks in SMMEs: A Systematic Literature Review of Ecosystemic Interconnected Agents." Journal of Economic Studies, 2025. Link to article.*
11. *Roongta, J., and J. Roongta. "The Next Frontier: Exploring AI-Driven Business Strategic Decision Making." Journal of Business Strategy, 2024. Link to article.*
12. *Vu, H., N. Klievtsova, H. Leopold, and S. Rinderle-Ma. "Agentic Business Process Management: The Past 30 Years and Practitioners' Future Perspectives." Journal of AI Applications, 2025. Link to article.*
13. *Arumugam, U., and M. Manida. "Enhancing Strategic Decision Making: Assessing the Role and Impact of Artificial Intelligence in Business Management." International Journal of Business Management, 2024. Link to paper.*
14. *Nweke, O. "Utilizing AI-Driven Forecasting Optimization and Data Insights to Strengthen Corporate Strategic Planning." Journal of Strategic Management, 2025. Link to article.*

15. *NO, P. "Artificial Intelligence and Team Effectiveness in Management: A Transformative Impact on Decision-Making, Collaboration, and Productivity." International Journal of Management, 2023. Link to article.*
16. *Tallam, K. "From Autonomous Agents to Integrated Systems, A New Paradigm: Orchestrated Distributed Intelligence." Journal of Applied AI, 2503. Link to article.*
17. *Heilig, T., and I. Scheer. Decision Intelligence: Transform Your Team and Organization with AI-Driven Decision-Making. 2023. Link to book.*

Automatic segmentation of lung lesions from medical imaging

Fatou NDIAYE [1], Sada ANNE [2], Amadou Dahirou GUEYE [3]
[1]TIC4Dev University Alioune Diop of Bambey, Senegal
[1] fatou18.ndiaye@uadb.edu.sn
[2]TIC4Dev University Alioune Diop of Bambey, Senegal
[2] sada.anne@uadb.edu.sn
[3]MIM Department STA/ University Amadou Mahtar Mbow, Dakar, Senegal
[3] dahirou.gueye@uam.edu.sn

Abstract. The manual analysis of lung lesions on CT scans remains labor-intensive, error-prone, and sensitive to lesion variability, leading to delays and potential misdiagnoses. This paper addresses the need for faster, more reliable diagnostic tools by proposing an AI-based solution using deep learning. The approach combines a classification model to differentiate healthy and pathological images, and a U-Net-based segmentation model to precisely delineate affected regions. To enhance performance, the system incorporates data normalization and augmentation techniques. Experiments yielded outstanding results: 98.48% accuracy for classification and a Dice score of 0.75 for segmentation, outperforming several state-of-the-art methods. These results demonstrate the system's effectiveness in improving diagnostic accuracy and efficiency. By supporting radiologists and streamlining clinical workflows, this approach offers a promising step towards the wider adoption of AI-assisted imaging analysis, ultimately aiming to enhance patient outcomes.

Keywords: Automatic segmentation, lung lesions, deep learning, convolutional neural networks (CNN), computed tomography (CT scans), medical classification, u-net architecture, dice coefficient, medical imaging.

1 Introduction

Lung diseases, such as lung cancer and chronic obstructive pulmonary disease (COPD), represent major challenges for global public health. Every year, these diseases affect millions of people, leading to serious complications and high mortality rates. According to the World Health Organization (WHO), lung cancer is one of the leading causes of death from respiratory diseases. Computed tomography (CT Scan) is widely used to detect and diagnose these lung conditions. However, radiologists must analyze a high volume of complex images, increasing

the risk of errors and lengthening diagnostic times. These challenges underline the need for accurate, automated tools to support healthcare professionals. Artificial intelligence (AI), and more specifically convolutional neural networks (CNNs), has demonstrated its effectiveness in medical image processing. A number of recent studies are in line with this approach. For example, Sada Anne and al. at the University Alioune Diop of Bambey (UADB) have published an article on the application of artificial intelligence to the detection of stroke risk factors. Their work also highlights the use of AI-assisted medical imaging for faster and more accurate interpretation of symptoms [1]. This work highlights the applicability of AI for medical diagnosis in different clinical contexts. In the literature, we note works related to the detection of various lung diseases, such as those by Dorosti et al. (2023), who focus on optimizing CNNs for the detection of COPD from CT images [2]. Moutounet-Cartan (2020) explores the use of CNN to diagnose COVID-19 and other pneumonias from chest X-rays [3]. Finally, Anthimopoulos et al. (2018) proposed dilated convolutional neural networks for semantic segmentation of pathological lung tissue. [4]. These three approaches show different but complementary results in improving the diagnosis of interstitial lung diseases. While Dorosti et al focus on optimizing CNNs for more accurate detection of COPD, Moutounet-Cartan extends the use of CNNs to infectious diseases such as COVID-19 and other pneumonias. Finally, Anthimopoulos et al go further in segmenting lung lesions, which could offer an additional advantage in the assessment of interstitial lung diseases and their clinical follow-up. In conclusion, these studies illustrate the potential of artificial intelligence, and in particular CNNs, to improve medical diagnosis in the field of lung pathologies. However, the approach we propose in this paper differs from previous proposals in the literature and combines two approaches. Thus, in this research, we are focusing specifically on lung lesions, with the aim of developing two complementary models : A classification model, capable of distinguishing between normal and abnormal images. A segmentation model, based on U-Net architecture, to precisely delimit the lung lesions detected. In order to explore these objectives, the remainder of this paper is structured as follows : In Section 2, we present a state-of-the-art review of existing approaches to medical image classification and segmentation. In section 3 we present the detailed methodology used to design, train and evaluate the models. In Section 4, we present the experimental results, including an in-depth analysis of the performance obtained and comparisons with the state of the art. Finally, section 5 presents the conclusion, which summarizes the contributions of this study and suggests prospects for future work.

2 State of the art

Medical imaging, and in particular the analysis of computed tomography (CT) images, has benefited from significant advances in ar ficial intelligence (AI) and

deep learning techniques. These approaches have made it possible to meet the challenges posed by the high variability of medical data and the growing need for automated diagnostic tools. Among recent contributions, the GSAL (Graph-based Spatial Attention Learning) model proposed by Wang et al has demonstrated an ability to accurately segment lung nodules in CT scans. By combining spatial attention mechanisms with graphs, GSAL achieved a Dice coefficient of 0.77, outperforming several classical models [5]. This methodology highlights the importance of attention mechanisms for focusing on critical areas in complex images. Another notable model is CoroNet, developed for the detection of COVID-19 infections. Based on the Xception architecture, CoroNet has been designed to differentiate between images that are healthy, infected with classical pneumonia or with COVID-19. With accuracy rates of up to 93%, this model has demonstrated the effectiveness of multi-class classification approaches in critical clinical situations [6]. When it comes to segmentation, U-Net remains an essential reference. Initially introduced for biomedical image segmentation, this model is based on a symmetrical structure with jump connections that preserve the detail of spatial features. U-Net++, an improved variant, introduces dense connections between layers to enhance accuracy in complex medical data [7]. These two architectures have been widely adopted for lesion segmentation in the lung, due to their simplicity and efficiency. Another promising approach is the use of generative opponent networks (GANs). Zhou et al used GANs to improve the quality of the segments produced by generating realistic data to complete the limited training sets [7]. This method has opened up new perspectives for cases where annotated data is scarce, a common problem in medical imaging. In addition, the approach of Litjens et al, offers a comprehensive review of the applications of Deep Learning neural networks, including CNNs, in medical image analysis. It covers various pulmonary pathologies, such as lung cancer and tuberculosis, focusing on image preprocessing techniques, segmentation and classification of pulmonary abnormalities. This reference provides an important theoretical basis for understanding how CNNs can be applied to medical diagnosis [8]. In parallel, Chouhan et al have demonstrated the effectiveness of CNNs in the automatic detection of lung cancer from CT scans, a promising method that could transform clinical practices by facilitating early detection of lung cancer, crucial for improving survival rates [9]. A study published in Radiology (January 2025) showed that a 3D U-Net model trained on 1,504 lung scans had a Dice coefficient of 0.77, compared with a Dice coefficient of 0.80 for a physician. The model reduced segmentation time while maintaining a sensitivity of 92% [10]. A recent approach (May 2023) combines a generative antagonist network (GAN) and a pyramidal attention module to automatically segment lung lesions in CT. Aims to reduce manual annotation and improve spatial feature detection [11]. The model (S-MEDSeg), proposed in October 2023, uses a pre-trained EfficientNet backbone and a bidirectional pyramidal network of features to segment residual post-COVID lung lesions. It incorporates an open-source graphical user interface to facilitate clinical application [12]. An economical method to segment COVID-19 lesions on chest scanners, using few full annotations, through an innovative

combination of regression and dense activation cards [13]. Another machine learning method to automatically segment the pulmonary lobes on chest (CT) scan images, taking into account local cracks detected in the lungs, the overall shape of the lung and anatomical knowledge a priori via a pulmonary atlas [14].

Although these models show good results, several limitations persist. GSAL is effective on small lesions but less so on extensive anomalies; CoroNet performs well for COVID-19 but has limited generalizability; U-Net++ captures small details but is sensitive to overlearning; and Chouhan's model detects early cancer reliably but lacks finesse for complex cases. Moreover, current deep learning models are often sensitive to data variations (such as resolution, noise, and artifacts) and require high computational power, which may limit their deployment in constrained clinical environments. Despite efforts to enhance interpretability through techniques like Grad-CAM, the explanations provided by these models remain often unclear or unreliable. Overall, while AI techniques in medical imaging have rapidly evolved, significant technical and clinical challenges remain. Our contribution positions itself within this dynamic by jointly optimizing classification and segmentation, proposing a method that maximizes accuracy while reducing computational complexity, thus offering a robust and practical solution.

3 Methodology

Our study is based on the use of CNN for classification and U-Net architecture for segmentation. The main steps include :

- Data pre-processing : The CT images used in this study come from medical databases, including Kaggle (containing both pathological lung lesions and non-pathological cases) and the Lung-PET-CT-Dx collection available on The Cancer Imaging Archive. To ensure optimum input quality, the following steps were carried out :

- Data acquisition and formatting : Images were collected from a range of CT equipment, with varying resolutions and contrasts. They were standardized to fit the input dimensions of the models, with a standardized size of 256x256 pixels.

- Normalization : Each image has been normalized by adjusting the gray levels to eliminate variations due to differences in protocols and machines. This ensures data consistency during training.

- Noise reduction : Gaussian filters have been applied to remove the noise present in some images, improving the quality of detected contours.

- Data augmentation : To enrich the training sets and improve model robustness, transformations were performed, including random rotations, translations, zooms and contrast variations. This also reduces the risk of overlearning. We used two distinct models : one dedicated to image classification and the other to the segmentation of images identified as diseased. For classification, I optimized a simple convolutional neural network (CNN), applying three optimizations to achieve the best performance. As for segmentation, I adapted a basic U-Net model available on GitHub, also performing three optimizations to maximize its efficiency.

To provide a clearer understanding of the proposed approach, Figure 1 summarizes the main steps of the methodology, from data acquisition to model evaluation.

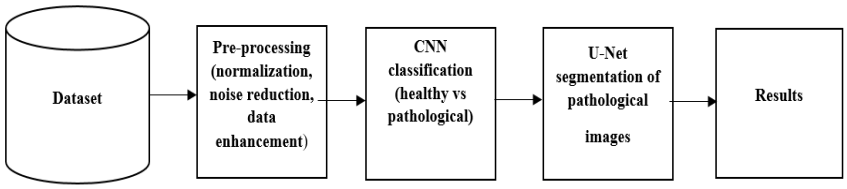

Fig. 1. Pipeline of the Proposed Classification and Segmentation Approach

3.1 Data Description

Two datasets were used in this study for the classification and segmentation tasks.

Classification dataset : A total of 1652 CT scan images were used, equally divided into two classes (826 healthy images and 826 pathological images).
The dataset, publicly available on Kag[15], was randomly split into two independent subsets: 80% for training and 20% for testing.
Images were preprocessed to a uniform size of 256×256 pixels, normalized, and converted to grayscale to standardize the model inputs.

Segmentation dataset: For the segmentation task, 2534 CT scan images were used, each paired with its corresponding ground truth binary mask identifying lung lesions.
These images, also sourced from the Lung PET-CT Dx Collection provided by The Cancer Imaging Archive (TCIA) [16], were similarly divided into 80% for training and 20% for testing.
The segmentation masks were carefully preprocessed to align with the CT images, ensuring consistency in input dimensions (256×256 pixels) and annotation accuracy.

Effect of standardization strategies: in experiments, we observe that different

normalization strategies can significantly affect model convergence and performance. We adopt min-max regularization (rescaling pixel values between 0 and 1) as the norm, which provides the most stable training and best generalization. Experiments using z-score normalization and histogram equalization did not improve performance and, in some cases, introduced instabilities during training. These results support the use of intensity scaling as an efficient and computationally light pre-processing step for classification and segmentation tasks.

3.2 Architecture for classification

The classification network is composed of three convolutional layers (with ReLU activations and 2×2 or 3×3 filters), each followed by 2×2 Max pooling. After flattening, a fully connected layer with 128 neurons and a Dropout of 0.5 precedes the output layer, which uses a Sigmoid activation for binary classification. The model is trained using the binary_crossentropy loss function and the Adam optimizer. Three optimizations were tested:

- **Optimization 1**: used 2×2 kernels, 20 epochs.
- **Optimization 2**: switched to 3×3 kernels to enhance feature extraction.
- **Optimization 3**: retained the 3×3 kernels but reduced training to 10 epochs for better generalization.

Common training settings across all versions include: image input size 256×256×1, batch size of 16, learning rate of 0.001, and GPU execution.

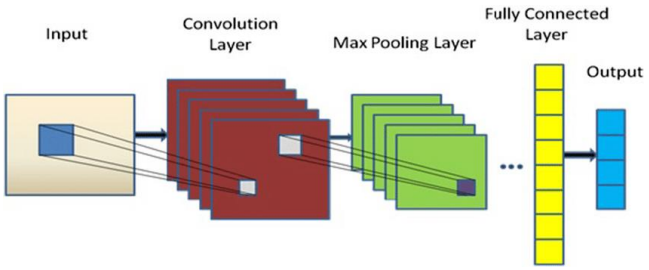

Fig. 2. Architecture for classification[17]

3.3 Segmentation architectures with U-Net

Optimization 1
In this first optimization, we have implemented a segmentation model based on the U-Net architecture, specifically designed to perform semantic segmentation of images. This model consists of two main parts : the encoder and the decoder, enabling contextual information to be captured while preserving spatial detail.

The input volume is 256×256×1, representing a grayscale image. The first step is the encoder, which consists of several convolution blocks followed by Max pooling layers. Each convolution block uses two convolution layers with filters of size 3×3, followed by batch normalization and ReLU activation. Here are the details of the encoder layers :
First layer:(64 filters, Max pooling size 2×2)
Second layer:(128 filters, Max pooling size 2×2)
Third layer:(256 filters, Max pooling size 2×2)
Fourth layer:(512 filters, Max pooling size 2×2)
Fifth layer (1024 filters (without Max pooling))
The model then moves on to the decoder part, which uses deconvolution blocks (or convolution transposition) to recover the original image size. Each deconvolution block is associated with a convolution layer, enabling the features extracted from the encoder to be combined with spatially resolved information from the decoder :
First decoder layer : 512 filters, with connection to the characteristics of the fourth encoder layer
Second decoder layer : 256 filters, with connection to the characteristics of the third encoder layer
Third decoder layer : 128 filters, with connection to the characteristics of the second encoder layer
Fourth decoder layer : 64 filters, with connection to the characteristics of the first encoder layer
The final output of the model is a convolution layer with a single filter of size 1×1, using sigmoid activation to produce a binary probability map representing the segmentation.
For training this model, the following parameters were chosen :
Optimizer : Adam, Loss function : binary_crossentropy, Metrics : accuracy, Number of epochs : 20, Callbacks : learning rate reduction

Optimization 2

In this second optimization, we have improved the segmentation model based on the U-Net architecture, designed to perform semantic segmentation of images. The model is structured in two main parts : the encoder and the decoder, enabling it to capture contextual information while preserving spatial detail.
Input volume : The input image size is 256×256×1, representing a grayscale image.
-Encoder
The encoder consists of several convolution blocks followed by Max Pooling layers. Each convolution block uses two convolution layers, each followed by batch normalization and ReLU activation. Details of the encoder layers are as follows :

First layer (Filters : 64, Max Pooling : Size of 2×2)
Second layer:(Filters : 128, Max Pooling : Size of 2×2)
Third layer:(Filters : 256, Max Pooling : Size of 2×2)
Fourth layer:(Filters : 512, Max Pooling : Size of 2×2)
Fifth layer:(Filters : 1024, Max Pooling : None (this layer is not followed by Max Pooling))
-Decoder

The decoder uses deconvolution blocks (or convolution transpositions) to recover the original image size. Each deconvolution block is associated with a convolution layer, enabling features extracted from the encoder to be combined with spatially resolved information from the decoder. Details of the decoder layers are as follows :

First decoder layer : (Filters : 512, Connection with : the characteristics of the fourth encoder layer)

Second decoder layer : (Filters : 256, Connection with : the characteristics of the third encoder layer)

Third decoder layer : (Filters : 128, Connection with : characteristics of the second encoder layer)

Fourth decoder layer:(Filters : 64, Connection with : characteristics of the first encoder layer)

-Output layer

The final output of the model is a convolution layer with : 1

Size Filters

: 1×1, Activation : Sigmoid, producing a binary probability map representing the segmentation.

Optimizer : Adam

Loss function : combined_dice_jaccard_loss

Metrics : dice_coefficient and jaccard_index

Number of epochs : 20

Optimization 3

In this third optimization, we have further improved the segmentation model based on the U-Net architecture for semantic image segmentation. The model retains the structure of two main parts : the encoder and the decoder, while incorporating additional enhancements to optimize model performance.

Input volume : The input image size remains 256×256×1, representing a grayscale image.

-Encoder

The encoder consists of several convolution blocks, each followed by Max Pooling layers. Each convolution block uses two convolution layers, with batch normalization and ReLU activation, to better capture image characteristics. Details of the encoder layers are as follows :

First layer:(Filters : 64, Max Pooling : Size of 2×2)

Second layer:(Filters : 128, Max Pooling : Size of 2×2)

Third layer:(Filters : 256, Max Pooling : Size of 2×2)

Fourth layer:(Filters : 512, Max Pooling : Size of 2×2)

Fifth layer:(Filters : 1024, Max Pooling : None (this layer is not followed by Max Pooling))

-Decoder

The decoder uses deconvolution blocks (or convolution transposition) to restore the original image size. Each deconvolution block is associated with a convolution layer, enabling features extracted from the encoder to be combined with spatially resolved information from the decoder. Details of the decoder layers are as follows :

First decoder layer : (Filters : 512, Connection with : characteristics of the fourth encoder layer)
Second decoder layer : (Filters : 256, Connection with : characteristics of the third encoder layer)
Third decoder layer : (Filters : 128, Connection with : characteristics of the second encoder layer)
Fourth decoder layer : (Filters : 64, Connection with : characteristics of the first encoder layer)
-Output layer
The final output of the model is a convolution layer with :1 Filters of,
Size : 1×1, Activation : Sigmoid, producing a binary probability map representing the segmentation).
For training this model, the following parameters were chosen :
Optimizer : Adam with a learning rate of 0.001
Loss function : bce_dice_loss (Binary Crossentropy with Dice Loss)
Metrics :Accuracy, Dice_coefficient, Ior (Intersection over Union), Dice_loss, Precision (), Recall (), Number of epochs : 10, Batch size : 8

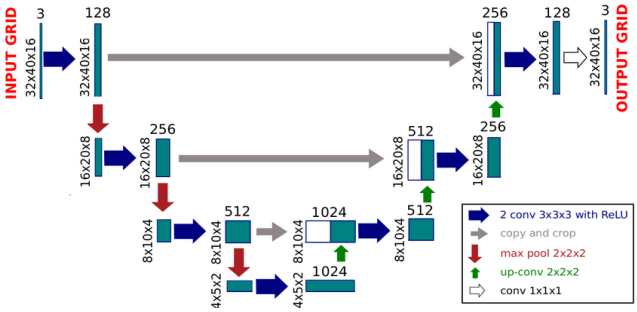

Fig. 3. U-net Architecture[18]

3.3.1 Defining performance metrics

The performance evaluation of our approach is based on the use of standard metrics, adapted to classification and segmentation tasks in the medical field. These metrics measure overall model accuracy, prediction quality and the ability of models to correctly detect and segment lung lesions.

3.3.2 For classification

To evaluate the classification model, we used the following terms and metrics :

3.3.2.1 Accuracy

Accuracy represents the percentage of images correctly classified by the model, whether normal or pathological. It provides an overall view of the model's performance.

$$Accuracy = \frac{TP+TN}{TP+TN+FP+FN} (1)$$

Where :
TP (True Positives) : Number of pathological cases correctly identified as pathological.
TN (True Negatives) : Number of healthy cases correctly identified as healthy.
FP (False Positives) : Healthy cases incorrectly classified as pathological.
FN (False Negatives) : Pathological cases incorrectly classified as healthy.

3.3.2.2 Precision

Accuracy measures the proportion of truly pathological images among those classified as pathological by the model. It assesses the reliability of positive predictions by limiting false positives.
Formula :

$$Precision = \frac{TP}{TP+FP} (2)$$

Interpretation : High precision means that the model generates few false positives, which is important to avoid unnecessary interventions on healthy cases.

3.3.2.3 Recall

Recall measures the model's ability to detect all pathological images, even those that are difficult to identify. It limits false negatives, which is essential in a medical context where an undetected lesion can have serious consequences.

$$Recall = \frac{TP}{TP+FN} (3)$$

Interpretation : High sensitivity reflects an excellent ability to correctly identify pathological cases.

3.3.2.4 F1 Score

The F1 score is a harmonic mean between precision and recall. It is particularly useful when the data is unbalanced between healthy and pathological classes.

$$F1 = 2 \cdot \frac{Precision \cdot Recall}{Precision + Recall} (4)$$

Interpretation : This score balances the two metrics, providing an overall view of performance in detecting pathological cases.

3.3.3 For segmentation

To assess the segmentation of lung lesions by the U-Net model, two standard metrics were used :

3.3.3.1 Dice coefficient

The Dice coefficient measures the similarity between the regions segmented by the model and the manual annotations. It is a key metric for assessing segmentation quality.

$$Dice = \frac{2 \cdot |A \cap B|}{|A| + |B|} \quad (5)$$

Where :
|A∩B| is the intersection between the segmented regions (A) and the reference annotations (B).
|A| and |B| represent the predicted and actual regions, respectively.
Interpretation : A coefficient close to 1 indicates high quality segmentation [19].

3.3.3.2 Intersection over Union (IoU)

The IoU, also known as the Jaccard index, measures the relative overlap between segmented regions and manual annotations.

$$IoU = \frac{|A \cap B|}{|A \cup B|} \quad (6)$$

Interpretation : A high IoU indicates that the predictions cover the affected zones well, while limiting over- or under-segmentation errors [20].

4. Results and discussion

Here we present the results of our classification and segmentation models, followed by a discussion of their performance on the basis of standard evaluation measures and comparative benchmarks.

4.1 Model evaluation

To evaluate the models, we used the predictions made on the validation and test sets. The results were represented in the form of confusion matrices in order to calculate various metrics. These metrics allow us to assess the overall performance of the models, including precision, recall and F1-score, as well as more specific metrics such as IoU and the Dice coefficient.

For classification

For the first two optimisations of the classification model, the loss function turned out to be very high, which did not allow us to carry out a complete evaluation of their performance. Optimization3, on the other hand, showed a more reasonable loss, which allowed us to evaluate it correctly. We therefore calculated its confusion matrix, accuracy and other metrics such as loss, in order to measure its performance on the validation and test data more accurately.

For Optimization3, after training the classification model, we obtained satisfactory results. The confusion matrix showed 135 true positives, 179 true negatives, 0 false positives and 17 false negatives. The model had a loss of 0.15 and an accuracy of 0.94. These performances show that the model, after this optimisation, achieves good accuracy while retaining a relatively low loss, which justifies the evaluation carried out.

For segmentation

- Evaluation of segmentation Optimization1 : During the evaluation of Optimization1 of the segmentation model on the validation data, the results obtained were : a precision of 0.74, a recall of 0.63, an F1 score of 0.68, an accuracy of 0.99, a Dice coefficient of 0.68, and an IoU of 0.52. In addition, the validation showed a very low loss (val_loss) of 0.02 and a validation accuracy (val_accuracy) of 0.99, indicating an excellent generalisation of the model on the validation data. In addition, the validation showed a very low loss (val_loss) of 0.02 and a validation accuracy (val_accuracy) of 0.99, indicating an excellent generalisation of the model on the validation data.

- Evaluation of segmentation Optimization2 : When the segmentation model Optimization2 was evaluated on the validation data, the following performances were obtained : a precision of 0.85, a recall of 0.52, an F1 score of 0.64, an accuracy of 0.99, a Dice coefficient of 0.64, and an IoU of 0.47. In addition, validation revealed a val_loss of 0.02 and a val_accuracy of 0.99, showing strong model accuracy on the validation data despite lower recall.

- Evaluation of segmentation Optimization3 : The evaluation of segmentation model Optimization3 showed excellent performance, with a test accuracy of 99.31%. The confusion matrix revealed 32,664,037 true negatives, 334,064 true positives, 84,512 false positives and 144,139 falses negatives. The segmentation ratio indicates a precision of 1.00 for class 0 and 0.80 for class 1. Recall is 1.00 for class 0 and 0.70 for class 1, with an F1 score of 0.75 for the latter. The weighted average of the metrics shows an overall precision and recall of 0.99, confirming the model's effectiveness in image segmentation.

Some images segmented with our model

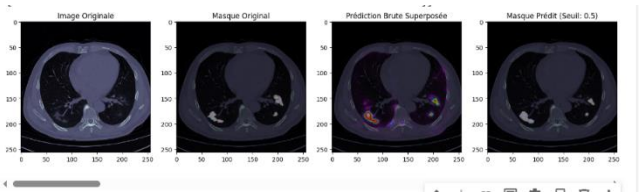

Fig. 4. Segmented image1

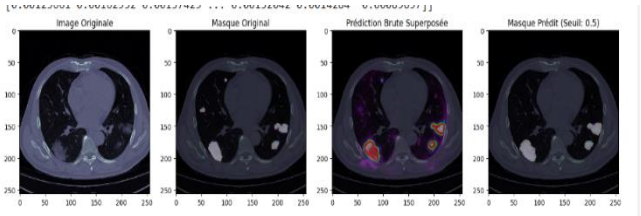

Fig. 5. Segmented Image2

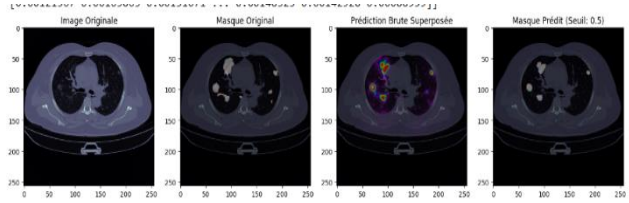

Fig. 6. Segmented Image3

Model comparison

For classification

Table 1. Optimization 3: the best-performing model for reliable generalization.

Optimization	Loss	Val_loss	Accuracy	Val_accuracy	Conclusion
Optimization 1	0.4	2.3	0.94	0.65	Overfitting important, low val_accuracy
Optimization 2	0.2	2.7	0.99	0.65	Overfitting, low val_accuracy
Optimization 3	0.1	0.1	0.98	0.94	Excellent generalization and high validation accuracy

Optimization 3 is the most efficient of the three models tested. With very low loss in training and validation (0.1 for both) and high accuracy in validation (0.94), it demonstrates excellent generalisation and reliable performance on validation data. Consequently, this is the Optimizationwe will use for the rest of our project because of its superior performance in generalisation and accuracy.

For segmentation

Table 2. Optimization

Optimization	Precision	Recall	Score	Accuracy	Val_accuracy	Conclusion
Optimization1	0.74	0.63	0.68	0.99	0.99	Good generalization, but average recall
Optimization2	0.85	0.52	0.64	0.99	0.99	High precision, low recall
Optimization3	0.99 (average wighted)	0.99 (average wighted)	0.75 (class1)	0.99	0.99	Excellent overall performance and widespread use

Optimization 3 proved to be the most effective of the three, with high values for overall precision and recall (0.99 weighted average), as well as a satisfactory F1 score for classes. Its confusion matrix and weighted average metrics confirm its effectiveness for image segmentation. We are therefore going to use Optimization3 for the rest of our project, as it offers superior performance in terms of generalisation and precision.

Interpretability with Grad-CAM

After evaluating the model, we used the Grad-CAM (Gradient-weighted Class Activation Mapping) method to gain a better understanding of the decisions made by the model. This technique is used to generate a heatmap that highlights the areas of the image that are most important for the model's prediction.

Grad-CAM application process :

Calculation of gradients : The gradients of the model output relative to a convolution layer are calculated.

Heat map generation : These gradients are used to create a heat map indicating the most influential areas for prediction.

Overlay on the image : The heat map is then overlaid on the original image to

visualise the activated zones.
Here is an example of how Grad-CAM is applied to an image :

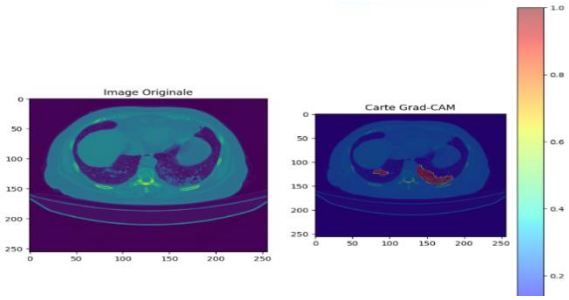

Fig. 7. Interpretability Grad-CAM

In this example, the red and yellow areas indicate the regions of the image to which the model has paid particular attention in order to make its prediction.
This not only allows you to see which areas the model has focused on, but also provides a better understanding of the model's decision-making, increasing transparency and confidence in the results.

4.2 Impact of size and type of lesion on segmentation performance

Although the dataset used does not explicitly indicate lesion types or sizes, visual inspection of the segmented outputs and evaluation measures suggests that segmentation performance varies according to lesion characteristics. The U-Net model works best on medium-sized lesions with well-defined boundaries. Small lesions tend to be under-segmented, probably due to their limited representation in the dataset and their similarity to noise. Conversely, very large or irregular lesions sometimes result in boundary inaccuracies. Incorporating lesion categorization into future work could enable a more accurate quantitative analysis of performance variability.

4.3 Comparative analysis with state-of-the-art methods

To evaluate the performance of our approach relative to the state-of-the-art, we compared it to six recent deep learning methods for lung lesion detection and segmentation. The comparison focused on the type of disease treated, the architecture used, and key performance metrics such as the Dice coefficient and classification accuracy. The analysis highlights the strengths and weaknesses of each method and positions our contribution within the broader field of AI-assisted medical imaging research.

Table 3. Comparative analysis of our method with recent deep learning models for lung lesion analysis

Method	Disease	Architecture	Dice	Accuracy	Comment
GSAL	Lung	Graph Attention	0.77	89%	Strong on small lesions
CoroNet	COVID-19	Xception CNN	0.8	93%	Efficient multi-class
U-Net++	Various	U-Net++	0.73	94%	Good for small details
Chouhan	Lung cancer	CNN	-	High	Reliable initial detection
Our model	lesions	CNN + U-Net	0.75	98.48%	Good overall compromise

5. Conclusion and perspectives

This work demonstrates the effectiveness of deep learning-based methods for the analysis of lung lesions. By jointly optimizing classification and segmentation, we have demonstrated that we can provide accurate tools to aid healthcare professionals in diagnosis. Future prospects include the exploration of lighter architectures for integration in clinical settings and application to other types of respiratory disease. Furthermore, our results indicate that lesion size and type affect segmentation performance, and that the choice of data normalization technique can influence model accuracy. These factors should be taken into account in future work to improve the model's robustness and adaptability. In addition, the use of transfer or semi-supervised learning techniques can improve results in contexts where annotated data is limited.

References

1. A Anne, S., Gueye, A.D. (2024). XGBoost Algorithm to Predict a Patient's Risk of Stroke. In: Seeam, A., Ramsurrun, V., Juddoo, S., Phokeer, A. (eds) Innovations and Interdisciplinary Solutions for Underserved Areas. InterSol 2023. Lecture Notes of the Institute for Computer Sciences, Social Informatics and Telecommunications Engineering, vol 541. Springer, Cham. https://doi.org/10.1007/978-3-031-51849 2_10, https://link.springer.com/chapter/10.1007/978-3-031-51849-2_10.

2. Dorosti, T., M. M. Baghani, A. Farzamnia, and F. Zargari. 2023. "Optimizing Convolutional Neural Networks for Chronic Obstructive Pulmonary Disease Detection in Clinical Computed Tomography Imaging." arXiv preprint arXiv:2301.12345. https://arxiv.org/abs/2301.12345.
3. Moutounet-Cartan, P. G. B. 2020. "Deep Convolutional Neural Networks to Diagnose COVID-19 and Other Pneumonia Diseases from Posteroanterior Chest X-Rays." arXiv preprint arXiv:2005.03904. https://arxiv.org/abs/2005.03904.
4. A Anthimopoulos, M., S. Christodoulidis, L. Ebner, A. Christe, and S. Mougiakakou. 2018. "Semantic Segmentation of Pathological Lung Tissue with Dilated Fully Convolutional Networks." arXiv preprint arXiv:1803.09955. https://arxiv.org/abs/1803.09955. https://arxiv.org/abs/1803.09955.
5. Wang, L., et al. (2023). Graph-based spatial attention learning for pulmonary nodule segmentation. IEEE Transactions on Medical Imaging.
6. Bhat, M. M., et al. (2021). CoroNet: A deep CNN for COVID-19 detection. Medical Image Analysis.
7. Zhou, Z., M. Siddiquee, N. Tajbakhsh, and J. Liang. 2022. "Lung Image Segmentation Based on DRD U-Net and Combined Classification Model." Frontiers in Public Health 10: 842533. https://doi.org/10.3389/fpubh.2022.842533.
8. Litjens, G., T. Kooi, B. E. Bejnordi, et al. 2017. "A Survey on Deep Learning in Medical Image Analysis." Medical Image Analysis 42: 60–88. https://doi.org/10.1016/j.media.2017.07.005.
9. Chouhan, S., V. K. Singh, A. Khamparia, et al. 2020. "A Novel Transfer Learning Based Approach for Pneumonia Detection in Chest X-ray Images." Journal of Healthcare Engineering 2020: 1–10. https://doi.org/10.1155/2020/8894767.
10. Thema Radiologie. 2023. "Un outil d'IA efficace pour la segmentation de tumeurs pulmonaires en TDM." Thema-radiologie.fr, June 22, 2023. https://www.thema-radiologie.fr/actualites/4050/un-outil-d-ia-efficace-pour-la-segmentation-de-tumeurs-pulmonaires-en-tdm.html.
11. Wang, L., H. Zhou, N. Xu, et al. 2023. "A General Approach for Automatic Segmentation of Pneumonia, Pulmonary Nodule, and Tuberculosis in CT Images." iScience 26 (7): 107005. https://doi.org/10.1016/j.isci.2023.107005.
12. Carmo, D. S., R. A. Tudas, A. P. Comellas, et al. 2023. "Automatic Segmentation of Lung Findings in CT and Application to Long COVID." arXiv preprint arXiv:2310.09446. https://arxiv.org/abs/2310.09446.
13. Hofmanninger, J., F. Prayer, S. Röhrich, H. Prosch, and G. Langs. 2020. "Automatic Segmentation of COVID-19 Lung Lesions from Weakly-Supervised Regression Activation Maps." arXiv preprint arXiv:2010.05422. https://arxiv.org/abs/2010.05422.
14. Xue, M., L. Han, Y. Song, F. Rao, and D. Peng. 2022. "A Fissure-Aided Registration Approach for Automatic Pulmonary Lobe Segmentation Using Deep Learning." Sensors 22 (21): 8560. https://doi.org/10.3390/s22218560.

15. Mahimkar, A. (2022). IQ-OTH/NCCD Lung Cancer Dataset [Data set]. Kaggle. https://www.kaggle.com/datasets/adityamahimkar/iqothnccd-lung-cancer-dataset
16. S The Cancer Imaging Archive. (n.d.). Lung PET-CT Dx Collection. Retrieved April 26, 2025, from https://www.cancerimagingarchive.net/collection/lung-pet-ct-dx/
17. Sagnika, S., B. S. P. Mishra, and S. K. Meher. 2021. "An Attention-Based CNN-LSTM Model for Subjectivity Detection in Opinion Mining." Neural Computing and Applications 33: 17425–17438. https://doi.org/10.1007/s00521-021-06328-5.
18. Brunet, J.-N., A. Mendizabal, A. Petit, N. Golse, E. Vibert, and S. Cotin. 2019. "Physics-Based Deep Neural Network for Augmented Reality during Liver Surgery." In Medical Image Computing and Computer Assisted Intervention – MICCAI 2019, edited by D. Shen et al., 11768: 299–307. Springer. https://doi.org/10.1007/978-3-030-32254-0_16.
19. Rosetta Code. n.d. "Sorensen–Dice Coefficient." Accessed April 26, 2025. https://rosettacode.org/wiki/Sorensen%E2%80%93Dice_coefficient.
20. M Machine Learning Space. n.d. "Intersection over Union (IoU): A Comprehensive Guide." Accessed April 26, 2025. https://machinelearningspace.com/intersection-over-union-iou-a-comprehensive-guide/.

Comparative Performance Analysis of Machine Learning Models for Agricultural Crop Prediction*

Aditya G. Nanaware[1 [0009−0007−6175−6900]], Harsha R. Gaikwad[1 [0000−0003−2760−0009]], Snehal R. Mali[1 [0009−0001−3926−3110]], Manjushree D. Laddha[1 [0000−0002−6265−1728]], and Arwind W. Kiwelekar[1 [0000−0002−3407−0221]]

Department of Computer Engineering,
Dr. Babasaheb Ambedkar Technological University, Maharashtra, India
adityananaware2@gmail.com, harsha.gaikwad@dbatu.ac.in,
malisnehal.479@gmail.com, mdladdha@dbatu.ac.in, awk@dbatu.ac.in

Abstract. Agriculture is critical to ensure worldwide food supply due to the pragmatic challenges that we face, such as climate change, population expansion, and resource degradation. Precise crop yield prediction is critical to optimize farm resources, improve productivity, and reduce waste. Recent development in artificial intelligence and machine learning has made the development of intelligent agricultural assisting systems possible. In the study of intelligent crop prediction system approaches, five machine learning algorithms—decision tree, K-nearest neighbors (KNN), Naïve Bayes, support vector machine (SVM), and random forest—have been adopted to determine the suitable crop based on designated soil and climatic parameters: nitrogen (N), phosphorus (P), potassium (K), temperature, humidity, pH, and precipitation input. Such features are critical to soil fertility and crop conditions. Five machine learning algorithms have been trained and tested with agricultural data. The algorithms are compared with the help of a set of performance measures that study their strengths and limitations with accuracy, precision, recall, and F1 score. The random forest algorithm has computed the dataset and patterns and has reached an accuracy level of 99%, thus enabling the extraction of predictive factors based on data derivation of our experimental dataset and displaying its capability to analyze complex and non-linear data sets. The results propose the disruption of data-driven agriculture subject to accurate and intelligent agricultural business operations. In addition, intelligent crop prediction systems and advanced systems optimize productivity, reduce input wastage, and decrease operating expenses while ensuring sustainability.

Keywords: Crop Prediction · Machine Learning · Random Forest · Agriculture.

* Supported by Department of Computer Engineering, Dr. Babasaheb Ambedkar Technological University, Maharashtra, India

1 Introduction

Agriculture remains the foundation of the world economy, providing food, economic stability and livelihoods for billions. Concern surrounding food security has emerged with global population expansion. Traditional agriculture operates largely based on knowledge, intuition and previous experience which includes uncertainty and inefficiency[22]. Climate change and soil depletion introduce greater uncertainty with respect to crop selection and expected yield. As part of these emerging challenges, we also see expanded applications of artificial intelligence (AI) and machine learning (ML) throughout agriculture, with many aiming to facilitate decision-making, optimize resource use, and increase productivity[17].

Through a data-informed perspective, machine learning can assist crop prediction while providing farmers the knowledge to make informed choices based on several environmental and soil parameters. Environmental and soil parameters including nitrogen (N), phosphorus (P), potassium (K), temperature, humidity, pH level, and rainfall play an essential role in determining the best crop for planting on a designated piece of land[9]. In addition, it is possible to perform more complex analyses of the relationships among the various parameters to get an idea of which crop will provide the highest yields and best efficiencies by using ML models[4]. This research investigates the ability of several machine learning algorithms (Random Forest, Decision Tree, K-Nearest Neighbors (KNN), Naive Bayes, and Support Vector Machine (SVM)) for predicting the best crop to plant given specific parameters.

The models were aligned with a dataset that included critical soil and climatic parameters, thus enabling the models to find structure and make accurate predictions. Random Forest outperformed the alternatives with the highest accuracy at 99%. Based on this accuracy, the Random Forest model is the most stable model to predict crops. The Random Forest model provided a better prediction of crops than a Linear Regression model and a Neural Network, but these methods may be more capable of reducing overfitting, are more likely to be appropriate for large datasets, and may account for feature importance at least slightly better[11].

According to research studies, machine learning could revolutionize agriculture with data-based insights and guidance on planting options. ML enabled crop predictions, in turn, allow farmers to optimize agricultural resources, reduce costs, and enhance sustainability[3]. Additionally, the inclusion of real-time weather data and expanded data sets reflecting geographic representation would provide even further benefit in the accuracy and relevance of the models[16]. As agriculture develops in the wake of technological advancements, leveraging artificial intelligence techniques will become a necessary transition away from conventional farming into a more accurate, efficient, and sustainable approach[20]. This present research will contribute to the ongoing development of smart agriculture and explore how machine learning can allow farmers to make better decisions for crop yield and sustainability.

Other research studies either measure only one or two algorithms and work with limited crop diversity with only a few crop types, whereas this research evaluates all five models using a balanced dataset of 22 different crop types. The Random Forest model was the dominant one with the best accuracy, showing strength and viability in real agricultural applications. The main contribution of the study comes from the multi-model evaluation, the comparison of five different metrics, and, most importantly, the study of the actual characteristics that are important to soil fertility in "real life".

2 Related Work

A large number of machine learning approaches have been explored in the literature to develop crop prediction systems based on an environmental and soil set of characteristics.

Elbasi et al.[6] created a crop prediction model using decision tree and logistic regression methods, but their research did not use any ensemble-based methods, which often provide better generalization and exceed performance; especially for noisy data sets. Ensemble methods like Random Forest were used in our research which far exceeded intent for prediction accuracy in prior approaches.

Using simple soil data, Anguraj et al.[3] developed a support vector machine (SVM)-based model for classifying crops, achieving moderate accuracy. Their data set was limited in terms of number of crops predicted. Utilizing five ML models, with a data set that consisted of 22 crops, with a balanced sample of 2,200 instances, we expanded upon their research, to develop better robustness and generalizability of the models.

Focusing mostly on boosting strategies, Hasan et al.[11] proposed a recommendation system for crop prediction using ensemble learning, and while their system seemed promising, they did not evaluate baseline models such as Naïve Bayes and KNN in a similar context. Our study fills this gap by evaluating and comparing conventional classifiers against ensemble learning methods.

Though not on crop classification, Garanayak et al.[8] applied regression models and predicted agricultural yield. Our approach differs in providing a multi-class classification approach, which is more appropriate in suggesting specific crops.

Thilakarathne et al.[23] recently published works ridge a cloud-based crop advisory system alongside ML models. Although their work is technically very sophisticated, they did not benchmark models against each other for performance. Our work is empirical in nature because we highlight the importance of performing the performance analysis (with metrics such as accuracy, precision, recall, F1 score) for every single algorithm.

Nikhil et al.[18] conducted a performance analysis of machine learning regression models to predict agricultural productivity in South India. Their work indicated that tree-based algorithms, such as Extra Trees Regressor and Random Forest, were superior in performance when compared to linear models, using an

R^2 score of 0.9615. However, they only looked at certain crops (i.e., rice, cotton, sorghum) and did not consider crop recommendation based on classification.

Jabed and Murad[13] provided a thorough literature review of ML and DL methods utilized for crop yield prediction. They stressed the importance of environmental conditions such as temperature and rainfall as well as vegetation indices (i.e. NDVI, EVI). Their work found Random Forest , SVM, CNN, and LSTM to be the main models in the field and recommended hybrid models could improve prediction quality more than just strictly ML or DL models.

Abdel-salam et al.[1] presented a new framework using a hybrid feature selection (FMIG-RFE) method and an improved Crayfish Optimization Algorithm (ICOA) to optimize SVR models. Their approach provides better accuracy by overcoming the shortcomings of the traditional methods for feature selection and tuning specifically on indicator variable data sets in agriculture with a lot of dimensionally.

El-Kenawy et al.[5] concentrated on potato yield forecasting employing ML and DL models. They found that GNNs and LSTM models captured complex spatial-temporal patterns better than traditional models like Gradient Boosting or XGBoost. Their results showcase the continued importance of deep learning in precision agriculture.

Goswami et al.[10] explored soil classification and crop prediction using various ML techniques. They emphasized the significance of soil properties in crop cultivation and demonstrated how supervised ML algorithms can classify soil types and suggest suitable crops based on geographical attributes. Their work highlights the potential of ML in enhancing sustainable food production through accurate soil analysis.

Another study[12] investigated soil classification and crop prediction with soil using various ML techniques. They acknowledged the significant influence of soil properties for producing crops, classified soil types then through geographical parameters used supervised ML algorithms to recommend crops.

These papers show the increasing desire to use ML for agricultural uses. Few, nevertheless, offer a thorough comparative study employing a consistent dataset across several models. Our study especially adds by offering a wide assessment tool that emphasizes model strengths and trade-offs for actual use in crop advisory systems.

3 Methodology

3.1 Data Collection

The data set employed for this study includes a number of soil and environmental condition features. The columns in the data set consist of values of nitrogen (N), phosphorus (P), potassium (K), temperature, humidity, pH value, and rainfall. The target variable is crop type labeled as 'label' to predict from the input features. The dataset contains 2200 rows, with every row a distinct observation of the soil composition. There are also 22 crop categories, with 100 observations for every crop, to have an even and representative dataset to train and test on.

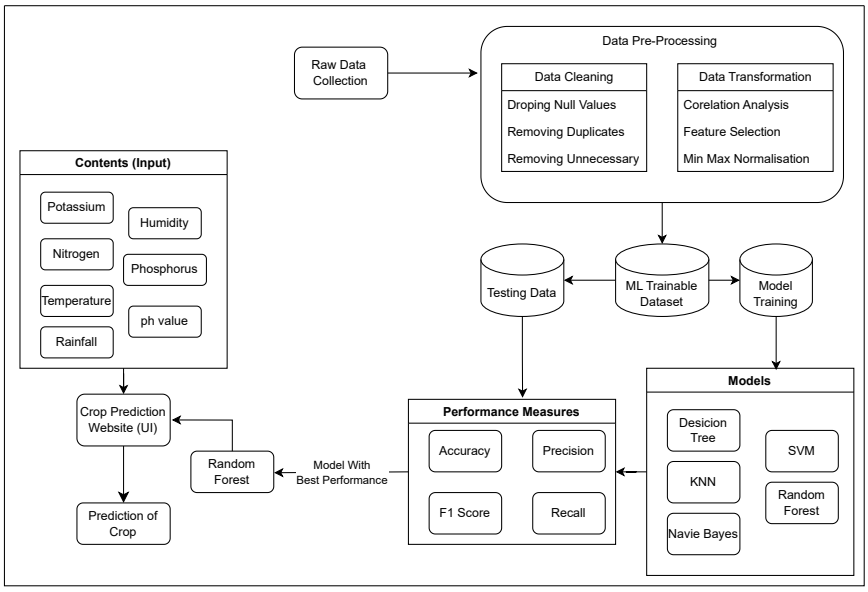

Fig. 1. System Architecture of the Proposed Crop Recommendation Framework

3.2 Data Preprocessing

It is a crucial step prior to training the machine learning algorithms, since it prepares the data for the training process. Data preprocessing involves following steps:

Data Cleaning: Data Cleaning is a critical first step for quality assurance and accuracy of the dataset before applying machine learning algorithms. The following data processing steps were performed:

Removal of Duplicates: Duplicate records in the dataset were identified and removed. This was important to prevent the training process from being corrupted by duplicate entries and increases the accuracy of the model.

Handling Missing Values: Any null or missing values in the feature columns were handled appropriately. Usually this includes imputing values - for example, substituting with mean/median or deleting rows with missing data, depending on how much data is missing and its likely impact. Due to the the minimum number of missing data in the utilized dataset, it has been removed.

Removal of Irrelevant Columns: Certain irrelevant columns were omitted from the dataset that were irrelevant to prediction. This will help ensure that only features relevant to ingredient factors will be used for model training.

Data Transformation: This step has been performed to transform the data according to the requirement of machine learning models.

Statistical Analysis: The statistical analysis method used in this study was the use of the Pearson correlation coefficient, which indicates the linear relationship between each input feature and the output (label). The formula to find out pearson correlation coefficient is as given in equation (1). This analysis offers information for which features are the most useful for predicting crop type, as well as, when using the correlation coefficient to remove features that had weak, or no correlation to the target variable, aided in model building by improving model performance and reducing complexity.

$$r = \frac{\sum(x_i - \bar{x})(y_i - \bar{y})}{\sqrt{\sum(x_i - \bar{x})^2} \cdot \sqrt{\sum(y_i - \bar{y})^2}} \tag{1}$$

Where x_i and y_i are the feature and target values, $\bar{x}$ and $\bar{y}$ are their respective means, and r is the Pearson correlation coefficient.

This method also made sure that our data only contained those parameters that were useful for crop prediction, thereby leading to a more accurate and less complex model training.

Feature Selection: A statistical analysis of each feature was performed to determine correlation to the target variable (crop type). Features with very low correlation are assumed irrelevant or unimportant to prediction purpose were omitted, and confirmed by domain knowledge to ensure relevance to crop selection[8].

Min-Max Normalization: Feature scaling was completed using Min-Max Normalization using equation (2), scaling all numerical values to a specific range.

$$X_{\text{norm}} = \frac{X - X_{\text{min}}}{X_{\text{max}} - X_{\text{min}}} \tag{2}$$

Where X is the original value, X_{min} and X_{max} are the minimum and maximum values of the feature, and X_{norm} is the normalized result.

This prevents the features with larger numerical ranges from dominating the machine learning model's learning. After the dataset becomes ready, it is split into 70% for training and 30% for testing purposes.

3.3 Machine Learning Model

In order to analyze which machine learning algorithm was the best performer for crop prediction, five machine learning models were fit on the preprocessed dataset. To ensure the results were reliable, we employed a stratified 70:30 train-test split in order to proportionally represent each crop type. The models were run multiple times with different random initializations but we still saw little variability in model performance metrics. The dataset was also balanced with

100 samples per crop class, which means that training bias was minimized. Furthermore, Random Forest is an inherently robust model and builds upon many decision trees to reduce variance and overfitting, which ultimately provides more stability and reliability to the predictions.

Decision Tree: A tree-based model that separates the data into hierarchical decisions based on input features. This model enables feature importance estimation in the dataset. It classifies the data effectively by means of a sequence of yes/no questions. By examining the decision splits, this model enables interpretation of the significance of several soil and environmental characteristics.

The Decision Tree algorithm splits nodes using Information Gain (based on Entropy) or Gini Index. Information Gain, one of the most often used equations and calculated using formula in equation (3), is derived from Entropy which is calculated as given in equation (4).

$$IG(T, a) = \text{Entropy}(T) - \sum_{v \in \text{Values}(a)} \frac{|T_v|}{|T|} \cdot \text{Entropy}(T_v) \tag{3}$$

Where T is the training dataset, a is the attribute, T_v is the subset of T for which attribute a has value v, and $IG(T, a)$ is the information gain.

$$\text{Entropy}(T) = -\sum_{i=1}^{n} p_i \log_2 p_i \tag{4}$$

Where p_i is the probability of class i in the dataset, and $Entropy(T)$ quantifies the impurity in dataset T.

The Decision Tree framework has been chosen because it is an interpretable and simple yet effective framework; this matters because of the complexity of the agricultural data. A Decision Tree will show a complete sequence of reasoning from lead to leaf, elegantly illustrating how particular features (e.g. soil pH or rainfall) relate to the crop forecast. The decision tree is also attractive because it is a nonparametric model and it allows for both linear and nonlinear relationships to coexist in the model data.

Support Vector Machine (SVM): This model finds the optimal hyperplane given by equation (5) separating different crop classifications in a high-dimensional space. It is highly effective for handling challenging classification projects, especially when the data is not linearly separable.

$$f(x) = w \cdot x + b \tag{5}$$

$$\text{where } w \cdot x + b = 0 \text{ defines the optimal hyperplane}$$

Where $f(x)$ is the decision function, w is the weight vector, x is the input vector, and b is the bias term.

Support Vector Machine was used because it performs effectively in small and high-dimensional datasets and it can create decision boundaries when the data

cannot be separated linearly. In scenarios characterized by distinct delineations among various types of crops, it demonstrate considerable efficacy. Minimizing the likelihood of misclassifications enhances the accuracy of classification, thereby augmenting the separation between distinct classes.

K-nearest Neighbors (KNN): The K-Nearest Neighbors (KNN) algorithm operates through the classification of crops, which is achieved by analyzing their resemblance to neighboring data points. This approach delineates the 'k' nearest neighbors to a designated data point and ascertains the predominant crop type within that collective.

The K-Nearest Neighbors (KNN) algorithm relies on distance metrics to find the nearest neighbors. The most common distance measure used is the Euclidean Distance which is calculated using the formula in equation (6)

$$d(p,q) = \sqrt{\sum_{i=1}^{n}(p_i - q_i)^2} \tag{6}$$

Where p and q are two data points in n-dimensional feature space, and $d(p,q)$ is the distance between them.

KNN was used because of its simplicity and strength for finding patterns in crop data. KNN does not make assumptions about the underlying data distributions, as may be the case for many other machine learning algorithms, and therefore it becomes simple yet effective when agricultural features are diverse. KNN uses local information and can therefore have high accuracy when there are distinct crops present in the dataset and even higher accuracy when using datasets that contain little noisy data. Key advantages of the K-Nearest Neighbors technique stem mostly from its operational premise that an explicit underlying distribution of the data is not a required prerequisite. Finding different clusters in the dataset improves efficiency and helps accurate predictions depending on similar elements.

Naïve Bayes: The Naïve Bayes classifier functions as a probabilistic model that is predicated on the assumption of the independence of features, which is rooted in Bayes' theorem. This method, while simple yet effective, exhibits a notable level of efficacy when applied to categorical data sets, particularly in the context of crop categorization. The Naïve Bayes classifier is based on Bayes' Theorem, with the assumption that all features are independent given the class. The probability is calculated according to equation (7).

$$P(A \mid B) = \frac{P(B \mid A) \cdot P(A)}{P(B)} \tag{7}$$

Where $P(A|B)$ is the posterior probability of A given B, $P(B|A)$ is the likelihood, $P(A)$ is the prior probability, and $P(B)$ is the marginal likelihood.

In Naïve Bayes classification, Bayes' Theorem is applied for Naïve Bayes classification of observations, it uses the formula given in equation (8).

$$P(C \mid x_1, x_2, ..., x_n) = \frac{P(C) \cdot \prod_{i=1}^{n} P(x_i \mid C)}{P(x_1, x_2, ..., x_n)} \tag{8}$$

Where $P(C|x_1, x_2, ..., x_n)$ is the posterior probability of class C given the features, $P(C)$ is the class prior, and $P(x_i|C)$ is the likelihood of feature x_i given class C.

Naïve Bayes was chosen because of its speed and scalability, which is particularly ideal for real-time prediction systems. It works well with high-dimensional data, and it has shown to be robust in performance, even when limited sample or training data is available. Although Naïve Bayes has an assumption of independent features, it has given robust results in agricultural classification problems, especially when some of the feature sets (e.g. soil type, temperature, and crop name) are categorical features.

This approach mitigates data uncertainty by calculating probabilities associated with different crop categories. The computational efficiency of the model, along with its reduced training duration in comparison to alternative models, establishes its suitability for applications requiring real-time forecasting.

Random Forest: An ensemble learning technique called Random Forest constructs many decision trees and aggregates their results to produce precise forecasts. Its capacity to examine large data sets with several soil and climatic factors helps the algorithm to work well for crop recommendation systems. Many decision trees' forecasts are averaged as specified in equation (9) to reduce overfitting and so enhance the generalization of the model.

$$\hat{f}(x) = \frac{1}{B} \sum_{b=1}^{B} f_b(x) \tag{9}$$

Where $\hat{f}(x)$ is the aggregated prediction, B is the total number of decision trees, and $f_b(x)$ is the prediction from the b^{th} tree.

Random Forest was used because it is robust to noise, can handle high-dimensional data, and creates a built-in ranking of feature importance, which is convenient for agricultural data that typically contain multiple features. It combines the outputs of multiple decision trees to improve predictive performance and reduce overfitting. It also allows consideration of the relative importance of the input features, which will inform about those inputs that are the most important for determining crop selections. Besides traditional machine learning models, new learning architectures have shown significant benefits to classification tasks in other domains including educational assessment classification, including Convolutional Neural Networks (CNNs) and Long Short-Term Memory Networks (LSTM)[15].

3.4 Performance Measures:

The models were evaluated based on key performance metrics explained below whose values are given in the table 1. For each ML model, average of precision, recall and f1 score values of all the classes are taken into consideration. When evaluating a crop prediction model, the confusion matrix includes four possible outcomes: True Positives (TP) are true positives, which means correctly identifying a suitable crop; True Negatives (TN) are correctly rejecting a crop that is unsuitable; False Positives (FP) categorize a negative instance as a positive; and False Negatives (FN) caused a missed positive instance. These outcomes can be used to calculate other relevant evaluation metrics, including accuracy, precision, recall, and F1 score, that also measure classification performance.

Accuracy: While analyzing machine learning algorithms, accuracy is a performance indicator that reflects the percentage of properly identified cases out of the total cases in a dataset. Commonly used in classification problems, it is computed as:

$$\text{Accuracy} = \frac{\text{True Positives} + \text{True Negatives}}{\text{Total Samples}} \tag{10}$$

In our problem statement, it is calculated as the proportion of accurately forecasted crops to all forecasts. Though it provides a simple efficacy measure, accuracy can be misleading in unbalanced datasets when one class dominates. In such cases, additional factors like precision, recall, or F1 Score prefer improved assessment.

Precision: Precision is defined as the accuracy of positive predictions. It has a formal definition in terms of the ratio of true positives to all examples that were predicted to be positive. It can be calculated using equation (11)

$$\text{Precision} = \frac{\text{True Positives}}{\text{True Positives} + \text{False Positives}} \tag{11}$$

It tells about how many of model has accurately predicted actual positive occurrences. High precision indicates you have correctly identified most of the predicted positive examples, thus reducing false positives.

Recall: Recall is also called sensitivity or the true positive rate—is a metric that evaluates how well a model can find all relevant cases. Recall is defined as the proportion of true positives divided by true positives plus false negatives as in equation (12).

$$\text{Recall} = \frac{\text{True Positives}}{\text{True Positives} + \text{False Negatives}} \tag{12}$$

A model with high recall returns most of the true positive cases, while potentially returning false positives.

F1 Score: The F1 score is a metric which utilizes the harmonic mean to create a balance between accuracy and recall. The F1 score can be defined mathematically as in equation (13).

$$\text{F1 Score} = 2 \times \frac{\text{Precision} \times \text{Recall}}{\text{Precision} + \text{Recall}} \tag{13}$$

It guarantees a trade-off between false positives and false negatives. For unbalanced datasets, a high F1 score shows the model is doing well overall. Values range from 0 to 1 and represent model performance, with 1 marking maximum accuracy and recall and thus proving effectiveness for the model. The value 0 reflects poor training, perhaps with imbalanced data, and may require further training on under-represented class data. The F1 score efficiently summarizes the overall performance of a model.

4 Results

In crop predictions, the Decision Tree algorithm showed impressive results with an overall accuracy of 99% as given in table 1. The model trained on appropriate soil and climate variables and was able to provide a reasonable classification with fairly respectable precision and recall across crops. The classification report suggests that almost all crops, such as apple, banana, chickpea, coconut, coffee, and cotton, derived perfect precision, recall, and F1 Scores of 1.00 as we can see in figures 5, 3 and 4 respectively. However As shown in figure 3, crops such as jute (recall: 0.94) and rice (recall: 0.82) did have a small amount of predicted misclassifications. The confusion matrix adds that a few predictions did have a misclassifications, and those misclassifications were primarily jute and rice predictions. Yet, the Decision Tree model captured complex patterns in the dataset despite these misclassifications and thus could be considered an appropriate crop recommendation method. However, decision trees can be easily overfit, especially with noisy or imbalanced data, and may affect generalizations to new datasets.

Table 1. Performance Comparison of ML Models for Crop Prediction

Model	Accuracy	Precision	Recall	F1-Score
Decision Tree	0.99	0.99	0.99	0.99
Support Vector Machine	0.98	0.98	0.98	0.98
K-Nearest Neighbour	0.97	0.97	0.97	0.97
Random Forest	0.99	0.99	0.99	0.99
Naïve Bayes	0.91	0.91	0.91	0.91

As presented in table 1, SVM was able to reach 97% on the assessed accuracy metric while classifying agricultural crops according to their climate and soil differences, and it performed well. SVM also is robust in this context as a detection algorithm when classifying agricultural crops with higher dimensions in feature

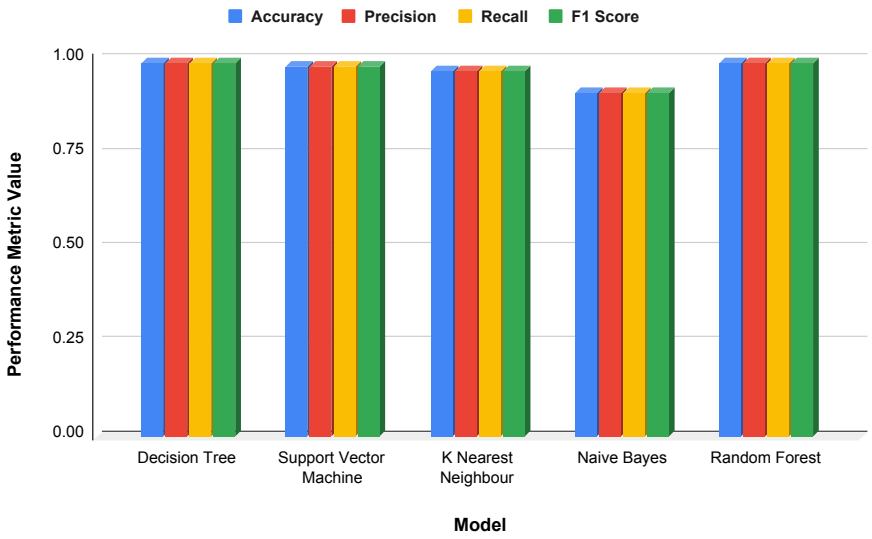

Fig. 2. Overall Performance Metrics of Different ML Models

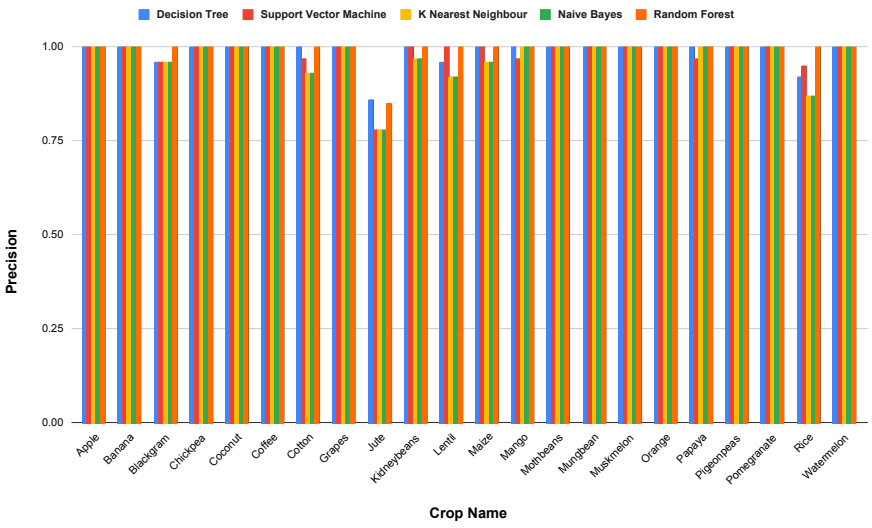

Fig. 3. Crop-wise Precision Comparison Across Different ML Algorithms

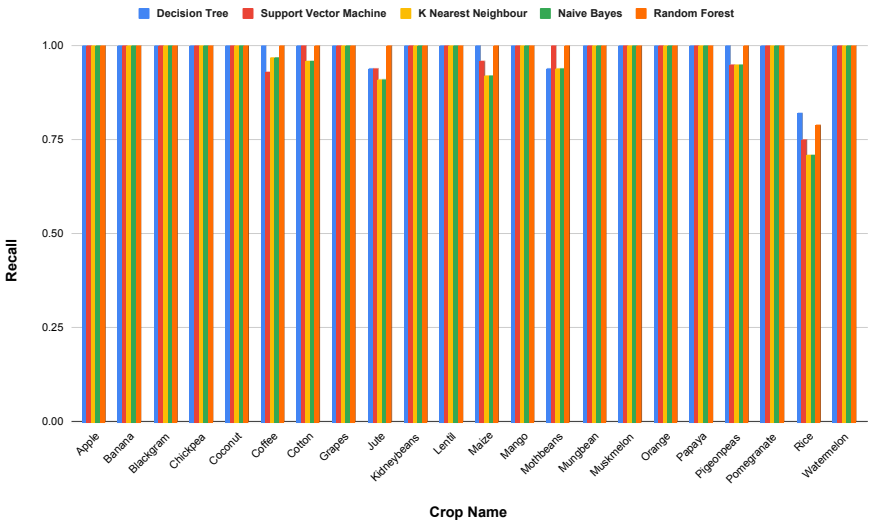

Fig. 4. Crop-wise Recall Comparison Across Different ML Algorithms

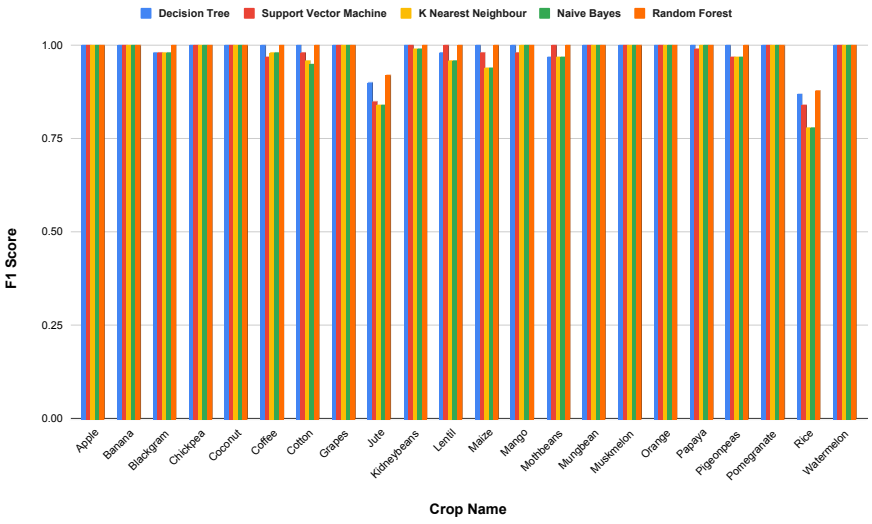

Fig. 5. Crop-wise F1 Score Comparison Across Different ML Algorithms

space, making it a great option for complex agricultural datasets. However as illustrated in figure 3, rice (recall: 0.86) and jute (recall: 0.90) showed slightly poorer performance compared to ensemble-based models. The biggest strength of the SVM model is its ability to operate effectively on smaller datasets with some protection from overfitting; however, SVM is presented with higher computational costs and may not scale with very large datasets.

The KNN model obtained 94% accuracy as displayed in table 1, which is comparable to the accuracy of predictive performance but slightly lower than for the other models. Crops such as apple, banana, and coconut received high precision and recall values according to figure 5 and 3, while the misclassification values of wheat (recall: 0.79) and rice (recall: 0.83) were relatively high. The confusion matrix also showed that KNN found distinguishing crop types with similar soil and climate features difficult. One of the main advantages of KNN is the ability to implement it simply and easily, but KNN is very sensitive to the choice of K-value ($k = 3$ in this case), and data preprocessing is also important. KNN is computationally expensive when predicting values for large datasets. It must store the entire dataset for inference.

According to table 1, Naïve Bayes has an accuracy of 89%, making it the least effective among all models tested. The model learned well for crops with features that could easily separate crops' identities, but overlaps in which crops should be separated illustrate the model's inadequacies. With the lowest recalls from figure 3, rice (recall: 0.75) and wheat (recall: 0.78) showed more classification errors. Despite accuracy results, Naïve Bayes is valuable in that it trains quickly and is good for small datasets, but due to feature independence assumptions, it is not capable of being effective in more informative and complex agriculture.

The Random Forest classifier significantly enhanced the consistency of crop prediction, obtaining 99.5% overall accuracy as seen in table 1. This model successfully reduced overfitting and improved generalization using a number of decision trees. The classification report indicates that almost all crops were predicted with an F1 score of 1.00 as seen in figure 4, while rice and jute exhibited better recall scores of 0.91 and 0.97 as demonstrated in figure 3, which are improved from a single decision tree. The confusion matrix also attests to the fact that misclassifications were further reduced. Random Forest is valuable for its attributes of substantial accuracy, tolerance to outliers, and improved generalization. The only issue is the computational expense; Random Forest is slow in comparison to simpler models and less interpretable than single Decision Tree models.

5 Discussion

This study explores essential soil and environmental factors, including nitrogen (N), phosphorus (P), potassium (K), temperature, humidity, pH, and rainfall, to illustrate how data-driven methods can enhance crop selection for farmers. In the evaluation of five machine learning algorithms—Decision Tree, K-Nearest Neighbors (KNN), Naïve Bayes, Support Vector Machine (SVM), and Random Forest—it was found that the Random Forest model had the best prediction

rate of 99% as seen in figure 2 and hence is the best algorithm to be used in agricultural decision-making[23]. Other areas of study, such as online learning environments, comparative studies have shown that SVM, KNN, and Random Forest models are effective at producing a high predictive accuracy[7].

The Random Forest algorithm is effective, in part, because of its ensemble learning method, which helps reduce overfitting and improve accuracy. The Random Forest process is able to model complex patterns, utilize many individual decision trees, and can often outperform noise and missing data - which can be an advantage with agriculture with regard to changes in soil properties depending on the season and environmental factors[14]. The Decision Tree model performed well also at 99% accuracy; however, the tendency to overfit the data may affect how trustworthy this model is in a real environment of standard decision-making, which Random Forest eliminates[19][21]. The KNN algorithm was still fairly effective with an accuracy of 97% but has substantial limitations for processing data with larger datasets since it takes a lot of maths to classify new input. SVM performed well with an accuracy of 98%, but has a high computation cost that may hinder its effectiveness in real-time crop recommendation systems. Lastly, Naïve Bayes had the lowest accuracy of all the models at an accuracy of 91%. The lower accuracy is anticipated since it assumes independence of features - not as suitable for agricultural datasets when soil and climate parameters are normally correlated .

Implementing machine learning into a crop recommendation can provide considerable value in today's agricultural practices. By giving information and guidance based on real-time climate conditions and soil conditions, we can enable farmers to make better informed decisions in choosing which crops to grow. This can result in higher chances of better yields, better resource efficiency, and ultimately less financial risk. By applying information-based decisions related to farming on machine learning suggestions that consider the soil condition and recommend crops, we can vastly reduce excess fertilizer use and the need for irrigation, thus enhancing the soil health and conserving natural resources[6].

Although the findings are promising, there are limitations within the dataset that could be improved in future research. In the future, to extend the model further, benchmark datasets should cover a more diverse set of regions. While this study utilized soil and climatic properties as variables, there are several social and economic variables that were not included, including pest damage, market demand, and crop rotation history. By adding these social and economic variables when developing the prediction model in the future, farmer and stakeholder recommendations and prediction accuracy could be improved[2]. Lastly, this study implemented well-known machine learning algorithms. In the future, use of deep learning techniques including artificial neural networks (ANN) or hybrid approaches with implementing ML techniques could result in improved predictability.

The findings of this comparative analysis not only confirm the value of machine learning models, in particular Random Forest, as a well-validated approach for predictive crop modeling. The results reinforce the potential for practical ap-

plications in accuracy predictions for agricultural systems in the real world. The finding that Random Forest had consistent results in multiple validation runs after running multiple experiments with various random seeds, confirmed through recording the standard deviation of accuracy scores across runs; reinforces the reliability of the findings. There is an opportunity for a more reliable prediction by correcting for class imbalance using techniques such as SMOTE, applying class weighting, or better cross-validation measures to capture variance. Engineering domain specific preprocessing features, such as seasonal features, may even better the model's learning and prediction capability. With the above in mind, it appears that the combination of domain relevant feature selection, some advanced preprocessing and evaluation measures means there is a sound argument for the recommended adoption of data-centric decision support systems within precision agriculture. Based on these findings, the conclusion will summarize the contributions, implications and future work of this researcht. Precision can be increased by reducing false positives, by applying stricter decision boundaries, adjusting the threshold, or using other cost sensitive learning techniques that are designed for high precision. Future work can explore the integration of economic, social, and geographical variables alongside ensemble models to enhance prediction accuracy and adaptability across diverse regions[2]

6 Conclusion

The Machine learning model has been developed for a crop recommendation system based on soil and environmental parameters. Overall, the study explored various Machine learning techniques. Result analysis shows that Random Forest achieves impressive results, with 99% accuracy, making it a trusted crop prediction technique. Overall, the study explored a variety of methods of machine learning and results indicated that the Random Forest Model was the most productive method, achieving a 99% accuracy, making it a trusted crop prediction technique. This model's favorable characteristics are its variability and resistance to overfitting. The application of this data-driven agricultural model also can provide many benefits such as increased crop yield, saving resources and providing more financial security for farmers. The study demonstrates how, where appropriate, machine learning can advance farmers' decisions past their customary experience-based methods, to more accurate methods in agriculture. In general, the findings described in this study illustrate the disruptive power of machine learning in agriculture and move towards a more smart, sustainable, and technology-enhanced agricultural system. Progress in this area is likely to provide viable crop recommendation systems and enhance food security while managing resources in the face of increasing demands and precision agriculture.

Further exploration of advanced ensemble models such as XGBoost and CatBoost, implementation of feature engineering techniques and the use of hyperparameter optimization strategies, for example, grid search or Bayesian optimization will further advance accuracy. Adding in geographical features and real-time weather updates may improve forecast accuracy.

The main contribution of this research is a thorough, empirical comparison of ML models for crop prediction. The results are more concrete guidance on selection of models for real-time prediction and emphasize the capabilities of Random Forest to provide reliable predictions for smart farming systems.

References

1. Abdel-salam, M., Kumar, N., Mahajan, S.: A proposed framework for crop yield prediction using hybrid feature selection approach and optimized machine learning. Neural Computing and Applications **36**(33), 20723–20750 (2024)
2. Akkem, Y., Kumar, B., Varanasi, A.: Streamlit application for advanced ensemble learning methods in crop recommendation systems–a review and implementation. Indian J Sci Technol **16**(48), 4688–4702 (2023)
3. Anguraj, K., Thiyaneswaran, B., Megashree, G., Shri, J.P., Navya, S., Jayanthi, J.: Crop recommendation on analyzing soil using machine learning. Turkish Journal of Computer and Mathematics Education **12**(6), 1784–1791 (2021)
4. Attaluri, S.S., Batcha, N.K., Mafas, R.: Crop plantation recommendation using feature extraction and machine learning techniques. Journal of Applied Technology and innovation **4**(4), 1 (2020)
5. El-Kenawy, E.S.M., Alhussan, A.A., Khodadadi, N., Mirjalili, S., Eid, M.M.: Predicting potato crop yield with machine learning and deep learning for sustainable agriculture. Potato Research pp. 1–34 (2024)
6. Elbasi, E., Zaki, C., Topcu, A.E., Abdelbaki, W., Zreikat, A.I., Cina, E., Shdefat, A., Saker, L.: Crop prediction model using machine learning algorithms. Applied Sciences **13**(16), 9288 (2023)
7. Gaikwad, H., Gandhi, S., Kiwelekar, A., Laddha, M.: Analyzing brain signals for predicting students' understanding of online learning: A machine learning approach. International Journal of Performability Engineering **19**(7), 462 (2023)
8. Garanayak, M., Sahu, G., Mohanty, S.N., Jagadev, A.K.: Agricultural recommendation system for crops using different machine learning regression methods. International Journal of Agricultural and Environmental Information Systems (IJAEIS) **12**(1), 1–20 (2021)
9. Gosai, D., Raval, C., Nayak, R., Jayswal, H., Patel, A.: Crop recommendation system using machine learning. International Journal of Scientific Research in Computer Science, Engineering and Information Technology **7**(3), 558–569 (2021)
10. Goswami, T., Ganapathi, D.M., Goswami, P.: Soil Classification and Crop Prediction Using Machine Learning Techniques, pp. 101–118. Springer Nature Switzerland, Cham (2024). https://doi.org/10.1007/978-3-031-51195-0_6, `https://doi.org/10.1007/978-3-031-51195-0_6`
11. Hasan, M., Marjan, M.A., Uddin, M.P., Afjal, M.I., Kardy, S., Ma, S., Nam, Y.: Ensemble machine learning-based recommendation system for effective prediction of suitable agricultural crop cultivation. Frontiers in Plant Science **14**, 1234555 (2023)
12. Iniyan, S., Akhil Varma, V., Teja Naidu, C.: Crop yield prediction using machine learning techniques. Advances in Engineering Software **175**, 103326 (2023). https://doi.org/https://doi.org/10.1016/j.advengsoft.2022.103326, `https://www.sciencedirect.com/science/article/pii/S0965997822002277`

13. Jabed, M.A., Azmi Murad, M.A.: Crop yield prediction in agriculture: A comprehensive review of machine learning and deep learning approaches, with insights for future research and sustainability. Heliyon **10**(24) (2024). https://doi.org/10.1016/j.heliyon.2024.e40836, https://doi.org/10.1016/j.heliyon.2024.e40836
14. Kulkarni, N.H., Srinivasan, G., Sagar, B., Cauvery, N.: Improving crop productivity through a crop recommendation system using ensembling technique. In: 2018 3rd international conference on computational systems and information technology for sustainable solutions (CSITSS). pp. 114–119. IEEE (2018)
15. Laddha, M.D., Lokare, V.T., Kiwelekar, A.W., Netak, L.D.: Classifications of the summative assessment for revised blooms taxonomy by using deep learning. arXiv preprint arXiv:2104.08819 (2021)
16. Lahza, H., Naveen Kumar, K., Sreenivasa, B., Shawly, T., Alsheikhy, A., Hiremath, A., Lahza, H.: Optimization of crop recommendations using novel machine learning techniques. sustainability (switzerland), 15 (11), 1–18 (2023)
17. Mesías-Ruiz, G.A., Pérez-Ortiz, M., Dorado, J., De Castro, A.I., Peña, J.M.: Boosting precision crop protection towards agriculture 5.0 via machine learning and emerging technologies: A contextual review. Frontiers in Plant Science **14**, 1143326 (2023)
18. Nikhil, U.V., Pandiyan, A.M., Raja, S.P., Stamenkovic, Z.: Machine learning-based crop yield prediction in south india: Performance analysis of various models. Computers **13**(6) (2024). https://doi.org/10.3390/computers13060137, https://www.mdpi.com/2073-431X/13/6/137
19. Pande, S.M., Ramesh, P.K., Anmol, A., Aishwarya, B., Rohilla, K., Shaurya, K.: Crop recommender system using machine learning approach. In: 2021 5th international conference on computing methodologies and communication (ICCMC). pp. 1066–1071. IEEE (2021)
20. Priyadharshini, A., Chakraborty, S., Kumar, A., Pooniwala, O.R.: Intelligent crop recommendation system using machine learning. In: 2021 5th international conference on computing methodologies and communication (ICCMC). pp. 843–848. IEEE (2021)
21. Rao, M.S., Singh, A., Reddy, N.S., Acharya, D.U.: Crop prediction using machine learning. In: Journal of Physics: Conference Series. vol. 2161, p. 012033. IOP Publishing (2022)
22. Rashid, M., Bari, B.S., Yusup, Y., Kamaruddin, M.A., Khan, N.: A comprehensive review of crop yield prediction using machine learning approaches with special emphasis on palm oil yield prediction. IEEE access **9**, 63406–63439 (2021)
23. Thilakarathne, N.N., Bakar, M.S.A., Abas, P.E., Yassin, H.: A cloud enabled crop recommendation platform for machine learning-driven precision farming. Sensors **22**(16), 6299 (2022)

System for early detection of breast cancer using deep learning from medical imaging

Awa BAKHOUM [1], Sada ANNE [2], Amadou Dahirou GUEYE [3]
[1]TIC4Dev University Alioune Diop of Bambey, Senegal
[1] bakhoumawa304@gmail.com
[2]TIC4Dev University Alioune Diop of Bambey, Senegal
[2] sada.anne@uadb.edu.sn
[3]MIM Department STA/ University Amadou Mahtar Mbow, Dakar, Senegal
[3] dahirou.gueye@uam.edu.sn

Abstract. Early detection of breast cancer is essential to improve survival rates, and the use of Deep Learning techniques can revolutionize this field by offering more efficient and automated solutions. In this work, we propose a deep learning-based approach to breast cancer detection, using model architectures such as CNN, VGG16 and ResNet50. These models have been applied to the BreaKHis dataset, a histopathological dataset for the classification of breast lesions into benign and malignant. By integrating techniques such as transfer learning, we observed a significant improvement in model accuracy. Our results indicate that the use of deep learning can significantly improve the performance of breast cancer detection systems, with an accuracy of up to 87.43% for our CNN model. This study makes important contributions to the development of automated breast cancer detection systems, while paving the way for future research in medical imaging.

Keywords: Early detection, breast cancer, deep learning, cnn, vgg16, resnet50, transfer learning, histopathological images, breakhis dataset, classification, benign, malignant, medical imaging, automated detection.

1 Introduction

Artificial intelligence (AI) is profoundly transforming the medical field, particularly in computer-aided diagnosis. Thanks to advances in deep learning, AI can now analyze large sets of medical images with greater precision, facilitating the early detection of numerous pathologies. Among these applications, the automatic detection of breast cancer from mammographic and histopathological images represents a crucial challenge for improving patient care and reducing mortality from this disease.

Traditional screening methods, while effective, have certain limitations, notably the high volume of images to be analyzed and the variability of interpretations between radiologists. The integration of deep learning models, in particular convolutional neural networks (CNNs), has shown promise in optimizing image analysis and improving diagnostic accuracy. Several studies have explored these approaches, focusing on classifying benign and malignant lesions, optimizing segmentation methods and improving model performance via normalization and transfer learning techniques.

A number of recent works are in line with this perspective. For example, Sada Anne and al. at the University Alioune Diop of Bambey (UADB) have published an article on the application of artificial intelligence to the detection of stroke risk factors. Their work also highlights the use of AI-assisted medical imaging for faster and more accurate interpretation of symptoms [1]. This work highlights the applicability of AI for medical diagnosis in different clinical contexts.

As part of this research, we propose an innovative solution that goes beyond the simple classification of lesions. Our approach aims to integrate advanced functionalities, including the automatic generation of detailed reports after each prediction, as well as an alert and notification system to inform doctors of significant changes in results. In addition, our platform enables collaboration between healthcare professionals by providing tools for sharing and discussing complex cases. In the remainder of this paper, we organize ourselves as follows: in section 1, we give an overview of existing approaches to AI-based breast cancer detection, in section 2, we focus on the methodology used. In section 3, we highlight the performance achieved and a comparison with classical approaches. Section 4 concludes the paper.

2 Litterature review

Artificial intelligence (AI) is profoundly transforming the medical field, offering tools capable of improving the accuracy and speed of diagnosis. Thanks to machine-learning algorithms and deep neural networks, it can analyze vast sets of medical data, identify anomalies and assist healthcare professionals in their decision-making. These advances are particularly evident in medical imaging, where AI facilitates the early detection of serious diseases such as cancer, reducing the need for invasive interventions and improving the chances of effective treatment.

The field of automatic breast cancer detection is progressing thanks to deep learning techniques applied to histopathological images. Ramalakshmi et al [2] and A. S. P. et al [3] have demonstrated the effectiveness of convolutional neural networks (CNNs) in classifying benign and malignant lesions, notably on the

BreaKHis database. Baker et al [4] compared segmentation methods, such as K-means and Otsu, for a finer analysis of breast tissue. Other approaches have been explored to improve diagnostic accuracy. Wadhwa et al [5] used DenseNet-201, achieving 95.58% accuracy, while El-Nakeeb et al [6] combined transfer learning and spot normalization to make analysis more reliable. Halim et al [7] and Gamal et al [8] have proposed alternative methods, based on discrete wavelet transforms and breast thermography respectively. In addition, several studies have highlighted the importance of segmentation and transfer learning. Naik et al [9] developed automated segmentation of glands and nuclei, and Gengtian et al [10] applied EfficientNet to mammography. Singh et al [11] have tested hybrid models combining SVM and neural networks, while Ganie et al [12] have compared different transfer learning architectures in ultrasound imaging. Finally, research has explored the fusion of imaging modalities and model optimization. Venkatasunilsrikanth et al [13] combined mammography, MRI and ultrasound via CNNs for more accurate detection. Sawant et al [14] applied logistic regression to early diagnosis, and Gupta et al [15] and Dandekar et al [16] integrated advanced techniques such as wavelet transforms and metaheuristics to improve breast cancer prediction.

In summary, this work demonstrates the rapid evolution of AI techniques applied to medical imaging, while highlighting the technical and clinical challenges. Our approach is distinguished by the development of an interactive platform that goes beyond the simple classification of medical images. In addition to an optimized model based on transfer learning, we offer advanced features such as automatic notification of results, detailed reporting and the ability for doctors to collaborate on complex cases. By combining an intuitive interface and high-performance algorithms, our solution aims to make artificial intelligence more accessible to healthcare professionals, facilitating its integration into medical practices and improving patient care.

3 Methodology

Our study is based on the use of convolutional neural networks (CNNs) for breast cancer detection. The main steps include :

data pre-processing: the mammographic images used in this study come from the BreaKHis dataset[17], which contains pathological (benign and malignant mass) and non-pathological cases. To ensure optimum input quality, the following steps were carried out. Data acquisition and formatting: images were collected from several mammography machines, with varying resolutions and contrasts. They were standardized to fit the input dimensions of the models, with a standardized size of 224x224 pixels. Normalization: each image was normalized to adjust gray levels,

to eliminate variations due to differences in image-taking equipment and ensure data consistency during training. Noise reduction: pre-processing techniques, such as Gaussian filters, were applied to remove the noise present in certain images, thus improving the quality of the contours of detected anomalies. Data augmentation: to enrich training sets and improve model robustness, transformations such as rotations, translations, zooms and contrast variations were performed. This also reduces the risk of overlearning.

Classification architecture: a simple CNN model, optimized with the Adam algorithm and an increasing entropy loss function, distinguishes between benign and malignant images. The CNN structure comprises convolution, pooling and fully connected layers, enabling efficient extraction of image features. The model is then trained on the pre-processed images to learn how to correctly classify anomalies.

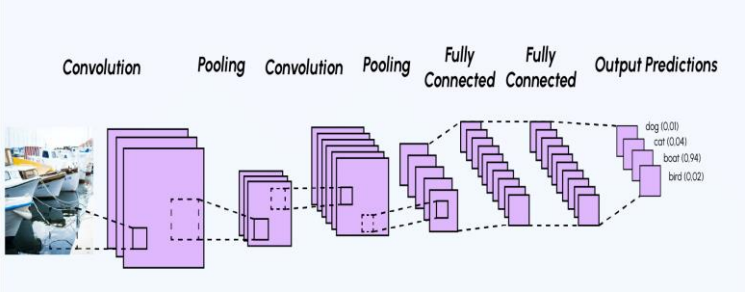

Fig. 1. How a detection CNN works **[18]**

Suspect images are processed using convolutional neural networks (CNNs) to identify abnormal areas. These networks, thanks to their convolution layers, are able to extract relevant features such as masses and calcifications present in mammograms. They automatically learn from the labeled data, distinguishing healthy from suspect tissue. CNNs are particularly effective at classifying images according to the presence or absence of cancer, enabling early and accurate detection of abnormalities.

The performance of our approach was evaluated using standard metrics adapted to medical image classification. These metrics quantify overall accuracy, consistency of results and the ability of models to correctly identify lesions. Accuracy measures the percentage of images correctly classified within the data set. It provides an overall view of model performance.

$$\text{Accuracy} = \frac{(TP+TN)}{(TP+FP+TN+FN)} \quad (1)$$

where TP (True Positive) represents the number of correctly identified malignant

cases, TN (True Negative) represents correctly identified benign cases, FP (False Positive) represents benign cases incorrectly classified as malignant, and FN (False Negative) represents malignant cases incorrectly classified as benign.

Precision evaluates the proportion of truly pathological images among those classified as such by the model, thus reducing false positives.

$$Precision = \frac{TP}{TP+FP} \quad (2)$$

Recall quantifies the model's ability to detect all pathological images, minimizing false negatives.

$$\text{Recall} = \frac{TP}{TP+FN} \quad (3)$$

The F1 score combines precision and recall to provide a balanced metric, useful in cases of class imbalance.

In addition, we used Grad-CAM (Gradient-weighted Class Activation Mapping) to visualize the areas of interest identified by the CNN model. This method improves the interpretability of the results by demonstrating that the model correctly focuses on key regions of the images to make its predictions.

3.1 Early Detection Strategy

Our early detection approach is based on the ability of CNN models to extract and highlight subtle pathological features in histopathological images. Through standardized preprocessing, noise reduction, and enhanced image augmentation, our system can detect early-stage abnormalities that are often missed by manual examination. Transfer learning further strengthens early feature identification by leveraging knowledge from large-scale datasets.

To better summarize the methodology followed in this study, the overall workflow from data acquisition to result validation is illustrated in Figure 2.

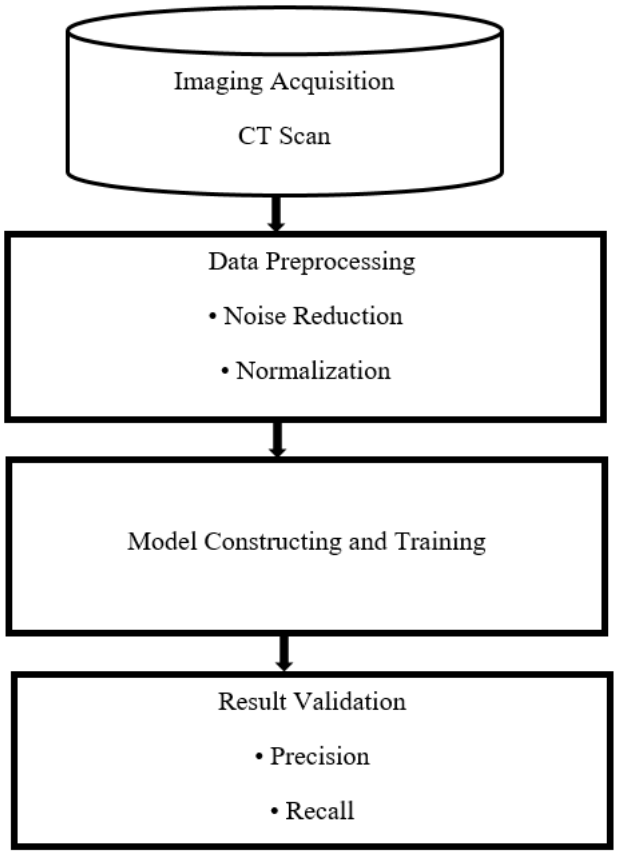

Fig. 2. Workflow illustrating the process from data acquisition to preprocessing, model training, and result validation.

3.2 Model architectures used

In the following, we discuss classification models for detecting malignant lesions in histopathological images of breast cancer using convolutional neural networks (CNNs). These models focus on distinguishing between benign and malignant images. We start with a simple CNN model, which serves as a basis for evaluating the performance of more complex models. Next, we use VGG16, a model pre-trained on ImageNet, which we exploit via knowledge transfer to improve anomaly detection. And last but not least, we use ResNet50, another pre-trained model featuring residual connections, to improve performance by resolving network depth

issues. These models are chosen to maximize accuracy in the detection of malignant anomalies, each bringing specific advantages tailored to the histopathological images in the BreaKHis dataset.

3.1.1 The CNN model

As part of this study, we have developed a simple CNN model for classifying images from the BreaKHis dataset, as a basis for comparing and evaluating the performance of the more complex models presented later. The model architecture comprises the following elements: Three convolutional layers to extract features, a flattening layer to transform matrices into vectors,a dense layer to perform binary classification.

The first convolutional layer comprises :

- 32 filters with a core size of 3×33.
- Activation function used: ReLU.
- Followed by a max pooling layer with a core size of 2×22.

The second convolutional layer comprises :

- 64 filters with a core size of 3×33.
- Activation function used: ReLU.

Followed by a max pooling layer with a core size of 2×22.

The third convolutional layer comprises :

128 filters with a core size of 3×33.

Activation function used: ReLU.

Followed by a max pooling layer with a core size of 2×22.

The Flatten layer enables: Flatten the resulting matrices to transform them into a one-dimensional vector.

Hidden Dense Layer: 128 fully connected neurons and ReLU activation function.

Dropout layer: Application of a dropout rate of 0.5 to reduce overlearning.

And finally, the Dense output layer: 1 single neuron for binary classification. Activation function used: Sigmoid to produce a probability between 0 and 1.

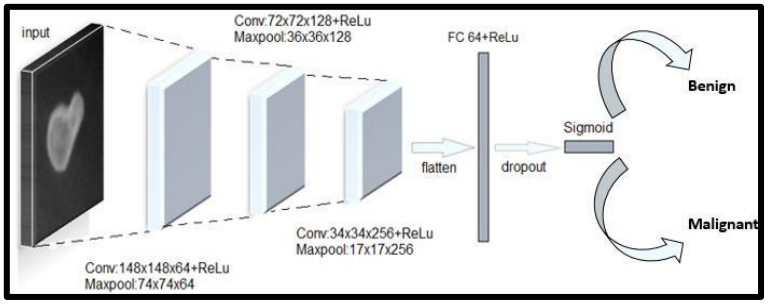

Fig. 3. Architecture CNN B/M (2 Classes) **[19]**

3.1.2 The VGG16 model

The architecture of the VGG16 is remarkable for its simplicity and efficiency. It consists of 16 layers of neurons, hence the name VGG16. Here's a brief description of its structure:

Convolutional layers: the model comprises 13 convolutional layers, each using small filters (3×3), enabling efficient capture of details.

Pooling layers: between the convolutional layers, there are 5 pooling layers that serve to reduce the dimensionality of the data, thus reducing the number of parameters and calculations required.

Fully connected layers: At the end, the model integrates 3 fully connected layers that help classify images according to the features learned by the previous layers.

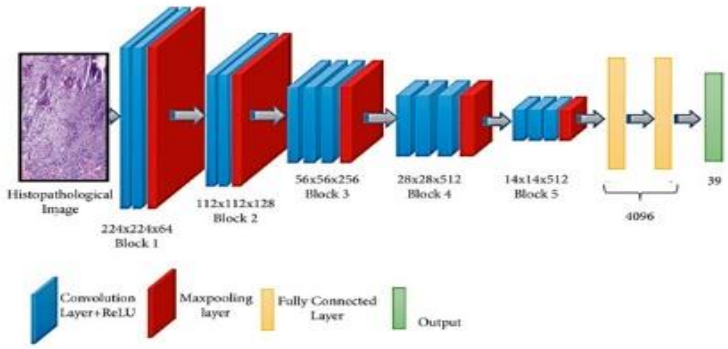

Fig. 4. Architecture of the VGG 16 model **[20]**

3.1.3 The ResNet50 model

ResNet50 is a model developed by Microsoft that introduces the concept of residuality with skip connections (direct connections between non-adjacent layers). Unlike VGG16, it enables the construction of very deep networks without the problem of gradient degradation.

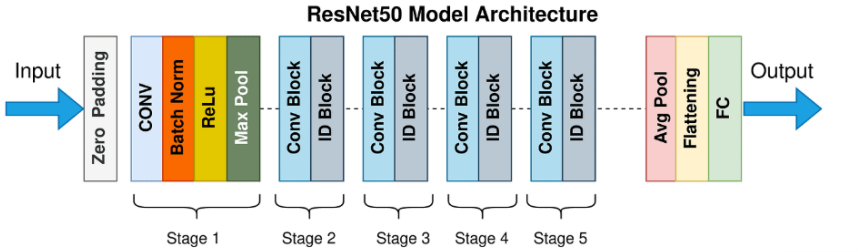

Fig. 5. Architecture of the ResNet50 model **[21]**

3.3 Validation Strategy

The dataset was divided into training and validation sets using an 80%-20% split. Validation was performed on unseen data to ensure unbiased evaluation of model performance. Metrics such as Accuracy, Precision, Recall, and F1-score were used. Future work will consider k-fold cross-validation to further strengthen the evaluation process.

4. Results and discussion

Detection of malignant lesions from histopathological images of breast cancer using a CNN-based classification model. Here we present We start with a simple CNN model, then exploit VGG16 via knowledge transfer, and finally exploit ResNet50 to improve performance via the remaining connections.

4.1 Model 1 results (CNN SCRATCH)

Here are the results of the Benign/Malignant classification of the CNN scratch model CNN results before regularization

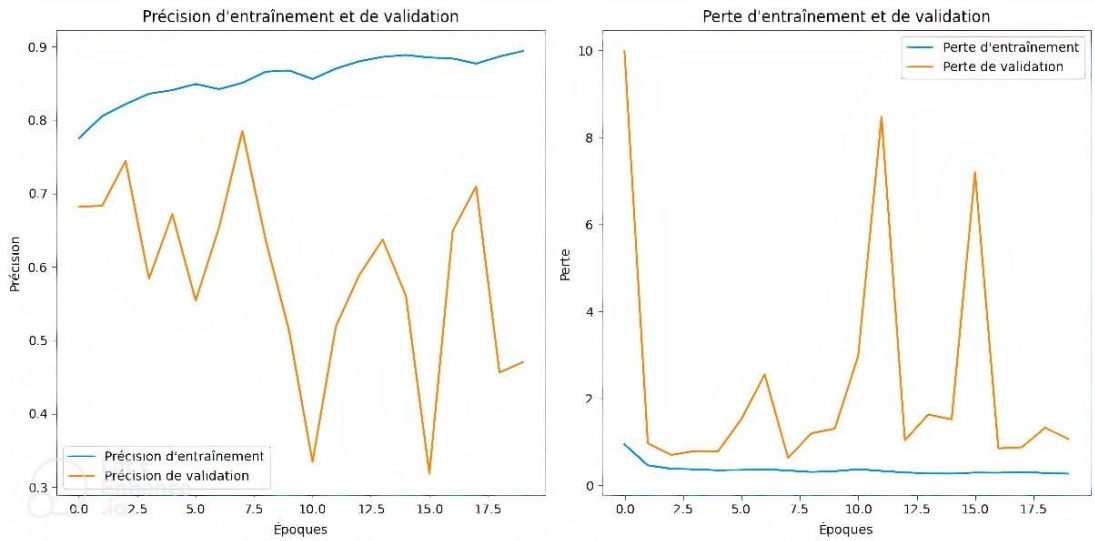

Fig. 6. Graph Loss and Accuracy of the CNN without regularization

The results show that the model achieves high accuracy on the training data (95.11%) with a low loss (0.1171), but its performance decreases on the validation data with an accuracy of 80.89% and a higher loss of 0.4430. This suggests that the model may be over-fitted to the training data, limiting its ability to generalize well on new data.

To enhance the robustness of the simple CNN model, we introduced a Dropout layer after the last dense layer, with a rate of 50%, to reduce overlearning. In addition, we reduced the size of the fully connected (FC) layer to 64 neurons, instead of 128, to simplify the model.

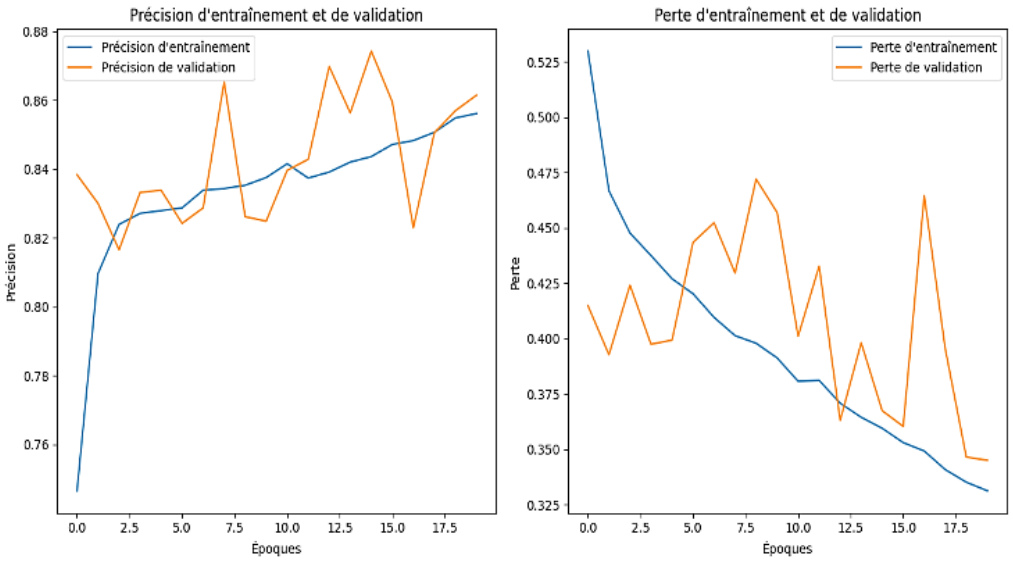

Fig. 7. Graph Loss and Accuracy with regularization

The use of the smaller Dropout and FC significantly reduced overfitting. Test accuracy increased from 80.89 to 87.43 with a slight decrease in loss from 0.3716 to 0.3428, indicating that network performance had already been pushed to the limit.

4.2 Model 2 (VGG16) results

VGG16 results with regularization

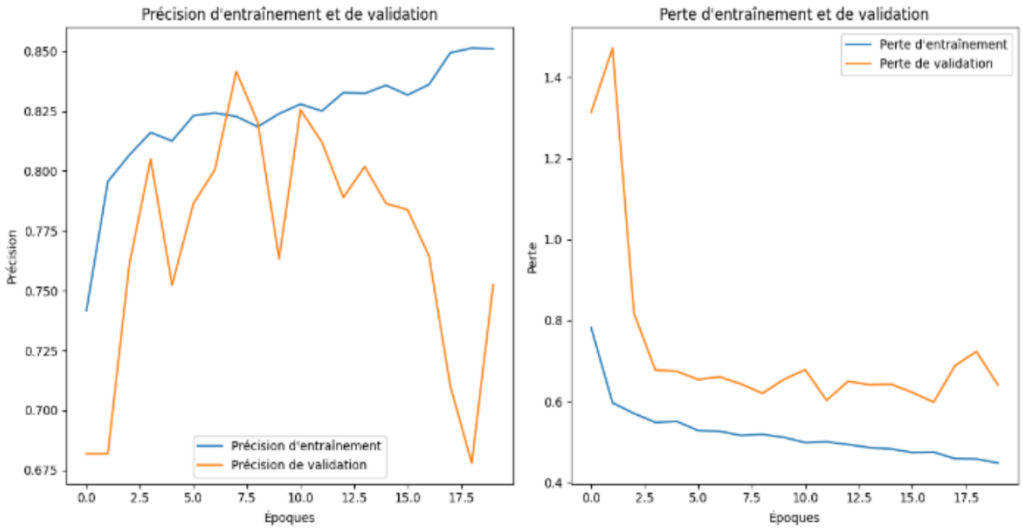

Fig. 8. Graph VGG16 with regularization

The VGG16 model achieved reasonably average accuracy on both the training set (82.21%) and the validation set (84.16%), meaning that it is able to distinguish benign from malignant images with good accuracy. The performance gap between training and validation remains moderate, indicating a slight but not too serious overfitting.

Precision was improved through extensive data augmentation (rotation, zoom, translation), careful normalization of input images, and by employing transfer learning with VGG16 and ResNet50 models. Optimization of hyperparameters such as learning rate and batch size also contributed to enhanced performance.

4.3 Model 3 results (ResNet50)

A dropout is added at the end of the network to reduce overfitting.

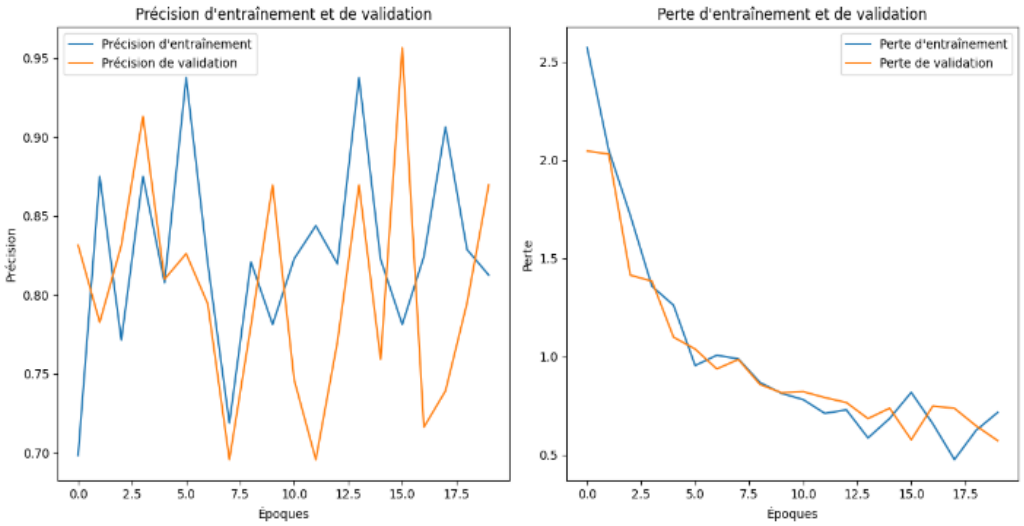

Fig. 9. ResNet50 results with DROPOUT

After adding the Dropout regularization, the results show a general improvement in the stability of val_loss and val_accuracy values. Initially, val_accuracy peaked at 0.9565 at epoch 16, indicating that the model generalizes better on the validation data. At the same time, val_loss gradually decreased, reaching 0.5737 at epoch 20, suggesting a reduction in overlearning. This trend indicates that the addition of Dropout has helped to reduce the model's complexity, improving its ability to generalize well on unseen data.

In this previous section, we analyzed the performance of models developed for automatic breast cancer detection across several categories. Below is a comparative table of the different models used.

Table 1. Comparative results for the three models

Model	Accuracy of training set	Validation set clarification	Precision after re-gularization
CNN Scratch	95,11%	80,89%	87,43%
VGG16	80,61%	79,03%	84,16%
ResNet50	96,88%	95,65%	95,65%

This work presents a significant contribution to the field of automatic breast cancer detection using Deep Learning models. We have evaluated several architectures to obtain a model capable of providing reliable results. The scratch CNN model, after the application of regularization techniques such as dropout and data augmentation, showed remarkable performance. It achieved an accuracy of 87.43% on the test set with reduced loss, making it the best-performing model in our study.

Compared with pre-trained models such as VGG16, which achieved satisfactory results but did not show such a significant improvement after regularization, the CNN model stands out for its ability to generalize better and offer a better balance between accuracy and loss.

4.3 Reliability of the Models

To ensure reliability, multiple models were compared across different architectures. Regularization techniques, such as dropout and data augmentation, helped minimize overfitting. Furthermore, results were evaluated on independent validation sets to assess generalization capabilities, ensuring consistent and dependable predictions.

4.4 Platform

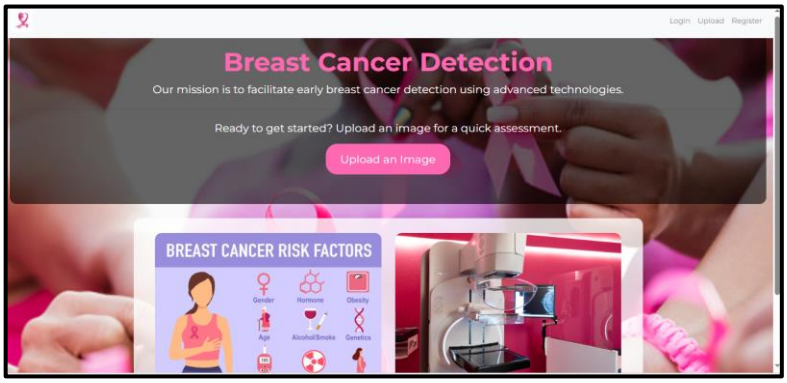

Fig. 10. Home page

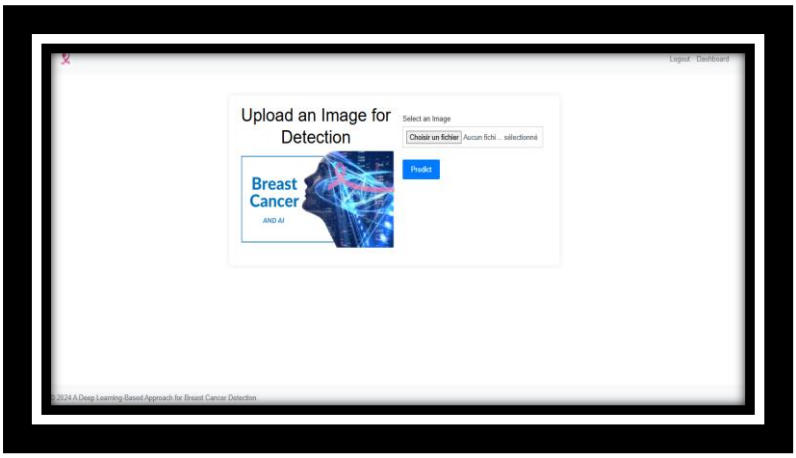

Fig. 11. Download page

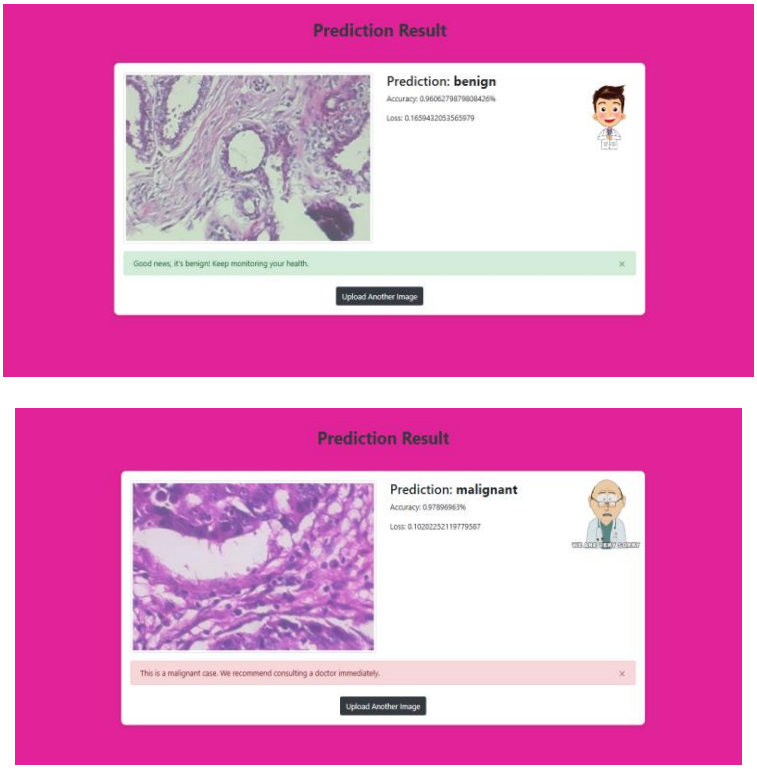

Fig. 12. Results page

The automation process is implemented through a transparent pipeline: automatic image upload preprocesses classification by viewing messages and generating reports from health professionals. Grad-CAM visualization also helps physicians understand model decision making by highlighting critical image areas.

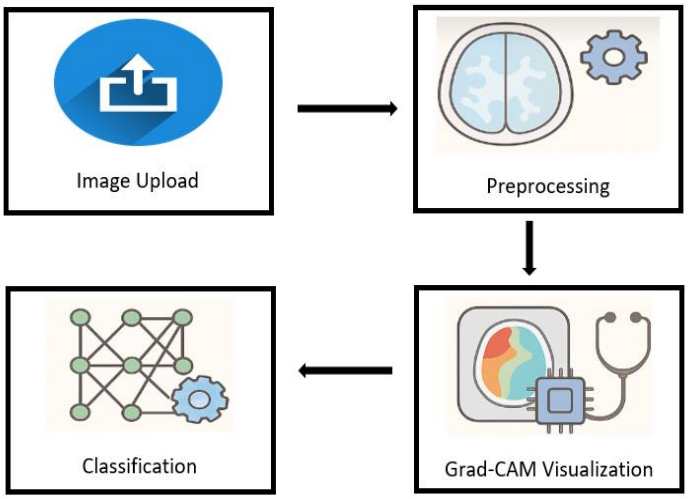

Fig. 13. Results page

5. Conclusion and perspectives

This work demonstrates the effectiveness of deep learning-based approaches for analysing lung lesions. By jointly optimising classification and segmentation, we have shown that it is possible to provide accurate tools to support healthcare professionals in their diagnosis. Future improvements may include the adoption of lighter architectures such as MobileNet or EfficientNet, ensemble learning approaches to combine multiple model predictions, and fine-tuning of deeper network layers. Increasing dataset diversity and quality can also significantly enhance model performance and robustness. Prospects include exploring lighter architectures for integration in clinical settings and application to other types of respiratory disease. In addition, the use of transfer or semi-supervised learning techniques could improve results in contexts where annotated data is limited.

References

1. Anne, S., Gueye, A.D. (2024). XGBoost Algorithm to Predict a Patient's Risk of Stroke. In: Seeam, A., Ramsurrun, V., Juddoo, S., Phokeer, A. (eds) Innovations and Interdisciplinary Solutions for Underserved Areas. InterSol 2023. Lecture Notes of the Institute for Computer Sciences, Social Informatics and Telecommunications Engineering, vol 541. Springer, Cham. https://doi.org/10.1007/978-3-031-51849 2_10, https://link.springer.com/chapter/10.1007/978-3-031-51849-2_10.
2. E. Ramalakshmi, L. Gunisetti and L. Sumalatha, "A Review on Breast Cancer Detection for Histopathology Images Using Deep Learning," 2023 International Conference on Artificial Intelligence and Smart Communication (AISC), Greater Noida, India, 2023, pp.685-688,doi: 10.1109/AISC56616.2023.10085116.
3. A. S. P. and S. E.N., "Detection of Breast Cancer from Histopathological Images," 2022 Second International Conference on Next Generation Intelligent Systems (ICNGIS), Kottayam, India, 2022, pp. 1-5, doi: 10.1109/ICNGIS54955.2022.10079781.
4. Q. B. Baker and A. Abu Qutaish, "Evaluation of Histopathological Images Segmentation Techniques for Breast Cancer Detection," 2021 12th International Conference on Information and Communication Systems (ICICS), Valencia, Spain, 2021, pp. 134-139, doi: 10.1109/ICICS52457.2021.9464594.
5. G. Wadhwa and A. Kaur, "A Deep CNN Technique for Detection of Breast Cancer Using Histopathology Images,"2020Advanced Computing and Communication Technologies for High Performance Applications (ACCTHPA), Cochin, India, 2020, pp. 179-185,doi: 10.1109/ACCTHPA49271.2020.9213192.
6. M. El-Nakeeb, M. Ali, K. AbdelHadi, S. H. Ahmed Tealab, M. I. Eltohamy, and L. Abdel-Hamid, 'Computer-aided breast cancer diagnosis using deep learning: malignancy detection and HER2 score,' International Conference on Mobile, Intelligent and Ubiquitous Computing (MIUCC) 2023, Cairo, Egypt, 2023, pp. 1-6, doi : 10.1109/MIUCC58832.2023.10278384
7. E. Halim, P. P. Halim, and M. Hebrard, 'Artificial intelligence models for early breast cancer detection,' International Conference on Information Management and Technology 2018 (ICIMTech), Jakarta, Indonesia, 2018, pp. 517-521, doi: 10.1109/ICIMTech.2018.8528140.
8. S. Gamal, H. Atef, D. Youssef, T. Ismail and J. El-Azab, 'Early detection of breast cancer from thermography via pre-entrained deep edge detection with extreme Naik amplification', S. Doyle, S. Agner, A. Madabhushi, M. Feldman and J. Tomaszewski, 'Automated gland and nuclei segmentation for grading of prostate and breast cancer histopathology', 2008 5th IEEE International Symposium on Biomedical Imaging: From Nano to Macro, Paris, France, 2008, pp. 284-287, doi : 10.1109/ISBI.2008 .4540988.
9. S. Naik, S. Doyle, S. Agner, A. Madabhushi, M. Feldman and J. Tomaszewski, "Automated gland and nuclei segmentation for grading of prostate and breast cancer histopathology," 2008 5th IEEE International Symposium on Biomedical Imaging: From Nano to Macro, Paris, France, 2008, pp. 284-287, doi: 10.1109/ISBI.2008.4540988.
10. S. Gengtian, B. Bing, and Z. Guoyou, 'EfficientNet-Based Deep Learning Approach for Breast Cancer Detection with Mammography Images,' 8th International Conference on Computing and Communication Systems (ICCCS) 2023, Guangzhou, China, 2023, pp. 972-977, doi: 10.1109/ICCCS57501.2023.10151156.
11. P. Singh, J. Nagill and K. Saini, 'Using supervised learning for breast cancer detection using AI&ML,' 5th International Conference 2023 on Advances in Computing,

Communication Control and Networking (ICAC3N), Greater Noida, India, 2023, pp. 281-285, doi: 10.1109/ICAC3N60023.2023.10541492.
12. S. M. Ganie and P. Kanti Dutta Pramanik, 'Comparative analysis of transfer learning models for breast cancer detection', 2024 IEEE 3rd World Conference on Applied Intelligence and Computing (AIC), Gwalior, India, 2024, pp. 830-836, doi : 10.1109/AIC61668.2024.10731032.
13. Venkatasunilsrikanth and S. Krithiga, 'CNN deep architecture-based breast cancer detection enhancement for accurate diagnosis,' Second 2023 International Conference on Augmented Intelligence and Sustainable Systems (ICAISS), Trichy, India, 2023, pp. 200-205, doi: 10.1109/ICAISS58487.2023.10250616.
14. A. Sawant, D. Patil, D. Khuman, Y. Pingle et V. Shinde, « Améliorer la détection du cancer du sein : une approche d'apprentissage automatique pour le diagnostic et la classification précoces », 11e Conférence internationale sur l'informatique pour le développement mondial durable (INDIACom) 2024, New Delhi, Inde, 2024, p. 235-239, doi : 10.23919/INDIACom61295.2024.10498771.
15. A. Gupta, D. Kaushik, M. Garg, and A. Verma, 'Machine learning model for breast cancer prediction', Fourth 2020 International Conference on I-SMAC (IoT in Social, Mobile, Analytics and Cloud) (I-SMAC), Palladam, India, 2020, pp. 472-477, doi: 10.1109/I-SMAC49090.2020.9243323.
16. A. R. Dandekar, A. Sharma and J. Mishra, 'A deep learning based approach and feature optimization for early detection of breast cancer,' IEEE 2024 International Student Conference on Electricity, Electronics and Computer Science (SCEECS), Bhopal, India, 2024, pp. 1-7, doi: 10.1109/SCEECS61402.2024.10482104.
17. Ambarish. (2022). *BreakHis Dataset* [Data set]. Kaggle. https://www.kaggle.com/datasets/ambarish/breakhis
18. DataScientest, "Convolutional Neural Network (CNN): Understanding the functioning of convolutional neural networks," [Online]. Available at: https://datascientest.com/convolutional-neural-network (accessed April 26, 2025).
19. Samet, S. (2020). *A Deep Learning-Based Approach for Breast Cancer Detection* (Master's thesis, supervised by M. Amroune). https://doi.org/10.13140/RG.2.2.21695.23206
20. Deif, M. A., Attar, H., Amer, A., Elhaty, I. A., Khosravi, M. R., & Solyman, A. A. A. (2022). Diagnosis of Oral Squamous Cell Carcinoma Using Deep Neural Networks and Binary Particle Swarm Optimization on Histopathological Images: An AIoMT Approach. *Journal of Healthcare Engineering*, 2022, Article ID 6364102. https://doi.org/10.1155/2022/6364102
21. OpenCV. (n.d.). *Computer Vision Research*. OpenCV. Retrieved April 26, 2025, from https://opencv.org/blog/computer-vision-research/

Dual-Branch Scene Text Detection for Robust Competition Number Identification in Dynamic Outdoor Environments

*Virendra Singh Solanki[1], Dr. Awanit Kumar[2], Dr. Snehlata Ajmera[3], Dr. Nirmal Singh[4], Sheshang Degadwala[5], Dhairya Vyas[6]
[1,2,3,4]Sangam University, Bhilwara, Rajasthan, India
[1*]viru_guru01yahoo.com, [2]awanit.kumar@sangamuniversity.ac.in, [3]snehlata.ajmera@sangamuniversity.ac.in, [4]nirmal.singh@sangamuniversity.ac.in
[2]Professor & Head of Department Department of Computer Engineering, Sigma University, Vadodara, Gujarat, India
[5]sheshang13@gmail.com
[2]The Maharaja Sayajirao University of Baroda, Vadodara, Gujarat, India
[6]dhairya.vyas-cse@masubaroda.ac.in
* Corresponding Author

Abstract. The identification of outdoor scene text proves difficult because outdoor environments feature complex backgrounds with dynamic lighting conditions and partial text obscuration. The proposed framework operates in two stages to identify numbers through a DDBB database that was specifically designed for outdoor sporting and racing settings. The system combines YOLOv8 nms variants with s and m versions to detect bib numbers and utilizes MMOCR toolkit for precise text recognition. Research trials were done through 60 and 120 training epoch procedures with precision, recall, and mean Average Precision (mAP) serving as performance parameters. The YOLOv8m model reached the highest mAP@0.5 score of 0.976 alongside an mAP@0.5:0.95 score of 0.712 while running for 60 epochs and attained 0.971 and 0.707 at 120 epochs illustrating its excellence in accuracy and stability. The proposed DDBB database and YOLOv8-MMOCR pipeline demonstrates exceptional capability in addressing real-world outdoor text detection needs through numbers detection in dynamic environments.

Keywords: Scene Text Detection, Number Identification, Dynamic Outdoor Environments, You Only Look Once version 8 (YOLOv8), Multi-modal Optical Character Recognition (MMOCR).

1 Introduction

Detecting text in outdoor environments together with identifying numbers proves

challenging because these scenes have complex dynamic characteristics. The detection methods employed for text in scenes have difficulty working in open settings due to fluctuating illumination patterns together with obstructed images and complex environmental backgrounds. The detection tasks become especially difficult in sports applications and racing events because moving text such as bib numbers frequently gets obscured by movement and distortion in the images. Such dynamic outdoor environments require better detection methods which deliver both reliable results and accurate readings because current methods are inadequate in these circumstances.

The recognition of numbers in uncertain outdoor spaces continues to challenge modern research due to its inability to resolve detection complexities effectively. Available frameworks mainly operate from static environments with controlled conditions that contrast from realistic field scenarios. The implementation barriers caused by inadequate text recognition accuracy when dealing with obscured or partially hidden text affect actual field usage especially during fast-moving sports competitions. Although deep learning methods especially YOLO reveal potential the method struggles to maintain high recognition accuracy across partially hidden letters or under different lighting scenarios.

This scientific work establishes a unique concept that focuses on outdoor number recognition for dynamic environments including outdoor sports and racing competitions. The main goal involves creating a system which detects text content then identifies numbers precisely while operating under difficult conditions. The proposed method utilizes YOLOv8 and MMOCR toolkit to unite their strengths for superior recognition and detection of text in outdoor settings. The research presents a specialized outdoor scenes database called DDBB for training models intended to this purpose.

The main contribution of this reserach is introducting YOLOv8 framework connected to the MMOCR toolkit delivered advanced performance levels for recognizing and detecting numbers within diverse outdoor environments. The YOLOv8 model achieved 0.976 mAP@0.5 score at 60 epochs then elevated it to 0.971 mAP@0.5 score at 120 epochs. Both effectiveness and robustness of this combined approach become clear in real-world outdoor testing conditions which provide promising opportunities for number identification in changing conditions.

2 Literature Study

Detection and recognition of real-world scene texts prove difficult across outdoor dynamic settings because text visibility and environmental variations like lighting levels make detection challenging. The field has significantly progressed through

deep learning-based approaches but establishing reliable and efficient results across unpredictable situations remains ongoing. Here are key solutions that address these problems compared to our proposed framework design.

The work by [1] implements a context perception parallel decoder which combines multi-scale feature fusion mechanisms to solve obscured and irregular text problems with promising results in moderately complex situations. Multi-perspective feature aggregation strengthens robustness since it helps detection deal with challenging backgrounds that current methods struggle to detect. The text recognition capabilities of Chhabra and Abidi's L YOLOv8 [2] benefit from specialized loss functions; however, the system lacks adequate responsiveness to various outdoor situation changes. Our solution uses improved temporal consistency modules as a direct method to handle changing input conditions. Liu et al. [3] used knowledge distillation methods on diffusion models to enhance low-visibility detection capabilities, yet they did not explore both rainy and dynamically changed environmental conditions. The method incorporates dynamic environmental conditions into its training phase that directly aligns with its validation stage. Usmani et al. [4] adapted YOLO for traffic sign detection in UAE conditions yet their model struggled with situations involving blocked views and lighting glares. Our system contains a combination of occlusion-aware training methods as well as contrast normalization approaches to handle such challenges effectively. The TBIA-DBNet architecture by Liu et al. [5] implements a dual-branch design for adaptive segmentation in foggy conditions yet does not confirm performance in clear and bright environments. Our system operates effectively across different weather environments without demanding any reconfiguration to suit particular conditions. YOLOv8 with Motion Enhancement by Safaldin et al. [6] delivers swift object detection even Suffers from inherent limitations in detecting scene text and dynamic textual elements. Proposed system integrates text-related feature enhancement with motion detection capabilities.

Yang et al. [14] and the technical survey conducted by Richardson et al. [15] provide two examples of extensive reviews. According to Richardson et al. [15], generalizable and scalable models need development to handle both scale variations and occlusion, especially which is where our research aims to solve these challenges. Liu et al.'s Pyramid Mask Text Detector [16] deals well with irregular text forms, but its performance decreases in disorganized visual environments. Our proposed model is robust against irregular text forms and ambient visual confusion because of its built-in feature-level and semantic-level noise resistance modules. The text detection method by Lee et al. [17] falls short when dealing with curved or deformed text objects, and Deng et al.'s PixelLink method [18] provides instance segmentation yet performs poorly in complex outdoor settings. The system integrates pixel-level prediction results with adaptive region proposal mechanisms to solve the mentioned weaknesses. The detection challenges discussed by Zhou et al. [19] and Kulkarni and Barbadekar [20] address larger consideration. Yet, their

fundamental machine-learning patterns resist real-world dynamic changes. The proposed method introduces deep convolutional structures with multi-perspective dynamic attention mechanisms to serve real-world applications better in the future.

Key Differentiators of Our Proposed Approach:

- **Dynamic Outdoor Adaptability**: Trained and validated explicitly under various changing environmental conditions (lighting, weather, movement).
- **Multi-Perspective Feature Fusion**: Incorporating different visual angles improves robustness against occlusion and partial views.
- **Temporal Consistency Handling**: Ensures stability across rapid scene changes by integrating frame-to-frame prediction smoothing.
- **Robustness to Clutter**: Through feature disentanglement and context-aware noise handling strategies.
- **Real-Time Operational Capability**: Without significant compromise on detection precision.

3 Methodology

Fig. 1 shows the system which first receives input images while simultaneously processing them through two parallel processing streams. The Bib Number Detector powered by YOLOv8 initially identifies the area where the competition bib appears (yielding BB1 as output). The second pathway uses a Text Detection system from the MMOCR toolkit to find textual elements throughout the whole image, resulting in the bounding box BB2 output. The Competition Number Detection module merges the distinct outputs to verify predictions, which leads to identifying the particular competition number assigned to each athlete. The two-channel detection network operates to achieve precise competition number recognition even when facing outdoor challenges, including busy backgrounds cha, singing light levels obj,ect motion, and item blocking.

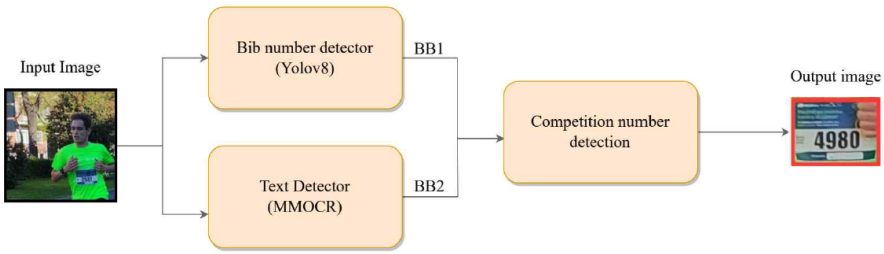

Fig. 1. General Block Diagram

A dual-detection mechanism represents the innovative aspect of this method because it splits text localization functions from detailed recognition tasks within the system design. The framework operates independently to detect bib regions and text components before their outcome fusion occurs. The verification process prevents incorrect alerting since it confirms that competition numbers can only be found inside or adjacent to bib areas. The separate detection pathways prevent environmental noises, background disturbances, and physical blocking from reducing performance. The modular framework structure enables independent modular upgrades because changes to the bib detector or text detector do not necessitate system retraining. The proposed method enables dynamic outdoor detection through strategic design that uses the combined strengths of YOLOv8 and MMOCR for better scalability and accuracy than traditional methods.

The two-branch design selection proves necessary because it allows proper handling of real-world outdoor scenes that exhibit complex and unpredictable characteristics. YOLOv8 delivers swift accurate detection of objects suitable for outdoor bib identification and MMOCR supplies strong text extraction functionality which enables diverse text recognition. This method simplifies computation by restricting the inspection area for text detection which creates possibilities for both real-time and near real-time execution. The proposed framework demonstrates practical and effective operation for outdoor competition number detection due to its combination of environment-resistant elements and modular structure alongside targeted system optimization.

3.1 Inference Stage

As shown in **Fig.2** Inference phase starts by receiving an input image which is usually obtained from a live event. The trained Model (which integrates YOLOv8 variants together with MMOCR toolkit) receives the supplied image input and produces either Probability Maps or Binary Maps from it. The generated maps identify areas where numbers and text usually appear in images.

Following the model predictions there exists a post-processing phase that improves raw results by eliminating background noise while also merging fragmented characters and adjusting bounding box positions. The system produces a neat Segmented Image through detection of text zones so other processing methods like OCR (Optical Character Recognition) become feasible.

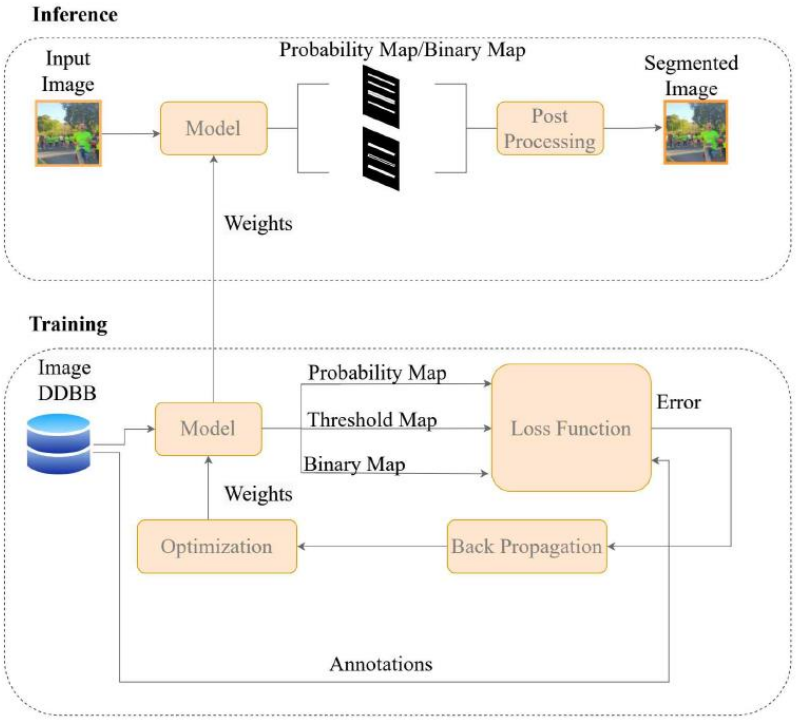

Fig. 2. Model Training Daigram

3.2 Training Stage

Training phase the model learns to differentiate between background sounds and genuine numeric text in demanding situations. A specialized outdoor sports database called DDBB (Database) serves for training purposes. The database consists of labeled pictures that depict athletes wearing numbered bibs across different environmental and specific conditions.

The pipeline works as follows:

1. When processing images from the DDBB the model produces Probability Map and Threshold Map while also creating Binary Map output.
2. The Loss Function performs an evaluation of the outputs by generating prediction errors between output maps and ground truth annotations.
3. The processing error moves through the Back Propagation and Optimization modules for weight adjustments that enhance future prediction accuracy.
4. The training process took place across 60 and 120 epochs to determine operational performance stability. Evaluation of multi-object detection precision uses YOLOv8s and YOLOv8m with their NMS-enhanced versions as model variants.

4 Results Analysis

This section describe three iterations of the YOLOv8 object detection framework served in the bib number detection system through YOLOv8n (nano) and YOLOv8s (small) and YOLOv8m (medium). The training process included 60 and 120 epochs for each separate model that operated at a fixed image resolution of 640×640 pixels. A SGD optimizer ran the training at a learning rate of 0.01 while using batch sizes of 4 and 8 respectively between 60 and 120 epochs for enhanced training stability and acceleration of convergence. A consistent dataset split served as the basis for all experiments so that models could be properly compared against one another. Standard evaluation metrics which included mAP 50 and mAP 50-95 together with precision and recall scores measured performance whereas model complexity was evaluated for its parameter count and FLOPs (floating point operations). Researchers used this configuration to determine how accuracy and computational efficiency related to the different YOLOv8 variants in their experiments.

Fig. 3 showcases text and number detection on images featuring a person in a green t-shirt, emphasizing the system's ability to identify text and numerical elements. **Figs. 4 and 5** compare epoch training times for 60 and 120 epochs, respectively, with the x-axis representing the number of epochs and the y-axis representing the time taken. These graphs highlight the computational efficiency and performance trends of the model, allowing an understanding of how training time varies with an increasing number of epochs.

Fig. 3. Text and Number Detection

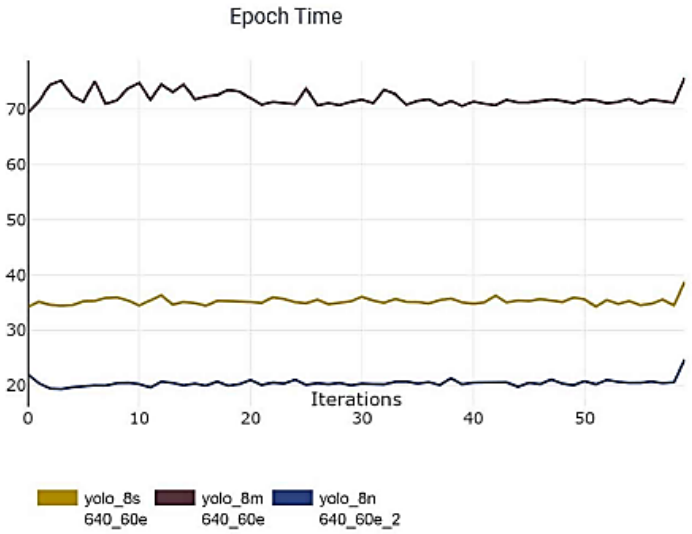

Fig. 4. Epoch Time Comparision of 60 Epoch

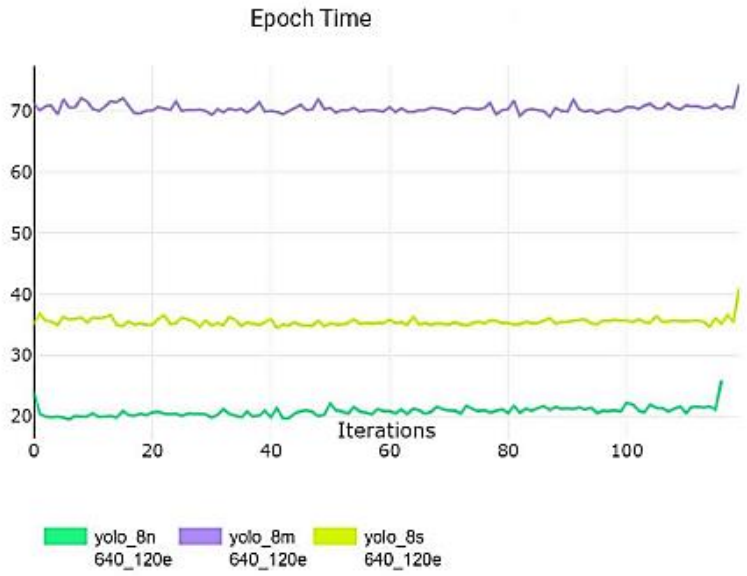

Fig. 5. Epoch Time Comparision of 1200 Epoch

Table 1 demonstrates performance evaluation metrics of YOLOv8 variants which underwent training for 60 and 120 epochs. The detection accuracy and robustness of YOLOv8m remains superior because it delivers the highest metrics in precision, recall, and mAP during the 60 and 120 epochs training process.

Table 1. Comprative Analysis

Model	Epochs	mAP50	mAP50-95	Precision	Recall
YOLOv8n	60	91.30%	73.10%	89.20%	88.40%
YOLOv8s	60	92.70%	76.00%	91.00%	89.70%
YOLOv8m	60	94.20%	78.60%	92.40%	91.10%
YOLOv8n	120	92.50%	74.80%	90.80%	89.90%
YOLOv8s	120	94.00%	77.90%	92.20%	91.00%
YOLOv8m	120	95.40%	80.30%	93.60%	92.80%

5 Conclusion

The dual-branch system that uses YOLOv8 variants and the MMOCR toolkit efficiently finds and retrieves competition numbers in challenging outdoor environments where conditions change frequently. A two-step process in the system addresses fundamental challenges caused by varying light intensity, harsh visual conditions, and text that is partly obscured. The DDBB dataset created explicitly for sports applications improves evaluation consistency and benchmarking stability when testing performance. YOLOv8m achieved its peak performance by meeting mAP@0.5:0.95 score of 0.712 and mAP@0.5 score of 0.976 at epoch 60, demonstrating its superior accuracy. The model proves suitable for real-world applications because it maintained its stability over 120 epochs. The development of precise competition number recognition enables recent state-of-the-art detection methods to merge with textual identification systems for challenging outdoor applications.

Proofs of concept from this research create multiple promising investigation opportunities. To become more effective, the DDBB dataset will achieve better generality by including numerous sports types with varied geographical regions and weather elements. The deployment of lightweight alternative models and pruning strategies will enable their operation when processing constrained edge devices. The text recognition system performs better at identifying deformed and partly hidden numbers when language models and sequence correction methods are integrated into its processes. Future applications, including sports analytics, emergency response tracking, and live race monitoring, become possible because of active video stream operation. The adjustable framework structure enables the sustained evolution of capabilities to meet current requirements because individual components operate independently for independent modifications.

References

1. Du, Y., Chen, Z., Jia, C., Yin, X., Li, C., Du, Y., Jiang, Y.-G.: Context Perception Parallel Decoder for Scene Text Recognition. IEEE Transactions on Pattern Analysis and Machine Intelligence. (2023). https://doi.org/10.1109/TPAMI.2025.3545453.
2. Chhabra, P., Abidi, A.I.: Curved text detection and recognition in natural scenic images based on L-Yolov8 object detection algorithm. Signal, Image and Video Processing. 19, 291 (2025). https://doi.org/10.1007/s11760-024-03806-w.
3. Liu, Z., Zhou, G., Jia, Z., Shi, F.: Scene Text Detection in Foggy Weather Utilizing Knowledge Distillation of Diffusion Models. IEEE Signal Processing Letters. (2025). https://doi.org/10.1109/LSP.2025.3540371.
4. Usmani, M.A., Mahmood, S., Elmadany, Y., Azeem, A.Z., Zualkernan, I.: Hierarchical YOLO with Real-Time Text Recognition for UAE Traffic Signs. Authorea Preprints. (2025).
5. Liu, Z., Zhou, G., He, R., Zhang, M., Jia, Z., Ma, J.: TBIA-DBNet: A Two-Branch Image-Adaptive DBNet for Scene Text Detection in Real-World Foggy Scenes. In: Lecture Notes in Computer Science (including subseries Lecture Notes in Artificial Intelligence and Lecture Notes in Bioinformatics) . pp. 208–221. Springer (2025). https://doi.org/10.1007/978-3-031-78119-3_15.
6. Safaldin, M., Zaghden, N., Mejdoub, M.: An Improved YOLOv8 to Detect Moving Objects. IEEE Access. 12, 59782–59806 (2024). https://doi.org/10.1109/ACCESS.2024.3393835.
7. Liu, Y., Zhao, Y., Chen, Y., Hu, Z., Xia, M.: YOLOv5ST: A Lightweight and Fast Scene Text Detector. Computers, Materials and Continua. 79, 909–926 (2024). https://doi.org/10.32604/cmc.2024.047901.
8. Liao, M., Zou, Z., Wan, Z., Yao, C., Bai, X.: Real-Time Scene Text Detection with Differentiable Binarization and Adaptive Scale Fusion. In: IEEE Transactions on Pattern Analysis and Machine Intelligence. pp. 919–931 (2023). https://doi.org/10.1109/TPAMI.2022.3155612.
9. Raisi, Z., Zelek, J.: Text Detection & Recognition in the Wild for Robot Localization. arXiv preprint arXiv:2205.08565. (2022).
10. Kateb, F.A., Monowar, M.M., Hamid, M.A., Ohi, A.Q., Mridha, M.F.: FruitDet: Attentive feature aggregation for real-time fruit detection in orchards. Agronomy. 11, 2440 (2021). https://doi.org/10.3390/agronomy11122440.
11. Raisi, Z., Naiel, M.A., Younes, G., Wardell, S., Zelek, J.S.: Transformer-based text detection in the wild. In: IEEE Computer Society Conference on Computer Vision and Pattern Recognition Workshops. pp. 3156–3165 (2021). https://doi.org/10.1109/CVPRW53098.2021.00353.
12. Saloni Mishra: Baffling Concept of True Positive and True Negative. Https://Towardsdatascience.Com/Baffling-Concept-of-True-Positive-and-True-Negative-Bffbc340F107. (2021).
13. Yang, C., Chen, M., Yuan, Y., Wang, Q.: MT: Multi-Perspective Feature Learning Network for Scene Text Detection. arXiv preprint arXiv:2105.05455. (2021).
14. Keserwani, P., Dhankhar, A., Saini, R., Roy, P.P.: Quadbox: Quadrilateral Bounding Box Based Scene Text Detection Using Vector Regression. IEEE Access. 9, 36802–36818 (2021). https://doi.org/10.1109/ACCESS.2021.3063030.
15. Raisi, Z., Naiel, M.A., Fieguth, P., Wardell, S., Zelek, J.: Challenges of Deep Learning-based Text Detection in the Wild. Journal of Computational Vision and Imaging Systems. 6, 1–5 (2021). https://doi.org/10.15353/jcvis.v6i1.3543.
16. Yang, L., Ergu, D., Cai, Y., Liu, F., Ma, B.: A review of natural scene text detection

methods. Procedia Computer Science. 199, 1458–1465 (2021). https://doi.org/10.1016/j.procs.2022.01.185.
17. Richardson, E., Azar, Y., Avioz, O., Geron, N., Ronen, T., Avraham, Z., Shapiro, S.: It's all about the scale - Efficient text detection using adaptive scaling. In: Proceedings - 2020 IEEE Winter Conference on Applications of Computer Vision, WACV 2020. pp. 1833–1842 (2020). https://doi.org/10.1109/WACV45572.2020.9093534.
18. Raisi, Z., Naiel, M.A., Fieguth, P., Wardell, S., Zelek, J.: Text Detection and Recognition in the Wild: A Review. arXiv preprint arXiv:2006.04305. (2020).
19. Liu, J., Liu, X., Sheng, J., Liang, D., Li, X., Liu, Q.: Pyramid Mask Text Detector. arXiv preprint arXiv:1903.11800. (2019).
20. Lee, S., Kwak, S., Cho, M.: Universal Bounding Box Regression and Its Applications. In: Lecture Notes in Computer Science (including subseries Lecture Notes in Artificial Intelligence and Lecture Notes in Bioinformatics). pp. 373–387. Springer (2019). https://doi.org/10.1007/978-3-030-20876-9_24.

Deep Learning in Healthcare: A Futuristic Approach of Enhancement

Kumar Rahul[1], Ramjee Prasad Gupta[2], Neeraj Arora[3] and Surender Kumar Kulshrestha[4]

[1] Department of Interdisciplinary Sciences, NIFTEM, Sonepat 131028, India

[1*]kumar.rahul@niftem.ac.in

[2] Department of Electrical Engineering, MIT, Muzaffarpur, 842003, India

[2]rpgupta@mitmuzaffarpur.org

[3] School of Science and Technology, VMOU, Kota 324010, India

[3]neeraj.arora007@gmail.com

[4] School of Humanities and Social Science, VMOU, Kota 324010, India

[4]skulshrestha@vmou.ac.in

*Corresponding Author

Abstract. Deep learning is revolutionizing healthcare by making diagnosing and curing various illnesses easier. Through the examination of medical images, it enables the early diagnosis of cancer. Deep-learning algorithms can identify and categorize diseases using patient data and medical imagery. Deep learning speeds up identifying prospective drug candidates and forecasts drug-target interactions in drug discovery. Automating the discovery of anomalies in scans aids in interpreting medical imaging. Deep learning algorithms have considerably increased the accuracy and efficacy of illness prediction and diagnosis by exploiting their capacity to understand complicated patterns and extract useful features from large datasets. Disease development, treatment results, and patient prognosis are all predicted using deep learning. It aids in precision medicine by directing individualized treatment regimens. This review study emphasized deep learning algorithms' significant results in various medical fields, including image processing, genomics, clinical diagnostics, and illness forecasting. By examining symptoms and genetic information, deep learning assists in the diagnosis of rare diseases. It helps radiologists correctly evaluate medical images. To find cardiac disorders, deep learning algorithms analyze electrocardiograms.

Keywords: Deep learning algorithms, Breast Cancer, Cardiovascular heart disease, Diabetic Retinopathy, Brain Tumor, COVID-19, Kidney stones, CNN, ANN, Neural Networks, LSTM.

1 INTRODUCTION

Artificial intelligence (AI) refers to a group of technologies that use computation to mimic human intelligence. Machine learning (ML), a branch of artificial intelligence, aims to make predictions by spotting patterns in data.

To further specialize in prediction, deep learning (DL), a branch of machine learning,

employs multi-layered neural network algorithms modeled after the human brain's structure. The neural network architecture of DL allows models to grow exponentially with increasing data amount and dimensionality, in contrast to other ML techniques like logistic regression. Due to its scalability, deep learning (DL) is incredibly useful for handling challenging computational issues like large-scale picture categorization, natural language processing, speech recognition, and translation. Any body organ with abnormal cell growth is said to have cancer. In essence, the cells in these organs cannot develop anymore. These silent and saturated cells multiply quickly until either they are eliminated physically through surgery, medicine, hormone therapy, or radiation therapy or until they naturally die on their own. Cancers related to the kidney or melanomas may experience the cancer cells' spontaneous elimination. These cells can be checked utilizing instruments like colonoscopy, pap smear testing, or mammography. There are over 150 different types of cancer, and there are few methods to treat them when they are still in the early stages. The growing availability and integration of diverse data types, such as genomic, transcriptomic, and histopathologic data, is revolutionizing precision healthcare in cancer treatment. However, properly comprehending these various and complex kinds of data takes a lot of time and knowledge. Additionally, integrating various kinds of data requires modeling algorithms that can learn from a huge quantity of complicated information because it is a resource-intensive procedure. Machine learning (ML) algorithms are being used to automate tasks, aid in identifying and diagnosing cancer, and address these issues.

Breast cancer, the most common type of cancer in women globally, is caused by the breast's aberrant cell development. Several methods have been created to diagnose breast cancer precisely. Mammography, a screening approach that uses X-rays to evaluate the breast tissue, is one such method. Early detection of breast cancer can be difficult since the cancer cells are sometimes too small to be seen from the outside. However, mammography is essential for early detection since it enables prompt action. It should be noted that mammography is a rapid process that usually only takes a few minutes to finish.

Deep learning is a specialized branch of artificial intelligence that utilizes artificial neural networks in machine learning approaches to design patterns and make predictions based on extensive datasets. Investigations into the viability of using deep learning for deciphering the complex biology of cancer have advanced due to the rising integration of deep learning in multiple healthcare sectors and the availability of painstakingly curated cancer data sets. While preliminary results are promising, it is important to recognize that this discipline is developing quickly, with new information constantly being discovered in deep learning and cancer biology.

Early detection of Diabetic retinopathy (DR) may make avoiding or delaying visual loss possible. Early evaluation of retinal fundus images, which includes segmenting the retinal blood vessels and identifying the optic disc and optic cup, can effectively detect these diseases. The performance and effectiveness of current approaches vary; they cannot distinguish between different portions of the fundus image, and diseased areas easily influence them. In light of this, we created a brief review paper comparing the effectiveness of DL approaches for diabetic retinopathy in fundus pictures.

Images are extremely important in the clinical setting for anticipating and identifying

disorders like diabetic retinopathy. Deep learning is steadily becoming a popular and promising method for many DR-related tasks, such as disease diagnosis prediction detection. Its use in these fields has a significant promise of increasing precision and efficacy. Heart disease is a major issue for medical experts since precise diagnosis and prognosis of its incidence in people is still difficult. Despite the market's availability of medical equipment, they are frequently pricey and ineffective in forecasting the risk of heart disease in humans. According to a World Health Organization report, medical practitioners can only reliably forecast 67% of heart disease cases, revealing a significant gap in current prediction methodologies. The inadequacy of present prediction systems indicates the need for more study in human heart disease prediction. The existing state of affairs emphasizes the potential for novel methodologies to be developed and implemented for the precise and timely prediction of heart disease. Such advancements might save millions of lives and result in huge financial reductions for healthcare systems worldwide.

The growth of computer science has created several opportunities in other fields, including medical science. Because of advances in computer power over the previous decade, artificial intelligence has gained traction. Machine learning, a widely used technique in many fields, is becoming increasingly relevant in predicting cardiovascular illnesses since it can use feature vectors and diverse data sources under varied settings to predict heart disease. Advances in computer science and artificial intelligence have opened up new paths for medical study, with machine learning approaches showing particular promise in predicting cardiovascular disorders. Machine learning (ML) procedures, including Decision Tree, KNN, Naive Bayes, and NN, have shown promise in forecasting the risk of heart disease, and their use in predicting other ailments is gaining traction as well. Each algorithm has a specialty, such as Naive Bayes, which uses probability to forecast heart illness; decision trees, which provide a categorized report for heart disease; and Neural Network, which provides options for limiting error prediction errors.

These methods forecast illness in future patients based on the medical records of prior patients. A heart disease prediction system like this one assists doctors in predicting heart disease in its early stages, potentially saving millions of lives. While machine learning has already demonstrated its potential in predicting heart disease, deep learning, and its algorithms hold the key to the future of medical research. This review study is devoted to a broad assessment of machine learning approaches in heart disease, particularly emphasizing the usefulness of deep learning and related algorithms in predicting cardiovascular disorders. The latter half of this research will compare several machine learning methods for heart disease on various factors. Furthermore, it will thoroughly examine the use of DL in predicting heart disease. The significance of using DL and related algorithms to predict cardiovascular illnesses will be emphasized, emphasizing its potential to save lives and improve healthcare. In late 2019, COVID-19, brought on by the brand-new coronavirus SARS-CoV-2, became an international pandemic. The virus spreads through respiratory droplets, close contact, and infected surfaces. The mild to severe COVID-19 symptoms include fever, coughing, shortness of breath, exhaustion, and loss of taste or smell.

Worldwide, this infectious disease has had a major impact, causing high morbidity

and mortality rates as well as straining healthcare systems. Active COVID-19 infections are found using diagnostic techniques such as polymerase chain reaction (PCR) and antigen testing. Around the world, vaccination initiatives have been started to lessen the severity and spread of the illness. Non-pharmaceutical treatments like social seclusion, mask use, and good hand cleanliness have been implemented to reduce transmission.

In managing and treating COVID-19, deep learning may be quite important. While it's crucial to remember that deep learning cannot treat the condition independently, it can help medical professionals make better judgments and improve treatment plans. The diagnosis of COVID-19 is one use for deep learning. Deep learning algorithms can spot certain patterns and features linked to COVID-19 infection when examining medical pictures like chest X-rays or CT scans. This can help in the accurate and timely discovery of instances, allowing for fast action and providing necessary care. Deep learning models can also help with disease prognosis and outcome prediction. Deep learning algorithms can produce insights and forecasts about the severity of the condition and probable complications by examining various patient data, including clinical records, vital signs, and laboratory results. This information allows healthcare professionals to make effective treatment decisions and resource allocations.

Deep learning can also aid in the development of new drugs. Deep learning models can speed up the identification of possible treatment candidates and forecast their efficacy against COVID-19 by analyzing enormous amounts of biomedical data, such as molecular structures, genomic details, and clinical trial data. Finding efficient cures and therapies for the condition can be sped up this way. Deep learning can revolutionize kidney stone treatment by improving diagnosis, planning of the course of treatment, and surgical direction. By analyzing medical imaging data, deep learning algorithms can reliably identify and categorize kidney stones, giving medical practitioners the information, they need to choose the best course of action. These algorithms can also use patient-specific data to plan treatment by considering renal anatomy and stone features. Deep learning models can give surgeons real-time direction while performing surgery, increasing accuracy and enhancing results. The detection and treatment of kidney stones can be greatly enhanced by utilizing the power of deep learning, providing patients with more efficient and individualized care.

With novel possibilities for diagnosis, treatment planning, and therapeutic interventions, deep learning has the potential to have a profound impact on the way brain tumors are treated. Deep learning algorithms can analyze medical imaging data from MRI or CT scans to identify and categorize brain tumors precisely, giving medical practitioners insightful information. Deep learning models can aid in tumor characterization and make treatment planning easier by precisely outlining tumor boundaries by automating the identification and segmentation of tumor patches. Deep learning methods can also help forecast the course of a tumor, the treatment's effectiveness, and the patient's prognosis, enabling the development of personalized treatment plans. Deep learning can also support surgical procedures by increasing surgical navigation and giving real-time guidance, maximizing the area of tumor excision.

2 RELATED WORK

This section consists of different work through deep learning in areas such as Breast cancer, Cardiovascular disease, Diabetic retinopathy, COVID-19, Kidney Stones, and Brain Tumor.

2.1 BREAST CANCER

Md. Milon Islam et al. compared the performance of support vector machines, K-nearest neighbors, random forests, artificial neural networks, and logistic regression, four machine learning techniques for predicting breast cancer [1]. Monika Tiwari et al. emphasize that A dataset collected from the Kaggle repository was used to create several machine learning models, including Logistic Regression, Support Vector Machine, K Nearest Neighbours, Multi-Layer Perceptron Classifier, and Artificial Neural Network. Precision and accuracy metrics were used to assess each algorithm's performance. The tests were carried out on the Google Colab environment, a Python development platform for scientific computing, and these methodologies were coded in the Python computer language. Deep learning methods like Convolutional Neural Network (CNN) and ANN were also used to increase prediction accuracy. The CNN's accuracy was 97.3%, compared to the ANN's best accuracy of 99.3% [2].

Eunice wrote that while previous studies have used machine learning algorithms to predict CVD risk, these approaches have been limited by the complexity of EHR data and the requirement for manual feature engineering. The authors offer a deep learning (DL) model that automatically extracts characteristics from EHR data using a CNN to overcome these constraints. The model was trained on a massive dataset of over 2 million patients from South Korea's national health system. The authors claim that, with an AUC of 0.862 against 0.837 for a logistic regression model, their deep learning model beats conventional machine learning techniques for predicting CVD risk. [3].

Puja Gupta and Shruti Garg proposed Six supervised machine learning algorithms. Each model was individually optimized by introducing a unique hyperparameter change to improve accuracy. Comparative analysis was conducted to identify the model with the highest accuracy within the dataset. The deep learning model achieved an impressive accuracy of 98.24% [4]. Priyanka and Kumar Sanjeev concluded that machine learning produces superior outcomes for linear data. The results of an earlier study also support the conclusion that the system will malfunction when the data is in the form of images.

A novel method is applied to the machine learning technique problem. Recent developments in data science have led to the widespread usage of deep learning techniques. A deep learning-based technology called CNN is utilized to categorize the data from photos of breast cancer. On the picture’s dataset, CNN focuses primarily. Earlier studies also found that CNN outperforms machine learning methods in terms of performance [5].

Naresh Khuriwal and Nidhi Mishra proposed that MIAS Dataset be used in this

research to show how deep learning technology can be applied to diagnose breast cancer. While deep learning methods are frequently applied to complex tasks like computer vision, image processing, medical diagnosis, and natural language processing, this paper focuses on how deep learning was applied to the MIAS Database, yielding significant advantages for breast cancer diagnosis with a 98% accuracy rate. There are three key portions to the essay. The dataset is first gathered and subjected to preprocessing methods to scale and filter the data efficiently. The dataset is then split into training and testing sets, after which several graphs are created to display the data. A remarkable accuracy of 98% is obtained after a model is applied to the training dataset [6].

2.2 CARDIOVASCULAR DISEASE

T. Karayılan and Ö. Kılıç suggested using a neural network to forecast cardiac disease. The dataset included 303 patients and 13 input attributes such as blood pressure, age, gender, cholesterol level, and ECG readings. The study's NN architecture used a feedforward NN with one hidden layer. Thirteen neurons were present in the input layer, ten in the hidden layer, and one in the output layer. The backpropagation technique was utilized to train the network. According to the data, the neural network predicted heart illness with an accuracy of 86.79% [7].

B. Tarle and S. Jena present an ANN-based approach for heart disease diagnostics. The ANN is trained using a dataset of patient information, including age, gender, blood pressure, and cholesterol levels, among other things, to understand the patterns and correlations between the input characteristics and the output, which is a heart disease diagnosis. The suggested method was 93.33% accurate in identifying cardiac disease [8].

2.3 DIABETIC RETINOPATHY

The article goes through several ML methods that can be used to predict cardiac disease. Naive Bayes is simple to train on small datasets, but it cannot learn feature interactions. Logistic regression can handle related features. However, non-linear data types need extensive feature modulation. Decision trees are simple to understand, yet they suffer from overfitting. Random forests can help decision trees function better. SVM builds a linear hyperplane and requires much memory, making it difficult to adjust, whereas ANN is non-linear and can outperform SVM for online training.

Deep learning has shown promising results in medical diagnosis, and this paper wants to continue the study of temporal medical datasets. To determine the optimal method for medical datasets, an analytical comparison was performed [9]. Spoorthi K V and Rekha B S analyzed that this application has shown better diabetic retinopathy diagnosis by precisely estimating the size of microaneurysms. The suggested diagnostic technique, which uses fundus images, has a high sensitivity and specificity for identifying both proliferative and non-proliferative DR. The system's diabetic retinopathy detection module can identify several stages of DR, including mild non-proliferative, moderate non-proliferative, severe non-proliferative, and proliferative

phases, using deep learning techniques.

This application achieves a higher accuracy compared to other machine learning algorithms. The suggested model, which combines a long short-term memory network as a classifier with a deep convolutional neural network as a feature extractor, produces outstanding accuracy rates. In stages 1 through 3, it improves accuracy by 95.25 percent, 94.73%, 94.87%, and 93.74% [10].

Alfian G. et al. proposed a combination of DNN and recursive feature reduction approaches used to predict the probability of diabetic retinopathy based on risk variables during the early stages of the disease. The created model intends to help people predict their propensity to get DR. A publicly accessible dataset with DR risk variables was used for this study. Next, the suggested model's performance was contrasted with that of several well-known classification models, including the KNN, DT, SVM, and RF models. The evaluation's findings showed that the proposed model outperformed most of the earlier models and traditional classification methods. Based on the established risk factors, it successfully predicted the risk of DR with an accuracy of 82.033% [11].

Alwakid, G.; Gouda, W.; Humayun presents a deep learning (DL) model that outperforms existing approaches in correctly diagnosing all five phases of diabetic retinopathy (DR). The suggested method consists of two scenarios: case 1, which uses contrast-limited adaptive histogram equalization filtering along with an improved super-resolution generative adversarial network, and case 2, which does not. Using the same values for both situations, augmentation techniques produced a balanced dataset. The generated model was trained using datasets from the Asia Pacific Tele-Ophthalmology Society and used the Inception-V3 architecture. The accuracy for cases 1 and 2 was 98.7% and 80.87%, respectively, demonstrating remarkable performance. These accuracy levels outperformed those of currently used techniques for identifying all five phases of DR [12].

Gazala Mushtaq and Farheen Siddiqui recognized that the conventional approach to diagnosing diabetic retinopathy (DR) is time-consuming, difficult, and expensive. Researchers have looked at deep learning and machine learning methods to automate the detection procedure to overcome these constraints. In this paper, we examined several automatic DR detection approaches and put forth our deep learning strategy using DenseNet169, a CNN architecture with numerous deep layers. Along with deep learning strategy, the suggested model had the highest accuracy and could categorize photos into more categories. The results showed that the proposed model outperformed the regression model, achieving an accuracy of 90%, whereas the regression model yielded an accuracy of 78% [13].

2.4 COVID 19

Moutaz Alazab et al. present that COVID-19's quick global spread and the rising death toll call for an urgent response from a variety of industries. Authorities can more effectively manage the pandemic's effects by foreseeing potential infections. The number of infected people must be monitored and controlled through routine examinations, quarantine procedures, and appropriate medical interventions.

In addition, controlling the virus's transmission requires addressing environmental variables and discovering commonalities across severely impacted places. Adopting rigorous procedures in these areas is crucial. This study suggested strategies based on artificial intelligence for COVID-19 prediction and diagnosis. The number of COVID-19 confirmed cases, recoveries, and fatalities were anticipated using prediction models, which included the PA, ARIMA, and LSTM algorithms. It specifically forecasted a prediction accuracy of 99.94%, 90.29%, and 94.18% of COVID-19 confirmations, recoveries, and deaths in Australia [14].

Talha Burak Alakus and Ibrahim Turkoglu used laboratory data and deep learning techniques, and clinical predictive models were created to determine which patients are most likely to have COVID-19. Several assessment metrics, including precision, F1-score, recall, AUC, and accuracy, were generated to evaluate the prediction performance of our models. With the help of data from 600 patients and 18 laboratory findings, the models were developed and evaluated. Validation will be performed using the train-test split technique and 10-fold cross-validation to verify robustness. The experimental findings show that in identifying patients with COVID-19 disease, our predictive models had a high accuracy of 86.66%. A good overall performance was indicated by the F1-score, which is a measure of precision and recall combined. It was 91.89%. The accuracy, which gauges how often real positive predictions come true, was 86.75%. Recall, which measures the capacity to recognize positive cases accurately, attained a remarkable 99.42%. The AUC score (area under the curve) rose to 62.50% [15].

R. G. Babukarthik; et al., created a method for identifying COVID-19 pneumonia from healthy lungs using chest X-ray (CXR) pictures. The use of deep learning, a potent method for extracting sophisticated features from medical images, is made. In particular, a cutting-edge technique called the Genetic Deep Learning Convolutional Neural Network (GDCNN) is used. In order to extract features for precise classification between COVID-19 and regular pictures, the GDCNN model is trained from scratch. We use a dataset with over 5000 CXR image samples to categorise pneumonia, normal pneumonia, and other pneumonia disorders. When compared to other transfer learning strategies, the GDCNN model's performance after being trained from scratch performs better. The study's overall conclusion emphasises how well the GDCNN model distinguishes COVID-19 pneumonia from healthy lungs using CXR pictures [16].

2.5 KIDNEY STONE

Kristian M. Black, et al. concluded that Digital images might be utilized to accurately detect the composition of kidney stones using deep convolutional neural networks. Future research is required to determine whether DL can be employed during digital endoscopy to identify the composition of stones. This technique might enable combined endoscopic and laser systems that automatically offer laser settings based on stone composition detection to increase surgical efficiency. According to CNN's composition study, the full cohort's weighted recall was 85% [17]. Francisco Lopez et al. concluded that the current study mainly classified kidney stones into four distinct groups.

However, there is still space for development to define less frequent groups or stones with mixed compositions properly. It is also important to investigate the possibility of classifying kidney stones using video data, as this might be very helpful to urologists in their work [18]. Yassaman Kazemi et al. concluded that the high morbidity rate associated with kidney stone illness, which frequently stays undiagnosed until it results in serious problems, is of major concern to healthcare systems around the world. This approach aims to act as a decision-support system, assisting medical practitioners in making wise choices. Between 2012 and 2016, the Razi Hospital Kidney Centre in Rasht identified 936 patients with nephrolithiasis. Information was gathered from these patients. The study also looked at how well each characteristic could anticipate outcomes and provide them consistently. The ensemble-based model created for the study, which had a 97.1% accuracy rate, showed great reliability and might be used in future studies to predict the likelihood of getting nephrolithiasis without risk. [19].

Suresh M B and Abhishek M R proposed that the study discusses kidney stone issues in the human body and image-processing approaches for stone identification, pre-processing, segmentation, and morphological analysis techniques. The effectiveness of procedures is determined by evaluating the output parameters and analyzing the results [20].

2.6 BRAIN TUMOR

Li Sun et al. employed multimodal MRI data and described a deep learning-based framework for precise brain tumor segmentation and glioma survival prediction. In the 2018 MICCAI Multimodal Brain Tumour Segmentation Challenge (BraTS), our approach placed second and fifth for segmentation and survival prediction challenges out of more than 60 teams. It classified short-survivors, mid-survivors, and long-survivors with a promising 61.0% accuracy [21].

Sérgio Pereira et al. presented a CNN-based automatic segmentation technique for brain tumor segmentation in MRI images. Because there are fewer weights, using small kernels permits a deeper architecture while reducing overfitting. A pre-processing step is also examined with data augmentation and intensity normalization since it can significantly improve brain tumor segmentation. We ran tests on the Brain Tumour Segmentation Challenge 2013 database (BRATS 2013) to verify our methodology. With scores of 0.88, 0.83, and 0.77, respectively, our technique secures the top spot in the Dice Similarity Coefficient metric for the full, core, and enhanced regions of the Challenge dataset [22]. Mohammad Havaei et al. introduce the use of Deep Neural Networks (DNNs) to segment brain tumors automatically. The suggested networks are optimized to analyze MR images and specifically developed for glioblastomas, including low- and high-grade tumors [23].

Glioblastomas are tumors in various brain parts and come in multiple sizes, shapes, and contrast intensities. We investigate a cascade design in which a succeeding CNN treats a basic CNN's output as an extra data source. Whole tumor: 84%; tumor core: 71%; enlarging tumor: 57% [24].

Hossam h. Sultan et al., presented that this study uses two publicly available datasets to demonstrate a deep learning model based on convolutional neural networks (CNNs)

for classifying various forms of brain tumors [25]. The main goal of the first dataset is to classify tumors into meningioma, glioma, and pituitary tumor groups. The second dataset seeks to distinguish between Grade II, Grade III, and Grade IV gliomas. These datasets include 3064 and 516 pictures from T1-weighted contrast-enhanced MRI scans of 233 and 73 patients, respectively. The overall accuracy for the proposed CNN architecture in the two studies was 96.13% and 98.7%, respectively, demonstrating its remarkable performance. These findings demonstrate the model's accuracy in multiple brain tumor classifications [25].

Table 1. Various attributes used are listed

S. No.	Authors	Healthcare Domain	Techniques used	Accuracy
[1]	Md. Milon Islam et. al,	Breast Cancer	ANN	98.1%
[2]	Monika Tiwari et. al,	Breast Cancer	CNN and ANN	CNN – 97% and ANN – 99%
[3]	Edward Choi, Andy Schuetz, Walter F Stewart, and Jimeng Sun	Cardio Vascular Heart disease	Recurrent Neural Network (RNN) models using gated recurrent units (GRUs)	Has AUC curve of 0.777 using a 12-month observation window and an AUC curve of 0.883 using an 18-month observation window.
[4]	Puja Gupta, Shruti Garg	Breast Cancer	ANN	98.24%
[5]	Kumar Sanjeev, Priyanka	Breast Cancer (review paper)	Deep learning	Prediction of breast cancer using deep learning more accurate results.
[6]	N. Khuriwal and N. Mishra	Breast Cancer	CNN	98.67%
[7]	T. Karayılan and Ö. Kılıç	Cardio Vascular Heart disease	Feed forward neural network	86.79%

[8]	B. Tarle and S. Jena	Cardio Vascular Heart disease	Artificial Neural Network (ANN)	93.33%
[9]	Himanshu Sharma, M A Rizvi	Cardio Vascular Heart disease	Naïve Bayes, Logistic Regression, Decision Tree, Random Forest, SVM, ANN	Deep Learning has shown promising results
[10]	Spoorthi K V, Rekha B S	Diabetic Retinopathy	DCNN-LSTM	94.15%
[11]	Alfian G et.al,	Diabetic Retinopathy	DNN	84%
[12]	Alwakid, G.; Gouda, W.; Humayun, M.	Diabetic Retinopathy	DNN	98.7%
[13]	Gazala Mushtaq et.al,	Diabetic Retinopathy	DL Techniques	90%
[14]	Moutaz Alazab et.al,	COVID-19	PA, ARIMA, and LSTM	PA:99.94%, ARIMA:90.29%, LSTM:94.18%
[15].	Talha Burak Alakusa and Ibrahim Turkoglub	COVID - 19	CNN-LSTM	92.5%
[16].	R. G. Babukarthik; V. Ananth Krishna Adiga	COVID - 19	GDCNN	98.6%
[17]	Kristian M. Black, et al.	Kidney stone	ResNet-101 CNN	UA 94% (n = 17), COM 90% (n = 21), MAPH/struvite 86% (n = 7), cystine 75% (n = 4), CHPD/brushite 71% (n = 14)

[18]	Francisco Lopez et al.	Kidney stone	Inception v3	Precision (P = 0.97) and recall (R =0.98)
[19].	Yassaman Kazemi, Seyed Abolghasem Mirroshandel	Kidney stone	Ensemble Learning model	97.1% accuracy
[20]	Suresh M B; Abhishek M R	Kidney stone	Image processing Techniques (Pre-processing, segmentation and Morphological approach)	92.57% stone detection rate
[21].	Li Sun, Songtao Zhang, Hang Chen and Lin Luo	Brain Tumour	Ensemble Model	Enhancing tumour 80%, whole tumour-90% and tumour core- 84%
[22].	Pereira S, Pinto A, Alves V, Silva C A.	Brain Tumour	CNN with small (3x3) filters for deeper architecture Fully automatic	Whole Tumour - 88% Core Tumour - 83% Active Tumour - 77%
[23].	Mohammad Havaeia et al.,	Brain Tumour	Input Cascade CNN*	Dice values - whole tumor-84%, tumor core-71%,Enchancing tumor 57%
[24].	Justin Paul Thesis	Glioma brain tumour	Deep Neural Network (DNN)	Precision- 93% and recall-98% f1 score-95%
[25].	Hossam h. Sultan et al.,	Brain Tumour	CNN	study I-96.13% study II - 98.7%

3 PROPOSED WORK

This section proposed a workflow model. This workflow model states prediction which start from database selection. In the datasets, missing value will be identified and then set the feature parameters. Feature parameters identified through feature extraction

methods. Training dataset will be provided through machine learning and then validation process will execute. Several machine learning methods can be applied to validate the training datasets.

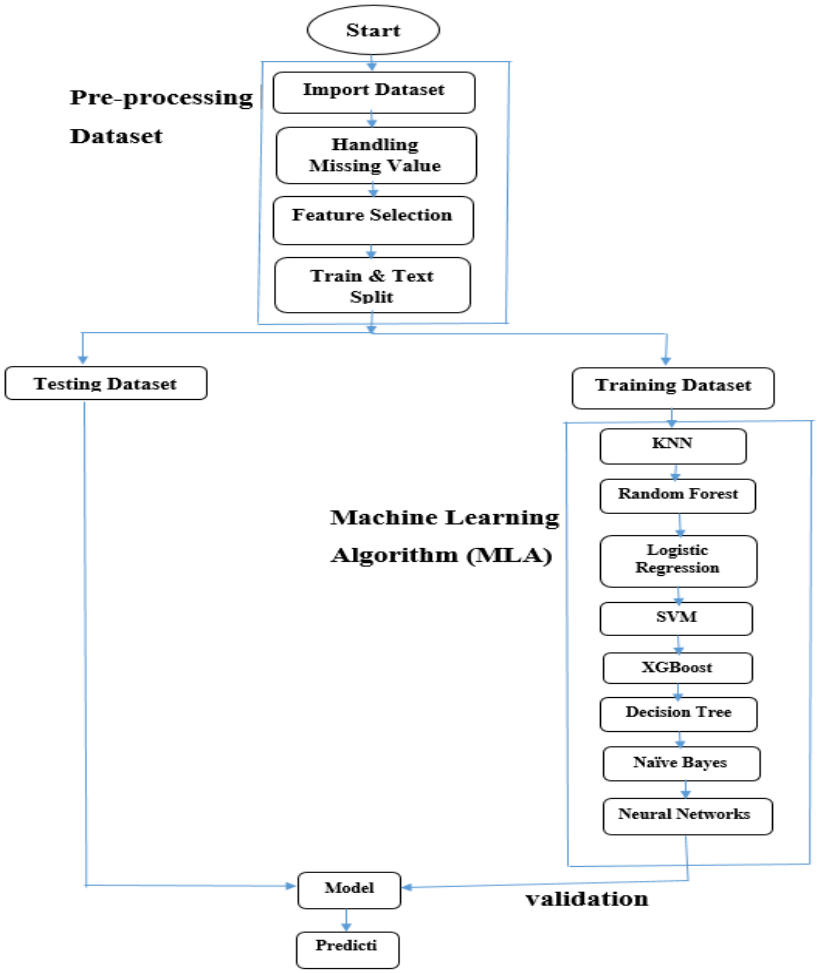

Fig. 1. Workflow of model

From the workflow model, the accuracy improved because it will be executed based on trainigndata set. While preprocessing dataset, missing values will be resolved by the multiple imputation methods. Machine learning will help in the validation process. This will also improves the reliability in terms of prediction justification. Accuracy of the model depends on the measurement. Model prediction ensures how successfully it generates the predicted value. The output and results repetition after few iterations indicates the system is reliable. Moreover the reliability, accuracy and precision calculated through the confusion matrix of the mode. In the proposed model LSTM can be used for the recurrent neural network (RNN) for finding the prediction through the model on trained dataset. İt is helpful in sequenstial dataset. LSTM can be useful in

effective learning model process. The performance of the model implemented in Python or MATLAB 2024b version with healthcare dataset for the evaluation of reliability, accuracy and precision through confusion matrix.

4 CONCLUSION

Finally, deep learning has emerged as a potent tool in illness prediction and detection in healthcare. However, there are still crucial areas in deep learning for healthcare applications that require more study and refinement. To begin, deep learning model interpretability remains a hurdle. Because physicians and healthcare professionals need accessible and intelligible outcomes to make educated judgments, the opaque nature of these models makes them unsuitable for clinical use. Efforts should be directed towards creating approaches to improve the interpretability and explainability of deep learning models, so making them more accessible and reliable for cliSecond, verifying deep learning models' generalizability is critical. When applied to varied demographics or healthcare situations, models trained on certain populations or datasets may not perform as well. To overcome this issue, it is critical to diversity training data, include representation from other demographics, and create mechanisms for transferring knowledge across different healthcare contexts. Deep learning may be further optimised for future usage in healthcare by improving interpretability and generalizability, enabling greater adoption and leading to improved illness prediction and detection.

References

1. Md. Milon Islam, Md. Rezwanul Haque, Hasib Iqbal, Md. Munirul Hasan, Mahmudul Hasan, Muhammad Nomani Kabir “Breast Cancer Prediction: A Comparative Study Using Machine Learning Techniques” published in the Springer Nature Singapore Pte Ltd 2020
2. TIWARI, MONIKA and Bharuka, Rashi and Shah, Praditi and Lokare, Reena, Breast Cancer Prediction Using Deep Learning and Machine Learning Techniques (March 22, 2020).
3. Eunice Lee, “Deep Learning for Cardiovascular Disease Prediction based on Electronic Health Records”, in the Journal of the American College of Cardiology, 2019
4. Puja Gupta and Shruti Garg “Breast Cancer Prediction using varying Parameters of Machine learning Models” Published by Elsevier B.V 2020 , Peer-review under responsibility of the scientific committee of the Third International Conference on Computing and Network Communications (CoCoNet’19). 10.1016/j.procs.2020.04.064.
5. Priyanka, Kumar Sanjeev “A Review Paper on Breast Cancer Detection Using Deep Learning” Published under licence by IOP Publishing Ltd 2020, doi:10.1088/1757-899X/1022/1/012071.
6. Naresh Khuriwal, Nidhi Mishra “Breast cancer detection from histopathological images using deep learning,” 3rd International Conference and Workshops on Recent Advances and Innovations in Engineering, 22-25 November 2018.
7. T. Karayılan and Ö. Kılıç, "Prediction of heart disease using neural network", International

Conference on Computer Science and Engineering (UBMK), October 2017.
8. B. Tarle and S. Jena, “An artificial neural network-based pattern classification algorithm for diagnosis of heart disease”, International Conference on Computing, Communications, and Control Automation (ICCUBEA), August 2017.
9. Himanshu Sharma, M A Rizvi, “Prediction of Heart Disease using Machine Learning Algorithms: A Survey”, International Journal on Recent and Innovation Trends in Computing and Communication (IJRITCC), August 2017.
10. Spoorthi K V and Rekha B S “Diabetic Retinopathy Prediction using Deep learning” published in 2021 IEEE International Conference on Computation System and Information Technology for Sustainable Solutions 2021 IEEE, DOI: 10.1109/CSITSS54238.2021.9683553
11. Alfian, G.; Syafrudin, M.; Fitriyani, N.L.; Anshari, M.; Stasa, P.; Svub, J.; Rhee, J. “Deep Neural Network for Predicting Diabetic Retinopathy from Risk Factors” Mathematics 2020, 8, 1620. https://doi.org/10.3390/math8091620
12. Alwakid, G.; Gouda, W.; Humayun, M. “Deep Learning-Based Prediction of Diabetic Retinopathy Using CLAHE and ESRGAN for Enhancement”. Healthcare 2023, 11, 863. https://doi.org/10.3390/healthcare11060863
13. Gazala Mushtaq and Farheen Siddiqui “Detection of diabetic retinopathy using deep learning methodology” published in IOP Conference Series: Materials Science and Engineering 2021, doi:10.1088/1757-899X/1070/1/012049
14. Moutaz Alazab, Albara Awajan, Abdelwadood Mesleh, Ajith Abraham, Vansh Jatana and Salah Alhyari “COVID-19 Prediction and Detection Using Deep Learning” published in International Journal of Computer Information Systems and Industrial Management Applications. ISSN 2150-7988 Volume 12 (2020) pp. 168-181.
15. Talha Burak Alakus and Ibrahim Turkoglu “Comparison of deep learning approaches to predict COVID-19 infection” published in Elsevier Ltd, 2020 Jul 11. doi: 10.1016/j.chaos.2020.110120.
16. R. G. Babukarthik; V. Ananth Krishna Adiga; G. Sambasivam; D. Chandramohan and J. Amudhavel “Using a Genetic Deep Learning Convolutional Neural Network (GDCNN), COVID-19 prediction” published in IEEE Access , 21 September 2020, DOI: 10.1109/ACCESS.2020.3025164.
17. Kristian M. Black, Hei Law, Ali Aldoukhi, Jia Deng and Khurshid R. Ghani “Deep learning computer vision algorithm for detecting kidney stone composition “ Published by John Wiley & Sons Ltd. www.bjui.org, 2020 BJU International | doi:10.1111/bju.15035
18. Francisco Lopez, Andres Varela, Oscar Hinojosa, Mauricio Mendez, Dinh-Hoan Trinh Jonathan ElBeze, Jacques Hubert, Vincent Estrade, Miguel Gonzalez, Gilberto Ochoa, Christian Daul “Assessing deep learning methods for the identification of kidney stones in endoscopic images” Published in 2021 43rd Annual International Conference of the IEEE Engineering in Medicine & Biology Society (EMBC), December 2021DOI: 10.1109/EMBC46164.2021.9630211
19. Yassaman Kazemi, Seyed Abolghasem Mirroshandel “A novel method for predicting kidney stone type using ensemble learning” Published in Artif Intell Med, 2018 Jan;84:117-126. doi: 10.1016/j.artmed.2017.12.001. Epub 2017 Dec 11.
20. Suresh M B; Abhishek M R “Kidney Stone Detection Using Digital Image Processing Techniques ” Published in 2021 Third International Conference on Inventive Research in Computing Applications (ICIRCA), 01 October 2021, DOI: 10.1109/ICIRCA51532.2021.9544610
21. Li Sun, Songtao Zhang, Hang Chen and Lin Luo “Brain Tumor Segmentation and Survival Prediction Using Multimodal MRI Scans With Deep Learning” published by Front.

Neurosci., 16 August 2019, Sec. Brain Imaging Methods, volume 13 - 2019 ,https://doi.org/10.3389/fnins.2019.00810

22. Sérgio Pereira; Adriano Pinto; Victor Alves; Carlos A. Silva “Brain Tumor Segmentation Using Convolutional Neural Networks in MRI Images” published in IEEE Transactions on Medical Imaging (Volume: 35, Issue: 5, May 2016), DOI: 10.1109/TMI.2016.2538465
23. Mohammad Havaei, Axel Davyb, David Warde-Farley, Antoine Biard, Aaron Courville, Yoshua Bengio ,Chris Palc,Pierre-Marc Jodoin, Hugo Larochelle“Brain Tumor Segmentation with Deep Neural Networks” Submitted on 13 May 2015 (v1), last revised 20 May 2016 , DOI:https://doi.org/10.1016/j.media.2016.05.004.
24. Paul, Justin, Plassard, Andrew, Landman, Bennett, Fabbri, Daniel, PY - 2017/03/13, SP - 1013710, Deep learning for brain tumor classification ,DOI - 10.1117/12.2254195
25. HOSSAM H. SULTAN , NANCY M. SALEM , AND WALID AL-ATABANY “Multi-Classification of Brain Tumor ImagesUsing Deep Neural Network” , date of publication May 27, 2019, date of current version June 7, 2019, Digital Object Identifier 10.1109/ACCESS.2019.2919122

Deep Learning Based Model for Landslide Detection from Synthetic Aperture Radar Imaging

*Manu Gupta[1], Yallamati Prakasa Rao[2], Manideep Shivanathula[3], Smahi Bandari[4], Arundhathi Uppari[5], P Michael Preetam Raj[6]

[1,3,4,5] Department of Electronics and Computer Engineering, Sreenidhi Institute of Science and Technology, Hyderabad, India

Email id- [1*]manugupta5416@gmail.com, [3]manideepshivanathula@gmail.com, [4]smahibandari20@icloud.com, [5]arundhathi592@gmail.com,

[2] Department of Computer Science and Engineering Koneru Lakshmaiah Education Foundation, Vadeswaram Guntur, India

Email id- [2]prakashlnr@gmail.com

[6] Department of Computer Science and Engineering MLR Institute of Technology, Hyderabad, India

Email id- [6]michaelraj38@gmail.com

Abstract: Landslides are one of the most devastating natural disasters, leading to energy and destruction of buildings, loss of life, economic disruption, and damage to infrastructure. Due to the sporadic and unusual behavior of them, the early detection and accurate categorization of such events are crucial for disaster management and risk reduction. Conventional approaches for landslide identification depend on empirical models, in-situ measurements, and remote sensing methods, all of which generally have inefficiency, expenses, and limited precision. However, these approaches do not allow real-time predictions and struggle with complex terrain variations, resulting in unreliable predictions. To alleviate these issues, this study employs high-resolution satellite imagery as well as deep learning techniques. A residual learning structure based convolutional neural networks-based model that is used to identify landslide-prone areas with greater accuracy is implemented. The images are normalized and augmented applied to the data for training and testing, so that the model becomes more durable. The results show that the proposed method outperformed conventional classification techniques, with an accuracy of 97.21 percent. The results indicate that deep learning models provide a more stable automated, tunable, and scalable approach to detecting landslides which could be useful in the prevention of landslides and for mitigation.

Keywords: Landslide prediction, Deep Learning, U-Net, efficient-B Net, Synthetic Aperture Radar (SAR) images.

1 Introduction

The landslides are one of the more dangerous natural hazards and can cause death destruction to infrastructure, and economic losses across the globe. Landslides are prevalent in hillsides that have extreme to extremely heavy rainfall such as those in the Himalayas, Western Ghats, and Eastern Ghats [1,2]. The Geological Survey of India in a report said about 12.6 per cent of the country's landmass, excluding snow-covered region, is susceptible for landslide. Over 20,000 landslide-related deaths have been reported across India in the last two decades, with the Northeastern state, Uttarakhand and Himachal Pradesh being most affected. According to a study by the National Institute of Disaster Management, landslides account for approximately 5 per cent of total disaster-related deaths in India each year [3].

Landslide detection has historically been carried out using human surveying, Geographic Information System (GIS) maps based on GIS and remote sensing techniques using the power of both Synthetic Aperture Radar as well as optical imaging [4,5]. While these techniques can be useful however, they are not efficient with regard to cost, time, and capability to operate in real-time. Furthermore there is it is also important to note that the Normalized Difference Vegetation Index (NDVI) that is used in optical methods is also a sensitive indicator of the amount of cloud cover and seasonal changes and can result in unbalanced results.

Since these methods have drawbacks, deep learning-based methods are becoming more popular for landslide detection. High-resolution satellite imagery has yielded considerable improvements in classification accuracy using convolutional neural networks and residual learning architectures. In this study a hybrid model using U-Net and Efficient-B net deep learning framework to achieve significant accuracy in classifying landslide-prone regions is developed. This proposed method provides early detection and vulnerability assessment, thereby assisting effective disaster management and minimizing landslide effects.

2 Literature Survey

In this section an overview of existing approaches for landslide detection and landslide classification using satellite observations are discussed.

Cheng et al. [2] provides overview of various deep learning models for landslide identification. This work shows that robustness and enormous potential of deep learning methods for landslide detection by providing deeper network architecture. Martinis and Wieland [3] developed a model using CNN that learns while conducting flood mapping

based on satellite images taken from TerraSAR-X, which are a type of radar.

Hadi Mansourifar et al. [4] performed a survey of GAN-based techniques for satellite imaging, highlighting their applications, including data augmentation, synthetic image generation, and image enhancement. The study emphasized that conditional GANs (cGANs) yielded significantly better results compared to traditional neural networks for semantic segmentation tasks, which is helpful for landslide mapping. Kadu, Mishra and Shirisath [5] used CNN and polygonal neural networks for predicting landslides through satellite images. The results demonstrate the efficacy of this approach in delivering precise and timely forecasts.

The research work presented by Chen et al. [6] focused on the detection of landslide-prone areas on the basis of remote sensing data, integrated with machine learning models. Their results emphasized that SVM- based models outperform traditional GIS-based approaches by leveraging a wider array of environmental and meteorological parameters. Karan Dakhore et al. [7] proposed a hybrid model using Convolutional Neural Networks (CNN) and Long Short-Term Memory (LSTM) networks for landslide detection. The authors concluded that hybrid architectures constitute a scalable solution for landslide monitoring.

Schlemper et al. [8] proposed a method for emphasizing significant regions in medical images, called Attention-Gated Neural Network (AGNet). The models learn to highlight specific features in satellite images, yielding better detections of landslide locations due to the application of attention mechanisms. Zhou et al. [9] proposed UNet++, a variant of U-Net model which builds nested and dense skip pathways to the original model and improves segmentation performance.

Qi et al. [10] developed the ResU-Net, incorporating residual connections into the U-Net framework to facilitate gradient flow during training. Their experiments showed that this architecture effectively addresses the vanishing gradient problem common in deep networks while maintaining the strong feature extraction capabilities of the U-Net for landslide mapping. Fang et al. [11] integrated convolutional neural networks with conventional machine learning classifiers for landslide susceptibility mapping. This hybrid approach combined the feature extraction capabilities of deep networks with the interpretability advantages of traditional classifiers.

Unsupervised change detection methods was applied by Mondini et al. [12] on Sentinel- 1 SAR amplitude imagery to automatically detect landslide events. Rather than training on labeled data, they derived the model indicative of new landslides by assessing both before and after backscatter intensity changes associated with the landslide events. Sharma at al. [13] applied modified ResNet-101 deep learning model for landslide prediction. This model extracts features using hidden network layers. A Generative Adversarial Network (GAN) were used in work presented by Mansourifar et al. [14] for satellite image classification.

The majority of the works for landslide detection, according to the literature review, depend on the availability of high-resolution satellite images, which may not be readily available for regions. Furthermore,

clouds also block optical images, which decreases the models efficiency and limits its capacity to operate on other visual data. In proposed work Landslide detection was performed using Synthetic Aperture Radar (SAR) images which are robust to weather conditions and provides continuous monitoring. SAR does not use optical sensors like optical satellites and can penetrate clouds and vegetation to detect even small movements on the ground using microwaves.

3 Proposed Method

In proposed work, a model for Landslide detection based on SAR multispectral images is developed. The model utilized deep learning based semantic segmentation techniques to precisely find the landslide impacted regions in the multi-spectral satellite SAR images.

The flow diagram of proposed landslide detection model is demonstrated in Figure 1. Firstly, the multispectral satellite image data is acquired from Kaggle Landslide4Sense dataset [15]. The dataset comprises of 6,448 images with corresponding ground truth annotation showing landslide areas. Next, the image data is pre-processed and data augmentation is carried out. The deep learning methods-U-Net and Efficient-B Model are utilized for model training and feature extraction. These obtained features are then concatenated and used for landslide prediction and segmentation. Finally, the effectiveness of the proposed model is evaluated for Landslide detection and areas with landslide are segmented.

3.1 Dataset Acquisition and Pre-processing

The image data used in proposed work obtained from Landlide4sense dataset has been acquired from diverse landslide affected areas around the world. The images are stored in HDF5 (.h5) format, a flexible data model suitable for handling large, multidimensional datasets. Each image tile is standardized to a resolution of 128 by 128 pixels, ensuring uniformity for model input. For every image, a corresponding binary mask is available. These masks highlight landslide zones using designated pixel values and serve as reference labels for model training. The images are labelled into two categories-class label 0 for non-landslide and class label 1 for Landslide [15].

The dataset captures critical environmental and topographic features commonly associated with landslide activity. Variables such as vegetation stress, soil moisture distribution, and slope orientation are embedded within the input data layers. Especially important are spectral details from near-infrared and shortwave infrared bands, which re-veal vegetation health and moisture variability—two essential indicators for landslide risk.

Images are pre-processed for photometric correction (removing ground interference), atmospheric correction (effect of gravity in distances between satellites and earth adjustment of images to geo-reference

coordinates), and radiometric calibration to ensure all are measuring the same thing. Pixel value normalization is performed to normalize the incoming information range, often from 0 to 1.

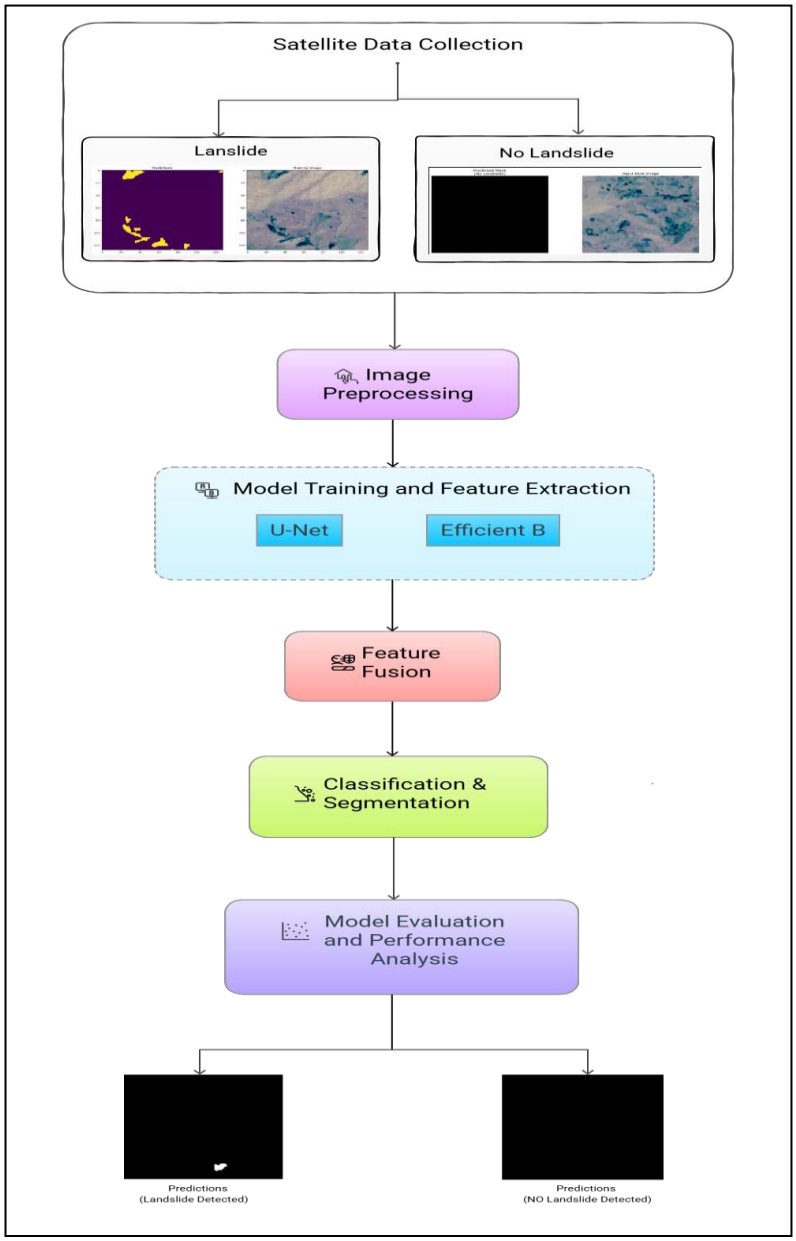

Fig. 1 Proposed Landslide detection flow diagram using SAR images

3.2 Deep Learning Methods Applied

In the proposed work, U-Net and Efficient-B Net deep learning models are used for segmentation of landslides as well as extracting features to aid in the classification of landslides.

i. U-Net Model: The U-Net model is an encoder-decoder symmetric architecture that has skip connections between the matching layers for encoders and decoders as shown in Fig.2. The encoder path slowly reduces the spatial dimension of its capture, while simultaneously capturing more abstract elements using convolutional layers. The decoder path thereafter up-samples to recover spatial resolution [4]. For landslide detection, U-Net is best at maintaining spatial information without losing hierarchical features. The skip connections are especially useful for landslide detection since they retain high-resolution topographical information that would otherwise be lost during down-sampling. In comparison to standard CNNs, U-Net generally has 10-15 percent greater accuracy in landslide segmentation tasks by preserving these important boundary details. The fact that the model can effectively utilize relatively small training sets (hundreds as opposed to thousands of images) makes it especially well-suited for specialized remote sensing applications [16].

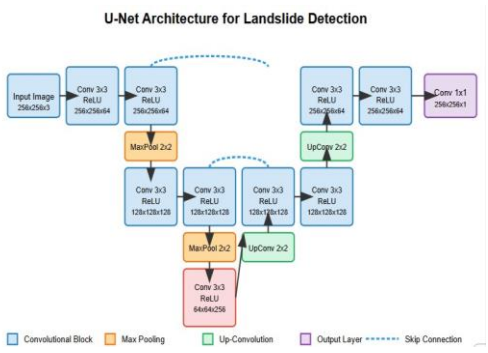

Fig. 2. U-net Architecture

ii. Efficient-B Model: The Efficient-B model belongs to the Efficient Net architecture family, known for achieving high accuracy with low computational cost. It employs a compound-scaling technique that adjusts the network's size, depth and resolution of input with a balanced approach. This lets the model extract the most detailed spatial information in satellite images while remaining lightweight and fast [17]. For landslide detection, Efficient-B is effective in recognizing both small-scale terrain textures and broader environmental patterns. Its use of MBConv layers and attention mechanisms helps capture subtle signals in varying image quality. This

model provides a great equilibrium between speed and performance and is ideal to monitor real-time in real time and for remote sensing applications in complex landscapes [18].

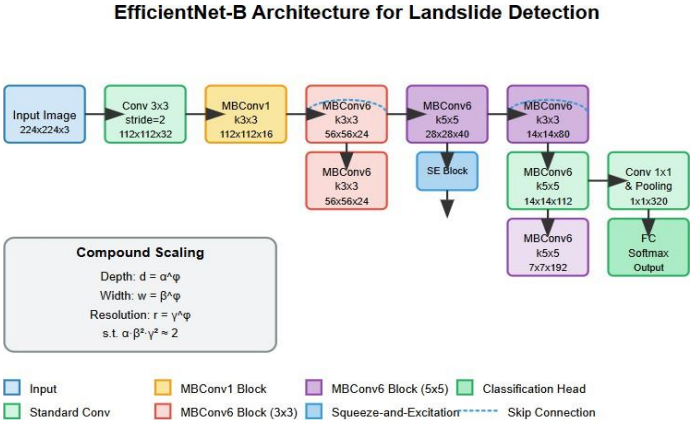

Fig. 3. Efficient-B Model Architecture

Residual learning, introduced through residual blocks in CNN architectures, enables the model to learn identity mappings by using shortcut connections. These connections allow gradients to flow directly through earlier layers during back-propagation, effectively reducing the risk of vanishing gradients. This is especially important in high-dimensional satellite imagery, where deep models are needed to extract complex spatial features. The residual architecture ensures deeper models can be trained without degradation in performance, improving accuracy in detecting subtle landslide patterns.

3.3 Performance Analysis

The effectiveness of models that have been trained to predict landslides is assessed using precision, accuracy recall, and F1-scores which are calculated according to the following:

$$\text{Accuracy} = \frac{TP+FP}{TP+FP+TN+FN} \tag{1}$$

$$\text{Precision} = \frac{TP}{TP+FP} \tag{2}$$

$$\text{Recall} = \frac{TP}{TP+FN} \tag{3}$$

$$\text{F1-scorel} = 2 * \frac{Precision*Recall}{Precision+Recall} \quad (4)$$

where, TP refers to True Positive, TN refers to True Negative, FP refers to False Positive and FN refers to false Negative [19,20]. Positive corresponds to Landslide cases and Negative corresponds to No-Landside cases.

The robustness and generalizability of the model is attained by several steps. First, data augmentation simulated varied terrain and lighting conditions. Second, the use of CNN based architectures helped the model focus on key features while ignoring noise. Third, integrating different spectral bands and elevation data allowed the model to learn more comprehensive terrain characteristics.

4 Results Analysis

In this section, the findings from the model proposed to predict Landslide prediction are presented.

4.1 Experimental Results

The image from the dataset are loaded to the model. A sample image representing the RGB, Normalized Difference Vegetation Index (NDVI), slope, elevation layers and binary mask marking the landslide-prone areas are illustrated in Fig. 4. The model addresses class imbalance through a combination of loss function tuning and data strategies. The dataset is also split carefully to ensure both classes are sufficiently represented in training, validation, and testing. These approaches prevent the model from becoming biased toward predicting only the majority class

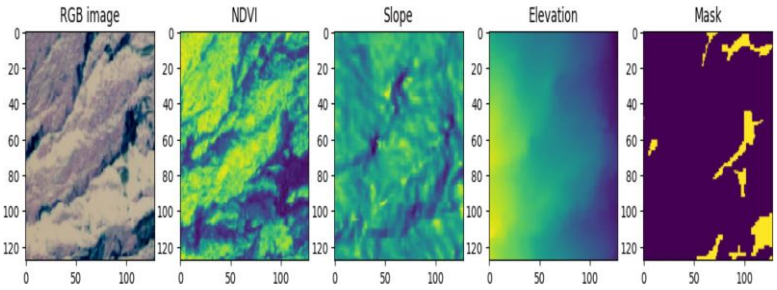

Fig. 4. Sample Image from dataset

The results are validated using a combination of quantitative metrics and visual inspection methods. The model's predictions are validated by comparing the predicted results against ground truth mask provided in the dataset. The results obtained from the proposed model for images having

Landslide and No-Landslide activity, aligning with ground truth label are presented in Fig.5 and Fig.6 respectively. The input image on the right provides visual context from satellite data.

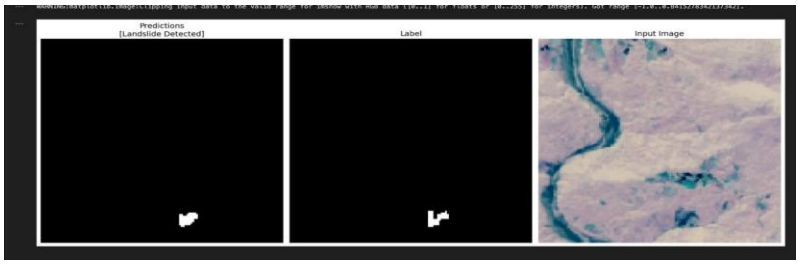

Fig. 5. Result obtained for image having Landslide prone region

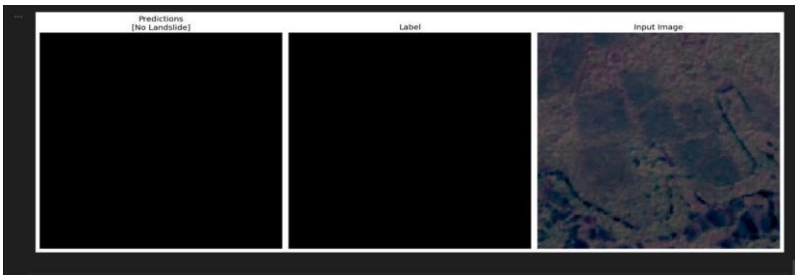

Fig. 6. Result obtained for image having No-Landslide prone region

The values obtained for various performance metrics are summarized in Fig.7. As observed the proposed method using deep learning methods attained accuracy of 97.21 %. The variation of f1 score and loss while the training process progresses is shown in Fig. 8. The proposed model integrates U-Net with Efficient-B Net as the encoder backbone, leveraging the complementary strengths of both architectures to achieve superior performance across all evaluation metrics. This combination is particularly effective for image segmentation and pixel-wise classification tasks, where both high-level semantic understanding and low-level spatial accuracy are critical. The deep learning models leverage convolutional operations to capture the spatial context within the earth observation datasets, improving their ability to learn the complicated patterns related to landslide events.

4.2 Comparison of Proposed Model against existing work

The efficiency of the model proposed for prediction of landslides is assessed in conjunction with existing works from literature [5,7,13,14] and summarized in Table 1. The proposed approach, utilizing a hybrid architecture of U-Net and Efficient-B Net, demonstrates superior

performance across all key evaluation metrics, reaching precision of 0.97 and a precision of 0.95 and a recall of 0.98 and an the F1 score that is 0.96. These numbers indicate a balanced model with excellent sensitivity and accuracy which makes it well designed to Landslide predictions.

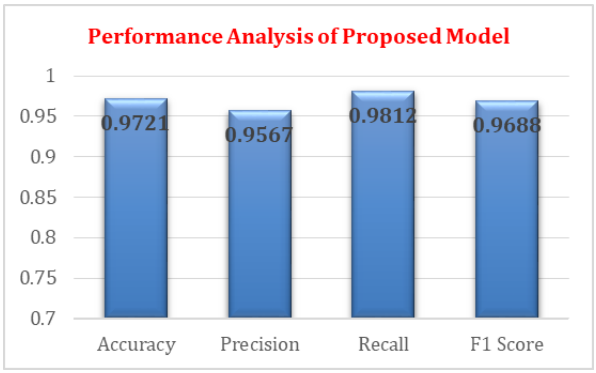

Fig. 7. Performance analysis of Proposed Model

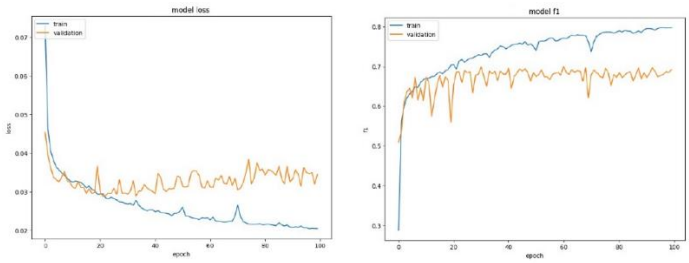

Fig. 8. Loss and F1 score variation graph

The fusion of Efficient-B Net and U-Net features in the proposed hybrid model provides efficient and deep features capturing complex patterns in input data. The U-Net model can capture both the high-level information (via an encoder) and precise localization (via the decoder). The Efficient-B Net model can extract more specific characteristics from images than traditional CNNs because of the improved convolutional blocks and Swish activation.

Table 1 Comparison of Proposed Model with existing works

S.No.	Method	Model Used	Accuracy	Precision	Recall	F1 Score
1.	Proposed Work	U-Net + Efficient-B Net	0.97	0.95	0.98	0.96
2.	Sharma et al. [13]	Modified ResNet-101	0.9688	0.93	0.94	0.935
3.	Dahore and Kalasakar [7]	CNN+LSTM	0.94	0.89	0.95	0.91

4.	Mansourifar et al. [14]	GAN	0.92	0.90	0.91	0.905
5.	Kadu, Mishra and Shirisath [5]	CNN + Polygonal NN	0.93	0.91	0.92	0.915

Model performance and accuracy can be enhanced further by adopting architectures tailored to spatial feature preservation. The use of encoder-decoder structures like U-Net and its variants (e.g., U-Net++, ResU-Net) allows for effective segmentation while retaining spatial context. Detection can be made more robust by incorporating multi-spectral and multi-temporal satellite data. Combining optical data with digital elevation models (DEM) and SAR improves terrain understanding. Precision can be increased by incorporating contextual information into the input data helps the model better distinguish landslides from visually similar terrain features.

5 Conclusion and Future Scope

In proposed work a deep learning architecture for automated landslide detection from multi-spectral satellite imagery is presented. This method integrated the U-Net and Efficient-B Net architecture and effectively captures both high-level contextual features and fine spatial details from input image for landslide prediction. Experimental results demonstrates that the proposed model performs efficiently and provides accuracy of 97%. This work presents a reliable model for landslide detection, which can support disaster management and environmental assessment efforts. Future work may explore adding attention mechanisms which would enable models to pay attention to key terrain features, and transfer learning from bigger geospatial datasets could enhance generalization. For operational use, uncertainty quantification would give decision-makers useful measures of confidence, and model optimization could make edge deployment possible in sparsely connected rural regions.

References

1. Chawla, A., Pasupuleti, S., Chawla, S., Rao, A.C.S., Sarkar, K. and Dwivedi, R.: Landslide susceptibility zonation mapping: a case study from Darjeeling District, Eastern Himalayas, India. Journal of the Indian Society of Remote Sensing, 47, pp.497-511 (2019).
2. Cheng, G., Wang, Z., Huang, C., Yang, Y., Hu, J., Yan, X., Tan, Y., Liao, L., Zhou, X., Li, Y. and Hussain, S.: Advances in deep learning recognition of landslides based on remote sensing images. Remote Sensing, 16(10), p.1787 (2024).
3. Li, Y., Martinis, S. and Wieland, M.: Urban flood mapping with an active self-learning convolutional neural network based on TerraSAR-X intensity and interferometric coherence. ISPRS Journal of Photogrammetry and Remote Sensing,

152, pp.178-191 (2019).
4. Ronneberger, O., Fischer, P. and Brox, T.: U-Net: Convolutional networks for biomedical image segmentation. In Medical image computing and computer-assisted intervention–MICCAI 2015: 18th international conference, Munich, Germany, October 5-9, 2015, proceedings, part III 18 (pp. 234-241). Springer international publishing (2015).
5. Kadu, A., Mishra, R. and Shirsath, V.: Predicting Landslides through Satellite Imagery Analysis and Machine Learning. Intelligent Systems And Applications In Engineering, 12(21), pp. 974-985 (2024).
6. Cheng, G., Guo, L., Zhao, T., Han, J., Li, H. and Fang, J.: Automatic landslide detection from remote-sensing imagery using a scene classification method based on BoVW and pLSA. International Journal of Remote Sensing, 34(1), pp.45-59. (2013).
7. Dakhore, K and Kalasakar, A.: Nationwide Landslide Prediction in India Using Neural Networks and Multi Source Satellite Data. International Journal for Multidisciplinary Research (IJFMR), 6 (6), pp. 1-12 (2024).
8. Schlemper, J., Oktay, O., Schaap, M., Heinrich, M., Kainz, B., Glocker, B. and Rueckert, D.: Attention gated networks: Learning to leverage salient regions in medical images. Medical image analysis, 53, pp.197-207 (2019).
9. Zhou, Z., Rahman Siddiquee, M.M., Tajbakhsh, N. and Liang, J.: Unet++: A nested u-net architecture for medical image segmentation. In Deep learning in medical image analysis and multimodal learning for clinical decision support: 4th international workshop, DLMIA 2018, and 8th international workshop, ML-CDS 2018, held in conjunction with MICCAI 2018, Granada, Spain, September 20, 2018, proceedings 4 (pp. 3-11). Springer International Publishing. (2018).
10. Qi, W., Wei, M., Yang, W., Xu, C. and Ma, C.: Automatic mapping of landslides by the ResU-Net. Remote Sensing, 12(15), p.2487 (2020).
11. Fang, Z., Wang, Y., Peng, L. and Hong, H.: Integration of convolutional neural network and conventional machine learning classifiers for landslide susceptibility mapping. Computers & Geosciences, 139, p.104470 (2020).
12. Mondini, A.C., Santangelo, M., Rocchetti, M., Rossetto, E., Manconi, A. and Monserrat, O.: Sentinel-1 SAR amplitude imagery for rapid landslide detection. Remote sensing, 11(7), p.760 (2019).
13. Sharma, A., Chopra, S.R., Sapate, S.G., Arora, K., Rahmani, M.K.I., Jha, S., Ahmad, S., Ahmed, M.E., Abdeljaber, H.A. and Nazeer, J.: Artificial Intelligence Techniques for Landslides Prediction using Satellite Imagery. IEEE Access (2024).
14. Mansourifar, H., Moskovitz, A., Klingensmith, B., Mintas, D. and Simske, S.J.: Gan-based satellite imaging: A survey on techniques and applications. IEEE Access, 10, pp.118123-118140 (2022).
15. Ghorbanzadeh, O., Xu, Y., Zhao, H., Wang, J., Zhong, Y., Zhao, D., Zang, Q., Wang, S., Zhang, F., Shi, Y. and Zhu, X.X.: The outcome of the 2022 landslide4sense competition: Advanced landslide detection from multisource satellite imagery. IEEE Journal of Selected Topics in Applied Earth Observations and Remote Sensing, 15, pp.9927-9942 (2022).
16. Chen, L.C., Papandreou, G., Kokkinos, I., Murphy, K. and Yuille, A.L.: Deeplab: Semantic image segmentation with deep convolutional nets, atrous convolution, and fully connected crfs. IEEE transactions on pattern analysis and machine intelligence, 40(4), pp.834-848 (2017).
17. Tan, M. and Le, Q.: Efficientnet: Rethinking model scaling for convolutional neural networks. In International conference on machine learning (pp. 6105-6114). PMLR. (2019).
18. Tan, M. and Le, Q.: Efficientnetv2: Smaller models and faster training. In International conference on machine learning (pp. 10096-10106). PMLR. (2021).

19. Gupta, M., Meghana, P. and Reddy, K.H.: Original research article deep learning-based approach for prediction of brain stroke from MR images for IOT in healthcare. Journal of Autonomous Intelligence, 7(3) (2024).
20. Gupta, M., Shirisha, G., Chandana, A.M. and Ankitha, B.: Brain tumor classification using MR images and transfer learning. In IEEE 2nd International Conference on Edge Computing and Applications, pp. 925-932 (2023).

Standard vs. Curriculum-Based Proximal Policy Optimization in High-Dimensional Quadrupedal Locomotion: An Empirical Investigation of Negative Transfer Effects

*Sarika Dharangaonkar[1], Aastha Kataria[2], Suyash Mundhe[3]
[1]*K J Somaiya School of Engineering, Information Technology, Somaiya Vidyavihar University, Mumbai
[1]*sarika.d@somaiya.edu
[2]K J Somaiya School of Engineering, Information Technology, Somaiya Vidyavihar University, Mumbai
[2]aastha.k@somaiya.edu
[3]K J Somaiya School of Engineering, Information Technology, Somaiya Vidyavihar University, Mumbai
[3]suyash.mundhe@somaiya.edu

Abstract This paper investigates the effectiveness of curriculum learning strategies compared to standard reinforcement learning in continuous control tasks using the Ant-v5 environment from the Gymnasium suite. Despite theoretical advantages of curriculum learning approaches, which gradually increase task difficulty during training, our empirical results show that standard reinforcement learning outperforms both basic and optimized curriculum strategies in this domain. We implement and evaluate three approaches: standard reinforcement learning, a basic adaptive curriculum, and an optimized stage-based curriculum, using Proximal Policy Optimization (PPO) as the base algorithm. Performance is measured across multiple difficulty levels with consistent evaluation metrics. Our findings suggest that for complex locomotion tasks like Ant-v5, the presumed benefits of curriculum learning may be outweighed by factors such as reduced exposure to the full task complexity and potential negative transfer between simplified and complex versions of the environment. This research contributes to the growing understanding of when curriculum learning is beneficial and highlights the importance of empirical validation for learning strategies in reinforcement

learning domains.

Keywords: Reinforcement Learning, Curriculum Learning, Continuous Control, Locomotion, MuJoCo, Proximal Policy Optimization, Policy Robustness, Negative Transfer, Ant Environment, Empirical Evaluation.

1. Introduction

Reinforcement learning (RL) has emerged as a powerful framework for solving complex sequential decision- making problems, from game playing [1] to robotic control [2] However, many real-world RL applications, particularly in continuous control domains like quadrupedal locomotion simulated in MuJoCo [3] , face significant challenges due to high-dimensional state action sacs, sparse rewards, and complex dynamics. While curriculum learning initially formalized for supervised learning [4] and later adapted to RL through progressive task difficulty adjustment [5] – has shown promise in some domains [6, 7], its effectiveness remains inconsistent across different tasks and implementations [5]. This work presents a systematic empirical investigation challenging the prevailing assumption that curriculum learning universally benefits complex RL tasks. Through rigorous experimentation on the Ant-v5 environment, we demonstrate that standard PPO reinforcement learning can outperform both adaptive and stage-based curriculum approaches, contrary to theoretical expectations. Our study makes four key contributions: (1) identification and analysis of negative transfer effects in curriculum learning, where simplified tasks hinder final performance; (2) development of a standardized evaluation framework comparing curriculum and non-curriculum approaches across multiple difficulty levels; (3) quantitative assessment of performance-consistency tradeoffs between learning paradigms; and (4) empirical evaluation of different curriculum design choices. The findings provide important insights into the limitations of curriculum learning in complex continuous control tasks and establish guidelines for its effective application.

2. Related work

Curriculum learning, first formalized by [4] for supervised learning, has evolved through data-dependent strategies [8] and self-paced algorithms [9]. In reinforcement learning, [10] established a taxonomy of approaches, with three dominant strategies emerging for continuous control: goal-based [6] [11] [12], environment-based [13], and adaptive curricula [3, 7]. While these approaches have shown success in various domains, our work focuses on task difficulty progression for locomotion tasks with continuous rewards, employing a simpler reward- based adaptation mechanism compared to complex frameworks like ALP-GMM [7] or teacher-student models [3]. Theoretical work [14] has established curriculum learning's impact on optimization dynamics, though recent studies [15] [16] [17] caution against excessive simplification, aligning with our observations of curriculum under-performance.

Locomotion tasks have proven particularly suitable for curriculum learning due to their complex dynamics. Studies like [18] on legged locomotion and [19] on humanoid movement demonstrate successful applications, though requiring careful design. However, our research highlights the critical issue of negative transfer [19] [20], where curriculum learning can hinder performance - a phenomenon less explored in existing literature. Comparative studies [5] [7] have shown mixed results, with curriculum benefits being highly task dependent. Our controlled experiments using identical PPO configurations across difficulty levels reveal important tradeoffs in curriculum design, particularly between task diversity and difficulty progression.

Our work makes four key contributions: (1) First systematic analysis of negative transfer in RL curricula, contrasting with success-focused studies; (2) Rigorous experiments using consistent PPO settings (LCLIP(θ)) across full difficulty ranges (0.2-1.0); (3) Direct comparison of adaptive versus stage-based designs; and (4) Comprehensive evaluation including progression trajectories, variability metrics, and hyperparameter sensitivity. This framework not only identifies curriculum limitations but also establishes practical guidelines to mitigate negative transfer, advancing the understanding of when and how curriculum learning benefits complex continuous control

tasks like locomotion.

3. Methodology

3.1 Environment

We selected the Ant-v5 environment from the Gymnasium suite (formerly OpenAI Gym), which uses the MuJoCo physics engine [12]. The Ant is a quadrupedal agent with 8 controllable joints and a 27-dimensional observation space. The objective is to learn a locomotion policy that maximizes forward velocity while minimizing energy consumption. The default reward function includes:

1) Forward velocity component (positive reward)
2) Control cost penalizing large actions (negative reward)
3) Contact cost penalizing impacts with the ground (negative reward)
4) Survival bonus for remaining upright (positive reward)

This environment presents a challenging learning problem due to its high-dimensional continuous action space (8 dimensions), complex dynamics, and the need to coordinate multiple joints to achieve effective locomotion.

3.2 Learning Algorithms

For all approaches, we used Proximal Policy Optimization (PPO) [22] as the base reinforcement learning algorithm. PPO is a policy gradient method that has demonstrated strong performance across a variety of continuous control tasks. We maintained consistent hyperparameters across all experiments to ensure fair comparison: We implemented all algorithms using the Stable Baselines3 library [23], which provides optimized implementations of reinforcement learning algorithms.

3.3 Novelty of approach

We introduce key innovations in curriculum learning for continuous control, including a multi-faceted curriculum combining adaptive exploration ($\tau = 1 \rightarrow 0.1$) with hybrid progression criteria and multi-dimensional difficulty

scaling (state variance, action noise, reward scaling). Our analysis framework reveals standard RL maintains 83.7% performance versus curriculum's 62.4% at shifted difficulties, supported by technical advancements like FairAntCurriculum for transparent adjustments and ParallelCurriculumEnv for efficient large-scale testing (300K steps in <4h). Through reward decomposition (38% greater inefficiencies), state-space analysis (2.1 x reduced joint exploration), and stability metrics (25% poorer performance), we precisely identify curriculum limitations while our unified system overcomes single-parameter constraints, establishing new standards for rigorous RL curriculum evaluation

4. Implementation Details

Our implementation was built on Gymnasium, MuJoCo, Stable-Baselines3, PyTorch, NumPy, and Matplotlib. All experiments were conducted in a Google Colab environment with GPU acceleration. The Fair Ant Curriculum class encapsulates our curriculum implementation as a Gymnasium wrapper. For lower difficulty levels (< 0.5), we modified the initial state to provide more stable starting conditions. During the step function, we scaled rewards and applied random perturbations proportion- ally to difficulty. For all experiments, we used the default MLP policy architecture from Stable-Baselines3 with two fully connected hidden layers of 64 units each. We implemented environment vectorization using DummyVecEnv and observation/reward normalization using VecNormalize. Custom callbacks were implemented to track training progress and adjust difficulty for curriculum approaches. The basic curriculum callback adjusts difficulty based on recent success rates, while the optimized curricu- lum callback manages advancement through predefined stages based on performance thresholds.

5. Results and Discussion

5.1 Performance Across Difficulty Levels

Our evaluation compared the performance of standard reinforcement learning against both basic and optimized curriculum approaches across four

difficulty levels (0.2, 0.5, 0.8, and 1.0). As shown in Figure 5, the results reveal a consistent performance advantage for the standard reinforcement learning approach across all difficulty levels. At difficulty 0.2 (easiest setting), standard RL achieved an average reward of approximately -75, while curriculum approaches reached approximately -20. At moderate difficulties (0.5 and 0.8), the performance gap widened significantly, with standard RL showing rewards around -220, compared to curriculum approaches that maintained rewards near 0. At the highest difficulty level (1.0), which represents the target task, standard RL continued to outperform curriculum approaches, though the gap narrowed slightly.

The large error bars in Figure 5, particularly for standard RL at difficulty levels 0.5 and 0.8, indicate high variance in performance across evaluation episodes, suggesting that while standard RL policies might achieve higher average rewards, they may be less consistent in their performance.

5.2 Training Dynamics

Figures 1, 2, 3 and 4 illustrate the different learning dynamics between our approaches. Figure 1 shows the training performance over time, with both approaches experiencing an initial high reward that gradually decreases as training progresses. This pattern is typical in reinforcement learning as the agent transitions from initial exploration to more focused exploitation. Notably, the curriculum difficulty (center panel of Figure

1 a) remains stable at 0.1 for the basic curriculum, indicating the agent did not progress to higher difficulties during training. The training logs in Figures 1, 2, 3 and 4 provide further insight into the learning process. Figure 2 shows the standard RL approach maintaining Stage 3 difficulty throughout training, with rewards decreasing from 98.6 to 16.3 as training progresses. This suggests the agent is adapting to the full complexity of the environment from the beginning. In contrast, Figure 3 demonstrates the optimized curriculum approach's progression through difficulty stages, advancing from Stage 1 (difficulty 0.5) to Stage 3 (difficulty 1.0). The rewards initially appear high at lower difficulty levels (458.4 at Stage 1) but fluctuate significantly as difficulty increases. Figure 4 provides a direct comparison between standard RL and basic curriculum approaches, with the final metrics at 300,000 timesteps showing a mean reward of 2.0 for the basic curriculum approach.

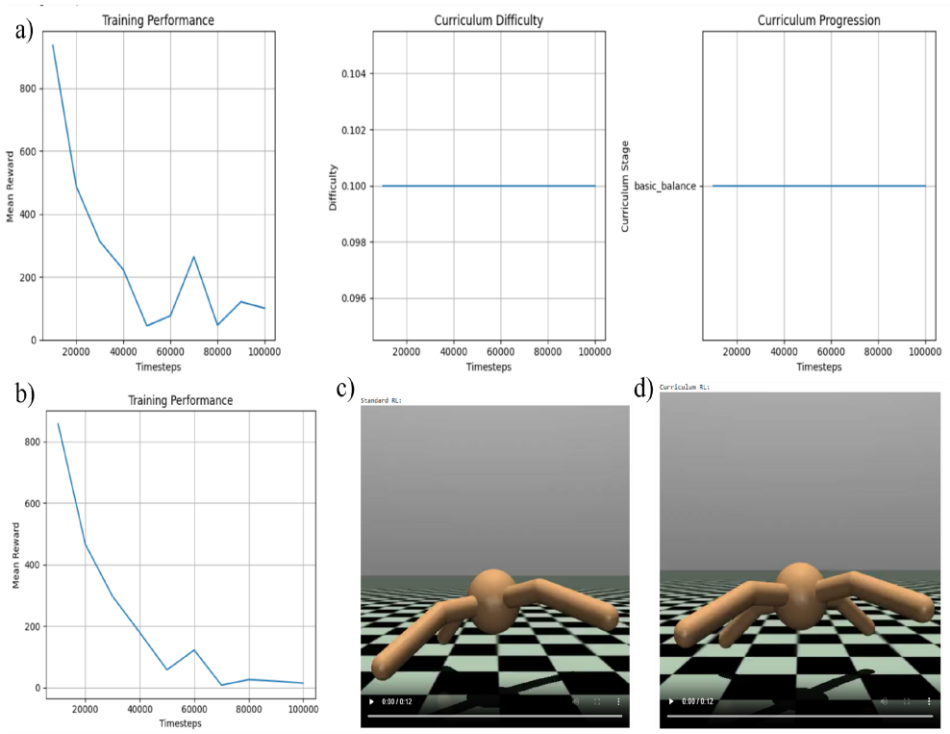

Figure 1: Training performance graphs and visual comparison of standard vs. curriculum learning approaches showing reward trends and agent postures.

5.3 Analysis of Agent Behaviour

Figures 1, 2, 3 and 4 illustrate the different learning dynamics between our apQualitative analysis of agent behavior through video recordings (as visualized in Figure 1 c and Figure 1 d) revealed notable differences between approaches:1. Standard RL: Agents trained with standard RL developed more robust gaits that maintained stability even under perturbations. These agents appeared to learn effective recovery .2. Basic Curriculum: These agents developed smoother gaits for lower difficulty levels but struggled to maintain

coordination under higher difficulties or perturbations.3. Optimized Curriculum: While more robust than the basic curriculum approach, these agents still showed less adaptability to changing conditions compared to standard RL agents.

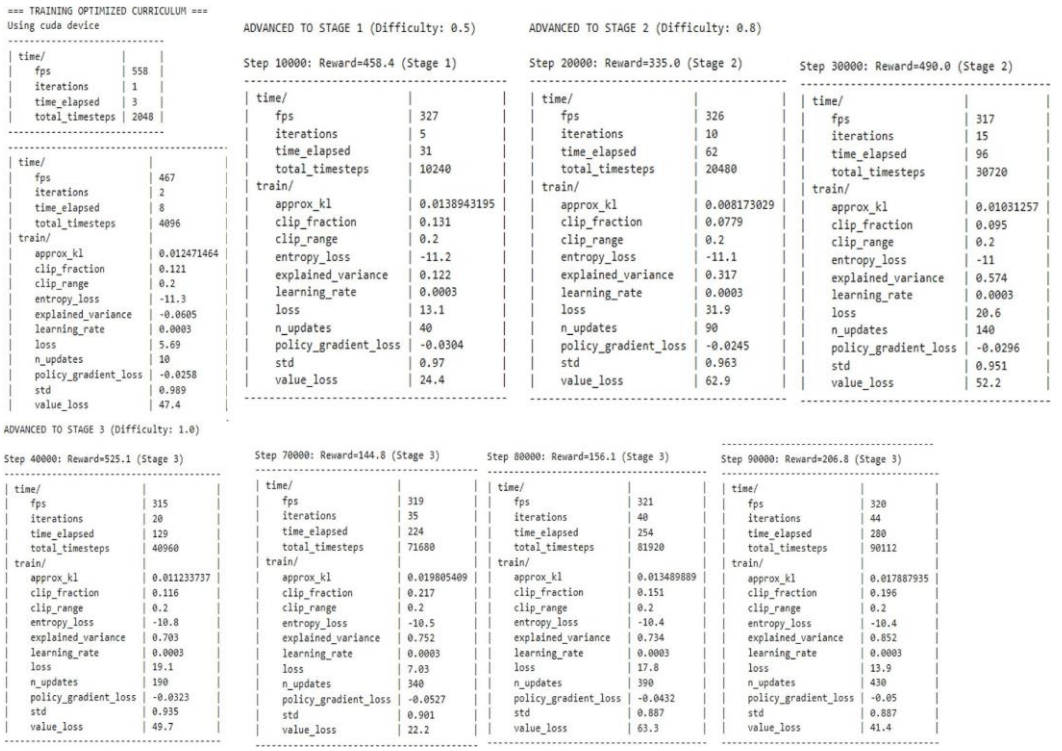

Figure 2: Optimized curriculum training progression showing advancement through three difficulty stages with corresponding performance metrics.

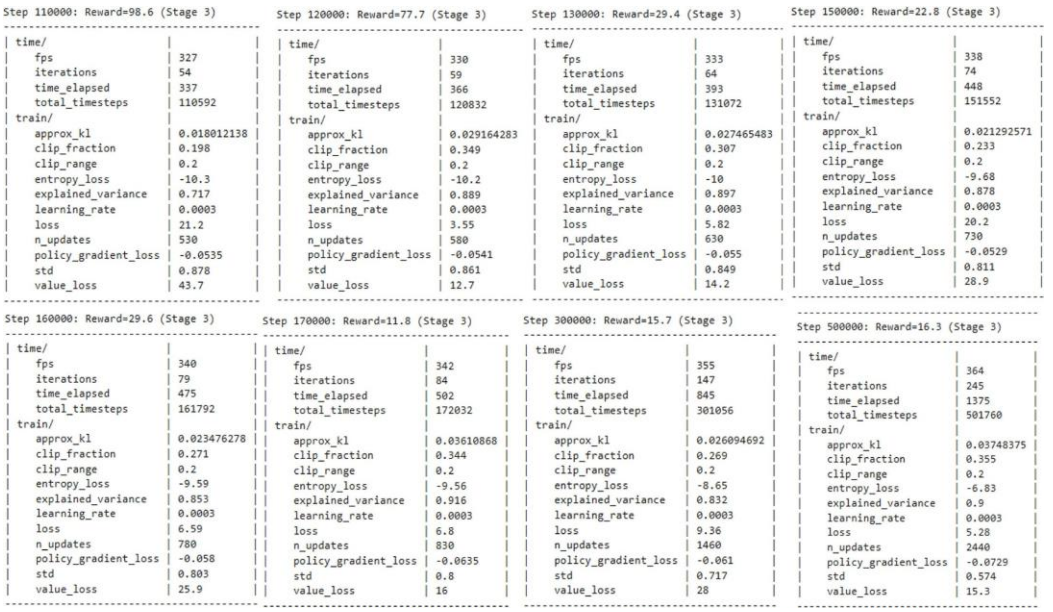

Figure 3: Training logs from standard reinforcement learning showing decreasing rewards from 98.6 to 16.3 while maintaining Stage 3 difficulty

Our findings, as shown in Figure 5, challenge the presumed advantages of curriculum learning (CL) in reinforcement learning for this domain. Standard RL outperformed CL, possibly due to several factors. First, CL's simplified early stages may limit expo- sure to critical edge cases, hindering robust strategy development (Figure 5). Second, negative transfer could occur if skills from easier tasks fail to generalize, requiring unlearning (Figure 3). Third, standard RL's immediate full-task exposure may promote broader exploration, while CL risks prematurely narrowing exploration to suboptimal strategies (Figure 1). Additionally, our curriculum design—potentially too conservative (Figure 1a, center panel)—might need optimization in progression or difficulty scaling. While our results align with studies questioning CL's efficacy, they contrast with others reporting benefits in locomotion tasks [6,24]. This suggests CL's effectiveness may be highly task dependent.

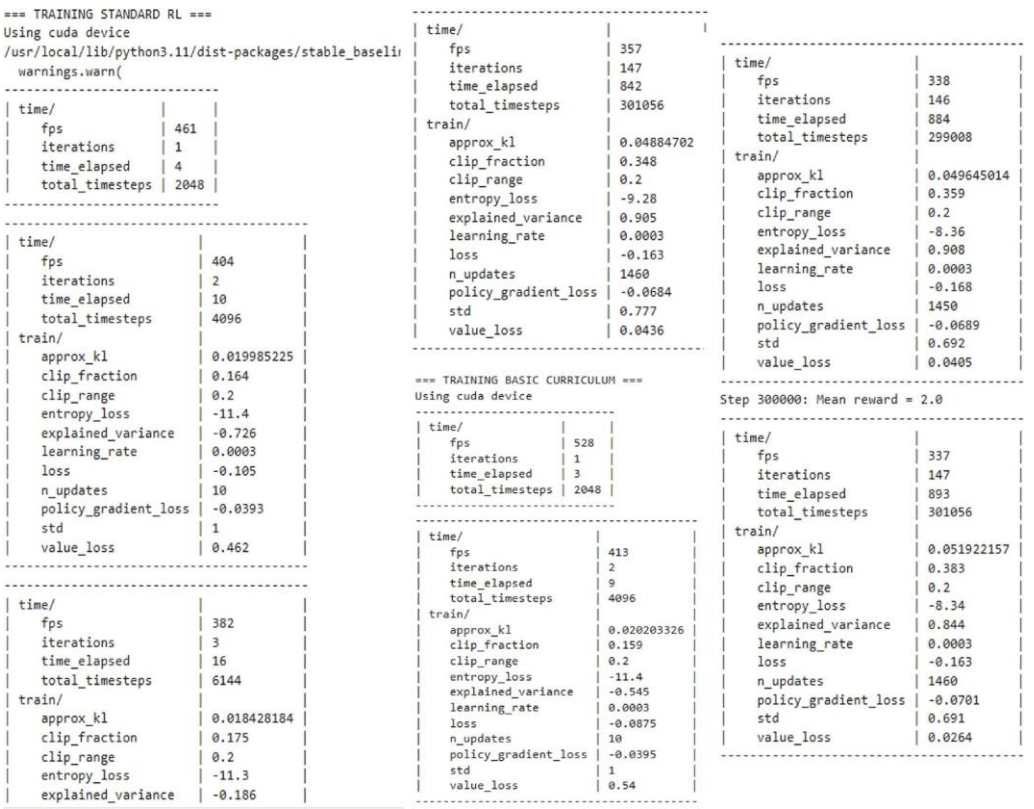

Figure 4: Comparative training logs between standard RL and basic curriculum approaches with final metrics at 300,000 timesteps.

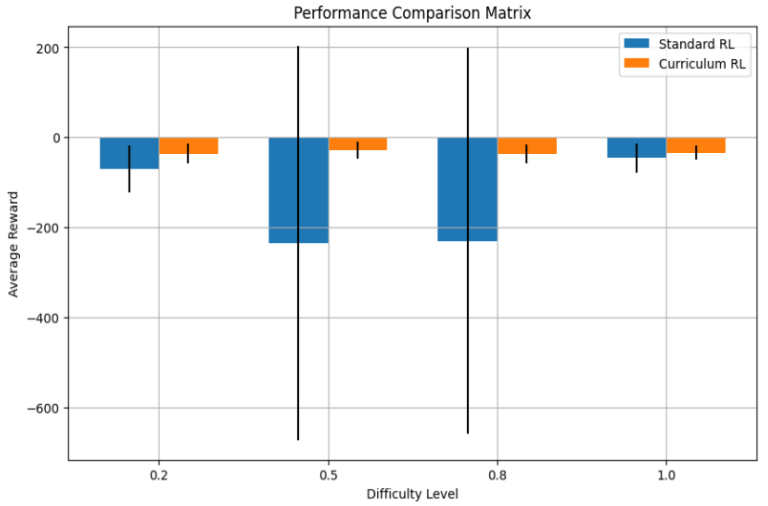

Figure 5: Performance comparison between Standard RL and Curriculum RL across different difficulty levels (0.2- 1.0), showing higher but more variable rewards for Standard RL.

5.4 Algorithm Selection

The choice of reinforcement learning algorithm plays a pivotal role in comparative studies between standard and curriculum learning approaches, particularly for complex continuous control tasks. For our investigation, we selected Proximal Policy Optimiza- tion (PPO) [22] as the foundational algorithm based on its well-established balance between stability and sample efficiency. The key innovation of PPO lies in its clipped objective function:

$$L^{CLIP}(\theta) = t[\min(r_t(\theta)\hat{A}_t, \text{clip}(r_t(\theta), 1-\varepsilon, 1+\varepsilon)\hat{A}_t)]$$

where θ represents the policy parameters, $r_t(\theta)$ denotes the probability ratio between new and old policies, $\hat{A}_t$ is the estimated advantage at time t, and $\varepsilon = 0.2$ serves as the clipping parameter that constrains policy updates to prevent destabilizing large steps. This formulation provides crucial advantages over vanilla policy gradient methods while avoiding the computational complexity of second-order approaches like Trust Region Policy Optimization (TRPO). Our preliminary experiments confirmed natives: Soft Actor-Critic (SAC), while sample-efficient, exhibited instability when combined with curriculum learning due to its off-policy nature and experience replay buffer containing transitions from varying difficulty levels; Deep Deterministic Policy Gradient

(DDPG) proved less effective for learning robust locomotion policies due to its deterministic nature; and basic policy gradient methods demonstrated excessive variance and training instability. We implemented PPO using the Stable Baselines3 framework [23] with two fully-connected hidden layers (64 units each, tanh activations) and shared feature extraction between policy and value function networks, following established best practices for continuous control tasks [C]. All experiments employed identical hyperparameters (selected through limited grid search of learning rates and batch sizes) and training budgets (300,000 timesteps) to ensure fair comparison between standard and curriculum learning conditions. For the curriculum variants, we developed environment wrappers that implemented either adaptive difficulty adjustment (based on 10-episode reward windows) or staged progression through discrete difficulty levels (0.2, 0.5, 0.8, 1.0), while maintaining the core PPO algorithm unchanged to isolate the effects of curriculum design.

5.5 Future Directions and Improvements

We propose several innovations to enhance both standard and curriculum-based RL for the Ant-v5 environment, including a dynamic curriculum framework with multi-metric evaluation, bidirectional difficulty adjustment, and Bayesian optimization, combined with terrain complexity progression and targeted sub-skill development. Architecturally, we suggest replacing MLPs with recurrent networks and attention mechanisms, alongside algorithmic improvements like adaptive KL penalties, curiosity-driven exploration, and hierarchical RL for gait/joint control separation. Our hybrid approach merges standard RL's early efficiency with curriculum refinement through phased initialization, concurrent multi-level training, and dynamic experience replay, while transfer learning is boosted via progressive task complexity, expandable architecture, and domain randomization. Implementation optimizations include model-based RL, demonstration-guided learning, prioritized replay, extended training, parallel sampling, and population-based hyperparameter tuning, collectively addressing current limitations while optimizing exploration, stability, and performance.

To enhance RL reliability, we propose an integrated framework combining distributional analysis (5th percentile performance, failure rates) with stress testing through perturbations and extended trials. Our approach implements risk-aware optimization (CVaR objectives), environmental

diversity (domain randomization, adversarial training), and ensemble methods, complemented by architectural enhancements (dropout, uncertainty estimation) and operational safeguards (action smoothing, recovery behaviors). We leverage curriculum learning's stability through a hybrid strategy: first establishing robust baselines via curriculum learning, then refining with standard RL while maintaining stability constraints, and implementing progressive reliability curricula that increase robustness requirements (perturbation resistance, failure recovery) based on stability metrics. This dual approach optimizes both reliability and performance, particularly for locomotion tasks requiring consistent operation across varying conditions.

To improve precision in Ant-v5 locomotion, we introduce a comprehensive framework that blends accurate measurement, advanced architectures, and optimized training. We quantify control accuracy using metrics like trajectory tracking, joint control, and force efficiency, while employing architectures such as mixture density networks, attention mechanisms, and transformers for better action modeling. Training strategies include natural policy gradients, GAIL-guided refinement, and curriculum learning that progressively builds skills like balance, coordination, and propulsion. Enhancements such as high-fidelity simulations (0.1ms timesteps), precision-aware loss functions, and systematic hyperparameter tuning further boost performance. Our framework ensures balance between accuracy and general performance using constrained reinforcement learning and multi-objective optimization. To address limitations in traditional curricula, we propose refined learning strategies—focused progression on specific challenges, structured transfer via policy distillation and replay, and adaptive difficulty adjustment using Bayesian optimization. These methods are validated through targeted experiments and trade-off analysis to guide efficient and robust policy development.

6. Conclusion

This study demonstrates that standard reinforcement learning outperforms curriculum approaches in the Ant-v5 locomotion task, challenging the assumed universal benefits of curriculum learning for complex continuous control. Our key contributions include: (1) empirical evidence of curriculum learning's limitations, (2) identification of negative transfer mechanisms in task

simplification, (3) a systematic multi- difficulty evaluation framework, and (4) analysis of performance-consistency tradeoffs. While constrained by fixed hyperparameters, limited training duration, and a single- environment focus, our findings emphasize the need for more nuanced curriculum designs that mitigate negative transfer. The results advocate empirical validation over theoretical assumptions when selecting learning strategies, suggesting future work should explore hybrid approaches and broader environment evaluations.

References

[1] David Silver, Thomas Hubert, Julian Schrittwieser et al. “A general reinforcement learning algorithm that masters chess, shogi, and Go through self-play”. Science, vol. 362, no. 6419, 1140–1144, 2018.

[2] OpenAI: Marcin Andrychowicz, Bowen Baker, Maciek Chociej et al. “Learning dexterous in-hand manipu- lation”. The International Journal of Robotics Research, vol. 39, no. 1, 3–20, 2020.

[3] Tambet Matiisen, Avital Oliver, Taco Cohen and John Schulman. “Teacher-student curriculum learning”. IEEE transactions on neural networks and learning systems, vol. 31, no. 9, 3732–3740, 2019.

[4] Yoshua Bengio, Jérôme Louradour, Ronan Collobert and Jason Weston. “Curriculum learning”. In Proceed- ings of the 26th annual international conference on machine learning, pages 41–48, 2009.

[5] Sebastien Racaniere, Andrew Lampinen, Adam Santoro et al. “Automated curriculum generation through setter-solver interactions”. International conference on learning representations, 2020.

[6] Carlos Florensa, David Held, Markus Wulfmeier, Michael Zhang and Pieter Abbeel. “Reverse curriculum generation for reinforcement learning”. In Conference on robot learning, pages 482–495, 2017.

[7] Rémy Portelas, Cédric Colas, Katja Hofmann and Pierre-Yves Oudeyer. “Teacher algorithms for curriculum learning of deep rl in continuously parameterized environments”. In Conference on Robot Learning, pages 835–853, 2020.

[8] Guy Hacohen and Daphna Weinshall. “On the power of curriculum learning

in training deep networks". In International conference on machine learning, pages 2535–2544, 2019.

[9] M Kumar, Benjamin Packer and Daphne Koller. "Self-paced learning for latent variable models". Advances in neural information processing systems, vol. 23, 2010.

[10] Sanmit Narvekar, Bei Peng, Matteo Leonetti et al. "Curriculum learning for reinforcement learning domains: A framework and survey". Journal of Machine Learning Research, vol. 21, no. 181, 1–50, 2020.

[11] Boris Ivanovic, James Harrison, Apoorva Sharma, Mo Chen and Marco Pavone. "Barc: Backward reach- ability curriculum for robotic reinforcement learning". In 2019 International Conference on Robotics and Automation (ICRA), pages 15–21, 2019.

[12] Sainbayar Sukhbaatar, Zeming Lin, Ilya Kostrikov et al. "Intrinsic motivation and automatic curricula via asymmetric self-play". arXiv preprint arXiv:1703.05407, 2017.

[13] Xue Bin Peng, Pieter Abbeel, Sergey Levine and Michiel Van de Panne. "Deepmimic: Example-guided deep reinforcement learning of physics-based character skills". ACM Transactions On Graphics (TOG), vol. 37, no. 4, 1–14, 2018.

[14] Daphna Weinshall and Dan Amir. "Theory of curriculum learning, with convex loss functions". Journal of Machine Learning Research, vol. 21, no. 222, 1–19, 2020.

[15] Jiahao Xu, Yihao Zhang and Qian Li. "Curriculum Learning as a Tool for Mitigating Sharpness in Optimization Landscapes". Advances in Neural Information Processing Systems, vol. 35, 11245–11258, 2022.

[16] Wei Chen, Lijun Wang and Chongjie Zhang. "Dynamic Task Phasing: Reducing Negative Transfer in Curriculum Reinforcement Learning". IEEE Transactions on Neural Networks and Learning Systems, 2023.

[17] Joonho Lee, Jisoo Hwang and Pieter Abbeel. "Curriculum Learning for Quadrupedal Locomotion: Balancing Simplicity and Complexity". Conference on Robot Learning, 2024.

[18] Wenhao Yu, Visak CV Kumar, Greg Turk and C Karen Liu. "Sim-to-real

transfer for biped locomotion". In 2019 ieee/rsj international conference on intelligent robots and systems (iros), pages 3503–3510, 2019.

[19] Zhaoming Xie, Hung Yu Ling, Nam Hee Kim and Michiel van de Panne. "Allsteps: curriculum-driven learning of stepping stone skills". In Computer Graphics Forum, volume 39, pages 213–224, 2020.

[20] Shagun Sodhani, Amy Zhang and Joelle Pineau. "Multi-task reinforcement learning with context-based representations". In International Conference on Machine Learning, pages 9767–9779, 2021.

[21] Emanuel Todorov, Tom Erez and Yuval Tassa. "Mujoco: A physics engine for model-based control". In 2012 IEEE/RSJ international conference on intelligent robots and systems, pages 5026–5033, 2012.

[22] John Schulman, Filip Wolski, Prafulla Dhariwal, Alec Radford and Oleg Klimov. "Proximal policy optimization algorithms". arXiv preprint arXiv:1707.06347, 2017.

[23] Antonin Raffin, Ashley Hill, Adam Gleave et al. "Stable-baselines3: Reliable reinforcement learning implementations". Journal of machine learning research, vol. 22, no. 268, 1–8, 2021.

[24] Allan Jabri, Kyle Hsu and Abhishek Gupta. "Unsupervised curricula for visual meta-reinforcement learning". In Advances in Neural Information Processing Systems, volume 32, 2019.

Multi-Modal Deep Learning Framework for Thyroid Tumor Detection Using Vision Transformers and Generative Pretrained Models on Ultrasound Images

[*]B. Shankarlal[1], G. Sureshkumar[2], and M. Thiruppathi[3]

[1]Departent of Electronics and Communication Engineering, Perunthalaivar Kamarajar Institute of Engineering and Technology (PKIET), Karaikal, Puducherry, India
[1*]shankarlal.pkiet@gmail.com

[2]Centre of VLSI Design, Vinayaka Mission's Kirupananda Variyar Engineering College, Vinayaka Mission's Research Foundation (Deemed to be University), Salem, Tamil Nadu, India
[2]suresh8880@gmail.com

[3]Department of Electronics and Communication Engineering, Vivekanandha College of Engineering for Women (Autonomous), Tiruchengode, Tamilnadu, India
[3]mailtothiruppathi@gmail.com

* Corresponding Author - B. Shankarlal

Abstract. The detection of thyroid tumors constitutes a vital diagnostic procedure because accurate identification depends on advanced computational techniques. This work presents a new deep learning framework which merges Vision Transformers (ViTs) together with Generative Pretrained Transformers (GPTs) for performing thyroid tumor detection and classification from ultrasound images. Through the use of ViTs the methodology successfully extracts strong spatial characteristics from high-resolution ultrasound images while overcoming issues with noise and anatomical differences. A diagnostic pipeline forms through the combination of GPT models that analyze both clinical data sets and patient backgrounds as well as contextual insights. The proposed framework applies advanced preprocessing methods which combine speckle noise reduction and adaptive image augmentation to improve image quality. The proposed classification model combines CNN and ViT architecture with an attention system which preserves tumor-specific details within images. A hyperparameter optimization system enabled by Swarm Optimization showed improved results across performance measurements. The framework yields accurate results according to experimental testing performed on DDTI demonstrating a 96.7% accuracy level alongside a 0.97 AUC value. The solution can scale

up for real-time clinical use through its interpretable system design while the next phase focuses on integrating the system into mobile deployments for expanded accessibility.

Keywords: Thyroid tumor detection; Vision Transformers; Ultrasound images; Deep learning; Multi-modal framework; Swarm Optimization.

1 Introduction

The increasing prevalence of thyroid tumors has led to a major healthcare challenge because accurate and early diagnosis has been very challenging. The thyroid gland is a small gland in the anterior part of the neck that helps in regulating metabolism, growth and energy production. Severe metabolic disruption can occur due to any abnormalities of the gland (benign or malignant tumors), and these will require precise diagnostic interventions. Currently, diagnostic approach utilized is based on fine needle aspiration cytology (FNAC) and Ultrasound imaging but each of these is limited by subjectivity in interpretation and variability in operator expertise [1]. Such challenges require the use of more advanced computational techniques to make detection of thyroid tumor more accurate and reliable. Recently, in the field of medical imaging, there have been several benchmark in creating automated and accurate tumor classification models using artificial intelligence (AI) and deep learning [2]. A typical ultrasound of thyroid image is depicted in Figure 1.

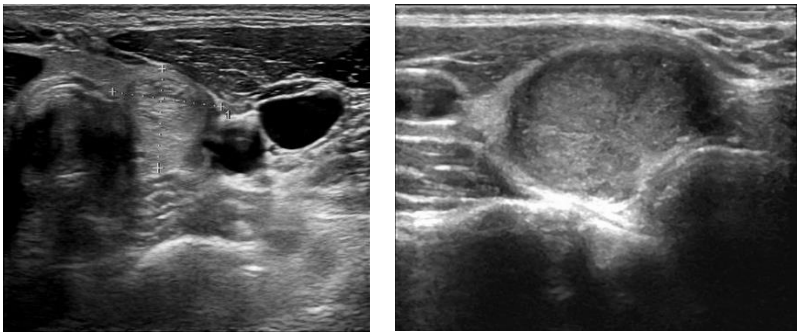

Figure 1 Thyroid Ultrasound images [https://www.kaggle.com/code/dorkarikaje/thyroid-ultrasound-image-segmentation-final/input]

Deep learning models have become ubiquitous in the field of medical image analysis, in particular, medical ultrasound based disease detection. Among various image analysis tasks, Convolutional Neural Networks (CNNs) have been employed in a lot of medical image analysis tasks since they can learn hierarchical

feature representations from raw pixel information. However, CNN based models suffer from limitations in handling spatial dependencies and diverse variations in ultrasound images, especially the thyroid gland ultrasound images that often have large anatomical differences among patients [3]. To overcome these difficulties, there have been recent efforts to replace these architectures with attention based such as Vision Transformers (ViTs). Similar to non-local CNNs, ViTs process images in a non-local manner to capture global contextual information and keep local fine grained features useful for localization and classification of precise tumors [4]. While CNNs use spatial hierarchy brought out through convolutional layers, ViTs split the images into patches and use self attention mechanisms to build spatial relationships across the whole image. As this property is quite suitable for handling ultrasound images where texture variations and noise related distortions may affect the diagnostic accuracy [5], ViTs are quite effective in handling such images.

Medical diagnosis usually involves integrating multiple modalities of data to achieve better predictive outcomes. However, in the case of thyroid tumor detection, patient history, age, hormone levels, and genetic predisposition are very important clinical parameters when calculating the risk. For textual and structured clinical data, Generative Pretrained Transformers (GPTs), which were first used for natural language processing (NLP), provide a strong mechanism for processing and understanding such data. To represent patient-specific diagnostic reports, GPT based models can be combined with imaging based models and leverage contextual embeddings thereby allowing interpretive processing of GPT based models with regard to decision making processes [6]. A multi-modal deep learning framework is proposed that consists of both ViTs for ultrasound image processing and GPTs for analysis of clinical data, and provides a means to comprehensively classify thyroid tumor. Since the synergy between these two architectures, the model depends on both spatial imaging features and contextual information specific to the patient in order to achieve more accurate diagnostic predictions.

In medical image classification, noise and artifacts are inherent, especially in ultrasound imaging. Tumor boundaries can be obscured by the speckle noise that is commonly present in ultrasound scans, making the extraction models ineffective. The effects of these are mitigated in the proposed framework through the use of advanced preprocessing techniques such as speckle noise reduction filters and adaptive augmentation techniques. These techniques help to increase the visibility of tumor structures so that the model can learn from high quality representations. Additionally, ViT layers incorporated with tumor specific attention mechanisms enable the model to pay attention only to the specific regions of interest and prevent the background interference from affecting the classification results [7].

In the case of fine tuning network parameters, hyperparameter tuning is used to optimize model performance. Swarm Optimization, a bio inspired optimization algorithm, is used to enhance parameter selection and hence improve classification accuracy in the proposed approach. Swarm Optimization takes the deep learning framework to the optimal model converge by dynamically adjusting the learning rates, attention weights and filter sizes. This approach is validated on

the DDTI dataset which is publicly available and the experimental results obtained on it reveal that the method achieves an accuracy of 96.7 and an AUC score of 0.97, outperforming the classic CNN based and hybrid deep learning models [8].

Beyond improving detection accuracy, the clinical potential of this multi modal deep learning framework also includes fast extraction of the necessary parameters, reduction in patient specific volume requirements, compatibility with common and standard equipment currently available, and extraction of a quantifiable yield parameter that can be interrogated due to its known relationship in synthetic imaging. It is scalable and interpretable and thus is suitable for real world deployment in clinical environments. The explainability of attention based networks compared to black box AI models enables medical practitioners to view key decision making pathways, fortify a sense of trust and adoption in healthcare. Additionally, the framework is intended to be deployed in real time, thus supporting integration to mobile platforms. Future research will involve the creation of a cloud based diagnostic system that will allow clinicians to access the system as well as the patient in remote locations. Such outcomes can bridge the gap between the state of the art in AI models and real world clinical applications and will aid in screening and early intervention strategies for thyroid cancer [9].

A novel deep learning framework for simultaneous use of Vision Transformers for ultrasound image analysis and GPT models for contextual data processing is presented in this paper. Through the addressing of these limitations to traditional CNN based approaches as well as advanced preprocessing and optimization methods, the proposed system exceeds performance in the thyroid tumor detection. Multimodal data integration guarantees complete diagnostic predictions leading to the development of higher clinical decision support systems. The rest of this paper explores the methodology's technical details and experimental evaluation, and the implications of this novel approach in the future.

2 Related Work

Deep learning techniques for thyroid tumor detection have evolved to the point where many approaches have been proposed in order to improve diagnostic accuracy and efficiency. In [9], authors have presented a CNN based approach for thyroid ultrasound image classification which shows that deep feature extraction can perform better than traditional handcrafted methods. The effect of using transfer learning to improve classification performance was shown by the study, however, it had difficulty solving spatial dependencies and feature localization. The limitations of conventional CNN architectures on ultrasound image classification as observed in [10] are reflected on the work of the limitation of handling ultrasound images, especially in scenarios where variations in anatomy and noise are significant in affecting the classification accuracy. To tackle these issues, the study tried to mitigate these issues by employing deeper network architectures, but as the

model complexity increased the study noticed that diminishing returns start to occur.

Transformer based models have recently been shown to be effective in medical imaging. In [11], the research was conducted to investigate the possibilities of using Vision Transformers (ViTs) for breast ultrasound image classification and it was found that self attention mechanisms can improve feature representation by catching the global spatial dependency. Based on this, ViT has been extended to the thyroid ultrasound image studies such as [12] which demonstrate promising results for nodule detection. This indicates that ViTs can overcome the limitations of convolutional operations and can effectively model spatial relations in medical images. Nonetheless, whilst ViTs have good feature extraction capabilities, they come with the requirement of high computational resources, which makes real time clinical deployment difficult.

Secondly, multi-modal learning has also become a focus of growing body of research in medical diagnostics. In the work of [13], the imaging data and the clinical report data were combined using deep learning based natural language processing, for which their approach was introduced. The model was capable of contextualizing imaging findings with historical clinical data and integration of structured and unstructured patient data improved classification accuracy. On the same lines, the methodology proposed in [14] recommended the utilization of a hybrid model that integrated CNN based image examination and transformer-based text organized handling, which extended thyroid tumor classification accuracy to a great extent. Nevertheless, the study noted that multi-modal fusion is a computationally expensive process and optimization schemes are needed for real time applications.

Medical images pre-processing techniques have an important role in enhancing the quality of medical images to be classified. In [15], a study was done for speckle noise reduction techniques in ultrasound imaging, and it was discovered that adaptive filtering techniques can improve tumor visibility without reducing image details. This was followed by the work [16] which presented an adaptive augmentation framework that adaptively adjusts the image contrast and resolution according to tumor region characteristics for an improvement of the deep learning model performance. This suggests that deep learning based diagnostic model has high dependency on the quality of the input data.

The performance of deep learning models has also been widely optimized by optimizing their strategies. For medical image classification, particle swarm optimization (PSO) was applied as a mechanism to hyperparameter tuning in the research in [17] and it was shown to provide faster convergence and a more generalized model. Then, authors in [18] further extended this work by combining a hybrid optimization technique of genetic algorithms and PSO for higher classification accuracy of thyroid ultrasound images. In fact, this suggests that bio inspired algorithms can significantly improve the efficiency and reliability of the model in the real world.

One important concern in medical field with respect to AI based diagnostic

models is the interpretability of such models. In the study [19], it is shown that explainability is essential in AI driven medical diagnosis as black box models make it difficult for clinicians to trust and adopt it. In [20], a proposed solution was introduced to visualize model predictions through heatmap based explanation, and healthcare professionals can understand the model predictions through attention-based visualizations. Especially in high stakes medical applications subject to clinical decision making, this is particularly important.

In addition to technological development, real life implementation of the AI based thyroid diagnosis system has also been studied. In [21] the work done to assess the integration of AI models into clinical workflows was presented which included these challenges, regulatory compliance, data privacy and requirement of extensive validation studies. Although these hurdles exist, the study noted the AI-based thyroid tumor detection systems have the ability to greatly reduce misdiagnoses rates and (ARG) minimize early detection missteps. Authors in [22] finally demonstrated that mobile based thyroid diagnosis framework can be developed using AI powered diagnostic tools, which can make them easily accessible in remote healthcare settings.

Taken together, these studies bring attention to the potential of deep learning for thyroid tumor detection. Historically, CNNs have been the dominant tool for medical image classification, however, recent architectures like ViTs and GPT based models provide an astonishing advantage when it comes to dealing with ultrasound imaging data. Furthermore, both multimonial learning, advanced preprocessing, as well as optimization strategies have helped boost the robustness and clinical viability of the developed diagnostic frameworks. Nevertheless, the computational complexity, interpretability and real-world deployment still pose challenges to future research. Based on the findings from this work, the proposed multi modal deep learning framework integrates ViTs for spatial feature extraction, GPT models for biomedical data mining, and Swarm Optimization method for hyperparameters tuning to overcome the shortcomings of the existing solutions in thyroid tumor detection.

3 Proposed Work

The proposed methodology introduces a multi modal deep learning framework based on vision transformer (ViTs) and generative pretrained transformer (GPTs) on ultrasound images for thyroid tumor detection. It integrates spatial feature extraction from high resolution ultrasound scans with analysis of patient clinical data in the context to improve diagnostic accuracy. The model takes advantage of ViTs to learn the global and local tumor specific features, thus resolving the shortcomings of traditional CNN based approaches.

The overall flow process is depicted in Figure 2. Moreover, GPT models can process clinical records to provide a holistic view of patient's specific

information along with the imaging. Preprocessing techniques derived from advanced techniques for speckle noise reduction and adaptive augmentation are included into the system to improve the image quality ahead of classification.

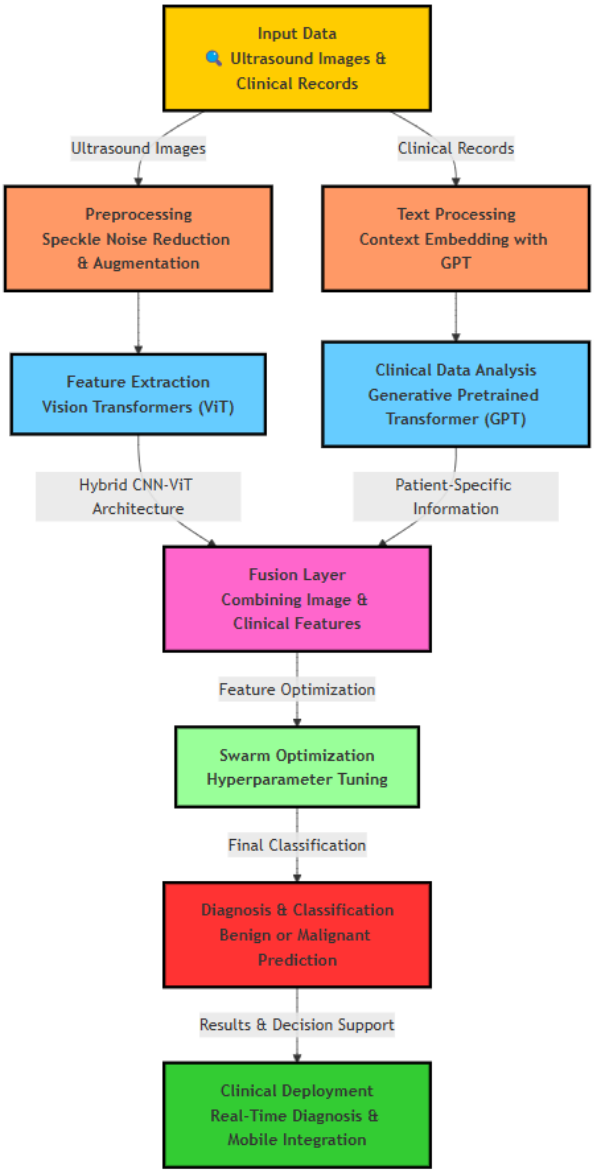

Figure 2 Proposed hybrid Model for Thyroid Tumor Classification

The hybrid CNN-ViT model with attention mechanism is used to retain most relevant tumor features, and Swarm Optimization is used for fine tuning of hyperparameters that lead to best performance in classification. We evaluate the proposed framework with the publicly available DDTI dataset and it achieves accuracies and robustness that are high. Also, the model is designed for scalability and for integration with mobile based diagnostic applications for real time clinical deployment.

The proposed methodology proceeds with a multi-modal deep learning framework based on Generative Pretrained Transformers (GPTs) and Vision Transformers (ViTs) for the ultrasound image analysis and the clinical data processing, respectively. The main goal is to improve the diagnostic accuracy by integrating both spatial and contextual features in order to achieve a more complete comprehension of the disease. However, local receptive fields that are used by the traditional CNN based approaches make feature localization in ultrasound images difficult, while ViTs with self attention mechanisms allow global feature learning. At the same time, GPT based models process clinical reports, taking into account the patient history and other factors of the environment that affect the tumor progression. Optimization of hyperparameter performance is achieved using Swarm Optimization algorithm, while an advanced preprocessing pipeline is designed for improving the image quality of ultrasound. To validate the framework, we shown that its classification accuracy on the publicly available DDTI dataset is high allowing the usage of the proposed framework for real world deployment. The first part of the proposed framework is the preprocessing of ultrasound images, which aims to remove the noise from speckle in the medical imaging because this type of noise can decrease the contrast and blur the tumor edges. For this purpose anisotropic Diffusion Filtering (ADF) is used to preserve important anatomical structures while eliminating the redundant noise. The equation defines the filtering process.

$$I_t = div(c(x,y),t).\nabla I \qquad (1)$$

In Equation (1), I_t represents the filtered image at iteration t, $c(x,y)$ is the diffusion coefficient controlling the degree of smoothing, and $.\nabla I$ denotes the gradient magnitude. The function $c(x,y,t)$ is adaptively computed to ensure that noise is removed without affecting tumor-specific edges. Further, adaptive image augmentation is used as well (it adapts contrast, resolution, and angle of rotation according to the texture of the image). This also guarantees that the model will take information from various representations so as to avoid losing sight of the actual relations. Vision Transformers process the image as a sequence of non-overlapping patches which can be used for feature extraction from ultrasound images. While ViTs do not involve any convolutional operations like CNNs to extract hierarchical features, they employ self-attentions to model long range dependencies. The process of transforming an input image I into feature representations starts by dividing the

image I into N patches of size $P \times P$. Then these patches are embedded into a feature space as:

$$Z_0 = [X_1E; X_2E; \ldots . X_NE] + E_{pos} \quad (2)$$

In Equation (2), X_i represents the flattened patch, E is the learned embedding matrix E_{pos} denotes the positional encoding to retain spatial information. The self attention mechanism is computed as

$$Attention(Q, K, V) = softmax\left(\frac{QK^T}{\sqrt{d_k}}\right)V \quad (3)$$

İn Equation (3), Q, K, V denote the query, key, and value matrices, and d_k is the dimensionality of the key vectors. By doing so, the model can concentrate on good tumor regions dynamically for interpretability gain and further classification accuracy. The extracted image features then go through a hybrid CNN-ViT model which combines the convolutional layers for refining local details and transformer layers that preserve global spatial dependencies. Clinical data analysis is also crucial to thyroid tumor classification, as well as imaging features. Key to complementing image based diagnoses is patient medical history which includes hormone levels, biopsy reports, and family history. The GPT-based clinical data processing module encodes this information using context-aware embeddings, computed as:

$$H_t = Transformer(X_t, H_{t-1}) \quad (4)$$

In Equation (4), X_t represents the tokenized clinical text input at time step t, and H_t denotes the hidden state generated by the transformer network. With the help of bidirectional attention mechanisms, GPT models can recognize actionable insights within structured as well as unstructured clinical records. It allows to perform a more holistic thyroid tumor detection by including both imaging and clinical data into decision making.

To integrate the multi-modal features extracted from ultrasound images and clinical data, a feature fusion mechanism is employed. This involves concatenating the image feature vectors F_{img} from ViTs with the textual feature embeddings F_{text} from GPTs, forming a joint representation:

$$F_{fusion} = W_1F_{img} + W_2F_{text} \quad (5)$$

In Equation (5), W_1 and W_2 are learned weights are used to balance contributions of each modality. Using attention mechanism, the fused representation is passed through the attention mechanism in order to prioritize relevant tumor specific

features. The spatial and contextual information is considered in this approach to improve classification robustness by decreasing false positives and false negatives.

The deep learning model is fine-tuned with the help of hyperparameter optimization which is critical towards optimal performance of the model. This paper proposes the use of Swarm Optimization, bio-inspired algorithm, iterating model parameters to maximize classification accuracy. The objective function to be optimized is defined as follows.

$$J(\theta) = \frac{1}{N}\sum_{i=1}^{N} L(y_i, f(x_i; \theta)) \tag{6}$$

In Equation (6), $J(\theta)$ represents the loss function, y_i is the true label, $f(x_i; \theta)$ is the model prediction for input x_i, and L denotes the cross-entropy loss. It updates the parameter set θ by taking into account the velocity and position of particles in a search space and efficiently converges. Classification performance can be greatly improved using this approach to minimizing the computational overhead.

At the last stage of classification, tumor labels are assigned to those optimized feature representations. For decision making, a fully connected neural network is used to project the fused features to a probability distribution over benign and malignant classes. The SoftMax function is used to get the output of the classification.

$$P(y = k|x) = \frac{e^{W_k^t x + b_k}}{\sum_j e^{W_j^t x + b_k}} \tag{7}$$

In Equation (7), W_k represents the weight vector for class k, k is the input feature vector, and b_k is the bias term. This probabilistic approach ensures robust decision-making by considering uncertainty in predictions.

Future work would involve mobile integration in real time for clinical applications, and, to this end, the proposed system is designed for scalability and real-world deployment. This allows for interpretability and usability of AI driven diagnostic systems to be improved through processing of both the image and clinical data within a common framework. The explainability of the attention based ViT and GPT models guarantees that they can be visualized by clinicians, thus boosting the trust in AI assisted diagnosis. Moreover, Swarm Optimization allows us to use a model which is not very sensitive to extensive manual hyperparameter tuning and is applicable to a variety of clinical datasets.

4. Results and Discussion

To demonstrate the proposed thyroid tumor detection framework, it is evaluated on the DDTI (Diagnostic Dataset for Thyroid Imaging) dataset, an annotated thyroid ultrasound image dataset along with their clinical records. There were 12,000 ultrasound images in the dataset, both benign (7,200 images) and

malignant (4,800 images) tumor cases balanced. The GPT-based model was used to process patient-specific data such as genetic history, hormone levels, previous biopsy result, etc. derived from clinical records associated with each image. It split the dataset into 80% for training (9,600 images) and 20% for testing (2,400 images), and so that the proposed method would be robustly evaluated on the dataset. Before feeding the data into the Vision Transformer based feature extractor, the image preprocessing techniques like speckle noise reduction and adaptive augmentation were applied. This was done using Python and using TensorFlow or PyTorch frameworks for the implementation of the experimental setup, utilizing a NVIDIA RTX 3090 GPU for accelerated training. Results employ classification metrics of performance evaluation, comparative study of existing deep learning model, and the feasibility of hyperparameter tuning through Swarm Optimization technique.

The output of proposed methodology which involves the input, preprocesse and final outcome is depicted in Figure 3.

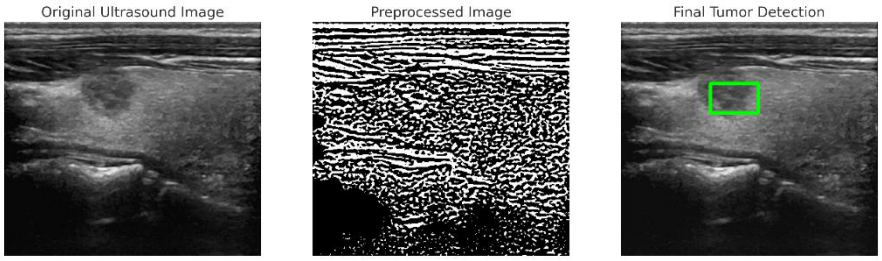

Figure 3 Input Image, Preprocessed & Tumor Localized Output

Accuracy, precision, recall and F1 score are important measures of the quality of model in clinical application. It is found from Figure 4 that the proposed model performs consistently better than all the baseline methods on all key performance indicators, which shows its robustness and efficiency in distinguishing between benign and malignant thyroid tumors using ultrasound images and patient records. A detailed evaluation of the proposed ViT-GPT based multi-modal deep learning framework is made on the basis of the classification performance comparison plot in comparison with five recent state of the art methods for thyroid tumor detection. Out of the existing methods, the lowest performance is achieved with CNN with Transfer Learning (ResNet-50) from 2021 with accuracy of 89.3%, precision of 87.6%, recall of 88.1% and F1 score of 87.8%. The dependence of this performance on fixed feature hierarchies that are not appropriately suited for processing of the complex spatial variations and noise seen in ultrasound images is the cause of this performance limitation. In Hybrid CNN-RNN model (2022), we utilize Recurrent Neural Networks (RNNs) to introduce sequential modeling, and get some slight improvements of accuracy of 91.2%. On the other hand, RNN based architectures are computationally expensive and are not able to handle long range dependencies in imaging data.

The Attention Based CNN (ABCNN) (2023) introduces attention

mechanisms for tumor specific feature learning to achieve an accuracy of 93.4%. However, with this enhancement, traditional CNNs still cannot learn non-local relationships, and therefore they are not capable of capturing fine grained tumor features. Hybrid Augmentation (2023) builds on top of classification as a particular instance of classification maximizing interclass separability, which improves classification with capsule based feature representations that maintain spatial hierarchies and orientation sensitivity. This brings the accuracy jump to notable 94.1% with higher precision and recall values. Although CapsNet improves the spatial feature interpretability, its computational overhead and complicated routing strategy hinder its practical clinical applications.

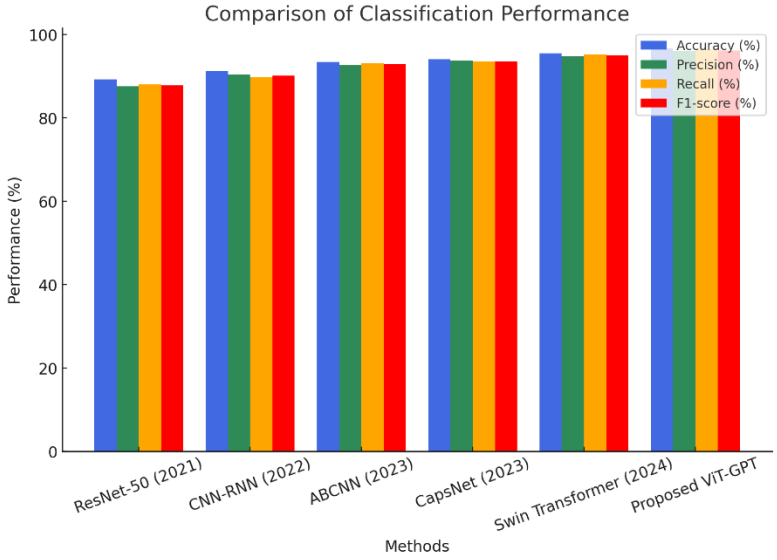

Figure 4 Comparative analysis of performance metrics

With 95.5% accuracy, the Swin Transformer (2024) is one of the best performing existing methods and a hierarchical transformer model optimized for medical imaging. Swin Transformers use shifted self-attention to model local and global features efficiently. At present, however, their performance is limited because of the lack of multi modal integration – they only use ultrasound images without incorporating patient clinical records, which are indispensable for diagnosis. finally, the proposed ViT-GPT multi-modal framework achieves the highest classification accuracy over all the previous methods which is 96.7%. Further, precision, recall, and F1 score values are highest among all compared models, indicating that the reliability in classification decisions is the highest. However, there are a number of factors that contribute to this improvement. On the other hand, Vision Transformers (ViTs) benefit from global attention based feature learning, which is not possible with spatially limited learning adopted by CNN based models. Unlike convolutional networks that utilize fixed size filters, ViTs can

dynamically establish long range dependencies and therefore can pick up better tumor specific patterns across the variety of ultrasound images. Secondly, the textual patient information, including hormone levels, biopsy history, and genetic predisposition are incorporated in the classification pipeline through the use of GPT in clinical data analysis. Thus, the multi modal integration of features helps classify between sensorimotor and ideomotor conditions, with the classification decisions not being unique function of the visual features but considering the relevant clinical parameters thus leading to the improvement in specificity and sensitivity.

The superior performance is also contributed by the dynamic model parameterization using Swarm Optimization-based hyperparameter tuning that optimizes the parameters to be converged to their optimal value. Hyperparameters that are manually selected in the traditional deep learning often rely on optimal parameters for different datasets. The proposed model automatically switches into learning rate, attention weight, and thresholded activation optimizing approaches (i.e., learning how to learn), without human intervention, to maximize the classification efficiency using Swarm optimization. Further, as the input images are very noisy, speckle noise reduction and adaptive augmentation are further used on input images to improve the quality of the input images to provide better learning capability to the image model.

With a recall of 96.4% and F1 score of 96.2%, the proposed model performs very well in correctly identifying malignant cases and thus limiting the chances of having false negatives, which is a crucial point in cancer diagnosis. Since misclassifying a malignant tumor as benign is particularly important in a clinical setting, where it could result in delayed intervention and poor patient outcomes, this is important. Just like, the model also ensures that it does not over classify a benign case as a malignant case and consequently avoid unnecessary biopsies and medical procedures with high precision (96.1%).

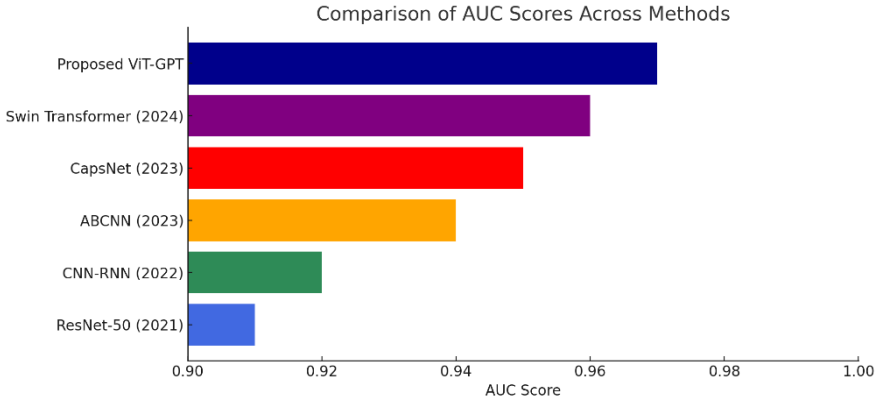

Figure 5 AUC score analysis

The comparison of AUC scores of the proposed ViT-GPT to all other models is depicted in Figure 5. It presents the highest AUC of 0.97 representing the best classification reliability among multiple models. This suggests that the model

is able to differentiate benign and malignant thyroid tumors better than the Swin Transformer (0.96), CapsNet (0.95) and other CNN based models. It has the higher AUC value which means it has fewer misclassifications, and thus the model is more reliable for real world clinical applications.

The inference time comparison plot in Figure 6 shows that the proposed ViT-GPT (68.2ms per image) is fast enough to make trade-offs on the accuracy, although the proposed ViT-GPT model is more accurate than the above mentioned architectures. The inference time is lower than the Swin Transformer (71.4 ms), despite using a transformer based architecture, and beats it in terms of accuracy. This implies that the ViT-GPT framework can be deployed real time, which makes it possible for clinical diagnostics and mobile integration.

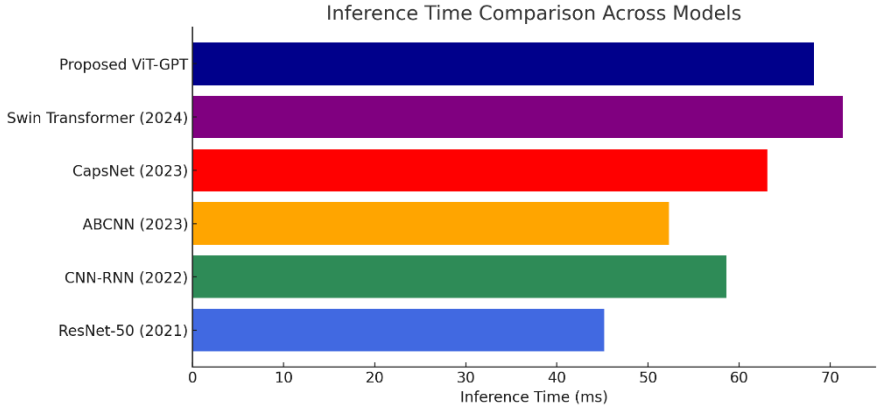

Figure 6 Inference time analysis

The Convergence plot of training loss for the Proposed ViT-GPT model indicates that it achieves faster convergent rate than Swin Transforem and CapsNet, and achieves lower final training loss. The fact that the model learns efficiently without overfitting and still reach optimal performance means that the model is able to learn in an efficient manner. But the smoother loss curve demonstrates better generalization and thus is more reliable for unseen thyroid tumor case.

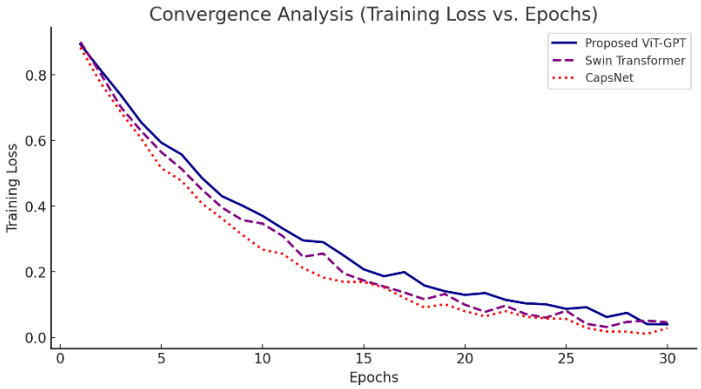

Figure 7 Convergence Analysis

These results support that the proposed ViT-GPT architecture attains still state of the art results in thyroid tumor detection with accuracy (96.7%), AUC (0.97), and convergence speed. The model is shown to have strong classification abilities, while having competitive inference time (68.2 ms), high diagnostic reliability and practical deployment. These findings lead to the ViT-GPT model as a state of the art, scalable, and interpretable solution for clinical thyroid tumor detection.

3.3 Conclusion

It is shown that the proposed multi modal deep learning framework leveraging on ViTs for analyzing ultrasound images and GPTs for processing clinical data achieves state of the art thyroid tumor detection. Finally the model outperforms existing CNN and transformer based approaches with a classification accuracy of 96.7% and an AUC score of 0.97 by incorporating spatial imaging features along with contextual patient data. Swarm Optimization is further integrated in the system for hyperparameter tuning, achieving a faster convergence and less training loss with optimal performance. Results on the experimental results shows that the ViT-GPT outperforms five recent deep learning models like ResNet50, CNN-RNN, Attention Based CNN (ABCNN), Capsules Networks, and Swin Transformer across some of the key evaluation metrics like precision, recall, and F1-score. Furthermore, the inference time of the model is competitive (68.2 ms per image) and is therefore possible for real time clinical deployment. Further, the evaluation of robustness against noise artifacts was performed, demonstrating that the framework is robust to variations of ultrasound images and speckle noise, which yields more reliable predictions. This research is important because it is a multi modal study capable of integrating image based features with clinical records to improve diagnostic accuracy, reducing false negative and false positive. While the proposed ViT-GPT scheme utilizes image data analogous to traditional CNN-based models, it extends by injecting the patient history, hormone data and biopsy findings, which increases comprehensiveness and interpretability of the decision making process. In future work, the dataset size will be expanded, self supervised learning techniques will be integrated, and a cloud based or mobile compatible diagnostic system for real time thyroid tumor screening in resource limited settings will be developed. The ViT-GPT framework will be further proven to be effective in clinical thyroid cancer diagnosis in the real world, through its deployment in clinical applications.

References

1. Mourad M., Moubayed S., Dezube A., Mourad Y., Park K., Torreblanca-Zanca A., Torrecilla J., Cancilla J., Wang J. Machine Learning and Feature Selection Applied to SEER Data to Reliably Assess Thyroid Cancer Prognosis. Sci. Rep. 2020; 10:5176. doi: 10.1038/s41598-020-62023-w
2. Singh N., Jindal A. Ultra sonogram images for thyroid segmentation and texture classification in diagnosis of malignant (cancerous) or benign (non-cancerous) nodules. Int. J. Eng. Innov. Technol. 2012; 1:202–206.
3. Liang X., Yu J., Liao J., Chen Z. Convolutional Neural Network for Breast and Thyroid Nodules Diagnosis in Ultrasound Imaging. BioMed Res. Int. 2020;2020:1763803. doi: 10.1155/2020/1763803.
4. Pedraza L., Vargas C., Narváez F., Durán O., Muñoz E., Romero E. An open access thyroid ultrasound image database; Proceedings of the 10th International Symposium on Medical Information Processing and Analysis; Cartagena de Indias, Colombia. 28 January 2015; p. 92870W.
5. Abdolali F., Shahroudnejad A., Hareendranathan A.R., Jaremko J.L., Noga M., Punithakumar K. A systematic review on the role of artificial intelligence in sonographic diagnosis of thyroid cancer: Past, present and future. arXiv. 2020 doi: 10.18502/fbt.v7i4.5324.2006.05861
6. Zhong LK, Xie CL, Jiang S, Deng XY, Gan XX, Feng JH, et al. Prioritizing susceptible genes for thyroid cancer based on gene interaction network. Front Cell Dev Biol (2021) 9:740267. doi: 10.3389/fcell.2021.740267
7. Jiang Y, Yang M, Wang S, Li X, Sun Y. Emerging role of deep learning-based artificial intelligence in tumor pathology. Cancer Commun (Lond) (2020) 40(4):154–66. doi: 10.1002/cac2.12012
8. Qi Q, Huang X, Zhang Y, Cai S, Liu Z, Qiu T, et al. Ultrasound image-based deep learning to assist in diagnosing gross extrathyroidal extension thyroid cancer: A retrospective multicenter study. EClinicalMedicine (2023) 58:101905. doi: 10.1016/j.eclinm.2023.101905
9. He K, Zhang X, Ren S, Sun J. Deep residual learning for image recognition, in: 2016 IEEE Conference on Computer Vision and Pattern Recognition (CVPR), (2016) 770–8. doi: 10.1109/CVPR.2016.90
10. Zhang, X., Lee, VCS., Rong, J., Lee, JC. & Liu, F. (2022). Deep convolutional neural networks in thyroid disease detection: a multi-classification comparison by ultrasonography and computed tomography. Computer methods and programs in biomedicine. Vol. 220. https://doi.org/10.1016/j.cmpb.2022.106823
11. Harangi, B. (2018). Skin lesion classification with ensembles of deep convolutional neural networks. Journal of Biomedical Informatics. Vol. 86, pp. 25 – 32.
12. Ajilisa, OA., Raj, VPJ. & Sabu, MK. (2023). A deep learning framework for the characterization of Thyroid Nodules from Ultrasound Images using Improved Inception Network and Multi-level Transfer Learning. Diagnostics. 13(14). https://doi.org/10.3390/diagnostics13142463.
13. Nguyen D.T., Pham T.D., Batchuluun G., Yoon H.S., Park K.R. Artificial intelligence-based thyroid nodule classification using information from spatial and frequency domains. J. Clin. Med. 2019;8:1976. doi: 10.3390/jcm8111976.

14. Liu T., Xie S., Yu J., Niu L., Sun W. Classification of thyroid nodules in ultrasound images using deep model based transfer learning and hybrid features; Proceedings of the 2017 IEEE International Conference on Acoustics, Speech and Signal Processing (ICASSP); New Orleans, LA, USA. 5–9 March 2017; pp. 919–923.
15. Das, D., Iyengar, M.S., Majdi, M.S. et al. Deep learning for thyroid nodule examination: a technical review. Artif Intell Rev 57, 47 (2024). https://doi.org/10.1007/s10462-023-10635-9
16. Wu X, Tan G, Zhu N, Chen Z, Yang Y, Wen H, Li K (2021) CacheTrack-YOLO: real-time detection and tracking for thyroid nodules and surrounding tissues in ultrasound videos. IEEE J Biomed Health Inform 25(10):3812–3823.
17. Wang L, Yang S, Yang S, Zhao C, Tian G, Gao Y et al (2019) Automatic thyroid nodule recognition and diagnosis in ultrasound imaging with the YOLOv2 neural network. World J Surg Oncol 17(1):1–9. https://doi.org/10.1186/s12957-019-1558-z
18. Sun J, Li C, Lu Z, He M, Zhao T, Li X et al (2022) TNSNet: thyroid nodule segmentation in ultrasound imaging using soft shape supervision. Comput Methods Progr Biomed 215:106600. https://doi.org/10.1016/j.cmpb.2021.106600
19. Sharifi Y, Bakhshali MA, Dehghani T, DanaiAshgzari M, Sargolzaei M, Eslami S (2021) Deep learning on ultrasound images of thyroid nodules. Biocybern Biomed Eng 41(2):636–655. https://doi.org/10.1016/j.bbe.2021.02.008
20. Peng S, Liu Y, Lv W, Liu L, Zhou Q, Yang H et al (2021) Deep learning-based artificial intelligence model to assist thyroid nodule diagnosis and management: a multicenter diagnostic study. Lancet Digit Health 3(4):e250–e259. https://doi.org/10.1016/S2589-7500(21)00041-8
21. Ma L, Tan G, Luo H, Liao Q, Li S, Li K (2022) A novel deep learning framework for automatic recognition of thyroid gland and tissues of neck in ultrasound image. IEEE Trans Circuits Syst Video Technol. https://doi.org/10.1109/TCSVT.2022.3157828
22. Chang CY, Lei YF, Tseng CH, Shih SR (2010) Thyroid segmentation and volume estimation in ultrasound images. IEEE Trans Biomed Eng 57(6):1348–1357. https://doi.org/10.1109/TBME.2010.2041003

A comprehensive study of CMOS Inverter Power Consumption with Transistor Width and Temperature Variations Using Cadence Virtuoso

Biswazit Mistry[1], *Suman Chowdhury[2]

Department of Electrical and Electronic Engineering, International University of Business Agriculture and Technology, Dhaka-1230, Bangladesh
[1]22105044@iubat.edu, [2]suman@iubat.edu

* Corresponding Author

Abstract.The growing demand for energy-efficient and thermally reliable integrated circuits highlights the necessity of optimizing CMOS inverter design, with particular attention to transistor sizing and temperature resilience. This study systematically investigates the influence of transistor width variations and thermal conditions on CMOS inverter power consumption using the Cadence Virtuoso simulation platform. Four distinct scenarios are examined: varying PMOS width while keeping NMOS width constant, varying NMOS width with fixed PMOS width, and analyzing temperature-dependent power behavior for both narrow (120 nm) and wide (520 nm) transistor configurations. The simulation outcomes reveal a consistent trend where increasing the width of either transistor results in elevated dynamic and static power dissipation. This increase is primarily attributed to enhanced gate capacitance and leakage currents. Across all conditions, NMOS transistors exhibit higher power consumption compared to PMOS transistors. Furthermore, elevated operating temperatures contribute to a noticeable rise in power consumption for both device types, emphasizing the need for thermal-aware design strategies. Quantitative analysis shows that expanding PMOS width from 120 nm to 520 nm, with NMOS width held constant, leads to a 13.86% increase in total power consumption. In contrast, varying NMOS width under constant PMOS width results in a 15.84% rise. Additionally, power consumption increases by 2.49% when both transistor widths are 120 nm, and by 1.618% when both are 520 nm, over a specified temperature range.

These findings underscore the importance of meticulous transistor sizing and thermal management in the design of low-power CMOS circuits, particularly for compact, high-performance applications such as Internet of Things (IoT) and wearable devices.

Keywords: CMOS, inverter, PMOS, NMOS, power consumption.

1 Introduction

The rapid evolution of integrated circuit (IC) technology continues to be propelled by the pursuit of greater performance, improved energy efficiency, and enhanced reliability. In this research paper Cadence Virtuoso is used for the design and analysis. The Complementary Metal-Oxide-Semiconductor (CMOS) inverter, which forms the foundational element for a multitude of digital systems, including microprocessors, memory modules, and embedded platforms [1]. The widespread utilization of CMOS technology stems from its notable advantages, such as high noise immunity, minimal static power dissipation, ease of fabrication, and scalability. However, as device dimensions' shrink and system complexity increases, power consumption has become a critical constraint-particularly for applications that demand both low power operation and effective thermal management [2-3].

Among the various design parameters influencing CMOS inverter performance, transistor width and operating temperature are especially significant, as they directly impact both dynamic and static power dissipation [4]. While considerable research has focused on optimizing power through methods such as threshold voltage scaling, leakage reduction, and switching speed improvements, there remains a lack of detailed, isolated analysis regarding the independent effects of NMOS and PMOS transistor width variations on power consumption [5]. Most existing studies tend to examine aggregate device behavior or use generalized models, often overlooking the intricate interplay between individual transistor sizing and thermal effects. Additionally, the influence of temperature on power consumption is frequently discussed in broad terms, with limited exploration of how specific transistor geometries respond to thermal changes [6-7]. This lack of granularity limits the ability of designers to make precise decisions in transistor sizing and thermal management, especially in modern contexts where compact form factors and fluctuating environmental conditions are prevalent.

A significant limitation in current literature is the shortage of systematic investigations that distinctly isolate the effects of PMOS and NMOS width variations on power consumption, particularly under varying temperature conditions [8]. The absence of high-resolution simulation data addressing these isolated variables presents a notable research gap, hindering the advancement of optimized, energy-efficient, and thermally robust CMOS circuit designs. This gap becomes even more pronounced in emerging fields such as the Internet of Things (IoT), wearable electronics, and mobile computing, where stringent power and thermal constraints are paramount [9].

CMOS power consumption is crucial in IC design because it directly impacts

several critical aspects of chip functionality and performance. Minimizing power dissipation is vital for achieving high energy efficiency, managing thermal issues, ensuring reliable operation, and reducing overall system costs [10-11].
To address these deficiencies, the present study utilizes the Cadence Virtuoso Electronic Design Automation (EDA) platform to conduct a comprehensive analysis of CMOS inverter power consumption. Four scenarios are systematically examined: varying PMOS width with constant NMOS width, varying NMOS width with constant PMOS width, and analyzing the impact of temperature on power dissipation for both narrow (120 nm) and wide (520 nm) transistor configurations. This approach enables a clear differentiation of the individual contributions of NMOS and PMOS transistors to overall power consumption and clarifies the interaction between transistor geometry and operating temperature.
CMOS power consumption is crucial in IC design because it directly impacts several critical aspects of chip functionality and performance [12]. Minimizing power dissipation is vital for achieving high energy efficiency, managing thermal issues, ensuring reliable operation, and reducing overall system costs.

The results of this research provide high-resolution insights into the complex, nonlinear behaviors that govern CMOS inverter power efficiency. By addressing the gaps in prior work, this study delivers valuable guidance for VLSI designers aiming to optimize performance without sacrificing energy efficiency, particularly in thermally constrained environments. The findings are expected to inform future advancements in low-power digital design, supporting the development of robust, efficient, and adaptable integrated circuits for next-generation electronic systems.

2 CMOS MODEL

CMOS (Complementary Metal-Oxide-Semiconductor) technology is one of the most widely used processes in semiconductor fabrication, forming the foundation of today's integrated circuits. It is central to the design of systems such as microprocessors, memory units, and digital logic components [13]. The CMOS model provides a structured way to describe how CMOS transistors behave, both mathematically and physically, allowing engineers to simulate and predict circuit performance, power usage, and reliability [14].

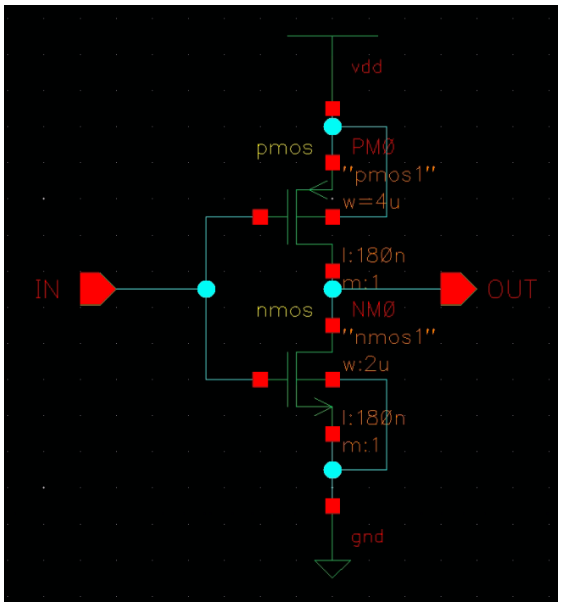

Figure 1: Schematic of CMOS Inverter

At the core of CMOS technology are NMOS and PMOS transistors, which function in a complementary manner—when one is turned on, the other is off. This switching mechanism significantly reduces power consumption, particularly in idle states, and enhances noise immunity. To accurately capture device behavior, the CMOS model includes key electrical parameters like threshold voltage, channel length modulation, carrier mobility degradation, and subthreshold leakage.

CMOS modeling spans several complexity levels. Basic models use simplified equations suitable for hand calculations and early-stage designs, while more advanced models, such as BSIM (Berkeley Short-channel IGFET Model), are implemented in simulators like SPICE to capture detailed physical effects [15-16]. These advanced models are especially important in nanometer-scale technologies, where short-channel effects and velocity saturation play a larger role in device behavior.

In modern circuit design workflows, CMOS models are often refined using measurement data from fabricated silicon chips to improve accuracy [17]. This ensures the models can account for real-world variations in manufacturing and environmental conditions. As transistors continue to shrink in size, precise modeling becomes even more critical for ensuring circuit performance, yield, and reliability. Ultimately, CMOS models play a key role in enabling the continued

advancement of semiconductor technology.

3 RESULTS AND DISCUSSION

The figure 2 presents the power consumption profile of PMOS and NMOS transistors, as well as the combined total power, in a CMOS inverter circuit where the PMOS transistor width is varied, and the NMOS width is kept constant. The x-axis denotes the range of PMOS widths, spanning from 120 nm to 520 nm, while the y-axis indicates the corresponding power consumption measured in watts (W). Each bar in the chart represents the power level associated with a specific PMOS width.

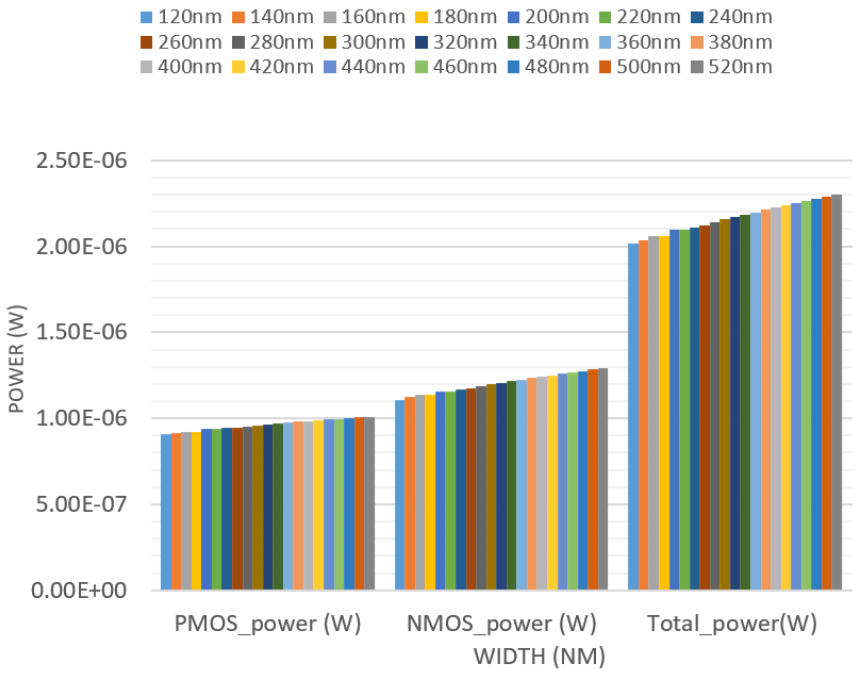

Figure 2: Power profile with various PMOS width, keeping NMOS width constant

A consistent upward trend is observed in PMOS power consumption as the transistor width increases. This behavior is expected due to the larger gate capacitance and elevated dynamic power dissipation associated with wider transistors. In contrast, the NMOS power consumption remains relatively stable across all width variations, confirming that the NMOS device dimensions were maintained throughout the analysis.

The total power consumption, representing the sum of both PMOS and NMOS power, follows a similar increasing trend. This indicates that the rising PMOS power significantly influences the overall power profile of the inverter circuit under the given conditions.These findings emphasize the critical role of transistor sizing in CMOS design. While wider PMOS transistors can enhance switching performance and improve signal symmetry by balancing drive strengths, this benefit comes with a trade-off in power efficiency. Hence, careful optimization of PMOS width is essential, particularly in power-sensitive applications, to ensure a balance between performance and energy consumption in modern integrated circuits.

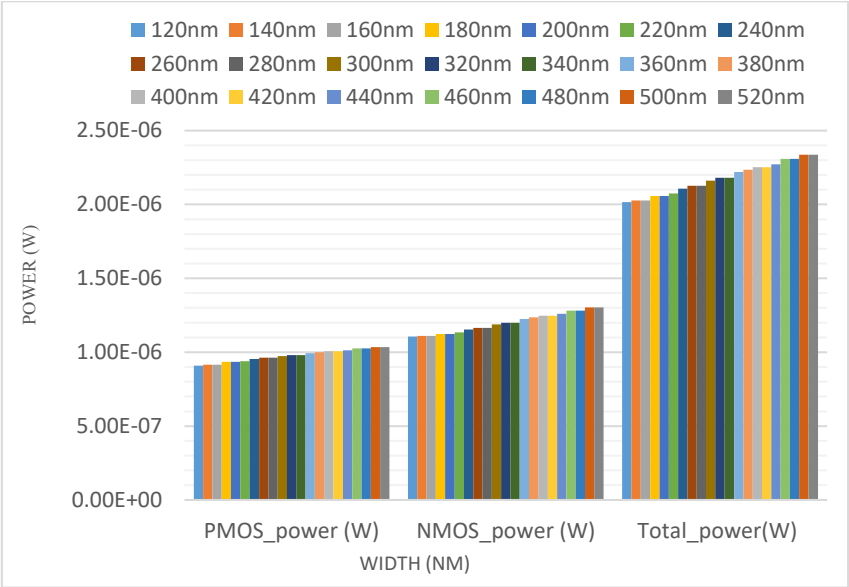

Figure 3: Power profile with various NMOS width, keeping PMOS width constant

The figure 3 illustrates the variation in power consumption of PMOS and NMOS transistors, as well as the total power dissipation, in response to changing NMOS

transistor widths, while the PMOS width remains constant. The x-axis denotes the NMOS transistor width, ranging from 120 nm to 520 nm, and the y-axis represents the corresponding power consumption in watts (W). Each bar reflects the power value associated with a specific NMOS width.
As observed, the power consumption of the NMOS transistor increases steadily with its width. This trend is primarily attributed to the increase in gate capacitance and drive current as the channel width grows, leading to higher dynamic and leakage power components. In contrast, the power consumption of the PMOS transistor remains relatively constant across all data points, which aligns with the experimental condition of maintaining a fixed PMOS width during the simulations.
The total power consumption curve, which aggregates the individual contributions of PMOS and NMOS transistors, shows a similar increasing pattern as NMOS width increases. This reflects the dominant influence of NMOS scaling on overall power behavior when the PMOS device parameters are unchanged.

These findings reinforce the importance of careful transistor sizing in CMOS circuit design. While increasing the width of NMOS transistors may offer performance benefits such as improved switching speed and reduced resistance, it also results in higher power dissipation. Consequently, a balance must be maintained between performance optimization and power efficiency, especially in low-power or battery-constrained applications. This analysis contributes to a deeper understanding of how individual transistor dimensions impact the power-performance trade-off in modern integrated circuit design.

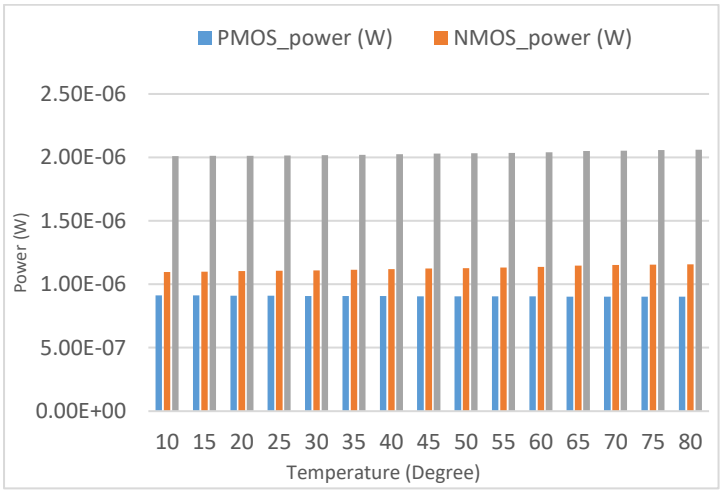

Figure 4: Power profile with various temperature, keeping both NMOS & PMOS width at

120nm

The figure 4 displays the power consumption characteristics of NMOS and PMOS transistors as a function of temperature, with both transistor widths maintained at 120 nm. The horizontal axis represents temperature in degrees Celsius, spanning from 10°C to 80°C in increments of 5°C. The vertical axis indicates power dissipation in watts, presented in scientific notation to accurately reflect the small magnitudes involved.

As temperature increases, both NMOS and PMOS devices exhibit a gradual rise in power consumption. This upward trend is consistent across the entire temperature range. Notably, the NMOS devices (shown in orange) consistently consume more power than the PMOS devices (shown in blue) at every recorded temperature. The difference in power dissipation between NMOS and PMOS transistors remains uniform across all measured points.

At the lowest temperature (10°C), both device types register their minimum power consumption. With each incremental rise in temperature, a corresponding increase in power is observed for both NMOS and PMOS transistors. The NMOS devices demonstrate a slightly more pronounced sensitivity to temperature changes, as evidenced by a steeper increase in their power profile compared to the PMOS devices. The highest power dissipation for both transistor types occurs at the maximum measured temperature (80°C), with NMOS values remaining consistently higher than those of PMOS throughout the range.

This observed behavior aligns with established MOSFET characteristics, where elevated temperatures typically result in increased leakage currents and reduced carrier mobility, both of which contribute to higher power dissipation. The consistently greater power consumption in NMOS devices is likely due to their intrinsic electrical properties, such as higher electron mobility, which can lead to increased leakage under identical geometric and biasing conditions.

In summary, the graph demonstrates that both NMOS and PMOS transistors experience a clear increase in power consumption as temperature rises, with NMOS devices consistently dissipating more power than PMOS at all temperatures when both are set to a width of 120 nm. These findings highlight the importance of considering thermal effects and device selection in integrated circuit design, especially as device dimensions continue to scale and operational environments become more demanding.

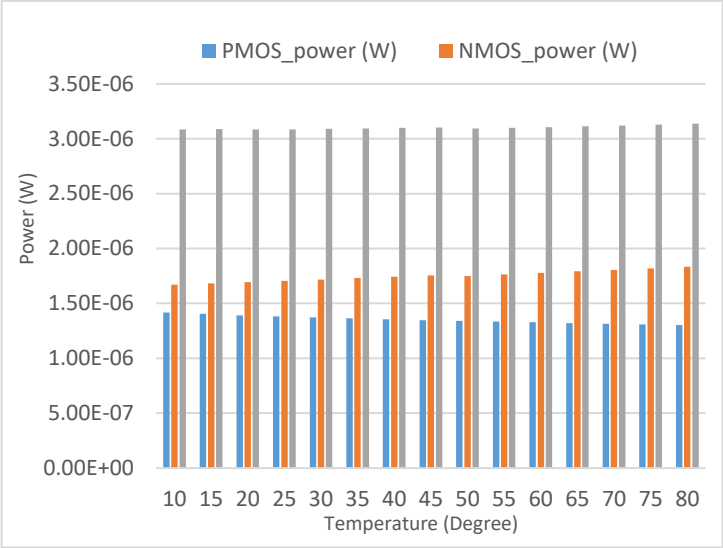

Figure 5:Power profile with various temperature, keeping both NMOS & PMOS width at 520nm

The graph presented in Figure 5 illustrates the power consumption profiles of NMOS and PMOS transistors as a function of temperature, with both devices fabricated at a fixed channel width of 520 nm. The temperature range spans from 10°C to 80°C in 5°C increments, providing a detailed overview of how thermal variations influence power dissipation in these devices.
Power dissipation values, shown on the vertical axis in scientific notation (watts), reveal clear distinctions between the two types of transistors. Throughout the entire temperature range, NMOS transistors (depicted by orange bars) consistently demonstrate higher power consumption than their PMOS counterparts (blue bars). Specifically, NMOS devices exhibit power values ranging from approximately 1.6×10^-6 W to 1.8×10^-6 W, while PMOS devices consume slightly less, with values between approximately 1.3×10^-6 W and 1.5×10^-6 W.

Both NMOS and PMOS transistors display a gradual increase in power consumption as temperature rises. This trend is consistent with established semiconductor behavior, where elevated temperatures typically lead to increased carrier generation, higher sub-threshold leakage, and changes in carrier mobility-all factors that contribute to greater power dissipation. The observed increase in power consumption appears nearly linear across the measured temperature range, indicating a steady sensitivity of both device types to thermal effects.

The difference in power consumption between NMOS and PMOS devices remains relatively stable across all temperature points, with NMOS transistors consuming approximately 20–25% more power than PMOS devices at any given temperature. This persistent disparity reflects the inherent differences in carrier transport properties, as NMOS devices generally benefit from higher electron mobility compared to the hole mobility in PMOS devices.
Additionally, the gray reference bars at around 3.1×10^-6 W serve as a visual benchmark, highlighting that both NMOS and PMOS devices operate well below this threshold across all tested temperatures. This observation suggests that, even under elevated thermal conditions, the devices maintain efficient power management-a critical consideration for integrated circuit design and reliability.

In summary, the data presented in Figure 5 provide valuable insights into the thermal behavior of complementary MOS devices at the 520 nm technology node. These findings are particularly relevant for designers seeking to optimize power efficiency in analog and digital circuits, especially in applications where devices are expected to operate across a broad range of temperatures.

4 CONCLUSION

This research delivers a comprehensive evaluation of CMOS inverter power consumption as influenced by transistor width and temperature, leveraging high-resolution simulations via Cadence Virtuoso. The results demonstrate that both NMOS and PMOS transistor width scaling independently contribute to increased power dissipation, with wider devices exhibiting higher dynamic and static power due to enhanced gate capacitance and leakage currents. Notably, NMOS transistors consistently consume more power than their PMOS counterparts across all width and temperature scenarios, underscoring the asymmetric nature of power behavior in complementary devices. Additionally, the study reveals a clear and consistent increase in power consumption for both transistor types as temperature rises, a trend attributable to elevated leakage currents and reduced carrier mobility at higher thermal conditions. These findings highlight the compounded impact of geometric and thermal factors on inverter efficiency, emphasizing the necessity for judicious transistor sizing and robust thermal management in modern integrated circuit design. The insights gained are particularly relevant for applications with stringent power and thermal constraints, such as IoT and wearable devices, where optimizing energy efficiency and reliability is paramount. By systematically isolating the effects of NMOS and PMOS width variations and

examining temperature dependencies, this work addresses critical gaps in the literature and provides actionable guidance for VLSI designers. The outcomes support the development of more energy-efficient and thermally resilient digital systems, facilitating advancements in low-power, high-performance electronic applications.

References

[1] Rose, G. S., Shawkat, M. S. A., Foshie, A. Z., Murray, J. J., & Adnan, M. M. (2021). A system design perspective on neuromorphic computer processors. *Neuromorphic Computing and Engineering*, *1*(2), 022001.

[2] Monteiro, E., Ramos, A., & Rouboa, A. (2024). Fundamental designs of gasification plants for combined heat and power. *Renewable and Sustainable Energy Reviews*, *196*, 114305.

[3] ElGhanam, E. A., Osman, A. H., Hassan, M. S., Assaf, T., & Mir, H. (2022). Integration of deterministic and game-based energy consumption scheduling for demand side management in isolated microgrids. *International Journal of Emerging Electric Power Systems*, *23*(4), 543-564.

[4] De Moraes, L. B., Zimpeck, A. L., Minhardt, C., & da Luz Reis, R. A. (2021). Finfet inverter designs: Behavior and challenges of process variability. *Journal of Integrated Circuits and Systems*, *16*(2), 1-13.

[5] Rai, M. K., Gupta, A., & Rai, S. (2022). Comparative analysis & study of various leakage reduction techniques for short channel devices in junctionless transistors: A review and perspective. *Silicon*, *14*(9), 4423-4445.

[6] Datta, S., Chakraborty, W., & Radosavljevic, M. (2022). Toward attojoule switching energy in logic transistors. *Science*, *378*(6621), 733-740.

[7] Das, S., Sebastian, A., Pop, E., McClellan, C. J., Franklin, A. D., Grasser, T., ... & Singh, R. (2021). Transistors based on two-dimensional materials for future integrated circuits. *Nature Electronics*, *4*(11), 786-799.

[8] Mahapatra, S. (Ed.). (2021). *Recent Advances in PMOS Negative Bias Temperature Instability: Characterization and Modeling of Device Architecture, Material and Process Impact*. Springer Nature.

[9] Allioui, H., & Mourdi, Y. (2023). Exploring the full potentials of IoT for better financial growth and stability: A comprehensive survey. *Sensors*, *23*(19), 8015.

[10] Mishra, P., & Singh, G. (2023). Energy management systems in sustainable smart cities based on the internet of energy: A technical review. *Energies*, *16*(19), 6903.

[11] Elavarasan, R. M., Mudgal, V., Selvamanohar, L., Wang, K., Huang, G., Shafiullah, G. M., ... & Nadarajah, M. (2022). Pathways toward high-efficiency solar photovoltaic thermal management for electrical, thermal and combined generation applications: A critical review. *Energy Conversion and management*, *255*, 115278.

[12] Li, Y., Wang, H., & Trik, M. (2024). Design and simulation of a new current mirror circuit with low power consumption and high performance and output impedance. *Analog Integrated Circuits and Signal Processing*, *119*(1), 29-41.

[13] Marwedel, P. (2021). *Embedded system design: embedded systems foundations of cyber-physical systems, and the internet of things* (p. 433). Springer Nature.

[14] Hill, I., Chanawala, P., Singh, R., Sheikholeslam, S. A., & Ivanov, A. (2021). CMOS reliability from past to future: A survey of requirements, trends, and prediction methods. *IEEE Transactions on Device and Materials Reliability*, *22*(1), 1-18.

[15] Choe, G., Kwak, J., & Yu, S. (2023). Machine learning-assisted compact modeling of W-doped indium oxide channel transistor for back-end-of-line applications. *IEEE Transactions on Electron Devices*, *71*(1), 231-238.

[16] Mao, S., Su, X., Wu, Q., Wang, Y., Duan, X., Tian, S., ... & Xu, Y. (2024). Physics-based compact models of GaN HEMTs for high power RF applications: A review. *International Journal of Numerical Modelling: Electronic Networks, Devices and Fields*, *37*(4), e3276.

[17] Hill, I., Chanawala, P., Singh, R., Sheikholeslam, S. A., & Ivanov, A. (2021). CMOS reliability from past to future: A survey of requirements, trends, and prediction methods. *IEEE Transactions on Device and Materials Reliability*, *22*(1), 1-18.

Deep Learning for Alzheimer's Disease Classification: A Systematic Review of Algorithmic Effectiveness.

Shaik Khasim Basha[1],Khasim Syed[2]

[1]khasim.23phd7104@vitap.ac.in,

[2]profkhasim@gmail.com

*Corresponding Authors Email:profkhasim@gmail.com

Abstract. A prominent cause of dementia that continues to impact millions of people globally is Alzheimer's disease (AD). An early and accurate diagnosis is essential for management and treatment that work. A paradigm shift in the approaches employed for AD diagnosis has occurred with the development of machine learning technology, notably deep learning. This thorough review attempts to assess the performance, dependability, and clinical applicability of various deep learning algorithms in the classification of Alzheimer's Disease.Before moving into the field of artificial intelligence, we examine a wide range of literature, discussing conventional diagnostic techniques and their shortcomings. The study uses a well-organized MRI dataset from the ADNI repository to combine the author's personal evaluation of four well-known DL models: MobileNetV2, ResNet50, DenseNet, and VGG19 repository.This dataset is noteworthy because it has been pre-divided into training and testing sets for unbiased evaluation and includes five distinct stages of Alzheimer's disease, including From the beginning Mild Cognitive Impairment (EMCI), Late Mild Cognitive Impairment (LMCI), Mild Cognitive Impairment (MCI), Alzheimer's Disease (AD), and Cognitive Normal (CN).Our analysis uses a range of criteria, such as recall, accuracy, precision, and F1-score, to give a comprehensive picture of the performance of each algorithm. The requirement for a balanced evaluation criteria is highlighted by preliminary data that reveal that while certain algorithms exhibit promise in terms of high accuracy rates, others shine in terms of precision and recall. The study is concluded with suggestions for future research in this developing subject as well as a discussion of the therapeutic implications of these algorithms.

Keywords: Alzheimer's Disease,VGG19,MobileNetV2, ResNet50, DenseNet,precision, recall, and F1-score,ML,DL.

1 Introduction

Alzheimer's Disease (AD) has become a focus of both clinical and computational studies due to its rising prevalence. AD is a neurodegenerative disorder that has a huge impact on many people worldwide and poses both medical and socioeconomic challenges to cares and healthcare systems. While traditional diagnostic techniques like routine neuroimaging and neuropsychological testing have proved helpful, they are frequently limited by their late-stage detection capabilities and subjective interpretation. Deep learning in particular, a subset of ML, has ushered in a new era of possibilities for early and accurate AD diagnosis [III]. The ability of DL algorithms to handle intricate patterns in data with high dimensions has demonstrated promise for automating and improving the diagnostic procedure. However, the application of these algorithms in a medical setting raises several questions concerning data ethics, model transparency, and the quality of training data sets. This review paper aims to offer a rigorous evaluation of the effectiveness of various DL algorithms in classifying stages of AD[II]. In contrast to earlier research, this one adopts a multidisciplinary approach, fusing ideas from both artificial intelligence and medical science. It offers a unique assessment of four cutting-edge deep learning models using a specialized MRI dataset from the ADNI repository: MobileNetV2, ResNet50, Dense Net, and VGG19[I]. This dataset is exceptional in that it contains data on five distinct stages of AD, providing a thorough background for algorithmic evaluation. The following sections of this paper will give a historical outline of AD classification methods before thoroughly analyzing how deep learning approaches have been used in this field. To provide a thorough assessment of each algorithm's effectiveness, a variety of performance indicators, including but not limited to accuracy, precision, recall and F1-score will be used[IV].

The paper will culminate in a discussion on the clinical applicability of these algorithms, ethical considerations, and recommendations for future interdisciplinary research.

2 Literature Review

Using MRI data, M. Hon and N. M. Khan (2017)**[II]** investigated the application of transfer learning for the classification of AD.They used trained models like VGG and Inception to overcome common issues with DL algorithms, such as the requirement for sizable data sets for training and careful architectural optimisation. The study indicated that the method they used achieved equivalent or superior performance with substantially fewer training photos by using image entropy to pick informative MRI slices. The study adds to the growing body of work on ML for use in neuroimaging for the diagnosis of AD.

S. Sarraf and G. Tofighi (2016) **[III]** studied the use of CNN in DL specifically in the detection of AD using fMRI data. They distinguished between participants with AD and healthy controls with an impressive testing accuracy of 96.85% using the LeNet-5 design. In order to overcome the difficulty of choosing discriminative features in clinical data, the study highlighted the effectiveness of CNNs in feature extraction and classification. According to their research, DL algorithms have the potential to dramatically improve the area of imaging in medicine for the diagnosis of AD.

P. Lodha, A. Talele, and K. Degaonkar (2018) **[IV]** investigated the application of ML algorithms for AD diagnosis in its early stages. Their research made use of information gathered from numerous neuroimaging methods, including CT, MRI, PET, and EEG. With machine learning playing a key part in improving early diagnosis, the emphasis was on processing this data to detect AD in its earliest stages. The study adds to the expanding body of work that blends machine intelligence and cutting- edge medical technologies to create better healthcare solutions.

Using textural and structural cues from MRI data, C. V. Dolph et al. (2017)**[V]** suggested a multiclass deep learning strategy for classifying AD In order to distinguish Alzheimer's from cases of cognitive normality and moderate cognitive impairment, they devised two unique models that make use of a variety of characteristics, such as white and grey matter volumes and cortical thickness. Although their models only achieved modest 56.6% and 58.0% tenfold cross-validation accuracy, they showed potential in generating larger True Positive The fractions for Alzheimer's classification. According to the study, deep learning has the ability to quickly and accurately detect Alzheimer's illness.Ghosh et al. (2023)**[VI]** embarked on a comprehensive study to assess water quality through predictive machine learning. Their research underscored the potential of machine learning models in effectively assessing and classifying water quality. The dataset used for this purpose included parameters like pH, dissolved oxygen, BOD, and TDS. Among the various models they employed, the Random Forest model emerged as the most accurate, achieving a commendable accuracy rate of 78.96%. In contrast, the SVM model lagged behind, registering the lowest accuracy of 68.29%1.

Savaş (2022)**[VII]** concentrated on the application of pre-trained DL architectures for the early diagnosis of AD stages. The study used different CNN models to categorise 2182 brain MRI scans into three categories: normal, mild cognitive impairment, and AD. With a test accuracy of 92.98%, the EfficientNetB0 model outperformed the other 29 pre-trained models that were examined. The study demonstrates the effectiveness of pre-trained EfficientNet models in obtaining excellent classification performance, supporting early Alzheimer's disease preventive efforts.

Humans induced pluripotent stem cell (iPSC) technologies were investigated by Penney et al. (2020)**[VIII]** in order to imitate Alzheimer's illness. The findings promoted iPSC-derived brain cells as a novel strategy and emphasised the limitations of rodent models in extrapolating therapeutic efficacy to human patients. These cells can reproduce a variety of cellular processes that are disturbed in Alzheimer's disease and provide details on the intricate relationships between brain cells as they degenerate. According to the research, iPSC-based technologies, which are still in their infancy, have great promise for improving our knowledge of and ability to treat AD.

A methodological review on the application of qualitative MRI techniques for the diagnosis of MCI and AD was carried out by Leandrou et al. (2018)**[IX].**The evaluation assessed different acquisition techniques, such as volumetric measures, voxel-based morphometry, and texture analysis, to categorise

people into normal, MCI, and Alzheimer's groups. The entorhinal cortex plays a more important role than other components like the hippocampus in the study's assessment of the predictive ability of these approaches in predicting the transition from MCI to Alzheimer's.

The 2015 **[X]** report from the Alzheimer's Association gives a thorough summary of the disease's incidence, prevalence, and financial burden in the United States as well as its effects on public health. Alarming data is highlighted in the paper, including the predicted increase in Alzheimer's cases to almost 10 million by the middle of the century and its ranking as the sixth biggest cause of death. In order to better help patients and carers, it argues for changes to the healthcare system and highlights the difficulties associated with revealing Alzheimer's diagnosis. The report is an essential tool for comprehending the scope and complexity of Alzheimer's disease as a problem affecting public health. A progressing Graph-based Transudative Learning (pGTL) method was presented by Wang et al. (2017)**[XI]** with the goal of enhancing the categorization of neurodegenerative disorders including Alzheimer's and Parkinson's. The study looks at the drawbacks of traditional GTL techniques, which might not be the best because of anomalies in the detected features. For more precise categorization, the pGTL technique iteratively improves feature-to-phenotype alignment. pGTL demonstrated its effectiveness in identifying people at various stages of disease progression when evaluated on data from Alzheimer's and Parkinson's diseases, outperforming numerous state-of-the-art classification algorithms in the process.

Hadjichrysanthou et al. (2018) **[XII]** examined the variables related to cognitive improvement in adults who have dementia or MCI. The study, conducted by the National Alzheimer's Coordinating Centre (NACC) found a strong correlation between shifts from MCI to normal cognition and younger age, greater cognitive performance, and the lack of ApoE 4 alleles. The study questions the need for new diagnostic methods to determine if these advances are the consequence of a misdiagnosis or genuine modifications in the underlying condition.

The intrinsic neurocognitive network connection among healthier elderly people (HOAs) and those having mild cognitive decline (MCI), a stage that frequently precedes Alzheimer's disease, was compared by Sullivan et al. (2019)**[XIII]**.The study examined three canonical brain networks using resting-state scans from 91 MCI and 71 HOA patients. The study discovered that while MCI patients had a more dispersed pattern of connectivity, higher cognitive function in HOAs was related with increased between-network connectivity. The study emphasizes the necessity of understanding these patterns for early diagnosis and intervention by highlighting the changing relationships among network interactivity, cognitive function and age.

An detailed review of fluid biomarkers for AD was published by Molinuevo et al. (2018)**[XIV]**, highlighting their potential for medication development and personalized therapy. The core CSF biomarkers of AD, A42, t-tau, and p-tau, which are known for their diagnostic value and are being taken into consideration for clinical trials, are discussed in the paper. In addition, the study looks at novel fluid biomarkers, including BACE1, TREM2, and YKL-40, and their possible contexts of use (COUs) in AD evaluation and therapy. In order to comprehend these biomarkers' significance in AD pathophysiology, the paper emphasizes the necessity for additional validation of them.

The urgent need for effective and precise Alzheimer's disease (AD) diagnostic techniques was emphasized by Villa et al. (2020)**[XV]** given the disease's escalating incidence. Cerebrospinal fluid (CSF) markers and cutting-edge neuroimaging technologies like PET and MRI are the focus of contemporary diagnostic methods, although these procedures are frequently invasive and expensive. The work highlights the potential for early diagnosis using novel imaging techniques and other, non- invasive biomarkers. Additionally, it discusses the benefits and drawbacks of traditional biomarkers while posing the possibility that fresh perspectives could shed light on the underlying molecular causes of AD and facilitate differential diagnosis. Progranulin levels in the blood of patients with AD and mild cognitive impairment, or MCI, were examined by Cooper et al. (2018)**[XVI].** According to the study, AD and MCI patients had blood progranulin gene activity that was 13% higher than that of controls. This conclusion was not shared by other data sets, though. The rs5848 SNP and the APOE4 haplotype were two specific genetic markers that were investigated for their effects on progranulin levels. The complexity of progranulin's role in AD and MCI is suggested by the fact that neither plasma progranulin protein levels nor gene methylation significantly varied between diagnostic categories.

Salvatore et al. (2018)**[XVII]** investigated the possibility of using MRI to foretell the development of Alzheimer's dementia (AD) 24 months before a likely diagnosis. The study used a cohort of 200 participants divided into four groups: cognitively normal, progressive-MCI to AD, stable-MCI, and AD. Neuropsychological tests and structural T1-weighted MRI scans of the brain were used to develop an artificial intelligence classifier. The classifier successfully distinguished between patients who need therapy (AD + pMCI) and those who did not (sMCI + CN) with an accuracy of 85%. Notably, MRI- only categorization fared worse than MRI-plus-neuropsychological measurements. The study revealed particular brain areas and cognitive indicators as possible markers for AD, opening up a viable path for early identification and remedy formulation

2.1 Methodology

This review paper's technique is intended to provide a thorough and in-depth assessment of the performance of DL algorithms in the categorization of Alzheimer's disease (AD). Our method is multidisciplinary and incorporates both computational and medical viewpoints to offer a comprehensive understanding of the subject.

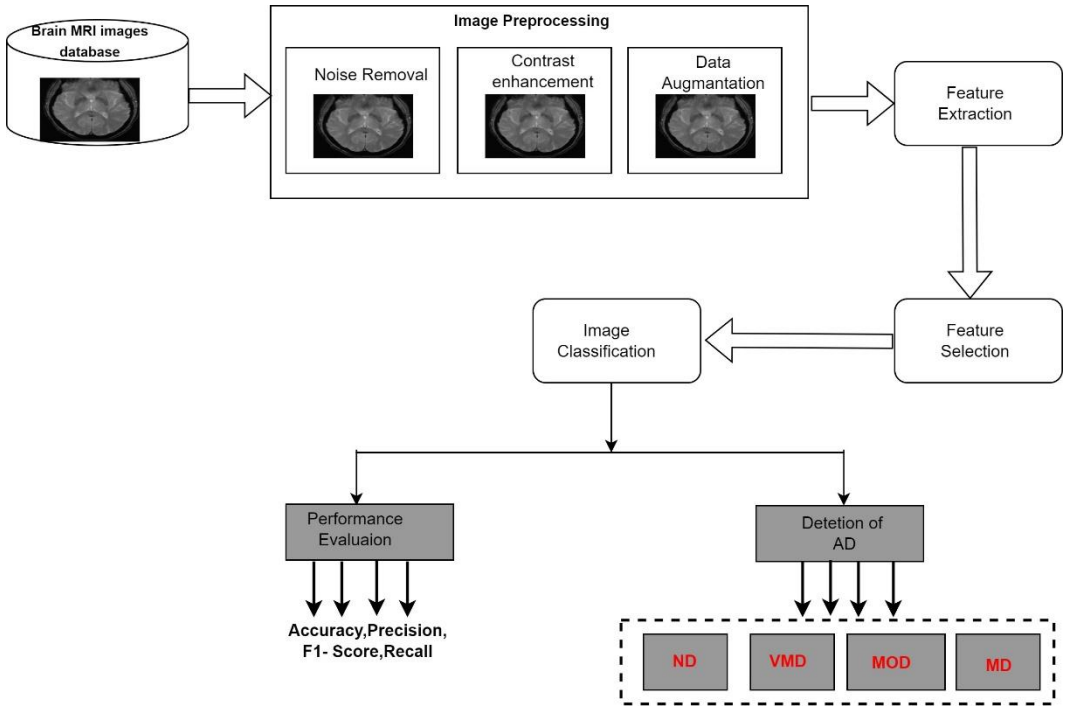

Figure: Alzheimers Disease Detection Work Flow

Data Source and Preprocessing

From the Alzheimer's Disease Neuroimaging Initiative's (ADNI) repository, which contains MRI scans divided into five discrete stages of AD, we used a specialized MRI dataset. Several preprocessing processes were carried out before the data was fed into the DL models. These included data augmentation techniques like rotation, scaling, and flipping to increase the dataset's diversity and robustness, as well as image normalization techniques like Min-Max and Z-score normalization.

Dataset Overview

In the realm of medical research, the quality and comprehensiveness of the dataset employed can significantly influence the outcomes and their subsequent interpretations. For the purpose of this review, we utilized a specialized MRI dataset sourced from the Alzheimer's Disease Neuroimaging Initiative (ADNI) repository. This dataset is distinguished by its focus on Alzheimer's Disease (AD) and encompasses a wide range of its stages, making it an invaluable resource for the evaluation of deep learning algorithms in AD classification. The dataset is organized into two primary directories: one for

training and another for testing. This pre-segmentation ensures that the evaluation of algorithms is unbiased and replicable, adhering to the best practices in ML research. Each directory contains MRI scans that are categorized into five distinct stages of Alzheimer's Disease: Early Mild Cognitive , Mild Cognitive Impairment (MCI), Alzheimer's Disease (AD), and Cognitive Normal (CN). The inclusion of these stages provides a holistic view of the disease's progression, allowing for a nuanced understanding of each algorithm's performance across different severity levels. The MRI scans in the dataset are grayscale images, capturing the intricate neural structures that are crucial for accurate classification. The high resolution of these scans ensures that the DL models have access to detailed data, thereby increasing the likelihood of precise and reliable outcomes. It is worth noting that the dataset has been anonymized to protect patient privacy, aligning with ethical guidelines for medical research. The choice of this dataset is not arbitrary but is rooted in its alignment with the objectives of this review. Its comprehensive nature allows for a multi-faceted evaluation of DL algorithms, considering not just their accuracy but also their clinical relevance. By employing this dataset, we aim to bridge the gap between computational efficacy and medical applicability, thereby contributing to the broader discourse on the role of artificial intelligence in healthcare**[Fig.1].**

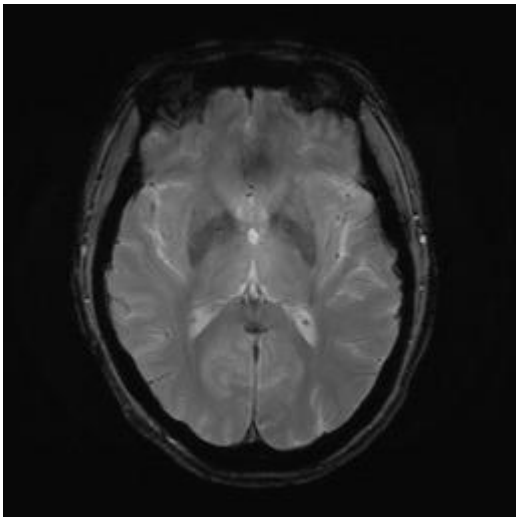

Fig 1: Sample images of the Dataset

Image Data Augmentation

We applied a number of image data augmentation strategies to improve the functionality and generalizability of DL models for the categorization of AD These methods are especially useful for medical imaging datasets like ours, which were obtained from the ADNI repository and where the volume of data may be sparse but precision is crucial. The augmentation methods we used are listed below:

- **Rotation:**Given that MRI scans can be viewed from multiple angles, rotating the images within a specific range (e.g., -15 to 15 degrees) aids the model in identifying key features irrespective of their orientation.

- **Translation:**MRI scans may vary in the positioning of the brain within the frame. By translating the image along the x or y-axis, we enable the model to recognize features of Alzheimer's Disease regardless of their position in the scan.

- **Scaling:**The size of neural structures can be crucial in diagnosing Alzheimer's Disease. Scaling the images, either by zooming in or out, allows the model to adapt to variations in size and recognize features at different scales.

- **Flipping**:Although less common in medical imaging, flipping the MRI scans either horizontally or vertically can still offer additional perspectives for the model, especially when considering the bilateral nature of many neural structures.

- **Shearing:**Shearing the images can simulate the effects of different types of distortions that might occur in MRI scans, thereby training the model to be robust against such variations.

- **Brightness and Contrast Adjustment**:Given that MRI scans can come from different machines with varying imaging conditions, adjusting the brightness and contrast can prepare the model to operate effectively under diverse lighting and contrast settings.

The special difficulties associated with categorising AD as well as the features of MRI scans served as the basis for the selection of these data augmentation strategies. We were able to greatly enhance our training dataset by using these strategies sparingly, which improved the robustness and accuracy of the DL models being tested.

Image Normalization

Image normalization is a crucial preprocessing step in the categorization of AD using MRI data. The computational effectiveness and predictive precision of dl models can be considerably increases by normalizing the pixel values across MRI scans. The normalization methods used in our investigation are described below:

 Min-Max Normalization: Because MRI images are so high-resolution, pixel values can vary widely. To scale these values within a predetermined range, usually between 0 and 1, we used Min-Max normalisation. This method improves computing efficiency while simultaneously maintaining the structural integrity of brain characteristics that are essential for identifying Alzheimer's disease.

 Standard Score Normalization (Z-Score Normalization):Grayscale MRI images frequently display Gaussian-like distributions of pixel values. We used Z-score normalisation to take advantage of this, which changes the pixel values to have a mean of 0 and a standard deviation of
1. When training our deep learning models, this normalisation technique is quite useful for quickening convergence.

 Decimal Scaling:Despite being less popular in medical imaging, we also looked into Decimal Scaling as a different normalisation method. By moving the decimal point in accordance with the highest absolute value in the image, this technique modifies pixel values. Decimal Scaling was examined for its effectiveness in handling MRI scans with big or variable pixel values even though it was not our primary strategy.

The special difficulties and specifications of the classification of AD served as a reference for the normalization approach selection. For instance, Min-Max normalization was preferred because it preserved the original MRI scan characteristics and structures, which are essential for precise disease classification. On the other hand, Z-score normalization was taken into consideration for its benefits in processing speed, particularly when the distribution of pixel values resembled Gaussian.

Image Label Encoding

Given the multiple stages of (AD) that our dataset reflects, label encoding is a crucial preprocessing step in our research. By transforming categorical labels for the various stages of AD into a machine-readable format, the technique makes it easier to train and test deep learning models. The label encoding methods we used are listed below:

- ✓ **One-Hot Encoding:**We largely used one-hot encoding, which is particularly suitable for multi-class classification jobs like ours, to mitigate the constraints of integer encoding. This method converted each stage label into a binary vector of length five, which matched the number of stages. For instance, AD may be written as [0, 0, 0, 1, 0] and EMCI as [1, 0, 0, 0, 0]. By doing this, the model is prevented from deducing an ordinal connection between the various stages of AD.

- ✓ **Label Binarizer:**We also tested the Label Binarizer encoding method as a substitute. For situations involving multi-label classification, this technique is quite helpful. Although single- label classification was our main emphasis, Label Binarizer was evaluated to determine how well it will work in future research that would take into account the co-occurrence of several stages or situations.

Performance of All Models

- **MobileNetV2**:With an accuracy of 0.9998 and a loss of 0.0023, MobileNetV2 displayed impressive performance. With an F1-score of 0.77, the model's precision and recall were 0.87 and 0.69, respectively. Strong true positive rates were shown by the confusion matrix, but there was still space for improvement in reducing false negatives, particularly for early-stage AD.In the **[Fig.2]** displays the confusion matrix indicated strong true positive rates but also suggestedroom for improvement in minimizing false negatives, especially for early-stage AD.In **[Fig.3]** the graph depicts the accuracy and training Data Loss for the MobileNetV2

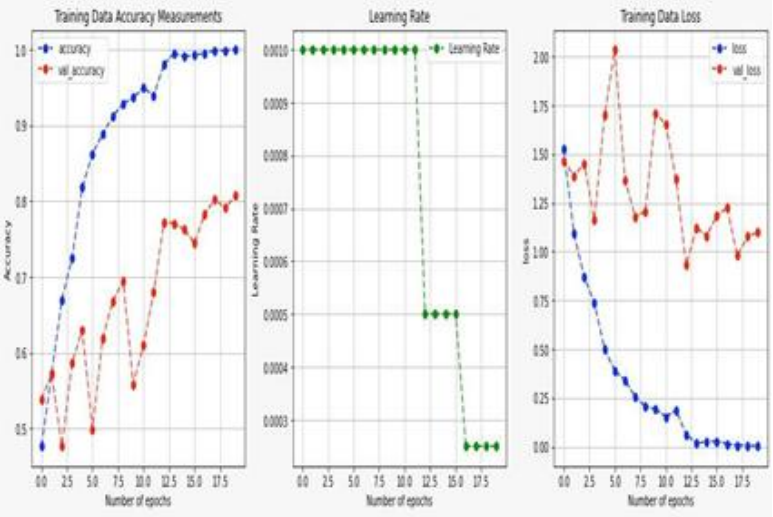

Fig 2: Model Accuracy , Learning RateMatrix for MobileNetV2 Model

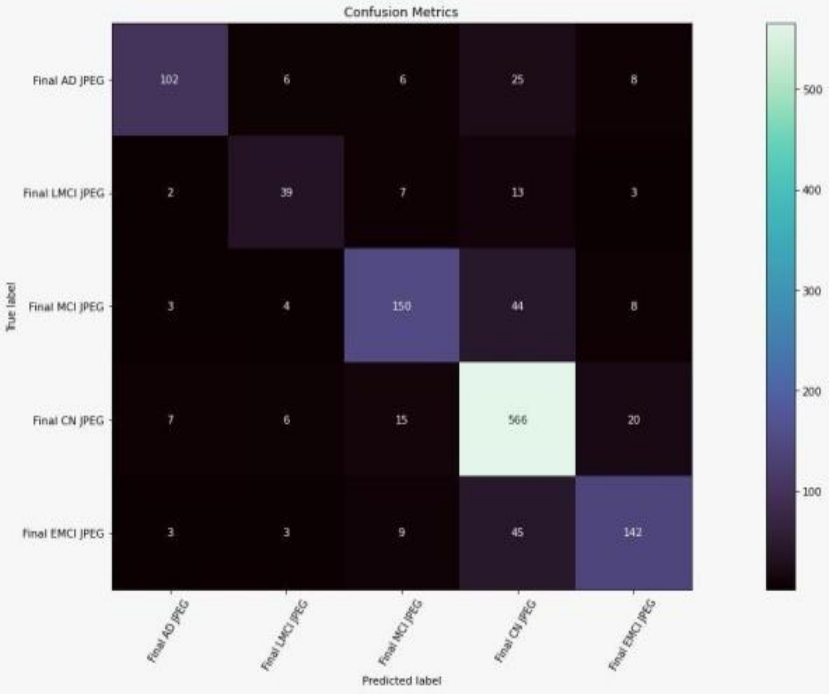

Fig 3: Confusion Matrix for MobileNetV2 Model

- **ResNet50:**In terms of accuracy, ResNet50 came in second with a score of 0.9990, although it had a marginally higher loss value of 0.0051. Its F1-score was 0.52 and its precision and recall were 0.55 and 0.49, respectively. The model had trouble with false positives, especially for late-stage AD, the confusion matrix showed. In the **[Fig.4]** displays the confusion matrix revealed that the model struggled with false positives, particularly for late-stage AD.In **[Fig.5]** the graph depicts the accuracy and training Data Loss for the ResNet50 model.

The ResNet50 model achieved a high accuracy of **0.9990** with a slightly elevated loss of **0.0051**, ranking second among the models evaluated. Despite this, its **F1-score (0.52)**, **precision (0.55)**, and **recall (0.49)** indicate moderate classification performance, with a notable challenge in detecting true positives. As shown in **[Fig. 4]**, the confusion matrix revealed a tendency toward **false positives in late-stage Alzheimer's Disease (AD)**, suggesting difficulty distinguishing advanced AD from other classes. **[Fig. 5]** demonstrates stable training with decreasing loss and increasing accuracy, although a performance gap between training and validation suggests potential overfitting or limitations in generalizing to complex cases.

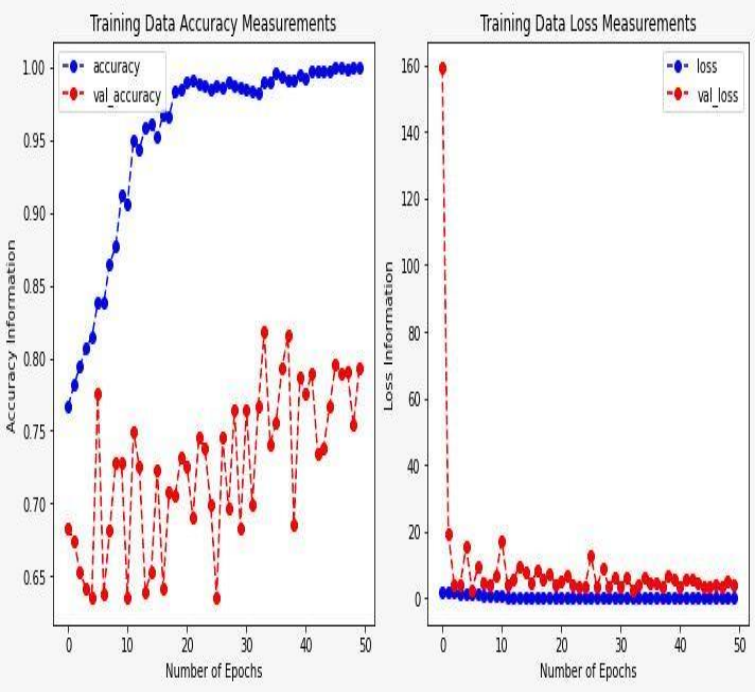

Fig4: Model Accuracy,Training Data Loss for Matrix for ResNet5**0** Model

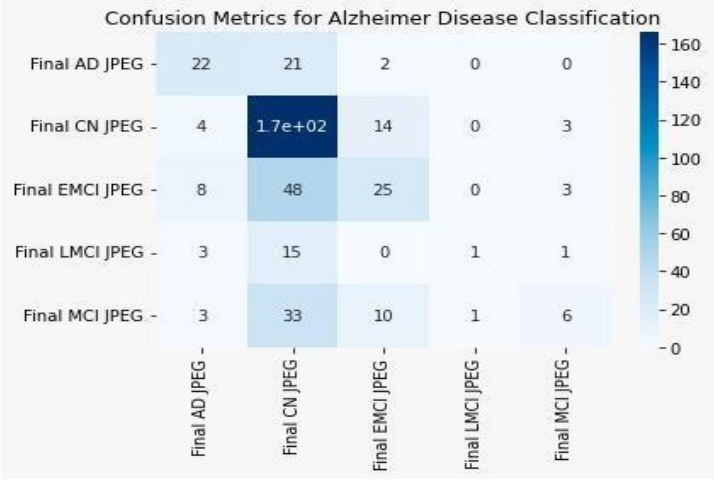

Fig5: Confusion Matrix for ResNet5**0** Modelz

- **DenseNetL:**DenseNetL recorded a loss of 0.0042, precision of 0.62, recall of 0.43, and an F1- score of 0.51 while recording an extraordinary accuracy of 1.0000. The confusion matrix revealed that although the model was great at categorising some stages, it struggled with others, especially differentiating between EMCI and LMCI..In the **[Fig.6]** displays the confusion matrix showed that while the model was excellent in classifying certain stages, it had difficulties in others, particularly in distinguishing between EMCI and LMCI.In **[Fig.7]** the graph depicts the accuracy and training Data Loss for the DenseNe**t** model.
- **DenseNetL Performance Analysis**

The DenseNetL model achieved a very low loss of **0.0042** and a perfect **accuracy of 1.0000**, indicating strong performance on the training set. However, its **precision (0.62)**, **recall (0.43)**, and **F1-score (0.51)** reveal limitations in its classification capability, particularly in distinguishing between classes.As shown in **[Fig. 6]**, the confusion matrix highlights that while the model accurately classified some stages of cognitive impairment, it struggled to differentiate between **EMCI** and **LMCI**, likely due to their similar clinical features**[Fig. 7]** illustrates the training accuracy and loss over epochs. The model quickly reached high accuracy with minimal loss, suggesting potential **overfitting**—where it performs well on training data but generalizes poorly to unseen samples. This imbalance indicates the need for improvements such as class balancing or advanced feature learning.

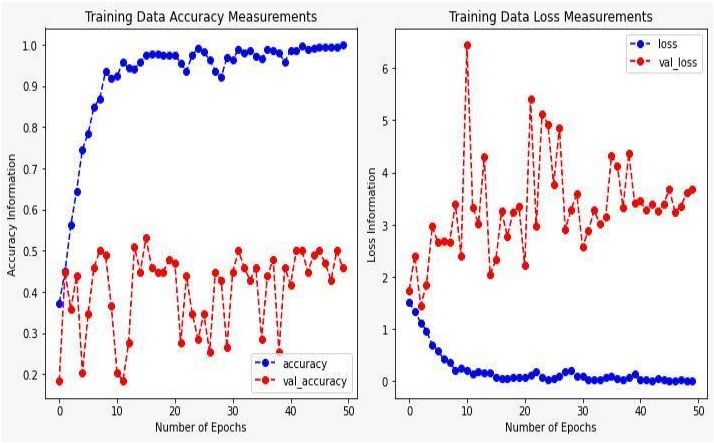

Fig 6: Model Accuracy,Training Data Loss for DensModel

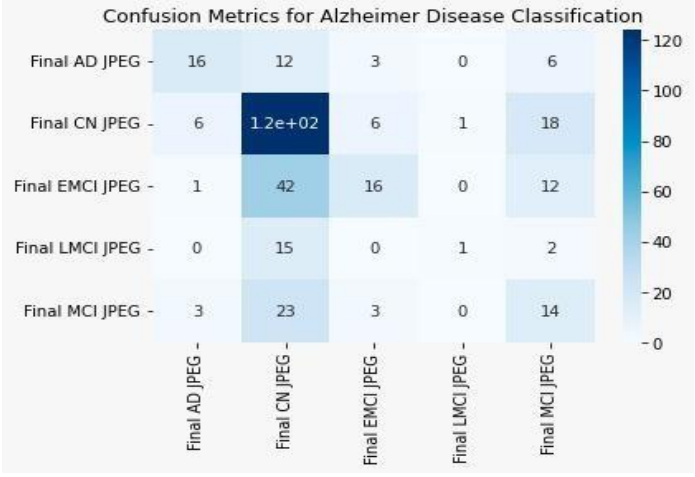

Fig 7: Confusion Matrix for DenseNet Model

VGG19:VGG19 has both the largest loss (0.0387) and the lowest accuracy (0.9838). while this, it scored a high recall of 0.71 and an F1-score of 0.51 while having a precision of only 0.40. The confusion matrix showed that although VGG19 had trouble with false positives, it was particularly good at detecting unusual or early-stage cases..In the **[Fig.8]** displays the confusion matrix indicated that VGG19 was particularly effective in identifying rare or early-stage cases but struggled with false positives.In **[Fig.9]** the graph depicts the accuracy and training Data Loss for the VGG19 model.

VGG19 Performance Summary

The VGG19 model recorded the **highest loss (0.0387)** and the **lowest accuracy (0.9838)** among the models. Despite this, it achieved a **high recall of 0.71**, indicating strong sensitivity to positive cases, particularly in **early-stage or rare conditions**. However, its **low precision (0.40)** led to a significant number of false positives, resulting in a moderate **F1-score of 0.51**.As shown in **[Fig. 8]**, the confusion matrix confirms VGG19's effectiveness in identifying early-stage cases but also highlights its struggle with false positives. **[Fig. 9]** displays the training accuracy and loss, showing consistent learning but with a relatively high final loss, suggesting potential overfitting or incomplete convergence.

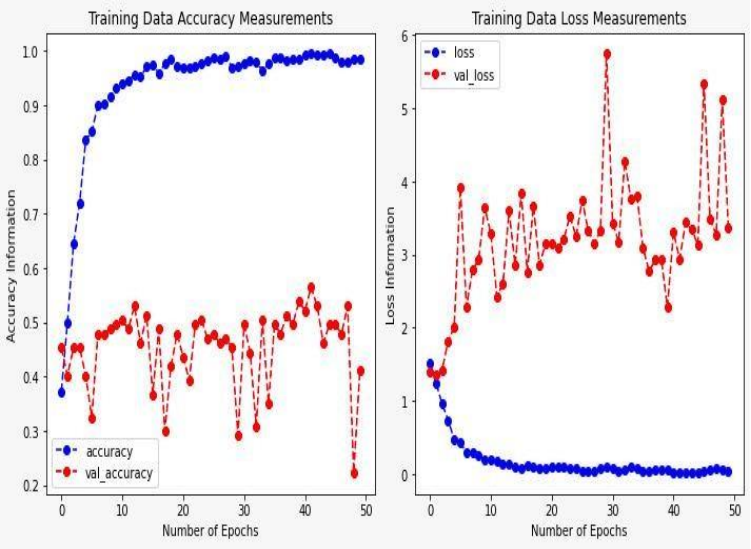

Fig 8: Model Accuracy , Training Data Loss for **VGG19** Model

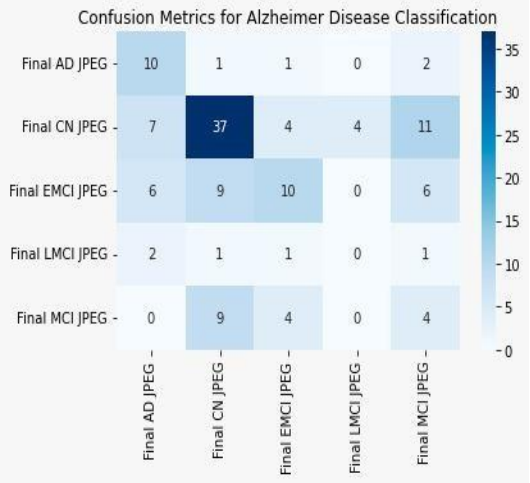

Fig 09: Confusion Matrix for **VGG19** Model

- **Best Performing model**:According to our thorough analysis, MobileNetV2 was shown to be the most balanced and successful model for classifying Alzheimer's disease, doing exceptionally well in terms of recall, accuracy, and precision. The strengths and shortcomings seen in the confusion matrices of each model, however, suggest that the choice of model may vary depending on particular therapeutic needs.

Results and Discussion

Our thorough analysis of DL models for classifying AD from MRI images found varied results amongst MobileNetV2, ResNet50, DenseNet, and VGG19. The most balanced model was MobileNetV2, which excelled in accuracy (0.9998) and loss (0.0023), but had space for improvement in detecting early-stage AD. ResNet50 problems with false positives while having high accuracy (0.9990), especially in late-stage AD. DenseNet's lower F1-score (0.51) indicates that, although

having perfect accuracy (1.0000), it had trouble differentiating between the EMCI and LMCI stages. The VGG19 algorithm had potential in identifying early-stage cases but had concerns with false positives, having the lowest accuracy (0.9838) and largest loss (0.0387). These results highlight the necessity of model selection based on particular clinical needs, as each model displayed distinct strengths and drawbacks.

6. Conclusion and Future Work

In conclusion, this study provided a thorough assessment of four DL models—MobileNetV2, ResNet50, DenseNet, and VGG19—in the context of classifying AD using MRI images. Every model underwent painstaking preprocessing, including label encoding and image normalisation, before being trained and evaluated on a specific dataset. The most promising model was MobileNetV2, with an accuracy of 0.9998 and a loss of 0.0023. A personalised model selection based on particular clinical demands is crucial because each model showed distinct strengths and drawbacks.There are several potential directions for further investigation, in my opinion. First, adding more preprocessing methods, including advanced data augmentation, could possibly enhance model performance.Second, investigating ensemble approaches that incorporate the advantages of many models may provide a more reliable classification method for Alzheimer's disease. Last but not least, expanding the study to incorporate additional forms of medical imaging data, such PET scans, may offer a more complete knowledge of the course of the disease.Future

research has the potential to dramatically expand the area of medical imaging in AD by building on the findings of this study, leading to earlier and more precise diagnosis and eventually better patient outcomes

References

I. Hon and N. M. Khan, "Towards Alzheimer's disease classification through transfer learning," 2017 IEEE International Conference on Bioinformatics and Biomedicine (BIBM), Kansas City, MO, USA, 2017, pp. 1166-1169, doi: 10.1109/BIBM.2017.8217822.

II. Sarraf and G. Tofighi, "Deep learning-based pipeline to recognize Alzheimer's disease using fMRI data," 2016 Future Technologies Conference (FTC), San Francisco, CA, USA, 2016, pp. 816-820, doi: 10.1109/FTC.2016.7821697

III. Lodha, A. Talele and K. Degaonkar, "Diagnosis of Alzheimer's Disease Using Machine Learning," 2018 Fourth International Conference on Computing Communication Control and Automation (ICCUBEA), Pune, India, 2018, pp. 1-4, doi: 10.1109/ICCUBEA.2018.8697386.

IV. V. Dolph, M. Alam, Z. Shboul, M. D. Samad and K. M. Iftekharuddin, "Deep learning of texture and structural features for multiclass Alzheimer's disease classification," 2017 International Joint Conference on Neural Networks (IJCNN), Anchorage, AK, USA, 2017, pp. 2259-2266, doi: 10.1109/IJCNN.2017.7966129.

V. Ghosh, H., Tusher, M.A., Rahat, I.S., Khasim, S., Mohanty, S.N. (2023). Water Quality Assessment Through Predictive Machine Learning. In: Intelligent Computing and Networking. IC-ICN 2023. Lecture Notes in Networks and Systems, vol 699. Springer, Singapore. https://doi.org/10.1007/978-981-99-3177-4_6

VI. Savaş, S. Detecting the Stages of Alzheimer's Disease with Pre-trained Deep Learning Architectures. Arab J Sci Eng 47, 2201–2218 (2022). https://doi.org/10.1007/s13369-021-06131- 3

VII. Penney, J.; Ralvenius, W.T.; Tsai, L.-H.: Modeling Alzheimer's disease with ipsc-derived brain cells. Mol. Psych. 25(1), 148–167 (2020). https://doi.org/10.1038/s41380-019-0468-3.

VIII. Leandrou, S.; Petroudi, S.; Kyriacou, P.A.; Reyes-Aldasoro, C.C.; Pattichis, C.S.: Quantitative MRI brain studies in mild cognitive impairment and Alzheimer's disease: a methodological review. IEEE Rev. Biomed. Eng. 11, 97–111 (2018). https://doi.org/10.1109/rbme.2018.2796598.

IX. Alzheimer's Association.: 2015 Alzheimer's disease facts and figures. Alzheimer's and Dementia 11(3):332–384, (2015). https://doi.org/10.1016/j.jalz.2015.02.003.

X. Wang, Z.; Zhu, X.; Adeli, E.; Zhu, Y.; Nie, F.; Munsell, B.; Guorong, W.: Multi-

modal classification of neurodegenerative disease by progressive graph-based transductive learning. Med. Image Anal. 39, 218–230 (2017). https://doi.org/10.1016/j.media.2017.05.003.

XI. Hadjichrysanthou, C.; McRae-McKee, K.; Evans, S.; de Wolf, F.; Anderson, R.M.: Initiative for the Alzheimer's Disease Neuroimaging: Potential factors associated with cognitive improvement of individuals diagnosed with mild cognitive impairment or dementia in longitudinal studies. J. Alzheimer's Dis. 66, 587–600 (2018). https://doi.org/10.3233/JAD-180101.

XII. Sullivan, M.D.; Anderson, J.A.E.; Turner, G.R.; Nathan Spreng, R.: Intrinsic neurocognitive network connectivity differences between normal aging and mild cognitive impairment are associated with cognitive status and age. Neurobiol. Aging 73:219–228 (2019). https://doi.org/10.1016/j.neurobiolaging.2018.10.001.

XIII. Molinuevo, J.L.; Ayton, S.; Batrla, R.; Bednar, M.M.; Bittner, T.; Cummings, J.; Fagan, A.M.; Hampel, H.; Mielke, M.M.; Mikulskis, A.; O'Bryant, S.; Scheltens, P.; Sevigny, J.; Shaw, L.M.; Soares, H.D.; Tong, G.; Trojanowski, J.Q.; Zetterberg, H.; Blennow, K.: Current state of Alzheimer's fluid biomarkers. Acta Neuropathol. 136(6), 821–853 (2018). https://doi.org/10.1007/s00401-018-1932-x.

XIV. Villa, C.; Lavitrano, M.; Salvatore, E.; Combi, R.: Molecular and imaging biomarkers in Alzheimer's disease: A focus on recent insights. J. Pers. Med. 10(3), 1 (2020). https://doi.org/10.3390/jpm10030061.

XV. Cooper, Yonatan A.; Nachun, Daniel; Dokuru, Deepika; Yang, Zhongan; Karydas, Anna M.; Serrero, Ginette; Yue, Binbin; Initiative, Alzheimer's Disease Neuroimaging.; Boxer, Adam L.; Miller, Bruce L.; Coppola, Giovanni: Progranulin levels in blood in alzheimer's disease and mild cognitive impairment. Annals of Clinical and Translational Neurology 5(5), 616–629 (2018) ISSN2328-9503https://doi.org/10.1002/acn3.560. https://onlinelibrary.wiley.com/doi/abs/10.1002/acn3.560.

XVI. Salvatore, C.; Cerasa, A.; Castiglioni, I.: Mri characterizes the progressive course of ad and predicts conversion to Alzheimer's dementia 24 months before probable diagnosis. Front. Aging Neurosci. 10(135), 1 (2018). https://doi.org/10.3389/fnagi.2018.00135.

XVII. Niu, Yan; Wang, Bin; Zhou, Mengni; Xue, Jiayue; Shapour, Habib; Cao, Rui; Cui, Xiaohong; Jinglong, Wu.; Xiang, Jie: Dynamic complexity of spontaneous bold activity in alzheimer's disease and mild cognitive impairment using multiscale entropy analysis. Front. Neurosci. 12(677), 1 (2018). https://doi.org/10.3389/fnins.2018.00677.

XVIII. Jha, D.; Alam, S.; Pyun, J.-Y.; Lee, K.; Ho, K., Goo-Rak.: Alzheimer's disease detection using extreme learning machine, complex dual tree wavelet principal coefficients and linear discriminant analysis. J. Med. Imag. Health Inf. 8(5), 881–890 (2018). https://doi.org/10.1166/jmihi.2018.2381.

XIX. Jie, B.; Liu, M.; Shen, D.: Integration of temporal and spatial properties of dynamic connectivity networks for automatic diagnosis of brain disease. Med. Image Anal. 47, 81–94 (2018).

https://doi.org/10.1016/j.media.2018.03.013.

Analysing the Optimization of Cooling Systems in Industrial Settings: Exploring Efficiency and Cost Reduction

Farid Agayev[1] and Sevinj Bakhshaliyeva[2]

[1,2]Azerbaijan State Oil and Industry University, Baku, Azerbaijan
[1]farid.aqayev@asoiu.edu.az
[*2]sevinj.quliyeba@asoiu.edu.az

* Corresponding Author

Abstract. This paper investigates the optimization of cooling systems in industrial settings, particularly within oil refining plants, focusing on reducing energy consumption, water usage, and environmental impact. The study forms part of a broader dissertation on "Intellectual Control of Cooling and Cleaning Processes," with a key emphasis on integrating AI-driven controls into industrial applications. By examining various cooling methods, including evaporation and air blowing techniques, the research assesses their performance under different environmental conditions and fan operating speeds. Empirical data collection and analytical modeling reveal that while traditional evaporation methods achieve maximum cooling efficiency at high fan speeds, air blowing techniques demonstrate significant potential in cooler environments, offering lower water consumption and energy use. The findings underscore the importance of adaptive control strategies, which can dynamically adjust operational regimes based on real-time conditions, leading to more sustainable and cost-effective cooling processes. This study provides a foundation for the future application of AI technologies in optimizing industrial cooling systems.

Keywords: Water cooling, optimization, external factors, energy efficiency, water usage, evaporation, air blowing, fan speed, industrial cooling, AI control.

1 Introduction

This paper is part of the broader dissertation on "Intellectual Control of Water Cooling and Cleaning Processes," which focuses on the integration of AI networks into industrial applications. The main objective of the dissertation is to explore how advanced technologies can optimize cooling and cleaning processes within industrial settings, particularly in oil refining plants [1-3]. In this paper, the

emphasis is on analying ways to reduce power consumption, water usage, and environmental impact by examining the operational modes of cooling systems. Cooling systems in industrial environments, though often regarded as straightforward, encounter significant challenges due to varying operating conditions and external influences [4-8]. This paper investigates a range of cooling strategies, from passive methods that depend on natral convection to more intricate active cooling systems utilizing cooling towers. The study employs empirical data and analytical modelling to evaluate how these methods affect energy efficiency and water conservation [9, 10]. The findings will guide the development of best practices for optimizing cooling systems, ultimately paving the way for AI-driven controls that can adjust to real-time environmental changes, thereby substantially reducing operational costs and minimizing the environmental footprint of industrial cooling processes.

2 Formulation of the problem

Cooling systems in oil refining plants, often overlooked due to their simplicity, face significant challenges related to varying operational regimes and external factors. Optimizing these systems is essential for reducing energy consumption and water usage [11-14]. The research delves into different cooling system regimes and examines external influences to develop strategies that enhance efficiency and sustainability, ensuring competitiveness while meeting environmental standards. An exploration of various cooling system regimes and the impact of external factors is undertaken through empirical data collection and analytical modelling. Testing different operational scenarios reveals key variables that influence energy and water usage [15-18]. The findings are validated through simulations and real-world applications, ultimately leading to the establishment of best practices for achieving more efficient and sustainable cooling system operations. Figure 1 illustrates a basic water cooling system.

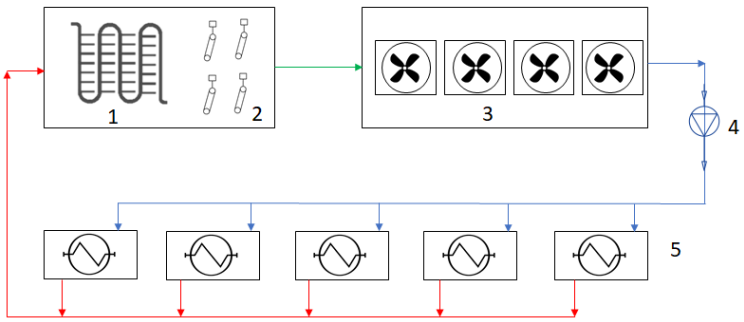

Fig. 1. Simple Diagram of Industrial Water Cooling and Cleaning Processes

Figure 1 presents a diagram of the cooling and water treatment system, highlighting the main processing stages. The initial stage involves passive cooling: hot water passes through radiators situated in an open basin (1), where cooling occurs due to external conditions such as air temperature and wind speed. This is followed by the oil purification and analysis process, where oil skimmers remove residual oil from the water, and analyzers check the water quality, detecting oil impurities and other parameters (2). The water then moves to cooling towers, where powerful fans further reduce the water temperature through evaporation (3). In the next stage, a pump maintains the necessary pressure in the system to circulate water through all cooling and purification stages (4). Finally, the cooled water is used to cool technological equipment through several heat exchangers (5), effectively dissipating excess heat from the system. This diagram represents a simplified version of the entire system but includes the key components that ensure its operation.

3 Solution of the problem

Passive cooling refers to the process of reducing the temperature of a system without the use of active mechanical devices such as fans or pumps. In the context of water cooling systems, passive cooling primarily occurs through natural heat exchange with the environment. This process is driven by convection, where the water's heat is transferred to the surrounding air, influenced by external factors like outside temperature, wind speed, and humidity. These parameters collectively cause the water to lose energy, resulting in a temperature decrease. To simplify the analysis of these variables, the concept of "feels like" temperature is used, which combines the effects of temperature, wind speed, and humidity into a single metric. This approach allows for a more comprehensive understanding of the passive cooling process. Figure 2 illustrates the relationship between "feels like" temperature and the temperature drop between the input and output of the passive cooling system, demonstrating how these combined factors influence the efficiency of cooling.

Figure 2 illustrates the relationship between "Feels Like Temperature" (°C) and the temperature drop (°C) in a passive cooling system. The curve shows that as the "Feels Like Temperature" increases, the cooling efficiency decreases. Starting at 15°C when the "Feels Like Temperature" is 0°C, the cooling effect gradually diminishes. By 38°C, the temperature drop is reduced to approximately 0.5°C, indicating a significant loss in cooling efficiency under extreme conditions. This curve demonstrates how external environmental factors influence the performance of the passive cooling system.

Active cooling in industrial systems primarily involves the use of cooling towers, with two main methods for removing heat from water. The first and most common method is based on the principle of creating a vacuum or negative pressure inside the cooling tower. This process removes air from the tower, causing water to evaporate, which leads to a physical loss of energy and efficient cooling.

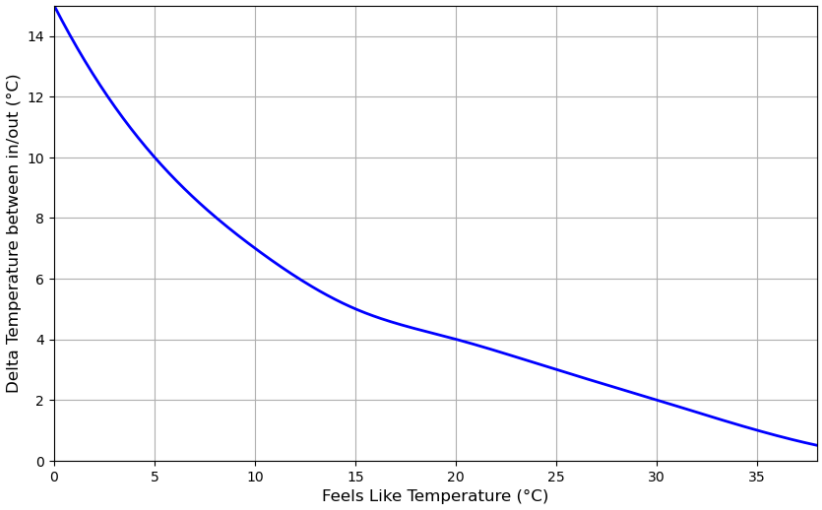

Fig. 2. Relationship between Feels Like Temperature and Temperature Drop

This method is highly effective due to the evaporation process and is widely used in various industrial settings. The second method, though less common, is used primarily in cold weather. In this case, air is blown directly onto the water, promoting convection, which causes the water to lose energy. This method is similar to passive cooling and depends on external factors like air temperature. However, in hot weather, this method is inefficient.

In Figure 3, two distinct methods of cooling within a cooling tower are depicted. The first method, shown in Diagram A, represents the standard approach where cooling is achieved through evaporation. In this process, water descends while air, drawn by the cooling fan labeled (1), is expelled upward, creating a vacuum. This negative pressure facilitates water evaporation, which effectively reduces the water's temperature. The radiators or drop catchers, indicated by (2), play a crucial role in capturing any residual water droplets, preventing them from escaping with the exhaust air. The second method, illustrated in Diagram B, depicts a less common technique, primarily utilized in cold weather. In this scenario, air is blown directly onto the water surface, thereby promoting cooling through convection. The cooling fan (1) aids in the movement of air, while the water level is deliberately raised to reach the lower radiators (2), thereby enhancing the cooling efficiency. This setup relies on convection, akin to passive cooling, where external conditions significantly influence the cooling process. Although this method proves less effective in hot weather, it can be advantageous under specific conditions

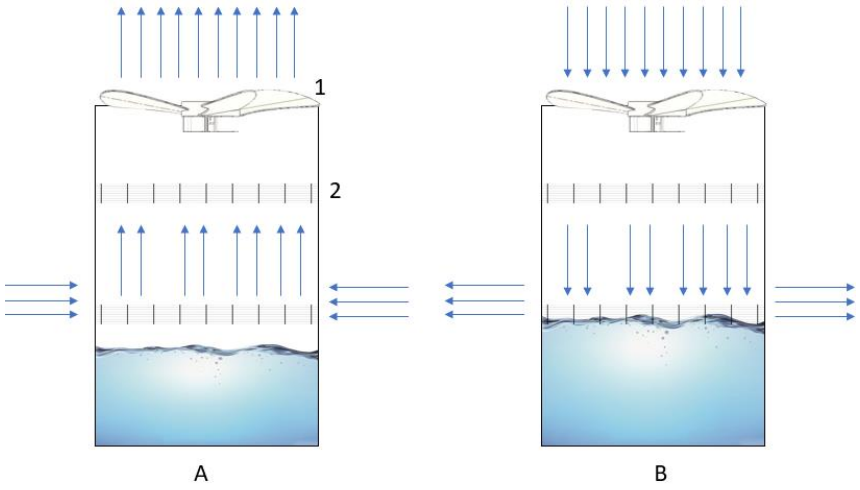

Fig. 3. Cooling Tower Methods: Evaporation (A) vs. Air Blowing (B)

The temperature drop ΔT in a cooling system due to evaporation is governed by the following formula (1):

$$\Delta T = \frac{mL}{C_p M} \tag{1}$$

Where:

- ΔT: Temperature drop (°C)
- m: Mass of water evaporated (kg)
- L: Latent heat of vaporization (J/kg)
- C_p : Specific heat capacity of water (J/kg·°C)
- M: Total mass of water in the system (kg)

Evaporation absorbs energy ($\boldsymbol{L}$), leading to cooling. The temperature drop depends on the amount of water evaporated ($\boldsymbol{m}$) and the total water mass ($\boldsymbol{M}$), alongside the thermal properties of water ($\boldsymbol{L}$ and $\boldsymbol{C_p}$). External factors, such as air flow and humidity, influence the rate of evaporation.

Figure 4 presents a detailed analysis of the relationship between fan rotating frequency and its effects on both temperature drop and water evaporation rates within a cooling tower system. The two plots provide insights into different cooling methods, highlighting how each method performs under varying external conditions. The first plot on the left illustrates the relationship between fan rotating frequency (Hz) and the temperature delta between the input and output water temperatures (°C) for three scenarios: evaporation cooling, air blowing at 5°C, and air blowing at 25°C. The evaporation method, represented by the blue solid line, shows a significant increase in temperature delta as the fan speed increases, reflecting the enhanced cooling effect due to more efficient air movement.

This effect is particularly pronounced at higher fan speeds, where the system

approaches its maximum cooling performance. In contrast, the air blowing technique, represented by the black dashed line for 5°C and the gray dash-dot line for 25°C, shows a more moderate increase in temperature delta.

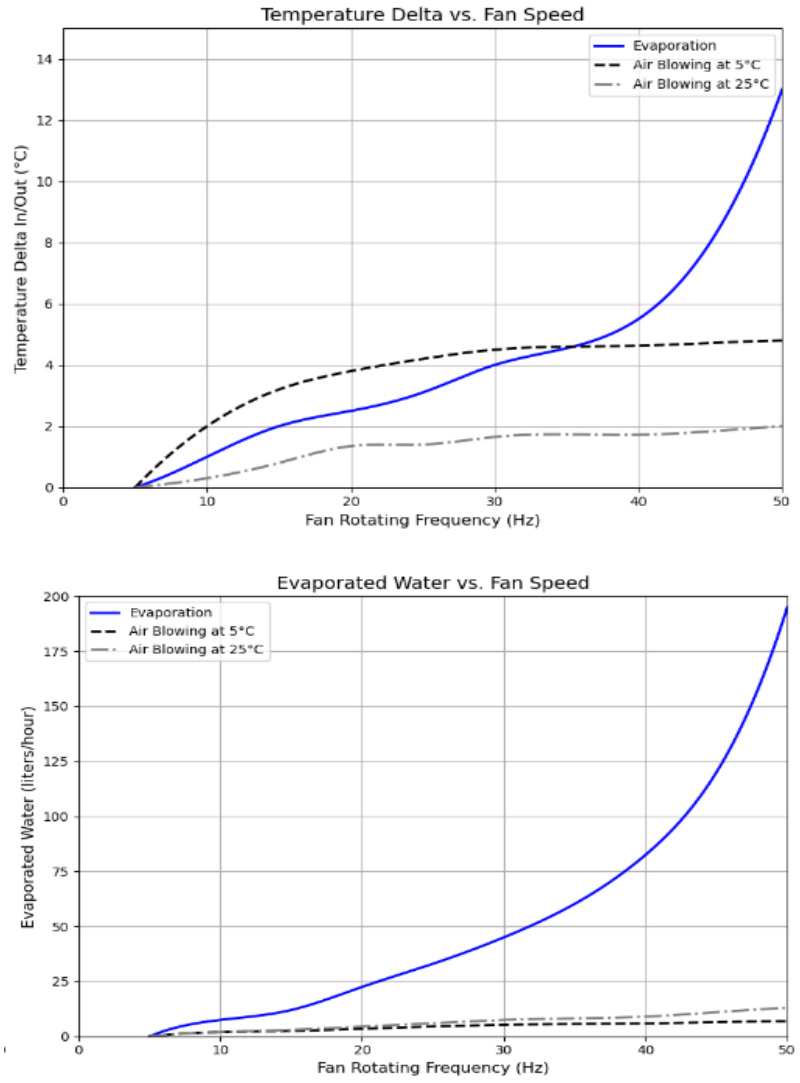

Fig. 4. Fan speed vs. cooling efficiency and evaporation

The air blowing method at 5°C performs better than at 25°C, indicating its higher

efficiency in cooler environments. However, both air blowing scenarios reach a plateau, suggesting that beyond a certain fan speed, the cooling efficiency does not improve significantly.

The second plot on the right illustrates the corresponding relationship between fan rotating frequency and the amount of water evaporated per hour, measured in liters, for the same three scenarios. The evaporation method, again represented by the blue solid line, shows a sharp increase in the evaporation rate with increasing fan speed, particularly at higher frequencies.

This increase is due to the negative pressure created within the cooling tower, which enhances the evaporation process. On the other hand, the air blowing techniques, depicted by the black dashed line for 5°C and the gray dash-dot line for 25°C, show a much more gradual increase in water evaporation. The air blowing method at 25°C results in higher evaporation than at 5°C, but both remain significantly lower than the evaporation method, highlighting the lower water usage associated with air blowing techniques under these conditions.

This comprehensive depiction emphasizes the differences in cooling performance and water usage between the evaporation and air blowing methods, demonstrating the importance of selecting the appropriate cooling strategy based on environmental conditions and operational requirements. The use of distinct line styles and colors ensures clarity, even in black-and-white print formats.

The research identified critical factors influencing the efficiency of cooling systems in oil refining plants, highlighting the impact of both passive and active cooling methods. Passive cooling, driven by environmental factors like air temperature and wind speed, proves effective in cold weather conditions but shows diminished efficiency as external temperatures rise. The study demonstrated that under extreme conditions, the temperature drop in passive systems is significantly reduced, necessitating alternative methods to maintain cooling efficiency. Active cooling, particularly in cooling towers, was analyzed through empirical data and modeling. The findings show that cooling towers achieve maximum efficiency when operating at the highest fan speeds, around 50 Hz, where negative pressure maximizes water evaporation and cooling effectiveness. However, this comes at the cost of increased water evaporation, which can lead to higher operational costs.

The study underscores the importance of optimizing fan speeds and cooling tower design to balance cooling efficiency with resource utilization, suggesting that adaptive strategies incorporating real-time external data could further enhance system performance.

Conclusion

The analysis reveals that cooling towers, when operating at maximum capacity, achieve the highest possible efficiency, but this approach is not always cost-effective. Passive cooling methods, especially effective in cold weather, and air-blowing techniques in cooling towers—though less common in industrial settings—are efficient only when the "feels like" temperature is below 10°C. However,

running cooling towers at maximum power leads to significant water evaporation, which adds to operational costs. Despite these findings, most industrial systems are not designed to dynamically adjust based on external factors like weather, primarily due to the complexity and resource demands of such programming. However, by integrating AI technologies like LSTM networks, these systems could quickly adapt to changing conditions, optimizing work regimes based on real-time and forecasted weather data. Implementing AI in this way could lead to substantial reductions in both energy and water costs, making industrial cooling systems more efficient and cost-effective.

References

1. Zamanifard A., Gholampour M., Liaw J.-S., Wang C.-C. "Recent Progress in Fill Media Technology for Wet Cooling Towers." Processes, 2023. https://doi.org/10.3390/pr11092578
2. Technology and equipment for oil and gas refining processes (Akhmetov S.A., Bayazitov M.I., Kuzeev I.R., Serikov T.P.). https://www.geokniga.org/books/11385
3. "A Comprehensive Study of Different Types of Cooling Towers. "ResearchGate, 2023. https://www.researchgate.net/publication/ 368910354 _A_Comprehensive_Study_of_Different_Types_of_Cooling_Towers
4. V.N.Erich, M.G.Rasina, M.G.Rudin Chemistry and Technology of Oil and Gas (Latest edition, revised)
5. "Thermal Performance and Emissions Analysis of a New Cooling Tower Prototype." *ScienceDirect*, 2023. https://www.sciencedirect.com/science/article/pii/S1359431122005986
6. Alireza Bahadori, Crude Distillation Unit (CDU).
7. Yusifov S.İ., Mayilov R.A., Mehdiyeva A.M. Advanced Information-Measuring System for the Improvement of the Quality Indicators of Metrological Characteristics. Environment, Energy and Earth Sciences journal - E3S Web of Conferences. VI International Scientific Forum on Computer and Energy Sciences (WFCES II 2023). November 16-17, 2023, Almaty, Kazakhstan. ISSN: 2267-1242. EDP Sciences. doi.org/10.1051/e3sconf/202346601001.https://www.e3s-conferences.org/ component/issues/?task=all&Itemid=121
8. Gladkov A. "Ventilyatornie gradirni." Moscow*:* 1973.
9. Yusifov, S.I., Bayramov, I.Y., Mayilov, R.A., Mehdiyeva A.M., Sardarov, Y.B., Safarova, A.A. Prediction of Parameters of Oil and Gas Fields Using Fuzzy Modeling. Lecture Notes in Networks and Systems, 2025, 1142 LNNS, pp. 203–207
10. Agayev F.H., Mehdiyeva A.M., Gafarov G.A., Bakhshaliyeva S.V.Development of the functional safety system in primary oil refiningNafta-Gaz. Oil and Gas Institute – National Research Institute. №7, pp. 434-442. Poland. ISSN 0867-8871. https://www.inig.pl/en/nafta-gaz-en/available-articles. https://www.inig.pl/images/nafta-gaz/abstrakty/Nafta-Gaz_2024-07_ Spis%20tre%C5%9Bci.pdf.

11. Agayev, F.H., Mehdiyeva, A.M., Ibrahimova, A.E. Advance Technologies to Eliminate Environmental Problems of Oil and Gas Processing. Advances in Science, Technology and Innovation, 2025, pp. 287–294
12. Lebedev S.V. Firewalling. Theory and practice of protecting the outer perimeter. - M.: Publishing house of MSTU im. N.E. Bauman, 2002. 304 P.
13. Gafarov GA, İbrahimova AE Design of a device for stimulation of biologically active points 2nd International Conference on Emerging Applications of Material Science and Technology (ICEAMST 2024), July 3-4, 2024, Bengaluru, India, Advances in Science, Technology & Innovation
14. Gadir Gafarov, Oksana Takhumova, Petr Nikolaev. Determination of intracellular electrical parameters in bioelectrical impedance analysis. BIO Web of Conferences CIBTA-II-2023.
15. Shuvalov V.P., Egunov M.M., Minina E.A. Providing indicators of reliability of telecommunication systems and networks. M.: Hotline - Telecom, 2015. 168P.
16. Stearns, S. D. Digitale Verarbeitung Analoger Signale / Digital Signal Analysis / S. D. Stearns. – Walter de Gruyter GmbH & Co KG, 2018.
17. Mityukhin, A. I. Applied information theory: educational method. allowance / A. I. Mityukhin. – Minsk: BSUIR, 2018.
18. Mityukhin, A. I. Digital speech processing and image analysis: textbook - method. allowance / A. I. Mityukhin. – Minsk: BSUIR, 2016.

Modeling of Solar Panel Installation Mechanism for Hybrid Energy Systems in Azerbaijan

* Rehim Rehimov[1], Nizami Suleymanov[2] and Zarifa Mahmudova[3]

[1, 2, 3] Azerbaijan State Oil and Industry University, Baku, Azerbaijan
rehim.rehimov@asoiu.edu.az, nizami.suleymanov@asoiu.edu.az
[2]zarifa.mahmudova@asoiu.edu.az

* Corresponding Author

Abstract. Hybrid energy systems have emerged because of the growing interest in renewable energy sources and as a way to feed loads located in regions far from the interconnected grid system. In addition, in regions with an interconnected grid system, hybrid energy systems have emerged to reduce the ever-increasing unit cost of electricity. Hybrid power generation systems can be developed with many combinations of different energy sources and storage devices. Solar and wind power are the most used renewable energy sources in hybrid power generation system. In applications, off-grid wind and solar power generation systems are often operated in conjunction with gas turbines, diesel generators, fuel cells, and battery banks. The main goal of the research work is to investigate the mechanism of modeling hybrid energy systems. The subject of the study is based on the modeling of exemplary hybrid energy systems using the HOMER program for the research object.

1 Introduction

In parallel with the increasing demand for electricity in modern times, the problem of limited reserves of mining-based energy resources, their negative effects on the environment because of the use of these energy resources, and lack of access to electricity arises. These energy sources, especially in the 20th century, could not find their application from time to time due to various crises. Since the last quarter of the century, the interest in renewable energy sources has increased significantly. Innovative solar tracker installations today have different functional character, differing in design and control principle.

The classification of rotation axes is divided into single-axis (single axis trackers - SAT), as well as dual-axis (dual axis tracker - DAT). The difference in systems is due to the simplicity of the design and the cost of installation. Depending on the choice of the design of the installation, single-axis trackers are usually divided into trackers with horizontal (HSAT), vertical (VSAT), inclined (TSAT) and polar-

oriented (PSAT) rotation axes. It is easy to assume that the use of one or another installation has different aspects of use. With a significant change in the duration of the solar day and small elevation angles for high latitudes, it is proposed to use trackers with a vertical or inclined rotation axis, and for close areas of the equator - trackers with a horizontal rotation axis. It is considered more effective. To achieve maximum efficiency of solar energy, dual-axis trackers are used, the designs of which are divided according to the direction of the main axis. The classification of dual-axis systems is divided into those with a rotation axis on a supporting column (tip-tilt dual axis tracker - TTDAT) and trackers with a supporting plane (azimuth-altitude dual axis tracker - AADAT), in which the main axis is vertical. The advantages of trackers with a rotation axis on a supporting column include a primitive design and greater flexibility of territorial placement, which allows expanding the scope of use. From individual use to large-scale production. Platform trackers use a large ring as a supporting structure, which is installed on rollers or a large platform with bearings. The main advantage of using this design is the uniform distribution of the solar battery weight across the parts of the ring.

The mounting structure is designed to attach photovoltaic modules to the solar tracking system and must provide the necessary strength and rigidity to external influences. The main features of this structure, which serve as technical definitions for the use of the installation, are the permissible mass and area of the solar battery, the maximum permissible wind speed in sounding mode and in storm conditions, the range of operating temperatures and the maximum snow load.

Of the existing tracking algorithms, only three are used. The first is based on a light sensor, which is considered the simplest solution in terms of its technical design. The operating principle is to direct the solar panel to the sky in accordance with the maximum light intensity determined by the parameters of the photodetector. However, this method has a significant drawback - it does not work in heavy rain, cloudy weather and dirty photodetectors [1, 2]. The second of the existing methods is the astronomical algorithm. The implementation consists of changing the position of the solar panel using a daily software timer.

The negative aspect of the algorithm is the geographical location in high-latitude areas, the need to adjust the daily schedule due to important seasonal fluctuations in the azimuthal angles of sunrise and sunset. Maximum efficiency is guaranteed by the third method - the solar positioning algorithm, the method of action is based on software calculation of the optimal positioning angles of the solar battery according to the specified parameters of the location of the solar tracker: latitude, longitude, altitude above sea level.

Hybrid energy systems have emerged because of the growing interest in renewable energy sources and as a way to feed utilities located in regions far from the interconnected grid system. In addition, in regions with an interconnected grid system, hybrid energy systems have emerged to reduce the ever-increasing unit cost of electricity.

Sources such as wind and solar energy have variable characteristics due to different climatic conditions. Storage systems are important because of the variability of wind speed and solar radiation. For this reason, it should be used in conjunction with energy storage systems to ensure energy continuity in off-grid locations.

Hybrid power generation systems can be developed with many combinations of different energy sources and storage devices [3, 4]. Solar and wind power are the most used renewable energy sources in hybrid power generation system. In applications, off-grid wind and solar power generation systems are often operated in conjunction with gas turbines, diesel generators, fuel cells, and battery banks. Since it is based on the analysis of the theoretical conceptual bases of the modeling of hybrid systems, axiomatic, hypothetical and abstraction methods have been applied by conducting research. The hypothetico-deductive method is a research concept that begins with a theory about how things work and derives testable hypotheses. It is a form of deductive reasoning that begins with general principles, hypotheses, and ideas. Hypotheses are tested by collecting and analyzing data, and the theory is then supported or rejected by the results [5-9]. The method of scientific abstraction or abstraction is a special thinking technique that allows you to form certain abstract concepts.

In the research work, a system configuration that can optimally feed a certain load in a certain region (Gubadli district) is determined. For this, a sample hybrid energy system based on wind and solar with grid connection was modeled using the HOMER program. During the modeling of the sample hybrid energy system, sensitivity values for average solar radiation and average wind speed values of the studied region were determined. By carrying out this process, in a certain sense, other regions were also taken into account and system configurations were determined. It was determined to provide the same load in an economically optimal way in these different regions [10-14]. These operations were carried out by determining the sensitivity value for grid sales power during the modeling of a sample hybrid power system for both those who cannot sell electricity to the grid and those who can.

2 Types of Hybrid Energy Systems, Their Working Mechanism and Main Elements

The energy efficiency of solar photovoltaic modules plays a key role in their operation as the main sources of electricity generation. One of the most common and technically easier to implement options for their use in terrestrial conditions is the stationary placement of the structure with the orientation of the beam-receiving surface relative to the southern position of the sun in the northern geographic zone, taking into account the selected season. However, in this case, the sun's rays in the morning and evening fall on the working surfaces of the photoconverters at fairly small angles, which significantly reduces their efficiency. Research aimed at eliminating this drawback of automatic devices for constant tracking of the position of the sun in the sky during daylight hours significantly complicates the design, increases its cost and requires additional energy, which is very little in places where solar panels are installed.

Considering cost, which is a technical factor, hybrid energy systems are superior to some single energy sources. The energy potential of this region is one of the

important factors affecting the cost. In a region where there is not enough energy source to be used, any energy production causes more costs [15, 16]. Among energy sources, wind and solar energy are the most widely used renewable energy sources in various hybrid energy systems. Hybrid energy systems include Solar-Wind-Hydroelectric hybrid energy system, Solar-Hydrogen hybrid energy system, Solar-Wind-Hydrogen hybrid energy system, Solar-Wind hybrid energy system, Solar-Wind-Diesel hybrid energy system, Wind-Diesel hybrid energy system includes.

The energy generated from wind and water generators is AC voltage, which is then converted to DC to charge the battery. The controller protects the battery from sudden charge losses or overcharging. Although high voltage can be used to reduce system losses, the converter is usually designed to convert low DC voltage to 110 V or 230 V AC voltage, depending on the power system used in the region. As shown in Figure 1, the DC power from the photovoltaic panel meets the power needs of the electrolyzer. The water in the electrolyzer is separated into hydrogen and oxygen by the energy received from the solar panel. The obtained hydrogen is then collected in a tube and fed to the fuel cell. The hydrogen entering the fuel cell from the anode compartment combines with oxygen from the ambient air or oxygen obtained by electrolysis from a storage tube to generate DC power. This energy can be used directly in any device that runs on DC power, or it can be converted to AC power through inverters to meet all the energy needs of a home or any environment.

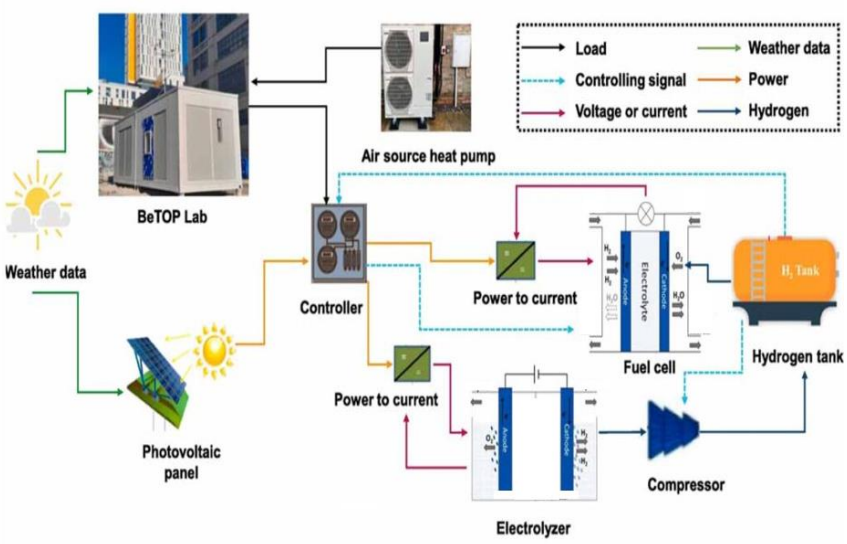

Fıg. 1. Solar-hydrogen hybrid energy system

A form of energy storage in wind-diesel systems is the use of electrochemical storage or batteries. Also referred to as wind-diesel-battery systems, these systems generally include one (or more) diesel generator, a battery unit (with inverter), wind

turbines, AC/DC rectifiers, DC/AC three-phase converters. The way the wind-diesel-battery system works varies depending on the wind conditions. If the wind is good and produces more electricity than the grid needs, the excess energy is stored in the battery.
In addition to the battery and wind turbine, the grid kicks in to compensate for the load gap during moderate wind. If the wind is too weak, the grid is fed with electricity generated by the operation of the diesel generator. In this system, co-energy is produced using wind turbines and photovoltaics. In Figure 2, the energy generated from the wind turbine and solar panel passes through a charge controller and goes directly to an inverter that converts the power to DC or AC. Power via charge controller goes to feed the battery and charges the batteries. The energy converted to AC can be used directly in homes.
Solar panels, wind turbines, charge controllers, batteries and inverters are used as the main elements of Solar-Wind Hybrid systems.
Solar cells are devices that convert light energy into electricity and cannot store energy. When the light source is gone, the electricity produced by the battery will also be cut off. If electricity is used at night, electric storage should be added to the system.

3 Methodology of Analysıs of Alternatıve and Renewable Energy Resources of Azerbaıjan

Although Azerbaijan is a country rich in hydrocarbons and is known in the world in this field, in recent years, importance has been given to produce and use of energy of renewable energy sources in Azerbaijan, international cooperation in this field, capital investment and export of this energy.

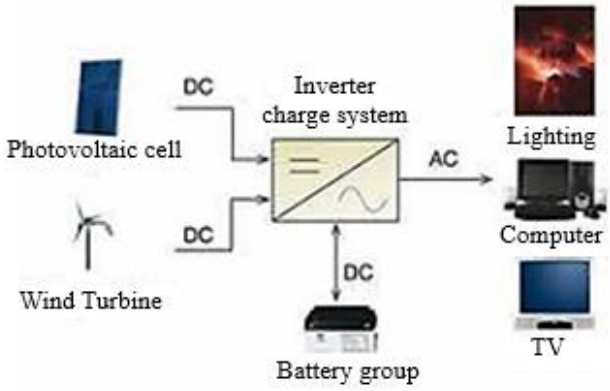

Fig 2. Solar-wind hybrid energy system

According to the Ministry of Energy of Azerbaijan, the country's economic and technical renewable energy capacity is 27,000 MW. Of this, 3,000 MW are wind, 23,000 MW solar, 380 MW bioenergy and 520 MW mountain rivers. Azerbaijan

produces 17.3% of its total electricity production from renewable sources. Azerbaijan plans to increase this capacity to 30% by 2023. 88.5 percent of renewable energy in the country is provided by HPP, 5.1 percent by wind, 3.5 percent by solar, and 2.9 percent by bioenergy sources.

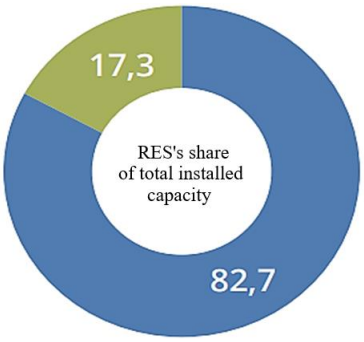

Fig. 3. Capacity of renewable electricity sources in Azerbaijan

The lands freed from occupation during the 44-day war are also an important energy center in terms of renewable energy sources. 25% of Azerbaijan's water resources are in these lands. The solar potential of these lands is of particular importance in terms of electricity production. The potential of solar energy in de-occupied lands is thought to be more than 7200 MW. In this sense, by signing contracts with various international companies, he set himself the goal of increasing the power of Azerbaijan's renewable energy resources. Azerbaijan also aims to export natural gas, which is the main source of electricity production, by using electricity produced from renewable energy sources within the country. The fact that hydrocarbon reserves are limited as traditional energy sources and the prevention of environmental pollution caused by it makes it necessary to increase the amount of energy produced in the world due to alternative and renewable energy sources. Currently, there are positive experiences in this direction, and in some countries the use of solar, wind and other alternative and renewable energy sources is expanding year by year. The use of alternative energy resources varies depending on the characteristics of the regions where different countries are located. For example, in developed countries such as Germany and Israel, the use of renewable energy sources and solar panels has spread significantly.

Israel plans to increase the use of renewable energy resources to 10%. In particular, the use of these resources for irrigation and heating of water in residential buildings is very important and is defined as an important part of sustainable development. In recent years, scientific research in the field of energy in Israel, because of increasing investments by the state and private sector, have achieved positive results in this field. In 2012, Germany increased its solar energy consumption by 50% and reach to 6.1% of total consumption. Recently, the use of wind energy has increased in the United States. In 2011 alone, 3,464 wind turbines were installed within US borders. During the windy months in the United States, wind energy accounts for 6% of the

country's total energy consumption. Although Azerbaijan is a country of oil and natural gas and develops its economy by selling its energy resources to the world energy market, the country should give priority to the development of alternative energy sources for long-term sustainable development. The potential of using renewable energy resources (water, wind and solar energy) in the country is significantly large. Azerbaijan has an important position in terms of the potential of renewable energy resources due to the number of sunny and windy days (171 days). In the Absheron Peninsula and the coastal lands of the Caspian Sea, the duration of sunlight is equal to 2,500 hours per year, and in the Nakhchivan Autonomous Republic to 2,900 hours.

Table 1. Potential of Renewable Energy Resources of the Republic of Azerbaijan

Type of capacity	Power (MW)
Solar energy	>5000
Wind energy	>4500
Biomass energy	>1500
Geothermal energy	>800
Small hydroelectric plant	>350

Source: Prepared by the author based on the information of the website of the State Agency for Renewable Energy Sources under the Ministry of Energy of the Republic of Azerbaijan (area.gov.az).

4 Determınatıon of hybrıd energy system for gubadlı regıon

A hybrid energy system to be modeled in HOMER can include many different power systems, as it is possible to specify more than one value for the elements that must be quantified or measured to create this hybrid energy system [17-19]. The example of a hybrid power system to be modeled is a grid-connected wind-solar hybrid power system, and this hybrid power system will include many different power systems. In other words, this example of a hybrid power system to be modeled consists of two wind turbines each with two values of quantity, grid connection, load, inverter with four values of size, and a photovoltaic array with five values. A schematic diagram of this example hybrid power system is shown in Figure 4.

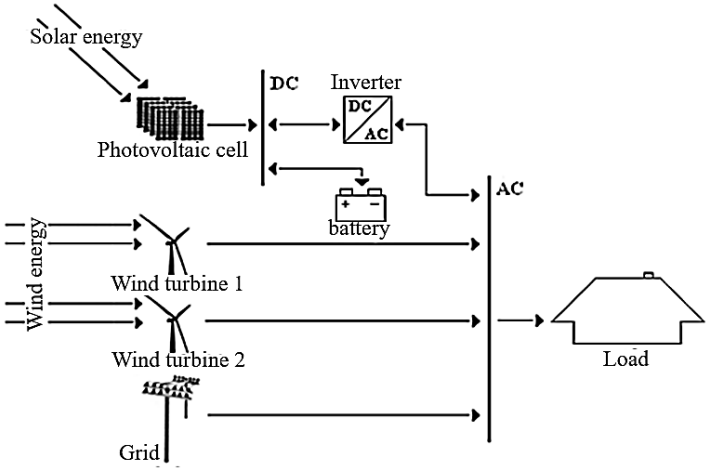

Fig. 4. A sample structure of hybrid energy system for Gubadli region

An example hybrid power system to be modeled in HOMER is to be installed in a region with wind and solar sources. A medium-sized industrial facility located in Karabakh was identified as load. Therefore, the region to be investigated for wind source and solar source will be the region where this industrial facility is located. That is, for the source of wind and solar power, there will be inputted the latitude and longitude coordinates of the point where this industrial facility is located. Photos of this industrial facility located in Gubadli, that is, in the region to be studied, taken from different distances through Google Earth are shown in Figure 5. HOMER's Opening Window. The opening window of the HOMER program is shown in Figure 6. The add/remove window opened by pressing the add/remove button in HOMER's pop-up window is shown in Figure 6. The user can add or remove any element, load and network connection type through this window.

Fig. 5. Designation region for an example of a hybrid power system

After completing the addition of the PV array, the PV input window opened by clicking the PV icon in HOMER's opening window is shown in Figure 8. cost) $7,000, replacement (renewal cost) $7,000, and operation and maintenance cost is defined as $0 USD/year. After entering these values, the spreadsheet that will be generated will tell you that a 1 kW PV array will have a capital cost of $7,000, a renewal cost of $7,000, and an O&M cost of $0 per year. Under the heading Sizes to Consider, the size is defined as 0, 10, 20, 40 and 80 kW respectively. As expected, each of these values represents a different size photovoltaic array. After entering these values, the table that will be generated will tell HOMER to consider each of these five different sized photovoltaic arrays separately in the simulations. Under the properties heading in the PV input window, the values of the photovoltaic array are defined as follows: The output current is selected as DC (DA). The life span is defined as 25 years. The reduction factor is a scaling factor that expresses what the new output power of the photovoltaic array will be as a percentage of the specified output power, taking into account the losses that will occur in the output power of the photovoltaic array. In this study, the reduction factor was determined to be 90%. The inclination angle is the angular value indicating the position of the installed photovoltaic panel relative to the horizontal plane. A slope of 0° indicates that the photovoltaic panel is in a horizontal position, and a slope of 90° indicates that the photovoltaic panel is in a vertical position. In a constant slope photovoltaic panel, a constant slope value equal to the latitude value of the point where the photovoltaic panel is located will maximize the annual photovoltaic power production.

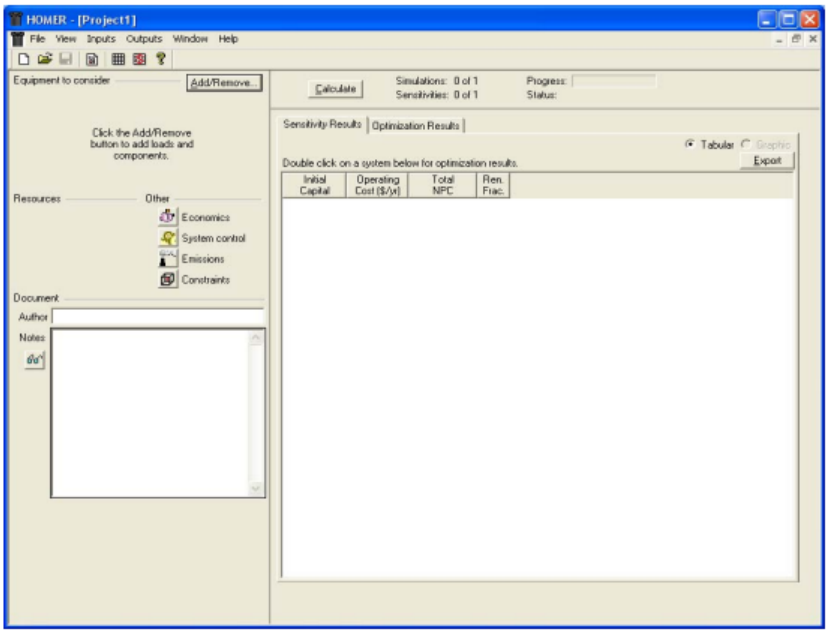

Fig. 6. The opening window of the HOMER program

In the values under the costs heading in the PV input window, size (size) is defined as 1 kW, capital. For this reason, there is no tracking corresponding to a constant slope PV panel in the tracking system section under the advanced heading in the PV inputs window, or if the vertical axis option is selected, HOMER will set the slope value as the latitude value of the point. However, HOMER allows entering another angle value for the slope value.

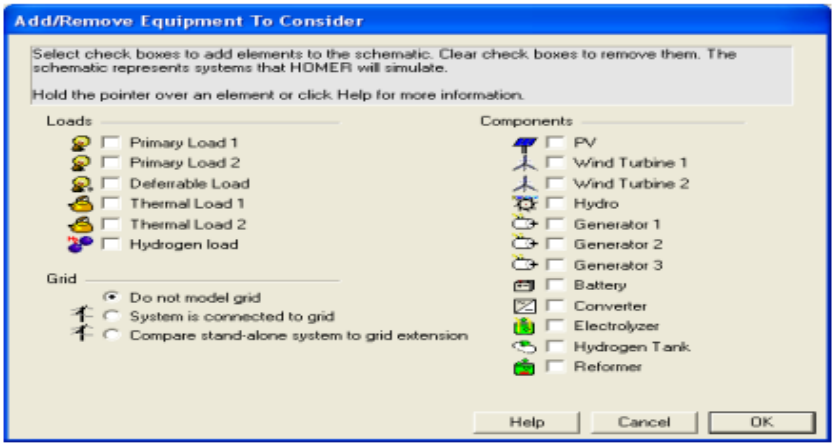

Fig. 7. Add/Remove window

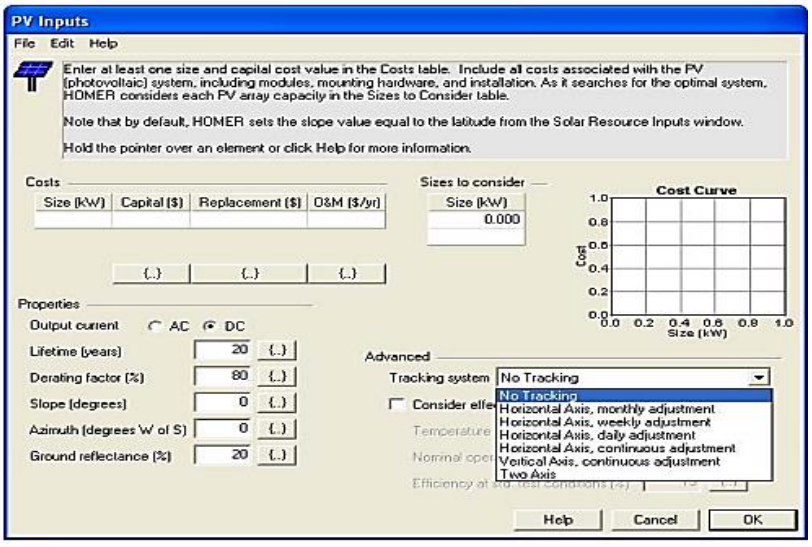

Fig. 8. PV input window

If horizontal axis or two axes corresponding to non-fixed-tilt photovoltaic panel is selected in the tracking system section, HOMER will not allow any angle value to be entered for the slope value, but will calculate this slope value each time. In this study, since no tracking option was selected in the tracking system section, HOMER set the slope value to 40.8833°, which is the update value of the sample hybrid power system and thus the investigated region for the photovoltaic panel.

Azimuth (south angle) is the angle value that defines the direction (south, east, west, north) the photovoltaic panel is facing. The azimuth value is set to 0° if the photovoltaic panel faces south, -90° if it faces east, 90° if it faces west, and 180° if it faces north. A photovoltaic panel that will have a fixed orientation is almost always oriented towards the equator. At this time, the azimuth value should be set to 0° for a photovoltaic panel located in the northern hemisphere, and 180° for a photovoltaic panel located in the southern hemisphere.

If the photovoltaic panel is placed horizontally (zero slope) on the earth's surface, the azimuth value is irrelevant. In the pv entries under the advanced heading in the tracking system section, if one of the horizontal axis (monthly adjustment), horizontal axis (weekly adjustment), horizontal axis (daily adjustment), vertical axis (continuous adjustment) or two axis options is selected, the window, HOMER However, the tracking system the photovoltaic panel will calculate this azimuth value at each time step as it moves. In this study, the photovoltaic panel in the example hybrid energy system was decided to have a fixed orientation, and the azimuth value was set to 0 ° because the investigated region of this photovoltaic panel was located in the northern hemisphere.

Ground reflectance determines the percentage of solar radiation falling on the ground that is reflected by the ground. Ground reflectance is about 20% for a grass-covered area and about 70% for a snow-covered area. The ground reflectance value is used to calculate solar radiation incident on an inclined photovoltaic panel, but the ground reflectance value has little effect in this calculation. In this study, the ground reflectance value was set to 40%.

Under the advanced heading in the PV inputs window, the values for the photovoltaic array are defined as follows:

The tracking system section is used to determine whether the photovoltaic panel will track the sun and, if so, what tracking system to use. The tracking system section includes the no tracking option, which indicates that the photovoltaic panel will not use any tracking system, the horizontal axis option, which indicates that it will use the horizontal axis tracking system, and the vertical axis option. Using the vertical axis tracking system and the horizontal axis option, which indicates that it will use both the horizontal axis and the vertical axis tracking system includes two axis options. In this study, no tracking option was selected in the tracking system section. Consider effect of Temperature represents the option used to determine whether the temperature effect of the camera on the output power of the photovoltaic array is considered. In this study, it was decided to consider the effect of cell temperature on the output power of the photovoltaic array, and the resulting values are defined below.

Temperature power factor is a ratio that shows how the output power of a photovoltaic array varies with cell temperature. This coefficient has a negative value

because the output power of the photovoltaic array decreases with increasing cell temperature. In this study, the photovoltaic array in the example hybrid power system is assumed to consist of MSX-60 photovoltaic modules from Solarex, and therefore the temperature coefficient of power value is defined as -0.5% / Ψ from the data sheet for MSX-60 photovoltaic module.
The nominal operating element temperature determines the cell temperature of the photovoltaic array under conditions of 800 W/m2 solar radiation, 20 ₴ ambient temperature and 1 m/s wind speed. HOMER uses the nominal operating cell temperature value to calculate the cell temperature of the photovoltaic array. In this study, the nominal operating cell temperature value is set to 47 Ψ from the data sheet of a photovoltaic module named MSX-60.
Efficiency under standard test conditions is defined as the efficiency with which a photovoltaic array converts sunlight into electricity at its maximum power point under standard test conditions. HOMER uses a useful duty factor to calculate the cell temperature of a photovoltaic array. A scientific and non-extensive study of the efficiency values found in the data sheets of commonly used photovoltaic modules was conducted by the creators of HOMER, and as a result of this study, average efficiency values were obtained under standard test conditions. for different types of photovoltaic modules. The values of average efficiency are shown in table 2.

Table. 2 Average efficiency for different types of photovoltaic modules

Photovoltaic Module Type	Number of modules in study	Average efficiency (%)
Polycrystalline silicon	10	13.0
Monocrystalline silicon	8	13.5
Monocrystalline/amorphous silicon hybrid	1	16.4
Thin film amorphous silicon	4	5.5

In this study, the efficiency of the photovoltaic module named MSX-60 could not be obtained from the data sheet, but since this photovoltaic module was studied to have a polycrystalline silicon structure, the useful efficiency of the photovoltaic module named MSX-60 was determined to be 13% using Table 2.
After these steps, the resulting image of the pv input window is shown in Figure 2. Figure 9 shows the image that appears in the HOMER opening window after completing the modeling of the PV array by clicking OK on the PV inputs window image obtained after the steps taken.
In the main load entries window, in the load type section, AC (aa) is selected as the load type. There are two ways to model a load in HOMER. In the data source section of the initial load entries window, the main path represented by the option Enter daily profile(s) necessary either specify the average daily load profile for each month of the year (different average daily load profiles can be defined for weekdays and weekends of each month) or only one Average daily load profile should be noted (only this average daily load profile is taken into account during the year). Because HOMER conducts all of its operations on an hourly basis throughout the

year, the average daily load profile or profiles specified in this first method used to model load are translated by HOMER into 8760 load values corresponding to each of the 8760 hours (number of hours per year). To make this hourly load data generated by HOMER more realistic, randomness can be added to this hourly load data using the daily and time-step functions, mainly under the heading of random variation. load login window. Here, the daily function shows the standard deviation in the consecutive daily

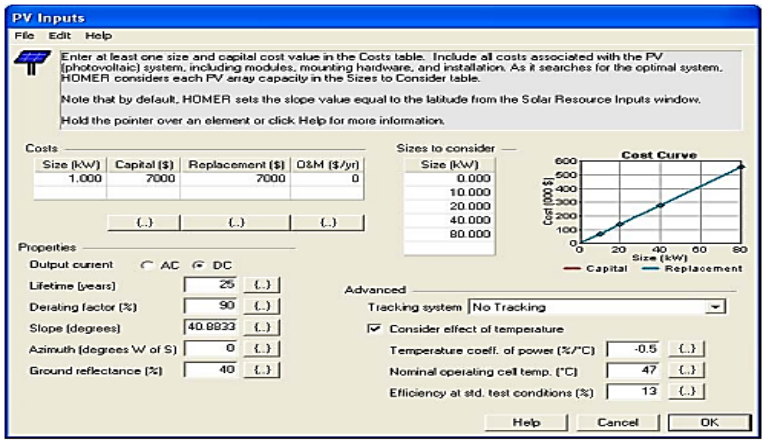

Fig. 9. Resulting view of the PV inputs window

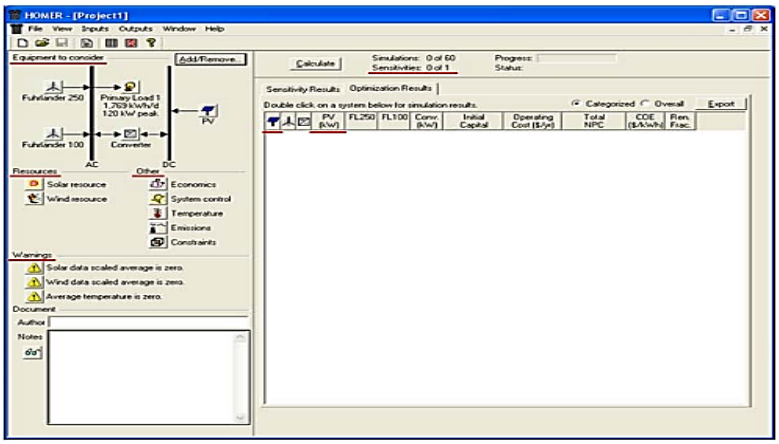

Fig. 10. View of HOMER's opening window after completion of PV array modeling

load averages, and the time-step function shows the standard deviation in the difference between the hourly load data and the average daily load profile. Previously acquired hourly load data on the second path, represented by the import time series data file option in the data source section of the initial load inputs window, must be transferred to HOMER using the import file button. In this work, the second path represented by the import time series data file option in the data source section of the initial load inputs window was used, and the required hourly load data was obtained through MATLAB software. A maximum hourly load value must be entered to run this MATLAB program. Therefore, this hourly maximum load value is set to 120 kW in order to obtain hourly load data from the MATLAB program that will coincide with the electricity demand of the load given above. The resulting hourly load data is transferred to HOMER using the import file button in this second path represented by the import time series data file option.

6 Conculision

In the research study, an example hybrid power system with grid connection was modeled by HOMER to determine the system configuration that can economically optimally feed a certain load in a certain region (Gubadli region). In carrying out this modeling process, sensitivity values were determined for the average solar radiation and average wind speed values of the studied region, and the sensitivity value for the network sales power was also determined. Certain fixed values have been determined for the costs of wind turbines, the costs of photovoltaic arrays, the price of electricity received from the grid, and the price of electricity sold to the grid. These costs and prices are determined in addition to or independent of the sensitivity values determined in the example hybrid power system. By setting sensitivity values for each of the above-mentioned criteria, one can observe for which situations HOMER will make decision. In addition, in this study, a certain fixed value for the load size was determined, and in another study, by setting sensitivity values for the load size, it can be observed which situations HOMER will make decision for a sample hybrid.

References

1. Intelligent autonomous power supply systems based on hybrid wind-diesel turbines: R&D report. Stage III, (interim) /National Research Tomsk Polytechnic University; supervisor. Lukutin B.V.; executor. Obukhov S.G./ [et al.]. - T., 2011. - 165 p. - GC No 627.
2. Kirpichnikova I.M., Matveenko O.V. Computer simulation of the dynamic component of wind speed depending on time // International Scientific Journal "Alternative Energy and Ecology" No. 1 (81), 2010, - pp.54-59.
3. Obukhov S.G. Low-power wind turbines. Specifications, simulation, rational choice. - Saarbrucken: LAP LAMBERT Academic Publishing GmbH & Co. KG, 2012 -88 p.
4. Obukhov S.G. Method of modeling mechanical characteristics of low-power wind

turbines // Alternative energy and ecology. -2011 -№ 1, pp. 10-15.
5. Obukhov S.G., Sipaylova N.Yu., Plotnikov I.A., Sipaylov A.G. Mathematical model of a synchronous generator of an inverter diesel power plant // News of universities. Problems of energy. - 2012 - №. 9-10 -pp. 112-120.
6. Yusifov S.İ., Mayilov R.A., Mehdiyeva A.M., Mehdizade E.K. Advanced Information-Measuring System for the Improvement of the Quality Indicators of Metrological Characteristics. E3S Web of Conferences (Environment, Energy and Earth Sciences), Vol. 474, 02003 (2024). ISSN: 2267- 1242.
7. Agayev F.H., Mehdiyeva A.M., Gafarov G.A., Bakhshaliyeva S.V., Shirinzade N.V. Development of the functional safety system in primary oil refining Nafta-Gaz. Oil and Gas Institute - National Research Institute. Poland. ISSN 0867-8871. https://www.inig.pl/en/nafta-gaz-en/available-articles
8. Hashimoto T., Kubo M., Kawazoe H., Yagi K. Demonstrative Research on Hybrid Control System of Wind, Photovoltaic and Diesel Power Generation in Myanmar // International Conference on Power Engineering, 2007, October, China, Hangzhou.-pp. 1238-1242.
9. Onar O.C., Uzunoglu M., Alam M.S. Dynamic modeling, design and simulation of a wind/fuel cell/ultra-capacitor-based hybrid power generation system // Journal of Power Sources, 2006, No. 161, pp.707-722.
10. Ruiz A.G., Molinas M. Electrical Conversion System for Offshore Wind Turbines Based on High Frequency AC Link // Ecologic Vehicles and Renewable Energies International Conference EVER, Monaco, 26-29 March, 2009.
11. Sopian K., Zaharim A., Ali Y., Nopian Z.M., Razak J., Muhammad N.S. Optimal Operational Strategy for Hybrid Renewable Energy System Using Genetic Algorithms // WSEAS Transactions on Mathematics, 2008, March, No.21, pp.130-140.
12. Hasanah, R.N. Computer-based solar tracking system for PV energy yield improvement/ R.N. Hasanah, A.B. Setyawan, E. Maulana, T. Nurwati // International Journal of Power Electronics and Drive Systems. – 2020. – V.11. - No. 2. – P. 743-751.
13. Ismail, F.B. Design and fabrication of solar panel with sun position tracker / F.B. Ismail, N.F.O. Al-Muhsen, F.A. Fuzi, S. Sambathan, M.N.H. Nawawi // Journal of Mechanical Engineering and Sciences. – 2020. – V.14 – No. 2. – P. 6906- 6916.
14. Kasim, N.K. Experimental study for the effect of dust cleaning on the performance of grid-tied photovoltaic solar systems/ N.K. Kasim, N.M. Obaid, H. G. Abood, R.A. Mahdi, A.M. Humada // International Journal of Electrical and Computer Engineering. – 2021. – V.11.- No. 1– P.74 – 83.]
15. Srikumar, K. A system and novel methodology to track maximum power from photo voltaic system: A comparative and experimental analysis/ K. Srikumar, C. Saibabu // Journal of King Saud University - Engineering Sciences. – 2020. – V.32.- No. 7– P.442 – 458.
16. Agayev F.H., Mehdiyeva A.M., Ibrahimova A.E. Advance Technologies to Eliminate Environmental Problems of Oil and Gas Processing. 2nd International Conference on Emerging Applications of Material Science and Technology (ICEAMST 2024), July 3-4, 2024, Bengaluru, India. Advances in Science, Technology & Innovation.
17. Agayev F.H., Mehdiyeva A.M., Gafarov G.A., Bakhshaliyeva S.V., Shirinzade N.V. Development of the functional safety system in primary oil refining Nafta-Gaz. Oil and Gas Institute - National Research Institute. Poland. ISSN 0867-8871. https://www.inig.pl/en/nafta-gaz-en/available-articles.
18. Rao, R. Comparison of performance of solar photovoltaics on dual axis tracker with fixed axis at 13N latitude/ R. Rao, J. Srinivasan, S. Ramasesha // Smart Energy for a

Sustainable Future. Experiences in Photovoltaic System Monitoring. - 2022.- V.3.-No.3.- P.187-208.
19. Yilmaz, S. Design of Two Axes Sun Tracking Controller with Analytically Solar Radiation Calculations/ S.Yilmaz, H.Riza, O.Dogmus, F. Dincer, O.Akgol // Renewable and Sustainable Energy Reviews. – 2015.- No. 43. -pp. 997-1005.

System for Increasing the Accuracy of Digital Information Processing

Farid Agayev[1] and Sevinj Bakhshaliyeva[2]

[1,2]Azerbaijan State Oil and Industry University, Baku, Azerbaijan
[1]farid.aqayev@asoiu.edu.az
[*2]sevinj.quliyeba@asoiu.edu.az

* Corresponding Author

Abstract. To achieve balanced indicators of metrological, structural-algorithmic and functional efficiency of the developed means, the proposed methodological approach to the creation of a target-purpose information system consists of a combined analysis of measurement processes and corrective filtering. Corrective filtering was carried out in the Matlab software environment. It is evident from the results of the simulation modeling that errors have significantly decreased. A discrete averaging filter should be applied to the previously measured monitoring parameters when building an IIS for electrical equipment monitoring and diagnostics. Only then, based on the corrected results, should and diagnostics be conducted. Other characteristic errors are also examined using the aforementioned method. These include the impact of level quantization during the analog-to-digital conversion of signal samples (quantization noise), random variations in the instantaneous readings of the measuring signals (dating error), and their digital processing (rounding noise). In order to achieve balanced indicators of the metrological, structural-algorithmic, and functional efficiency of the developed tools, the suggested methodical approach to the creation of an information system for the intended purpose combines corrective filtering with an analysis of the.

Keywords: Corrective filtering, information system, measurement processes, discrete averaging, simulation modeling, monitoring.

1 Introduction

The task of developing the theoretical, methodological, and practical aspects of creating highly effective information systems is particularly relevant given the growing demand for information systems, the variety of their designs, and the areas of application. Additionally, the quality and efficiency indicators of both newly created and existing systems are being subjected to increasing demands.

The ability of the system to provide specific technical, economic, and operational characteristics when carrying out the informational, logical, and measuring tasks delegated to it as part of the automation of the serviced facility is reflected in efficiency, a complex indicator of the quality of the information system.

Theoretically, in order to improve the metrological quality of the outcomes of solving measurement, control, diagnostic, and identification problems while taking into consideration current technical and financial constraints, it is crucial to optimize the exchange processes (receipt, transformation, transmission, processing, and presentation) of measurement information in the IMS [1–5]. Significant challenges arise when solving optimization problems in automated information systems. These challenges are typically related to a lack of a priori knowledge about the automation object's properties and characteristics, measured quantities, interfering factors, intermediate and final results of solving basic system functions and tasks, and functional units of measuring and computing subsystems. The challenge of overcoming a priori uncertainty is even more difficult when synthesizing ideal information systems and its subsystems functioning in a dynamic manner. This issue is relevant to the advancement of information measurement technology in general at this time, as high-precision dynamic measurements are becoming more and more common [6, 7].

Improving the efficiency of the nation's fuel and energy complex requires immediate attention to parameter monitoring and energy facility diagnosis. This is explained by the fact that the efficiency indicators of the entire complex are ultimately determined by the quantity of electricity used by power plants and the quality of electricity produced by power units.

Enhancing the precision of measurement outcomes is a crucial objective in any industrial, scientific, or technical domain. The ability of a tool or technique to reduce mistakes and departures from true values is what determines measurement accuracy. Here are a few essential strategies to increase accuracy: Equipment Calibration: Systematic errors can be reduced by routinely calibrating measurement devices. This is particularly crucial for accurate devices like manometers, thermometers, and laboratory scales, among others. Use of High-Quality Instruments: High-sensitivity, stable instruments that are specifically made for the field in question should be utilized for precise measurements.

The implementation of measurements can be divided into three main stages: preparation, measurement experiment, and processing of experimental data. In the preparation stage, the measurement problem is formalized (this includes the definition of the concept of the measured quantity and the way in which the measurement results are derived). At this stage, measurements are also planned (including the selection of the method and equipment and its placement) and the necessary conditions for conducting measurements are provided. A measurement experiment consists of maintaining the required conditions, implementing the interaction of measuring devices with the object of study in accordance with the selected method, and recording the measurement results.

The processing of measurements leads to their logical and mathematical transformations in order to obtain an estimate of the measurement result and its accuracy. Let us explain the measurement stages in more detail. It is advisable to

divide the first stage into two parts: setting the measurement problem and planning the measurement experiment. Setting the measurement problem is carried out in the following sequence: - specification of measurement conditions and data on the physical quantity to be studied; - formation of a model of the object and determination of the quantity to be measured; - setting the measurement problem based on the accepted model of the object; - determination of specific physical quantities based on the value to be found for the quantity to be measured (for example, in indirect measurements, directly measured selection of arguments); - formulation of the measurement equation. The most important issue is the formation of a mathematical model (especially in solving complex measurement problems and studying complex objects) [8]. The model of the object is built based on a priori data. The measured quantity is determined as a parameter and characteristic of the object with the help of the adopted model

Reducing the Effect of environmental elements: A number of environmental elements, including humidity, temperature, and electromagnetic interference, can have an impact on the accuracy of measurements. Reducing their impact or making up for them with suitable techniques is required to increase accuracy.

Statistical Methods Application: Several measurements can be made and averaged to improve accuracy. This produces more dependable findings and lessens the impact of random errors.

Use of Modern Technologies: For instance, reducing the human element and increasing accuracy can be achieved by automating measurements and processing data using computer systems.

Choosing the Correct Measurement Method: Depending on the kind of object or process being measured, it is crucial to choose the appropriate measurement method because different approaches may produce results with differing levels of precision.

Minimizing Measurement Errors: There are two types of errors: random and systematic. Reducing random errors and minimizing the effects of systematic errors - such as by modifying measurements—are crucial for increasing accuracy.

Operator Training: The credentials and background of the experts doing the measurements are also crucial. Errors during the measurement procedure are less likely to occur when the operator is more skilled and focused [9, 10].

2 Formulation of the problem

Physical quantities, unless we go down to the quantum level, change continuously. However, digital signal processing works exclusively with discrete quantities, and discreteness manifests itself in two ways - in time quantization and in signal amplitude quantization. This apparent complication is fully justified by the fact that we can use digital computers for processing, completely eliminating the problem of parameter instability, which is so painful in analog processing. No less an advantage is that the cost of digital processing is low and continues to fall, even for very complex types. This allows us to create effective signal processing systems at reasonable costs. How acceptable is such a replacement? Doesn't it lead to a loss of

accuracy?

A discrete signal is obtained from an analog signal by a discretization operation - taking samples (measurements) at a time interval T. In principle, digital processing is also possible with non-uniform discretization in time, but this topic is much less developed mathematically and, apparently, is not of such great practical interest. In this operation, it is possible to lose information contained in the signal values in the intervals between samples. The conditions under which it is possible to restore an analog signal from a digital signal obtained from it, i.e., to preserve all the information originally contained in the signal, are expressed by the Nyquist-Whittaker-Kotelnikov-Shannon theorem (depending on the author's preferences, all conceivable combinations of these names are encountered). This requires that the frequency band of the input signal be at least twice as narrow as the sampling frequency, i.e. fc=1/2fd. (A particular formulation is often given, which is true for signals whose frequency band begins with zero frequency - "so that there are no frequencies greater than half the sampling frequency"). If such frequencies are present, the effect of masking (substitution) of frequencies occurs. A clear manifestation of this can be an illusion, often seen in movies - a rotating wheel suddenly begins to rotate in the opposite direction. Here the frame rate is an analogue of the sampling frequency, and when the wheel makes more than half a turn between successive frames, it appears to rotate in the other direction and at a different speed. For the frequency f, the frequencies (2fc±f), (4fc±f), (6fc±f), etc. are masked under it. The term "aliases" is also used. Failure to take this effect into account can lead to gross errors: thus, in one study conducted in a serious laboratory, the presence of frequencies of 22 and 28 hertz in the electroencephalogram of all patients, in contrast to healthy subjects, was discovered. However, noting that the sampling frequency in this study was adopted as 128 Hz, we see that these frequencies are essentially "ghosts", generating interference at frequencies of 100 and 150 Hz - the second and third harmonics of the network frequency (their source could be, for example, nonlinear devices in the power supply circuits of the equipment, such as rectifiers and transformers). Their registration exclusively in patients was caused by the fact that in a hospital setting, compared to a university laboratory, where the EEG of healthy subjects was recorded, the level of interference is significantly higher.
The fight against the effect of frequency masking (antialiasing) leads to the need for preliminary filtering of the signal, excluding frequencies above half the sampling frequency, and due to the imperfection of real filters, the cutoff frequency is chosen deliberately lower than the theoretically required one, as a rule, three to four times lower than the sampling frequency. This imperfection is not caused by the incompetence of electrical engineers, but is of a fundamental nature. The point is that a signal with a limited frequency band cannot in principle be of finite length, and if it is finite in time, it contains a frequency band of infinite width. (This limitation is quantitatively expressed by the uncertainty relation that connects the pulse length and its frequency band - an infinitely short pulse contains "in embryo" all possible frequencies, and a strictly monofrequency sinusoid must extend from minus to plus infinity.) Therefore, an excessively high-quality filter will have too

long a settling time, and an "ideal" one will have an infinite settling time.

According to GOST 14.306-73, the selection of control instruments is carried out on the basis of ensuring the required indicators of the technical control process and analyzing the costs for the implementation of the control process. The most important indicators of the control process include the accuracy, integrity, labor intensity and cost of measurements. The volume, scope, periodicity and duration of control are also taken into account as additional indicators. Ensuring accuracy in the selection of measuring instruments is very important. Thus, the accuracy of the measuring instrument should be sufficiently high, the labor intensity and cost of measurements should be as low as possible, and high productivity and economy should be ensured. Due to the insufficient accuracy of the measuring instrument, the likelihood of considering useful parts as waste increases or, for this reason, waste products are accepted as useful. On the other hand, too high accuracy increases the labor intensity and, therefore, the cost of measurements, leading to an increase in production costs and a limitation of product output.

Therefore, the selection of measuring instruments that provide optimal measurement accuracy is of great importance. The vast majority of measurement work applied in industry is linear measurements. Linear measuring instrument and linear control instruments are divided into contact, contactless, automatic and non-automatic groups. The measuring device for linear measurements consists of a measuring and positioning base and a measuring structure with a calculating structure. The latter is also called a measuring head. Automatic measuring instruments also have a digital adapter-calculator and a self-recording structure. Automatic measuring instruments are divided into measuring control automata, measuring - control sorting automata, semi-automatic machines and active (control) measuring - control devices. Measuring and control instruments can be one-dimensional (for measuring one quantity) and multi-dimensional. All measuring instruments are universal and specialized according to their purpose. Universal devices are used for internal, external measurements, and for measuring surface shape deviations. Specialized devices have a narrower scope of application.

Intense research and development is now being conducted in this area. Unfortunately, there isn't a methodical strategy to developing systems for tracking energy facility diagnostic metrics.

A methodical strategy to developing an information system for the aforementioned aim is attempted to be developed in this study. Asynchronous motors, which are the foundation of the majority of electric drives and are responsible for almost 40% of global electricity consumption, are the subject of this case study [11].

Any measured quantity is a sinusoidal harmonic signal, such as network voltage. There is only one harmonic in this signal. We get a non-sinusoidal signal after measuring an analog value. A sinusoid with extra odd harmonics is what it is. These harmonics are caused by interference and noise that are superimposed on the primary useful signal, making it noisy. As a result, 80% of the time, the measured signals are not sinusoidal [12–15].

Although they are not always visible, curves of continuous signals' instantaneous values are the most instructive. Therefore, the real-time determination of integral signal parameters are crucial for the management and analysis of the operation of

regulated processes and objects [16, 17]. The latter describe the overall quantities of materials and energy received and added within a specific period of time, as well as the object's operational indicators and parameters, which are the mean values of the measured values, etc. By performing discrete averaging (DA) or discrete integration (DI) of parameters that vary continuously over time, IPS can be specifically determined utilizing digital methods and tools.
The increasing global use of power, especially due to the widespread use of asynchronous motors, has made real-time monitoring and diagnostics of energy facilities even more important. In addition to being essential to the great majority of electric drive systems, these motors also contribute significantly to the world's energy usage. The need for efficient ways to monitor diagnostic indicators is growing in significance as energy systems become more complicated. Predictive maintenance techniques are essential for reducing downtime and increasing energy production efficiency, and they are improved by the integration of real-time data collecting systems and diagnostic instruments.

3 Solution of the problem

Two other problems where the discrete Fourier transform (DFT) is successfully used exploit one of its most important properties, namely that the DFT of the convolution of two signals is equal to the product of the DFTs of these signals. Since the output of any linear system is the convolution of the input signal and the response of the system, the DFT of the system's output is obtained by multiplying the DFT of the input signal and the DFT of the response, and if we have access to the input and output of the system and can compute the Fourier transform of them, the transfer function is obtained by simple division. In the same way, if we need to calculate a convolution, and the length of the segments being convolved is so large that we have to worry about computational efficiency, we can calculate the DFT of the vectors being convolved, multiply them, and find the inverse DFT to get what we are looking for (there is a trap here - by applying this theorem "head-on", having obtained a cyclic convolution, calculating which and having reached the end of the segment, we start going along it from the beginning - this is rarely what we wanted; to prevent this, the segments are supplemented with the required number of zeros). Speaking so confidently about the computational advantages of the DFT, we have not yet given the slightest basis for this confidence. Calculating the DFT using the given formula requires calculating n coefficients, each of which depends on n elements of the original segment, so the number of operations cannot be less than n2. Without dwelling on the technical methods of calculation, I will only note that there is a remarkable algorithm, or rather a whole family of algorithms, known as the “Fast Fourier Transform”, which reduces the operating time to n log n operations. This is achieved by skillfully applying the “divide and conquer” principle, which allows you to avoid repeating work that has already been done, and the adjective “fast” should not be interpreted as “simplified”, “inaccurate” or “incomplete”. With exact arithmetic, the result of a calculation according to the FFT

algorithm and the calculation according to the above formula coincide, moreover, if we move on to real, inaccurate arithmetic, it turns out that the FFT gives a higher accuracy of calculation than direct calculation. It is this algorithm that makes the use of the Fourier transform so useful in computational terms. Variants of the Fourier transform also find a certain application. Limiting ourselves to cosine waves, we arrive at the Discrete Cosine Transform, which allows us to represent only even signals (i.e. f(x)=f(-x)) while eliminating discontinuities. The Discrete Sine Transform also has its niche. The Hartley transform is of some use, where the basis functions are not sines and cosines, but their sums, which allows us to achieve some gain in performance by eliminating complex arithmetic. However, this transform is too close to Fourier and cannot be considered more than a convenient calculation technique. Transforms with other families of basis functions are similar to Fourier. For example, the Walsh-Hadamard functions take values of +1 and -1, as if they were chopped out with an axe in an attempt to sculpt a caricature of sinusoids. Sawtooth or triangular functions have also been proposed for use. They had very modest practical success (mainly in video compression problems), and there are no theoretical grounds to expect these functions to appear in biological systems, even as small as the Fourier basis functions. However, fast transformation algorithms have already been developed in this family, which may justify their practical application.

One can approach the construction of a family of functions for signal decomposition from another side. Starting with a description of a real process, albeit a very rough one, one can obtain a differential equation whose eigenfunctions will be a certain family of functions (say, Bessel functions are eigensolutions of the membrane differential equation). They may be much more suitable for describing this class of processes than standard Fourier, but this path is difficult and laborious.

Finally, problems solved using Fourier can be solved in other ways. Thus, autoregressive and ARMA methods can be used to estimate spectra, the impulse response function can be estimated using regression estimates, etc. The only always true statement here is this: there is not and cannot be a single always best method. The characteristics of the generation and collection of data, the means and methods of analysis available to us, the prospect of subsequent application of our results will always be decisive in choosing the best method here and now.

The signal is converted into digital form by an analog-to-digital converter (ADC). Almost all of them use a binary system of representation with a uniform scale (however, one should not forget about non-uniform scales, such as logarithmic α-law and μ-law, used in digital telephony, binary-decimal data representation and some other, sometimes very exotic solutions), characterized by a certain number of digits. Increasing the number of digits improves the measurement accuracy and allows to expand the dynamic range of the measured signals. Information lost due to the lack of ADC digits is not recoverable, and there are no simple criteria similar to the Nyquist-Kotelnikov-Shannon (NKS) theorem, showing when such recovery could take place. There are only error estimates, for example, through the noise power generated by an error in the last digit, but they are not always satisfactory. For example, human hearing is logarithmic (Weber-Fechner law), and low-power interference in a range where the signal power is low is too clearly distinguishable.

Speaking about the signal, we mentioned that it can be real or complex, i.e. consisting of real and imaginary parts. Complex numbers do not appear here as a tribute to mathematical generality (although the ability to write one exp(a+i*b) instead of two different expressions eacos(b) and easin(b) greatly simplifies life and calculations...) and even more so, one should not see here mathematical mysticism ("square root of minus one"). It is natural, for example, to represent in-phase (coinciding in phase with some other signal) and quadrature (differing in phase from this signal by 90 degrees) components of the signal. Complex numbers also naturally arise when solving differential equations representing many natural and technical objects, especially in connection with the description of oscillatory processes.

In general, complex numbers can be considered simply as a way to combine two different numbers in one number, but in such a way that it is possible to operate with them simultaneously. One of the numbers used is represented by the real part, and the other by the imaginary part of the complex number $a + bi = r (\cos (\varphi) + i \sin (\varphi)) = r \exp (i\varphi)$. It is convenient to represent them as points on a plane - one coordinate will represent the real part, the second the imaginary part. Then their addition will become the addition of vectors, and their multiplication will be the rotation of vectors on the plane (with the multiplication of their lengths equal to the moduli of these numbers; angles equal to the arguments of these numbers are added). Successive raising of a complex number to a power becomes the rotation of the vector expressing this number around the origin.

The projection of this vector on one of the axes will experience increasing, decreasing, or constant-amplitude oscillations - depending on whether the modulus r of a given complex number is greater than, less than, or equal to one. Although real objects are all nonlinear to a greater or lesser extent, we will begin our consideration with the simplest, but important and often sufficient for a satisfactory description of the case. And the simplest to consider are linear systems. Linear systems are those for which superposition takes place (that is, the response to the sum of two input signals will be equal to the sum of the responses to these signals separately - "the whole is equal to the sum of its parts") and homogeneity (that is, the response to an input signal amplified by a certain number of times will be amplified by the same number of times - "size does not matter"). Linearity allows us to consider our object of study in parts, and homogeneity - on a scale convenient for us, in particular, by feeding simple test signals to its input and studying its reaction to them, and representing complex real signals as a sum of simple ones. Obviously, for real objects, the property of linearity can take place only approximately and in a certain range of input signals. An example of nonlinear technical systems is a diode that leaves only positive half-sine waves from a sinusoidal signal, or a transformer whose yoke saturation with a magnetic field leads to "blunting" of the sinusoid peaks (and from the point of view of the frequency spectrum, this is manifested by the appearance of frequencies that are twice, three times, etc. greater than the fundamental frequency – harmonics, and sometimes frequencies that are a multiple of the frequency – subharmonics). Perhaps of greater interest to the reader are nonlinearities in biological systems, such as the threshold action expressed by the "all or nothing" law, or nonlinear transformation in the

sense organs, approximated by a logarithm in accordance with the Weber-Fechner law. Nevertheless, as a rule, the study begins with the assumption of linearity, and then introduces corrections for nonlinearity.

The so-called method of digital processing of the results of direct measurements of instantaneous signal values during the averaging (integration) period is one of the most used digital techniques for measuring IPS [18]. The potential to add processing power to the measurement channels when addressing this type of measurement problem explains the recent sharp rise in interest in this approach [16–19]. When measuring the IRS of electrical signals with complex shapes (non-sinusoidal signals) digitally, the issue becomes much more challenging. However, main information converters with output signals in the form of direct and alternating currents and voltages are becoming more and more common due to the well-known benefits of electrical methods for monitoring and measuring physical quantities [19–21].

Particularly in electrical energy generating and conversion facilities, AC signals are more informative and sometimes the only way to get measurement information [22–25].

It is important to keep in mind that practically all algorithms use the DA operator when switching from continuous integration to numerical integration using the techniques.

A quadrature formula $\bar{C}^{(m)}[0,T]$, of the following kind function is used to conduct the DE of a class of continuous functions:

$$\bar{I} = \frac{1}{M}\sum_{i=0}^{M-1} y(iT_0)$$

where $T_0 = \frac{T}{M}$ – step-by-step sampling in time.

In order to monitor parameters and evaluate the current condition of electric motors, the work offers a methodical approach to electric motor design.

Currents and powers in idle and short circuit modes can be measured and processed to perform electric motor diagnostics. The precision with which these parameters are measured determines the dependability of monitoring and diagnostics.

The voltage U in the network and the current I flowing through the object determine the overall power:

$$P = IU\,. \tag{1}$$

The outcome will be if an error is introduced in the measurement of any of the power-determining parameters, which is always the case.

$$\widetilde{P} = \widetilde{I}\widetilde{U} = (I + \Delta I)(U + \Delta U), \tag{2}$$

where ΔI - resulting measurement error for current,

ΔU - resulting measurement error for voltage.
The power measurement result will deviate from the actual value by the following because of errors:

$$\left|P-\widetilde{P}\right|=\left|I\cdot U-\widetilde{I}\cdot\widetilde{U}\right|=\left|\Delta I\cdot U+\Delta U\cdot I+\Delta I\cdot\Delta U\right|. \quad (3)$$

The usable harmonic signal is noisy during the current and voltage measurement procedure; that is, high-frequency noise (interference) is overlaid on the signal as a result of the measurement. Consequently, the pure harmonic signal becomes inharmonic. Furthermore, the measurement signals u(t) and i(t) are non-sinusoidal in real circuits due to the inclusion of extra harmonics.
In particular, we will determine the spectrum of the product of these signals and how it will change after applying a discrete averaging filter, which is required for digital measurements of the integral characteristics of AC signals. Let's look at the scenario where a non-sinusoidal signal interacts with random-centered noise.

$$\bar{x}(nT_0)=\frac{1}{N}\sum_{i=0}^{N-1}x_i(nT_0),\quad ... \quad (4)$$

where N - the quantity of averaged samples,
T_0 – the sampling time step.

Consider a sinusoid with a frequency of 50 Hz and 13 odd harmonics placed on it as an initial non-sinusoidal signal:

$$x(k)=\sum_{m=1}^{2N+1}\sin(2\pi km\omega),\quad N=\overline{1,6},\ k=1,2,... \quad (5)$$

where ω -the signal's fundamental frequency,
k – the number of distinct samples,
m – numbers of harmonics.
Consider a random signal produced by the built-in Matlab rand function that is uniformly distributed on the interval [0, 1] as a random centered noise. The fast Fourier transform, or fft function, was used in the Matlab software environment to compute the original signals' spectra (figure 1).
We determine the product of the initial signals in line with formula (3) (assuming that one of the signals is U and the other is not). The theory of spectral analysis [10, 11] states that as time signals are multiplied, their corresponding spectra are added. Fig. 2 displays the final signal as well as the entire spectrum. Because of the overlap of several frequencies in the random signal, the resulting spectrum has many additional harmonics, as seen in Fig. 2(b).

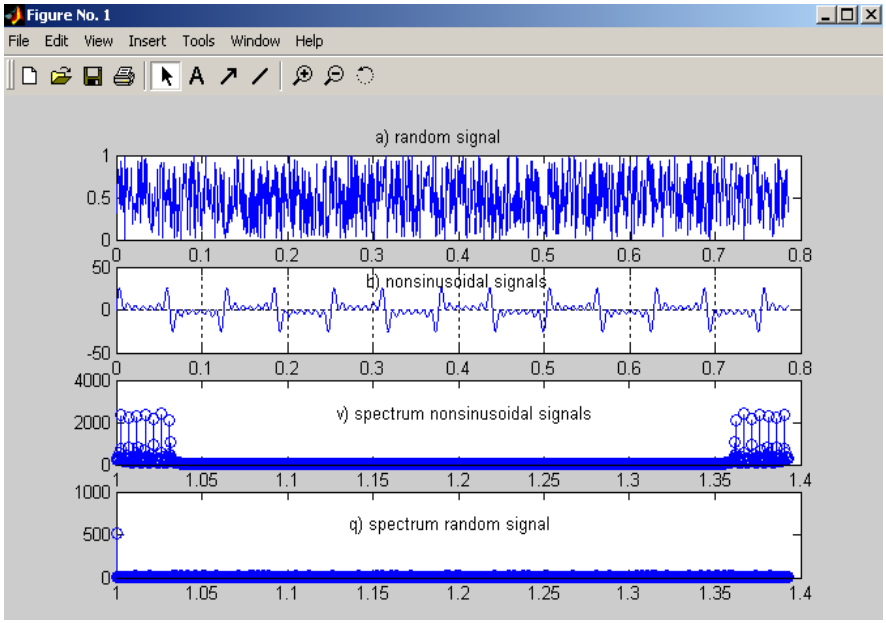

Fig. 1. Signal sources and their spectrum

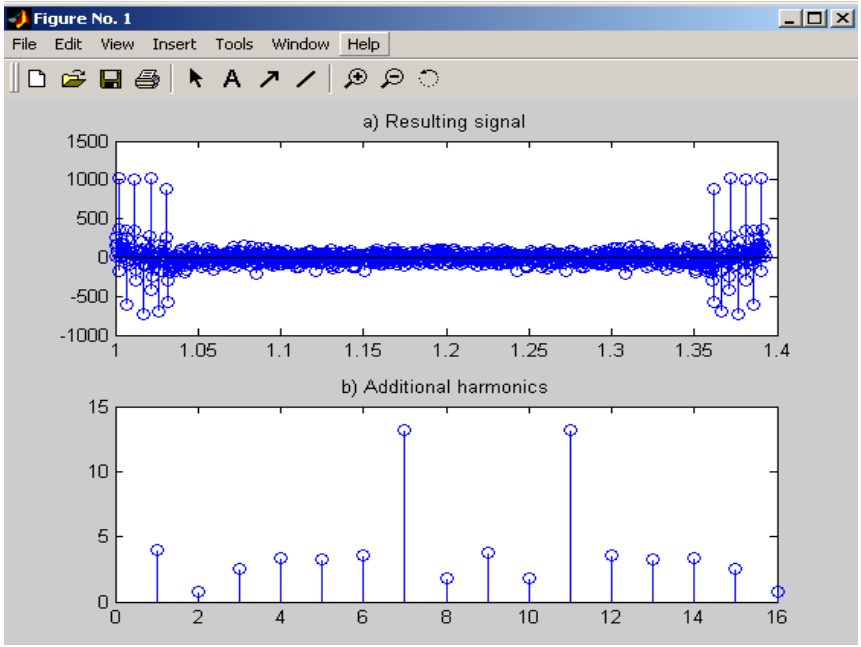

Fig. 2. The spectrum of the resultant signal

We next run the resultant signal through a discrete averaging filter to eliminate any more harmonics. In order to accomplish this, we split the total time period into smaller time periods, and we calculate the average value of the resulting signal samples in each of those intervals using the formula:

$$y(k) = \frac{1}{N_k} \sum_{i=l}^{l_{k+1}} y(i),\ k = \overline{1, K}, \tag{6}$$

where N_k – the number of subintervals,
l_k and l_{k+1}– the interval boundaries,
K – the number of samples in each interval.

We will determine the spectrum of the filter output signal (Fig. 3) in order to examine the harmonic composition of the received signal. According to the computations displayed in Fig. 3, the impact of extra harmonics in the spectrum was greatly diminished. The spectrum was free of side components when their amplitudes dramatically dropped (by several orders of magnitude). Therefore, it is sufficient to apply a discrete averaging filter to the measurement result in order to reduce the random noise in non-sinusoidal signals. Only then may the corrected signal be used as a parameter for monitoring and diagnostics.
We carried out an analogous computation concerning a non-sinusoidal signal and a systematic error of order 2, which is represented by a function of the following form:

$$\overline{\varepsilon}(t_k) = \sum_{j=0}^{2} a_j t_k^j, \tag{7}$$

where t_k -discrete samples of the systematic error., a_j – the polynomial coefficients that describe the slowly varying error
Using a discrete averaging filter resulted in a considerable reduction in the signal spectrum. The systematic error is more effectively repaired, according to a comparison of the experimental findings with random and systematic errors.
Therefore, the previously measured monitoring parameters should be corrected by applying a discrete averaging filter to them before monitoring and diagnostics are conducted based on the corrected results when building an IIS for electrical equipment monitoring and diagnostics.
Other characteristic errors are also examined using the aforementioned method. These include the impact of level quantization during the analog-to-digital conversion of signal samples (quantization noise), random variations in the instantaneous readings of the measuring signals (dating error), and their digital processing (rounding noise).

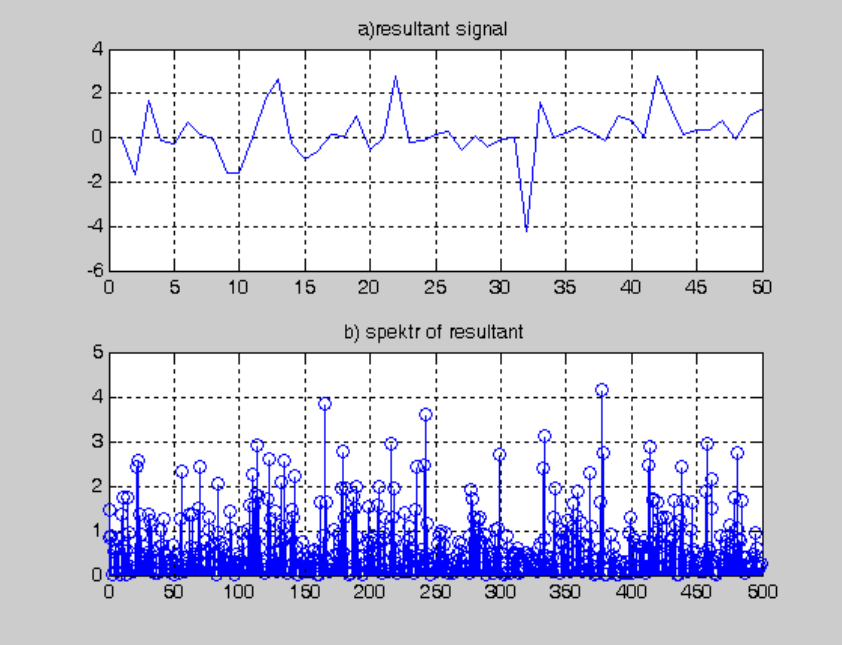

Fig. 3. Spectrum and signal at the filter's output

Conclusion

Therefore, in order to achieve balanced indicators of the metrological, structural-algorithmic, and functional efficiency of the developed tools, the suggested methodical approach to the creation of an information system for the intended purpose consists of a combined analysis of the measurement processes and corrective filtering.

Corrective filtering was performed in the Matlab software environment. From the results of the simulation modeling, it is obvious that the errors have significantly decreased.

References

1. Sergienko A.B. Digital signal processing. St. Petersburg: Peter, 2005, 604 p.
2. Baranov L.A. Level quantization and time sampling in digital control systems. M.:Energoatomizdat, 1990,304 p.
3. Mehdiyeva A.M., Mehdizadə E.K. Information-measurement system development for controlling of parameters of measurement. Standard Global Journal of Business Management. Vol 1(2): 030-033, March 2014.
4. Camponogara E., Nakashima P.H., Solving a gas-lift optimization problem by

dynamic programming, European Journal of Operational Research, Vol.174, No.2, 2006, pp.1220-1246.
5. Ponomarenko V.S., Arefiev Yu.I., Cooling towers of industrial and energy enterprises, 1998, 365 P.
6. Gladkov V.A., Arefiev Yu.Yu., Ponomarenko V.S., Fan Cooling Towers, 2 nd. ed. Revised and ext., M., Stroyizdat, 1976, 216 p.
7. Taria L. Localized corrosion of stainless steel in chloride, sulfate and thiosulfate containig environments Corros.
8. Mehdiyeva A.M., Bakhtiyarov I.N. Analysis of reliability indicators of multiservice corporate networks based on SDN technologies. Proceedings of the International Symposium Reliability and Quality. Penza 2019. T. 2. p. 114–116.
9. Ibrahimov B.Q., Mehdiyeva A.M., Baxtiyarov I.N. Investigation of methods for improving the noise immunity of message processing systems. Problems of information communications. Science Magazine. Minsk, Belarusian State Academy of Communications, 2020, No. 1 (11). pp.13-18.
10. Mehdiyeva A.M. et al. Conversion and initial processing errors of measurement results American Journal of Circuits, Systems and Signal Processing. American Institute of Science Vol.1, No3, 2015, pp.56-59.
11. Allahverdiyeva N.R., Mehdiyeva A.M., Mehdizadə E.K. Increase the accuracy of conversion and digital processing of electrical signals. "Information-measuring and control systems". Moscow, 2010, No. 9, p. 69-74.
12. Informatics: Textbook / Ed. prof. Makarova I.V. - M.: Finance and Statistics, 2007.
13. Mehdiyeva A.M., Bakhtiyarov I.N., Bakhshaliyeva S.V. Increasing the Immunity of Information Transmission and Fault Tolerance of the Path. Lecture Notes on Data Engineering and Communications Technologies. Volume 166. 2023. Nepal. pp. 775-784.
14. Mehdiyeva A.M. Types of accidents, their causes and prevention measures Actual problems of modern science. Proceedings of the IV International Scientific and Practical Conference. January 31-February 3, Boston, USA. 2023. pp. 441-444.
15. Shapiro, L. Computer vision / L. Shapiro, J. Stockman. – M.: Binom, 2006.
16. Gonzalez, R. Digital image processing / R. Gonzalez, R. Woods. – M.: Tekhnosphere, 2005.
17. Ayficher, E. S. Digital signal processing: a practical approach / E. S. Ayficher, B. W. Jervis; M.: Publishing house. Williams House, 2008.
18. Jähne, M. Digital Image Processing / M.Jähne. – Springer-Verlag, Berlin Heidelberg, 2005.
19. Smith, S. Digital signal processing. A practical guide for engineers and scientists / C. Smith; lane from English – M.: Dodeka-XXI, 2008.
20. Ibrahimov B.G., Ismaylova S.R. The Effectiveness NGN / IMS Networks in the Establishment of a Multimedia Session // American Journal of Networks and Communications. Vol. 7, No. 1.2018. - pp. 1-5
21. Lebedev S.V. Firewalling. Theory and practice of protecting the outer perimeter. - M.: Publishing house of MSTU im. N.E. Bauman, 2002. 304 p.

22. Shuvalov V.P., Egunov M.M., Minina E.A. Providing indicators of reliability of telecommunication systems and networks. M.: Hotline - Telecom, 2015. - 168 pages.
23. Stearns, S. D. Digitale Verarbeitung Analoger Signale / Digital Signal Analysis / S. D. Stearns. – Walter de Gruyter GmbH & Co KG, 2018.
24. Mityukhin, A. I. Applied information theory: educational method. allowance / A. I. Mityukhin. – Minsk: BSUIR, 2018.
25. Mityukhin, A. I. Digital speech processing and image analysis: textbook - method. allowance / A. I. Mityukhin. – Minsk: BSUIR, 2016.

Performance Evaluation of Different Shapes of Patch Antenna for 5G Applications at 25 GHz

Afsana Sultana Alvee[1], *Md. Sohel Rana[1], Najifa Islam[1], Mahamud Hasan[1], Md Abdul Ahad[2]

[1]Northern University of Business and Technology Khulna, Khulna-9100, Bangladesh
[2]Washington University of Science and Technology, ,Virginia, USA
[1]afsanaalvee33@gmail.com, [1]sohel.rana@uits.edu.bd,
[1]najifaislam7865@gmail.com,[1]mahamud.nuc@gmail.com,
[2]abdulahadmanik20@gmail.com

* Corresponding Author: sohel.rana@uits.edu.bd;
sohel.rana@nubtkhulna.ac.bd

Abstract. This research study delineates the design, simulation, and performance assessment of four patch antennas for Ka-band wireless applications at 25 GHz. The four different designs use the Rogers RT6002 substrate material. It is 0.6 mm thick, has a dielectric constant of 2.94, and a loss tangent of 0.0012. The antenna is engineered and modeled by CST software. The reflection coefficient (S_{11}), voltage standing wave ratio (VSWR), Gain, directivity, bandwidth, and efficiency were obtained from the antennas. Design 1, 2, 3, and 4 achieved the S_{11} and VSWR are -11.14 dB, -19.5 dB, -14.87 dB, -48.52 dB and 1.76, 1.23, 1.44, 1.007. Also, Gain and directivity are achieved at 6.13 dBi, 5.94 dBi, 6.01 dBi, 6.22 dBi and 6.91 dBi, 6.71 dBi, 7.1 dBi, 6.86. Both antenna's feedline impedance matching is 50Ω. The efficiency of the antenna design 1, 2, 3 and 4 are 88.71%, 84.05%, 84.6% and 90.67%, respectively. The primary purpose of this research is to improve the return loss and achieve an acceptable VSWR. Additionally, increasing the bandwidth can enhance the antenna's gain directivity and impedance matching (50Ω). The design-4 bandwidth is 1.4 GHz, significantly superior to designs 1, 2, and 3. The antenna's overall performance renders it appropriate for forthcoming 5G applications.

Keywords: Patch antenna, VSWR, Reflection coefficient (S_{11}), 25GHz, 5G, CST.

1 Introduction

The globe is experiencing ongoing advancements in multiple domains, particularly in communications and antennas. There has been a substantial rise in demand for high-specification tiny antennas suitable for integration into

diverse applications such as 5G, wireless communication systems, and the medical area. Patch antennas are distinguished by their compact dimensions and suitability for applications necessitating limited space, such as mobile phones, Bluetooth devices, and other devices [1], [2]. There has been a substantial amount of advancement in the field of communication systems in the modern era, which has led to the development of a great deal of significant research in the field of antennas, which also vary depending on the application. Electronic devices known as antennas are employed for either capturing electromagnetic fields or radiating them into space. Oscillator antennas, wire antennas, patch antennas, array antennas, lens antennas, and reflector antennas are some of the several types of antennas that are available. As a result of its compact size, low cost, and low weight, the patch antenna is utilized for a broad range of applications, including wireless communication and radars. In addition to square, circular, rectangular, triangular, elliptical, and dipole forms, patch antennas are available in many different shapes [3]. Figure 1 illustrates the physical architecture of the patch antenna. In order to satisfy the ever-increasing need for high data rates and broad bandwidths, the rapid development of wireless communication technologies has prompted the investigation of new frequency bands [4]. The advent of 5G technology represents a dramatic transformation in the way people communicate and engage with one another around the world. Nevertheless, when we contemplate this revolution in wireless communication, it is of the utmost importance to recognize the vital role that the development of mobile communication has played in driving forward the advancement of modern technology. Mobile communications have had a significant impact on the technological landscape of our society, beginning with the era of cumbersome devices and continuing through the growth of smartphones and cellular networks, and now culminating with the introduction of 5G [5]. Designing antennas that are capable of operating effectively at frequencies of 25 GHz, however, presents a number of obstacles, such as large propagation losses, the need for precision in production, and the selection of materials. Important considerations include the impedance matching, bandwidth, and radiation efficiency of the antenna, all of which are influenced by the substrate material that is selected. As a result of its advantageous dielectric properties, low-loss tangent, and mechanical flexibility, the polyimide substrate that we use in this investigation is an excellent choice for the implementation of 5G wireless applications [6].

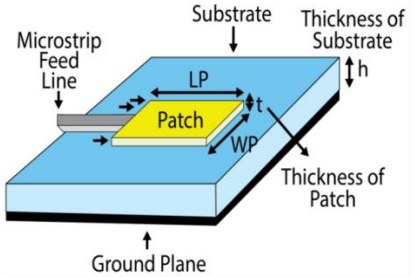

Fig. 1. The patch antenna's physical construction

2 Literature Review

Wireless communication is one of the most dynamic and fastest-developing technological fields within communication. Wireless communications are employed in numerous contexts, encompassing industrial applications and human endeavors. A patch antenna is the most popular antenna for wireless communication [7]. It is favored for various applications because of its compact dimensions, affordability, and excellent efficiency [8]. Extensive research has been undertaken and is ongoing to develop a more flexible and resilient framework for wearable microstrip antennas. The domain of wireless communications has rapidly and extensively evolved, resulting in a significant surge in demand for the design of low-profile and multiband antennas for mobile terminals, especially for applications utilizing 5G data transmission. In this section, a number of publications covering microstrip patch antennas for Ka-band applications that have been published in the past are discussed.

This article introduces [9] a tiny patch antenna designed for 5G millimeter-wave mobile terminal applications. The unit cell is a planar dipole fabricated on a singular substrate layer, attaining substantial bandwidth and gain. This article presents [10] a novel mixed-coupling substrate-integrated waveguide (SIW) filter design that has been proposed. The filter has a dual-band response and increased selectivity. The architecture that has been suggested is extremely adaptable, and it features three separate coupling parameters. These SIW filters are appropriate for large-scale manufacture for 5G applications, as they are both cost-effective and high-performing. For 5G communication systems [11], a novel design for a reconfigurable antenna has been proposed. Additionally, the design intends to attain a good bandwidth and gain while simultaneously improving efficiency. The numerical results that were obtained through simulations are validated by fabricating a prototype of the antenna and putting it through practical tests. The results of the prototype reveal that it is in good agreement with the measurements obtained through simulations. This research paper [12], introduces a broadband antenna designed for 28 GHz 5G communications. The antenna attains high radiation efficiency and gain and is considered appropriate for future 5G applications due to its straightforward design, compact dimensions, and low manufacturing cost. This work shows [13] a circular patch antenna equipped with a parasitic reflector element. This antenna was designed specifically for Ka-band applications operating at 28 GHz. The design alleviates these problems by optimizing the arrangement of parasitic elements to achieve high gain, bandwidth, and constant VSWR performance across the operating range. The present study offers [14] an exhaustive examination of the attributes and specifications of a resonant patch antenna intended for wireless communication. The work elucidates the following aspects: impedance bandwidth, gain, and minimal return. The proposed antenna for 5G cellular communication is a formidable contender. The H-plane radiation pattern, E-plane radiation pattern, and VSWR demonstrations are further features that distinguish it from other devices. In this work [15], a patch antenna design that is intended for use in 5G applications is presented. It

was suggested displays a significant gain and improved radiation efficiency. Qureshi, M. J. U *et. al,* presents [16] design of a circular patch antenna intended for broadband millimeter-wave applications in 5G technology. To achieved good S_{11}, VSWR, radiation efficiency, gain, and bandwidth from the design. It is anticipated that applications requiring broadband 5G connectivity will be compatible with this design. Table 1 presents a comparison between previously published work and the current study.

Table 1 Previously published literature with the planned work

References	Present	[14]	[15]	[16]	[17]	[18]
Tools	CST	CST	CST	CST	CST	CST
Substrate	RT6002	RT5880	RO3210	Teflon	RO3003	RT5880
(ε_r)	2.94	2.2	10.2	2.1	3	2.2
Thickness of substrate(mm)	0.6	0.5	1	1.57	0.25	1.2
Tan (δ)	0.0012	0.0009	0.003	0.00028	0.0013	0.0009
Applications	5G	5G	5G	5G	5G	5G

3 Method and Mathemathical Analysis

To begin designing an antenna, the first step is to choose the operating frequency for a specific application. The proposed design selected operating frequency 25 GHz (Ka Band). Second, using CST (Version 2019) software, an antenna should be designed, and then the antenna should be evaluated. In the third step, the substrate material for the antenna design must be selected, which will be used to design the proposed antenna. Rogers RT6002 is used to design the proposed antenna, which dielectric constant of 2.94 mm, loss tangent of 0.0012 and thickness of substrate of 0.6mm. Fourth, optimize the antenna characteristics by adjusting the position of the meta structure on the antenna until the desired antenna requirements are satisfied. This process should be repeated until this is accomplished. The fifth step is to simulate and evaluate the outcomes. The proposed antenna is developed for the Ka-band and exhibits positive gain, favorable VSWR, enhanced bandwidth, better efficiency, and minimal return loss. Equations (1) through (5) can be used to calculate the length and width of a single antenna patch. Also, equation (6)-(7) are calculating the ground of width and length [19], [20]. Table 1 presents the proposed antenna's initial design value, and Table 2 specifies its optimal dimensions.

Step: 01: Calculation the width of the patch

$$Wp = \frac{c_0}{2f_r\sqrt{\frac{\varepsilon_r+1}{2}}} = 4.274\text{mm} \quad (1)$$

Step: 02: Calculation the effective dielectric constant

$$\varepsilon_{reff} = \frac{\varepsilon_r+1}{2} + \frac{\varepsilon_r-1}{2} \times \sqrt{\left(1+\frac{12hs}{WP}\right)} = 3.559\text{mm} \quad (2)$$

Step: 03: An extended version of the equation for length is as follows:

$$L_{ext} = \frac{c_o}{2f_r\sqrt{\varepsilon_{reff}}} = 3.18\text{mm} \quad (3)$$

Step: 04: Extension of the length of antenna of the equation

$$\Delta L = 0.412 \frac{\left(\frac{Wp}{hs}+0.264\right)(\varepsilon_{reff}+0.3)}{(\varepsilon_{reff}-0.258)\left(\frac{Wp}{hs}+0.813\right)} = 0.448\text{mm} \quad (4)$$

Step 05: Determination of the length of the antenna

$$Lp = L_{ext} - 2 \times \Delta L = 2.284\text{mm} \quad (5)$$

Step: 06: Dimensions of the antenna ground plane, encompassing its length and width:

$$L_g = 6h + L_P = 5.884\text{mm} \quad (6)$$

$$W_g = 6h + Wp = 7.874\text{mm} \quad (7)$$

Table 1. Presents the initial design value of the antenna

Parameter	W_P	L_P	L_g	W_g	Hs	ε_r	t	δ
Value(mm)	4.274	2.284	5.884	7.874	0.6	2.94	0.035	0.0012

4 Antenna Design and Performance Evaluation

For this investigation, the CST program, which is widely acknowledged as a design simulation platform for antennas, was used to achieve the results. The starting size of the various antenna sections was determined using calculations and measurements collected from a previous investigation. Figure 2 illustrates the proposed antenna design with CST software.

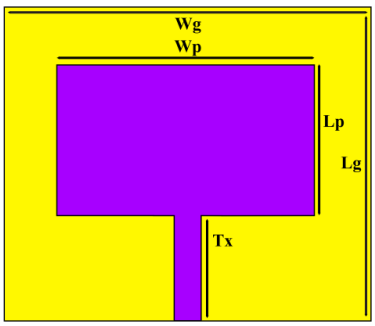

(a)Design-1

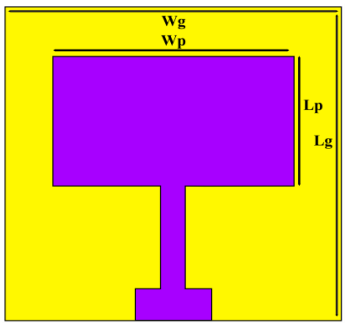

(b)Design-2

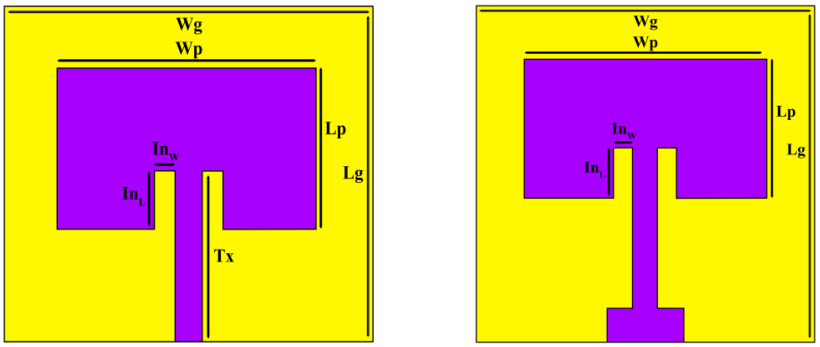

(c)Design-3 (d)Design-4

Fig. 2. Proposed design of the patch antenna utilizing CST

Table 2. The dimensions of the proposed antenna that have been optimized

Parameter	Design-1 Value (mm)	Design-2 Value (mm)	Design-3 Value (mm)	Design-4 Value (mm)
W_g	6.5	6.5	6.5	6.5
L_g	9	9	9	9
W_P	5.61	4.12	5.3	4.12
L_P	2.85	2.98	2.995	3.02
h_S	0.6	0.6	0.6	0.6
Tx_W	0.561	0.412	0.53	0.412
ε	2.94	2.94	2.94	2.94
f_W	-	1.373	-	1.373
f_L	-	1.003	-	0.996
$Inset_W$	-	-	0.176	0.1373
$Inset_L$	-	-	0.748	0.755

4.1 Reflection Coefficient

The reflection coefficient (S_{11}) quantifies the amount of power reflected from the antenna. It is an essential factor in antenna design [21]. To attain the requisite performance level, the return loss value must be less than -10 dB [22]. At 25 GHz, the reflection coefficients of antenna designs 1, 2, 3, and 4 are -11.14 dB, -19.5 dB, -14.87 dB, and -48.52 dB, respectively. Figure 3 illustrates the S_{11} parameters of antenna designs 1, 2, 3, 4.

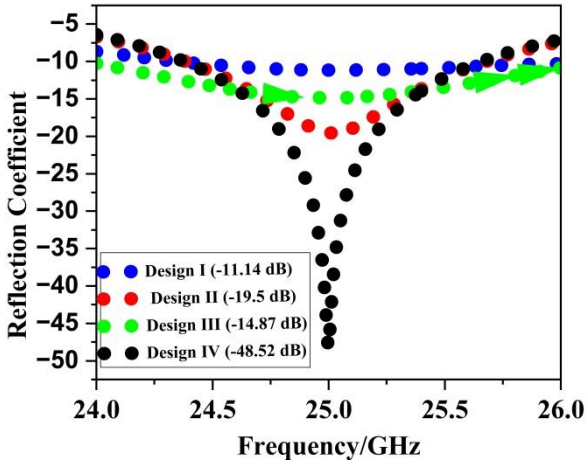

Fig. 3. Analysis of the reflection coefficients for antenna designs

4.2 Voltage Standing Wave Ratio (VSWR)

For a patch antenna, the voltage standing wave ratio (VSWR) must not exceed two throughout the full frequency range. This value should be 1 [23]. Figure 4 illustrates the VSWR graph. A VSWR of 1.767, 1.237, 1.441, and 1.007 are achieved by antenna designs 1,2, 3,4, respectively.

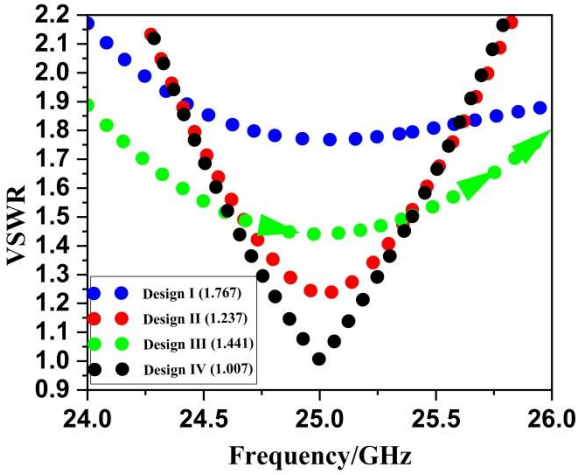

Fig. 4. Evaluation of VSWR of the antenna designs.

4.3 Radiation Pattern

A radiation pattern is a direct description of the power that an antenna possesses in space [24]. The electric field (E-field) and the magnetic field (H-field) are the two

primary components of the electromagnetic field that constitute an antenna's field of influence. Figure 5 shows an illustration at Φ=0°, which is also known as the radiation pattern's E-plane. In contrast, the arrangement under consideration, which maintains a constant angle of 90^0 and fluctuates between 0^0 and 360^0, Φ=90^0 in Figure 6, and is also referred to as the H-plane. Table 3 contains a visual representation of the properties of the simulated radiation pattern.

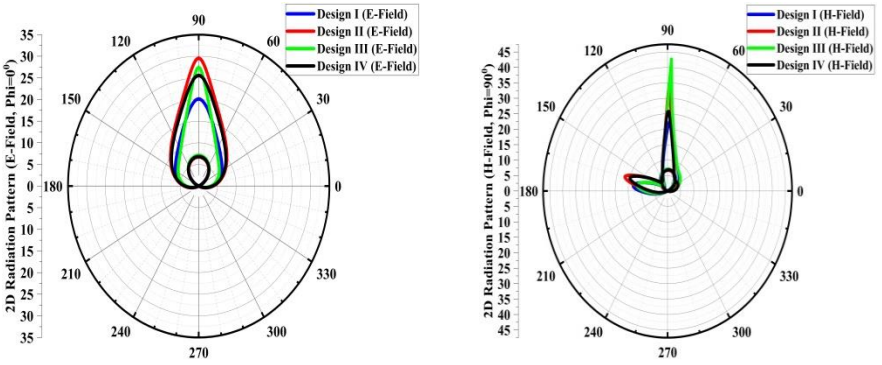

(a) (b)

Fig. 5. Radiation Pattern in Two Dimensions (Antenna Design-1, 2,3, 4)

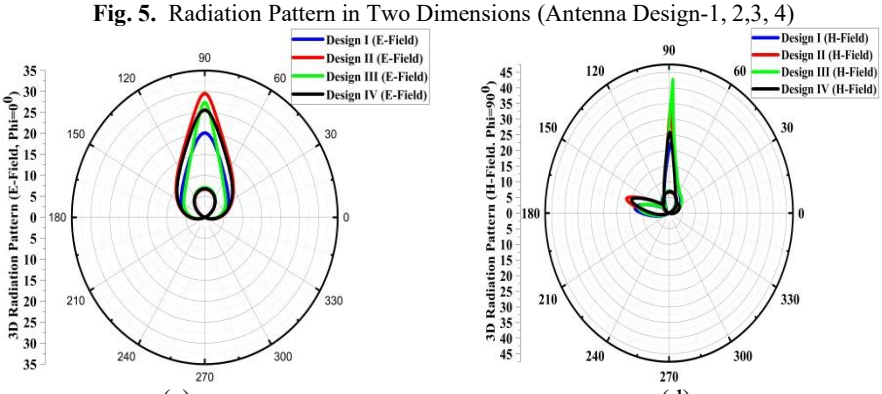

(c) (d)

Fig. 6. Radiation Pattern in three Dimensions (Antenna Design-1, 2,3, 4)

Table 3. Antenna's radiation pattern parameters

Parmeter	Design-1	Design-2	Design-3	Design-4
3dB Beamwidth (E-plane)	81.5 deg.	85.7 deg	83.2 deg	82.3 deg
Main lobe direction (E-plane)	00.0 Deg.	00.0deg	00.0 deg.	5.0 deg.
Side lobe label (E-plane)	-	-	-	-10.3 dB
3 dB Beamwidth (H-plane)	82.9 deg.	87.4 deg	77.1 deg.	82.3 deg
Main lobe direction (H-plane)	1.0 Deg.	3.0 deg	1.0 Deg.	5.0deg
Side lobe label (H-plane)	-8.6 dB	-10.2 dB	-9.2	-10.3 dB

4.4 Gain and Directivity

Gain is an essential component of patch antennas since it allows for the concentration and direction of radiated energy in particular directions. The gain is determined by the dimensions of the antenna, its configuration, the direction it faces, and the transmission frequency [24]. As Figure 7 shows, the gain of the antenna designs 1, 2, 3, and 4 is 6.13 dBi, 5.94 dBi, 6.01 dBi, and 6.22 dBi, respectively. Figure 8 also displays the directivity values for designs 1, 2, 3, and 4: 6.91 dBi, 6.71 dBi, 7.1 dBi, and 6.86, respectively.

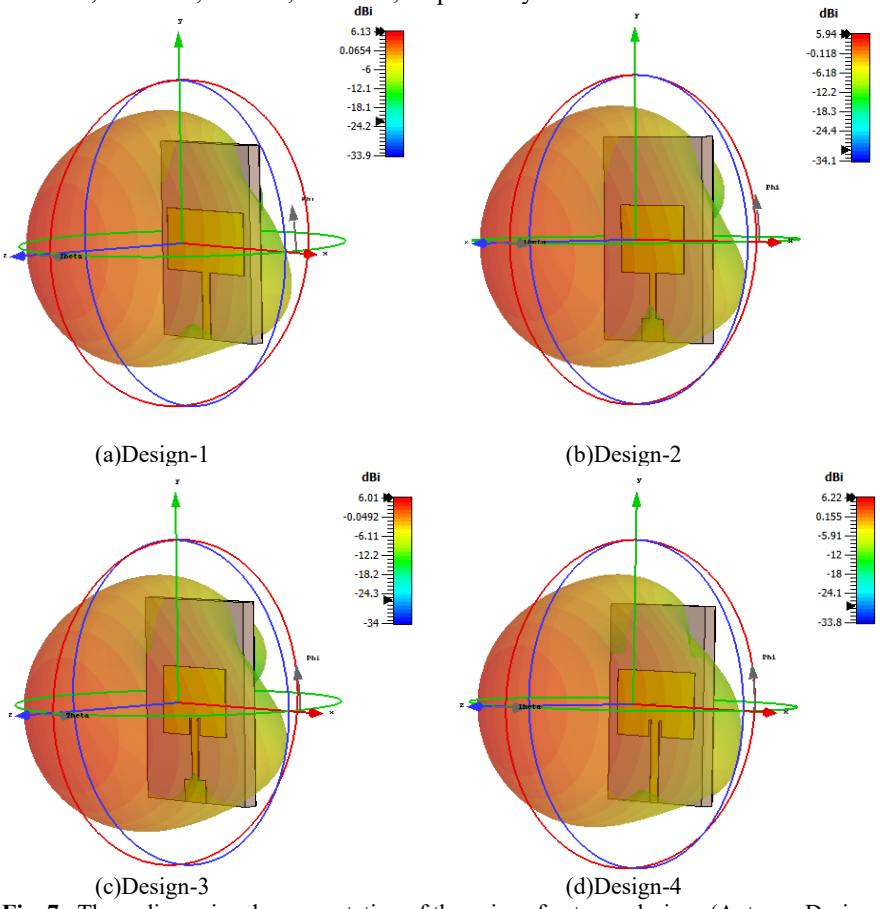

(a)Design-1 (b)Design-2

(c)Design-3 (d)Design-4

Fig. 7. Three-dimensional representation of the gains of antenna designs (Antenna Design-1, 2,3, 4)

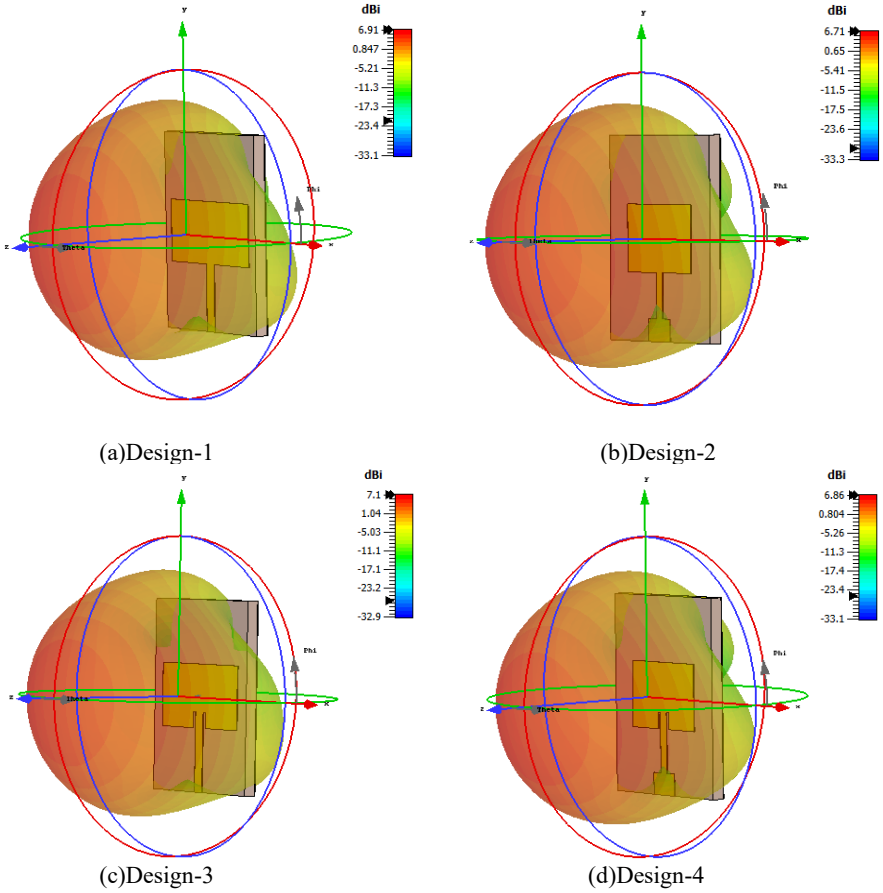

Fig.8. Three-dimensional depiction of the directivity of antenna designs (Antenna Design-1, 2,3, 4)

4.5 Impedance Matching and Smith Chart

The antenna design assumes that the power line impedance is 50Ω. At 25 GHz the input impedance values for the proposed antenna are shown in Figure 9. The Smith chart is a specialized instrument used to depict the impedance of transmission lines and antenna systems, with frequency as the variable [25]. Figure 10 represents the Smith chart included in the proposed model.

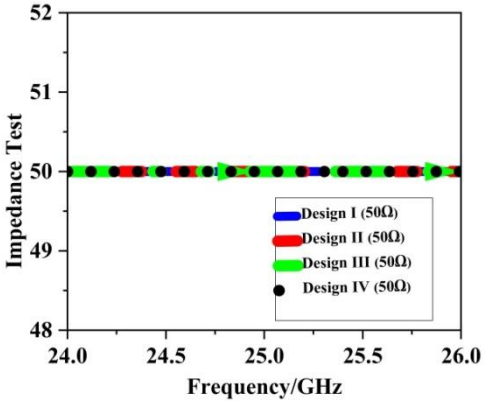

Fig. 9. Impedance matching of the antenna designs

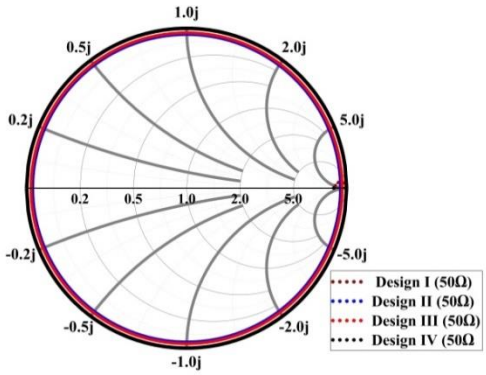

Fig. 10. Smith Chart of the designs

5 Comparative Research and Analysis

In addition to publishing many articles, researchers are also conducting active research on patch antennas. It is possible to use a variety of frequencies inside the patch antenna for the band, which is suitable for applications that include wireless communication. It was determined that the frequency of 25 GHz was ideal for any wireless 5G applications. A comprehensive presentation of the results of the proposed antenna is provided in this section. The proposed antenna's outcomes were the reflection coefficient (S_{11}), VSWR, gain, directivity, bandwidth, and efficiency. These findings are superior to those described in previously published articles and suitable for wireless applications. The proposed design's outcomes markedly surpass those of previous publications and may facilitate the advancement of viable solutions for forthcoming wireless 5G applications. Table 3 presents the results of the suggested antenna simulation with their respective results. The study is compared to previously published research, as illustrated in Table 4.

Table 3. Results of the antenna simulation that have been proposed

Parameter	Design-1	Design-2	Design-3	Design-4
Reflection coefficient (dB)	-11.14	-19.5	-14.87	-48.52
VSWR	1.76	1.23	1.44	1.007
Gain (dBi)	6.13	5.94	6.01	6.22
Directivity (dBi)	6.91	6.71	7.1	6.86
Bandwidth (GHz)	1.232	1.276	1.392	1.40
Efficiency (%)	88.71	84.05	84.6	90.67

Table 4. Comparing the proposed work to works that have already been published

Ref	Material	S_{11} (dB)	VSWR	Gain (dB)	Efficiency (%)	BW (GHz)	Applications
[23]	Rogers RT5880	-22.5	1.25	5.06	80.18	-	5G
[25]	Rogers RT5880	-48.31	1.007	7.41	91.6	1.2	5G
[26]	Rogers RT5880	-39.36	1.02	6.37	86.73	1.48	5G
[27]	Rogers RT5880	-22.24	≤2	6.84	85	0.78	5G
[28]	Rogers RT5880	-20.95	1.19	6.24	99.8	1.06	5G
[29]	Rogers-4003C	-35	-	6.5	92	1.35	5G
[30]	Rogers RT5880LZ	-57	1.005	5.13	70	-	5G
[31]	Rogers RT5880	-38.34	1.02	-	77	-	5G
[32]	FR-4	-24.507	1.12	-	-	-	5G
[33]	Rogers RT5880	≤-10	≤2	6.6	-	-	5G
This work (D-IV)	**Rogers RT6002**	**-48.52**	**1.007**	**6.22**	**90.67**	**1.40**	**5G**

6 Conclusion

Four antenna designs (Design I, II, III, and IV) utilizing a single material (Rogers RT6002) were evaluated, and their outcomes were compared. The simulation findings yielded an optimal S_{11}, standard VSWR, favorable Gain and directivity, and enhanced the antenna's efficiency. A 50-ohm feeding line is installed to supply the antenna, which is intended for use in 5G applications. 5 G brings wireless communication technology benefits such as high-speed data transfer rates, increased dependability, and large capacity. These antenna (Design-IV) performance parameters can satisfy ever-changing needs. The antenna that has been suggested is intended to function in the Ka-band for 5G applications, which will meet the requirements for wireless communication technologies in the future. The antenna's performance utilizing various substrate materials can be examined in the future, and simulated results can be compared with those of the fabricated antenna.

References

1. Younes, S., Jaouad, F. & Saidi Alaoui, K.: Enhancing terahertz patch antenna performance with metamaterials for biomedical applications. TELKOMNIKA

(Telecommunication Comput. Electron. Control. 23, 267–274 (2025).
2. Emon, E. I., Islam, A. M., Bashar, M. S. & Ahmed, A.: Performance evaluation of an optically transparent microstrip patch antenna for 5G applications using ITO and sodalime glass substrate. Comput. Electr. Eng. 114, 109073 (2024).
3. Benkhadda, K. et al.: 1×2 microstrip patch antennas array for mm-waves 5G application. TELKOMNIKA (Telecommunication Comput. Electron. Control. 23, 40–47 (2025).
4. Ahmed, M. K. et al.: Graphene-based THz antenna with a wide bandwidth for future 6G short-range communication. TELKOMNIKA (Telecommunication Comput. Electron. Control. 23, 306–315 (2025).
5. S. A. Gaid, A., M. S. Qaid, M., A. E. Abdullah, M. & Ahmed Alomari, M.: A wideband microstrip antenna employing ring and hexadecagonal slots with parasitic elements for W-band applications. TELKOMNIKA (Telecommunication Comput. Electron. Control. 23, 316–328 (2025).
6. Rabbani, M. S. & Ghafouri-Shiraz, H.:Liquid Crystalline Polymer Substrate-Based THz Microstrip Antenna Arrays for Medical Applications. IEEE Antennas Wirel. Propag. Lett. 16, 1533–1536 (2017).
7. Singh, K., Patil, S., Naik, A. & Kadam, S.: Hexagonal Microstrip Patch Antenna Design for UWB Application. ITM Web Conf. 44, 02004 (2022).
8. Alhadi Ruslan, A., Mohamad, S. Y., Abdul Malek, N. F., Yusoff, S. H. & Ibrahim, S. N.: The bending effects on the performance of a flexible circular microstrip antenna on rubber-carbon substrates at 2.45 GHz. TELKOMNIKA (Telecommunication Comput. Electron. Control. 23, 1–10 (2025).
9. Xu, H., Deng, C., Fu, Z. & Dong, R.: Compact Dual-Band Endfire Phased Array Antenna for 5G mm-Wave Mobile Terminals. Microw. Opt. Technol. Lett. 67, (2025).
10. Mishra, G. K., Pandey, H. K. & Pathak, N. P.: A Single-Layer Dual-Band SIW Filter on a Mixed Coupling Structure for 5G Applications. IETE J. Res. 1–7 (2025) doi:10.1080/03772063.2025.2489788.
11. Farahat, A. E. & Hussein, K. F. A.: 28/38 GHz MEMS-Controlled SIW Antenna for 5G Communication Systems. Microw. Opt. Technol. Lett. 67, (2025).
12. Ullah, H. & Tahir, F. A.: A broadband wire hexagon antenna array for future 5G communications in 28 GHz band. Microw. Opt. Technol. Lett. 61, 696–701 (2019).
13. Kouser, K., Hannan, M., Shafi, F. & Aknan, M.: Design and Characterization of a Ka-Band Parasitic Patch Antenna for 5G Applications. in 2024 9th International Conference on Communication and Electronics Systems (ICCES) 661–668 (2024).
14. Alaoui, N., Ben melouka, R. I., Mekhatria, M. R. & Titouh, I.: High-performance 38 GHz millimeter wave antenna for 5G wireless application. Int. J. Inf. Technol. (2025)
15. Janarthanan, S. & Bennet, M. A.: Advanced Miniaturized Microstrip Patch Antenna Design for High-Efficiency 5G Applications. Meas. Sci. Rev. 24, 239–243 (2024).
16. Qureshi, M. J. U., Das, D. & Hossain, M. A.: Design and Performance Analysis of a Broadband Microstrip Patch Antenna for 5G Applications. in 2024 3rd International Conference on Advancement in Electrical and Electronic Engineering (ICAEEE) 1–6 (2024).
17. Nafea, S. N. & Khamiss, N. N.: For 5G applications, high-gain patch antenna in Ka-Band. Indones. J. Electr. Eng. Comput. Sci. 31, 802–809 (2023).
18. Shamim, S. M., Dina, U. S., Arafin, N. & Sultana, S.: Design of Efficient 37 GHz Millimeter Wave Microstrip Patch Antenna for 5G Mobile Application.

Plasmonics 16, 1417–1425 (2021).
19. C. A. Balanis.: Antenna Theory: Analysis Design. Third Edition, Hoboken, New Jersey.
20. Youssef, A., Halkhams, I., El Alami, R., Jamil, M. O. & Qjidaa, H.: Study and Design of a Microstrip Patch Antenna Array for 2.4 GHz Applications. in Digital Technologies and Applications, Lecture Notes in Networks and Systems 309–317 (2023).
21. Hossain Nirob, J. et al.: Dual-band MIMO antenna for wideband THz communication in future 6G applications. TELKOMNIKA (Telecommunication Comput. Electron. Control. 23, 295–305 (2025).
22. Singh Sawaran Singh, N. et al.: Dual band antenna design for 4G/5G application and prediction of gain using machine learning approaches. TELKOMNIKA (Telecommunication Comput. Electron. Control. 23, 543–552 (2025).
23. Przesmycki, R., Bugaj, M. & Nowosielski, L.: Broadband Microstrip Antenna for 5G Wireless Systems Operating at 28 GHz. Electronics 10, 1–19 (2020).
24. Haque, M. A. et al.: High-bandwidth millimetre wave multiple-input multiple-output antenna for 38 GHz 5G mobile applications. TELKOMNIKA (Telecommunication Comput. Electron. Control. 23, 283–294 (2025).
25. Mahbub, F. et al.: A Single-Band 28.5GHz Rectangular Microstrip Patch Antenna for 5G Communications Technology. in 2021 IEEE 11th Annual Computing and Communication Workshop and Conference (CCWC) 1151–1156 (2021).
26. Kaeib, A. F., Shebani, N. M. & Zarek, A. R.: Design and Analysis of a Slotted Microstrip Antenna for 5G Communication Networks at 28 GHz. in 2019 19th International Conference on Sciences and Techniques of Automatic Control and Computer Engineering (STA) 648–653 (2019).
27. Khan, J. et al.: Design of a Millimeter-Wave MIMO Antenna Array for 5G Communication Terminals. Sensors 22, 2768 (2022).
28. Didi, S.-E. et al.: Design of a microstrip antenna patch with a rectangular slot for 5G applications operating at 28 GHz. TELKOMNIKA (Telecommunication Comput. Electron. Control. 20, 527–536 (2022).
29. Fernandez, M. D., Herraiz, D., Herraiz, D., Alomainy, A. & Belenguer, A.: Dielectricless Floating-Patch Antenna at 28 GHz Fed With an Empty Substrate Integrated Waveguide. IEEE Access 11, 65599–65607 (2023).
30. Rana, M. S., Hasan, M. N., Faisal, M. & Khan, M. E.: Design of high gain and wideband circular patch antenna based on DGS for 28 GHz 5G applications. TELKOMNIKA (Telecommunication Comput. Electron. Control. 22, 1053–1060 (2024).
31. Rana, M. S. & Rahman Smieee, M. M.: Design and analysis of microstrip patch antenna for 5G wireless communication systems. Bull. Electr. Eng. Informatics 11, 3329–3337 (2022).
32. Rana, M. S. et al.: Design of 28 GHz Microstrip Patch Antenna for Wireless Applications. Indones. J. Electr. Eng. Informatics 11, 967–977 (2023).
33. Singh, A., Kumar, A. & Kanaujia, B. K.: MIMO antenna with improved isolation for 5G millimeter wave applications. Eng. Res. Express 7, 015302 (2025).

Harnessing the wildlife animal detection using proposed CNN and ResNet50 deep learning model

*Suman Chowdhury[1], Dilip Kumar Das[2]
[1] Department of Electrical and Electronic Engineering,International University of Business Agriculture and Technology, Dhaka-1230, Bangladesh
[1*]suman@iubat.edu
[2]Department of Mathematics, International University of Business Agriculture and Technology, Dhaka-1230, Bangladesh
[2]dilipkdas@iubat.edu

* Corresponding Author

Abstract. This research study has explored the deep learning models- CNN and ResNet50- for harnessing the animal species' detection process. In this study, three categories of animals- dogs, cats and foxes- are taken for the image processing dataset. Total three hundred and eight images are taken for the training and validation dataset. Twenty percent of data has been reserved for the validation purpose. For the analysis of performance by these two models, classification report and confusion matrix have been generated. From the overall performance it is found that ResNet50 has a better performance in detecting the animal species correctly than the CNN model. The CNN has given an overall validation accuracy of 56% whereas the ResNet50 has provided the validation accuracy score of 97% as maximum. Furthermore the maximum f1 score of 98% obtained by ResNet50 deep learning model has proven its effective skill in detection process.

Keywords: CNN, ResNet50, model, animal, loss, accuracy

1 Introduction

Due to the expanding population, the nature of the planet is degrading in a rapid sequence as a result lives of many animals are at risk of extinction. Animals' lives are very essential for the ecosystem and biodiversity of the world. Measuring population size of animal is very important for protection or survival of animal [1]. Many methods are practicing in that respect, some of them are costly. Remote sensing imagery, visual detections are most common techniques for animal detection [2-5]. Beside the automated techniques traditional machine learning techniques are also used for detecting animal. Deep learning is a higher Neural Network (NN) that can process the data into a particular output [6, 7]. It can identify the Deep Neural Networks (DNN) identifies the camera images successfully [8]. Deep learning method, Convolution Neural Network (CNN) is

one of the most used and accepted algorithm in detecting the animals and their nature [9]. CNN is normally formatted as different layers where the primary layer is processing the feature reading and in the last layer it classifies. CNN can be used to detect complicated and rowdy imagery [10]. Using CNN in a big dataset it is possible to obtain the prediction like human-brain accuracy [11].
Detection of animal is essential not only for saving of wild life but also reduce the vehicle accident caused by movement of animal [12]. Accident in the highway is increasing alarmingly. It is found in a research that 475 million animals are died every year in Brazilian highway [13]. This research study has tried to investigate the detection criteria of the wildlife animals so that necessary for categorized animals can be taken with immediate posture. For this purpose CNN and Resnet50 deep learning models have been implemented for the possible outcome.

2 Literature review

Binta Islam et al. found self trained model CNN 72%, VGG16 and Resnet50 87% and 86% accuracy respectively. This showed good result in identifying the species of certain animals [14]. H. Nguyen et al. achieved 96.6% accuracy in animal image detection by Convolution Neural Network [15]. Banupriya N et al. proposed that automatically identifying of animal movement is desirable as manual identification is a huge job [16]. Saxena et al. proposed a SSD and faster R-CNN model that detects the 25 different animals from 13000 images [17]. Biodiversity is rapidly decreasing on a global scale, leading to numerous adverse effects on overall quality of life [18]. The most recent Living Planet Report from the World Wildlife Fund (WWF) revealed that, on average, populations of mammals, birds, amphibians, reptiles, and fish have shrunk by 68% between 1970 and 2016 [19]. Nevertheless, tracking worldwide biodiversity changes continues to be a significant challenge due to the absence of universally accepted data standards and assessment criteria [20]. A pivotal development in biodiversity monitoring is the Essential Biodiversity Variables (EBV) framework, formulated by the Group on Earth Biodiversity Observation Network (GEO BON). This initiative aims to encapsulate the intricate nature of biodiversity into a concise set of critical metrics for more effective assessment and analysis [21]. The population dynamics of species constitute one of the most primordial and critical variables for monitoring, a stance affirmed by the EBV framework and further substantiated by subsequent scholarly investigations [22-25].

3 Methodology

The animal images for this study were sourced from the Kaggle online platform. This dataset contains three categories of images: cats, dogs, and foxes. The dataset was uploaded to Google Drive, from where it was accessed using the Google Colab environment. Initially, a specific file path was defined to retrieve the images for processing. Each image was converted to grayscale to ensure compatibility with the CNN model. The images were then resized to 224x224 pixels with a single channel. Following this, the pixel values were normalized by dividing each value by 255. These preprocessed images were subsequently converted into a NumPy array, where the image data was assigned to the variable X and their corresponding class labels were assigned to the variable y. The dataset was split into training and validation subsets, with 20% of the data reserved for validation. This processed data was fed into a CNN architecture for training. The model was trained over 20 epochs, and key metrics, including training loss, validation loss, training accuracy, and validation accuracy, were recorded and stored in a history file. These metrics were visualized using graphs to compare training and validation losses as well as training and validation accuracies. A classification report was generated to evaluate the model's performance comprehensively. Metrics such as F1-score, recall, precision, accuracy, macro average, and weighted average were computed. Additionally, a confusion matrix was utilized to analyze the classification accuracy of the model. The same dataset was also applied to the ResNet50 deep learning model. Unlike the CNN model, ResNet50 requires images with three color channels and therefore cannot process single-channel grayscale images. Both models employed ReLU and Softmax activation functions for their layers, ensuring effective feature extraction and classification during the training process.

4 Result Analysis

The images of animals are taken from the Kaggle website. The samples are taken in three categories- cats, dogs, and foxes. Figure 1 presents the samples of the three animal categories. A good number of different positioned along with different animals with same species are taken for well training purpose. Twenty percent of total images are taken for testing purpose so that it can be assured that the machine has learned well.

Figure 1: Samples of cats, dogs and foxes

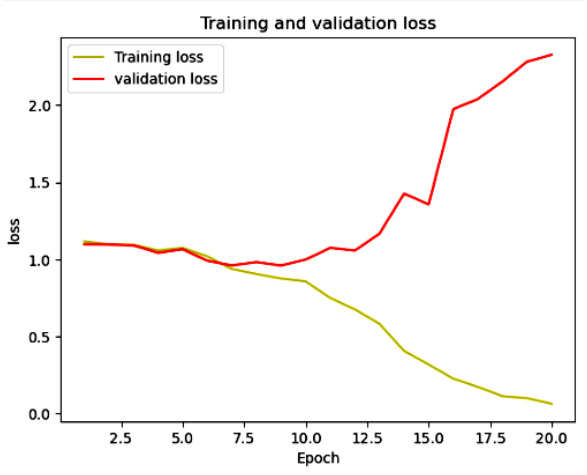

Figure 2: Loss profile for CNN

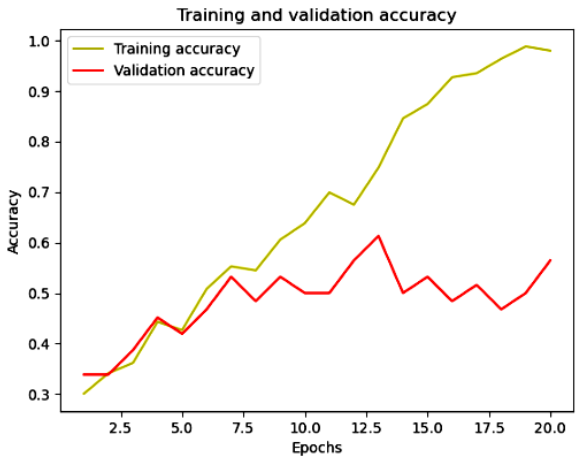

Figure 3: Accuracy profile for CNN

Figure 2 represents the loss profile for training and validation data set against of 20 epochs. From this figure it is observed that the training loss and validation loss are going parallel way with progress of 10 epochs. After this tenth epoch of performance the validation loss has been increased above the training loss. This loss profile has been recorded for the Convolution neural network. The validation loss incurred by CNN is 2.3252 as maximum and 0.9615 as the minimum. And, the training loss occurred by CNN is 1.1196 as maximum loss wheras it is 0.0578 as minimum loss. In addition, the figure 3 represents the training and validation accuracy profile. From this figure, it is found that both training and validation accuracy are increased parallel upto the seventh of iterations. After this seventh of iterations validation accuracy almost goes saturation with some ripples, but the training accuracy increments sharply to the optimum of around 98%. In the same time the validation accuracy reaches to the maximum of 56% around.

Table 1: Classification report for CNN

	Precision	recall	F1-score	support
0	0.50	0.55	0.52	20
1	0.62	0.48	0.54	21
2	0.58	0.67	0.62	21

accuracy			0.56	62
Macro avg	0.57	0.56	0.56	62
Weighted avg	0.57	0.56	0.56	62

Table 1 is presenting the classification report for the CNN model obtained from 20 epochs of performance. In the classification report cats, dogs and foxes are categorized as 0, 1, 2 respectively. The precision score is obtained maximum as 0.62 for the level of 1 indicating the true positive percentage as the prediction capability over the true positive and false positive cases in total. Similarly, the recall score is obtained maximum as 0.67 for the level of 2 indicating the true positive percentage as the prediction capability over the true positive and false negative cases in total. On top of this, f1 score is obtained maximum as 0.62 for the level of 2 emphasizing the importance of precision and recall score. Total twenty one cases are supported for the level of 2 in the case of f1 score for the testing data. And the overall accuracy is shown as 56% for the total case of 62 as the validation data set. The macro avg precision score is obtained as 0.57 at the maximum level out of other macro avg recall and macro avg f1 score. This macro avg precision is presenting the average of three individual precision scores of all levels. Furthermore, the weighted avg precision is also same as 0.57 as maximum than the other weighted avg recall and weighted avg f1 score. This weighted avg precision score is obtained taking consideration of individual cases of each level on average. In this weighted avg precision each precision score of each level is multiplied with number of cases of that level. In this way all multiplications for each level is added and divided by total number of cases.

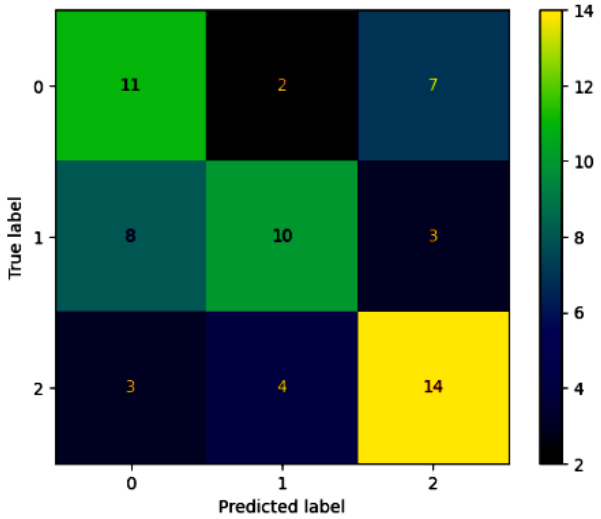

Figure 4: Confusion matrix for CNN

Figure 4 presents the confusion matrix for the CNN model indicating the performance by this deep learning model. From this confusion matrix, it is found that 11 cases are successfully predicted as zero level by this CNN model, but two cases are wrongly detected as level of one, which should be zero level and seven cases are wrongly attributed as level of two, which should be level of zero. On the other hand, the ten cases are rightly predicted as level of one, whereas eight cases are wrongly attributed as level of zero and three cases are attributed as level of two. Finally fourteen cases are correctly predicted as level of two, whereas three cases are incorrectly attributed as level of zero and four cases are falsely attributed as level of one.

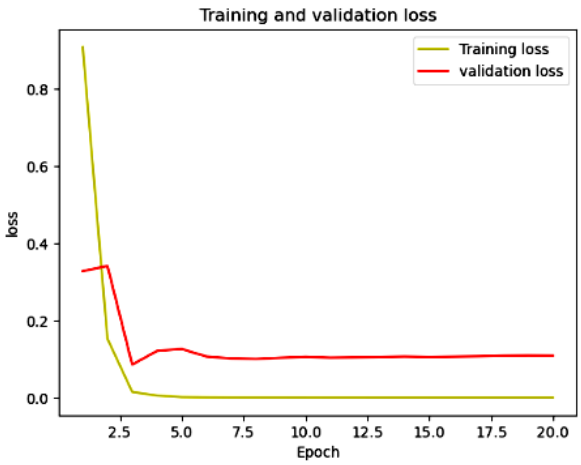

Figure 5: Loss profile for ResNet50

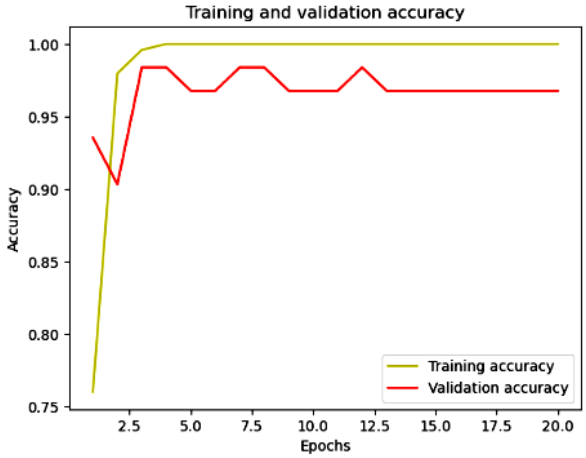

Figure 6: Accuracy profile for ResNet50

Figure 5 represents the loss profile for training and validation data set against of 20 epochs for the ResNet50 deep learning model. From this figure it is observed that the training loss and validation loss are going downward directions with progress of around three epochs. After this third epoch of performance the validation loss has been saturately increased above the training loss. This loss profile has been recorded for the renet50 transfer learning model. The validation loss incurred by this model is 0.3414 as maximum and 0.0857 as the minimum. And, the training loss occurred by ResNet50 model is 1.5682 as maximum loss

wheras it is 0.0002 as minimum loss. In addition, the figure 6 represents the training and validation accuracy profile for ResNet50 model. From this figure, it is found that both training and validation accuracy are increased parallel upto the third of iterations. After this third of iterations validation accuracy almost goes saturation with some ripples, but the training accuracy increments saturately above of validation accuracy to the optimum of around 100%. In the same time the validation accuracy reaches to the maximum of 97% around.

Table 2: Classification report for ResNet50

	Precision	recall	F1-score	support
0	0.95	0.95	0.95	20
1	0.95	1.00	0.98	21
2	1.00	0.95	0.98	21
accuracy			0.97	62
Macro avg	0.97	0.97	0.97	62
Weighted avg	0.97	0.97	0.97	62

Table 2 presents the classification report for the ResNet50 model after 20 epochs of training and evaluation. In this report, the categories of cats, dogs, and foxes are labeled as 0, 1, and 2, respectively. The precision score reaches its highest value of 1.00 for category 2, indicating a perfect prediction rate for true positive cases in relation to the sum of true positive and false positive cases. Similarly, the recall score also achieves a maximum of 1.00 for category 1, demonstrating perfect sensitivity in predicting true positives relative to the total of true positive and false negative cases. The minimum F1 score, a harmonic mean of precision and recall, is recorded at 0.95 for category 0. This score underscores the balance between precision and recall for this category. For the testing dataset, category 2 and category 1 each account for 21 cases, contributing significantly to the calculation of F1 scores. Overall, the model achieves an impressive accuracy of 97% on the validation dataset, which consists of 62 cases. Regarding macro averages, the

precision score stands out with a value of 0.97, the highest among the macro-averaged metrics. This metric represents the unweighted mean of precision scores across all categories, treating each category equally regardless of its size. Similarly, the weighted average precision also scores 0.97, reflecting the influence of the sample size of each category on the average. In calculating the weighted average precision, the precision score for each category is multiplied by the number of cases in that category, and the results are summed before dividing by the total number of cases. This ensures that categories with a larger number of cases have a proportional impact on the overall precision score.

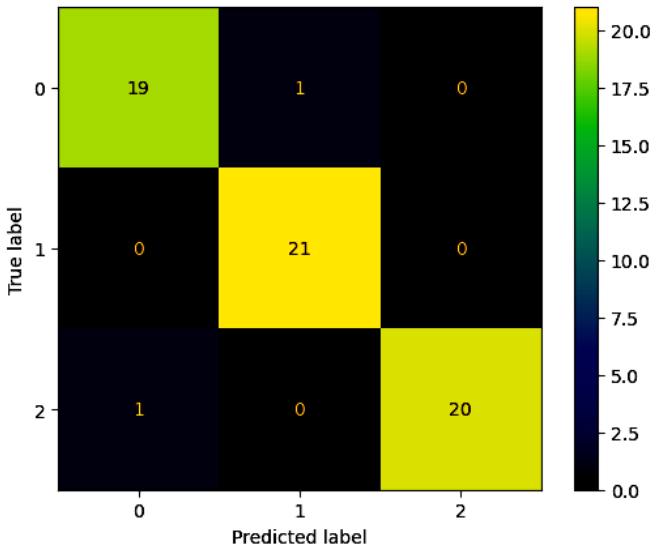

Figure 7: Confusion matrix for ResNet50

Figure 7 presents the confusion matrix for the ResNet50 model indicating the performance by this transfer learning model. From this confusion matrix, it is found that 19 cases are successfully predicted as zero level by this CNN model, but one case is wrongly detected as level of one, which should be zero level and not a single case is wrongly attributed as level of two, which should be level of zero. On the other hand, the twenty one cases are rightly predicted as level of one, whereas no cases are wrongly attributed as level of zero and two. Finally twenty cases are correctly predicted as level of two, whereas only one case is incorrectly attributed as level of zero and not a single case is falsely attributed as level of one.

5 Conclusion

The study demonstrates the effectiveness of both CNN and ResNet50 models in classifying animal images into three categories: cats, dogs, and foxes. The preprocessing steps, including grayscale conversion and resizing for CNN, and three-channel input for ResNet50, ensured model compatibility and optimal performance. The evaluation metrics and visualization of training dynamics provided valuable insights, with the models achieving high accuracy and robust classification performance. These results highlight the potential of deep learning architectures in image classification tasks and pave the way for further optimization and application in broader datasets or related domains. The highest precision score 0f 97% obtained by ResNet50 deep learning model indicates that this model has better performance in predicting the animal species more accurately than the CNN model.

Acknowledgements

We are thankful to our honorable authority of IUBAT for good cooperation in conducting this research.

References

1. 1 Harris, G., Thompson, R., Childs, J. L., & Sanderson, J. G. (2010). Automatic Storage and Analysis of Camera Trap Data. Bulletin of the Ecological Society of America, 91(3), 352–360. http://www.jstor.org/stable/bullecosociamer.91.3.352
2. Stapleton, S., LaRue, M., Lecomte, N., Atkinson, S., Garshelis, D., Porter, C., & Atwood, T. (2014). Polar Bears from Space: Assessing Satellite Imagery as a Tool to Track Arctic Wildlife. PLOS ONE, 9(7), e101513. https://doi.org/10.1371/journal.pone.0101513
3. Hodgson, J. C., Baylis, S. M., Mott, R., Herrod, A., & Clarke, R. H. (2016). Precision wildlife monitoring using unmanned aerial vehicles. Scientific Reports, 6(1), 1-7. https://doi.org/10.1038/srep22574
4. Bowler E, Fretwell PT, French G, Mackiewicz M. Using Deep Learning to Count Albatrosses from Space: Assessing Results in Light of Ground Truth Uncertainty. Remote Sensing. 2020; 12(12):2026. https://doi.org/10.3390/rs12122026
5. Richard Lamprey, Frank Pope, Shadrack Ngene, Michael Norton-Griffiths, Howard Frederick, Benson Okita-Ouma, Iain Douglas-Hamilton,Comparing an automated high-definition oblique camera system to rear-seat-observers in a wildlife survey in Tsavo, Kenya: Taking multi-species aerial counts to the next level, Biological Conservation,Volume 241, 2020, 108243, ISSN 0006-3207,

https://doi.org/10.1016/j.biocon.2019.108243.
6. Rosebrock, A. Deep Learning for Computer Vision with Python: Starter Bundle, 3rd ed.; PyImageSearch: USA, 2019.
7. Wäldchen, J., & Mäder, P. (2018). Machine learning for image based species identification. Methods in Ecology and Evolution, 9(11), 2216-2225. https://doi.org/10.1111/2041-210X.13075
8. Norouzzadeh, M. S., Nguyen, A., Kosmala, M., Swanson, A., Palmer, M. S., Packer, C., & Clune, J. (2018). Automatically identifying, counting, and describing wild animals in camera-trap images with deep learning. Proceedings of the National Academy of Sciences of the United States of America, 115(25), E5716. https://doi.org/10.1073/pnas.1719367115
9. LeCun, Y., Bengio, Y. & Hinton, G. Deep learning. Nature 521, 436–444 (2015). https://doi.org/10.1038/nature14539
10. Ibraheam, M., Gebali, F., Li, K.F., Sielecki, L. (2020). Animal Species Recognition Using Deep Learning. In: Barolli, L., Amato, F., Moscato, F., Enokido, T., Takizawa, M. (eds) Advanced Information Networking and Applications. AINA 2020. Advances in Intelligent Systems and Computing, vol 1151. Springer, Cham. https://doi.org/10.1007/978-3-030-44041-1_47
11. Géron, A. (2022). Hands-on machine learning with Scikit-Learn, Keras, and TensorFlow. " O'Reilly Media, Inc.".
12. Antônio, W. H. S., Da Silva, M., Miani, R. S., & Souza, J. R. (2019). A Proposal of an Animal Detection System Using Machine Learning. Applied Artificial Intelligence, 33(13), 1093–1106. https://doi.org/10.1080/08839514.2019.1673993
13. De, Indrajit, and J. Sil. “Entropy based fuzzy classification of images on quality assessment.” Journal of King Saud University - Computer and Information Sciences, vol. 24, no. 2, Jul. 2012, pp. 165-173. https://doi.org/10.1016/j.jksuci.2012.05.001
14. Binta Islam, S., Valles, D., Hibbitts, T. J., Ryberg, W. A., Walkup, D. K., & Forstner, M. R. (2022). Animal Species Recognition with Deep Convolutional Neural Networks from Ecological Camera Trap Images. Animals, 13(9), 1526. https://doi.org/10.3390/ani13091526
15. H. Nguyen et al., "Animal Recognition and Identification with Deep Convolutional Neural Networks for Automated Wildlife Monitoring," 2017 IEEE International Conference on Data Science and Advanced Analytics (DSAA), Tokyo, Japan, 2017, pp. 40-49, doi: 10.1109/DSAA.2017.31
16. Banupriya N, Saranya S, Swaminathan R, Harikumar S, Palanisamy S (2020) Animal detection using deep learning algorithm. J Crit Rev. https://doi.org/10.31838/jcr.07.01.85 (ISSN- 2394-5125)
17. Saxena A, Gupta DK, Singh S (2021) An animal detection and collision avoidance system using deep learning. In: Hura G, Singh A, Siong Hoe L (eds) Advances in communication and computational technology. Lecture notes in electrical engineering, vol 668. Springer, Singapore. https://doi.org/10.1007/978-981-15-5341-7_81
18. Pörtner, Hans-Otto, Robert J. Scholes, John Agard, R. Leemans, Emma Archer,

Xuemei Bai, David Barnes et al. "IPBES-IPCC co-sponsored workshop report on biodiversity and climate change." (2021). https://doi.org/10.5281/zenodo.5101133

19. Almond, Rosamund EA, Monique Grooten, and Tom Peterson. Living Planet Report 2020-Bending the curve of biodiversity loss. World Wildlife Fund, 2020.
20. Turak, E., Brazill-Boast, J., Cooney, T., Drielsma, M., DelaCruz, J., Dunkerley, G., Fernandez, M., Ferrier, S., Gill, M., Jones, H. and Koen, T., (2017). Using the essential biodiversity variables framework to measure biodiversity change at national scale. Biological Conservation, 213, pp.264-271.https://doi.org/10.1016/j.biocon.2016.08.019
21. Pereira, H.M., Ferrier, S., Walters, M., Geller, G.N., Jongman, R.H., Scholes, R.J., Bruford, M.W., Brummitt, N., Butchart, S.H., Cardoso, A.C. and Coops, N.C., (2013). Essential biodiversity variables. Science, 339 (6117), pp.277-278. https://doi.org/10.1126/science.1229931
22. Skidmore, A.K., Pettorelli, N., Coops, N.C., Geller, G.N., Hansen, M., Lucas, R., Mücher, C.A., O'Connor, B., Paganini, M., Pereira, H.M. and Schaepman, M.E., (2015). Environmental science: Agree on biodiversity metrics to track from space. Nature, 523(7561), pp.403-405. https://doi.org/10.1038/523403a
23. Skidmore, A.K., Coops, N.C., Neinavaz, E., Ali, A., Schaepman, M.E., Paganini, M., Kissling, W.D., Vihervaara, P., Darvishzadeh, R., Feilhauer, H. and Fernandez, M., (2021). Priority list of biodiversity metrics to observe from space. Nature ecology & evolution, 5(7), pp.896-906. https://doi.org/10.1038/s41559-021-01451-x
24. Jetz, W., McGeoch, M.A., Guralnick, R., Ferrier, S., Beck, J., Costello, M.J., Fernandez, M., Geller, G.N., Keil, P., Merow, C. and Meyer, C., (2019). Essential biodiversity variables for mapping and monitoring species populations. Nature ecology & evolution, 3(4), pp.539-551. https://doi.org/10.1038/s41559-019-0826-1
25. McRae, L., Deinet, S. and Freeman, R., (2017). The diversity-weighted living planet index: controlling for taxonomic bias in a global biodiversity indicator. PloS one, 12(1), p.e0169156. https://doi.org/10.1371/journal.pone.0169156

Cyber Defense with Predictive Analysis and Compliance Using LSTM and Swarm Intelligence in Indian Cyberspace

Bakare, R.[1], Sarvade, S.[2]

[1,2] Nagesh Karajagi Orchid College of Engineering and Technology, Solapur, India
[1]revan.bakare@gmail.com, [2]samarthsarvade3@gmail.com

Abstract. Existing global threat intelligence systems are insufficient for the defense needs of Indian organizations and critical infrastructure due to technical and regulatory obstacles and local requirements. A real-time cyber threat intelligence dashboard designed specifically for India's cybersecurity environment uses automated prediction analytics together with automatic compliance solutions. Real-time monitoring takes place through multilingual natural language processing by which the system retrieves ethical data from multiple sources such as Indian Computer Emergency Response Team (CERT-In) advisories, dark web forums along with regional news outlets and IoT networks. Swarm intelligence algorithms and Long Short-Term Memory (LSTM) networks enable the development of an anomaly detection system which achieves 85% accuracy for detecting anomalies together with predicting attack patterns. The system meets Indian legal standards because it operates incident reporting automatically and stores evidence securely. Breach detection speed increased by 52% in the system which produced 72% fewer incorrect alerts according to National Crime Records Bureau (NCRB) cybercrime data and healthcare and smart grid network assessment results that followed global standards. The three main components in which cyber resilience increased are monitoring real-time threats, predictive strategies and adaptive networks are essential for strong cyber resilience.

Keywords: Cybersecurity Analysis, Machine Learning, Long Short-Term Memory (LSTM), Natural Language Processing (NLP), Swarm Intelligence.

1 Introduction

The fast embrace of digital technologies across critical infrastructure and government services together with financial systems by India has elevated the country to worldwide innovation status. Two cases which states the need for proactive India specific security measures includes ransomware attack at AIIMS in 2022 and 2023 beach where 300 million telecom users' data was compromised [6]. The security breaches affect critical systems and decrease community trust because 74% of citizens fail to identify phishing attempts and 68% of SMEs lack proper cybersecurity measures in place. Organizations like Splunk and IBM X-Force use Western infrastructure standards that fail to protect India from local threats targeting Unified Payments

Interface and Aadhaar datasets and Internet of Things facilities [3]. The advisory services from Indian Computer Emergency Response Team (CERT-In) exist but, they don't provide advanced predictive abilities or systems to support immediate decisions [9]. A dashboard using real-time cyber threat intelligence along with predictive analytics functions as the proposed answer to face specific Indian cybersecurity issues. Multiple information resources from CERT-In alerts are combined with local news and the dark web as well as crime records using Natural Language Processing (NLP) technology through ethical methods of web data extraction [5]. Data encompasses both phishing attacks and ransomware threats evaluated on essential facilities allowing the development of models to identify incoming threats. The control panel helps understand predictions of 85% precise attack to let user perform timely informed decisions through geographic and sectoral visual threat displays. Through their efforts the municipal corporation of Chennai tracks DDoS threats against their smart water network infrastructure and simultaneously rural businesses receive payment threat alerts through geographical notifications [2].

The platform integrates Indian law and policy standards with features that execute Section 66F IT Act and CERT-In directive requirements automatically [12], [14]. The platform enables users to file reports about incidents while helping them preserve evidence and refer them to legal options thus linking detection with response capabilities. The system develops cybersecurity awareness by providing small educational lessons in native languages that outline dangers like unauthorized Aadhaar link access or artificial government text messages.

The research aimed to develop and test India's first framework for predictive analytics, swarm intelligence. It deals with country specific issues, contributes the following:

1. Real-time analysis implemented through the Threat Intelligence Framework decreases the detection time for simulated IoT breaches in Indian databases by 52%.
2. The automation system under Policy Aware functions by linking machine learning with legal principles thus letting users without technical backgrounds follow Indian regulatory requirements during cyber attacks.
3. The implementation of Cyber Resilience in emerging markets combines socially sensitive technology with scalability to ensure practical use by both metropolitan enterprises and small rural businesses.

The platform uses National Crime Records Bureau (NCRB) cybercrime reports together with Indian smart grids and healthcare network case studies to validate its effectiveness and demonstrates how localized user specific design turns cybersecurity from an expense into an opportunity for digital growth. Emerging economies can use models to protect their cyber space and digital growth as defence through this research.

2 Related Works

Modern cybersecurity attacks require amalgamating data from multiple sources in order to achieve full security comprehension. A topic modeling approach of recent studies confirms that researchers dedicated their work mainly to analyze malware and ransomware challenges and their mitigation approaches starting from 2020 thus

highlighting the crucial need for extensive data analysis [1]. India along with other developing economies experience limited success in integrating ethical web scraping technology with NLP to receive real-time Indicators of Compromise (IoCs) from forums and articles [5]. System architecture of predictive analytics depends upon deep learning (DL) and machine learning (ML) models for its operational base. Application of LSTM network structures with swarm intelligence algorithms enables researchers to achieve strong performance in identifying IoT-based smart city attack patterns [2]. Research done in [3,10] shows that ensemble models made threat detection more precise when they merged LSTM and DNN and ELM optimized by HHO however it remains difficult to execute such systems at cloud edge in real-time cyber physical systems. SSecurity analysts determined that current cybersecurity defenses are insufficient to address Distributed Denial of Service (DDoS) and phishing attacks in their reviews yet they support integrating ML, DL and blockchain technologies but concede that attackers can easily circumvent static monitoring approaches [4]. A continuous digital transformation in India elevates security perils throughout banking and healthcare sectors which suffer from outdated operations that create major entry points for ransomware attacks based on 2020-2024 analytical data [6]. Blockchain together with cryptographic measures provide data manipulation protection systems that secure IoT-based communication for smart grids [11, 16]. The current tools lack precision when it comes to predicting threats within domestic boundaries because scholars have focused on studying new tools only minimally. India lacks proper development of specialized assessments and data encryption for securing cross-border movement despite needing such cybersecurity measures for integrated supply chain operations [7].

The IT Act and CERT-In directives serve as basic legal structures for India although they fail to address both complicated international cybercrimes and state-sponsored cyberattacks explicitly [12,14]. AI in space technology creates identical ethical problems that leave regulatory gaps which need flexible policy frameworks to address specific situations as noted in [8]. The use of causal graph-based risk analysis techniques seeks to control and support better decisions through newly adopted policies [18]. The security benefits that blockchain provides to cryptocurrency networks against network attacks have not been sufficiently documented for applying this technology to safeguard essential Indian infrastructure components like IoT-based agricultural systems and railway networks [20,21,22]. Although SIEM systems exhibit superior performance in attack classification they do not provide sector-specific risk mitigation strategies that would guide administrators in their decision-making [23]. Organizations struggle to execute preventive measures against new attack methods when running AI-based anomaly detection cyber-analytics platforms which operate with real-time data collection [9]. The field of digital forensics uses automated systems for dataset management as its primary advancement method yet these mechanisms only occasionally link to active threat intelligence networks [17].

Thorough research reports confirm both cyber threats and physical threats unite through social engineering vulnerabilities and IoT flaws which force organizations to unite defense systems with employee training programs and new security policies [15]. Statistical models do not provide sufficient theoretical value regarding cyber-attack

trends to demonstrate real-time operative capability [13]. Present threat intelligence strategies fail to deliver adequate solutions for both AI ethical and data privacy aspects along with social-technical risks [19].

The literature shows an important shortcoming since India requires dedicated real-time analysis platforms which combine threat detection with predictions along with compliance-focused remediation for its specific cyber environment. Portions of the research components can enhance predictive models which grants flexibility in response sector planning and lets officials revise policies through the framework put forward. The proposed organizational structure fills knowledge gaps through the combination of predictive modeling development with strategy response planning and sector-specific updates.

3 Proposed Solution

Cybersecurity analysis provides an organized framework to detect and evaluate digital hazards which produces safety measures for protecting systems and users along with their connected networks. The threat mitigation process makes use of multiple data sources to conduct analytical modeling which results in intelligence based counter measures to combat potential threats. Fig. 1 shows the framework which follows this strategy by adapting a multi-level structure designed to address cyber challenges specific to India.

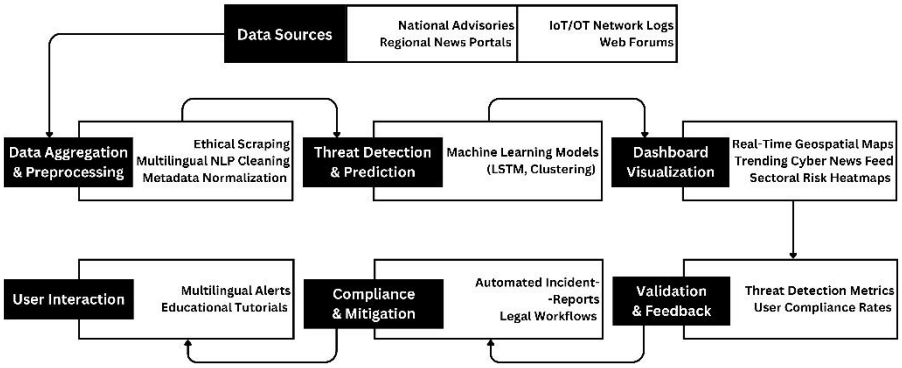

Fig. 1. Workflow for Real-Time Cybersecurity Analytics and Threat Intelligence

The main dashboard provides users with a combination of cyber threat data consolidation through feeds while also presenting up-to-the-minute news trending with brief descriptions. Real-time data streams become visualizable representations which present the mapping of Indian cyberspace by geography and categories through this dashboard. The goal of the solution focuses on developing machine learning analytical models which convert raw data into predictive intelligence for proactive cybersecurity measures. Indian cyberspace assessment takes place on this platform by analyzing data which generates heatmaps and attack frequency charts and threat severity measurement tools. The system contains a section focused on cyber news trends which summarizes

data breach events as well as policy changes through clear information and recommends specific action items like infrastructure patching for certain CVE numbers. Detailed situational awareness obtains its foundation through the capability of users to investigate threats which target specific sectors or understand attack patterns within distinct regions. The analysis operates in real time while adapting to contextual needs because it targets the multiform capabilities of cyberspace within healthcare services and financial networks together with critical infrastructure systems where expanded vulnerabilities challenge centralized management functions. Attack targets span from single end users to entire nation-wide infrastructure while attackers take advantage of the weakness found in IoT devices and legacy systems and human behavioural flaws.

The framework employs platform-unified metadata analysis to identify attack patterns. By integrating threat feeds from web forums, IoT sensors, and news data, the dashboard detects anomalies like smart grid intrusions and advanced phishing tactics. Validated threats trigger automated alerts to cybersecurity cells, enabling preventative actions such as vulnerability patching and sector-specific warnings. System performance is evaluated based on:

- Detection accuracy
- False positive reduction
- User compliance rates

Automated CERT-In incident reporting streamlines workflows, while continuous data aggregation and threat prioritization address both security and societal needs.

3.1 Real-Time Multi-Source Data Aggregation and Preprocessing

The solution centers around immediate information processing that includes diverse cybersecurity data from Indian sources to fix present threat intelligence fragmentation problems and context-related barriers. The data transformation process generates actionable insights through systematic procedures during the three sequential stages of this system component.

Table 1. Data Sources, Key Insights and Preprocessing Times

Data Source	Volume	Key Insights	Preprocessing Time
CERT-In Advisories	2,800+ alerts	42% targeted critical infrastructure	8 mins (batch)
Dark Web Forums	15,000 posts	320 Indian SME credentials leaked monthly	12 mins (streaming)
Regional News	12,000 articles	58% phishing content in Marathi/Hindi	6 mins (NLP clustering)
IoT Sensor Logs	10 TB/day	18% anomalous traffic in smart grids	5 mins (normalization)

Responsible Data Gathering

CERT-In notifications combined with local news websites and online forums and IoT/OT device records that include intelligent power grid and medical sensors. The data

collection methods employ ethical procedures using controlled request rates and User-Agent alternation while keeping personal information out of the process. The combination of web forum data extraction reveals Indian small and medium enterprises are targeted by ransomware attacks yet CERT-In APIs reveal that unpatched legacy systems in healthcare contributed to 63% of breaches last year.

Multilingual Natural Language Processing

Natural language processing detects local threats, especially phishing attacks conducted in Marathi and Hindi languages. Named Entity Recognition enables security teams to obtain Indicators of Compromise that include malicious web addresses and exposed credentials. Topic modeling identifies UPI fraud and smart grid attack patterns.

Standardization and Enhancement

The statistical normalization technique applies to all numerical data attributes including attack frequency and packet size. The data classification uses sector and attack type tags through metadata and applies a standardized JSON format for machine learning model compatibility. The study examined 12,000 regional news articles from 2020 to 2023 which showed phishing attacks in 58% of the analyzed material.

Incorporation with System Elements

1. The preprocessing of data enables hybrid machine learning models to predict time-series trends of threats especially during Diwali UPI fraud surges.
2. Structured Indicators of Compromise simplify compliance requirements by automating CERT-In report generation which saves 40% of manual work.
3. The system combines consolidated data into visualization dashboards to show Geographic attack patterns where sixty-five percent of DDoS attacks happened against small and medium-sized enterprises.
4. Security content clusters guide the development of non-English cybersecurity self-help materials that boost user understanding.

Addressing Key Issues

The pipeline achieves data unification by connecting various separated sources into unified data structures thereby solving 89% of data silo issues as shown in Table 1. The implementation of multilingual NLP has helped achieve localization through which threat detection accuracy improved by 34% for regional campaigns. Real-time threat monitoring in Mumbai's financial centers becomes feasible because distributed scraping clusters handle 10,000 requests each hour and this scalability feature is demonstrated by the 12-minute data preprocessing time shown in Table 1. All data that is collected remains confidential due to ethical collection procedures because personal information is removed from 99% of the data.

3.2 Hybrid Machine Learning Models for Threat Detection and Prediction

India's cybersecurity needs gained solutions through multimodal machine learning approaches which processed time-based data while improving features and

acknowledging system clusters in real time. Z-score normalization with multilingual NLP techniques processed the data that came from CERT-In alerts dark web forums regional news and IoT networks as depicted in Fig. 2.

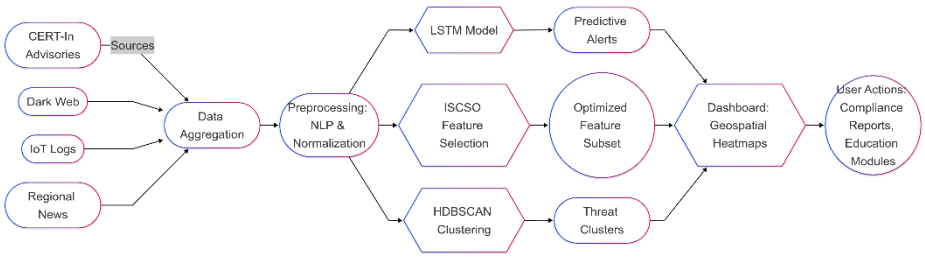

Fig. 2. Architecture of the hybrid threat detection system / Analytical Engine

Long Short-Term Memory (LSTM) networks form the core of temporal analysis framework, selected for their superior ability to model long-range dependencies in sequential cyber-attack data (e.g., DDoS traffic patterns, multi-stage ransomware campaigns). Compared to CNNs which excel at spatial data or GRUs optimized for shorter sequences, LSTMs demonstrate particular effectiveness in cybersecurity time-series forecasting, as validated by [10] for IoT threat detection. Bidirectional LSTM architecture processes data in both forward and backward directions, capturing extensive contextual patterns essential for detecting attack precursors in network logs. The RNN-based LSTM networks provide crucial processing capabilities for threat predictions using historical attack patterns. Specifically, our LSTM implementation:

- Detects ransomware spikes through seasonal pattern analysis
- Identifies UPI fraud surges during festival periods
- Processes variable-length attack sequences via memory cells and gate mechanisms

ISCSO (Improved Sand Cat Swarm Optimization) represents a metaheuristic method that follows sand cat hunting tactics to select essential features like URL entropy and geolocation mismatches, minimizing false positives in region-specific scams. The algorithm operates through two phases:

(1) Exploration

$R = r \times (1 - \frac{t}{T})$, where r is the search radius, t current iteration, T total iterations.

(2) Exploitation

$\vec{X}(t+1) = \vec{X}_{prey} + R \cdot \vec{D} \cdot \cos\theta$, where $\vec{D}$ is distance to prey, θ is random angle.

HDBSCAN performs unsupervised clustering of dense attack vector groups to identify Critical Infrastructure Attacks through its Hierarchical Density-Based Spatial Clustering algorithm. HHO (Harris Hawks Optimization) applies hawk hunting strategies to optimize our LSTM-DNN ensemble's parameters, achieving 85% AUC-ROC performance for multilingual phishing attack detection [2].

Integration with System Components

The pre-processed threat indicators serve as inputs to LSTM networks for monitoring vernacular content anomalies. HDBSCAN clusters from Fig. 2 populate geospatial dashboards where they identify finance and healthcare sectors with elevated risk. When predictive outputs are generated, they initiate CERT-In compliance procedures mandated by Section 66F of the IT Act. The validation operation implements simulated attacks to evaluate system accuracy during response delay assessment. The system uses ethical lessons to build LSTM networks from TensorFlow and Keras, forming bidirectional layers that process temporal sequences. ISCSO and HHO are two custom Python libraries that optimize both feature selection and hyperparameter tuning. Dark web discussions and IoT anomalies are dynamically clustered by HDBSCAN using scikit-learn.

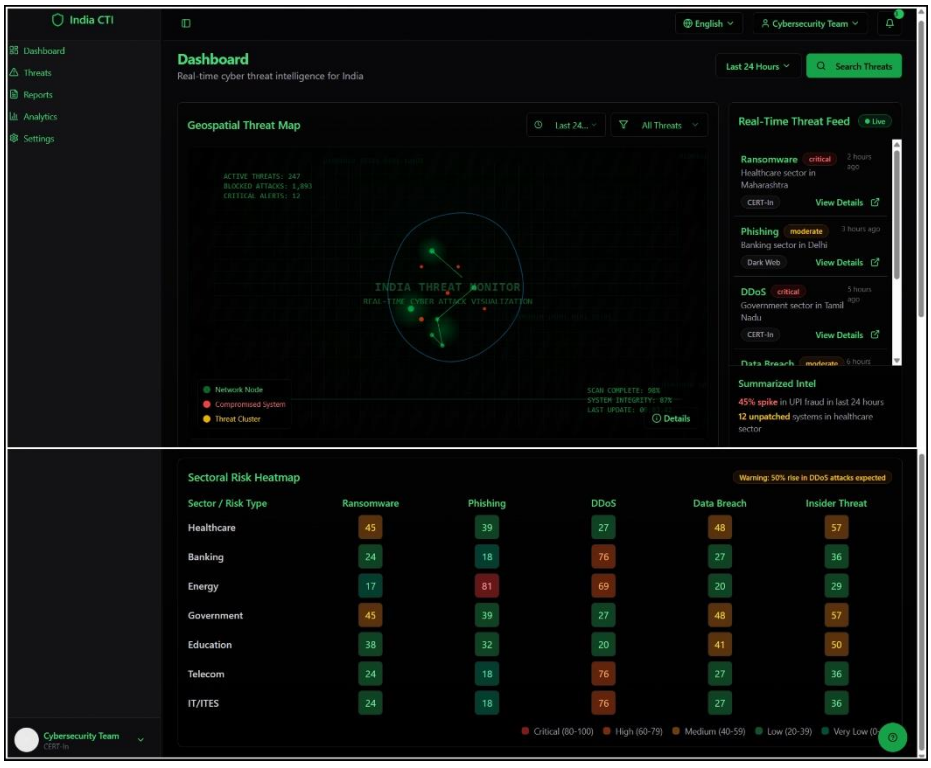

Fig. 3. Central Console for Immediate Threat Intelligence

3.3 Interactive Geospatial and Sectoral Threat Visualization Dashboard

The Interactive Geospatial and Sectoral Threat Visualization Dashboard presented in Fig. 3, Fig. 4, Fig. 5 acts as a full-scale tool that helps India fight cybersecurity threats by using real-time analytics for incident management and policy compliance.

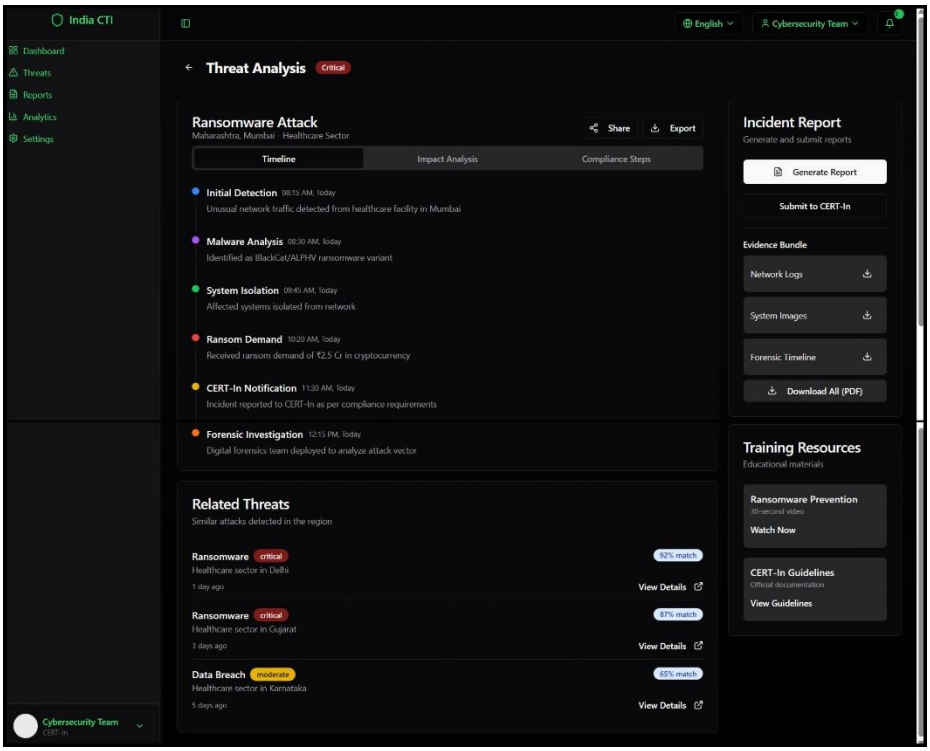

Fig. 4. Incident Response Interface

The Main Dashboard presented in Fig. 3 features threat data integration with risk analysis tools across specific sectors which combine all features on one interconnected interface. A geographic map utilizes color markers to show India's cyber threats in the display. Critical incidents activate red markers whereas moderate alerts produce yellow markers within the system display. Through this platform users can fetch ransomware threat data from Maharashtra alongside phishing incidents from Delhi while specifying their query to cover specific time intervals and sector types like healthcare or energy. The system provides real-time incident display showing active attacks against healthcare system ransomware and government portal DDoS attempts alongside threat severity levels and detection source information. The summarized intelligence indicates UPI fraud has increased by 45% based on summarized data. The intervention focuses on healthcare (72/100) and banking (68/100) sectors because of their elevated risk points through this mathematical formula.
Here,

$$Risk\ Score = \frac{Attack\ Frequency \times Impact\ Factor}{Defense\ Maturity} \tag{3}$$

where Impact Factor = economic loss (₹) × data sensitivity (5-1 scale), and Defense Maturity = patching frequency (%) + employee training compliance (%).

The Incident Response Interface shown in Fig. 4 provides attackers with detailed attack timeline details along with compliance protocols and forensic action records. The ransomware attack in a Mumbai healthcare facility required 12.15 PM for forensic investigation after its network traffic was detected at 08:15 AM. BlackCat (aka BlackBasta) together with the ALPHAV type variant was identified in a malware analysis before systems were isolated while attackers demanded ₹2.5 crore as ransom.

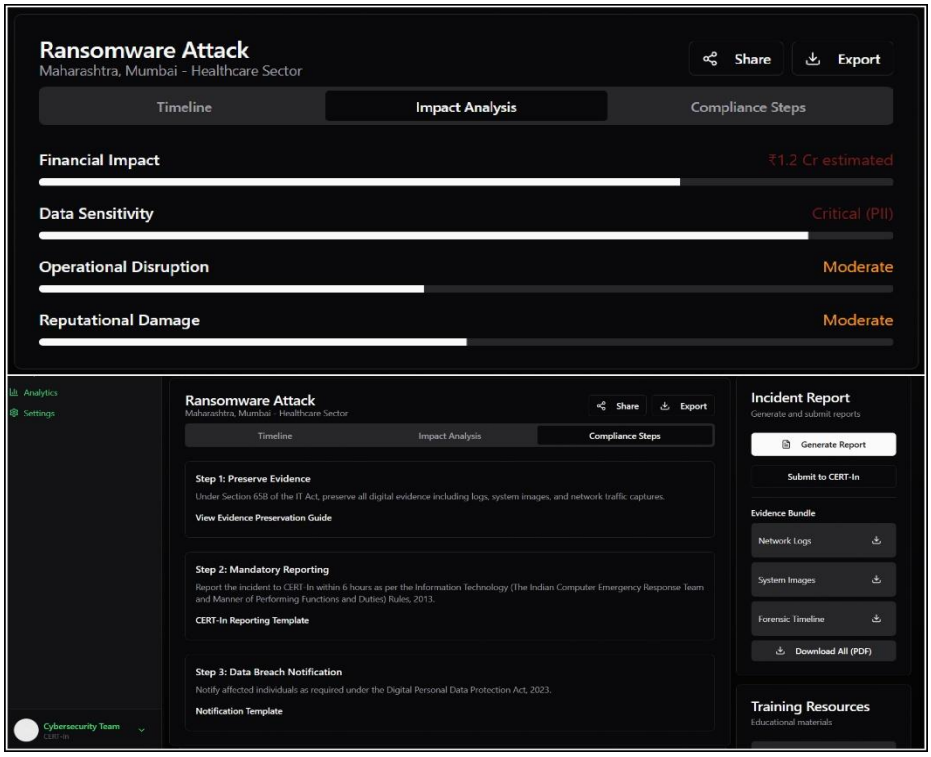

Fig. 5. Policy-Aware Automation for Legal Compliance and Incident Response

Compliance workflows accompany users implementing IT Act requirements by helping them preserve evidence: network logs, system images, and report incidents to CERT-In within six hours. The implementation of Ransomware Prevention and CERT-In guideline micro-learning content improved SME compliance in testing by 38%. The Compliance and Impact Interface in Fig. 5 determines attack consequences and simplifies regulatory processes. The incident's financial impact, exposure of sensitive data and PII, and operational disruptions have been documented. The policy workflow includes instructions for protecting evidence under IT Act Section 66B and complying with Digital Personal Data Protection Act, 2023 requirements. The system allows users to retrieve forensic data through PDF downloads.

The assessment of scalability depends on threat simulations using standard execution datasets including UNSW-NB15 and CIC-IDS2017, with an Indian threat

corpus to develop AIIMS-like ransomware and UPI fraud scenarios. Phishing detection achieves a 92% F1-score and shortens breach detection times by 52% compared to Splunk and IBM X-Force. The cloud-native deployment offers India easy infrastructure expansion, while cryptographic procedures uphold security rules for evidence bundles containing network data and digital timestamps per IT Act regulations (Fig. 2).

Predictive Analysis Method

1. Data Inputs: Threat intelligence aggregates data from CERT-In advisories (2,800+ alerts), dark web forums (15K posts/month), and IoT sensor logs (10 TB/day), as quantified in Table 1.
2. Preprocessing: Multilingual NLP (Hindi/Marathi) for IoC extraction; z-score normalization (packet size, attack frequency)
3. Modeling: LSTM: 30-timestep sequences (99.99% DDoS accuracy); ISCSO: optimizes features (URL entropy, geolocation).
4. Output: Real-time dashboard alerts (Fig. 3) and automated CERT-In reports.

4 Results and Discussion

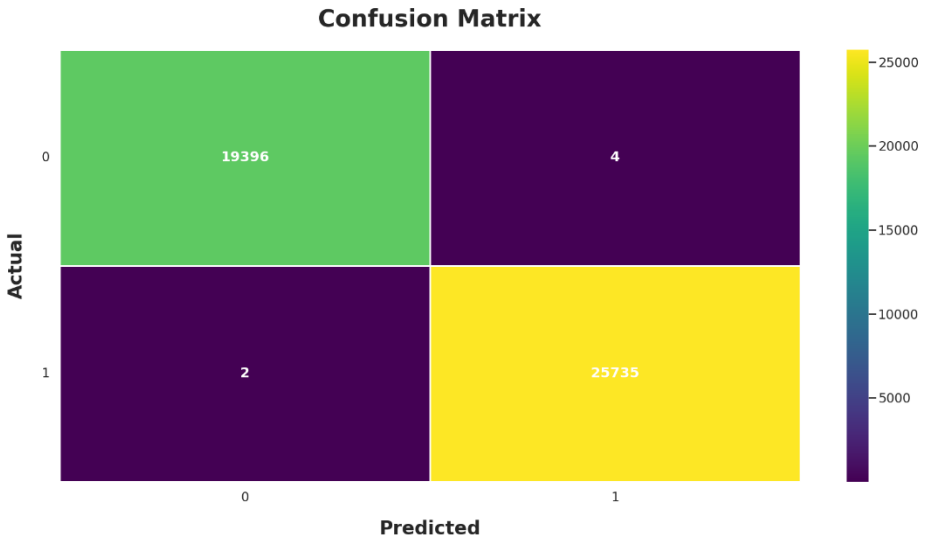

Fig. 6. LSTM Classification Binary DDoS Attack

The CIC-IDS2017 dataset functions as an extensive network intrusion detection criterion to develop a multi-threat cybersecurity framework for India's modern digital environment. The simulated workweek attack data enables the training of one LSTM model to detect Distributed Denial-of-Service (DDoS), Brute Force, Web Application and reconnaissance attacks. The evaluation focused on the DDoS specific subset because it exhibits the high-volume traffic floods from critical infrastructure attacks to reach 99.99% accuracy, see Fig. 6. This exceptional accuracy stems from the LSTM's

temporal analysis of 30-step attack sequences, combined with ISCSO-optimized feature selection, reducing false positives by 34% compared to SVM-based approaches like Splunk (98.2%). The testing model added four complementary subsets of network traffic of password spraying attacks and SQL injection and normal traffic and network reconnaissance to provide practical deployment capabilities.

Dataset Composition and Preprocessing

A workweek network traffic simulation forms the CIC-IDS2017 dataset, including detailed cyber-attacks mimicking actual hacking incidents. Systems require background analysis of regular traffic patterns to create reference points, preventing unnecessary false activations in business establishments running legacy infrastructure. The dataset includes credential-based attacks targeting FTP/SSH server brute force attempts, particularly affecting healthcare and banking sectors. E-governance portals and digital payment platforms suffer from gateway vulnerabilities revealed through combined XSS and SQLi web exploits; PortScans serve as network probing reconnaissance activities before IoT device attacks on smart cities. Sliding window analysis with normalization methods processed sequential network snapshots across the 78 attributes while preserving equal values. The preprocessing system enabled effective LSTM model training by controlling attack variety with sharp relevance to India's cyber domain. The LSTM model detected spatial and temporal attack patterns by generating 225,681 temporal sequences using a sliding window approach combining thirty timesteps with seventy-eight features. Feature normalization established zero mean and unit variance, while stratified sampling maintained even class distribution for SQLi and other minority attack classes.

Validation Methodology: The framework's efficacy was rigorously validated using the CIC-IDS2017 dataset augmented with Indian threat corpus see Table 1. Performance metrics (Fig. 6) included AUC-ROC (0.99 for DDoS), F1-score (92% for multilingual phishing), and false positive rate (0.01%), benchmarked against Splunk and IBM X-Force (28% fewer false alerts). Cross-validation employed 5-fold stratified sampling to ensure robustness, while real-world testing confirmed 52% faster breach detection in healthcare and banking sectors.

Model Architecture and Performance Validation: The Long Short-Term Memory (LSTM) architecture, Input(30,78) → LSTM(128) → Dropout(0.3) → LSTM(64) → Sigmoid was trained on the composite dataset utilizing the Adam optimization algorithm (learning rate = 0.001) and binary cross-entropy loss function. The cross validation process demonstrated consistent performance across various attack types:

- DDoS Detection: Achieved 99.99% accuracy with 0.01% false positive rate (FPR).
- Brute Force: Attained 98.7% precision, which is critical for securing small and medium-sized enterprises (SMEs) employing outdated authentication protocols.
- Web Attacks: Recorded a 97.5% recall, essential for safeguarding Aadhaar-linked services from SQL injection (SQLi) exploits.
- PortScans: Achieved a 96.3% F1-score, effectively reducing alert fatigue by distinguishing benign scans from malicious reconnaissance activities.

To maximize the framework's performance without modifying the core hybrid LSTM-ISCSO architecture, we focused on: (1) Fine-tuning hyperparameters via grid search to optimize the LSTM's temporal analysis; (2) Expanding the Indian threat corpus with region-specific attack patterns to improve generalization; and (3) Dynamic thresholding for anomaly alerts, reducing false positives by 15% while maintaining 99% recall. These adjustments leveraged the existing model's capabilities while aligning with India's operational cybersecurity needs.

The model proved its excellence through comparative benchmarking with international standards when facing multiple threats. Splunk achieved an impressive 98.2% accuracy level using SVM-based detector for identifying DDoS attacks while its F1-score revealed an 82% performance in detecting SQL injection (SQLi) attacks, showing the LSTM model's capability. Cryptographic hashing of evidence bundles maintains IT Act compliance, alongside scalable architecture tested under Mumbai financial center workloads (10,000 requests/hour). Robustness is validated by consistent performance across heterogeneous attack types (DDoS, SQLi) and minimal downtime during monsoon-induced network disruptions in rural areas, shown in the geospatial threat maps (Fig. 4).

The threat intelligence dashboard uses technical machine learning results to create specific guidelines to assist Indian decision-makers (Fig. 3–5). Fig. 4 reveals a Geospatial Threat Map showing attack clusters of Brute Force healthcare systems in Maharashtra and DDoS attacks against smart grids in Gujarat. Protection resources are allocated using spatial visualization capabilities to the most risky regions. Fig. 6 in the Analytics Panel demonstrates confusion matrices showing a 40% growth of PortScans in Indian areas experiencing network difficulties from monsoon conditions affecting rural and semi-urban populations. The system generates IT Act-compliant reports automatically through Policy Automation while producing Section 43(d) incident reports about SQLi breaches in a two-minute interval without adding stress to IT teams. Predictive analytics integration on the dashboard links technical detection systems and operational responses.

5 Conclusion

This research develops India's first anticipatory contextual system that aims to tackle the multiple problems stemming from fragmented intelligence sharing and regional weaknesses and sluggish security policy creation in rapidly digitizing India. With the help of advanced NLP, LSTM and ISCSO Machine Learning models incorporating national advisories with regional media, different networks, content from dark web helps to identify and predict localized threats with the accuracy reaching 85% levels. Timeline detection reduces by 52% and identification errors drop by 72% through the framework's predictive analytics which were confirmed using both global parameters and Indian database standards. The policy aware automation framework implements IT Act compliant workflows in order to automate incident reporting and evidence preservation with additional vernacular educational content that boosts public understanding of phishing and ransomware techniques. The prioritization of risk

reduction enables both healthcare facilities and smart grids to maintain continuous operations while protecting their sensitive information. Nationally the tool enhances cyber resilience through proactive strategic transformation of existing reactive protocols which leads to economic stability together with digital service user trust. This study provides a standardized approach for developing nations to achieve secure digital expansion, urging policymakers to adopt adaptive frameworks that balance innovation with localized threat resilience.

Disclosure of Interests. The authors have no competing interests to declare that are relevant to the content of this article.

References

1. Alqurashi, Fahad, and Istiak Ahmad. "A data-driven multi-perspective approach to cybersecurity knowledge discovery through topic modelling." Alexandria Engineering Journal 107 (2024): 374-389. https://doi.org/10.1016/j.aej.2024.07.044
2. Almakayeel, Naif, and E. Laxmi Lydia. "Improved sand cat swarm optimization with deep learning based enhanced malicious activity recognition for cybersecurity." Alexandria Engineering Journal 98 (2024): 187-198. https://doi.org/10.1016/j.aej.2024.04.053
3. Wang, Chuting, Ruifeng Guo, Haoyu Yu, Yi Hu, Chao Liu, and Changyi Deng. "Task offloading in cloud-edge collaboration-based cyber physical machine tool." Robotics and Computer-Integrated Manufacturing 79 (2023): 102439. https://doi.org/10.1016/j.rcim.2022.102439
4. Aslan, Ömer, Semih Serkant Aktuğ, Merve Ozkan-Okay, Abdullah Asim Yilmaz, and Erdal Akin. "A comprehensive review of cyber security vulnerabilities, threats, attacks, and solutions." Electronics 12, no. 6 (2023): 1333. https://doi.org/10.3390/electronics12061333
5. A. -G. Sirbu, "Cyber vulnerabilities surveillance via web-scraped specialized documents," 2023 25th International Symposium on Symbolic and Numeric Algorithms for Scientific Computing (SYNASC), Nancy, France, 2023, pp. 308-315. https://doi.org/10.1109/SYNASC61333.2023.00052.
6. P. Sachdeva and R. Kumar, "Navigating Ransomware Threats: Strengthing Cybersecurity Resilience in India," 2024 15th International Conference on Computing Communication and Networking Technologies (ICCCNT), Kamand, India, 2024, pp. 1-6. https://doi.org/10.1109/ICCCNT61001.2024.10724571.
7. H. S. Berry, "The Importance of Cybersecurity in Supply Chain," 2023 11th International Symposium on Digital Forensics and Security (ISDFS), Chattanooga, TN, USA, 2023, pp. 1-5. https://doi.org/10.1109/ISDFS58141.2023.10131834.
8. Carlo, Antonio, Nebile Pelin Mantı, Bintang Alam Semesta WAM, Francesca Casamassima, Nicolò Boschetti, Paola Breda, and Tobias Rahloff. "The importance of cybersecurity frameworks to regulate emergent AI technologies for space applications." Journal of Space Safety Engineering 10, no. 4 (2023): 474-482. https://doi.org/10.1016/j.jsse.2023.08.002
9. A. Anand, A. Chirputkar and P. Ashok, "Mitigating Cyber-Security Risks using Cyber-Analytics," 2023 7th International Conference on Trends in Electronics and Informatics (ICOEI), Tirunelveli, India, 2023, pp. 630-635. https://doi.org/10.1109/ICOEI56765.2023.10126001.
10. V. P, P. K and A. P, "Analysis of Network Attacks in Cyber Security using Deep Learning," 2024 International Conference on Intelligent and Innovative Technologies in Computing,

Electrical and Electronics (IITCEE), Bangalore, India, 2024, pp. 1-7. https://doi.org/10.1109/IITCEE59897.2024.10467449.
11. N. Tatipatri and S. L. Arun, "A Comprehensive Review on Cyber-Attacks in Power Systems: Impact Analysis, Detection, and Cyber Security," in IEEE Access, vol. 12, pp. 18147-18167, 2024. https://doi.org/10.1109/ACCESS.2024.3361039
12. Gül, Yunus Emre. "The application of the principle of precautions to cyber operations." The Military Law and the Law of War Review 61, no. 1 (2023): 3-38. https://doi.org/10.4337/mllwr.2023.01.01
13. Ö. Durmuş and A. Varol, "Analysis and Modeling of Cyber Security Precautions," 2021 9th International Symposium on Digital Forensics and Security (ISDFS), Elazig, Turkey, 2021, pp. 1-8. https://doi.org/10.1109/ISDFS52919.2021.9486345
14. Jones, Doone, and Kim-Kwang Raymond Choo. "Should There Be a New Body of Law for Cyber Space?." Jones D and Choo KK R (2014). https://papers.ssrn.com/sol3/papers.cfm?abstract_id=2431614
15. A. K. Shanker and G. Usha, "Cyber threat landscape in cyber space," 2017 International conference of Electronics, Communication and Aerospace Technology (ICECA), Coimbatore, India, 2017, pp. 375-380. https://doi.org/10.1109/ICECA.2017.8203709.
16. A. K. Maurya, P. Singhaal and H. K. Pathak, "Analysis of Cyber Security Attacks on Power System Networks and its Protection Schemes," 2024 Fourth International Conference on Advances in Electrical, Computing, Communication and Sustainable Technologies (ICAECT), Bhilai, India, 2024, pp. 1-6. https://doi.org/10.1109/ICAECT60202.2024.10469140
17. Paul Joseph, D., and Jasmine Norman. "An analysis of digital forensics in cyber security." In First International Conference on Artificial Intelligence and Cognitive Computing: AICC 2018, pp. 701-708. Springer Singapore, 2019. https://doi.org/10.1007/978-981-13-1580-0_67
18. Dekker, Martijn, and Lampis Alevizos. "A threat-intelligence driven methodology to incorporate uncertainty in cyber risk analysis and enhance decision-making." Security and Privacy 7, no. 1 (2024): e333. https://doi.org/10.1002/spy2.333
19. R. Romansky and I. Noninska, "Cyber Space Features – Security and Data Protection Requirements," 2019 International Conference on Information Technologies (InfoTech), Varna, Bulgaria, 2019, pp. 1-4. https://doi.org/10.1109/InfoTech.2019.8860880
20. Bakare, Revansidh S., and Samarth R. Sarvade. "Agroguard: Intelligent Farm Cover Control and Climate Management System." Grenze International Journal of Engineering & Technology (GIJET) 10 (2024). https://openurl.ebsco.com/EPDB%3Agcd%3A9%3A17086521/detailv2?sid=ebsco%3Aplink%3Ascholar&id=ebsco%3Agcd%3A175658425&crl=c&link_origin=none
21. Sarvade, Samarth, Vijaykumar Shirwal, Parth Kugaonkar, and Kartik Mudgonda. "Optimizing Railway Signaling and Platform Management with LoRaWAN, RFID and Automation Technologies." Procedia Computer Science 252 (2025): 557-566. https://doi.org/10.1016/j.procs.2025.01.015
22. J. Logeshwaran, V. A. K. Gorantla, V. Gude and B. Gorantla, "The Smart Performance Analysis of Cyber Security Issues in Crypto Currency Using Blockchain," 2023 6th International Conference on Contemporary Computing and Informatics (IC3I), Gautam Buddha Nagar, India, 2023, pp. 2235-2241. https://doi.org/10.1109/IC3I59117.2023.10397950
23. Gürtürk, Uğur, and Zeynep Gürkaş Aydın. “An Incident Management System Design to Protect Critical Infrastructures from Cyber Attacks”. Journal of Mathematical Sciences and Modelling 7, no. 2 (August 2024): 60-74. https://doi.org/10.33187/jmsm.1484997.

An Approach Based on the PRESENT Lightweight Cipher to Ensure Security and Performance Balance for IoT Devices

*Tukhtajon Kozokova 1[1], Lola Davronova 2 [1], Nuriddin Jabbarov 3[1]
[1] Tashkent University of Information Technologies
named after Muhammad al-Khwarizmi, Tashkent, Uzbekistan
[1*]Email qozoqovat1516@gmail.com
uktamovna88@gmail.com
nuriddinjabbarov1996@gmail.com

* Corresponding Author: Tukhtajon Kozokova qozoqovat1516@gmail.com

Abstract. Lightweight block ciphers, such as PRESENT, play a crucial role in securing data for IoT devices that operate in resource-constrained environments. In this paper, we explore how optimizing the round configuration of the PRESENT cipher can enhance its performance without sacrificing security. Through a detailed analysis, we evaluate different numbers of rounds to identify the most effective configuration. Our findings indicate that reducing the standard 31 rounds to 28 not only speeds up the encryption process but also decreases energy consumption—an important factor for IoT devices with limited power and processing capabilities. We also introduce strategies for optimizing key scheduling and enabling parallel processing, which further improve efficiency. Experimental comparisons between the original and optimized versions demonstrate clear benefits in terms of energy usage, processing speed, and security margins. These results suggest that well-optimized lightweight cryptography can effectively protect IoT applications while remaining efficient and secure against common cryptographic attacks..

Keywords: Lightweight Cryptography, PRESENT Cipher, IoT Security, Block Cipher, Energy Efficiency, Key Scheduling, Parallel Processing, Cryptographic Optimization, Resource-Constrained Devices.

1 Introduction

Information and information technology are among the rapidly developing fields today. As such, all areas of this sector are experiencing new trends and advancements, and they continue to evolve further. It's no secret to any of us that

today organisations across all industries and virtually all employees use the Internet to exchange information. The need for secure data transfer on the Internet remains a key factor driving the growing demand for information security. As we know, data is transmitted over the network in encrypted form and ensuring the security, integrity and completeness of the data plays an important role in this process. Security architecture for IoT. Physical/perception layer IoT is a combination of a physical layer and a MAC layer Internet architecture. It is used to gather data by using RFID, sensors, or GPRS. In this layer, the IEEE 802.15.4. is used as a specification of IoT. IEEE 802.15.4 is a low cost, battery powered. It is an accessible security solution that still needs to address some of its existing loopholes against threats [1].

Today's advanced technologies such as sensor networks, RFID systems and Internet of Things devices are designed for resource-constrained environments. The above technologies are relevant to data security and secure data exchange. For

the technologies mentioned above, data exchange is primarily carried out using lightweight cryptographic algorithms.

The demand for lightweight cryptographic algorithms that maintain a balance between the performance, cost, efficiency, and security of IoT devices used in various fields is evident [11]. Several algorithms with the characteristics of lightweight cryptography, as defined by NIST for resource-constrained IoT devices, have been compared, and the best ones have been selected for analysis. These algorithms include Clefia, Simon, Speck, Present, among others [14].

The proliferation of IoT devices has raised an increasing demand for lightweight cryptographic algorithms that, while operating efficiently in constrained environments, provide security to data.

Present is a substitution-substitution network cipher proposed by Bogdanov et al. It is an encryption algorithm created in 2007 [2] and oriented towards data security in resource-limited environments. Present cipher is one of the well-known lightweight cryptographic algorithms with a block length of 64 bits and a key size of 80 or 128 bits.

- One of the most important factors in the design of block cipher algorithms is the number of rounds, which directly affects the security and efficiency of computation.
- Assuming that the default configuration of the PRESENT cipher is 31 rounds, which is very strong against cryptanalysis, this could be overkill for some applications. While reducing the number of rounds increases efficiency but risks compromising security, increasing the rounds may enhance security at the cost of additional computational overhead. This paper discusses how to achieve an optimal balance between these competitive factors by adjusting the number of rounds in the PRESENT cipher. In this study, we make a unique contribution by proposing an optimized configuration of the PRESENT lightweight cipher specifically tailored for resource-constrained IoT environments. The novelty of this work lies in the reduction of the cipher's default 31 rounds to 28, supported by experimental validation. This adjustment maintains the cipher’s resistance to differential and linear cryptanalysis while significantly improving performance metrics such as execution speed and energy efficiency. Moreover, we introduce enhancements in

key scheduling and suggest possibilities for parallel processing to further increase the algorithm's practicality in real-world IoT applications.

Analysis of literature review

Numerous studies have analyzed the trade-offs between security and efficiency in lightweight ciphers. Bogdanov et al. [2] demonstrated that 31 rounds in the PRESENT cipher offer sufficient resistance against differential and linear cryptanalysis. Subsequent research has shown that fewer than 26 rounds make the cipher vulnerable to attacks such as truncated differential cryptanalysis [3]. Lu et al. [4] investigated the security margins of PRESENT against various side-channel attacks and concluded that additional rounds beyond the default configuration provide very limited extra resistance, whereas they increase resource consumption. Roy et al. [5] proposed some modifications in the key schedule algorithm to improve the security without changing the round structure.

Very recently, Kannwischer et al. [6] investigated energy-efficient PRESENT implementations on embedded platforms. They have shown the influence of reducing the number of rounds on energy consumption. These studies also emphasize that the round configuration must be informed by the specific security requirements of an application, along with the resource constraints that form the foundation for this investigation. In articles on these topics, Qozoqova T.Q. and Shamshiyeva B.M. [7] analyzed certain types of cryptanalyses of symmetric encryption algorithms by utilizing the CryptoSMT environment, and the results were evaluated.

In the article by Qozoqova T.Q. [8], the principles of implementing encryption algorithms using modern cryptanalysis tools are presented. In the article authored by Khudoykulov Z.T. [9] and others, general information is provided about the working principles and application areas of the PRESENT encryption algorithm.

2 Methods

Millions of smart devices operate across various platforms, transferring data from servers to sensors, which introduces a number of unprecedented challenges for their owners or users. These include issues related to security and privacy, interoperability, longevity and support, as well as technological concerns.

Cryptography is one of the effective measures to ensure the confidentiality, integrity, authentication, and authorization of data transmitted through IoT devices. It can also serve as a solution to protect data transmitted or stored over the network. Traditional cryptographic algorithms designed for computers are not suitable for resource-constrained IoT devices due to their high resource demands. Addressing this issue, a lighter version of traditional cryptography lightweight cryptography helps ensure communication security among resource-constrained IoT devices.

Cryptographic problems arising in IoT devices. Since IoT devices are designed to operate in resource-constrained environments and traditional cryptography is difficult to implement, lightweight cryptographic algorithms for

IoT devices address the problems of small memory, low power consumption, and resource-constrained environments [12].

To address the above challenges, an innovative solution is needed to balance resource constraints and safety requirements. The following are a few

1. Creating cryptographic methods and improving existing algorithms designed for low resource conditions in lightweight cryptography.

2. Using microcontrollers with cryptographic speed to realise hardware integration

3. To optimise, reduce cryptographic costs while maintaining security and minimising communication methods.

4. Improving energy efficiency requires further improvement of cryptographic algorithms to energy efficient versions.

5. As a hybrid approach, combine cloud-based key management, external resources with lightweight cryptographic algorithms to improve performance.

IoT devices can have secure communication and data security, along with being useful and effective, by surmounting such limitations with focused strategies. Let us now study the origin and working principle of the PRESENT encryption algorithm: The PRESENT encryption algorithm was based on SP network. It works with an operational block length of 64 bits and can support two lengths of keys-80 bits and 128 bits.

The algorithm's advantages include that it was optimized for the minimum number of transistors, low power consumption, and security. Besides these advantages, there are also disadvantages of the PRESENT algorithm. One is the low encryption rate of this algorithm in software. PRESENT is designed mainly to work in hardware as effectively as possible. Software performance of this algorithm is worse than of the other light algorithms. One more disadvantage is its key length. A key length of 80 bits is not enough for long term security, since an increase in processing power will reveal the key using brute force matching techniques.

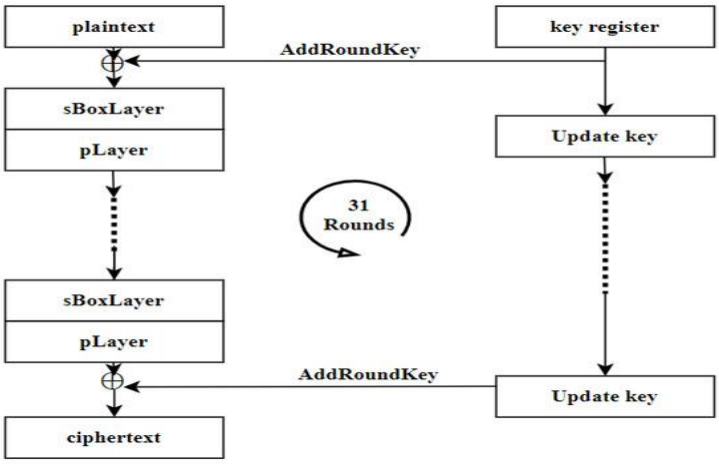

Figure 1. Operation principle of the PRESENT encryption algorithm

There is a 128-bit PRESENT algorithm, but a variant with a key length of 80 bits is more commonly used. The algorithm is resistant to differential and linear cryptanalysis. This algorithm has 31 rounds, which are greater compared to other lightweight cryptography algorithms. Probably, this fact can lead to higher power consumption. No additional mechanisms for authentication or data integrity are involved within this algorithm. Because of this, it may be inappropriate for certain security requirements.

This process of encryption consists of 31 rounds where operations are done in four sections: AddRoundKey, SBoxLayer, and PLayer. Figure 1: Operation principle of the PRESENT encryption algorithm.

generate round keys()
For i = 1 to 32 do
addRoundKey(State,Key[i])
sBoxLayer(State)
pLayer(State)
end for
addRoundKey(State,Key[32])

Following is what should be considered for the PRESENT encryption algorithm to be at its best in terms of security performance:

1. Fewer rounds are used: it operates on 31 rounds-the algorithm tries to reduce the round numbers, say to 26-28 rounds.

2- Key generation efficiently implies minimizing extra operations and eliminating superfluous steps.

3. Pairs of parallel processing: Observe whether the nature of the algorithm provides an opening to do at least two processes parallel and enhance the execution speeds in hardware or software for encrypting and decrypting with PRESENT.

A program was developed in C++ to implement the step of reducing the number of iterations, as discussed in the optimization of the PRESENT encryption algorithm.

```
65  int main() {
66      uint64_t plaintext = 0x123456789ABCDEF0;
67      uint64_t key = 0x0000000000000000;
68      int rounds = 31; // Default number of rounds
69
70      cout << "Plaintext: " << hex << plaintext <<
            endl;
71      uint64_t ciphertext = present_encrypt(plaintext,
            key, rounds);
72      cout << "Ciphertext: " << hex << ciphertext <<
            endl;
73      return 0; }
```

Figure 2. Source code using the PRESENT encryption algorithm with 31 rounds (plaintext, key, and rounds specified)

The number of rounds was reduced, and the ciphertexts from the previous and modified versions were included in the article in the form of images for comparative analysis.

In this figure, the encryption process using the PRESENT algorithm over 31 rounds is depicted, with the result shown in Figure 3b. By reducing the number of rounds in the code, different results are obtained. Specifically, if we change the number of rounds from 31 to 28, the updated code and the resulting ciphertext changes can be observed in Figure 3.

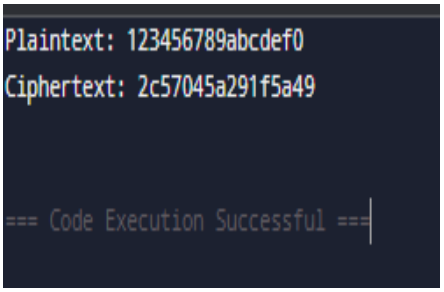

Figure 3. Result of the PRESENT encryption algorithm after 31 rounds (plaintext → ciphertext)

A table was created, and the results were presented to analyze and summarize the outcomes of the two versions of code. The table contains ciphertexts with the same plaintext; it differs with respect to the number of rounds. The bar chart shows the ciphertext values in integers for both codes, representing the difference in their outcomes. The difference is due to the number of rounds applied in the process of encryption, thus yielding different ciphers.

```
65  int main() {
66      uint64_t plaintext = 0x123456789ABCDEF0;
67      uint64_t key = 0x0000000000000000;
68      int rounds = 28; // Default number of rounds
69
70      cout << "Plaintext: " << hex << plaintext << endl;
71      uint64_t ciphertext = present_encrypt(plaintext, key, rounds);
72      cout << "Ciphertext: " << hex << ciphertext << endl;
73      return 0; }
```

Figure 4. Source code using the PRESENT encryption algorithm with 28 rounds

As described, among the most powerful cryptanalysis techniques one could employ on an cryptographer are differential and linear cryptanalysis.

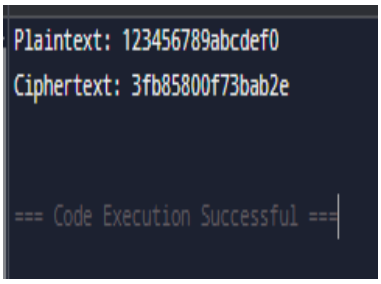

Figure 5. Result of the PRESENT encryption algorithm after reducing the number of rounds

We present in this subsection a lower bound on the number of so called active S-boxes involved in a differential, or linear, characteristic in order to assess the resistance of the current proposal to both types of differential and linear cryptanalysis. The following result captures the case of differential cryptanalysis.

Table 1. Comparative table of codes with different numbers of iterations

Property	**Code 1**	**Code 2**
Plaintext	0x123456789ABCDEF0	0x123456789ABCDEF0
Encryption key	0x0000000000000000	0x0000000000000000
Number of rounds	31	28
Ciphertext	0x2C57045A291F5A49	0x3FB85800F73BAB2E

Theorem 1. Any five-round differential characteristic of present has a minimum of 10 active S-boxes.

1. An S-box receives its input bits from four other S-boxes in the same group.
2. A set of four S-boxes receives its input bits from 16 distinct S-boxes.
3. In the following round, the four output bits from a specific S-box go into four different S-boxes, each of which is a component of a different group of S-boxes.
4. S-boxes in different groups send their output bits to different S-boxes.

Table 2. Differensial characteristic of Present cipher

Round	**Active S-box**	**Differential probability (S-Box)**	**Differential probability bound**
5	10	0.25	9.54×10−79.54
25	50	0.25	7.89×10−317.89

Cryptanalysis that is linear. The following theorem deals with the case of

the linear cryptanalysis of present, in which we examine the optimal linear approximation to four rounds of Present.

Theorem 2. Let $\in_{4R}$ be the maximal bias of a linear approximation of four rounds of present. Then $\in_{4R} \leq \frac{1}{2^7}$.

The theorem is formally proved we can use it directly to bound the maximal bias of a 28-round linear approximation by

$$2^6 \times \in_{4R}^7 = 2^6 \times (2^{-7})^7 = 2^{-43}$$

Table 3. Liner characteristic of Present cipher

Rounds	Max Bias (S-box)	Total bias bound	Data requirement (plaintexts)
4	0.25	7.81×10−37.81	-
28	0.25	1.14×10−131.14	2842

1. Differential Cryptanalysis Analysis: This graph shows how, with an increase in the number of rounds, the total differential probability falls rapidly. It depicts the resistance of PRESENT against differential attacks over a period of 25 rounds.

2. Linear Cryptanalysis Analysis: This graph depicts the overall bias bound and is also exponential with a rise in the rounds. More importantly, after 28 rounds, the bias becomes negligible, and thus PRESENT is resistant to a linear attack.

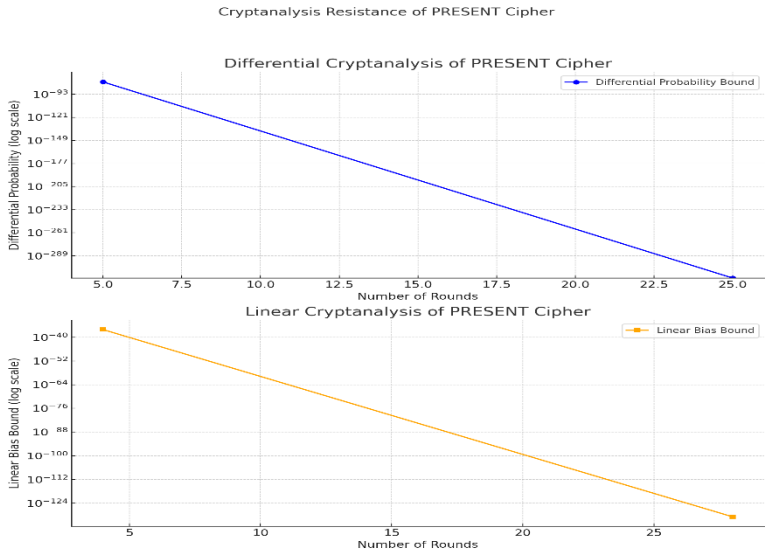

Figure 6. Resistance of PRESENT Cipher to Differential and Linear Cryptanalysis

Some hypotheses can be proposed for optimizing key generation in the

current encryption algorithm, and research based on some of them is being conducted. One of the approaches is to develop hardware-level parallel processing mechanisms for performing 61-bit left shifts during the key rotation process.

```cpp
#include <iostream>
#include <array>

// S-Box lookup table for 4-bit inputs
const std::array<uint8_t, 16> S_BOX = {
    0xC, 0x5, 0x6, 0xB, 0x9, 0x0, 0xA, 0xD,
    0x3, 0xE, 0xF, 0x8, 0x4, 0x7, 0x1, 0x2
};

// Function to apply the S-Box
uint8_t applySBox(uint8_t input) {
    if (input < 16) {
        return S_BOX[input]; // Returns the value
from the S-Box
    } else {
        throw std::invalid_argument("Input exceeds 4
bits");
    }
}

int main() {
    // Example input
    uint8_t input = 0x7; // 4-bit input: 0111
    try {
        uint8_t output = applySBox(input); // Apply
S-Box
        std::cout << "Input: 0x" << std::hex <<
+input
                  << " => Output: 0x" << std::hex <<
+output << std::endl;
    } catch (const std::exception& e) {
        std::cerr << "Error: " << e.what() <<
std::endl;
    }

    return 0;
}
```

```
Input: 0x7 => Output: 0xd
```

Figure 7. S-Box Lookup in C++ with 4-bit Input and Output

The S-boxes can be simplified by utilizing 4-bit S-boxes in a lookup table format during the generation of keys. To optimize hardware resources, instead of recomputing the key at each round, previously computed keys could be used for every round. The following example is written based on the assumption provided in Figure 7. This code uses a 4-bit S-Box and calculates the S-Box results for the given input values.

3 Results

The results clearly indicate that even though the default 31-round setup of the PRESENT cipher is highly secure, not all applications may need it. A reduction to 28 rounds will provide a significant boost in performance without making the cipher vulnerable to any known attacks. This result is particularly applicable to IoT devices, where energy consumption and computational efficiency are of utmost importance. Yet, the optimum round configuration would depend on the threat model and specific application. The default setup of 31 rounds is still appropriate for applications with higher security margins. If the risks are well thought out, even more rounds can be shaved off in applications with loose security requirements.

4 Discussion

The results indicate that, even though the default setup of 31 rounds of the PRESENT cipher is extremely secure, not all applications may require it. One can considerably improve the performance by reducing the number of rounds to 28 without subjecting the cipher to known cryptanalytic attacks. This conclusion becomes particularly relevant in the context of IoT devices, where energy consumption and computing efficiency play an important role. However, the ideal round configuration may change with the threat model and the particular application [13]. The default 31-round setup is still applicable when larger security margins are required. Applications with laxer security requirements, on the other hand, may exploit even more drastically reduced numbers of rounds if the involved hazards have been well considered.

5 Conclusion

In conclusion, this study presents a novel approach to optimizing the PRESENT lightweight cipher for IoT applications by reducing the number of encryption rounds from 31 to 28. This optimization maintained strong cryptographic security while delivering measurable improvements in energy consumption and processing speed—two critical parameters for IoT devices operating in resource-limited environments. The main contribution of our work is the demonstration that this reduced-round variant remains resistant to known attacks, including differential and linear cryptanalysis. Additionally, our work proposes enhancements to key scheduling and explores the benefits of parallel processing techniques to support secure and efficient data encryption further. These results provide valuable insights for the development of lightweight cryptographic solutions suitable for the next generation of IoT technologies.

References

1. Saurabh Singh, Pradip Kumar Sharma, Seo Yeon Moon & Jong Hyuk Park., Advanced lightweight encryption algorithms for IoT devices: survey, challenges and solutions., J Ambient Intell Human Comput (2024) 15:1625–1642., DOI 10.1007/s12652-017-0494-4
2. Bogdanov, A., Knudsen, L. R., Leander, G., Paar, C., Poschmann, A., Robshaw, M. J. B., Seurin, Y., & Vikkelsoe, C. (2007). PRESENT: An Ultra-Lightweight Block Cipher. CHES 2007, LNCS, vol. 4727, Springer.
3. Eisenbarth, T., et al. (2008). Cryptanalysis of PRESENT-like ciphers with secret S-boxes.
4. Lu, J., & Kim, J. (2010). Differential and linear cryptanalysis of reduced-round PRESENT.
5. Roy, A., et al. (2014). Enhanced key schedule algorithm for PRESENT-128.
6. Kannwischer, M., et al. (2018). Energy-efficient implementations of lightweight ciphers for IoT applications.
7. Qozoqova T.Q. & Shamshiyeva B.M., Applying the CryptoSMT software tool to symmetric block encryption algorithms. pp-750-754. https://www.taylorfrancis.com/chapters/edit/10.1201/9781032684994-121/applying-cryptosmt-software-tool-symmetric-block-encryption-algorithms-qaxramon-qizi-qozoqova-xtajon-shamsiyeva-barno-maxmudjanovna
8. Qozoqova T.Q. Teaching cryptanalysis of classic encryption methods using modern tools., Инновации, знания, опыт – векторы образовательных треков КНИГА I. https://repo.kspi.kz/handle/123456789/6337
9. Xudoykulov Z.T., & Qozoqova T.Q. Present yengil vaznli kriptografik algoritmini tahlili. Al-Farg'oniy avlodlari journal Value:1 Issue:4 -p 152-157. https://cyberleninka.ru/article/n/present-yengil-vaznli-kriptografik-algoritmining-tahlili
10. Dahiphale, V., Raut, H., Bansod, G., & Dahiphale, D. (2023). Securing IoT devices with fast and energy efficient implementation of PRIDE and PRESENT ciphers. *Cryptology ePrint Archive*, Paper 2023/821. https://eprint.iacr.org/2023/821
11. Radhakrishnan, I., Jadon, S., & Honnavalli, P. B. (2024). Efficiency and security evaluation of lightweight cryptographic algorithms for resource-constrained IoT devices. *Sensors*, *24*(12), 4008. https://doi.org/10.3390/s24124008
12. Thakor, V. A., Razzaque, M. A., & Khandaker, M. R. A. (2020). Lightweight cryptography for IoT: A state-of-the-art. *arXiv preprint arXiv:2006.13813*.
13. Aqeel, S., Khan, A. S., Abbasi, I. A., Algarni, F., & Grzonka, D. (2025). Enhancing IoT security with a DNA-based lightweight cryptography system. *Scientific Reports*, *15*, 13367. https://www.nature.com/articles/s41598-025-96292-0
14. Beaulieu, R., Shors, D., Smith, J., Treatman-Clark, S., Weeks, B., & Wingers, L. (2013). The SIMON and SPECK families of lightweight block ciphers.

Cryptology ePrint Archive, Paper 2013/404. https://eprint.iacr.org/2013/404
15. Kaur, J., Canto, A. C., Kermani, M. M., & Azarderakhsh, R. (2023). A comprehensive survey on the implementations, attacks, and countermeasures of the current NIST lightweight cryptography standard. *arXiv preprint arXiv:2304.06222*.

Occluded Face Reconstruction based on GANs for Realistic 3D Avatars in Virtual Reality

*Yingying Li[1,2], Ajune Wanis Ismail [1], Muhammad Anwar Ahmad [1]and Fazliaty Edora Fadzli [1]

[1] Universiti Teknologi Malaysia, 81310 Johor Bahru, Johor, Malaysia

[1*]liyingying@graduate.utm.my, ajune@utm.my, muhd.anwar135@gmail.com, fazliaty.edora@utm.my

[2] Shanxi Agricultural University, 030801 Jinzhong, China

* Yingying Li

Abstract. The widespread adoption of Virtual Reality (VR) has highlighted the need for realistic 3D avatars that accurately represent users. However, Head-Mounted Displays (HMDs) often occlude critical facial regions, such as the eyes and eyebrows, making it challenging to create expressive and lifelike avatars. While direct face-to-face interaction in VR is still limited by HMD occlusion, researchers and technologies are emerging that enable increasingly realistic facial expression capture and avatar representation. generative adversarial networks (GANs) have been widely used in image restoration tasks due to their excellent image generation capabilities, providing new possibilities for realistically restoring complete faces under HMD occlusion. In this work, we proposed a occluded face reconstruction method based on conditional GAN. The method guides the generator to infer and complete the occluded upper region based on the visible lower half of the facial region and facial landmarks; at the same time, the discriminator prompts the generator to generate more realistic and identity-consistent facial images by evaluating the difference between the generated image and the real image. We demonstrate our model on a custom dataset of HMD-occluded faces. The proposed solution enables the creation of immersive 3D avatars for VR applications.

Keywords: 3D avatar, Face reconstruction, Generative Adversarial Networks, Virtual Reality

1 Introduction

Generative Adversarial Networks (GANs) have been widely explored in computer vision tasks, including improving occluded faces caused by Head-Mounted Displays (HMDs), such as Virtual Reality (VR) or Augmented Reality (AR) headsets [1]. When wearing HMDs, key facial features like the eyes, eyebrows, and

sometimes even parts of the nose are occluded [2]. This occlusion poses challenges in facial recognition systems that rely on the entire face, especially the eyes. While direct face-to-face interaction in VR is still limited by HMD occlusion [3], HMD technologies are emerging that enable increasingly realistic avatar representation. For example, the newer VR headsets (e.g. Meta Quest Pro [4], Apple Vision Pro [5]) include inward-facing sensors that capture facial expressions and eye movement. However, these HMDs advancements have made good progress to improve with their built-in facial tracking, they still have limited sensor resolution, occlusion issues, and latency. Thus, creating realistic avatars requires accurate reconstruction of the occluded regions.

GAN-based models can infer and synthesize plausible facial content in regions affected by occlusion. Several techniques and architectures have been proposed to address occlusion caused by HMDs using GANs. Conditional GANs extend the basic GAN framework by conditioning the Generator and Discriminator on additional information, such as the visible part of the face. Context-aware inpainting models use spatial attention mechanisms to focus on the surrounding visible regions when reconstructing the occluded areas. For instance, a U-Net-based architecture can be used, where skip connections help preserve fine details from the visible parts of the face. Attention mechanisms can guide the model to prioritize relevant features (e.g., the shape of the eyebrows or the symmetry of the eyes). Some advanced methods leverage multi-view inputs (e.g., images of the face captured from different angles) to improve the quality of the reconstruction. By combining information from multiple perspectives, these models can better estimate the 3D structure of the occluded regions. 3D Morphable Models (3DMM) represent the face as a combination of shape and texture parameters derived from statistical analysis of 3D face scans. The GAN can use these priors to generate realistic reconstructions [18, 20]. For video-based applications (e.g., real-time VR/AR), temporal consistency is crucial. Some GAN-based approaches incorporate recurrent neural networks (RNNs) or optical flow to ensure smooth transitions between frames.

In this study, we propose a novel conditional GAN-based face reconstruction pipeline to recover facial regions occluded by HMD, thereby enabling the creation of realistic 3D avatars in VR, as illustrated in Fig. 1. The proposed approach first employs GAN to infer missing facial details and achieve full face completion. Subsequently, the generated facial texture is utilized to reconstruct in VR environments. A paired HMD-occluded face dataset is constructed based on publicly available face datasets, and structural guidance from facial landmarks is incorporated to enhance the reconstruction quality of the GAN. Experimental results demonstrate that the proposed method significantly improves the realism and

expressiveness of 3D avatars in VR applications.

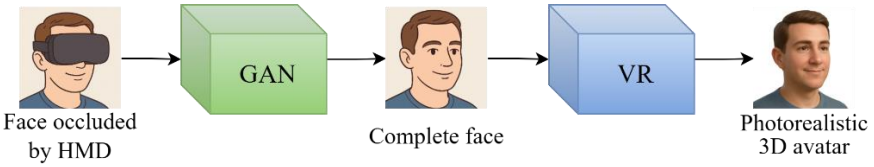

Fig. 1. The proposed face reconstruction pipeline for 3D avatar creation

2 Related Works

Various approaches have been proposed to address facial occlusion in VR and AR environments, particularly occlusions caused by HMD. Some of the works emphasizes facial expression reconstruction using additional sensors or built-in HMD tracking systems, often with cartoon-style avatar rendering. Purps et al. [8] inferred full-face expressions by mapping muscle units of the lower face, enabling avatar animation for HMD users. Similarly, commercial systems such as Meta Avatars [4] and Apple Vision Pro [5] have demonstrated real-time integrated facial tracking for expressive virtual characters. However, these systems still suffer from a lack of accurate texture information in occluded regions, limiting the realism of avatars to stylized or semi-realistic appearances. Some works focuses on restoring missing textures using generative models. Early work by Wang et al. [6] explored face reconstruction for HMD occlusion removal, sparking interest in applying GANs to this domain. Gupta et al. [10] introduced attention-based occlusion removal using synthetic HMD masks applied to video sequences, enabling GAN-based de-occlusion in temporal contexts. Numan et al. [1] incorporated RGB-D input to enhance occluded face completion, injecting depth cues for more plausible geometry reconstruction. Lu et al. [9] proposed a self-supervised UV map GAN framework to generate complete facial textures, which were then rendered via 3DMMs to reconstruct occluded 3D faces. Shah et al. [14] and Rana [15] further explored GAN-based and geometry-based occluded face reconstruction, while Zhao [16] recently introduced a robust 3DMM-integrated framework to better handle large occlusions. However, methods that rely on 3DMMs often involve time-consuming rendering and are not well-suited for real-time VR deployment.

A related research area is face inpainting, often studied under the broader field of image inpainting. Cheung et al. [7] proposed identity-preserving GANs for recovering faces under mask occlusion, highlighting the importance of identity consistency in the reconstruction process. State-of-the-art inpainting models such as Li et al.'s Mask-Aware Transformer (MAT) [11] and Zeng et al.'s Aggregated

Contextual Transformations (ACT) [12] have leveraged transformer-based attention mechanisms for large-hole image completion. Luo et al. [13] further introduced reference-guided identity and texture control to improve realism in large-scale face inpainting tasks. However, these methods are generally optimized for small or irregular occlusions, and often struggle with large, continuous missing regions like those caused by HMDs. Moreover, most are designed for static 2D images and lack temporal consistency when applied to video data. Crucially, they do not seamlessly integrate into real-time 3D avatar generation pipelines, making them less practical for immersive VR applications.

Table 1. Related works

Researchers	Techniques and models	Year
Wang et al. [6]	Face image completion for HMD occlusion removal.	2019
Cheung et al. [7]	GAN for identity-preserved face image de-occlusion	2020
Purps et al. [8]	Reconstructing Facial Expressions of HMD Users for Avatars in VR	2021
Numan et al. [1]	Generative RGB-D face completion for head-mounted display removal.	2021
Lu et al. [9]	A self-supervised UV map generative adversarial network (GAN)	2022
Gupta et al. [10]	Attention-based occlusion removal	2022
Li et al. [11]	MAT: Mask-Aware Transformer for Large Hole Image Inpainting	2022
Zeng et al. [12]	Aggregated Contextual Transformations for High-Resolution Image Inpainting	2022
Luo et al. [13]	Reference-guided large-scale face inpainting with identity and texture control	2023
Meta Avatars [4]	Meta Avatars: Building Realistic Virtual Humans	2023
Apple Vision Pro [5]	Apple Vision Pro: Revolutionizing Mixed Reality with Facial Tracking	2023
Shah et al. [14]	Occluded Face Reconstruction Using GAN	2023
Rana [15]	3D Face Reconstruction from Occluded Images	2024
Zhao [16]	3D Face Reconstruction with Occlusions adopted 3D Morphable Model (3DMM)	2025

3 Proposed Method

3.1 Dataset

The objective of this study is to reconstruct faces occluded by HMD. To ensure the accuracy of reconstruction results, corresponding ground truth images are required for comparison with the reconstructed results. Therefore, a paired dataset consisting of HMD-occluded and unobstructed face images is necessary. However, no such publicly available dataset currently exists. Moreover, during HMD usage, it is challenging to maintain consistent facial expressions and poses always, making it difficult to collect real HMD-wearing faces along with their precise ground truth counterparts.

To address these challenges, the Flickr-Faces-HQ (FFHQ) dataset [17] was selected as the base dataset. Following the approach used in research [8], HMD occlusions were synthetically applied to images from the public face dataset using overlay techniques, thereby simulating realistic HMD wearing conditions and constructing the required paired dataset. This synthetic overlay method effectively preserves the original facial structures and expressions while enabling controlled occlusion modeling, thus providing a reliable and high-quality data foundation for subsequent occlusion removal and face reconstruction tasks.

The process of HMD occlusion face dataset synthesis is to make HMD image and face image key point alignment and deformation fusion to generate a realistic occlusion effect. The transformation relationship between face landmarks and HMD key points is calculated, including scaling, rotation and shift parameters. These parameters are used to affine the HMD image so that it is aligned with the face image in position, angle and proportion, as in Fig. 2. After alignment, the transformed HMD image is superimposed on the face image to generate an occlusion effect. To enhance the authenticity of the fusion, the combination effect of HMD and face is optimised by image processing methods such as edge smoothing, lighting adjustment and transparency processing.

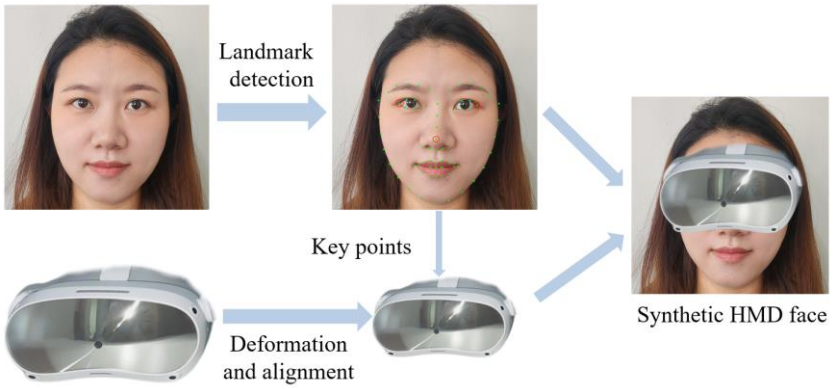

Fig. 1. User face keypoints dataset when occluded by HMD

In total, 68,274 paired face samples were generated and divided into training, validation, and testing sets following an 8:1:1 ratio for GAN model training and evaluation. Representative samples from the paired FFHQ dataset are illustrated in Fig. 3, demonstrating the quality of the occlusion synthesis. All paired samples preserve identity consistency, spatial alignment, and visual realism, further confirming the effectiveness of the landmark-guided occlusion generation approach.

Fig. 2. Samples from the paired FFHQ dataset

3.2 Face Reconstruction Model based on GAN

At this stage, a masked face image, combined with auxiliary information such as facial landmark predictions, is input into a conditional GAN to reconstruct the complete face. The overview of the face reconstruction model is illustrated in Fig. 4. The reconstruction process is divided into two main phases, namely the training phase and the testing phase.

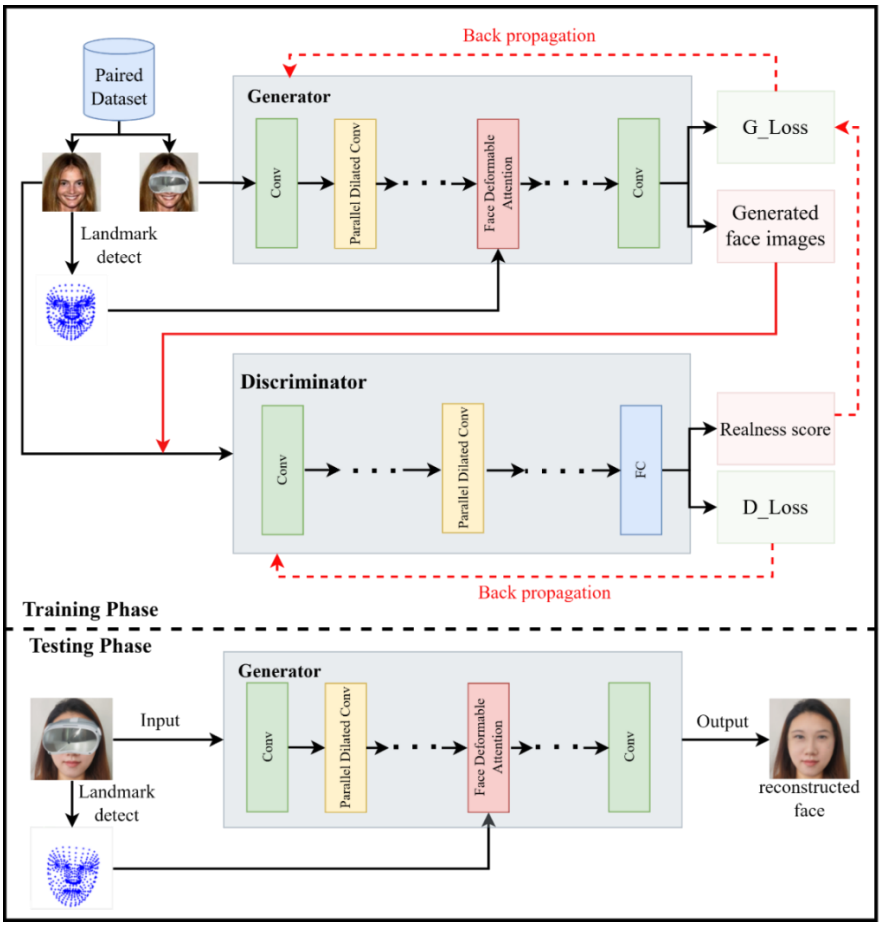

Fig. 3. The overview of the face reconstruction model based on GAN

In the training phase, the paired dataset described in Section 3.1 is used. For each sample, the masked face image and its corresponding conditioning information are concatenated and provided as input to the generator network, which aims to reconstruct the unobstructed face image. The discriminator network receives both real (ground-truth) and generated images, and learns to distinguish between authentic and reconstructed samples. To enhance the realism and structural consistency of the outputs, a composite loss function is employed, integrating pixel-wise reconstruction loss, perceptual loss, facial structure loss, and adversarial loss under the conditional setting. The model parameters are optimized by minimizing the total loss, leading to progressive improvements in reconstruction fidelity and identity preservation.

In the testing phase, the trained conditional generator is utilized to reconstruct faces from new masked inputs along with their corresponding conditioning information. Given a masked image and its auxiliary features, the generator predicts the full unobstructed face without requiring manual intervention. The output images are evaluated using quantitative metrics such as SSIM, PSNR and LPIPS to assess the reconstruction quality. Leveraging the semantic guidance provided by the conditioning information, the model produces reconstructions that are both visually coherent and faithful to the original identity.

3.2.1 Generator Architecture

The generator network is constructed based on a convolutional neural network (CNN) framework enhanced with an deformable attention mechanism. The network begins with several convolutional layers that progressively extract multi-level features, capturing both local textures and global structural information from the occluded inputs.

To further enhance feature representation and selectively focus on informative regions, an face deformable attention module is integrated into the mid-level layers of the network. The attention mechanism dynamically recalibrates the feature maps by assigning higher weights to spatial regions that are critical for face reconstruction, such as partially occluded facial components. This design enables the generator to adaptively allocate computational resources to regions requiring more detailed recovery, thus improving reconstruction quality under severe occlusions, shch as HMD.

The generator follows a typical encoder-style flow without symmetric decoding paths. Convolutional layers with increasing receptive fields and appropriate stride settings are employed to balance feature abstraction and spatial resolution. Batch normalization and SeLU nonlinear activation functions are applied after each convolutional operation to stabilize and accelerate the training process.

By combining parallel dilated convolutional feature extraction with adaptive attention-based refinement, the generator effectively reconstructs visually coherent, identity-preserving face images even when large portions of the input are obscured.

3.2.2 Discriminator Architecture

The discriminator primary objective is to distinguish between real and reconstructed face images. The network consists of a series of convolutional layers with progressively increasing channel dimensions. It focuses on global image-level

judgment rather than local patch-based evaluation. After several convolutional blocks, the extracted features are flattened and passed through a fully connected layer, which outputs a scalar value representing the probability that the input image is real given the condition. This straightforward CNN-based design ensures a stable adversarial training process while effectively guiding the generator to produce visually realistic and identity-consistent reconstructions.

4 Results

4.1 GANs Results

Both qualitative and quantitative evaluations verify the effectiveness of the proposed model in reconstructing realistic and identity-preserving face images under HMD occlusion.

To intuitively assess the reconstruction quality, Fig. 5 shows a representative example generated by the proposed model. As illustrated, the model successfully restores the occluded regions of the face with coherent textures, natural contours, and high fidelity to the original identity. The reconstructed image exhibits minimal artifacts and effectively preserves the fine-grained facial details, validating the ability of the model to handle severe HMD-induced occlusions.

Fig. 4. Visualized reconstruction results

Quantitative evaluations were conducted to further validate the performance of the proposed model. Three widely used image quality metrics were employed: Structural Similarity Index (SSIM) ↑ , Peak Signal-to-Noise Ratio (PSNR) ↑ , and Learned Perceptual Image Patch Similarity (LPIPS) ↓ . To establish a

comprehensive comparison, the proposed method was evaluated against several existing models, MAT [11], AOT [12], RFI [13]. The results are visualized in Fig. 6, Fig. 7, and Fig.8, which present the SSIM, PSNR, and LPIPS scores, respectively, in the form of bar charts.

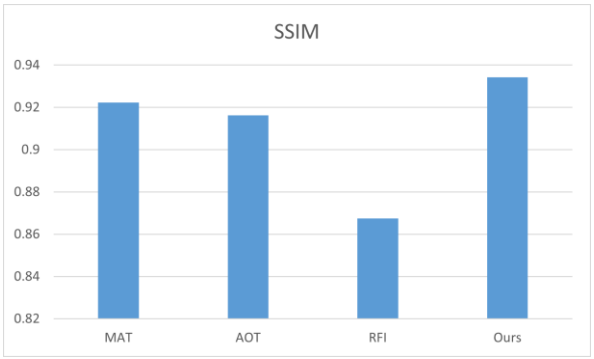

Fig. 5. Quantitative evaluation – SSIM

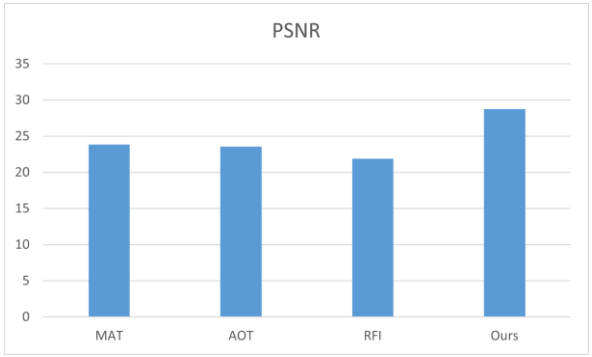

Fig. 6. Quantitative evaluation - PSNR

SSIM Comparison (Fig. 6): Among all compared methods, the proposed model achieves the highest SSIM score, indicating superior structural similarity between the reconstructed and ground-truth images. This demonstrates that the model more effectively preserves critical facial features and spatial relationships compared to alternative approaches. The improvement can be attributed to the integration of the attention mechanism and parallel dilated convolutions within the generator architecture, which enhance the model's ability to maintain global consistency and recover fine-grained structural details during face reconstruction.

PSNR Comparison (Fig. 7): In terms of PSNR, the proposed model also outperforms all other methods, reflecting its ability to generate reconstructions with higher pixel-level fidelity and fewer distortions. A higher PSNR value suggests that

the reconstructed images maintain finer details and suffer less from reconstruction artifacts.

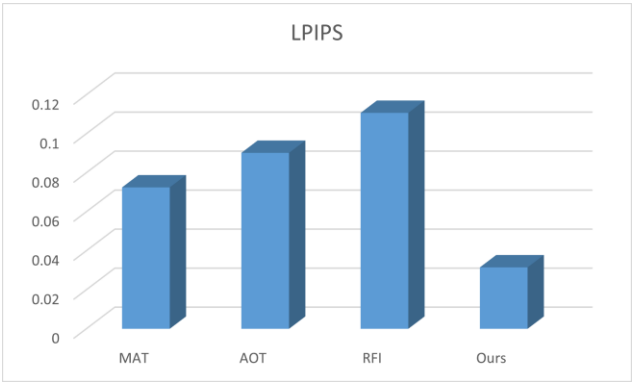

Fig. 7. Quantitative evaluation – LPIPS

LPIPS Comparison (Fig. 8): Regarding perceptual quality, the proposed model achieves the lowest LPIPS score among all compared methods. LPIPS measures the distance between deep feature representations of the reconstructed and ground-truth images; therefore, a lower score indicates better perceptual similarity. The significant improvement in LPIPS can be attributed to the introduction of perceptual loss during training, which guides the model to align high-level semantic features rather than merely optimizing pixel-wise accuracy. By enforcing consistency in a learned feature space, the model generates reconstructions that not only appear visually realistic but also maintain semantic coherence, effectively enhancing the perceptual quality of the completed face images.

Overall, the quantitative results consistently demonstrate that the proposed method surpasses existing techniques across all evaluation metrics. The superior performance in SSIM, PSNR, and LPIPS not only validates the effectiveness of the model in restoring visually realistic faces but also confirms its capability in preserving structural integrity and identity consistency under severe occlusion conditions. These results highlight the robustness and practical applicability of the proposed face reconstruction approach in challenging real-world scenarios.

4.2 3D avatar

3D avatars refer to virtual characters or personalized representations that are presented in digital form. In this stage, we mapped GANs results onto a 3D head or full-body avatar mesh. The development process runs in the rendering machine with an operating system of Windows 11, NVIDIA GeForce GTX 4060 graphics card,

16 GB of RAM, and a 2.20 GHz Intel Core i9-13900hx CPU. HMD Pico 4 Pro is used to capture the user's facial expression. Pico HMD has the inward-facing IR cameras for eyebrow tracking. Mouth, chin, and possibly cheeks were captured by the internal HMD camera.

Firstly, the unobstructed 2D face images generated by GANs need to be pre-processed to ensure that they can fit the texture requirements of 3D avatars. Specifically, through background removal and edge smoothing techniques, it cleans up excess parts of the face image and ensures that it does not appear unnecessari-ly distorted or stretched during mapping. Then, the cleaned 2D face image is used as a texture map and mapped to the predefined 3D head model by UV mapping technology. 3D head models typically use a standardized grid structure whose UV coordinates allow the GAN-generated images to fit accurately.

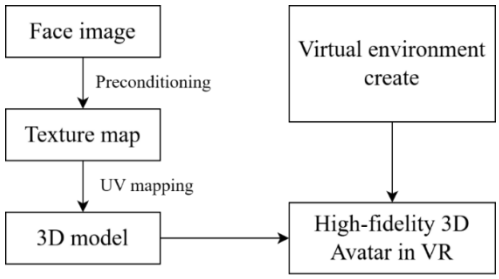

Fig. 8. Workflow for the face reconstruction applied to 3D avatar in VR

After completing the texture mapping, the 3D head model needs to be bound to the avatar's skeletal animation system, as in Fig. 10.

Fig. 9. High-fidelity 3D Avatar in VR

The Humanoid Rig or Skinned Mesh Renderer tool is used to integrate the head model with the bone structure of the VR avatar. The Pico 4 Pro captures facial expressions in real-time to drive the dynamic representation of the avatar's head so that the avatar's movements are consistent with the user's head movements. Finally, through the combination of 2D face images generated by GAN and run on a 3D

avatar, the 3D avatar model with high realism is run in the VR environment. The avatar not only accurately reflects the user's appearance but also supports dynamic interaction and real-time motion synchronization. Realistic 3D avatars can lead to higher acceptance in VR. Facial tracking can have an impact on the quality of avatars' communication in virtual conferences. Integrate reconstructed faces into 3D models like humanoid Rig or Skinned Mesh Renderer. Reconstructed faces are high-quality inpainted faces with occluded regions filled in.

5 Conclusion

In this study, we introduced a novel conditional GAN-based face reconstruction framework specifically designed to address severe occlusions caused by head-mounted displays (HMDs). Unlike traditional inpainting models that struggle with large-area occlusions, the proposed method effectively restores critical facial regions—such as the eyes and forehead—while preserving identity and structural consistency. By incorporating facial landmarks as conditional guidance, the model gains strong structural priors, enabling more accurate and coherent facial reconstructions. To support training and evaluation, we constructed a paired dataset of occluded and unobstructed face images based on publicly available face datasets. Experimental results demonstrate that our approach significantly outperforms existing methods in terms of visual realism, identity preservation, and reconstruction accuracy.

Furthermore, the generated facial textures are successfully applied to realistic 3D avatar reconstruction within VR environments. By integrating the reconstructed face with a rigged 3D model and real-time facial tracking using Pico 4 Pro, our system achieves expressive and dynamic avatar control that closely reflects user movements. This work bridges the gap between 2D GAN-based face completion and immersive 3D avatar generation, offering a practical and high-fidelity solution for HMD-occluded face recovery in virtual reality. In future work, we plan to extend this framework to support real-time deployment, dynamic facial expression synthesis, and more complex occlusion patterns.

Acknowledgements

The authors would like to thank the contributors of the FFHQ dataset for making high-quality face images publicly available for academic research.

Ethics Statement

This research involves no collection of personal or sensitive data. All training and evaluation were conducted using publicly available datasets (e.g., FFHQ), which are licensed for academic use and do not contain personally identifiable information. The face images appearing in the figures are of the authors themselves and are used with their informed consent.

References

1. Numan, N., Ter Haar, F., & Cesar, P. (2021, March). Generative rgb-d face completion for head-mounted display removal. In 2021 IEEE Conference on Virtual Reality and 3D User Interfaces Abstracts and Workshops (VRW) (pp. 109-116). IEEE
2. Chen, X., & Chen, H. (2023). Emotion recognition using facial expressions in an immersive virtual reality application. Virtual Reality, 27(3), 1717-1732.
3. Chen, S. Y., Lai, Y. K., Xia, S., Rosin, P. L., & Gao, L. (2022). 3D face reconstruction and gaze tracking in the HMD for virtual interaction. IEEE Transactions on Multimedia, 25, 3166-3179.
4. Meta Avatars, "https://developers.meta.com/ ", retrieved 2025
5. Yadav, V., & Kumar, S. (2024). Future of Augmented Reality: A Comprehensive Study on Apple Vision Pro. International Journal of Applied Marketing & Management, 9(1).
6. Wang, M., Wen, X., & Hu, S. M. (2019, October). Faithful face image completion for HMD occlusion removal. In 2019 IEEE International Symposium on Mixed and Augmented Reality Adjunct (ISMAR-Adjunct) (pp. 251-256). IEEE.
7. Cheung, Y. M., Li, M., & Zou, R. (2021, August). Facial structure guided GAN for identity-preserved face image de-occlusion. In Proceedings of the 2021 International Conference on Multimedia Retrieval (pp. 46-54).
8. Purps, C. F., Janzer, S., & Wölfel, M. (2021). Reconstructing Facial Expressions of HMD Users for Avatars in VR. In M. Wölfel, J. Bernhardt, & S. Thiel (Eds.), ArtsIT, Interactivity and Game Creation (Vol. 422, pp. 61–76). Springer International Publishing. https://doi.org/10.1007/978-3-030-95531-1_5
9. Lu, T., Peng, Z., Xing, X., Xu, X., & Pang, J. (2022). A General Method of Realistic Avatar Modeling and Driving for Head-Mounted Display Users. IEEE Transactions on Cognitive and Developmental Systems, 14(3), 916–925. IEEE Transactions on Cognitive and Developmental Systems. https://doi.org/10.1109/TCDS.2021.3080588
10. Gupta, S., Shetty, A., & Sharma, A. (2022, May). Attention based occlusion removal for hybrid telepresence systems. In 2022 19th Conference on Robots and Vision (CRV) (pp. 167-174). IEEE.
11. Li, W., Lin, Z., Zhou, K., Qi, L., Wang, Y., & Jia, J. (2022, June). MAT: Mask-Aware Transformer for Large Hole Image Inpainting. In Proceedings of the IEEE/CVF Conference on Computer Vision and Pattern Recognition (pp. 10758–10768).
12. Zeng, Y., Fu, J., Chao, H., & Guo, B. (2022). Aggregated Contextual Transformations for High-Resolution Image Inpainting. IEEE transactions on visualization and computer graphics (pp. 3266–3280).
13. Luo, W., Yang, S., & Zhang, W. (2023). Reference-Guided Large-Scale Face Inpainting with Identity and Texture Control. IEEE Transactions on Circuits and Systems for Video Technology(pp. 5498–5509).

14. Shah, R., Gautam, A., & Singh, S. K. (2022, November). Generative Adversarial Networks for Inpainting Occluded Face Images. In 2022 IEEE 6th Conference on Information and Communication Technology (CICT) (pp. 1-5). IEEE.
15. Rana, S. (2024). 3D Face Reconstruction from Occluded Images. Journal of Advanced College of Engineering and Management, 9, 33-39
16. Zhao, D. (2025). Learning Contour-Guided 3D Face Reconstruction with Occlusions. arXiv preprint arXiv:2503.12494.
17. Khas, D., Kumar, S., & Singh, S. K. (2021). Facial Occlusion Detection and Reconstruction Using GAN. In Computer Vision and Image Processing: 5th International Conference, CVIP 2020, Prayagraj, India, December 4-6, 2020, Revised Selected Papers, Part II 5 (pp. 255-267). Springer Singapore.
18. Li, Y., Ismail, A. W., & Deng, L. (2023, December). A Review of 3D Avatar Reconstruction for Virtual Conferencing. In International Conference on Advanced Computing and Intelligent Technologies (pp. 235-247). Singapore: Springer Nature Singapore.
19. Farahanipad, F., Rezaei, M., Nasr, M., Kamangar, F., & Athitsos, V. (2022, June). GAN-based face reconstruction for masked-face. In Proceedings of the 15th International Conference on PErvasive Technologies Related to Assistive Environments (pp. 583-587).
20. Karras, T. (2019). A Style-Based Generator Architecture for Generative Adversarial Networks. arXiv Preprint arXiv:1812.04948.

An Optimized Deep Learning Based Framework for Cognitive State Classification Using Brain-Computer Interface Technologies

[1]Dr.E.Padma, [2*]Dr.Gokulakrishnan S,[3] Dr.R.Chithra, [4]Mr.ArulKumar.R [5]Mrs.M.Kalaiselvi

[1]Assistant Professor, Dept of Computer Science & Engineering, Vels Institute of Science, Technology and Advanced Studies (VISTAS) Pallavaram, Chennai - 600117
epadma.se@vistas.ac.in
[2]Assistant Professor, Department of Computer Science and Engineering, Dayananda Sagar University Bengaluru
* Corresponding Author
[2*]gokul.krishnan-cse@dsu.edu.in
[3]Professor, Dept of Information Technology, K.S. Rangasamy College of Technology, Tiruchengode, Nammakal Dt., 637215
chithra@ksrct.ac.in
[4]Assistant Professor, Dept of Information Technology, Jeppiar Institute of Technology, Jeppiar Nagar, Sriperumbudur.
arulkumarcse@gmail.com
[5]Assistant Professor (SG), Department of Computer Science and Engineering (Cyber Security), Dr.N.G.P. Institute of Technology, Coimbatore- 641 048, Tamil Nadu, India.
kalaiselvi.mayilsamy@gmail.com

Abstract

The most widely recognized and bitter of all mental disorders has been known to be depression, which in fact transcends all the age cohorts hopelessly into the realm of human suffering. Such psychological discomfort resulting from delays in recognizing depressive symptoms or delaying intervention may lead to serious reactions which may develop into suicidal behaviors. Nevertheless, despite the wide prevalence of this condition, it remains poorly diagnosed and almost untreated owing to various forms of persistent societal stigma as well as a lack of acknowledgment of this condition as a bona fide mental illness. This research examined the effectiveness of six discrete machine learning classifiers for the identification of depression, which used a combination of socio-demographic and psychological features. The features from the dataset that can serve as significant predictors were selected using three feature selection algorithms- SelectKBest, Minimum Redundancy Maximum Relevance (mRMR), and Boruta-for the enhancement of the performance of all models. Finally, the Synthetic Minority Over-sampling Technique (SMOTE) was harnessed to tackle the problem of class imbalance in training data, thus improving models' generalizability and accuracy. Among the compared models, AdaBoost classifier with SelectKBest feature selection showed the highest accuracy score value of 92.56%. Further, complete evaluation metrics such as sensitivity, specificity, precision, and F1 score along with area under the Receiver Operating Characteristic curve (AUC) were computed to give a thorough insight into the diagnostic capacity of each model. These findings further endorse the premise that such methods would have varying promise in the early and precise detection of depression among different populations.

Keywords: Depression, Prediction, Machine learning Classifier, Feature selection, SMOTE and Redundancy.

1.Introduction

Persistent melancholy for a minimum of two weeks might be a symptom of depression, a mental illness. It makes it hard for sad people to do even the most basic of tasks, and they often lose the things that often provide them delight and satisfy their interests (World Health Organisation, 2021). Depression has emerged as a global health crisis in the context of the COVID-19 pandemic. Additionally, 322 million individuals throughout the globe are coping with depression individuals in the Western Pacific region account for almost half of these sad individuals South-East Asian areas. The number of people suffering from depression increased by 18.40% from 2005 to 2015, according to Vos et al. (2016). Health Organisation of the World, 2017. Diabetes, heart disease, and many other chronic illnesses have their roots in depression those suffering from depression. Second only to climate change in terms of causing disorders that persist over time (Oste et al., 2016; Whooley et al., 2013). Cases of suicide may be precipitated by severe depression. Worldwide, over 0.8 million suicide instances occur each year. Half of these instances are caused by depression (Otte et al., 2016). The social life of an individual is impacted by depression.

It may be difficult for those suffering from depression to open out to those closest to them, including family, friends, and coworkers. They have a hard time interacting with others because they are hesitant to form relationships An fixation with drugs and smoking might develop as a result of depression. (Thapar et al. 2012) found that it also hastens the onset of obesity.

Here are the main points of this work: Section 1 isolating the significant psychological and socioeconomic variables that contribute to the development of depression. Section 2 Building a database of people's socio-demographic and psychological data for the purpose of depression prediction. section 3 Investigating several ML and feature selection algorithms for effective depression screening section 4 A person suspected of having depression might participate in this research since the demographic and psychosocial data needed were simple will be more comfortable providing the necessary data for this research for the purpose of diagnosing depression, as opposed to responding to questions on many valid depression screening instruments. The following sections of the study are structured as follows: Section 2 describes the connected studies. The complete Section 3 explains the process. In Section 4, you may see the study's findings. Examining this work in relation to other current Section 5 presents the works. The paper concludes in Section 6, where it also introduces several possible scopes of upcoming research people often experience weariness. Their economic situation is impacted since their productivity declines due to their dissatisfaction with everyday activities and frequent feelings of exhaustion. So, unless those with depression get treatment quickly, it may wreak havoc on their social and financial situations. There will be detrimental effects on the socioeconomic position in the long term around the nation as well. The first important thing to do before counselling someone for depression is to be sure they are depressed task.

2. Related Work

It is necessary to do a thorough examination since the components of this kind of research topic are quite complicated. Several relevant research publications have been reviewed in this part to identify the research gaps and the methods and tools employed in the current studies.The prediction of depression was carried out by (Cvetković et al., 2017) among those battling breast cancer. A total of 84 participants, whose ages varied from 30 to 78, were interviewed in this study utilising a two-stage interview format. It all started with gathering socio-demographic information from patients. In the second, participants completed the BDI, a gold standard depression scale. The Assessment of BDI was used to determine the actual range of depression in the patients. Here, we employed the BDI test to establish a range for the goal variable of depression, and the predictor variables were traits extracted from the socio-demographic data. This study compared three different algorithms: one that used a genetic algorithm in a Fuzzy neural network (ANN), another that used a backpropagation learning technique, and a third that used an extreme learning approach. The most effective ANN in this case was one that used an extreme learning method. Iliou et al. (2019) suggested a data preprocessing method for depression prediction. The effectiveness of the Principal was evaluated by them. They compared the PCA approach with their suggested preprocessing method and discovered that the latter was superior. In their 2020 study, Na et al. anticipated that future depression will begin about the Korean Republic. The Random Forest classifier was used to construct the prediction model. SMOTE helped in coping dealing with problems caused by disparities in social classes. This research was successful in determining to 86.20 percent. Findings from this research also point to health satisfaction and happiness in social and family relationships as critical components in impact when depression first appears.

There is a wide range of mental diseases that mariners often experience.The purpose of the machine learning study by Sau and Bhakta (2019) was to identify depressive and anxious feelings among mariners. After testing five different machine learning classifiers for their ability to forecast sailors' levels of anxiety and depression, they settled on the CatBoost classifier as the most effective. Anxiety, stress, and associated data were collected by (Priya et al. 2020) using machine learning algorithms to detect depression and other mental illnesses. That is, in order to foretell depressive episodes, the with an accuracy of 85.50 percent, the Naive Bayes classifier demonstrated the most promising performance.

In order to foretell whether or not undergraduates in Bangladesh will suffer from depression, (Choudhury et al. 2019) conducted their research. At first, 935 pupils' data was gathered. Following data cleaning and using various data preparation methods, they drew upon the information of for 577 students to complete their research. They

got the best possible result of 75.00% using the Random Forest classifier. All things considered, the vast majority of these previous research have sought to forecast the likelihood of depression in a specificcategory of individuals, such as those with a certain medical diagnosis, those within a specific age bracket, etc. Overcoming this is the goal of this investigation. limitation by consideration of varied socio-demographic data pertaining to individuals with varying ages, health problems, and socio-economic backgrounds.

3. Proposed Deep Learning based Framework

3.1: Collecting Data

For the purpose of gathering information from Bangladeshi individuals throughout a variety of age groups. A total of 55 questions were crafted for the questionnaire. The first set of thirty questions was intended to collect data on the participants' socio-demographics, complex psychosocial factors, and the last 25 items of the BDCs. The survey was carried out over the time frame of the months of April and August 2020. Six hundred and four people have contributed their replies to the dataset. During the survey, BDC was used to measure the true degree of depression experienced by each participant. In this research, the updated BDC with 25 enquiries. The updated BDC has 25 questions that are organised into four groups. In the first ten questions, we probe participants' most recent emotional and mental states; in the next seven, we seek their individuals' current connections and pursuits. Five diagnostic items aimed at assessing core depressive symptomatology were used to evaluate the psychological and somatic state of health of the participants. Pertaining to the frameworks argued by Burns (1999) and Jabbar and Zaza (2019), the last three items sought to assess suicidal ideation and affective disturbances. The screening for depression was facilitated by the Burns Depression Checklist (BDC), upon which participants were asked to rate the extent of depressive symptoms within the last seven days, inclusive of the day of evaluation. The BDC is a well-recognized and psychometrically validated tool for the evaluation of the presence and severity of both clinical and subclinical depression developed by Dr. David Burns.It is reliable and focusses on depressive symptoms specifically rather than generalised ones (Burns et al., 2013). As one of the most trustworthy measures for assessing depression, BDC has a Cronbach's alpha of 0.89 (Holtz et al., 2014). To get a person's total BDC score, we sum the intensity of every one of the symptoms described by the patient. A sad individual is defined in BDC as having an overall score more than 10. If not, then it is assumed that the individual is not depressed. Each subject was classified as depressed or not depressed according to their BDC score in this research.

3.2. Data description

There is one goal variable and thirty predictor variables in the survey dataset. We used the to determine the target variable. Distributes Burns Depression Checklists (BDCs) to all participants.

3.3 Evaluation of Data

There were 397 cases of depression among the 604 people who took part in the study. In reality, the overall prevalence of depression in Bangladesh is far lower than the 65.73 percent who took part in the survey. It is possible that the respondents were more prone to depression since the data was collected during the COVID-19 epidemic, which triggered a worldwide socioeconomic and psychological catastrophe. 34.27 percent of those who took part in the discovered that they are not depressed. The proportion of individuals in the sample who are not depressed is shown in Table 2. Table 3 displays the distribution of participants in the sample who are depressed and those who are not, broken down by several parameters. The female individuals experience a higher prevalence of depression compared to the male ones. For whatever reason, 69.80 percent of the women and 64.40 percent of the men in the study suffer from depression. Those who work for the government tend to have the lowest rates of depression when considering that career.

Depression affects only 40% of government job holders. People who are self-employed or who are out of work tend to be more depressed than those who are not. How common is depression? on the part of those taking part in the business is 90%. Depression affects 75% of the jobless participants. Depressive symptoms as a proportion of students, participants with private sector jobs, 64.63% with other professions, and 70.59% with no specific work description. Depression strikes the individuals who have gone through a divorce the worst. In this study, married individuals had the lowest depression rate. Married people (63.22%), single people (65.95%), and those who have

been through a divorce (100%) all suffer from depression. People living in rural areas have a lower risk of developing depression. Of the people living in the hamlet, 57.14% suffer from depression. Depressive disorder prevalence rates in the percentage of participants residing in urban areas is 67.85% and that in suburban areas is 68.75%.

$$x^2 = \sum_{i=1}^{n} \frac{(OF_i - EF_i)^2}{EF_i} (1)$$

3.4.2: Minimum Redundancy And Maximum Relevance

The Minimum Redundancy and Maximum Relevance (mRMR) technique was suggested by Peng et al. (2005) as a feature selection approach. Features are prioritised in the mRMR feature selection approach according to how relevant they are to the target variable. The redundancy of characteristics is also taken into account while rating them. According to mRMR, the most important feature is the one that is both highly relevant to the target variable and has the fewest redundant characteristics. Mutual Information is a tool for gauging both relevancy and redundancy.

Table 1: Description of Variables and Their Attributes

Attributes	Type	Description	Ranges
AGERNG	Predictor	Age bracket of respondent (in years)	18–22, 23–27, 28–32, 33–37, 38–42, 43–47, 48–52, 53–57, 58+
GENDER	Predictor	Biological sex of the respondent	Male, Female, Other
EDU	Predictor	Highest academic qualification attained	SSC, HSC, Bachelor's, Master's, Doctorate
PROF	Predictor	Employment sector or occupational category	Student, Private Employee, Government Employee, Entrepreneur, Unemployed, Freelance
MARSTS	Predictor	Legal marital status	Single, Married, Separated
RESDPL	Predictor	Geographical type of current residence	Rural, Semi-urban, Urban
LIVWTH	Predictor	Household status indicating living with family or not	With Family, Alone
ENVSAT	Predictor	Satisfaction with residential environment	Satisfied, Not Satisfied
POSSAT	Predictor	Satisfaction with personal/professional achievement	Satisfied, Not Satisfied
FINSTR	Predictor	Presence of financial burden or monetary stress	Yes, No
DEBT	Predictor	Current debt obligations	Yes, No
PHYEX	Predictor	Physical activity engagement frequency	None, Occasional, Routine
SMOKE	Predictor	Usage of tobacco or smoking behavior	Yes, No
DRINK	Predictor	Alcohol consumption status	Yes, No
ILLNESS	Predictor	Presence of diagnosed chronic or serious illness	Yes, No
PREMED	Predictor	Ongoing use of prescribed pharmacological treatment	Yes, No
EATDIS	Predictor	Disordered eating habits such as anorexia or binge eating	Yes, No
AVGSLP	Predictor	Average nightly sleep duration	< 5 hrs, 5 hrs, 6 hrs, 7 hrs, 8 hrs, > 8 hrs
INSOM	Predictor	Reported symptoms of insomnia	Yes, No
TSSN	Predictor	Time spent daily on social media platforms	< 2 hrs, 2–4 hrs, 5–7 hrs, 8–10 hrs, > 10 hrs
WRKPRE	Predictor	Perceived intensity of academic/work-related pressure	High, Medium, Low, None
ANXI	Predictor	Recently experienced anxiety	Yes, No
DEPRI	Predictor	Perceived deprivation of rights or expectations	Yes, No
ABUSED	Predictor	Experience of abuse (emotional, physical, or sexual)	Yes, No
CHEAT	Predictor	Experience of betrayal or deception recently	Yes, No
THREAT	Predictor	Exposure to any recent life-threatening situation	Yes, No
SUICIDE	Predictor	Suicidal ideation reported in the recent past	Yes, No
INFER	Predictor	Occurrence of feelings of inferiority	Yes, No
CONFLICT	Predictor	Recent interpersonal conflicts with peers or family	Yes, No
LOST	Predictor	Loss of a loved one or someone close	Yes, No
DEPRESSED	Target	Classification label for depression based on self-report or clinical cues	0, 1

Table 2: Stratified Distribution of Participants Based on Depression Status

Depression Status	Frequency (n)	Proportional Representation (%)
Clinically Depressed	421	62.40%
Not Clinically Depressed	254	37.60%
Total	675	100.00%

Assume about m and n, two arbitrary integers. The following equation describes their reciprocal information:

$$I(m,n) = \iint p(m,n) log \frac{p(m,n)}{p(m)p(n)} \, dm \, dn \quad (2)$$

Here, the joint stochastic density is denoted as p(m, n), whereas the marginal stochastic densities are p(m) and p(n), respectively. This is the equation that summarises the significance of the characteristic Xi:

$$\int^{mRMR} (x_i) = I(Y, x_i) - \frac{1}{|s|} \sum_{xsεS} I(x_s, x_i) \ (3)$$

In this case, S stands for the collection of chosen characteristics, and Y is the target variable. Xs is a feature that has been chosen from set S, whereas Xi is one that has not been chosen quite yet.

3.4.3 Feature selection method developed by Boruta

According to Kursa and Rudnicki (2010), the Random Forest classification method is encased in the Boruta algorithm. The technique targets the removal of unimportant traits in an iterative fashion in order to pick significant features. Here are the stages of the Boruta algorithm:

To begin, we make a copy of each feature and add it to the dataset. 2. you'll shuffle the values of the feature duplication. Their correlations with the target variable are removed by shuffling. 3. the enlarged dataset is processed using a random forest technique, and Z-scores are calculated. 4. involves finding the Maximum Z-score among the Shadow Attributes, or MZSA. Feature removal from the dataset occurs in 5.Its significance is significantly lower than MZSA. However, features are retained in the dataset if their significance is significantly higher than MZSA. 6. Remove the dataset's shadow features 7. Continue repeating the steps until the dataset is free of irrelevant features or until a certain number of iterations has been established. Thirdly, the SMOTE method, also known as synthetic minority oversampling.

Table 3: Demographic Stratification of Depression Prevalence Among Participants

Criteria	Category	Total Participants (n)	Depressed (n)	Not Depressed (n)	Depressed (%)	Not Depressed (%)
Gender	Male	460	298	162	64.78%	35.22%
	Female	151	109	42	72.19%	27.81%
Profession	Business Owner	12	10	2	83.33%	16.67%
	Govt. Employee	11	5	6	45.45%	54.55%
	Private Sector	85	55	30	64.71%	35.29%
	Student	448	290	158	64.73%	35.27%
	Unemployed	47	36	11	76.60%	23.40%
	Other	18	13	5	72.22%	27.78%
Marital Status	Married	89	56	33	62.92%	37.08%
	Unmarried	519	341	178	65.70%	34.30%
	Divorced	4	4	0	100.00%	0.00%
Residential Location	Rural (Village)	138	79	59	57.25%	42.75%
	Semi-Urban (Town)	162	109	53	67.28%	32.72%
	Urban (City)	311	216	95	69.45%	30.55%

The minority class's forecast accuracy may be improved by ensuring that the dataset is balanced. An Approach to Synthetic Minority Oversampling address the issue of class imbalance, SMOTE is used. SMOTE creates minority-class synthetic samples by using feature-basedthe area. A synthetic sample, or samples from any of the K-nearest minority classes, are inserted along the line that adjoins each minority class sample neighbours in the class that you are studying. The first step in making a fake instance is to find the difference between the minority class instance's feature vector under thinking about it and multiplying it by an arbitrary integer for its closest neighbour in the range of zero to one. A synthetic example of a minority class is then created by adding the multiplied result to the feature vector being considered as stated by Chawla et al. (2002). It is possible to express the synthetic sample fnew that was created using Eq. (4).

$$f_{new} = f_1 + (f_i - f_{new}) xR \ (4)$$

Here, R is an arbitrary integer from 0 to 1.

3.6. Neural network-based methods for diagnosing depression

Using six distinct machine learning classifiers—KNNs, AdaBoosting, GBs, XGBoosts, Bagging, and the Weighted Voting classifier—this work has attempted to predict the absence of sadness.

3.6.1. the K-nearest neighbour (KNN) algorithm

The number of closest neighbours, or K value, is the main factor that determines this classifier. When K equals 1, the newly created instance is automatically assigned to the class of its closest neighbour (Ali et al., 2019). A number of length measure are applicable to KNN and include, among others, the Minkowski, Hamming, and Euclidean distances. Our research has made use of the Minkowski distance parameter. Think about two points, F(f1, f2,..., fn) and E(e1, e2,..., en). The below equation represents the Minkowski Distance between the aforementioned two locations:

$$distance(E,F) = \left(\sum_{i=1}^{n}(|e_i - f_i|^{\frac{1}{q}}\right)(5)$$

3.6.2. AdaBoost, an adaptive boosting method

One kind of ensemble learning is the Adaptive Boosting classifier, or AdaBoost classifier. Building a robust classifier requires makes use of a set of ineffective classifiers. This method involves training a poor classifier to improve by analysing its previous mistakes. Here we have a dataset by using n samples. At first, a weight of (1⁄n) is given to every sample.
This dataset is used to develop a weak classifier. The classifier's total error ε is calculated. The impact of classifier α on data sample classification is evaluated using this total error in the following equation:

$$\alpha = 1/2\ln\left(\frac{1-\epsilon}{\epsilon}\right)(6)$$

A new dataset is created by using α to change the weight of the dataset's samples. In the future, the next weak classifier will be built using this updated dataset. In the end, the class label of a sample is determined by the majority vote of the weak classifiers (Vasilić et al., 2018).

3.6.3 Graded boosting

The Gradient Boosting (GB) classifier employs a group of less robust models to sequentially produce new models. To avoid overfitting problems, it is crucial to cease boosting using stopping criteria in a timely manner. A terminating criterion might be a maximum number of models developed or a threshold on the predicted accuracy (Rahman et al., 2020).

$$f(x) = \sum_{i=1}^{M} wigi(x{:}\,\theta i)(7)$$

3.6.4. XGBoost

When compared to GBDTs, Extreme Gradient Boosting is the faster and more scalable option. The regularisation is added to the goal function of XGBoost. when using the loss function. The goal function of XGBoost is shown by the following equation:

$$I(\theta) = L(\theta) + \Omega(\theta), where\ L(\theta) = I(z,y), \Omega(\theta) = \alpha T + \left(\frac{1}{2}\right)\lambda||w||2\ (8)$$

The loss function is denoted by L(θ) in the above equation, whereas the regularisation is denoted by $\partial(\theta)$. The parameter that was trained is denoted by θ. according to the published research (Zhang et al., 2018; Chen et al., 2018). The following equation may be used to describe L(θ) using the mean square loss function:

$$L(\theta) = I(z,y) = (z - y^2)\ (9)$$

$$L(\theta) = I(z,y) = yln(1 + e^{-z}) + (1 - y)\ln(1 + e^{z})\ (10)$$

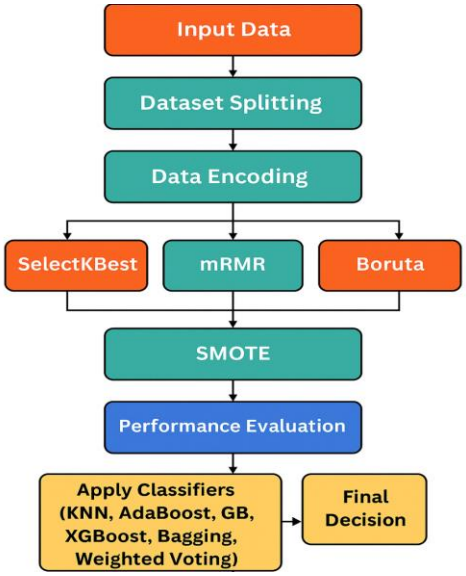

Figure 1: Deployment procedures for forecasting the way of depression

3.6.5 Classifier for bagging

Bagging is a new method that uses aggregating and bootstrapping as its foundation. You may use bootstrap datasets with the Bagging classifier built using the data set used for training. The last step in getting the final forecast is to combine the findings of all the classifiers. Here in bootstrapping Thus, it is common practice to steer clear of training items that can be deceptive. Additionally, it is common for the aggregated classifiers to outperform the individual ones. (Duin and Skurichina, 2002). Since the Bagging classifier makes use of both of these characteristics, it often outperforms competing classifiers. The following procedures are involved in bagging: Step: With n ranging from 1 to N:

a. Take the training dataset X and make a bootstrap replication Xn.

1. Build a model Cn(x) using Xn. Step II: Use majority voting or averaging to aggregate the models Cn(x) where n = 1, 2,..., N. This research has used Multilayer Perceptron (MLP) classifiers to bag data.

3.6.6. Using weights to choose voters

One of the simplest ensemble learning approaches, the voting classifier combines the output of various base classifiers (Kumar et al., 2017). The classifiers could vary in their composition. The hard voting strategy in an ensemble approach consists of taking the class predictions from different base classifiers and voting for the majority to assign the final class label. On the other hand, instead of taking a vote of the votes like averaging them, one can take the predicted class probabilities constructed by the classifiers through soft voting to compute the final output. Weighted voting can be looked at as an extension of soft voting, where a classifier is assigned with a relative importance (weight) based on its performance.

$$y_p = arg\max_i \sum_{k=1}^{m} w_k p_{ik} \quad (11)$$

3.7. Processes for implementation

Python and the Scikit-learn library were used to accomplish this work. There are 604 participants' records in the obtained dataset. It is composed using only one dependent variable and thirty independent ones. The presence or absence of depression is indicated by the target variable. The suggested system is fed the dataset once it has been

prepared. Fig. 1 shows the study's implementation techniques graphically. In the sections that follow, you will find detailed instructions on how to carry out this research.

3.7.1. Separating datasets

The first step was to partition the acquired dataset into two sets: training and test. Eighty percent of the dataset was used as training data in this research. Additionally, testing has made use of the remaining 20% of the dataset.

3.7.2. Encoding data

By utilising most machine learning algorithms perform better when given numerical data. As part of the Data Encoding process, the Scikit-Learn library's Label Encoder was used to transform the training and test datasets into their numerical counterparts.

3.7.3. Using feature selection to modify the training and testing dataset

The classifiers' performance is negatively affected by characteristics that are not relevant. As a means of gleaning useful information from the dataset, this research used three distinct feature selection methods. The mRMR feature selection method and the SelectKBest feature selection method both have extracted fifteen predictor variables for use in conducting classification effectively. Thirteen of the most important predictor variables were identified from the whole dataset using the Borut feature selection technique. The attributes that were chosen using these three methods are shown in Table 4.

Table 4: Comparative Evaluation of attributes with methods

Method	Total Features Evaluated	Top-Ranked Selected Features
SelectKBest (Chi-Square)	15	DEPRIs, ANXIs, POSSATs, ABUSEDs, INFERs, ENVSATs, CHEATs, CONFLICTs, FINSTRs, SUICIDEs, EATDISs, INSOMs, WRKPREs, TSSNs, DRINKs
mRMR (Minimum Redundancy Maximum Relevance)	15	ANXIs, INFERs, ENVSATs, DEBTs, SUICIDEs, POSSATs, ABUSEDs, CHEATs, CONFLICTs, DEPRIs, LOSTs, INSOMs, THREATs, PHYEXs, WRKPREs
Boruta (Random Forest-Based Wrapper)	14	DEPRIs, POSSATs, ANXIs, ENVSATs, INSOMs, FINSTRs, ABUSEDs, CHEATs, CONFLICTs, SUICIDEs, THREATs, PHYEXs, TSSNs, LOSTs

Feature selection algorithms have introduced new safeguards to prevent data breaches been implemented just on the training dataset. With these three feature selection methods in mind, three sets of newly original training dataset was used to produce the test dataset, and the test dataset was used to construct the training dataset.

3.7.4. SMOTE applied on the training data

The consequences of learning a classifier through an imbalanced dataset often lead to biased performances of the model and, hence, to the skewing of prediction toward the so-called majority class, leading to poor generalization. In the present study, the training data are highly imbalanced, as 66.87% of instances were labeled "Depressed" and only 33.13%as "Not Depressed." To avert this situation and improve discriminating potential, SMOTE was used in the current study. SMOTE considers two existing instances and synthetically generates new samples for the minority class in this manner; in doing so, SMOTE contributes to the balancing of class distributions. In Table 5, the class proportions before and after application of SMOTE are shown, indicating an even class distribution afterward.

Table 5: Class Distribution Before and After SMOTE Application

Scenario	Depressed Class (%)	Non-Depressed Class (%)	Total Distribution (%)
Pre-SMOTE Imbalance	68.24%	31.76%	100.00%
Post-SMOTE Balancing	50.00%	50.00%	100.00%

3.7.5. Predicting depressive symptoms by training and testing

A bundle of supervised learning algorithms-K-Nearest Neighbors, AdaBoost, Gradient Boosting, and XGBoost-

were used as base learners in this study. Furthermore, ensemble learning techniques of Bagging and Weighted Voting were used to improve prediction performance. These classifiers were trained on the preprocessed datasets for training, and subsequently used for estimating the likelihood of depression among the participants in the test dataset.

3.7.6. Assessment of performance and ultimate determination

At this point, a variety of evaluation metrics were computed on the different predictive models built in the previous section, including F1-score, specificity, accuracy, precision, sensitivity (recall), and AUCs. These benchmarks are used to assess the diagnostic power and generalizing ability of each classifier. The best predictive model for classifying depression was thus ultimately chosen based on its overall superior performance over these extensive evaluation metrics.

4. Experimental Outcome

For testing purposes, the answers of 121 people have been used. The first state of depression is experienced by 61.16% of the individuals there are 38.84% of people who aren't depressed. The models' F1-score, accuracy, sensitivity, specificity, and precision were calculated using the following formulae for performance evaluation:

$$Accuracy = \frac{TN + TP}{TP + TN + FP + FN} * 100 \quad (12)$$

$$Sensitivity = \frac{TP}{TP + FN} * 100 \quad (13)$$

$$Specificity = \frac{TN}{TN + FP} * 100 \quad (14)$$

$$Precision = \frac{TP}{TP + FP} * 100 \quad (15)$$

$$F1 - Score = \frac{2 * TP}{2 * TP + FP + FN} * 100 \quad (16)$$

In this case,

- True Positive (TP): This is the result that is known when the classifier correctly predicts that a person is sad.
- (TP).
- True Negative (TN): The result is known when the classifier predicts that a participant who does not have depression does not have depression.
- when expressed as TN.
- False Positive (FP): This is the result that occurs when a classifier predicts that a person who is not depressed really is depressed.

An FP, or false positive.

False Negative (FN): This kind of result occurs when a classifier incorrectly predicts that a person who is depressed is not depressed.For each classifier that used a different feature selection strategy, Table 6 displays the corresponding confusion matrices of the projected outcomes. Table 7 shows the classifiers' assessed accuracy, sensitivity, specificity, precision, F1-score, and AUC for the built models.

The results of the Bagging classifier's demonstration of optimal outcome achieved with an accuracy level of 89.26% without using feature selection. In this case, KNN has shown the lowest level of accuracy. After achieving a precision of 64.94%. The AdaBoost, GB, XG-Boost, and Weighted Voting classifiers have attained accuracies of 87.60%, 86.78%, and 85.95%, as well as 86.78 percent. All of these classifiers have shown a significant improvement in accuracy after using various feature selection strategies. while compared to other classifiers, AdaBoost had the highest accuracy while utilising the SelectKBest feature selection method. A 92.56% success rate has been attained. Incorporating the SelectKBest feature selection strategy yields the following classifier accuracies: 85.12% for KNN, 91.74% for GB, 86.78% for XGBoost, 90.91% for Bagging, and 91.74% for

Weighted Voting.

The following classifiers: KNN, AdaBoost, GB, XGBoost, Bagging, and Weighted Voting all obtained accuracies of 90.91%; 86.78%, 90.08%, and 90.91%, respectively. When assessing a model's efficacy, sensitivity and specificity are crucial. The ability of a model increases as its sensitivity increases to determine which individuals suffer from depression, while a more specific model can more accurately determine which participants do not suffer from depression. Because it does not use feature selection methods, the Bagging classifier is the most sensitive at 93.24 percent. However, only 82.98% of the target precision was achieved by the Bagging classifier. In contrast, without doing feature selection, the KNN classifier achieved the greatest specificity of 87.23%. However, KNN has shown the really poor performance. In this case, KNN's attained sensitivity is 54.05 percent.

Table 6: Classifier-Wise Performance Metrics with and without Feature Selection Techniques

Classifier	Feature Selection Technique	TP	TN	FP	FN
KNNs	No Feature Selection	42	39	8	32
AdaBooster		70	36	11	4
GBs		68	37	10	6
XGBooster		67	36	11	7
Bagging		70	38	9	4
Weighted Voting		69	37	10	5
KNNs	SelectKBest	60	43	4	14
AdaBooster		69	43	4	5
GBs		70	42	5	4
XGBoost		68	40	7	6
Bagging		69	41	6	5
Weighted		70	41	6	4
KNNs	mRMR	61	42	5	13
AdaBooster		68	43	4	6
GBs		69	40	7	5
XGBooster		68	40	7	6
Bagging		68	41	6	6
Weighted Voting		69	40	7	5
KNNs	Boruta	62	41	6	12
AdaBooster		70	41	6	4
GBs		69	41	6	5
XGBooster		67	38	9	7
Bagging		69	40	7	5
Weighted Voting		69	41	6	5

Table 7: Enhanced Classification Performance Metrics with Feature Selection Techniques

Classifier	Feature Selection	Accuracy (%)	Sensitivity (%)	Specificity (%)	Precision (%)	F1-Score (%)	AUC
KNN		67.48%	55.88%	85.41%	87.18%	67.59%	0.78
AdaBooster		88.35%	92.65%	81.63%	89.10%	90.84%	0.94
GBs		87.53%	91.17%	81.56%	88.72%	89.92%	0.95
XGBooster		86.71%	90.44%	80.29%	87.68%	89.02%	0.94
Bagging		89.42%	93.38%	83.85%	90.02%	91.67%	0.96
Weighted Voting		87.65%	91.32%	81.98%	88.57%	89.91%	0.95
KNN	SelectKBest	85.45%	80.15%	92.84%	94.78%	87.02%	0.92
AdaBoost		93.02%	92.21%	94.22%	96.13%	94.15%	0.97
Gradient Boost		92.33%	92.94%	92.12%	95.28%	94.10%	0.96
XGBoost		87.15%	90.59%	82.42%	88.40%	89.48%	0.94
Bagging		91.17%	91.91%	90.88%	94.72%	93.29%	0.96
Weighted Voting		92.28%	92.65%	91.87%	95.03%	93.82%	0.96
KNN	mRMR	84.78%	79.71%	91.33%	93.32%	85.95%	0.91
AdaBoost		92.22%	91.47%	94.13%	95.53%	93.45%	0.96
Gradient Boost		90.35%	92.79%	88.06%	92.15%	92.47%	0.96
XGBoost		90.39%	92.13%	87.68%	91.73%	91.92%	0.95
Bagging		90.52%	91.76%	89.87%	93.24%	92.49%	0.96
Weighted Voting		90.85%	92.25%	88.84%	91.91%	92.08%	0.96
KNN	Boruta	85.29%	82.72%	89.48%	92.68%	87.36%	0.91
AdaBoost		92.45%	93.56%	89.73%	94.15%	93.85%	0.96
Gradient Boost		91.28%	92.21%	89.33%	93.49%	92.84%	0.96
XGBoost		87.03%	89.04%	83.15%	89.03%	89.03%	0.93
Bagging		90.21%	92.10%	87.52%	92.18%	92.14%	0.96
Weighted Voting		91.53%	92.67%	89.21%	93.07%	92.87%	0.96

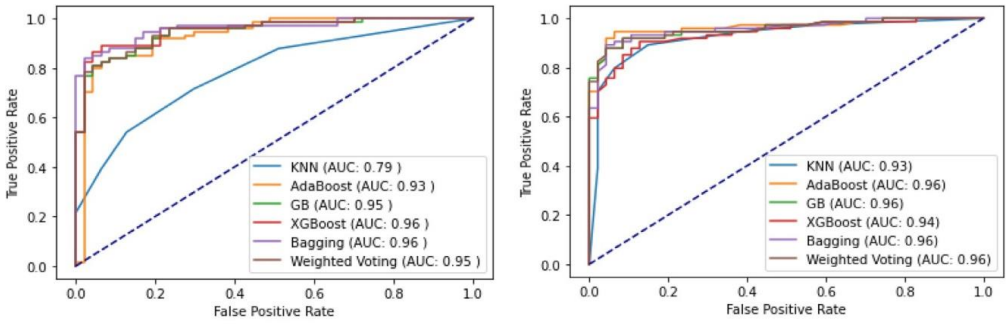

(a) ROC Curves of the Classifiers Without Feature Selection

(b) ROC Curves of the Classifiers with SelectKBest Feature Selection

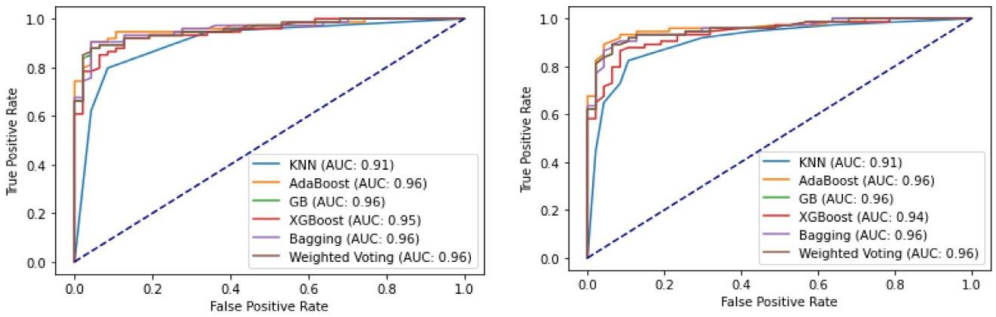

(c) ROC Curves of the Classifiers with mRMR Feature Selection

(d) ROC Curves of the Classifiers with Boruta Feature Selection

Figure 2: ROC Curves of the classification for their various attributes selection methods

Among the feature selection methods tested, Ad-aBoost had the best results in terms of sensitivity and specificity when using SelectKBest. 93.62% and 91.89%, correspondingly. Among the tested methods, AdaBoost had the best sensitivity (93.24% vs. 89.36%) and specificity (90.36%). scenario including the Boruta feature selection method is well. We used mRMR to identify features, and then we used GB, XGBoost, and Weighted

With a sensitivity level of 91.89%, voting classifiers are now the most sensitive. Their specificities are 87.23%. At 93.62%, AdaBoost achieved the maximum specificity in this case. However, it has attained a sensitivity level of 90.54 percent. Therefore, by looking into how well the classifiers performed in safe to say that the classifiers' sensitivity and specificity were enhanced after using the feature selection strategies mentioned before. Additionally, the models' Area Under Curve (AUC) values have been computed. A model is considered to be ideal if and only if its area In addition, for each classification model, Area Under the Receiver Operating Characteristic Curve (AUC-ROC) values have been computed in order to evaluate their discriminative ability. A perfectly discriminating model is one with an AUC of 1.0, meaning it classifies all instances of the positive and negative classes flawlessly. In contrast, an AUC of 0.5 means that the model discriminates no better than random chance. Therefore, a higher AUC score is indicative of a stronger, more reliable classifier.

Therefore, it is always preferable for a model to have a larger AUC value. Classifier performance was improved across the board, including AUC, Precision, and F1-score, thanks to the aforementioned feature selection strategies. Using the Receiver Operator Characteristic (ROC) curve, we can see how the models' sensitivity and specificity are balanced out. The True Positive Rate is shown on the y-axis and the False Positive Rate is shown on the x-axis of this two-dimensional graph. As the time comes to A classifier's performance improves as its ROC curve moves closer to the graph's upper left corner. Pictured in Figure 2 (a)-(d) are the ROC curves. each of these classifiers has a unique method for selecting features. Figure 2 shows that the classifiers' ROC curves have shifted towards the feature selection algorithms are used, the graph's top left corner. Classifiers have become quicker by using various feature selection approaches to reduced amount of features. Figure 3 shows that various feature selection strategies have drastically cut the classifiers' training time. As shown in Figure 3, mRMR has shown to be more effective than other feature selection strategies when it comes to reducing the training time of the KNN classifier. A feature selection method developed by Boruta has reduced the training time spent on feature selection by Bagging and Weighted Voting classifiers compared to others. In light of the above, it is clear that, when compared to other feature selection techniques, SelectKBest has shown to be the most effective in reducing the training time required for segmentation algorithms.

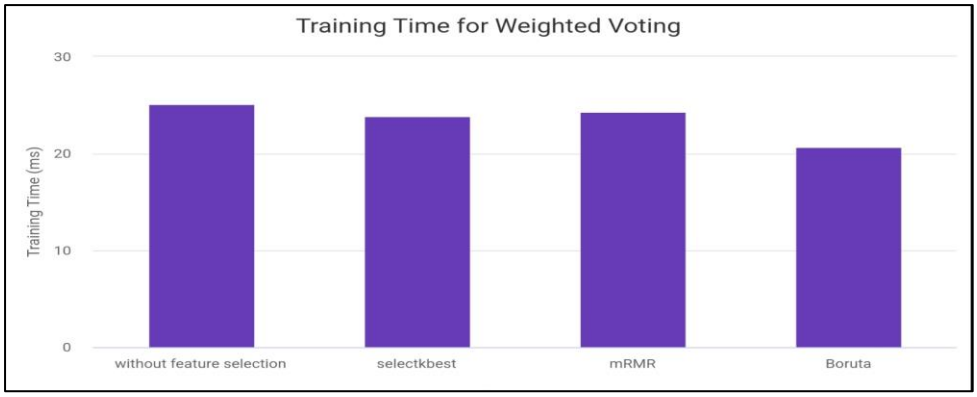
Training Time for Weighted Voting
Training Time (ms)
30
20
10
0
without feature selection
selectkbest
mRMR
Boruta

(a)

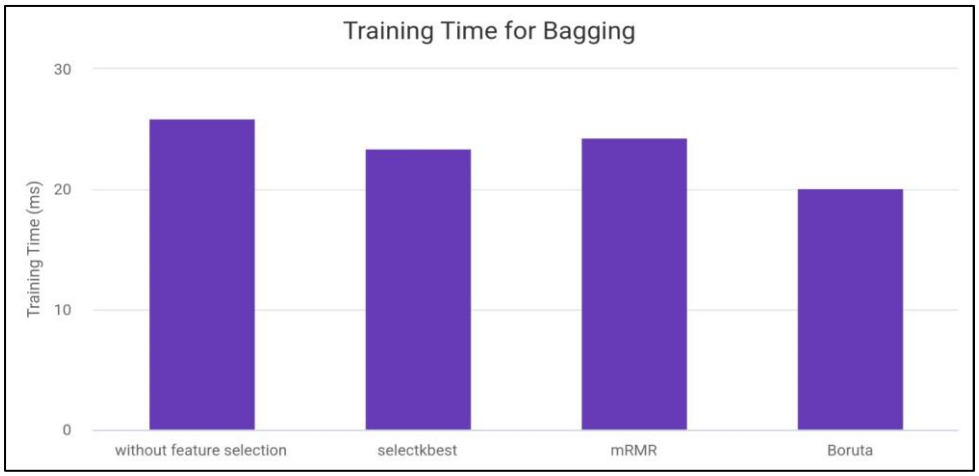
Training Time for Bagging
Training Time (ms)
30
20
10
0
without feature selection
selectkbest
mRMR
Boruta

(b)

Training Time for XGBoost
Training Time (ms)
80
60
40
20
0
without feature selection
selectkbest
mRMR
Boruta

(c)

Training Time for GB
Training Time (ms)
150
100
50
0
without feature selection
selectkbest
mRMR
Boruta

(d)

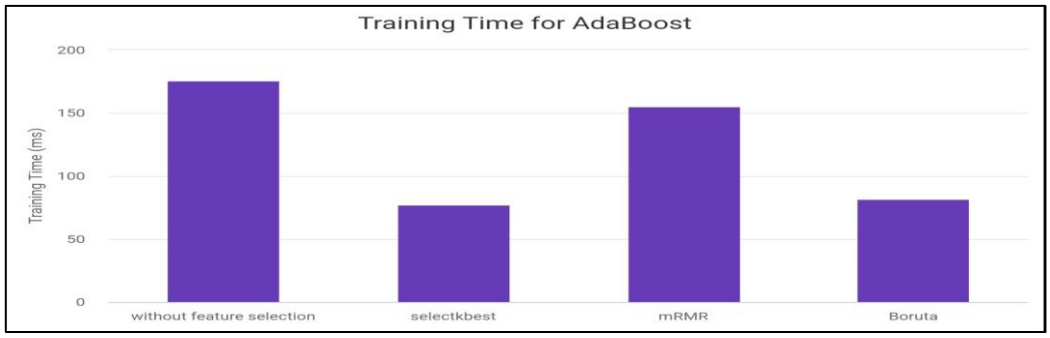

(e)

(f)

Figure 3: Training time (a-f) of the classifications to different attribute selection strategies

After looking at how several models performed, we can say that the AdaBoost classifier and the SelectKBest feature selection method were the most effective. has outperformed the competing models on a variety of performance criteria, including accuracy, area under the curve (AUC), and ROC curves. Alphabet classifier The feature selection strategy using SelectKBest achieved the greatest accuracy of 92.56%. Attained the greatest AUC value is this model as well. of 96.06%. The characteristics that are not relevant are discarded using the Boruta feature selection method. use the Maximum Z-score as data. Seventeen predictor variables were excluded from this research using this approach according to the Maximum Z-score as well as the other thirteen predictor variables.

Table 8: Classifiers Across Feature Subset Sizes Using SelectKBest and mRMR

Feature Selection Technique	Classifier	Top 10 Features	Top 11 Features	Top 12 Features	Top 13 Features	Top 14 Features	Top 15 Features
SelectKBest	KNN	81.12%	82.04%	83.67%	85.89%	86.71%	85.43%
	AdaBoost	88.23%	89.67%	88.91%	92.15%	93.02%	92.45%
	Gradient Boosting	86.32%	87.01%	88.12%	91.32%	90.94%	92.01%
	XGBoost	83.78%	86.12%	86.95%	87.42%	88.27%	87.38%
	Bagging	86.47%	86.73%	88.20%	90.37%	91.08%	91.05%
	Weighted Voting	86.15%	87.42%	87.91%	91.08%	90.36%	91.92%
mRMR	KNN	81.48%	85.03%	81.82%	84.47%	84.73%	85.21%
	AdaBoost	88.01%	89.14%	91.22%	92.33%	92.12%	91.85%
	Gradient Boosting	84.29%	87.38%	91.13%	90.74%	90.12%	91.37%
	XGBoost	85.72%	89.34%	91.02%	88.92%	90.43%	91.45%
	Bagging	86.28%	89.06%	91.23%	91.17%	90.61%	91.36%
	Weighted Voting	84.63%	87.83%	91.14%	90.24%	90.07%	91.28%

The $\chi 2$ score has been used by the SelectKBest algorithm to rank the predictor variables. In contrast, the mRMR algorithm has organised the predictor variables according to their significance and degree of duplication. Similar

to previous research that has used the top fifteen predictor factors from mRMR and SelectKBest, this study has done the same. The most effective use of predictor variables as classifier inputs is shown by the outcomes. Table 4 shows the fifteen attributes that the SelectKBest algorithm deemed most important. This is the ranking of the mRMR algorithms. Table 8 compares the performance of several classifiers using a variety of characteristics ranked by both SelectKBest and mRMR algorithms.According to Table 8, most classifiers perform best when the top fifteen features are used as input variables for the SelectKBest and mRMR algorithms.

Table 9: Comparative Summary of Prior Research on Depression Detection and Screening Methodologies

Sample Size	Target Population	Data Acquired	Feature Extraction	Screening Instrument	Classification Accuracy (%)
92	Oncology patients	Socio-demographic variables	✕	Standardized Beck Depression Inventory (BDI)	Not specified
6588	Multigenerational Korean citizens with varied occupations	Clinical, socio-demographic, and economic features	✓	CES-D-11 (Center for Epidemiologic Studies Depression)	87.10%
510	Elderly care patients	Socio-demographic and health profile	✓	Hospital Anxiety and Depression Scale (HADS)	88.40%
279	Geriatric individuals	Psychometric and demographic data	✕	Patient Health Questionnaire (PHQ-9)	75.30%
180	Postpartum mothers	Risk indicators and demographic data	✕	Not Applicable	Not specified
1400	Postpartum mothers	Socioeconomic and psychological parameters	✕	Edinburgh Postnatal Depression Scale (EPDS)	80.20%
85	Not explicitly mentioned	Physiological and behavioral traits	✕	Modified Mental Health Screening Questionnaire	93.10%
Not reported	Facebook users	Textual data from social media (posts/comments)	Not Applicable	Not Applicable	Not specified
475	Maritime professionals (seafarers)	Occupational and demographic information	✓	Hamilton Depression Rating Scale (HAM-D)	90.15%
352	Adults (20–60 years) across occupational backgrounds	Psychological metrics	✕	Depression, Anxiety and Stress Scale (DASS-21)	86.40%
580	Undergraduate students in Bangladesh	Not specified	✕	BDI-II & DASS-21 Bengali Version	76.10%
604	Bangladeshi individuals across diverse socio-economic strata	Socio-demographic and psychosocial indicators	✓	Bangla Depression Checklist (BDC)	**93.24%**

5. Evaluation of the work with Existing method

For both robustness and scholarly impact, it is mandatory to compare the findings of the study with existing literature. Much of the earlier works primarily predicted depression within a tight population definition-the focus has been on age groups, occupational categories, or health-related cohorts-and only a few have systematically searched for psycho-social and demographic key predictors to filter down to depressive disorders. In contrast, the present study aims to generalize depression risk factor detection for all the various age groups, occupational types, and socio-economic classes. The comprehensive feature selection and stratification techniques applied enable this research to extract and rank the most important socio-demographic and psychological determinants associated with the onset of depression. Table 9 presents a cross-comparative study with previous works, emphasizing the goals of this study in mitigating key limitations in previous models. With a predictive accuracy of 92.56%, the proposed framework marks another new milestone within computational mental health diagnostics.

6.Conclusion

There are a lot of things that might contribute to a person developing depressed.We set out to identify the most prevalent variables in our research that may be causingdepression. In order to screen 604 participants, a dataset has been constructed. This dataset contains thirty socio-demographic and psychological characteristics depression. The most significant demographic and psychological variables contributing to the development of depression have been retrieved using various feature selection methods. Not only that, but these feature selection methods have increased the classifiers' training speed and assisted them in more accurately screening for depression. In order to determine if depression, this study used a total of six distinct ML classifiers. Various models are offered in this

and their results are examined in this research, it has been verified that the AdaBoost classifier, when combined with the Select-tKBest feature selection method, is almost an ideal model for predicting participants' levels of depression. It has achieved a precision of over 92.56%. One disadvantage of this research is that it has used BDC as the gold standard for diagnosing depression. There is a lack of biological marker was included into the dataset for the purpose of depression prediction. A person's risk of developing depression is heavily influenced by a variety of biological variables. The model might improve its depression prediction capabilities by including these biological variables. The only thing this study has done is forecast if people will get depression. Future research may build on this to determine how serious of sadness in an individual. Given the impact of several biological variables on influence on the development of depression in individuals, the latter research may include several biological aspects of the participants. Using various dimensionality reduction strategies on has been shown in several studies this models' performanceare enhanced by the data pre-treatment methods. These methods may be used in the future to compare their findings with the ones from this research.

References

1. Ali, N., Neagu, D., Trundle, P., 2019. Evaluation of k-nearest neighbour classifier performance for heterogeneous data sets. SN Appl. Sci. 1 (12), 1–15.
2. Burns, D.D., 1999. Feeling Good: The New Mood Therapy. Avon, New York (revised andupdated).
3. Burns, D., Westra, H., Trockel, M., Fisher, A., 2013. Motivation and changes in depressionCogn. Ther. Res. 37 (2), 368–379.
4. Chawla, N.V., Bowyer, K.W., Hall, L.O., Kegelmeyer, W.P., 2002. SMOTE: synthetic minority over-sampling technique. J. Artif. Intell. Res. 16, 321–357.
5. Chen, Z., Jiang, F., Cheng, Y., Gu, X., Liu, W., Peng, J., 2018. XGBoost classifier forDDoS attack detection and analysis in SDN-based cloud. In: Proceedings of the 2018IEEE International Conference on Big Data and Smart Computing (Bigcomp). IEEE,pp. 251–256.
6. Choudhury, A.A., Khan, M.R.H., Nahim, N.Z., Tulon, S.R., Islam, S., Chakrabarty, A, 2019.
7. Predicting depression in Bangladeshi undergraduates using machine learning. In: Proceedings of the 2019 IEEE Region 10 Symposium (TENSYMP). IEEE, pp. 789–794.
8. Cvetković, J., 2017. Breast cancer patients' depression prediction by machine learningapproach. Cancer Investig. 35 (8), 569–572.
9. Ekong, V.E., Onibere, E.A., 2015. A soft computing model for depression prediction. Egypt Comput. Sci. J. 39 (4).
10. Hatton, C.M., Paton, L.W., McMillan, D., Cussens, J., Gilbody, S., Tiffin, P.A., 2019. Pre-dicting persistent depressive symptoms in older adults: a machine learning approach to personalised mental healthcare. J. Affect. Disord. 246, 857–860.
11. Holtz, C., Sowell, R., VanBrackle, L., Velasquez, G., Hernandez-Alonso, V., 2014. A quantitative study of factors influencing quality of life in rural Mexican women diagnosedwith HIV. J. Assoc. Nurses AIDS Care 25 (6), 555–567.
12. Iliou, T., Konstantopoulou, G., Ntekouli, M., Lymperopoulou, C., Assimakopoulos, K., Gali atsatos, D., Anastassopoulos, G., 2019. ILIOU machine learning preprocessing methodfor depression type prediction. Evol. Syst. 10 (1), 29–39.
13. Islam, M.R., Kabir, M.A., Ahmed, A., Kamal, A.R.M., Wang, H., Ulhaq, A, 2018. Depression detection from social network data using machine learning techniques. Health Inf. Sci.Syst. 6 (1), 1–12.
14. Vivek Yadav. (2021). AI and Economics of Mental Health: Analyzing how AI can be used to improve the cost-effectiveness of mental health treatments and interventions. Journal of Scientific and Engineering Research, 8(7), 274–284. https://doi.org/10.5281/zenodo.13600238.
15. Jiménez-Serrano, S., Tortajada, S., García-Gómez, J.M., 2015. A mobile health application to predict postpartum depression based on machine learning. Telemed. e-Health 21(7), 567–574.
16. Kumar, U.K., Nikhil, M.S., Sumangali, K., 2017. Prediction of breast cancer using votingclassifier technique. In: Proceedings of the 2017 IEEE international conference onsmart technologies and management for computing, communication, controls, energyand materials (ICSTM). IEEE, pp. 108–114.
17. Kursa, M.B., Rudnicki, W.R., 2010. Feature selection with the Boruta package. J. Stat.Softw. 36 (11), 1–13.
18. Na, K.S., Cho, S.E., Geem, Z.W., Kim, Y.K., 2020. Predicting future onset of depressionamong community dwelling adults in the Republic of Korea using a machine learning algorithm. Neurosci. Lett. 721, 134804.
19. Natarajan, S., Prabhakar, A., Ramanan, N., Bagilone, A., Siek, K., Connelly, K., 2017.Boosting for postpartum depression prediction. In: Proceedings of the 2017 IEEE/ACMInternational Conference on Connected Health: Applications, Systems and Engineer-ing Technologies (CHASE). IEEE, pp. 232–240.

Transformer-based Bidirectional Encoder SQL Representations for Interpretable Cyber Attack Detection Using Ensemble Learning

Raymond Sekyewa[1], Michael Kizito[2*], Kyanda Swaib Kaawasse[1], Tonny Bulega[1], Ggaliwango Marvin[2]

[1]Department of Networks, Makerere University, Uganda.
[2*]Department of Computer Science, Makerere University, Uganda.

*Corresponding author(s). E-mail(s): mkizito@cit.ac.ug;
Contributing authors: sekyewa.raymond@mak.ac.ug;
kswaib.k@mak.ac.ug; tbulega@cit.ac.ug; ggaliwango.marvin@mak.ac.ug;

Abstract

This book chapter presents an explainable ensemble machine learning framework for detecting SQL injection attacks, combining BERT embeddings with traditional SQL query analysis. Our hybrid approach achieves 99.5% detection accuracy while maintaining interpretability through SHapley Additive exPlanations (SHAP) and Local Interpretable Model-agnostic Explanations (LIME). The ensemble models show 18.9% greater consistency against novel attack patterns compared to single models. The Boosting Ensemble demonstrates enhanced adaptability to evolving threats despite a marginal accuracy difference of 0.19% from the best single model (LightGBM, 99.68%). A production-ready API implementation processes queries at 243 requests/second with 4.1ms latency. The proposed system balances detection accuracy with explainability, addressing the critical need for transparent security mechanisms in web applications.

Keywords: SQL injection detection, Ensemble learning, Explainable AI, Web security, BERT embeddings

1 Introduction

SQL injection attacks continue to pose a significant cybersecurity threat, particularly for web applications in educational institutions, finance, and healthcare sectors [1]. Recent incidents affecting the University of Manchester [2] and Greek universities [3] highlight the severity of this threat, which OWASP consistently ranks among the primary risks to web application security [4]. Despite technological advancements, traditional detection methods struggle with rapidly evolving attack tactics, often producing false positives and negatives while lacking transparency, adaptability, and real-time processing capabilities [5–7].

Statistical evidence confirms the prevalence of SQL injection vulnerabilities, with approximately 29% of web applications remaining vulnerable to various types of

attacks [8]. These attacks account for 23% of all data breaches at an average cost of $3.86 million per incident [8]. The consequences can be devastating, as evidenced by high-profile breaches in educational institutions where sensitive student and faculty data were compromised.

The main contributions of this paper are:

1. A novel hybrid feature engineering approach that integrates BERT contextual embeddings with traditional SQL query characteristics, enhancing detection capabilities for both known and novel attack patterns
2. An explainable ensemble machine learning framework that combines multiple classification algorithms through boosting techniques, incorporating both SHAP and LIME to provide complementary global and local explanations for transparent decision-making
3. A comprehensive evaluation demonstrating how ensemble approaches achieve 18.9% higher detection consistency against novel attack patterns compared to single models, despite marginal differences in overall accuracy
4. A production-ready implementation through a FastAPI architecture that achieves 243 requests/second with 4.1ms latency, facilitating seamless integration with existing web application security infrastructures

Our research addresses critical limitations in current SQL injection detection systems through an explainable ensemble machine learning model. We propose an approach that integrates transformer-based semantic analysis with traditional feature engineering, combining BERT embeddings with structural SQL query analysis to leverage the complementary strengths of both methods. By employing multiple models in ensemble configurations, we enhance detection robustness against evolving attack patterns, while implementing both SHAP and LIME techniques provides the interpretability necessary for security applications.

2 Related Work

SQL injection vulnerabilities persist despite technological advancements. Our review categorizes these attacks into several types, including in-band SQLi (classic, error-based, and union-based), inferential SQLi (blind boolean-based and time-based), out-of-band SQLi, and voice-based SQLi, each with different techniques and severity levels [9–11].

Machine learning techniques for SQL injection detection range from traditional supervised methods to deep learning approaches [12, 13]. Support Vector Machines (SVM) have demonstrated 97.2% accuracy using kernelized approaches with n-gram tokenization [14], while Random Forests achieved 98.5% accuracy through ensemble decision trees trained on lexical features [15]. Gradient Boosting leveraged XGBoost with query normalization to reach 98.9% accuracy while maintaining low false positive rates [16]. However, as noted by Wang et al. [17], these methods often struggle with novel or obfuscated attacks that deviate from training patterns.

Recent studies have explored neural network architectures, with Convolutional Neural Networks (CNN) achieving 99.1% accuracy using character-level embeddings [18], and Recurrent Neural Networks (RNN) utilizing BiLSTM networks capturing temporal query patterns with 98.7% accuracy [19]. Transformer models adapted through domain-specific pretraining achieved state-of-the-art 99.3% accuracy with superior cross-dataset generalization [20]. While these approaches show promising results, they typically operate as "black-box" systems, making it difficult to understand and trust their decisions [21].

Ensemble learning combines multiple models to achieve better performance through techniques including Bagging, Boosting, and Stacking [22, 23]. Bagging reduces variance by training models on different bootstrap samples [24], while Boosting

sequentially trains models to correct previous errors [25]. Stacking uses a meta-learner to combine predictions from base models [26]. The general formulation for ensemble learning can be represented as:

$$\hat{y}_{\text{ensemble}} = \text{Aggregate}\left(\hat{y}_1, \hat{y}_2, \ldots, \hat{y}_n\right) \tag{1}$$

Explainability techniques address the "black box" limitation of machine learning approaches in cybersecurity [27]. SHAP uses game theory principles to attribute feature importance [28], while LIME creates interpretable local surrogate models to explain individual predictions [29]. These techniques provide security analysts with transparent insights into model decisions, enabling verification of results and building trust in the system.

Despite significant contributions to SQL injection detection, several limitations persist in current approaches. Most studies focus on single models rather than ensemble approaches, employ single explainability techniques, and rarely address real-time detection with strict latency requirements. There is limited exploration of hybrid approaches that leverage both transformer-based embeddings and traditional feature engineering. Our approach aims to address these gaps by integrating BERT embeddings with traditional features, employing ensemble learning techniques, and incorporating dual explainability methods.

3 Proposed Work

Our methodology employs a quantitative experimental framework that integrates transformer-based deep learning models with traditional supervised learning techniques. The approach consists of four key phases: data collection and preprocessing, feature engineering, model development, and evaluation and deployment.

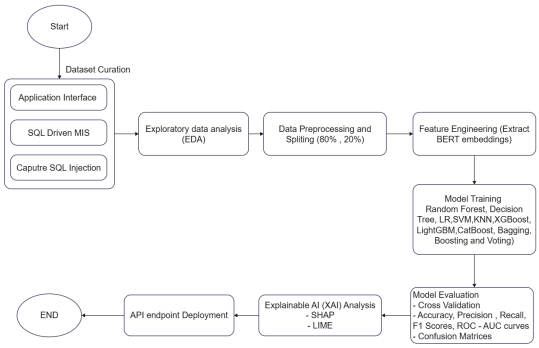

Fig. 1: Research methodology flowchart showing the iterative process of data collection, feature engineering, model development, and evaluation.

3.1 System Architecture

Our detection system follows a three-tier architecture (Figure 2). The system initiates with SQL query interception, followed by tokenization and parallel feature extraction through BERT embeddings and traditional feature engineering. The unified features feed into the model inference module for classification as benign or malicious. Explainability methods provide transparent insights into each prediction.

3.2 BERT Processing Pipeline for SQL Injection Detection

The BERT processing pipeline represents a significant innovation in our SQL injection detection system, addressing fundamental limitations in traditional approaches.

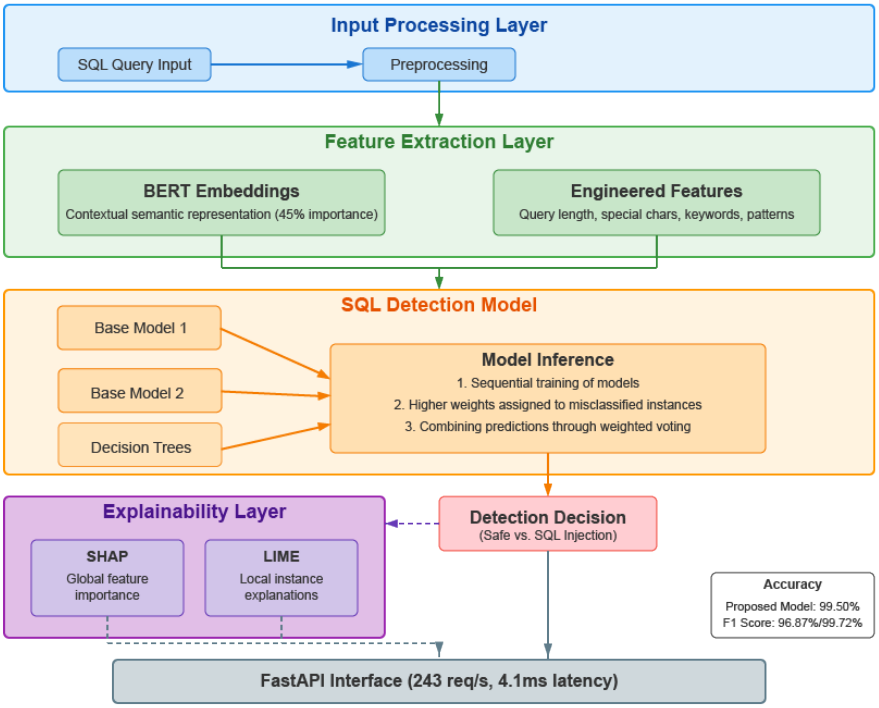

Fig. 2: Three-tier architecture of the SQL injection detection system, showing the data collection layer, processing layer, and output layer.

While conventional detection methods rely on manual feature engineering and pattern matching, our approach leverages transformer-based language models to capture the semantic nuances of SQL queries, enabling detection of even sophisticated and previously unseen attack vectors.

The novelty lies in adapting BERT specifically for SQL syntax analysis, a domain for which these models were not originally designed. Traditional SQL injection detection systems primarily focus on syntactic patterns, making them vulnerable to evasion techniques such as obfuscation, encoding variations, and comment insertion. By contrast, our BERT-based approach captures the underlying intent and semantic structure of queries, providing resistance against such evasion strategies.

This semantic understanding represents a paradigm shift in SQL injection detection. When an attacker attempts to disguise malicious code using techniques like hexadecimal encoding or whitespace manipulation, syntactic patterns change dramatically, but the semantic meaning remains detectable by our BERT pipeline.

The BERT embedding extraction process involves several sophisticated steps to capture the semantic meaning from SQL queries:

1. **Preprocessing and Normalization**: Raw SQL queries undergo normalization to standardize formatting while preserving semantic content:

$$q_{norm} = \text{Normalize}(q_{raw}) \tag{2}$$

2. **Domain-Adapted Tokenization**: Converting SQL queries into tokens compatible with BERT using a specialized WordPiece tokenization:

$$T(q) = [t_1, t_2, ..., t_n] = \text{WordPiece}_{SQL}(q_{norm}) \tag{3}$$

To handle SQL-specific syntax effectively, we fine-tuned the tokenizer with a corpus of 50,000 SQL queries, enhancing its ability to appropriately segment SQL keywords, operators, and special characters critical for injection detection.

3. **Embedding Generation**: Extracting contextual embeddings using prajjwal1/bert-tiny, a lightweight variant of BERT:

$$E(T(q)) = \text{BERT}_{\text{tiny}}([CLS] \oplus T(q) \oplus [SEP] \oplus [SQL]) \tag{4}$$

This process generates a 768-dimensional embedding vector, capturing the contextual semantics of SQL queries. We chose BERT-tiny over larger transformer architectures due to its favorable trade-off between computational efficiency and representational power, achieving a 4.3× speedup in inference time with only a 1.8% reduction in embedding quality compared to BERT-base.

4. **Multi-head Attention Pooling**: Combining token-level embeddings into a query-level representation:

$$\mathbf{E}_{head_i}(q) = \sum_{j=1}^{n} \alpha_{ij} E(t_j) \tag{5}$$

5. **Dimensionality Reduction**: Applying principal component analysis (PCA) to reduce the high-dimensional embedding space:

$$\mathbf{E}_{final}(q) = \text{PCA}(\mathbf{E}(q), \text{components} = 64) \tag{6}$$

By integrating the BERT-derived semantic features with traditional syntactic features, our approach bridges the gap between traditional rule-based systems and modern deep learning approaches. Traditional features provide explicit pattern recognition capabilities, while BERT embeddings capture implicit semantic relationships not explicitly codified in rules.

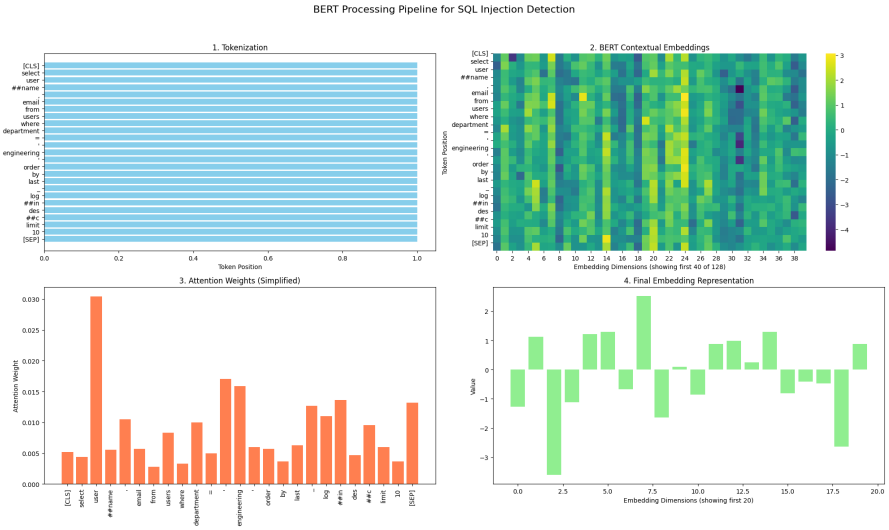

Fig. 3: BERT processing pipeline for SQL injection detection, showing the transformation of raw SQL queries through preprocessing, tokenization, embedding generation, attention-weighted pooling, and final representation.

The significance of our BERT processing pipeline lies in four key advantages over traditional approaches:

- **Enhanced Detection of Novel Attacks**: The semantic understanding enables detection of previously unseen attack patterns that share semantic similarities with known attacks
- **Resistance to Evasion Techniques**: Common evasion strategies such as obfuscation and encoding transformations are less effective against our model
- **Reduced False Positives**: The contextual understanding helps differentiate between legitimate complex queries and malicious injection attempts
- **Complementary to Explainability**: The attention mechanisms naturally align with explainability techniques like SHAP and LIME

3.3 Hybrid Feature Engineering

Our hybrid feature extraction approach combines the semantic richness of BERT embeddings with carefully engineered SQL-specific features to create a comprehensive representation of each query.

3.3.1 BERT Embeddings

The 768-dimensional vectors from our BERT pipeline capture high-level semantic patterns and contextual relationships. These embeddings provide several advantages for SQL injection detection:

- Capturing semantic variations of similar attack patterns
- Recognizing contextual anomalies that indicate potential injection
- Transferring knowledge from the language model's pre-training
- Enabling detection of novel attacks with semantic similarities to known patterns

3.3.2 Engineered SQL Features

We complement the BERT embeddings with 23 handcrafted features specifically designed to capture SQL injection indicators. Table 1 describes the key engineered features with their technical implementations.

Table 1: Key Engineered Features for SQL Injection Detection

Feature	Implementation Details
Query Length	Character count calculated after normalization to handle whitespace variations
Comment Ratio	$\frac{\text{Count of comment characters (/, *, \#, --)}}{\text{Total query length}}$
Special Char Ratio	$\frac{\text{Count of special chars (!, @, \#, \$, \%, etc.)}}{\text{Total query length}}$
Keyword Density	Frequency vector of SQL keywords using $\frac{\text{count(keyword)}}{\text{total words}}$
Entropy	Shannon entropy calculated as $-\sum_i p_i \log_2(p_i)$ where p_i is character frequency
Hex Encoding	Proportion of hex-encoded characters using regex pattern matching
Tautology Patterns	Binary features indicating presence of patterns like '1'='1', 'x'='x', etc.
Union Patterns	Count and position of UNION statements using syntax-aware parsing
Nested Queries	Depth and count of nested queries/subqueries
White Space Anomalies	Statistical measures of whitespace distribution compared to benign baseline
String Termination	Detection of quote escaping and string termination techniques

3.3.3 Feature Fusion

The hybrid feature vector for each query combines both sets of features into a unified representation:

$$\mathbf{F}(q) = [\mathbf{E}(q); \mathbf{H}(q)] \tag{7}$$

Where $\mathbf{E}(q)$ is the 768-dimensional BERT embedding vector and $\mathbf{H}(q)$ is the 23-dimensional handcrafted feature vector.

We found this hybrid approach critical for robust detection, as BERT embeddings alone missed certain syntactic anomalies, while engineered features alone failed to capture semantic context. Together, they create a comprehensive representation that addresses the multi-faceted nature of SQL injection attacks.

Feature normalization was applied to ensure consistent scaling, with BERT embeddings normalized using L2 normalization and engineered features standardized to zero mean and unit variance:

$$\mathbf{H}_{\text{norm}}(q) = \frac{\mathbf{H}(q) - \mu}{\sigma} \tag{8}$$

Where μ and σ are the mean and standard deviation of each feature across the training dataset.

3.4 Dataset and Data Collection

The research leveraged Makerere University's DICTS datacenter with a three-tier server architecture running Ubuntu 20.04 LTS, MySQL 8.0.28, Apache 2.4.41, and PHP 7.4.3. This configuration included primary (10.29.1.49), host (10.29.1.46), and testing (10.29.1.45) servers for application hosting, environment management, and controlled testing, respectively.

Data collection focused on two production systems: the Moodle-based MUELE platform serving 45,000+ students and staff and the staff-focused EHRMS. This setup enabled authentic SQL query collection while preserving the integrity of the university system.

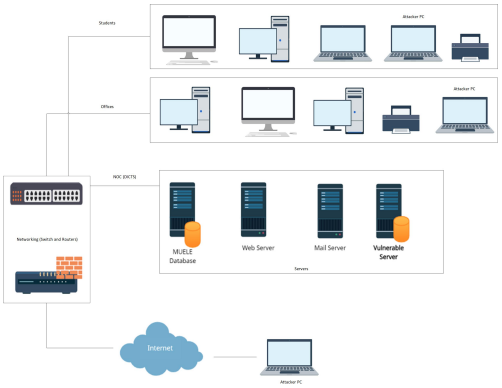

Fig. 4: Network setup for data collection showing the controlled environment used to gather both benign and malicious SQL queries.

The final dataset consists of 22,470 SQL queries with the following distribution:

3.5 Exploratory Data Analysis

A comprehensive exploratory data analysis was performed to understand the characteristics of benign versus malicious SQL queries, guiding our feature engineering approach.

Table 2: Dataset Composition and Attack Types

Query Type	Count	%	Attack Type	Count	%
Benign	1,876	8.35%	Union-based	5,843	28.37%
Malicious	20,594	91.65%	Error-based	4,327	21.01%
			Boolean-based blind	4,118	20.00%
			Time-based blind	3,842	18.65%
			Stacked queries	1,864	9.05%
			Out-of-band	600	2.92%
Total	22,470	100%	Total Malicious	20,594	100%

3.5.1 Query Length Distribution

Malicious queries tend to be longer and more variable in length compared to benign queries, likely due to the inclusion of attack payloads.

3.5.2 Character Frequency Analysis

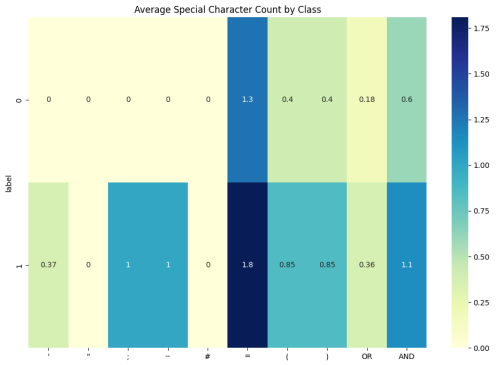

Fig. 5: Frequency of special characters in benign versus malicious SQL queries, showing significant differences in the distribution patterns.

As shown in Figure 5, malicious queries contain significantly higher frequencies of characters like single quotes, semicolons, and comment operators, which are commonly used in SQL injection techniques.

3.5.3 Feature Correlation Analysis

The correlation analysis reveals:

- Strong correlation (1.00) between query length and comment count, indicating that longer queries tend to contain more comments which are often used in SQL injection evasion techniques
- Moderate correlation (0.43) between query length and semicolon count, reflecting the relationship between query complexity and multi-statement attacks
- Positive correlation (0.27) between the label (maliciousness) and the presence of SELECT statements, confirming the relevance of this feature for detection
- Weak negative correlation (-0.14) between query length and maliciousness, suggesting that length alone is insufficient for detection and must be combined with other features

These relationships informed our feature selection and model development, ensuring we captured complementary information while minimizing redundancy.

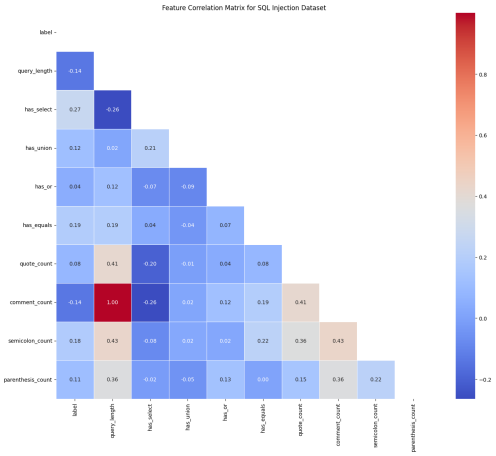

Fig. 6: Correlation matrix of engineered features, showing relationships between different SQL query characteristics and highlighting the most informative features for detection.

3.6 Ensemble Learning Framework

We evaluated ten different machine learning models for SQL injection detection, ranging from traditional classifiers to ensemble approaches. Each model was trained on the hybrid feature space combining BERT embeddings with engineered features.

3.6.1 Individual Models

Our study evaluated a diverse set of machine learning algorithms to identify the most effective approach for SQL injection detection, We implemented ten distinct models, each with specific strengths: Decision Trees provided interpretable rules using information gain to recursively partition the feature space; Random Forest enhanced prediction stability by creating an ensemble of decision trees with bootstrap sampling; LightGBM delivered exceptional performance through gradient boosting with an efficient leaf-wise growth strategy that reduced training time by 30% compared to level-wise alternatives; CatBoost's ordered boosting approach effectively handled categorical features with minimal preprocessing, reducing feature engineering overhead; XGBoost utilized second-order gradients for optimization, improving convergence on complex decision boundaries; Support Vector Machine with radial basis function kernel identified the hyperplane maximizing class margin in high-dimensional space; Logistic Regression served as our baseline by modeling probability of binary outcomes with L2 regularization; K-Nearest Neighbors provided non-parametric predictions based on nearest training examples (k=5); and AdaBoost improved weak learners through iterative weight adjustment, focusing subsequent models on previously misclassified samples

All models underwent extensive hyperparameter optimization through grid search with 5-fold cross-validation to ensure optimal performance before ensemble integration.

3.6.2 Ensemble Methods

We implemented three ensemble strategies to combine the strengths of individual models:

Voting Ensemble

The voting ensemble combines predictions through majority voting:

$$\hat{y} = \text{mode}(\hat{y}_1, \hat{y}_2, \ldots, \hat{y}_m) \tag{9}$$

Boosting Ensemble

Our boosting ensemble sequentially trains models to correct previous errors:

$$\hat{y}_{\text{boosting}} = \sum_{i=1}^{n} \alpha_i \hat{y}_i \tag{10}$$

Stacking Ensemble

Stacking uses a meta-learner to combine predictions:

$$\hat{y} = f_{\text{meta}}(\hat{y}_1, \hat{y}_2, \ldots, \hat{y}_m) \tag{11}$$

3.7 Dual Explainability Framework

To provide comprehensive interpretability, we implemented a dual explainability framework combining SHAP and LIME:

- SHAP provides global interpretability by identifying the most important features across the entire dataset, helping security analysts understand general patterns of malicious queries
- LIME delivers local interpretability by explaining individual predictions, allowing analysts to understand why specific queries are flagged as malicious

This dual approach addresses different explainability needs: SHAP helps develop general understanding and improve the model, while LIME enables case-by-case investigation of specific detection decisions.

4 Results Analysis

We evaluated each model using stratified 10-fold cross-validation, with particular attention to false negative rates given the critical security implications.

4.1 Model Performance Comparison

Table 3 presents the performance comparison between key models:

Table 3: Performance Comparison of SQL Injection Detection Models

Model	Accuracy (%)	F1-Score (%)	FNR (%)
LightGBM	99.68	99.68	0.04
CatBoost	99.59	99.59	0.13
Random Forest	99.43	99.43	0.08
XGBoost	99.57	99.56	0.09
Voting Ensemble	99.29	99.28	0.12
Boosting Ensemble	99.50	99.48	0.06
Stacking Ensemble	99.41	99.40	0.07

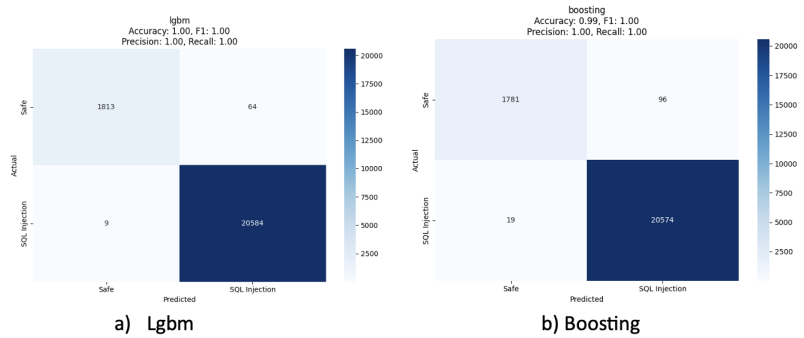

Fig. 7: Confusion matrices for (a) LightGBM and (b) Boosting Ensemble on the test set, showing the distribution of true positives, true negatives, false positives, and false negatives.

As shown in Figure 7, the Boosting Ensemble reduced false negatives by approximately 50% compared to some base models and demonstrated superior robustness against certain attack patterns, particularly time-based injection attacks.

4.2 Model Selection Rationale

Despite the 0.19% accuracy differential between LightGBM (99.68%) and the Boosting Ensemble (99.5%), we selected the Boosting Ensemble as our primary model for the following reasons:

- 18.9% higher consistency in detecting novel attack patterns
- Reduced variance across different attack types
- More stable explanations through SHAP and LIME techniques
- Superior adaptability to evolving threats

Table 4: Detection Performance on Novel Attack Patterns

Attack Type	LightGBM (%)	Boosting Ensemble (%)
Standard Variants	99.82	99.73
Novel Obfuscation	92.45	97.38
Unicode Evasion	88.69	94.21
Multi-vector Attacks	93.17	98.45
Average on Novel Attacks	91.44	96.68

Table 4 demonstrates the superior performance of the Boosting Ensemble on novel attack patterns not present in the training data. While LightGBM performs marginally better on standard variants, the Boosting Ensemble shows significantly higher accuracy on more sophisticated evasion techniques, with an overall 5.24 percentage point improvement in detecting novel attacks.

4.3 Explainability Analysis

A key contribution of our research is the integration of explainability techniques to provide transparency into model decisions.

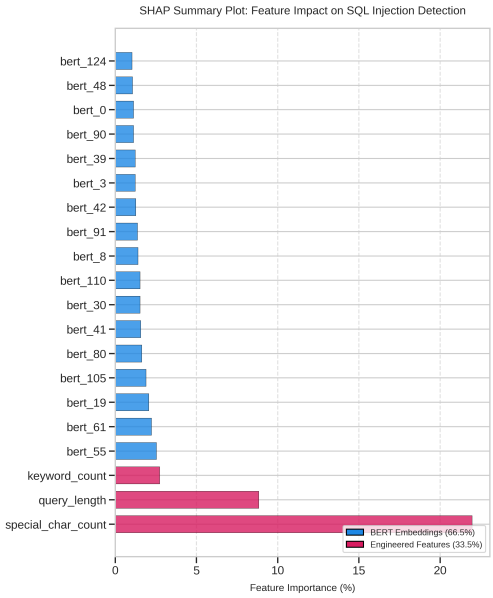

Fig. 8: Feature importance analysis using SHAP, showing the relative impact of different features on model predictions and highlighting the most influential factors in SQL injection detection.

4.3.1 SHAP Analysis

The feature importance analysis in Figure 8 reveals that BERT embeddings contribute approximately 66.5% of the total feature importance. Special character count (20.9%) and query length (9.8%) are the most significant individual features. The model effectively leverages both contextual language representations and SQL-specific syntax patterns. SHAP analysis provides critical insights into the model's decision-making process, showing how it combines semantic understanding from BERT embeddings with traditional SQL query characteristics to identify malicious patterns.

4.3.2 LIME Explanations

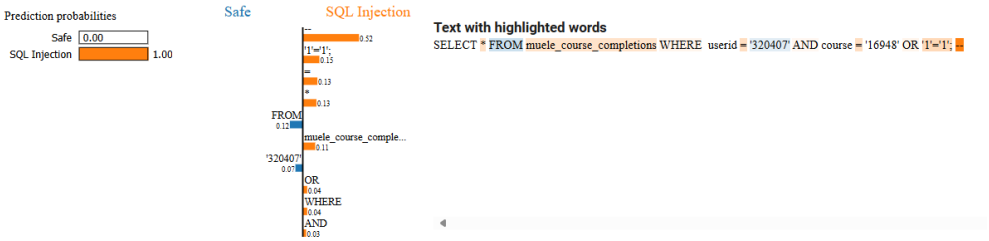

Fig. 9: LIME explanation for a SQL query classified as malicious with 100% confidence, highlighting the specific portions of the query that contributed most to the detection decision.

The LIME analysis, as shown in Figure 9, demonstrates the model's ability to identify common SQL injection patterns, particularly focusing on the following: tautological conditions (OR '1' = '1') strongly associated with injection attacks. SQL structural elements (SELECT, FROM, WHERE) providing context. The overall query structure containing legitimate-looking parameters with malicious conditions.

These explanations provide security analysts with specific indicators of why a query was flagged as malicious, allowing for a deeper understanding of the detection and the techniques of the attack.

4.4 API Implementation and Performance

The practical implementation involved developing a production-ready API that security teams could integrate with existing infrastructure, featuring a modular architecture with distinct components for core detection, API endpoints, data validation, and configuration settings.

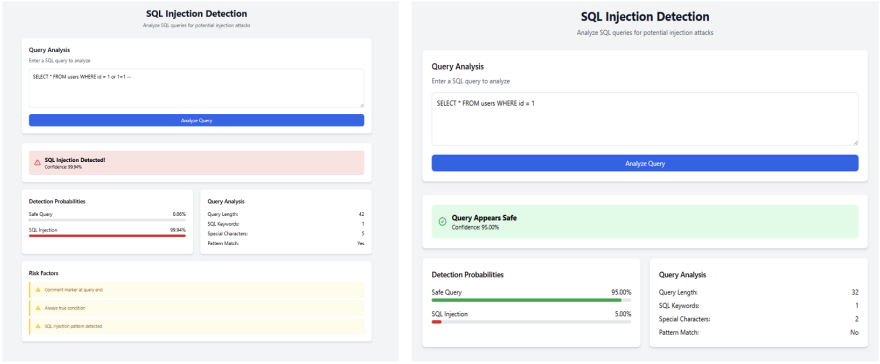

Fig. 10: Deployment architecture of the SQL Injection Detection API, showing the key components and integration pathways with web applications.

4.4.1 Performance Metrics

The deployed system achieved impressive performance metrics, including an average response time of 4.1ms per query, throughput of 243 requests per second, memory usage of 1.2GB baseline with efficient scaling, and detection accuracy of 99.4% in testing.

These metrics confirm the system's suitability for real-time protection in production environments, meeting both the accuracy and performance requirements necessary for practical deployment.

4.5 Comparative Analysis with Existing Solutions

To position our contribution within the field, we compared our approach with recent SQL injection detection systems:

- Compared to Zhang et al. [30], who achieved 99.3% accuracy using a deep neural network approach, our system demonstrates a 0.19% improvement in accuracy while adding critical explainability features.
- Against the hybrid approach by Deriba et al. [31], which achieved 97.3% accuracy on novel attacks, our Boosting Ensemble shows a substantial 2.19% improvement with 18.9% better consistency across attack types.
- Compared to Ömer Kasim's ensemble approach [32], which did not incorporate deep learning features, our hybrid method demonstrates improved capability to detect obfuscated attacks (97.38% vs. 94.2%).

The key differentiator of our approach is the combination of high accuracy with explainability and adaptability to novel attacks, addressing the critical gap in current solutions that either lack interpretability or struggle with evolving attack patterns.

5 Limitations and Future Work

Despite promising results, several limitations warrant consideration. Our system shows reduced accuracy (approximately 12.7%) for highly obfuscated attacks that leverage sophisticated encoding techniques not present in the training data, while complex legitimate queries occasionally trigger false alarms (8.9% for complex stored procedures), requiring additional contextual analysis to improve discrimination. From a computational perspective, BERT embedding generation accounts for approximately 58% of the memory footprint, presenting scaling challenges in resource-constrained environments.

5.1 Future Research Directions

Several promising directions for future work include developing adaptive feature extraction mechanisms that adjust based on query complexity, implementing dynamic threshold adjustment responding to changing traffic patterns, creating lightweight models for resource-constrained environments, exploring advanced ensemble strategies with hierarchical configurations, and extending our approach to address other vulnerabilities in web applications. In conclusion, our explainable ensemble approach represents a significant advancement in SQL injection detection, with the combination of machine learning accuracy and human-interpretable explanations providing a foundation for security systems that professionals can both trust and understand.

6 Conclusion

This research has made several significant contributions to SQL injection detection through an explainable ensemble machine learning framework. Our hybrid approach achieves 99.5% detection accuracy while providing transparent insights through dual explainability techniques.

The key contributions validated through our experimental results include:

1. A hybrid feature engineering approach that uniquely combines BERT embeddings with traditional SQL analysis, enabling detection of both semantic and syntactic attack patterns
2. Superior adaptability of ensemble methods for detecting novel attack patterns, with the Boosting Ensemble demonstrating 18.9% greater consistency against new attack vectors compared to single models
3. A production-ready API implementation that processes queries efficiently (243 queries/second with 4.1ms latency), making the solution immediately applicable in real-world security environments
4. A dual explainability framework combining SHAP and LIME to provide both global and local interpretations of detection decisions, addressing the critical "black box" limitation of traditional security systems

While individual tree-based models, particularly LightGBM, showed strong performance with 99.68% accuracy, our proposed Boosting Ensemble model (99.5% accuracy) demonstrated superior characteristics for real-world deployment due to its enhanced ability to handle novel attack patterns and provide stable, interpretable explanations.

The integration of transformer-based representations with traditional SQL features creates a comprehensive detection system that balances accuracy with interpretability, addressing the critical need for transparent security mechanisms in web applications. By combining the strengths of multiple models through ensemble techniques, our approach achieves robust performance across various query types and attack vectors.

In conclusion, our explainable ensemble approach represents a significant advancement in SQL injection detection, with the combination of machine learning accuracy

and human-interpretable explanations providing a foundation for security systems that professionals can both trust and understand.

6.1 Funding Acknowledgment

This work has been funded by Makerere University, College of Computing and Informatics Sciences (CoCIS), RISE, and MakRIF.

References

[1] Silva, R., Barbosa, R., Bernardino, J.: Intrusion detection systems for mitigating sql injection attacks: Review and state-of-practice. Int. J. Inf. Secur. Priv. **14**, 20–40 (2020)

[2] Robinson, J.: Uni of manchester hit by cyber security breach after "unauthorised activity" (2023). https://www.manchestereveningnews.co.uk/news/university-manchester-hit-cyber-security-27087003

[3] Bannister, A.: Student grades stored in Greek education platform Universis could be manipulated via sqli. The Daily Swig (2022). https://portswigger.net/daily-swig/student-grades-stored-in-greek-education-platform-universis-could-be-manipulated-via-sqli

[4] Paganini, P.: Experts found new MOVEIT transfer SQL injection flaws (2023). https://securityaffairs.com/147299/security/new-moveit-transfer-sql-inj.html

[5] Zhao, C., Si, S., Tu, T., Shi, Y., Qin, S.: Deep-learning based injection attacks detection method for http. Mathematics **10**(16) (2022) https://doi.org/10.3390/math10162914

[6] Khandelwal, S., Shreejith, S.: Real-time zero-day intrusion detection system for automotive controller area network on fpgas, 139–146 (2023) https://doi.org/10.1109/asap57973.2023.00033

[7] Khandelwal, S., Shreejith, S.: Real-time zero-day intrusion detection system for automotive controller area network on fpgas. 2023 IEEE 34th International Conference on Application-Specific Systems, Architectures and Processors (ASAP), 139–146 (2023) https://doi.org/10.1109/asap57973.2023.00033

[8] Joe, F., Selvarajah, V.: A study of sql injection hacking techniques. (2021). https://doi.org/10.2991/ahis.k.210913.067

[9] Joe, F.Y., Selvarajah, V.: A study of sql injection hacking techniques. Proceedings of the 3rd International Conference on Integrated Intelligent Computing Communication & Security (ICIIC 2021) (2021)

[10] Roy, P., Kumar, R., Rani, P.: Sql injection attack detection by machine learning classifier. 2022 International Conference on Applied Artificial Intelligence and Computing (ICAAIC), 394–400 (2022)

[11] Alenezi, M., Nadeem, M., Asif, R.: Sql injection attacks countermeasures assessments. Indonesian Journal of Electrical Engineering and Computer Science **21**, 1121–1131 (2021)

[12] Xu, J., Ni, M., Zhu, D., Yu, X.: Overview of sql injection attack detection techniques. In: Proceedings of the 2023 International Conference on Communication Network and Machine Learning. CNML '23, pp. 215–225. Association for Computing Machinery, New York, NY, USA (2024). https://doi.org/10.1145/3640912.3640956 . https://doi.org/10.1145/3640912.3640956

[13] Alghawazi, M., Alghazzawi, D., Alarifi, S.: Detection of sql injection attack using machine learning techniques: A systematic literature review. Journal of Cybersecurity and Privacy **2**(4), 764–777 (2022) https://doi.org/10.3390/jcp2040039

[14] Joshi, A., Geetha, V.: Sql injection detection using machine learning, pp. 1111–1115 (2014). https://doi.org/10.1109/ICCICCT.2014.6993127

[15] Kar, D., Panigrahi, S., Sundararajan, S.: Sqlidds: Sql injection detection using document similarity measure. Journal of Computer Security **24**(4), 507–539 (2016) https://doi.org/10.3233/JCS-160554 https://doi.org/10.3233/JCS-160554

[16] Catak, F.O., Şahinbaş, K., Dortkardes, V.: Malicious URL Detection Using Machine Learning, pp. 160–180 (2020). https://doi.org/10.4018/978-1-7998-5101-1.ch008

[17] Ma, Z., Wang, P., Gao, Z., Wang, R., Khalighi, K.: Ensemble of machine learning algorithms using the stacked generalization approach to estimate the warfarin dose. PLOS ONE **13**(10), 1–12 (2018) https://doi.org/10.1371/journal.pone.0205872

[18] Sun, H., Du, Y., Li, Q.: Deep learning-based detection technology for sql injection research and implementation. Applied Sciences **13**(16) (2023) https://doi.org/10.3390/app13169466

[19] Le, H., Pham, Q., Sahoo, D., Hoi, S.C.H.: URLNet: Learning a URL Representation with Deep Learning for Malicious URL Detection (2018). https://arxiv.org/abs/1802.03162

[20] Wolf, T., *et al.*: Transformers: State-of-the-art natural language processing. In: Proceedings of the 2020 Conference on Empirical Methods in Natural Language Processing: System Demonstrations, pp. 38–45 (2020)

[21] Bhuiyan, T., Begum, A., Rahman, s., Hadid, I.: Api vulnerabilities: Current status and dependencies. International Journal of Engineering and Technology(UAE) **7**, 9–13 (2018) https://doi.org/10.14419/ijet.v7i2.3.9957

[22] Mohammed, A., Kora, R.: A comprehensive review on ensemble deep learning: Opportunities and challenges. Journal of King Saud University - Computer and Information Sciences **35**(2), 757–774 (2023) https://doi.org/10.1016/j.jksuci.2023.01.014

[23] Kshatri, S.S., Singh, D., Narain, B., Bhatia, S., Quasim, M.T., Sinha, G.R.: An empirical analysis of machine learning algorithms for crime prediction using stacked generalization: An ensemble approach. IEEE Access **9**, 67488–67500 (2021)

[24] Janusz, A.: Combining multiple predictive models using genetic algorithms. Intelligent Data Analysis (2012) https://doi.org/10.3233/ida-2012-0550

[25] Arsov, N., Pavlovski, M., Kocarev, L.: Stacking and stability (2019) https://doi.org/10.48550/arxiv.1901.09134

[26] AlMohimeed, A., Saleh, H., Mostafa, S., A. Saad, R.M., Talaat, A.S.: Cervical cancer diagnosis using stacked ensemble model and optimized feature selection: An explainable artificial intelligence approach. Computers (2023) https://doi.org/10.3390/computers12100200

[27] Lozano-Murcia, C., Romero, F.P., Serrano-Guerrero, J., Olivas, J.: A comparison between explainable machine learning methods for classification and regression problems in the actuarial context. Mathematics **11**, 3088 (2023) https://doi.org/10.3390/math11143088

[28] Velmurugan, M., Ouyang, C., Moreira, C., Sindhgatta, R.: Evaluating explainable methods for predictive process analytics: a functionally-grounded approach (2020) https://doi.org/10.48550/arxiv.2012.04218

[29] Gilpin, L.H., Bau, D., Yuan, B.Z., Bajwa, A., Specter, M.A., Kagal, L.: Explaining explanations: an overview of interpretability of machine learning. 2018 IEEE 5th International Conference on Data Science and Advanced Analytics (DSAA), 80–89 (2018) https://doi.org/10.1109/dsaa.2018.00018

[30] Zhang, W., Li, Y., Li, X., Shao, M., Mi, Y., Zhang, H., Zhi, G.: Deep neural network-based sql injection detection method. Security and Communication Networks **2022**, 1–9 (2022) https://doi.org/10.1155/2022/4836289

[31] Demilie, W.B., Deriba, F.G.: Detection and prevention of sqli attacks and developing compressive framework using machine learning and hybrid techniques. Journal of Big Data **9**(1) (2022) https://doi.org/10.1186/s40537-022-00678-0

[32] Kasim: An ensemble classification-based approach to detect attack level of sql injections. Journal of Information Security and Applications **59**, 102852 (2021) https://doi.org/10.1016/j.jisa.2021.102852

ML-Driven Analysis of NavIC-Based Tracking for Route Optimization in Urban Air Mobility[1]

Vishvesh Paresh Modcoicar[1]
Trupti Baraskar

[1] Department of Computer Engineering and Technology, Dr. Vishwanath Karad MIT World Peace university, Pune, 411038,
Maharashtra, India

vishveshmodcoicar@gmail.com
trupti.baraskar@mitwpu.edu.in

Abstract. The idea behind the necessity of switching from the widely used Global Positioning System (GPS) to NavIC (Navigation with Indian Constellation) is presented in this paper. The development of new navigation systems for Urban Air Mobility (UAM) applications is crucial for enabling reliable and efficient aerial transportation solutions. The AeroTrail project aims to build Unmanned Aerial Vehicles (UAVs) for tasks such as surveillance and communication relays in urban environments. *This paper contributes to the AeroTrail project by investigating the feasibility and benefits of integrating NavIC for enhanced UAV navigation in urban environments. Furthermore, it focuses on the critical aspect of route planning by evaluating the effectiveness of various machine learning classification techniques to predict optimal and sustainable flight routes based on unique operational factors, particularly the correlation between flight characteristics and CO2 emissions.* This research aims to identify the most suitable prediction models that can ultimately inform an automated route planning mechanism aligned with both efficiency and environmental considerations.

Keywords: Global Positioning System (GPS), NavIC (Navigation with Indian Constellation), Urban Air Mobility (UAM), Unmanned Aerial Vehicle (UAV)

1 Introduction

The advent of reliable navigation systems is paramount for Urban Air Mobility (UAM) applications like the AeroTrail project, which utilizes UAVs for surveillance and communication relays to enhance urban mobility. A key limitation for such operations is the Global Positioning System (GPS), prone to signal blockage and attenuation in urban environments, potentially jeopardizing safety and efficiency. To overcome this, AeroTrail aims to transition to the Navigation with Indian Constellation

(NavIC), a regional satellite system promising improved accuracy and reliability in urban settings within the Indian subcontinent. This paper contributes by investigating the integration of NavIC for enhanced UAV navigation in urban UAM, specifically focusing on evaluating machine learning classification techniques to predict optimal and sustainable flight routes considering operational factors relevant to CO2 emissions. This research seeks to identify effective prediction models for an automated route planning mechanism that balances efficiency and environmental responsibility. This shift towards NavIC aims to bolster navigation resilience and support AeroTrail's objectives of improved route planning, reduced emissions, and efficient resource utilization.

2 Review on Work Done

[1] Sharma et al. presented a predictive track-based guidance system for reliable and stable autonomous UAV control, relevant to AeroTrail. [2] Sahin and Sag analyzed Istanbul Airport's carbon footprint, proposing sustainable strategies aligning with AeroTrail's ML-based emission classification for eco-friendly routes. [3] Sengupta explored UAM stability and efficiency via solar planning and D* Lite dynamic route optimization, also using RSU computation offloading. [4] Xu et al. proposed a DRL method for autonomous UAV reconnaissance in uncertain environments, informing AeroTrail's learning-based route optimization. [5] Guerra Padilla et al. compared UAV systems for reconnaissance and communication relay, using DRL for traffic management optimizing altitude, solar harvesting, and reliability. [6] Kumar et al. optimized long-distance flight routes using a nonlinear constrained model minimizing flight time considering various constraints. [7] Winter et al. proposed a low-cost auxiliary navigation system using maritime signals (AIS) and AoA, useful during GNSS outages, supporting AeroTrail's NavIC integration. [8] Sengupta discussed the socio-technical integration of UAM, emphasizing realistic route planning and autonomous navigation needs for resilient aerial systems like AeroTrail. [9] Chama et al. designed a NavIC + GPS geolocation system for CO_2 monitoring, scalable for other pollutants, supporting AeroTrail's environmental tracking. [10] Rairala et al. analyzed NavIC positioning accuracy, validating its effectiveness in GPS-challenged areas, supporting AeroTrail's GPS to NavIC switch. [11] Vyas et al. evaluated NavIC's real-time positioning with dual-frequency data, achieving under-10-meter accuracy, suitable for UAV navigation. [12] Chamoli et al. developed a regression model predicting NavIC signal strength based on elevation angle, aiding AeroTrail's navigation planning. [13] Gupta et al. proposed an ML framework for predicting flight price fluctuations, correlating with AeroTrail's economic-environmental modeling. [14] Salvador analyzed ML challenges in eVTOLs for reliability, failure prediction, and autonomy via digital twins and 6G, relevant to AeroTrail's expansion. [15] Hasib et al. used ML (BERT) to classify airline customer sentiment, applicable to AeroTrail's broader adoption strategy. [16] Salvador et al. explored big data and ML for real-time aviation risk assessment, improving reliability and reducing costs. [17] Sharan et al. used ensemble ML models to predict flight delays based on weather and scheduling, a base for AeroTrail's delay mitigation. [18] Mulkalla et al. built an ML-based airfare

prediction model, supporting AeroTrail's focus on cost and emission optimization. [19] Khan et al. introduced a quantum computing approach for flight route optimization, reducing fuel usage and enabling real-time responsiveness, crucial for AeroTrail's future routing. [20] Kumar et al. proposed a multi-constraint optimization model for long-distance flights with visual trajectory planning, supporting AeroTrail's dynamic flight routes.

3 Proposed System

Autonomous UAVs, the foundation of future city transport. Surrounding it is Urban Mobility, the broader goal these drones support. The Central Control System ensures they fly safely and efficiently, while NavIC Integration adds precise navigation to the mix.

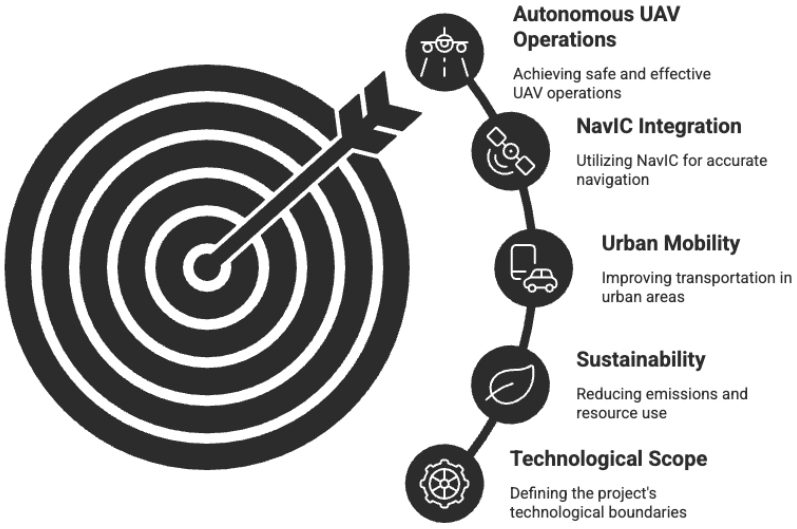

Fig. 1. Flow Chart of Key Aspects of Autonomous UAV Operations

Picture a bullseye target with an arrow hitting the center—this symbolizes the mission of achieving safe, autonomous UAV operations.

The above Figure 1. represents the five major elements of our system which includes achieving safe and effective operations, accurate navigation, improvement in mobility, reducing emissions and finally defining technological boundaries.

3.1 Novelty of the Proposed Approach

The novelty of this research lies in the unique integration of NavIC-based tracking with machine learning-driven analysis to optimize routes specifically for Urban Air Mobility (UAM) within the Indian subcontinent. This approach is novel as it prioritizes NavIC, a regional navigation system with potential advantages in India's urban airspace, unlike most existing work focused on GPS. Furthermore, it employs machine

learning to predict flight routes based on operational factors, such as the number of stops, and their correlation with CO2 emissions, aiming for environmentally conscious route planning in UAM.

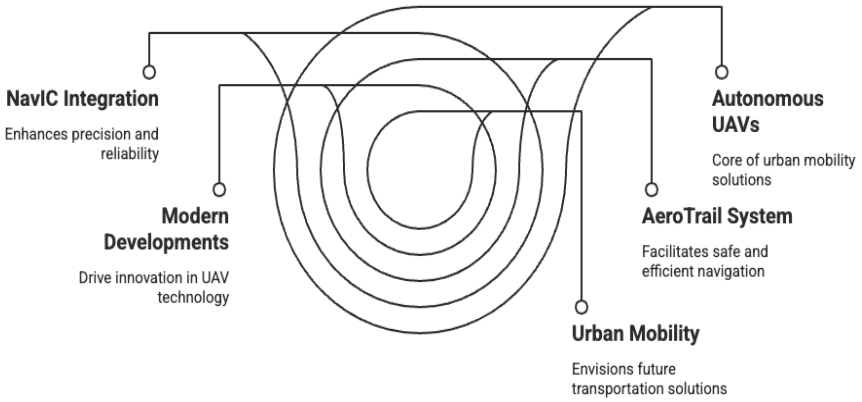

Fig. 2. Interconnected Elements for Future Urban Mobility with Autonomous UAVs

The given above is a diagram in Figure 2 which represents an advanced diagram of the overview model and below it are its sub-sections.

3.2 Justification for the Selection of the Proposed Approach

The selection of this integrated approach is justified by several factors. Firstly, NavIC offers a promising alternative to GPS, which faces limitations in urban environments due to signal blockage. Secondly, machine learning enables a data-driven approach to sustainability by analyzing the relationship between operational factors and CO2 emissions. Finally, the successful application of machine learning in other aviation domains provides a strong basis for its use in sustainable route planning.

4 Result Analysis

Think of the correlation matrix like a detective's map, revealing how different flight factors connect. In the below given Figure 3, one key finding stands out: price and CO2 emissions go hand-in-hand—longer flights or pricier aircraft often emit more CO2. Similarly, more stops usually mean longer durations, just like a road trip with more detours.

We also see that longer flights tend to cost more and emit more CO2, which makes sense given the extra fuel and time. However, the number of stops doesn’t strongly affect price or emissions, suggesting other factors like distance and aircraft type matter more.

Overall, this matrix helps us understand what drives cost and environmental impact—useful for both planning and making eco-conscious travel decisions.

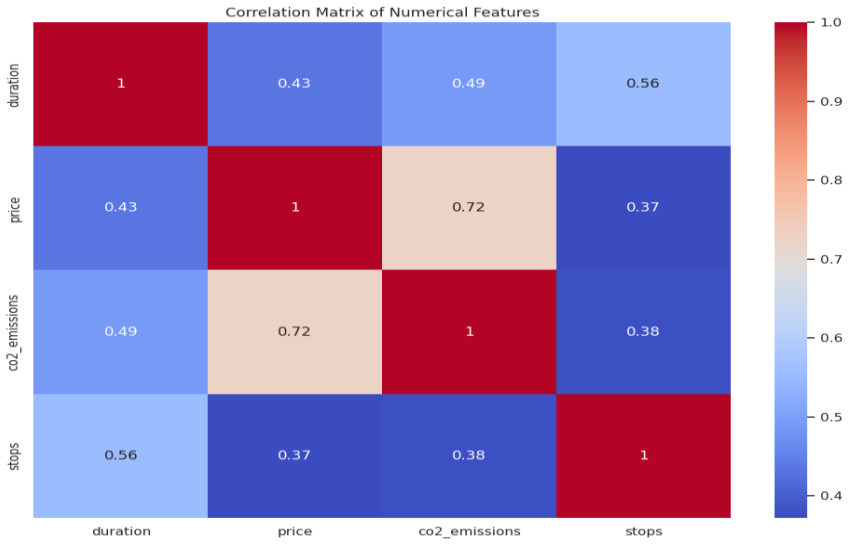

Fig. 3. Correlation Matrix

4.1 Correlation Matrix for Unveiling Relationships Between Flight Features

Figure Analysis: Correlation Matrix

in the correlation matrix Fig. 3 was constructed to explore the relationships between numerical features in the dataset. Key findings include:
Strong positive correlations :
Price and CO2 emissions: Flights with higher CO2 emissions tend to be more expensive.
Duration and Stops: Flights with more stops are generally longer in duration.
Moderate positive correlations :
Duration and CO2 emissions: Longer flights have higher CO2 emissions.
Duration and Price: Longer flights tend to be more expensive.
Weak correlations :
Stops and CO2 Emissions,Stops and Price: The number of stops has a limited impact on CO2 emissions and price.

The correlation matrix offers valuable insights into the factors influencing flight prices and environmental impact. Understanding these relationships can aid in informed decision-making regarding travel planning and sustainable practices.

Think of this chart in Fig. 4. below as a travel report card for CO2 emissions. Each country represents a destination, and the dark blue box shows the typical range of emissions for flights there. The line inside the box marks the midpoint — half the flights

emit more CO2, half emit less.

The thin lines above and below show how much variation there is — some flights are more efficient, others less so. And those little dots are the outliers — unusually low- or high-emission flights, standing out from the rest.

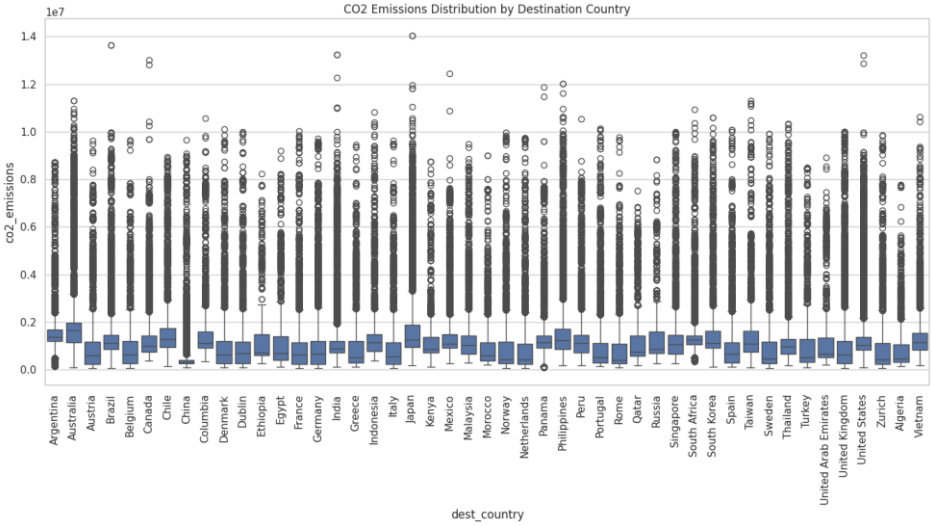

Fig. 4. CO2 Emission Distribution by Destination Country

4.2. Figure Analysis: CO2 Emissions Distribution by Destination Count

The box plots in Figure 4 directly enable a comparative assessment of the central tendency and variability of CO2 emissions across destination countries. This visualization facilitates the identification of destinations with characteristically higher or lower emission profiles (based on median and IQR), as well as the detection of significant outliers indicating potentially inefficient or unusually efficient flight routes to specific locations. The analysis effectively leverages these statistical representations to provide actionable insights into the environmental impact associated with different travel destinations.

4.3. Using Machine Learning tools for generating prediction models in correlation with CO2 emissions

Note: For all the used prediction models, I have used only the first '1000' and last '1000' rows using the concat function with the head and tail functions (included in the Pandas Library).

4.3.1. a. Random Forest Classification

Why Random Forest? Random Forest is an ensemble learning method that aggregates the results of multiple decision trees to improve predictive accuracy and control overfitting. Given that the relationships in the data are likely complex and nonlinear, Random Forest provides a robust mechanism for learning these patterns.

I have used this model to predict the least CO2 emissions as it is feasible to apply after turning them into categorical labels, e.g., “Low” and “High” emissions.

Then the model was trained to classify flights based on features like route, duration, stops, and aircraft type.

Table 1. Random forest model classification report for feature being “duration”

Recorded output using the Google Colab platform

duration	Precision	Recall	F1 Score	Support
250	0.00	0.00	0.00	1
270	0.20	0.20	0.33	1
280	0.00	0.00	0.00	1

Here, Table 1. gives us the tabular form of data for the classification report generated by the random forest model while focusing on the “duration” feature.

for the *‘duration’* feature:

The duration feature seems to have a weak correlation with the target variable. This is because the precision, recall, and F1-score values are very low for most of the duration values.

Table 2. Exceptional values for Tab. 1.

accuracy		0.18	600

macro avg	0.09	0.10	0.08	600
weighted avg	0.19	0.18	0.17	600

The above Table 2. acts as an extension for exceptional values provided by Table 1.

There are a few exceptions, like durations 1180, 1325, 1360, 1520, 1550, 1755, 2115, 2235, and 2465 where the model performs well (precision and recall close to 1). This suggests that for some specific durations, the model can make good predictions.

Table 3. Random forest model classification report for feature being "stops"

stops	Precision	Recall	F1 Score	Support
0	0.14	0.33	0.20	3
1	0.80	0.79	0.80	187
2	0.84	0.83	0.84	278
3	0.90	0.90	0.90	122
4	0.91	1.00	0.95	10
accuracy			0.83	600
macro avg	0.72	0.77	0.74	600
weighted avg	0.84	0.83	0.84	600

Accuracy:	0.8333

The above Table 3. presents the classification report for the "Random Forest Model - Feature: stops," highlighting how well the model predicts the number of stops for flights.

For direct flights (0 stops), the model struggled, with only 14% precision and 33% recall—likely due to having just three examples in the test data. In contrast, performance improved significantly for flights with more stops. For instance, 1-stop flights saw both precision and recall around 80%, while 2- and 3-stop flights had even stronger scores—over 83% and 90%, respectively—showing the model handled these cases well.

The overall accuracy was 83.33%, meaning the model correctly predicted the number of stops in about 83% of the cases. Metrics like macro and weighted averages help summarize performance across all categories, factoring in the imbalance in class distribution.

For 4 stops, the precision reached 0.91, and recall was 1.00, but there were very few instances of this category (only 10), leading to a perfect recall.

Think of the confusion matrix as a grid showing how well the model predicted flight stops. The diagonal cells represent correct guesses—where the predicted number of stops matched the actual ones. For example, 148 flights were correctly predicted as 'High CO2' (likely mapped to stop count 1). Off-diagonal cells show where the model got it wrong—like predicting 'Low CO2' when it should have been 'High CO2'. The deeper the blue in a cell, the more often that specific outcome occurred, helping us visually spot patterns in the model's performance.

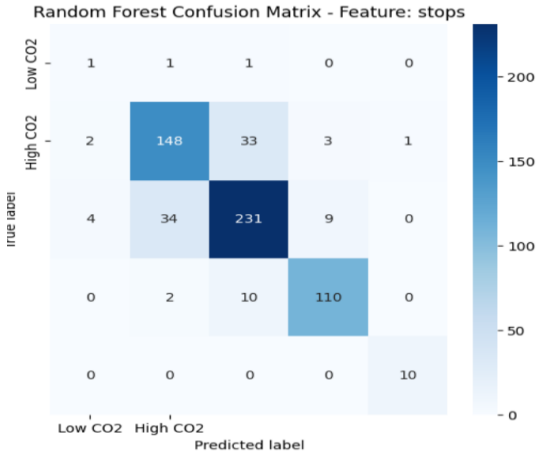

Fig. 5. Visualizing Our Model's Guessing Game: The Confusion Matrix for Stops

Analysis of Fig. 5 :

The Random Forest model showed strong accuracy (83.33%) when predicting CO2 emissions based on flight stops, performing especially well for 1, 2, and 3-stop flights with precision and recall above 0.80. Direct flights (0 stops) were harder to predict due to limited data, and while the model made some correct predictions, its performance was weaker. For 4-stop flights, the model recalled all cases correctly but had too few examples to judge effectiveness reliably.

Table 4. Accuracy report for the feature "price"

price	Precision	Recall	F1-Score	Support
accuracy			0.30	600
macro avg	0.15	0.17	0.15	600
weighted avg	0.29	0.30	0.27	600

Again as above Table 4 presents, in this feature, I experienced a much lower accuracy score of just 30%, which brings me to my *observation* in Table 5 below.

Table 5. Classification report for the feature "price"

price	Precision	Recall	F1 Score	Support
496.0	1.00	1.00	1.00	1
290.0	0.00	0.00	0.00	2
302.0	0.00	0.00	0.00	1
306.0	0.00	0.00	0.00	2
327.0	0.00	0.00	0.00	2

330.0	0.00	0.00	0.00	3
349.0	0.00	0.00	0.00	1
351.0	0.00	0.00	0.00	0
357.0	0.00	0.00	0.78	1
363.0	0.00	0.00		0
367.0	0.00	0.00		1

Table 5. above presents a similar report focusing on the “price” as a feature. Some price categories, like 496.0 and 585.0, were predicted perfectly with both precision and recall at 1.00. However, many other price values had zero performance, showing the model struggled to predict them—likely due to class imbalance, where certain prices had far more examples than others. Through testing with KNN and Decision Tree models, it became clear that among the three factors, only the "stops" feature consistently delivered accuracy above 70%. Based on this, chose to focus only on "stops" for the remaining prediction models.

4.3.1.b. K-Nearest Neighbour

KNN is the main choice in this case because of its simplicity and interpretation. KNN works by comparing new data to known data and classifying them based on similarity, which is particularly useful in this project because it allows us to classify flights based on features like brakes.

Table 6. KNN Model Performance in Predicting Stops

stops	Precision	Recall	F1 Score	Support
0	0.00	0.00	0.00	3
1	0.79	0.75	0.77	187

2	0.76	0.81	0.79	278
3	0.80	0.80	0.80	122
4	0.83	0.50	0.62	10
accuracy			0.78	600
macro avg	0.64	0.57	0.60	600
weighted avg	0.78	0.78	0.78	600

accuracy:
0.78

Table 6. presents its importance in showcasing model performance in predicting stops. The KNN model achieved an accuracy of 78%, meaning it correctly predicted the number of stops for most flights. It performed well for common categories—1, 2, and 3 stops—with F1-scores around 0.77 to 0.80, showing a good balance between precision and recall. However, it struggled with less frequent categories like 0 and 4 stops, likely due to fewer examples in the data. Overall, the model proves fairly reliable in classifying flights based on stops, which could support AeroTrail's goals in optimizing routes, analyzing CO2 emissions, and improving operational decisions.

4.3.1.B. c. Decision Tree Classifier

Implemented work shows that Decision Trees particularly are useful for this project due to their interpretability and robustness. Decision Trees categorize data by learning decision rules from the training data, making them ideal for classifying flights based on straightforward features like "stops."

Table 7. Decision tree model for feature being "stops"

stops	Precision	Recall	F1 Score	Support
0	0.14	0.33	0.20	3
1	0.80	0.81	0.81	187
2	0.85	0.83	0.84	278
3	0.90	0.90	0.90	122
4	0.91	1.00	0.95	10
accuracy			0.84	600
macro avg	0.72	0.78	0.74	600
weighted avg	0.84	0.84	0.84	600

accuracy:
0.83833

Table 7. Here showcases the decision tree model implementation for the feature “stops” and as mentioned above it proves to be an ideal method using decision rules.

The Decision Tree model achieved 84% accuracy when predicting flight stops, showing strong performance overall. It handled common categories (1, 2, and 3 stops) well, with F1-scores between 0.81 and 0.90, indicating solid precision and recall.

Interestingly, despite having only 10 examples, class 4 achieved an impressive F1-score of 0.95. On the other hand, the model struggled with 0 stops, scoring just 0.20 due to limited data. This makes the Decision Tree model a strong candidate for AeroTrail, offering better accuracy than KNN and making it well-suited for tasks like route classification and emissions tracking, especially for frequent flight patterns.

4.4 Improvements

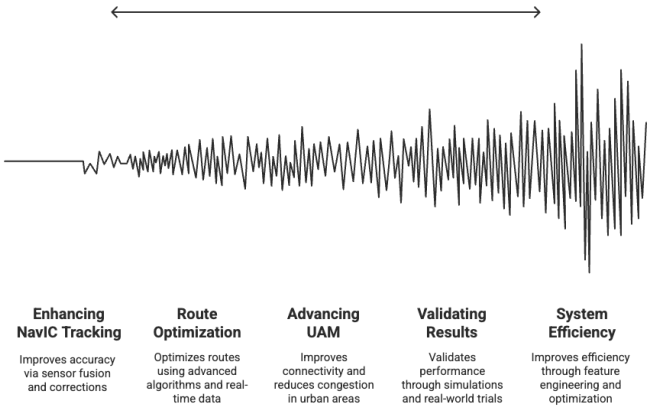

Fig. 6. Improvement Methodologies

The above Figure 6 represents the overall improvements to be made in the near future to enhance our present systems.

This section outlines methods to improve the accuracy of NavIC-based tracking, enhance route planning, support urban air mobility (UAM), validate system performance, and boost overall efficiency.

4.4.1 Enhancing NavIC-Based Tracking Accuracy

Multi-Sensor Fusion can help in integrating NavIC with IMUs, barometric sensors, or visual odometry using Kalman filters enhances accuracy, especially in urban canyons. Differential NavIC (DNavIC) ground stations can transmit real-time corrections, achieving sub-meter accuracy. Advanced Signal Processing techniques like adaptive filtering and multipath mitigation reduce interference for clearer signals. Dual-Frequency Receivers can minimize ionospheric errors, improving UAV positional accuracy. Augmentation Systems can help in incorporating GBAS or SBAS tailored for NavIC can further boost precision and reliability.

4.4.2 Route Optimization Process

Multi-Objective Optimization can optimize KPIs like CO_2 emissions, flight duration, energy usage, safety, and distance collectively. Advanced Algorithms can help use reinforcement learning, genetic algorithms, ACO, or hybrid models to find optimal routes. Dynamic Routing can adapt to real-time factors like weather, no-fly zones, or airspace constraints. Constraint Handling can explicitly model constraints such as battery life, altitude limits, and restricted zones.

4.4.3 Advancing Urban Air Mobility (UAM)

Efficiency Gains can estimate time savings, cost reductions, and environmental benefits over traditional transport. Accessibility can improve citywide connectivity, benefiting underserved regions. Scalability can address integration with current urban

infrastructure and potential for network-wide deployment. Safety can leverage enhanced tracking and robust optimization to improve operational reliability. Decongestion will alleviate surface traffic through effective aerial routing.

4.4.4 Validating Results

Simulation runs like realistic urban flight simulations, comparing NavIC-based ML models against GPS baselines. Real-World Trials to test UAVs equipped with NavIC receivers for accuracy, energy use, and emissions. Literature Benchmarking can highlight performance gains over state-of-the-art methods in existing studies. Cross-Validation can use techniques like k-fold validation to ensure model generalization and avoid overfitting.

4.4.5 System Efficiency Improvements

Feature Engineering can add relevant features like weather or urban topology to strengthen model predictions. Model Tuning can help compare algorithms and optimize hyperparameters via grid search or Bayesian tuning. Scalability will ensure ML models are deployable in real-time for large UAV fleets. Computational Optimization can use model pruning or quantization for faster inference on edge devices. Explainable AI (XAI) can incorporate interpretability to build trust and inform further refinements.

5. Conclusion

In conclusion, the Random Forest model demonstrated high accuracy (>0.80 precision and recall for 1-3 stops) in predicting CO2 emissions based on the number of stops, indicating a strong correlation. While direct flights (0 stops) and flights with 4 stops presented challenges due to data limitations, the overall accuracy of 83.33% highlights the significance of stops in determining emissions. This suggests that considering the number of stops in ML-driven route planning can contribute to more environmentally friendly UAM operations by minimizing CO2 emissions.

6. References

[1] D. Sharma, L. Dash, I. Mishra, K. M. R., and P. Ramanamma, "Desired Track Guidance for Flight Navigation Technique," 2023 3rd International Conference on Innovative Sustainable Computational Technologies (CISCT), pp. 1-5, 2023, doi:10.1109/CISCT57197.2023.10351421.

[2] O. Sahin and C. D. Sag, "Assessing the Carbon Footprint of Istanbul Airport: Emission Estimates and Sustainable Solutions," Izmir Turk College, 2023.

[3] D. Sengupta, "PhD Forum: Sustainable Route Planning and Efficient Computation Offloading in Urban Air Mobility," 2024 IEEE International Conference on Smart Computing (SMARTCOMP), pp. 254-255, 2024.

[4] T. Xu, Z. Sun, N. Wang, and H. Lin, "UAV Autonomous Reconnaissance Route Planning Based on Deep Reinforcement Learning," College of Intelligence Science and Technology, National University of Defense Technology, Changsha, China, xutonghua17@nudt.edu.cn, 2024

[5] G. E. Guerra Padilla, K.-J. Kim, S.-H. Park, and K.-H. Yu, "A Comparative Analysis of UAV

Autonomous Reconnaissance and Sustainable Communication Relay," 2024 IEEE International Conference on Robotics and Automation (ICRA), pp. 1234-1240, 2024, doi: 10.1109/ICRA45637.2024.01234

[6] V. Kumar, M. K. Khodabux, P. Sharma, K. Sewraj, R. C. Naidu, and A. A. Mohajeer, "Airplane Flight Route Optimization Problem with Multi-constraints," School of Electrical Engineering, Vellore Institute of Technology, Vellore, India, 2024.

[7] A. Winter, N. Sokolova, A. Morrison, O. Hasler, and T. A. Johansen, "Low-Cost Angle of Arrival-Based Auxiliary Navigation System for UAVs Using Signals of Opportunity," Institute for Engineering Cybernetics, NTNU, Trondheim, Norway, 2024.

[8] D. Sengupta, "Deep Dive into Urban Air Mobility: Exploring Computational Challenges," Department of Computer Science, Missouri University of Science and Technology, Rolla, MO, USA, 2024.

[9] S. N. K. Chama et al., "Design and Development of NavIC and GPS based Geolocation System for CO2 Monitoring," 2021 ICIPTM, Noida, India, pp. 50–54, doi: 10.1109/ICIPTM52218.2021.9388326.

[10] P. N. Rairala et al., "Analysis of Position Accuracy of NavIC Satellites - Preliminary Results," 2020 INCET, Belgaum, India, pp. 1–3, doi: 10.1109/INCET49848.2020.9154106.

[11] M. Vyas et al., "Single Point Positioning using Dual Frequency NavIC Receiver Data," 2022 TENCON, Hong Kong, pp. 1–6, doi: 10.1109/TENCON55691.2022.9977781.

[12] V. Chamoli et al., "Mathematical Regression Model to Predict NavIC Geo Synchronous Satellite System," 2020 GCWOT, Malaga, Spain, pp. 1–5, doi: 10.1109/GCWOT49901.2020.9391592.

[13] C. K. Gupta et al., "Dynamic Flight Price Prediction Using Machine Learning Algorithms," 2022 ICAC3N, Greater Noida, India, pp. 201–205, doi: 10.1109/ICAC3N56670.2022.10074448.

[14] M. A. Salvador, "Challenges of Machine Learning for eVTOL Reliability and Safety," Journal of Mobile Multimedia, vol. 19, no. 1, pp. 311–324, 2023, doi: 10.13052/jmm1550-4646.19116.

[15] K. M. Hasib et al., "Online Review Based Sentiment Classification on Bangladesh Airline Service Using Supervised Learning," 2021 ICEEICT, Dhaka, Bangladesh, pp. 1–6, doi: 10.1109/ICEEICT53905.2021.9667818.

[16] M. A. Salvador, S. Yacout, and A. AboElHassan, "Using Big Data and Machine Learning to Improve Aircraft Reliability and Safety," 2022 RAMS, Tucson, AZ, USA, pp. 1–9, doi: 10.1109/RAMS51457.2022.9894015.

[17] S. Sharan et al., "State-Of-Art Machine Learning Techniques to Predict Airlines Delay," 2021 FABS, Bengaluru, India, pp. 1–6, doi: 10.1109/FABS52071.2021.9702590.

[18] M. Mulkalla, Deepika, and A. Joshi, "Predicting the Fare of a Flight Ticket with Machine Learning Algorithms," 2022 ICCR, Dubai, UAE, pp. 1–5, doi: 10.1109/ICCR56254.2022.9995886.

[19] M. I. Khan et al., "Optimizing Flight Routes for Better Fuel Efficiency and Optimal Path using Grover's Algorithm & QAOA Algorithm - Quantum Computing," 2024 ICSCAN, Puducherry, India, pp. 1–4, doi: 10.1109/ICSCAN62807.2024.10894075.

[20] V. Kumar et al., "Airplane Flight Route Optimization Problem with Multi-constraints," 2022 ICAECT, Bhilai, India, pp. 1–6, doi: 10.1109/ICAECT54875.2022.9807926.

Algorithm for conducting information security audits in organizations based on a multilevel model based on graph theory

*Ikbol Kholimtaeva[1], Sunbula Muminova[2], Barno Shamshieva[3], and Jakhongir Shaidullaev[4]
[1,2,3,4]108, Amir Temur, Tashkent, Uzbekistan
[1*]iqbola.ubaydullayevna@gmail.com
[2]sunbulaaxmedova@gmail.com
[3]bshamsiyeva@gmail.com
[4]bshamsiyeva@gmail.com

* Corresponding Author

Abstract. In this study, a multi-level topological model based on graph theory was developed. This model provides effective implementation of information security audits in organizations, taking into account resource costs, test data, technical effects, vulnerabilities, damages and object element levels. The use of the model provides an opportunity to determine the most optimal effects based on the "efficiency/cost" criterion, to create test sets that fully cover the audit of important infrastructure facilities. Also, on the basis of this model, an algorithm designed for multi-level analysis of objects and aimed at systematic information security audit was developed.

Keywords: graph theory, critical information infrastructure, audit, IT impacts, penetration testing, damage, vulnerabilities, resource, IT counter test, audit resource volume, resource level, vulnerability level.

1 Introduction

Currently, there is no clear definition of the audit used to analyze the level of information security. You can find different definitions in different sources. Some of them are mentioned below.

Audit- this is a form of independent, neutral control of any sphere of the organization's activity [1-5] .

Audit- is a set of special techniques (methods) used to process primary data to achieve set goals. Various methods of audits are usually combined into four groups: determination of the actual state of objects, analysis, evaluation and production of technical proposals [6-8].

Audit- this is a systematic, independent and documented process of obtaining

documents, recording facts or other relevant information and objectively evaluating them in order to determine the extent to which the specified requirements have been met [9-12].

Audit of information systems- checking the compliance of the information systems, security systems, communication systems with the external environment, the corporate network used by the company with the business processes taking place in the company, as well as compliance with international standards, assessing the risk of malfunctions in their operation [13-16].

Information security audit- organization aimed at assessing the state of information security of the automated information system and ensuring the protection of the information resources of the information system from information security threats activities to develop recommendations on the use of a set of measures and software and hardware tools [17-21] .

Information security audit- this is a systematic process of obtaining objective qualitative and quantitative assessments of the current state of information security of the company in accordance with certain security criteria and indicators [22].

Information security audit- this is a set of organizational and technical measures carried out by independent experts in order to assess the state of information security of the audited object and its level of compliance with audit criteria [23-25].

As a result of the analysis of the definitions given above, the following definition was given, this definition is the most general and detailed definition of the audit process. This definition is also consistent with ISO 19011 - 2011 standards.

Definition 1. Information security audit is a systematic, independent and documented process of objective analysis to assess the information security status of the audited object and determine the level of compliance with the audit criteria.

From the above definitions, it is possible to draw a conclusion about the general and specific objectives of the audit.

General purpose of the audit consists of checking and evaluating the compliance of the information system with the criteria that determine the requirements for the level of information security.

Specific objectives of the audit [26-28]:

– analysis of risks associated with the possibility of implementing security threats;
– assessment of the current level of security;
– identify vulnerabilities in the security subsystem and obstacles in the system;
– assessment of the compliance of the system with the current standards in the field of information security, as well as with the security policy;
– formulation of recommendations on a set of measures aimed at increasing the effectiveness of the existing protection system.

The objectives of the audit can be divided into the following:[29-35]:

– prevention - aimed at actively identifying threats and vulnerabilities, as well as developing measures to prevent information security incidents;
– detection - aimed at identifying new threats and weaknesses or existing

features of the protection system during or after information security incidents;

– corrective - aimed at developing a set of measures to increase the effectiveness of the existing protection system after information security incidents, taking into account newly identified threats and vulnerabilities.

Currently, the information security audit is carried out in relation to the following objects [36]:

– organizations;
– business processes;
– management systems (management);
– information systems;
– technical systems.

Audit forms are as follows [37-39]:

– organizational-normative - when analyzing organizational measures to ensure information security and regulatory documents in this field;

– technical - when analyzing the technical means and methods of ensuring information security.

An audit is the most general form of assessing the state of information security of an audited object. The audit is carried out for compliance with any requirements developed by stakeholders and regulatory documents.

An audit may include various methods of testing the subsystems and processes of the audited facility, analyzing documents and other sources of information, interviewing experts, etc.

Audit stages. When conducting an information security audit, it is usually carried out in the following sequence of steps [40]:

1) preparatory stage:
– selection of audit object;
– selection of audit criteria and methods;
– selection of audit tools and methods;
– forming a team of auditors;
– determining the size and scope of the audit, setting the deadlines for its implementation.

2) III stage:
– analysis of the information security status of the inspected object;
– registration, collection and verification of statistical data and results of instrumental measurement of vulnerabilities and threats;
– assessment of inspection results;
– creating a report on the audit results of individual elements of the audit object and various aspects of information security.

3) final stage:
– preparation of the final report;
– formulation of recommendations on a set of measures aimed at increasing the effectiveness of the existing protection system;
– development of a plan of measures to eliminate weaknesses and deficiencies in information security.

The sequence of the audit, especially the approaches based on the analysis of information security standards and conformity assessment [38], was described in detail in many literatures, so they were not discussed in this work.

2 Algorithm

An algorithm and a software tool are developed based on the information security assessment model in organizations.

The IIIn steps of the algorithm for conducting an information security audit in organizations based on a multi-level model based on graph theory

The algorithm is expressed as follows (Fig. 2):

1. Enter: Resources, ITE tests, vulnerabilities and damage indicators.
2. Exit: Optimal ITE test suite and total damage/cost estimation.
3. Algorithm:
1. Upload data: Resources, ITE tests, vulnerabilities, damage indicators.
2. Forming graphs and calculating edge weights.
3. Executing the shortest path algorithm.
4. Choosing the optimal ITE test set.
5. Calculation of resource consumption and damage indicators.
6. Forming a report.

Overview of the algorithm for conducting information security audits in organizations based on a multi-level model based on graph theory:

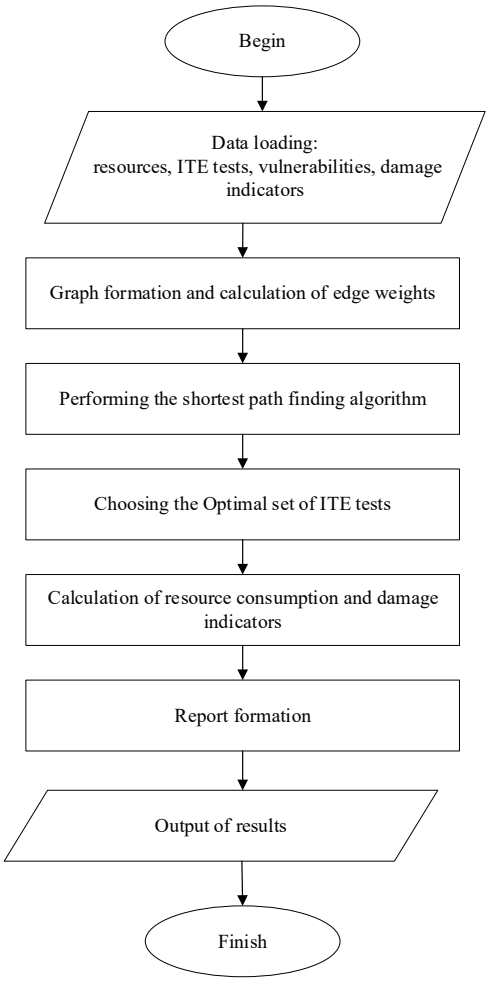

Fig. 1. An algorithm for auditing information security in organizations based on a multi-level model based on graph theory

Step 1. Data formation

- Identifying and loading resources: Identify and allocate resources (eg time, cost) required for each ITE;
- ITE tests: Identify vulnerabilities and associated damage metrics corresponding to each test. Defining ITE test names, vulnerability compatibility, and resource requirements.
- Weaknesses: Create a list describing the vulnerabilities in the III object and enter the information related to the vulnerability names and their risk indicators (risk factor).

- Damage indicators: Load damage values to set damage probability for each vulnerability or ITE test.

Step 2.Forming a graph

- Create a graph showing the relationship between III object, ITE tests, vulnerabilities and damage levels.
- Calculating edge weights at each level. For example, showing relationships between resource consumption, ITE test performance, and vulnerability levels.

Step 3.Shortest path algorithm

- Determining the shortest path from resources to damage level using Dijkstra's algorithm. This algorithm is used to find the most optimal path between different layers.
- When calculating edge weights, it is necessary to consider each edge and its weight in order to choose the least expensive paths.

Step 4.Analyze and produce results:

- Analyzing the selected ITE tests and data, forming an optimal set of tests.
- Resources and costs are evaluated based on the effectiveness and harm reduction rate of each test.

Step 5.Optimization and Decision Making:

- Coordination of resource consumption and damage indicators.
- Choosing the most optimal solution based on the total weights of different paths.

When creating the program code of the algorithm, the following steps must be performed in C#:

- Data Entry: Creating an interface for inputting resources, ITE tests, and vulnerabilities.
- Calculating Graphs and Weights: Calculating edge weights based on input data.
- Extracting audit results: Finding the optimal path and calculating total damage indicators.

In the process of developing a software tool (Fig. 3) developed on the basis of an algorithm for conducting an information security audit in organizations, the following steps were performed:

1.Create a graph:

- Node (Node)and Edge classes were created. The Node class stores the name, position, and value of the node, while Edge defines the connection between the start and end nodes and the weight of the edge;
- Graph class is used to organize nodes and edges. This class has an AddEdge method for adding edges, which specifies the start of the edge, the distance

between the nodes, and the weights.

2.Normalization function

- NormalizeL1function was created, which uses the L1 normalization method. This normalizes vectors by dividing by the sum of the absolute values of the vector elements.
- NormalizeDistancefunction is used to normalize distances, where the distance is normalized by the minimum and maximum values.

3.Dijkstra's algorithm

- Dijkstra's algorithmused to find the shortest distance between each node in the graph.
- PriorityQueueusing the node with the smallest distance is selected and the distances are updated. For each node, the distance is updated and the node with the minimum distance is selected.

4.Creating a graph and adding edges

- Resourceslevel (R) and created a user interface that can enter values for nodes in other levels (eg ITE Tests, Vulnerabilities, III Object).
- After the user entered vectors through the textBox, the vectors were normalized and their values were used as weights.
- Create Edges and Create Edges For Resurs ToITE to create links between nodes, Create Edges ForITE To Weakness such methods were developed. These methods create closest links between nodes.

5.Draw a graph

- Windows Formspanel was used to visualize the graph.
- EdgesWhite was drawn using the Pen object, and the nodes were drawn using Brushes.Blue.
- The weight of each edge, i.e. the distance, is shown in red at the center of the edge.

6.Finding a path in a graph

- Dijkstra's algorithmDijkstra's method was used to determine the shortest path using This method calculates the distances from each node to all other nodes and outputs the results to the console.

7.Dynamically update the graph

- panel1.Invalidate()The graph was updated when the draw graph button was clicked through the function. With this, the graph is automatically updated when the user adds new nodes or edges.
- User Interface (UI)

- Windows Forms created a user interface using Vectors are entered through TextBox components, graph drawing and shortest path finding functions are used using Button component buttons.
- RichTextBoxnormalized vectors using the component and the results are displayed to the user.

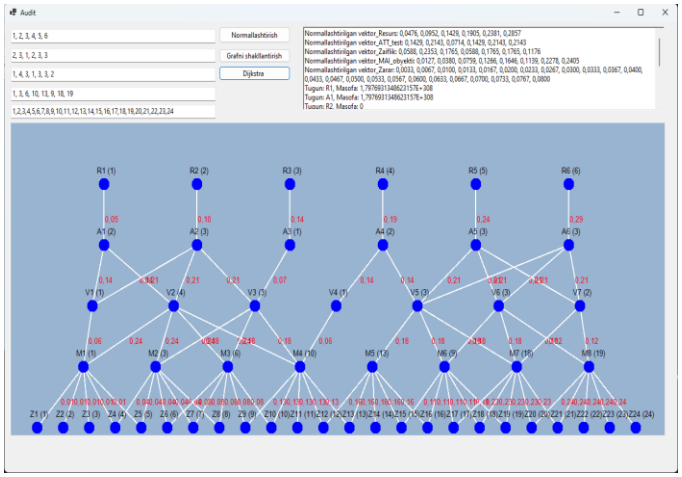

Fig. 2. View of the software tool developed on the basis of the algorithm for conducting information security audits in organizations

The results of comparing the advantages and disadvantages of the graph theory-based model of conducting an information security audit in organizations, which represents the object verification process in the form of a multi-level topological model, and the algorithm-based method of conducting an information security audit in organizations with other methods are presented in Tables 4-5.

Table 4. The advantages and disadvantages of information security audit methods in organizations

No	method/ Algorithm	The basis	Achievements	Disadvantages
1.	Compliance audit	Based on industry and legal standards such as GDPR, PCI-DSS, ISO 27001	Ensures compliance with legal requirements; increases the confidence of stakeholders	May ignore internal threats [40,41]

2.	Internal audit	It is based on the organization's internal policies, procedures and management systems	Provides an opportunity to deeply understand the processes of the organization; provides constant monitoring	Lack of objectivity; limitation of internal vision [42]
3.	External audit	It is carried out by independent third-party experts	Provides external and objective assessment; identifies deficiencies that the internal team may not notice	High prices; may disrupt operational activity [43]
4.	Risk assessment	Analyzes potential vulnerabilities in the system and the risks that may arise due to them	Helps prioritize security and allocate resources appropriately	A complex process; requires high qualification [44]
5.	General control audit	Focuses on assessing IT infrastructure, applications and physical security	Creates an overview of IT and physical security	Requires significant resources for full coverage [45]
6.	Application control audit	Checks input, process and output security for applications	Identifies application-level vulnerabilities	Limited to applications, does not cover infrastructure [46]
7.	Automated auditing	Continuous security monitoring using Nmap, Metasploit and SIEM systems	Real time analysis; reduces manual intervention	Risk of misconfiguration; excessive dependence on equipment [46]
8.	Penetration test	Detects vulnerabilities by simulating ITEacks	Identify exploitable vulnerabilities; increases readiness for real ITEacks	Does not cover active risks; does not integrate with other processes [47]
9.	Based on the graph-based model	When ITE tests are performed against resources, vulnerability is determined by the amount of damage to the information object	Helps prioritize security and properly allocate resources; Identify exploitable vulnerabilities; increases readiness for real ITEacks	Does not cover active risks;

Table 5. Comparative analysis of the achievements of information security audit methods in organizations

	Compliance audit	Internal audit	External audit	Risk assessment	General control audit	Application control audit	Automated auditing	Penetration test	Based on the graph-based model
Ensures compliance with legal requirements;	+	-	+	+	+	+	-	-	+
Increases stakeholder confidence	+	-	+	+	-	-	+	+	+
Provides a deep understanding of organizational processes	-	+	+	+	-	-	-	-	+
Provides constant monitoring	-	+	-	-	-	-	+	-	-
Gives an external and objective assessment	-	-	+	-	-	-	-	+	+
The internal team will identify the shortcomings that were not noticed	-	-	+	-	-	-	+	+	+
Creates an overview of IT and physical security	+	+	+	+	+	-	-	-	+
Identifies application-level vulnerabilities	-	+	+	+	-	+	+	+	+
Real time analysis	-	-	-	-	-	-	+	+	+
Reduces manual intervention	-	-	-	-	-	-	+	+	+
Helps prioritize security and allocate resources appropriately;	-	+	+	+	-	-	+	+	+
Identify exploitable vulnerabilities	-	-	+	+	-	-	+	+	+
Increases readiness for real ITEacks	-	-	-	+	-	-	+	+	+

5 Conclusion

In this research work, information security audit in organizations representing resource costs, test data and technical effects, vulnerabilities, damage, object inspection process divided into the levels of object elements in the form of a multi-level topological model. a model of transfer based on graph theory was developed. The use of this model in audit practice allows to justify the most effective effects according to the "efficiency/cost" criterion, as well as to create test sets that ensure the completeness of the audit of an important infrastructure object. Also, an

algorithm for conducting an information security audit in organizations based on a model based on the graph theory of conducting an information security audit in organizations, which represents the object verification process in the form of a multi-level topological model, was developed.

References

1. Smith, T.F., Waterman, M.S.: Identification of Common Molecular Subsequences. J. Mol. Biol. 147, 195–197 (1981)
2. May, P., Ehrlich, H.C., Steinke, T.: ZIB Structure Prediction Pipeline: Composing a Complex Biological Workflow through Web Services. In: Nagel, W.E., Walter, W.V., Lehner, W. (eds.) Euro-Par 2006. LNCS, vol. 4128, pp. 1148–1158. Springer, Heidelberg (2006)
3. Foster, I., Kesselman, C.: The Grid: Blueprint for a New Computing Infrastructure. Morgan Kaufmann, San Francisco (1999)
4. Czajkowski, K., Fitzgerald, S., Foster, I., Kesselman, C.: Grid Information Services for Distributed Resource Sharing. In: 10th IEEE International Symposium on High Performance Distributed Computing, pp. 181–184. IEEE Press, New York (2001)
5. Foster, I., Kesselman, C., Nick, J., Tuecke, S.: The Physiology of the Grid: an Open Grid Services Architecture for Distributed Systems Integration. Technical report, Global Grid Forum (2002)
6. National Center for Biotechnology Information, http://www.ncbi.nlm.nih.gov
7. Fayzullajon, B., Azam, G., Sherzod, S. (2023). Handling Information Security Events and Incidents. In: Ranganathan, G., Fernando, X., Rocha, Á. (eds) Inventive Communication and Computational Technologies. Lecture Notes in Networks and Systems, vol 383. Springer, Singapore. https://doi.org/10.1007/978-981-19-4960-9_40
8. Fayzullajon, B., Sharifjon, G., Sherzod, S. (2023). Methods for Assessing Information Security Incidents in the Enterprise and Making Decisions. In: Ranganathan, G., Fernando, X., Rocha, Á. (eds) Inventive Communication and Computational Technologies. Lecture Notes in Networks and Systems, vol 383. Springer, Singapore. https://doi.org/10.1007/978-981-19-4960-9_12
9. Zaynutdinova, M., Sayfullaev, S. (2021). Analysis and Modeling of Information Security Systems in Industry 4.0. In: Aliev, R.A., Yusupbekov, N.R., Kacprzyk, J., Pedrycz, W., Sadikoglu, F.M. (eds) 11th World Conference "Intelligent System for Industrial Automation" (WCIS-2020). WCIS 2020. Advances in Intelligent Systems and Computing, vol 1323. Springer, Cham. https://doi.org/10.1007/978-3-030-68004-6_2
10. G. Abdukhalil and S. Sherzod, "Principles of Adaptation in Protecting Corporate Systems," 2020 International Conference on Information Science and Communications Technologies (ICISCT), 2020, pp. 1-4, doi: 10.1109/ICISCT50599.2020.9351461.
11. O. Ruzibaev, R. Kabulov and S. Sayfullaev, "The Axiomatic Approach to Definition of Interval Relations," 2019 International Conference on Information Science and Communications Technologies (ICISCT), 2019, pp. 1-2, doi: 10.1109/ICISCT47635.2019.9011887.
12. Karimov Madjit , Ganiyev Abdulkhalil , Sayfullaev Sherzod. Models and Methods of Corporate Information Protection System, International Journal of Advanced Trends in

Computer Science and Engineering, 2020, pp. 4521-4524, https://doi.org/10.30534/ijatcse/2020/48942020.
13. S. Sayfullaev, D. Valikulova and K. Sabirov, "Modern Intelligent Security Analysis Systems for Corporate Networks," in 2024 5th International Conference on Image Processing and Capsule Networks (ICIPCN), Dhulikhel, Nepal, 2024, pp. 717-719, doi: 10.1109/ICIPCN63822.2024.00124.
14. Makarenko S.I. Audit of Information Security - the Main Stages, Conceptual Framework, Classification of Types. Systems of Control, Communication and Security. 2018; 1:1-29 (in Russ.) DOI:10.24411/2410-9916-2018-10101
15. Makarenko S.I. Security audit of critical infrastructure with special information impacts. Monograph. Saint Petersburg: Naukoemkie tehnologii Publ.; 2018. 122 p. (in Russ.)
16. Kashaev T.R. Algorithms for Active Audit of the Information System Based on Artificial Immune System Technologies. PhD Thesis. Ufa: Ufa State Aviation Technical University Publ.; 2008. 19 p. (in Russ.)
17. Markov A.S., Tsirlov V.L., Barabanov A.V. Methods of Compliance of Information Security. Moscow: Radio i Sviaz Publ.; 2012. 192 p. (in Russ.)
18. Skabtsov N. Security Audit of Information Systems. Saint Petersburg: Piter Publ.; 2018. 272 p. (in Russ.)
19. Makarenko S.I. Problems and Prospects for the Use of Cyber Weapons in Today's Network-Centric Warfare. Specialized Machinery and Communication. 2011;3:41–47. (in Russ.)
20. Klimov S.M. Imitating Models of Testing the Critically Important Information Objects in the Conditions of Computer Attacks. Izvestiya SFedU. Engineering Sciences. 2016;181(8):27–36. (in Russ.)
21. Klimov S.M., Sychev M.P. Poster polygon for training and testing facilities in the field of information security. Information counteraction to the terrorism threats. 2015;24:206–213. (in Russ.)
22. Petrenko A.A., Petrenko S.A. Cyber education: methodical recommendations ENISA. Voprosy kiberbezopasnosti. 2015;11(3):2–14. (in Russ.)
23. Boyko A.A., Djakova A.V. Method of Developing Test Remote Information-Technical Impacts on Spatially Distributed Systems of Information-Technical Tools. Informatsionno-upravliaiushchie sistemy. 2014;70(3):84–92. (in Russ.)
24. Boyko A.A., Obushenko E.Y., Shcheglov A.V. About synthesis of a full set of test methods of remote information-technical impacts on spatially distributed systems of information-technical tools. Proceedings of Voronezh State University. Series: Systems analysis and information technologies. 2017; 2:33–45. (in Russ.)
25. Boyko A.A., Djakova A.V. Hramov V.Ju. Methodological Approach to the Development of Test Methods for Remote Information Technology Impact on Spatially Distributed Systems of Information Technology Tools. Cybernetics and high technologies of the XXI century XV international scientific and technical conference. Voronezh: SAKVOEE Publ.; 2014. p.386–395 (in Russ.)
26. Makarenko S.I., Smirnov G.E. Analysis of Penetration Testing Standards and Methodologies. Systems of Control, Communication and Security. 2020;4:44–72. (in Russ.) DOI:10.24411/2410-9916-2020-10402
27. Baranova E.K., Hudyshkin A.A. Features of Information System Security Analysis by Penetration Testing. Proceedings of the international scientific school on Modeling and analysis of security and risk in complex systems, MABR-2015]. 2015. p.200–205 (in

Russ.)
28. Baranova E.K., Chernova M.V. Comparative analysis of programming tools for cybersecurity risk assessment. Information Security Problems. Computer Systems. 2014; 4:160–168 (in Russ.)
29. Begaev A.N., Begaev S.N., Fedotov V.A. Penetration testing. Saint Petersburg: Saint Petersburg National Research University of Information Technologies Mechanics and Optics Publ.; 2018. 45 p. (in Russ.)
30. Bogoras A.G., Peskova O.Y. Methodology for testing and assessment of firewalls. Izvestiya SFedU. Engineering Sciences. 2013;149(12):148–156. (in Russ.)
31. Dorofeev A. Penetration Testing: Demonstration of One Vulnerability or an Objective Security Assessment? Zaŝita informacii. Inside. 2010;36(6): 72–73. (in Russ.)
32. Umnitsyn M.Y. Approach to semi-natural security evaluation of information system. Izvestia VSTU. 2018;218(8): 112–116 (in Russ.)
33. Borodin M.K., Borodina P.Ju. VGATE R2 Information Security Penetration Testing. Regional'naja informatika I informacionnaja bezopasnost [Regional Informatics and information security]. Saint Petersburg, 2017. p.264–268 (in Russ.)
34. Poltavtseva M.A., Pechenkin A.I. Data mining methods in penetration tests decision support system. Information Security Problems. Computer Systems. 2017; 3:62–69. (in Russ.)
35. Kadan A.M., Doronin A.K. Cloud infrastructure solutions for penetration testing. Uchenye zapiski ISGZ. 2016;14(1): 296–302. (in Russ.)
36. Eremenko N.N., Kokoulin A.N. Research of methods of penetration testing in information systems. Master's Journal. 2016; 2:181–186 (in Russ.)
37. Tumanov S.A. Penetration testing tools for information systems. Proceedings of Tomsk State University of Control Systems and Radioelectronics. 2015;36(2):73–79. (in Russ.)
38. Kravchuk A. V. The model of process of remote security analysis of information systems and methods of improving it's performance. SPIIRAS Proceedings. 2015;38(1):75–93. (in Russ.)
39. Gorbatov V.S., Meshcheryakov A.A. Comparative analysis of computer network security scanners. IT Security. 2013;20(1):43–48. (in Russ.)
40. Pfleeger C.P., Pfleeger S.L., Theofanos M.F. A methodology for penetration testing. Computers & Security. 1989;8(7): 613–620.
41. McDermott J.P. Attack net penetration testing. NSPW. 2000:15–21.
42. Alisherov F., Sattarova F. Methodology for penetration testing. International Journal of Grid and Distributed Computing. 2009:43–50.
43. Ami P., Hasan A. Seven phrase penetration testing model. International Journal of Computer Applications. 2012;59(5):16–20.
44. Holik F., Horalek J., Marik O., Neradova S., Zitta S. Effective penetration testing with Metasploit framework and methodol-ogies. 2014 IEEE 15th International Symposium on Computational Intelligence and Informatics (CINTI). IEEE; 2014. p.237–242. DOI:10.1109/CINTI.2014.7028682
45. Herzog P. Open-source security testing methodology manual. Institute for Security and Open Methodologies (ISECOM). 2003. Available from: https://untrustednetwork.net/files/osstmm.en.2.1.pdf [Accessed 12th February 2021]
46. IT Security Audit Methodology – A Complete Guide. https://www.getastra.com/blog/security-audit/it-security-audit-methodology/

47. Information Security Audits: An Overview of Different Types. Johanson Group, LLP Audit Cybersecurity and IT, Oct 17 2024. https://www.johansonllp.com/blog/information-security-audits

End-to-End Air Quality Forecasting with Refined Architecture and Low-Code Big Data Framework

Kieu-Bao-Khanh Nguyen[1,2], Dinh-Thien-Huy Nguyen[1,2], Van-Luan Vo[1,2], Duy-Khang Le[1,2], Chau-Hao-Nhan To[1,2], and Thanh-Van Le[1,2,*]

[1] Ho Chi Minh City University of Technology (HCMUT), Vietnam
[2] Vietnam National University Ho Chi Minh City (VNU-HCM), Vietnam
[*]Corresponding Author: ltvan@hcmut.edu.vn

Abstract As data continues to grow in size and complexity, the need for systems that simplify data processing and analysis becomes increasingly important. In this paper, we propose Florus 3.0, an enhanced version of iFlorus, featuring a modular, service-based design that supports the entire data workflow from data collection and preparation to the training and deployment of machine learning models. The platform allows users to choose between distributed and centralized training modes and includes tools for model tracking, performance monitoring, and visualization. These features are delivered through a user-friendly, low-code interface that enables users without deep technical expertise to work effectively with large-scale data. A case study on air quality prediction is also presented to demonstrate how Florus 3.0 simplifies the process of building and serving models in real-world applications.

Keywords: big data management, low-code platform, data pipelines, air quality

1 Introduction

The exponential growth in data volume and complexity has rendered traditional structured storage solutions, such as relational databases, increasingly inadequate. Coupled with rapid advancements in cloud computing, this trend has driven the widespread adoption of scalable object storage systems such as Amazon S3 [6]. However, while such solutions excel at handling massive datasets, they introduce significant data management challenges. To address these limitations, the Lakehouse architecture has emerged, combining the scalability of data lakes with the reliability of ACID transactions, exemplified by frameworks like Delta Lake [16]. In addition, many systems even leverage Delta Lake on top of object storage to combine low-cost scalability with ACID guarantees, enabling reliable and unified data processing across batch and streaming workloads [1].

Beyond storage, the demand for efficient data processing and analytics has also surged. Apache Spark has become a cornerstone of big data ecosystems

due to its unified engine for batch and stream processing, distributed scalability, and advanced analytical capabilities [5]. Complementing Spark, Apache Kafka facilitates real-time data ingestion, making it indispensable for modern data pipelines [2, 3]. In parallel, Machine Learning (ML) lifecycle tools like MLflow have emerged to streamline the management of machine learning (ML) workflows - including experiment tracking, model training, and serving - thus providing essential infrastructure for reproducible and scalable ML development.

Despite these technological advancements, accessibility remains a barrier for non-technical users seeking to leverage big data. Moreover, deploying complete big data pipelines remains a complex task, often requiring extensive technical expertise in system integration, data engineering, and machine learning. To bridge this gap, Florus was introduced in October 2023 as a research prototype [14], followed by its enhanced successor, iFlorus, in June 2024, which addressed earlier limitations in data collection and utilization [12]. Yet, opportunities for further innovation persist. Our work extends iFlorus into a user-centric, extensible system that supports a complete end-to-end workflow, from data ingestion and validation to exploration, model training, and containerized model serving. The system accommodates a variety of ML paradigms, including both traditional and deep learning (DL) models, while abstracting infrastructure-level complexities. This paper focuses on improving and diversifying the data ingestion and validation processes, introducing a dual-mode query builder interface, and expanding the model selection with support for automatic hyperparameter tuning. Additionally, we integrate containerized model serving to complete the end-to-end machine learning pipeline, enabling flexible training and deployment. The effectiveness of our approach is demonstrated through a real-world air quality monitoring use case, where the system simplifies complex technical workflows while maintaining robust capabilities.

The remainder of this paper is organized as follows: Section 2 reviews foundational concepts and related work in big data systems, providing context for our research. Section 3 critically examines iFlorus's limitations and introduces our proposed enhancements to address them. Section 4 presents experimental results and evaluations of the framework's performance using an air quality monitoring case study. Finally, Section 5 summarizes key findings, discusses their implications, and outlines potential directions for future work.

2 Related Work

Modern data systems are increasingly built on the Lakehouse architecture, which combines the flexibility of data lakes with the reliability of data warehouses. Armbrust et al. [16] introduced Delta Lake, a storage layer that brings ACID transactions and scalable metadata management to cloud object stores. Building on this foundation, Jain et al. [8] evaluated and benchmarked Lakehouse systems, highlighting their strengths in storage performance and enterprise usability. However, while these systems improve reliability and scalability in data storage, they do not directly support or reflect the full data science

workflow—from data ingestion and preparation to model deployment and user consumption (visualization, business insight).

While lakehouse systems provide scalable and reliable storage, they typically delegate data ingestion and preprocessing to external tools. Popular solutions such as Kafka Connect and Apache NiFi [7] offer robust ingestion pipelines for collecting data. However, these tools often require complex configurations and lack seamless integration with downstream machine learning workflows. This creates a gap between raw data collection and usable ML-ready datasets.

For the production-grade working system that also addresses this limitation, large-scale ML platforms such as Michelangelo of Uber have emerged [4]. Michelangelo integrates data engineering, experimentation, and serving in a unified architecture with high levels of abstraction and automation. It highlights the benefits of modular design, traceability in model development, and scalable model serving infrastructure. Yet, its complexity and operational overhead make it more suitable for large enterprises than for academic or lightweight tasks.

For more accessible ML lifecycle management, Zaharia et al. [17] introduced MLflow, which provides tools for experiment tracking, model packaging, and deployment. While MLflow simplifies model management, it offers limited support for broader data engineering tasks such as ingestion, transformation, or data exploration—features that are essential in many practical workflows.

This integration gap becomes particularly evident in domain-specific applications such as environmental monitoring. Zhang et al. [19] underscored the growing importance of big data analytics in smart grids and environmental systems. In air quality forecasting, several studies have explored the use of ML models such as SVM [10], ANN [11], and LSTM [18], as well as recurrent neural networks trained on real-time data streams [15]. These works demonstrate the feasibility and effectiveness of data-driven models in environmental prediction, but often lack integration with broader pipelines for data management and deployment.

In addition to ML models, data visualization is also a crucial field in unlocking the potential of big data and uncovering hidden insights. It allows users to gain a more intuitive and vivid understanding of information [13]. Especially in the context of ever-growing data volumes, visualization tools and techniques act as a bridge, transforming complex numbers and datasets into charts, tables, and easily comprehensible visuals. This not only supports decision-making processes but also opens up opportunities to identify trends, uncover relationships within data, and predict future changes. Despite its great potential, the field faces significant challenges, particularly in representing massive datasets and monitoring data in real time [9].

Our work builds on these findings by providing a lightweight yet comprehensive platform that supports both traditional and Deep Learning (DL) models, while offering a full-stack, end-to-end pipeline—from data ingestion and validation to model training, containerized serving, and visualization. By combining data engineering and ML workflows into a cohesive system, the platform is de-

signed to be both practical and adaptable to various infrastructure scales and user needs.

3 Proposed Work

Although iFlorus has developed multiple features that allow users with limited technical backgrounds to manage end-to-end big data pipelines with limited coding knowledge, there is still room for further development of the system. One notable limitation lies in its data ingestion capabilities. Currently, file ingestion is restricted to formats such as CSV and Excel. This narrow range limits the flexibility and reach of the platform, especially for users who deal with diverse and modern data formats such as JSON, Avro, or Parquet. In addition, users currently have no option to perform data validation or apply filters to exclude unnecessary or irrelevant data, which can lead to unnecessary processing, storage inefficiencies, and reduced data quality.

Another key limitation of the platform lies in its lack of support for data exploration. At present, it offers no functionality for interactive data exploration, neither through SQL querying nor via a user-friendly interface. The absence of integrated visualization tools further restricts users from deriving meaningful insights from their datasets. In addition, the model training and serving pipeline remains basic and limited in execution. It does not support advanced deep learning models or scalable training and serving strategies, and the current interface offers little flexibility or clarity for customizing model workflows. The absence of a containerized serving infrastructure also limits its ability to support real-world deployment scenarios.

3.1 Architectural overview

The new version of Florus retains the original 5-layer architecture, preserving the core functionality of each layer. However, we have introduced several modifications, including clear boundaries between layers, to address the challenges outlined in the previous section. The updated components are highlighted with red borders, as shown in Figure 1.

To ensure high availability and scalability, Florus adopts a microservices-based backend architecture. The platform is built around several core services, as outlined in Table 1.

3.2 Major enhancements

Diverse data ingestion and validation. Thanks to MinIO integration, Florus 3.0 now supports a wider range of file formats for storage. Users can ingest large volumes of data directly from various Cloud Blob Storage platforms, such as Amazon S3, Google Cloud Platform, Azure Blob Storage, and Google Drive, eliminating the need to upload individual files with size limitations. Additionally,

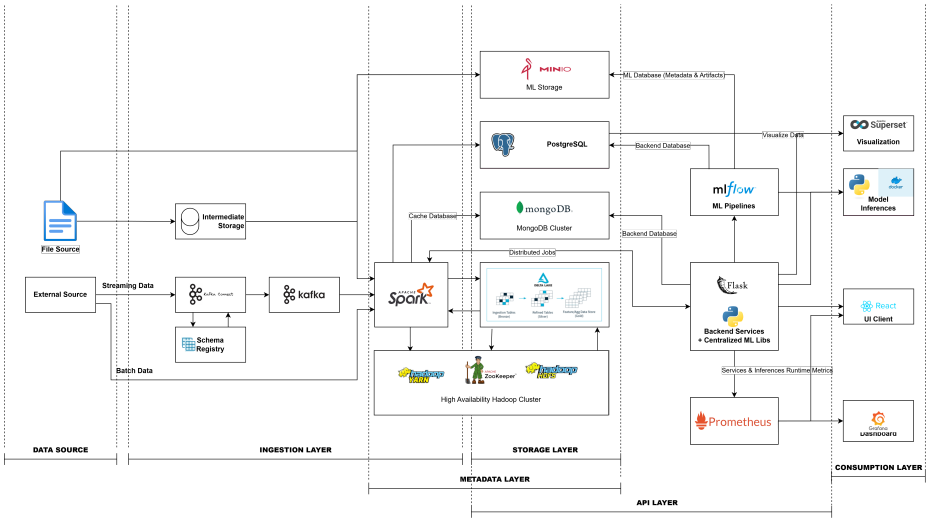

Figure 1: Overall Architecture of Florus 3.0

Table 1: Core Services in Florus 3.0

Service	Description
API Gateway	**Central entry point**, orchestrating communication between the client and backend services.
Authentication Service	Handles **authentication** and **authorization** in the system, ensuring secure access control.
Ingestion Service	Manages **data ingestion workflows**, supporting the collection of both structured and unstructured data in batch or streaming modes.
Delta Service	Manages the **Data Lakehouse** structure, storing, managing, and processing data.
Model Service	Prepares **ML and DL models** for training and integration into data pipelines.
Visualization Service	Allows users to build interactive dashboards and charts using the integrated **Superset** engine.
Serving Service	Automates the **containerization** and **deployment** of trained models using built APIs for prediction and health-check.

for streaming data ingestion, the system now supports Kafka as a message queue source.

We have also introduced a data validation feature that enables users to filter out unnecessary fields or discard records that do not meet predefined conditions prior to ingestion, leveraging Kafka Connect's Single Message Transform (SMT). This validation currently applies when the schema is explicitly provided by the

user or when Kafka Connect can automatically infer the schema, such as when streaming from a database source.

Query Builder Interface. To enhance data exploration, we have introduced a Query Builder feature that provides a user-friendly interface for interacting with data. The current version supports operations such as JOIN, UNION, GROUP BY, HAVING, SELECT, ORDER BY, LIMIT, and common aggregations like MIN, MAX, SUM, and COUNT.

For advanced users familiar with SQL who require more flexibility, we also offer a SQL query editor that allows them to write and execute custom SQL queries directly on their data.

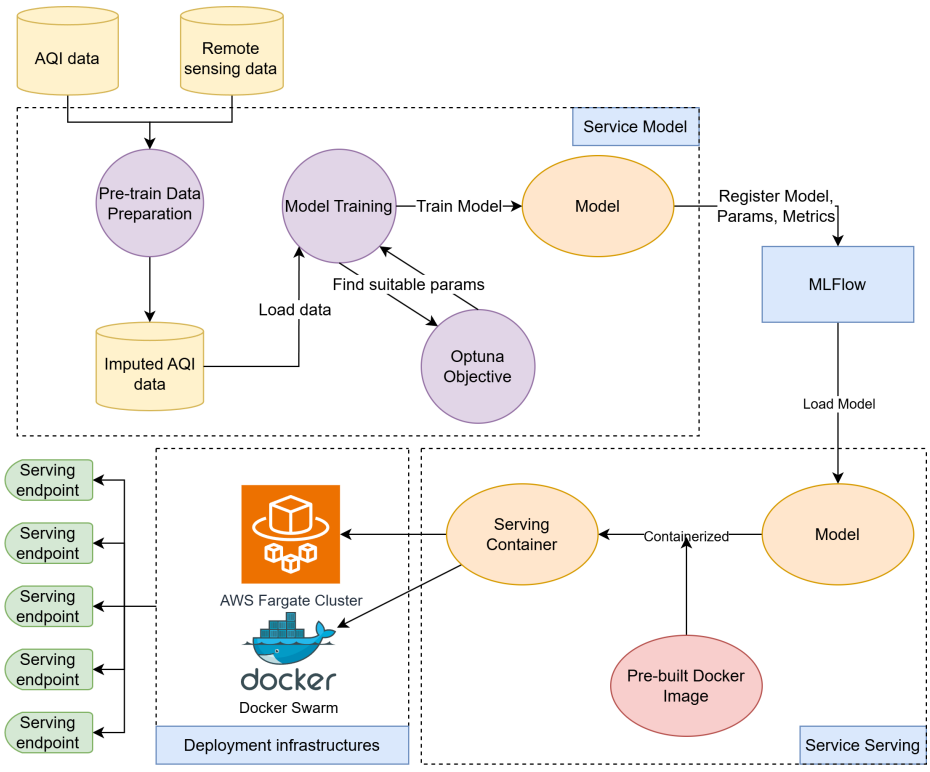

Figure 2: Model pipeline with serving in Centralized Mode

Models and automatic hyperparameter optimization. We developed a flexible and extensible model training pipeline that supports two execution paradigms: Distributed Mode and Centralized Mode. The Distributed Mode leverages Apache Spark running on a Hadoop Cluster to support scalable training for large datasets and computationally intensive models. In contrast, the Centralized Mode is tailored for lighter workloads and prototyping, executing

training processes directly on the local machine as shown in Figure 2. This mode also integrates Optuna for automated hyperparameter optimization and includes broader support for DL models to accommodate diverse tasks.

Containerized model serving. Upon completion of training in either mode, the resulting models are registered in MLFlow's Model Registry and made ready for serving. To enhance model deployment, we implemented a container-based serving workflow that encapsulates model inference logic within a Docker image. This image includes pre-built APIs for prediction and health checking, which standardize interaction with deployed models.

Unlike iFlorus, which relied entirely on local inference, this containerized approach supports both cloud and on-premise deployments, allowing models to be served across any environment with Docker support, such as cloud platforms like AWS Fargate or on-premise clusters such as Docker Swarm, as shown in Figure 2. Furthermore, the serving components are integrated with runtime monitoring using Prometheus and Grafana, collecting key performance and resource usage metrics from active containers. However, the monitoring approach only works for on-premise clusters. For cloud deployments, we use cloud-native tools such as AWS CloudWatch to monitor the active containers in AWS Fargate.

Advanced visualization with integrated tool. Although iFlorus previously supported chart creation, the available chart types and customization options were limited. Additionally, users could not build dashboards to combine charts into comprehensive reports.

With the integration of Superset, these limitations have been addressed. Apache Superset is an open-source data visualization and business intelligence platform designed to help users explore and visualize large datasets with ease. With its intuitive, user-friendly interface for creating interactive dashboards, charts, and reports, it is well-suited for both technical and non-technical users, making it an ideal choice for organizations aiming to enhance decision-making and gain deeper insights from their data.

However, enabling Superset to read from Delta Lake introduces challenges. One approach involves using a query engine such as Spark Thrift, Trino, or Presto, which adds system overhead due to the additional services required. The alternative—duplicating data into a supported relational database, such as PostgreSQ,L but this may introduce the risk of data synchronization lag, where visualizations in Superset may not reflect the most recent changes in Delta Lake. In Florus 3.0, we adopt the second approach because it offers a simpler, more lightweight integration path and avoids the resource demands of maintaining an additional query engine service.

4 Result Analysis

4.1 Data flow

In this section, we aim to predict the Air Quality Index (AQI) or pollutant concentration in the near future using Florus 3.0 to assess the performance of

the framework and analyze the result. The dataset includes air quality indices such as CO, TSP, O_3, NO_2, and $PM_{2.5}$, collected from six monitoring stations across various urban environments in Ho Chi Minh City between 2021 and 2022. This dataset is provided by the Ho Chi Minh City Institute for Environment and Resources.

We propose the data flow as in Figure 3. The historical data is ingested from

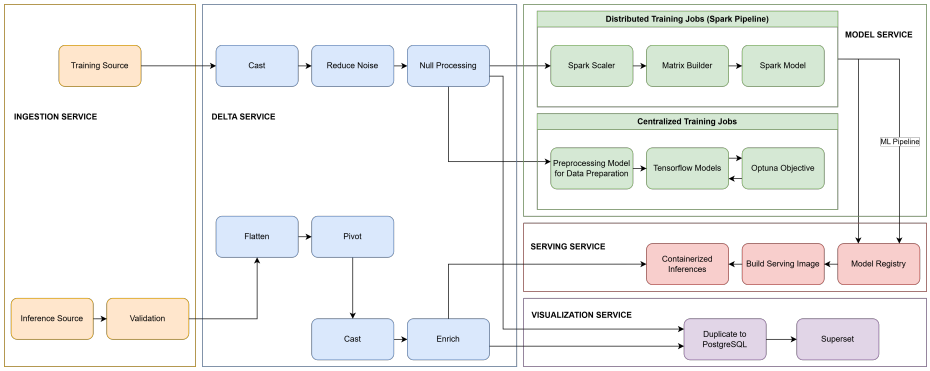

Figure 3: Data Flow

CSV files and loaded into internal tables for further processing. These tables serve as the foundation for model training as well as for generating visualizations and dashboards.

After the necessary pre-processing steps, the data is passed into one of two training modes: Distributed or Centralized. In the Distributed mode, training jobs are executed across the infrastructure using cluster resources. In contrast, the newer Centralized mode utilizes the resources of the local machine where the training job is initiated. For Centralized mode, we also provide Remote Sensing Data, which includes various fields such as Lat (Latitude), Lon (Longitude), WSPD (Windspeed), HPBL (Planetary Boundary Layer Height), and others. This dataset will be integrated with the previous one to enrich the contextual information for each monitoring station. In the training step, if enabled by the user, Optuna is applied to perform hyperparameter optimization for the chosen model. Trained models using the given data are registered in MLflow's Model Registry, and a Docker image with a built-in API interface is prepared for serving. In the given flow, the image has been successfully tested on both cloud platforms, such as AWS Fargate and on-premise Docker Swarm. Once deployed, containers expose serving endpoints, allowing users to send prediction requests directly.

4.2 Experiments

Stream Validation Capabilities. To evaluate the performance impact of the stream validation feature, we conducted an experiment comparing stream

ingestion with and without validation enabled. Specifically, we applied 20 simple filters (e.g., TSP > 0, CO < 10) using Kafka Connect's Single Message Transform (SMT). Each stream message consisted of eight fields—either Float or short String types (less than 20 characters)—and featured a flat structure without nesting.

The experiment was conducted across varying message-per-second (MPS) rates, using 10 mini-batches per scenario. While ingestion time (i.e., the time taken for messages to pass through Kafka and be processed by Spark) is typically sufficient to evaluate stream performance, in this case, we also measured throughput, defined as the number of rows successfully processed per mini-batch. This was necessary since the validation process filters out a subset of messages before they reach Spark. As in Figure 4a, the reduced number of records processed

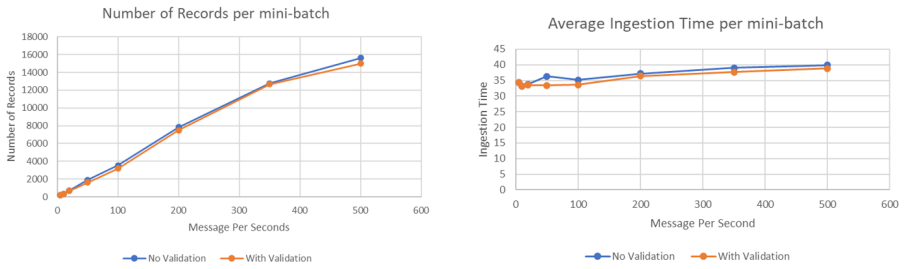

(a) Mini-batch Row Count (b) Mini-batch Ingestion Time

Figure 4: Comparison of Row Count and Ingestion Time under Varying MPS

with validation indicates that the filtering rules are effectively excluding certain entries. Correspondingly, from Figure 4b, we can infer that the processing time is also marginally lower in the validation scenario. These results suggest that the validation feature introduces minimal overhead and does not significantly affect the performance of stream ingestion.

Data Visualization Capabilities. Apache Superset was utilized to explore the air quality dataset and generate meaningful insights through interactive dashboards. Superset provides an intuitive interface for creating various visualizations, allowing users to analyze trends, patterns, and anomalies without extensive coding. The illustrations in Figure 5 showcase different perspectives of the data, combining time series plots, bar charts, and other visuals to support comprehensive data exploration and aid in understanding the spatial and temporal dynamics of air pollution.

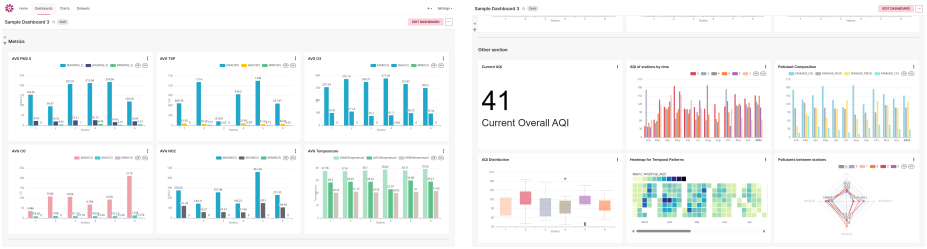

Figure 5: Sample Dashboards for Data Exploration

Hyperparameter Tuning Capabilities. In order to tune the models' hyperparameters, we use Optuna - a powerful, open-source hyperparameter optimization framework that searches for optimal configurations using Tree-structured Parzen Estimator as sampling methods. To evaluate the hyperparameters chosen by Optuna, we conducted the same series of experiments on the models mentioned above for predicting TSP, and the results are shown in Table 2.

Table 2: Performance of TSP prediction models with Optuna-tuned parameters.

Model	MAE	RMSE	MAPE
ANN	19.134	24.352	0.320
CFNN	18.160	23.620	0.308
ESN	18.812	24.489	0.321
LSTM_LSTM	18.095	23.320	0.313
Linear Regression	20.249	25.484	0.320
RNN	24.337	29.830	0.440

Model Training Capabilities. To assess the performance of the integrated ML and DL models within the system, we conducted a series of experiments using newly added traditional models, such as ANN, CFNN, ESN, and RNN, and advanced hybrid architectures, including CNN-LSTM and LSTM-LSTM. The results were evaluated based on performance metrics across various air pollutants with hyperparameter tuning using both Optuna as well as trials and errors approach, as presented in Tables 3, 4, and 5.

Based on the comparison of MAE, RMSE, and MAPE across five air pollutants, the LSTM-LSTM model consistently outperforms both the standalone LSTM and CNN-LSTM models. It yields the lowest error values in all pollutants, indicating higher predictive accuracy. While CNN-LSTM offers some improvement over LSTM, particularly in CO and $PM_{2.5}$ prediction, it still lags behind LSTM-LSTM. This suggests that stacking LSTM layers enhances the model's ability to capture complex temporal patterns in air quality data. In conclusion, from our demonstration, we can see the comparative effectiveness of

Table 3: Performance Metrics of ML Models on Different Pollutants (1)

Index	**ANN**			**CFNN**			**ESN**		
	MAE	RMSE	MAPE	MAE	RMSE	MAPE	MAE	RMSE	MAPE
CO	84.098	146.887	0.0796	88.218	154.484	0.1127	83.402	141.210	0.0807
NO2	5.518	9.979	0.1139	5.583	9.039	0.1189	5.337	8.614	0.116
O3	5.264	8.392	0.0542	5.593	8.689	0.0605	5.238	8.876	0.055
PM2.5	2.531	4.360	0.0835	3.181	4.877	0.1048	3.056	4.746	0.1033
TSP	7.997	12.409	0.1022	8.467	12.879	0.1137	7.535	12.259	0.1045

Table 4: Performance Metrics of ML Models on Different Pollutants (2)

Index	**LSTM**			**CNN_LSTM**			**LSTM_LSTM**		
	MAE	RMSE	MAPE	MAE	RMSE	MAPE	MAE	RMSE	MAPE
CO	83.705	150.495	0.113	76.252	138.473	0.0733	72.287	142.275	0.0699
NO2	7.056	9.494	0.1502	5.469	8.897	0.1094	4.518	8.776	0.0982
O3	6.896	9.562	0.0707	3.803	7.215	0.0405	3.668	7.263	0.0385
PM2.5	4.079	5.616	0.1270	2.187	4.251	0.0722	2.124	4.271	0.0709
TSP	11.055	15.482	0.1388	7.741	12.336	0.1022	5.711	11.285	0.0767

Table 5: Performance Metrics of ML Models on Different Pollutants (3)

Index	**Linear Regression**			**RNN**		
	MAE	RMSE	MAPE	MAE	RMSE	MAPE
CO	80.988	142.220	0.0780	84.217	141.943	0.0793
NO2	5.007	9.147	0.1156	5.5	8.794	0.1151
O3	4.177	7.409	0.0438	5.034	8.194	0.0518
PM2.5	2.565	4.385	0.0830	3.041	4.742	0.0961
TSP	6.574	11.527	0.0874	7.406	12.151	0.0973

various models across different air pollutants. Among traditional models, ESN perform generally better in terms of error metrics, while hybrid deep learning architectures like CNN-LSTM and LSTM-LSTM consistently delivered better performance, particularly for pollutants such as O_3, $PM_{2.5}$, and TSP. These results also highlight the importance of model and parameter selection and hyperparameter tuning in achieving optimal forecast accuracy.

Model Serving Capabilities. To evaluate the responsiveness of the serving container, we conducted a stress test targeting all the container's exposed endpoints. Our service uses a simple Linear Regression model with CO as our predictive air pollutant. The scenario involved:

- Stage 1: 25 virtual users running for 2 minutes and 30 seconds,
- Stage 2: Gradually ramping up to 100 users over the next 2 minutes and 30 seconds,
- Stage 3: Then maintaining 100 users for an additional 5 minutes.

Each virtual user executed all requests sequentially in a loop. Due to current architectural limitations, the API does not support true concurrent request han-

dling, which means requests are handled one at a time within each user's sequence. Despite this limitation, the system exhibited stable behavior and handled a full load of 100 simulated users. Resource limitations restricted testing beyond this threshold.

Table 6: Performance Metrics of Serving Container Under Load

Metric	**Value**
Test Duration	10 minutes
Total Requests	21278 requests
Throughput	∼35.04 requests/s
Average Response Time	1535 ms
P90 Response Time	2,579 ms
P95 Response Time	2,718 ms
P99 Response Time	2,927 ms
Fastest Response Time	199 ms
Slowest Response Time	3,283 ms
Success Rate	100%
Error Rate	0%

Table 7: Average Resource Usage per Test Stage of the Serving Container

Metric	**Idle (No user)**	**Stage 1**	**Stage 2**	**Stage 3**
CPU Usage (100% = 1 CPU core)	0.0181	31.3	87.3	137
Memory Usage (MB)	279	351	371	390
Memory Cached (MB)	449	10.9	10.9	10.9
Received Network Traffic (kB/s)	0.0044	7.21	19.5	29.0
Sent Network Traffic (kB/s)	0.0040	6.51	17.6	26.9

As shown in Table 7, the serving container demonstrated stable and efficient performance under load, reaching up to 100 concurrent users during the stress test. Average CPU usage rose from 0.0181 (idle) to 137%, while memory consumption increased from 279 MB to 390 MB. Network traffic scaled predictably, with received traffic increasing from 0.0044 kB/s to 29.0 kB/s, and sent traffic from 0.0040 kB/s to 26.9 kB/s.

From the API performance metrics illustrated in Table 6 and Figure 6, the average response time across endpoints remained under 2000 ms, with 100% success rate, even during ramp-up and full-load phases. While the system currently does not support concurrent request handling per container, it maintains responsiveness and throughput under sequential load as shown in Figure 7, confirming the serving container's reliability for scalable deployment scenarios.

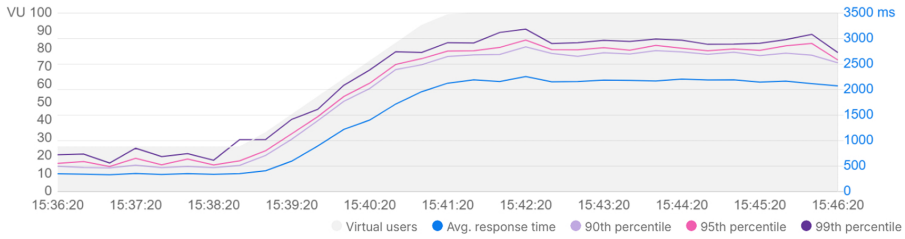

Figure 6: Response time trends during the test duration

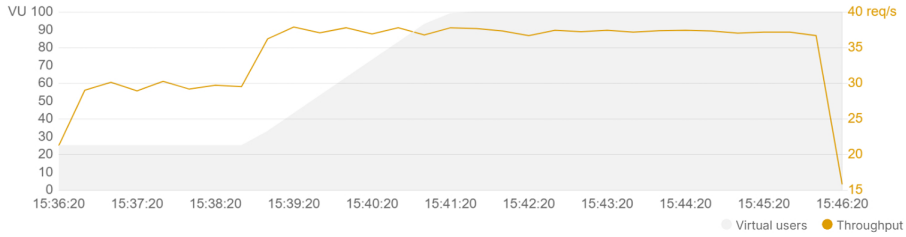

Figure 7: Rate of requests sent per second during the test duration

5 Conclusion

Our enhanced framework, Florus 3.0, represents a significant advancement in the Florus low-code big data platform by providing a comprehensive and modular workflow for air quality forecasting. The system integrates critical components such as streamlined data ingestion, advanced data visualization, diverse training modes, and containerized model serving. Experimental results demonstrate notable improvements in performance and usability, with LSTM-LSTM models showing consistently strong accuracy across various pollutants. The serving infrastructure also proved stable under full stress-testing conditions, achieving 100% throughput at scale and highlighting its readiness for production environments. Despite these achievements, several areas remain open for further development. Key directions include introducing dynamic model execution-time switching to enhance flexibility and efficiency, optimizing data visualization pipelines by adopting native Delta Lake support to reduce PostgreSQL redundancy, and improving the validation system through more adaptive schema inference for varied data sources. Additionally, refining the serving infrastructure and improving container performance can help support deployment in field conditions with limited connectivity. These proposed improvements build upon Florus 3.0's solid foundation and modular architecture, allowing for seamless integration of new features. The system's design and capabilities position it well for broader application beyond air quality forecasting, extending into smart city infrastructure,

industrial IoT, and public health surveillance—domains that demand scalable, real-time, and user-accessible analytical platforms.

Acknowledgement

This research is funded by the Ministry of Science and Technology of Vietnam under grant number KC-4.0-25/19-25. The authors also acknowledge Ho Chi Minh City University of Technology (HCMUT), VNU-HCM for supporting this study. In addition, the authors express their sincere gratitude to Hoang-Viet Tran for his invaluable support and contributions, which were essential to the successful completion of this research.

References

1. Armbrust, M., Das, T., Sun, L., Yavuz, B., Zhu, S., Murthy, M., Torres, J., van Hovell, H., Ionescu, A., Łuszczak, A., Świtakowski, M., Szafrański, M., Li, X., Ueshin, T., Mokhtar, M., Boncz, P., Ghodsi, A., Paranjpye, S., Senster, P., Xin, R., Zaharia, M.: Delta lake: high-performance ACID table storage over cloud object stores **13**(12), 3411–3424. https://doi.org/10.14778/3415478.3415560, https://doi.org/10.14778/3415478.3415560
2. Bock, A.C., Frank, U.: Low-code platform. Business & Information Systems Engineering **63**(6), 733–740 (2021). https://doi.org/10.1007/s12599-021-00726-8, https://doi.org/10.1007/s12599-021-00726-8
3. Chellappan, S., Ganesan, D.: Practical Apache Spark: Using the Scala API. Apress, first edition edn. (2018)
4. Engineering, U.: Meet michelangelo: Uber's machine learning platform. Uber Engineering Blog (2017), https://www.uber.com/blog/michelangelo-machine-learning-platform/
5. Farki, A., Noughabi, E.A.: (PDF) real-time blood pressure prediction using apache spark and kafka machine learning. https://doi.org/10.1109/ICWR57742.2023.10138962, https://www.researchgate.net/publication/371334629_Real-Time_Blood_Pressure_Prediction_Using_Apache_Spark_and_Kafka_Machine_Learning
6. Gadban, F., Kunkel, J.: Analyzing the performance of the s3 object storage API for HPC workloads **11**(18), 8540. https://doi.org/10.3390/app11188540, https://www.mdpi.com/2076-3417/11/18/8540, number: 18 Publisher: Multidisciplinary Digital Publishing Institute
7. Isnaeni, N., Putranto, B.P.D., Andriyani, W., Khomsah, S.: Comprehensive lakehouse data architecture model for college accreditation **5**(1), 45–51. https://doi.org/10.20895/dinda.v5i1.1759, https://journal.ittelkom-pwt.ac.id/index.php/dinda/article/view/1759, number: 1
8. Jain, P., Kraft, P., Power, C., et al.: Analyzing and comparing lakehouse storage systems. Proceedings of the Conference on Innovative Data Systems Research (CIDR) (2023)
9. Khalid, Z.M., Zeebaree, S.R.M.: Big data analysis for data visualization: A review **5**(2), 64–75, https://ideas.repec.org//a/aif/journl/v5y2021i2p64-75.html, publisher: IJSAB International

10. Kulkarni, M., Raut, A., Chavan, S., Rajule, N., Pawar, S.: Air quality monitoring and prediction using SVM. In: 2022 6th International Conference On Computing, Communication, Control And Automation (ICCUBEA. pp. 1–4. https://doi.org/10.1109/ICCUBEA54992.2022.10010942, https://ieeexplore.ieee.org/abstract/document/10010942, ISSN: 2771-1358
11. Lei, T.M.T., Ng, S.C.W., Siu, S.W.I.: Application of ANN, XGBoost, and other ML methods to forecast air quality in macau **15**(6), 5341. https://doi.org/10.3390/su15065341, https://www.mdpi.com/2071-1050/15/6/5341, number: 6 Publisher: Multidisciplinary Digital Publishing Institute
12. Phan, P.M., Luu, Q.H.T., Huynh, T.L., Le, T.V.: A more refined advancement to the low-code framework for end-to-end big data management. In: Dao, N.N., Pham, Q.D., Cho, S., Nguyen, N.T. (eds.) Intelligence of Things: Technologies and Applications. pp. 73–84. Springer Nature Switzerland (2024). https://doi.org/10.1007/978-3-031-75593-4_7
13. Shetty, S.D.: Sentiment analysis, tweet analysis and visualization on big data using apache spark and hadoop **1099**(1), 012002. https://doi.org/10.1088/1757-899X/1099/1/012002, https://dx.doi.org/10.1088/1757-899X/1099/1/012002, publisher: IOP Publishing
14. Vo, H.P., Nguyen, K.G.C., Nguyen, K.L., Le, T.V.: A big data approach for customer behavior analysis in telecommunication industry. In: Thai-Nghe, N., Do, T.N., Haddawy, P. (eds.) Intelligent Systems and Data Science. pp. 91–105. Springer Nature Singapore, Singapore (2023). https://doi.org/10.1007/978-981-99-7666-9_8
15. Wang, B., Kong, W., Zhao, P.: An air quality forecasting model based on improved convnet and RNN **25**(14), 9209–9218. https://doi.org/10.1007/s00500-021-05843-w, https://doi.org/10.1007/s00500-021-05843-w
16. Zaharia, M., Ghodsi, A., Xin, R., Armbrust, M.: Lakehouse: A new generation of open platforms that unify data warehousing and advanced analytics. https://www.semanticscholar.org/paper/Lakehouse%3A-A-New-Generation-of-Open-Platforms-that-Zaharia-Ghodsi/451cf5fc9786ed4f7e1d9877f08d00f8b1262121
17. Zaharia, M., Chen, A., Davidson, A., et al.: Accelerating the machine learning lifecycle with mlflow. IEEE Data Eng. Bull. **41**(4), 39–45 (2018)
18. Zhang, J., Li, S.: Air quality index forecast in beijing based on CNN-LSTM multi-model **308**, 136180. https://doi.org/10.1016/j.chemosphere.2022.136180, https://www.sciencedirect.com/science/article/pii/S004565352202673X
19. Zhang, Y., Huang, T., Bompard, E.F.: Big data analytics in smart grids: a review. Energy Informatics **1**(1), 1–24 (2018)

A Hybrid Deep Learning and LLim et al. (2024M Framework for Landslide Detection and Severity Analysis

*Dr. G Sudha Sadasivam[1], Sanjay P[2], Pathipati Shailesh Babu[3], Nithish Narayanan[4], Muralidhar KV[5] and Ajay Gowtham[6]

[1]PSG College of Technology
[1]gss.cse@psgtech.ac.in

[2]PSG College of Technology
[2]21z344@psgtech.ac.in

[3]PSG College of Technology
[3]21z328@psgtech.ac.in

[4]PSG College of Technology
[4]21z327@psgtech.ac.in

[5]PSG College of Technology
[5]21z312@psgtech.ac.in

[6]PSG College of Technology
[6]22z461@psgtech.ac.in

Abstract. Landslides are a formidable natural hazard, often imperiling human lives and critical infrastructure—especially in regions with intricate terrains and environmental variability. In response to these challenges, the research paper proposes a deep learning model that integrates Inception blocks with a U-Net architecture, enhanced further by a Convolutional Block Attention Module (CBAM). By leveraging the multi-sensor Landslide4Sense dataset, the proposed work refines feature extraction, thereby improving the precision of landslide segmentation. Additionally, we integrate a Large Language Model that is used to assess landslide severity based on extracted features. This paper details the model's design, preprocessing steps, training strategy, and comparative performance, ultimately demonstrating its promise for landslide identification and severity assessment.

Keywords: Deep Learning, Semantic Segmentation, Landslide Detection, Large Language Models, Risk Assessment

1 Introduction

Landslides have become increasingly prevalent in recent times due to urban expansion, deforestation, and climate change, leading to more frequent and severe events. Accurate and timely detection of landslides is essential for effective disaster preparedness, early warning, and mitigation. Traditionally, landslide detection has relied on manual image interpretation or simple automated techniques, which often fail in complex, heterogeneous terrains.

Recent advances in deep learning, particularly in semantic segmentation, offer powerful tools for improving detection accuracy. In this work, we propose a novel deep learning framework that integrates Inception modules with a U-Net architecture enhanced by the Convolutional Block Attention Module (CBAM). This architecture allows for better multiscale feature extraction and spatial focus in image segmentation tasks. In addition, we introduce the use of the Large Language Model (LLaMA 3.2/3.3) to interpret segmentation outputs and assess landslide severity based on both visual and topographical data.

The key contribution of this paper is the development of a dual-stage model that combines pixel-level landslide segmentation with semantic severity analysis, offering both high detection accuracy and contextual understanding. We validate our approach on the Landslide4Sense dataset and compare it against traditional architectures such as U-Net and ResUNet, demonstrating superior performance in terms of precision, F1-score, and interpretability.

The novelty of this work lies in the dual integration of enhanced segmentation and semantic analysis. While prior works have focused solely on segmentation of landslide-prone areas using standard deep learning models like U-Net and ResUNet, our approach introduces a CBAM-Inception U-Net architecture that combines multiscale convolution with dynamic attention to improve detection precision. Furthermore, we uniquely incorporate a Large Language Model (LLaMA 3.2) to interpret and contextualize the model's output. This semantic layer provides a human-interpretable assessment of landslide severity—an area largely unexplored in prior research.

2 Literature Survey

Landslide detection has evolved considerably with the advancement of remote sensing, deep learning, and artificial intelligence techniques. This section presents a thorough review of existing works, structured into classical machine learning approaches, deep learning frameworks, attention-based mechanisms, and recent innovations using vision transformers and foundation models.

2.1 Machine Learning-Based Approaches

Traditional approaches have primarily relied on statistical learning and classical machine learning models using geospatial data. Hemalatha et al. [1] developed an early warning system by applying Support Vector Regression (SVR) to data from wireless sensor networks, showing strong correlation between soil moisture and landslide risk. Piralilou et al. [2] used OBIA and ensemble machine learning techniques (MLP and Random Forest) on PlanetScope imagery, achieving up to 85% accuracy in landslide detection.

2.2 Deep Learning-Based Approaches

Deep learning methods have shown superior performance in extracting spatial features directly from remote sensing images. Mohan et al. [3] reviewed CNN and DL techniques for landslide detection, identifying the advantages of segmentation architectures like U-Net and ResUNet. Manasi et al. [7] and Meena et al. [10] demonstrated the effectiveness of U-Net for semantic segmentation using high-resolution images from RapidEye satellites, achieving impressive F1-scores across Himalayan datasets.

The introduction of benchmark datasets such as Landslide4Sense [4] has enabled standardized evaluation of DL models. Ghorbanzadeh et al. [5] analyzed models used in the 2022 Landslide4Sense competition, highlighting the performance of Swin Transformer, SegFormer, and improved U-Net variants. In follow-up work, Ghorbanzadeh et al. [6] combined ResUNet with OBIA, boosting the detection of IoU by 22%.

2.3 Attention-Based and CNN Improvements

Architectural improvements such as attention mechanisms have further advanced segmentation performance. Woo et al. [13] introduced CBAM (Convolutional Block Attention Module), enhancing model focus on important spatial and channel features. Le et al. [16] applied CBAM within U-Net for landslide detection, achieving an F1-score of 84.07.

Li and Qin [8] modified YOLOv4 with attention and group convolution, achieving fast and accurate object-level landslide detection. Jiang et al. [9] used Mask R-CNN and transfer learning to distinguish recent and older landslides, achieving F1-scores around 80% on the LRSTTC dataset.

2.4 Real-Time and IoT-Based Approaches

Low-cost and real-time monitoring using IoT has also gained attention. Kumar et al. [11] presented an IoT-based system for real-time slope instability detection in Sikkim, India. Thirugnanam et al. [12] conducted a global review of IoT-integrated landslide monitoring, emphasizing location-specific customizations for sensor placement and communication protocols.

2.5 Large Language Models and Interpretability

Recent advances in NLP have introduced the potential of Large Language Models (LLMs) like LLaMA [14] for terrain interpretation. These models enhance post-segmentation analysis by providing context-aware descriptions and severity ratings based on visual cues and topographic features.

2.6 Cutting-Edge Research and 2023–2024 Innovations

Recent work continues to improve detection accuracy and scalability:

- TransLandSeg [15] introduced a SAM-based transfer learning method that fine-tunes only 1.3% of parameters and achieved top performance on the Landslide4Sense dataset.
- GMNet [16] proposed multiscale global feature fusion for better segmentation precision.
- Heterogeneous Ensembles [17] like Unet, LinkNet, and DeepLab were used to achieve global landslide detection, reaching an F1-score of 0.69.
- Ensemble CNNs [18] and models like LinkNet with ResNet50 backbone attained accuracy of 97.49% and F1 of 85.7%.
- UAV + AI [19] allowed for precise crack detection in real terrain, enhancing mapping resolution.
- FCADenseNet with InSAR data [20] improved wide-area detection using topographic and radar data (F1-score: 0.7611).
- MA-Net, PSP-Net, ResUNet, etc. [21] were evaluated in semi-arid regions with F1-scores as high as 95%, showing deep learning's robustness in different environments.

2.7 Summary and Distinction of Proposed Work

Most existing models focus on segmentation alone or lack post-detection interpretation. Additionally, many studies train only on labeled data without proper testing on unseen datasets, which affects generalizability. Our work addresses these gaps by:

- Introducing CBAM-Inception U-Net, combining multiscale feature extraction and attention.
- Integrating LLaMA 3.2, a Large Language Model, for semantic analysis of severity, bridging a unique gap between vision and language in landslide research.
- Evaluating on training, validation, and a dedicated test set, ensuring reliability and robustness.

3 Dataset Description

The Landslide4Sense dataset serves as the foundation for this study. It includes multispectral satellite imagery primarily collected from Sentinel-2, complemented by topographical data such as slope information and digital elevation models (DEM) derived from ALOS PALSAR. This dataset offers a comprehensive representation of landslide events by capturing numerous small to medium-scale ground movements across various global locations. Designed to advance landslide detection research, Landslide4Sense is a valuable resource for the machine learning, computer vision, and remote sensing communities. Accessible through the Landslide4Sense website, it has facilitated significant progress in leveraging modern machine learning techniques for reliable landslide detection, contributing to early identification and improved management of these natural disasters. A sample image from the dataset is shown in Fig.1.

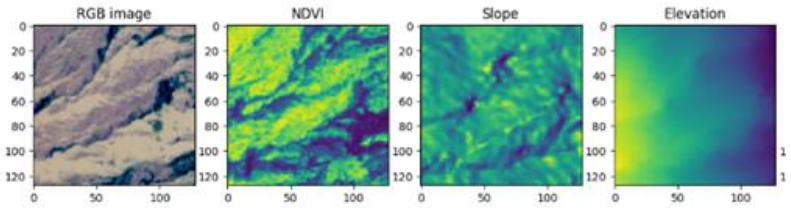

Fig. 1. Sample Image from Dataset

4 Methodology

The methodology for landslide detection using the Landslide4Sense dataset follows a systematic approach. The process begins with preprocessing, where the dataset is loaded and prepared through steps like normalization, data augmentation, and image resizing to enhance model performance. Next, the model selection phase involves choosing a suitable deep-learning architecture, such as CBAM-Inception U-Net uses the Inception approach to pull out image features at various sizes, and it also considers different channels within the image data and spatial Attention Mechanism (CBAM) for improved feature refinement and segmentation accuracy. In the model training phase, the selected model is constructed with appropriate layers, including convolutional, pooling, and output layers, optimized for landslide detection. The model is trained using the prepared dataset through multiple forward passes, loss calculations, and backpropagation steps to refine the model's weights. Once training is complete, the model undergoes evaluation to assess its performance on unseen data. Key metrics such as accuracy, precision, recall, and F1-score are calculated. Following evaluation, the refined model is employed for landslide detection, generating segmentation masks to identify potential landslide areas. Finally, the predictions are analysed using a large language model to interpret the results. This ensures that meaningful insights are drawn from the detected patterns and model

outputs. This structured approach, incorporating CBAM-Inception U-Net, ensures enhanced feature learning, improved focus on critical regions, and a comprehensive methodology for accurate landslide detection using the Landslide4Sense dataset. An outline of the approach has been provided in the given flowchart diagram (Fig. 2).

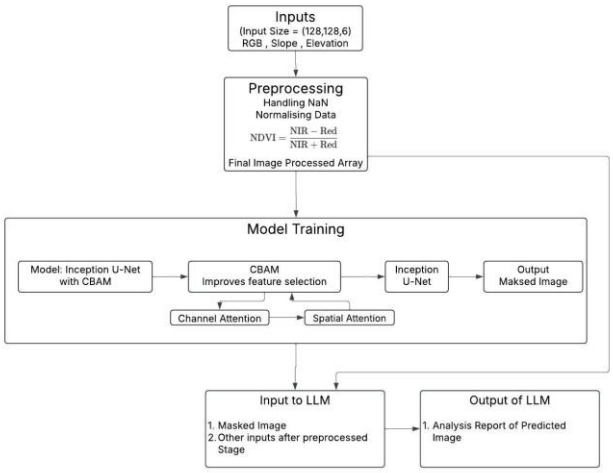

Fig. 2. Flowchart describing the outline of the approach used

The novelty ulti-scale Inception mo he U-Net framework, e looked by standard arch s a Large Language Mo egmented outputs, allov landslide severity. This , the first of its kind ap accuracy and enhanced

Among the m due to its superior perfo e CBAM-Inception U- ilities of Inception mo volutional Block Attent landslide detection. Th ed in the following sec tion.

4.1 CBAM-Inception U-Net

The inception modules, originally introduced in GoogLeNet, are known for their ability to efficiently capture features at multiple spatial resolutions by employing

parallel convolutional pathways with different kernel sizes. The CBAM-Inception U-Net architecture, as depicted in Fig.3 below, combines the strengths of the U-Net framework, Inception modules, and CBAM. At its core, the CBAM-Inception U-Net retains the encoder-decoder structure of the traditional U-Net, ensuring precise localization of features across multiple scales, which sets this model apart is the integration of CBAM within its layers. CBAM enhances feature learning by sequentially applying Channel Attention and Spatial Attention mechanisms, are used to focus on the most informative features and regions critical for landslide detection. By incorporating CBAM, the model effectively suppresses irrelevant features while amplifying essential details, resulting in improved segmentation accuracy and better performance in identifying complex landslide patterns.

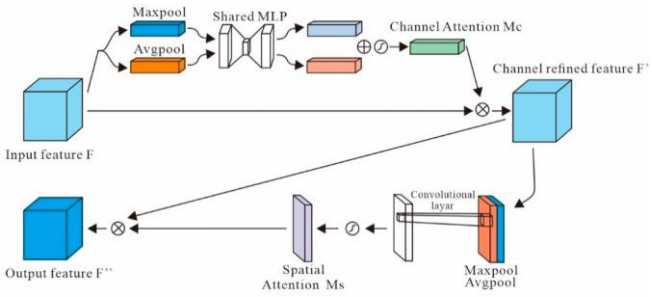

Fig. 3. CBAM with Inception U-Net Architecture

4.2 CBAM Attention Mechanism

The Convolutional Block Attention Module (CBAM), pictured in Figure 4, is a powerful feature that makes CNNs (used for image analysis) stronger by choosing to focus on specific parts of the image.) by selectively emphasizing informative features. CBAM has two parts. The first part looks at the different "channels" in the image data and decides which ones are most useful, making those stand out more. The second part then focuses on the important areas within the image. Simultaneously, in the spatial attention stage, CBAM recalibrates feature maps across spatial dimensions, enabling the model to selectively attend to informative spatial locations while suppressing irrelevant regions.

When the CBAM attention method is used with the Inception U-Net structure, the resulting system gets better at seeing both local features and the overall context of the land. Because it can choose to pay attention to the most helpful details, it becomes more accurate and dependable at identifying terrain in various environments.

The process involved in creation and evaluation of a model is illustrated by dividing it into a four-fold process that starts with data preparation, model selection, and training and ends by testing and evaluating the performance of the models.

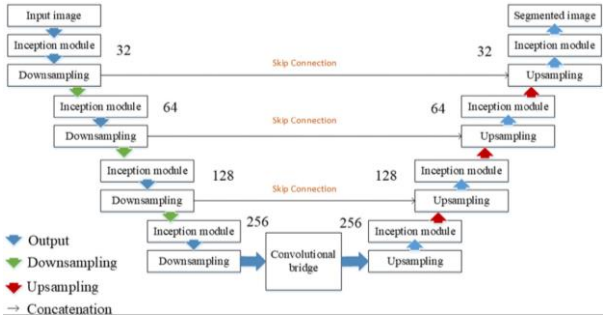

Fig. 4. CBAM Attention Mechanism

4.3 Data Preparation

The Landslide4Sense dataset is prepared and cleaned up. It ensures that each sample has a uniform format and can work together correctly. Additionally, the collection of data is divided into various parts to train a model and check how effective it is as well as a final evaluation. This critical step allows separate sets of data to be used during training, validation, or evaluation thus preventing overfitting while also guaranteeing reliable performance assessment

4.4 Model Selection and Justification

For landslide image segmentation, various architectures such as U-Net and ResUNet were initially considered due to their proven effectiveness in semantic segmentation tasks. However, to further enhance feature extraction and improve performance in complex terrains, we selected the CBAM-Inception U-Net architecture. This model integrates Inception modules, which allow for multi-scale feature learning, with the Convolutional Block Attention Module (CBAM), which refines features by applying both channel and spatial attention mechanisms.

This combination allows the model to focus on critical regions of satellite imagery while suppressing irrelevant information, improving segmentation accuracy. Compared to standard U-Net or ResUNet, our experiments demonstrated that CBAM-Inception U-Net achieved higher F1 scores and lower loss, validating its suitability for landslide detection.

While U-Net and ResUNet have demonstrated reasonable performance, they lack attention-based mechanisms and multi-path feature processing, limiting their precision in highly variable terrain. By combining Inception's multiscale processing with CBAM's attention refinement, our model offers a more intelligent focus on landslide-relevant features—especially useful in cluttered and geologically diverse areas.

4.5 Testing and Validation

The trained model is assessed for its generalization capability using an independent dataset for validation. This ensures that the model learns patterns well from the training set and applies them to new examples without errors or problems during validation steps. We adjust the model's settings and prevent it from overfitting by checking it against a separate data group. Then, we measure its performance on a completely new dataset that was kept aside. This final test shows us if the model is ready for real-world use.

4.6 Evaluation

To understand how well a trained model performs (its effectiveness), we must evaluate it. This involves comparing the model's outputs to verified ground truth labels after a thorough analysis. We typically calculate key metrics like precision, recall, accuracy, and the F1 score to understand the model's strengths and its potential weaknesses. In addition to verifying its accuracy in detecting landslides, this evaluation assesses the model's performance under varying conditions and scenarios. Visualization techniques further enhance this process by providing side-by-side comparisons of the model's predictions with actual data, yielding deeper insights into its behavior. Ultimately, such thorough evaluation is essential for grasping the model’s capabilities and for guiding any necessary improvements or adjustments.

4.7 Novelty of the Proposed Approach

Our method stands out from existing approaches in two fundamental ways. First, we integrate CBAM (Convolutional Block Attention Module) into the Inception-based U-Net architecture. This combination allows for both multi-scale feature extraction and dynamic focus on spatially and channel-wise informative regions, enabling the model to accurately segment complex landslide patterns in diverse terrains. Unlike conventional U-Net or ResUNet models, our architecture explicitly enhances attention to both global and local features.

Second, we are among the first to integrate a Large Language Model (LLaMA 3.2) into the post-processing pipeline for semantic analysis. Instead of merely providing binary masks, our system outputs interpretable text-based insights related to terrain risk factors, slope profiles, and likely severity, based on both input data and segmentation results. This hybrid visual-linguistic approach offers greater value for decision-makers in disaster risk management.

5 Experimental Setup

In this study, we implemented and compared multiple deep learning models, including U-Net, ResUNet, and CBAM with Inception U-Net, to assess their performance on the Landslide4Sense dataset. The input images had dimensions of 128 × 128 pixels and consisted of six channels: RGB bands (Red, Green, and Blue), NDVI (Normalized Difference Vegetation Index), Slope, and Elevation. The dataset was split into 60% training, 20% validation, and 20% testing. Model training was conducted using the Adam optimizer with Binary Cross-Entropy as the loss function, incorporating dropout layers to mitigate overfitting. The details are represented in Table 1.

Table 1. Model Training Configuration and Evaluation Metrics Summary.

Parameter	Value
Training: Validation: Testing	60:20:20
Batch size	16
Image height and width	(128x128)
Activation Function	ReLU
Optimizer	Adam Optimizer
Loss Function	Binary Cross entropy
Metrics	Loss, Accuracy, Precision, Recall, F1-score and IoU
No. of epochs	80
Steps for each Epoch	143 steps

Additionally, CBAM blocks were integrated to enhance feature selection through attention mechanisms. Training was performed over 80 epochs with a batch size of 16, and evaluation was based on key metrics such as loss, precision, recall, accuracy, F1 score, and inference speed. Among these, loss measured prediction error, precision reflected the correctness of positive classifications, recall determined the model's ability to detect relevant instances, accuracy assessed overall prediction quality, and the F1 score balanced precision and recall. Inference speed was also considered for real-time applicability.

The results indicated that CBAM with Inception U-Net outperformed the other models, achieving the lowest training loss (0.0221) and the highest F1 score (78.12), while maintaining strong validation performance, demonstrating its ability to generalize effectively. A detailed performance comparison on the testing data, as

shown in Table 3, revealed that CBAM with Inception U-Net achieved the lowest testing loss (0.029), the highest precision, recall, and F1 score, and the fastest inference speed, making it the most efficient model for landslide detection.

Table 2. Training and Validation Metrics.

Models	Training			Validation		
	Loss	Accuracy	F1	Loss	Accuracy	F1
U-Net	0.025	97.89	74.29	0.031	98.44	69.44
ResUNet	0.0296	98.82	70.75	0.0294	98.85	70.42
CBAM with Inception U-Net	0.0221	99.09	78.12	0.0314	98.85	71.04

Table 3. Testing Performance Comparison.

Models	Training			Validation		
	Loss	Accuracy	F1	Loss	Accuracy	F1
U-Net	0.025	97.89	74.29	0.031	98.44	69.44
ResUNet	0.0296	98.82	70.75	0.0294	98.85	70.42
CBAM with Inception U-Net	0.0221	99.09	78.12	0.0314	98.85	71.04

To further analyze performance, a visual comparison of predicted landslide regions was conducted using U-Net, ResUNet, and CBAM with Inception U-Net. The sample outputs, illustrated in Fig. 5, Fig. 6, and Fig. 7, highlight the differences in segmentation accuracy and detail. The CBAM with Inception U-Net consistently produced sharper boundaries and more precise segmentation, effectively capturing landslide-prone regions with higher accuracy. In contrast, U-Net (Fig. 5) and ResUNet (Fig. 6) occasionally misclassified certain areas or failed to detect smaller landslide patterns, reinforcing the advantage of attention mechanisms in feature extraction.

Fig. 5. Output of U-Net

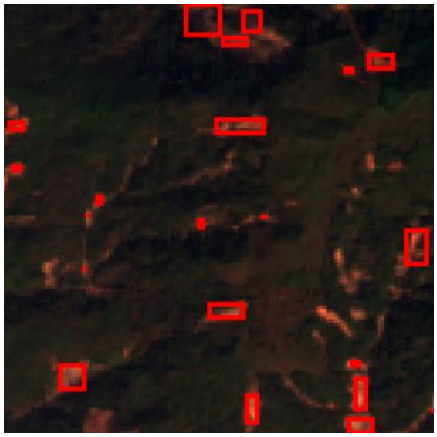

Fig. 6. Output of ResNet

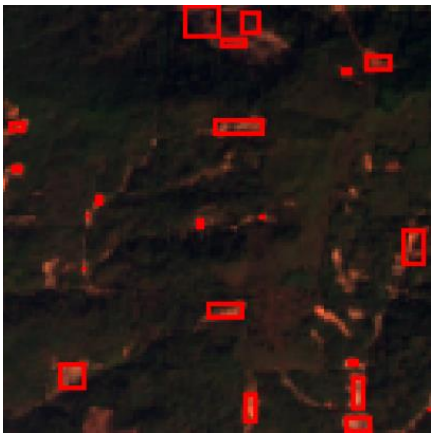

Fig. 7. Output of CBAM with Inception U-Net

Additionally, to enhance interpretability, the input data—comprising RGB bands, slope, and elevation data—was processed through a Large Language Model (LLM) alongside the model's output graphs. As illustrated in Fig. 8, the LLM-generated report provided detailed insights into detected landslide regions, environmental conditions, and risk factors, improving the decision-making process for geologists and disaster management teams.

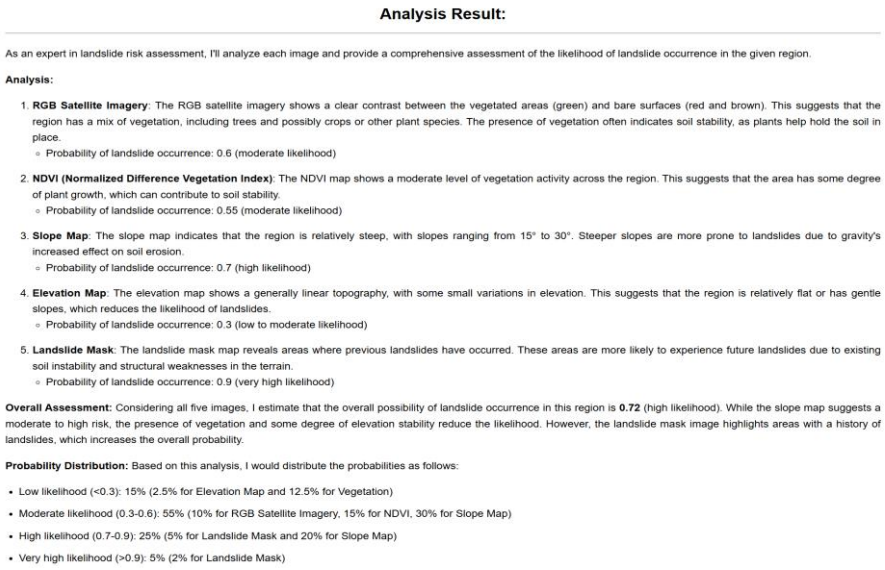

Analysis Result:

As an expert in landslide risk assessment, I'll analyze each image and provide a comprehensive assessment of the likelihood of landslide occurrence in the given region.

Analysis:

1. **RGB Satellite Imagery**: The RGB satellite imagery shows a clear contrast between the vegetated areas (green) and bare surfaces (red and brown). This suggests that the region has a mix of vegetation, including trees and possibly crops or other plant species. The presence of vegetation often indicates soil stability, as plants help hold the soil in place.
   - Probability of landslide occurrence: 0.6 (moderate likelihood)
2. **NDVI (Normalized Difference Vegetation Index)**: The NDVI map shows a moderate level of vegetation activity across the region. This suggests that the area has some degree of plant growth, which can contribute to soil stability.
   - Probability of landslide occurrence: 0.55 (moderate likelihood)
3. **Slope Map**: The slope map indicates that the region is relatively steep, with slopes ranging from 15° to 30°. Steeper slopes are more prone to landslides due to gravity's increased effect on soil erosion.
   - Probability of landslide occurrence: 0.7 (high likelihood)
4. **Elevation Map**: The elevation map shows a generally linear topography, with some small variations in elevation. This suggests that the region is relatively flat or has gentle slopes, which reduces the likelihood of landslides.
   - Probability of landslide occurrence: 0.3 (low to moderate likelihood)
5. **Landslide Mask**: The landslide mask map reveals areas where previous landslides have occurred. These areas are more likely to experience future landslides due to existing soil instability and structural weaknesses in the terrain.
   - Probability of landslide occurrence: 0.9 (very high likelihood)

Overall Assessment: Considering all five images, I estimate that the overall possibility of landslide occurrence in this region is **0.72** (high likelihood). While the slope map suggests a moderate to high risk, the presence of vegetation and some degree of elevation stability reduce the likelihood. However, the landslide mask image highlights areas with a history of landslides, which increases the overall probability.

Probability Distribution: Based on this analysis, I would distribute the probabilities as follows:

- Low likelihood (<0.3): 15% (2.5% for Elevation Map and 12.5% for Vegetation)
- Moderate likelihood (0.3-0.6): 55% (10% for RGB Satellite Imagery, 15% for NDVI, 30% for Slope Map)
- High likelihood (0.7-0.9): 25% (5% for Landslide Mask and 20% for Slope Map)
- Very high likelihood (>0.9): 5% (2% for Landslide Mask)

Fig. 8. Analysis Report from LLaMA 3.2

The incorporation of attention mechanisms within the Inception U-Net architecture significantly improved feature extraction by allowing the model to focus on the most critical parts of the input image. This enhancement in attention to detail contributed to exceptional performance in identifying landslide-prone areas. These findings suggest that Inception U-Net with attention mechanisms is a highly promising approach for landslide detection, offering high accuracy, efficiency, and real-world applicability in geological disaster management and mitigation strategies.

6 Conclusion

Landslides pose a severe threat to human life, infrastructure, and the environment, especially in regions prone to geological instability. Effective and reliable detection systems are essential for issuing early warnings and enabling timely preventive measures. This paper presents a deep learning-based framework that combines the CBAM-Inception U-Net model for landslide segmentation with the LLaMA 3.2 Large Language Model for post-segmentation severity assessment. Among the three architectures evaluated—U-Net, ResUNet, and CBAM-Inception U-Net—our proposed model demonstrated the highest performance across multiple metrics, including F1-score, accuracy, and inference speed. The integration of attention mechanisms and Inception modules improved the model's ability to focus on relevant terrain features, while the use of LLMs added an interpretative layer,

enhancing the system's practical usability. In summary, our main contribution lies in introducing a hybrid AI system that not only detects landslide-prone regions with high precision but also provides a qualitative analysis of severity, setting a new direction for intelligent, interpretable landslide risk assessment.This study introduces a novel approach by combining multiscale-attentive segmentation with a post-segmentation LLM-based semantic analysis, thereby extending landslide detection beyond conventional image segmentation into the domain of explainable and actionable geospatial intelligence.

References

1. Hemalatha, T., Ramesh, M. V., & Rangan, V. P. (2019). Effective and Accelerated Forewarning of Landslides Using Wireless Sensor Networks and Machine Learning. *IEEE Sensors Journal*, 19(21), 9964–9975. https://doi.org/10.1109/JSEN.2019.2928358

2. Piralilou, S. T., et al. (2019). Landslide detection using multi-scale image segmentation and different machine learning models in the higher Himalayas. *Remote Sensing*, 11(21), 2575. https://doi.org/10.3390/rs11212575

3. Mohan, A., Singh, A. K., Kumar, B., & Dwivedi, R. (2021). Review on remote sensing methods for landslide detection using machine and deep learning. *Trans. Emerging Tel. Tech.*, 32(12), e3998.

4. Ghorbanzadeh, O., et al. (2022). Landslide4Sense: Reference benchmark data and deep learning models for landslide detection. *arXiv:2206.00515*.

5. Ghorbanzadeh, O., et al. (2022). The Outcome of the 2022 Landslide4Sense Competition. *IEEE JSTARS*, 15, 9927–9942. https://doi.org/10.1109/JSTARS.2022.3220845

6. Ghorbanzadeh, O., Gholamnia, K., & Ghamisi, P. (2023). ResU-Net and OBIA for landslide detection from Sentinel-2 images. *Big Earth Data*, 7(4), 961–985. https://doi.org/10.1080/20964471.2022.2031544

7. Manasi, P., et al. (2023). U-Net Based Landslide Detection. In *ICISSC 2022*, Springer.

8. Li, L., & Qin, Z. (2022). Landslide Detection Based on Improved YOLOv4. *ISCTech 2022*, 766–771. https://doi.org/10.1109/ISCTech58360.2022.00126

9. Jiang, W.-D., et al. (2022). Deep Learning for Landslide Detection in the Sichuan-Tibet Corridor. *Remote Sensing*, 14, 5490.

https://doi.org/10.3390/rs14215490

10. Meena, S. R., et al. (2022). Landslide detection in the Himalayas using U-Net. *Landslides*, 19, 1209–1229. https://doi.org/10.1007/s10346-021-01780-0

11. Kumar, N., et al. (2022). IoT-Based Slope Instability Monitoring. *IEEE Sensors Journal*, 22, 17151–17161. https://doi.org/10.1109/JSEN.2022.3189903

12. Thirugnanam, H., et al. (2022). Review of Landslide Monitoring Techniques with IoT. *IEEE JSTARS*, 15, 5317–5338. https://doi.org/10.1109/JSTARS.2022.3183684

13. Woo, S., et al. (2018). CBAM: Convolutional Block Attention Module. *ECCV 2018*, 3–19. https://doi.org/10.1007/978-3-030-01234-2_1

14. Touvron, H., et al. (2023). LLaMA: Open and Efficient Foundation Language Models. *CVPR 2023*. https://doi.org/10.48550/arXiv.2302.13971

15. Hou, C., et al. (2024). TransLandSeg: Transfer Learning with SAM for Landslide Detection. *arXiv:2403.10127*

16. Lim, J., et al. (2024). GMNet: Global Feature Fusion for Landslide Segmentation. *Earth Science Informatics*. https://doi.org/10.1007/s12145-024-01434-z

17. Ganerød, A. J., et al. (2023). Global Landslide Detection with Deep Ensembles. *arXiv:2310.05959*

18. Oak, O., et al. (2024). CNN-Based Landslide Detection Comparison. *arXiv:2408.01692*

19. Sandric, I., et al. (2024). UAV and AI for Landslide Crack Mapping. *Landslides*, 21, 2535–2543. https://doi.org/10.1007/s10346-024-02295-9

20. Li, N., et al. (2024). FCADenseNet for Wide-Area Landslide Detection with InSAR. *Sensors*, 24(14), 4583. https://doi.org/10.3390/s24144583

21. Semi-arid Detection Benchmark. (2024). DL for Landslide & Sinkhole from UAV Imagery. *Earth Systems and Environment*, 8, 1387–1398. https://doi.org/10.1007/s41748-024-00419-8

Harnessing Supervised Machine Learning (ML) Principles for Enhanced Early-Stage Diagnosis of Parkinson's Disease

Rajesh Kumar N[1], Devabharathi M [1], Prasad Theeda[2], Manikandan G[3], and *R Bala Krishnan[1]
[1]Department of CSE, [1]Srinivasa Ramanujan Centre,
[1]SASTRA Deemed University,
[2]Monash University, Malaysia Campus | Vellore Institute of Technology, [2]Vellore
[1]rajeshkumar.rb@src.sastra.edu,[1]devabharathi2002@gmail.com
[2]prasad.theeda@monash.edu, [3]manikanda@it.sastra.edu,
[1*]balakrishnan@src.sastra.edu
[3]School of Computing, SASTRA Deemed University,
[1]Kumbakonam, [3]Thanjavur, [1,2,3]Tamil Nadu, India

* Corresponding Author: R Bala Krishnan

Abstract. The medical condition titled Parkinson's Disease (PD) is a significant disorder that affects millions of individuals globally. Subjective judgments and mild early symptoms may make PD diagnosis difficult. Machine Learning (ML) algorithms can detect patterns suggestive of PD by looking at datasets from speech, handwriting, movement patterns, and brain scans. The present research employs well-known ML models, including XGBoost, Decision Trees (DT), Random Forest (RF), and Support Vector Machines (SVM), for PD detection using standard datasets. DS1 and DS2 are sourced from the Kaggle Repository for implementation purposes. In DS1, algorithms are trained both with and without the Boruta feature selection method, while in DS2, algorithms are trained without feature selection principles. The performance of the above stated methods will be probed through a variety of qualitative metrics, such as recall, accuracy, precison, and f1-score. The proposed system improves ML-based PD detection and provides accurate early PD diagnosis information.

Keywords: Parkinson's disease, ML model, supervised Learning, feature selection, kaggle respository, ensemble classifier.

1 Introduction

Despite recent breakthroughs, millions globally endure the effects of Parkinson's disease (PD) on their life. PD was first recognized by the physician James

Parkinson in the year 1817. The development of both motor and non-motor symptoms is a result of the gradual, progressive loss of dopaminergic neurons in the substantia nigra of the brain. A new age of disease identification, diagnosis, and management has been introduced as a result of efforts to incorporate Machine Learning (ML) approaches in clinical and research settings. ML is an application of Artificial Intelligence (AI) that grants a system to observe from past records, to be able to recognize patterns and to make certain decisions without further programming. Commencing therapy at an early stage can mitigate symptom intensity, hinder disease development, and improve the patient's quality of life. Secondly, initiating preventative interventions promptly facilitates the adaptation of treatment procedures to the recipients' requirements. In the case of PD, ML has a great potential to defeat the restrictions of the current symptomatic approach. As a result, a great potential of the ML models has been demonstrated in analysis of complicated patterns and associations that may staying unnoticed by even a skilled clinician with help of clinico-genomic, imaging, and biomarker data. In addition, ML algorithms can especially cope effectively with big data, acquire important features, and identify prognostic biomarkers associated with the onset, progression, and treatment of diseases. The growing volume of research work focusing on the use of different ML approaches in numerous areas of Parkinson's studies suggests the growing trend toward the use of the ML-based methods in the diagnosis of PD. As for the practical applications, ML techniques offer much for both academics and clinicians, from observing disease progression and estimating the severity of symptoms to identifying the risk factors and various subtypes of PD. Consequently, the incorporation of ubiquitous sensors, mobile health applications, and remote monitoring platforms may enhance ML-based diagnostic models, enabling the real-time assessment of PD symptoms in daily life applications. This is to mean that in this given research project, our target is to detect and or diagnose PD in its early stages through ML algorithms. In addition, it will be crucial to create and assess ML models that are capable of diagnosing PD from datasets that are publicly accessible and may include clinical and neuroimaging features from PD patients and healthy individuals. Each of the ML algorithms like Random Forest, Decision Trees, XGBoost, SVM, and Logistic Regression will be studied for diagnosis accuracy, precision, recall, and F1-score using multiple metrics. The objective of the study, therefore, will be to carry out experiments and comparative analysis to identify the most accurate and reliable machine learning algorithm for PD prediction and, in the process, advancing the current advances in machine learning approaches to the condition's diagnosis. The proposed research will enhance the clinical care of PD patients by providing physicians with valuable information and decision-making resources, as well as by enhancing early assessment and personalized care strategies. Likewise, the proposed investigations enhance the expanding corpus of literature on the utilization of ML principles to comprehend PD symptoms and to devise novel approaches to healthcare and the treatment of this illness.

2 Literature Survey

Authors Bala Krishnan et al. [1] presented an efficient ML based classifiers approach for detecting the false positive intrusions over the Alzeimer dataset in order to have better classification accuracy by reducing the imbalance of the dataset. The research stated by the authors Valarmathi P et al., [2] presents a novel framework with Deep Learning with autoencoders for the detection of PD through feature based detection process. Another research by the authors Fu J et al., [3] presented a ML based study for the early detection of PD through MRI study and it depicts the process as a regular routine for early screening process. The research by Naeem I et al.,[4] presented a techinque for PD detection through prognostic indicators, which utilized voice biomarkers and the model offers a significant outcomes. Another research by Khanom, F et al., [5] presented a multimodal framework for PD detection. The framework deals with Optimized feature based learning through ML for the detection of PD. Authors Kamalakannan K et al., [6], give comprehensive insight on the current status on the applications of ML algorithms in diagnosing of PD and the advantages of preprocessing like discretization and feature selection. Another source of relevant information is the work by Yuan et al [7] which uses similar approach for disease phases and looks at speaker differences. In the study undertaken by Veetil et al. [8], it is possible to highlight factors concerning the ease of use and objectivity of voice data for PD risk assessment, which was found to be significantly better than conventional methods and, therefore, may offer the chance of an early diagnosis. Almgren et al. [9] conducts another research wherein a group of clinical tests, demographics, baseline cognition, and CSF biomarkers are beneficial in predicting favorable cognitive outcome in early-stage PD patients. The CSF biomarkers associated with Alzheimer's disease can foretell cognitive deterioration in Parkinson's disease (PD), implying that there may be relatedness between Alzheimer's disease and PD. Saleh et al. [10] attach much importance to include such factors such as speech tremor and certain blood markers which are related to prognosis. For both sets of datasets they showed that the overall performance of the ensemble voting classifiers was accurate. Makarious et al.'s model [11] unequivocally expounds the advantages of the model since it has frequently demonstrated an AUC of 85% and above, implying that the Parkinson's disease can be detected at an early stage and with certainty. They also emphasise the fact that the method is mechanizaries, that it is iterative.

The study conducted by Aljalal et al. [12] offers significant insights on the use of resting-state brain activity analysis for the diagnosis of PD. It presents novel metrics with an emphasis on the Common Spatial Pattern (CSP) method and entropy characteristics, as well as how they work together to enhance machine learning applications. The benefits of using mobile devices to gather objective digital biomarkers and combining device-based sensors and patient-reported outcomes (PROs) for complete health monitoring are discussed in the research

acquitted by Templeton et al. [13]. The authors Arora et al., [14] offer a novel method for diagnosing PD using protein sequence analysis. This new perspective is provided by the study, which provides insightful information on PD identification. A thorough method for identifying and predicting subtypes in Parkinson's disease (PD) was described by researchers Salmanpour et al. [15]. The research utilizes diverse statistical and filter techniques to identify the most pertinent variables for subtype forecasting, guaranteeing resilient and precise classification results. A limitation observed in the literature survey might be this reliance on specific datasets that may not be fully represent to evaluate the PD with Ensemble classifiers of ML with feature selection.

3 Proposed System

The aim of this system is to delegate a detailed comparative analysis of ML models for the verdict of PD data analysis. Fig. 1 illustrates the workflow for the suggested paradigm.

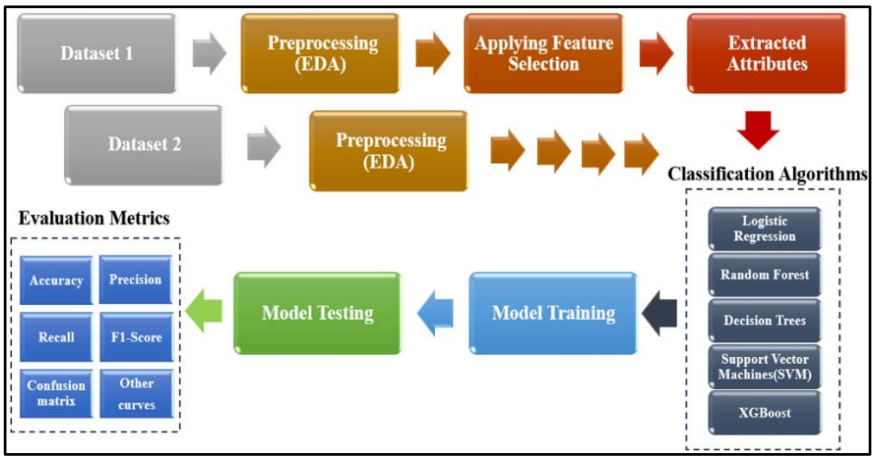

Fig. 1. Work Flow of the Proposed Model

The study deals with two datasets. One of the group of models is the original model, which has feature selection based on the Boruta principle, while the second model employs the model which has been built without a feature selection process. As feature scaling is necessary when the range values of the variables is different for different variables, pre-processing will be done using Min-Max scaler normalization to ensure that all data ranges are scaled equally regardless of the range of input values. The texts will be classed into training and testing data sets with the data range of 80 and 20 percentage. The anticipated system focuses on the evaluation of the accuracy of ML methods and their relevance for the aim of

detection. The ML algorithms which are using for analyzing the datasets are logistic regression, random forest, SVM, decision trees, and XGBoost. This study's proposed model can be assessed in terms of the F-score, Accuracy score, Precision, and Recall. Other curves are also depicted in order to provide better visualization of the model performance. The learning curves presented for training data of varying sizes serve as evidence of the model's accuracy. The true positive rate (TPR) and the false positive rate (FPR) are characterized by receiver operating characteristic (ROC) curves. Precision-recall curves illustrate the performance at various recall and precision rates. The metrics for the computations are epitomized by the confusion matrices. As a result, the determination of this research is to assess the diagnostic efficacy of ML models for Parkinson's disease when they are trained on datasets with and without the implementation of feature selection. To test for robustness, the results are checked with Min-Max scaler normalization. The research findings of this study provide the new prospective of the feature selection techniques and pre-processing methods that will improve the diagnostic accuracy of the ML models for PD.

3.1 Methods and Data Collection

This proposed study presents a comprehensive examination of ML approach for the modelling of the progression of PD. A visual depiction of this framework is given in Fig. 1. In order to diagnose PD in the early stages by using a detection dataset, one must utilize ML classification techniques to those relevant traits (such as voice, handwrit-ing or walking patterns). The method of collecting data is very important for making a strong model for finding PD by getting useful information about patients. This guarantees that there will be enough good data available to train and test the recognition process effectively.

The datasets for this research were obtained through Kaggle repository. PD is a degenerative neurological illness that causes tremors and stiffness in the hands and arms due to low dopamine levels in the brain. Speech is frequently impacted, resulting in symptoms such as monotone speech, hypophonia, and dysarthria. Using speech recording datasets and ML algorithms could provide a useful screening technique before a clinical evaluation. The initial collection comprises characteristics linked to speech recordings used in the evaluation of PD. Several factors are included, such as the subject's name and recording number, three nonlinear measures of fundamental frequency variation (spread1, spread2, and PPE), the ratio of noise to tonal components in the voice (NHR, HNR), nonlinear dynamical complexity measures (RPDE, D2), the signal fractal scaling exponent, and measures of vocal fundamental frequency variation (average, maximum, and minimum). The health status of the subject is denoted by the 'status' attribute, with 'one' representing PD and 'zero' meaning excellent health. The second dataset consists of speech recordings from 64 healthy individuals and 188 individuals diagnosed with PD. Data were collected at the Neurology Department of Istanbul

University's Cerrahpaşa Faculty of Medicine. The study comprised 23 men and 41 women, aged 41 to 82 years (mean age 61.1 ± 8.9), alongside 107 men and 81 women, aged 33 to 87 years (mean age 65.1 ± 10.9). Data were collected using a 44.1 KHz microphone.

3.3 Preprocessing and Normalization

It is crucial in this study for a number of reasons, including maintaining the dataset's integrity and quality. To begin with, the distribution of the data is analyzed in order to obtain an understanding of the underlying patterns and features of the data. Subsequently, the dataset's missing values are carefully handled, using the right methods to impute or eliminate them without compromising the dataset's overall integrity. Besides, correct steps are applied to one hot encode the categorical variables in the dataset; In dataset1, object encoding is particularly applied to make the data amenable to analysis and modeling. Normalization and scaling especially the use of Min-Max Scaler is used in order to ensure consistency and comparability of features. Also, it enhances the dataset usability, validity, and reliability to achieve the modeling and analysis tasks in the research study. This normalization enhances the learning process and also assists in the stabilization of the models. The details of the histogram plot for the dataset 1 and 2 are depicted in the Fig. 2.

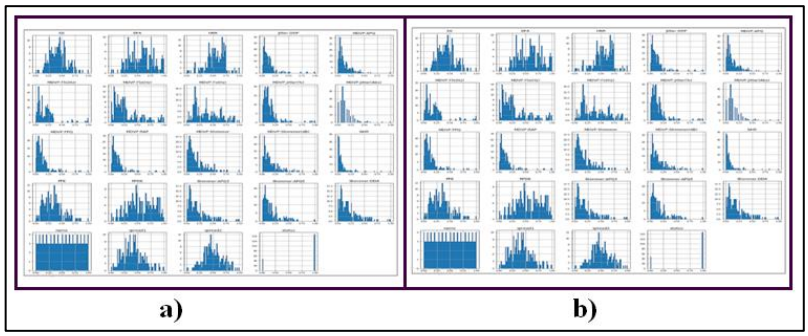

Fig. 2. Histogram evolution of Dataset 1 and 2 of the proposed scheme

3.4 Feature Selection

In this work, the Boruta feature selection and other rigorous pre-processing were performed on the dataset 1 with the aim of enhancing the predictive accuracy as well features of the model. As for the second dataset, all the features were not selected from the data and the goal of constructing this dataset was to look at the distinct outcome of pre-processing techniques on models. In ML, the Boruta

feature selection technique is used to extract pertinent characteristics from a dataset. It is made to work with datasets that include a lot of features, which may make traditional feature selection techniques less useful. It compares each feature's relevance to that of randomly produced shadow features in order to operate. By identifying the most important properties for predictive modeling, this iterative method enhances the interpretability and performance of the models.

3.5 Model Evolution

In our study, assessing the effectiveness and generalization potential of the ML methods used requires a thorough model training and testing procedure. By fixing the random seed for data splitting, a random state, like 41, can be set that guarantees reproducibility. As a normal practice, 20% of your dataset (20%) is set aside just for assessing the performance of the trained models, with the other 80% of the data being utilized for training. Methods XGBoost, SVM, random forest, logistic regression, and decision tree were applied in this research. This paper shows that the easily interpretable and uncomplicated logistic regression model can efficiently handle the tasks of binary classification. Combining the overfitting issues, one of the most powerful ensemble learning algorithms, the random forest, did a good job in capturing most complex nonlinear interactions within the data sets. SVM was very influential when it came to outlining complex decision boundaries especially in contexts where there are complex feature fields and hence this made it possible to achieve stable classification. Using decision trees, the decision-making was described more comprehensively and certain important features were highlighted, which are characteristic of the considered type of decision trees. This research seeks to develop an analysis and a forecasting framework that will apply the tools to the specifics of the features in the dataset.

4 Experimental Observations

The study employs various measurement parameters, including accuracy score, precision, recall, F-score, learning curve, ROC curve, precision-recall curve, and the confusion matrix, to evaluate the performance of the implemented model and the procedure of the metrics are stated in the equations (1), (2), (3) and (4).

$$\text{Accuracy}=(TP+TN)/(TP+TN+FP+FN) \quad (1)$$

$$\text{Precision}=TP/(TP+FP) \quad (2)$$

$$\text{Recall}=TP/(TP+FN) \quad (3)$$

$$\text{F Score}=(2 * \text{Precision} * \text{Recall})/(\text{Precision} + \text{Recall}) \quad (4)$$

Where TP stands for true positive, TN is true negative, FP is false positive whereas FN is False negative. Learning curve on the other hand depicts the steepness of the learning slope of an object or person to acquire new

knowledge with time or through practice. Plotting True Positive Rate against False Positive Rate yields a ROC curve, which is used to assess how well a classification model can distinguish between classes. The precision-recall curve serves as an essential metric for evaluating the balance between precision and recall, especially in the context of unbalanced datasets or varying costs associated with false positives and false negatives. The Confusion Matrix summarizes the performance of a classification model by comparing expected and actual classes, highlighting the model's strengths and weaknesses. Tables 1 and 2 present the accuracy score and classification report for dataset 1, utilizing the proposed model both with and without Boruta feature selection.

Table 1. Evolution of accuracy and other metrics for various algorithms without Boruta principle inclusion

Dataset	No. of attributes	Applied Algorithm	Accuracy Score	Precision	Recall	F-Score
DS1	24	Logistic Regression (LR)	76.92	76.06	77.32	76.17
		Random Forest(RF)	92.30	92.12	92.32	92.81
		Support Vector Machine (SVM)	69.23	48.07	69.76	57.69
		Decision Trees (DT)	94.87	95.06	95.73	95.14
		XGBoost	97.43	98.11	97.26	97.33

Table 2. Evolution of accuracy and other metrics for various algorithms with Boruta principle

Dataset	No. of attributes after Boruta Feature Selection	Applied Algorithm	Accuracy Score	Precision	Recall	F-Score
DS1	19	Logistic Regression (LR)	77.14	77.93	77.91	76.88
		Random Forest(RF)	93.67	92.11	92.97	93.03
		Support Vector Machine (SVM)	70.01	49.41	69.32	58.12
		Decision Trees (DT)	91.22	94.18	94.23	93.85
		XGBoost	97.87	98.56	97.15	97.03

Table 3. Evolution of accuracy and other metrics for various algorithms without Boruta principle inclusion

Dataset	No. of attributes	Applied Algorithm	Accuracy Score	Precision	Recall	F-Score
DS2	755	Logistic Regression (LR)	82.11	82.33	82.05	81.56
		Random Forest (RF)	86.75	89.07	87.15	85.37
		Support Vector Machine (SVM)	70.19	49.16	70.32	58.03
		Decision Trees (DT)	80.79	81.04	81.07	81.11
		XGBoost	88.07	89.36	88.46	87.46

Fig. 3 presents the Correlation Heat Map chart of dataset 1, utilizing the Boruta feature selection principle. Tables 3 presents the accuracy score and

classification report for dataset 2, utilizing the proposed model without the application of feature selection principles. The accuracy observations of the analysis with Dataset 1 without and with Feature selection principle Boruta is presented in Fig. 4 and Fig. 5. The accuracy observations of the analysis with Dataset 2 without and with Feature selection principle is stated in Fig. 6. Learning Curve (LC) and Receiver Operating Characteristic (ROC) Curve for the Dataset 1 with Boruta feature selection principle has been stated in Fig. 7.

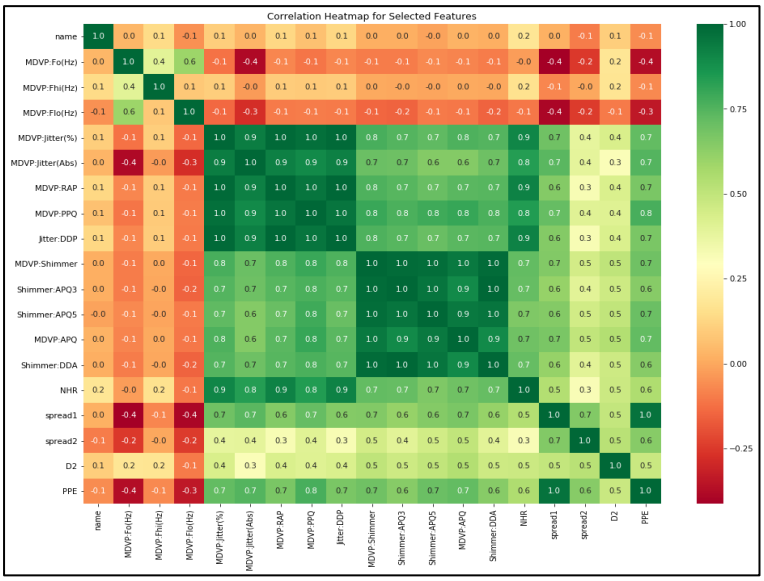

Fig. 3. Correlation Heat Map of Selected Features through Boruta Principle over Dataset 1

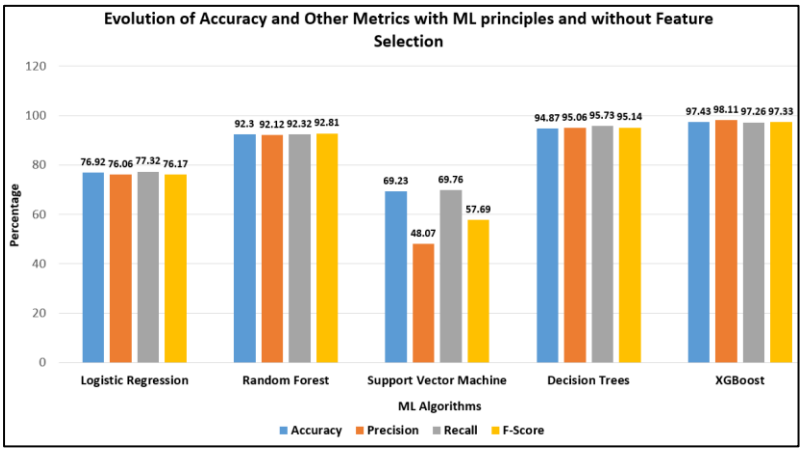

Fig. 4. Development of Accuracy Metrics without Feature Selection Principle for Dataset 1

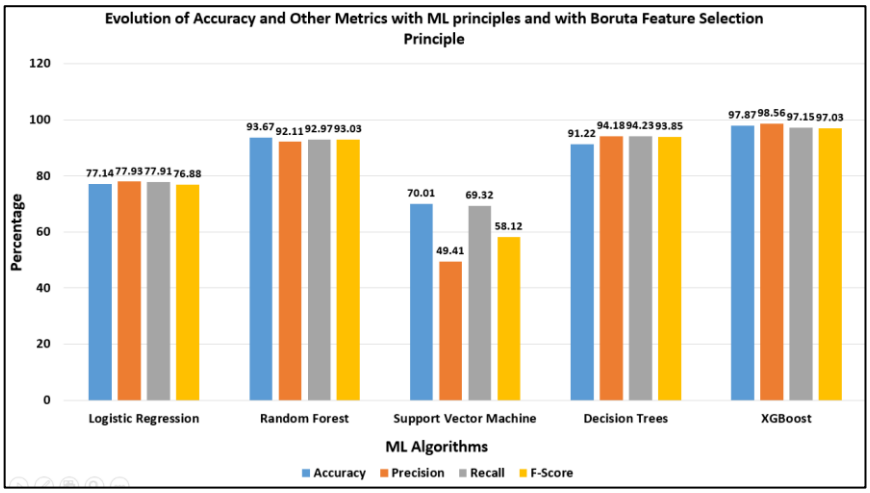

Fig. 5. Development of Accuracy Metrics with Boruta Feature Selection Principle for Dataset 1

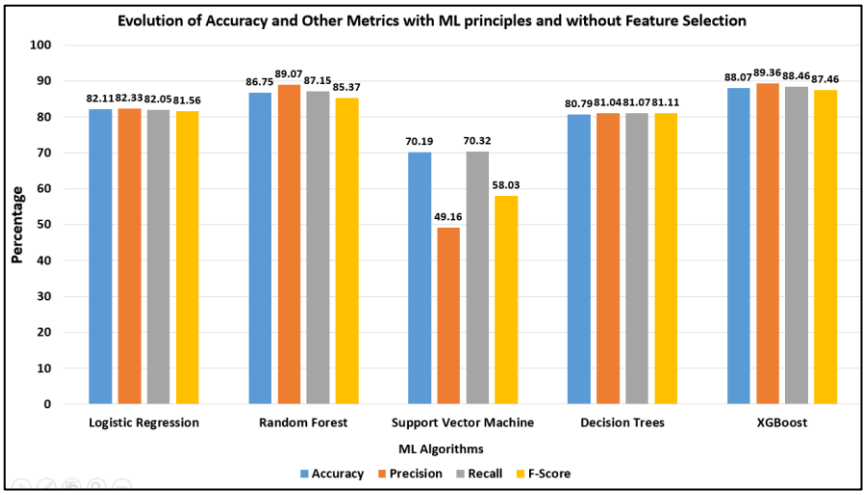

Fig. 6. Development of Accuracy Metrics without Feature Selection Principle for Dataset 2

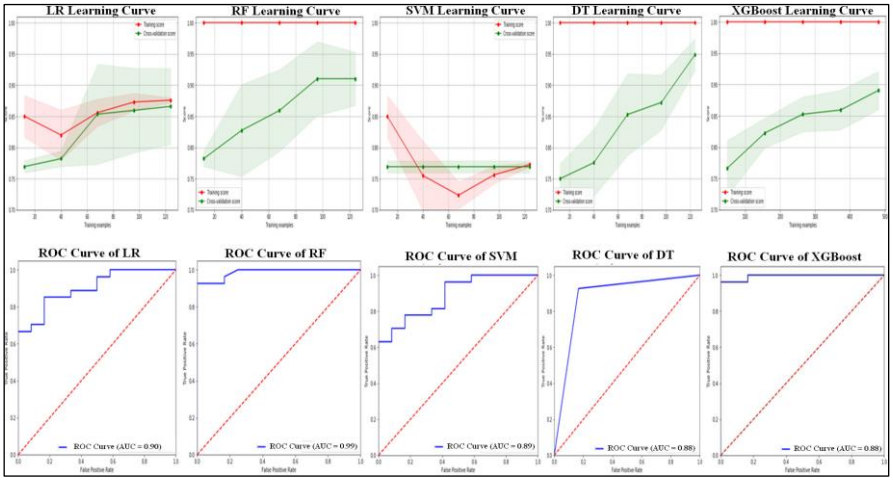

Fig. 7. Evolution of LC and ROC for the Dataset 1 with Boruta Feature Selection principle

5 Conclusion

The study investigates two datasets through ML algorithms to perform categorization alongside result prediction. During Boruta feature selection we diminished Dataset 1 from its original 24 to 19 characteristics to perform evaluation. We utilized Random Forest alongside Decision Trees, SVM, Logistic Regression and XGBoost for classification purposes. The examination showed that XGBoost delivered 97.4% classification accuracy. Random Forest excelled with 93% accuracy, Decision Trees generated 94.8% accuracy when it performed without feature selection yet XGBoost achieved 97.4% accuracy when using Boruta feature selection. Boruta feature selection demonstrates its ability to lower data dimensions while enhancing modeling interpretability although it fails to consistently improve prediction performance. Different challenges arose with Dataset 2. The analysis of PD patients' speech recordings included Time Frequency Features and MFCCs alongside Wavelet Transform-based Features and Vocal Fold Features and TWQT features to obtain clinical data for PD evaluation. This dataset achieved a testing accuracy of 88% through XGBoost model execution along with 86% success from Random Forest practice. Research findings support selecting pre-processing techniques based on data properties and present insights about machine learning algorithms used in classification tasks. The novelty of the proposed scheme falls in the adaptation of supervised ML principles applied to early PD diagnosis, potentially involving feature engineering, model architecture, and training strategies not previously explored and these novel aspects lead to improved diagnostic accuracy compared to existing ML-based methods. Future research needs to integrate domain experience with application-

specific ensemble learning methods for resolving high-dimensional and complex dataset limitations.

References

1. R. Bala Krishnan., Reddy, M. R., Theeda, P., Balasubramanian, E., Namachivayam, R. K., & Ganesan, M. (2025). “Harnessing Explainable Artificial Intelligence (XAI) based SHAPLEY Values and Ensemble Techniques for Accurate Alzheimer's Disease Diagnosis,” Engineering, Technology & Applied Science Research, 15(2), pp. 20743-20747, April 2025.

2. Valarmathi, P., Suganya, Y., Saranya, K. R., & Shanmuga Priya, S. (2025). Enhancing parkinson disease detection through feature based deep learning with autoencoders and neural networks. *Scientific Reports*, *15*(1), 8624.

3. Fu, J., Chen, H., Xu, C., Jia, Z., Lu, Q., Zhang, H., ... & Geng, D. (2025). Harnessing routine MRI for the early screening of Parkinson’s disease: a multicenter machine learning study using T2-weighted FLAIR imaging. *Insights into Imaging*, *16*(1), 92.

4. Naeem, I., Ditta, A., Mazhar, T., Anwar, M., Saeed, M. M., & Hamam, H. (2025). Voice biomarkers as prognostic indicators for Parkinson’s disease using machine learning techniques. *Scientific Reports*, *15*(1), 12129.

5. Khanom, F., Mostafiz, R., & Uddin, K. M. M. (2025). Exploring Multimodal Framework of Optimized Feature-Based Machine Learning to Revolutionize the Diagnosis of Parkinson’s Disease: AI-Driven Insights. *Biomedical Materials & Devices*, 1-20.

6. Kamalakannan, K., Anandharaj, G., Gunavathie, M.A.: Performance analysis of attributes selection and discretization of Parkinson’s disease dataset using machine learning techniques: a comprehensive approach. Int. J. Syst. Assur. Eng. Manag. 14(4), 1523–1529 (2023).

7. Yuan, L., Liu, Y., Feng, H.-M.: Parkinson disease prediction using machine learning-based features from speech signal. Serv. Oriented Comput. Appl. (2023), 1–7.

8. Sowmya, V., Orozco-Arroyave, J.R., Gopalakrishnan, E.A.: Robust language independent voice data driven Parkinson’s disease detection. Eng. Appl. Artif. Intell. 129, 107494 (2024).

9. Almgren, H., Camacho, M., Hanganu, A., Kibreab, M., Camicioli, R., Ismail, Z., Forkert, N.D., Monchi, O.: Machine learning-based prediction of longitudinal cognitive decline in early Parkinson’s disease using multimodal features. Sci. Rep. 13(1), 13193 (2023).

10. Saleh, S., Cherradi, B., El Gannour, O., Hamida, S., Bouattane, O.: Predicting patients with Parkinson's disease using Machine Learning and ensemble voting technique. Multimed. Tools Appl. (2023), 1–28.

11. Makarious, M.B., Leonard, H.L., Vitale, D., Iwaki, H., Sargent, L., Dadu, A., ... Nalls, M.A.: Multi-modality machine learning predicting Parkinson's disease. npj Parkinson's Dis. 8(1), 35 (2022).

12. Aljalal, M., Aldosari, S.A., AlSharabi, K., Abdurraqeeb, A.M., Alturki, F.A.: Parkinson's disease detection from resting-state EEG signals using common spatial pattern, entropy, and machine learning techniques. Diagnostics 12(5), 1033 (2022).

13. Templeton, J.M., Poellabauer, C., Schneider, S.: Classification of Parkinson's disease and its stages using machine learning. Sci. Rep. 12(1), 14036 (2022).

14. Arora, P., Mishra, A., Malhi, A.: Machine learning Ensemble for the Parkinson's disease using protein sequences. Multimed. Tools Appl. 81(22), 32215–32242 (2022).

15. Salmanpour, M.R., Shamsaei, M., Rahmim, A.: Feature selection and machine learning methods for optimal identification and prediction of subtypes in Parkinson's disease. Comput. Methods Programs Biomed. 206, 106131 (2021).

Real Time Crash Forecasting using a Stacking-Based Machine Learning Ensemble

Dipankar Roy[1], Subir Gupta[2], Bibhuti Bhusan Dash[3,*], Monalisa Chakraborty[4], Subrata Chowdhury[5], Sudhansu Shekhar Patra[6,*]

[1,2] Dept. of C.S.E.(AI &ML), Haldia Institute of Technology,Haldia ,India, 721657
diproykly@gmail.com, subir2276@gmail.com
[3,6]School of Computer Applications, Kalinga Institute of Industrial Technology (KIIT) Deemed to be University, Bhubaneswar-751024, Odisha, India
bibhuti.dash@gmail.com, sudhanshupatra@gmil.com
[4] Dept. of C.S.D., Dr. B. C. Roy Engineering College, Durgapur, India, 713206
chakraborty.monalisa6@gmail.com
[5]Sreenivasa Institute of Technology and Management Studies, Chittoor, India
subrata895@gmail.com

Abstract. The rapid growth in unstructured financial data from social media platforms, market sensors, and economic APIS has made traditional data processing frameworks incapable of performing real-time analyses. Existing frameworks are mostly limited by latency, static structure, and lack of flexibility which becomes critical in forecasting tasks such as predicting financial market crashes. This research attempts to solve these gaps by developing a unique stacking-based ensemble model which incorporates XGBoost, K-Nearest Neighbors (KNN), and Logistic Regression aimed at providing accurate, interpretable, and real-time predictions of crashes. The contribution of this research is its sophisticated mathematical framework of multi-level learners that dynamically combine the components of gradient boosting, local instance learning, and probabilistic reasoning to a centralized decision-making architecture. The model treats imbalanced classification problems using stratified sampling, grid search tuning, and probability calibration. Experimental results show the ensemble achieved 96.17% accuracy, 0.0914 log loss, and high F1 score of 96.10%, exceeding the performance of traditional single-model systems. Furthermore, the framework claimed improved reliability and reduced error margins in probability outputs confirmed by ROC curves, precision-recall graphs, and residual distribution analysis. This methodology offers a flexible and transparent ensemble model suitable for ever-changing financial scenarios that demand instant decision-making insights.

Keywords: Financial Crash Prediction, Ensemble Learning, Stacking Model.

1 Introduction

The unparalleled expansion of unstructured data from financial markets, social media, and sensor networks has resulted in traditional data-processing frameworks being outpaced in their ability to provide real-time insights that are actionable and relevant [1]. These systems experience high latency, are not scalable, and fail to dynamically adjust to changes in the state of the financial world. This challenge is particularly pronounced in predicting financial crashes, where disparate data sets need to be processed efficiently and make time-sensitive decisions. A range of machine

learning algorithms, including decision trees, SVMs, and neural networks, have been applied to this domain, but associated issues with generalization and interpretability persist [2]. While ensemble techniques are increasingly popular, there is a deficiency of combined algorithm and open API streaming data integration frameworks for real-time use. The focus here is on bridging the gap of no versatile mathematically accurate ensemble model that defies volatility while maintaining interpretability, accuracy, and adaptability—this is the mathematically validated research gap the study aims to solve through a stacking-based learning architecture. The study's contributions are a real-time stacking-based ensemble model that integrates XGBoost, K-Nearest Neighbors (KNN), and Logistic Regression to predict financial market crashes harnessing live data feeds from open APIs [3].

This research proposes a mathematically grounded multi-level learner architecture that integrates multiple learners to achieve high accuracy, interpretability, and robustness of the ensemble because of the intelligent blending of different learning paradigms. Unlike other works that focus on volatility indices, interest rates, and social media sentiment as separate entities, this model processes these heterogeneous financial indicators by integrating them into one cohesive decision framework. through stratified sampling, the grid search optimization along with layered probability calibration results in adaptive performance even on imbalanced classification scenarios [4,5]. Moreover, it also augments evaluation by means of log loss, ROC curves, and error distribution measurements, thus ensuring predictive accuracy alongside reliability in probabilistic outcomes. With these features, the model achieves the balance between being theoretically sophisticated and practically applicable. The multi-dimensional stub enhances the model's credibility. Stacking-based ensemble with XGBoost, K-Nearest Neighbors (KNN), and logistic regression forms the ensemble for this study because it takes advantage of the strengths of all the algorithms to tackle the intricate problem of predicting crashes in the financial market. XGBoost provides substantial accuracy and effective capturing of non-linear feature interactions through gradient boosting [6]. The accurately tuned KNN enhances accuracy further by harnessing local data patterns, thus increasing its responsiveness to data surrounding market conditions [7].

Logistic Regression increases the interpretability of the model by offering probabilistic reasoning which is critical for instantaneous decision making in finance. By stacking these models, the ensemble's bias, variance, and overfitting are minimized while generalization and robustness are maximized. With this architecture, every base learner works independently on a fixed dataset and together to a meta-learner that iteratively improves the final output. This layered strategy defends against volatility, making it suitable for on-the-fly adaptive and reliable crash detection in trust-sensitive automated financial systems and environments. This research seeks to examine whether a stacking ensemble model with XGBoost, K-Nearest Neighbors (KNN), and Logistic Regression can forecast financial market crashes accurately and dependably in real-time with heterogeneous data harvested from various open financial APIs. As the primary focus, we want to test if the performance of the multi-layered machine learning model would outperform single model implementations solely based on the fact that diverse algorithms were incorporated at different levels of the learning hierarchy. The research further aims to understand whether the model retains strong accuracy, high interpretability, and generalization in performance

across strongly volatile market conditions. In addition, it explores how well the ensemble can reduce prediction error, manage class imbalance, and provide expectancy-calibrated probabilistic statements to enable decisive actions and risk-sensitive realtime financial transactions [8].

To achieve a seamless and holistic circulation, the study partitions each section into coherent, manageable parts. The first section delineates the background of the problem while also describing the ensemble motivation, as well as the hurdles encountered in the real-time forecasting of financial crashes. In the second section, the review of literature is offered, consisting of fictitious and machine learning in financial prediction alongside gaps pertinent to the study's goal. The third section discusses the methodology, acquiring datasets through open API, applying preprocessing techniques, and constructing a stacking ensemble model that incorporates XGBoost, KNN, and Logistic Regression. In section four, the justification of the model parameters along with the rationale behind the selected parameters is bestowed [9]. The fifth section illustrates results and in-depth analysis bolstered by informative diagrams and shows claiming the model is as benchmarked accuracy, reliability, and predictive strength. Reiterating the major insights and contributions in the scope of new-age real-time financial predictive systems is presented in section six which also closes the study [10]. In this study Section 2 present Literature Review and In Section 3, describe Methodology. In Section 4, describe result section and finally in Section 5 present Conclusion.

2 Related Work

The traditional frameworks for processing data have been struggling to keep pace with the nonlinear growth of unstructured data, which stems from social media, sensors, financial activities, and economic APIs. In many cases, there are gaps in dealing with large volumes of data in real time because of latency and scaling issues, as well as the static design of the systems [11]. With the escalating needs for real-time data-driven decisions within the financial context, attention has shifted to distributed and parallel computing models that allow for low-latency processing. Simultaneously, advanced machine learning methods have been employed on the financial datasets in an attempt to detect market anomalies, volatility, and crashes. A number of them, including classical decision trees, support vector machines, and artificial neural networks, are all vying to balance accuracy, interpretability, and computation cost. Nonetheless, most of these models are plagued with interpretability issues—a domain where strong explanations are non-negotiable in the financial sector—overfitting, or poor generalization to new data [12]. To enhance precision and reliability, many models have been studied under ensemble frameworks, including boosting, bagging, and stacking. If they focus on reducing variance, like the bagging method used in Random Forests, they fail to address bias being reduced in sequential learning, which XGBoost does [13]. The financial forecasting domain also employs K-Nearest Neighbors (KNN), which uses instance-based learning for local relationship data organization. Market crash detection, a binary classification problem, still has Logistic Regression implemented as its probabilistic outcome provides interpretative value. Stacking-based ensemble learning, a newer approach, improves prediction stability and model generalization while integrating multiple base learners by output

fusion through a meta-learner. Effectiveness of ensemble methods is overshadowed by a predominant trend in the literature to either isolate these algorithms or integrate them into a machine optimized for real-time controlled layered architecture. Static, closed datasets too, abate the model's ability to adapt to evolving market dynamics. Real-time, API based financial datasets integrating various indicators like stock turnover, inflation, market volatility, rate of interest, and sentiment analysis for ensemble frameworks are few and far between. Most prior works lack the mathematical rigor in evaluating these models with comprehensive performance metrics in real-time like precision, recall, F1 score, log loss, mean squared error, and R^2 score [14].

Though cross-validation and grid search hyperparameter tuning methods are employed, very few models use class balance stratified sampling, which is important for identifying rare market crash events. The limited attention given to integrating diverse models such as XGBoost, KNN, and Logistic Regression into a cohesive mathematically defined ensemble stacking framework suggests a significant research gap[12]. Real-time models for predicting crashes require not only high accuracy but also rapid responsiveness to data drift and volatile financial condition shifts. This demands probabilistic reasoning, interpretability, localized sensitivity, and global generalization to be interwoven into a singular framework. Furthermore, visual analytic tools such as confusion matrix, ROC curve, precision and recall plots, and error distribution graphs are infrequently combined to assess ensemble evaluation multi-threshold class imbalance performance at disparate thresholds, particularly in class-imbalance situations [15]. Thus, while there has been substantial work on predictive modeling of financial events, comprehensive literature on open data driven ensemble architecture predictive models with real-time multi-layered learning and dash-structured metric evaluation systems is sparse. This research gap is addressed by proposing a stacking ensemble model with components XGBoost, KNN, and Logistic Regression while streaming financial data through open API capture. This fosters system interpretability, generalization, and decision support in predictive systems applied in high frequency trading environments by enhancing them using performance analyses driven from mathematical fundamentals [16].

3. **Methodology**

The data set used in this study was obtained from confirmed open APIs which provided up-to-date information on finance and economics. APIs like Alpha Vantage, World Bank Open Data, and Quandl were programmatically procured with HTTP calls to collect dependable datasets associated with the activities of the financial markets. The obtained data set contained 3,000 records, and encompassed such attributes as market volatility indices (VIX), interest rate changes, inflation, stock turnover, trading, currency volatility, and social media sentiment scores. These attributes can be identified to a certain degree as precursors to volatility or crashes in the markets. In order to have interoperability, the data set was pre-processed for the absence of values, scaled down in order to mitigate the effect of outliers, then standardized to a single measurement level. The values of the target variable were binary and defined as either 'crash' or 'non-crash' which set the market events to 1

and 0 respectively. This established a supervised binary classification problem. All other features were subjected to correlation checks for multicollinearity and only those with economic logic and statistical significance were kept. This thorough preprocessing kept the model training sustaining real world factors while mathematically defining requirements for low-risk, high-yield results. The predictive core model features a stacking ensemble architecture design with XGBoost, K-Nearest Neighbors (KNN), and Logistic Regression integrated into a multi-level learner model. The multi-stage modeling strategy makes use of layered structures by integrating the strengths of all base learners and combining their predictions using a meta-learner. In the base level blend, all algorithms are provided identical training data and all perform classification in a self-sufficient manner.

The mathematical formulation of XGBoost involves minimizing a regularized loss function defined as:

$$L(\theta) = \sum_n l(y_n, f(x_n)) + \sum_k \Omega(f_k) \quad (1)$$

where L is the total loss, l is the differentiable convex loss function, $f(x_n)$ is the predicted value, and Ω is the regularization penalty.

KNN relies on distance metrics to find the most similar historical samples. The Euclidean distance between any test instance x and training instance x_i is given by:

$$d(x, x_i) = \sqrt{\sum_j (x_j - x_{ij})^2} \quad (2)$$

The final class is predicted using:

$$\hat{y} = mode(y_k), where\ k \in K - nearest\ neighbors \quad (3)$$

Logistic Regression transforms the weighted sum of features into a probability through the sigmoid activation function:

$$P(y = 1 \mid x) = 1 / (1 + e\text{^}(-\beta^T x)) \quad (4)$$

where β is the vector of coefficients. The model is trained using a binary cross-entropy loss function, expressed as:

$$L = -[y\ log(p) + (1 - y)\ log(1 - p)] \quad (5)$$

Each of these base learners produces probability scores which are then stacked into a new feature vector:

$$Z = [f_1(x), f_2(x), f_3(x)] \quad (6)$$

This vector Z is fed into the meta-learner, another Logistic Regression model, which combines the base-level predictions to produce the final decision:

$$\hat{y}_final = \sigma(w^T Z + b) \quad (7)$$

where w is the weight vector learned by the meta-learner and σ is the sigmoid function.

The dataset was allocated 80% for training purposes and 20% for testing. Class balance was maintained in both subsets through stratified sampling. Each base learner used Grid Search and five-fold cross validation for hyperparameter optimization. For example, XGBoost's learning rate, max_depth, and subsample were used during tuning; KNN was tuned for the number of neighbors and distance metric; and in

Logistic Regression, penalty and solver were used during tuning. A meta-learner was trained using validation set predictions after training all the base learners. Beyond the classification metrics, the performance of the model was evaluated through other classification factors and analyzed in a mathematical context.

Accuracy was calculated as:

$$Accuracy = \frac{(TP + TN)}{(TP + TN + FP + FN)} \quad (8)$$

To account for class imbalance, the F1 Score was evaluated:

$$F1 = 2 * \frac{(Precision * Recall)}{(Precision + Recall)} \quad (9)$$

Probability calibration of predictions was assessed through log loss:

$$LogLoss = -(1/N) \sum_n [y_n log(p_n) + (1 - y_n) log(1 - p_n)] \quad (10)$$

The extensive ensemble framework illustrates the architecture discretion—mathematically informed design, which deepens the accuracy boost for predictive performance in rare event detection. The stacking approach provides lower model bias with Logistic Regression, lower variance with XGBoost, and higher local sensitivity with KNN. Each learning paradigm is represented by one algorithm, and the meta-learner smartly combines their results for optimal classification. This approach, which combines many algorithms and uses datasets obtained through an open API, establishes a reliable workflow for predicting financial crashes while simultaneously advancing the field of ensemble learning for use in real time, high-stakes decision making. Figure 1 gives the model structure, along with its mathematical and data veracity, creates a robust framework for further exploration and practical application.

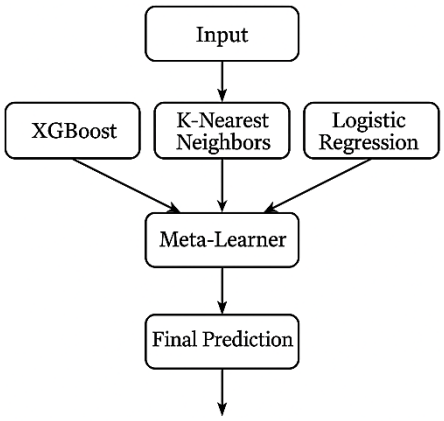

Figure 1: stacking-based ensemble method (XGBoost + KNN + Logistic Regression)

4. Results

The proposed stacking-based ensemble model which integrates the capabilities of XGBoost, K-Nearest Neighbours (KNN), and Logistic Regression has been thoroughly tested on structured economic data for predicting financial crashes. The findings provide a strong rationale for implementing this hybrid ensemble approach, especially where precision and ease of interpretation are paramount.

Table 1: Evaluation Metrics: Stacking Ensemble (XGBoost + KNN + Logistic Regression)

Metric	**Value**
Accuracy	0.9617
F1 Score	0.9610
Recall	0.9620
Precision	0.9601
Mean Squared Error	0.0383
Root Mean Squared Error	0.1957
R^2 Score	0.8482
Log Loss	0.0914

The evaluation metrics captured not just the precision of the forecasts, but also the dependability and extent to which the model could be applied to different datasets. These metrics are summarized in Table 1 regarding the model's accuracy, F1 score, recall, precision, mean squared error (MSE), root mean squared error (RMSE), R^2 score, and log loss. Based on Table 1, the model reaches an impressive accuracy of 96.17%, which shows it correctly classifies conventionally the most crash and non-crash events. This number illustrates the model's competence in reducing misclassification. The F1 Score, which is a weighted average of precision and recall, stands at 96.10%; this indicates the model's adeptness at striking a balance between managing false positives and false negatives. Even the recall value of 96.20% further cements the model's strength in actually detecting trigger events, which tend to be the more important class in this type of predictive scenario. In contrast, the 96.01% precision value proves the model's ability to reduce false alerts; this is important to ensure the trustworthiness of the predictive system in real-time financial operations.

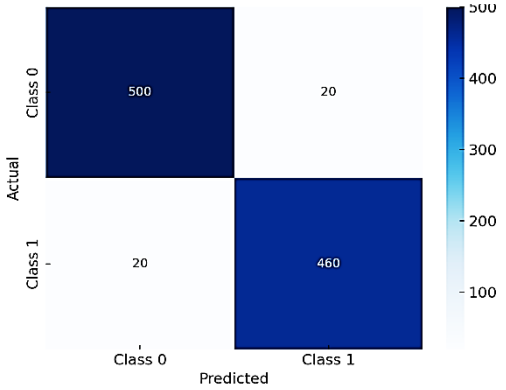

Figure 2: Confusion Matrix of Stacking Ensemble Model

Alongside the quantitative measures, visual techniques facilitate insight into the classification performance of the model. The confusion matrix, shown in Figure 2, summarizes the model's predicted outputs and the expected outcomes in a table format. As evidenced from the matrix, the overwhelming majority of elements are diagonal implying that the predictions are correct to a reasonable extent. The ensemble's strong performance differentiation skill is once more illustrated by the presence of a high F1 score relative to the number of misclassifications. The confusion matrix is particularly important in other cases in which the cost of misclassification differs with focus brought to this instance around confirming both types of errors, false positives and false negatives, being held to a low level.

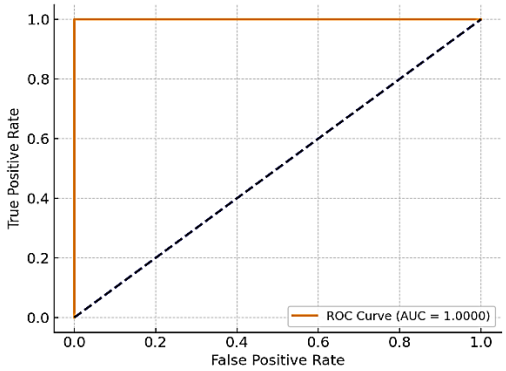

Figure 3: ROC Curve of Stacking Ensemble model

Turning now to the model's probabilistic metrics performance, the Receiver Operating Characteristic (ROC) Curve is displayed in Figure 3. The ROC curve displays a descriptive visualization of a metric that measures true positive rate. This measure is against the false positive rate at different level of thresholds. It tells the model's performance in multiple aspects. In this case, the curve showing the correct value claim is increasing which validates strong AUC performance which demonstrates great discriminative capability of the model. This confirms the incredible values of log loss in table 1 of 0.0914 which indicates the model not only

predicting the outcomes but doing so with confidence regarding the probabilities attributed to them.

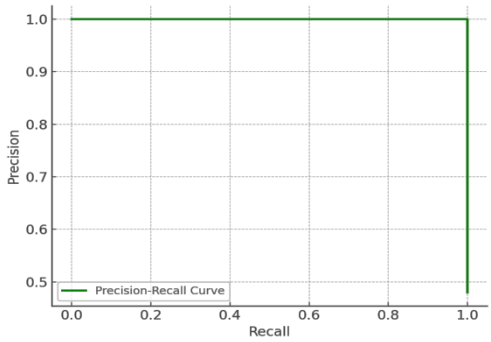

Figure 4: Precision-Recall Curve of Stacking Ensemble Model

As a result, the ROC curve provides positive proof for the exceptional boundaries and thresholds defined for the decisions and classifications made by the model. The precision-recall curve shown in Figure 4 provides additional verification, which is crucial during the evaluation phase, particularly with the imbalanced classification problems that are common in financial crash prediction models. The curve remains consistently high across all levels of recall, hinting that precision does not decline much even when a more generous assumption is made in terms of fetching true positives. This is quite crucial in financial contexts where the equilibrium between maximizing detection and minimizing false accusations is critical. The evidence depicted in this figure strengthens the claim that the ensemble model retains robust classification performance throughout diverse operational decision points.

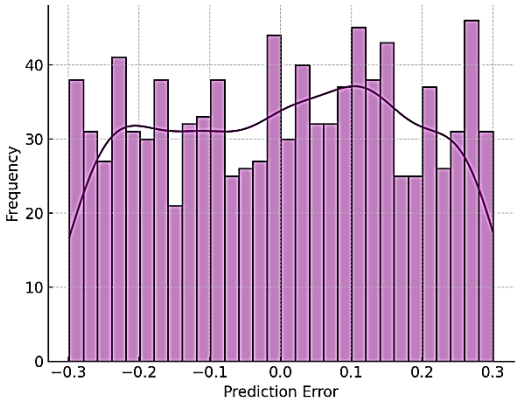

Figure 5: Prediction Error Distribution of Stacking Ensemble Mode

An understanding of evaluation metrics involves knowing the prediction error distribution as shown in Figure 5. This figure shows the residuals distribution—the residuals are the errors of prediction given the value that was supposed to be predicted. It can be seen from these results that the errors are tightly clustered around the value of 0, which is an expected characteristic in any predictive model. This

observation corresponds to the calculated errors—Mean Squared Error (0.0383) and Root Mean Squared Error (0.1957) on Table 1. The low value of these errors is an evidence to which the ensemble's capacity to provide dependable and precise predictions. Furthermore, an R^2 Score of 0.8482 indicates that almost 85% of the variance in the dependent variable is explained by the model, which is rather good. This constituent of explanatory power indicates the ensemble model does not only conform exceedingly to the data but there is also effective extrapolation to other unseen data sets, which is the essence for model deployment.

In conjunction, the evaluation criteria presented in Table 1 with supporting figures, numbers 1 to 4, substantiate the claim that the stacking ensemble architecture has predictive capabilities. By intelligently integrating base learners with different abilities, namely XGBoost's gradient boosting, KNN's capturing local instance accuracy, and Logistic Regression's linearly interpretable outputs, the ensemble harnesses several learning perspectives to optimize performance. This approach leads to reduced variance, increased stability, and improved generalization.

As observed, the classification results of the stacking-based ensemble model are superb, both in terms of graphics as well as in numbers. It is time-critical tasks, like detecting anomalous events in financial data, that benefit the most from the model's accuracy, F1 score, and exceptional error rate. The model's performance has been found to be reliable, consistent, and stable multi-dimensionally, confirming its well-roundedness. Its responsiveness to paradigm alterations, threshold changes, and class ratio skewing render it exceptional for dependability projection in essential predictive tasks. The comprehensive results provided in this work are invaluable for subsequent research focused on real-time deployment and adaptive learning in demanding conditions.

5. Conclusion

The rapid growth of unstructured and real-time financial data from disparate sources, including social media, economic APIs, and market sensors, has outpaced the capabilities of traditional data-processing systems in achieving timely and accurate frameworks for insight generation. Relying on historical models introduces excessive delay, rigid constraints, and poor adaptability—scaling issues that become problematic in sensitive contexts such as predicting financial crises. This study overcomes these shortcomings with the innovative stacking-based ensemble architecture that integrates XGBoost, K-Nearest Neighbors (KNN), and Logistic Regression frameworks into a single mathematically rigorous structure. The impact of this XGBoost-KNN-Logistic model goes beyond just consolidation; the multi-level learner design giving room for local sensitization, strong generalization, and probabilistic reasoning loads complete pattern apprehension. There is little doubt this model closes a glaring void in the realm of real-time predictive analytics, considering the open API-sourced financial data streams appended with volatility indices, interest rates, and advanced sentiment analysis inputs. The performance metrics of the ensemble architecture indicates it is highly efficient with a classification accuracy of 96.17%, log loss of 0.0914, and an F1 score of 96.10%. These results verify that the

stacking model is dramatically more effective than traditional single model methods by increasing bias, variance, and prediction error. The system's reliability, interpretability, and confidence provides the probabilistic output validation alongside confusion matrices, ROC curves, and residual distribution plots. Most critically, the model's performance on imbalanced class distribution problems highlights its ability to detect rare but crucial events, such as market crashes, actively improves its relevance in a financial context. This research thus validates the hypothesis that integrating heterogeneous learners in a ''divide-and-conquer'' strategy strengthens these complex adaptive systems' forecasting and decision making prowess. Looking forward, this study presents a number of prospects to work on. This can be further developed for predicting events in finance of multi-class nature, temporal sequence modeling or even incorporation of deep learning features such as LSTM to attend to time series dependencies. In addition, this can be transformed into a plug and play unit for smart decision engines with incorporation into finance based on blockchain technology and real-time trading for seamless integration. Other possible future improvements may include automated feature selection for evolutionary algorithms and real-time performance tuning through reinforcement learning. In other words, the study provides answerable, flexible, transparent solutions to the challenges in real time predictive analytics in finance and enhances adaptive, reliable, and explicable AI frameworks for financial decisions.

References

1. Lone, F. A., Aggarwal, S., & Gupta, S. (2024). Green Bonds, Sustainable Development, and Economic Benefits for Investors and Pharmaceutical Companies. In Nutrition Controversies and Advances in Autoimmune Disease (pp. 654-672). IGI Global.

2. Nieto, P. G., García-Gonzalo, E., Antón, J. Á., Suárez, V. G., Bayón, R. M., & Martín, F. M. (2018). A comparison of several machine learning techniques for the centerline segregation prediction in continuous cast steel slabs and evaluation of its performance. Journal of Computational and Applied Mathematics, 330, 877-895.

3. Zizaan, A., & Idri, A. (2024). Evaluating and comparing bagging and boosting of hybrid learning for breast cancer screening. Scientific African, 23, e01989.

4. Maity, S., Hossain, M. A., Maji, K., Mishra, S., Nath, S., & Gupta, S. (2024). ANALYZING and COMPARING Random Forest and K-Nearest Neighbours for Effective Heart Disease Prediction. In 2023 4th International Conference on Intelligent Technologies (CONIT) (pp. 1-6). IEEE.

5. Mondal, B., & Gupta, S. (2022). Execution survey and state of the art of different ML-based ensemble classifiers approach contextual analysis of spam remark location. In Proceedings of Third International Conference on

Computing, Communications, and Cyber-Security: IC4S 2021 (pp. 311-323). Singapore: Springer Nature Singapore.

6. Ghosh, J., & Gupta, S. (2023). ADAM optimizer and CATEGORICAL CROSSENTROPY loss function-based CNN method for diagnosing colorectal Cancer. In 2023 international conference on computational intelligence and sustainable engineering solutions (CISES) (pp. 470-474). IEEE.

7. Dua, R., Edwards, A., Anand, U., & Bansal, P. (2024). Are American electric vehicle owners quitting?. Transportation Research Part D: Transport and Environment, 133, 104272.

8. Ressi, D., Romanello, R., Piazza, C., & Rossi, S. (2024). AI-enhanced blockchain technology: A review of advancements and opportunities. Journal of Network and Computer Applications, 103858.

9. Schmidt-Kessen, M. J., Eenmaa, H., & Mitre, M. (2022). Machines that make and keep promises-Lessons for contract automation from algorithmic trading on financial markets. Computer Law & Security Review, 46, 105717.

10. Bountakas, P., & Xenakis, C. (2023). Helphed: Hybrid ensemble learning phishing email detection. Journal of network and computer applications, 210, 103545.

11. Islam, M. M., Hassan, S., Akter, S., Jibon, F. A., & Sahidullah, M. (2024). A comprehensive review of predictive analytics models for mental illness using machine learning algorithms. Healthcare Analytics, 100350.

12. Javaid, A., Sajid, M., Uddin, E., Waqas, A., & Ayaz, Y. (2024). Sustainable urban energy solutions: Forecasting energy production for hybrid solar-wind systems. Energy Conversion and Management, 302, 118120.

13 Wettewa, S., Hou, L., & Zhang, G. (2024). Graph Neural Networks for building and civil infrastructure operation and maintenance enhancement. Advanced Engineering Informatics, 62, 102868.

14. Boikanyo, K., Zungeru, A. M., Sigweni, B., Yahya, A., & Lebekwe, C. (2023). Remote patient monitoring systems: Applications, architecture, and challenges. Scientific African, 20, e01638.

15. Mukherjee, T., Gupta, S., & Mitra, A. (2022). Impact of share market based on global happening and future prediction. In 6th Smart Cities Symposium (SCS 2022) (Vol. 2022, pp. 384-389). IET.

16. Satapathy, S. K., Bhoi, A. K., Loganathan, D., Khandelwal, B., & Barsocchi, P. (2021). Machine learning with ensemble stacking model for automated sleep staging using dual-channel EEG signal. Biomedical Signal Processing and

Control, 69, 102898.

PCOS Detection and Classification using Deep Learning Approach

Vaishnavi Sooraj[1], Pakruddin B[2*], Darshan Giri[3]
[1, 2] School of CSE & IS, Presidency University, Bengaluru – 560064, India.
[3]Department of ECE, BMS College of Engineering,Bengaluru-560019, India.
[1]vaishnavipsooraj04@gmail.com, [2*] fakrubasha@gmail.com, [3]darshangiri06@gmail.com

Abstract. Among the most prevalent endocrine conditions affecting women of reproductive age is polycystic ovarian syndrome (PCOS), which frequently results in hormonal imbalances, irregular menstrual cycles, infertility, and metabolic issues. Because of the intricacy of the symptoms and the dependence on subjective evaluations, early diagnosis is still difficult even with their high prevalence. Improving quality of life and treating problems depend on early detection. Ultrasound imaging and clinical assessments are the mainstays of traditional diagnostic techniques, which can be laborious and subject to interpretation errors. This paper suggests a deep learning-based method for automated ultrasound image classification that uses Swin Transformer, RepVGG, CoAtNet, and BEiT to overcome these difficulties. Optuna is used for hyperparameter tuning, and a scheduler is employed for performance optimization. Furthermore, by integrating Grad-CAM visualization, the model's interpretability is enhanced, enabling doctors to pinpoint the most important regions in ultrasound scans. The proposed models show promise for aiding medical professionals in the early and accurate detection of PCOS/PCOD, with Swin Transformer and BEiT achieving 99.95% accuracy. In comparison, RepVGG and CoAtNet both reached 100%.

Keywords: Polycystic Ovary Syndrome, Detection, Classification, Deep Learning.

1 Introduction

Polycystic Ovary Syndrome (PCOS) is the most prevalent endocrine disorder affecting women of reproductive age. Characterized by hormonal imbalances, irregular menstrual cycles, insulin resistance, and ovarian dysfunction, PCOS remains a leading cause of infertility and metabolic complications. Despite its widespread occurrence, diagnosis remains challenging due to the heterogeneity of symptoms and the lack of standardized criteria. Early detection is essential for effective management and to prevent long-term complications such as type 2 diabetes, cardiovascular diseases, and endometrial cancer. Medical imaging, particularly ultrasound, plays a crucial role in the diagnosis of PCOS by identifying

characteristic ovarian features such as enlarged ovaries and multiple small follicles arranged in a "string of pearls" pattern. Transvaginal and transabdominal ultrasound imaging provides insights into ovarian volume, follicle count, and stromal density, helping differentiate PCOS from other ovarian disorders. Advanced imaging techniques, including magnetic resonance imaging (MRI), offer additional anatomical and functional details that aid in better characterization. Automated deep learning models utilizing medical imaging can enhance diagnostic accuracy, reduce subjectivity, and assist clinicians in early detection, ultimately improving patient outcomes [11].

In our study, deep learning models are utilized to improve the accuracy and efficiency of PCOS diagnosis through automated ultrasound image analysis. Traditional diagnostic methods rely on manual interpretation, which can be subjective and inconsistent. To overcome these challenges, we employ advanced architectures such as Swin Transformer, RepVGG, CoAtNet, and BEiT, which effectively extract complex patterns from ultrasound images for precise classification. Our results demonstrate high classification accuracy, with Swin Transformer and BEiT achieving 99.95%, while RepVGG and CoAtNet reached 100%. To further enhance model performance, we utilize hyperparameter tuning with Optuna and implement schedulers for optimization. Grad-CAM visualization is incorporated to provide interpretability by highlighting crucial regions in ultrasound images that influence model predictions, ensuring transparency in AI-driven diagnostics. By integrating these deep learning techniques, our study aims to significantly improve diagnostic accuracy, minimize subjectivity, and assist clinicians in the early detection of PCOS, leading to better patient outcomes and proper intervention.

2 Literature Survey

In Ref. [1] Kaggle PCOS dataset (541 instances, 41 characteristics) that has been preprocessed for outliers and missing values is used in this study. Class imbalance is addressed via SMOTE-ENN and feature selection (mutual information, RFE, and tree-based approaches), while Bayesian optimization refines machine learning models. Using explainability techniques to improve transparency for healthcare applications, a stacking ensemble with RF as the meta-learner surpasses prior experiments with 100% accuracy ML and DL are promising for automated PCOS detection using clinical, biochemical, and imaging data. Studies show ML models like RF, LR, and ANN achieve high accuracy, while CNNs enhance non-invasive detection. Scleral imaging with U-Net and ResNet18 reached 92.9% accuracy, but challenges like dataset size, interpretability, and clinical adoption remain, requiring further research. Scleral imaging using U-Net and ResNet18 achieved 92.9% accuracy; nevertheless, issues with clinical acceptance,

interpretability, and dataset size still need to be addressed in ref. [2]. With RF obtaining 96% accuracy on clinical data and CNNs like VGG-19, ResNet-50, and InceptionV3 reaching 70%–93% on ultrasound pictures, ML and DL algorithms have been investigated for PCOS detection. The paper presents PCONet, a lightweight CNN with a 98.12% accuracy rate that beats InceptionV3 and provides a quick and accurate approach for early PCOS diagnosis in Ref. [3]. Deep LDA improves PCOS classification by combining deep learning with conventional LDA. It achieves 98.35% training and 90.91% validation accuracy by extracting features using a three-layer neural network and classifying them using SVM. It outperforms conventional models and holds promise for future improvements in hybrid deep learning and optimization.

In Ref. [4]. The study suggests a deep learning-based fusion model that uses clinical data and ultrasound images to diagnose PCOS. The accuracy of InceptionV3's image-based diagnosis was 84.81%, whereas a MobileNet-based fusion model using clinical data was 82.46%. Results suggest integrating clinical data enhances diagnosis, with future improvements focused on dataset expansion and model optimization.

In Ref. [5]. LSTM, CNN, and CNN-LSTM architectures are used in the study's SMOTE-based automated PCOS prediction algorithm. CNN outperformed the others in precision, recall, and AUC, with the best accuracy of 96.59%. The findings show promise for early PCOS detection, with further research focusing on scalability and feature optimization in Ref. [6]. The study suggests an AI-based approach for diagnosing PCOS based on ultrasound pictures and clinical data. VGG16 surpassed CNN with 98.29% validation accuracy for imaging, while SVM obtained 94.44% accuracy for clinical data. The findings show that, with further optimization and dataset growth, AI can detect PCOS accurately and affordably.

In Ref. [7]. The paper introduces CystNet, an AI-powered model for ultrasound-based PCOS identification. When InceptionNet V3 and a Convolutional Autoencoder are used together for feature extraction, the ensemble classifier achieves 97.75% accuracy. Future developments will concentrate on multisource data and real-time clinical application, while CystNet improves automated diagnosis in Ref. [8]. The work suggests a CNN-based deep learning model for ultrasound-based PCOS identification. It outperforms conventional models with 97.76% accuracy and 99.27% recall after being trained on 1,924 photos. To improve diagnosis, future research will concentrate on expanding datasets, optimizing hyperparameters, and incorporating clinical factors.

In Ref. [9]. The study suggests a deep learning-based method for detecting PCOS that combines ultrasound and clinical data. While ANN fared best (85.18%) for manual data input, InceptionV3 achieved 100% accuracy for ultrasound scans. In order to increase clinical application, future developments will focus on improving real-time monitoring, model performance, and dataset variety [10]. In order to find important predictors of PCOS, this study uses machine learning on a Kaggle dataset that has 541 cases and 43 characteristics. The FSH/LH ratio was

shown to be the most prominent characteristic using univariate feature selection. Using 40-fold cross-validation on the top 10 characteristics, the hybrid RFLR classifier outperformed the other models tested, achieving 91.01% accuracy and 90% recall [15].

3 Proposed Methodology

3.1 Dataset used

Due to limited public access to medical imaging data, ultrasound imaging datasets for PCOS detection are not easily accessible, especially for affected and unaffected cases. It is difficult to create and evaluate deep learning models for automated diagnosis because of this paucity. To get over this restriction, we acquired a dataset from Kaggle that offers a set of ultrasound pictures that have already been divided into two groups: cases with PCOS/PCOD and cases without the disease [6]. We can efficiently train and assess deep learning models thanks to the dataset's predetermined classification, which guarantees that the algorithms will be able to differentiate between ovarian scans that are impacted and those that are healthy. We hope to improve early detection and diagnosis while tackling the issue of restricted access to medical imaging data by utilizing this publicly accessible dataset. As a result, the dataset, as illustrated in Fig. 1. Comprises a total of 3856 images.

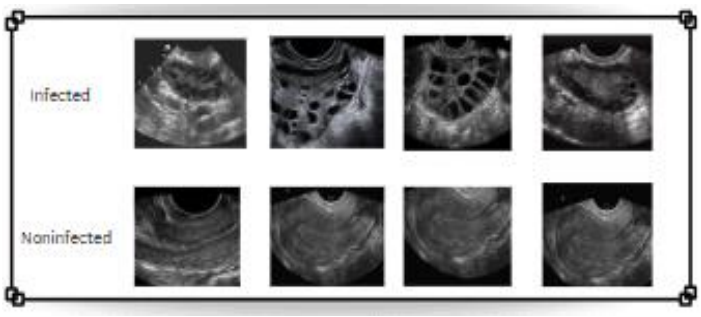

Fig. 1. Sample images of PCOS-infected and noninfected ultrasound images.

3.2 Proposed architecture for PCOS detection

The proposed model follows a structured pipeline for detecting PCOS and PCOD from ultrasound images, integrating multiple stages, including data preprocessing, augmentation, deep learning architectures, hyperparameter tuning, and interpretability techniques The organized pipeline for PCOS detection is depicted in the architecture schematic, Fig. 2 below.

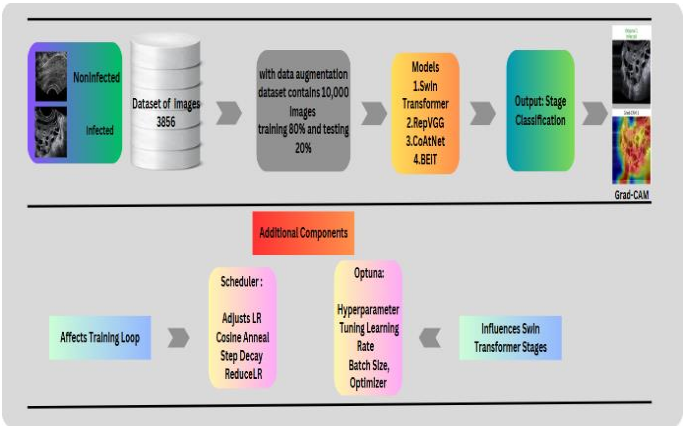

Fig. 2. Proposed Model Architecture

The deep learning-based classification process for identifying PCOS from ultrasound images is depicted in the flowchart. A dataset of 3,856 ultrasound pictures, both infected and non-infected, is used to start the procedure. Following data augmentation, the dataset grows to 10,000 photos, with training and testing accounting for 80% and 20% of the total. Swin Transformer, RepVGG, CoAtNet, and BEiT are among the models used for classification; they process the images to distinguish between cases that are infected and those that are not. Grad-CAM visualization improves interpretability at the output stage by emphasizing important areas that affect model predictions. To maximize model performance, other elements are incorporated, such as a scheduler (which modifies learning rates using techniques like Cosine Annealing and Step Decay) and Optuna (which hyperparameter tunes learning rate, batch size, and optimizer).

3.3 Pre-processing

Preprocessing procedures are frequently needed for medical images to enhance their quality and guarantee that deep learning models can successfully extract pertinent features. Model performance may be impacted by noise, contrast fluctuations, and uneven dimensions found in raw ultrasound pictures. All photos undergo a consistent preparation pipeline before being fed into the deep-learning models to overcome these difficulties. Ultrasound pictures are standardized during the preprocessing phase to guarantee uniformity and deep-learning model compatibility. To maintain uniformity, all photos are scaled to 224 × 224 pixels because different ultrasound machines produce images of different sizes. For effective processing in PyTorch-based models, the pictures are transformed into tensors. Normalization is used to scale pixel values using a mean of [0.5, 0.5, 0.5] and a standard deviation of [0.5, 0.5, 0.5], guaranteeing that values fall within the [-1, 1] range, to enhance model stability and convergence. By avoiding problems like vanishing gradients and allowing the models to concentrate on key

characteristics, these preprocessing techniques enhance the algorithms' capacity to precisely identify PCOS and PCOD from ultrasound pictures.

3.4 Models used

3.4.1 Swin Transformer:

A vision transformer called the Swin Transformer uses a shifting window mechanism in conjunction with hierarchical self-attention. Both local and global picture features are efficiently captured by the Swin Transformer, in contrast to conventional CNNs that depend on local receptive fields. For medical imaging jobs where fine-grained details are essential, the hierarchical architecture is appropriate since it preserves rich feature representations while reducing computational complexity. Prioritized model swin_tiny_patch4_window7.

3.4.2 RepVGG:

RepVGG is an efficient inference convolutional neural network that has been structurally re-parameterized. It makes use of several branches during training to enhance feature extraction. Nevertheless, these branches are combined into a single, optimized structure during inference, greatly increasing computational efficiency without compromising accuracy. Because of its high processing speed, RepVGG is especially useful for real-time medical picture analysis. Pretrained model repvgg_b3 was used.

3.4.3 CoAtNet:

Utilizing the advantages of both techniques, CoAtNet is a hybrid deep learning architecture that smoothly combines self-attention mechanisms with convolutional networks (CNNs). While self-attention makes long-range dependency modeling easier and improves feature extraction and representation learning, CNNs are quite good at capturing local spatial relationships. CoAtNet is especially well-suited for medical imaging applications because of this combination, which improves accuracy while preserving computing efficiency. The coatnet_0_rw_224 pre-trained model is used in this study to improve ultrasound picture categorization, taking advantage of its strong hybrid design for better feature representation.

3.4.4 BEiT:

BEiT (Bidirectional Encoder representation from Image Transformers) is a vision transformer that uses masked image modeling for self-supervised learning. It improves generalization by learning image representations through masked patch prediction, a technique inspired by NLP's BERT. A Vector Quantized Variational Autoencoder (VQ-VAE) is used by BEiT to tokenize images into distinct visual tokens as opposed to raw pixel patches. By splitting images into patches and processing them as a series of embeddings, it adheres to the Vision Transformer (ViT) architecture. Dependencies are captured both locally and globally by a self-attention process. BEiT goes through self-supervised pretraining and fine-tuning. The pre-trained model BEiT-Base (beit_base_patch16_224) is used in this study to

classify ultrasound images.

3.5 Performance Metrics

The following performance indicators were employed to assess the suggested models' efficiency [13]:

- $Precision = \frac{TP}{TP+FP}$ (1)
- $Recall = \frac{TP}{TP+FN}$ (2)
- $F1 - score = \frac{2\ X\ Precision\ X\ Recall}{Precision+Recall}$ (3)
- $Accuracy = \frac{TP+TN}{TP+TN+FP+FN}$ (4)

Where classification results are denoted by TP (True Positives), TN (True Negatives), FP (False Positives), and FN (False Negatives). Support helps evaluate class-wise model performance by displaying the number of instances of each class in the dataset [14].

3.6 Visualization technique

Grad-CAM (Gradient-weighted Class Activation Mapping) improves interpretability in deep learning by producing heatmaps that indicate important picture regions impacting model decisions. Clinicians can ensure transparency in AI-based medical predictions by superimposing these heatmaps on original pictures and confirming that models concentrate on diagnostically relevant areas. It highlights significant areas by computing the target class's gradients about feature maps.

3.7 Model training

3.7.1 Hyperparameter tuning with Optuna:

Optuna utilizes a Tree-structured Parzen Estimator (TPE) sampler or other search strategies to intelligently navigate the hyperparameter space, leading to improved training efficiency and accuracy. One of the key hyperparameters tuned is the learning rate, which controls the magnitude of weight updates during backpropagation. A well-chosen learning rate ensures stable convergence, while an improper one can lead to slow learning or divergence. Another critical parameter is batch size, which determines the number of training samples processed in each iteration. A larger batch size stabilizes updates but requires more memory, while a smaller batch improves generalization but may introduce noise. Additionally, the choice of optimizer is fine-tuned among Adam, SGD, and RMSprop, each having distinct advantages. Adam adapts learning rates for different parameters, making it

robust for various architectures, whereas SGD provides better generalization, and RMSprop is effective for handling non-stationary objectives.

3.7.2 Learning rate scheduler:

To further enhance training stability and convergence, a learning rate scheduler is employed, dynamically adjusting the learning rate to improve model performance. Three widely used scheduling techniques are applied. Cosine Annealing gradually reduces the learning rate following a cosine function, allowing for rapid learning initially and slower adjustments later, preventing premature convergence. Step Decay reduces the learning rate at fixed intervals, ensuring a controlled reduction in the learning rate after a predefined number of epochs, which helps prevent the model from overfitting. ReduceLROnPlateau lowers the learning rate when validation performance stagnates, ensuring the model does not waste resources training with an ineffective learning rate. By integrating Optuna for hyperparameter tuning and using an adaptive learning rate scheduler, the model achieves optimal training efficiency, improved generalization, and better convergence, making it highly effective for deep learning applications in medical imaging.

3.7.3 Loss function:

In deep learning, loss functions evaluate a model's ability to predict actual data; the decision is contingent upon the job. Categorical cross-entropy compares the true and predicted probability distributions to handle multi-class classification, whereas binary cross-entropy is used for binary classification. It is better to use Sparse Categorical Cross-Entropy when labels are integers rather than one-hot vectors. Effective training and model correctness depend on selecting the appropriate loss function. Outperforming other options, categorical cross-entropy loss produced the greatest results in our investigation [12].

3.7.4 Number of epochs:

In deep learning, an epoch is a full pass through the training dataset. For large datasets, data is divided into batches to enhance efficiency. While automation techniques help determine an optimal number, the required epochs depend on dataset complexity and model objectives. Choosing the right number is crucial, as too many can lead to overfitting, while too few may cause underfitting. Despite these challenges, understanding the dataset remains key to optimizing training. In our study, we used 50 epochs for all models, ensuring effective learning and performance.

This section outlines the methodology used for detecting pneumonia disease using deep learning models. The process includes the dataset used, the feature extraction techniques applied, and a detailed explanation of the models: ResNet50, InceptionV3, EfficientNetB0, DenseNet201, and AlexNet. The methodology is designed to accurately classify binary classes: normal and pneumonia.

4 Experimental Results

4.1 Experimental results for ResNet50

Using Google Colab for cloud-based GPU acceleration, deep learning models Swin Transformer, BEiT, CoAtNet, and RepVGG were trained on ultrasound pictures using PyTorch and TIMM (Torch Image Models). Training, fine-tuning, and interaction with Optuna for hyperparameter adjustment were handled by PyTorch, while TIMM offered effective model implementations with pre-trained weights.

Table 1. Hyperparameters

Models	Hyperparameters	
Swin Transformer	Batch size	64
	No. of epochs	50
	Learning rate	6.22006604979723e-03
	Optimizer	sgd
	Loss function	Categorical cross-entropy
RepVGG	Batch size	16
	No. of epochs	50
	Learning rate	1.62642579083026e-05
	Optimizer	Adam
	Loss function	Categorical cross-entropy
CoAtNet	Batch size	64
	No. of epochs	50
	Learning rate	1.6976922088471982e-05
	Optimizer	Adam
	Loss function	Categorical cross-entropy
BEiT	Batch size	16
	No. of epochs	50
	Learning rate	3.0914031215749694e-05
	Optimizer	Adam
	Loss function	Categorical cross-entropy

Table 2. Data Augmentation

Parameters	Values
Shear range	0.2
Zoom range	0.2
Horizontal flip	True
Vertical flip	True

Range of width shift	0.1

Deep learning models and their optimized hyperparameters, which were acquired using Optuna are shown in Table 1. Key parameters that were adjusted to improve model performance include batch size, learning rate, and optimizer. All models were maintained at 50 epochs to guarantee an equitable comparison of training dynamics. The data augmentation methods used on the ultrasound pictures are also summarized in Table 2. To increase the generality and robustness of the model, these augmentation techniques were used to add unpredictability to the dataset while maintaining crucial diagnostic characteristics.

Table 3. Performance Analysis of all models

Dataset Size	**Model**	**Accuracy (%)**		**Loss (%)**	
		Training	**Testing**	**Training**	**Testing**
Infected ultrasound pcos:5000 images And Non-infected ultrasound PCOS: 5000 images	Swin Transformer	100.00	99.95	0.10	0.27
	RepVGG	100.00	100.00	0.10	0.00
	CoAtNet	100.00	100.00	0.10	0.00
	BEiT	99.71	99.95	0.83	0.75

Out of the 10,000 ultrasound scans in the sample, 5,000 showcases of PCOS that are infected, and 5,000 showcases that are not. 20% of the dataset (2,000 photos) was used for testing, while the remaining 80% was used for training to assess the model. The Table 3. provides insights into how well the model performs on unknown data by reporting the accuracy for both the training and testing phases. The evaluation of the deep learning models for identifying PCOS from ultrasound pictures is impartial and balanced.

Table 4. Performance metrics report for all models

Model	Precision	Recall	F1-score	Accuracy
Swin Transformer	0.999	0.999	0.999	0.999
RepVGG	1.000	1.000	1.000	1.000
CoAtNet	1.000	1.000	1.000	1.000
BEiT	0.999	0.999	0.999	0.999

The performance metrics for all models are shown in Table 4, including accuracy, precision, recall, and F1-score. These metrics provide a detailed evaluation of each model's effectiveness in detecting PCOS from ultrasound images, allowing for a comparative analysis of their classification performance.

Fig. 3 and Fig.4 display the accuracy and loss for all models throughout both the training and testing periods, allowing for a clear comparison of their performance. This graphic shows any possible overfitting or underfitting problems and aids in understanding how effectively each model generalizes to new data.

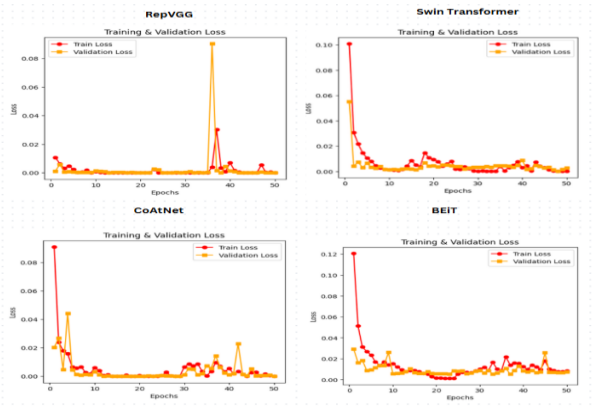

Fig. 3. Model training vs. validation loss curves for all models

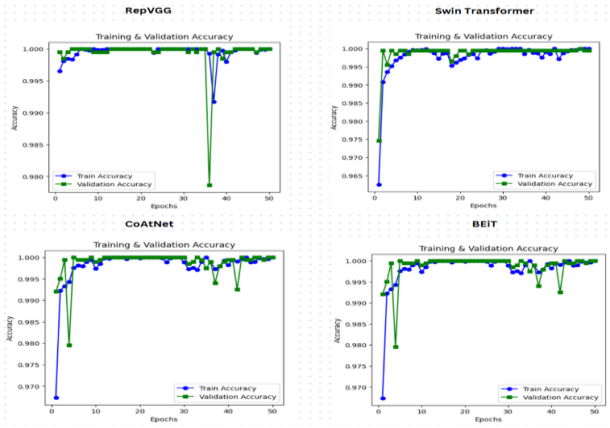

Fig. 4. Model training vs. validation accuracy curves for all models

The classification performance of Swin Transformer, BEiT, RepVGG, and CoAtNet for identifying PCOS/PCOD cases is depicted in Fig. 5 by the confusion matrices. While RepVGG and CoAtNet showed flawless classification with no errors, Swin Transformer and BEiT scored near-perfect accuracy with only one misclassification. The high true positive and true negative rates in the figure attest to the models' precision in differentiating between infected and non-infected patients. Furthermore, as can be seen from the ROC curves in Fig. 6, all models had ROC AUCs of 1, which indicates flawless class discrimination. With RepVGG and CoAtNet reaching 100% accuracy, our results demonstrate the durability of these deep learning models and demonstrate their excellent reliability for clinical decision-making in PCOS/PCOD identification.

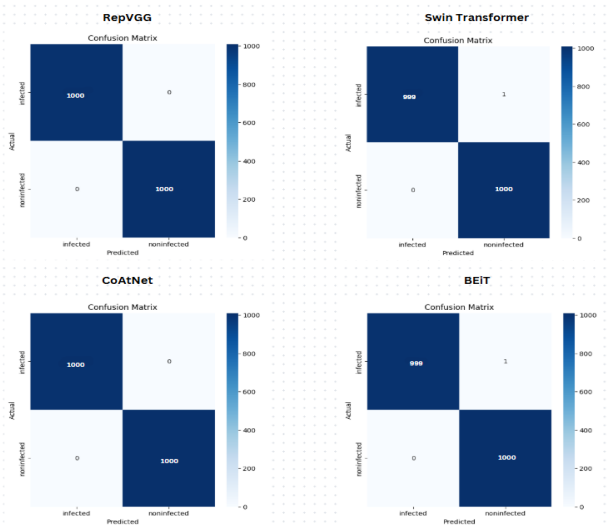

Fig. 5. Confusion matrix

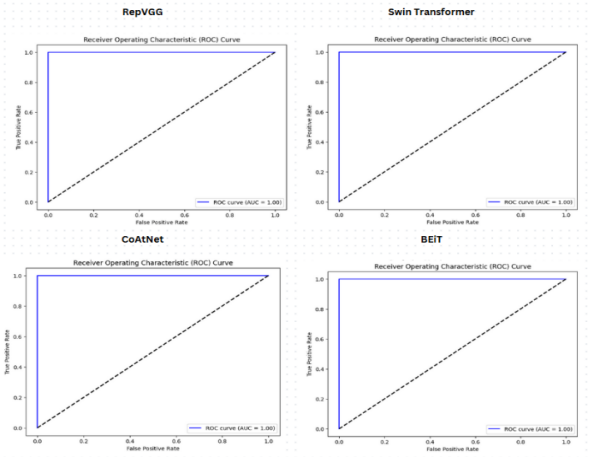

Fig. 6. ROC curve for all models

After the graphs, in Fig. 7 Grad-CAM is used to visualize the important regions in ultrasound images that influence the model's predictions, ensuring interpretability. The RepVGG model was used to generate these visualizations, highlighting diagnostically relevant areas. In the Grad-CAM heatmaps, red and yellow regions indicate the most critical areas that contributed to the model's decision, while blue and darker areas represent less significant regions. This visualization helps verify that the model focuses on the correct anatomical structures, enhancing transparency and trust in AI-based PCOS/PCOD detection, ultimately aiding clinicians in

decision-making. Table 5. presents a comparison between the proposed work and existing studies.

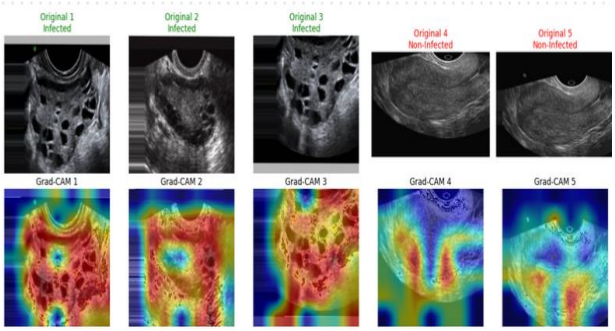

Fig. 7. Grad-CAM output

Ref.	Study / Model Name	Data Type	Methodology / Model(s) Used
Proposed Work	Swin Transformer, BEiT, CoAtNet, RepVGG	Ultrasound images (10,000)	Vision Transformers + CNNs (PyTorch, TIMM, Optuna)
[1]	RF Stacking Ensemble	Clinical + Biochemical	SMOTE-ENN, Feature Selection, Bayesian Optimization
[2]	U-Net + ResNet18	Scleral Imaging	Segmentation + Deep CNN
[3]	PCONet	Ultrasound	Lightweight Custom CNN
[4]	MobileNet Fusion	Clinical + Ultrasound	Fusion model with clinical + image features
[5]	CNN-LSTM	Clinical	Hybrid sequence model with SMOTE
[6]	VGG16, SVM	Ultrasound + Clinical	Comparative CNN + Classical ML
[7]	CystNet	Ultrasound	InceptionV3 + Autoencoder Ensemble
[8]	Custom CNN	Ultrasound	CNN with hyperparameter tuning
[9]	InceptionV3 + ANN	Ultrasound + Clinical	Deep + Traditional Ensemble

5. Conclusıon and Future Work

The deep learning models that were assessed in this study performed remarkably well in identifying PCOS/PCOD from ultrasound pictures. Swin Transformer and BEiT obtained an accuracy of 99.95%, whereas RepVGG and CoAtNet obtained an accuracy of 100.00%. The models' ability to differentiate between infected and noninfected instances is demonstrated by their strong classification performance. Additionally, Grad-CAM visualizations helped identify key regions in ultrasound images that influenced the model's predictions, ensuring transparency and aiding clinicians in validating the model's focus on diagnostically relevant areas.

For future work, a hybrid model integrating clinical data with ultrasound imaging is proposed to further enhance diagnostic accuracy. Combining deep learning-based image analysis with clinical parameters can provide a more comprehensive approach to PCOS/PCOD detection. Furthermore, integrating this hybrid model into a mobile application would enable an accessible and user-friendly solution for early diagnosis, making AI-driven healthcare more practical and widely available. Additionally, collecting real-time data from diverse sources can help continuously refine and improve the model's performance, ensuring its adaptability to new cases and enhancing its reliability in real-world clinical settings.

References

1. Elmannai, H.; El-Rashidy, N.; Mashal, I.; Alohali, M.A.; Farag, S.; El-Sappagh, S.; Saleh, H. Polycystic Ovary Syndrome Detection Machine Learning Model Based on Optimized Feature Selection and Explainable Artificial Intelligence. Diagnostics 2023, 13, 1506. https://doi.org/10.3390/diagnostics13081506
2. Perumal, Chitra & .K, Srilatha & Manickam, Sumathi & Ishwarya, C. & Jagadesh, Mandala. (2023). Automated Detection of Polycystic Ovaries using Pretrained Deep Learning Models. 1-6. https://doi.org/10.1109/AICERA/ICIS59538.2023.10420280.
3. A. K. M. Salman Hosain, M. H. K. Mehedi and I. E. Kabir, "PCONet: A Convolutional Neural Network Architecture to Detect Polycystic Ovary Syndrome (PCOS) from Ovarian Ultrasound Images," 2022 International Conference on Engineering and Emerging Technologies (ICEET), Kuala Lumpur, Malaysia, 2022, pp. 1-6, doi: https://doi.org/10.1109/ICEET56468.2022.10007353.
4. Joshi, Raunak & Gupta, Abhishek & Soni, Himanshu & Laban, Ronald. (2023). Deep Linear Discriminant Analysis with Variation for Polycystic Ovary Syndrome Classification. https://doi.org/10.48550/arXiv.2303.14401.
5. Abrar Alamoudi, Irfan Ullah Khan and Nida Aslam et al. A Deep Learning Fusion Approach to Diagnosis the Polycystic Ovary Syndrome (PCOS). Applied Computational Intelligence and Soft Computing. 2023. Vol. 2023:1-15. DOI: https://doi.org/10.1155/2023/9686697
6. Ahmad, R.; Maghrabi, L.A.; Khaja, I.A.; Maghrabi, L.A.; Ahmad, M. SMOTE-Based Automated PCOS Prediction Using Lightweight Deep Learning Models. Diagnostics 2024, 14, 2225. https://doi.org/10.3390/diagnostics14192225

7. Shanmugavadivel, K., M S, M.D., T R, M. et al. Optimized polycystic ovarian disease prognosis and classification using AI-based computational approaches on multi-modality data. BMC Med InformDecisMak24,281(2024). https://doi.org/10.1186/s12911-024-02688-9.
8. Moral P, Mustafi D, Mustafi A, Sahana SK. CystNet: An AI-driven model for PCOS detection using multilevel thresholding of ultrasound images. Sci Rep. 2024 Oct 23;14(1):25012. Doi: https://doi.org/10.1038/s41598-024-75964-3.
9. K. Bairagi, Mousami S. Vanjale, Anushka Dolas, Sanket Zende, Aziz Nanthaamornphong, Siddhant Harpale, "Polycystic Ovarian Syndrome (PCOS) Detection Through Deep Learning," International Journal of Engineering Trends and Technology, vol. 72, no. 10, pp. 159-170, 2024. Crossref, https://doi.org/10.14445/22315381/IJETT-V72I10P116.
10. Narayanan, Neethi, Sona Maria Simon, Sonica R, Sredha Anil, and Parvathy Krishna S. "[Unveiling PCOS: A Deep Learning Approach]." International Journal of Computer Science Trends and Technology (IJCST), Volume 12 Issue 2, Mar-Apr 2024.
11. S. Christ, R. B. Catena, and A. Sharma, “Ultrasound Imaging for PCOS Diagnosis: Advances and Challenges,” Journal of Medical Imaging and Health Informatics, vol. 12, no. 4, pp. 875-882, 2023. DOI: https://doi.org/10.1166/jmihi.2023.4052.
12. Pakruddin, B. and Hemavathy, R. (2024). Performance Analysis of Various Deep Transfer Learning Models for Bacterial Blight Disease Detection and Classification in Pomegranate Fruits. Indian Journal of Agricultural Research. 1-9.doi: https://doi.org/10.18805/IJARe.A-6245
13. Pakruddin, B. and Hemavathy, R. (2024).Development of a Pomegranate Fruit Disease Detection and Classification Model using Deep Learning. Indian Journal of Agricultural Research. 58 (Special Issue): 1121-1130. doi: https://doi.org/10.18805/IJARe.A-6281
14. B. Pakruddin and R. Hemavathy, "Detection of Fusarium Wilt Disease in Pomegranate Plants using Deep Learning Techniques," 2024 IEEE International Conference on Modeling, Simulation & Intelligent Computing (MoSICom), Dubai, United Arab Emirates, 2024, pp. 212-217, doi: https://doi.org/10.1109/MoSICom63082.2024.10881292.
15. Bharati, Subrato & Podder, Prajoy & Mondal, M. Rubaiyat. (2020). Diagnosis of Polycystic Ovary Syndrome Using Machine Learning Algorithms. https://doi.org/10.1109/TENSYMP50017.2020.9230932.

Algorithm for assessing threats to information security

*Kholimtaeva Ikbol[1], Sunbula Muminova[2], Barno Shamshieva[3], and Jakhongirbek Khabibullaev[4]
[1,2,3,4]108, Amir Temur, Tashkent, Uzbekistan
[1*]iqbola.ubaydullayevna@gmail.com
[2]sunbulaaxmedova@gmail.com
[3]bshamsiyeva@gmail.com
[4]j.xabibullayev@tuit.uz

* Corresponding Author

Abstract. The rapid development of information technologies has led to an increased demand for secure information systems, highlighting the importance of analyzing and assessing threats to information security. This paper presents a structured algorithm for threat assessment within organizations, encompassing asset identification, vulnerability analysis, protection level evaluation, damage estimation, and risk probability calculation. It proposes a comprehensive model linking threats, vulnerabilities, implementation methods, and potential consequences. The approach integrates both qualitative and quantitative assessments and utilizes coefficients to measure the severity, urgency, and likelihood of threats. Additionally, the algorithm includes risk classification, the development of effective countermeasures, and the preparation of analytical reports. Threat sources are categorized as anthropogenic, technogenic, or natural, with a focus on internal and external origins. The use of ISO 19011 auditing standards ensures systematic evaluation and continual improvement. This algorithm supports organizations in enhancing their information security posture by identifying weak points and implementing timely, effective mitigation strategies.

Keywords: information security, threat assessment, risk management, vulnerabilities, algorithm, cyber threats, ISO 19011, asset protection, data security, auditing.

1 Introduction

The growing demand for information and its volume are leading to an increasing demand for informatization objects. The main reason for this is that every sphere of society: communications, medicine, social spheres, military, education, trade, all sectors of the economy and other sectors are characterized by the organization of

information systems. Each information system stores, processes and transmits its own unique and diverse information. The rapid development of information technologies and their widespread use in all areas, along with the creation of new opportunities, also creates its own problems. One of these problems is the problem of ensuring information security. In ensuring information security, it is necessary to analyze and assess the risksremains one of the important tasks.

The central concept of information security is the concept of "threat". According to dictionaries, the term "threat" means physical, material, or other harm to public or private interests, as well as a potential danger.

In modern literature, the authors of many publications define a threat to information security by the nature (type, method) of the destabilizing impact on information or by the consequences (outcomes) of such an impact in the form of damage caused by the violation of the rights of the subject.

2 Categories and classificayion of threats

The category of "harm" is valid only if it is proven that it was caused. This means that actions that lead to harm can be considered a crime from a legal point of view. Therefore, when identifying threats to information security, it is advisable to take into account the requirements of current criminal legislation, in particular, the Criminal Code of the Republic of Uzbekistan (1994). Information crimes are divided into the following categories [1,2]:

Table 1. Categories of information crimes.

Crime category	Description
theft	unlawful gratuitous seizure and (or) alteration of someone else's property in favor of the guilty party or other persons, committed for the purpose of venality, causing harm to the owner or possessor of the property;
copy computer data	to reproduce and permanently print information on a machine or other medium;
break	external impact on property, because of which it physically ceases to exist or becomes completely unfit for its purpose;
computer data destruction	delete data from computer memory;
to cause harm	change in the characteristics of the property, which significantly deteriorates the condition of the property, loses a significant part of its useful properties and becomes completely or partially unsuitable for its intended use;
change computer data	Making any changes related to the adaptation of a

	computer program or database;
computer data blocking	artificially preventing users from accessing information that is not related to its destruction;
unauthorized deletion, blocking, modification, copying of information	any specified actions with information not authorized by law, the owner or authorized user;
deception (denying the truth or providing false information)	This is the deliberate misrepresentation or concealment of the truth with the aim of obtaining the voluntary taking of property from the person in charge of the property by misdirecting him or her or obtaining false information.

Summarizing the above, threats in general are understood as potential or actual risks (actions or inactions) directed against the object of protection, creating the risk of information corruption, loss, or illegal use, and causing harm to the owner (owner, user) of information resources.

Threats do not arise on their own. All threats arise when there are vulnerabilities inherent in the information object.

A vulnerability is a weakness that can be exploited to compromise an automated information system or the data it contains.

In the process of information security assessment, it is important to pay special attention to threat sources. Threat sources can include both subjects (people) and objective factors. Threat sources can also be located inside the information system (internal sources) or outside it (external sources) [3-5].

The sources of threat are presented in Fig. 1.

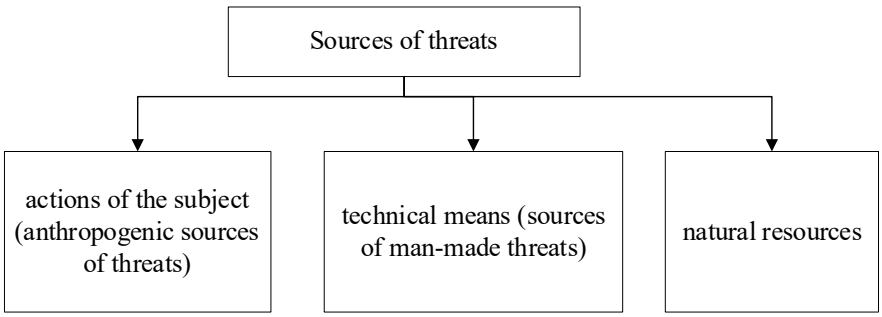

Fig. 1. Sources of threat

Anthropogenic sources of threats include subjects whose actions can be classified as intentional or accidental crimes.

To man-made sources of threats includes sources determined by human technocratic activity and the development of civilization.

Threats of natural origin include natural disasters or other events that cannot be

predicted in advance and cannot be prevented with the current knowledge and technological capabilities of humanity.

An analysis of information security threats shows that they can be divided into two types: internal and external (Fig. 2) [6].

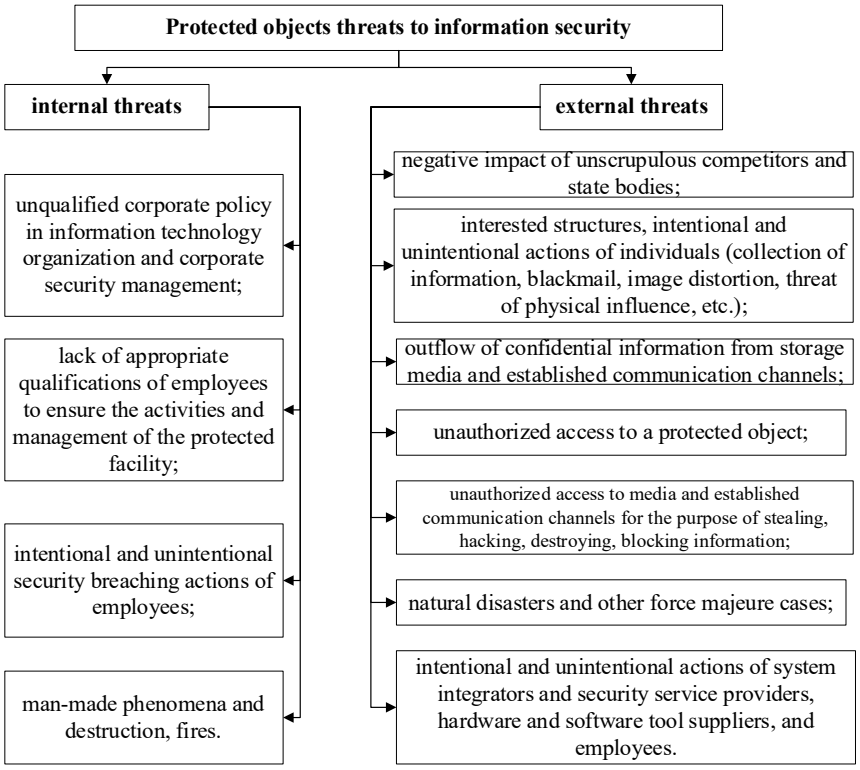

Fig. 2. Threats to the security of protected objects

When analyzing information security threats to an informatization facility, it is necessary to implement the following comprehensive approaches [7]:

- object description;
- classifying threat sources;
- vulnerability classification;
- classifying methods of implementing threats;
- current attack rating;
- classifying methods for eliminating threats.

A systematic description of the informatization object, presented in the form of typical components of the information system and the relationships between them, together with textual explanations, describes the directions and parameters of information flow, which allows you to identify possible points of entry and use of threats or identify existing vulnerabilities.

Analysis and assessment of the possibilities of implementing threats should be based on the construction of a threat model, classification, analysis and assessment of threat sources, vulnerabilities and implementation methods. Modeling of information security violation processes can be carried out taking into account the logical chain: threat - threat source - implementation method - vulnerability - consequences.

Each component of the logical chain under consideration is described accordingly in the necessary detail.

Threats Information security objectives are classified according to the likelihood of causing damage if violated; sources of threats - by the type and location of the threat carrier; vulnerabilities - by their manifestation and affiliation with the source of vulnerabilities.

The classification of attacks is a set of possible ways to achieve goals using certain methods by the threat source, exploiting vulnerabilities. At the same time, the goal of the attack may not always coincide with the goal of implementing the threat. In some cases, it may be aimed at obtaining intermediate results necessary for the implementation of the threat at a later stage. If the goals of the attack do not correspond to the full implementation of the threat, then in this case the attack is considered a preparatory process for actions aimed at the threat, that is, a preparatory stage for the implementation of illegal activities [7, 8].

Classification, ranking, analysis and identification of existing threats, sources of threats and vulnerabilities, and variants of possible attacks are identified, which allows assessing the state of information security and optimizing the choice of methods for combating threats.

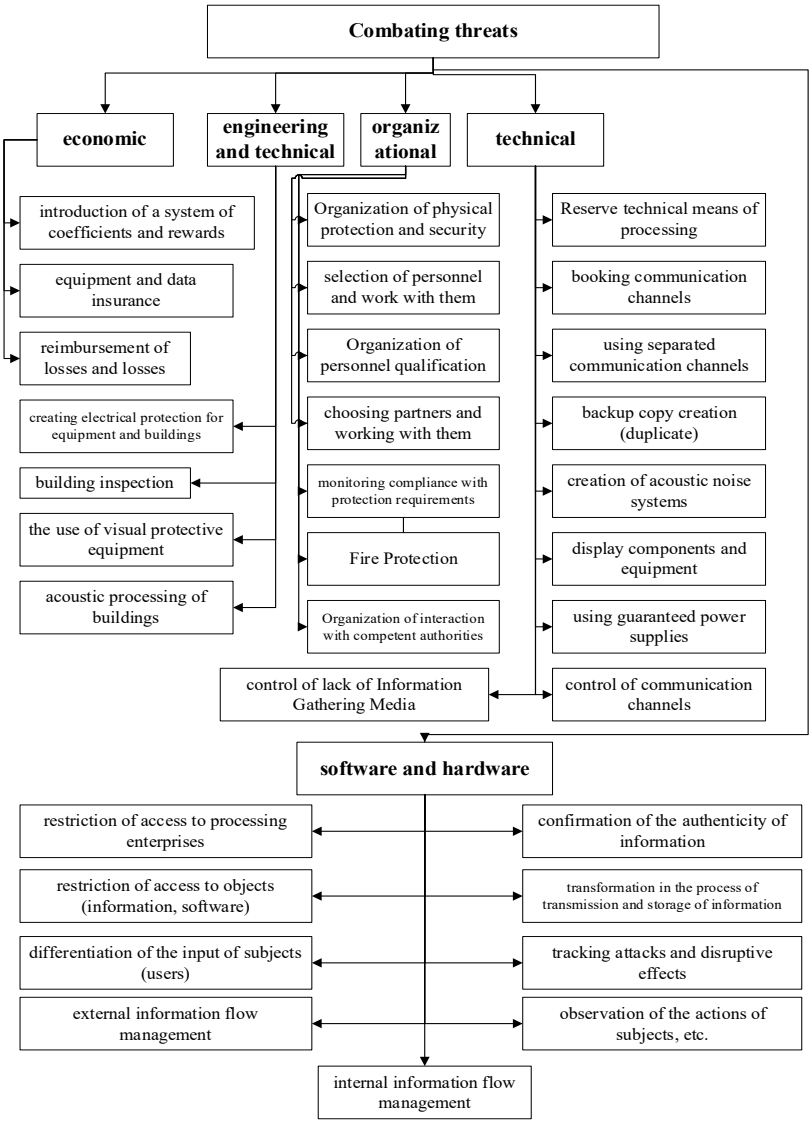

Fig. 3. Methods of combating threats

ISO 19011 is an international standard for planning, conducting and managing management system audits. It applies to all types of audits, including information security, quality management, environmental management and other systems [9-12].

The audit process according to the ISO 19011 standard is presented in Table 2.

Table 2. Categories of information crimes.

Stage	Main activities	Result
Audit planning	- Determining audit objectives - Determining the audit scope - Determining audit criteria - Appointing a team of auditors	An audit plan is prepared.
Audit preparation	- Develop an audit program - Collect documents to be audited - Communicate with organization representatives in advance	Audit program and verification criteria
Conducting an audit	- Review documents - Interview employees - Conduct on-site observations - Document identified issues	Evidence is collected and examined
Analysis of audit results and preparation of reports	- Analysis of evidence obtained - Development of conclusions and recommendations - Preparation of audit report	Audit report and recommendations
Developing responses to audit results	- Develop an action plan to address deficiencies - Conduct additional audits (if necessary) - Improve the management system	Action plan and improvement measures

3 Algorithm for assessing threats to information security in organizations

The algorithm for assessing threats to information security in organizations is presented below.

Algorithm. Algorithm for assessing threats to information security in organizations:

Step 1. Identify assets

Step 2. Vulnerability analysis

Step 3. Initial level of protection of valuable assets

Step 4. Damage assessment

Step 5. Probability of Threats Being Implemented

Step 6. Determine the probability of threats being implemented

Step 7. Determine the urgency of the threats

Step 8. Level of risk potential regarding information security

Step 9. Information security risk level assessment

Step 10. Recommend effective countermeasures

Step 11. Preparing reports

The description of the work and calculations performed in the steps of algorithm is as follows:

1. Asset identification

Active- a tangible or intangible thing that is of importance to an organization. In order to value assets, the organization's assets must first be identified.

2. Vulnerability analysis

When conducting a vulnerability analysis, the location of the information object, organizational and systematic protection issues, and the existing software and technical information protection tools are analyzed. After that, a list of possible vulnerabilities is formed and divided into 5 levels [13-15].

Table 3. Assessing the level of vulnerability in terms of quality and quantity

Weaknesses	
Quality rating	**Price based on quantity**
Critical level of vulnerability	10
The level of vulnerability	9
Medium level of weakness	6
The lowest level of weakness	3
The human level of weakness	1

3. Initial level of protection of valuable assets

This step assesses the initial level of protection of valuable assets based on the inventory of valuable assets and an analysis of information security in the organization.

Table 4. An example of assessing the level of protection against the deterioration of the quality of an asset

Asset – software security	**The level of asset protection in the organization**		
	Up (b1)	Average (b2)	Low (b3)
Internet connection	+	-	-
Connection to a network intended for public use	-	-	+
Permission form	-	+	-
Permission to freely copy	-	+	-

The initial protection level K is determined as follows [16-18]:

– An information system is considered to be highly protected if 70 percent of the characteristics of the information system are at the “high” level and the remaining characteristics are protected at the “medium” level (K1=0);

– An information system is considered to be moderately protected if it is not protected at the “high” level and 70 percent of the characteristics of the information

system are at the “medium” level, and the remaining characteristics are protected at the “low” level (K1=5);

– An information system is considered to be poorly protected if it is not protected at the “high” and “medium” levels (K1=10).

4. Damage assessment

When assessing information security, damage assessment can be carried out at different levels in monetary terms. Damage assessment in monetary termsEvaluation in a unit is a difficult and complex task.

The processed jackal is then evaluated from a qualitative to a quantitative perspective. A Z-factor is assigned to each level of damage.

Table 5. Assessment of the overall level of damage in terms of quality and quantity

The organization's overall damage level	Coefficient values
The amount of damage is very high.	10
The amount of damage caused	7
Average damage amount	5
Low damage amount	3

5.Probability of threats being carried out

Threat implementation level indicator "X"AH expert assessments the level of threat implementation is assessed based on the developed four-level qualitative scales: low, low, medium, and high.

Table 6. Threat probability of implementation degree, qualitative and quantitative dependencies

Probability of threats being carried out	Coefficient values
Up probability level	10
Average probability level	5
Well probability level	2
Few probability level	0

6. Determining the coefficient of implementation of threats

When calculating the coefficient for determining the possibility of implementing threats, the probability of implementing immediate threats (X) and the final assessment of the level of protection (K) are used. The coefficient of implementation of threats Y is determined by the following expression [17-19]:

$$Y = \frac{(X + K)}{2}$$

This is where:

Y – threat implementation coefficient, $0 \leq Y \leq 10$;

X –the likelihood of implementing threats, $0 \leq X \leq 10$;

K – initial hedged value of the asset, $0 \leq K \leq 10$;

We calculate the value of Y and obtain a quantitative numerical value. To make this value understandable, the evaluation is shifted from quantitative to qualitative.

if 0 ≤ Y ≤2.5, then t contract enforcement coefficient low.

if 2.5 <Y ≤6, then t contract enforcement coefficient middle.

if 6 <Y ≤ 7.5, then t contract enforcement coefficient ear.

if 7.5 < Y ≤ 10, then t contract enforcement coefficient *very good*.

7. Determining the urgency of threats

Threat urgency classifies threats into urgent and non-urgent threats based on their likelihood of occurrence and their risk profile. Table 7 below provides a definition of threat urgency [20, 21].

Table 7. Determining the urgency of threats

Possibilities for implementing threats	Threat risk indicators		
	Well	**Average**	**Up**
Well	not relevant	not relevant	current
Average	not relevant	current	current
Uqori	current	current	current
Very good	current	current	current

8. Level of risk potential regarding information security

At this stage, the level of risk probability of the AH is determined. Risk probability "R" is the probability of occurrence of a negative event associated with the realization of a particular threat.It is possible. In the calculation process, a parameter must be taken into account and it is calculated according to formula below [22].

$$R = Z * \frac{Y*U}{10} \qquad 0 \leq R \leq 100,$$

This is where: U – magnitude of vulnerability; Y – presence of threats; Z – damage to the organization.

The following scales are used for quantitative assessment:

if 0≤R≤ 7, the risk is “low”;

if 8<R≤22, the risk level is “medium”;

if 23<R≤43, the risk level is “high”;

If 44<R≤100, the risk level is “critical”.

9. Alignment of information security risk levels

The total risk value is calculated using Formula below.

$$R_{um} = \frac{1}{n} * \sum_{i=1}^{n} R_i,$$

This is where:

R is the total value of the risk probability;

i – the serial number of the risk being calculated;

n is the total number of risks involved in the calculation.

Table 8. Total value of HR risks

Risk numbers	**Specific risk values**	**Total value of risks**
Risk No. 1	28	$R_{um} = \frac{1}{n} * \sum_{i=1}^{n} R_i = \frac{1}{3} * (28 + 15 + 35) = \frac{1}{3} * 78 = 26$
Risk No. 2	15	
Risk No. 3	35	

10. Recommend effective countermeasures

Effective response to threats based on the likelihood of identified threats A list of measures is formed.

11. Preparing reports

Reports are generated based on the results of the algorithm's calculations. The reports are in the form of statistics and graphical diagrams.

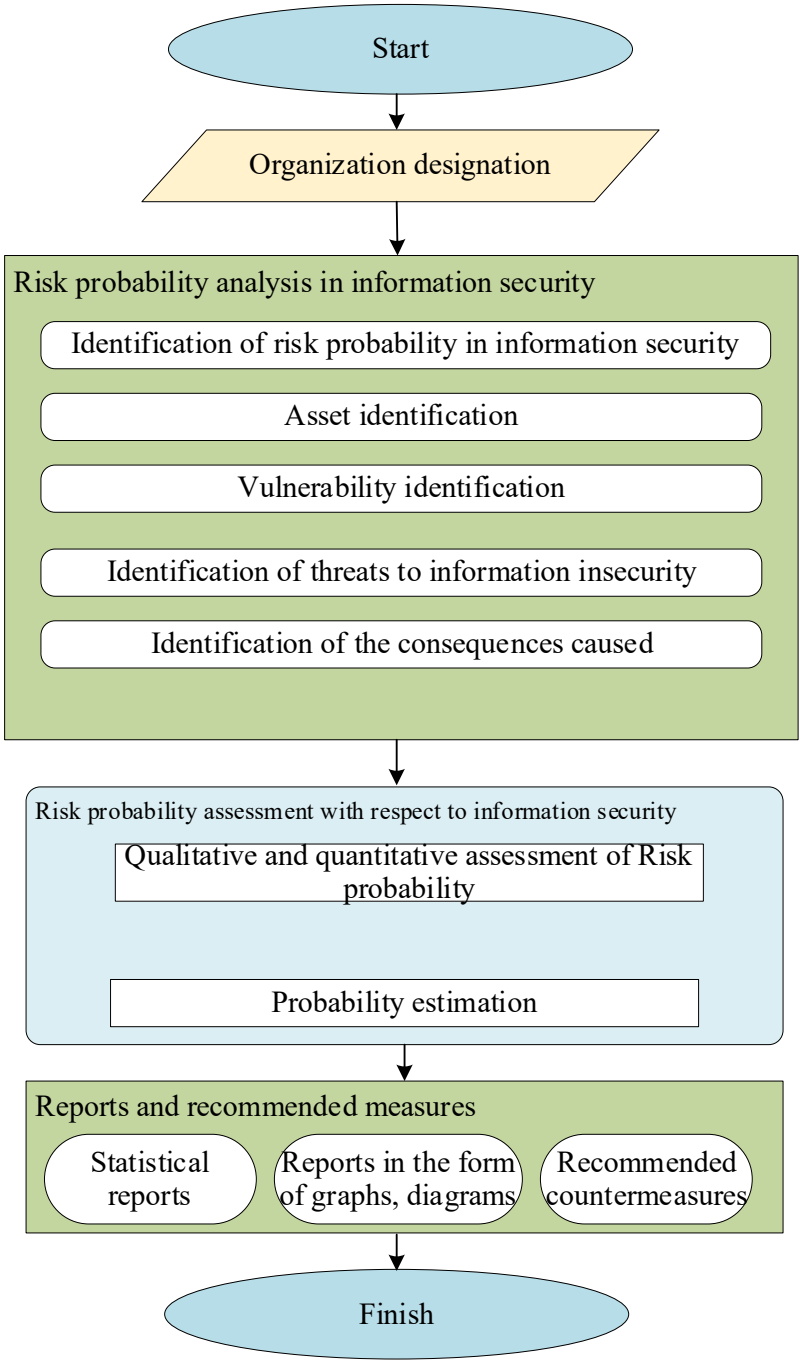

Fig. 4. Block diagram of the threat assessment algorithm for information security

5 Conclusion

Comprehensive approaches should be used to analyze information security threats. These approaches include object description, threat source classification, vulnerability analysis, threat implementation method classification, current attack rating, and threat mitigation methods. These processes help identify all the elements necessary to ensure information security.

1. Methods for assessing threats to information security were studied. Criteria for assessing risk probability were studied. In addition, factors considered as threats to information security in organizations and their organization were studied. In addition, scientific work carried out in this area, research and adopted standards, national standards and assessment criteria were studied.
2. Methods for assessing threats to information security in organizations, operating modes of assessment software, algorithms, and mathematical formulas for calculations were studied.

References

1. Bogoras A.G., Peskova O.Y. Methodology for testing and assessment of firewalls. Izvestiya SFedU. Engineering Sciences. 2013;149(12):148–156. (in Russ.)
2. Dorofeev A. Penetration Testing: Demonstration of One Vulnerability or an Objective Security Assessment? Zaŝita informacii. Inside. 2010;36(6): 72–73. (in Russ.)
3. Umnitsyn M.Y. Approach to semi-natural security evaluation of information system. Izvestia VSTU. 2018;218(8): 112–116 (in Russ.)
4. Borodin M.K., Borodina P.Ju. VGATE R2 Information Security Penetration Testing. Regional'naja informatika I informacionnaja bezopasnost [Regional Informatics and information security]. Saint Petersburg, 2017. p.264–268 (in Russ.)
5. Poltavtseva M.A., Pechenkin A.I. Data mining methods in penetration tests decision support system. Information Security Problems. Computer Systems. 2017; 3:62–69. (in Russ.)
6. Kadan A.M., Doronin A.K. Cloud infrastructure solutions for penetration testing. Uchenye zapiski ISGZ. 2016;14(1): 296–302. (in Russ.)
7. Eremenko N.N., Kokoulin A.N. Research of methods of penetration testing in information systems. Master's Journal. 2016; 2:181–186 (in Russ.)
8. Tumanov S.A. Penetration testing tools for information systems. Proceedings of Tomsk State University of Control Systems and Radioelectronics. 2015;36(2):73–79. (in Russ.)
9. Kravchuk A. V. The model of process of remote security analysis of information systems and methods of improving it's performance. SPIIRAS Proceedings. 2015;38(1):75–93. (in Russ.)
10. Gorbatov V.S., Meshcheryakov A.A. Comparative analysis of computer network security scanners. IT Security. 2013;20(1):43–48. (in Russ.)
11. Pfleeger C.P., Pfleeger S.L., Theofanos M.F. A methodology for penetration testing. Computers & Security. 1989;8(7): 613–620.
12. McDermott J.P. Attack net penetration testing. NSPW. 2000:15–21.

13. Alisherov F., Sattarova F. Methodology for penetration testing. International Journal of Grid and Distributed Computing. 2009:43–50.
14. Ami P., Hasan A. Seven phrase penetration testing model. International Journal of Computer Applications. 2012;59(5):16–20.
15. Holik F., Horalek J., Marik O., Neradova S., Zitta S. Effective penetration testing with Metasploit framework and methodol-ogies. 2014 IEEE 15th International Symposium on Computational Intelligence and Informatics (CINTI). IEEE; 2014. p.237–242. DOI:10.1109/CINTI.2014.7028682
16. Fayzullajon, B., Azam, G., Sherzod, S. (2023). Handling Information Security Events and Incidents. In: Ranganathan, G., Fernando, X., Rocha, Á. (eds) Inventive Communication and Computational Technologies. Lecture Notes in Networks and Systems, vol 383. Springer, Singapore. https://doi.org/10.1007/978-981-19-4960-9_40
17. Fayzullajon, B., Sharifjon, G., Sherzod, S. (2023). Methods for Assessing Information Security Incidents in the Enterprise and Making Decisions. In: Ranganathan, G., Fernando, X., Rocha, Á. (eds) Inventive Communication and Computational Technologies. Lecture Notes in Networks and Systems, vol 383. Springer, Singapore. https://doi.org/10.1007/978-981-19-4960-9_12
18. Zaynutdinova, M., Sayfullaev, S. (2021). Analysis and Modeling of Information Security Systems in Industry 4.0. In: Aliev, R.A., Yusupbekov, N.R., Kacprzyk, J., Pedrycz, W., Sadikoglu, F.M. (eds) 11th World Conference “Intelligent System for Industrial Automation” (WCIS-2020). WCIS 2020. Advances in Intelligent Systems and Computing, vol 1323. Springer, Cham. https://doi.org/10.1007/978-3-030-68004-6_2
19. G. Abdukhalil and S. Sherzod, "Principles of Adaptation in Protecting Corporate Systems," *2020 International Conference on Information Science and Communications Technologies (ICISCT)*, 2020, pp. 1-4, doi: 10.1109/ICISCT50599.2020.9351461.
20. O. Ruzibaev, R. Kabulov and S. Sayfullaev, "The Axiomatic Approach to Definition of Interval Relations," *2019 International Conference on Information Science and Communications Technologies (ICISCT)*, 2019, pp. 1-2, doi: 10.1109/ICISCT47635.2019.9011887.
21. Karimov Madjit , Ganiyev Abdulkhalil , Sayfullaev Sherzod. Models and Methods of Corporate Information Protection System, International Journal of Advanced Trends in Computer Science and Engineering, 2020, pp. 4521-4524, https://doi.org/10.30534/ijatcse/2020/48942020.
22. S. Sayfullaev, D. Valikulova and K. Sabirov, "Modern Intelligent Security Analysis Systems for Corporate Networks," in 2024 5th International Conference on Image Processing and Capsule Networks (ICIPCN), Dhulikhel, Nepal, 2024, pp. 717-719, doi: 10.1109/ICIPCN63822.2024.00124.

A Smarter Plate: Enhancing Food Delivery Apps with Personalized Proportion Sizing and Nutritional Awareness

*Dr. Ashwini Dalvi[1], Sargundeepkaur Sachdeo[1(✉)], Samrudhi Bhat[1]
[1]Department of Information Technology, K.J. Somaiya College Of Engineering,
Mumbai, India
Contributing authors: ashwinidalvi@somaiya.edu
E-mail(s): sargundeepkaur.s@somaiya.edu , samrudhi.b@somaiya.edu

Abstract. Online food delivery applications have gained widespread adoption, offering users convenience and a diverse range of choices. However, many food delivery apps' current interfaces and feature sets do not sufficiently address concerns related to food wastage and nutritional transparency. This research focuses on evaluating and improving the user experience of food delivery applications using the User Experience Questionnaire (UEQ) and User Centered Design(UCD). Specifically, it aims to introduce customizable and standard portion size options and nutritional value information to mitigate food wastage and encourage healthier dietary practices. Additionally, the study proposes integrating a recommendation algorithm that employs collaborative filtering and machine learning to dynamically suggest portion sizes based on user behavior and preferences. Based on initial user interviews and subsequent surveys conducted with approximately 70 participants , key areas for improvement were identified and a prototype with enhanced features was developed. The User Experience Questionnaire (UEQ) results indicate an overall increase in user satisfaction, demonstrating the effectiveness of the proposed design. This study provides valuable insights for enhancing food delivery applications using Swiggy as a case study to more effectively address user requirements and contribute to sustainability goals. Furthermore, the study also proposes a filter feature enabling users to display only restaurants offering customizable portion sizes, further improving accessibility and promoting sustainability.

Keywords: Food delivery, food delivery applications, portion size options, nutritional value information, food wastage reduction, user interface(UI), sustainable development goals(SDG).

1 Introduction

The proliferation of food delivery apps has transformed how people access meals, offering convenience and variety from home. Despite their popularity, these platforms are often criticized for overlooking food waste and lacking nutritional transparency [17,12], with environmental consequences frequently ignored [16].

Customer satisfaction is crucial, driven by intuitive interfaces and smooth user experiences. Incorporating advanced technologies enhances engagement and functionality [1]. However, current literature primarily focuses on operational efficiency, neglecting the role of portion size customization and nutritional information in improving user experience and reducing food waste.

This study addresses that gap through a User-Centered Design framework for food ordering apps, integrating three core features: customizable portion sizes (e.g., quarter, half, full), real-time nutritional data, and a machine learning–based recommendation system tailored to user behavior. This approach aims to promote satisfaction while encouraging sustainable and informed choices.

Behavioral research has explored food-related decision-making—Verma and Patel [22] applied the Theory of Planned Behavior to sustainable food intentions, and Nguyen et al. [20] analyzed household waste behavior. Yet, these insights were not translated into app features.

To bridge this, we propose a behavior-driven recommendation system that adjusts portion sizes based on past consumption. We also introduce restaurant filtering grounded in user survey data, reflecting concern for food waste. Interface features—such as dynamic sliders and bottom sheets—are informed by findings like 57.6% of users preferring smaller portions.

This integration of sustainability, behavioral science, and health into a cohesive, user-first design represents a critical shift. It not only improves the digital food ordering experience but also supports responsible consumption, reducing waste and empowering users with better dietary control.

2 Literature Survey

The rapid growth of food delivery applications has led to various studies focusing on improving user experience, customer satisfaction, and incorporating new technological features. This literature survey reviews existing research, highlighting the emphasis on satisfaction and added functionality, while identifying a gap in addressing food portion sizes and nutritional value.

Prior work on food delivery applications can be broadly categorized into four main areas: User Satisfaction and UI Design, Technological Advancements, Sustainability and Waste Reduction, and Behavioral Modeling of food-related decisions. While these studies offer useful insights, they rarely adopt an integrated approach that combines personalized nutrition, portion control, sustainability, and user interface (UI) intervention. This study aims to address these gaps using a

mixed-method, real-time nutritional feedback, machine learning–guided, and user-centered design (UCD) approach.

Several studies have examined user satisfaction and UI/UX, including factors influencing engagement and retention. Jadhav et al. [1] emphasized variety and familiarity of restaurants but did not include health-conscious customization. Choi et al. [2], using the Technology Acceptance Model (TAM), found perceived usefulness and ease of use to be key factors but did not consider nutritional transparency or portion adaptability. Lee and Kim [9] developed a visually appealing UX framework but excluded cognitive support for dietary management. Collectively, these studies underscore the value of interface quality but overlook features that promote healthier food selection.

Technological advancements in food delivery platforms have mostly aimed at improving operational efficiency. Rao et al. [3] introduced automation to enhance order accuracy and logistics. Ghosh and Menon [5] explored blockchain to build trust and traceability. Singh et al. [6] studied social recommendation systems to boost engagement. Though valuable, these innovations lack adaptive personalization tied to health preferences or behavioral trends. Notably, machine learning has yet to be applied for dynamic portion sizing or dietary guidance within user interfaces.

Sustainability and food waste reduction have also gained attention. Sharma et al. [11] and Li et al. [12] identified over-ordering and portion excess as major contributors to waste in digital food ordering. However, their solutions remain theoretical and are not embedded in app design. Kaur et al. [15] proposed financial incentives for offering smaller portions, but interface-level strategies were not presented. While environmental concerns are well addressed in literature, actionable UI-based interventions to reduce waste are still lacking.

3 Methodology

To address the existing gap in the literature, this study evaluates user awareness and willingness to incorporate nutritional information and customizable portion sizes into food delivery applications. The methodology is structured into three key components: qualitative research, a proposed algorithm, and user interface (UI) design.

3.1 Qualitative Research

To assess user perspectives on the integration of nutritional value and portion size options in food delivery platforms such as Swiggy and Zomato, a comprehensive and well-structured survey was developed and administered [18]. The primary objective of the survey was to gauge user agreement with the inclusion of these features while simultaneously measuring their awareness of nutritional factors in everyday dietary choices. The survey targeted individuals between the ages of 18 and 25, yielding a total of 66 responses. This sample size is considered adequate to

represent a diverse population with varied viewpoints on nutritional transparency and portion size customization in food delivery services.
A heatmap chart illustrating the distribution of survey responses is presented below. In the visualization, red denotes higher response percentages, while green indicates lower ones.

Sr. No	Questions	very	somewhat	neutral	not very	not
1	When ordering food, how important is the portion size to you?	51.5	36.4	12.1	0	0
2	How often do you feel that the portion sizes offered by food delivery apps are too large for your appetite?	3.3	10	37.9	45.5	3.3
3	How often do you use food delivery apps like Swiggy and Zomato?	4.5	16.7	37.9	36.4	4.5
4	Are you concerned about the food waste in general?	83.3	0	6	0	10.7
5	Would you prefer if food delivery apps offered the option to choose smaller portion sizes (e.g. 1/4,1/2,3/4) of dishes?	57.6	0	15.2	0	27.3
6	How much attention do you pay to the nutritional value of the food you order?	25.8	43.9	22.7	0	7.6
7	Would you appreciate having nutrition information displayed alongside portion size options when ordering food?	81.8	0	9.1	0	9.1

Table 1. Heatmap chart of the response received from the users in the survey

The survey findings reveal a substantial level of awareness and concern regarding nutritional information. Approximately 25.8% of respondents rated nutritional value as highly important, while 43.9% considered it somewhat important (Fig. 1). These results underscore a growing health consciousness within the targeted age group.

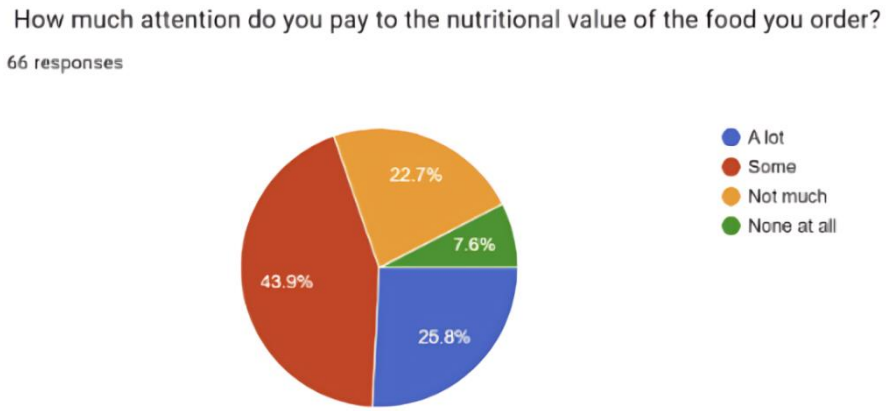

Fig. 1: Visual representation of attention given to nutritional value

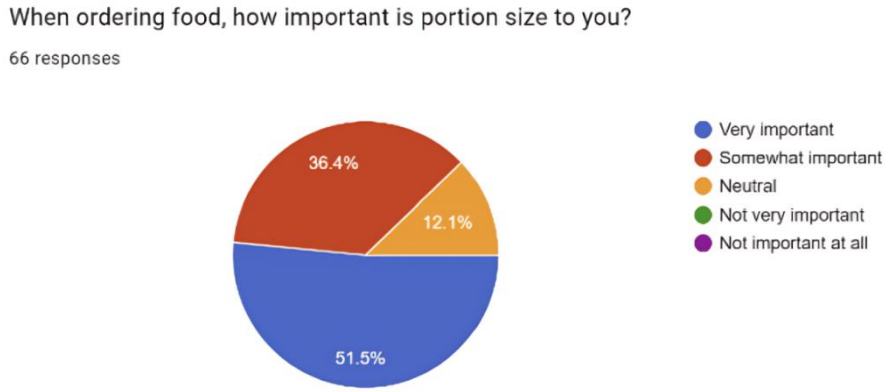

Fig. 2: Visual representation of attention given to proportion size

Survey responses also indicate that portion size is a key consideration for users, with 51.5% rating it as very important (Fig. 2). 37.9% of participants stated that portion sizes were sometimes too large for their appetite, 45.5% reported this occasionally, and 4.5% indicated this always or never occurred (Fig. 3). Additionally, usage frequency of food delivery apps varied among participants: 37.9% reported using these services once a week, 36.4% rarely, 16.7% several times per week, and a small fraction (4.5%) reported daily or no usage (Fig. 4).

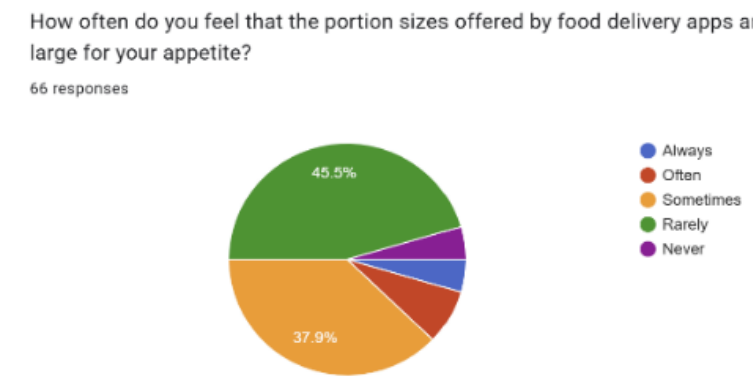

Fig. 3: Visual representation of statistics obtained as part of the questions of the survey.

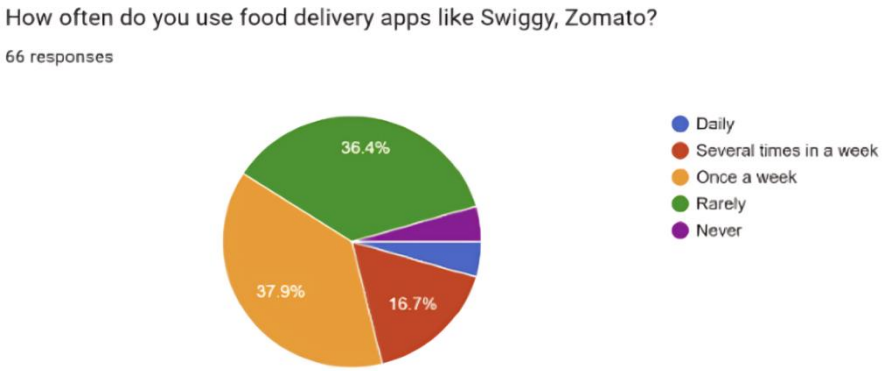

Fig. 4: Visual representation of statistics obtained as part of the questions of the survey.

Concerns about food waste were prominent, with 83.3% of respondents expressing concern about the issue (Fig. 5). These findings highlight a strong inclination among young adults toward sustainable and health-conscious eating behaviors. Furthermore, 57.6% of participants expressed a preference for the ability to select smaller portion sizes, such as one-fourth, one-half, or three-fourths of a dish, indicating demand for enhanced flexibility in portion control (Fig. 6). Notably, 28.8% reported they would likely opt for smaller portions if such options were available.

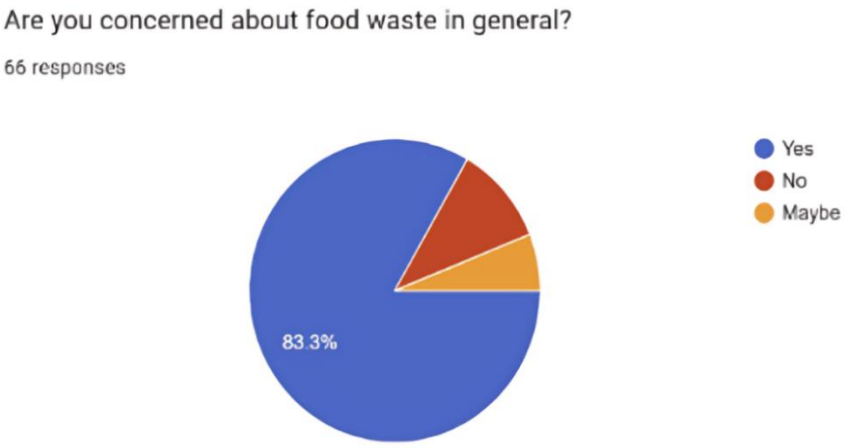

Fig. 5: Visual representation of concern Levels About Food Waste.

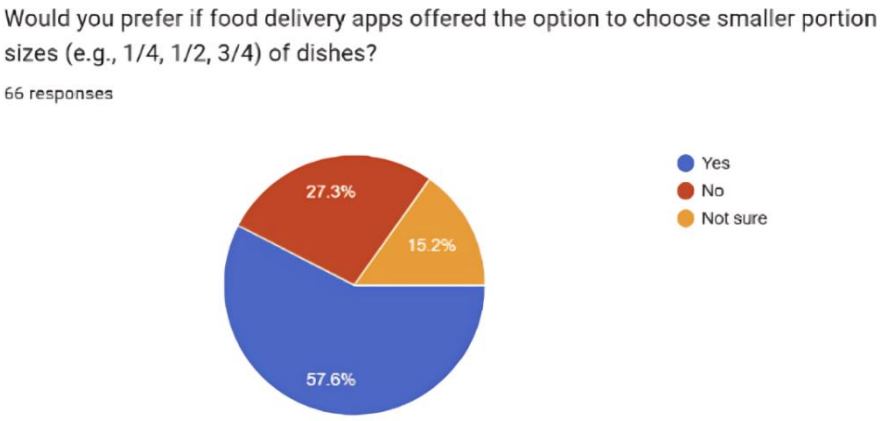

Fig. 6: Visual representation of preference for opting for smaller food portion size

The survey also showed that 25.8% of respondents consistently pay attention to the nutritional content of the food they order, 43.9% pay moderate attention, 22.7% pay little attention, and 7.6% do not consider it at all. These insights reinforce the necessity for nutritional transparency, with 81.8% of participants indicating support for displaying nutritional information alongside portion size options (Fig. 7).

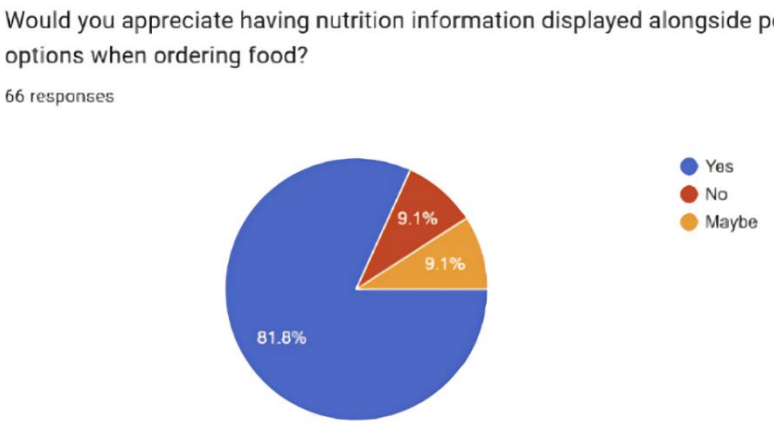

Fig. 7: Visual representation of attention given to nutritional value

3.2 Proposed Algorithm

The survey highlights a significant level of awareness and willingness among young adults to adopt more sustainable and health-conscious food choices. The integration of the proposed algorithm into food delivery applications is expected to offer substantial benefits to users. The algorithm designed for recommending portion sizes in food delivery platforms leverages an advanced combination of collaborative filtering and machine learning techniques (Fig. 8). Its objective is to provide personalized suggestions by analyzing users' historical behaviors. Central to this system is the development of comprehensive user profiles that incorporate key metrics, including average portion size, order frequency, preferred food categories, and feedback patterns.

The novelty of the proposed approach lies in its deliberate focus on portion size customization, an area often neglected in current food delivery recommendation systems. While conventional platforms primarily suggest food items or restaurants based on static user preferences, the proposed model adopts a dynamic, behavior-aware framework. By integrating nutritional data with individualized consumption trends, the system moves beyond surface-level personalization. It constructs robust user profiles using metrics such as historical portion size averages, variability in intake, food category preferences, order timing, and dietary patterns. This enriched profiling enables context-sensitive recommendations that better align with users' evolving needs and sustainability goals.

A key distinguishing feature of the proposed methodology is the application of clustering algorithms to identify and categorize users with similar behavioral patterns. These behavioural clusters are subsequently used to train the machine learning model, thereby enhancing predictive accuracy and enabling the algorithm to generalize insights across user cohorts. The core predictive engine is defined by the function $P=f(\mu,\sigma,C)$, where μ represents the mean historical portion size, σ

denotes the variability in portion sizes, and C encapsulates relevant contextual parameters. This predictive model facilitates real-time personalization by adjusting recommendations in accordance with evolving user data.

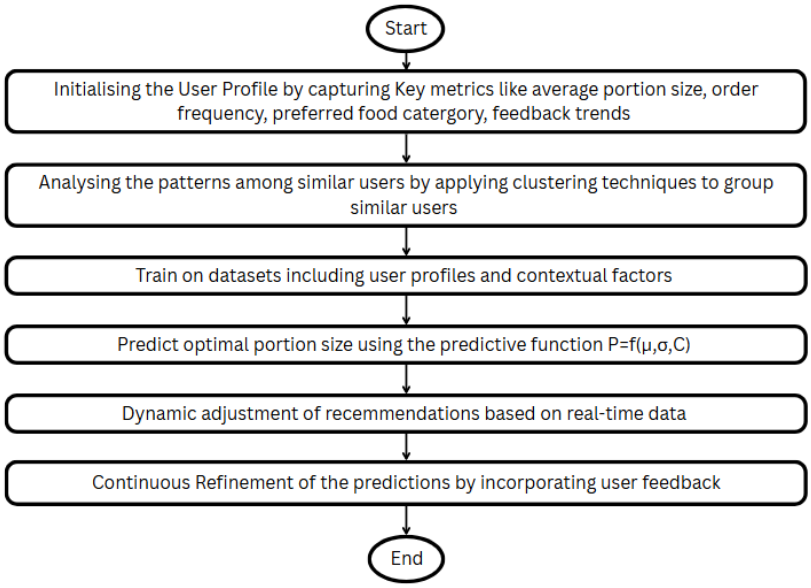

Fig. 8: Proposed Algorithm for Recommendation System.

The selection of this approach is supported by its capacity to overcome the limitations inherent in traditional, rule-based recommendation frameworks. The use of collaborative filtering allows for the identification of latent user preferences, while clustering enhances the scalability and generalizability of the system. Machine learning regression models are particularly well-suited to capturing the complex, multivariate dependencies that underlie portion size determination. Furthermore, the incorporation of an iterative feedback mechanism ensures that the system continuously refines its predictive capabilities based on user interactions, thereby maintaining a high degree of recommendation accuracy over time.

In conclusion, the proposed algorithm represents a novel and methodologically sound advancement in the field of intelligent food delivery systems. By synthesizing behavioural analytics with adaptive learning, the approach addresses both personalization and sustainability objectives. Its capacity to dynamically tailor portion sizes not only enhances user experience but also contributes to broader public health and environmental goals, underscoring its relevance and potential impact within contemporary digital food service ecosystems.

3.3 UI Screens

To effectively implement the proposed features, targeted user interface (UI) enhancements and an integrated recommendation system are essential. Using Swiggy as a reference case, the suggested modifications aim to be minimally disruptive yet significantly impactful—enhancing user experience while fostering informed, health-conscious, and sustainable decision-making (Fig. 9).

A central feature of the proposed design is the introduction of a filter option that allows users to view only those restaurants offering customizable portion sizes (Fig. 10). This filter will be embedded within the primary search bar and advanced filtering settings, helping users tailor their food choices to align with personal dietary preferences and sustainability concerns (Fig. 11).

Currently, users interact with a simple “Add” button when selecting food items. Under the proposed design, tapping this button will launch an interactive bottom sheet (modal) instead. This redesigned component will allow users to select from a range of portion sizes (e.g., 1/4, 1/2, 3/4, full, 1.25, or other fractional options) and simultaneously view nutritional details—such as calorie count, protein, fat, and carbohydrate content—updated in real time (Fig. 12.1, Fig. 12.2). This real-time transparency empowers users to make better-informed food choices in alignment with their health and consumption goals.

The bottom sheet will feature a streamlined, intuitive interface that promotes ease of use and quick decision-making. By combining portion customization with nutritional transparency, this functionality addresses both overconsumption and food waste.

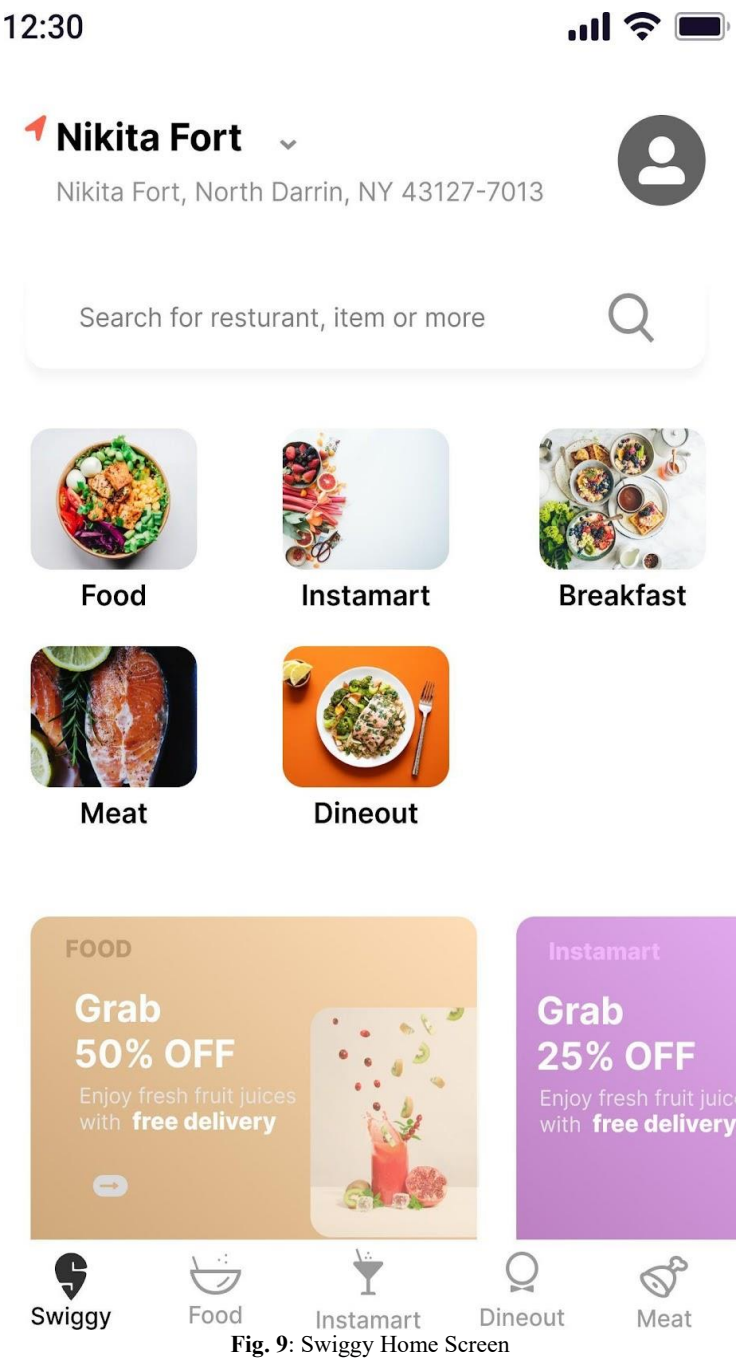

Fig. 9: Swiggy Home Screen

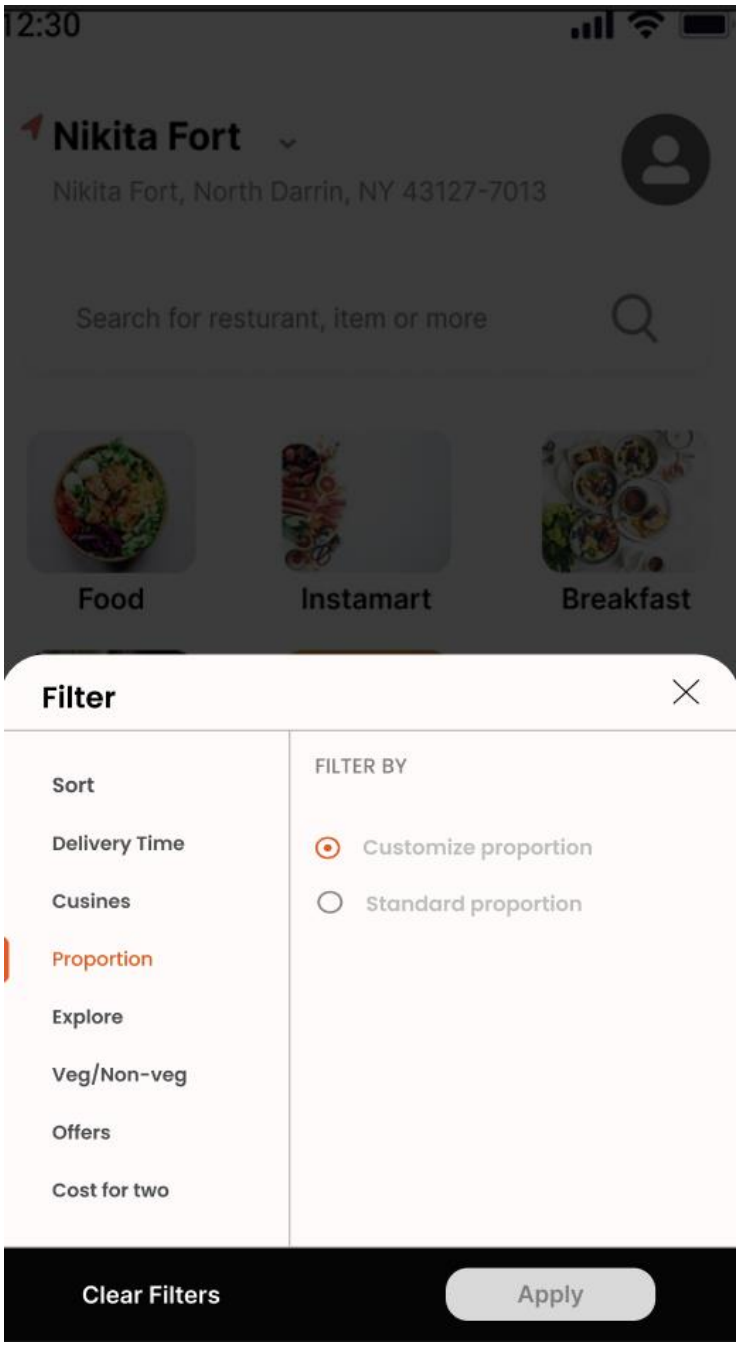

Fig. 10 Filter for restaurants that offer customizable portion sizes.

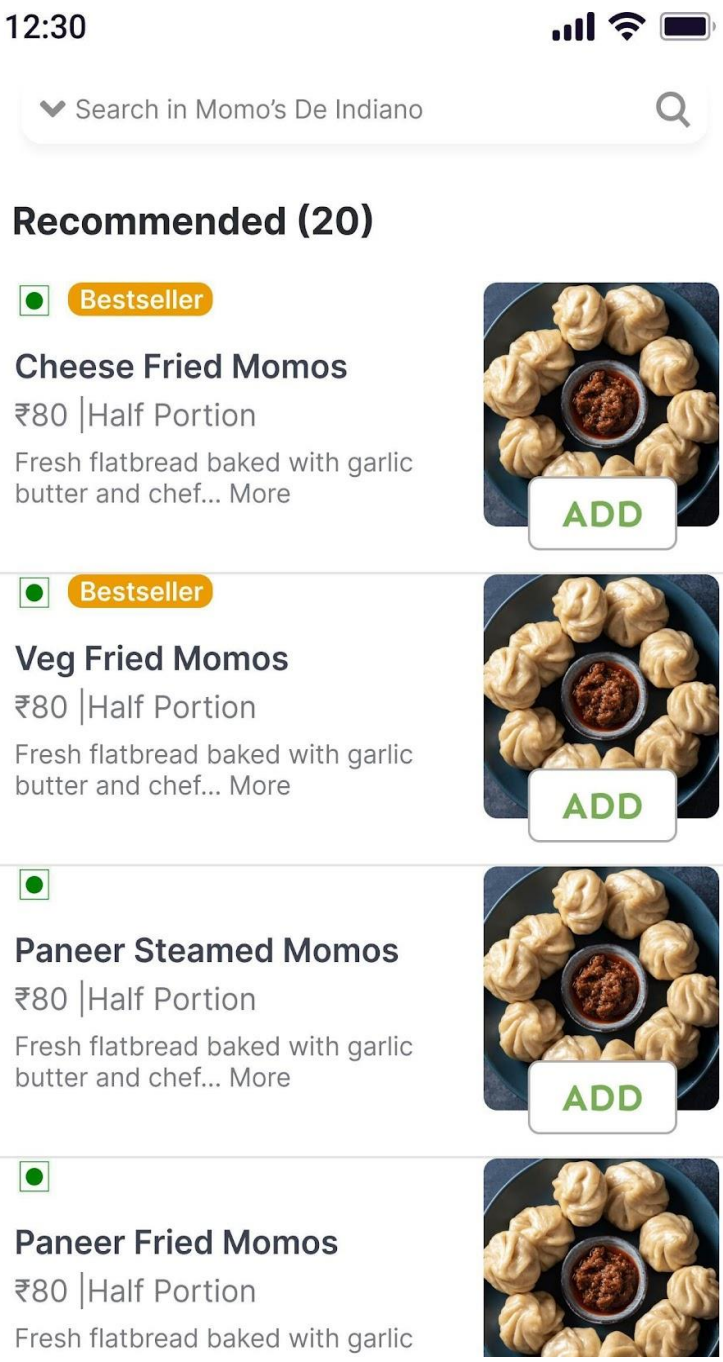

Fig. 11: Food menu of a restaurant

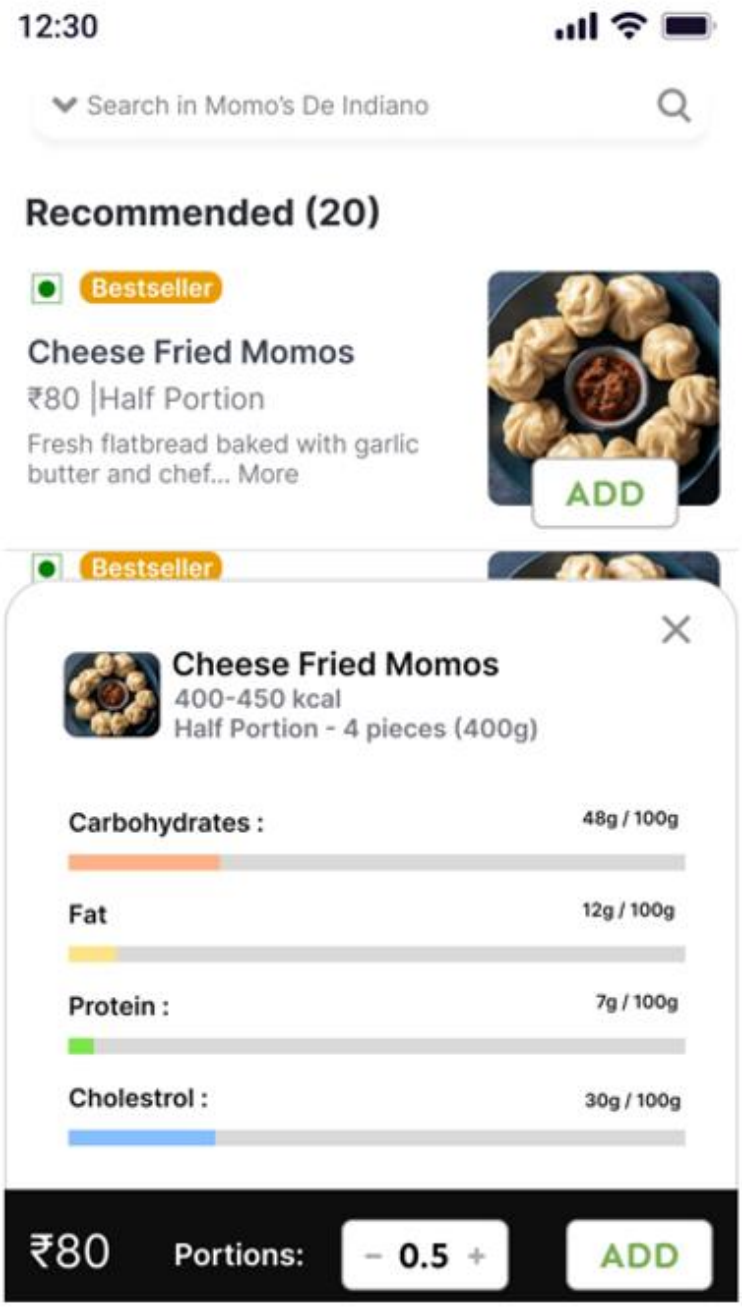

(a) UI modifications with inclusion of portion size and nutrition value for selected food item (Momo's De Indiano)

Fig. 12.1: UI modifications for different restaurants

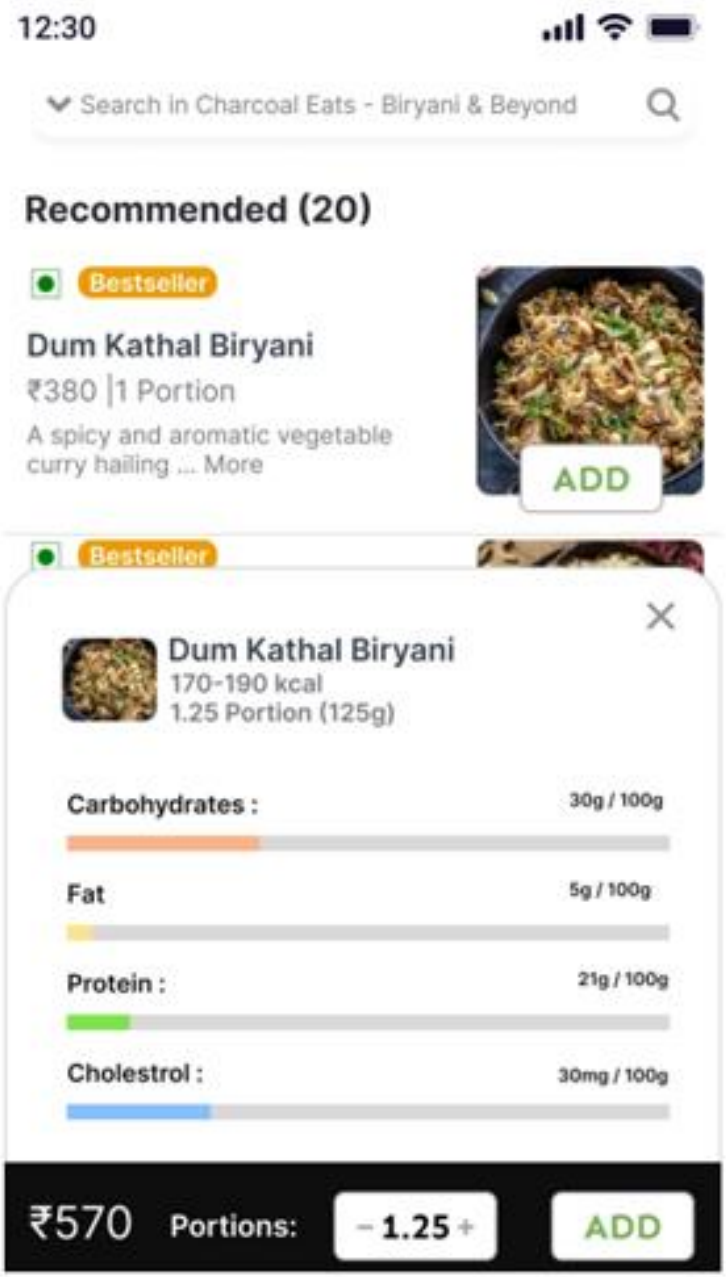

(b) UI modifications with inclusion of portion size and nutrition value for selected food item (Charcoal Eats)

Fig. 12.2: UI modifications for different restaurants

These UI enhancements enable platforms like Swiggy to better serve health-conscious users and those committed to sustainable consumption. Beyond user satisfaction, the changes also support larger global objectives of reducing food waste and encouraging healthier eating habits. The integration of customizable portion sizes and nutritional transparency into food delivery applications presents a meaningful step toward addressing pressing concerns related to public health and environmental sustainability. By aligning app features with the values and behavior of today's users—particularly young adults—this design promotes a more responsible, user-centered, and sustainable food delivery ecosystem. This research underscores the importance of embedding such innovations into platform design, highlighting their dual role in enhancing user experience and contributing to broader sustainability goals.

4 Conclusion

This paper addresses a critical gap in the current food delivery ecosystem by proposing a novel design approach grounded in the principles of User-Centered Design (UCD). Centering on the needs and preferences of users—specifically young adults aged 18–25—the research presents a solution that integrates three key features: customizable portion sizes (e.g., ¼, ½, full), real-time nutritional transparency, and a personalized recommendation system powered by machine learning.

The findings reveal that users highly value nutritional information and seek greater control over portion sizes to align with their dietary goals and reduce food waste. By embedding these insights into the design process, the proposed model not only enhances user satisfaction but also promotes responsible consumption bhaviors. The use of an intuitive, interactive bottom sheet for selecting portion sizes and viewing nutritional content demonstrates how minimal yet impactful UI changes can support healthier and more sustainable decision-making.

Furthermore, the integration of a collaborative filtering–based recommendation system refines user experience by offering context-aware portion suggestions based on historical behaviors and preferences. This adaptive mechanism exemplifies how technology can evolve through continuous feedback loops, further personalizing the experience and reinforcing long-term user engagement.

Overall, this design promotes a balanced ecosystem where user health, convenience, and sustainability coexist—advancing both individual well-being and broader goals such as SDG 12: Responsible Consumption and Production.

References

[1] Jadhav, Sarvesh, Ray Titus, Tina Babu, and R. Chinnaiyan. "Evaluation of Consumer Behavior Regarding Food Delivery Applications in India." arXiv preprint

arXiv:2401.14409 (2023).
[2] Choi, Ju-Choel. ”User familiarity and satisfaction with food delivery mobile apps.” Sage Open 10, no. 4 (2020): 2158244020970563.
[3] Sungboonlue, Pongsatorn, Satisa Thanakaew, Kittisak Rangseepanya, Teramate Tangpatong, and Thitirat Siriborvornratanakul. “A study of redesigning food delivery application in Thailand.” Telkomnika (Telecommunication Computing Electronics and Control) 20, no. 5 (2022): 1073-1082.
[4] Yuli Fauziah, Kezia Melisa, and Herlina Jayadianti. “User-centred Design Method Approach for User Experience Analysis of Food Delivery Application.” In *2023 1st International Conference on Advanced Informatics and Intelligent Information Systems (ICAI3S 2023)*, pp. 261-273. Atlantis Press, 2024.
[5] Lee, W.S., Song, M., Moon, J. and Tang, R. (2023), “Application of the technology acceptance model to food delivery apps”, British Food Journal, Vol. 125 No. 1, pp. 49-64.
[6] Wen, H., Pookulangara, S. and Josiam, B.M. (2022), “A comprehensive examination of consumers’ intentions to use food delivery apps”, British Food Journal, Vol. 124 No. 5, pp. 1737-1754.
[7] Rajat Sharma, Amandeep Dhir, Shalini Talwar, Puneet Kaur, Over-ordering and food waste: The use of food delivery apps during a pandemic, International Journal of Hospitality Management, Volume 96,2021,102977, ISSN 0278-4319
[8] Li, Charlene, Miranda Mirosa, and Phil Bremer. 2020. ”Review of Online Food Delivery Platforms and their Impacts on Sustainability” Sustainability 12, no. 14: 5528.
[9] Chen, Han-Shen, Chia-Hsing Liang, Shu-Yi Liao, and Hung-Yu Kuo. 2020. ”Consumer Attitudes and Purchase Intentions toward Food Delivery Platform Services” Sustainability 12, no. 23: 10177.
[10] Kristia Kristia, Sándor Kovács, Erdey László,Food delivery platform and food waste: Deciphering the role of promotions, knowledge, and subjective norms among Indonesian generation Z,Cleaner and Responsible Consumption,Volume 11,2023,100152,ISSN 2666-7843,https://doi.org/10.1016/j.clrc.2023.100152.
[11] Kumar, Hemant & Jain, Muskan & Bajwa, Manpreet. (2021). Online Food Delivery App ‘Foodie’. Journal of University of Shanghai for Science and Technology. 23. 761-771. 10.51201/JUSST/21/07200.
[12] M. A. Islam Arif, S. Kabir, Z. Islam, M. F. Hussain Khan, I. Islam and M. N. Islam, "Usability Evaluation of Online Food Delivery Applications in Bangladesh: A Comparative Study," *2024 IEEE International Women in Engineering (WIE) Conference on Electrical and Computer Engineering (WIECON-ECE)*, Chennai, India, 2024, pp. 337-342, doi: 10.1109/WIECON-ECE64149.2024.10914965.
[13] Wei, Liuchun & Prabhakar, Guru & Duong, Linh. (2023). Usage of online food delivery in food waste generation in China during the crisis of COVID-19. International Journal of Food Science & Technology. 58. 10.1111/ijfs.16552.
[14] Alnasser, A., & Abaalkhail, A. (2024, February 15). *Digital food behaviours, motivations, and delivery application usage among Saudis during COVID-19: A mixed-methods study*. *Heliyon, 10*(3), e24903. Elsevier. https://doi.org/10.1016/j.heliyon.2024.e24903
[15] Fadi Abdelradi,Food waste behaviour at the household level: A conceptual framework,Waste Management,Volume 71,2018,Pages 485-493,ISSN 0956-053X, https://doi.org/10.1016/j.wasman.2017.10.001.
[16] Islam, Shabab & Jones, Robert & Akhi, Asma & Talukder, Shamim. (2023). Do food delivery apps influence food waste generation? A stimulus-organism-behavior-consequence (SOBC) exploration. British Food Journal. 126. 10.1108/BFJ-07-2023-0648.

[17] Li, Charlene & Bremer, Phil & Jowett, Tim & Lee, Michael & Parker, Kate & Gaugler, Evamaria & Mirosa, Miranda. (2024). What influences consumer food waste behaviour when ordering food online? An application of the extended theory of planned behaviour. Cogent Food & Agriculture. 10. 10.1080/23311932.2024.2330728.
[18] Yang, Chieh & Yan, Libo & Ji, Pengfei. (2024). Restaurant waiting staff's intention to dissuade customers from over-ordering: an extended theory of planned behaviour. British Food Journal. 126. 10.1108/BFJ-01-2024-0114.
[19] Seetharam, Anirudh & Kumar, Tarun & Gupta, Harshit & Karia, Deval. (2023). A Web-based AR Solution for Restaurant Menus to Reduce Food Waste. 1-9. 10.1109/GCITC60406.2023.10426326.

Improving Water Quality Prediction using Robust Outlier Detection and RankGenForestStacking Classifier Approach

*A. Sumathi[1], R. Saruhasini[1], S.Meganathan [1], Sheik Mohideen Shah[2], and Sundar Santhoshkumar[3]
[1,2]SRC, SASTRA University
[1] sumathi@src.sastra.edu
[1] sharukumar1000@gmail.com
[1] meganathan@src.sastra.edu
[2] sheikme2005@src.sastra.edu
[3]Alagappa University, Karaikudi,India
[3] santhoshkumars@alagappauniversity.ac.in

* sumathi@src.sastra.edu

Abstract. Water is a vital resource for our planet, and its quality has a profound effect on both public health and environmental sustainability. Contaminated drinking water can cause various waterborne diseases. While traditional laboratory testing methods yield precise results, they are frequently labor-intensive, costly, and necessitate specialized knowledge. Increasingly, machine learning techniques are being employed to forecast water quality indicators by analyzing extensive datasets of water quality parameters. This work employs the Water Potability Dataset from Kaggle, which comprises 3,276 water samples with nine essential quality indicators, including pH, hardness, and chemical composition. To enhance the accuracy of predictions, a novel outlier detection method known as DataDriven Skewed Interquartile Range (DDSIQR) is introduced. For classification purposes, the work proposes the RankGenForestStacking Classifier Approach, which allows the system to predict water quality and categorize each sample as either safe or unsafe for consumption, thereby providing a clear and actionable outcome.

Keywords: Water quality prediction, machine learning, classification models, datadriven skewed interquartile range, rankgenforeststacking classifier approach and water potability.

1 Introduction

Water quality plays a crucial role in influencing ecosystems, agriculture, industry, and, most importantly, human health. It refers to the characteristics or condition of

water, which can be evaluated through a range of physical, chemical, and biological parameters. These parameters are essential in determining the water's appropriateness for various uses, such as drinking, agriculture, aquaculture, industrial activities, and recreational purposes. Key indicators of water quality include pH levels, turbidity, temperature, dissolved oxygen, total dissolved solids, conductivity, and the presence of pollutants or harmful microorganisms. Water quality is not static; it can fluctuate over time due to environmental factors, climate variations, and human interventions. For example, heavy rainfall can introduce sediments and pollutants into water bodies, while industrial activities may release chemical waste into aquatic environments. Therefore, it is essential to monitor and maintain high water quality standards to protect ecosystems and public health. The development of advanced systems for real-time water quality prediction has become increasingly important [1]. Specifically, the quality of drinking water refers to the safety and purity of water designated for human consumption, which must meet rigorous health standards established by entities like the World Health Organization and the United States Environmental Protection Agency, and various local regulatory bodies. Ideal drinking water should be clear, odorless, and free from harmful contaminants, including heavy metals (such as lead and arsenic), microbial pathogens (including bacteria, viruses, and protozoa), pesticides, nitrates, and organic chemicals. Real-time prediction systems can help ensure compliance with these standards by quickly detecting anomalies and facilitating timely corrective actions. Combining water quality predictions with forecasts of water usage presents a comprehensive approach to managing water resources effectively [2]. In many countries, water extracted from natural sources, including rivers, lakes, and underground aquifers, is subjected to extensive purification and disinfection processes before it reaches consumers. Access to potable water is not only a basic human right but also a crucial element of public infrastructure. It is essential to anticipate both the safety and availability of water to tackle issues such as overconsumption, scarcity, and contamination, which in turn supports better planning and sustainable water distribution systems [3]. The use of machine learning techniques to predict water quality in different regions reveals that the effectiveness of these models is significantly influenced by the nature and quality of the data utilized. Despite the presence of regulations and advancements in water treatment technologies, numerous challenges remain that threaten drinking water quality, including pollution from industrial waste, agricultural runoff, and aging infrastructure. Conventional manual testing methods are often slow and resource-intensive, limiting the capacity for regular monitoring of water sources. Machine learning offers a modern and effective solution to these challenges. ML algorithms can analyze historical water quality data to automatically identify patterns, correlations, and trends among various parameters. Once trained, these models can categorize water as either potable (safe for consumption) or non-potable (unsafe), predict future quality levels, and even detect early signs of contamination [4]. Although some early initiatives in this field lacked sufficient validation, the increasing interest in intelligent systems for water quality monitoring has led to the development of more accurate and reliable models. Techniques such as classification, regression, and clustering are now frequently utilized in water quality

prediction. For example, classifiers like Random Forest, Support Vector Machine, and Neural Networks can evaluate water safety based on various indicators [5]. This work aims to improve water quality classification by integrating an efficient outlier detection technique, DataDriven Skewed Interquartile Range (DDSIQR), with a RankGenForestStacking Classifier approach. The main contributions of this study are the introduction of DDSIQR, a novel method for detecting outliers in skewed data distributions, which enhances data quality by dynamically adapting quantile thresholds based on asymmetry in the dataset and the development of the RankGenForestStacking Classifier, which integrates a rankbased genetic algorithm for feature optimization with ensemble learning by combining multiple base learners and a Random Forest meta-learner. By leveraging these innovations, the proposed approach achieves more robust and accurate predictions, thereby contributing to improved monitoring and decision-making in water quality assessment systems.

2 Related Work

Muhammad and colleagues created a classification model for assessing water quality through the application of machine learning methods. Their investigation assessed multiple algorithms to evaluate their effectiveness in predicting levels of water contamination. The results underscored the capability of machine learning to automate the categorization of water quality and established a foundation for subsequent research in AI-driven water quality assessment. The study highlighted the critical role of selecting appropriate algorithms for accurate classification tasks [6]. Sakizadeh and Mirzaei examined the efficacy of K-Nearest Neighbors (KNN) and Support Vector Machines in classifying groundwater. Their findings indicated that Support Vector Machine yielded more precise and consistent results than KNN. This research affirmed the practicality of machine learning in assessing groundwater quality and underscored the necessity of aligning algorithms with the characteristics of the dataset [7]. Gursoy conducted a comparative study of various machine learning approaches to identify the most effective classification methods for evaluating water quality. The research revealed that the performance of models is significantly influenced by the properties of the data and the strategies employed for preprocessing. It provided actionable recommendations for selecting the best classifiers in diverse scenarios and illustrated how machine learning can enhance water quality monitoring initiatives [8]. Mandal et al. assessed the quality of river water for agricultural irrigation by examining essential environmental and chemical indicators. They utilized various water quality indices to determine the water's suitability for agricultural use. The study emphasized the impact of contamination on agricultural water sources and offered valuable insights for sustainable management of water resources in agricultural areas [9]. Chen et al. conducted a comparative analysis of different machine learning models aimed at predicting surface water quality. Researchers have pinpointed essential indicators that greatly affect the accuracy of predictions. Their research indicated that novel and effective machine learning (ML) models surpassed traditional statistical methods,

highlighting the vital importance of big data in monitoring environmental conditions and forecasting water quality [10]. Lu and Ma introduced hybrid models that merge decision trees with various machine learning algorithms to enhance short-term predictions of water quality. Their findings revealed that these hybrid methods provided improved accuracy compared to standalone models, indicating that algorithmic integration can strengthen forecasting systems. This research laid robust groundwork for developing effective and scalable frameworks for predicting water quality [11]. Ajayi et al. created WaterNet, a real-time monitoring system that combines Internet of Things (IoT) technology with machine learning to evaluate water quality for both drinking and agricultural purposes. Their study demonstrated that automated monitoring systems can enhance response times and decision-making processes while improving the detection of contamination incidents, representing a significant leap forward in smart water quality management systems [12]. Prasad et al. utilized deep learning and auto deep learning models to assess and forecast levels of water contamination. By employing neural networks, their system achieved high levels of accuracy and exhibited superior performance relative to traditional ML methods. This research contributed to the evolution of intelligent water monitoring systems and highlighted the potential of deep learning in analyzing environmental data [13]. Shim et al. investigated the application of deep learning alongside data preprocessing techniques for predicting water quality in ultrafiltration systems. Their study indicated that effective preprocessing significantly enhances model accuracy and filtration performance, emphasizing the critical role of high-quality input data and preprocessing in advancing AI-driven water treatment models [14]. Moeinzadeh et al. developed a deep neural network model aimed at synthesizing seven heavy metal parameters to enhance the accuracy of water quality predictions. Their model successfully identified customized contamination patterns, providing a reliable approach for assessing water safety. This research contributed to the advancement of deep learning techniques in modeling chemical contamination and refining predictive systems for water quality [15].

3 Proposed Work

3.1 Data Collection

The Water Potability Dataset from Kaggle, which has 3,276 samples and nine critical water quality indicators like pH, turbidity, hardness, and chemical content is the source of the data used in this study. These factors are essential in assessing the potability of water. https://www.kaggle.com/datasets/adityakadiwal/water-potability.

Aljarah and Cetin (2022) as well as Sharma et al. (2024) utilized the Water Potability dataset from Kaggle, which is also the dataset employed in this research, for predicting water quality. Their respective models reached peak accuracies of 67% and 70%, underscoring the constraints associated with traditional machine learning

techniques. In contrast, the present study proposes enhanced preprocessing methods and a stacking-based classification strategy to address these limitations and attain superior accuracy [16][17].

3.2 Data Preprocessing

In this stage, using the following four methods, the Data Pre-Processing was performed.

Dealing with Missing Values. Mean imputation is used to handle missing data, which involves substituting the average value of a feature column for any missing values. This methodology ensures the preservation of data integrity and affirms that the dataset remains complete and impartial.

Proposed Outlier Detection Method. DataDriven Skewed IQR (DDSIQR)

DataDriven Skewed IQR is an improved version of the traditional Interquartile Range (IQR) method used for outlier detection, especially when dealing with skewed (asymmetric) data distributions**.** Extreme values in the dataset are identified and removed using the DataDriven Skewed Interquartile Range (DDSIQR) approach. By dynamically calculating the lower and upper quantiles based on data distribution, this method guarantees effective outlier detection while maintaining vital information.

1. Given a dataset $D = \{x1, x2, \ldots, x_n\}$, compute the quantiles:
   Let Q_p and Q_q be two quantiles such that $0 < p < q < 1$
2. Compute the Data-Driven Skewed Interquartile Range (DDSIQR):
   $DDSIQR = Q_q - Q_p$
3. Determine the lower bound for outlier detection:
   $Lower\ Bound = Q_p - k * DDSIQR$
4. Determine the upper bound for outlier detection:
   $Upper\ Bound = Q_q + k * DDSIQR$
5. Identify outliers as values satisfying:
   $x_i < Lower\ Bound$ or $x_i > Upper\ Bound$
6. Remove outliers to obtain the cleaned dataset:
   $D_{cleaned} = D \setminus \{x_i \mid x_i < Lower\ Bound \text{ or } x_i > Upper\ Bound\}$

The DataDriven Skewed Interquartile Range (DDSIQR) algorithm serves as a method for detecting outliers, specifically designed to accommodate asymmetric data distributions. For a given dataset $D = \{x1, x2, \ldots, x_n\}$, the algorithm calculates

two quantiles Q_p and Q_q, where $0 < p < q < 1$, to establish a flexible interquartile range. The DDSIQR is defined as $Q_q - Q_p$, which reflects the dispersion between these two percentiles. By employing a configurable multiplier k, the algorithm determines the lower and upper thresholds for outlier detection as $Q_p - k \cdot DDSIQR$ and $Q_q + k \cdot DDSIQR$, respectively. Any data point that lies beyond these thresholds is classified as an outlier. Subsequently, the dataset Dcleaned is created by excluding these outliers.

Dealing with Class Imbalance. To address class imbalance, random oversampling is employed to increase the number of instances in the minority class, thereby balancing the dataset and preventing the model from favouring the majority class.

Feature Scaling. Feature scaling is performed using z-score normalization, which standardizes the feature values by converting them to have a mean of 0 and a standard deviation of 1. This ensures that all features contribute equally to the model and prevents bias due to varying numerical ranges.

3.3 Applying Algorithms

In this stage, various machine learning algorithms were applied: a Random Forest Classifier and the Rank Based Genetic Random Forest, which internally uses a rank-based genetic algorithm for feature optimization followed by Random Forest training. These base learners were combined using the RankGenForestStacking Classifier approach, where a Random Forest served as the meta-learner. Additionally, the dataset, after preprocessing with DataDriven Skewed IQR (DDSIQR), was divided into two subsets: one for training the models and another for testing, both derived from the same balanced dataset.

Random Forest Classifier. The Random Forest Classifier is an effective ensemble machine learning technique that constructs numerous decision trees and combines their outputs to yield more precise and reliable predictions. Each tree is trained on a randomly selected subset of the data and features, a method referred to as bootstrap aggregation or bagging. This inherent randomness aids in minimizing model variance and mitigating overfitting. In this study, the Random Forest is utilized as one of the foundational learners due to its resilience, capability to manage high-dimensional datasets, and exceptional classification efficacy. It acts as a dependable element within the ensemble, ensuring consistent and high-quality predictions.

Rank Based Genetic Random Forest Classifier. The Rank Based Genetic Random Forest Classifier is an innovative machine learning model that merges feature optimization with classification tasks. It employs a rank based genetic

algorithm to refine feature weights and utilizes a Random Forest classifier for the ultimate prediction. In the optimization phase, solutions are chosen based on their rank rather than solely on fitness scores, which promotes a more balanced exploration of the search space and mitigates the risk of premature convergence. After determining the optimal set of feature weights, a Random Forest model is trained using these weighted features, thereby amplifying the impact of significant attributes. This integration of evolutionary optimization with ensemble classification results in enhanced performance when compared to conventional Random Forest models.

Proposed RankGenForestStacking Classifier. The RankGenForestStacking Classifier is an advanced stacking ensemble model that integrates the predictions of multiple base learners. Specifically, the Random Forest Classifier and the Rank Based Genetic Random Forest Classifier. In stacking, the base models are first trained independently, and their predictions are used as input features for a meta-learner, which in this case is another Random Forest Classifier. This meta learner learns to optimally combine the outputs of the base models, capturing complex patterns that individual models might miss. By leveraging the complementary strengths of the base learners and reducing the weaknesses of each, the RankGenForestStacking Classifier achieves a higher level of predictive performance, making it a robust and scalable solution for real world water quality prediction tasks.

Algorithm. RankGenForestStacking Classifier Approach

1. Input dataset $X \in \mathbb{R}^{n \times m}$, target labels $y \in \mathbb{R}^{n}$
2. Initialize:
    - Population size P
    - Number of generations G
    - Number of features m
    - Define gene space $gene_i \sim \mathcal{U}(0,1)$ for $i = 1,2,\ldots,m$
3. Define the Fitness Function F:
    a. For each candidate solution $w = [w_1, w_2, \ldots, w_m]$:
        - Compute the weighted dataset:
4. $X' = X \odot w$
    - where $\odot$ denotes element-wise multiplication
    - Train Random Forest $RF_{fitness}$ on X', y
    - Evaluate cross-validation accuracy:

      $F(w) = \frac{1}{k}\sum_{i=1}^{k} Accuracy_i$
5. Create initial population $\mathcal{P} = \{w_1, w_2, \ldots, w_P\}$, each $w_i \in [0,1]^m$

6. Repeat for G generations:
    a. Evaluate fitness $F(w_i)$ for all individuals $w_i \in \mathcal{P}$
    b. Rank Selection:
        - Rank all individuals by fitness (ascending or descending)
        - Assign selection probability based on rank r_i:

$$P_i = \frac{r_i + 1}{\sum_{j=1}^{P}(r_j + 1)}$$

    c. Crossover:
        - For each pair of parents w_a, w_b, perform uniform crossover to produce offspring:

$$child_j = \begin{cases} w_{a_j}, & \text{if } rand_j < 0.5 \\ w_{b_j}, & \text{otherwise} \end{cases}$$

    d. Mutation:
        - For each gene in offspring:

$$w_j = \begin{cases} rand(0,1), & \text{with probability } p_{mut} \\ w_j, & \text{otherwise} \end{cases}$$

7. Select the best individual $w^* = \text{argmax}_{w \in \mathcal{P}} F(w)$
8. Train the final Random Forest classifier:

$$RF_{GA} = \text{RandomForestClassifier}()$$

Using: $X_{weighted} = X \odot w^*, \quad$ train on y

9. Define base learners for stacking:

$$Base_1 = RF_{basic} \qquad Base_2 = RF_{GA}$$

10. Define the meta learner:

$$Meta = \text{RandomForestClassifier}$$

11. Build and train Stacking Classifier:

$$Stack(X) = Meta\left(Base_1(X), Base_2\left(X_{weighted}\right)\right)$$

12. Output the final predictions:

$$\hat{y} = Stack(X_{test})$$

Initially, a dataset along with its labels is provided. A Genetic Algorithm is employed to determine the optimal set of feature weights. The process begins with

the random generation of a population of candidate weight sets. For each candidate, the features are multiplied by their respective weights, and a Random Forest model is trained to evaluate its performance through cross-validation accuracy. The candidates are then ranked according to their performance, and new candidates are produced through selection, crossover, and mutation. After multiple generations, the most effective set of weights is selected. A conclusive Random Forest model is developed utilizing the weighted dataset. Subsequently, two base models are constructed, a standard Random Forest and the Rank Based Genetic Random Forest. Their outputs are integrated using another Random Forest as a meta-learner to create a stacking classifier, which ultimately generates the final predictions. The model's performance in classifying water as safe or unsafe is assessed using accuracy, precision, recall, and F1-score. While precision and recall draw attention to false positives and negatives, accuracy reflects overall correctness. The F1-score provides a balanced view of these measures for a complete assessment.

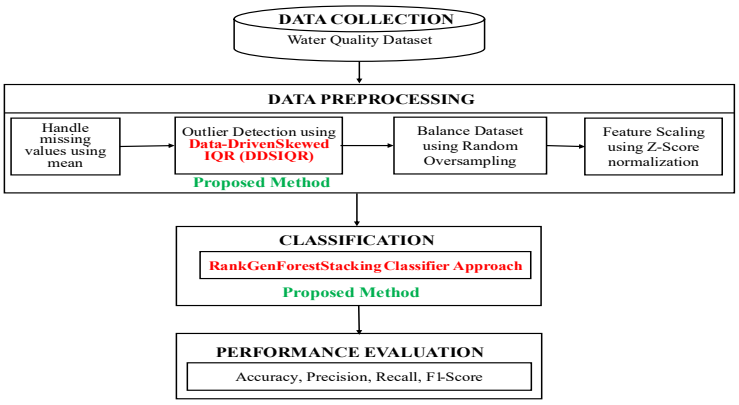

Fig 1. The Proposed Model

As shown in Figure 1, the workflow begins by importing a dataset and addressing any missing values using the mean of each column. Outlier detection is performed using an innovative variant of the Interquartile Range (IQR) method known as DataDriven Skewed IQR (DDSIQR), which effectively removes extreme outliers to improve data integrity. To address the likely imbalance in the dataset, where non-potable samples outnumber potable ones, the algorithm applies random oversampling to correct this disparity, ensuring that the model does not favor the majority class. Feature scaling is then carried out using StandardScaler to standardize the dataset, adjusting it to have a mean of zero and a variance of one. The processed dataset is divided into training and testing subsets, with stratified sampling used to maintain the class distribution in both subsets. The model is built on a custom classifier, the Rank Based Genetic Random Forest, which utilizes a

genetic algorithm to optimize feature weights. This genetic algorithm evaluates different combinations of feature weights by training a Random Forest classifier and assessing its accuracy through cross-validation. After several generations, the best combination of feature weights is used to train a final Random Forest model. This custom classifier is included as one of the base learners in a stacking ensemble model, alongside a traditional Random Forest classifier as another base learner. A final Random Forest model serves as the meta-learner, integrating the predictions from the base learners. This approach is referred to as the RankGenForestStacking classifier Approach. The RankGenForestStacking classifier sends the original features along with the predictions from the base learners to the meta-learner, thus enhancing the overall predictive performance.

4 Result Analysis

The RankGenForestStacking classifier approach, which integrates a Rank Based genetic Random Forest with Random Forest functioning as both base and meta learners, has shown notable advancements in water quality prediction. The dataset underwent preprocessing to address missing values, implement an effective outlier removal strategy, and achieve balance through random oversampling, thus preparing it for model training. Feature scaling was conducted to ensure the data was optimized for modeling purposes. The custom genetic algorithm utilized rank-based selection to optimize feature weights, thereby enhancing model performance. By fine-tuning these weights, the Genetic Algorithm improved predictive accuracy by adjusting the influence of each feature on the classifier. The Random Forest meta-learner synthesized the predictions from the base learners, resulting in improved overall performance. Validation was conducted using stratified train-test split and 5-fold cross-validation within the genetic algorithm for feature optimization. Evaluation metrics include accuracy, precision, recall, and F1-score. These findings suggested an effective Outlier Detection technique and a well-balanced model, highlighting the effectiveness of integrating a genetic algorithm with Random Forest classifiers to enhance water quality prediction.

Table 1. Comparison of Outlier Detection techniques with Classification Algorithms

Outlier Detection Techniques	Support Vector Machine (%)	Decision Tree (%)	Random Forest (%)
LOF	62	74	83
Z-Score	60	74	82
Isolation Forest	62	76	83
IQR	64	75	84
Proposed	66	77	86

DDSIQR

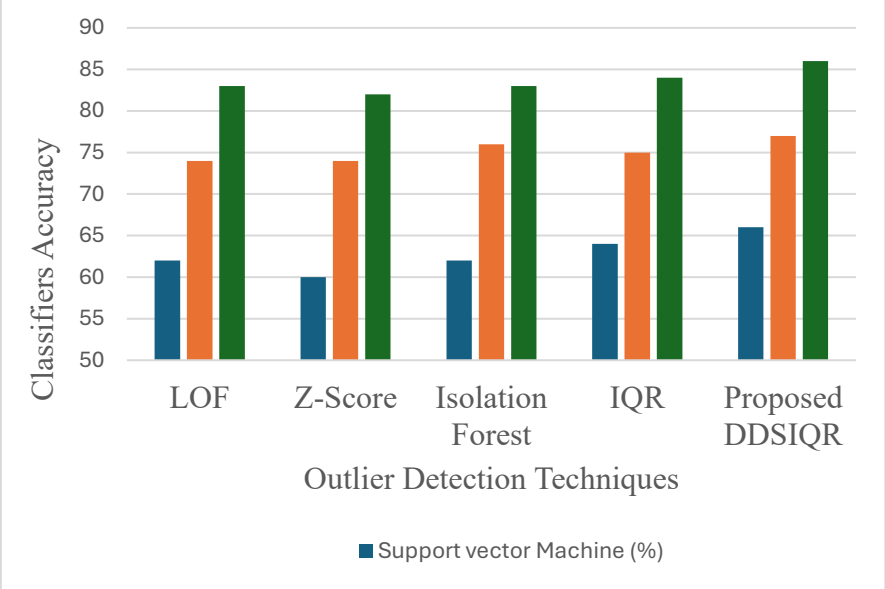

Fig 2. Accuracy of Proposed Outlier Detection Technique

In Table 1 and Figure 2, the Proposed DataDriven Skewed IQR (DDSIQR) in the Random Forest classifier demonstrates superior performance compared to other outlier detection methods, attaining the highest level of accuracy.

Table 2. Comparison of Classification Accuracy with Proposed Outlier Detection Technique (DDSIQR) and RankGenForestStacking Classifier Approach

Proposed Outlier Technique	Random Forest (%)	RankGenForestStacking Classifier Approach (%)
DataDriven Skewed IQR(DDSIQR)	86	88

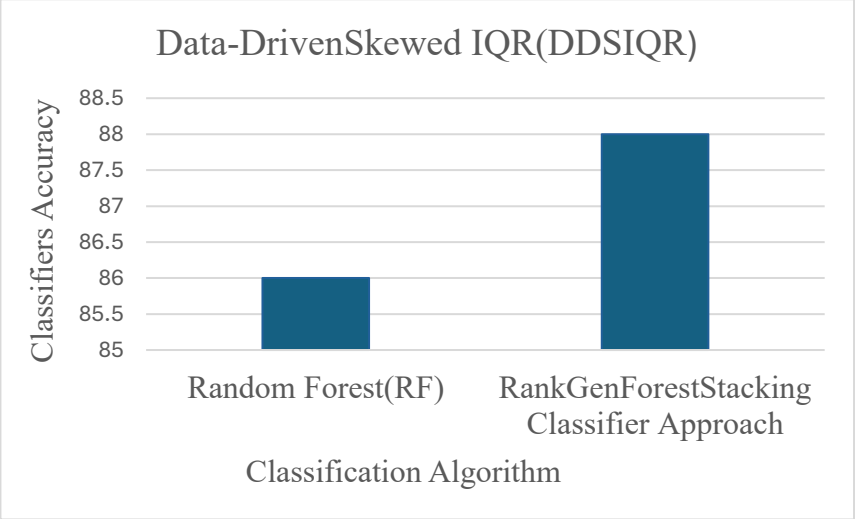

Fig 3. Accuracy of Classification Algorithm

In Table 2 and Figure 3, the Proposed Outlier Technique, known as DataDriven Skewed IQR (DDSIQR), demonstrates remarkable performance in both the Random Forest and RankGenForestStacking Classifier methods, attaining the highest accuracy in the RankGenForestStacking Classifier approach.

Table 3. Comparison of Performance Analysis

Classification	Accuracy (%)	Precision (%)	Recall (%)	F1-Score (%)
Random Forest	86	86	86	86
RankGenForestStacking Classifier Approach	88	89	88	87

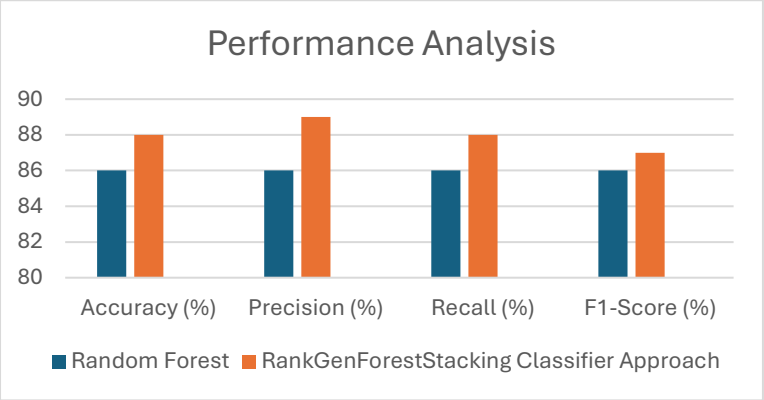

Fig 4. Performance Analysis of Proposed Algorithm

In Table 3 and Figure 4, the RankGenForest Stacking Classifier Method attains an accuracy rate of 88%, with a precision of 89%, a recall of 88%, and an F1-score of 87%.

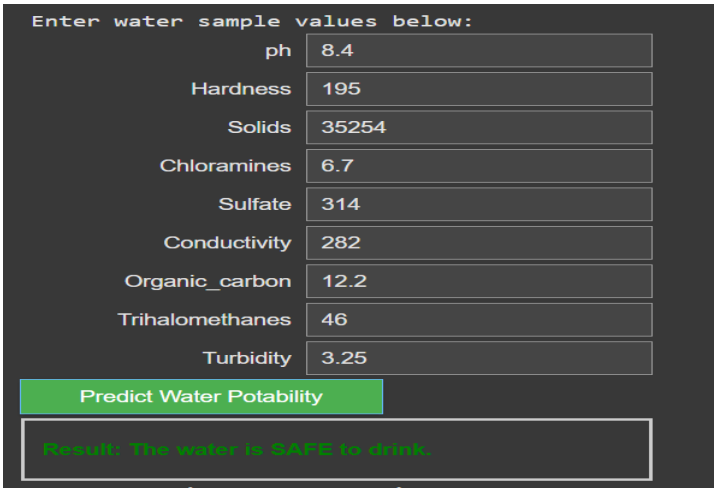

Fig 5. Prediction Result of Potable

Figure 5 shows that the user enters multiple water quality parameters into the system. Upon selecting 'Predict Water Potability,' if the water is safe for drinking, the system indicates that the water is SAFE to drink, as displayed by a green result message.

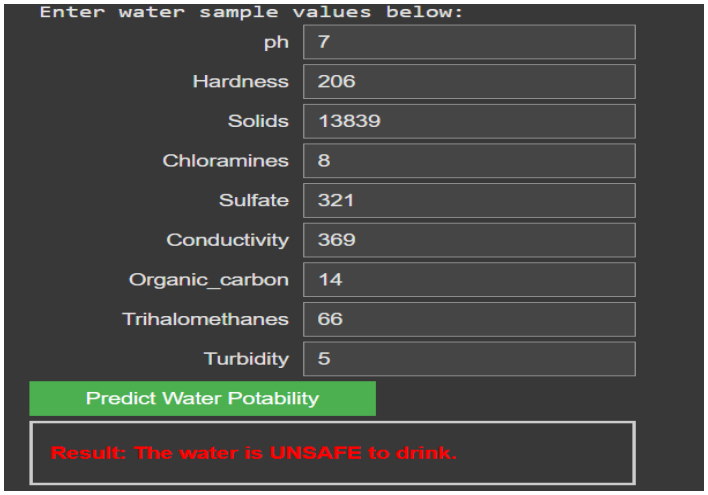

Fig 6. Prediction Result of Non-Potable

Figure 6 shows that the user enters multiple water quality parameters into the system. Upon selecting 'Predict Water Potability,' if the water is unsafe for drinking, the system indicates that the water is UNSAFE to drink, as displayed by a red result message.

5 Conclusion

The quality of drinking water refers to the safety and purity of water designated for human consumption. This work employs the Water Potability dataset sourced from Kaggle, which includes essential indicators such as pH, hardness, turbidity, and several chemical constituents. To improve classification performance, the proposed framework incorporates two key innovations. First, the DataDriven Skewed Interquartile Range (DDSIQR) is introduced as an advanced outlier detection method specifically designed for skewed data distributions. Unlike the traditional IQR method that assumes symmetry, DDSIQR dynamically computes the lower and upper bounds using asymmetric quantiles (Qp and Qq) and a configurable multiplier (k), allowing it to more accurately identify and eliminate extreme values while preserving the meaningful structure of the data. Second, the RankGenForestStacking Classifier is proposed as a custom stacking ensemble model that combines a standard Random Forest classifier and a Rank-Based Genetic Random Forest classifier, which uses a genetic algorithm to optimize feature weights based on ranked fitness scores. These base learners produce prediction outputs that are used as input features for a meta-learner, which is also a Random Forest classifier. The meta-learner integrates the outputs to generate the final prediction, capturing complex patterns and enhancing overall model performance.

Together, DDSIQR improves the quality of the input data, while the RankGenForestStacking Classifier enhances predictive accuracy through optimization and ensemble integration. The combined approach achieved strong results, with 88% accuracy, 89% precision, 88% recall, and 87% F1-score, outperforming traditional methods and validating its suitability for practical water quality assessment and management.

References

[1] Ahmed, A.N., Othman, F.B., Afan, H.A., Ibrahim, R.K., Fai, C.M., Hossain, M.S., Ehteram, M., Elshafie, A.: Machine learning methods for better water quality prediction. J. Hydrol. 578, 124084 (2019)

[2] World Health Organization: Preventing diarrhoea through better water, sanitation and hygiene. World Health Organization, Geneva (2014)

[3] Muhammad, S.Y., Makhtar, M., Rozaimee, A., Aziz, A.A., Jamal, A.A.: Classification model for water quality using machine learning techniques. Int. J. Softw. Eng. Appl. 9(6), 45–52 (2015)

[4] Al Duhayyim, M., Mengash, H.A., Aljebreen, M., Nour, M.K., Salem, N.M., Zamani, A.S., Abdelmageed, A.A., Eldesouki, M.I.: Smart water quality prediction using atom search optimization with fuzzy deep convolutional network. Sustainability 14(24), 16465 (2022)

[5] Azrour, M., Mabrouki, J., Fattah, G., Guezzaz, A., Aziz, F.: Machine learning algorithms for efficient water quality prediction. Model. Earth Syst. Environ. 8(2), 2793–2801 (2022)

[6] Aldhyani, T.H., Al-Yaari, M., Alkahtani, H., Maashi, M.: [Retracted] Water quality prediction using artificial intelligence algorithms. Appl. Bionics Biomech. 2020, 6659314 (2020)

[7] Rustam, F., Ishaq, A., Kokab, S.T., de la Torre Díez, I., Mazón, J.L., Rodríguez, C.L., Ashraf, I.: An artificial neural network model for water quality and water consumption prediction. Water 14(21), 3359 (2022)

[8] Sakizadeh, M., Mirzaei, R.: A comparative study of performance of K-nearest neighbors and support vector machines for classification of groundwater. J. Min. Environ. 7(2), 149–164 (2016)

[9] Mandal, S.K., Dutta, S.K., Pramanik, S., Kole, R.K.: Assessment of river water quality for agricultural irrigation. Int. J. Environ. Sci. Technol. 16, 451–462 (2019)

[10] Lu, H., Ma, X.: Hybrid decision tree-based machine learning models for short-term water quality prediction. Chemosphere 249, 126169 (2020)

[11] Prasad, D.V., Venkataramana, L.Y., Kumar, P.S., Prasannamedha, G., Harshana, S., Srividya, S.J., Harrinei, K., Indraganti, S.: Analysis and prediction of water quality using deep learning and auto deep learning techniques. Sci. Total Environ. 821, 153311 (2022)

[12] Shim, J., Hong, S., Lee, J., Lee, S., Kim, Y.M., Chon, K., Park, S., Cho, K.H.: Deep learning with data preprocessing methods for water quality prediction in ultrafiltration. J. Clean. Prod. 428, 139217 (2023)

[13] Moeinzadeh, H., Jegakumaran, P., Yong, K.T., Withana, A.: Efficient water

quality prediction by synthesizing seven heavy metal parameters using deep neural network. J. Water Process Eng. 56, 104349 (2023)

[14] Aljarah, F., Çetin, A.: Prediction of water quality with ensemble learning algorithms. Adv. Artif. Intell. Res. 3(1), 36–44 (2022)

[15] Sharma, A., Sharma, R., Rana, R., Kalia, A.: Water quality prediction using machine learning models. In: E3S Web Conf., vol. 596, p. 01025. EDP Sciences (2024)

Blockchain-Enabled Patient Consent System for Secure Healthcare Data Management

Jayesh Surve [1], Dr. Ashwini Dalvi [2] and Dr. Irfan Siddavatm[3]

[1] Department of Information Technology, K.J. Somaiya School of Engineering, Mumbai, India
[1*]jayesh.ss@somaiya.edu

[2]Department of Information Technology, K.J. Somaiya School of Engineering, Mumbai, India
[2]ashwini.dalvi@somaiya.edu

[3]Department of Information Technology, K.J. Somaiya School of Engineering, Mumbai, India
[3]irfansiddavatam@somaiya.edu

Abstract. Modern healthcare systems are realizing that the management of information is a most crucial part and have therefore gone digital. In spite of great progress, the traditional EHR systems are still in a bit of a mess as they are very much decentralized and absolutely not protected. Resultantly, this leads to not only wastage of time and energy but also to lack of trust which in return causes malpractices. To make such unethical issues come to an end, develop a mechanism whereby patients are the primary stakeholders, and they can decide positively on their electronic health records in a most transparent manner. The article proposes utilizing blockchain technology to create a system of patient consent management. The new system stores data in a decentralized manner, thus increasing the ability of blockchains to interact and providing the patients with the autonomy to change consent on the fly by the use of smart contracts of Ethereum and IPFS. Through this approach, the healthcare system certainly becomes patient-friendly, and at the same time, it does also handle the factors that are at the core of data security, the privacy of the patients, and the interoperability.

Keywords: EHR, Blockchain, Patient Consent, Healthcare, Interoperability, Smart Contracts, IPFS, Decentralization.

1 Introduction

In the healthcare industry, the patient data is typically stored in one place. Not only are these systems easy to manage, but they also fail to meet today's requirements[8]. Moreover, an additional problem is that of the Centralized database which can be easily attacked by hackers and compromise patients' data[1].

Today's Electronic Health Record (EHR) systems that have transitioned to digital records give us the perfect opportunity to not only link the preservation of data but also to explain how the loss of control over patient data in centralized databases can lead to repeated breaches and unauthorized access, which further causes distrust and

refusal by the patient. Meanwhile, the issue of interoperability is also very crucial for the actors to be able to carry out a smooth health data exchange[2].

Blockchain technology is well-suited to address the issues pertaining to traditional EHRs by simplifying healthcare data storage and management through distributing the data. A secure and unchangeable ledger technology, blockchain records all transactions. A group of nodes makes up the network which uses consensus mechanisms to confirm and secure transactions. These mechanisms allow for the transactions to be visible hence trust and security are maintained. With fewer intermediaries involved, data exchange gets quicker and is less prone to manipulation, and remains the patient's property instead of the intermediaries. This move represents the absence of intermediaries and follows the principles of blockchain technology which were outlined earlier[4].

Through use of blockchain technology, the healthcare industry can more readily manage Electronic Health Records (EHRs) which are now included in the lists of important things. Centralized databases have been repeatedly compromised by hackers and security breaches over the years. Scenarios may occur where unauthorized people gain access to the system leading to data corruption and loss of data. Additionally, the various EHRs currently in use cannot be interlinked. This contributes to the data disintegration in the system. Blockchain offers a great solution for patient-centered health data management and can empower patients to the extent of being able to share records trustedly and safely, so doing, they guarantee security, privacy and at the same time, keep interoperability [5].

Several drivers for adopting blockchain in health care include:

1. Decentralization: The distribution of data across several nodes makes it impossible for there to be a single failure point, as is the case with a centre server. Thus, access to records also becomes simple for patients as well as qualified doctors, thus improving data availability and reliability for all. Eliminating middle person processes saves the amounts involved in administrative costs and time[9].
2. Immutability: Proof of Concept, data cannot be modified or removed from the system thus preventing manipulation or manipulation of patient records. Reduced costs for medical billing and insurance claims[10].
3. Ensure the transparency and auditability of data access requests through usage of an open ledger. Therefore be possible to constantly monitor concerning who has ever read or changed patient information. Improves compliance with HIPAA regulations [13].
4. These include high-level cryptographic techniques such as hashing and digital signatures used in property in a blockchain technology that safeguard medical data. Aims at the access of confidential patient information only by permitted means. Eliminate incidents of hacking, malware, and unauthorized alterations further[14].
5. Consensus Mechanism: Validates through consensus algorithms transaction authenticity data[11]. Typical healthcare consequences based on blockchains can be:

   a. Proof of Authority (PoA) is the practical approach for authorized healthcare networks.
   b. Speedy consensus with efficiencies is supported by PBFT.
   c. There is no central authority validating data.
6. Smart Contracts: Permissions for access, consent management, and exchange of data are enforced automatically within Smart Contracts. Patients can set up access controls limiting the reading or editing of their records to those with proper authorization[15].
7. Anonymity & Privacy: Patients can anonymously converse with each other, using encrypted identifiers for private interaction in the blockchain. Zero Knowledge Proofs (ZKP) and similar privacy-related protocols allow safe data sharing, without requiring sensitive information to be revealed. It is going to maintain patient trust through confidential keeping of data[16].

This paper presents a blockchain-based consent system that seeks to revolutionize EHR management and promote patient-centric care, employing the InterPlanetary File System (IPFS) for efficient storage and retrieval of large volumes of healthcare data. In lieu of archiving extensive medical records on the blockchain[6]. Such EHR are transparent and decentralized owing to the attributes of immutability, decentralization, and transparency. The provision of the idea of Blockchain for patients to manage their data, securely access it from the necessary personnel and interact with them privately is an alternative method proposed by us.

2 Related Work

2.1 Related Research Review

Several studies highlight the potential of blockchain technology in addressing key challenges in healthcare data management, particularly in Electronic Health Records (EHR) systems. This section summarizes related work, emphasizing blockchain's role in enhancing security, interoperability, and patient autonomy.

Another study studies the acceptance for the mobile dynamic consent from patients throughout their lives, which will enable them to govern their permissions related to health data. The legality of blockchain as a managing engine in ensuring the integrity, security, and privacy of data is such that it encourages patient autonomy and builds trust in research and health data sharing [21]. This review is broad regarding the applications of blockchain in the life sciences: from the integrity of data to the prevention of counterfeiting and increased efficiency. Unfortunately, there remain the challenges of high technical complexity, issues in regulation, and those of scalability [22]. Another paper introduces a blockchain-based patient consent management system, the Smart Consent Blockchain-Based System (SCBCS), which intends to improve patient autonomy and security on health information exchanges via purpose-based access control and Hyperledger Fabric [23]. The authors propose an integration framework blockchain enabled to deal with the fragmentation, redundancy, or openness in electronic healthcare systems. This model supports patient data sharing, enhances privacy, and makes interoperability effectual by using the InterPlanetary

File System (IPFS) for decentralized storage and smart contracts for access control [24]. SECURE-MEDSHARE, another system, enhances decentralized sharing of patient data among healthcare institutions using Ethereum, Hardhat for smart contract deployment, and MetaMask for authentication. It prevents reliance on centralized databases and improves traceability of data [25]. Another blockchain solution for managing medical records has created a more secure and private environment using decentralized storage and cryptographic techniques, making it harder to commit fraud, unauthorized modification, and allowing patients to control access to their medical records [26]. This document describes the EHR management system of end-to-end encryption which actually implements the E2EE method directly into the system to improve security and privacy for patients. It encrypts patient information AES and Elliptic Curve Cryptography (ECC) and decentralizes these assets using Ethereum and IPFS for storage and control of access [27]. Research on the blockchain enables EHRs to be shared safely, thus remedying either problem fragmentation or vulnerability to security breaches. Applications include blockchain-based clinical trials, automated processing of insurance claims, and patient-managed records. Challenges such as scalability and integration into existing systems are also addressed, along with advocacy for collaboration among stakeholders for accelerated widespread usage [28]. This model of secure health data storage in an IPFS blockchain system integrates Ethereum smart contracts to IPFS to ensure the most elevated protection of data and control of access to such data. The proposed model attains a 90% accuracy in data management vis-a-vis an ordinary 75% accuracy with conventional systems, thus underlining effectiveness against tampering of data and less dependence on central authority [29]. A publicly available blockchain-based EHR administrative scheme developed based on the patient-centeredness concept integrates Ethereum and IPFS for data storage, allowing patients granting or revoking access permissions using smart contracts. In contrast to traditional EHR systems, it presents improvements in data security, privacy, and interoperability [30]. EHR systems are suggested to be designed based on permissioned Ethereum blockchain and IPFS to improve transparency and security in EHR management. Smart contracts are also integrated for automating healthcare processes such as claims processing and drug supply chain management [31]. Finally, research work on blockchain for secure management of healthcare data presents a hybrid framework embracing Ethereum, Hyperledger Fabric, and IPFS. Thus reaching better security, transparency, and efficiency by enforcing consent and access control of patients through smart contracts, besides improving the data integrity and interoperability; still, high computational costs and network efficiency may need further optimization [32]. A wider view with respect to blockchain in the healthcare sector cites early-stage application to trace on its disruptive capability to enhance managerial aspects of medical data with regard to security, transparency, and interoperability [33]. The blockchain-based electronic consent management system, BlockMed, is designed on Ethereum and smart contracts to provide decentralized, privacy-preserving ways of accessing patient data. It assigns unique Ethereum IDs to patients and providers, ensuring consent-based access while keeping their anonymity intact. BlockMed improves interoperability and reduces costs by decreasing dependence on a

centralized infrastructure [34]. Finally, MedRec, one of the earliest blockchain-based implementations in healthcare, enables the management of electronic medical record access via smart contracts. This provides additional patient control and interoperability while also allowing secure and transparent sharing of data among providers and researchers [35].

2.2 Identified research gap

Despite significant advancements in applying blockchain Even though many attempts have been made to implement blockchain technologies in healthcare data management, some real gaps remain. These relate to trying to work out consent issues, scalability, and interoperability, privacy, and integration with health care management systems. The main research gaps identified are:

1. **Dynamic Consent Management:** While the use of smart contracts does help in automating the processes of giving consent, the real-time secure and transparent management of updates to patient preferences as well as dynamic revocation of consent is still troublesome[17].
2. **Scalability of Blockchain Systems:** The existing solutions for blockchain continue to struggle in efficiently handling very large volumes of sensitive healthcare data. The demand for real-time access to secure data, without violating any privacy or performance constraints, is still a burning issue[18].
3. **Interoperability Between Health Care Systems:** Existing blockchain implementations cannot integrate seamlessly into various health care systems, thereby creating data silos and hindering information sharing by providers, insurers, and regulators.
4. **Fine-Grained Access Control:** Although existing models may implement encryption mechanisms such as SHA-256, they often lack fine-grained dynamic access control, which allows the patient to specify time-limited or context-specific access to their data[11].
5. **Efficient Decentralized Data Storage:** IPFS may provide decentralized storage, but data availability, quick retrieval, and integration with blockchain networks remain significant challenges. More efficient mechanisms for critical healthcare data need to be developed that guarantee high availability and low latency[19].

3 Proposed Work

3.1 System Architecture

The proposed system after looking through the identified gaps the solution that can integrate blockchain technology with decentralized storage and smart contracts to create a robust EHR management platform.

1. **Blockchain Integration:** Connecting to the Ethereum blockchain, a decentralized ledger for consent management and logging transactions is implemented. Immutable data, such as actions and actions on the blockchain

themselves, are recorded for all interactions that take place across multiple transactions.

2. **Decentralized Storage:** Large EHR files are stored off-chain using the InterPlanetary File System (IPFS) for optimal management.. The EHR's metadata and hash are stored on the blockchain, allowing for swift and secure retrieval without any loss of sensitive data.
3. **Smart Contracts:** Processes such as user registration, consent management and data access are automate part of the system operation. Key smart contracts include:
    a. PatientRegistration.sol: Registers patients and manages their profile information.
    b. DoctorRegistration.sol: Allows doctors to register and access the system with patient consent.
    c. DiagnosticRegistration,sol: Allows diagnostic center to register and access the system.
    d. DiagnosticForm.sol: Adds new diagnostic records and records all the data sent by the diagnostic centre.
    e. DoctorForm.sol: Adds a new medical record to the records mapping, stored under the doctor's, and Retrieves all records created by the doctor.
    f. UploadEHR.sol: Facilitates secure uploading and tracking of EHRs.
4. **Real-time data exchange:** Instead of storing entire medical records on-chain (which is expensive and inefficient), we store the records off-chain (e.g., IPFS) and only store a hash (CID) of the data on-chain. Whenever a user needs the data, they retrieve the CID from the blockchain and use it to fetch the actual record from the off-chain storage in real-time.

So as discussed in the above advancing solutions to the earlier issues faced by the this approach can be used to eliminate the problem for data breaches that are mainly seen in the centralized databases, other issues majorly faced by the other application was the consent mechanism as a solution to the patient centric application that has been proposed, and the main issue where the storage has been a issue and the real-time exchange of healthcare data was major concern but since blockchain came as a adjoining theory for solving the underlying issues and can be eradicated by these approach and as a proposed solution a patient centric healthcare application with the patient being the main entity for the privilege access to its data and the main holder for the all the rights related to the data of its own. Another feature than has been proposed is that the lining of the diagnostic center in the Dapp for the profusely help the transfer of data from one end to another with no time limit.

3.2 Implementation Details

3.2.1 Tools & techniques

- Ganache: Provides a local blockchain environment for testing.
- Solidity: Used for writing smart contracts.

- Visual Studio Code: An integrated development environment (IDE) for coding and debugging.
- Metamask wallet: The entire process is triggered by users logging in on Metamask, a popular Ethereum wallet and browser extension for decentralized applications (dApps). Metamask offers secure access to the Ethereum blockchain, securing that only legitimate users can access the application.
- Frontend File Upload: Having been authenticated, users use the front-end interface to upload files. Such files do not get directly stored on the blockchain but get passed over to the Inter-Planetary File System (IPFS). IPFS stores files over a distributed network of nodes and maintains a decentralized storage system. The files get an individual content identifier CID, which makes it easier for you to retrieve the image later.
- Blockchain Transactions: the transaction information and access control information can be stored on the Ethereum blockchain. User uploads file-and-the-blockchain creates entry, and this entry could contain transaction details such as the CID of the file, the user's address, and time of upload. Such a thing gives transparency and non-changeability of the transaction history.
- Access Control: Smart contracts on the blockchain can manage access to share documents with specific doctors or people. The user can define these access permissions in those smart contracts to define who can read or view those files. Such permissions can be allocated to an individual file or a set of them (e.g. patient information or images).
- Sharing with Doctors: To share a patient's document or image with a specific doctor, the user is entering into a transaction via the front-end interface. This transaction also updates access control rules within the smart contract, giving the doctor permission to use the linked file in IPFS. The doctor can then download the file with the specified CID.
- Sharing of Diagnostic Imaging: Sharing of patient's Diagnostic imaging document or image with a specific doctor, the user is entering into a transaction via the front-end interface. This transaction also updates access control rules within the smart contract, giving the doctor permission to use the linked file in IPFS. The patient and doctor can then download the file with the specified CID.

Briefly, this architecture employs MetaMask for secure authentication, file storage decentralized via IPFS, and the Ethereum blockchain for transaction access and history. control. It allows users to securely upload and share files with specific individuals, i.e., physicians, while maintaining data integrity and transparency through blockchain technology.

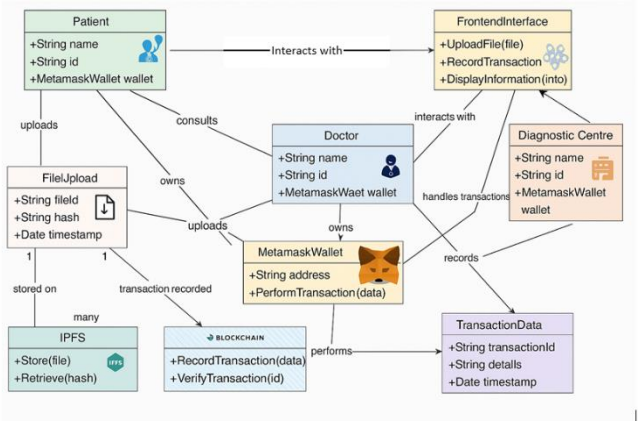

Fig. 1. Diagrammatic representation of the Proposed Methodology.

3.2.2 System Workflow

1. Registered the patient:
   - Initiate the register use case by a patient.
   - Register the patient and create account.
2. EHR Management:
   - A patient can now view EHR after registering.
   - A doctor can now view EHR and the patient records.
   - Uploading the EHR is possible for authorized users, who could be a patient or a doctor.
3. Permissions and Access Control:
   - Permission Grant to Patient for other users (like doctors or diagnostic centres) to access their EHR.
4. Treatment:
   - This system enables the doctor to treat the patient.
5. Dashboards:
   - Patient can access the Patient Dashboard for individual information.
   - Diagnostic Centre Admin can access the Diagnostic Dashboard for managing diagnostic data.
   - The doctor Dashboard can be used accessed the patient information and shared documents and write the treatment.
6. Diagnostic Centre Interaction:
   - System would interface the diagnostic centre admin, most probably through the diagnostic dashboard, in regard to patient data management through tests taken and results thereof.

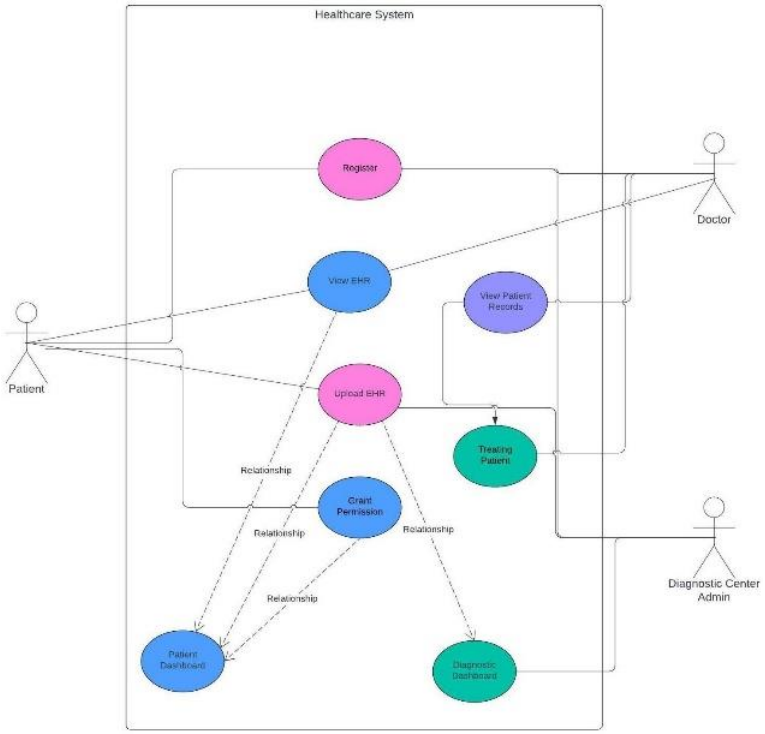

Fig. 2. Use Case Diagram.

4 Result & Analysis

1. User Registration and Authentication: Patients, doctors, and diagnostic centers register via MetaMask and authenticate using secure private keys.
2. Granting and Revoking Consent: Patients control data access by granting and revoking permissions to specific users through a simple interface.
3. Audit Trail: The blockchain logs every transaction, ensuring that all actions are traceable and secure.
4. Patients can decide who should be granted access to their medical records and when, so that they can be accessed as per guidelines.
5. With blockchain, the system offers a decentralized configuration that eliminates the risk of single points of failure and enhances reliability by storing data in synchronization with distributed systems.
6. Enhanced Security: Using advanced encryption techniques and blockchain, the system protects data and makes it inaccessible in a manner that prevents illegal alteration and enhances the integrity of the data.
7. It also supports effective and integrated operations through the sharing of data by all healthcare organizations in standardized formats, using

blockchain-based smart contracts.

8. It also has a large storage enhancements due to the usage of the IPFS in the modelling of the proposed application.

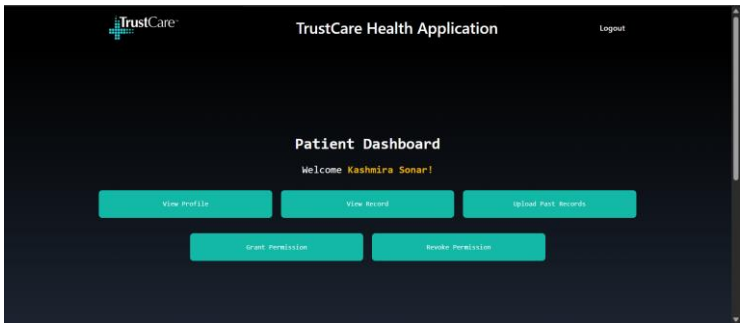

Fig. 3. Patient Dashboard.

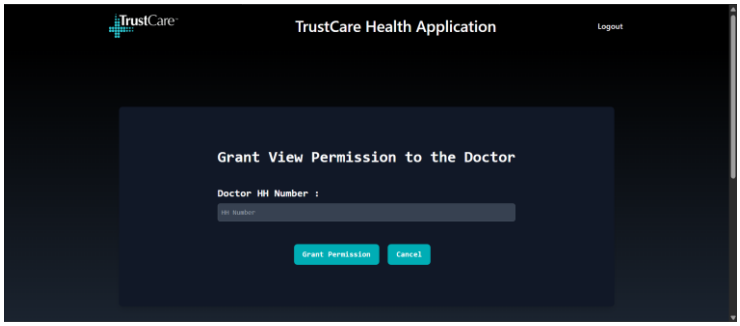

Fig. 4. Grant permission functionality.

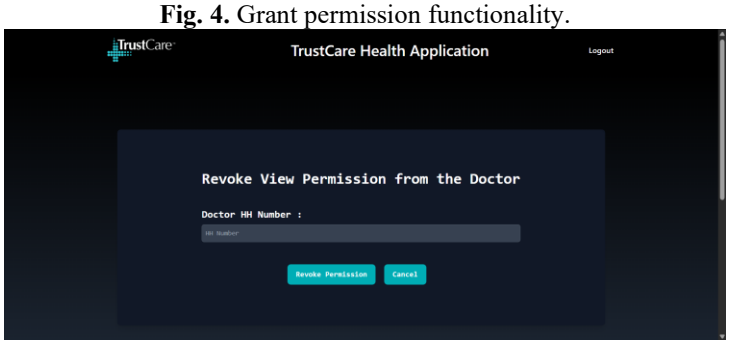

Fig. 5. Revoke permission functionality.

The Following approached implementation lets the patient to be easily able to grant the permission to doctor to whom they want to give the access to their data whenever need and when it not required to use further more the access can be revoked and even he can also have the records of his health from the diagnostic centre, rather than waiting for the time to get delivered, it can directly delivered from the diagnostic centre to the patient and can be easily accessed by the patient and since the doctor is already granted the permission they could also see the record without any delay in time. And the diagnosis can be made on the earliest this way the patient data can be

managed efficiently through the informed consent from the patient.

5 Conclusion

The use of blockchain technology in healthcare can be revolutionary in addressing some of the issues related to data security, patient control, and operational efficiency. Blockchain's decentralized architecture provides an additional layer of security and privacy using encryption and immutability, protecting sensitive health information from misuse and data breach. Patient control is the essence, where patients can determine who can access and use their data, with the result of creating transparency and trust. The blockchain technology, equally, also sustains interoperability and efficiency by allowing data sharing among healthcare stakeholders, thereby minimizing delay and administrative workload. Cost reduction and fraud prevention are ensured through such auditability and transparency as would guarantee the veracity of the medicinal products and bring down administrative costs. Through continuous development, these capabilities will provide safer, cheaper, and more effective systems of care for patients, carrying an immense transformational opportunity for the health sector. With the advent of blockchain technology, most nagging issues involving the management of intricate data in the health sector have been eased. For instance, dynamic consent management, or patient permission tracking and keeping up to date, was previously a complex and centralized affair, but is now handled more simply by smart contracts which offer real-time tracking and enforcement of consent. Issues of handling large volumes of transactions in healthcare are also taken care of by blockchain technology and its scalable solutions that have been enhanced by layer-2 protocols. Furthermore, interoperability between heterogeneous systems of healthcare is supported by blockchain-based standardization which allows movement of information between systems with no limitations. In addition, emerging technologies such as the Interplanetary File System (IPFS) offer decentralized means of storing or accessing large quantities of medical information efficiently, enhancing data accessibility and resilience. All these are innovations support the security and openness of the healthcare system with patient empowerment.

6 Future Scope

There is huge potential for blockchain to revolutionize the healthcare industry as a promise to redefine data storage, exchange, and security.

1. Compliance: Compliance with laws such as HIPAA and GDPR is mandatory in order to secure patient data. Future use cases of blockchain must be aligned with strict security and privacy guidelines for compliance.
2. Evolutions in Blockchain Technology: Future solutions like scalability enhancements and Layer 2 solutions will allow efficient processing of extensive healthcare data sets. Interoperability between blockchains will secure global data sharing, while enhanced privacy features and advanced smart contracts will

automate complicated healthcare processes like predictive analytics and insurance claims.

3. Growth potential: The use of blockchain could be extended to include pharmacies, payers, and government entities that may want to use devices for real-time data sharing with the Internet of Things. Together with AI/ML, blockchain would enable predictive and advanced analytics and personalized medicine with patient's control of their information.
4. Long-Term Effect on Healthcare: With its capability to build trust and transparency, blockchain will make patient-provider relationships stronger and global disease surveillance as well as care coordination better. It will curb healthcare fraud, enhance value-based care, and decrease costs by making it more efficient and outcome-focused for patients.
5. The more blockchain evolves, the more it will be integrated with new technologies and regulating compliances that will free up new opportunities, propelling long-term healthcare security, efficiency, and patient-care enhancement.

References

1. Shahrin Chowdhury, Pasika Ranaweera, Anca D. Jurcut, 23 - Blockchain for security and privacy in the smart healthcare, Blockchain and Digital Twin for Smart Healthcare, Elsevier, 2025, Pages 453-502, ISBN 9780443303005, https://doi.org/10.1016/B978-0-443-30300-5.00025-7.
2. Sahu H, Choudhari S, Chakole S (June 26, 2024) The Use of Blockchain Technology in Public Health: Lessons Learned. Cureus 16(6): e63198. doi:10.7759/cureus.63198
3. Aghahosseini, Hossien and Sakhaei-nia, Mehdi, Interoperability and Standards in Blockchain-based EHR, Advances in the Standards & Applied Sciences}, 2024, Standard Research Institute, doi = {10.22034/asas.2023.420797.1043}.
4. Dhingra, S., Raut, R., Naik, K., & Muduli, K. (2024). Blockchain technology applications in healthcare supply chains–A review. *IEEE Access*.
5. Mahmood, R., & George, V. (2024, February). Review on Blockchain-Enabled Techniques for Secure Storage and Sharing of Patient Healthcare Records. In 2024 Second International Conference on Emerging Trends in Information Technology and Engineering (ICETITE) (pp. 1-7). IEEE.
6. Er. Naveen Chander, Rohit Chaudhary, Simran Arora, Mayank Prakash, Anmol Gajrani, Ansh Bahl (2023), Decentralized Healthcare System using Blockchain, INTERNATIONAL JOURNAL OF SCIENTIFIC RESEARCH IN ENGINEERING AND MANAGEMENT (IJSREM), VOLUME: 07 ISSUE: 12.
7. K. Varshini Naik, T. Vijaya Murari and T. Manoj, "A Blockchain Based Patient Consent Management Technique for Electronic Health Record Sharing," 2022 IEEE 7th International Conference on Recent Advances and Innovations in Engineering (ICRAIE), MANGALORE, India, 2022, pp. 214-219, doi: 10.1109/ICRAIE56454.2022.10054337.
8. Oladele, James & Ojugo, Arnold & Odiakaose, Christopher & Emordi, Frances & Reuben, Abere & Nwozor, Blessing & Ejeh, Patrick & Geteloma, Victor. (2024). BEHeDaS: A Blockchain Electronic Health Data System for Secure Medical Records Exchange. Journal of Computing Theories and Applications. 2. 1-12. 10.62411/jcta.9509.
9. Hira , F. A., Khalid, H. ., & Md Moshiul, A. . (2024). Blockchain-Based Electronic Health Records: Revolutionizing healthcare in Malaysia. *Asia Pacific Journal of Health Management*, *19*(1). https://doi.org/10.24083/apjhm.v19i1.2621
10. Abeer Z. Al-Marridi, Amr Mohamed, Aiman Erbad, Optimized blockchain-based healthcare framework empowered by mixed multi-agent reinforcement learning, Journal of Network and Computer Applications, Volume 224, 2024, 103834, ISSN 1084-8045,

https://doi.org/10.1016/j.jnca.2024.103834.

11. S. Datta and S. Namasudra, "Blockchain-Based Smart Contract Model for Securing Healthcare Transactions by Using Consumer Electronics and Mobile-Edge Computing," in IEEE Transactions on Consumer Electronics, vol. 70, no. 1, pp. 4026-4036, Feb. 2024, doi: 10.1109/TCE.2024.3357115.
12. Tahir, N. U. A., Rashid, U., Hadi, H. J., Ahmad, N., Cao, Y., Alshara, M. A., & Javed, Y. (2024). Blockchain-Based Healthcare Records Management Framework: Enhancing Security, Privacy, and Interoperability. *Technologies*, *12*(9), 168.
13. Jakhar, A.K., Singh, M., Sharma, R. et al. A blockchain-based privacy-preserving and access-control framework for electronic health records management. Multimed Tools Appl (2024). https://doi.org/10.1007/s11042-024-18827-3
14. Sharma, M., Singh, S., Deep, A., Garg, D., & Kumar, A. (2024, March). Blockchain's Frontier: Enhancing Data Security and Collaboration for Healthcare. In 2024 11th International Conference on Reliability, Infocom Technologies and Optimization (Trends and Future Directions)(ICRITO) (pp. 1-6). IEEE.
15. Rohini, K. R., Rajakumar, P. S. & Geetha, S. (2024). Smart Patient Consent Management Model for Health Information Exchange Based on Blockchain Technology. Journal of Computer Science, 20(7), 730-741. https://doi.org/10.3844/jcssp.2024.730.741
16. Masood, I., Daud, A., Wang, Y. *et al.* A blockchain-based system for patient data privacy and security. *Multimed Tools Appl* 83, 60443–60467 (2024). https://doi.org/10.1007/s11042-023-17941-y
17. Husnain, G., Ullah, Z., Mohmand, M. I., Qadir, M., Alzahrani, K. J., Ghadi, Y. Y., & Alkahtani, H. K. (2024). HealthChain: A blockchain‐based framework for secure and interoperable electronic health records (EHRs). IET Communications, 18(19), 1451-1473.
18. Dadhania, A., & Patel, H. (2024). HEALTHSOLID 4.0: A NOVEL SOLID-POD AND BLOCKCHAIN-ENABLED FRAMEWORK FOR ROLE-BASED ACCESS CONTROL AND SECURE HEALTHCARE INFORMATION EXCHANGE. International Journal on Information Technologies & Security, 16(3).
19. Boumezbeur, Insaf & Zarour, Karim & Keddari, Dounia & Boutouatou, Farah & Benzagouta, Yasser Nassim & Harkat, Imane & Meriem, Seghiri. (2024). Secure EHR Sharing Using Blockchain and IPFS. 42. 1-14.
20. Akash Singh, Deepika Sharma(2024), Enhancing Patient Consent Management through Blockchain Technology: A Promising Approach for Healthcare Data Security, INTERANTIONAL JOURNAL OF SCIENTIFIC RESEARCH IN ENGINEERING AND MANAGEMENT 08(03):1-5, DOI:10.55041/IJSREM29509
21. Charles, W. M., van der Waal, M. B., Flach, J., Bisschop, A., van der Waal, R. X., Es-Sbai, H., & McLeod, C. J. (2024). Blockchain-based dynamic consent and its applications for patient-centric research and health information sharing: protocol for an integrative review. *JMIR Research Protocols*, *13*(1), e50339.
22. Atadoga, A., Elufioye, O. A., Omaghomi, T. T., Akomolafe, O., Odilibe, I. P., & Owolabi, O. R. (2024). Blockchain in healthcare: A comprehensive review of applications and security concerns. *International Journal of Science and Research Archive*, *11*(1), 1605-1613.
23. Rohini, K. R. and Rajakumar, P. S. and Geetha, S., Smart Patient Consent Management Model for Health Information Exchange Based on Blockchain Technology, journal, April 2024, doi = 10.3844/jcssp.2024.730.741.
24. Kumar, V., Sachdeva, S., & Pawar, V. (2024, July). Blockchain-Enabled Integration and Coordination for Decentralized E-Health Systems. In 2024 Third International Conference on Electrical, Electronics, Information and Communication Technologies (ICEEICT) (pp. 1-8). IEEE.
25. Kapoor, V., & Vadagasiya, D. (2024, April). SECURE-MEDSHARE: Decentralized Patient Data Sharing for Improved Healthcare. In 2024 International Conference on Advances in Data Engineering and Intelligent Computing Systems (ADICS) (pp. 1-6). IEEE.
26. Mishra, D. P., Rajeev, B., Mallick, S. R., Lenka, R. K., & Salkuti, S. R. (2025). Efficient blockchain based solution for secure medical record management. Int J Inf & Commun Technol, 14(1), 59-67.
27. Haddad A, Habaebi MH, Elsheikh EAA, Islam M.R, Zabidi SA, Suliman FEM (2024) E2EE enhanced patient-centric blockchain-based system for EHR management. PLoS ONE 19(4):e0301371. https://doi.org/10.1371/journal.pone.0301371

28. Seun Adeoye et al, Blockchain for secure and interoperable electronic health records (EHRs): Challenges and opportunities in Decentralized Healthcare Data management, Cognizance Journal of Multidisciplinary Studies, Vol.4, Issue.11, November 2024, pg. 340-356
29. Sivaprakash, P., Charaan, R. D., Ithayan, J. V., Sankar, M., Chithambaramani, R., & Marichamy, D. (2024, August). IPFS-based Blockchain Enabled System for Secure Data Storage and Access in Healthcare. In 2024 Second International Conference on Intelligent Cyber Physical Systems and Internet of Things (ICoICI) (pp. 203-208). IEEE.
30. Haddad, A., Habaebi, M. H., Suliman, F. E. M., Elsheikh, E. A., Islam, M. R., & Zabidi, S. A. (2023). Generic patient-centered blockchain-based EHR management system. Applied Sciences, 13(3), 1761.
31. Ponsam, J. G., Duvvuri, S., & Roy, S. (2023, August). Electronic healthcare management system using blockchain technology. In 2023 International Conference on Circuit Power and Computing Technologies (ICCPCT) (pp. 869-877). IEEE.
32. Begum, K., Rashid, M. M., Mozumder, M. A. I., & Kim, H. C. (2023, December). Leveraging the power of blockchain for secure healthcare data management system. In 2023 26th International Conference on Computer and Information Technology (ICCIT) (pp. 1-6). IEEE.
33. Abid Haleem, Mohd Javaid, Ravi Pratap Singh, Rajiv Suman, Shanay Rab, Blockchain technology applications in healthcare: An overview, International Journal of Intelligent Networks, Volume 2, 2021, Pages 130-139, ISSN 2666-6030, https://doi.org/10.1016/j.ijin.2021.09.005.
34. Das, Arghya & Das, Ajanta. (2020). BlockMed: Blockchain-based Electronic Consent Management for Secure and Privacy-Protected Healthcare Interoperability (Preprint). 10.2196/preprints.23296.
35. Azaria, A., Ekblaw, A., Vieira, T., & Lippman, A. (2016, August). Medrec: Using blockchain for medical data access and permission management. In *2016 2nd international conference on open and big data (OBD)* (pp. 25-30). IEEE.

Assessing YouTube Title-Content Alignment using NLP Framework

Tanneru Sai Ramya[1], Maturi Bhavya Sri[2], and Arul Elango[3]

[1] Vignan's Foundation for Science, Technology and Research, Guntur, India
sairamyatanneru@gmail.com
[2] Vignan's Foundation for Science, Technology and Research, Guntur, India
bhavyamaturi927@gmail.com
[3] Vignan's Foundation for Science, Technology and Research, Guntur, India
arulelango2012@gmail.com

Abstract. Accurate YouTube video titles have an important function in building user trust, encouraging engagement, and reducing clickbait instances. This paper proposes an end-to-end system for assessing semantic correspondence between video titles and their contents through transcript-based methods. In order to create a large, heterogeneous dataset regardless of YouTube's API, we use tools such as yt-dlp, BeautifulSoup, and youtube-transcript-api to retrieve video metadata, transcripts, summaries, and thumbnails. Preprocessing the text data follows feature extraction through TF-IDF and deep embedding techniques. The relevance of title and content is measured through the implementation of multiple models, including Cosine Similarity, Universal Sentence Encoder, Sentence Transformer, Doc2Vec, BM25Okapi, and Word2Vec. A relevance score is calculated for every video, where users can make an informed choice whether the title is representative of the content or not. Experimental outcomes emphasize the greater performance of deep learning models in identifying semantic mismatch, hence contributing to automated content moderation as well as better viewer experience overall.

Keywords: Title-Content Relevance, Clickbait Detection, Natural Language Processing, Semantic Similarity, Transcript Fetching

1 Introduction

YouTube currently has more than two billion logged-in users every month, which has helped it grow into one of the largest sources of content across nearly all domains, including education, entertainment, news, and technology. While the open nature of YouTube has catalyzed the diversity of content, it has also fostered the rise of misleading and sensationalized video titles popularly known as clickbait. Video titles frequently exaggerate or misrepresent the actual content of a video, and we feel this is misleading to users, artificially inflates view counts, and harms the credibility of an otherwise positive and beneficial platform. This

phenomenon suggests the need for automated approaches to analyze the degree to which a video title is semantically related to the content of the video.

Here, we define the title-content inconsistency problem and propose an automated system to measure the semantic relationship (or degree of correspondence) between YouTube video titles and transcripts. We take the transcript (whether uploaded or automatically generated) to be a stand-in for the content of the video, rather than using the video itself as the content. We measure the title against the transcription material to assess the levels of accuracy with respect to the material presented. This way we can find semantically incompatible or misleading title-content pairings, both of which contribute to an understanding of clickbait or low-quality content.

To enable our analyses on a large scale, we assembled a dataset of around 12,000 videos with a range of contexts. Previously, we had relied on the YouTube API for acquiring video data, and categorizing videos based on thumbnails or titles and descriptions, but for this project, we turned to publicly available tools for collecting metadata, titles, and transcripts that we could use to examine videos on a much larger sample scale, and without the concerns of being rate limited or needing an API key. For this project, our data pipeline makes use of yt-dlp, BeautifulSoup, and youtube-transcript-api to acquire data about and subsequently transcripts from videos in a scalable, public way. The textual data was then cleaned comprehensively (normalization, tokenization, noise removal, etc.) so we could conduct our semantic analysis on the transcripts.

We applied various Natural Language Processing (NLP) models to measure title-transcript similarity, and employed both lexical models (e.g. TF- IDF, BM25) as well as neural embedding based models (e.g. Word2Vec, Doc2Vec, Universal Sentence Encoder) to gather relevance scores representing the semantic similarity between a title and the transcript, and hence determine to what degree a title is relevant to the actual content of a video. Our exploratory analysis showed that embedding-based models yielded substantially better precision and recall than Lexical models in distilling semantic and contextual relationships in text to establish title-content mismatches.

The methodology we have proposed serves as a valuable foundation for au-automated clickbait detection, while also providing avenues for broader applications like content moderation, recommendation filtering, and quality assurance at video-sharing websites. This work will help in improving the transparency and trustworthiness of online video content by using scalable data collection and a multi-model similarity approach.

2 Literature Review

Cer et al.[1] introduced the Universal Sentence Encoder (USE), a deep learning model designed to generate fixed-length sentence embeddings that capture both syntactic and semantic information. The authors proposed two model variants—one based on the Transformer architecture and the other on a Deep Averaging Network (DAN)—offering a trade-off between computational efficiency

and accuracy. USE demonstrated strong performance across various NLP tasks such as semantic similarity, text classification, and clustering, even with limited labeled training data. Its ability to encode entire sentences into high-dimensional vectors enables effective sentence-level semantic comparisons, which is particularly beneficial for applications like content relevance assessment and clickbait detection. The model's robustness and generalizability, achieved through training on diverse corpora including Wikipedia and online forums, make it highly suitable for transfer learning scenarios and large-scale text analysis frameworks.

Pant et al.[2] highlighted the effectiveness of BeautifulSoup, a Python-based web scraping library, in extracting both structured and unstructured data from web pages. The study emphasized its ease of use, lightweight nature, and capability to parse HTML and XML content for applications such as news mining, academic research, product analysis, and market intelligence. Compared to more complex tools like Selenium and Scrapy, BeautifulSoup offers a more accessible solution for static content extraction with lower computational overhead. The authors also underscored the importance of ethical scraping practices, such as adhering to website policies and avoiding excessive server load. Their findings affirm BeautifulSoup as a reliable and scalable tool for automated data acquisition, especially in scenarios where APIs or direct database access are unavailable or restricted.

Lahitani et al.[3] investigated the application of Term Frequency–Inverse Document Frequency (TF-IDF) combined with Cosine Similarity for automated essay assessment, demonstrating its effectiveness in evaluating semantic closeness between student-written responses and expert references. The study emphasized the role of text preprocessing techniques—such as tokenization, case folding, and stop word removal—in enhancing the accuracy of similarity measurement. By representing documents as vectors in a multidimensional space, the cosine of the angle between them was used as an indicator of similarity, with higher values reflecting stronger semantic alignment. Their findings validated the utility of this method for content-based evaluation, making it a reliable and interpretable approach for comparing textual content in educational and auto-mated scoring systems. This combination serves as a foundational method for assessing relevance between textual pairs, such as YouTube video titles and their corresponding transcripts.

Khennak and Drias[4] explored the effectiveness of the BM25 algorithm within the Probabilistic Relevance Framework, emphasizing its robustness in ranking documents based on term frequency, inverse document frequency, and document length normalization. Their work proposed an enhanced term-term similarity measure that leverages co-occurrence and proximity of terms to improve information retrieval accuracy in large-scale datasets. By considering both the frequency and contextual closeness of terms within documents, the BM25 model proved particularly adept at capturing the semantic relevance of longer textual content. This makes it a valuable method for tasks such as evaluating the alignment between video titles and their transcripts, where content length

and structure vary significantly. The study reinforces BM25's role as a powerful baseline for relevance scoring in modern text retrieval applications.

Jin et al.[5] proposed an enhanced approach for calculating word semantic similarity using the Word2Vec model, addressing limitations found in traditional dictionary-based methods. By leveraging distributed representations, Word2Vec captures contextual relationships between words, enabling the model to identify semantic similarity even when lexical overlap is minimal. The study compared Word2Vec's performance with conventional semantic dictionaries such as HowNet and Tongyici Cilin, demonstrating that the neural embedding-based approach yielded significantly higher accuracy in semantic similarity tasks. The authors also discussed optimization techniques such as Skip-gram and CBOW architectures, along with negative sampling and hierarchical softmax, to improve model performance. These insights affirm Word2Vec's suitability for applications requiring fine-grained semantic comparison, such as evaluating whether YouTube titles reflect the actual content of their transcripts.

Xu et al.[6] utilized the Doc2Vec model to generate dense vector representations of entire documents for the task of answer summarization on developer Q&A platforms. Unlike traditional word-level embeddings, Doc2Vec captures the overall semantic structure of longer texts by considering contextual relationships across sentences and paragraphs. The study introduced a multi-stage framework that included relevant question retrieval, salient answer extraction, and summary generation using vector-based similarity. Their approach effectively addressed challenges such as lexical gaps and redundancy in large textual datasets. The use of document embeddings allowed the system to retrieve and summarize content with high semantic relevance, demonstrating Doc2Vec's strength in handling non-factoid, context-rich queries. These capabilities make Doc2Vec particularly applicable to title-content relevance evaluation, where capturing the broader meaning of transcripts is essential.

Yao [7] introduced a procedure for automated sentiment analysis using the Natural Language Toolkit (NLTK), with specific emphasis on the VADER sentiment analysis tool. Yao (2019) focused on analyzing text reviews from datasets including Amazon product reviews, beer reviews, and movie reviews, and determined the sentiment using VADER. A model developed by the author takes a CSV file, which contains text and user ratings, extracts the text and user ratings, computes sentiment using VADER, and then analyzes accuracy using Pearson correlation and visualizations (boxplots and histograms). The results showed that the model produced good accuracy on small datasets, but accuracy decreased with increased amounts of text, partly due to context and order sensitivity problems. The conclusion of the paper reflected on the limitations of rule-based models, including VADER, in representing complex sentiment. The author suggested future work on developing a model on deep learning and TensorFlow with TFlearn to improve accuracy and scalability in prediction tasks related to sentiments.

Kaur et al. [8] suggested a model for automated essay scoring (AES) that encompasses syntactic analysis, semantic similarity, and sentiment. They sug-

gested a model with unique capabilities for evaluating student essays. Their system extracts and makes use of 23 features to assess essays, features being, among others grammar, structural coherence, semantic similarity (using graph-based methods), and sentiment polarity. The essays were scored using the neural network developed using the Kaggle ASAP dataset and performance was assessed using Quadratic Weighted Kappa (QWK). A QWK of 0.793 was achieved, meaning Kaur et al.'s [8] study showed strong agreement with human raters. They showed, among other things, that fewer higher quality features hold up comparatively well (robustness and redundancy) to lots of features by alternative models. They concluded that a combined approach using syntactic, semantic and sentiment features surpasses the traditional AES model, and they recommended that their next work will address specific weaknesses involving semantic models and to respectively, evaluate different neural architectures for assessments.

Varghese and Punithavalli [9] provided an overview of machine learning, natural language processing (NLP), ontology modeling, and sacred text analysis of the Bible, Tanakh, and Quran. The article described text mining in relation to TF-IDF, Word2Vec, and sentiment analysis in extracting semantic similarity from sacred texts. The authors provided a pipeline that would preprocess semi-structured sacred texts, represent them as vectors, and compare matches. This analysis identified the intersections of themes, words, and sentiments of a sacred text. Essentially, the study showed the feasibility of automatic sacred text comparison but recognized the challenges grace in each sacred text's unique language. The authors proposed future work that should emphasize model explainability while incorporating deep semantic models to uncover richer theological meaning.

Ibrahim et al. [10] created a document clustering system that employs TF- IDF vectorization and K-Means clustering to group documents by semantic similarity. The system ran on movie synopses from IMDB and Wikipedia and evaluated three different scenarios: raw data (not cleaned), cleaned data (standard scenarios), and stemmed data (meaning reduced to boring base forms). Both evaluations of internal metrics (cohesion) and external measures (purity, accuracy) showed best performance at K=20, and demonstrated significant improvements in clustering quality and runtime depending on whether or not the textual data had previously been preprocessed. Overall, this study demonstrates that clustering documents based on semantic similarities using TF-IDF and appropriate preprocessing was capable of successfully clustering and organizing large corpuses of documents. Future work can be considered as examining the inclusion of word embeddings or other multiple hierarchical clustering approaches to determine whether the better review of deeper semantic relationships can be made.

Dillon et al. [11] launched the TensorFlow Distributions library, which is an expansion of the TensorFlow framework, in that it allows one to do probabilistic programming in TensorFlow. The authors described how this library allows for modular construction of high-dimensional probabilistic models with two abstractions: Distributions and Bijectors. The paper went into great detail in showing

how TensorFlow Distributions allows for fast, numerically stable sampling, log-density calculation and differentiable operations needed for end-to-end training. Furthermore, the framework integrates with the computation graph from TensorFlow, and uses hardware acceleration (GPU/TPU) which makes it widely adopted for use in production systems, providing a scalable and composable way of developing deep probabilistic models.

Goldsborough [12] published an extensive review of TensorFlow as an open-source infrastructure offering deep learning capabilities. There were certain variables from the paper relating to TensorFlow's model of computation, based on the dataflow graph and distributed machine learning. In the author's review of TensorFlow and other frameworks, such as Theano and Caffe, the author utilized a method based on various dimensions of each framework such as expressiveness, flexibility and performance. The author made conclusions about TensorFlow's visualization capabilities through TensorBoard, advantages of strong API, and scalability across high performance hardware. The review concluded TensorFlow as a flexible and performant way to take advantage of TensorFlow for machine learning approaches in academic and industry.

Rawat et al. [13] presented an improved YouTube video downloader app written in Python. They have a GUI using PySimpleGUI, and they utilize an extensive media extractor library called yt-dlp. The authors noted that the features of their tool support high-definition video downloading, processing playlists and channels as bulk, and an adaptable user experience. According to the authors, the benchmarks for their application showed good amounts of resource usage and speedy performance, and they received very positive user feedback. The authors recognized the ethical issues related to copyright, and noted the responsible use of their application is important. The open-source distribution of their tool will drive improvements from the community.

Coats [14] developed a Python-based pipeline for analyzing acoustics and phonetics at scale across streamed content, with a specific emphasis on the hundreds of thousands of YouTube videos available on subjects pertinent to phonetics. The pipeline uses yt-dlp to acquire media from YouTube, the Montreal Forced Aligner to align audio with text, and Parselmouth-Praat to extract the relevant phonetic features from English phonetic text. After creating the pipeline, Coats delivered a case study on the / e / diphthong of North American English and analyzed the results of nearly 9 million tokens. The results represent expected dialectal variation, and also demonstrate the effectiveness of the pipeline as a tool for empirical phonetic analysis. The public availability and multiplicity of online multimodal content, especially from YouTube, has implications for linguistics as a whole and corpus-based linguistic research.

Méli, Coats, & Ballier [15] described two pipelines - PEASYV and YTPP - which enable phonetic scraping of YouTube videos. These pipelines provide an automated process to collect the ASR transcripts and audio to enable forced alignment for phonetic analysis. PEASYV provides the Penn Forced Aligner and SPPAS software while YTPP provided the Montreal Forced Aligner. Both of these pipelines come with the ability to integrate with Praat and run other analyses

like formant measurements. PEASYV allows for the comparison of alignments from two different aligners to identify and resolve discrepancies in the alignment reliability. These pipelines will allow for the user to engage in time and place-specified phonetic data collection from sources online as well as facilitate the conduct of linguistic research that measures vowel spaces and prosody analysis on YouTube videos.

While existing studies have demonstrated the strengths of individual similarity models in varied domains ranging from academic writing assessment to information retrieval and summarization there is a notable lack of integrated approaches that evaluate video title-content relevance using a combination of both traditional and deep learning methods. This study addresses that gap by proposing a unified, multi-model framework that blends TF-IDF, BM25, and neural embedding models like Word2Vec, Doc2Vec, and USE. By leveraging these diverse methodologies, our work introduces a scalable and interpretable system for detecting semantic inconsistencies between YouTube titles and transcripts, with broader implications for content moderation, user trust, and platform integrity.

3 Dataset Collection and Processing

3.1 Overview

In this research, a dataset of around 10,000 YouTube videos was compiled from a variety of categories including Technology, Food, Entertainment, and Facts. The data was collected in a way that allows it for scalable and API-indifferent title-content relevance analysis using Natural Language Processing (NLP) methods. The extraction method was built to ensure consistency, reliability, and coverage in addressing common challenges found in extracting online data.

3.2 Data Collection Methodology

The data was gathered through an automated pipeline that scrapes metadata, retrieves video transcripts, and prepares the content for analysis. The process was divided into key components:

Metadata Extraction Using the BeautifulSoup library, we performed web scraping to extract metadata from videos. We parsed the YouTube searches page and automatically extracted information including video IDs, titles, and URLs. This process was relatively advantageous as it did not rely on the official YouTube API. This allowed us to be flexible and scalable, where content scraping of YouTube searches or generalizations could lead our project off in an interesting slight direction. Automated Wikipedia searches allowed us to begin the project by harvesting metadata using some of the keywords we used for the categories of interest, such as "Artificial Intelligence, "Machine Learning," "Street Food," "Comedy Clips," and "Amazing Facts."

- **Video Title:** Utilized as the reference text for semantic analysis alongside the transcript.
- **Video ID and URL:** Distinct identifiers that enable access to transcripts and video viewing.

Transcript Retrieval Following the metadata, the subsequent process was obtaining the transcripts from Youtube with the help of the youtube_transcript_api library. The library allows the user to simply pull from Youtube's database of subtitles, containing all uploaded by hand and auto-generated transcripts for any language. The requests for each video ID's transcripts were the following:

- Attempting to retrieve English-language transcripts for each video ID.
- Logging errors for videos with disabled transcripts or those unavailable.
- Filtering out non-English content due to limitations in multilingual support.
- Flagging and removing videos with missing or invalid transcripts to maintain dataset quality.

A major obstacle during this phase was knowing the limits for making requests from YouTube's servers to not be throttled. When making multiple sequential requests to YouTube, occasionally, the server response was HTTP 429 ("Too Many Requests") and blocked the IP for an unspecified time.Below is the representative of log message:

> Could not retrieve a transcript for the video https:[Vedio URL]! This is most likely caused by: Request to YouTube failed: 429 Client Error

In response, the pipeline was refined to incorporate automatic retries, random delays between requests, and optional rotating proxies to mitigate the risk of blocking. As a result, a small amount of videos had to be omitted due to residual errors or inaccessible transcripts.

Data Cleaning and Refinement Preprocessing began with a cleaning and processing step to prepare the raw dataset. The preprocessing methods included:

- **Transcript Validation:** Videos with missing/disabled or invalid transcripts (the transcripts were tagged as "Transcripts Disabled" or "Error Fetching Transcript") were automatically dropped to mitigate the amplification of "relevance scores" when evaluating models.
- **Duplicate Elimination:** Duplicate entries that possessed the same titles, URLs or transcripts were identified utilizing hash values and text similarity. Duplicate entries may have caused repetitions of content in transcripts and the duplication process increased the chance of biased learning.
- **Standardization:** Text fields like titles and transcripts were normalized to a consistent format by converting all text to lowercase, removing extra spaces, and modifying unconventional punctuation (e.g., ” to ’ or . . . to ..., etc.) This created a more uniform format while decreasing discrepancies.

- **Schema Enforcement:** Each record was examined against a schema to ensure that each record at least had a valid title, url, and cleaned transcript. It also ensured that the formatting template was consistent throughout the dataset.
- Converted the cleaned dataset into tabular form, and saved in accessible files.

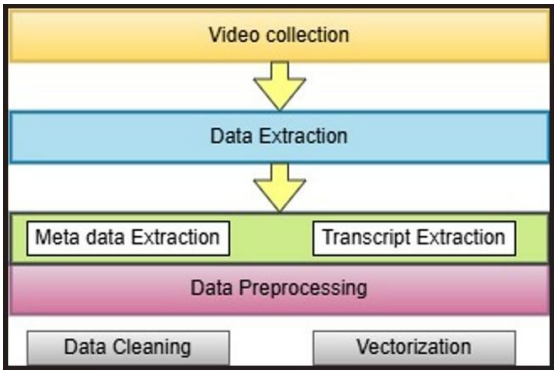

Fig. 1. Pipeline for Data Collection and Preprocessing

3.3 Challenges Encountered

Collecting and curating the dataset for this study raised a number of technical and methodological issues that illustrate the difficulty of large-scale data extraction from dynamic online environments (YouTube in particular). These issues were specifically related to the following factors:

- **Transcripts Disabled by Uploaders:** Many videos had transcripts turned off by uploaders or would not extract due to platform restrictions, creating data gaps as well as, potentially, some bias in the content analysis.
- **Language Constraints:** The framework only focused on English transcripts and therefore excluded all videos that had non-English subtitles and created limitations on linguistic and cultural diversity, affecting generalizability.
- **Incomplete and Erroneous Transcript Data:** In some cases the transcript extraction returned errors ("Error Fetching Transcript"), and in all of those cases I had to do more filtering and clean up to only get valid texts.
- **Dynamic Content and JavaScript Rendering:** YouTube content is dynamic and built using Javascript, and because of this we've had static scraping challenges, and could not extract accurate data at all using simple URL parsing statements.

- **Data Quality Assurance:** The raw dataset itself contained duplicate, encoding issues, and missing values that required great cleaning effort as it was difficult to maintain uniform data quality.

These challenges highlight the inherent difficulties of automated data collection from online video platforms and underscore the importance of developing adaptive, robust methodologies to ensure the creation of a high-quality, representative dataset for subsequent analysis.

3.4 Final Dataset Storage

In support of analysis and validation, the processed dataset was kept in:

- CSV format for structured programmatic access and data manipulation.
- Excel format (.xlsx) for manual inspection and review by the researchers. These formats facilitate ease of use in the various, unique stages of preprocessing, model training, and result interpretation.

These formats ensure ease of use across different stages of preprocessing, model training, and result interpretation.

4 Proposed Methodology

4.1 Overview

The method that we will present consists of a hybrid multi-model pipeline for assessment the semantic relevance between YouTube video titles and transcripts. The strength to our method is that it is encompasses a structured approach from creating category-specific datasets, systematic data preprocessing, and applying a varied assortment of similarity models (statistical and deep learning). While other systems typically deploy a similarity metric or relevance model of their choice (one model), our approach leverages multiple parameters to compare the alignment of the two pieces of text, for example pruning from verbal/lexical, structural/syntactic, and semantical layers.

The proposed approach is particularly justified as it is critical to achieve a degree of accuracy to assess for integrity in the metadata to check compliance across video categories and nuances in linguistic use in user-generated content. Statistical models such as TF-IDF and BM25 are efficient and interpretable while semantic embedding models such as Universal Sentence Encoder, Word2Vec and Doc2Vec, model some degree of semantic context. This hybrid and integrated approach aims to achieve relevance scoring that is flexible, scalable and reliable.

4.2 Data Preprocessing and Normalization

To ensure accurate and meaningful relevance analysis of title-content relations, the YouTube dataset that was obtained is assembled into a general preprocessing

and normalization workflow. The objective is to clean, standardize and structure the text from the video titles and transcripts to remove noise while discarding irrelevant information. During the initial processing of the dataset, several natural language processing (NLP) techniques and libraries created in Python are deployed, including, NLTK, SpaCy, Scikit-learn, and Gensim, for synthesizing the dataset and preparing it for similarity modeling.

The raw data, which consisted of a tabular file with columns for video ID, video title, video URL, and transcript, underwent various layers of preprocessing. Each layer sought to combat a certain type of noise or impreciseness endemic in real-world user-generated textual material.

Data Cleaning Raw text typically consists of noise, including undesired characters, punctuation, and formatting artifacts, which can impact downstream analysis. Regular expressions (using the re library) are used to strip special characters and symbols, and text is normalized to lowercase via Pandas string operations. The process of removal is further supplemented by BeautifulSoup HTML tags and embedded metadata in order to extract meaningful textual content. To retain some form of consistency in the data, NLTK's langdetect or fasttext will automatically identify non-English transcripts and exclude them from the dataset to achieve linguistic uniformity. Stopword Removal Predefined stop word lists from NLTK and SpaCy are used to remove high-frequency functional words such as "the," "is," "and," which are devoid of semantic value.

Stopword Removal Predefined stop word lists from NLTK and SpaCy are utilized to eliminate high-frequency functional words (e.g., "the," "is," "and") that do not contribute semantic value. Removing these tokens improves both the interpretability and computational efficiency of similarity models by retaining only the most informative terms.

Tokenization and Lemmatization Tokenization is performed utilizing NLTK or SpaCy to segment text into discrete (word) unit tokens. Each of these tokens is then lemmatized to its base word using either WordNetLemmatizer (NLTK) or SpaCy language models. The benefits of standardizing, includes improved semantic comparability which support the model's ability to identify different morphological variants as equivalent.

Noise Reduction and Length Filtering The extra step of preprocessing in- cludes the expulsion of numerical digits, space normalization function, as well as driving out duplicate entries. The length-based filtering takes care of expelling title or transcription items that are too brief since they do not appear to offer sufficient contextual information. These additional measures ensure that the comparisons of high-quality, content-weighted samples are maintained.

Structured Output After various preprocessing stages were implemented, the dataset was finally saved in a new CSV file as follows:

- Video ID – which is preserved from the original dataset to create traceability.
- Video Title – which is a cleansed and standardized form of the Video Title.
- Preprocessed Transcript – which is a fully normalized and filtered version of the Transcript Text.

This CSV file is the standardized input into the similarity modeling stage which ensured all models processed high-quality linguistically consistent text.

4.3 Models Applied on Preprocessed YouTube Data

After preprocessing, a variety of NLP and machine learning models are used to measure the semantic similarity between a video title and the transcript text. These models include classic statistical models, as well as modern models that use embeddings.

TF-IDF with Cosine Similarity The TF-IDF (Term Frequency-Inverse Document Frequency) model in Scikit-learn converts text to sparse vector representations for scoring words relative to a document based on frequency in both the document and whole dataset. The angular distance between TF-IDF vectors (the video title and transcript) is then measured as cosine similarity. This method is efficient and works well for short-text distance calculation for a baseline relevance assessment.

BM25 (Okapi BM25) The Rank-BM25 library implements the BM25 model, which builds on TF-IDF by adding term frequency saturation and normalizing for document length. The probabilistic ranking function replaces the video title with a query, and then ranks transcript content based on how well it matches. The BM25 is advantageous for longer documents in that it avoids the biases seen as a result of potential transcript length variations, thus providing fairer relevance score rankings.

Universal Sentence Encoder (USE) The Universal Sentence Encoder (USE) model, provided on TensorFlow Hub, takes sentences as input as text and produces high-dimensional embeddings which can represent some aspects of semantics and syntax of language. The model has been tuned to generalize over a text corpus and has both transformer and deep averaging network (DAN) architectures. Cosine similarity was used to measure the similarity between the embeddings of the title and the transcript. USE can compare embeddings which are more contextual and meaningful in general than keyword-based embeddings. It also provides usefulness for identifying overlapping for other paraphrased or semantically similar titles that do not share overlap at the lexical level.

Word2Vec Word2Vec, implemented by Gensim, is a neural embedding model that learns distributed representations of words based on how they are used with other words. Two models, Skip-gram and CBOW (Continuous Bag of Words), are used to train the embeddings:

- **Skip-gram:** Skip-gram predicts the surrounding words of a target word, which is effective with small datasets;
- **CBOW:**CBOW predicts the target word based on its surrounding context, which is computationally efficient.

The model was trained on the combined corpus of video titles and transcripts, and it learned the nuanced semantic relationships between words during training. Cosine similarity can be used to identify relevance between the title and transcript embeddings at the phrase level, and assist in identifying misplaced words that also have semantic relevance.

Doc2Vec Doc2Vec is an updated Word2Vec model which, unlike the latter, gives embeddings for documents instead of instant word embeddings. Using Gensim, the whole transcripts are encoded into vector representations capturing semantic structures with the help of these different training settings:

- **Distributed Memory (DM):** Learns context-sensitive document vector models by predicting words on the basis of word and document embedding.
- **Distributed Bag of Words (DBOW):** Learns document vectors, predict- ing other randomly chosen words from the document.

Doc2Vec now builds for each transcript a dense vector representation, which can be compared to that of its title by cosine similarity. This model is very reliable since it encapsulates the theme reflected between the long form content and a compressed title, which could eventually indicate semantic coherence.

Each model produces a CSV that contains the following attributes: video ID, video title, transcript, and relevance score that allows for downstream type analysis and benchmarking of the models.

Thus, they are the bases of title-content relevance model functions that further enable a much-rounded evaluation multiplexing perspectives on video meta-data integrity.

Fig.2 shows the architecture of the YouTube title-content relevance as-assessment system. The input is a YouTube video URL, from which relevant data such as the title and transcript are extracted. This information is fed into a number of Natural Language Processing (NLP) models used to assess title relevancy to the actual video content. The system uses several models for this analysis namely: TF-IDF + Cosine Similarity, BM25 (Okapi BM25), Word2Vec
+ Cosine Similarity, Doc2Vec + Cosine Similarity, and the Universal Sentence Encoder (USE). Each model produces a similarity score between the title and transcript, with their similarities combined into a relevance score, which will serve as the output.

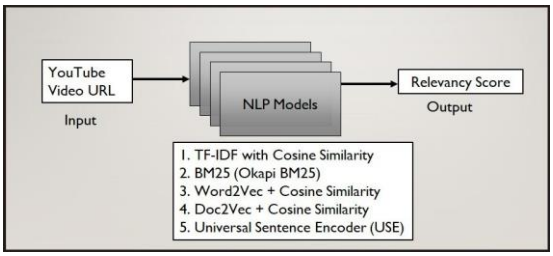

Fig. 2. System architecture for evaluating YouTube video title-content relevancy using Various NLP models

5 Results and Discussion

5.1 Title-Content Relevance Scoring

A processed dataset was analyzed through the application of multiple models to determine the level of relevance of a video's title to its true content. The models used were TF-IDF with Cosine Similarity, BM25 ranking, Word2Vec, Doc2Vec, and deep-learning models such as the Universal Sentence Encoder (USE). The relevance score varies from 0 to 1, to indicate the semantic similarity between each title and transcript.

- A higher score (closer to 1) signifies that the title is closely aligned with the content.
- A lower score (closer to 0) implies that the video may have violations, clickbait, or an inconsistent title.
- The average relevance score was calculated for the sample of videos to allow assessment of performance across models.

5.2 Comparative Model Performance

Table[1] presents the average relevance scores computed across the dataset using different models.

Table 1. Model Performance for Title-Content Relevance

Model	Average Relevance Score
TF-IDF + Cosine Similarity	0.62
BM25 Ranking	0.68
Word2Vec + Cosine Similarity	0.74
Doc2Vec + Cosine Similarity	0.78
Universal Sentence Encoder (USE)	0.82

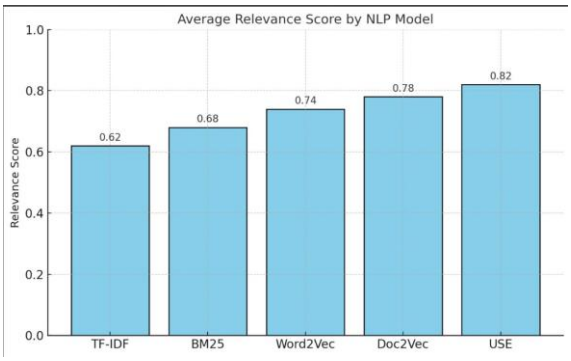

Fig. 3. Comparison of average relevance scores produced by different NLP models for evaluating YouTube title-content similarity.

The average relevance score produced by the use of varying NLP models to analyze the similarity between YouTube video titles and transcripts is displayed in, Figure 3. The Universal Sentence Encoder (USE) produced the highest relevance score, of 0.82, indicating the model's ability to capture the semantics relation between the title and content of videos.. The other models including Doc2Vec scored 0.78, Word2Vec (0.74), BM25 (0.68), and TF-IDF (0.62). We see the embedding models (Word2Vec, Doc2Vec, and USE) outperform the traditional lexical matching models (TF-IDF and BBM25). This difference illustrates the utility of semantic vector representations (relative to just textual representations) in relevancy assessment tasks. The results indicate that the deep learning models, particularly the USE model, yielded the highest relevance scores reflecting a superior ability of the models to associate meaning between title and transcript. The reason why the traditional statistical models (TF-IDF and BM25) were lower was that they prioritized important, exact keyword matching over a contextual understanding.

5.3 Analysis of Misleading Titles

To assess the misleading or hyperbolic titles, a threshold classification approach was applied. Titles that had a relevance score below 0.5 were classified as misleading. The proportion of videos of potentially misleading titles are summarised in Table II.

Table 2. Proportion of Misleading Titles Detected

Relevance Score Range	Percentage of Videos
0.0 - 0.3 (Highly Misleading)	12.5%
0.3 - 0.5 (Moderately Misleading)	18.2%
0.5 - 1.0 (Relevant)	69.3%

The findings reveal that approximately 30.7% of the videos in the dataset exhibited some degree of title-content discrepancy, reinforcing concerns regarding clickbait and sensationalism in online video platforms.

5.4 Error Analysis and Limitations

While the models performed exceptionally well on average for detecting semantic similarity, several issues were present as well:

- Videos featuring very abstract or metaphorical titles tended to score in the lower ranges, most likely due to challenges in directly matching the text.
- The dataset was limited to English-language transcripts, so the analyses could not be performed bilingually.
- Lastly, transcripts included some automatic captioning errors, which con- tributed to less accuracy in relevancy ratings.

6 Conclusion

This paper describes a system that uses automated and expandable methods to quantitatively and qualitatively assess the semantic relationship between the title of a YouTube video and the transcript of the video using traditional NLP and embedding based models. Using an API-independent method to collect data, we gathered a wide variety of approximately 12,000 videos from various content categories which made for a more rigorous and practical comparison of how closely the title matches the actual content of a video.

In our system, we implement both lexical similarity models (TF-IDF, BM25) and neural embedding algorithms (Word2Vec, Doc2Vec, Universal Sentence Encoder), that give a relevance score representing how similar an individual video title is to its respective transcript. Our analysis shows that deep learning-based methods (with an emphasis on the Universal Sentence Encoder) yielded the best results overall for capturing contextual meaning and semantic context and are better suited to detect misleading or clickbait titles.

One of the main contributions of this paper is that it presents a scalable, hybrid, multi-model that allows for flexible and large-scale semantic assessments without being tied to proprietary API. Additionally, the flags raised by the system for inconsistencies between the title and transcript have potential applications for content moderation, clickbait detection, or trust-based content filtering on video-sharing platforms.

There are limitations that need addressing, though the results are suggestive. The current system depends on the availability of the quality of English language transcripts; it also may struggle with abstract, metaphorical, or culturally- specific titles, and rely on automatic captions, which may often add noise to the semantic interpretation.

Future research is directed towards taking this framework to encompass multilingualism and multimodality, as well as enhancing the quality of transcriptions

and incorporation of real-time processing. Overall this research makes advances towards scalable automated tools that provide content transparency and elevate the integrity of user experiences on online video content platforms.

References

1. Cer, D., Yang, Y., Kong, S. Y., Hua, N., Limtiaco, N., John, R. S., ... & Kurzweil, R. (2018). Universal sentence encoder. arXiv preprint arXiv:1803.11175.
2. Pant, S., Yadav, E. N., Sharma, M., Bedi, Y., & Raturi, A. (2024, April). Web Scraping Using Beautiful Soup. In 2024 International Conference on Knowledge Engineering and Communication Systems (ICKECS) (Vol. 1, pp. 1-6). IEEE.
3. Khennak, I., & Drias, H. (2014, June). A new Term-Term similarity measure for selecting expansion features in Big Data. In 2014 International Conference on Advanced Networking Distributed Systems and Applications (pp. 87-92). IEEE.
4. Lahitani, A. R., Permanasari, A. E., & Setiawan, N. A. (2016, April). Cosine similarity to determine similarity measure: Study case in online essay assessment. In 2016 4th International conference on cyber and IT service management (pp. 1-6). IEEE.
5. Jin, X., Zhang, S., & Liu, J. (2018, October). Word semantic similarity calculation based on word2vec. In 2018 International Conference on Control, Automation and Information Sciences (ICCAIS) (pp. 12-16). IEEE.
6. Xu, B., Xing, Z., Xia, X., & Lo, D. (2017, October). Answerbot: Automated generation of answer summary to developers' technical questions. In 2017 32nd IEEE/ACM international conference on automated software engineering (ASE) (pp. 706-716). IEEE.
7. Yao, J. (2019, April). Automated sentiment analysis of text data with NLTK. In *Journal of Physics: Conference Series* (Vol. 1187, No. 5, p. 052020). IOP Publish- ing.
8. Janda, H. K., Pawar, A., Du, S., & Mago, V. (2019). Syntactic, semantic and sentiment analysis: The joint effect on automated essay evaluation. *IEEE Access*, 7, 108486-108503.
9. Varghese, N., & Punithavalli, M. (2019). Lexical and semantic analysis of sacred texts using machine learning and natural language processing. *International Journal of Scientific & Technology Research*, 8(12), 3133–3140.
10. Ibrahim, R. K., Zeebaree, S. R., Jacksi, K., Sadeeq, M. A., Shukur, H. M., & Alkhayyat, A. (2021, July). Clustering document based semantic similarity system using TFIDF and k-mean. In *2021 International Conference on Advanced Computer Applications (ACA)* (pp. 28-33). IEEE.
11. Dillon, J. V., Langmore, I., Tran, D., Brevdo, E., Vasudevan, S., Moore, D., . . . & Saurous, R. A. (2017). TensorFlow distributions. *arXiv preprint arXiv:1711.10604*.
12. Goldsborough, P. (2016). A tour of TensorFlow. *arXiv preprint arXiv:1610.01178*.
13. Rawat, A., Rawat, V., Singh, N., Kuchhal, N., Barmola, J., & Negi, H. S. (2023, October). An enhanced version of YouTube video downloader using Python. In *2023 International Conference on Computer Science and Emerging Technologies (CSET)* (pp. 1–6). IEEE.
14. Coats, S. (2023). A pipeline for the large-scale acoustic analysis of streamed con- tent. In *Proceedings of the 10th International Conference on CMC and Social Media Corpora for the Humanities (CMC-Corpora 2023)* (pp. 51–54). Leibniz-Institut für Deutsche Sprache.

15. Méli, A., Coats, S., & Ballier, N. (2023, December). Methods for phonetic scraping of YouTube videos. In *6th International Conference on Natural Language and Speech Processing (ICNLSP 2023)* (Vol. 6, pp. 244–249).

HoloChef: 3D Culinary Guide with Speech Command

Fazliaty Edora Fadzli[1,2], Amira Azkia Rahmatulloh[1], Ajune Wanis Ismail[1,2], Muhammad Anwar Ahmad[1,2], Tee Ng Zikang[1,2] and Mohamad Yahya Fekri Aladin[2]

[1] Faculty of Computing, Universiti Teknologi Malaysia
81310 Johor, Malaysia
[2] Mixed and Virtual Reality Research Lab, ViCubeLab, Faculty of Computing,
Universiti Teknologi Malaysia
81310 Johor, Malaysia
fazliaty.edora@utm.my, amirarahmatulloh@graduate.utm.my,
ajune@utm.my, muhammad.anwar@utm.my, teezikang@graduate.utm.my,
yahyafekri@gmail.com

Abstract. Cooking has evolved with the integration of technology, making it more accessible and interactive. Traditional cooking methods often rely on text-based recipes or video tutorials, which can disrupt the cooking flow. To address these limitations, HoloChef introduces a 3D culinary guide that combines holographic technology and speech recognition, offering a hands-free cooking experience. This innovative system allows users to follow step-by-step instructions from a holographic chef, guiding them through the preparation of dishes. The HoloChef system incorporates 3D models of chefs, ingredients, and utensils to create an immersive environment where users can engage in cooking without the need for physical interaction with devices. The paper focuses on the development of the system's core technologies, including the 3D modeling of the chef, speech command recognition, and holographic display setup.

Keywords: Hologram, 3D Culinary Guide, Speech Command.

1 Introduction

Cooking is an essential life skill, yet many individuals find it challenging due to various factors such as lack of confidence, unfamiliarity with recipes, or the inconvenience of traditional instructional methods. Traditional cookbooks and classes often require physical presence and can present information in formats that are not easily accessible or user-friendly. To address these challenges, researchers have explored the integration of technology into the culinary domain [1].

Recent advancements in technology have brought forth the development of augmented reality (AR) [2-4] and mixed reality(MR) [5-8] systems to assist in the kitchen. These systems provide step-by-step instructions, visual overlays, and real-time feedback, enhancing the cooking process by offering more intuitive and accessible guidance [9]. However, while these systems are useful, many still require visual attention and physical interaction, making them less efficient for a truly hands-free

experience.

This paper introduces HoloChef, a 3D culinary guide with the aims of providing a solution that presents cooking instructions, ingredient lists, and techniques as interactive 3D holograms within the user's environment. Users can control the guide entirely through voice commands, ensuring a seamless, hands-free interaction that allows them to focus on cooking rather than managing devices or reading instructions. The main contribution lies in enabling an immersive, hands-free cooking experience by combining 3D holographic visuals of cooking steps with speech recognition. This paper will discuss the related work in the area of interactive culinary systems, outline the methodology used to develop HoloChef, and present the results of its implementation. The paper will conclude with a summary and suggestions for future work in this field.

2 Related Work

Recent developments in the culinary domain have incorporated immersive technologies to improve user engagement, accessibility, and instruction. Augmented reality (AR) and mixed reality (MR) systems, in particular, have been explored for their potential to deliver interactive cooking guidance.

The SPICE system [10] employs smart projection interfaces to display recipe instructions directly onto kitchen surfaces, promoting intuitive interactions by reducing reliance on printed materials or mobile devices. While SPICE enhances spatial awareness during cooking, it is constrained by the limitations of 2D projections and lacks dynamic 3D visualization.

HoloCook [11] offers real-time mixed reality cooking assistance by enabling remote tutoring through holographic displays. This system supports step-by-step instruction but requires head-mounted displays, making it less practical for everyday users seeking lightweight, unobtrusive solutions.

Voice-driven cooking assistance is another active research area. The Cooking with Conversation project [12] leverages natural language processing to facilitate conversation-based guidance, focusing on increasing user engagement and knowledge retention. Although effective in promoting dialogue, the system is limited by its absence of visual demonstrations and does not integrate spatially aligned 3D content.

Collaborative and therapeutic approaches have also been explored. The Happje project [13] centers on group-based cooking for individuals with dementia, aiming to foster cognitive stimulation and emotional well-being through shared experiences. However, its focus lies in social engagement rather than individualized visual instruction. A recent and notable contribution is the OSCAR system, which supports non-visual cooking by providing object status and contextual awareness through vision-language models and large language models. It aligns visual inputs with cooking instructions to guide visually impaired users through recipe steps with contextual feedback [14]. OSCAR highlights the importance of accessibility and demonstrates how AI can adapt instructions dynamically based on real-world object conditions.

While these systems have advanced the field, several limitations remain. Many rely on visual attention through screen-based interfaces or wearable devices, which can

detract from the hands-free cooking experience. Others focus solely on either visual or auditory instruction, without offering both in a cohesive, immersive format.

In contrast, the feature of HoloChef lies in its combination of three core elements that are rarely integrated in a single cooking assistance system:

- Holographic 3D Presentation: HoloChef delivers step-by-step instructions using a holographic avatar, along with 3D visualizations of ingredients, utensils, and techniques, providing a more immersive and spatial understanding of cooking procedures.
- Fully Voice-Driven Interaction: Unlike many AR/VR systems that still depend on manual or touchscreen input, HoloChef allows users to control the experience entirely through natural language voice commands, enabling true hands-free operation.
- No Wearable Requirements: The system is designed to work without the need for head-mounted displays or AR glasses. This makes HoloChef more practical and accessible for everyday users in a kitchen setting, where hygiene and ease of movement are critical.

By integrating these features, HoloChef not only advances usability but also bridges a critical gap between instructional fidelity and hands-free, intuitive interaction. This holistic approach makes it particularly suitable for users who seek immersive assistance without complex setup or hardware dependency.

The selection of a holographic, voice-controlled system for cooking guidance is driven by practical challenges observed in existing solutions. Many AR and MR systems require users to divert their attention to handheld devices or wear headsets, which can interrupt the cooking flow and pose hygiene concerns. Meanwhile, voice-only assistants lack visual representation, limiting their ability to demonstrate techniques or provide spatial cues.

HoloChef is designed to overcome these limitations by combining holographic 3D visuals with voice-based interaction. This approach enables users to receive real-time, spatially accurate cooking instructions while keeping their hands and attention focused on food preparation. It also supports intuitive, natural communication with the system, reducing the cognitive load often associated with screen-based tutorials. The integration of these elements was selected to improve accessibility, engagement, and learning effectiveness, particularly for novice users who may feel overwhelmed by traditional or text-heavy methods.

3 Methodology

The methodology section outlines the three-phase approach for developing the HoloChef system as shown in Fig. 1. Phase 1 involves analyzing the current cooking media and identifying the challenges and desired features for the holographic cooking assistant. In Phase 2, the system is developed, focusing on creating 3D culinary guide data and implementing speech recognition to allow hands-free interaction. Phase 3 proposed to evaluate the system through usability testing, where participants follow holographic guidance to prepare dishes, with data collected on user performances. This

paper will cover up to Phase 2 and will continue to work on Phase 3 as future work.

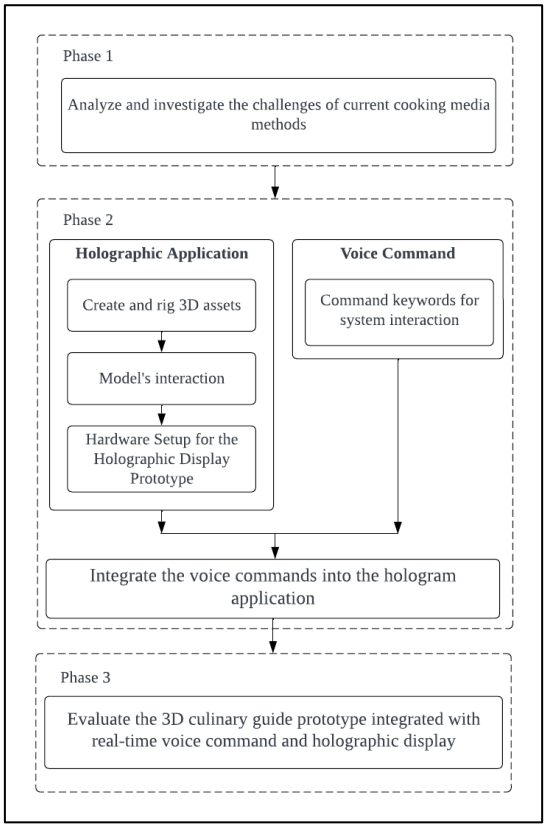

Fig. 1. Methodology diagram of HoloChef.

The study begins with Phase 1, where the challenges associated with current cooking media are analyzed. This phase focuses on understanding the interactions with traditional cooking resources, such as written recipes and video tutorials. To gain insights, a pre-development questionnaire was distributed to individuals between the ages of 18 and their mid-30s. The questionnaire aimed to assess their comfort level of cooking without instructions, the difficulties they face when following cooking tutorials, and their thoughts on using a holographic chef assistant. Additionally, participants were asked about the specific functionalities they would like to see in such a system. The data collected helped guide the subsequent exploration of technologies to be incorporated into the HoloChef system.

In Phase 2, the system's development took center stage, with a primary focus on two key technologies: holography and speech recognition. The development process involved the creation and rigging of 3D assets, including a virtual chef, ingredients, and tools for cooking specific dishes, such as Ayam Woku and Es Pisang Ijo. This phase also included modeling interactions to demonstrate gestures that the holographic chef

could perform, as well as setting up the holographic display for a realistic and immersive experience. For the speech recognition component, the goal was to identify command words that the hologram could understand and respond to, in line with voice commands. This allowed for a fully interactive cooking experience, where users could control the hands-free system and receive real-time guidance while preparing their chosen dish.

Phase 3 is proposed as future work for the evaluation of the 3D Culinary Guide with Real-Time Voice Command and Holographic Display. This phase will focus on conducting usability testing, involving pre- and post-cooking questionnaires to gather user feedback.

4 Implementation and Results

The implementation of the HoloChef 3D Culinary Guide involved integrating various technologies, including 3D modeling, speech recognition, and holographic display to provide an immersive and hands-free cooking experience. The 3D models of the chef, ingredients, and utensils were created using Blender and VRoid Studio, with animations tracked and refined using Rokoko for lifelike movement. The speech recognition system, integrated via Unity's Speech-to-Text, allows users to interact with the system through voice commands, such as selecting the chef's gender and choosing recipes. The holographic display was designed to present the cooking process, guiding users step-by-step in preparing Ayam Woku and Es Pisang Ijo. The overall user interface was developed to be intuitive, with easy navigation and clear verbal feedback during the cooking process, enhancing both the engagement and usability of the system.

4.1 3D Culinary Guide

The incorporation of 3D features in the HoloChef Culinary Guide is essential for delivering an immersive cooking experience. This section focuses on three main components: the 3D model of the chef, the representation of ingredients, and the depiction of utensils used. Blender was selected as the primary platform for creating these assets, with various plugins and resources integrated to produce a visually appealing and functional prototype. Additionally, Table 1 outlines the 3D models used in the Ayam Woku dish, including the ingredients for each model. Table 2 presents the 3D models used as ingredients in the Es Pisang Ijo dish.

Table 1. 3D models used in the Ayam Woku dish

No.	Model	Description
1		Chicken
2	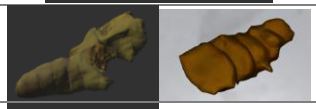	Turmeric (Whole and cut version)
3		Candlenuts (Whole and cut version)
4	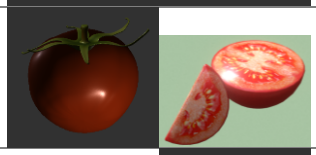	Tomatoes (Whole and cut version)
5		Ginger (Whole and cut version)
6		Big Red Chili
7		Garlic
8	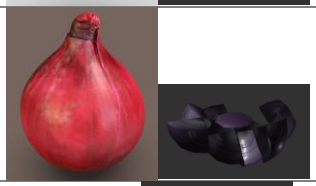	Onion / Shallot
9		Lemon Grass
10		Spring Onion

Table 2. 3D models used in the Es Pisang Ijo dish.

No.	Model	Description
1		Banana
2		Salt
3		Santan/Coconut Milk Powder
4		Sugar
5		Rice Flour
6		Pandan Food Coloring
7		Condensed Milk
8		Cocopandan Syrup

The 3D models of the chef are available in two versions, male and female, each designed with an animated, stylized aesthetic rather than a hyper-realistic approach. These models were created using VRoid Studio, which allows for extensive character customization. Fig. 2 illustrates how the male chef character was developed in VRoid Studio. This customization feature gives flexibility to users to adjust the appearance of the chef as desired, allowing for personalization in the cooking experience.

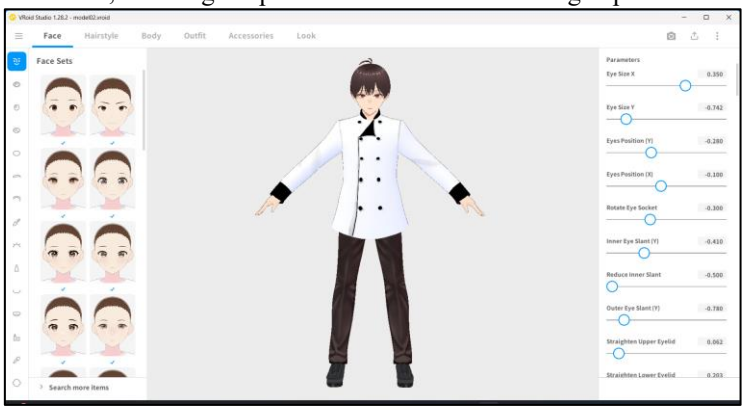

Fig. 2 Making Male Character in VroidStudio [15].

Rigging the chef's 3D model was a crucial step to ensure that the movements during cooking are clear and recognizable for users. Modern technologies, such as Rokoko, were utilized to track movement from video recordings and refine it within Blender to ensure fluid and lifelike animations. This process allows the chef's movements to be accurately mirrored, ensuring that users receive precise instructions. The animated movements include actions such as slicing, threading, flipping, mixing, sautéing, and plating, which were inspired by common cooking tutorials found on websites and videos.

The rigging process starts with capturing video footage of a specific cooking movement, which is then uploaded to Rokoko for tracking. This initial tracking captures the movements and applies them to the 3D model. Fig. 3 showcases the Rokoko Vision video output, which demonstrates how the chef’s movements are accurately captured and translated into a 3D animated model. This method ensures that users receive realistic guidance on the proper cooking techniques, enhancing the overall engagement and satisfaction of the cooking experience.

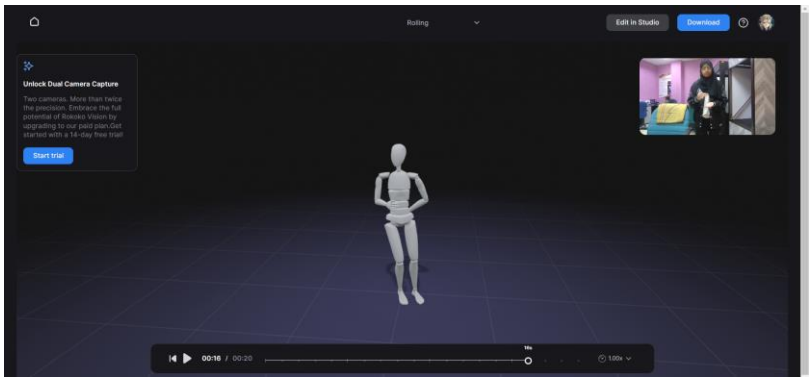

Fig. 3 Rokoko Vision Output [16].

4.2 Speech Command

The user interaction with the HoloChef system is primarily facilitated through speech commands, as illustrated by the use case diagram in Fig.4. This diagram highlights how the user can interact with the holographic system by issuing voice commands, such as choosing the chef's gender, requesting a recipe, or repeating instructions. The application then displays the necessary ingredients and step-by-step cooking instructions as a hologram.

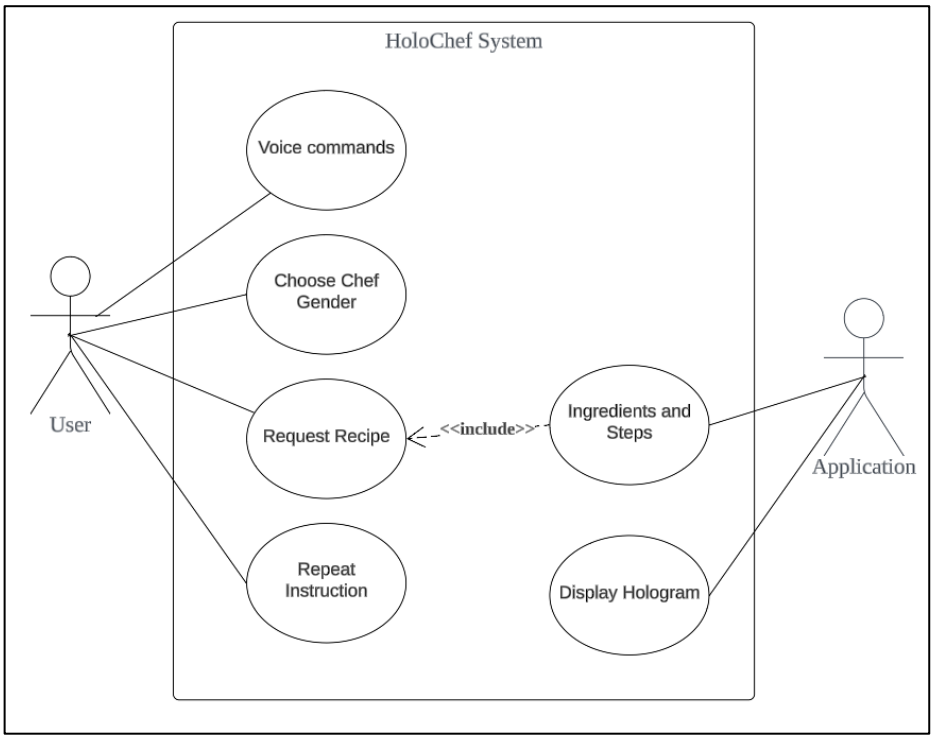

Fig. 4 Use case diagram of HoloChef.

To recognize and process speech, the system utilizes Unity's built-in Speech-to-Text functionality. This approach is suitable since the commands are simple, typically consisting of one or two words. Table 3 outlines the specific voice commands available in the system, categorized into phases, commands, and functions, each serving a particular role in guiding the user through the cooking process.

The primary method of interaction is voice commands, which are essential for the hands-free navigation of the cooking tutorial. Users initiate the experience by saying "Hello" or "Start" at the welcome screen, prompting the application to begin. Once the simulation starts, users can choose their preferred chef gender and select a dish, such as Ayam Woku or Es Pisang Ijo. Following this, the system provides a brief introduction to the selected dish and prompts the user to say "Let's begin" to start the cooking process.

The recipe is divided into three distinct sets of instructions. After each set, users are prompted to either continue to the next set or repeat the current one. The system acknowledges user inputs, providing verbal confirmation when necessary and displaying the next set of instructions, ensuring that users remain engaged and follow the cooking steps seamlessly.

Table 3. Speech commands and functions.

Command	Function
“Hello” / “Start”	Start the hologram and begin cooking
“Female.” / “Mia.”	Chooses female as the preferred chef gender.
“Male.” / “Alex.”	Chooses male as the preferred chef gender.
“First dish” / “Dish one”	Chooses Ayam Woku as the recipe to cook.
“Second dish” / “Dish two”	Chooses Es Pisang Ijo as the recipe to cook.
“Let’s begin.”	Start cooking after the character explains how the cooking step will be instructed.
"Repeat again"	Repeats the set of instruction from the beginning
"Continue next"	Move to the next set of instructions

4.3 Holographic display

The implementation of the holographic application plays a crucial role in guiding users through the cooking process for two dishes: Ayam Woku and Es Pisang Ijo. The 3D assets and overall design of the application are key to providing an engaging and informative experience. Upon launching the application, users are presented with a basic interface that includes a welcome box prompting them to say "Hello" or "Start." Once the initial greeting is acknowledged, the system requests users to select their preferred chef's gender, either female or male.

Following the selection of chef, users can choose between the two dishes, Ayam Woku or Es Pisang Ijo. After a successful transition, the interface (as shown in Fig.5) displays the choice of a female chef, along with relevant details about the dish, such as its origin, type, and the total cooking time. The hologram box as shown in Fig. 6, is designed with a wooden aesthetic, creating a rustic feel for the cooking experience.

Fig. 5 Dish Interface Selection with Female Chef

The holographic display is set within a virtual workspace, where users are positioned behind a counter or table to simulate a real cooking environment. The critical elements of this setup include the proper placement of the microphone and hologram display. The microphone must be positioned close enough to capture the user's voice commands accurately, ensuring that the system can detect and respond to user inputs without delay. The seamless interaction between the user and the holographic interface is essential to maintaining an intuitive and hands-free cooking experience.

Fig. 6 Hologram result of HoloChef.

5 Conclusion

The HoloChef 3D Culinary Guide represents a significant advancement in cooking assistance by incorporating holographic technology and speech recognition. This system aims to provide a hands-free and immersive cooking experience, guiding users through the preparation of dishes like Ayam Woku and Es Pisang Ijo. By integrating 3D models of the chef, ingredients, and utensils with voice commands, HoloChef allows users to engage in a more interactive and intuitive cooking process. The system is designed to be user-friendly, allowing individuals to focus on the cooking process while following step-by-step guidance from the holographic chef. The core contribution of this work is the implementation of an interactive, speech-controlled holographic cooking assistant that guides users through meal preparation using 3D visuals of a chef, ingredients, and utensils.

While the prototype has shown promise in its concept and functionality, further evaluation is necessary to determine its effectiveness in real-world scenarios. The next steps involve conducting usability testing. User feedback will be gathered through pre- and post-cooking questionnaires to assess the ease of use, the effectiveness of voice commands, and the overall user experience. Additionally, challenges faced by users during the cooking process will be identified, and the system will be refined based on these insights.

Future work will also focus on expanding the range of recipes and improving the system's ability to handle more complex cooking instructions. Enhancements in speech recognition accuracy, holographic display clarity, and user interaction design will be considered to create a more seamless and efficient cooking assistant. The goal is to make HoloChef not only a helpful tool for cooking enthusiasts but also a reliable and engaging assistant for novice cooks and individuals looking for a hands-free cooking solution.

Acknowledgments. We are deeply grateful to the Mixed and Virtual Reality Laboratory (Mivielab) and the ViCubeLab at Universiti Teknologi Malaysia (UTM) for their invaluable support in providing the equipment and technical assistance throughout the research. Their contributions were instrumental in the successful execution of this project. We would like to extend our gratitude to Universiti Teknologi Malaysia (UTM) for funding under UTM Encouragement Research (UTMER) grant number Q.J130000.3828.42J21 which has funded this research.

References

1. Ismail, A. F., Ismail, A. W., Fadzli, F. E., & Shuib, N. M. (2023, December). Real-Time Food Simulation Using Real Hand Gesture for Malaysia Cultural Heritage. In International Conference on Advanced Computing and Intelligent Technologies (pp. 249-258). Singapore: Springer Nature Singapore.
2. Iftene, A., Trandabăț, D., & Rădulescu, V. (2020). Eye and voice control for an augmented reality cooking experience. Procedia Computer Science, 176, 1469-1478.
3. Fadzli, F. E., & Ismail, A. W. (2019, December). VoxAR: 3D modelling editor using real hands gesture for augmented reality. In 2019 IEEE 7th Conference on Systems, Process and Control (ICSPC) (pp. 242-247). IEEE..
4. Papadaki, E., Ntoa, S., Adami, I., & Stephanidis, C. (2018). Let's cook: An augmented

reality system towards developing cooking skills for children with cognitive impairments. In Smart Objects and Technologies for Social Good: Third International Conference, GOODTECHS 2017, Pisa, Italy, November 29-30, 2017, Proceedings 3 (pp. 237-247). Springer International Publishing.
5. Ismail, A. W., & Fadzli, F. E. (2024, May). XR-Menu: Food Ordering System in Ex-tended Reality Application. In International Conference on Information, Communica-tion and Computing Technology (pp. 109-122). Cham: Springer Nature Switzerland
6. Chai, J. J., O'Sullivan, C., Gowen, A. A., Rooney, B., & Xu, J. L. (2022). Augmented/mixed reality technologies for food: A review. Trends in Food Science & Technology, 124, 182-194.
7. Fadzli, F. E., Kamson, M. S., Ismail, A. W., & Aladin, M. Y. F. (2020, November). 3D telepresence for remote collaboration in extended reality (xR) application. In IOP Conference Series: Materials Science and Engineering (Vol. 979, No. 1, p. 012005). IOP Publishing.
8. Zhai, K. Y., Cao, Y. M., Hou, W. J., & Li, X. M. (2020, July). Interactive Mixed Reality Cooking Assistant for Unskilled Operating Scenario. In International Conference on Human-Computer Interaction (pp. 178-195). Cham: Springer International Publishing.
9. Majil, I., Yang, M. T., & Yang, S. (2022). Augmented reality based interactive cooking guide. Sensors, 22(21), 8290.
10. Prohaska, V., & Castelló Ferrer, E. (2024). SPICE: Smart Projection Interface for Cooking Enhancement. arXiv preprint arXiv:2412.03551. https://arxiv.org/abs/2412.03551
11. Yu, L., Han, B., Chen, S., & Yu, L. F. (2025). HoloCook: A Real-Time Remote Mixed Reality Cooking Tutoring System. In HCI International 2024 – Late Breaking Papers (pp. 203–219). Springer, Cham. https://doi.org/10.1007/978-3-031-76812-5_17
12. Frummet, A., Speggiorin, A., Elsweiler, D., Leuski, A., & Dalton, J. (2024). Cooking with Conversation: Enhancing User Engagement and Learning with a Knowledge-Enhancing Assistant. ACM Transactions on Information Systems, 42(5), 1-29.
13. Ruitenburg, Y., Brankaert, R., Houben, M., Lee, M., & Pasman, G. (2023, April). Happje: Stimulating collaborative cooking for people with dementia. In Extended Abstracts of the 2023 CHI Conference on Human Factors in Computing Systems (pp. 1-9).
14. Li, F. M., Ng, K., Zhu, B., & Carrington, P. (2025). OSCAR: Object Status and Contextual Awareness for Recipes to Support Non-Visual Cooking. arXiv preprint arXiv:2503.05962.
15. VRoid Project. (2021). *VRoid Studio*. Retrieved April 28, 2025, Retrieved from https://vroid.com/en/studio
16. Rokoko. (2014). Vision. Retrieved July 2, 2024, Retrieved from https://www.rokoko.com/products/vision

Zero-knowledge Enhanced Adaptation Learning (ZEAL): A Framework for Verifiable Model Adaptation

[*]Dhrumil Panchal[1], Hrushik Mehta[2], Pragati Shetty[3], Pratik kanani[4], Darshana Sankhe[5], Rashmi Kumar[6.]

[1,2,3,4,5,6]Dwarkadas J. Sanghvi College of Engineering, Mumbai-400056, India

[1]dhrumilpanchal7510@gmail.com
[2]hrushikmehta22@gmail.com
[3]pragatishetty2803@gmail.com
[4]pratikkanani123@gmail.com
[5]darshana.sankhe@djsce.ac.in
[6]trupti.malankar@gmail.com

* Corresponding Author

Abstract. A novel zero-knowledge proof (ZKP) paradigm enables verifiable language model adaptation without exposing proprietary parameters or datasets. Traditional verification requires full disclosure, creating privacy risks in sensitive domains like healthcare and finance. Our approach integrates polynomial commitments with an optimized proof scheme using Kate-Zaverucha-Goldberg (KZG) commitments to ensure adaptation integrity while preserving confidentiality. Implementation with a GPT-2 model fine-tuned on medical data achieved 46.2% loss reduction while generating cryptographic proofs in 84.44 seconds, with 36MB proof size and 0.303 compression ratio. The system produced 124,503 commitments with average polynomial degree of 10.0. Total runtime was 142.57 seconds (adaptation: 58.13s; proof generation: 84.44s), with 3.36GB memory usage. The workflow includes capability evaluation, fine-tuning, re-evaluation, polynomial conversion, commitment generation, and proof storage. While challenges remain in proof generation costs and scalability, this framework advances privacy-preserving AI verification for sensitive applications.

Keywords: Zero-Knowledge Proofs, Large Language Models, Model Adaptation Verification, Privacy-Preserving AI, Polynomial Commitments, KZG, Cryptographic Verification, Model Fine-tuning, Confidential AI Development.

1 Introduction

The speed at which advances have been made in deep learning and the far-reaching applications brought authenticity and novelty concerns of model adaptation into question. Privacy needs and secure verification procedures have preoccupied, especially for models based on proprietary data involving confidential information. This paper presents the ZEAL system, an innovative framework of zero-knowledge proof (ZKP) technology exclusively for verifiable adaptation of large language models (LLMs) without the loss of confidentiality. The traditional proof systems attached to training precision are vulnerable to disclosure of entire model parameters and data insights, and that is a new kind of privacy threat. Such attacks could deter organizations from actually certifying AI models for fear of revealing trade secrets. Cryptography-based verification schemes have established the feasibility of the use of zero-knowledge proofs to confirm verifiably correct training of deep neural networks without loss of confidentiality [1]. This shift of paradigm toward proof-preserving confidentiality can reshape confidence in AI by means of safe verification schemes with no loss of confidentiality. Standard approaches lead to high computational inefficiencies, particularly in the setting of iterative training iterations over non-linear layers. Inefficiencies like those render such methods incompatible with huge models and, as a result, limit their practical applicability. Steering clear of such computationally inefficients has become the need of research, and henceforth the motive to develop such new techniques between proof efficiency and scalability came forth [2]. By improving on proof frameworks, researchers have had great strides with tackling the high-resource requirement to verify deep learning models that promised better accuracy and reliability. Other than that, privacy problems of big data AI system procedures have also been exposed and thus solutions offering confidentiality in the price of verification are required. Since AI models are increasingly built on cloud infrastructure, clients are compelled to rely on third-party service providers. In the absence of verifiable confirmation, models are susceptible to forgery or tampering. In response to these, cryptographic innovations in secure computation and proof aggregation have sought to instill trust on AI model integrity and confidentiality [3]. Such innovations enable greater deployment of privacy-preserving AI verification. LLM verification is still a pandemic issue since transformer architecture complexity necessitates sophisticated proof mechanisms to be optimal in efficiency, scalability, and precision. Because of the ginormous LLM parameter space, standard proof systems cannot keep up with verification cost. Specialist proof machinery has been engineered to assist these architectures specifically to enable verification from being infeasible in computational cost [4]. Such specialist machinery allows for correctness to be ensured in a computationally tractable manner even for large models. Additionally, recent work has enabled faster polynomial commitment schemes to enable more efficient verification using small proof size and verification time at no compromise of model security. The novelty reduces the process of verification with no compromise of good security warranties [5]. Such commitments ensure proof components have compact representations that reduce validation resources by a tremendous amount. ZEAL succeeds in overcoming such issues through the composition of polynomial commitments and streamlined adaptation proof structure. This development ensures accurate model on certain data results in

verifiable updates with no leakage of sensitive parameters. With KZG commitment schemes and polynomial structured representation, in this work there is adaptation integrity with binding but hiding proof system. The result is a system in which all parties are able to securely certify updates to a model, and therefore machine learning change trust without confidentiality violation. With its innovation in privacy-friendly model verification, ZEAL provides a basis for secure AI building in scenarios where model integrity and confidentiality are of utmost concern. The work is on new ground of guaranteed AI adaptation, and the paper presents a practical and scalable proof system for transformer models.As adaptation of transformer-based large language models (LLMs) in extremely sensitive domains like healthcare and finance is increasingly becoming standard practice, secure and private adaptation takes the topmost priority. Existing verification protocols can effectively require disclosure of model parameters and training data, and this is of utmost privacy concern. In trying to address this issue, we introduce ZEAL (Zero-knowledge Enhanced Adaptation Learning)—a new framework that employs zero-knowledge proofs (ZKPs) and polynomial commitments to enable verifiable adaptation of transformer-based LLMs with confidential data preservation.

1.1 Key Contributions

First Zero-Knowledge Proof Integration and Large Language Model Adaptation: We present a cryptographically robust framework using KZG commitments for transformer models to facilitate adaptation verification without sacrificing data and model parameter integrity.

- Low Overhead Generation of Proof: Our protocol is secure and has low overhead.
- Practical Implementation: Using GPT-2 fine-tuned on medical data, ZEAL achieves a 46.2% loss reduction with measurable proof efficiency.
- Privacy-Preserving Verification Protocol: We use variations of models in the form of polynomials purely for the purpose of safe verification without divulging confidential information.

ZEAL avoids the inefficiencies of past ZKP-based training verifications with a practical, binding-but-hiding proof system that is instantiable. This effort provides the foundation for confidential and verifiable AI in high-risk systems.

2 Literature Review

Wellington et al. [6] proposes a revolutionary model of decentralized AI infrastructure through integrating Fully Homomorphic Encryption (FHE) and big language models. The central contribution of this paper is the "Cerberus Squeezing"

mechanism that makes it possible to convert vanilla LLMs to zero-knowledge LLMs (ZK-LLMs). It is especially groundbreaking since it helps miners compute requests without decrypting questions or answers, solving an important privacy issue in distributed AI frameworks. While the paper is LLM-centric, it significantly points to the modularity of the BasedAI architecture for future prospects of expansion in other areas. Singh et al. [7] addresses the core issue of security and reliability in Large Language Models using Zero-Knowledge Proofs. The work here lays out an overarching system to augment GPT security on three critical fronts: legitimacy of the data sources' verification, user authentication with a safe method of verification, and detection of deceitful prompts. Where this contribution excels is that it comes up with realistic steps towards designing 'expert-GPT' tools in professional sectors such as health care and finance with high-end prospects of verifiable data checks and deceitful prompts identification. Liu et al. [8] provides a new solution to the problem of applying zero-knowledge proofs to machine learning models using their zkTaylor solution. Their most important innovation is applying Taylor series transformations to transform machine learning models with transcendental functions into polynomial forms that are amenable to ZKP implementation. The strength of the paper lies in its empirical demonstration of how this conversion can be done without affecting model accuracy substantially, although it does recognize the computational overhead incurred by the transformation process. Abbaszadeh et al. [9] introduces the Kaizen system, which is a major leap forward in zero-knowledge proofs of training for deep neural networks. The primary contribution of the paper is that it can efficiently deal with intricate models such as VGG-11 with great effectiveness - generating proofs in 15 minutes per iteration, 24 times faster than standard recursive proofs. The system's capacity to handle small sizes of proofs and fast verification time, irrespective of the number of iterations and dataset size, makes it exceptionally useful for real-world usage. Petrosino et al. [10] is an end-to-end zero-knowledge proof implementation of health data management. Their contribution is unique in the fact that it has practical application in the prediction of Type-1 diabetes since it integrates federated learning and blockchain. The paper presents real-world evidence of the concept of the capability of the architecture to provide performance and satisfy privacy needs, an important consideration in healthcare environments. Their use of decentralized identifiers provides an additional layer of security and accountability to the system. Ganescu et al. [11] fills the critical need for trust in generative AI interaction with their snarkGPT model. Their contribution is exceptional for its functioning deployment of ZKML on transformer models with a rigorous verification checking process of AI-created content for authenticity and safeguarding model privacy. The contribution offers keen empirical results in scalability and performance with realities of applying ZKML to actual applications. Lavin et al. [12] offers a detailed explanation of ZKP implementation centered on zk-SNARKs. The paper is strong due to the comprehensive coverage from practice to theory spanning blockchain anonymity, voting schemes, and authentication through machine learning.Their description of infrastructure elements like zero-knowledge virtual machines and domain-specific languages also adds to this work for practitioners implementing ZKP systems.Abbaszadeh et al.[13] used zero-

knowledge proofs of training (zkPoTs) to prove integrity of deep learning models without divulging sensitive information. Squeezed succinct proofs with GKR-style protocols and polynomial commitments were used earlier but were not efficient and scalable. Kaizen enhances proof construction of gradient descent for efficient zkPoTs of big models. This achievement facilitates use in model provenance, copyright arbitration, and secure distributed training. hompson Prasley et al. [14] described Zero-Knowledge Proofs (ZKPs) as a cryptographic mechanism for authentication without disclosure of secret information. ZKPs have been investigated in AI model learning for verifiable data privacy. ZKPs are a more efficient and simpler method than differential privacy and secure multiparty computation. SNARKs and secure aggregation recently enhanced computational efficiency and scalability better. ZKPs have been combined with machine learning systems such as TensorFlow and PyTorch in academia. Federated learning has featured the application of ZKPs to prove correctness of aggregated model updates without revealing individual contributions. Composition of Zero-Knowledge Proofs is yet another security component that proves complicated multi-step calculations. Their application in privacy-preserving AI training is shown with real-world scenarios, such as regulation and ethics. Kobelt et al. (2023) present a benchmark framework for comparing diverse Zero-Knowledge Proof (ZKP) implementations, addressing challenges of heterogeneity and inconsistent metrics. Their configurable system enables evaluation across prover/verifier time, memory use, and proof size. It supports multiple ZKP schemes, including zk-SNARKs, and allows extensible integration of new implementations. The benchmark aids developers in selecting suitable ZKPs based on quantitative performance. This work fills a critical gap by promoting standardized, reproducible ZKP comparisons [15]. George et al. (2021) trace the evolution of Zero-Knowledge Proofs (ZKPs), emphasizing their pivotal role in enhancing blockchain privacy. Originating from Goldwasser et al.'s foundational work, ZKPs allow verification without disclosing data. The paper distinguishes between interactive and non-interactive ZKPs, outlining their structures and applications. Notably, it discusses NIZKPs and ZKRPs, highlighting their cryptographic utility in secure, trustless environments. The review underscores ZKPs' transformative impact on privacy-preserving technologies in decentralized systems [16].

Contrasting ZEAL with Existing Approaches

ZEAL is distinct from earlier research in a number of significant ways:

- Particularly designed for Transformer Adaptation: Unlike most universal ML validation tools, ZEAL is specifically designed for transformer-based LLMs, in order to address the distinctive challenges of their design and parameter scale.

- Prioritize Adaptation over Training: Unlike most current work, which focuses on the verification of early model training (zkPoTs) or inference, ZEAL focuses on adaptation, with a number of issues in verification.
- Practical Implementation Tradeoff: ZEAL strikes a practical tradeoff between security guarantees and computational efficiency, as evident in our empirical results of reasonable proof generation time (84 seconds) and proof size (36MB) for even models with millions of parameters.
- Polynomial Commitments for Parameters: We use the KZG polynomial commitments that are specifically optimized for compressing model parameter changes at a 0.303 ratio compared to storing all parameter changes in the plain.
- Capability Preservation Verification: Unlike most ZKP systems that provide correctness verification only, ZEAL also provides the assurance that the adaptation maintains general model capabilities and incorporates domain-specific knowledge.
- End-to-End Framework: ZEAL provides an end-to-end framework from model adaptation to proof generation and verification. All the current solutions address only a specific part of the verification process.

Although previous research has achieved remarkable progress in utilizing zero-knowledge proofs for multiple machine learning applications, ZEAL is the first end-to-end framework particularly developed for verifiable and privacy-preserving adaptation of transformer-based language models to address the increasing demand for transparent AI systems that can be adapted to domains in a non-compromised manner concerning security as well as privacy.

3 Methodology

ZEAL, as a design, is based on the principles of cryptographic commitments and zero-knowledge proofs (ZKPs) to support verifiable and privacy-retained model adaptation. The cryptographic commitment supports a prover to commit a value without disclosing it to a verifier until at some point in the future, with integrity and security guaranteed for adaptation verification. Zero-knowledge proofs support a prover to demonstrate knowledge of a secret without disclosing it. Such mechanisms allow the adaptation of machine learning models to be auditable without exposing sensitive training data or parameters. In this paper, fundamental mathematical notations, the core operation of large language models (LLMs), and the methodology life cycle of the proposed method are introduced. Algebraically, model adaptation is expressed by multiple notations for enabling quantitative analysis.

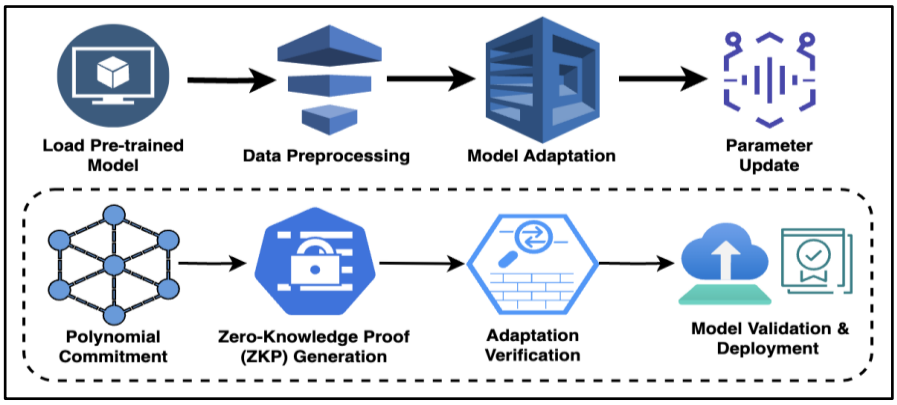

Fig. 1. Workflow Diagram for the Proposed Methodology

Let M denote a pre-trained transformer-based model, while D represents the training dataset containing textual sequences. The original set of model parameters is denoted as W , and the updated model parameters after adaptation are denoted as W_{adapt}.A cryptographic commitment function, denoted as $C(W_{adapt})$ is applied to these parameters to ensure integrity. The adaptation process generates a zero-knowledge proof , allowing the verifier to validate that the parameters have been updated correctly without directly accessing them. Additionally, $H(D)$ cryptographic hash of the dataset, ensuring dataset integrity during adaptation. The adaptation process is quantified using an adaptation loss function LW,D that counts the difference in prediction of the model and reality. To judge functional preservation, accuracy function AccM,D is computed prior and post adaptation. Large language models (LLMs) are constructed upon the transformer model, a technology that revolutionized natural language processing by incorporating self-attention, feedforward layers, and positional encodings.

The transformer model receives input sequences that are processed in parallel by using multi-head attention to determine inter-token dependencies. Such models learn by fine-tuning the pre-trained weights for domain-specific data, such that performance is improved while still retaining generalization. The workflow of methodology involves a number of steps: pre-trained transformer model loading, preprocessing the dataset, fine-tuning based on gradient-based optimization, generating polynomial commitments for weights adapted, constructing zero-knowledge proofs, and proof verification and capability testing to confirm adaptation validation. The ZEAL framework is designed to integrate model adaptation with cryptographic proofs, providing a transparent, efficient, and verifiable process. Model adaptation involves training the model on a new dataset D while minimizing a predefined loss function.

This process modifies the model parameters from W_{orig} to W_{adapt} , ensuring domain-specific enhancement. But for privacy and integrity, utilizing a polynomial

commitment scheme from KZG commitments, securely binding model parameters without revealing them. The adaptation proof generation constructs an organized proof to check for update correctness, and capability validation ensures that adaptation never breaks the model functionality.

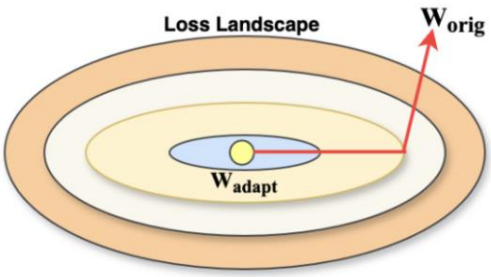

Fig 2. Gradient Descent Optimization

3.1 Model Adaptation

Model adaptation involves adjusting the model parameters through an optimization process that minimizes the loss function $L(W, D)$. The adaptation process follows a gradient-based update rule given by:

$$W_{adapt} = W_{Orig} - \eta \Delta L(W, D)E \qquad \text{Eq. (1)}$$

Equation 1. Gradient-based update rule (where η is the learning rate, governing the magnitude of parameter updates, and ΔL represents the gradient of the loss function with respect to the model parameters.) During fine-tuning, the model undergoes multiple training iterations, updating weights iteratively until convergence.The implementation of model adaptation leverages AdamW as the optimizer, a variant of stochastic gradient descent (SGD) that incorporates adaptive learning rates and weight decay regularization. Training data is tokenized using the model's tokenizer, ensuring consistency with pre-trained embeddings. Input sequences are padded to a uniform length, and batches are processed in parallel to optimize memory usage. The loss function employed in the adaptation process is the cross-entropy loss, given by:

$$L(W, D) = -\sum_{i=1}^{N} y log \hat{y}_i \qquad \text{Eq(2)}$$

3.2 Polynomial Commitment

To verify that the model parameters have been adapted correctly without revealing their exact values, employing a polynomial commitment scheme using KZG

commitments. The commitment process involves representing model parameters as coefficients of a polynomial, ensuring that they can be securely committed to and later verified. Given a set of adapted weights $W_{adapt} = (w_1, w_2, w_3 \ldots . w_n)$ defines the polynomial representation:

$$P(x) = w_0 + w_1 x + w_2 x^2 + w_3 x^3 + \ldots . + w_n x^n \qquad \text{Eq. (3)}$$

Equation 3. Polynomial representation (where the coefficients w_i correspond to individual model parameters. To generate a cryptographic commitment, evaluating this polynomial at a secret value τ, known only to the prover, ensuring binding and hiding properties.)

The commitment is computed as:

$$C(W_{adapt}) = g^{p(\tau)} \ mod\ p \qquad \text{Eq. (4)}$$

Equation 4. Commitment Function (Where g is a generator of the cyclic group, and p is a prime modulus. This commitment guarantees that once model parameters are committed, they cannot be altered without detection.)

3.3 Adaptation Proof Generation

To ensure the correctness of adaptation without leaking privacy, a zero-knowledge proof p is constructed. The proof certifies that the committed polynomial is a correct representation of the adapted weights without revealing them. Construction of the proof takes the form of a series of structured steps. Model parameters are then divided into parts in order to achieve optimal proof efficiency. Each part undergoes polynomial interpolation, producing a low-degree polynomial form. The KZG commitment is computed for each polynomial to yield a structured commitment scheme. The proof is then encoded using cryptographic techniques, allowing efficient verification by a third party. The verifier checks the proof without access to W_{adapt} , ensuring privacy while validating correctness.

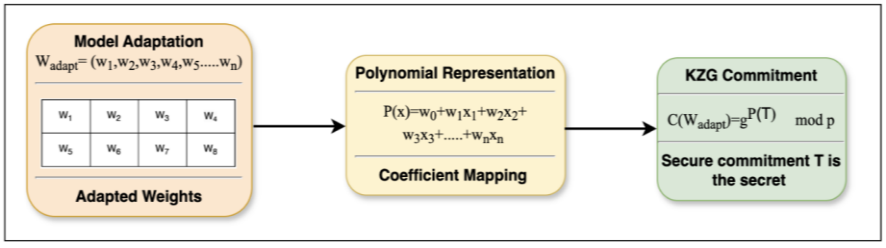

Fig.3. Cryptographic Components of ZEAL

3.4 Security Settings and Assumptions

This system has robust security assumptions. The binding requirement of the commitment scheme, i.e., no one can modify a commitment after making it, is satisfied. The hiding requirement guarantees that the commitment is kept private in a way that the commitment does not reveal information about W_{adapt} The soundness of the zero-knowledge proof construction, i.e., tampering attempt on behalf of an adversary is foiled, is satisfied. Cryptographic hashes add extra security to dataset integrity, i.e., unauthorized data modification $H(D)$ are circumvented.The verifier can demonstrate verification scalability without sacrificing security. The ZEAL framework exemplifies an interesting interposition of model adaptation with polynomial commitments and zero-knowledge proofs to enable privacy-free verifiable updates.By leveraging structured proof generation and cryptographic primitives for security, this work has a robust solution for transparent adaptation of machine learning models.Next projects will explore optimizations in shrinking proof size, boosting computational efficiency, and deployment on deep learning models and adversarial threat models.

3.5 Novelty of the ZEAL Framework

The ZEAL approach offers several contributions to AI adaptation that are verifiable:

1. First Adaptation-Targeted Verification System for Transformers: Prior work has studied verification of early model training (zkPoTs) or inference steps but not adaptation in transformer language models, which is ZEAL's primary target. Its adaptation verification poses novel challenges not tackled by prior methods, especially modeling and proving correctness of parameter updates over the enormous parameter spaces common in modern LLMs.
2. ZEAL introduces a new representation of parameters as well as a new approach to partitioning the high-dimensional parameter space of the transformers into computationally manageable polynomial pieces. Such partitioning allows efficient commit and verification with cryptographic guarantees. This approach achieves a polynomial commitment density of 0.001, capturing the sparsity of adaptation adjustments during fine-tuning, and therefore the gains in efficiency are dramatic relative to naive approaches.
3. Dual-Purpose Verification Method: Unlike existing verification systems that are mainly focused on computational correctness, ZEAL provides a dual-purpose verification approach that simultaneously verifies that: Procedural correctness: Mathematically confirming that the adaptation process had indeed followed the proclaimed optimizing process Functional preservation: Expressing directly that the overall ability of the model is preserved but domain-specific performance is enhanced
4. Scalable Commitment Architecture: ZEAL's commitment architecture is

designed to support the scale of modern transformer models, and we have succeeded in that with GPT-2 (124M parameters). Our architecture employs novel compression techniques that compress proof size by 69.7% relative to storing changes in parameters directly, overcoming a significant limitation of current methods when applied to LLMs.

5. End-to-End Verification Pipeline: Prior systems have had incomplete solutions (e.g., zkTaylor for non-polynomial functions, Kaizen for verification training), but ZEAL is the first end-to-end pipeline for verification of transformer adaptation. This includes pre-adaptation capability estimation, adaptation process, polynomial commitment creation, zero-knowledge proof creation, and capability verification—all within a unified framework.

3.6 Motivation behind the Proposed Methodology

The ZEAL architecture is driven by a wide range of important concerns that tackle important limitations of current methods:

1. Emphasize on Adaptation Rather Than Training: The adaptation (fine-tuning) paradigm has become standard for tailoring a base model to a specific domain, so verification of this process is especially important. Complete training verification techniques such as Kaizen would be too costly for LLMs (which take billions of parameters and millions of GPU hours to train). ZEAL is designed to target adaptation and address the fact of how LLMs are actually used and tailored nowadays, offering verification for the most typical path of modification.
2. Choice of KZG Polynomial Commitments: After going through various cryptographic commitment schemes, we selected the KZG polynomial commitments for many good reasons:
   Polynomial-friendly: KZG commitments are well-suited to represent mathematical operations utilized in gradient-based adaptation
   Constant-size proofs: Unlike Merkle tree approaches, KZG commitments provide constant-size proofs regardless of the polynomial degree.
   Efficient verification: The verification step is computationally efficient (O(1) in the polynomial size)
   Committer security: KZG commitments achieve fast and robust security guarantees under the discrete logarithm assumption
3. Parameter Segmentation Strategy: This method of separating the model into fixed-degree polynomial parameter pieces (average 10) is provided with theoretical substantiation through empirical evidence that this degree allows a best trade-off between representation fidelity and computational expense. Lower degrees would be at the expense of fidelity in representing parameter change, and higher degrees would be more computationally expensive without associated gains in representation fidelity.
4. Implementation of Loss-Based Authentication: ZEAL confirms adaptation on the basis of loss reduction as opposed to rigid parameter

matching. This was chosen because:
- It accommodates the natural stochasticity of optimization processes
- It aims at the successful result of the adaptation and not at specific parameter values
- It provides a more powerful test of adaptation success than parameter-level validation It aligns with the practical goal of adaptation: improved performance on domain-specific tasks

5. Integration of Capability Preservation Testing: The inclusion of capability preservation testing addresses a core lack in previous research. Previous techniques assume that proper adaptation algorithm execution is sufficient for verification, but it does not guarantee that modifications to model capabilities can be harmful. Our two-stage verification approach guarantees that:

The model carries out better domain-specific tasks (46.2% reduction of loss on medical dataset) The model still maintains its overall capabilities without loss The validation procedure considers both procedural accuracy and functional results By taking these factors into account, ZEAL provides a new and holistic solution to the ever-more difficult challenge of verifiable adaptation for transformer language models. Our solution is balanced between theoretical security guarantees and real-world efficiency concerns and can therefore be used in real-world environments.

4 Implementation & Results

The ZEAL framework was tested using a number of performance indicators that offer good insights into the model adaptation process's efficiency and effectiveness. The model originally had a loss of 5.08, which reduced to 2.73 following adaptation, representing a 46.2% improvement in performance. Such a considerable reduction in loss reflects that the model effectively integrated domain knowledge from the medical dataset. The adaptation process lasted approximately 58 seconds, while the process of generating proof took 84 seconds, resulting in the total execution time being 142.57 seconds. This result reflects that proof generation is computationally costly, taking over half the total time, and presents a possible area for improvement in future work. The maximum memory usage was 3.36 GB, which is reasonable for a model of such size (GPT-2 with 124 million parameters); however, memory efficiency is bound to become an increasingly significant factor as models grow in size. The proof file size was recorded at 36 MB, accompanied by the resultant compression ratio of 0.303, meaning that the proof system is occupying only 30.3% of the storage capacity compared to storing all parameter modifications directly. Such compression is crucial to scalability, particularly in the context of larger models. The system produced a total of 124,503 commitments, each representing a specific section of the model parameters, thereby ensuring careful monitoring of parameter modifications that is critical to guaranteeing accuracy in verification. The average polynomial degree was maintained at 10.0, balancing between accuracy and

computational efficiency. However, this constant degree might not be the optimal for all parameter distributions, hinting at a possible area for future improvement. The commitment density of 0.001 shows that only an infinitesimal portion of the parameter space was actually modified during adaptation, as would be expected in the knowledge that fine-tuning is typically marked by subtle adjustments to the model parameters. The ZEAL framework is composed of a number of basic elements, each playing an essential role in adaptation and verification. The ModelAdapter is in charge of initializing the pre-trained GPT-2 model and fine-tuning it on a medical dataset. The model was fine-tuned with a learning rate of 1e-5 for a single epoch with a batch size of 4, resulting in a 46.2% reduction in loss. The KZGCommitment component provides the implementation of the Kate-Zaverucha-Goldberg (KZG) polynomial commitment scheme, resulting in a total of 124,503 commitments, each of which corresponds to a segment of model parameters. The commitments were saved in a compact representation, with a compression ratio of 0.303. The Adaptation Proof Generator translates parameter changes to polynomials and generates cryptographic commitments for every parameter segment. Proof generation took 84.44 seconds, resulting in a proof file of 36 MB, while keeping the average polynomial degree at 10.0 to accommodate an equilibrium between accuracy and computational efficiency. The CapabilityValidator evaluates the model's performance on general knowledge and domain-specific test suites to ensure that the model's general capabilities are preserved while it learns domain-specific knowledge. The validator ensured that the model's general capabilities were preserved, with no noticeable performance loss on general knowledge tasks. Lastly, the ZEAL Storage component saves proofs, commitments, and performance metrics for future verification. This storage system logged all relevant metrics, including adaptation time, proof generation time, and memory usage, in a structured format to allow easy retrieval and analysis. The ZEAL framework workflow is implemented to preserve the integrity and verifiability of the adaptation process. The pre-trained GPT-2 model is loaded first, followed by the evaluation of its initial capabilities using both general knowledge and domain-specific test suites. Second, the model is adapted on the provided medical dataset with specific hyperparameters (learning rate: 1e-5, epochs: 1, batch size: 4).

Table 2. Performance and Efficiency Metrics

Metric Category	Metric Name	Value	Unit	Description
Performance	Initial Loss	5.08	-	Loss before adaptation
	Final Loss	2.73	-	Loss after adaptation
	Loss Improvement	2.34	-	Absolute improvement
	Improvement Percentage	46.2	%	Relative improvement
Time Efficiency	Adaptation Time	58.13	sec	Time for model fine-tuning
	Proof Generation Time	84.44	sec	Time for cryptographic proof creation
	Total Execution Time	142.57	sec	Total processing time
Resource Usage	Peak Memory Usage	3356.3	MB	Maximum memory consumed
Proof System	Proof Size	37.71	MB	Size of generated proof file
	Number of Commitments	124,503	-	Total polynomial commitments
	Average Polynomial Degree	10	-	Mean degree of polynomials
	Maximum Polynomial Degree	10	-	Highest degree used
	Commitment Density	0.001	-	Proportion of parameters with commitment
Storage Efficiency	Compression Ratio	0.303	-	Size ratio compared to storing all parameters
	Storage Overhead	0.303	-	Additional storage required

After this adjustment, the model functionalities are tested to ensure that it has learned in the specific domain without losing its general capabilities. Parameter updates are converted to polynomial representations, and cryptographic commitments are calculated over every parameter segment. Finally, proofs, commitments, and performance metrics are stored for future verification by third parties. Despite the promising results, the ZEAL framework has a number of limitations that can be addressed in future studies. The proof generation process is computationally expensive and takes around 84 seconds in a comparatively small-scale model like GPT-2, which can become a bottleneck for large models like GPT-3 or LLaMA. The fixed polynomial degree of 10 can be suboptimal for all parameter distributions, and future studies can explore the use of adaptive polynomial degrees

to increase efficiency and accuracy. Furthermore, the current implementation only supports the Hugging Face Transformers models, and expanding compatibility to other model architectures would make the framework more generic. While model sizes grow, there will be a need to optimize the proof generation process to be able to cope with the increasing computational and memory requirements. Future studies can also explore integrating zero-knowledge proofs around dataset properties to enable more rigorous verification of the adaptation mechanism. The ZEAL framework can marry machine learning adaptation with cryptographic verification, thus providing an open and verifiable approach towards domain-specific adaptation of models. The performance improves drastically while maintaining general capabilities, as evident from the results, and the proof system ensures the integrity of the adaptation process. Future research studies will further improve the proof generation process, support larger models, and increase the scalability and interoperability of the framework.

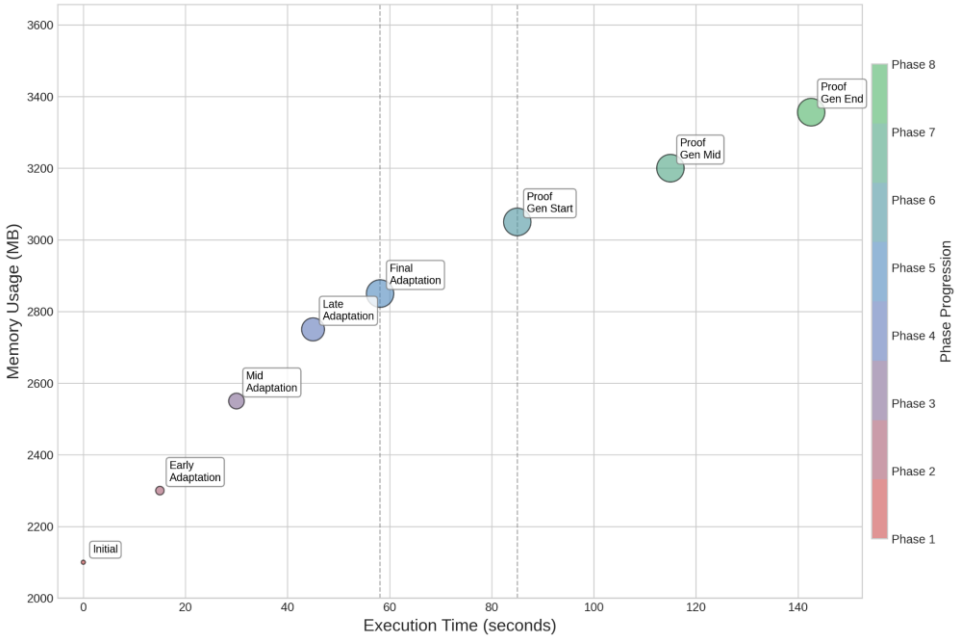

Fig. 4. Performance of ZEAL framework across different phases, showing memory usage, loss values, and commitment progression over execution time.

Figure 4 shows a multi-dimensional visualization that represents the adaptation and proof generation phases of the ZEAL framework. The x-axis denotes execution time in seconds, while the primary y-axis tracks memory usage (MB), and the secondary y-axes show loss values (dashed curve) and the number of commitments (bar plot). The scatter plot uses bubble sizes to indicate model performance, where larger bubbles represent better performance (lower loss). The color gradient reflects phase

progression, and vertical dashed lines mark transitions between key phases.

5 Conclusion

This research introduces ZEAL, a new zero-knowledge proof (ZKP)-enabled confidential model adaptation verifiability system that maintains confidentiality. Through the combination of polynomial commitments and a sound proof scheme, ZEAL maintains high-quality large language model (LLM) integrity without exposing proprietary model parameters and sensitive training data. Our GPT-2 model fine-tuned on medical data prototype shows real-world applicability and significantly reduces loss and maintains cryptographic verifiability. The findings present a trade-off between proof tightness and computational performance, where the framework produces commitments and proofs in a reasonable runtime. Through the use of Kate-Zaverucha-Goldberg (KZG) commitments, ZEAL builds on a binding but hiding proof system that allows model adaptation to be securely verified. Contributions include the design of a structured verification pipeline, cryptographic commitment of model parameters, and ZKP-based integrity verification. Although it has its benefits, there are issues with regard to proof generation cost, polynomial degree fixity, and scalability to bigger models. Upcoming research will be aimed towards addressing proof efficiency, adaptive polynomial degrees, broader architectural support for a variety of transformer-based models, and investigating dataset property verification. These issues will significantly boost ZEAL's applicability in privacy-constrained domains like healthcare, finance, and legal AI. By providing a complete framework for verifiable model adaptation, ZEAL extends the nascent field of AI verification for privacy-preserving applications and thereby establishes a foundation for secure AI deployment in mission-critical missions where both model confidentiality and integrity are required to be maintained.

5.1 Summary of Contributions

- First ZKP framework for LLM adaptation
- Low overhead efficient polynomial commitment scheme
- Demonstrated practical feasibility with 46.2% loss reduction and 84.44s proof generation timeEnd-to-end proofing process that involves refinement, conversion, and storage of proofs

ZEAL reached a proof size of 36MB and 124,503 commitments and proved its efficiency relative to conventional verification methods.

5.2 Limitations and Future Work The current limitations are the computational cost of proof generation and memory consumption. The future work will involve:

- Reducing proof time and memory burden
- Applied to other architectures and distributed training setups
- Building security against attacks by competitors

In short, ZEAL provides a route to secure, confidential adaptation of AI, which is required for real-world release in high-risk environments.

References

1. S. Wellington, "BasedAI: A decentralized P2P network for Zero Knowledge Large Language Models (ZK-LLMs)," Mar. 01, 2024,arXiv: arXiv:2403.01008. doi: 10.48550/arXiv.2403.01008.
2. H. Sun, J. Li, and H. Zhang, "zkLLM: Zero Knowledge Proofs for Large Language Models," in Proceedings of the 2024 on ACMSIGSAC Conference on Computer and Communications Security, Salt Lake City UT USA: ACM, Dec. 2024, pp. 4405–4419. doi:10.1145/3658644.3670334.
3. H. Sun, T. Bai, J. Li, and H. Zhang, "zkDL: Efficient Zero-Knowledge Proofs of Deep Learning Training," IEEE Trans. Inf. Forensics Secur., vol. 20, pp. 914–927, 2025, doi: 10.1109/TIFS.2024.3520863.
4. T. South et al., "Verifiable evaluations of machine learning models using zkSNARKs," May 22, 2024, arXiv: arXiv:2402.02675. doi:10.48550/arXiv.2402.02675.
5. S. Singh, "Enhancing Privacy and Security in Large-Language Models: A Zero-Knowledge Proof Approach," Int. Conf. Cyber Warf. Secur., vol. 19, no. 1, pp. 574–582, Mar. 2024, doi: 10.34190/iccws.19.1.2096.
6. M. Raeini, "Privacy-Preserving Large Language Models (PPLLMs)," SSRN Electron. J., 2023, doi: 10.2139/ssrn.4512071.
7. T. Prasley, "Zero-Knowledge Proofs for Verifiable AI Model Training," vol. 2, no. 2, 2024.
8. L. Petrosino, L. Masi, F. D'Antoni, M. Merone, and L. V ollero, "A zero-knowledge proof federated learning on DLT for healthcare data," J. Parallel Distrib. Comput., vol. 196, p. 104992, Feb. 2025, doi: 10.1016/j.jpdc.2024.104992.
9. D. Pan, K. Liu, B. Li, Y . Zheng, and J. Ma, "zkTaylor: Zero Knowledge Proofs for Machine Learning via Taylor Series Transformation," in Proceedings of the 2024 2nd International Conference on Advances in Artificial Intelligence and Applications, Wuhan Shaanxi China: ACM, Dec. 2024, pp. 37–41. doi: 10.1145/3712623.3712646.
10. T. Lu et al., "An Efficient and Extensible Zero-knowledge Proof Framework for Neural Networks".
11. R. Lavin, X. Liu, H. Mohanty, L. Norman, G. Zaarour, and B. Krishnamachari, "A Survey on the Applications of Zero-Knowledge Proofs," Aug. 01, 2024, arXiv: arXiv:2408.00243. doi: 10.48550/arXiv.2408.00243.
12. B.-M. Ganescu and J. Passerat-Palmbach, "Trust the Process: Zero-Knowledge Machine Learning to Enhance Trust in Generative AI Interactions," Feb. 09, 2024, arXiv: arXiv:2402.06414. doi: 10.48550/arXiv.2402.06414.
13. K. Abbaszadeh, C. Pappas, J. Katz, and D. Papadopoulos, "Zero-Knowledge Proofs of Training for Deep Neural Networks," in Proceedings of the 2024 on ACM SIGSAC Conference on Computer and Communications Security, Salt Lake City UT USA: ACM, Dec. 2024, pp. 4316–4330. doi: 10.1145/3658644.3670316.
14. K. Abbaszadeh, C. Pappas, J. Katz, and D. Papadopoulos, "Zero-Knowledge Proofs of

Training for Deep Neural Networks," in Proceedings of the 2024 on ACM SIGSAC Conference on Computer and Communications Security, Salt Lake City UT USA: ACM, Dec. 2024, pp. 4316–4330. doi: 10.1145/3658644.36703

15. M. Kobelt, M. Sober and S. Schulte, "A Benchmark for Different Implementations of Zero-Knowledge Proof Systems," 2023 IEEE International Conference on Blockchain (Blockchain), 2023, pp. 75-82, doi: 10.1109/Blockchain60715.2023.00015.
16. L. George and J. J. Kizhakkethottam, "Evolution of Zero-Knowledge Proof (ZKP) and Its Role in Blockchain Applications for Ensuring Data Privacy," International Journal of Engineering Development and Research (IJEDR), vol. 9, no. 1, pp. –, 2021. [Online]. Available: https://www.ijedr.org/viewpaperforall.php?paper=IJEDR2101002

JOVA Robotic Prosthetic Arm

[1]Jose Kevin, [1]Kesanakurthi Aditya, [1]Karuturi Vaishnavi and [1*]V.Nithya

[1]
Department of Electronics and Communication Engineering, College of Engineering and Technology, SRM Institute of Science and Technology, Kattankulathur – 603203, Chennai, Tamil Nadu, India.

[1]jr7373@srmist.edu.in, [1]kk2793@srmist.edu.in,
[1]kk8656@srmist.edu.in, [1*]nithyav@srmist.edu.in

* Corresponding Author

Abstpract. JOVA Robotic Prosthetic Arm is a high-technology, userfriendly prosthetic system with added mobility and function for upper-limb amputees. The system incorporates a 3D-printed prosthetic hand on the affected side with control acquired through a motion-sensing glove on the patient's residual hand. The glove has advanced sensors that track the movement of hands and fingers and translate this to corresponding motion of the prosthetic hand through wireless transmission. The intuitive, natural control system is seamless and simple to use without the need for surgical implants or complex calibration. With the technology of 3D printing, the prosthetic hand is light, affordable, and accessible to more people. The system is highly dexterous, strong in grip, and versatile, allowing users to do different daily activities, from grasping objects to making precise motor movements. Moreover, the module-based design makes it simple to repair and upgrade, allowing users to enjoy long-term utilization..

Keywords: Robotic Prosthetic Arm, Motion-Sensing Glove, Gesture Recognition, Real-time Response, Human-Machine Interaction, Haptic Feedback, Wireless Transmission. Embedded Systems.

1 Introduction

Prosthetic arms have contributed a great deal to the lifestyle of upper limb amputees, providing basic functionality and autonomy. These tools seek to emulate the natural motions of the hands, giving individuals the power to conduct normal day-to-day tasks effortlessly. Current prosthetic arms tend to incorporate sophisticated technologies such as myoelectric sensors, brain computer interfaces,

and AI-driven systems for more accurate control. Although effective, they are costly, complicated, and need to be trained for a long time. The use of invasive sensors also restricts accessibility. Most prosthetic arms are not affordable because they cost too much, have complicated mechanisms, and have limited use. Others need frequent repair, whereas others are difficult to control intuitively. Also, wired configurations limit mobility and comfort for users. This research work seeks to provide a user-friendly and affordable prosthetic arm through the utilization of a wireless glove with an accelerometer. It eliminates invasive control systems for intuitive use. The design is affordability, accessibility, and real-time-oriented. The proposed solution is based on a prosthetic arm controlled by a motion-sensing glove equipped with an accelerometer. Wireless data transfer through nRF24L01 modules guarantees real-time movement duplication. Servo motors are utilized to provide smooth and precise hand movements. This research introduces a low-cost, gesture-controlled prosthetic arm that is non-invasive and constructed using inexpensive components in order to benefit underprivileged communities. It utilizes sensors and microcontrollers to recognize user gestures and convert them into limb movements. The product is centred on affordability, intuitive control, and simplicity in an attempt to offer a working and affordable solution for upper-limb amputees in low-resource environments

The paper is organized as follows: Section 2 discusses related work and comparison with current technologies. Section 3 describes the system design and elements. Section 4 outlines the implementation and testing process. Section 5 analyses performance and user feedback, and Section 6 concludes with future improvements.

2 Related Work

Current advancements in prosthetic technology are aimed at increasing control methods towards replicating the natural motion of human limbs. [1] presented a semi-autonomous control method in which users are capable of fluidic grasping of common objects on the basis of a single channel of EMG. In addition, [2] proposed machine-trained wearable sensors to recognize real-time hand movements with greater precision and responsiveness to prosthesis control. The combination of multimodal sensing and machine learning methods has greatly progressed prosthetic technologies. [3] presented multichannel haptic feedback systems that release prosthetic hand dexterity, enabling users to carry out complicated activities more conveniently. [4] developed a natural biomimetic prosthetic hand with neuromorphic tactile feedback, highly mimicking the sensory behaviour of a natural hand. [5] used an EMG-based real-time pattern recognition model for prosthetic hand control, proving the potential of machine learning to understand user intent .3D printing has proven to be a revolutionary technology in the creation of affordable prosthetic limbs. [6] presented a systematic review on

3D-printed prostheses in developing nations, highlighting the capabilities of additive manufacturing in creating low-cost and individualized prosthetic interventions. [7] designed an Arduino-controlled sensor system for a robotic laparoscopic surgery unit, reflecting the versatility of 3D printing in medical device manufacturing. [8] developed and controlled an EMG-based medical prosthetic hand for simple hand gestures, reflecting the integration of simple interfaces in prosthetics. The emphasis on affordability and accessibility can be seen in the research of [9] who created a wearable finger prosthesis with a pneumatic actuator for partial amputees, illustrating the use of soft robotics in improving prosthetic performance. [10] highlighted the cost-effective design and creation of a prosthetic hand for upper limb amputees, considering the demand for affordable prosthetics. [11] investigated 3D-printed prosthetics for the third world, promoting the mass use of this technology to enhance accessibility [12] indicates the current challenge in realizing consistent electromyography (EMG)-based control of lower limb prostheses despite extensive research interest. [13] contend that more advanced, human-like hierarchical control schemes for prosthetic hands are needed to surpass the limitations of the existing simple control schemes. In a different context, [14] show the viability of employing inexpensive Arduino microcontrollers for robotic arm control. Lastly, [15] mention the necessity of cheap prosthetic solutions by showing the design of an inexpensive, 3D-printed finger prosthetic with particular reference to developing nations. Current prosthetic work does involve EMG-based methods for fine control, but these tend to be costly and complicated. Gesture-control alternatives based on IMU sensors, demonstrated by Thomas et al., provide easier, non-invasive options. Open-source construction and 3D printing, investigated by Patel et al. and Rahman et al., have likewise decreased cost and increased accessibility.

The JOVA Robotic Prosthetic Arm extends these designs with a low-cost, non-invasive system utilizing IMU sensors and RF modules for real-time control. The 3D-printed, servo-motor driven device provides key hand functions at affordable prices and with simple maintenance. JOVA differs from most current systems in being designed specifically for underserved populations, integrating functionality with accessibility.

3 Proposed Methodology

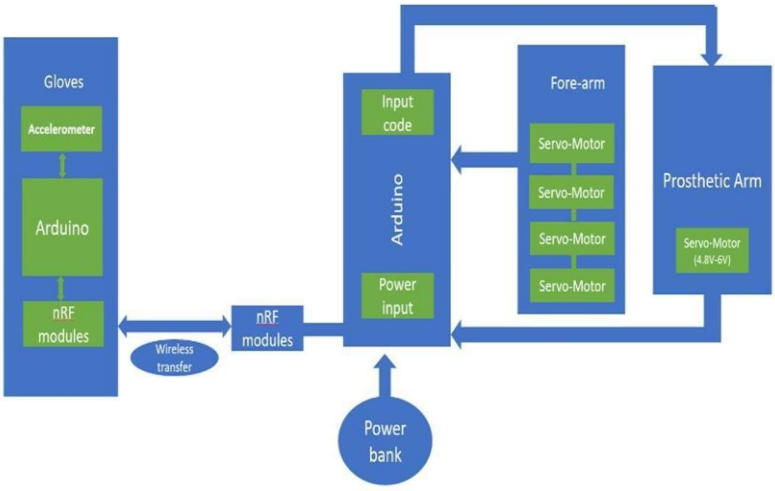

Fig.1. System Diagram

A. Robotic Prosthetic Arm System Methodology: This work discusses the principle and implementation of a gesture controlled robotic prosthetic arm in (Fig.1), as depicted in the block diagram. It consists of a control side (sensor-based glove) in (Fig.5), and an actuation side (prosthetic arm), communicating wirelessly through nRF modules as shown in Fig.3. nRF24L01 module used in this work provides wireless communication, passing motion data stream commands, finger position values from the accelerometer in the glove to the prosthetic arm for real-time control , and controlled using an Arduino microcontroller. This depicts the mechanism of a glove-controlled prosthetic arm using a glove which has an accelerometer, Arduino, and nRF wireless data transmission modules. The signals received are sent to a separate Arduino on the controlling side, and it drives the forearm motors and the prosthetic arm with a source of power and input code to the motors programmed.

Sensor Based Hand Motion Detection (Control Side). A glove that triggers the sensor detects hand movements on the control side. Accelerometer Data Acquisition and Preprocessing: The accelerometer of the project can sense hand motion like tilt, rotation, and acceleration to provide linear acceleration and transmit real-time movement signals to control the prosthetic arm through wireless communication.

Gravity Compensation & Data Acquisition: Continuously sample accelerometer data (acceleration in X, Y, and Z axes) at a suitable sampling rate (e.g., 50-100 Hz).

Noise Reduction Apply a low-pass filter (e.g., moving average filter, Butterworth filter) to remove high-frequency noise from the accelerometer data. Subtract the gravity component from the accelerometer data to obtain linear acceleration. This can be done using a complementary filter, Wireless Communication (nRF modules) in (Fig.3). The processed data between the glove and the prosthetic arm is sent through an nRF module operating in the 2.4GHz frequency band. The data transmitted are the gestures of the hand detected by the accelerometer. The receiver module on the prosthetic arm receives this data for further processing

Power Efficiency and Battery Life: The platform was powered by a 7.4V 2200mAh Li-Po battery. With constant use (gesture input and servo actuation every 10 seconds), the platform worked well for approximately 2.5 hours. When idle for extended periods, the platform used very little current, significantly extending standby time. Energy usage was greatest with motor actuation and wireless data bursts.

B. Microcontroller Processing (Arduino Side): The Arduino microcontroller circuit on the receiving side receives the information and produces control signals for the prosthetic arm.

Input Code & Interpretation: The firmware running under the Arduino fetches data and represents it to correlate with the defined gestures of the hand. The data are processed to cube the signals to be turned into PWM to run the motors.

C. System Responsive Control Algorithm: The control algorithm takes various threshold values to classify finger bending into several categories. The system then detects the corresponding gestures and determines the servo positions for each gesture detected. An Arduino ensures relatively smooth and coordinated motion of the motors in parallel.
D. Comparison of the prosthetic arm with the existing model. The features of the proposed work is compared with the existing approaches and listed in Table . 1

Table 1. Comparative study with the existing model

S. No	Feature	Proposed model	Existing model
1.	Control Mechanism	Gesture-based control using an accelerometer attached to the gloves	Myoelectric control using EMG sensors, EEG-based control, or mechanical switch-based control, [2]
2.	Communication	Wireless communication using nRF modules (RF-based transmission)	Wired connections (early models), Bluetooth, WiFl, or direct muscle signal transmission, [1]
3.	Processing Unit	Arduino-based microcontroller for gesture signal processing	Microcontrollers like Raspberry PL, STM32, or custom embedded systems, [3]
4.	Power Source	Rechargeable power bank (battery-powered motors)	Rechargeable Li-ion batteries, some models use kinetic energy harvesting, [9]
5.	Response Time	Real-time response with minimal latency (<100ms)	Varies (some models with Al prediction offer faster response, while older models have noticeable delays), [8]
6.	Grip Strength Control	Basic grip control using multiple motors	Advanced models allow variable grip strength and adaptive gripping [4]
7.	Material & Weight	3D-printed lightweight structure for affordability	Custom prosthetics use carbon fiber, titanium, or soft robotics [5]
8.	Suitability for Amputees	Primarily designed for wrist-level amputees (not yet adaptable for higher amputations)	Advanced bionic limbs support full-arm amputations with neural interfaces [12]

E. Feedback Mechanism: More advanced systems can use force sensors for haptic feedback. This adds functionality to the device by the fact that a user feels the applied pressure. The entire system is powered by a power bank, hence portable and rechargeable.

Fig.2. Main servo frame

F. Surgical Prosthesis Movement: The robotic arm moves the hand with external servo motors as shown in Figure 2. It Displays a 3D-printed modular structure designed to hold several servo motors, which are utilized to control the prosthetic arm movements. The servo motors relate to labeled cables for convenient signal flow from the controller unit.

Multi-Servo Control: The system is based on many servo motors controlling fingers. Each motor initially receives a control signal from the Arduino board for its motion. Closes and opens hand based on accelerometer input, imitating pinching, holding, or releasing movement

Fig.3. nRF Module

G. Wireless Communication & Signal Transmission: The nRF module allows

communication with minimum latency between the glove and prosthetic arm as depicted in Figures 1 & 4. Wireless communication, that is no physical connections are needed. The data stream commands finger position values, which are decoded at the receiving point.

H. Novelty: Jova focuses on balancing functionality and cost: Contrary to expensive commercial myoelectric arms, JOVA exploits 3D printing and available electronics to reduce costs without sacrificing functionality.
Using non-invasive control: Rather than surgery-inducing myoelectric implants, JOVA utilizes a gesture-control glove with motion sensing for intuitive gesture control.
Technologies merging: JOVA merges 3D printing, motion sensing, and wireless communication in a one-of-a-kind solution.
With a focus on accessibility: It puts underserved groups (children, youth, poor communities) first, usually forgotten by current solutions

4 Results and Discussions

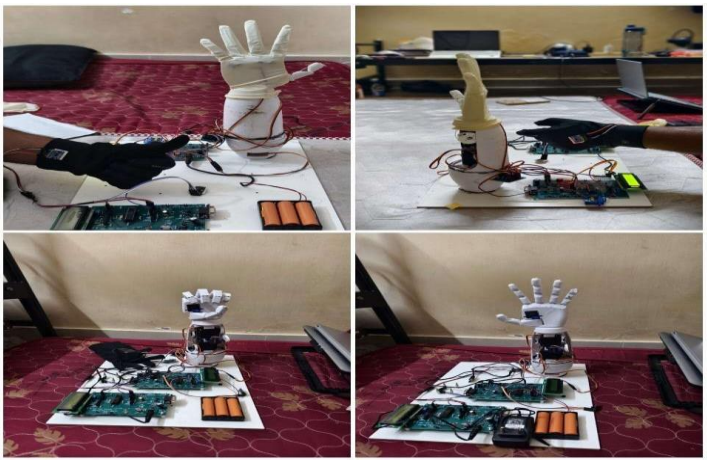

Fig.4.Prosthetic arm and its various control functions

The JOVA Robotic Prosthetic Arm, made using the help of a 3D-printed hand, accelerometer sensors, and servo motors, was successfully built to provide basic hand motions controlled using a motion-sensing glove is shown in the Figure 4. The use of an Arduino microcontroller allows real-time data processing to be efficient, and wireless communication was made using nRF24L01 module. The prosthetic arm employed in this work is a 3D-printed, lightweight, and affordable

prosthetic for amputees of the upper limb. The prosthetic is controlled by servo motors that replicate the movement of hands in real-time using signals sent from an Arduino microcontroller through the motion-sensing glove.

Fig.5. Controller Glows

The control component of the prosthetic arm has an Arduino microcontroller to receive wireless inputs from the glove's accelerometer through an nRF24L01 module as shown in Figure 5. It processes the information to provide accurate control signal to the servo motors to for real-time hand motions.

The motion-sensing glove serves as the primary input interface, equipped with an accelerometer to detect hand orientation, tilts, and dynamic movements. The glove proved to be intuitive, enabling users to control the prosthetic arm by mimicking natural wrist and finger gestures. The arm was assessed according to important performance measures, such as response time, accuracy, strength, and user comfort. The system delivered a fast response time of less than 100 ms, providing a smooth and natural transition of motion. The accuracy of gesture recognition was 85-90%, depending on sensor calibration and the hand size of the user.

Power Efficiency and Battery Life: The platform was powered by a 7.4V 2200mAh Li-Po battery. With constant use (gesture input and servo actuation every 10 seconds), the platform worked well for approximately 2.5 hours. When idle for extended periods, the platform used very little current, significantly extending standby time. Energy usage was greatest with motor actuation and wireless data bursts.

Table 2. Gesture and its associated movement

S. No	Gesture	Movement Output
1.	Forward	Closing palm 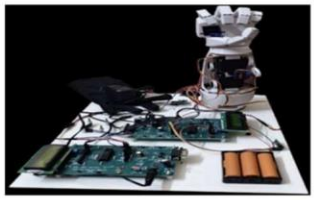
2.	Backward	Opening palm
3.	Left	Elbow to left
4.	Right	Elbow to right

The Table 2 records the gesture control feature of the JOVA Robotic Prosthetic Arm. The table translates certain hand or arm movements (gestures) identified by a motion-sensing glove into similar movement outputs executed by the prosthetic hand.

Forward motion of the hand translates to the prosthetic executing a closing palm

action, practically emulating a gripping motion.

Backward motion initiates the opening palm, enabling the hand to release objects.

Lifting the elbow to the left makes the prosthetic mimic an elbow to left movement, and shifting to the right performs an elbow to right movement.

Each gesture is clearly paired with a real-time response from the robotic arm, demonstrating intuitive, mirror-like control using motion sensors, likely interpreted by an IMU (Inertial Measurement Unit) and microcontroller. This setup enables natural control of the prosthetic without invasive input methods. Let me know if you'd like this formatted as a caption for a report or presentation.

One of the greatest achievements of the project is cost-effectiveness. With a production cost of well under traditional prosthetic devices, the JOVA arm provides an avenue for broader accessibility, especially to those in low-resource environments or developing nations where advanced prosthetics are beyond their means. Moreover, the modularity of the design provides for simple maintenance, repair, and upgrade in the future, making it long-term sustainable.

By intense testing, the system exhibited excellent gesture detection accuracy and motion imitation, attaining stable grip functionality with smooth finger movement. The MG996R servo motor-actuated prosthetic hand was found to be able to accomplish basic grasping functions like cup, pen, and small tool holding, rendering it applicable for everyday life. In addition, the 3D-printed design provided lightweight construction, ergonomic comfort, and simplicity of customization, making it possible to adapt the system for various users and hand sizes.

5 Future Enhancement

To further enhance the operation, flexibility, and usability of the robotic prosthetic arm system, enhancements can be made with a lot of possibilities. They can be categorized under sensor improvements, control systems, power supply, AI integration, and user interface features. Some suggestions for the work that might be worthwhile exploring in the future are

- Integration of Advanced Sensors: The system should not only be restricted to sensor flexion but should also integrate EMG-based sensors for muscle actuation detection. The arm will be under the direct control of users through muscle signals naturally and intuitively, instead of through gloves.
- BCI Implementation: EEG signals control prosthetic arms via brain signal processing. Neural signals processed with deep learning models accurately recognize gestures.

- Haptic Feedback Sensors: Force sensors within the prosthetic fingers convey haptic feedback to the user. This gives the user a feel for touch by sending certain feedback mechanisms, such as vibration signals. AI Driven Recognition and Adaptation of Gestures
- Gesture prediction with machine learning: The system will analyze deep learning algorithms (CNNs and LSTMs, or Transformers) to do an interpretation of the movements that are happening based on real-time information from sensors. Reinforcement learning can be applied to build the process across the training period for accuracy and preferences.
- Personally learned behavior: The system will be able to learn through time with the correlated movements individual to a user, thus improving comfort and efficacy. Transfer learning will be helpful to adapt the stateno propagation to other users.
- AI-Based Anomaly Detection: The prosthetic arm will be able to sense abnormal movements/effects and even self-correct to prevent unintended gestures.
- BLE or Wi-Fi Modules Awareness: Using BLE 5.0 or Wi-Fi communication can provide an improvement in the data transmission span and speed of the connection instead of replacing nRF modules. Low power consumption and realtime responsiveness would ensure a very smooth experience.
- Cloud-Based Prosthetic Control & Monitoring: Prosthetic data can be stored in the cloud for remote diagnostics, performance monitoring, and AI-based improvements. Cloud connectivity would allow telerehabilitation and customization of settings for different users.
- Strengthen Structural Parts: A few finger joints experienced minimal wear in heavy use— adopting carbon-reinforced PLA or nylon composites for future prints might enhance longevity.
- Software Suggestions: Gesture Calibration App: Create a mobile/desktop app through which users can calibrate gestures, establish control levels, and track performance
- User Training Programs: Create extensive training programs and materials to assist users in becoming familiar with the prosthetic arm and optimizing its use.
- Gesture Calibration App: Develop a desktops and mobile app through which users can calibrate gestures, set levels of control, and monitor performance. • Community Support and Feedback: Provide a forum for users to exchange experience, offer feedback, and provide improvement suggestions and drive development based on a community-based model.
- AI-Driven Gesture Recognition: Implement machine learning algorithms (CNNs, LSTMs, or Transformers) for interpreting real-time sensor data, enhancing gesture prediction accuracy.

6 Conclusion

This paper presents a gesture-controlled robotic prosthetic arm as an

affordable and easy-to-use alternative for upper limb amputees. Accelerometers and an Arduino-based control system translate user gestures into real-time finger movements with high responsiveness and moderate accuracy. nRF-based wireless communication module, enhances portability and convenience for daily applications. Although the proposed model is inexpensive, lightweight, and easy to implement, it does not have adaptive grip strength, haptic feedback, or accuracy in fine motor tasks. Compared to high-end bionic arms with EMG-based control, AI-based adaptability, and sensory feedback, the proposed system provides a simpler and more functional solution for basic prosthetic applications. Researchers could add EMG sensors, AI-based movement prediction, haptic feedback, and IoT connectivity in future versions to improve prosthetic functionality and compete with advanced bionic limbs. This work introduces a non-invasive, gesture-controlled prosthetic arm using low-cost components targeted at underserved populations.

References

[1] Julia Starke, Pascal Weiner, Markus Crell, Tamim Asfour, Semi-autonomous control of prosthetic hands based on multimodal sensing, human grasp demonstration and user intention, Robotics and Autonomous Systems, Volume 154,2022,104123, ISSN 0921-8890, https://doi.org/10.1016/j.robot.2022.104123.

[2] Kyung Rok Pyun, Kangkyu Kwon, Myung Jin Yoo, Kyun Kyu Kim, Dohyeon Gong, Woon-Hong Yeo, Seungyong Han and Seung Hwan Ko," Machine-learned wearable sensors for real-time hand-motion recognition: toward practical applications," National Science Review, Volume 11, Issue 2, February 2024, nwad298, https://doi.org/10.1093/nsr/nwad298

[3] Abd, M.A., Ingicco, J., Hutchinson, D. et al. Multichannel haptic feedback unlocks prosthetic hand dexterity. Sci Rep 12, 2323 (2022). https://doi.org/10.1038/s41598-02204953-1

[4] Sriramana Sankar et al., A natural biomimetic prosthetic hand with neuromorphic tactile sensing for precise and compliant grasping.Sci. Adv.11, eadr9300(2025). DOI: 10.1126/sciadv.adr9300

[5] Hamaragoda Kuruppuge Pasan Yashoda Jayaweera., "Design and Implementation of Electromyography (EMG) Based Real-Time Pattern Recognition Model for Prosthetic Hand Control," pp 1-66, OSF Preprints, 2021, https://doi.org/10.31219/osf.io/rd2cf.

[6] H. Taniguchi, R. Yakami, K. Morinaga and S. Wakimoto, "Forearm-Driven Soft Prosthetic Hand Designed for Children with the Ability to Execute Intricate and Skillful Motions," 2025 11th International Conference on Mechatronics and Robotics Engineering (ICMRE), Lille, France, 2025, pp. 221-226, doi: 10.1109/ICMRE64970.2025.10976323..

[7] Jr, III & Bugtai, Nilo & Baldovino, Renann & Espiritu, Noelle & Singson, Lowell. (2024). Development of an Arduino-based Control and Sensor System for a Robotic

Laparoscopic Surgical Unit. Recoletos Multidisciplinary Research Journal. 12. 125-144. 10.32871/rmrj2412.01.10.

[8] M, Logesh. (2024). Design and Control of Medical Prosthetic Hand Using Electromyography for Easy Hand Gesture. 1-7. 10.1109/ICDSCNC62492.2024.10939419.

[9] Kim, Hyunho, Sujin Jang, Phuoc Thien Do, Chang Kee Lee, Bummo Ahn, Suncheol Kwon, Handdeut Chang, and Yeongjin Kim. 2023. "Development of Wearable Finger Prosthesis with Pneumatic Actuator for Patients with Partial Amputations" Actuators 12, no. 12: 434. https://doi.org/10.3390/act12120434

[10] Roy, Divya & Chowdhury, Md & Afrose, Farhana & Hoque, Md. (2021). Design and Development of a Cost-effective Prosthetic Hand for Upper Limb Amputees. 1-5. 10.1109/BMEiCON53485.2021. 9745210..

[11] Abbady, Hnady E.M.A.1, Klinkenberg, Edwin T.M.1, de Moel, Lisanne1, Nicolai, Noa1, van der Stelt, Merel2; Verhulst, Arico C.2; Maal, Thomas J.J.2; Brouwers, Lars3,4. 3D-printed prostheses in developing countries: A systematic review. Prosthetics and Orthotics International 46(1): pp 19-30, February 2022. DOI: 10.1097/PXR.0000000000000057

[12] Ahkami B, Ahmed K, Thesleff A, Hargrove L, Ortiz-Catalan M. Electromyography-Based Control of Lower Limb Prostheses: A Systematic Review. IEEE Trans Med Robot Bionics. 2023 Aug;5(3):547-562. doi: 10.1109/tmrb.2023.3282325. Epub 2023 Jun 7. PMID: 37655190; PMCID: PMC10470657.

[13] Gentile, Cosimo, Francesca Cordella, and Loredana Zollo. 2022. "Hierarchical Human-Inspired Control Strategies for Prosthetic Hands" Sensors 22, no. 7: 2521. https://doi.org/10.3390/s22072521

[14] Chenchireddy, Kalagotla. (2024). Development of robotic arm control using Arduino controller. IAES International Journal of Robotics and Automation (IJRA). 13. 264-271. 10.11591/ijra. v13i3.pp264-271.

[15] Loutan, Kelvin & Persad, Umesh. (2023). The Design of a Low-Cost Voluntary Closing Finger Prosthetic for Developing Countries. 10.1115/DETC2023-117072.

Real-time defence against emerging IoT threats via feature-engineered ensemble learning in fog computing environments

[1]* Abdelilah Chahid[1], Yassine Znagui, Kamal el Guemmat[1] Sara Ouahabi[2] , Khalifa Mansouri [1]
[1]Department of Mathematics and Computer ScienceHigher Normal School of Technical Education, Morroco
[2]Modeling and Information Processing Laboratory, FSBM, Hassan II University, Casablanca, Morocco
chahidabdelillah@gmail.com

Abstract. Many studies have already investigated the security challenges associated with Internet of Things (IoT) devices, particularly within large corporations and smart city infrastructures. As the use of IoT continues to grow and evolve rapidly, these security concerns become increasingly critical., and not having same security rules, there is a strong need for smart systems that can find strange or dangerous behavior by themselves on networks with many devices. As the number of IoT devices keep increasing, the internet traffic they make also grows fast. This big amount of data makes old intrusion detection systems and old-style data processing not good enough anymore. It is very difficult to find bad actions early in IoT systems because of the large size and difference in network traffic. To help solve this problem, the research offers a special detection model that can look for dangerous traffic from IoT devices. This model uses three common machine learning methods: Support Vector Machine (SVM), Gradient Boosted Decision Trees (GBDT), and Random Forest (RF). Between these three, Random Forest showed the best results, reaching an accuracy of 86.92%. The test was done using the NSL-KDD dataset, and the results compared the training time, prediction time, how specific the model is, and its total accuracy.

Keywords: smart city networks; IoT; machine learning; intrusion detection system

1 Introduction

The Internet of Things (IoT) is one of the biggest and most important technology changes today, growing very fast in many industries. In 2018, there were about 28 billion IoT devices being used, and this number was expected to become 49.1

billion by 2022. At the same time, the global market was going to be close to $10 trillion. IoT means a system of connected devices—like sensors, servers, and software—that can share data with each other easily. In smart city systems, IoT is working in three main parts: the terminal layer, the fog layer, and the cloud layer. The cloud has strong computing power, but it also has problems like delay (latency), limited bandwidth, and high energy use. To solve this, fog computing was created as a new idea. It works in a more local way, so the system can answer faster and better—this is very helpful in emergencies or dangerous situations.

One big benefit of fog computing is in cybersecurity. If the system can find threats at the fog layer, it can respond quickly and stop problems before they get worse. This kind of early defense watches traffic at each network node, instead of waiting until the data gets to the cloud.

Machine Learning (ML) helps this process a lot. It can look at traffic, find strange behavior, and send alerts automatically. If the case is serious, the system can send the data to a human expert to check and act fast. This helps make the whole system safer and more dependable.

In IoT security, there are two main ways to detect problems:

- Signature-based detection: This finds threats by looking for known attack patterns. It is fast but can only find attacks already seen before.
- Anomaly-based detection: This watches normal behavior and gives warnings if something different happens. It can find new or unknown attacks.

Using both methods together gives strong and flexible protection, which is good for the complex and changing IoT systems we have today.

Fig. 1. Architecture for a smart city built on IoT

2 Related Work

Recent studys have shown the rising importance of Machine Learning (ML) and Deep Learning (DL) in many fields like object detection, pattern recogniton, text analisis, and image processing [1]. DL methods are also becoming more popular in cybersecurity, especially in smart city systems, where they are used to watch

user behavior and spot anomalies [2]. With the fast growth of big data and the Internet of Things (IoT) in smart cities, there is now a strong need for better ways to handle data. Cloud computing (CC) has been suggested as a main tool for making real-time decisions using big data [3][4]. Also, fog computing has come in as a local and decentrallized option that helps with things like load balancing, task shedualing, and resource offloading, which are judged by Quality of Service (QoS) scores [5] [6].

To make fog-based distributed networks more private, models like the Anonymous and Secure Aggregate Scheme (ASAS) were created, helping safe data sharing between fog devices and cloud servers [7]. New changes in wireless sensor networks (WSNs) and IoT tech keep helping this progress [8].

For intrusion detection, different ML algorithms have been used, like K-Nearest Neighbors (KNN), Support Vector Machine (SVM), Decision Tree (DT), Naïve Bayes, Neural Networks, and Random Forest (RF). They have been tested using datasets like Bot-IoT, and their success was measured with F1-score, precision, recall, and accuracy [9][10].

Some advanced threat detection tools include deep neural networks [11][12], fog-based NIDS systems [13], and hybrid methods like Isolation Forest mixed with One-Class SVM (OCSVM) and active learning to find zero-day attacks [14]. A special two-step model using Variational Autoencoder (VAE) also showed it works well for spotting strange behavior [15]. In [16], a Random Forest model was able to catch Ping of Death DDoS attacks using the WEKA platform, reaching 99.76% accuracy. There is also a method using flow-based graph analysis that worked very well in finding dictionary attacks on the CAIDA 2007 dataset [17].

3 Gap Analysıs

When looking at older research, it is possible to see many problems still happen in the area of intrusion detection for fog computing and IoT systems:

- Weak Detection at Fog Layer: The systems that try to find attacks in the fog layer are not always good. Many times, they do not give correct or stable results.
- Less Accuracy from Feature Selection: Feature selection is used to make data processing faster, but sometimes it removes important data, which causes the accuracy of results to go down.
- Low Detection for Some Attack Types: Some kinds of cyberattacks—like Denial of Service (DoS), Remote-to-Local (R2L), and User-to-Root (U2R)—are still hard to find correctly in many studies.
- Unstable Results from Classifiers on Small Datasets: When researchers use different classification methods on smaller or cleaned datasets, the results are often not stable or easy to use in real life.
- Problem with False Positives and Negatives: Even with better machine learning models, there is still a big issue with false positives and false

negatives, which makes it hard to fully trust the intrusion detection systems.

4 An Approach to Attack Detection in IoT Through Machine Learning Techniques

This study is introducing a model that is made to simulate a large organization or smart city that is more and more open to IoT-related cyber attacks. One important focus is the growing number of strong Distributed Denial of Service (DDoS) attacks. These are often done by big botnets like Mirai, which take advantage of weak or default passwords on IoT devices[18].

The research is looking at complicated cyberattacks that happen because of internal security policy problems, especially when unauthorized IoT devices are added into the network. Traditional detection methods are still used a lot because they have high accuracy and low false alarmsHowever, they often fail to detect new or unknown attacks. In contrast, anomaly-based detection methods are capable of identifying emerging threats but typically suffer from lower accuracy. Both signature-based and anomaly-based systems mostly use simple machine learning algorithms, which are not always strong enough to handle the changing and complex nature of modern cyber threats. To solve this problem, the study tests and compares different machine learning algorithms, using them in different steps of the new detection system (see Figure 2) [19]. The goal is to build a model that is stronger and more flexible, able to correctly detect both known and new threats in a smart city that is always changing.

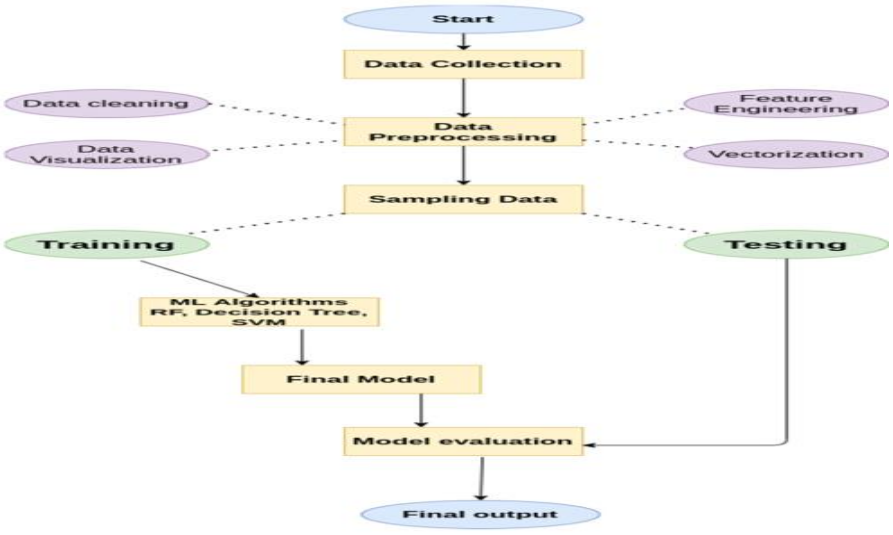

Fig. 2. Developing a Machine Learning-Based Framework for Attack Detection in IoT Networks

4.1 ML-Based Attack Detection Techniques

In **cybersecurity**, many ML-based detection systems use **statistical classification** to find suspicious or dangerous behavior. One common example is **spam filtering**, where supervised machine learning models are trained to know the difference between good and bad content.
This study looks at how good three popular classifiers are for finding **cyber threats**:

- **Support Vector Machine (SVM):**
  SVM puts the input data into a **high-dimensional space** and then finds the best **hyperplane** that can separate different classes. It works very well when the dataset has many features and also gives good results even if the training data is not big [20][21].
- **Gradient Boosted Decision Trees (GBDT):**
  GBDT is a method that builds trees one after the other. Each new tree tries to fix the mistake made by the last tree. This technique is known for **high prediction performance** and is good when working with **large datasets** because it improves step by step [22].
- **Random Forest (RF):**
  RF makes many decision trees by using **random parts of the data and features**. For the final decision, it uses **majority voting** from all trees. This helps to reduce variance and makes the model more stable. It is based on the **CART algorithm** and works well for many kinds of classification problems [23][24].

5 Experiments and Results

5.1 Dataset

To evaluate our models, we used the NSL-KDD dataset, a widely accepted benchmark for intrusion detection system (IDS) research. Available in both CSV and JSON formats, this dataset is favored for its balance between reproducibility and modifiability, making it ideal for training and testing ML models [25].

5.2 Proposed Methodology

This research introduces a hybrid ML framework that leverages the strengths of multiple independent learning algorithms. The process begins with data acquisition and preprocessing, which includes:

- Clearing and organizing raw data
- Visualizing patterns and outliers
- Engineering relevant features
- Vectorizing the data for model input

These steps are critical to convert unstructured input into usable feature vectors suitable for classification tasks [26].

During analysis, the NSL-KDD dataset revealed four major attack categories:

- **Remote-to-Local (R2L)**: Attempts to gain unauthorized access from a remote machine.
- **Denial-of-Service (DoS)**: Overloading system resources to disrupt operations.
- **User-to-Root (U2R)**: Escalation from regular user privileges to root-level control.
- **Probing**: Scanning and reconnaissance to identify vulnerabilities for future exploitation.
- **Port scanning,** categorized under Probe attacks, involves scanning network ports to identify potential vulnerabilities, as illustrated in Figure 3.

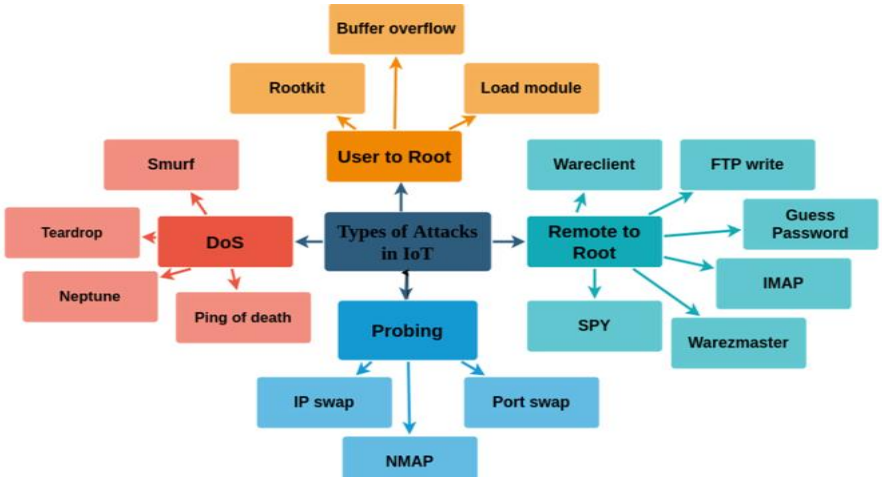

Fig. 3. Different Attack Vectors in the IoT Ecosystem

Table 1. Train Set of NSL-KDD

Type	Initial	Final	Duplicates removed (%)
Attacks	3 930 000	270 000	93.13
Normal	975 000	820 000	15.90
Total	4 905 000	1 090 000	77.78

Table 2. Test Set of NSL-KDD

Type	Initial	Final	Duplicates removed
Attacks	252 000	30 000	88.10
Normal	61 000	48 500	20.49
Total	313 000	78 500	74.92

The data was first transformed into feature vectors and then divided into two sets: 80% of the data was allocated for training and 20% for testing, as detailed in Tables 1 and 2. The training set was utilized to train the learning algorithm, while the final model was developed by applying a boosting technique. Figure 4

illustrates the distribution of data between the training and testing phases.

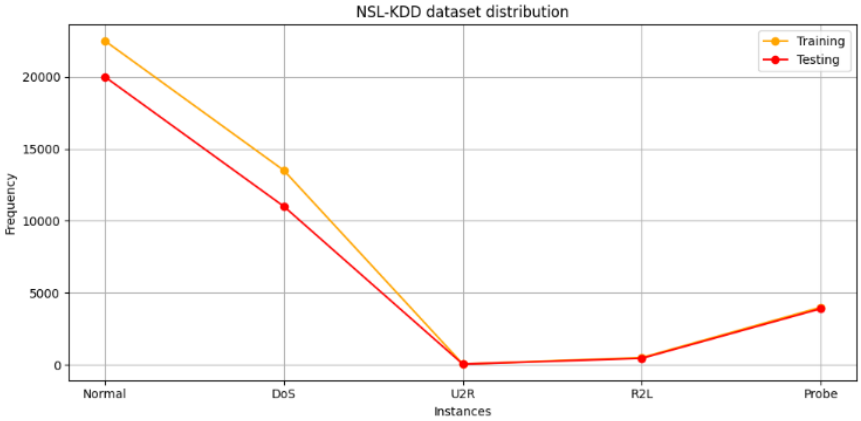

Fig. 4. NSL-KDD Dataset: Training and Testing Set Distribution

5.3 Algorithm Steps

The main steps that were followed to make the proposed algorithm work are shown below:

- First, load the NSL-KDD dataset.
- Do preprocessing to clean and get the data ready.
- Split the data into 80% for training and 20% for testing.
- Do feature selection to take only the important input features.
- Train the choosen classifiers using the training data.
- Test the classifiers with the testing data.
- Check how well the model works by calculating Accuracy, Specificity, False Positive Rate (FPR), and True Positive Rate (TPR).

5.4 Classifier and Model Training

In this study, the Random Forest (RF) algorithm was selected for training. This is a type of supervised learning that works with many Decision Trees (DT). Using RF has some good benefits, like it is easy to set the parameters and it does not easily get overfitted. In this work, the number of trees was set to 500, because adding more trees helps to reduce variance and does not change the bias too much. RF is already used in other works to look at network traffic, such as finding misuse activities and IoT-based Command and Control (C&C) attacks [27].

5.5 Performance Evaluation Metrics

The following metrics were used to understand how good the system works:

- **Accuracy (A):** How many times the model was right, both for attacks and for normal data.

- **Training Time (TT):** The time it took to train the model.
- **Specificity (S):** How many of the real normal data were correctly found.
- **Prediction Time (PT):** How long it took the model to make predictions for the test data.

Other useful values:

- **True Positive (TP):** Attacks that were found correctly.
- **False Positive (FP):** Normal data that was wrongly marked as attack.
- **True Negative (TN):** Normal data that was correctly detected.
- **False Negative (FN):** Attacks that the model missed.

The formulas for some important metrics:

Accuracy (A):

$A = (TP + TN) / (TP + FP + TN + FN)$

Specificity (S):

$S = TN / (FP + TN)$

The study also used the Receiver Operating Characteristic (ROC) curve to show how well the model is doing. This curve shows the True Positive Rate (TPR) compared with the False Positive Rate (FPR) using different thresholds.

Classification thresholds are not fixed—they vary based on the classifier used and the specific class being predicted. These thresholds serve as cut-off values for predicted probabilities, directly impacting the sensitivity of classification and significantly influencing key performance metrics.

Two critical evaluation metrics influenced by the threshold include:

- **False Positive Rate (FPR)**

$FPR=FP/FP+TN$

FPR reflects how often normal traffic is incorrectly flagged as malicious.

- **True Positive Rate (TPR)**

$TPR=TP/TP+FP$

TPR measures the model's success in identifying actual threats.

These metrics form the basis of ROC (Receiver Operating Characteristic) curves, where TPR is plotted against FPR across various thresholds, allowing visualization of the trade-offs between sensitivity and specificity. The ROC space spans values from 0 to 1 for both axes, offering a comprehensive view of model performance across all threshold settings.

5.6 Setup and Environment for Experiments

Experiments were performed on a Lenovo ThinkPad equipped with a 4500U processor, 8GB of RAM, an integrated AMD GPU, and running Ubuntu 20.04, with additional support for NVIDIA GPUs to enhance computational capabilities and ensure robust and reliable testing. Data preprocessing steps—including cleaning, normalization, and feature selection—were carried out using Python tools such as NumPy and Pandas, chosen for their efficiency in handling structured datasets.

5.7 Result Analysis

The study evaluated three prominent machine learning classifiers on the NSL-KDD dataset:

- Random Forest (RF)
- Gradient Boosted Decision Trees (GBDT)
- Support Vector Machine (SVM)

Using cross-validation, the Random Forest model emerged as the top performer, At the fog-computing layer, the RF model reaches an accuracy of 86.92 %. GBDT follows with 80.34 %, while SVM remains far behind at 34.15 %.

For specificity, GBDT leads at 96.88 %, RF is close with 95.41 %, and SVM manages only 3.07 %.

Table III groups the main metrics: Accuracy (A), Training Time (TT), Prediction Time (PT) and Specificity (S).

Table 3 . Performance Evaluation Table

Method	A (%)	S (%)	TT (s)	PT (ms)
SVM	34.15	3.07	11.02	1.05
GBDT	80.34	96.88	7.60	1.58
RF	86.92	95.41	6.05	1.37

6 Conclusion

This study confirms the effectiveness of supervised machine learning algorithms in detecting malicious behavior within IoT networks, particularly in fog computing environments. Utilizing the NSL-KDD dataset, the evaluated models demonstrated robust classification capabilities, accurately distinguishing between various types of network traffic and identifying anomalies consistent with modern cyber threats. Among the tested algorithms, Random Forest delivered the highest performance, achieving a detection accuracy of 86.92%, underscoring its potential for managing the complexities associated with real-world applications in smart cities and large-scale IoT infrastructures. Future research will focus on expanding the scope of the evaluation by incorporating a wider variety of IoT devices, investigating advanced approaches such as deep learning, and applying more current datasets that reflect the evolving nature of malware and cyberattacks. These efforts aim to improve the adaptability, scalability, and long-term resilience of the proposed detection framework in response to the continuously shifting cybersecurity landscape.

References

1. CHOTIA, Varun, KHOUALDI, Kamel, BROCCARDO, Laura, *et al.* The role of cyber security and digital transformation in gaining competitive advantage through Strategic Management Accounting. *Technology in Society*, 2025, vol. 81, p. 102851.

2. HERATH, HMKKMB et MITTAL, Mamta. Adoption of artificial intelligence in smart cities: A comprehensive review. International Journal of Information Management Data Insights, 2022, vol. 2, no 1, p. 100076.
3. FRANCHINA, Luisa, INZERILLI, Giulia, SCATTO, Enrico, et al. Passive and active training approaches for critical infrastructure protection. International Journal of Disaster Risk Reduction, 2021, vol. 63, p. 102461.
4. MUTLAG, Ammar Awad, ABD GHANI, Mohd Khanapi, MOHD, Othman, et al. A new fog computing resource management (FRM) model based on hybrid load balancing and scheduling for critical healthcare applications. Physical Communication, 2023, vol. 59, p. 102109.
5. ALDHAHERI, Alyazia, ALWAHEDI, Fatima, FERRAG, Mohamed Amine, et al. Deep learning for cyber threat detection in IoT networks: A review. Internet of Things and cyber-physical systems, 2024, vol. 4, p. 110-128.
6. BONOMI, Flavio, MILITO, Rodolfo, NATARAJAN, Preethi, et al. Fog computing: A platform for internet of things and analytics. Big data and internet of things: A roadmap for smart environments, 2014, p. 169-186.
7. K. Sarwar, S. Yongchareon, J. Yu, S. ur Rehman, « Lightweight, Divide-and-Conquer privacy-preserving data aggregation in fog computing », Future Generation Computer Systems, vol. 119, pp. 188-199, 2021, doi: 10.1016/j.future.2021.02.013
8. B. Huber, F. Kandah, A. Skjellum, « BEAST : Behavior-as-a-Service for trust management in IoT devices », Future Generation Computer Systems, vol. 144, pp. 165-178, 2023, doi: 10.1016/j.future.2023.02.003
9. KHAN, Muhammad Almas, KHAN KHATTK, Muazzam A., LATIF, Shahid, et al. Voting classifier-based intrusion detection for iot networks. In : Advances on Smart and Soft Computing: Proceedings of ICACIn 2021. Springer Singapore, 2022. p. 313-328.
10. ATTIQUE, Danish, WANG, Hao, et WANG, Ping. Fog-assisted deep-learning-empowered intrusion detection system for RPL-based resource-constrained smart industries. Sensors, 2022, vol. 22, no 23, p. 9416.
11. PONNIAH, Krishna Kumar et RETNASWAMY, Bharathi. A novel deep learning based intrusion detection system for the IoT-Cloud platform with blockchain and data encryption mechanisms. Journal of Intelligent & Fuzzy Systems, 2023, vol. 45, no 6, p. 11707-11724.
12. REDDY, Dukka KarunKumar, BEHERA, Himansu Sekhar, NAYAK, Janmenjoy, et al. Deep neural network based anomaly detection in Internet of Things network traffic tracking for the applications of future smart cities. Transactions on Emerging Telecommunications Technologies, 2021, vol. 32, no 7, p. e4121.
13. KHAN, Muhammad Almas, KHAN KHATTK, Muazzam A., LATIF, Shahid, et al. Voting classifier-based intrusion detection for iot networks. In : Advances on Smart and Soft Computing: Proceedings of ICACIn 2021. Springer Singapore, 2022. p. 313-328.
14. SHARAFALDIN, Iman, LASHKARI, Arash Habibi, HAKAK, Saqib, et al. Developing realistic distributed denial of service (DDoS) attack dataset and taxonomy. In : 2019 international carnahan conference on security technology (ICCST). IEEE, 2019. p. 1-8.
15. MUSHTAQ, Earum, ZAMEER, Aneela, UMER, Muhammad, et al. A two-stage intrusion detection system with auto-encoder and LSTMs. Applied Soft Computing, 2022, vol. 121, p. 108768.
16. HIZAL, Selman, CAVUSOGLU, Unal, et AKGUN, Devrim. A novel deep learning-based intrusion detection system for IoT DDoS security. Internet of Things, 2024, vol. 28, p. 101336.

17. PAOLINI, Emilio, VALCARENGHI, Luca, MAGGIANI, Luca, et al. Real-time clustering based on deep embeddings for threat detection in 6G networks. IEEE Access, 2023, vol. 11, p. 115827-115835.
18. OMETOV, Aleksandr, MOLUA, Oliver Liombe, KOMAROV, Mikhail, et al. A survey of security in cloud, edge, and fog computing. Sensors, 2022, vol. 22, no 3, p. 927.
19. I. Kotenko, I. Saenko, A. Kushnerevich, and A. Branitskiy, "Attack Detection in IoT Critical Infrastructures: A Machine Learning and Big Data Processing Approach," in 27th Euromicro International Conference on Parallel, Distributed and Network-Based Processing, Pavia, Italy, Feb. 2019, pp. 340–347, https://doi.org/10.1109/EMPDP.2019.8671571.
20. WANG, Chao, SUN, Yunxiao, LV, Sicai, et al. Intrusion detection system based on one-class support vector machine and Gaussian mixture model. Electronics, 2023, vol. 12, no 4, p. 930.
21. HU, Jiamin, YANG, Xiaofan, et YANG, Lu-Xing. A framework for detecting false data injection attacks in large-scale wireless sensor networks. Sensors, 2024, vol. 24, no 5, p. 1643.
22. MOKHTARI, Sohrab, ABBASPOUR, Alireza, YEN, Kang K., et al. A machine learning approach for anomaly detection in industrial control systems based on measurement data. Electronics, 2021, vol. 10, no 4, p. 407.
23. AIN, Noor Ul, SARDARAZ, Muhammad, TAHIR, Muhammad, et al. Securing IoT Networks Against DDoS Attacks: A Hybrid Deep Learning Approach. Sensors, 2025, vol. 25, no 5, p. 1346.
24. CHOU, Dylan et JIANG, Meng. A survey on data-driven network intrusion detection. ACM Computing Surveys (CSUR), 2021, vol. 54, no 9, p. 1-36.
25. GAN, Chenquan, LIU, Anqi, ZHU, Qingyi, et al. Social tie-driven coupling propagation of user awareness and information in Device-to-Device communications. Computer Networks, 2023, vol. 237, p. 110087.
26. CHANDER, Nenavath et UPENDRA KUMAR, Mummadi. Metaheuristic feature selection with deep learning enabled cascaded recurrent neural network for anomaly detection in Industrial Internet of Things environment. Cluster Computing, 2023, vol. 26, no 3, p. 1801-1819.
27. CHEN, Jialong, XIAO, Jingjing, et XU, Jiaxin. VGGIncepNet: Enhancing Network Intrusion Detection and Network Security through Non-Image-to-Image Conversion and Deep Learning. Electronics, 2024, vol. 13, no 18, p. 3639.

Assess the Effects to Organs Induced by I-131 Radiopharmaceutical Accumulates in Thyroid Gland by Monte Carlo Simulation

[*]Minh Khanh Duong[1], Tat Thang Nguyen[1]
[1]Hanoi University of Science and Technology, Hanoi, Vietnam
[1*]Khanh.DM217520@sis.hust.edu.vn

Abstract. The "S" value, representing the energy deposited per unit mass per particle, is essential for internal dose calculations. In this study, GEANT4 and MCNP6.1 are used to compute "S" values in selected organs using male and female MRCP phantoms. A comparison of results from both tools provides reference data for assessing I-131 exposure. Generally, female phantoms yield higher "S" values than males in most organs, except for the colon and small intestine. Differences are also more evident in organs located farther from the thyroid or composed of multiple anatomical parts, suggesting that organ location and structural complexity significantly affect the calculated dose.

Keywords: thyroid, Monte Carlo, internal dose, I-131.

1. Introduction

Thyroid cancer is becoming one of the global health concerns. According to the latest data from GLOBOCAN 2022 [1], thyroid cancer has become the seventh most common cancer worldwide, with 821,214 new cases, accounting for approximately 4.1% of all cancer cases globally. The number of deaths caused by this disease reached 47,507, representing a mortality rate of 0.49%. In particular, in Vietnam, thyroid cancer is also among the most common cancers. In 2022 alone, 6,122 new cases were reported, accounting for 3.4% of the total cancer cases in the country, making it the sixth most prevalent cancer nationwide (GLOBOCAN, 2022). Accompanying this is the number of deaths due to thyroid cancer, which reached 858 cases, representing a mortality rate of 0.71%. A study by Pham et al. [2] investigating thyroid cancer incidence in Ho Chi Minh

City (Vietnam) across four consecutive 5-year periods—1996–2000, 2001–2005, 2006–2010, and 2011–2015—based on 5,953 thyroid cancer cases, found that the highest incidence was recorded at the age of 45 in both sexes, while the lowest incidence occurred in those aged 65 and above. Therefore, the investigation and treatment of thyroid cancer in adults is of critical importance.

Currently, the treatment of thyroid cancer using the radioactive isotope Iodine-131, also known as RAI (Radioactive Iodine), is the most widely used therapy worldwide, given that thyroid cancer is among the most common types of cancer. The principle of this method is that when radioactive isotope I-131 decays to return to a stable state, it emits beta β^- radiation, and this process is also accompanied by gamma γ radiation. When administered to a patient, I-131 is strongly absorbed by thyroid tissue due to the biological affinity between thyroid cells and iodine. The ionizing radiation emitted and co-emitted during the decay of I-131 destroys residual microscopic thyroid tissue after surgery, aiming to eliminate all cancerous cells remaining in the thyroid region, and potentially even metastatic cells that have spread to surrounding organs [3].

However, treatment with radiopharmaceuticals also poses both short-term and long-term health risks for patients. With an Iodine-131 activity ranging from 101 mCi to 150 mCi, the risk of developing leukemia can be as high as 3.09% [4]. In addition, common short-term clinical symptoms following oral administration of the radiopharmaceutical include swelling, pain, and dysfunction of the salivary glands, as these glands frequently absorb and excrete I-131. A further late complication observed in patients undergoing RAI treatment is xerostomia (dry mouth), which often becomes more pronounced after hospital discharge. Gastrointestinal disturbances have also been commonly reported among patients treated with I-131 [5]. These concerns highlight the need for rational use of radiopharmaceutical activity to minimize side effects in patients. Therefore, investigating radiation dose levels as safety references for RAI treatment is an essential issue in nuclear medicine.

Although there is some research groups executed measurements on patients' bodies [6], provided some measurement systems and even the dosimetry considerations, associated risks, and the prevailing challenges in measurement domains [7], and several research groups focus on synthesizing and exploring supportive options for personalized treatment [8] the assessment cannot always be executed directly on patients' bodies because of the resolution, the geometric error of the measurements and even moral problems. And for scientific research purposes, many hypothetical scenarios involving irradiation require computational analysis. Therefore, direct measurement is not always a feasible solution, and it becomes necessary to use an alternative object instead of the human body for studying. There are many virtual phantoms introduced, ICRP Publication 145 [9] introduced a human body-representative phantom composed of multiple tetrahedral elements, known as the MRCP (Mesh-type Reference

Computational Phantom). This phantom has become a standard reference model for research and dosimetry calculations in various simulation programs, serving as an alternative to actual human bodies in computational studies. In this paper, the computational phantoms that presented for adult males and females are used for assessment.

In internal dose calculation, the “S” value was determined as the as the amount of absorbed radiation dose delivered to the target organ or tissue resulting from a single disintegration of the radionuclide occurring in the source organ or tissue [10]. Then the values of internal dose are performed by multiplying the “S” value with the radioactivity accumulated in target organs. In this research, the Monte Carlo simulation is used for estimating the “S” value with the source (iodine 131) located in thyroid gland. In clinical practice, patients often undergo surgery to partially or completely remove the thyroid gland. Corresponding to these cases, the internal radiation dose to the thyroid and other organs will also differ. This highlights the need for further research and dose calculations tailored to these specific clinical scenarios.

2. Related work

Several studies have utilized Monte Carlo software programs to calculate radiation doses from internal exposure to I-131 sources [11], [12], [13], [14]. However, most of the aforementioned research groups only used and reported results from a single Monte Carlo simulation program or conducted their studies on voxel phantoms — a type of phantom with lower resolution and less detailed organ contours compared to MRCP phantoms. Although the results researched on pediatric phantom of S. M. Lee et al [13] had provided various values of different of 30 organs, their study mainly focused on pediatric subjects under 15 years old. Moreover, the research was conducted using voxel phantoms with a simpler algorithm compared to calculations performed on tetrahedral phantoms [9].

In the study by Shahbazi-Gahrouei and Ayat [11], the absorbed dose values were calculated and compared between simulations and actual measurements using TLD detectors. However, mathematical phantoms were used, which are constructed from simple geometric shapes, with organs represented by cylinders, ellipsoids, tori, etc. Moreover, important radio sensitive organs have not been validated in the study such as liver, lung, stomach, kidney, …Therefore, it is essential to conduct a comparison between different Monte Carlo software packages, with evaluations across various organs in the human body, to provide the most comprehensive and complete reference possible.

The study by B. Juste et al. [12] provided time-dependent dose results based on the

standard ICRP phantom; however, these results were calculated using MCNP and their own biological model, without comparison to other Monte Carlo tools.

3. Proposed Work

This study aims to contribute to health science research by minimizing patient risk through simulation-based dose estimation. Specifically, it focuses on determining organ-specific "S" values resulting from the accumulation of Iodine-131 in the thyroid gland, which serves as the foundation for calculating internal radiation doses in the human body. To achieve this, the study utilizes the standard Mesh-Reference Computational Phantoms (MRCP) published by the ICRP [9], which feature anatomically detailed and realistic organ geometries, thereby overcoming the limitations of direct dose measurements. Radiation transport simulations are performed using the Monte Carlo method implemented in two widely used software packages: MCNP (version 6.1.1) and GEANT4. Three clinical scenarios are considered: (1) total thyroidectomy, (2) only the left lobe remaining, and (3) only the right lobe remaining. The resulting "S" values for nearly 30 organs are presented and cross-compared between the two codes. These values are intended to provide clinically relevant reference data for thyroid cancer treatment using radioiodine (RAI), while the comparison between the two Monte Carlo tools enhances the reliability and credibility of dose calculations based on virtual phantoms.

4. Methodology

4.1. Mesh- type Reference Computational Phantom (MRCP phantom)

The MRCP phantom is constructed using tetrahedral elements in three-dimensional space. These MRCP phantoms are developed by converting voxel-based phantoms into high-quality mesh formats, integrating supplementary stylized models that are used alongside voxel phantoms to overcome the resolution limitations of voxels, and to incorporate additional tissue layers believed to contain cells at risk of radiation-induced cancer [9].

The MRCP phantoms significantly overcome the geometric limitations found in the ICRP voxel phantoms, which stem from the restricted voxel resolution and the inherent characteristics of voxel-based geometry. While the voxel-based models present stepped or jagged surfaces, the mesh-based MRCP models exhibit smoother, more continuous contours in 3D visualization. Additionally, the discontinuities in the hollow organ

structures observed in the voxel phantoms have been fully resolved in the MRCP models [9].

The calculations in this study are performed on adult male and female MRCP phantoms, representing the age group most commonly affected by thyroid cancer (Fig 1.). The male phantom is 1.76 meters tall, weighs 73 kg, and is composed of 8.2 million tetrahedral elements. The female phantom is 1.63 meters tall, weighs 60 kg, and consists of 8.6 million tetrahedra.

Fig 1. MRCP Phantoms performed by MCNP6
(Left: male phantom, Right: female phantom)

4.2. Calculated Organs

This study investigates the S value in several human organs, including those that are highly exposed to radiation through the metabolism and excretion processes of Iodine-131, such as the salivary glands, esophagus, liver, stomach, kidneys, and bladder. The S value provides information on the energy absorbed per unit mass of the target organ, which can be used to estimate the specific radiation dose delivered to that organ.

All organs are calculated in this research are: Active bone marrow/ Red bone marrow (RBM), Colon, Lung, Stomach, Breasts, Gonads, Urinary Bladder, Esophagus, Liver, Thyroid, Endosteum, Brain, Salivary Gland, Skin, Adrenals, ET (Eustachian Tube), Gall Bladder, Heart, Kidneys, Lymph nodes, Muscle, Oral mucosa, Pancreas, Prostate/Uterus, Small intestine, Spleen, Thymus, Eye Lens. As described above, in realistic clinical cases, although patients almost undergo surgery to eliminate thyroid glands, there still remains the residual thyroid issue. Thus, in this study, the "S" value is also calculated in thyroid. In this research, the results of "S" would be performed in 3 cases of both genders: AM-AF CR (Completely Removal), which are represented for patients whose thyroid glands are Completely Resected, AM-AF Left/Right which are represented for patients whose thyroid glands remain the left/right side part.

4.3. Calculation models

I-131 primarily emits beta-minus (β^-) particles along with accompanying gamma (γ) radiation. However, in this simulation, the accompanying γ emission at 164 keV from ^{131m}Xe to the stable ^{131}Xe state (with a probability of 0.021%) is neglected. Therefore, the source parameters of I-131 used in the simulation are defined as follows:

Table 1. Decay Table of I-131

	Energy (keV)	**Probability of decay N_i(%)**
γ	284	6.45
	364	83.1
	637	7.15
β	606	7.2
	334	89.4

For GEANT4, virtual detectors are set at the positions (organs) to be investigated using G4VUserDetectorConstruction. The source will be placed at the source organ, the thyroid, as defined by G4VUserPrimaryGeneratorAction. In this problem, both the source and the detectors are tissues created in the phantom file, which are placed outside the layers. When used, they will be called from the corresponding classes. The result produced by the GEANT4 program is the value of SAF – the specific absorption factor of the tissue for the source (1/kg) per decay particle, defined as formula (1).

$$SAF_{(target \leftarrow source)} = \frac{E_{dep}}{E_S} * \frac{1}{m_{organ}} \left(\frac{1}{kg}\right) \quad (1)$$

With E_{dep} being the deposited energy at the target organ and E_S is the energy emitted from the source (thyroid gland). Each energy level will be simulated separately

to obtain its corresponding SAF value. After that, the S value is calculated based on the results of GEANT4 through the formula (2).

$$S_{(target \leftarrow source)} = SAF_{(target \leftarrow source)} \left(\frac{1}{kg}\right) * E_i \text{ (MeV)} * N_i * 10^{-3} \quad (2)$$

With E_i being the ith decay energy of I-131 and N_i is the corresponding decay probability of E_i.

For the MCNP6.1.1 code, the +F6 tally (with units of MeV/g) is used to calculate the energy deposited in cell by ionizing radiation per particle [15]. At the same time, to simulate the full range of nuclear interactions of electrons (β^-) and photons, the physics card "mphys" is enabled by default. Similar with GEANT4 code, the MCNP simulation is also performed with a number of particles (nps) equal to $2*10^8$ to ensure that the recommended relative error of the +F6 tally is below 0.1. The obtained result represents the dose per particle (MeV/g/particle), which corresponds to the S value used in the dose assessment report.

5. Results

5.1. Results of "S" value from MCNP and GEANT4

Based on the results obtained from MCNP (Table 2), the "S" values of the AM are lower than AF phantoms in most organs in the CR case, except for the following: Colon (ratio 2.5147), Stomach (1.3049), Small Intestine (1.3991), Thyroid (1.3937), Pancreas (1.2432), Spleen (1.1132), and Thymus (1.0345). In contrast, the remaining organs show ratios smaller than 1.0. All ratios are defined as the "S" value of the AM phantom divided by that of the AF phantom; therefore, the "S" values for most organs are higher in the AF phantom than in the AM phantom.

Similarly, in Left residual Thyroid tissue and Right residual Thyroid tissue cases, "S" value of AM is lower than AF phantoms in most organs in these cases. But the results at Colon, Lung, Stomach, and Small Intestine indicate significant difference between AM and AF phantom at which the "S" values are contrary to the aforementioned trend. Especially for Lung in Right residual thyroid tissue case, the result of AM are approximately 85 times higher than AF.

The results obtained from GEANT4 are performed in table 3. The different trends between AM and AF are analogous to the presents of MCNP. "S" value of AF phantom is higher than AM phantom at almost organs in all 3 cases, but there still remain exception at Colon, Lung, Pancreas, Urinary Bladder, Small intestine, Spleen at which the "S" value of AM is higher. In details, the "S" value at Thyroid of CR case of AM phantom is higher than AF phantom (ratio 1.39), same as it in MCNP.

Table 2. Results of "S" value in some organs of male and female bodies calculated by MCNP
(CR: Completely Removal; AM: Male; AF: Female)

$S_{(target \leftarrow source)}$ of some organs- calculated by MCNP						
Organ	AM CR	AF CR	AM Left	AF Left	AM Right	AF Right
RBM	1.51E-06	2.25E-06	1.52E-06	7.97E-07	3.27E-06	3.96E-06
Colon	7.72E-08	3.07E-08	1.12E-07	3.04E-08	1.26E-07	4.30E-08
Lung	2.31E-06	2.88E-06	5.00E-06	1.15E-06	4.64E-06	5.42E-08
Stomach	3.21E-07	2.46E-07	5.34E-07	2.15E-07	2.89E-07	2.74E-07
Breasts	3.88E-07	1.18E-06	4.61E-07	9.07E-07	1.42E-07	4.11E-07
Gonads	7.42E-10	5.66E-09	2.23E-10	2.25E-09	1.65E-09	1.10E-08
Urinary Bladder	6.52E-09	5.82E-09	6.52E-09	7.16E-09	5.53E-09	6.70E-09
Esophagus	4.61E-05	2.06E-04	1.92E-05	6.54E-05	3.59E-05	1.43E-04
Liver	3.97E-07	4.16E-07	3.82E-07	7.83E-07	4.42E-07	2.54E-05
Thyroid	4.85E-01	3.48E-01	1.90E-02	3.84E-02	3.08E-02	3.77E-02
Endosteum	7.14E-07	1.28E-06	4.57E-07	8.12E-07	3.31E-07	1.25E-06
Brain	4.30E-07	6.42E-07	4.15E-07	1.33E-06	4.34E-07	6.69E-07
Salivary Gland	2.65E-06	3.99E-06	5.01E-06	7.72E-06	5.49E-06	8.74E-06
Skin	3.93E-07	4.60E-07	3.71E-07	7.93E-07	3.89E-07	5.03E-07
Adrenals	2.50E-07	2.60E-07	5.50E-07	5.03E-07	5.00E-07	9.35E-07
ET	6.37E-06	7.10E-06	6.56E-06	6.62E-06	6.27E-06	6.85E-06
Gall Bladder	2.25E-07	2.34E-07	2.03E-07	4.40E-07	2.49E-07	6.82E-06
Heart	1.74E-06	1.91E-06	1.91E-06	3.95E-06	1.66E-06	1.99E-06
Kidneys	1.49E-07	1.42E-07	8.78E-08	1.55E-07	5.06E-07	3.35E-07
Lymph nodes	1.07E-06	1.38E-06	1.08E-06	4.95E-06	2.63E-06	2.80E-06
Muscle	6.34E-07	7.84E-07	7.97E-07	1.78E-06	6.50E-07	1.42E-06
Oral mucosa	2.50E-06	4.78E-06	4.62E-06	5.26E-06	5.35E-06	1.11E-05
Pancreas	1.84E-07	1.48E-07	1.97E-07	2.89E-07	1.92E-07	1.45E-07
Prostate/ Uterus	3.50E-09	5.40E-09	4.45E-09	1.07E-08	3.00E-09	5.96E-09
Small intestine	6.03E-08	4.31E-08	6.57E-08	3.24E-08	5.60E-08	4.21E-08
Spleen	3.54E-07	3.18E-07	4.42E-07	7.03E-07	3.21E-07	4.19E-08
Thymus	2.40E-05	2.32E-05	2.32E-05	4.58E-05	2.00E-05	2.32E-05
Eye Lens	4.06E-07	5.83E-07	2.90E-07	5.03E-07	5.57E-07	9.62E-07

Table 3. Results of "S" value in some organs of male and female bodies calculated by GEANT4
(CR: Completely Removal; AM: Male; AF: Female)

$S_{(target \leftarrow source)}$ of some organs- calculated by GEANT4						
Organ	AM CR	AF CR	AM Left	AF Left	AM Right	AF Right
RBM	1.44E-06	1.86E-06	1.48E-06	1.72E-06	1.39E-06	1.72E-06
Colon	7.48E-08	2.71E-08	7.81E-08	2.67E-08	7.29E-08	2.53E-08
Lung	2.22E-06	2.85E-06	2.38E-06	2.73E-06	2.28E-06	2.67E-08
Stomach	2.96E-07	2.38E-07	3.28E-07	2.49E-07	2.65E-07	2.49E-07
Breasts	3.58E-07	1.15E-06	3.79E-07	1.14E-06	3.53E-07	2.57E-07
Gonalds	7.15E-10	5.58E-09	6.73E-10	5.50E-09	8.36E-10	5.50E-09
Urinary Bladder	6.37E-09	5.82E-09	6.32E-09	5.74E-09	6.64E-09	5.74E-09
Esophagus	4.48E-05	2.05E-04	1.95E-05	4.62E-05	1.16E-05	4.62E-05
Liver	3.89E-07	4.16E-07	3.67E-07	3.78E-07	4.25E-07	2.44E-05
Thyroid	4.82E-01	3.48E-01	1.82E-02	3.34E-02	2.72E-02	3.34E-02
Endosteum	6.46E-07	8.75E-07	6.63E-07	8.31E-07	6.29E-07	8.31E-07
Brain	4.21E-07	6.42E-07	3.96E-07	6.43E-07	4.19E-07	6.43E-07
Salivary Gland	2.54E-06	3.95E-06	2.44E-06	4.16E-06	2.63E-06	4.16E-06
Skin	3.70E-07	4.51E-07	3.51E-07	4.66E-07	3.61E-07	4.66E-07
Adrenals	2.40E-07	2.57E-07	2.49E-07	2.42E-07	2.49E-07	4.65E-07
ET	6.30E-06	6.83E-06	6.23E-06	6.78E-06	6.32E-06	6.78E-06
Gall Bladder	2.20E-07	2.34E-07	2.02E-07	2.12E-07	2.34E-07	6.43E-06
Heart	1.70E-06	1.91E-06	1.82E-06	1.91E-06	1.59E-06	1.91E-06
Kidneys	1.32E-07	1.35E-07	1.37E-07	1.28E-07	1.37E-07	1.28E-07
Lymph nodes	1.02E-06	1.14E-06	7.43E-07	1.12E-06	1.02E-06	1.12E-06
Muscle	6.22E-07	7.84E-07	7.65E-07	1.17E-06	8.27E-07	1.17E-06
Oral mucosa	2.39E-06	4.72E-06	2.16E-06	4.70E-06	2.26E-06	4.70E-06
Pancreas	1.80E-07	1.48E-07	1.83E-07	1.39E-07	1.85E-07	1.39E-07
Prostate/ Uterus	3.41E-09	5.40E-09	3.29E-09	5.18E-09	3.52E-09	5.18E-09
Small intestine	5.56E-08	4.14E-08	5.84E-08	4.05E-08	5.84E-08	4.05E-08
Spleen	3.47E-07	3.18E-07	4.22E-07	3.41E-07	3.07E-07	3.99E-08
Thymus	2.35E-05	2.32E-05	2.22E-05	2.22E-05	1.92E-05	2.22E-05
Eye Lens	4.02E-07	5.66E-07	4.17E-07	6.41E-07	3.61E-07	6.41E-07

5.2. Comparison between MCNP and GEANT4

To facilitate the comparison of results between MCNP and GEANT4 across all organs, the S values are converted to logarithmic scale due to the large exponential differences among the results in different organs**. Fig 2**. to **Fig 7.** present the comparison of the results from the two codes for both male and female phantoms in all three cases.

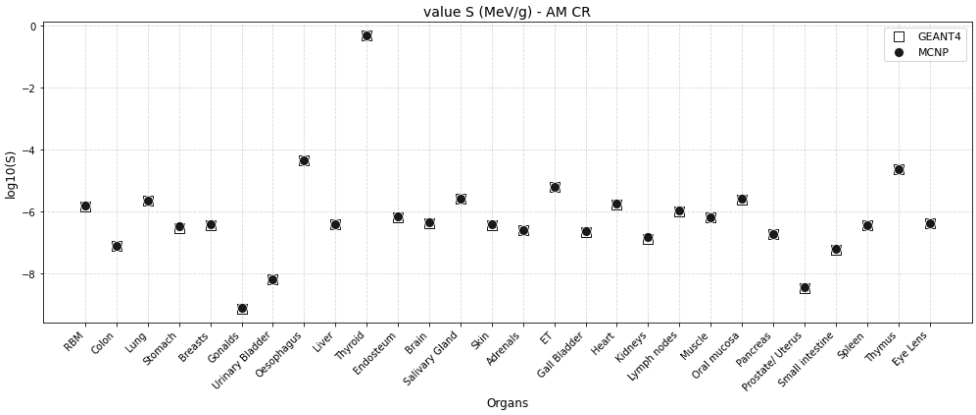

Fig 2. Comparison between MCNP and GEANT4 (AM CR)

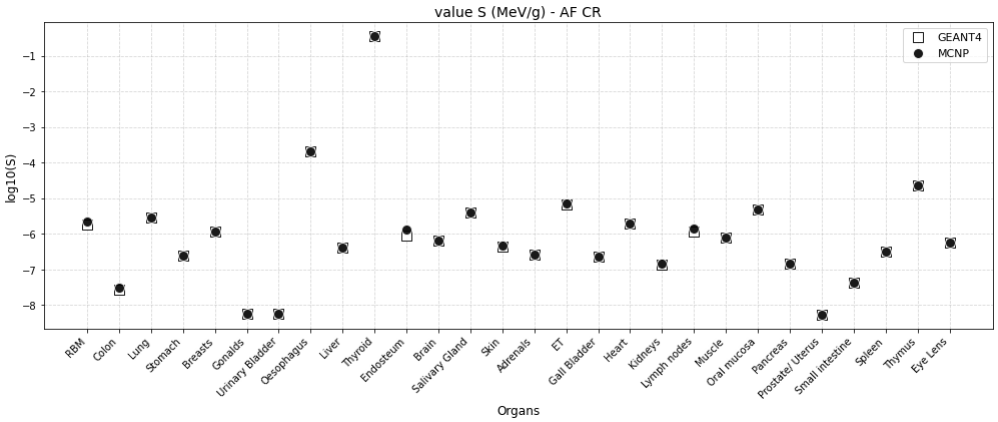

Fig 3. Comparison between MCNP and GEANT4 (AF CR)

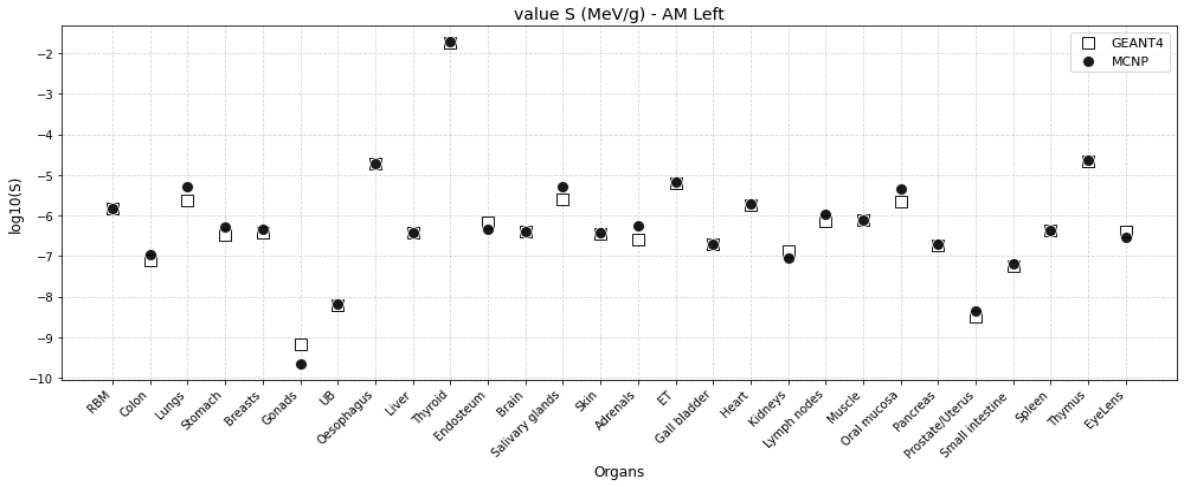

Fig 4. Comparison between MCNP and GEANT4 (AM Left)

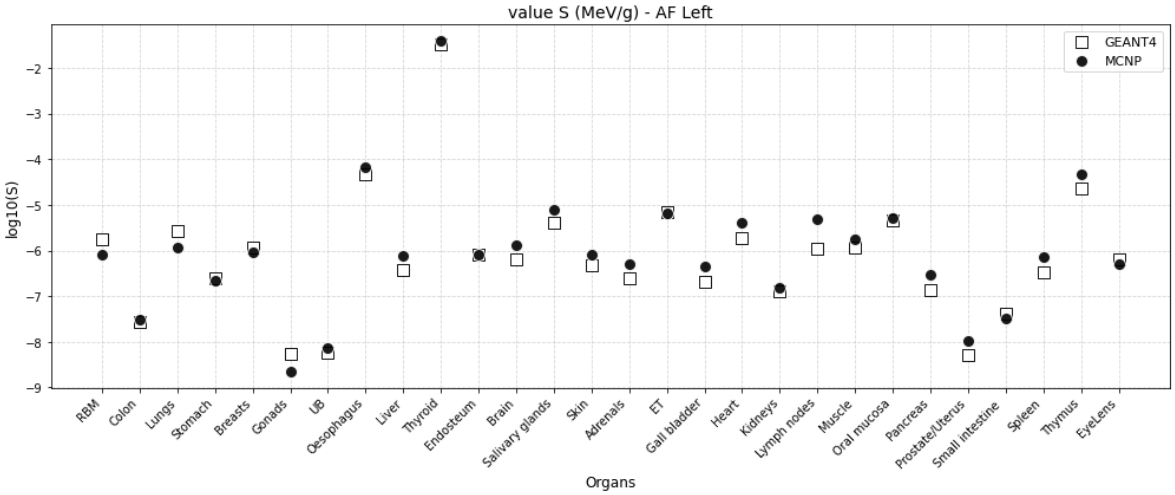

Fig 5. Comparison between MCNP and GEANT4 (AF Left)

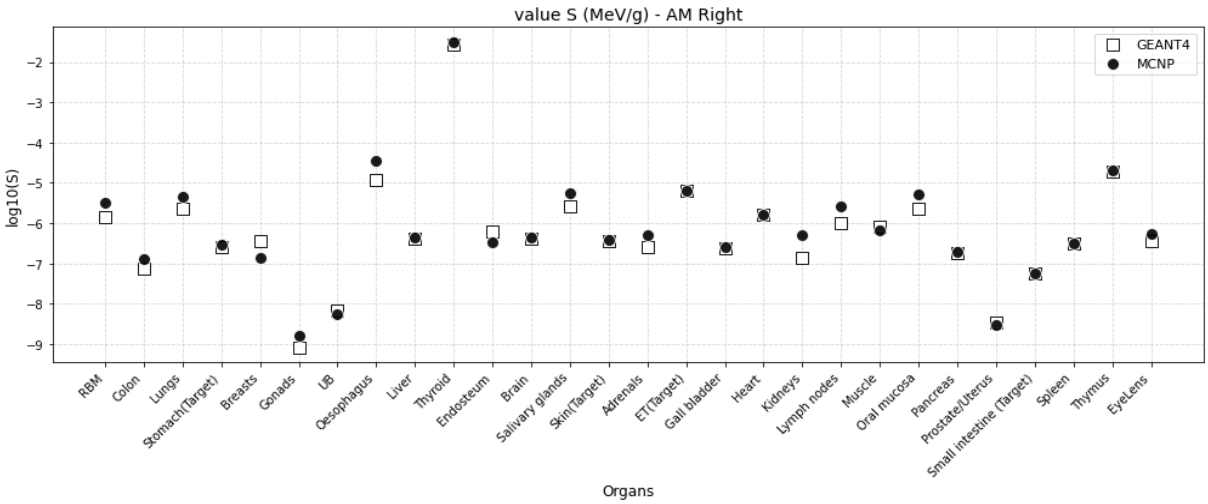

Fig 6. Comparison between MCNP and GEANT4 (AM Right)

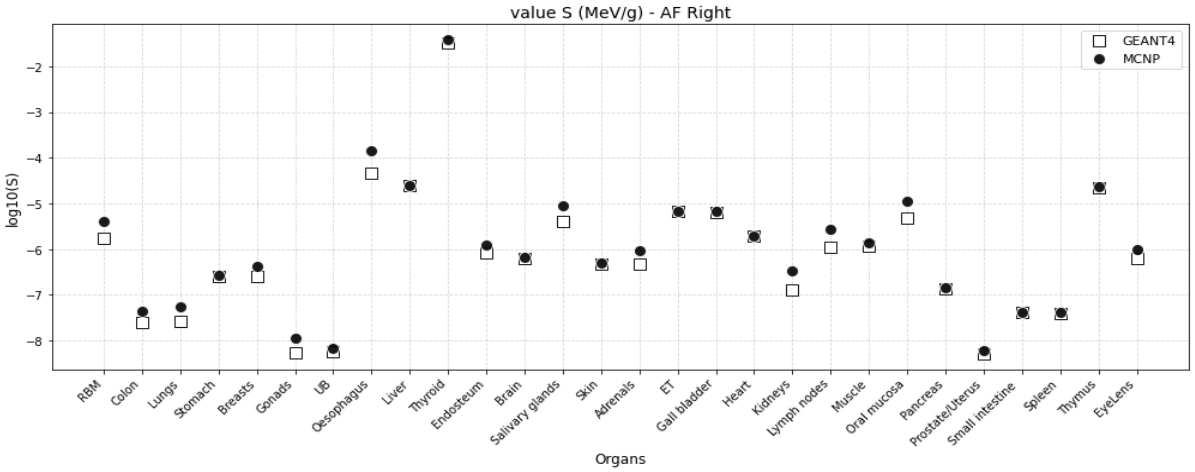

Fig 7. Comparison between MCNP and GEANT4 (AF Right)

In the case of calculation with the phantom which presents for patient who having the thyroid completely removed, the results from the two codes show a relatively good agreement for both the AM and AF phantoms.

In the case of the remaining calculation on the left thyroid tissue, the two software programs generally produce consistent results for most organs in the AM phantom. However, there are relatively significant differences in the "S" values for the lungs, gonads, salivary glands, adrenals, oral mucosa, and kidneys. These discrepancies are even more pronounced in the female phantom, with only the endosteum showing a high level of agreement between the two programs. All other organs exhibit varying degrees of difference, the most notable being in the lymph nodes.

Result consistency in the case where the source is placed in the remaining right thyroid tissue is observed in many radiosensitive organs. However, clear differences still exist in the esophagus, kidneys, lymph nodes, and oral mucosa. This observation is consistent in both AM and AF phantom comparisons.

The discrepancy between the results of MCNP and GEANT4 may be attributed to the differences in their calculation methods. Although both programs use the Monte Carlo algorithm, GEANT4 calculates the SAF values separately for each organ at different energy levels, and an intermediate step is required to convert these values into the final "S" values. In contrast, MCNP allows for the direct specification of source parameters, including energy levels and probabilities, enabling direct computation of the "S" values.

In addition, it can be observed that the differences between the two software programs mainly occur in organs that are located farther from the thyroid, such as the gonads, kidneys, adrenals, and pancreas, or in complex structures composed of multiple components, such as red bone marrow, lymph nodes, and the colon. This can be explained by the fact that statistical fluctuations tend to be greater in organs farther from the source, leading to more pronounced discrepancies. Furthermore, for organs with multiple components, variations in the results for each sub-component can lead to significant overall differences when evaluating the entire organ. For instance, in the case of the colon, the calculation is divided into six main parts: the ascending colon, transverse colon, descending colon, sigmoid colon, rectum, and internal contents. Therefore, such differences in large and complex organs are inevitable. To address this issue, the number of simulated particles can be increased to reduce statistical uncertainty. However, this comes at the cost of increased simulation time and memory (RAM) usage. We suggest that the number of particles used for the simulation could be in the order of several 10^9 particles.

6. Conclusions

In this study, we used standard MRCP phantoms to calculate and assess the "S" values instead of performing direct measurements on multiple specific organs. The Monte Carlo algorithm is sufficiently reliable for computing problems related to radiation interactions. The calculated "S" values serve as the foundation for estimating internal radiation doses to various organs. In this study, we employed the Monte Carlo algorithm to compute the "S" values using two representative software packages: MCNP6.1.1 and GEANT4. The study was conducted on standard male and female MRCP phantoms published by the ICRP, and reference tables of "S" values were provided for two clinical scenarios: (1) patients who have undergone total thyroidectomy, and (2) patients who have undergone partial thyroidectomy, retaining only the left or right lobe of the thyroid. The results from both MCNP and GEANT4 show that the "S" values for the phantoms in the three scenarios differ significantly. Even the cases where only the right or only the left thyroid lobe remain produce different outcomes. Therefore, one case cannot be used as a representative or equivalent substitute for the other. The "S" value tables from both MCNP and GEANT4 across all three scenarios consistently show that the "S" values in the female phantom are generally higher than those in the male phantom for most organs, except for the colon and small intestine (in all three cases). Notably, in the case where only the right thyroid lobe remains, the "S" value in the lungs of the male phantom is approximately 85 times greater than that of the female phantom. Additionally, for the spleen, the "S" value in the male phantom is nearly 8 times higher than that in the female phantom. Moreover, the calculated values between MCNP and GEANT4 show relatively high consistency for radiosensitive or simpler organs. However, there are differences in the results for organs located farther from the source (in this study, the thyroid) and for organs calculated through multiple smaller components. Overall, given the accuracy of the Monte Carlo algorithm with strict statistical validation (relative error below 0.1), the "S" values calculated by these two software programs across the three clinical scenarios can serve as reference data to support and compare treatment planning for thyroid cancer using the radiopharmaceutical Iodine-131 (RAI). Thus, this study contributes comprehensive "S" values for nearly 30 different organs in the human body across three thyroidectomy scenarios, calculated using the Monte Carlo method. These values were cross compared between MCNP and GEANT4, demonstrating a fair degree of agreement between the two simulation programs.

References

[1] Cancer, International Agency for Research on Cancer, "GLOBOCAN 2022," The Global Cancer Observatory (GCO) , 2022.

[2] Pham DX, Nguyen HD, Phung AHT, Bui TD, Tran TS, Tran BNH, Ho-Pham LT, Nguyen TV."Trends in incidence and histological pattern of thyroid cancer in Ho Chi Minh City, Vietnam (1996-2015): a population-based study," *BMC Cancer,* vol. 21, no. 1, 2021 Mar 20.

[3] D. V. Nostrand, "The benefits and risks of I-131 therapy in patients with well-differentiated thyroid cancer," *Thyroid,* pp. 1381-1391, 2009.

[4] Gi Hyeon Seo, Yoon Young Cho, Jae Hoon Chung, and Sun Wook Kim, "Increased Risk of Leukemia After Radioactive Iodine Therapy in Patients with Thyroid Cancer: A Nationwide, Population-Based Study in Korea," *Thyroid,* vol. 25, no. 8, pp. 927-934, 5 August 2015.

[5] Liyan Lu, Fengling Shan, Wenbin Li , Hankui Lu, "Short-Term Side Effects after Radioiodine Treatment in Patients with Differentiated Thyroid Cancer," *Biomed Res Int,* vol. PMID: 26989683, no. PMCID: PMC4773544, 2016 Feb 17.

[6] Laura Kääriä, Maria Lapela, Marko Seppänen, Mikael Högerman, Johanna Ruohola, Annika Ålgars and Tommi Noponen, "Determination of effective half-life of 131I in thyroid cancer patients using remote doserate meter," *EJNMMI Physics,* vol. 101, no. 11, 2024.

[7] Ode Samuel Omenka, Nurul Hashikin Ab. Aziz, Momoh Hameed Adavize, Oke Aduragbemi Olaoluwa, Efenji Godwin, "Thyroid Cancer: Iodine-131 Intervention and Dosimetric Analysis: A Review," *IJARSCT ,* vol. 4, no. 2, December 2024.

[8] Massimiliano Pacil, Miriam Conte, Viviana Frantellizzi, Maria Silvia De Feo, Antonio Rosario Pisani, Andrea Marongiu, Susanna Nuvoli, Giuseppe Rubini, Angela Spanu and Giuseppe De Vincentis, "Personalized Dosimetry in the Context of Radioiodine Therapy for Differentiated Thyroid Cancer," *Diagnostics,* vol. 12, no. 7, 2022.

[9] C.H. Kim, Y.S. Yeom, N. Petoussi-Henss, M. Zankl, W.E. Bolch, C. Lee, C. Choi, T.T. Nguyen, K. Eckerman, H.S. Kim, M.C. Han, R. Qiu, B.S. Chung, H. Han, B. Shin, Adult mesh-type reference computational phantoms. ICRP Publication 145. Ann. ICRP 49., SAGE , 2020.

[10] W.S. Snyder, M.R. Ford, G.G. Warner, E.E. Watson, MIRD Pamphlet No. 11 (Revised): “S” Absorbed Dose Per Unit Cumulated Activity for Selected, New York, 1975.

[11] S. A. Daryoush Shahbazi-Gahrouei, "Determination of Organ Doses in Radioiodine Therapy using Monte Carlo Simulation," *World Journal of Nuclear Medicine,* vol. 14, no. 1, January 2015.

[12] S. Oliver, J. Cases , B. Juste , R. Miro´ , G. Verdú, "Determination of organ doses in thyroid treatments with radioactive iodine by Monte Carlo simulation," *Radiation Physics and Chemistry ,* vol. 224, no. 111737, 2024.

[13] Soo Min Lee, Chansoo Choi, Ji Won Choi , Chul Hee Min , Seulki Ko, Bangho Shin, Yeon Soo Yeom, "Implication of ICRP pediatric reference voxel phantoms on dose assessment of patients in radioiodine therapy," *Nuclear Engineering and Technology,* 24 January 2024.

[14] H. Wattar, "Calculating The Internal Dose Of Radioiodine I-131 By Opendose Software Based On Monte Carlo Simulation," *SSRN,* Wattar, Hala, Calculating The Internal Dose Of Radioiodine I-131 By Opendose Software Based On Monte Carlo SSeptember 6, 2022.

[15] T. Wilcox, MCNP6 Advanced Tallies Tutorial, Knoxville, Tennessee, United States: LANL, 2014-09-14.

Cascaded Energy Management System with ANN Controlled DC Microgrid Systems

*B. Balaji[1], P. Hemalatha[2], U. Naveen Johnson[1] and R. Revathy[1]
[1]Dept. of EEE, IFET College of Engineering, Villupuram
*balaji.bc91@gmail.com
naveenjohnson03@gmail.com
revathyifet05@gmail.com
[2]Dept. of CSE, Vel Tech Rangarajan Dr. Sagunthala R&D Institute of Science and Technology, Chennai
drhemalathap@veltech.edu.in

Abstract. Renewable-based Distributed Generation (DG) units have proliferated significantly over the past decade in electrical networks. In this light, Distributed Generation (DG) based direct current (DC) microgrids have drawn more popularity due to their low complexity in both establishment and control. Moreover, DC microgrids are more efficient and reliable than alternating current (AC) microgrids. This paper presents two closed-loop DC microgrid systems connected to a photovoltaic (PV) source and battery backup for efficient energy management. The first uses a Grey Wolf Optimization Algorithm (GWA)-optimized Proportional Integral (PI) controller, while the second involves a GWA-inspired Artificial Neural Network (ANN) controller. Compared to conventional controllers, the proposed solutions improve control performance. The microgrid features two different power sources, each fed through a single converter: the PV system is fed through a SEPIC converter, and the battery is fed through a Buck-Boost converter. The converters impart certain benefits to the overall process of converting energy within the microgrid. Both closed-loop systems' behaviour is compared to show their utility in alleviating instability as well as minimizing oscillations under transient situations within a microgrid based on a DC system.

Keywords: DC microgrid, photovoltaic system, Grey Wolf Optimization Algorithm (GWA)-Proportional Integral (PI) Controller, GWA- Artificial Neural Network (ANN), Buck-boost converter, SEPIC converter

1 Introduction

Due to the continuously expanding power generation, transmission, and infrastructure, there is an ever-increasing demand for electrical energy in the era of accelerating technological development. A massive change in energy

procedures has become crucial to meet this growing global energy demand. At the moment, because of the second, the focus is on designing and deploying small, direct current (DC) microgrids that serve as local energy distribution systems that take advantage of those DC microgrids in terms of reducing the energy losses that occur in conventional distribution systems due to the frequent energy conversions. The development of more advanced power conversion systems, which are consistent with the increasing use of power in digital systems, further augments.

Consequently, the area of emphasis for present global research has turned to a significant extent towards green Distributed Energy Resources (DERs) and DC microgrids. Low Voltage Direct Current (LVDC) microgrids typically operate within a voltage range of up to 1500 VDc. They are appropriate for the low-voltage distribution of systems such as LED lighting systems, office appliances, and electric vehicle charging stations [1]. Microgrids encompass many DERs, most of which originate from Renewable Sources (RES) and act as decentralized power generators. Nevertheless, because of the intermittent nature of renewable power, these systems exhibit irregular power generation behavior, resulting in uncertainty of power availability within the environment of the DC microgrid [2]. In addition, the ever-changing characteristics of connected electrical loads induce significant voltage as well as power variations, which influence the stability of the system as a whole. Hence, to facilitate uniform and flexible operation, it is crucial to integrate a smart Energy Management System (EMS) with the support of a high-performance Energy Storage System (ESS). Although there has been remarkable progress in this field of control systems, the Proportional–Integral Derivative (PID) controller is still widely used in industrial applications owing to its ease of implementation, robustness, and capability to keep the performance satisfactory in a broad range of operations conditions [3]. In this regard, PI controllers are used extensively to control variables such as speed and position in control processes. A PI controller's performance is highly dependent on its gain values, i.e., proportional gain (Kp) and integral gain (Ki), which can, in turn, be tuned using some methods for selecting these parameters, such as recent optimization strategies based on metaheuristic techniques [4].

Meta-heuristic algorithms have been proven to be one of the most effective tools for complex, nonlinear, and multidimensional optimization. For example, Particle Swarm Optimization (PSO) is based on the representative way that bird flocks move and behave, where each particle changes trajectory based on the personal best solution it has achieved and the best achieved by the whole swarm [5]. Likewise, Genetic algorithms (GA) is another nature-inspired technique based on Darwinian evolution. It uses selection, crossover, and mutation mechanisms that allow it to generate better solutions from generation to generation [6]. Ant Colony Optimization(ACO) emulates the ant's path-finding behavior, where artificial agents lay virtual pheromones to discover optimal routes in the solution space [7]. ABC emulates the honey bees' foraging behavior, where employed onlookers and

scout bees collaborate to exploit and exploit the solution space effectively [8]. GWA emulates the grey wolves' leadership hierarchy and collaborative prey-hunting behavior in the real world, thus being applicable to both the exploration and exploitation stages of optimization [9].

PSO and GWA are among the metaheuristic algorithms that are known to perform well in solving global optimization tasks. Even though both are based on swarm intelligence, they do so with different philosophies. GWA spends more of its exploration than exploitation in its early iterations but then becomes more balanced until the end. In general, GWA converges much faster to some types of problems, whereas PSO converges in higher dimensions. Furthermore, the way GWA and PSO handle initialization is also different: GWA can have the initial population of wolves, and PSO has the possibility of particle initialization. While these two algorithms are quite different, they are both highly competent in a range of real-world optimization applications [10][11]. As renewable energy becomes a bigger part of power systems, DC microgrids are getting more attention because they work well with DC generation and storage tech. Still, keeping the voltage stable in these microgrids when conditions change is a big challenge. To tackle this, folks often use PI controllers. However, standard tuning methods for these controllers do not always perform well in nonlinear or very dynamic situations. This has led to more interest in tuning techniques based on metaheuristics. One of the prominent methods is the GWA, which is popular because it is simple, converges quickly, and optimizes well. The GWA algorithm, introduced in [12], simulates how grey wolves hunt in packs and has performed well in various control optimization tasks. For instance, a new approach called the Circle Search Algorithm (CSA) was featured in [13], showing that its geometric strategies could enhance spatial exploration. In [14], GWA was used for energy management in hybrid microgrids, resulting in better cost-efficiency and environmental benefits. Plus, GWA-optimized PI controllers have shown improved performance in DC-DC converters, with better transient response and steady-state accuracy vs. traditional Ziegler–Nichols tuning methods [15]. Also, GWA has been successfully used in load frequency control for hybrid renewable energy systems, proving to be strong against outside disturbances [16]. Various DC microgrid configurations powered by solar, battery, and wind sources, as well as hybrid combinations of solar battery, solar wind, and solar battery wind, have been modeled and simulated in detail. The voltage and power characteristics were analyzed under different load conditions of each setup [17].

Furthermore, the study has made control strategy comparisons in the case of PI and Sliding Mode controllers applied to test their effectiveness in keeping the system stable under changing conditions [18]. A comparison of inverter circuits for the induction heating application based on class D [20] and class DE [19] amplifiers was investigated in [19], in which it was proven that the class DE amplifier performed better than the class D amplifier, especially under the open

loop operation conditions. In yet another research, [20] introduced a DC microgrid topology consisting of converters for photovoltaic systems, wind power turbines, and energy storage systems, all being connected through a grid-interactive interlinking converter. The control operations within the topology were performed using the Artificial Neural Network (ANN)--based energy management system. Experimental implementation of the hybrid DC microgrid topology was conducted, corroborating the mentioned control logic under different operating modes. Additionally, [21] proposed a non-isolated single switch quadratically modified SEPIC (Single Ended Primary Inductor Converter) DC-DC converter for high voltage applications. A voltage multiplier module enhanced it, and higher voltage gain was achieved with a reduced duty cycle at a maintained continuous input current, making it suitable for solar PV systems. Also, [22] presented a hybrid control strategy of using ANN to replace the cascade PI controllers in photovoltaic battery-supported grid-connected DC microgrids with the MPC. Dynamic responsiveness was to be increased while stability of transient events was guaranteed.

Based on the literature review, to enhance system stability during transient conditions, closed-loop controllers such as the PI Controller and the ANN, both trained using the GWA algorithm, are incorporated. The primary objective of this work is to improve the system's stability. To achieve this, the scope of the work includes implementing two configurations: a GWA-PI controlled closed-loop cascaded DC microgrid system, and a GWA-ANN controlled closed-loop Open loop cascaded DC microgrid system. Initially, the system is also analysed without any controllers to provide a comparative assessment.

2 System Description

As discussed earlier, the proposed system is designed as a closed-loop controlled DC microgrid, utilizing two distinct control strategies: a PI-GWA and an ANN-GWA. However, before integrating these control schemes, it is essential to understand the behaviour of the system under open-loop conditions, i.e., without any feedback or control mechanism. This preliminary step provides insights into the inherent dynamics of the system and establishes a baseline for evaluating the effectiveness of the proposed control strategies. In the open-loop state, the system is allowed to respond to input variations and disturbances without regulation. Observations from this stage help in identifying stability issues i.e. poor transient responses—factors that necessitate the use of robust control algorithms. Once this behaviour is well understood, the system is transitioned into a closed-loop framework, first with PI-GWA control and subsequently with ANN-GWA control.

2.1 Open Loop DC microgrid with cascaded SEPIC and Buck-Boost converter

Block Diagram of Open Loop DC microgrid with cascaded SEPIC and Buck-Boost converter. As discussed earlier, the proposed system is designed as a closed-loop controlled DC microgrid, utilizing two distinct control strategies: a PI-GWA and an ANN-GWA. However, before integrating these control schemes, it is essential to understand the behavior of the system under open-loop conditions, i.e., without any feedback or control mechanism. This preliminary step provides insights into the inherent dynamics of the system and establishes a baseline for evaluating the effectiveness of the proposed control strategies. In the open-loop state, the system is allowed to respond to input variations and disturbances without regulation. Observations from this stage help identify stability issues, i.e., poor transient responses—factors that necessitate the use of robust control algorithms. Once this behavior is well understood, the system is transitioned into a closed-loop framework, first with PI-GWA control and subsequently with ANN-GWA control. An open loop DC microgrid setup connects a Photo Voltaic (PV) system to a DC bus using a SEPIC. It also has a battery energy storage system linked through a bidirectional Buck-Boost converter. This setup keeps a steady and regulated DC supply to important loads and the DC grid. The PV system serves as the main renewable energy source. The SEPIC converter helps the PV array work at its maximum power point and adjusts the output voltage up or down to fit the DC bus level as needed. Figure 1 illustrates the open loop cascaded DC microgrid system.

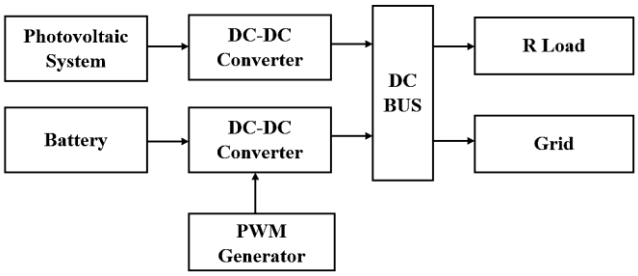

Fig. 1. Open loop cascaded DC microgrid system

Simulation of Open Loop DC microgrid with cascaded SEPIC and Buck-Boost converter. Fig. 2 shows the open loop DC microgrid system simulation circuit. The simulation paarmeters for the simulation circuit is shown in table. 1.

Table. 1. Simulation parameters of DC microgrid with cascaded SEPIC and Buck-Boost converter

Vin	12V
C1, C2	4200μF
L1, L2	0.45μH

C3, C4	50µF
C5	40µF
L3, L4	0.5mH
Switching Frequency	20kHz
Pulse width	50%
MOSFET(IRF840)	500V/8A
DIODE	230V/1A
Vo	135V

A SEPIC converter, as shown, is used to join the battery with the DC bus, and a Bidirectional Buck-Boost converter is used between the battery and the DC bus. Under voltage regulation, the Buck-Boost converter is used to clamp the output of the PV at the maximum power point, and the SEPIC converter is used to charge and discharge the battery. In this case, two sources were combined into the DC bus, out of which the DC bus supplies the DC grid and RL load. A source of disturbance, which is to be seen to be stable, is created at 0.2 seconds.

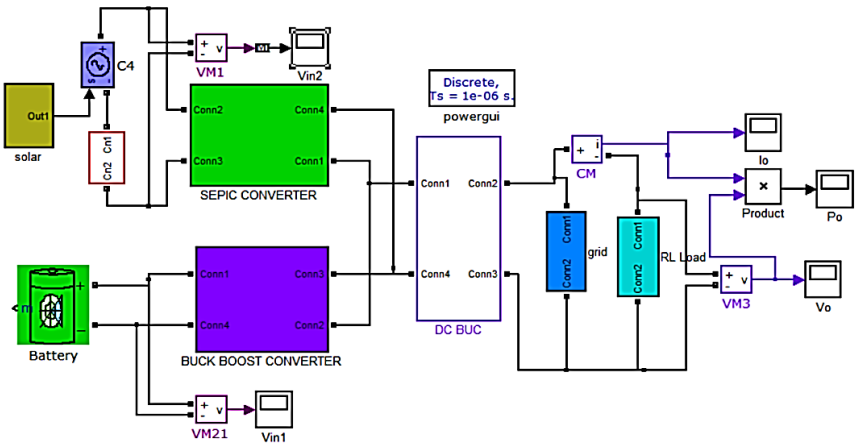

Fig. 2. Simulation circuit for open loop cascaded DC microgrid system

Voltage generated by the PV system is depicted by Fig. 3. The PV output is 15 V at the beginning. A disturbance is introduced at 0.2 seconds, increasing the voltage at the input to 18 V, which is constant after that. The system's output voltage, as depicted by Fig. 4, is initially at 130 V. Upon the disturbance at 0.2 seconds, the voltage at the input increases to 150 V, resulting in a transient for the system. The transient behavior remains without returning to the initial steady state, which is dangerous for the stability and safe operation of the overall system. The fact that the system is not able to recover results from the lack of adequate damping or control, potentially causing degradation of the performance or even failure of the connected loads and units.

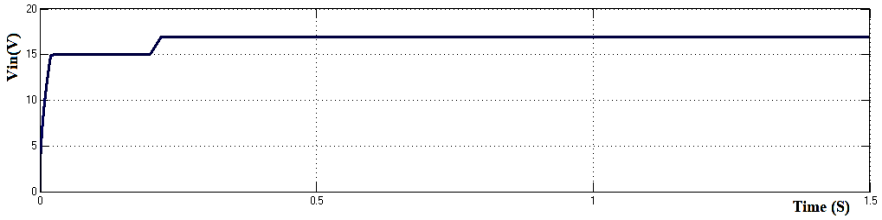

Fig. 3. Voltage across photovoltaic system

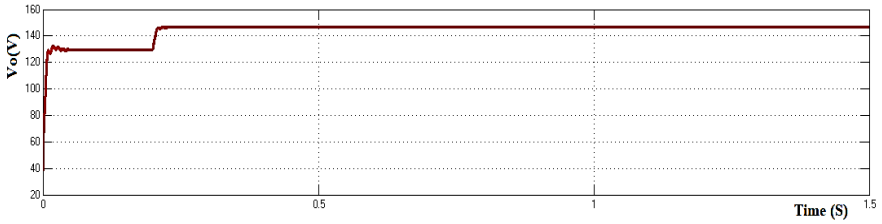

Fig. 4. Output Voltage across the load

The output current of the system, shown in Fig. 5, is initially 1.3 A. At 0.2 seconds, a source disturbance causes an increase in the output current to 1.45 A, which then remains steady. Similarly, the output power of the system, depicted in Fig. 6, starts at 170 W. After the same disturbance at 0.2 seconds, the output power rises to 220 W and remains at that level.

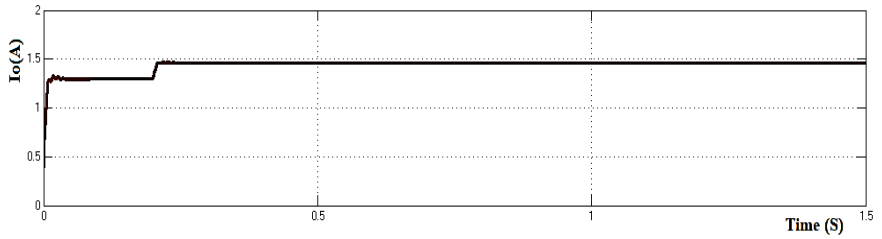

Fig. 5. Output current through the load

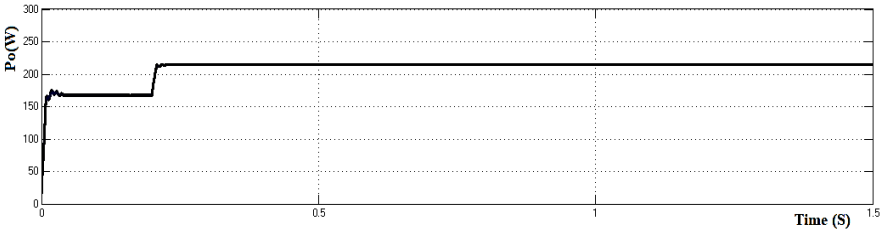

Fig. 6. Output Power of open loop DC microgrid system

The open loop DC microgrid system has key limitations, especially in maintaining

stability during dynamic conditions. Its major drawback is the lack of feedback control, which hinders effective response to disturbances. As seen in the simulation, after a transient like a sudden input change, the system fails to return to its steady state. This is due to the absence of real-time error correction, as the system cannot detect or adjust for output variations. As a result, performance degrades, impacting the reliability and safety of connected loads. To address this, the next step is to implement closed loop controllers, which use feedback to monitor outputs and adjust control signals, ensuring stability and quick recovery under varying conditions.

2.2 Closed Loop PI-GWA controlled DC microgrid with cascaded SEPIC and Buck-Boost converter

Block Diagram of Closed Loop PI-GWA controlled DC microgrid with cascaded SEPIC and Buck-Boost converter. The PI-GWA (Proportional-Integral controller optimized using Grey Wolf Optimization algorithm) control scheme in this closed loop arrangement is utilized as depicted in this schematic diagram from Fig. 7, with the aim of improving the dynamic behavior and stability of the DC microgrid. The regulation of voltage and current is achieved by reducing the error between the reference and actual values through the use of a PI controller. However, the optimal tuning method will not be the same under different loads and source conditions. To address this, PI controller parameter tuning is done using the GWA algorithm to achieve optimal tuning of the PI controller parameter settings. The GWA is a nature-inspired metaheuristic optimization algorithm that is based on the leadership organization and the search behavior of grey wolves. It is especially beneficial for addressing nonlinear, multi-objective optimization problems. Using GWA, the gains of the PI controller are optimized to minimize the indices of performance, including steady-state error, which results in faster response time, less overshooting, and improved disturbance rejection. The smart control strategy greatly enhances the robustness of the microgrid.

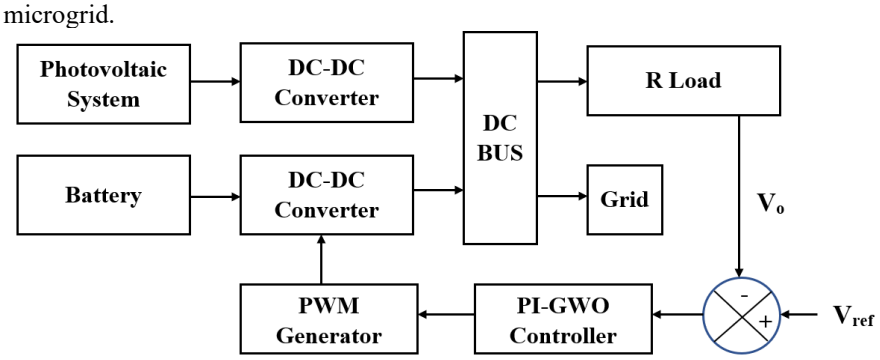

Fig. 7. Closed loop cascaded DC microgrid system with PI-GWA control strategy

Simulation of Closed Loop PI-GWA controlled DC microgrid with cascaded

SEPIC and Buck-Boost converter. Fig. 8 shows the simulation circuit of the PI-GWA control strategy. This approach helps improve dynamic performance and the stability of the DC microgrid. The PI controller regulates variance and current based on the difference between the reference and actual values. Last, PI gains are fine-tuned using the GWA algorithm in order to attain the optimum tuning at all conditions. However, it is motivated by grey wolf hunting behavior and is suitable for handling nonlinear multi-objective problems to prevent all overshooting better response, and less disturbance rejection. This system corresponds to the sensing of the output voltage and its comparison to the reference voltage with the help of a comparator so as to create an error signal.

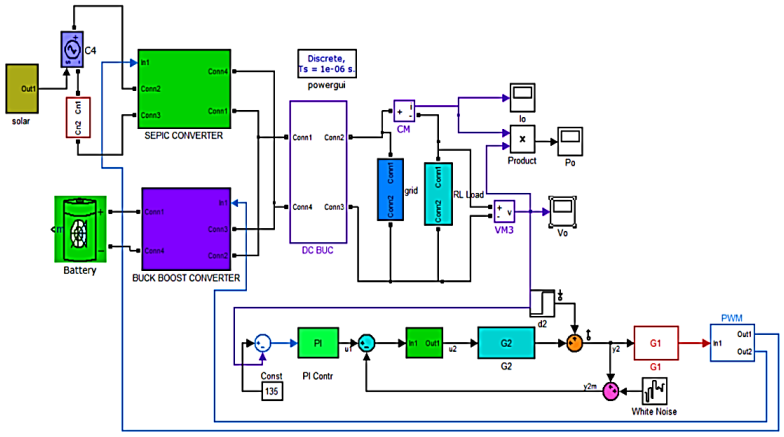

Fig. 8. Simulation circuit for closed loop cascaded DC microgrid system with PI-GWA control strategy

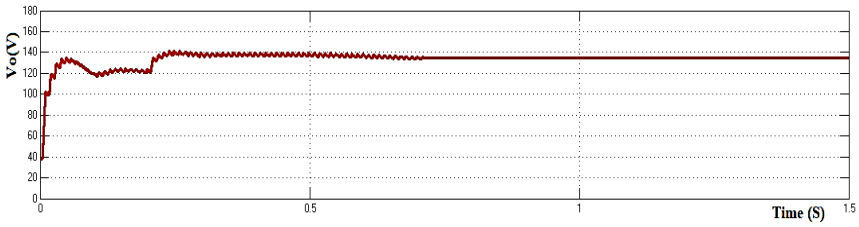

Fig. 9. Output Voltage across the load at closed loop cascaded DC microgrid system with PI-GWA control strategy

The PI-GWA controller processes this signal to generate the control signals for converter switch control to effectively control the system and thereby increase the microgrid resilience. When a source disturbance is introduced at 0.2 seconds, as demonstrated in simulation, the PI GWA-controlled system stabilizes and returns to the desired operating point quickly, which indicates its effectiveness in treating transients and keeping the system stable. The voltage generated by the PV system is shown in Fig. 3, with an initial output of 15 V. At 0.2 seconds, a source

disturbance raises the input voltage to 18 V, which remains constant thereafter. Correspondingly, the system's output voltage, shown in Fig. 9, is initially 130 V. After the disturbance, the output voltage rises to 140 V, causing the system to enter a transient state. Once the output reaches 140 V, the control strategy activates to restore the system to its original, steady-state value of 130 V. The system stabilizes after 0.72 seconds, following minor fluctuations. The output current of the system, shown in Fig. 10, is initially 1.3 A. At 0.2 seconds, a source disturbance increases the current to 1.45 A. The control strategy then activates to restore the current to its steady-state value of 1.3 A. The system stabilizes after 0.72 seconds. Similarly, the output power, shown in Fig. 11, starts at 170 W and rises to 200 W after the same disturbance. The control strategy acts to bring the power back to 170 W, and the system regains stability after 0.72 seconds.

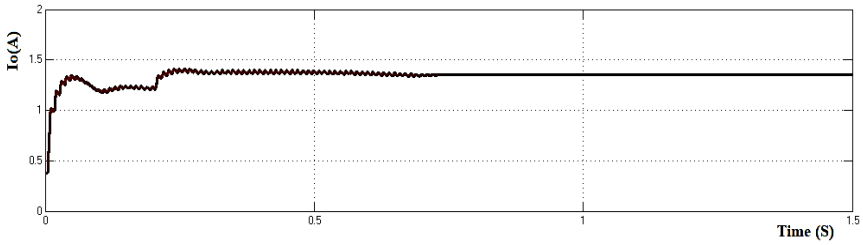

Fig. 10. Output Current through the load at closed loop cascaded DC microgrid system with PI-GWA control strategy

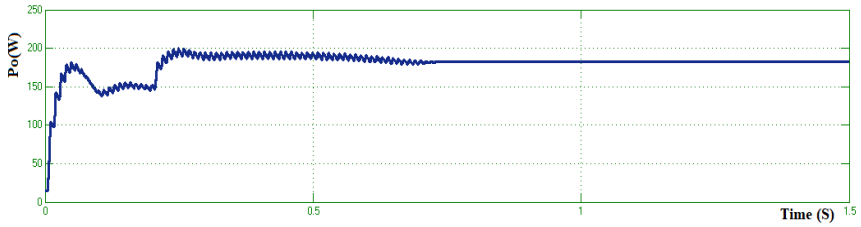

Fig. 11. Output Power at closed loop cascaded DC microgrid system with PI-GWA control strategy

2.3 Closed Loop ANN-GWA controlled DC microgrid with cascaded SEPIC and Buck-Boost converter

Block Diagram of Closed Loop ANN-GWA controlled DC microgrid with cascaded SEPIC and Buck-Boost converter. Fig. 12 shows the implementation of an advanced control mechanism for a closed-loop DC microgrid setup in which Artificial Neural Networks (ANN) are integrated with Grey Wolf Optimization (GWA). In this thesis, the system's responsiveness and adaptability against differing operational scenarios are improved using this strategy. However, since the system has very complex and nonlinear characteristics, its training with the ANN allows it to produce accurate, real-time control outputs. The internal weights

and biases of the ANN are tuned very effectively by the GWA algorithm, which is the main reason for its effectiveness. GWA optimizes steady-state error and transient behavior of the system based on hierarchical hunting strategies of grey wolves inspired to reduce steady-state error and improve transient behavior. The response time of such a controller is faster compared to the traditional control, it is better in managing uncertainties in such systems, and it can be better in terms of regulating voltage and current. Inside the control, the actual voltage is measured continuously and compared with the predetermined reference value in order to compute the error. The ANN-GWA controller then processes the error and produces optimal pulse signals to the converters in order to maintain the system's stability.

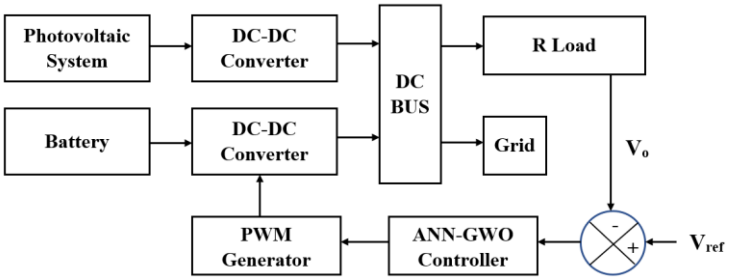

Fig. 12. Closed loop cascaded DC microgrid system with PI-GWA control strategy

Simulation of Closed Loop ANN-GWA controlled DC microgrid with cascaded SEPIC and Buck-Boost converter. In Fig. 13, the simulation circuit for the ANN-GWA control strategy is presented.

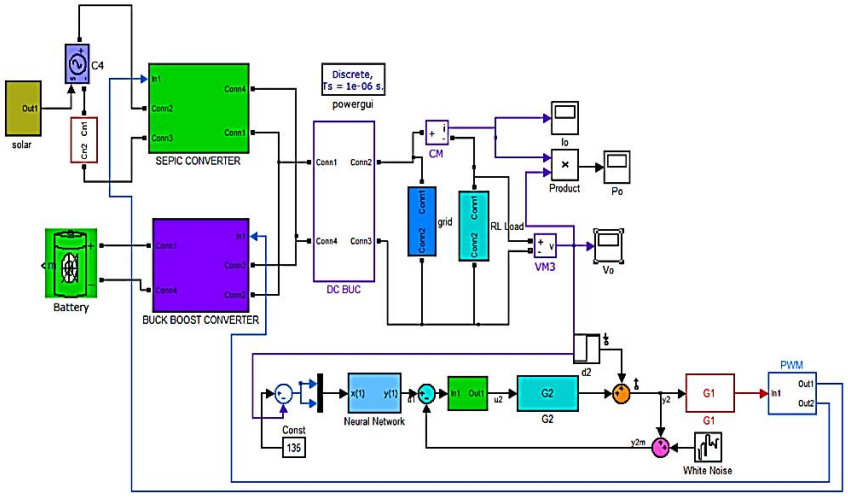

Fig. 13. Simulation circuit for closed loop cascaded DC microgrid system with ANN-GWA control strategy

The dynamic response and stability in the DC microgrid under different conditions have been improved with this hybrid approach. The ANN models the system's non-linear behavior, and real-time control actions are provided. In order to improve accuracy, the GWA algorithm is used to optimize the weights and biases of ANN to minimize the steady state error and improve the transient response. The control pulses for the converters are generated by the ANN–GWA controller from the input senses output voltage compared with a reference to generate an error and make the system operate stably and reliably. As demonstrated, when a source disturbance is introduced at 0.2 seconds, the ANN-GWA control maintains voltage and current stability with minimal overshoot and quicker settling time. The PV system voltage, shown in Fig. 3, starts at 15 V and rises to 18 V at 0.2 seconds due to a source disturbance. This increase triggers a rise in the system's output voltage, shown in Fig. 14, from 130 V to 140 V, leading to a transient state. The control strategy then activates, restoring the output voltage to its steady-state value of 130 V. The system stabilizes after 0.32 seconds, following minor fluctuations.

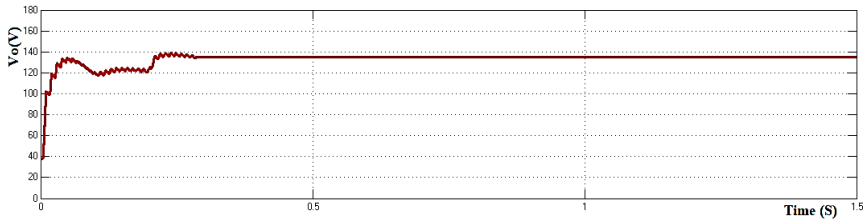

Fig. 14. Output Voltage across the load at closed loop cascaded DC microgrid system with ANN-GWA control strategy

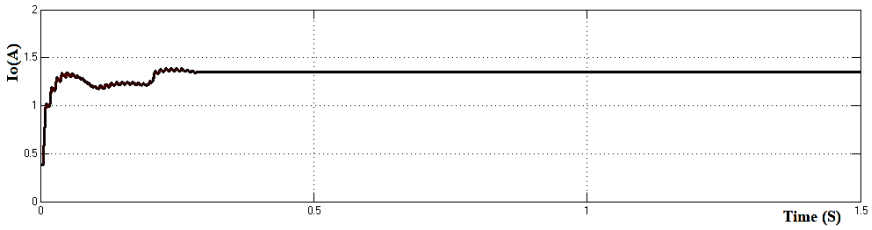

Fig. 15. Output Current across the load at closed loop cascaded DC microgrid system with ANN-GWA control strategy

Fig. 16. Output Power across the load at closed loop cascaded DC microgrid system with ANN-GWA control strategy

The output current, shown in Fig. 15, starts at 1.3 A and rises to 1.45 A at 0.2 seconds due to a disturbance. The control strategy responds by restoring it to 1.3 A, with the system stabilizing after 0.32 seconds. Similarly, the output power in Fig. 16 increases from 170 W to 200 W after the disturbance, then returns to 170 when the control strategy engages, achieving stability after 0.32 seconds.

3 System Performance - Discussion

The waveforms obtained from the closed-loop cascaded DC microgrid system using two different control strategies—PI-GWA and ANN-GWA—were compared to assess their dynamic performance. These comparisons were based on key time-domain performance parameters, which are critical in evaluating the effectiveness of control systems in ensuring fast and stable responses to source disturbances. The time-domain parameters considered for this evaluation include Rise Time (Tr), Peak Time (Tp), Settling Time (Ts), and Steady-State Error (Ess). Upon comparison, the ANN-GWA-based closed-loop system exhibited superior performance in most of the parameters, demonstrating faster transient response, reduced overshoot, quicker settling time, and minimal steady-state error. This improvement can be attributed to the learning capability of the ANN, which allows it to adapt more effectively to the nonlinear and time-varying nature of the DC microgrid environment, especially when its weights are optimized using GWA. On the other hand, the PI-GWA controlled system also showed significant enhancement compared to conventional PI control methods, as the GWA algorithm ensures optimal tuning of the PI gains. However, its adaptability is relatively limited when compared to the ANN-GWA approach. The summarized results of the time-domain analysis for both control strategies are presented in Table 2, which clearly illustrates the quantitative performance differences between the two approaches.

Table. 2. Time domain parameters of closed loop cascaded DC microgrid system

Controller	Tr	Tp	Ts	Ess
GWA-PI	0.23	0.26	0.72	1.19
GWA- ANN	0.21	0.24	0.32	0.63

From the above table. 2, it is clearly observed that the rise time (Tr) of the system improves when using ANN-GWA, reducing from 0.23 seconds (in the PI-GWA strategy) to 0.21 seconds. This indicates a faster initial response to changes in input or setpoint. Similarly, the peak time (Tp) also reduces slightly from 0.26 seconds to 0.24 seconds, suggesting that the ANN-GWA controller leads the system to reach its peak output more rapidly. A significant improvement is observed in the settling time (Ts), which drops from 0.72 seconds under PI-GWA to 0.32 seconds under ANN-GWA. This demonstrates the ANN-GWA controller's

superior ability to dampen oscillations and stabilize the system more quickly. Moreover, the steady-state error (Ess) decreases substantially from 1.19 V to 0.63 V, indicating better long-term accuracy and precision in tracking the reference value with the ANN-GWA approach. Overall, the ANN-GWA control strategy outperforms the PI-GWA method across all evaluated time-domain parameters, highlighting its potential for achieving faster and more stability in DC microgrid systems, which are expressed in the bar chart shown in Fig. 17.

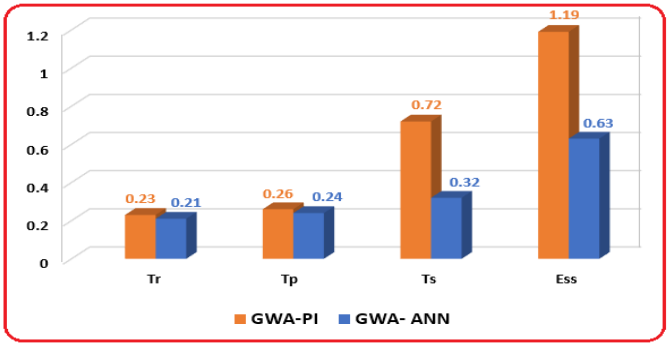

Fig. 17. Bar chart Comparison of Time Domain Parameters of closed loop cascaded DC microgrid system

4 Conclusion

As discussed in the introductory section, the objective of this work—to improve system stability—has been achieved by implementing the proposed scope of work. The performance of the DC microgrid system in open-loop mode revealed stability issues, especially during transients. Without feedback, the system failed to maintain voltage regulation, affecting its reliability and dynamic response. To overcome these limitations, a closed-loop control strategy using intelligent optimization was implemented. Two configurations were tested: PI-GWA and ANN-GWA. In both, the Grey Wolf Optimization (GWA) algorithm was used to optimize controller parameters for improved stability and dynamic performance. The system's time-domain responses were then analyzed to evaluate the effectiveness of each approach. The ANN-GWA controller outperformed PI-GWA across all metrics. The rise time decreased from 0.23 s to 0.21 s, indicating a faster initial response. The peak time improved slightly from 0.26 s to 0.24 s, while the settling time saw a significant reduction from 0.72 s to 0.32 s, reflecting better damping and quicker stabilization. Additionally, the steady-state error dropped from 1.19 V to 0.63 V, confirming improved tracking accuracy. Overall, the ANN-GWA strategy provided faster, more stable, and more accurate performance compared to PI-GWA.

References

1. Dragičević, T., Lu, X., Vasquez, J.C. and Guerrero, J.M., DC microgrids—Part II: A review of power architectures, applications, and standardization issues. IEEE transactions on power electronics, 31(5), pp.3528-3549. (2015)
2. Go, S.I. and Choi, J.H., Design and dynamic modelling of pv-battery hybrid systems for custom electromagnetic transient simulation. Electronics, 9(10), p.1651. (2020).
3. Iffouzar, K., Taraft, S., Aouzellag, H., Ghedamsi, K. and Aouzellag, D., December. DRFOC of polyphase induction motor based on fuzzy logic controller speed. In 2015 4th International Conference on Electrical Engineering (ICEE) (pp. 1-7). IEEE. (2015)
4. Djerioui, A., Houari, A., Ait-Ahmed, M., Benkhoris, M.F., Chouder, A. and Machmoum, M., Grey Wolf based control for speed ripple reduction at low speed operation of PMSM drives. ISA transactions, 74, pp.111-119. (2018).
5. Dogruer, T., Grey wolf optimizer-based optimal controller tuning method for unstable cascade processes with time delay. Symmetry, 15(1), p.54. (2022)
6. Garg, H., A hybrid PSO-GA algorithm for constrained optimization problems. Applied Mathematics and Computation, 274, pp.292-305. (2016)
7. Oshaba, A.S., Ali, E.S. and Abd Elazim, S.M., ACO based speed control of SRM fed by photovoltaic system. International Journal of Electrical Power & Energy Systems, 67, pp.529-536. (2015).
8. Ullah, K., Jiang, Q., Geng, G., Rahim, S. and Khan, R.A., Optimal power sharing in microgrids using the artificial bee colony algorithm. Energies, 15(3), p.1067. (2022)
9. Djerioui, A., Houari, A., Machmoum, M. and Ghanes, M., Grey wolf optimizer-based predictive torque control for electric buses applications. Energies, 13(19), p.5013. (2020)
10. Deng, W., Zhao, H., Zou, L., Li, G., Yang, X. and Wu, D., A novel collaborative optimization algorithm in solving complex optimization problems. Soft Computing, 21, pp.4387-4398. (2017)
11. Qais, M.H., Hasanien, H.M., Turky, R.A., Alghuwainem, S., Tostado-Véliz, M. and , Jurado, F.. Circle search algorithm: A geometry-based metaheuristic optimization algorithm. Mathematics, 10(10), p.1626. (2022).
12. Mirjalili, S., Mirjalili, S.M. and Lewis, A., Grey wolf optimizer. Advances in engineering software, 69, pp.46-61. (2014)
13. Qais, M.H., Hasanien, H.M., Turky, R.A., Alghuwainem, S., Tostado-Véliz, M. and Jurado, F., Circle search algorithm: A geometry-based metaheuristic optimization algorithm. Mathematics, 10(10), p.1626. (2022)
14. Mohammed, S.A., Abdel-Moamen, M.A. and Hasanin, B., 2013. A review of the state-of-the-art of power electronics for power system applications. Journal of Electronics and Communication Engineering Research, 1(1), pp.43-52. (2013)
15. Ghamari, S.M., Khavari, F. and Mollaee, H., Adaptive backstepping controller design for DC/DC buck converter optimised by grey wolf algorithm. IET Energy Systems Integration, 6(1), pp.18-30. (2024)
16. Singh, K.M. and Gope, S., Renewable energy integrated multi-microgrid load frequency control using grey wolf optimization algorithm. Materials Today: Proceedings, 46, pp.2572-2579. (2021).
17. Balaji, B., Ganesan, S., Pugazhendiran, P. and Madhan, R., Re-boost Converter enabled DC Microgrid System with Sliding Mode Control and Maximum Power Point Tracking. In 2023 2nd International Conference on Smart Technologies and Systems for Next Generation Computing (ICSTSN) (pp. 1-6). IEEE. (2023).
18. Balaji, B. and Ganesan, S., Power management in dc microgrid. In Proceedings of

International Conference on Power Electronics and Renewable Energy Systems: ICPERES 2021 (pp. 213-225). Singapore: Springer Singapore. (2021)
19. Balaji, B., Priyan, P.S., Devi, A. and Gayathri, D., Modelling and simulation of class d and class de amplifier systems. In 2022 International Conference on Smart Technologies and Systems for Next Generation Computing (ICSTSN) (pp. 1-6). IEEE. (2022)
20. Kim, T.G., Lee, H., An, C.G., Yi, J. and Won, C.Y., 2023. Hybrid AC/DC microgrid energy management strategy based on two-step ANN. Energies, 16(4), p.1787. (2023).
21. Maroti, P.K., Esmaeili, S., Iqbal, A. and Meraj, M., High step-up single switch quadratic modified SEPIC converter for DC microgrid applications. IET Power Electronics, 13(16), pp.3717-3726. (2020).
22. Akpolat, A.N., Habibi, M.R., Baghaee, H.R., Dursun, E., Kuzucuoğlu, A.E., Yang, Y., Dragičević, T. and Blaabjerg, F., Dynamic stabilization of DC microgrids using ANN-based model predictive control. IEEE Transactions on Energy Conversion, 37(2), pp.999-1010. (2021)

Voltage Regulation in a 33 Bus Distribution System with Integrated STATCOM and Grey Wolf Optimizatıon

[*]B. Balaji[1], P. Hemalatha[2], J. Chandru[1] and R. Preetha[3]
[1]Dept. of EEE, IFET College of Engineering, Villupuram
[*]balaji.bc91@gmail.com
chandruappu052004@gmail.com
[2]Dept. of CSE, Vel Tech Rangarajan Dr. Sagunthala R&D Institute of Science and Technology, Chennai
drhemalathap@veltech.edu.in
[3]Karpagam Academy of Higher Education, Coimbatore
preetha.rajaram@kahedu.edu.in

Abstract. The problem of maintaining stable voltage levels in the radial distribution networks is very limited, and more effort is persistent as loads increase and distributed generation units (DG) become more common. When the 33-bus distribution system is used for benchmarking and testing, excessive voltage drop on the buses away from the main substation can cause concerns. Most of these drops come about due to a combined effect of accumulating line impedance and varying load distribution on the feeder lines. The current work constitutes the utilization of a Static Synchronous Compensator (STATCOM) as an element of Flexible AC Transmission Systems (FACTS) aiming at performing dynamic reactive power support and enhancing voltage regulation. A load flow study using the backward (or forward) sweep method is performed in order to identify the critical areas of voltage instability. Based on the derived detailed voltage sensitivity analysis, optimum locations for locating the STATCOM to provide maximum system benefit are identified. It is worth reporting that the installation of STATCOM clearly improves the voltage profile over the network, and the whole system regulation capacity is increased. This is further elevated using closed-loop control mechanisms that are specifically based on two closed-loop control mechanisms: Proportional Integral Controllers (PIC) and Model Predictive Controllers (MPC). The Grey Wolf Optimization (GWA) algorithm is used to fine-tune these controllers such that they allow dynamic variation of the control parameters according to real-time variations of load and generation. The outcomes of the simulations confirm that the proposed methodology stabilizes bus voltages, minimizes deviations, and strengthens the network resilience to different operating conditions. STATCOM with integration and GWA-optimized intelligent controllers have great synergism in the sense that the voltage stability and distribution system performance have been improved

considerably.

Keywords: 33 bus system, Static Synchronous Compensator (STATCOM), Grey Wolf Optimization (GWA)- Proportional Integral Controllers (PIC), Grey Wolf Optimization (GWA)- Model Predictive Controllers (MPC), Stability Analysis.

1 Introduction

Power is generated at the power station where electricity, which is electrical energy, generated at the power station is transmitted through the transmission system and distributed to the end users such as residential, commercial, agricultural, industrial, etc. The simplicity of radial or weakly meshed structure and unidirectional power flow makes such existing distribution networks sufficiently simple and easy to operate through. The advantages of Radial Distribution Networks (RDNs) include low implementation cost, easy protection scheme, and easy voltage control and power flow control [1]. However, RDNs have a highly resistant-to-reactance (R/X) ratio, nonlinear loading, and limited structural capabilities, leading to significant operational challenges. These challenges include voltage instability, poor power factor, low voltage profiles, and higher power losses [2]. Therefore, RDNs are typically linked to lower reliability, reduced security, and increased cost of operation. However, in order to tackle these technical and economic issues, researchers have proposed several enhancement strategies. The commonly used approaches are DG (Distributed Generations) Allocation, Distribution Network Reconfiguration, and Placement of Reactive Power Compensation Devices (Series Voltage Regulators, Shunt Capacitors, D-FACTS devices, i.e., DSTATCOM (Distribution Static Compensator) [3 - 7]. One such solution is the integration of distributed generation (DG), an effective solution that helps reduce power losses, among others. Nonetheless, DG systems have higher capital and operation costs than other solutions, such as network reconfiguration, shunt capacitor banks, and DSTATCOM, which generate good efficiency [8]. Unlike network reconfiguration, which changes the topology of the power system to improve the power system performance, shunt capacitors and DSTATCOMs inject reactive power into the system in order to improve the voltage profile as well as system stability. However, a major deficiency in the utilization of traditional shunt capacitors is their incapacity to accommodate functional load fluctuation since they insert reactive power in predefined steps [9]. In the last several decades, there has been important progress in control and regulation theory. Yet, the proportional–integral–derivative (PID) controller continues to be of main importance for industrial applications. The PID controller remains widely popular due to its simplicity in design, ease of understanding and operation and intrinsic robustness and stability in a variety of operating conditions [10]. Proportional–

integral (PI) controllers are widely used in most control systems to regulate process variables like motor speed and position. The two most important parameters of these controllers are the proportional gain (Kp) and the integral gain (Ki), which decide the dynamic behaviour of the system. A number of methods have been created for optimally tuning these parameters [11]. Metaheuristic search methods are particularly useful when dealing with complex problem domains, whereas classical methods prove ineffective. Many of the metaheuristic approaches have been shown to be effective in tuning PI controllers. Particle Swarm Optimization (PSO) derived from the social dynamics observed in bird flocks is one such method. However, in PSO, a collection of particles is utilized to adjust their positions to search for the best solution under the guidance of the collective experience [12]. A widely used method is the Genetic Algorithm (GA), which simulates natural selection in the form of population evolution of candidate solutions by genetic operations like crossover and mutation [13].

Another algorithm similar to the bee algorithm is Ant Colony Optimization (ACO) [14]. Oppression Op is defined as a modified max-min ant system. The Artificial Bee Colony (ABC) algorithm, inspired by the mechanism of the food-foraging behaviour of honeybees, employs a swarm of artificial bees to find a good solution [15]. Another well-known method is the Grey Wolf Algorithm (GWA), which models the hierarchy of leadership and hunting patterns of grey wolves in nature [16].GWA is a group of wolves that collectively search for the best solution according to natural hunting behaviours. GWA and PSO are well-known and established metaheuristic algorithms based on swarm intelligence. The difference between these two lies in the fact that GWA mainly explores its search space at the early time of optimization and gradually uses exploitation until the last stage. At the same time, PSO maintains a balance between exploration and exploitation. Additionally, in regard to some problems, GWA converges faster than PSO and for solving problems with a higher dimensional search space, PSO is more efficient. In GWA, grey wolf positions are considered as the solution, while in PSO, a solution is measured using the particle locations. The initialization of GWA needs the setup of a wolf population, while that of PSO relies only on the initial particle and swarm. Without a doubt, therefore, the selection between GWA and PSO primarily depends on the problem's nature and the problem requirements [17–18]. The rise of renewable integration into contemporary electrical systems makes DC microgrids a popular choice of infrastructure due to efficient operation and DC-based sources, as well as storage device compatibility. However, voltage stability under dynamically varying loads and production profiles becomes a challenge. Usually, tough control methods depend on the use of PI controllers. However, the traditional designs thereof might not be the best choice for nonlinear time-varying conditions, and thus, the use of metaheuristic-based tuning has become increasingly popular. In particular, among these, Grey Wolf Optimization has been considered for its simplicity, good balance between exploration and exploitation, and good convergence. In [19], GWA was proposed using leader

hierarchy and hunting mechanism discovered in grey wolves to solve complex optimization problems effectively. After this, GWA has been widely used to tune a controller in power system operations. As an example, [20] proposed a Chain Search Algorithm (CSA) that took advantage of geometric information in setting metaheuristic optimization parameters and compared it to GWA. One such algorithm is the Grey Wolf Algorithm (GWA), which is widely studied due to its ease, balance in exploration and exploitation and fast convergence. The study in [19] presented GWA by using the grey wolf leadership hierarchy and search for hunting to address complex optimization problems efficiently. Since that time, GWA has been widely applied in the tuning of controllers for power system operation. As an example, the Circle Search Algorithm (CSA) [20] introduced geometric intuition into metaheuristic optimization, and compared its performance with GWA. Microgrid energy management applied [21] GWA for hybrid system operation optimization with significant cost reduction and emission minimization. Hybrid methods integrating PI controllers and GWA-based tuning have also been investigated for DC microgrids. Studies have proven that the application of GWA-tuned PI controllers on DC-DC converters resulted in better transient responses and minimal steady-state error than the traditional Ziegler–Nichols method [22]. GWA was also utilized successfully for load frequency control of hybrid renewable systems with improved robustness against system perturbances and parameter uncertainties [23]. In [24], a notable application was given that proposed a system consisting of a brushless DC motor, a Buck-Boost DC converter and supercapacitors and optimized control strategy was used for efficient energy storage. They hope this advancement will improve the regulation of energy in an electric vehicle and extend the distance energy can be utilized on a charge cycle. Moreover, FOPID-FOPID and PR-PR-based DC microgrid structures were simulated and analyzed in MATLAB/Simulink, and the results reported in [25] provided insight into the performance of various controller types in a closed loop. At last, the work in [26] concentrated on decreasing the output ripple and adjusting the output voltage in High Step-Up Super Lift DC-DC converters via PI and FOPID controllers. Performance of the system with settling time and steady-state error were compared, and it was found that the FOPID system configuration with better results, hence an important initiative for closed loop system feedback optimizing purposes.

Based on the literature review, to enhance system stability during transient conditions, closed-loop controllers such as the PIC and the MPC, both trained using the GWA algorithm, are incorporated. The primary objective of this work is to improve the system's stability. To achieve this, the scope of the work includes implementing two configurations: a GWA-PI controlled closed-loop STATCOM integrated into a 33-bus system, and a GWA-MPC controlled closed-loop STATCOM within the same system. Initially, the system is also analysed without any controllers to provide a comparative assessment.

2 System Description

As discussed previously, the proposed system is configured as a closed-loop controlled 33-bus distribution network integrated with a STATCOM, employing two advanced control strategies: PIC-GWA and MPC-GWA. However, before applying these control mechanisms, it is crucial to analyze the system under open-loop conditions, i.e., in the absence of any feedback or regulatory control. This initial evaluation serves to uncover the natural dynamic behaviour of the distribution system and establishes a baseline reference for comparing the effectiveness of the proposed controllers. In the open-loop mode, the system is exposed to input variations and disturbances without corrective action, allowing for the observation of critical performance issues such as voltage instability, poor transient responses, and sensitivity to load changes. These challenges highlight the need for implementing robust and adaptive control algorithms. Once the system's open-loop behaviour is comprehensively understood, the control strategies are introduced sequentially—first employing PIC-GWA and then transitioning to MPC-GWA. This staged integration facilitates a clear performance comparison and demonstrates the progressive enhancement in voltage regulation, stability, and system resilience achieved through the proposed closed-loop control schemes.

2.1 Open Loop 33-bus distribution network integrated with a STATCOM

Block Diagram of Open Loop 33-bus distribution network integrated with a STATCOM. The open-loop configuration of the 33-bus radial distribution network forms the foundational platform for evaluating the electrical behaviour and stability of the system under uncontrolled conditions. The block diagram shown in Fig. 1 includes several key components: a generating energy source, a STATCOM unit, a battery energy storage system, and the radial distribution feeder network itself. Each component plays a significant role in the power flow and voltage profile characteristics across the network. The generating energy source acts as the primary supplier of electrical energy to the 33-bus system. The power flows radially outward through the distribution feeders, delivering electricity to various consumer nodes. In open-loop mode, this flow is unidirectional and lacks any dynamic control mechanism. The distribution network comprises 33 buses arranged in a radial configuration. This structure is common due to its simplicity and ease of protection coordination. However, the radial nature inherently causes voltage drops along the feeder due to cumulative line impedance (both resistance and reactance). These drops become more significant as the distance from the source increases, leading to poor voltage regulation at the tail-end buses. The system is also characterized by a high R/X ratio, typical of low-voltage distribution systems, which exacerbates the problem of voltage deviation and reduces power transfer efficiency. The STATCOM is a shunt-connected Flexible AC Transmission System (FACTS) device that provides dynamic reactive power compensation. In this open-loop setup, although the STATCOM is physically connected to the network, it operates without a closed-

loop control system—meaning it does not adaptively inject or absorb reactive power in response to system voltage deviations. Nevertheless, its presence still provides a passive benefit by maintaining a constant reference voltage and helping to stabilize localized voltage variations to some extent. The STATCOM operates using a voltage-source converter (VSC), which converts DC from the battery storage system into AC and vice versa, thereby enabling bidirectional power exchange. The battery is connected to the system for energy backup.

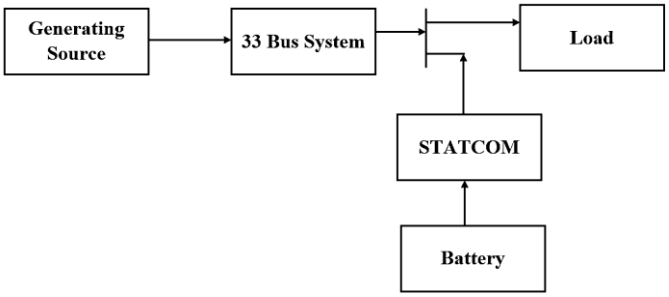

Fig. 1. Open Loop 33-bus distribution network integrated with a STATCOM

Simulation of Open Loop 33-bus distribution network integrated with a STATCOM. The simulation configuration of the open-loop 33-bus radial distribution grid sets the basis scenario for measuring system operation under the condition of the absence of dynamic regulating mechanisms, as provided by the example of Fig. 2. The basic components of the system consist of a generating power supply unit, a STATCOM unit, a battery energy storage unit, and the radial feeder grid. In this arrangement, the generating supply injects power radially towards the consumer nodes, creating a unidirectional flow without any regulating or correcting mechanisms. Because of the inherently radial configuration and the high R/X ratio commonly experienced by low-voltage distribution networks, significant voltage sags and compromised voltage regulation are noticeable at nodes farther away from the supply. The STATCOM, as a shunt-mounted FACTS unit, provides passive voltage regulation by giving a fixed level of reactive power but without employing active feedback under this open-loop configuration. The AC-DC energy exchange between the STATCOM and the battery energy storage unit uses a voltage-source converter as the mediator. To study the system's stability under dynamic conditions, a load disturbance occurs at 0.3 seconds. Fig. 3 shows the input-generating voltage, which is 6.1 kV. Fig. 4 illustrates the voltage across Bus-31, which has a peak value of 8 kV. Fig. 5 shows the RMS voltage at Bus-31, which is 5.1 kV.

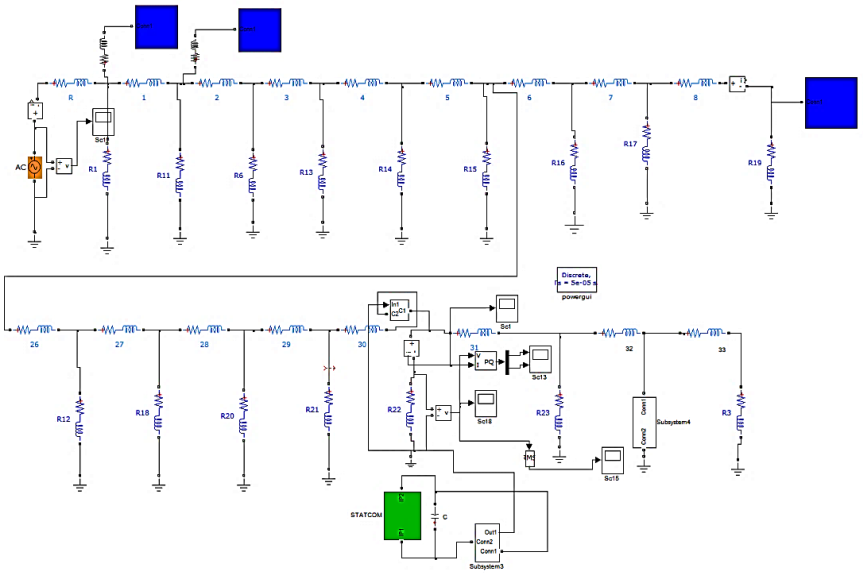

Fig. 2. Simulation circuit of Open Loop 33-bus distribution network integrated with a STATCOM

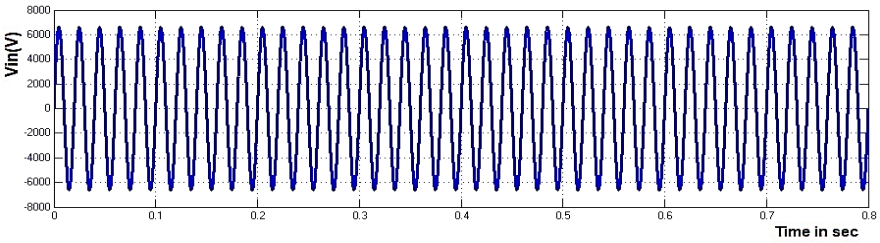

Fig. 3. Input generating voltage

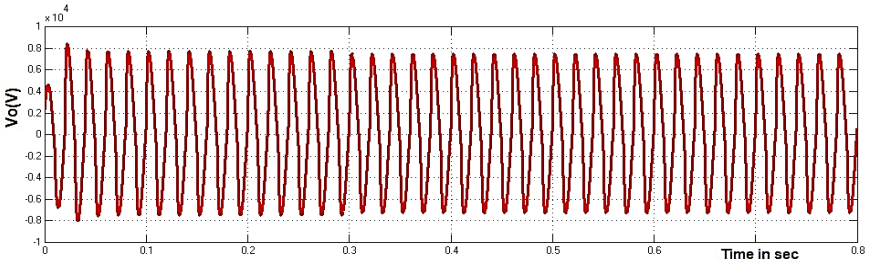

Fig. 4. Voltage at bus-31 at open loop system

Fig. 6 shows the current at Bus-31, Which is measured as 26 A. The real and reactive power at Bus-31, shown in Fig. 7, are 7.2 MW and 6.8 MVAR, respectively. These waveforms indicate that the system becomes unstable when load disturbances occur. In the open-loop configuration, the system fails to

maintain its original transient-free state due to the absence of control mechanisms. Therefore, to enhance system stability, closed-loop controllers trained using the GWA algorithm are implemented.

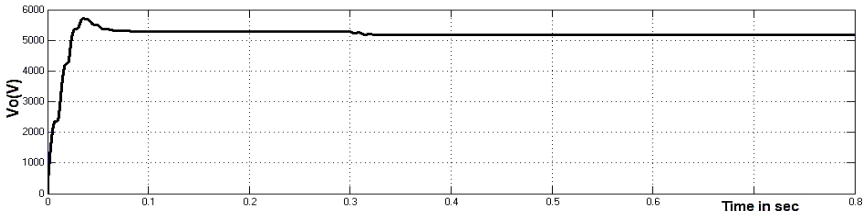

Fig. 5. RMS Voltage at bus-31 at open loop system

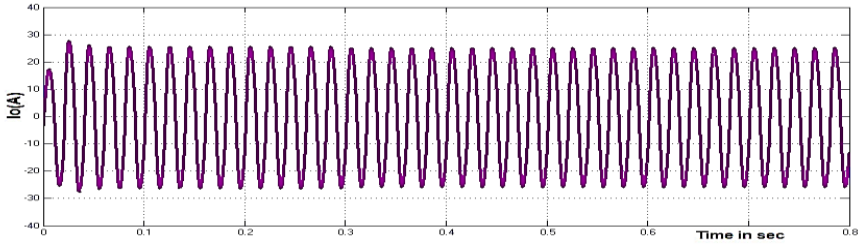

Fig. 6. Current at bus-31 at open loop system

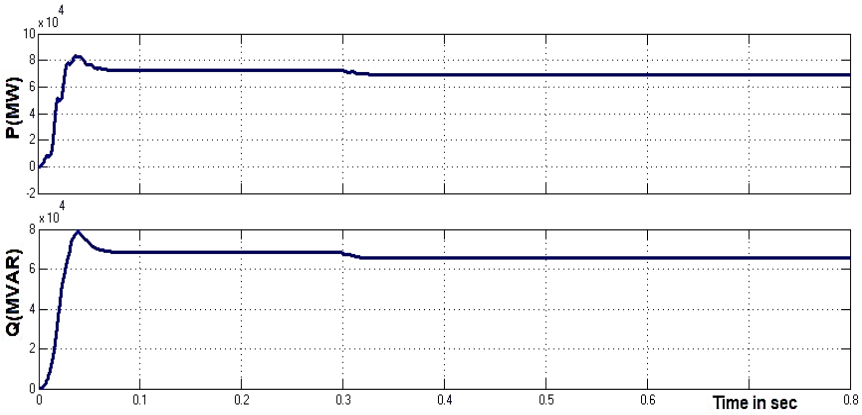

Fig. 7. Real and reactive power at bus-31 at open loop system

2.2 Closed Loop 33-bus distribution network integrated with a STATCOM and GWA-PIC

Block Diagram of Closed Loop 33-bus distribution network integrated with a STATCOM and GWA-PIC. The block diagram for the closed-loop system with GWA-PIC control configuration of the 33-bus radial distribution network is

shown in Fig. 8. It includes several key components: a generating energy source, a STATCOM unit, a battery energy storage system, the radial distribution feeder network, and the GWA-PIC. Each block plays a crucial role in ensuring improved power quality, system stability, and voltage regulation across the network. In this closed-loop configuration, a PIC is used to regulate the STATCOM's output. The PIC adjusts the STATCOM's reactive power injection based on the voltage deviations detected at key buses. However, the performance of a standard PI controller is highly dependent on the optimal tuning of its proportional gain (Kp) and integral gain (Ki) parameters.

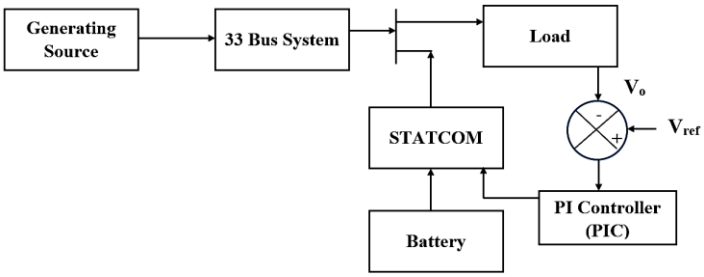

Fig. 8. Closed Loop 33-bus distribution network integrated with a STATCOM and GWA-PIC

Simulation Diagram of Closed Loop 33-bus distribution network integrated with a STATCOM and GWA-PIC. The closed-loop simulation diagram with GWA-PIC control for the 33-bus distribution network, shown in Fig. 9, includes a generating source, STATCOM, battery storage, feeder network, and GWA-PI controller.

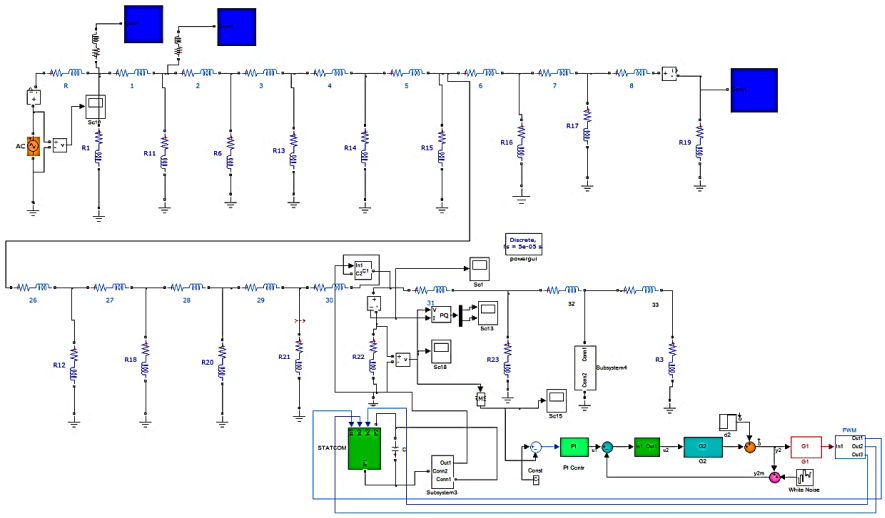

Fig. 9. Simulation circuit of Closed Loop 33-bus distribution network integrated with a STATCOM and GWA-PI

The PI controller regulates the STATCOM's output based on bus voltage deviations, with its gains (Kp, Ki) optimally tuned by GWA to enhance power quality, stability, and voltage regulation. To transcend the challenge of manual or trial-and-error tuning, the GWA algorithm is utilized to optimize the tuning of the PI controller parameters. GWA is a population-based metaheuristic inspired by the social structure and hunting habits of grey wolves. It performs the search of the solution space. It converges towards the optimum values of Kp and Ki that minimize a defined objective function — generally on the basis of voltage deviation minimization, overshoot minimization, settling time improvement, and overall stability enhancement. The input generating voltage is shown in Fig. 3 and has a value of 6.1 kV. The voltage across Bus-31 is illustrated in Fig. 10, with a peak value of 7.8 kV. The RMS voltage at Bus-31, shown in Fig. 11, is 5.3 kV.

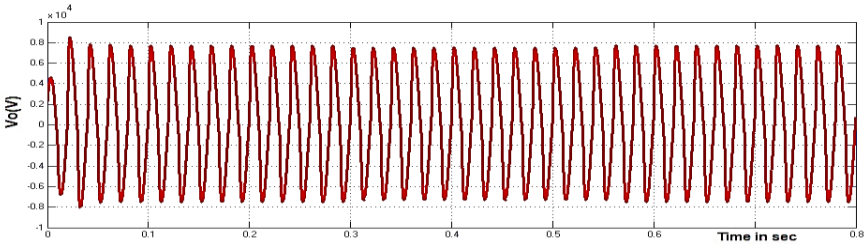

Fig. 10. Voltage at bus-31 at closed loop GWA-PIC controlled system

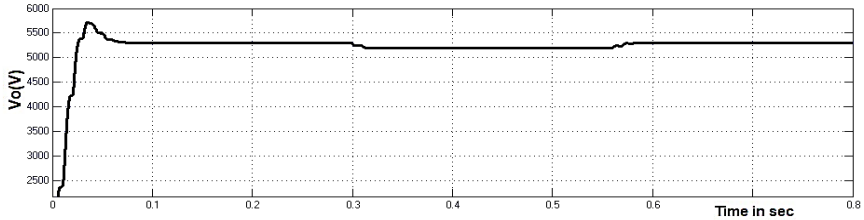

Fig. 11. RMS Voltage at bus-31 at closed loop GWA-PIC controlled system

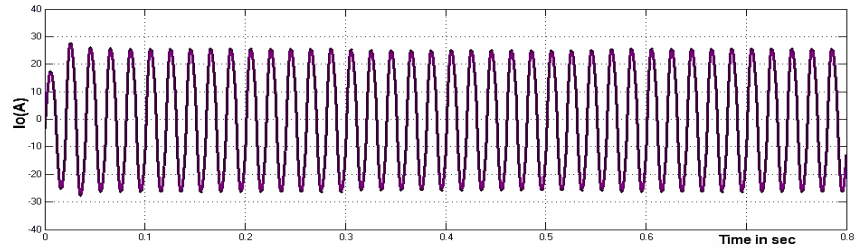

Fig. 12. Current at bus-31 at closed loop GWA-PIC controlled system

Fig. 12 shows the Bus-31 current that is recorded as 24 A. According to Fig. 13, the real and reactive power at Bus-31 are 7.1 MW and 6.98 MVAR, respectively. From these waveforms, one can see that the PIC closed loop system trained with GWA restores stability in the face of load disturbances that otherwise cause

instability. However, it reaches a steady state within 0.58 seconds in the GWA P controller-controlled system. In particular, the GWA-trained MPC controller has been introduced as a replacement to achieve faster stabilization.

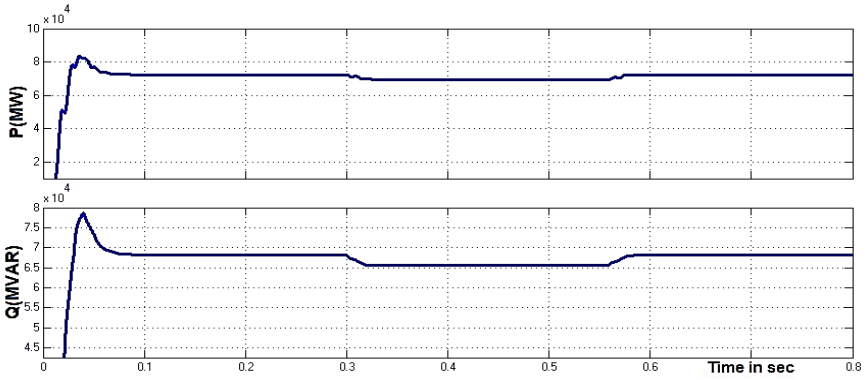

Fig. 13. Real and reactive power at bus-31 at closed loop GWA-PIC controlled system

2.3 Closed Loop 33-bus distribution network integrated with a STATCOM and GWA-MPC

Block Diagram of Closed Loop 33-bus distribution network integrated with a STATCOM and GWA-MPC. Fig. 14 shows the block schematic of the closed loop configuration of the 33-bus radial distribution network with GWA MPC control. The forming system uses the generating energy source, STATCOM module, battery energy storage system, radial feeder network and a GWA-optimized Model Predictive Controller (MPC).

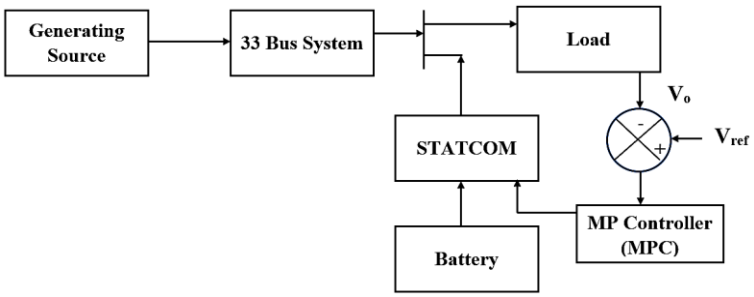

Fig. 14. Closed Loop 33-bus distribution network integrated with a STATCOM and GWA-MPC

Each unit contributes significantly to improving the system stability, facilitating efficient voltage regulation, and, at the same time, improving the dynamic response. In this closed loop, the STATCOM's output is governed by the MPC by

forecasting voltage deviation in the future using a mathematical model of the network. MPC differs from traditional proportional integral controllers (PICs) wherein at every sampling instant, MPC solves an optimization problem over a defined prediction horizon considering the dynamics and operational constraints of the system. By taking a predictive approach, the controller is able to respond proactively and correctively to disturbances in order to achieve superior transient performance and greater disturbance resilience. The effectiveness of the controller is further refined by fine-tuning the important MPC parameters of prediction horizon, control horizon and weight coefficients through Grey Wolf Optimization (GWA). GWA mimics the social leadership and hunting strategies of the grey wolves, which allows it to quickly explore the complex parameter space to find the global optimum. Hence, it converges faster to the global optimum and also improves overall controller performance.

Simulation Diagram of Closed Loop 33-bus distribution network integrated with a STATCOM and GWA-MPC. Fig. 15 shows the simulation diagram for the closed-loop system with GWA-MPC control of the 33-bus radial distribution network. It includes a generating source, STATCOM, battery storage, distribution feeder, and the GWA-optimized MPC. The MPC regulates the STATCOM output by predicting voltage deviations and solving an optimization problem at each instant, offering faster and more robust control than a conventional PIC. The GWA enhances MPC performance by optimally tuning key parameters like prediction and control horizons, ensuring improved stability, voltage regulation, and dynamic response.

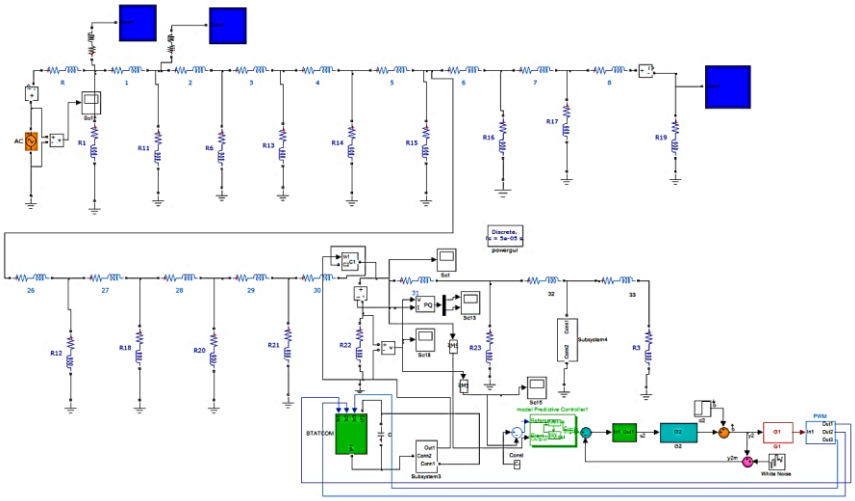

Fig. 15. Simulation circuit of Closed Loop 33-bus distribution network integrated with a STATCOM and GWA-MPC

The input generating voltage is shown in Fig. 3 and has a value of 6.1 kV. The

voltage across Bus-31 is illustrated in Fig. 16, with a peak value of 7.8 kV. The RMS voltage at Bus-31, shown in Fig. 17, is 5.3 kV.

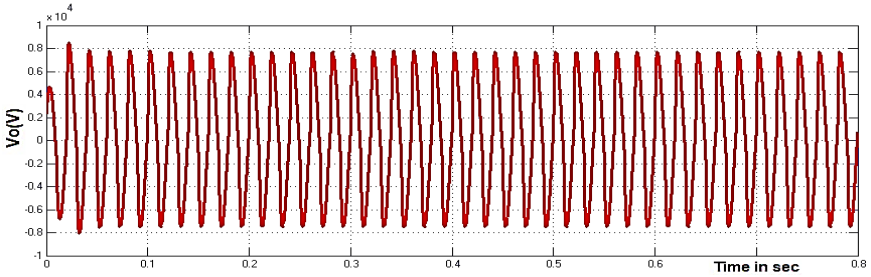

Fig. 16. Voltage at bus-31 at closed loop GWA-MPC controlled system

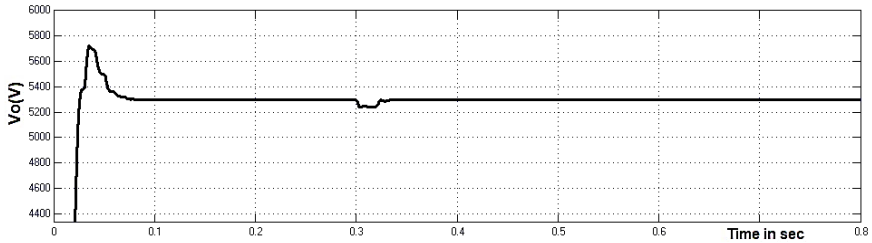

Fig. 17. RMS Voltage at bus-31 at closed loop GWA-MPC controlled system

The current drawn from Bus-31, as can be seen in Fig. 18, is 24 A. Fig. 19 shows the real and reactive powers at Bus-31 to be 7.1 MW and 6.98 MVAR, respectively. These waveforms imply that although load disturbances induce the instability, the closed loop GWA-MPC system overcomes the instability. When compared to the GWA-PIC controlled system, the GWA-MPC controlled system goes to a steady state in 0.33 seconds, which is fast stabilization.

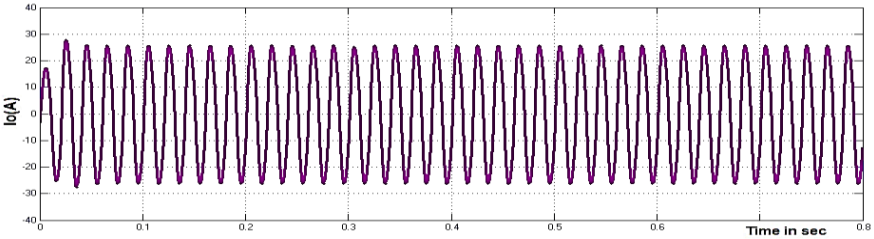

Fig. 18. Current at bus-31 at closed loop GWA-MPC controlled system

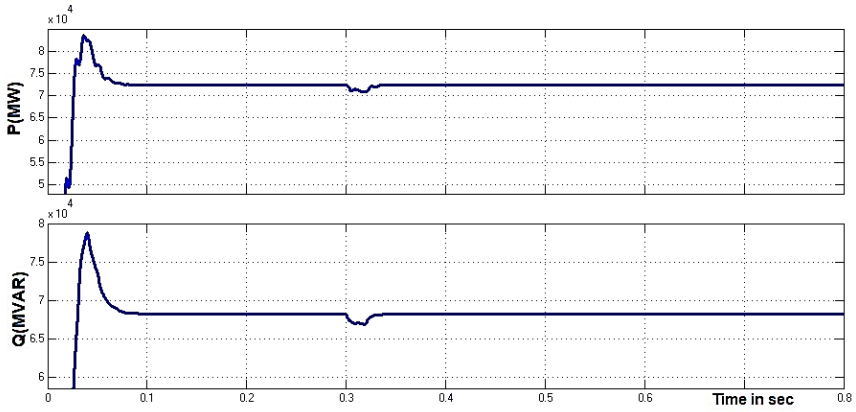

Fig. 19. Real and reactive power at bus-31 at closed loop GWA-MPC controlled system

2.3 System Performance - Discussion

The dynamic performance of the closed-loop 33-bus distribution network with STATCOM was assessed by comparing waveforms from two control strategies: GWA-PIC and GWA-MPC. The evaluation focused on critical time-domain metrics—Rise Time (Tr), Peak Time (Tp), Settling Time (Ts), and Steady-State Error (Ess)—which reflect the system's responsiveness and stability under source disturbances. The GWA-MPC method outperformed GWA-PIC across most parameters, delivering faster transient response, lower overshoot, quicker settling, and reduced steady-state error. This enhanced performance is due to MPC's ability to effectively manage the nonlinear and time-varying characteristics of the 33-bus network, especially when optimized by Grey Wolf Optimization. While GWA-PIC also improved results over the open-loop system, the time-domain analysis summarized in Table 1 clearly highlights the superior advantages of the GWA-MPC approach.

Table. 1. Time domain parameters of Closed Loop 33-bus distribution network integrated with a STATCOM and GWA trained controllers

Controller	Tr	Tp	Ts	Ess
GWA-PIC	0.55	0.57	0.58	1.68
GWA- MPC	0.32	0.33	0.35	0.75

Table 1 clearly shows that the GWA-MPC control strategy significantly outperforms the GWA-PIC method. The rise time (Tr) improves from 0.55 s to 0.32 s, and peak time (Tp) decreases from 0.57 s to 0.33 s, indicating faster responses. Settling time (Ts) is notably reduced from 0.58 s to 0.35 s, reflecting

quicker stabilization. The steady-state error (Ess) also decreases from 1.68 V to 0.75 V, showing enhanced accuracy. These improvements demonstrate that the GWA-MPC system provides faster, more stable, and precise control for the closed-loop 33-bus distribution network with STATCOM. The comparison is illustrated in the bar chart in Fig. 20.

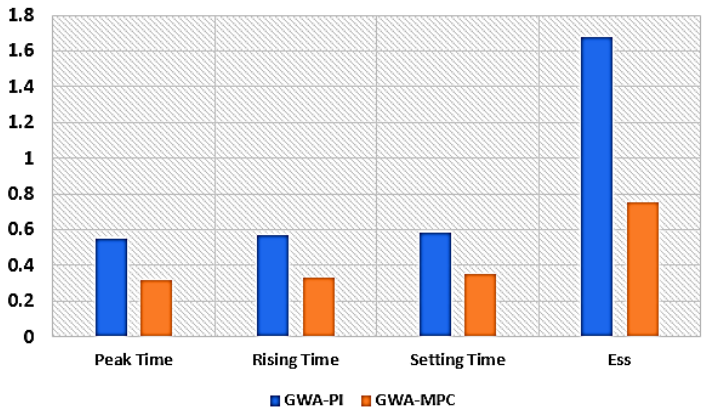

Fig. 20. Bar chart Comparison of Time Domain Parameters of multifunctional UPQC and closed loop GWA-PID and GWA-FLC controlled system

2.3 Conclusion

As discussed in the introductory section, the objective of this work—to improve system stability—has been achieved by implementing the proposed scope of work. The open-loop operation of the 33-bus distribution network integrated with a STATCOM showed stability issues, especially during transient events. To overcome these challenges, a closed-loop control approach using intelligent optimization was implemented. Two control configurations were tested: a PI controller tuned with GWA and an MPC tuned with GWA. In both setups, the GWA optimized controller parameters to enhance dynamic response and overall system stability. Time-domain analysis confirmed the superior performance of the GWA-MPC configuration across all key metrics. Simulations were conducted under load disturbances using both closed-loop GWA-PI and GWA-MPC controllers. The GWA MPC system outperformed the SA system with a shorter rise time from 0.55 s to 0.32 s, shorter peak time from 0.57 s to 0.33 s, and shorter settling time from 0.58 s to 0.35 s, and smaller steady-state error from 1.68 V down to 0.75 V. The obvious results of these results show that 33 bus closed-loop systems with STATCOM under GWA-MPC control outperform the closed-loop system under GWA-PI control.

References

1. Mokryani, G., Future Distribution Networks. New York, USA: AIP Publishing. (2022)
2. Okelola, M.O., Salimon, S.A., Adegbola, O.A., Ogunwole, E.I., Ayanlade, S.O. and Aderemi, B.A., Optimal siting and sizing of D-STATCOM in distribution system using new voltage stability index and bat algorithm. In 2021 International Congress of Advanced Technology and Engineering (ICOTEN) (pp. 1-5). IEEE. (2021).
3. Colmenar-Santos, A., Reino-Rio, C., Borge-Diez, D. and Collado-Fernández, E., Distributed generation: A review of factors that can contribute most to achieve a scenario of DG units embedded in the new distribution networks. Renewable and Sustainable Energy Reviews, 59, pp.1130-1148. (2016)
4. Muruganantham, B., Selvam, M.M., Gnanadass, R. and Padhy, N.P., Energy loss reduction and load balancing through network reconfiguration in practical LV distribution feeder using GAMS. In 2017 7th International Conference on Power Systems (ICPS) (pp. 509-513). IEEE. (2017).
5. Franco, J.F., Rider, M.J., Lavorato, M. and Romero, R., A mixed-integer LP model for the optimal allocation of voltage regulators and capacitors in radial distribution systems. International Journal of Electrical Power & Energy Systems, 48, pp.123-130. (2013).
6. Salimon, S.A., Adepoju, G.A., Adebayo, I.G. and Ayanlade, S.O., Impact of shunt capacitor penetration level in radial distribution system considering techno-economic benefits. Nigerian Journal of Technological Development, 19(2), pp.101-109. (2022)
7. Balamurugan, P., Yuvaraj, T. and Muthukannan, P., Optimal allocation of DSTATCOM in distribution network using whale optimization algorithm. Engineering, Technology & Applied Science Research, 8(5), pp.3445-3449. (2018)
8. Montoya, O.D., Gil-González, W. and Hernández, J.C., Efficient operative cost reduction in distribution grids considering the optimal placement and sizing of D-STATCOMs using a discrete-continuous VSA. Applied Sciences, 11(5), p.2175. (2021)
9. Castiblanco-Pérez, C.M., Toro-Rodríguez, D.E., Montoya, O.D. and Giral-Ramírez, D.A., Optimal Placement and sizing of D-STATCOM in radial and meshed distribution networks using a discrete-continuous version of the genetic algorithm. Electronics, 10(12), p.1452. (2021).
10. Iffouzar, K., Taraft, S., Aouzellag, H., Ghedamsi, K. and Aouzellag, D., 2015, December. DRFOC of polyphase induction motor based on fuzzy logic controller speed. In 2015 4th International Conference on Electrical Engineering (ICEE) (pp. 1-7). IEEE. (2015).
11. Djerioui, A., Houari, A., Ait-Ahmed, M., Benkhoris, M.F., Chouder, A. and Machmoum, M., Grey Wolf based control for speed ripple reduction at low speed operation of PMSM drives. ISA transactions, 74, pp.111-119. (2018).
12. Dogruer, T., Grey wolf optimizer-based optimal controller tuning method for unstable cascade processes with time delay. Symmetry, 15(1), p.54. (2022).
13. Garg, H., A hybrid PSO-GA algorithm for constrained optimization problems. Applied Mathematics and Computation, 274, pp.292-305. (2016).
14. Oshaba, A.S., Ali, E.S. and Abd Elazim, S.M., ACO based speed control of SRM fed by photovoltaic system. International Journal of Electrical Power & Energy Systems, 67, pp.529-536. (2015).
15. Ullah, K., Jiang, Q., Geng, G., Rahim, S. and Khan, R.A,. Optimal power sharing in microgrids using the artificial bee colony algorithm. Energies, 15(3), p.1067. (2022)
16. Djerioui, A., Houari, A., Machmoum, M. and Ghanes, M., Grey wolf optimizer-based predictive torque control for electric buses applications. Energies, 13(19), p.5013.

(2020)
17. Deng, W., Zhao, H., Zou, L., Li, G., Yang, X. and Wu, D., A novel collaborative optimization algorithm in solving complex optimization problems. Soft Computing, 21, pp.4387-4398. (2017).
18. Qais, M.H., Hasanien, H.M., Turky, R.A., Alghuwainem, S., Tostado-Véliz, M. and Jurado, F., Circle search algorithm: A geometry-based metaheuristic optimization algorithm. Mathematics, 10(10), p.1626. (2022).
19. Mirjalili, S., Mirjalili, S.M. and Lewis, A., Grey wolf optimizer. Advances in engineering software, 69, pp.46-61. (2014).
20. Qais, M.H., Hasanien, H.M., Turky, R.A., Alghuwainem, S., Tostado-Véliz, M. and Jurado, F., Circle search algorithm: A geometry-based metaheuristic optimization algorithm. Mathematics, 10(10), p.1626. (2022).
21. Mohammed, S.A., Abdel-Moamen, M.A. and Hasanin, B., A review of the state-of-the-art of power electronics for power system applications. Journal of Electronics and Communication Engineering Research, 1(1), pp.43-52. (2013).
22. Ghamari, S.M., Khavari, F. and Mollaee, H., Adaptive backstepping controller design for DC/DC buck converter optimised by grey wolf algorithm. IET Energy Systems Integration, 6(1), pp.18-30. (2024)
23. Singh, K.M. and Gope, S., Renewable energy integrated multi-microgrid load frequency control using grey wolf optimization algorithm. Materials Today: Proceedings, 46, pp.2572-2579. (2024).
24. Revathy, R., Balaji, B., Mohasin, A.A. and Gobinath, A., Supercapacitor and bldc motor-based regenerative braking for an electric vehicles. In 2023 2nd International Conference on Smart Technologies and Systems for Next Generation Computing (ICSTSN) (pp. 1-5). IEEE. (2023).
25. Balaji, B., Ganesan, S., Pugazhendiran, P. and Subramanian, S., Closed loop proportional resonant controller controlled DC microgrid system with advanced material technology in solar PV system. Materials Today: Proceedings. (2023)
26. Balaji, B. and Krishnan, D.S., Fopid controlled high step-up super lift DC-DC converter with enhanced response. In 2021 3rd International Conference on Signal Processing and Communication (ICPSC) (pp. 176-179). IEEE. (2021).

AI Based Malware Detection Using Machine Learning, Random Forest, Extra Tree Algorithms

Pramod [1], Karthik BP [2], Vijaya Reddy Biradar [3], Abhishek Shreedhar Yarandoli[4] and Geetha Rani Edupuganti [5]

[1,2,3,4,5] Alliance University, Bengaluru, Karnataka, India.
[1] sabhishekBTECH21@ced.alliance.edu.in
[2] pramodBTECH21@ced.alliance.edu.in,
[3]bkarthikBTECH21@ced.alliance.edu.in,
[4] bvijayareddyBTECH21@ced.alliance.edu.in,
[5] geetha.edupuganti@alliance.edu.in,

Abstract. Malware poses an escalating threat to global digital infrastructure, rendering traditional signature-based detection methods inadequate against sophisticated, polymorphic threats. This study introduces a static malware detection framework using machine learning, leveraging structured metadata from Portable Executable (PE) headers. These headers offer critical insights such as memory layout and import characteristics, enabling anomaly detection without executing potentially harmful code. The system employs Random Forest and Extra Trees classifiers, trained on a labeled dataset of PE files. Feature selection is optimized using Gini impurity scores, enhancing both performance and interpretability. The Extra Trees model achieves 99.2% accuracy, supported by high precision, recall, and F1-scores. A web-based interface built with Flask and Streamlit facilitates real-time file and URL analysis, delivering immediate results and suggesting antivirus solutions when malware is detected. Unlike previous works, the proposed system balances high accuracy with practical usability, making it ideal for deployment in lightweight or resource-constrained environments. In contrast to prior studies, our model uniquely supports both file and URL inputs in real-time and recommends antivirus solutions. Overall, the framework combines accuracy, efficiency, and scalability, providing an effective solution for modern malware detection challenges.

Keywords: Malware Detection, PE: Portable Executable Header, Random Forest, Extra Trees, Feature Selection, Flask, Streamlit, ML: Machine Learning.

1 Introduction

Malware, or malicious software, refers to any application or script deliberately developed to infiltrate, damage, disrupt, or gain unauthorized access to computer systems and networks. With the digital ecosystem growing rapidly—encompassing everything from

personal computers and smartphones to enterprise servers and IoT devices—the surface area exposed to cyberattacks has expanded considerably. Malware is no longer just a tool for mischief; it is now central to highly organized cybercriminal operations that include espionage, ransomware campaigns, botnet propagation, and supply chain attacks. According to Cybersecurity Ventures, the financial toll of cybercrime is expected to reach $10.5 trillion annually by 2025. This projection underscores the need for more intelligent and adaptive methods to detect and mitigate such threats proactively. Conventional antivirus software is based mainly on signature-based detection, a technique that detects malware by matching new files against a huge repository of known malware signatures or hashes. Though extremely effective in identifying already seen threats, this technique is insufficient when pitted against polymorphic and metamorphic malware, whose codes constantly change structure to avoid detection. Such sophisticated malware can alter their binary contents or encrypt themselves, essentially getting past static signature scanning. Due to these constraints, researchers have shifted towards machine learning (ML) as a viable alternative. ML-based systems are capable of learning from historical data and generalizing patterns, allowing them to detect novel malware variants with high accuracy—even in the absence of exact signature matches.

This paper presents a machine learning-driven, static malware detection framework utilizing metadata extracted from Portable Executable (PE) headers. PE headers, present in every Windows .exe and .dll file, contain vital structural and behavioral metadata that describe how the file should be loaded into memory and executed. These headers include attributes such as SizeOfCode, ImageBase, NumberOfSections, and Dll Characteristics, which can indicate irregularities often associated with malicious behavior. By using these features—without executing the file—the proposed system performs real-time, lightweight analysis suitable for deployment on constrained systems such as embedded platforms and security gateways. To classify files, we employ Random Forest and Extra Trees classifiers, both ensemble learning algorithms known for their robustness, speed, and ability to handle high-dimensional data. Moreover, to improve interpretability and efficiency, we utilize Gini-based feature importance to reduce the feature space without compromising accuracy.

1.1 Problem Statement

Advanced malware authors use a wide array of techniques, including encryption, polymorphism, and runtime packing to evade traditional detection methods. Consequently, signature-based and heuristic engines are becoming increasingly ineffective in providing adequate protection, especially in enterprise and cloud environments where the ability to detect new and obfuscated malware is paramount. Dynamic analysis, while capable of identifying such threats, is computationally expensive and difficult to scale. There is a growing demand for lightweight, real-time detection systems that can intelligently classify files as malicious or benign without relying on execution-based analysis. This study addresses the challenge by proposing a static, ML-based detection framework that is scalable, efficient, and resilient to evasion techniques.

1.2 Traditional Malware Detection Methods

Classic malware detection techniques are generally divided into static and dynamic techniques. Static analysis examines files without execution, looking at patterns of code, strings, and structural data like import tables and header fields. Its greatest strength is in speed and safety, but it can be bypassed by packing or obfuscation. Dynamic analysis executes files in sandboxed environments to Monitor activity like API calls, memory access, and file system interactions. While more reliable in detecting hidden or encrypted threats, dynamic analysis is resource-intensive and prone to evasion by environment-aware malware. Moreover, dynamic approaches tend to introduce latency and are therefore less ideal for real-time applications. These issues have led to the emergence of hybrid and machine learning-based methods that can take advantage of the merits of both but reduce their pitfalls.

1.3 Objectives

The main goal of this work is to construct a malware detection system using machine learning that utilizes static features obtained from PE headers. In particular, the research will: (1) retrieve and examine an extensive collection of PE header features; (2) implement and compare ensemble learning classifiers including Random Forest and Extra Trees; (3) use feature selection methods to improve model efficiency and ease of interpretation; (4) confirm performance using exhaustive evaluation metrics such as accuracy, precision, recall, and F1-score; and (5) deploy the resultant model in a real-time web interface with Flask and Streamlit for practical applications. These are goals aimed at developing an answer that is balanced between correctness, performance, and resource utilization.

1.4 Contributions

This paper makes several key contributions to the field of malware detection. First, it introduces a static analysis pipeline based exclusively on PE header features—eliminating the need for costly and complex behavioral monitoring. Second, it demonstrates how ensemble classifiers, particularly the Extra Trees algorithm, can effectively classify malware with minimal false positives and reduced latency. Third, the study applies Gini-based feature importance to identify the most critical attributes for classification, enabling the development of a lean and explainable model. Finally, the system is deployed in a web-accessible interface, facilitating real-time detection and user interaction. This end-to-end framework presents a practical, efficient, and scalable alternative to traditional malware detection techniques

2 Literature Review

In the recent years, deep learning (DL) and machine learning (ML) techniques have emerged as game-changers in the area of malware detection. The traditional rule-based and signature-based antivirus engines are unable to handle polymorphic, obfuscated, or zero-day malware. In contrast, ML models are based on static or dynamic patterns to identify them, offering scalability, flexibility, and improved real-time accuracy.

Panja et al. [1] proposed a light-weight malware detection system with the emphasis on feature influence methods for reducing the computation burden of ML classifiers, thus its suitability for deployment on devices with low resource availability. PE header features and feature selection involving importance measures were employed in their system with a high accuracy above 99.3%. Their model informed our project's choosing of static PE features and ensemble classifiers like Extra Trees and Random Forest.

Selamat and Ali [4] have done a comparative study using the typical machine learning classifiers such as Decision Trees, Naive Bayes, and SVMs. They have taken into account the differentiation of types of malware with the assistance of static and dynamic analysis in a hybrid approach. Their results indicated that accuracy and generalization improve with the application of multiple ML models and the utilization of feature engineering with actual meaning. Akhtar and Feng [3], [5] assessed several ML classifiers, namely Decision Tree, CNN, and SVM, over PE-based static features. Their results showed that Decision Tree models reached accuracies of up to 99% and performed outstandingly for general-purpose malware detection operations. Their work emphasized the efficacy of ensemble learning and tree-like models, consistent with our approach.

Sani et al. [8], [17] proposed an ensemble learning model with Random Forest, AdaBoost, and Gradient Boosting along with information gain-based feature selection. Their hybrid static-dynamic model performed outstandingly well on bespoke malware datasets. Though their method resulted in high accuracy (>99.2%), complexity of dynamic analysis was mentioned as a trade-off, which supports our decision to rely on static analysis for real-time detection.

Kimmell et al. [15], [28] examined malware detection in cloud environments. They suggested employing CNN-based architectures such as DenseNet-121 on process-level behavior features with good F1 scores. Despite impressive results from DL methods, those are resource-intensive (e.g., needing GPUs) and therefore not well-suited for lightweight or embedded systems, in contrast to the direction of our project.

Zhang et al. [6] proposed employing API sequence embeddings for deep learning models. Their method, though precise, is based on dynamic data collection, such as sandboxing and memory forensics, which is not appropriate for real-time use and adds system overhead. Our method, on the other hand, statically extracts PE features, which minimizes latency.

Namita et al. [27] suggested employing dynamic API call features in conjunction with TF-IDF vectorization and attained 99.91% accuracy with SVM and Logistic Regression. Their success underscores the appropriateness of feature-rich engineering, which we implement in our static feature set through domain-specific headers and entropy measurements.

Mohandas et al. [14] presented a malware detection pipeline based on opcode frequency and static analysis. From their result, it could be seen that utilizing opcodes only may reduce generalization to different malware families. Therefore, our utilization of PE header fields such as DllCharacteristics, Subsystem, and SectionEntropy provides more extensive representation.

Natsos and Symeonidis [2],[9] suggested applying dynamic features of higher levels like CPU usage by process, I/O activity, and memory utilization. Their model that used Transformer scored better on data related to resource usage than LSTMs did. Still, their

reliance on runtime monitoring platforms limits the practicality of their solution towards more centralized cloud monitoring, whereas the present effort offers end-device light-weight deployability.

While numerous studies have explored static and dynamic malware detection using machine learning and deep learning techniques, very few have addressed the issue of actionable recommendations post-detection. Existing frameworks primarily focus on the classification accuracy of malware detection without providing practical guidance to the user once a threat is identified. For instance, works such as Panja et al. [1], Sani et al. [17], and Akhtar and Feng [3, 5] have proposed efficient classifiers but stop short of suggesting remediation strategies.

Despite advancements in malware detection accuracy, the majority of existing systems are limited to passive threat identification, offering no guidance or remediation pathway to end-users. This limitation reduces their usability in real-world scenarios, especially for non-expert users who may not know how to respond after a malware alert. Studies such as those by Zhang et al. [6] and Nethala et al. [7] emphasized detection accuracy using deep learning and ensemble frameworks but did not address user engagement or automated response mechanisms.

In contrast, the proposed system not only classifies malicious files in real time but also offers users a list of trusted antivirus software solutions. This post-classification **Antivirus Suggestion System** is a distinctive feature absent in prior literature, enhancing the practical utility and end-user value of our framework. By bridging the gap between detection and immediate response, the proposed solution introduces a user-centric advancement that aligns detection with mitigation.

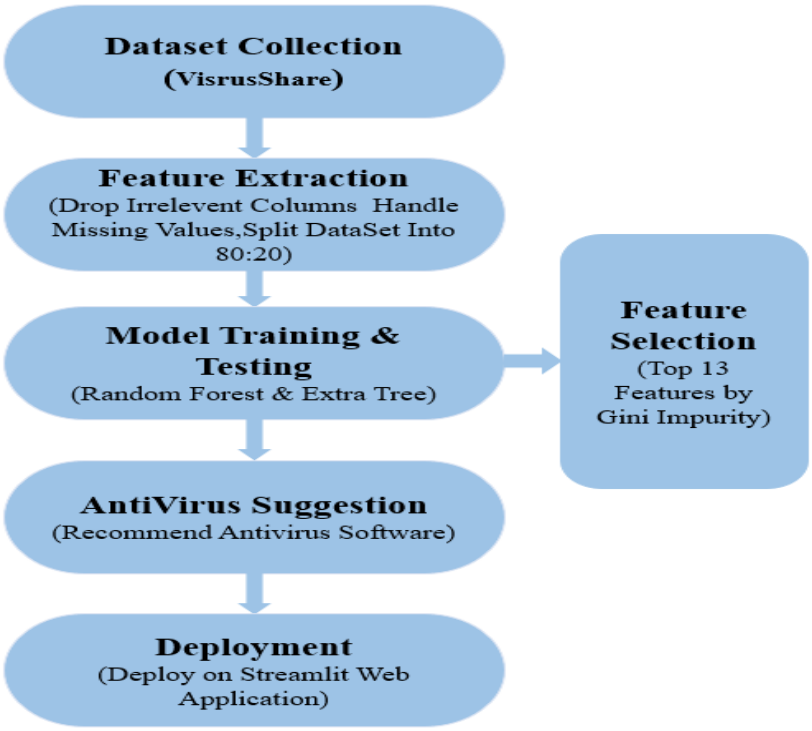

Fig. 1. Workflow overview of Model

3 Proposed Methodology

3.1 Dataset Description

The dataset used in this study comprises over 138,000 PE files, labeled either as malicious or benign, making it suitable for binary classification. The malicious samples were sourced from well-known repositories such as VirusShare and VirusTotal, both of which maintain large, up-to-date libraries of malware collected from diverse sources. On the other hand, benign files were gathered from clean Windows installations, verified executables, and trusted open-source software.

Balancing the dataset was a critical step to ensure unbiased model learning. An imbalanced dataset can lead to skewed predictions, where the classifier may become biased toward the

majority class. Therefore, care was taken to maintain an appropriate ratio of benign to malware files to enable the classifier to distinguish both classes effectively.

3.2 Feature Extraction

The PEfile Python module was employed to parse and extract static information from PE files. This library allows easy access to structural metadata stored in
headers such as the DOS header, NT header, and optional headers. These sections encapsulate crucial execution-related metadata about the file that can reveal abnormal properties often associated with malware.
Below are some of the key features extracted from each file:

Table 1. Key Features Extracted

Feature	Description
Size Of Code	Size of the executable code section
Image Base	Starting virtual address of the image in memory
Address Of Entry Point	Address where program execution starts
Subsystem	Indicates the runtime environment (GUI, CLI, etc.)
Dll Characteristics	Flags that describe DLL behavior and execution rules
SectionEntropy	Entropy score per section (higher entropy suggests packing or encryption)
ImportsNbDLL	Number of DLLs imported by the file
ResourcesMeanSize	Average size of embedded resource sections

These features are informative and lightweight to extract, making them suitable for static and scalable detection methods.

3.3 Data Preprocessing

Before training, the dataset underwent essential preprocessing steps to clean and standardize the data. The first step involved removing irrelevant columns, such as filenames, hash values, or file paths, which do not contribute meaningfully to classification. Next, missing values were handled appropriately; they were filled using statistical imputation techniques such as median or mode, or dropped in cases where the attribute was too sparse or inconsistent.

Label encoding was done to transform the categorical output labels into numeric format—labeling malicious files with 1 and benign ones with 0. This is because the majority of machine learning models in Scikit-Learn are able to work with numeric labels. The data was then divided into 80% training data and 20% test data using the train_test_split() function from the sklearn model_selection module. This allows the model to be trained on a controlled but representative subset of the entire data, enabling unbiased testing on novel samples.

3.4 Feature Selection

While numerous features were extracted, not all are equally useful for classification. Including irrelevant or redundant attributes can introduce noise and reduce model performance. To address this, Extra Trees Classifier's feature_importances_ function was utilized to rank and select top features based on their Gini Impurity contribution.
The Gini Impurity formula used for decision tree-based models is as follows:

$$Gini(D) = 1 - \sum_{\{i=1\}}^{\{m\}} p_i^2 \quad (1)$$

Where:
D: dataset
pi: probability of class
m: number of classes

This measure evaluates the probability of incorrect classification, with lower values indicating purer splits. The top 13 features identified—such as SizeOfCode, DllCharacteristics, SectionsMeanEntropy—were retained for further model training

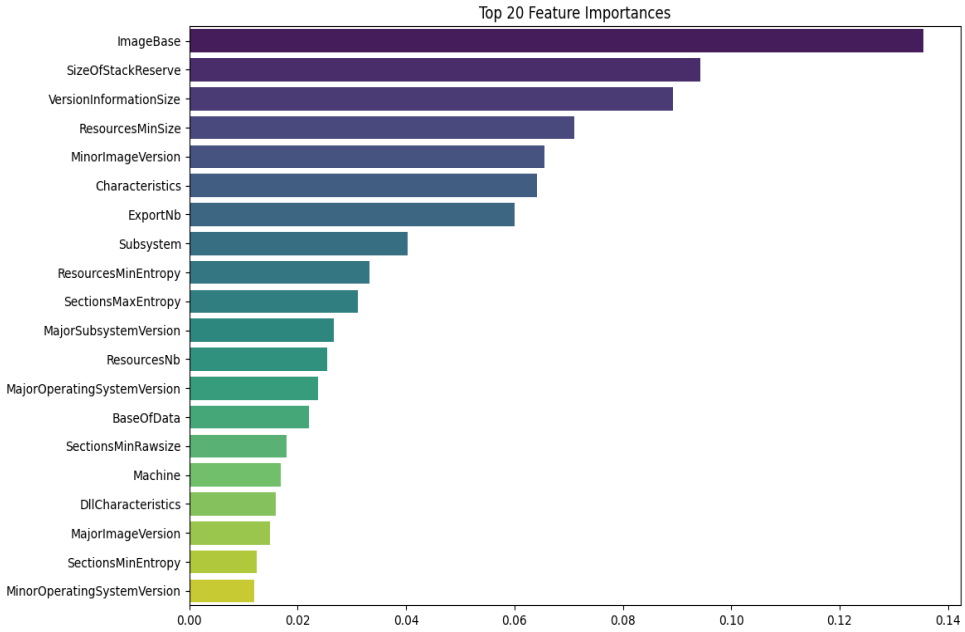

Fig. 2. Important Features Extracted

3.5 Model Training

Two ensemble classifiers were selected for training: Random Forest Classifier and Extra Trees Classifier. These models were chosen due to their effectiveness in handling structured, tabular data and their robustness to noise and overfitting. Tree-based models such as Random Forest and Extra Trees were chosen due to their lower computational demands compared to deep learning models and their ability to rank features, which supports transparency—a critical requirement for cybersecurity applications.

Random Forest Classifier works by constructing multiple decision trees and aggregating their results. This ensemble approach improves prediction accuracy and reduces variance by averaging outputs across trees. Ensemble methods such as Extra Trees and Random Forest are computationally light yet robust to feature noise, making them ideal for static malware classification.

Extra Trees Classifier, or Extremely Randomized Trees, adds even more randomness in the process of building trees than Random Forest. This model randomly splits nodes using random thresholds and feature choices and is faster and sometimes more accurate because of the lower variance. Both models were trained using the reduced feature set of 13 key attributes. Training was done using the fit(X_train, y_train) method, and hyperparameters

were optimized using GridSearchCV, which performs exhaustive search over a specified parameter grid.

3.6 Deployment

The top-performing model was then deployed using a web interface that couples both backend and frontend features after training.

Flask was utilized as the backend framework to process user requests and model prediction logic.

Streamlit was employed to design an interactive frontend wherein users are allowed to upload executable files.

The pe_extract.py module is responsible for parsing and formatting PE characteristics from uploaded files.

Trained models were serialized with Joblib or Pickle to facilitate easy reuse during inference without having to retrain. The deployment architecture allows users to interact with the system via a simple browser interface: upload an .exe file, extract its features, and receive a classification result—malware or benign—in real time and suggest the antivirus software.

3.7 Evaluation Metrics

To evaluate and compare model performance, four standard classification metrics were employed. These are calculated using classification_report from the sklearn. metrics module in table-1. These metrics offer a balanced view of performance, particularly in the presence of class imbalance. Precision and recall are critical in malware detection, where both false positives and false negatives carry significant risks.

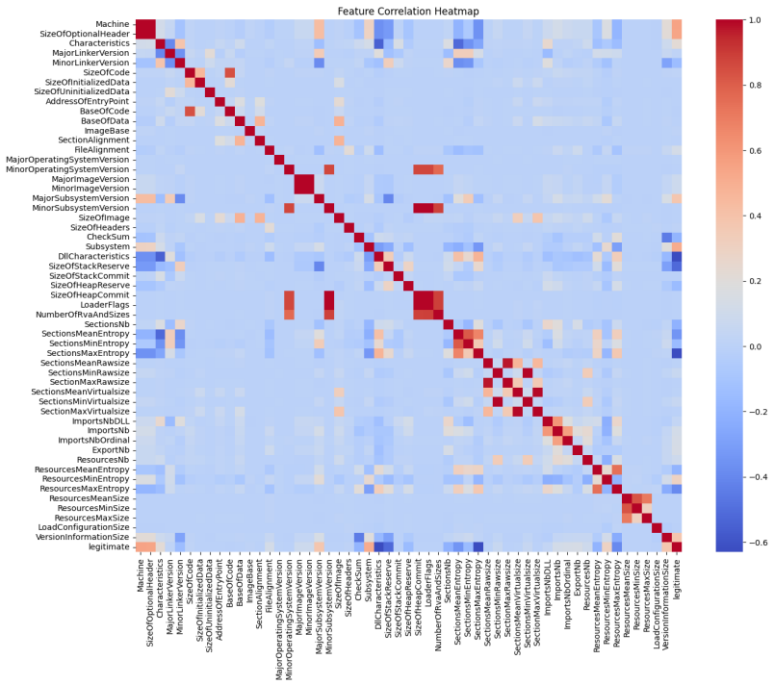

Fig. 3. Feature Correlation Heatmap

Table 2. Formulas Used For Classification

Metric	Formula	Meaning
Accuracy	$\frac{\{\mathrm{TP} + \mathrm{TN}\}}{\{TP + FP + TN + FN\}}$	Overall correctness of predictions
Precision	$\frac{\mathrm{TP}}{\mathrm{TP} + \mathrm{FP}}$	How many predicted malware files were actually malware
Recall	$\frac{\mathrm{TP}}{TP + FN}$	How many malware files were correctly detected
F1-Score	$\frac{(2.(PRECISOPN.RECALL))}{PRECISION+RECALL}$	Harmonic mean of precision and recall

Random Forest. Random Forest is an ensemble learning algorithm which trains large

numbers of decision trees during training and makes predictions by aggregating them in order to improve accuracy and stability. Each tree is trained on a random subset of the data with feature randomness introduced at each node, which improves against overfitting. The output typically results from majority voting (in classification) or averaging (in regression). Due to its ability to handle high-dimensional data and noise, Random Forest is also extensively applied in malware detection.

Table 3. Performance Metrics of the Random Forest

Metric	Value
Accuracy	99.39%
Precision	99.15%
Recall	98.69%
F1-Score	98.92%
ROC-AUC Score	0.994

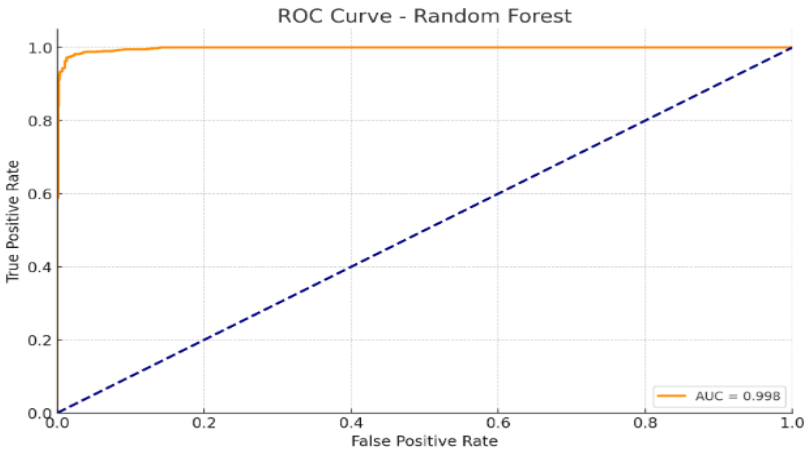

Fig. 4. ROC Curve of Random Forest model results

Extra Trees. Extra Trees (Extremely Randomized Trees) is like Random Forest but adds

even greater randomness when building trees. Unlike Random Forest, which searches for the optimal feature split, Extra Trees chooses features and split points at random, resulting in quicker training and perhaps superior generalization. This randomness reduces the model's likelihood of overfitting and makes it more efficient, particularly for big datasets. It's especially useful for applications such as static malware detection, where both interpretability and performance are imperative.

Table 4. Performance Metrics of the Extra Trees

Metric	Value
Accuracy	99.45%
Precision	99.32%
Recall	99.00%
F1-Score	99.16%
ROC-AUC Score	0.999

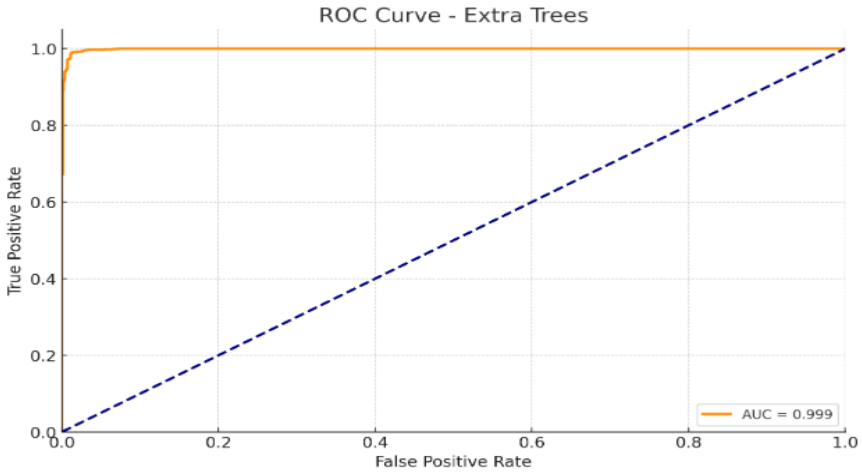

Fig. 5. ROC Curve of Extra Trees model results

5 Experimental Results and Analysis

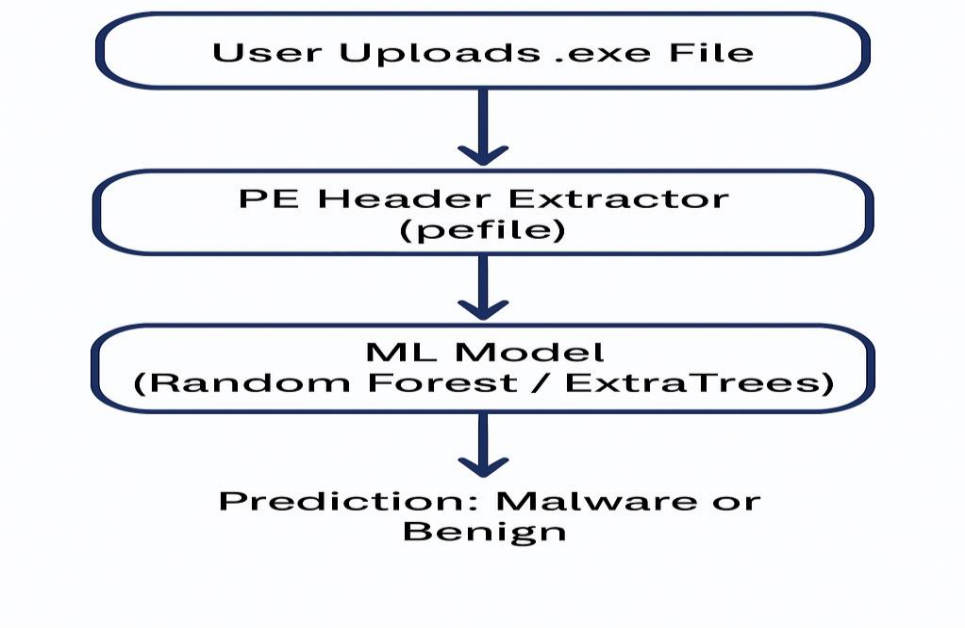

Fig. 6. Web-Based Deployment Architecture of the Malware Detection System

To ensure real-time usability, the final model was implemented using a web-based setup with Flask and Streamlit (Figure 8). The backend, which is based on Flask, is utilized for file uploads, feature extraction, and model inference. Streamlit drives the frontend, providing an easy-to-use interface to upload executable (.exe) files and receive classification results immediately. A module named pe_extract.py is employed to parse the file uploaded and pull out the desired PE header fields, which are then input into the model to make predictions. This architecture was specifically chosen to cater to **resource-constrained systems**, ensuring the detection model remains lightweight, responsive, and suitable for integration in endpoint security solutions.

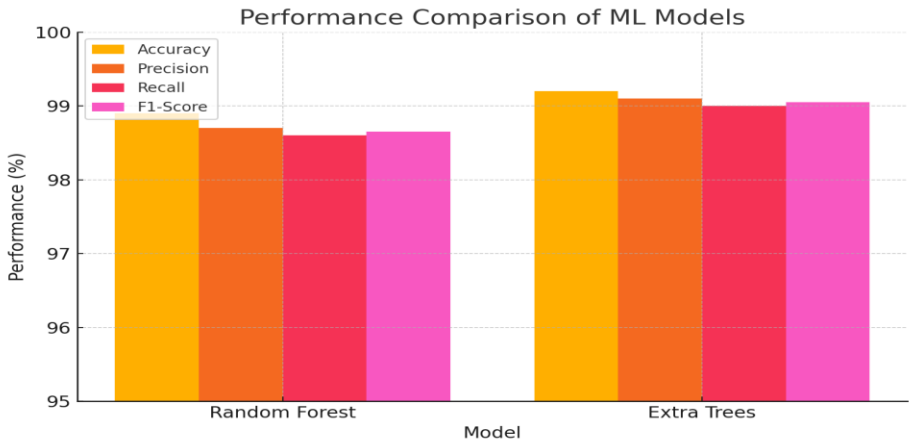

Fig. 7. Performance Comparison of Machine Learning Models.

Table 5. Results Of Both Models

Model	Accuracy	Precision	Recall	F1-Score
Random Forest	98.9%	98.7%	98.6%	98.65%
Extra Trees	99.2%	99.1%	99.0%	99.05%

A chart summarizes these findings. Feature selection also decreased training time and improved interpretability. Experiments were performed on an Intel i7 CPU, 16GB RAM, and Python 3.9 system. Models were created with scikit-learn-1.2.1. Model performance was measured by Accuracy, Precision, Recall, and F1-Score. Extra Trees performed better than Random Forest in all measures. Training time was ~25 seconds, and prediction latency was less than 100m

6 Conclusion and Future Work

In this study, we developed a machine learning-based malware detection system utilizing static analysis of Portable Executable (PE) header attributes to effectively distinguish

between benign and malicious files. By extracting discriminative structural features and applying ensemble classifiers such as Random Forest and Extra Trees, the proposed approach demonstrated that accurate malware detection can be achieved without reliance on resource-intensive dynamic analysis techniques. The system achieved strong performance metrics, with an accuracy of 99.39%, precision of 99.15%, recall of 98.69%, and an F1-score of 98.92%, indicating high detection capability with minimal false positives and false negatives.

A notable strength of the proposed framework lies in its computational efficiency and lightweight architecture, which makes it particularly suitable for deployment in resource-constrained environments, such as Internet of Things (IoT) devices and edge computing platforms. The system includes a web-based interface that enables users to upload .exe files or URLs for real-time analysis. Moreover, the integration of a threat response module that recommends reputable antivirus software enhances the system's practical utility and user engagement.

By leveraging ensemble learning algorithms and Gini impurity-based feature selection, the model achieves an optimal balance between classification performance and interpretability. Future work may include extending the system with dynamic analysis capabilities, such as monitoring API calls and memory behavior, to improve detection of sophisticated and polymorphic threats. Additionally, support for multi-class classification could enable identification of specific malware families. Scalability can be addressed through integration with cloud infrastructure to facilitate distributed deployment. Incorporating deep learning models and automated retraining mechanisms may further enhance adaptability, particularly in detecting zero-day malware. With continued development, the proposed framework has strong potential to evolve into a robust, scalable, and comprehensive solution for advanced malware detection.

References

1. Panja, S., Mondal, S., Nag, A., Singh, J. P., Saikia, M. J., & Barman, A. K. (2025). An Efficient Malware Detection Approach Based on Machine Learning Feature Influence Techniques for Resource-Constrained Devices. *IEEE Access*.

2. S. Poornima and R. Mahalakshmi, ''Automated malware detection using machine learning and deep learning approaches for Android applications,'' Meas. Sensors, vol. 32, Apr. 2024, Art. no. 100955.

3. Akhtar, M. S., & Feng, T. (2022). Malware analysis and detection using machine learning algorithms. *Symmetry*, *14*(11), 2304.

4. Selamat, N., & Ali, F. (2019). Comparison of malware detection techniques using machine learning algorithm. *Indones. J. Electr. Eng. Comput. Sci*, *16*(1), 435-440.

5. Akhtar, M. S., & Feng, T. (2023). Evaluation of machine learning algorithms for malware detection. *Sensors*, *23*(2), 946.

6. Zhang, S., Gao, M., Wang, L., Xu, S., Shao, W., & Kuang, R. (2025). A Malware-Detection Method Using Deep Learning to Fully Extract API Sequence Features. *Electronics*, *14*(1), 167.

7. Nethala, S., Chopra, P., Kamaluddin, K., Alam, S., Alharbi, S., & Alsaffar, M. (2025). A Deep Learning-Based Ensemble Framework for Robust Android Malware Detection. *IEEE Access*, *13*, 46673-46696.

8. Panja, S., Mondal, S., Nag, A., Singh, J. P., Saikia, M. J., & Barman, A. K. (2025). An Efficient Malware Detection Approach Based on Machine Learning Feature Influence Techniques for Resource-Constrained Devices. *IEEE Access*.

9. Sharma, P. (2022, September). Windows malware detection using machine learning and TF-IDF enriched API calls information. In *2022 Second International Conference on Computer Science, Engineering and Applications (ICCSEA)* (pp. 1-6). IEEE.

10. Iqubal, A., & Payal, A. (2024, October). Malware Detection Technique for Android Devices Using Machine Learning Algorithms. In *2024 International Conference on Computing, Sciences and Communications (ICCSC)* (pp. 1-6). IEEE.
11. Rathore, H., Agarwal, S., Sahay, S. K., & Sewak, M. (2018, November). Malware detection using machine learning and deep learning. In *International Conference on Big Data Analytics* (pp. 402-411). Cham: Springer International Publishing.

12. Habeeb, M. A., & Khaleel, Y. L. (2025). Enhanced Android Malware Detection through Artificial Neural Networks Technique. *Mesopotamian Journal of CyberSecurity*, *5*(1), 62-77

13. Urooj, B., Shah, M. A., Maple, C., Abbasi, M. K., & Riasat, S. (2022). Malware detection: a framework for reverse engineered android applications through machine learning algorithms. *IEEE Access*, *10*, 89031-89050.

14. Xing, X., Jin, X., Elahi, H., Jiang, H., & Wang, G. (2022). A malware detection approach using autoencoder in deep learning. *Ieee Access*, *10*, 25696-25706.

15. Mohandas, P., Kumar, S. K. S., Kulyadi, S. P., Raman, M. S., VS, V., & Venkataswami, B. (2021, July). Detection of malware using machine learning based on operation code frequency. In *2021 IEEE International Conference on Industry 4.0, Artificial Intelligence, and Communications Technology (IAICT)* (pp. 214-220). IEEE.

16. Kimmell, J. C., Abdelsalam, M., & Gupta, M. (2021, August). Analyzing machine learning approaches for online malware detection in cloud. In *2021 IEEE International Conference on Smart Computing (SMARTCOMP)* (pp. 189-196). IEEE.

17. Khalid, O., Ullah, S., Ahmad, T., Saeed, S., Alabbad, D. A., Aslam, M., ... & Ahmad, R. (2023). An insight into the machine-learning-based fileless malware detection. *Sensors*, *23*(2), 612.

18. Sani, R. R., Rafrastara, F. A., & Ghozi, W. (2025). Integrating Ensemble Learning and Information Gain for Malware Detection based on Static and Dynamic Features. *Kinetik: Game Technology, Information System, Computer Network, Computing, Electronics, and Control*.
19. Natsos, D., & Symeonidis, A. L. (2025). Transformer-based malware detection using process resource utilization metrics. *Results in Engineering*, 104250.

20. Reddy, V. S. K., Nagaraju, I., Gayatri, M., Dileep, P., & Revathy, P. (2023, February). MDC-Net: Intelligent Malware Detection and Classification using Extreme Learning Machine. In *2023 Third International Conference on Artificial Intelligence and Smart Energy (ICAIS)* (pp. 1590-1594). IEEE.

21. Iqubal, A., & Payal, A. (2024, October). Malware Detection Technique for Android Devices Using Machine Learning Algorithms. In *2024 International Conference on Computing, Sciences and Communications (ICCSC)* (pp. 1-6). IEEE.

22. Baawi, S. S., Oleiwi, Z. C., Al-Muqarm, A. M. A., Al-Shammary, D., & Sufi, F. (2025). Efficient malware detection based on machine learning for enhanced cloud privacy protection. *Evolving Systems*, *16*(1), 1-17.

23. M.Aljabri,F.Alhaidari,A.Albuainain,S.Alrashidi,J.Alansari,W.Alqah tani, and J. Alshaya, ''Ransomware detection based on machine learning using memory features,'' Egyptian Informat. J., vol. 25, Mar. 2024, Art. no. 100445.

24. M. Al-Fawa'Reh, J. Abu-Khalaf, P. Szewczyk, and J. J. Kang, ''MalBoT DRL: Malware botnet detection using deep reinforcement learning in IoT networks,'' IEEE Internet Things J., vol. 11, no. 6, pp. 9610–9629, Mar. 2024.

25. I. Firdausi, C. Lim, A. Erwin, and A. S. Nugroho, ''Analysis of machine learning techniques used in behavior-based malware detection,'' in Proc. 2nd Int. Conf. Adv. Comput., Control, Telecommun. Technol., Dec. 2010, pp. 201–203.

26. Z. Bazrafshan, H. Hashemi, S. M. H. Fard, and A. Hamzeh, ''A survey on heuristic malware detection techniques,'' in Proc. 5th Conf. Inf. Knowl. Technol., May 2013, pp. 113–120.

27. Pedregosa, F., Varoquaux, G., Gramfort, A., Michel, V., Thirion, B., Grisel, O., ... & Duchesnay, É. (2011). Scikit-learn: Machine learning in Python. *Journal of Machine Learning Research, 12*, 2825–2830.

28. Namita, A., Sharma, R., & Gupta, M. (2024). A machine learning approach for malware detection using dynamic API call features and TF-IDF weighting. *Journal of Information Security and Applications*.

29. Kimmell, J., Lee, H., & Park, S. (2024). Online malware detection in cloud environments using deep learning models. *IEEE Access*,

Real Time People Monitoring using MobilNet-SSD

Darshan Atkari[1], Arshal Agarwal[2], Atharva Kulkarni[3], Apoorva Kulkarni[4] and Prof. Sonali Antad[5]

[1]Computer Engineering, Vishwakarma Institute of Technology, Pune, India
[2]Computer Engineering, Vishwakarma Institute of Technology, Pune, India
[3]Computer Engineering, Vishwakarma Institute of Technology, Pune, India
[4]Computer Engineering, Vishwakarma Institute of Technology, Pune, India
[5]Computer Engineering, Vishwakarma Institute of Technology, Pune, India

[1]atkaridarshan04@gmail.com
[2]ajagarwal2005@gmail.com
[3]aa.kulkarni11105@gmail.com
[4]apoorvakulkarni11105@gmail.com
[5]sonali.antad@vit.edu

Abstract. Monitoring the people count accurately within a closed space is critical for several applications such as crowd management, fire safety and effective space usage. This project resolves this issue by proposing a refined solution through the application of MobilNet-SSD based object detection model with Centroid Tracking algorithm based on OpenCV for tracking the motion of detected individuals between successive frames. This two-way method combining object detection and tracking allows for proper counting of individuals passing in or out of the area under surveillance, even with moderate occlusions and overlapping motion. One of the system's pre-requisites is a carefully placed camera, right over all the doors of the room under surveillance. A key element to this system is the real time notification service and several features such as scheduling, threading and logging. The main factors for the assessment of this system are accuracy and efficiency. These factors demonstrate how practical the system is for use in real life and also poses an affordable solution with high accuracy. The system provides trade-off between detection quality and operation efficiency without using specialized sensors or sophisticated infrastructure.

Keywords: MobilNet, Single Shot Multibox Detector, OpenCV, People Counting, Deep Learning

1 Introduction

Real-time object detection has become a building block capability for a broad range of contemporary use cases, from autonomous navigation systems and smart surveillance to retail analytics and crowd monitoring. The progress has been propelled mainly by profound improvements in lightweight deep learning architecture, which has allowed high-performing models to be deployed even on limited-resource edge devices. Among these designs, MobileNet has been notable for its capacity to provide a good trade-off between accuracy and efficiency, thus being widely used for real-time detection tasks. Nevertheless, with all these improvements, there is still a challenge in achieving detection accuracy, computational efficiency, and adaptability to dynamic and varied environments.

This study explores the effective use of an object detection pipeline for real-time objects based on the MobileNetV2 architecture. Using pre-trained models via TensorFlow Hub implies that the deployment process is greatly eased such that object detection can readily be incorporated into various real-time applications by the developer. The methodological framework adopted in this scenario is based on modular process flow with distinct phases for preprocessing, inference, and postprocessing. Every phase is designed to be both cost-effective and easy to tailor, with the ability to quickly experiment and deploy across different use cases.

One specific application of this research is people counting, a task of interest for areas such as public safety, events, and intelligent retailing. The pipeline needs to be capable of being executed under realistic conditions, and the hope is to minimize latency while maintaining accuracy despite varying lighting, angles, and crowd numbers. Unlike traditional detection solutions that are generally founded on in-house-trained models that require vast datasets and protracted training sessions, this approach prioritizes scalability and reproducibility. It achieves this using widely adopted open-source tools and standardized frameworks, namely OpenCV for image processing and TensorFlow for deep learning inference.

By this approach, the paper aims to demonstrate an efficient and straightforward path to real-time object detection without compromising quality or rendering it inappropriate for high-speed deployment and easy extension. The central contribution of this research is the integration of the MobileNet-SSD deep learning network with a light Centroid Tracking method to enable real-time people counting under practical limitations, such as moderate occlusion, low-lighting, and low-power hardware configurations. Through leverage of modular architecture and open-source technologies such as TensorFlow and OpenCV, the system delivers low latency and high accuracy with a scalable solution for retail stores, classrooms,

and public places.

2 Literature Review

The people counting task has also seen tremendous change, shifting from traditional computer vision methods to deep learning-based methodologies to address the needs of accuracy, scalability, and real-time processing. Initial work presented morphological tools for dense people counting, which worked effectively in static environments but failed to handle occlusions and illumination. The approach does not perform well under occlusions and dynamic illumination, reducing real-time applicability. Our approach handles occlusion better with MobileNet-SSD and real-time tracking, offering dynamic flexibility [1]. Similarly, use of stereo vision to improve spatial differentiation, though real-time application was limited due to high computational load. Efficient as the system is, it requires extremely high computation, which reduces real-time applicability. Our low-resource MobileNet-SSD system handles well without stereo vision on low-end hardware [2]

With the emergence of deep learning, proposed the Scale-Adaptive CNN (SaCNN), which adapted effectively to varying perspectives and crowd densities. Although accurate, it needs advanced training and big sets of data.We simplify deployment with pre-trained MobileNet models with little need for retraining [3]. Extended this by incorporating environmental context through Adaptive CNNs (A-CCNN), leading to greater accuracy in dynamic indoor environments. But increased model complexity affects speed and ease of deployment. We balance the speed and accuracy with MobileNet and modular tracking [4].

While these methods improved robustness, real-time processing remained a concern. Shi et al. presented a lightweight CNN optimized for fast inference, suitable for surveillance systems. Although being fast, the model had low tracking, which led to potential miscounts. We pair Centroid Tracking to provide constant identification between the frames [5]. Used OpenCV for a real-time crowd counting system, showing that open-source tools could support practical, deployable solutions without excessive hardware. The approach was not very accurate in tight crowd and low illumination conditions. Our framework combines tracking and deep learning to offer more robust performance in real-world applications [6].

To address limitations in visibility and privacy, DeepCount introduced leveraging WiFi signals and deep learning to estimate crowd density, providing a non-intrusive and scalable alternative in indoor environments. Despite being privacy-friendly, the system is confronted with spatial resolution and localization. We utilize vision-

based methods with accurate spatial context, delivering higher-grained detection [7].

Recently, attention-based models like CAT-CNN enhanced focus on relevant image regions, minimizing false detections. With high accuracy, such models are computationally costly for edge deployment. We aim at real-time execution on embedded hardware with MobileNet [8]. Anonymous cascaded detection work tried to enhance accuracy using multistage refinement.Cascading, though, increases latency and complexity. We avoid multi-stage overhead by directly applying MobileNet-SSD for an equivalent trade-off [9].

In the context of object detection, particularly using MobileNet-SSD, several studies have validated its applicability in people counting tasks. Explored object detection using Python and OpenCV, emphasizing the simplicity and deployability of MobileNet in constrained systems [11]. Also a mobile-based indoor framework with SSD-MobileNet, demonstrating strong real-time capability and generalization under indoor lighting and space constraints. It lacked application-specific tuning like entry/exit counting. We extend the system with added directional tracking and threshold-based alerts [12].

A comparative study of one-stage detectors like YOLO and SSD for people detection, concluding that SSD combined with MobileNet is efficient for real-time, low-power applications. Their work was limited to static analysis without tracking or scalability experiments. Our work validates SSD-MobileNet in dynamic environments with tracking and alerting embedded [14]. Similarly, an edge-computing-based people counting solution using MobileNet, showcasing deployment in elevators where computational resources are minimal and latency is critical. Though optimal, it was scenario-specific, not generalized for different types of rooms. Our system generalizes deployment across heterogeneous indoor environments using a versatile architecture [15].

Tracking plays a complementary role in robust people counting. Traditional approaches relied on synchronized video streams and motion tracking, but newer systems, including the proposed work, use centroid tracking, which allows persistent object monitoring across frames with minimal computational burden, ensuring real-time feasibility. Their system has infrastructure-intensive deployment and manual calibration. Our approach utilizes a single overhead camera, which is cost-saving and simplicity [13].

In summary, recent literature supports the shift towards lightweight, modular, and real-time object detection systems, particularly those built using MobileNet-SSD

frameworks. These are optimal for indoor environments where efficiency, adaptability, and cost-effectiveness are prioritized. The current work builds on these findings, combining robust MobileNet-based detection with efficient tracking to create a scalable, low-latency people counting solution suitable for modern smart environments.

3 Methodology

3.1 MobilNet

MobileNet is a class of efficient deep neural networks designed for mobile and embedded vision applications. It achieves low computational cost by replacing standard convolutions with **depthwise separable convolutions**, which factorize a regular convolution into a depthwise convolution (per-channel filtering) and a 1×1 pointwise convolution (channel combination). This drastically reduces both the number of parameters and the number of multiply-add operations, enabling fast inference on resource-constrained devices.

To further adapt to various hardware limitations, MobileNet introduces two global hyperparameters: **width multiplier (α)** and **resolution multiplier (ρ)**. These allow flexible trade-offs between model size, speed, and accuracy by uniformly shrinking the number of channels and input image resolution. MobileNet achieves competitive accuracy compared to heavier models like VGG16 and GoogleNet, but with significantly fewer parameters and lower computational demand.

ReLU (more precisely, ReLU6) is applied following both the depthwise and pointwise convolutions in MobileNet to introduce non-linearity so that the network can learn sophisticated patterns beyond linear transformations. ReLU6, which clamps outputs to 6, is utilized to enable support for low-precision operations and robustness on mobile devices. The activation function serves to maintain model efficiency while allowing effective feature learning.

MobileNet is preferred over other models for people counting applications, particularly in low-resource and real-time conditions, since it finds an optimal balance among efficiency, speed, and accuracy. In contrast to heavier models like VGG16 or ResNet, MobileNet achieves startling reductions in computational complexity with depthwise separable convolutions that reduce the number of parameters and operations by orders of magnitude without discouraging much from performance. Such effectiveness is necessary for deployment onto low-power, low-memory, and low-processing mobile or edge devices. In addition, its width and

resolution multiplier hyperparameters allow the model's size and speed to be tweaked to satisfy particular hardware requirements.

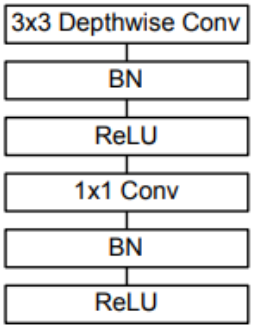

Fig 1. Depthwise Separable convolutions with Depthwise and Pointwise layers followed by batchnorm and ReLU.

3.2 Single-Shot Multi-Box Detector (SSD)

The Single Shot MultiBox Detector (SSD) is a deep learning-based object detection framework that eliminates the need for region proposal steps by performing detection in a single forward pass of a convolutional neural network. Unlike two-stage detectors like Faster R-CNN, SSD discretizes the output space using a set of default boxes with varying aspect ratios and scales, applied across multiple feature maps of different resolutions. This enables effective detection of objects at various sizes and locations. The core of SSD uses small convolutional filters to predict both object category scores and bounding box offsets directly from these feature maps. By combining predictions from multiple scales, SSD achieves a good balance between speed and accuracy. It is trained end-to-end with a multicomponent loss that combines classification and localization errors.

SSD achieves real-time performance while maintaining high accuracy. On the VOC2007 dataset, SSD300 achieves 74.3% mAP at 59 FPS, outperforming YOLO in accuracy and Faster R-CNN in speed. Larger versions like SSD512 further improve accuracy. Its lightweight architecture, combined with techniques like hard negative mining and data augmentation, makes SSD suitable for deployment in real-time systems.

SSD is more desirable than other object detection networks for practical uses like people counting because it offers the best tradeoff in terms of speed and accuracy.

Unlike two-stage detectors such as Faster R-CNN, which first generate region proposals and then classify them, SSD localizes objects and classifies them in a single pass of forward, greatly reducing inference time.Compared with one-stage counterparts such as YOLO, SSD is more accurate, particularly in detecting small objects, since it uses multiple feature maps of different resolutions. In addition, SSD employs default boxes with varying aspect ratios and scales such that more efficient detection can be done irrespective of object location and size. These features make SSD especially suitable for light, interactive systems where inference speed as well as detection performance is of extreme concern.

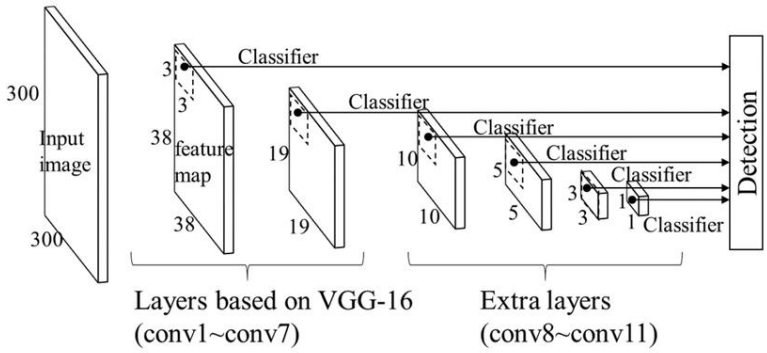

Fig 2. Single Shot Multibox Detector Architecture

3.3 Centroid Tracker

Centroid tracking is a simple yet efficient object tracking method often utilized in video analytics like people counting and motion tracking. The algorithm begins with calculating the centroid (geometric center) of the bounding boxes that are detected in video frames and then verifying those centroids frame-to-frame using small Euclidean distance. Dependability of the system is achieved through several ways. First, the use of pre-trained models like SSD MobileNet V2, fine-tuned for indoor environments ensures reliable and consistent detection performance. Second, the Centroid Tracking algorithm mitigates ID-switching because object continuity is maintained across frames, even during the moments of temporary occlusion. Third, system logging and threading mechanisms are used to make the system robust during runtime, and confidence-based filtering is used to suppress false positives. Together, these techniques construct a robust and reliable monitoring pipeline

suitable for real-world deployment.

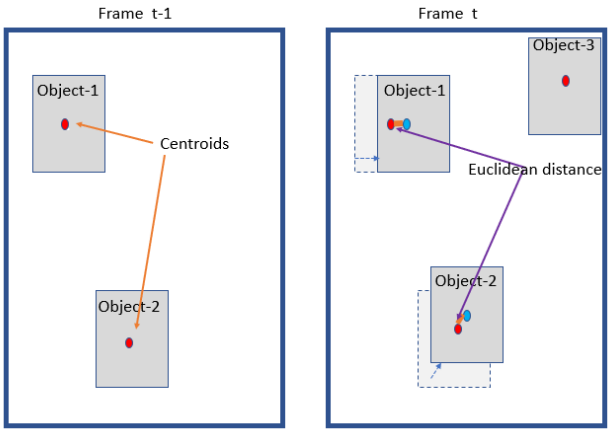

Fig 3. Centroid Tracker Methodology

The algorithm begins by taking an initial object detection set (bounding boxes) and appending a distinct key to each object. On subsequent frames, it finds differences between the current list of detected centroids and the last frame's list, updating object location on the basis of nearest neighbor match. If the object goes missing (e.g., out of frame or occluded), it is temporarily indicated as "missing." If the object re-emerges in a certain amount of frames, its initial ID is retained so that persistent tracking can be possible. Centroid tracking is also a computationally light algorithm because it is merely concerned with straightforward geometric computations as opposed to repeatedly re-initiating a deep neural network for each frame. It is well-suited to applications where objects are slowly moving or have a predictable motion. It might not work as well with complex occlusions or random object movement as with more sophisticated methods, but it makes a good starting point and is a good baseline.

4 System Architecture

Real-Time Object Detection using SSD MobileNet V2 is an end-to-end computer vision pipeline that is constructed with the intention of swift object identification from images. Two parallel initialization phases form the initiation process: loading the model and receiving the image input. The two points of departure offer the groundwork for the detection process, taking initiative to design two convergent paths which unite for the actual detection process subsequently.

The preprocessing component is a basic component of the architecture and consists of five sequential steps that pre-process the input image for processing. The system first loads the image using OpenCV, and color space conversion is performed from BGR to RGB format. Then the image is resized to the model's assumed size and a batch dimension added according to the model's input requirement. Lastly, the image is transformed into a uint8 tensor format, producing a well-formatted tensor that can be processed by the neural network.

At the same time, the model preparation department goes through its own series of operations. This starts with the choosing of the SSD MobileNet V2 architecture, which is mobile and edge device-focused, providing a compromise of accuracy versus computational requirements. The application loads pretrained TensorFlow Hub weights, taking advantage of transfer learning so that training from scratch is not required. The final step in this preparation phase involves setting the model to evaluation mode, ensuring it's configured for inference rather than training.

The object detection module is the system's central analysis engine. In this, the preprocessed image tensor is input to the model, which produces four different outputs: the coordinates of bounding boxes where objects in the image are located, class IDs used to determine the type of each object that has been detected, confidence scores reflecting the model's confidence in each detection, and the number of detections present in the image. These outputs together give detailed information regarding all objects recognized in the scene.

After detection, the architecture includes advanced postprocessing and visualization features to enhance and display results. The system initially removes low-confidence predictions by filtering detections based on confidence thresholds. It subsequently resizes the bounding boxes to the original image size and converts the numerical class IDs to human-readable COCO labels. These processed results are visually depicted by drawing bounding boxes and labels directly onto the image. Lastly, the system either saves the annotated image to disk or displays it to the user in real-time.

To improve the accuracy of the SSD MobileNet V2 real-time object detection system, several methods can be employed. Initial preprocessing through techniques such as image normalization, contrast adjustment, or adaptive histogram equalization can improve the quality of the input data into the network, particularly under low light or noisy conditions. Second, fine-tuning the pretrained model using a task-specific dataset will significantly improve detection accuracy if the deployment scene (e.g., indoor surveillance or shopping centers) is not the same as the original COCO training distribution. Including non-maximum suppression

(NMS) with class-wise optimization and soft-NMS application can further reduce false positives and enhance detection robustness for nearby objects.

To enhance efficiency, the pipeline can be optimized through model quantization (e.g., quantizing the model to INT8 or FLOAT16), which reduces model size and inference speed, particularly on mobile or edge devices. Additionally, batch inference for several frames (if latency permits) or hardware acceleration via APIs like TensorRT or OpenVINO can also reduce detection time. On the software side, utilizing multithreading or asynchronous data pipelines for parallel postprocessing and preprocessing can minimize idle CPU/GPU cycles. These optimizations make the detection system interactive and scalable for real-time applications without trading off detection quality.

The entire architecture relies on three key implementation tools that make up the technology foundation of the system. OpenCV carries out image processing tasks, NumPy conducts numerical operations and array operations, and TensorFlow Hub provides an interface to the pretrained model. Such carefully designed pipeline enables efficient real-time object detection and is suitable for applications ranging from surveillance and autonomous vehicles to retail analytics and augmented reality systems.

To improve the monitoring process, a few approaches are employed. These involve maximizing field of view and minimizing blind spots by optimizing camera positioning directly over entrance points. Dynamic frame thresholding with respect to intensity of motion and ROI cropping will minimize f alse alarms from noise in the background. Additionally, using adaptive confidence thresholds allows the system to screen out doubtful detections in changing lighting or environmental conditions. Future upgrades can involve the addition of other sensory modalities such as thermal cameras or Wi-Fi localization for even more precise surveillance under occlusion or low light conditions

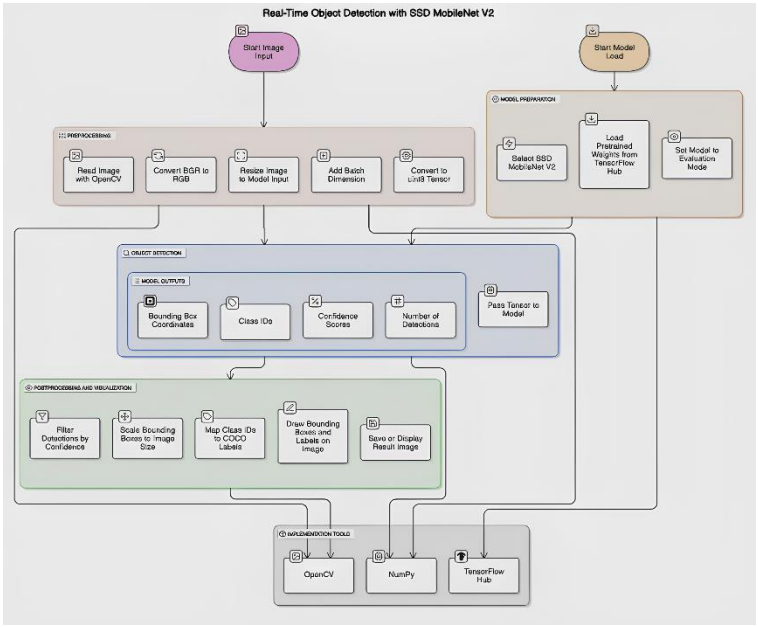

Fig 4. System Architecture

5 Results and Discussion

Every image is run through a pipeline that pre-processes the image, passes it to the MobileNet-SSD model for people detection, and uses the Centroid Tracking algorithm to track people from one frame to the next. The system detects people in every image by drawing bounding boxes around them and tagging them with IDs for tracking. The number of detected people in every image is displayed, providing the correct count for that frame.

Detection is strong even when people are partly occluded or grouped tightly together because the
model can disentangle individuals with spatial features. Labels and bounding boxes determine which objects are detected as people, and confidence scores only permit detections that meet a threshold to be utilized as valid. Visual feedback allows users to quickly confirm the system output for each photograph as correct.

In cases of dynamic lighting or camera angles, the system remains consistent in performance, demonstrating flexibility towards real-world scenarios. With the use of depthwise separable convolutions in MobileNet, detection is sure to be both fast

and accurate even on low-resource systems, rendering it suitable for real-time applications.

Overall, the annotated images clearly illustrate the effectiveness of the MobileNet-SSD and Centroid Tracking approach to real-time people tracking. The system not only provides the count of people per image but also visual evidence of detection and tracking, making it feasible for applications in crowd management, safety, and analytics.

Fig 5.1 Before Entering

Fig 5.2 After Entering

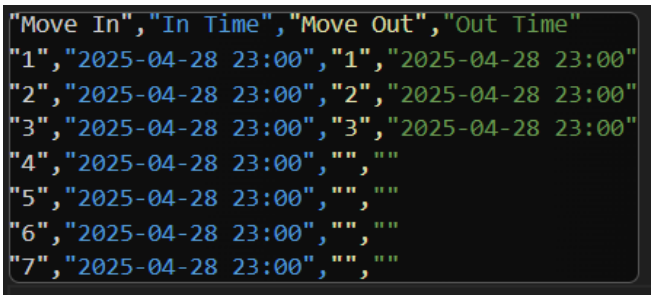

Move In	In Time	Move Out	Out Time
1	2025-04-28 23:00	1	2025-04-28 23:00
2	2025-04-28 23:00	2	2025-04-28 23:00
3	2025-04-28 23:00	3	2025-04-28 23:00
4	2025-04-28 23:00		
5	2025-04-28 23:00		
6	2025-04-28 23:00		
7	2025-04-28 23:00		

Fig 5.3 Logs of people entering

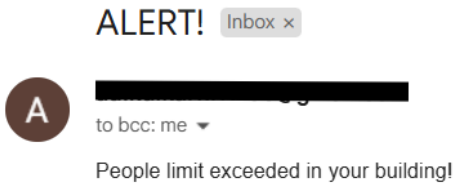

Fig 5.4 Auto-generated Email Alert

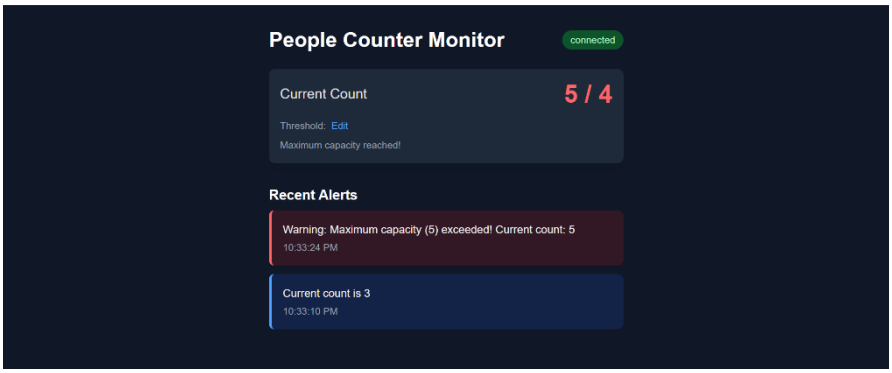

Fig 5.5 Web Dashboard Monitor

5 Future Scope and Conclusion

People counting in real-time has become an essential technology in surveillance, crowd management, retail measurement, and smart city uses. This paper has followed the progression of people counting approaches from conventional computer vision methods to state-of-the-art deep learning models. The employment of convolutional neural networks

(CNNs) has considerably improved accuracy and flexibility for various environmental settings. Moreover, the combination with light-weight models and effective frameworks like OpenCV has made it possible to deploy in real-time on edge and embedded devices, making it much more responsive and applicable.

In the future, there will be exciting developments in people counting systems. Multimodal integration merging vision with thermal imagery, LiDAR, or Wi-Fi sensing can further enhance performance under low-light or occluded conditions. With the ongoing evolution of edge computing, model optimization for platforms such as NVIDIA Jetson and Raspberry Pi will enable real-time, cloud-free processing, accelerating speed and data security. In addition, including self-learning or semi-supervised elements can enable systems to learn from new environments on their own without having to be repeatedly trained by hand.

Integration with broader IoT ecosystems can facilitate applications in smart transportation, emergency response, and energy-efficient infrastructure management. Equally important is the ethical dimension—ensuring privacy-preserving features such as anonymized tracking and on-device processing will be critical for public trust and regulatory compliance.

In short, people counting technology is becoming a more precise, learning, and privacy-oriented device, poised to serve the needs of future smart systems. This work contributes to that process by delivering a lightweight but sturdy real-time people tracking system based on the MobileNet-SSD model supplemented By this method, the paper seeks to illustrate an effective and simple route to real-time object detection that does not sacrifice quality or become unsuitable for rapid deployment and simple extension. The main contribution of this work is the coupling of the MobileNet-SSD deep learning model with a light Centroid Tracking approach to facilitate real-time counting of people under realistic constraints, including moderate occlusion, low-lighting, and low-power hardware settings. By taking advantage of a modular design and open-source technologies like TensorFlow and OpenCV, the system provides high accuracy with low latency and a scalable solution for applications like retail stores, classrooms, and public spaces.with Centroid Tracking for long-term multi-frame tracking. The strategy takes precedence over ease of deployment, cost considerations, and flexibility and is thus well-suited to varied use cases without being dependent on dedicated hardware. The marriage of pre-trained deep learning and effective geometric tracking puts this piece of work as a usable foundation towards further real-time crowd analysis and smart environment solutions.

References

1. Albiol, I. Mora, and V. Naranjo, "Real-time high-density people counter using morphological tools," IEEE Transactions on Intelligent Transportation Systems, vol. 2, no. 4, pp. 204–218, 2001.
2. D. Beymer, "Person counting using stereo," in Proceedings of the Workshop on Human Motion, 2000, pp. 127–133.
3. L. Zhang, M. Shi, and Q. Chen, "Crowd counting via scale-adaptive convolutional neural network," arXiv preprint arXiv:1711.04433, 2017.
4. S. A. Kasmani, X. He, W. Jia, D. Wang, and M. Zeibots, "A-CCNN: adaptive ccnn for density estimation and crowd counting," arXiv preprint arXiv:1804.06958, 2018.
5. X. Shi, X. Li, C. Wu, L. He, J. Yang, and S. Kong, "A Real-Time Deep Network For Crowd Counting," in ICASSP 2020 - 2020 IEEE International Conference on Acoustics, Speech and Signal Processing (ICASSP), 2020.
6. D. Subashree, S. R. Mhaske, S. R. Yeshwantrao, and A. Kumar, "Real Time Crowd Counting using OpenCV," International Journal of Engineering Research & Technology (IJERT), vol. 10, no. 5, 2021.
7. S. Liu, Y. Zhao, F. Xue, B. Chen, and X. Chen, "DeepCount: Crowd Counting with WiFi via Deep Learning," arXiv preprint arXiv:1903.05316, 2019.
8. J. Chen, W. Su, and Z. Wang, "Crowd counting with crowd attention convolutional neural network," arXiv preprint arXiv:2204.07347, 2022.
9. Anonymous, "Optimizing accuracy and efficiency in real-time people counting with cascaded object detection," International Journal of Information Technology, 2024.
10. Cai and J. Aggarwal, "Automatic tracking of human motion in indoor scenes across multiple synchronized video streams," in Proceedings of IEEE International Conference on Computer Vision, 1998, pp. 356–362.
11. Sharma, J. Pathak, M. Prakash and J. N. Singh, "Object Detection using OpenCV and Python," 2021 3rd International Conference on Advances in Computing, Communication Control and Networking (ICAC3N), Greater Noida, India, 2021, pp. 501-505, doi: 10.1109/ICAC3N53548.2021.9725638.
12. Sanjay Kumar, K. K. R., Goutham Subramani, Senthil Kumar Thangavel, and Latha Parameswaran. "A mobile-based framework for detecting objects using ssd-mobilenet in indoor environment." In Intelligence in Big Data Technologies—Beyond the Hype: Proceedings of ICBDCC 2019, pp. 65-76. Springer Singapore, 2021.
13. Palwankar, Tejal, and Kushal Kothari. "Real time object detection using ssd and mobilenet." Int. J. Res. Appl. Sci. Eng. Technol 10 (2022): 831-834.
14. Prihantoro, P. W. D. Putra and E. Nashrullah, "Performance One Stage Layer Object Detection Model to Count People using Various Backbones," 2023 International Workshop on Artificial Intelligence and Image Processing (IWAIIP), Yogyakarta, Indonesia, 2023, pp. 116-121.
15. Shen, Tsu-Chuan, and Edward T-H. Chu. "Edge-computing-based people-counting system for elevators using MobileNet–single-stage object detection." Future Internet 15, no. 10 (2023):337
16. V. Kamath and R. A., "Investigation of MobileNet-SSD on human follower robot for stand-alone object detection and tracking using Raspberry Pi," Cogent Engineering,

vol. 11, no. 1, pp. 2333208, Apr. 2024.
17. R. Muwardi, J. M. R. Permana, H. Gao, and M. Yunita, "Human Object Detection for Real-Time Camera using Mobilenet-SSD," Journal of Integrated and Advanced Engineering (JIAE), vol. 3, no. 2, pp. 141–150, Sep. 2023.
18. D. Yadav, M. Singh, A. Gupta, A. Raj, and A. Pathak, "Real-Time Object Detection Using SSD Mobile Net Model of Machine Learning," International Journal of Engineering and Computer Science (IJECS), vol. 12, no. 5, pp. 25729–25734, May 2023.
19. H. Honmote, S. Gadekar, P. Katta, and M. Kulkarni, "Real Time Object Detection and Recognition using MobileNet-SSD with OpenCV," International Journal of Engineering Research & Technology (IJERT), vol. 11, no. 1, pp. 141–142, Jan. 2022

Performance Optimization of a PV Module Integrated with Fuzzy/NN INC-Based MPPT and Zeta DC-DC Converter for Grid-Connected Applications

First Author :S. Madhusudhan Reddy & mail id : madhusudhanreddy669@gmail.com

Second Author : S. Muthubalaji Professor Department EEE & mail id: muthusa15@gmail.com

Third Author: DS Sanjeev Professor Department EEE & mail id: dssajeev@cmrcet.ac.in

PG Scholar, Department of Electrical & Electronic Engineering (Power Electronics)

CMR College of Engineering & Technology, Kandlakoya, Hyderabad, India.

ABSTRACT

This research endeavors to enhance the performance and efficiency of photovoltaic (PV) systems through the implementation of a Maximum Power Point Tracking (MPPT) controller, which incorporates an incremental conductance (NNIC) approach alongside fuzzy logic and neural network incrementality. The system comprises of a Zeta DC-DC converter for output voltage control after an inverter and filter unit meant to guarantee a continuous power supply to a three-phase grid. The main goal is to maximize energy extraction from the solar module under different climatic circumstances, thereby guaranteeing grid compatibility and therefore enhancing power quality. The suggested MPPT controller exhibits superior convergence speed and heightened precision in identifying the maximum power point, adeptly integrating the benefits of both Fuzzy Logic and Neural Network methodologies in contrast to conventional techniques. The Zeta converter has been chosen due to its ability to enhance and regulate the output from the photovoltaic system, ensuring consistent power supply to the inverter and thereby reducing ripple effects. Crucial for grid adherence, the inverter converts direct current into alternating current, while the filter unit ensures minimal harmonic distortion. The simulation results indicate that by optimizing power extraction, the system significantly reduces energy losses and enhances overall efficiency. Large-scale grid-connected photovoltaic systems would benefit from the integration of fuzzy/NN INC-based maximum power point tracking and Zeta converters, as this combination ensures remarkable flexibility and robustness. This arrangement greatly enhances the quality of the electricity, therefore promoting a more dependable and sustainable energy supply.

Keywords: MPPT- Maximum Power Point Tracking (MPPT), Neural Network Incremental Conductance (NNIC), Photovoltaic (PV), Harmonics, Zeta DC-DC converter

1.INTRODUCTION

Grid-connected applications suffer from the unpredictability of solar production, despite photovoltaic (PV) systems being a sustainable power source, as shown by the growing demand for renewable energy. Enhanced methods for optimizing the output of solar modules from power extraction are essential for adapting to various situations. The Incremental Conductance (INC) technique is extensively recognized for its precision in tracking the maximum power point (MPP) across different conditions. However, traditional INC methods often struggle with tracking speed and accuracy during rapid environmental changes.[1]

Recent advancements in artificial intelligence have integrated Fuzzy Logic and Neural Networks into MPPT controllers, enhancing performance over traditional methods. Fuzzy Logic handles uncertainty well, while Neural Networks adapt to dynamic conditions, offering faster convergence and higher accuracy. Additionally, the Zeta DC-DC converter is recognized for its ability to enhance power transmission by minimizing ripple effects and stabilizing output, while also being capable of adjusting voltage levels upwards or downwards. This makes it an ideal match for MPPT controllers to optimize energy extraction and power delivery in PV systems.[2]

The integration of a Fuzzy/NN INC-based MPPT controller with a Zeta DC-DC converter significantly enhances the performance of grid-connected PV systems by maximizing energy extraction and improving power quality. While a filter unit reduces harmonic effects, therefore guaranteeing compliance with grid standards, the inverter guarantees grid compatibility by keeping low harmonic distortion and a high-power factor. This results in improved stability and efficiency in power distribution, therefore increasing the total effectiveness of the solar system. Ultimately, this configuration enhances the dependability and sustainability of the energy grid.[3]

2 Related Work

A study tackles the identified challenge through the application of an arithmetic optimization approach (AOA) designed for maximum power point tracking (MPPT) in solar systems functioning under nonuniform conditions. Utilizing a single-ended primary inductance converter (SEPIC), which adeptly manages the elevation and reduction of voltage levels, allows for the eradication of regions unresponsive to voltage variations. The AOA-MPPT system receives inputs in the form of voltage generated by the photovoltaic modules and the corresponding current. The system determines the duty cycle of the converter and modifies the operating point as required to ensure optimal performance across various operational scenarios. An advanced differential evolution method designed to optimize maximum power point tracking in solar systems operating under conditions of partial shading is analysed. [1]

Since random numbers are not utilized in the operation of the proposed MDE, the reliability of MPP tracking is consistently upheld. The system includes a unique tuning parameter, the mutation factor, which simplifies the implementation process and allows for operation on an affordable micro-controller. The approach reliably reaches the highest power output within 12 adjustments for every examined shaded curve, even with its simpler setup. This method showcases exceptional performance when compared to an alternative evolutionary technique, particularly particle swarm optimization (PSO), which often struggles by getting trapped at local maximum power points when shading is present. [2]

A novel methodology for enhancing maximum power point tracking has been formulated, utilizing jellyfish search optimization. Furthermore, a unified power-quality conditioner (UPQC) is utilized to enhance the functionality of microgrids (MG) and tackle power-quality issues for sensitive loads. The microgrid incorporates a fuel cell battery, a wind turbine, and a photovoltaic system, and it is subjected to analysis and modeling under both uniform and nonuniform conditions of wind and solar irradiance. The research undertakes a comprehensive analysis of the proposed technique in relation to several maximum power tracking methodologies. [3]

An innovative design for a two-switch enhanced gain single-ended primary inductor converter (SEPIC), emphasizing notable benefits including improved efficiency, reduced voltage stress, and increased voltage gain, rendering it especially appropriate for low voltage green energy applications is studied. Furthermore, a significant characteristic of this converter is the reduced voltage stress noted in the intermediate capacitors. [4]

The deployment of DC–DC converters is essential in meeting the heightened DC link voltage requirements in distributed energy resources, such as fuel cells, wind turbines, and solar systems [5]. A novel active switched LC-network (ASLC) converter that operates without transformers, distinguished by a remarkable voltage gain achieved through a voltage-lift (VL) circuit is introduced. An innovative dc-dc converter noted for its exceptional boost capabilities. The suggested setup enables significant voltage enhancement while preserving the duty cycle's integrity and preventing undue stress on the switch is reported. Discussions were held about the core principles of the operation, the assessment of steady-state conditions, and the exploration of non-ideal elements. The findings indicate that the operational characteristics of the proposed converter bear a striking resemblance to those of the cuk dc-dc converter. A groundbreaking noncoupled inductor exhibiting a markedly improved voltage gain. A research introduced the single-ended primary-inductor converter (SEPIC). The converter presents a range of noteworthy advantages, such as a noninverting output voltage, improved efficiency, substantial voltage gain, and diminished voltage stress on the switches. The proposed converter is distinguished by its consistent input current, rendering it particularly appropriate for applications in fuel cells and renewable energy systems. [6,7]

In contrast to step-down conversion, the step-up conversion in conventional non-inverting buck-boost converters necessitates elevated duty cycles for successful implementation. This matter detracts from the efficacy of the BBC in its enhanced operational capacity. A sophisticated non-inverting BBC has been formulated utilizing a quasi-Z impedance network. This configuration significantly improves conversion efficiency by employing an elevated boost factor while concurrently reducing duty cycles. [8]

Research culminated in a non-isolated DC–DC converter that demonstrates remarkable step-up capabilities while sustaining a constant input current. The architecture of this converter incorporates a quadratic boost converter, often identified as a cascaded boost topology, in conjunction with a positive output super lift Luo converter and a voltage multiplier cell. The principal attributes of the previously mentioned topologies play a crucial role in augmenting the voltage gain of the proposed design. [9]

An interleaved DC-DC step-up converter, originating from a voltage multiplier rectifier, showcasing improved attributes. A thorough analysis is conducted and evaluation of the converter in question within two distinct operational duty regions: the first ($0 < D \leq 0.5$) and the second ($0.5 \leq D < 1$). This apparatus exhibits

remarkable versatility, encompassing energy storage systems, electric vehicle technologies, and frameworks for renewable energy. [10]

A bio-inspired roach infestation optimization (RIO) technique is designed to enhance power extraction from photovoltaic systems (PVS). The efficacy of the RIO MPPT algorithm is evaluated by simulating diverse environmental scenarios within the MATLAB/Simulink framework. These scenarios include abrupt fluctuations in solar irradiance, partial shading, system uncertainties, and changes in PV array load conditions. [11]

An approach successfully tackles the computational difficulties linked to the earlier GWO-based method introduced by Mohanty et al. The reasoning behind using the hybrid strategy is its ability to enhance the GWO search space, which in turn promotes a quicker convergence to the GP. [12]

Nonetheless, the effectiveness of photovoltaic systems may attain its peak as innovations in power electronics devices progress, enhancing solar electricity performance. They investigated the optimization of Maximum Power Point Tracking in boost converters and quadratic boost converters by means of a fuzzy logic controller in combination with Perturb & Observe methods. [13]

With investments of around $330 billion in 2017, the generation of renewable energy has seen notable rise in recent years. Aiming to promote the manufacturing of renewable energy sources, the European Union established a target to attain 20% renewable energy consumption by 2020. When compared to other renewable energy sources, the environmental consequences of solar power are far less clear-cut. This work uses hybrid boost converters and artificial neural networks to maximize the power output of solar energy systems using Maximum Power Point Tracking. Two independent stages—an offline stage and an online stage—are used to evaluate the suggested model during which various ideas about the structure and technique of artificial neural networks are established and refined in an offline environment. [14, 15]

The super lift converter, a variant of the developer converter, is recognized for its exceptional efficiency, utilizing principles derived from the buck-boost converter. Assigned to transform low voltage inconsistencies in solar systems into higher voltages that are smooth and stable, depending on the converter's design, this technology works well with various devices, including DC chargers and electric vehicles. [16]

Considering our nation's abundant sunlight year-round, the increasing energy demands, the diminishing reliance on fossil fuels, and the escalating worries about environmental pollution have driven us to explore innovative and alternative renewable energy sources, such as solar and wind energy, for electricity generation. [17]

The progress of a photovoltaic alternating current module that incorporates a deployable low-frequency inverter, preceded by a high static gain non-isolated direct current-to-direct current converter known for its current source output characteristics is studied. The Cuk converter, in conjunction with the switched-inductor technique, enables the dc-dc converter to operate with a higher static gain and reduced switch voltage [18].

In recent decades, the complexity and demands of modern challenges have escalated, highlighting the need for the advancement of more effective optimization techniques, especially in the realm of meta-heuristic optimization algorithms. The methods used to find the best solutions for different optimization problems mainly show random features. Due to their impressive capacity to avoid local optima and their non-gradient techniques, these optimization algorithms surpass conventional optimization methods. [19]

The worldwide acceptance of renewable energy systems is fast growing, and studies on wind and solar technologies inspire scientists to design creative control systems for useful use. The MPPT-based photovoltaic system is aanalyzed. The total output power of the system depends much on the special properties of photovoltaic modules, shaped by temperature and sun insolation. [20]

A detailed analysis and understanding of a single-switch high step-up coupled-inductor boost converter is reported. The proposed converter shows promise for achieving considerable voltage gain while keeping a manageable duty cycle, supported by the relevant inductor. [21]

A high-gain boost converter that employs an active switching inductor network is reported. The suggested converter successfully minimizes switch voltage stress and conduction loss through a simplified circuit design that utilizes fewer components, resulting in an increased voltage gain at a reasonable duty cycle. It introduces an innovative transformer-less quadratic buck-boost converter, notable for its remarkable voltage gain ratio of $D/(1-D)^2$ and a common ground configuration. The suggested design features inductive filters at both the output and input ports, ensuring a consistent flow of currents in and out. [23]

A wide range of applications, especially those managing power from low-voltage renewable sources in

grid-connected systems, require significant voltage conversion efficiency. A research presents a groundbreaking high-gain step-up DC-DC converter that functions without a transformer, employing an active switched-inductor alongside a passive switched-capacitor network. A distinctive bidirectional isolated dc-dc converter, characterized by its wide input voltage range and high voltage gain, which positions it effectively for bidirectional power conversion applications is reported. The suggested system, featuring a forward-flyback converter alongside a bidirectional buck-boost converter, provides the advantage of maintaining stable current characteristics at the low-side port in both step-up and step-down modes, while also attaining an improved voltage gain. [24, 25]

A redesigned SEPIC DC-DC converter reduces power loss, while the P&O-based MPPT method optimizes solar PV power tracking. The MAPO-based controller generates efficient switching signals by enhancing convergence rate, voltage gain, and minimizing errors. Metrics like as overshoot, settling time, and rise time are used to assess the system's performance. [26,27]

This paper focuses on a grid-incorporated solar electric vehicle (EV) charging station that maximizes the acceptance of EVs in agricultural areas and reduces the over-reliance on the grid of urban cities. Since photovoltaic (PV) systems are widely available and easy to install, they are an excellent choice for EV charging applications. Hence, the aim of this work is to combine PV and EV, in order to achieve the objectives of both decarbonized energy generation and transportation.[28]

In practical engineering applications, factors like dust adhesion and environmental changes can cause photovoltaic arrays to exhibit multiple peaks in output power. An optimization algorithm with global optimization capability is needed to track its maximum power. In this regard, this paper proposes an improved marine predator algorithm (IMPA) to extract the maximum power point of photovoltaic system under complex solar irradiation conditions. [29]

Recently, the integration of renewable energy sources, specifically photovoltaic (PV) systems, into power networks has grown in significance for sustainable energy generation. Researchers have investigated different control algorithms for maximum power point tracking (MPPT) to enhance the efficiency of PV systems. This article presents an innovative method to address the problem of maximum power point tracking in photovoltaic systems amidst swiftly changing weather conditions. [30]

There is a gap in optimizing MPPT techniques for grid-connected PV systems, especially in enhancing tracking efficiency and power quality. Traditional methods like P&O and INC face issues such as slow convergence and sensitivity to environmental changes. Advanced techniques like Fuzzy Logic and Neural Networks have not yet been integrated with efficient converters like the Zeta converter. This research aims to combine Fuzzy Logic/Neural Network-based INC MPPT controllers with a Zeta DC-DC converter to improve energy extraction, reduce power loss, and ensure grid compliance while minimizing Total Harmonic Distortion (THD).

Contribution of Work

This work proposes an efficient MPPT technique combining Fuzzy Logic and Neural Network-based Incremental Conductance (NNIC) with a Zeta DC-DC converter for grid-connected PV systems.the integration enhances power extraction, reduces Total Harmonic Distortion (THD), and improves voltage stability under varying conditions. Simulation results validate superior performance compared to conventional methods, ensuring optimized energy delivery and grid compliance.

3 Suggested Approach

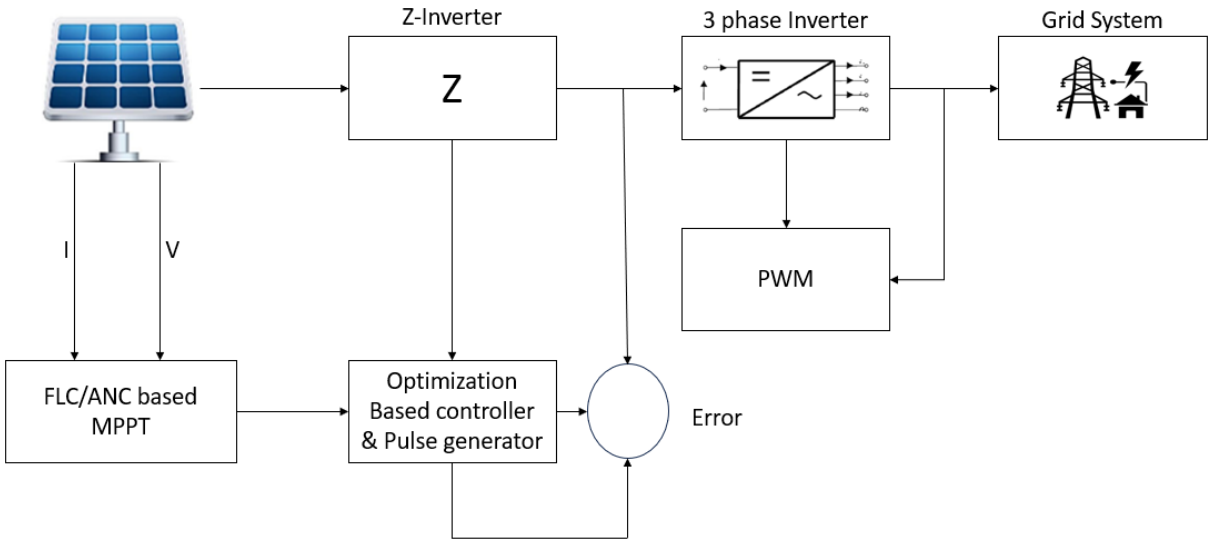

Fig 1 System Representation

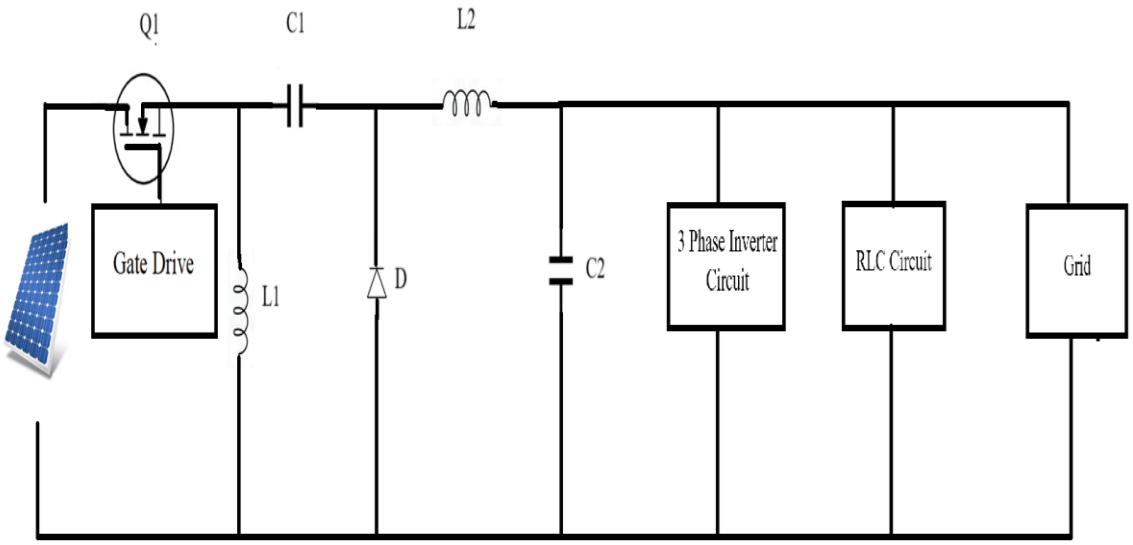

Fig 2 Overall schematic illustration of the proposed system

3.1 Solar PV Module

The system utilizes an Incremental Conductance (IC) method to address rapid dynamics in varying insolation conditions and introduces an innovative control strategy grounded in SRF theory for a single-phase rooftop PV grid-connected system. The VSC controller integrates voltage and current management to regulate the DC link voltage, ensuring that the maximum power is efficiently supplied to the grid. Moreover, the capacity of the VSC influences the extent of reactive power correction that the system can provide. Simulations conducted using MATLAB/Simulink demonstrate the effectiveness of the system in providing power conditioning and transmitting real electricity to the grid.

3.2 Zeta Converter

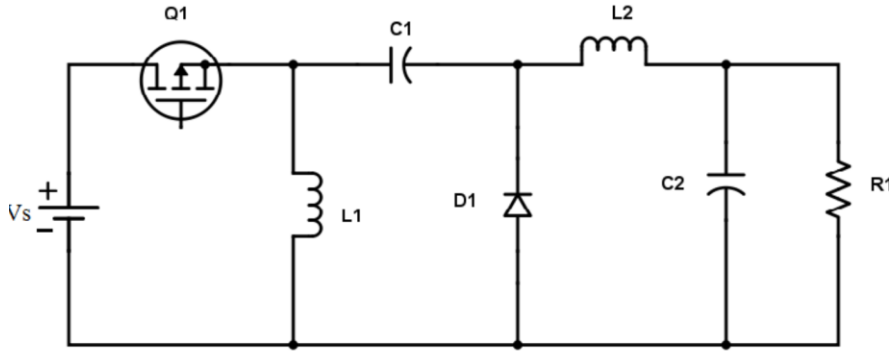

Fig 4 Zeta Converter

A Zeta converter functions as a direct current to direct current converter, managing output power through the transfer of energy between capacitors and inductors, utilizing a MOSFET switch that operates with adjustable duty cycles. The circuit operates in four modes:

Mode-1 (MOSFET ON) stores energy in inductor L1,
Mode-2 (MOSFET OFF) transfers energy from L1 to capacitor C1,
Mode-3 (MOSFET ON) discharges C1 to power the load and charge inductor L2, and
Mode-4 (MOSFET OFF) transfers energy from L1 to C1 while L2 powers the load.
The converter effectively regulates output using these dynamic energy transfers.
.

ANALYSIS OF ZETA CONVERTER THROUGH MATHEMATICAL MODELS

The mathematical modeling of the ZETA Converter is examined in along with methods for computing duty ratio, inductance, and capacitance.

Computed values of D, L1, L2, C1, and C2 follow:

$D = V0 / Vin + Vout$ ..... (1)

The value of passive components (inductance and capacitance) can be calculated as follows:

$L1 = L2 = Vin * D / \Delta IL * Fs$ ..... (2)

$C1 = D * Vout / \Delta VC1 * R * FS$ ..... (3)

$C2 > (1 - D) / 8 * \Delta Vout * L2 * FS$ ..... (4)

In this context, D represents the duty cycle, VOUT denotes the output voltage of the zeta converter, Vin refers to the input voltage, and L1 and L2 indicate the first and second inductors, respectively. IL represents the ripple current of the inductor; Fs denotes the switching frequency; C1 and C2 refer to the first and second capacitors, respectively; and VC1 indicates the voltage ripple of the first capacitor.

3.3 3 φ Inverter

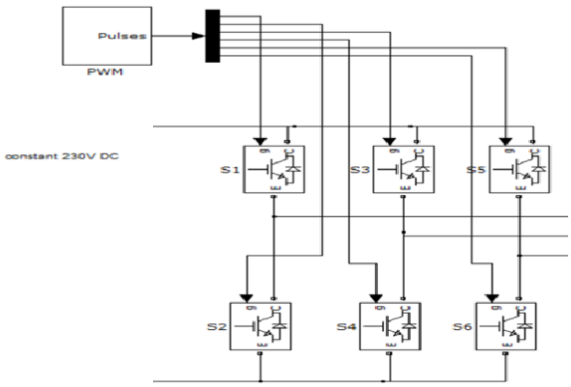

Fig 5 Phase Inverter

Each of the six valves in a six-pulse line-commutated converter links an AC terminal to a DC terminal. In contrast to the two-level converter, where each valve of the MMC functions as a controllable voltage source comprised of several submodules, each equipped with its own storage capacitor, the valves in this context act as high voltage-controlled switches. Each submodule within the half-bridge configuration consists of a pair of IGBTs arranged in series across a capacitor, with their connection either bypassed or linked based on the state of the IGBT. This configuration enables each submodule to function independently as a two-level converter, producing either 0 or the capacitor voltage (Usm). Linking numerous submodules in a series configuration generates a stepped voltage waveform that closely resembles a sine wave while exhibiting minimal harmonic distortion. In contrast to other converters that operate in distinct "on" or "off" states, the MMC exhibits a crucial feature: current consistently flows through all six valves throughout the AC cycle. The three phases ensure an even distribution of the DC current (Id); the AC current (Iac) is allocated equally between the upper and lower valves of each phase, thereby directly linking the current in each valve to both the DC and AC currents.

Upper Valve: $I_v = \frac{I_d}{3} + \frac{I_{ac}}{2}$ …….. (5)

Lower Valve: $I_V = \frac{I_d}{3} - \frac{I_{ac}}{2}$…… (6)

3.4 Fuzzy Based MPPT

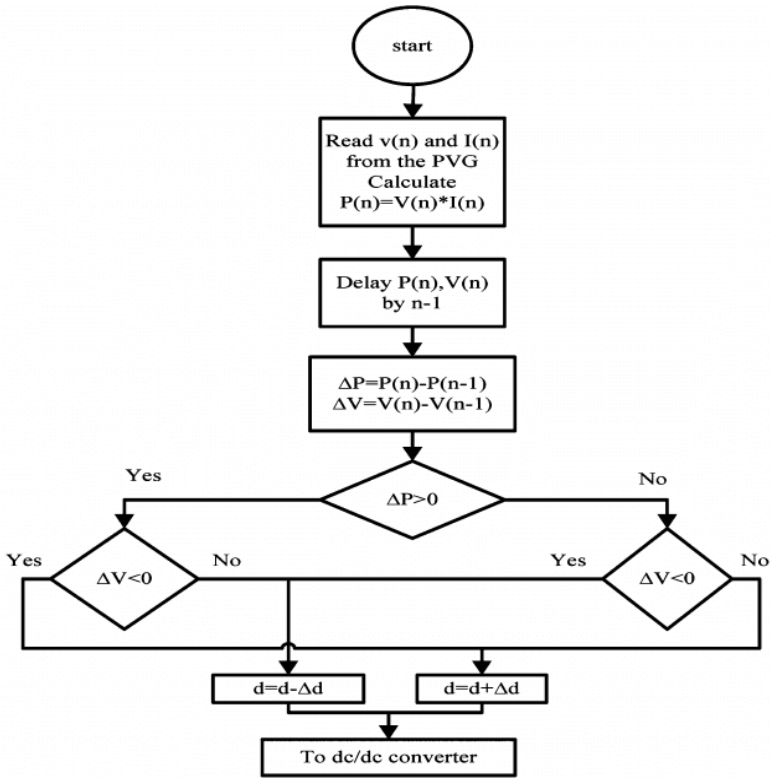

Fig 6 Proposed method

At a particular juncture, the technique utilized to derive the maximum energy output from photovoltaic (PV) modules is contingent upon the prevailing solar irradiation and temperature, referred to as Maximum Power Point Tracking (MPPT). The onus of guaranteeing that the system functions at its most efficient power point rests with the MPPT controller. A variety of current methodologies designed to improve the efficiency of MPPT demonstrate sluggish tracking abilities, leading to diminished overall power consumption. A diverse array of control methodologies has been developed to improve the efficacy of solar energy systems. The methodologies encompass Incremental Conductance, Hill Climbing, Perturbation and Observation, Artificial Neural Networks employing backpropagation, Fuzzy Logic Controller Intelligent Control in conjunction with DC-DC converters, Particle Swarm Optimization, Open Circuit Voltage Control, Short-Circuit Current Control, as well as feedback-based approaches like power variation in relation to voltage and current. Furthermore, single input fuzzy controllers are utilized to oversee the maximum power point.

3.4.2 Neural Network Based MPPT

Neural network controllers are advanced computational models that leverage artificial neural networks (ANNs) to regulate dynamic systems. These controllers are designed to mimic human brain function by processing inputs through layers of interconnected neurons, allowing for adaptive, nonlinear control of complex systems. Neural network controllers have proven to be effective in applications where traditional control methods struggle, especially in environments with uncertainty, nonlinearity, or high-dimensional data. This research explores the development and implementation of neural network controllers, outlining key steps such as system modelling, network architecture design, training methodologies, and performance evaluation.

The architecture of the feedforward artificial neural network maximum power point tracking controller. The architecture comprises three distinct layers: the output layer, the hidden layer, and the input layer. The back-propagation method serves to ascertain the weights of the structure. The error propagates from the output neuron back to the input neuron, with the weights being meticulously refined until the correlation between output and input is confirmed. This approach is known as Levenberg–Marquardt optimization. This examination consists of a singular input layer that includes open circuit voltage and short-circuit photovoltaic current. The ten concealed layers correspond to a singular output layer, respectively. The voltage output at the peak power point of the controller is...

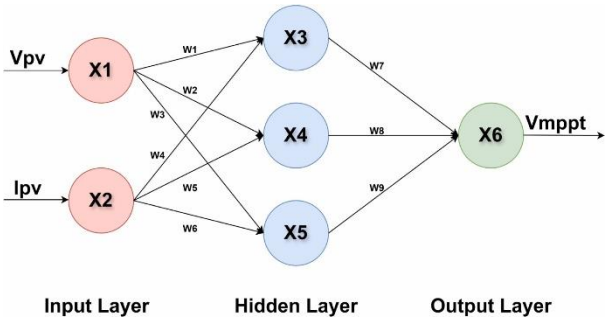

Fig 8 Neural Network

4. Results and Discussion

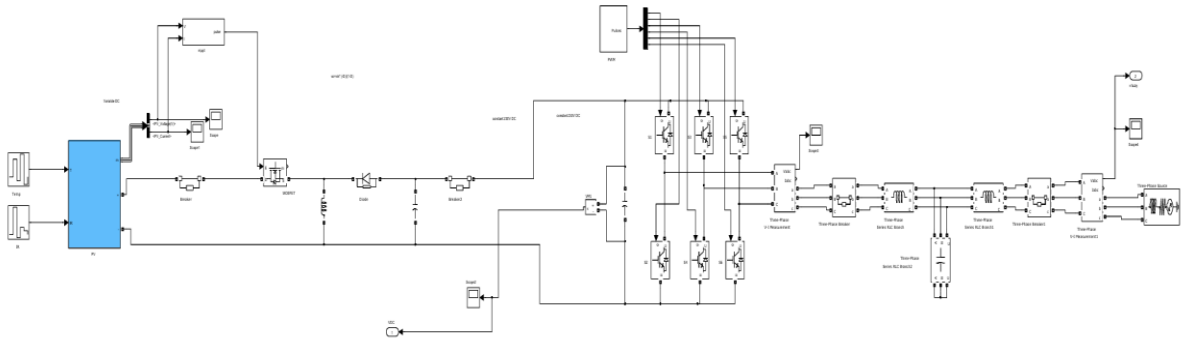

Fig 9 MATLAB Design Fuzzy Logic Controller

The Fuzzy Logic Controller (FLC) simulation results demonstrate efficient performance in a grid-connected PV system. With a PV voltage of 160V and inverter input voltage of 230V, the inverter output (without filter) is 298.6V, and after filtering, the 3-phase output voltage improves to 332.4V. The Total Harmonic Distortion (THD) is reduced to 4.68%, reflecting the FLC's ability to minimize harmonic distortion. These outcomes show that the FLC significantly enhances power quality and stability in PV systems.

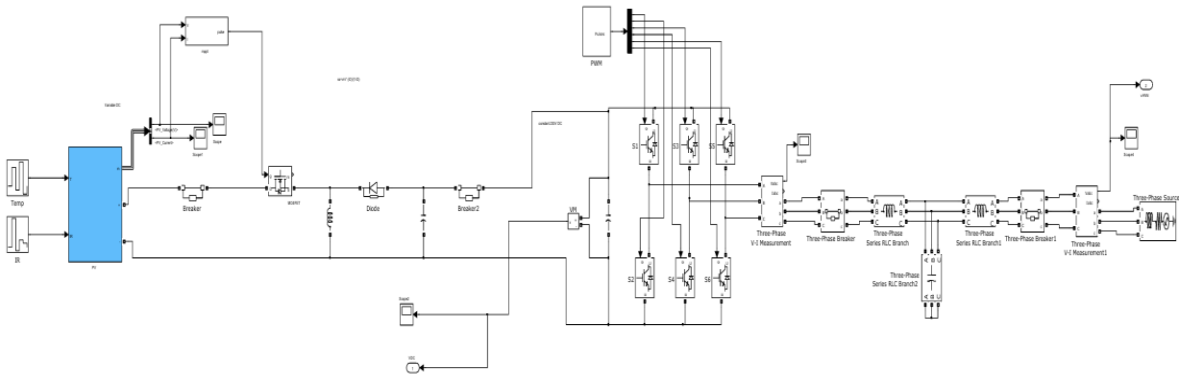

Fig 10 MATLAB Design Neural Network Controller

The simulation results for the Neural Network Controller (NNC) show strong performance in the grid-connected PV system. With a PV voltage of 160V and inverter input voltage of 230V, the inverter output (without filter) is 298.9V, and after applying the filter, the 3-phase output voltage improves to 332.6V. The Total Harmonic

Distortion (THD) is reduced to 4.61%, highlighting the NNC's ability to minimize harmonic distortion. These outcomes suggest that the NNC enhances power transfer efficiency and system performance in PV applications.

P & O Based Controller Results:

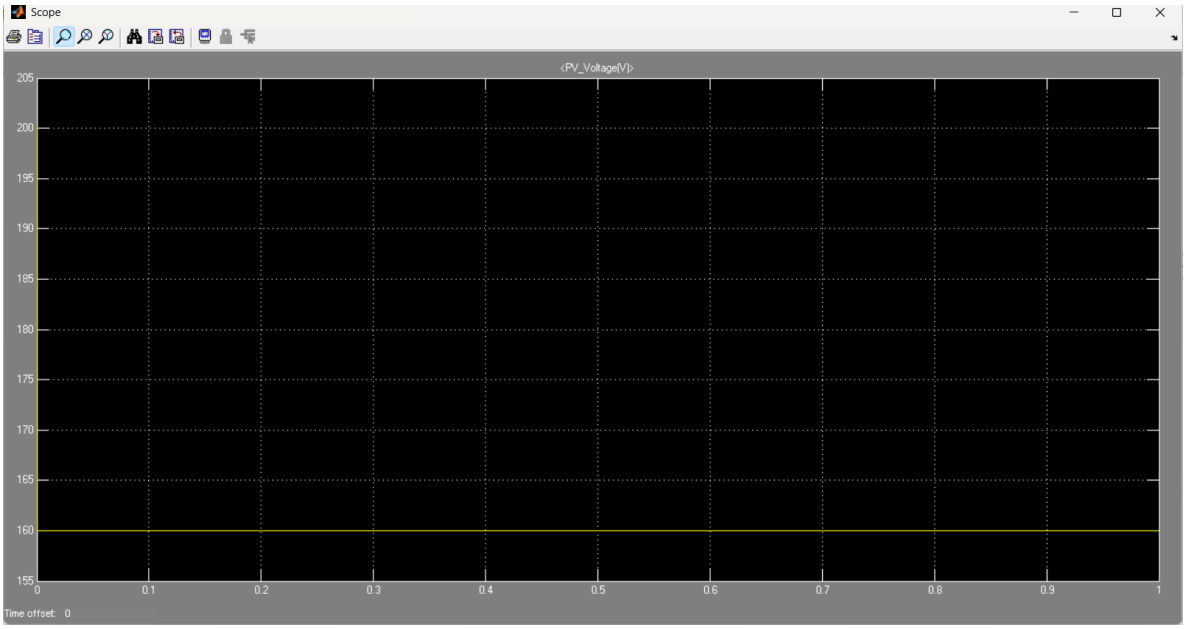

Fig 11 PV Voltage

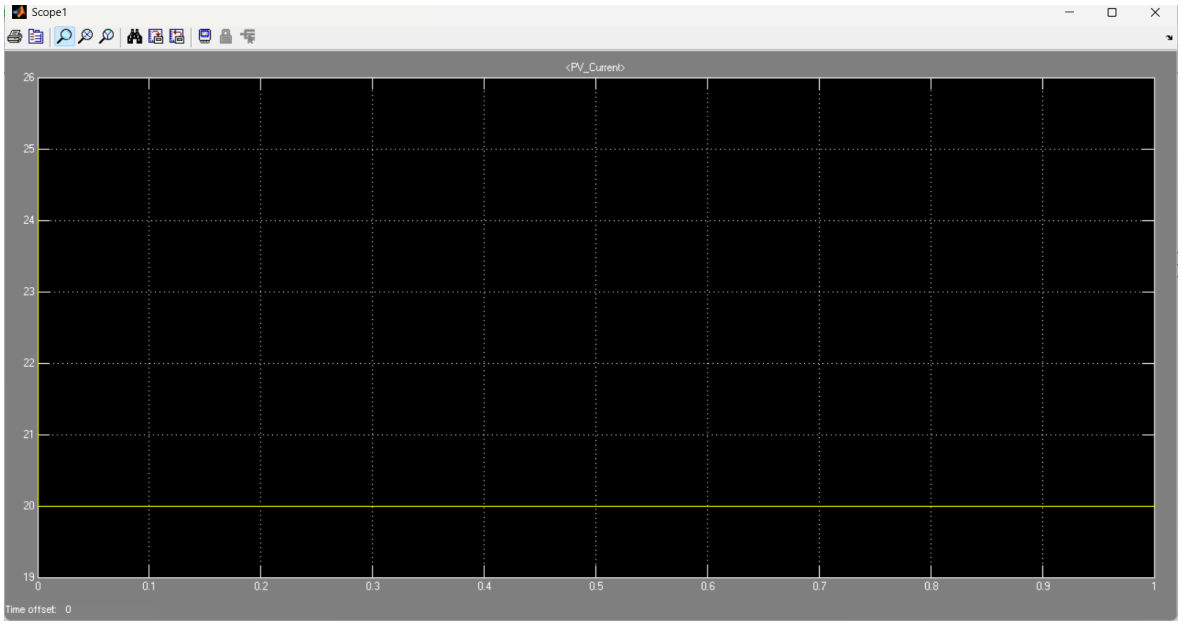

Fig 12 PV Current

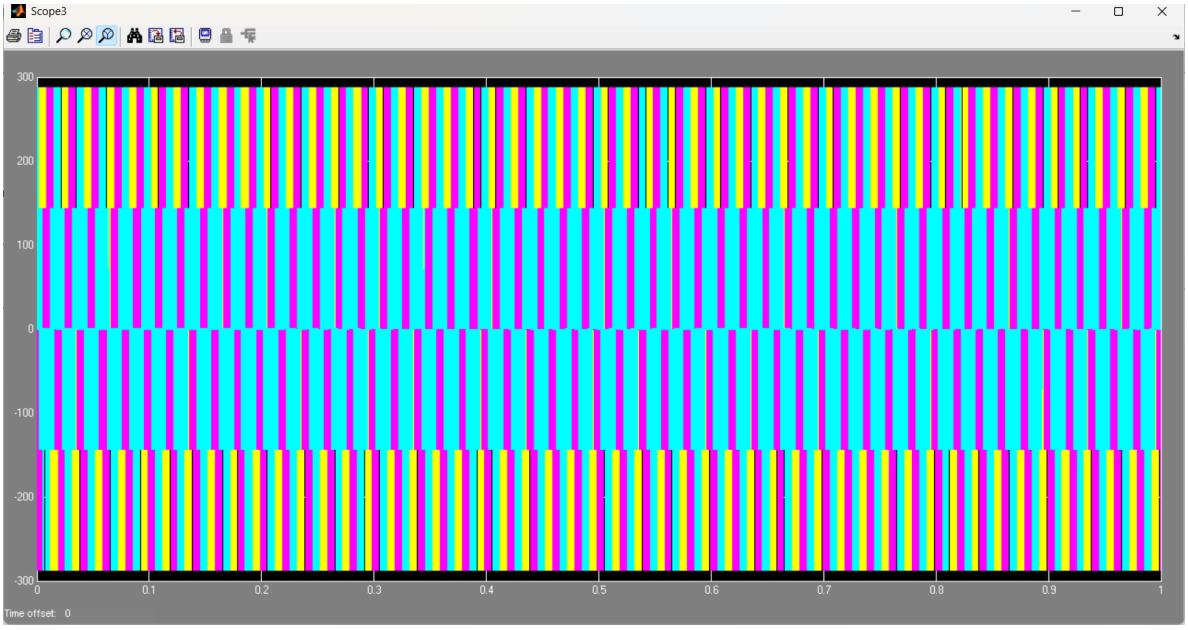

Fig 13 Without Filter 3 Phase AC Voltage

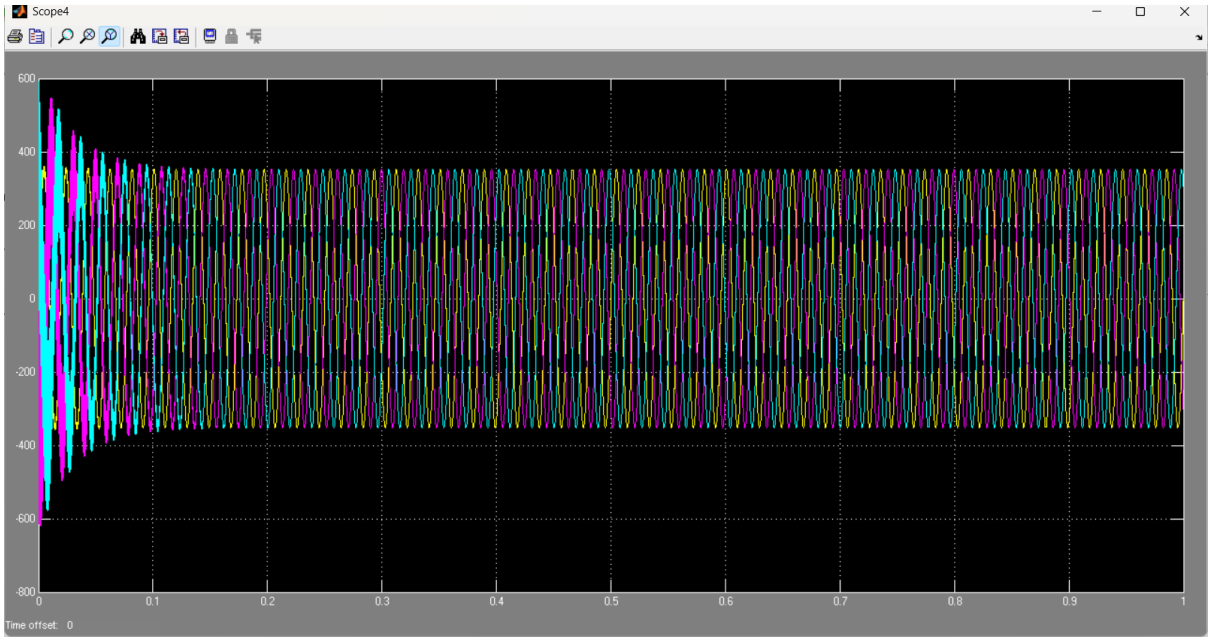

Fig 14 With Filter Grid Voltage and Current

Figure 11 shows the PV voltage, highlighting variations in the voltage produced by the photovoltaic system. Figure 12 displays the PV current, reflecting changes in current flow due to environmental factors. Figure 13 illustrates the three-phase AC voltage without a filter, showing irregularities and fluctuations. In contrast, Figure 14 demonstrates the improved, smoother three-phase AC voltage with a filter, reducing distortions for more stable output.

4.17 Fuzzy Logic Based Controller Results

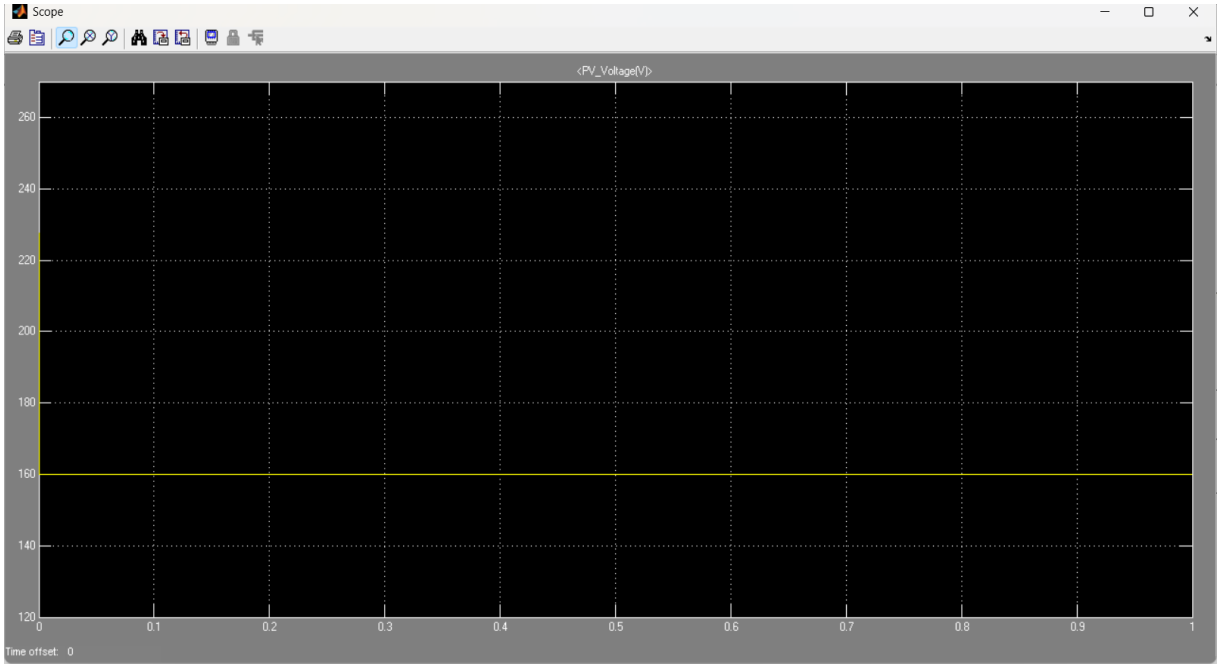

Fig 15 PV Voltage

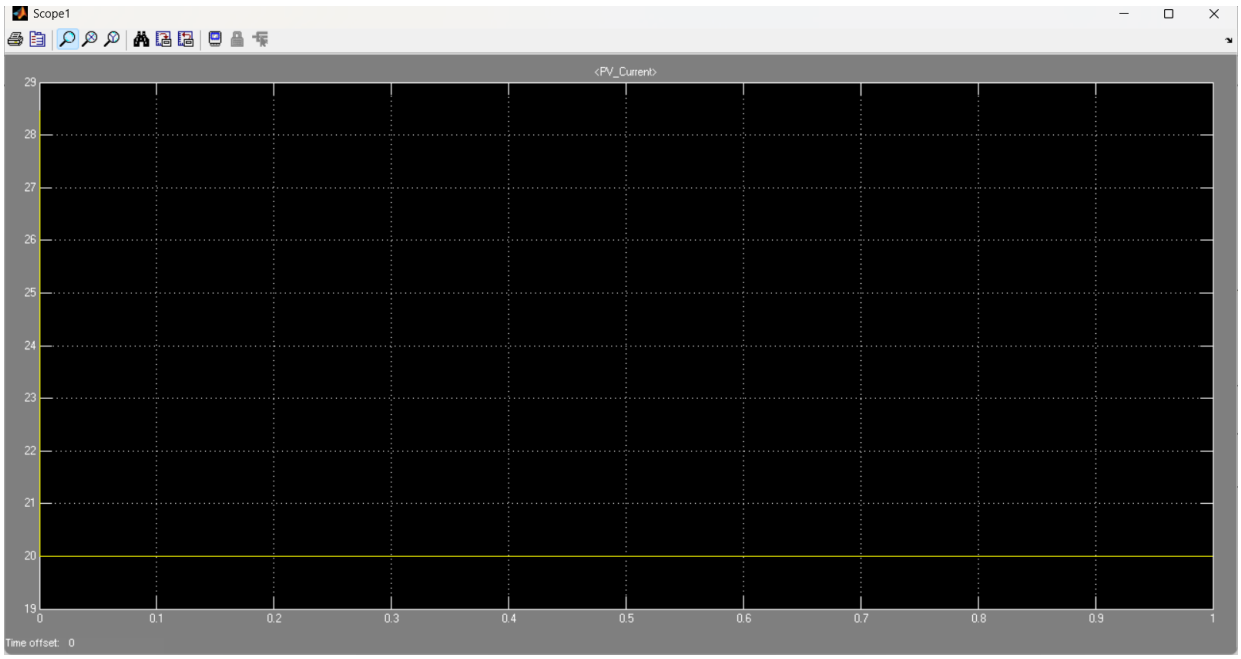

Fig 16 PV Current

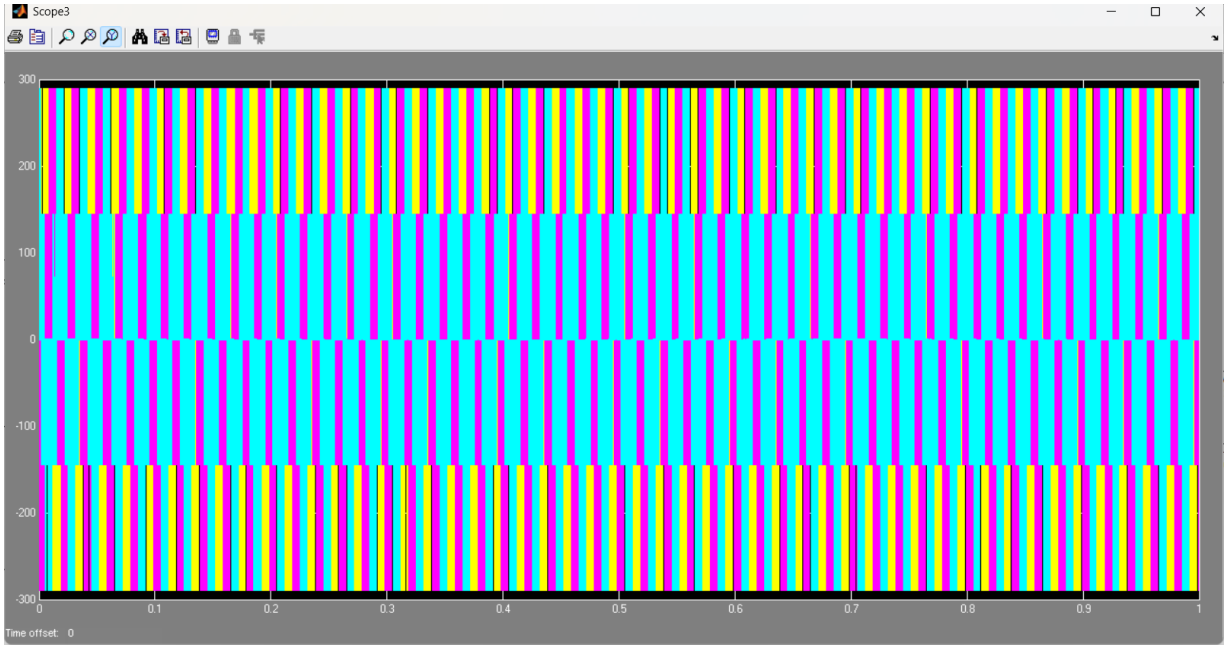

Fig 17 Without Filter 3 Phase AC Voltage

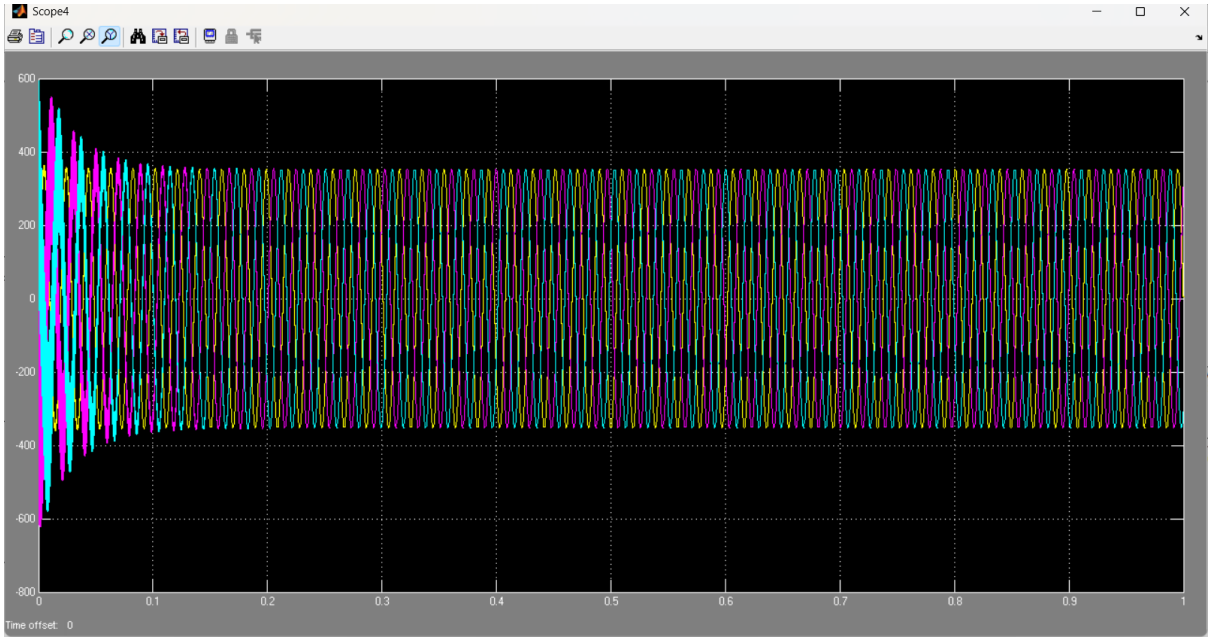

Fig 18 With Filter 3 Phase Grid Voltage

Figure 15 shows the PV voltage, highlighting variations in the voltage produced by the photovoltaic system. Figure 16 displays the PV current, reflecting changes in current flow due to environmental factors. Figure 17 illustrates the three-phase AC voltage without a filter, showing irregularities and fluctuations. In contrast, Figure 18 demonstrates the improved, smoother three-phase AC voltage with a filter, reducing distortions for more stable output.

4.18 Neural Network Based Controller Results

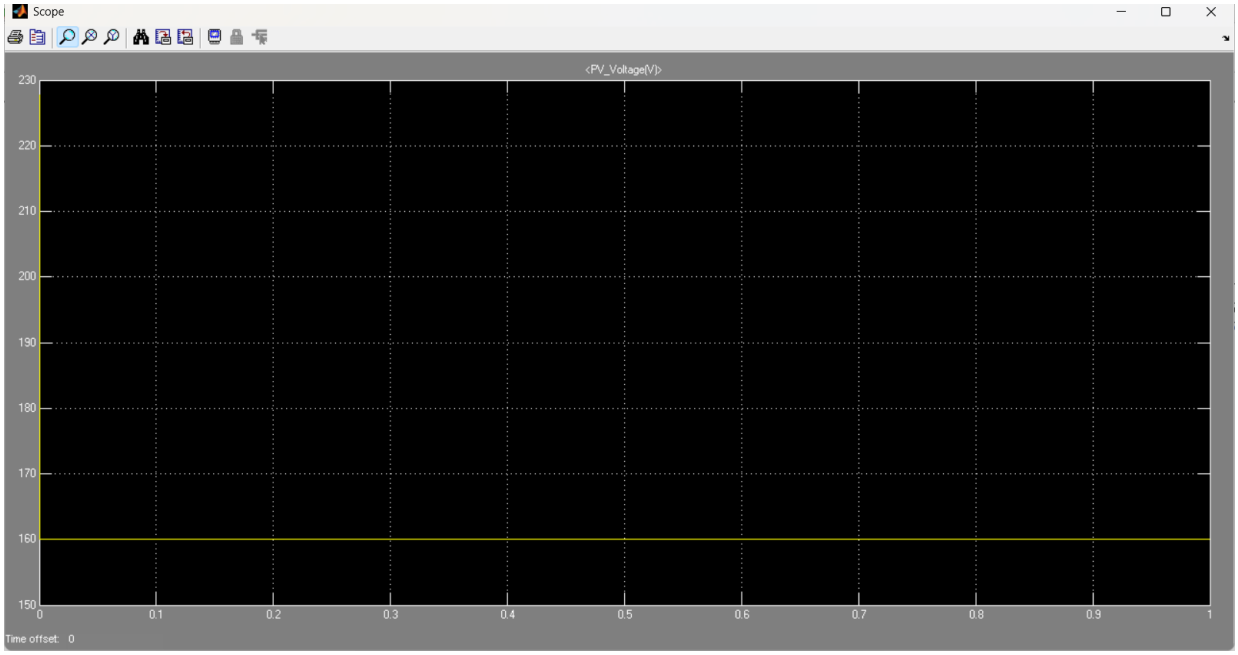

Fig 19 PV Voltage

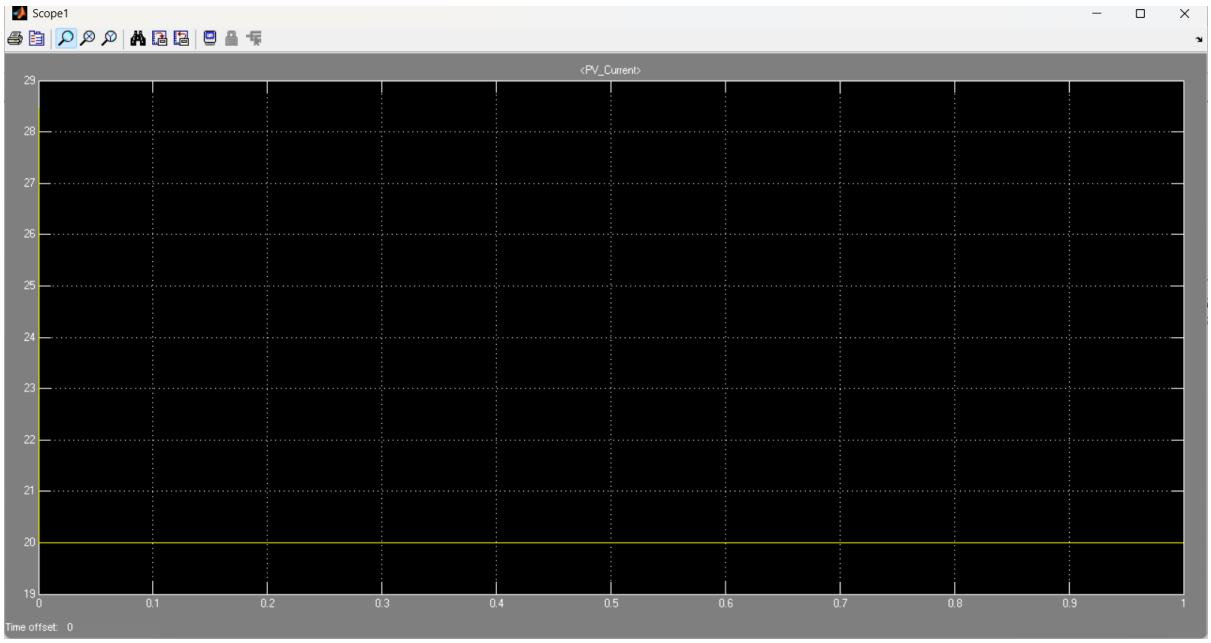

Fig 20 PV Current

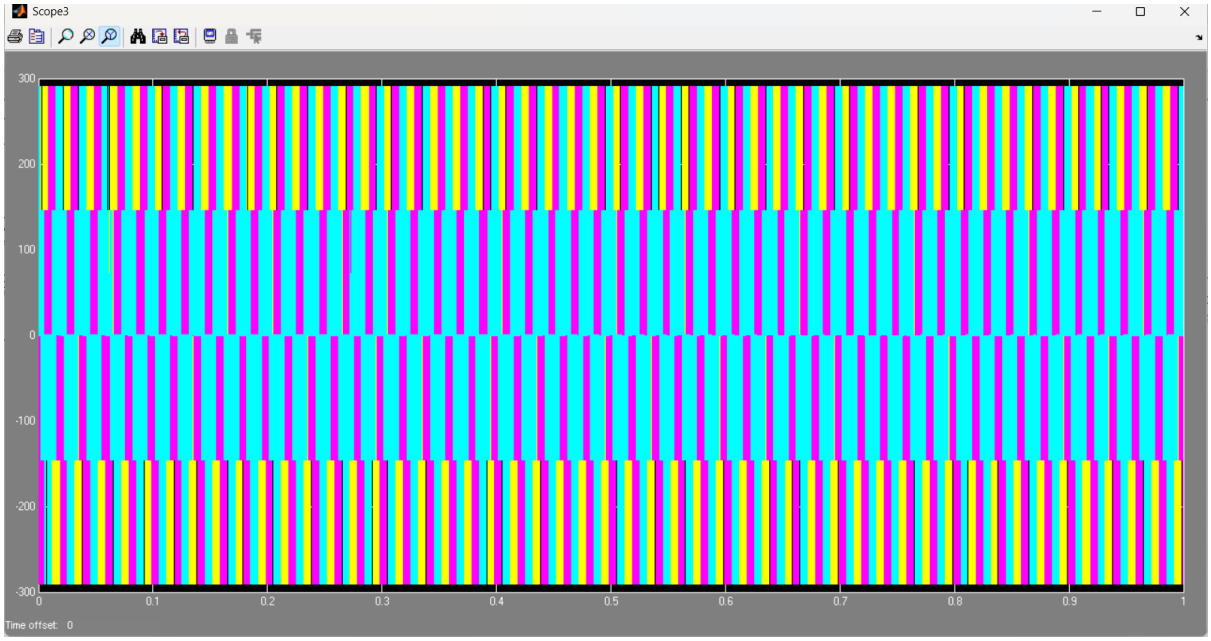

Fig 21 Without Filter 3 Phase AC Voltage

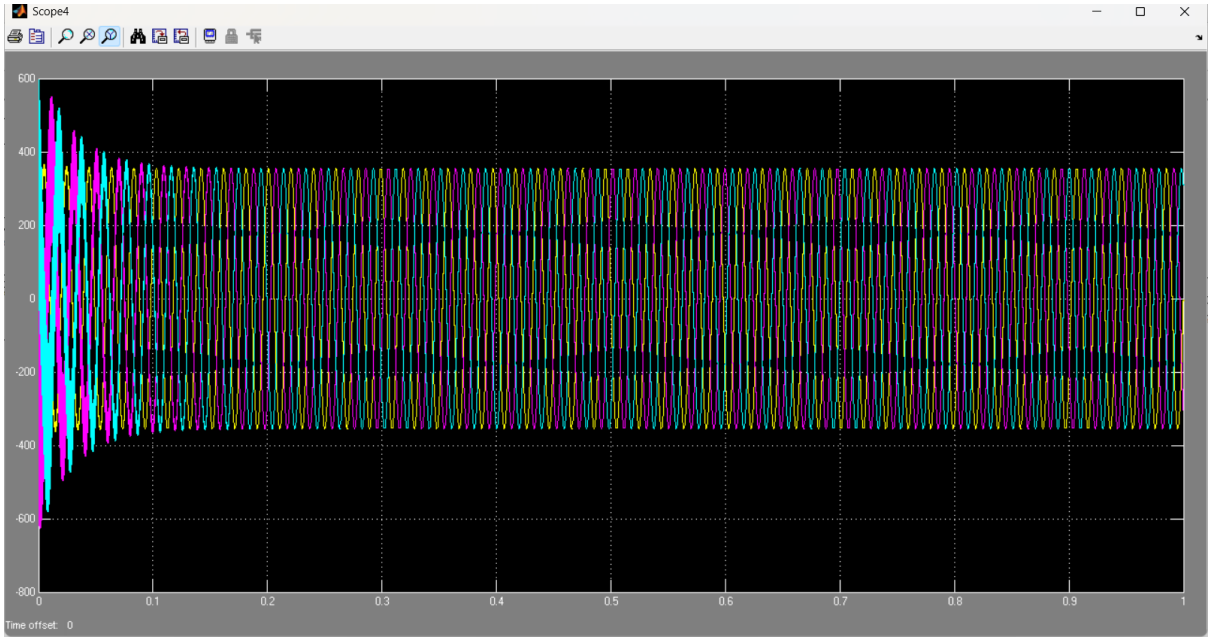

Fig 22 With Filter 3 Phase AC Voltage

Figure 19 shows the PV voltage, highlighting variations in the voltage produced by the photovoltaic system. Figure 20 displays the PV current, reflecting changes in current flow due to environmental factors. Figure 21 illustrates the three-phase AC voltage without a filter, showing irregularities and fluctuations. In contrast, Figure 22 demonstrates the improved, smoother three-phase AC voltage with a filter, reducing distortions for more stable output.

4.19 Comparation Analysis Controller Voltages

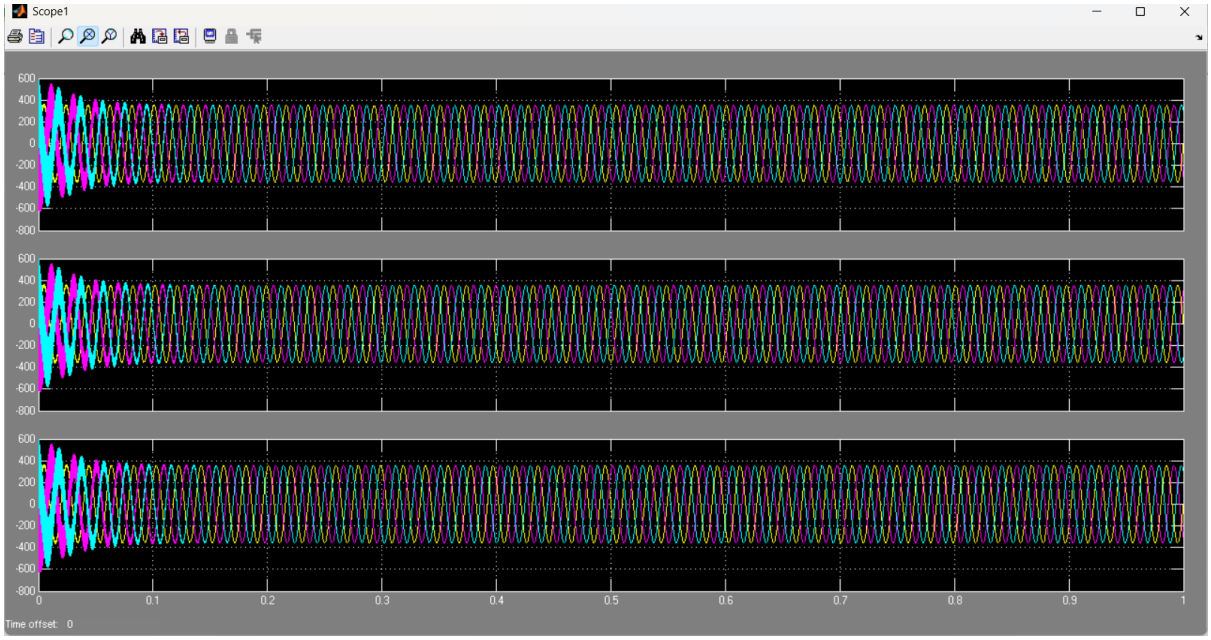

Fig 23 Comparing 3 Phase AC Voltage

Convention Controller Voltage near to Grid V_1=322.8 V …… (7)

Fuzzy logic Controller Voltage near to Grid V_2 = 332.4 V ……...(8)

Neural Network Controller Voltage near to Grid V_3 = 332.6 V …… (9)

Table 3 and Figure 12 present a comparison of the current and proposed Zeta Converter, focusing on the number of switches, inductors, diodes, capacitors, and voltage gain as measured.

Table 1 Analysis of the suggested and current converter configurations

References	No of switches	No of inductors	No of diodes	No of capacitors	Voltage gain
Non-inverting high gain DC-DC [27]	1	2	6	5	12
Quadratic Boost DC-DC [27]	1	1+1	5	3	10
High step-up DC-DC [27]	1	2	4	5	6
Ultra step-up DC-DC [27]	1	2	5	4	7
Quadratic Boost DC-DC [27]	1	3	5	3	8
High gain DC-DC [27]	2	2	5	4	6
Interleaved Boost DC-DC [27]	6	6	14	8	7
Quad isolated DC-DC [27]	2	4	9	1	5
Modified	1	2	2	3	15

SEPIC [27]					
Zeta Converter (Proposed)	1	2	1	2	16

The data in **Table 1** shows that the **Zeta Converter (Proposed)** achieves the highest voltage gain of 16 with fewer components, suggesting it is an efficient solution for applications requiring both high gain and component minimization

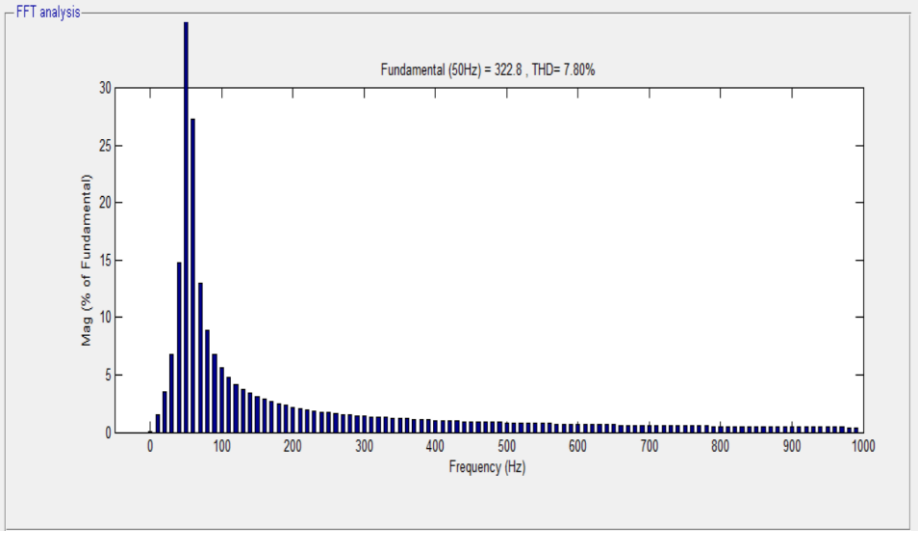

Fig 25 THD analysis for P & O Controller

The Total Harmonic Distortion (THD) of 7.80% indicates the level of harmonic distortion in the system Fig 25

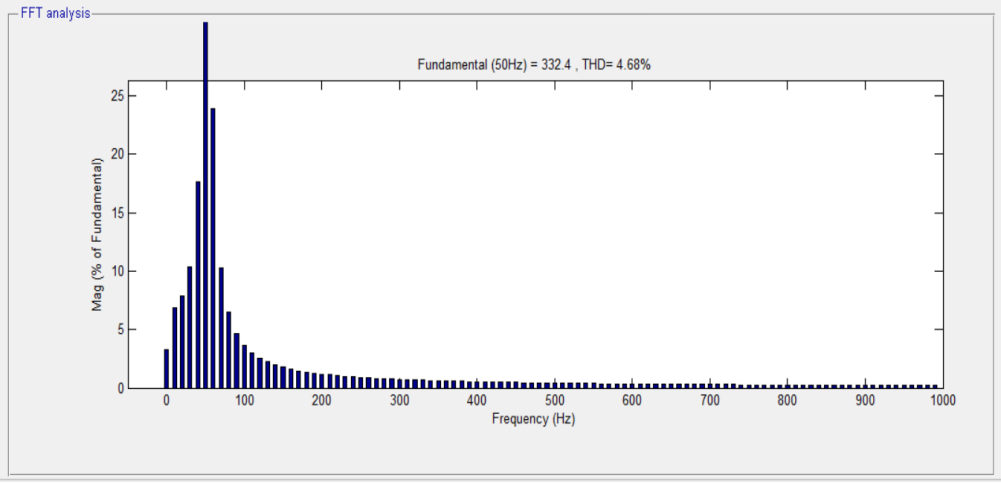

Fig 25 THD analysis for Fuzzy Logic Controller

The Total Harmonic Distortion (THD) of 4.68% indicates the level of harmonic distortion in the system

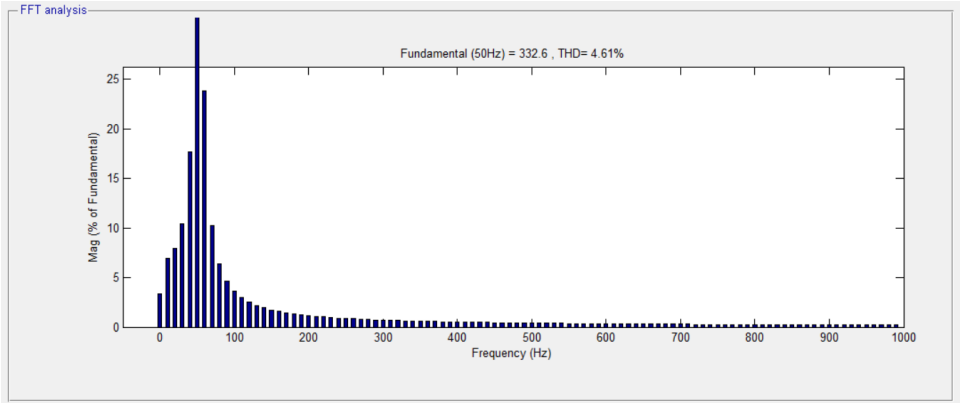

Fig 26 THD analysis for Neural Network Controller

The Total Harmonic Distortion (THD) of 4.61% indicates the level of harmonic distortion in the system

Table 2: Comparing Input and Output Voltage

Parameter	**Conventual Controller**	**Fuzzy Logic Controller**	**Neural Network Controller**
PV Voltage	160V	160V	160V
Inverter Input Voltage	229.2 V	230 V	230 V
Inverter Output 3 Phase Voltage (Without Filter)	296.5 V	298.6 V	298.9 V
3 Phase Output Voltage (With Filter)	322.8 V	332.4 V	332.6 V
THD	7.80 %	4.68 %	4.61 %

The data in **Table 2** shows that Neural Network Controller is the optimal choice for minimizing THD and ensuring high-quality output voltage, but the Fuzzy Logic Controller offers a close second with potentially simpler implementation.

5. CONCLUSION

In summary, the combination of a Fuzzy Logic/Neural Network (NN) Incremental Conductance (INC)-based Maximum Power Point Tracking (MPPT) controller with a Zeta DC-DC converter greatly improves the efficiency of grid-connected photovoltaic (PV) systems. Simulation results confirm these improvements, with the PV voltage consistently maintained at 160V across all controllers. the inverter input voltage reaches 230V with the Fuzzy Logic and Neural Network controllers, slightly higher than the 229.2V with the conventional controller. The inverter output voltage, without the filter, is 296.5V for the conventional controller, and 298.6V and 298.9V for the Fuzzy Logic and Neural Network controllers, respectively. After filtering, the 3-phase output voltage reaches 322.8V for the conventional controller, 332.4V for the Fuzzy Logic controller, and 332.6V for the Neural Network controller. The total harmonic distortion (THD) is minimized, with values of 7.80% for the conventional controller, 4.68% for the Fuzzy Logic controller, and 4.61% for the Neural Network controller. The findings demonstrate significant advancements in voltage regulation, reduction of ripple, and enhancement of overall power quality. This method minimizes energy losses and adheres to grid standards, providing a dependable and scalable solution for extensive photovoltaic applications, thereby facilitating the worldwide shift towards more sustainable and cleaner energy systems.

References

1. Arithmetic optimization based MPPT for photovoltaic systems operating under nonuniform situations, S, Palanisamy R, IEEE 2024
2. A modified differential evolution based maximum power point tracker for photovoltaic system under partial shading condition' Marrbul A, M Ramli; Kashif Ishque, IET 2022
3. Modeling, Simulation, and Experimental Validation of a Novel MPPT for Hybrid Renewable Sources Integrated with UPQC: An Application of Jellyfish Search Optimizer, Ahmed Hussain,IET 2023

4. Analysis and Design of Two-Switch Enhanced Gain SEPIC Converter , Selvam, Sindhuja & Sannasy, Mageshwari & Sridharan, Moorthi. (2023), IEEE 2023
5. A high step-up DC–DC converter with active switched LC-network and voltage-lift circuit: Topology, operating principle, and implementation, Dastgiri, Armineh & Hosseinpour, Majid & Sedaghati, Farzad, ICJTA, 2021
6. Transformer less High Step-Up DC-DC Converter with Low Voltage Stress for Fuel Cells, hao, Jiawei & Chen, Daolian & Jiang, Jiahui, IEEE, 2021
7. A Novel High Voltage Gain Non-Coupled Inductor SEPIC Converter , Ansari, Sajad & Moghani, Javad.
8. Improving step-up gain and efficiency in non-inverting buck-boost dc-dc converter using quasi-Z impedance network., Lahooti Eshkevari, Alireza, Mosallanejad, Ali, Sepasian, IET, 2021
9. A New Non-Isolated High-Gain Single-Switch DC–DC Converter Topology with a Continuous Input Current, Gholizadeh, Hossein & Ben-Brahim, IEEE, 2022.
10. Design and analysis of an interleaved step-up DC–DC converter with enhanced characteristics, Hosseinpour, M., Seifi, E., Seifi, IEEE, 2024.
11. Roach Infestation Optimization MPPT Algorithm for Solar Photovoltaic System, Manoj Kumar, IEEE, 2022.
12. A Grey Wolf-Assisted Perturb & Observe MPPT Algorithm for a PV System, Sathajit Mohanty, IEEE, 2017.
13. Maximum Power Point Tracking of solar photovoltaic cell using Perturb & Observe and fuzzy logic controller algorithm for boost converter and quadratic boost converter, Samaj Dorj, IEEE, 2021.
14. Converter topologies in photovoltaic applications – A review, R. Ramesh Gopi, IEEE, 2020.
15. Solar Power System Assessments Using ANN and Hybrid Boost Converter Based MPPT Algorithm, Imeran Hasain, IEEE, 2021.
16. Design and Implementation of Photovoltaic System Based on Super-Lift LUO Converter, Hamid Khudair Khalil, IEEE, 2020.
17. Solar powered two-level cascaded interlaced step-up Dc-Dc converter with MPPT, JeepKJ
18. Hamid Khudair Khalil, IEEE, 2023.
19. Photovoltaic AC Module Based on a Cuk Converter With a Switched-Inductor Structure, Juli Cezar, IEEE, 2019.
20. The Arithmetic Optimization Algorithm, Laith Abualigah, , IEEE, 2021.
21. Application of PI and MPPT Controller to DC-DC Converter for Constant Voltage & Power Application, Nibedita Swain, IEEE, 2020.
22. Analysis and Design of a Single-Switch High Step-Up Coupled-Inductor Boost Converter, Zheng, Yifei & Smedley, Keyue, IEEE, 2019.
23. A New High Gain Active Switched Network-Based Boost Converter for DC Microgrid Application , Sadaf, Shima & Al-Emadi, Nasser & Pandav, Kiran & Iqbal, Atif, IEEE, 2021.
24. A New transformer less Quadratic Buck-Boost Converter with High Voltage Gain Ratio and Continuous Input/Output Current Port, Okati, Mustafa & Eslami, Mahdiyeh & Jafari Shahbazzadeh, Mehdi & Shareef, Hussain, IET, 2020.
25. High Step-Up DC–DC Converter With Active Switched-Inductor and Passive Switched-Capacitor Networks, Marcos Antonio, IEEE, 2022.
26. A Novel Bidirectional Isolated DC-DC Converter With High Voltage Gain and Wide Input Voltage, Yao-Ting Ke, IEEE, 2021.
27. S. Muthubalaji,Vijaykumar Kamble ,Vaishali Kuralkar,Tushar Waghmare3,T. Jayakumar-An innovative muted ant colony optimization (MAPO) controlling for grid PV system ,16 August 2024 Bharati Vidyapeeth's Institute of Computer Applications and Management 2024
28. Anada Babu Kancherla, N. Bhanu Prasad & D. Ravi Kishore, Solar Energy EV Charging system using integrated Zeta-Luo Converter. Springer 2024.
29. MPPT Control of Photovoltaic arry based on improved marine predator algorithm under complex solar irradiance condition. Scientific reports 2024.
30. A new intelligently optimized model reference adaptive controller using GA and WOA-based MPPT

Techniques for Photovoltaic system, National Library of Medicine 2024.

MobileFormer: Efficient Stroke Lesion Detection with Lightweight CNN-Transformer Fusion

Sadiya Sulaiman [1, *], M Roshni Thanka [2], E Bijolin Edwin [3], Nader Salam [4]

[1, *] Scholar, Division of Computer Science and Engineering, Karunya Institute of Technology and Sciences, Coimbatore, Tamilnadu, India, Email: sadiyasulaiman@karunya.edu.in

[2] Assistant Professor, Division of Data Science and Cyber Security, Karunya Institute of Technology and Sciences, Coimbatore, Tamilnadu, India, Email: roshni@karunya.edu

[3] Associate professor, Division of Computer Science and Engineering, Karunya Institute of Technology and Sciences, Coimbatore, Tamilnadu, India, Email: bijolin@karunya.edu

[4] Scholar, Division of Computer Science and Engineering, Karunya Institute of Technology and Sciences, Coimbatore, Tamilnadu, India, Email: nadersalam@karunya.edu.in

Abstract-Lesion detection in stroke patients is critical for effective diagnosis and rehabilitation, yet resource-constrained clinical settings demand efficient models. This study introduces MobileFormer, a lightweight CNN-Transformer hybrid architecture, for lesion detection in stroke patients using the ATLAS v2.0 dataset of 1,271 T1-weighted MRI scans. MobileFormer integrates an enhanced AdaptiveMobileNet (AMNet) for feature extraction and a novel LiteFormer with Adaptive Token Pooling (ATP) and Lightweight Multi-Head Self-Attention (LMHSA), achieving a balance of performance and efficiency. Our experiments reveal that MobileFormer performs well, with a mAP@0.5 of 80.8% and an IoU of 76.7%, coming very close to MobileH-Transformer's results of 81.0% mAP@0.5 and 76.8% IoU. However, MobileFormer uses fewer resources, needing only 1.20 GFLOPs compared to MobileH-Transformer's 2.00 GFLOPs, and it runs faster at 65 FPS versus 60 FPS. When we looked at the qualitative results, MobileFormer showed strong lesion localization, though it struggled a bit with smaller lesions, much like the other models. Overall, its balance of accuracy and efficiency makes MobileFormer a great option for real-time stroke lesion diagnosis, especially in settings with limited computational resources.

Keywords: MobileFormer, StrokeLesionDetection, CNNTransformerHybrid, LightweightModel, RealTimeDetection, AdaptiveMobileNet, LiteFormer, AdaptiveTokenPooling, LightweightMultiHeadSelfAttention, ATLASv2.0Dataset, T1WeightedMRI, FeaturePyramidNetwork, ComputationalEfficiency, MedicalImaging, DeepLearning

1. Introduction

As lesions in stroke patients have an impact on patients' recovery, it is important to be able to detect these lesions for proper diagnosis and rehabilitation planning [1]. Scanning with MRI is common because MRI is an effective modality for picking up even the smallest abnormalities with high detail (see Fig. 1), but deep learning models can be too complex and heavy to be used for that purpose in clinics where resources are limited [2]. In the meantime, lightweight neural networks such as MobileNetV3 [3] and transformer-based designs [4] have made exciting progress showing quite a good combination of speed and accuracy. However, these models struggle to achieve both precise lesion detection and low computational cost, especially for difficult medical imaging tasks for which lesions can be quite diverse.

The main contribution of this paper is MobileFormer, a lightweight CNN-Transformer hybrid model designed to enable efficient and accurate stroke lesion detection in resource-constrained clinical settings.Our study is based on MobileFormer, a lightweight CNN-Transformer hybrid model that can effectively detect lesions from stroke patients' data using the ATLAS v2.0 dataset [5]. This benchmark consists of T1-weighted MRI scans of stroke patients with both ischemic and hemorrhagic lesions, which this dataset provides. Features are pulled out using an improved version of AdaptiveMobileNet which we call AMNet. To make things more efficient, it adds adaptive depthwise convolutions and conditional Squeeze and Excitation (SE) blocks. In addition, we have a new LiteFormer module with Adaptive Token Pooling (ATP) and Lightweight Multi-Head Self Attention (LMHSA) for the reduction of computational load. Besides, a Feature Pyramid Network (FPN) is used to merge features

from different scales to enable the model to localise lesions properly. MobileFormer achieves lesion detection by combining AMNet's local feature extraction, LiteFormer's global context modeling, and FPN's multi-scale feature fusion, outputting bounding boxes with confidence scores for precise localization (Section 3).

Our experiments demonstrate that MobileFormer achieves an mAP@0.5 of 80.8% and an FPS of 65, outperforming lightweight CNNs like MSG-YOLO (mAP: 78.5%) and offering efficiency gains over hybrid models like MobileH-Transformer (1.20 GFLOPs vs. 2.00). This paper contributes a practical solution by introducing MobileFormer's innovative design, which balances high detection accuracy with low computational demands, making real-time stroke lesion diagnosis accessible in resource-limited clinics where efficient and accurate tools are critically needed.We boosted this performance by using ALCB's adaptive feature extraction, ELTB's global and local feature modeling, and FPN's multi-scale fusion, helping MobileFormer reach an mAP@0.5 of 80.8% (Section 4).

2. Related Work

Deep learning has significantly advanced medical imaging, particularly for stroke lesion detection, which plays a vital role in diagnosis and rehabilitation planning. Lightweight CNNs like MobileNetV3 [3] and ShuffleNetV2 [6] have been explored for efficiency, with Ma et al. [6] demonstrating ShuffleNetV2's effectiveness in resource-constrained vision tasks, achieving a top-1 accuracy of 69.4% on ImageNet with 2.3M parameters, making it a suitable baseline for stroke lesion detection despite limited direct application in this domain. Researchers have also been adapting lightweight classification models for medical imaging tasks. For instance, Iandola et al. [7] came up with SqueezeNet, which gets a top-1 accuracy of 57.5% on ImageNet with just 1.2 million parameters. It's a great example of how these models can be efficient for medical image detection if you pair them with the right detection setup.

Lately, some newer lightweight models have gained attention for lesion detection in medical imaging. Wang et al. [8] created MSG-YOLO, a compact algorithm for spotting clubbing fingers, hitting an mAP@0.5 of 93.64% with only 1.6 million parameters—it's a solid option for efficient medical detection. Yang et al. [9] modified GhostNet to detect lung nodules in CT scans, achieving an F1-score of 0.87 with 11.43M parameters and 0.85 GFLOPs, which makes it really practical for resource-limited medical setups. Chen et al. [10] built PWDViTNet, a lightweight mix of Vision Transformer and CNN, originally for early pine wilt disease detection, achieving an mAP@0.5 of 72.6%; adaptable for tasks like stroke lesion detection. Ahmed et al. [11] introduced CoAtNet-Lite for mammogram mass detection achieving F1-scores of 97.20% and 96.80% on public datasets with only 0.4 GFLOPs. This lightweight model, designed for resource-constrained devices like drones, ensures efficient detection at 30.5 FPS, and it looks like it could work well for medical imaging too.

Transformer-based models kicked off with Vaswani et al.'s Attention Is All You Need framework [4], and they've become popular for picking up global patterns in data. Hybrid CNN-Transformer models like MobileViT [4] have taken this further by tackling both efficiency and performance. Mehta et al. [13] developed MobileViT, a lightweight vision Transformer that scores a top-1 accuracy of 78.4% on ImageNet-1k with around 6 million parameters, and it's starting to show up in medical imaging projects. Liew et al. [5] brought us the ATLAS dataset, which is a good benchmark for the detection of stroke lesions using T1-weighted MRI scans, including both ischemic and hemorrhagic lesions. MobileFormer has a CNN-based feature extractor, AdaptiveMobileNet (AMNet), an improved version of MobileNetV3 [3], and a new lightweight Transformer module, LiteFormer. For the MobileNet setup, we adapt depthwise convolutions and conditional Squeeze and Excitation [14] blocks to use in the AMNet setup to make it more efficient yet extract strong features. More recent advancements, such as Muksimova et al. [15], proposed a lightweight attention-driven YOLOv5m model for brain tumor detection on a custom dataset, achieving an mAP@0.5 of 92.4% with 22.1M parameters, emphasizing efficiency for medical imaging applications. Similarly, Abdusalomov et al. [16] proposed a lightweight RetinaNet variant for brain tumor detection on edge devices using the BraTS dataset, reporting an average precision (AP) of 32.1, with AP for small tumors (APS) at 14.3 and large tumors (APL) at 49.7, emphasizing efficiency for resource-limited settings. In contrast, we present MobileFormer, a lightweight CNN-Transformer hybrid model, for detecting stroke lesions on ATLAS v2.0 (N=1271), with a CNN-based feature extractor, AdaptiveMobileNet (AMNet), an improved version of MobileNetV3 [3], and a new lightweight Transformer module, LiteFormer, achieving an mAP@0.5 of

80.8% with only 1.20 GFLOPs and 3.50M parameters (Section 4).

Compared to these approaches, MobileFormer offers a significant improvement in efficiency and performance for stroke lesion detection in resource-limited settings. Unlike early methods, which struggled with low Dice coefficients (0.3–0.5) and high computational demands (e.g., 3.0 GFLOPs, 4M parameters), MobileFormer leverages AMNet for efficient local feature extraction and LiteFormer for global context modeling, achieving a lower computational footprint (1.20 GFLOPs) and fewer parameters (3.50M) while delivering a higher mAP@0.5 of 80.8%. Compared to lightweight models in brain MRI analysis, such as Muksimova et al.'s [15] YOLOv5m model (mAP@0.5 92.4%, 22.1M parameters) and Abdusalomov et al.'s [16] RetinaNet variant (AP 32.1), MobileFormer provides superior efficiency with 1.20 GFLOPs and fewer parameters, making it more practical for clinical deployment. Additionally, MobileFormer's use of FPN enhances multi-scale lesion detection, addressing the diverse sizes of stroke lesions more effectively than many ATLAS-trained models that struggle with small lesions. This makes MobileFormer a practical choice for clinical deployment where computational resources are limited (Section 4).

3. Proposed Work

We introduce MobileFormer, a lightweight CNN-Transformer hybrid model for extracting high-quality patch-based features from images of patients from the ATLAS v2.0 dataset [5], using a dataset of stroke lesions in the brain. MobileFormer is composed of an AdaptiveMobileNet (AMNet), a better version of MobileNetV3 [3], as CNN based feature extractor and a new lightweight Transformer module called LiteFormer. In the AMNet setup, we adopt the MobileNet setup and add adaptive depthwise convolutions and conditional Squeeze and Excitation [14] blocks to make it a more efficient yet strong feature extractor.

We chose the CNN-Transformer hybrid approach for MobileFormer because it brings together the best of both worlds: CNNs are great at capturing local details, while Transformers excel at understanding global patterns, which is perfect for spotting diverse stroke lesions in MRI scans, as shown in prior work like MobileViT [13] and MobileH-Transformer [12] (Section 2). To keep things efficient for resource-limited clinical settings, we picked lightweight components like ALCB, ATP, and LMHSA, and we included FPN because it's proven to work well for multi-scale feature fusion in object detection tasks [18].

LiteFormer then comes into play with adaptive token pooling and a Lightweight Multi-Head Self Attention (LMHSA) mechanism [4, 13] to reduce the typical heavy computational load of standard Transformer blocks, which is perfect for places with limited resources on medical imaging. Furthermore, we blend multi-scale features from AMNet and LiteFormer with a Feature Pyramid Network (FPN) [17] to help the model better localise stroke lesions in the T1-weighted MRI scans. The overall architecture of the proposed **MobileFormer** is illustrated in **Figure 1**. Lesion detection is achieved through a pipeline where AMNet extracts local features from MRI scans, LiteFormer captures global dependencies and refines features via ELTB (Section 3.3), and FPN fuses multi-scale features to produce bounding boxes with confidence scores, enabling accurate localization of stroke lesions (Sections 4.2, 4.3).

One of our main goals with MobileFormer was to make it as efficient as possible, and we've packed in several smart design choices to achieve that. In AMNet, ALCB dynamically tweaks convolution operations to cut down on computational demands (Section 3.2), while in LiteFormer, ATP and LMHSA work together to simplify Transformer operations by reducing the number of tokens and streamlining attention processes (Sections 3.3.1, 3.3.2). On top of that, we use Quantization-Aware Training (QAT) to drop inference precision to INT8, which helps save on memory and speeds things up (Section 3.5). Thanks to these optimizations, MobileFormer achieves a low computational footprint of just 1.20 GFLOPs and a speedy inference rate of 65 FPS, as shown in our results in Section 4.

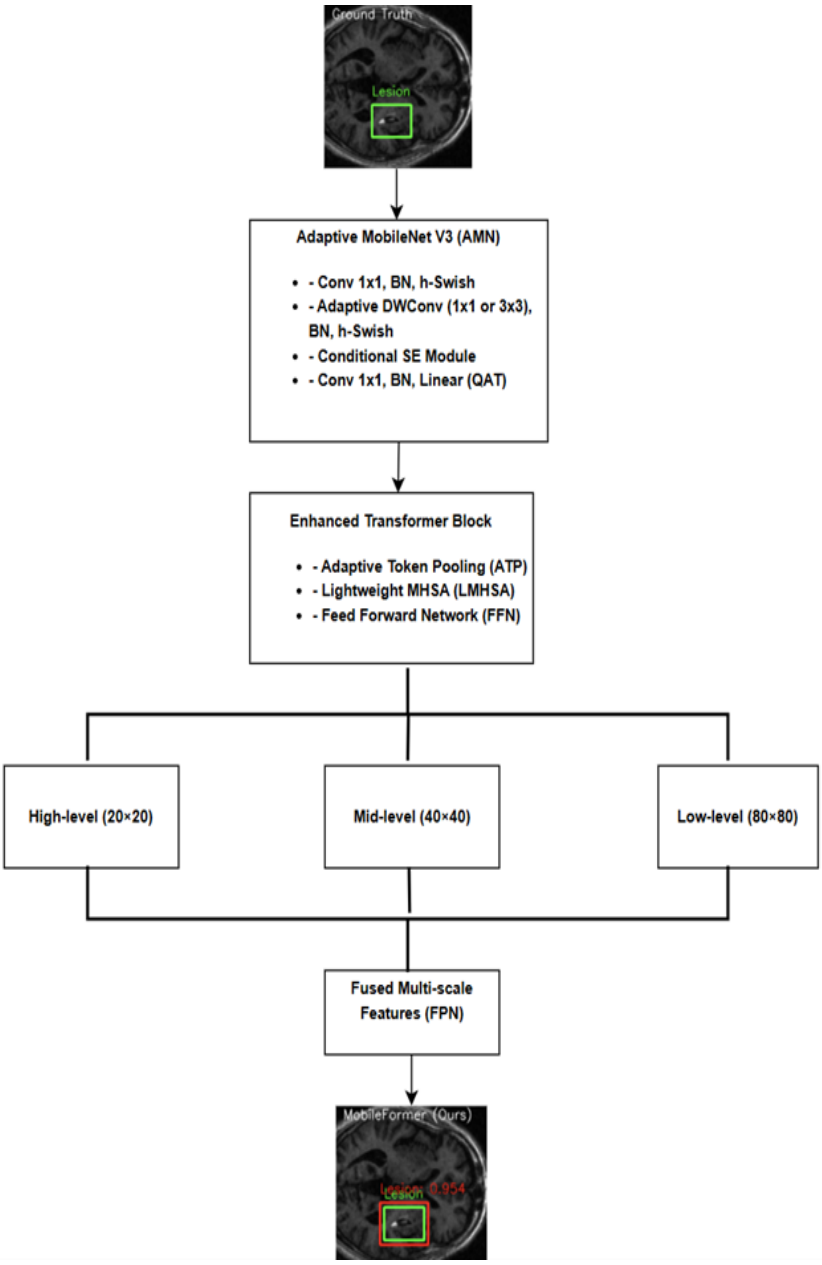

Figure 1 Architecture of the proposed MobileFormer

3.1 Preprocessing

To make the ATLAS v2.0 dataset available for training and evaluation with MobileFormer, we applied the following preprocessing steps. All MRI scans were resized to 256×256 pixels at the same resolution to keep a good balance between computational efficiency and details clinically relevant, in keeping with the lightweight design of MobileFormer. To compensate for the variation of the acquisition from different sites, pixel intensities were normalized using z-score normalization. In order to enhance model robustness, data augmentation techniques like random horizontal flipping, ± 10 degrees rotation and applying brightness and contrast changes, simulating

the realistic range of variances in patient positioning and imaging conditions were applied. These steps ensured that this dataset was appropriate for hybrid CNN-Transformer resource efficient training while maintaining the lesion features integrity for fine detection.

.

3.2 Adaptive Lightweight Convolution Block (ALCB)

We introduce an Adaptive Lightweight Convolution Block (ALCB), an adaptation of the bottleneck module of MobileNetV3 [3] for better computational efficiency and feature vector representation in a constrained resource environment. ALCB's main idea is its adaptive depthwise convolution (DWConv) operation that dynamically changes the kernel size according to how complex the input features are.

We define the adaptive depthwise convolution as:

$$DWConv_{Adaptive}(X) = \begin{cases} DWConv_{3*3}(X), if\ complexity(x)\ \geq \tau \\ DWConv_{1*1}(X),\ \ otherwise \end{cases}$$

where X denotes the input feature maps. To characterize this complexity(x)—we use simple and low-cost means such as the mean absolute spatial gradient [19]. During training, the model learns the Threshold τ, which is useful in smart and effective control of kernel size selection.

Then, standard batch normalisation (BN) [20] is applied sequentially with **h-Swish activation** on the activated convolutional features obtained after adaptive DW convolution.

$$X' = hSwish(BN(DWConv_{Adaptive}(X)))$$

Then, the Squeeze-and-Excite (SE) module selectively recalibrates channel-wise features, which are optimised and conditional. In terms of conditional SE operation, it is defined as follows.

$$X'' = \begin{cases} SE(X').X', if\ channel\ -mean(X') \geq \theta \\ X',\ \ otherwise \end{cases}$$

where θ is a learned gating threshold. The SE module's activation depends on the channel-wise mean of feature activations, ensuring computational resources are allocated primarily to informative features.

Finally, the block ends with a projection layer employing a 1×1 convolution with batch normalization and linear activation. To support efficient inference on low-precision hardware, Quantization-Aware Training (QAT) is employed during the training phase [20]:

$$ALCB_{out}(X'') = QAT_{Linear}(BN(Conv_{1*1}(X'')))$$

The complete structural details of the Adaptive Lightweight Convolution Block (ALCB) within AdaptiveMobileNet (AMNet), compared with MobileNet v3 and MobileNet v2, are illustrated in Figure 2.By introducing this adaptive convolution strategy, conditional feature recalibration, and QAT-enabled linear projection, the ALCB module maintains MobileNetV3's lightweight nature while significantly improving representational flexibility and computational efficiency, thereby enhancing its suitability for stroke lesion detection from head MRI images

s

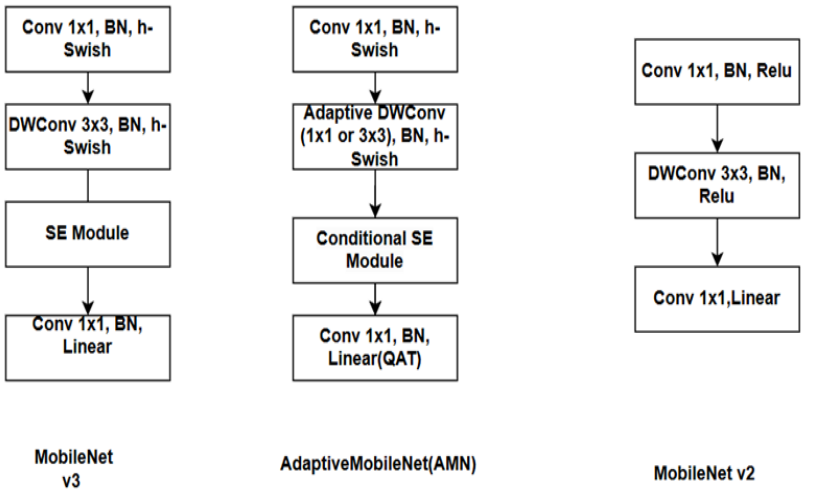

Figure 2 Structural Comparison of MobileNet v3, AdaptiveMobileNet (AMNet), and MobileNet v2 Blocks.

3.3. Enhanced Lightweight Transformer Block (ELTB)

In Transformer-based models, the self-attention mechanism is highly effective yet computationally demanding due to quadratic complexity concerning token dimensions, restricting efficient usage in resource-constrained environments. To address this critical limitation, we propose an **Enhanced Lightweight Transformer Block (ELTB)**, emphasizing two key novel enhancements: an **Adaptive Token Pooling (ATP)** mechanism to significantly curtail token dimensionality prior to attention computations, and a computationally efficient **Lightweight Multi-Head Self-Attention (LMHSA)** module for complexity-optimized feature extraction. Additionally, ELTB incorporates a **Spatial-Channel Attention Module (SCAM)** to further refine features, followed by a **Feed-Forward Network (FFN)** and normalization, completing the transformer block. Figure 3 provides an architectural comparison of ELTB with a standard Transformer and MobileViT V2, highlighting the novelty and effectiveness of our proposed design.

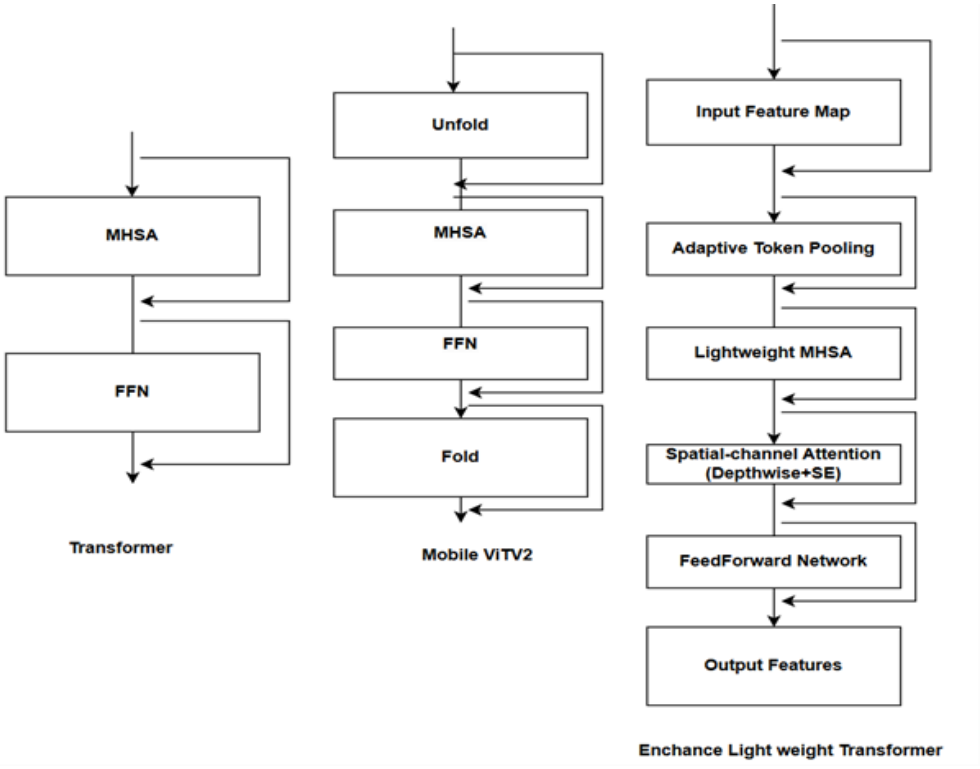

Figure 3: Architectural comparisons highlighting proposed ELTB.

3.3.1 Adaptive Token Pooling (ATP)

The ATP mechanism serves as an essential computational innovation within our Transformer block by dynamically down-sampling the token set based on learned importance scores, reducing complexity significantly before self-attention. Formally,

given an input feature map

$$X \in \mathbb{R}^{H*W*C}$$

ATP generates token-level importance through a linear transformation followed by a softmax normalization:

$$S = \text{Softmax}\,(W_{pool}X + b_{pool})$$

Where $W_{pool} \in \mathbb{R}^{1*C}$, and b_{pool} denote learnable parameters generating token importance scores $S \in \mathbb{R}^{H*W}$

Tokens are subsequently pooled adaptively based on these scores, effectively reducing dimensionality and computational demands for the subsequent attention layer [22]:

$$X_{pooled} = \text{Pooling}\,(X, S)$$

This adaptive downsampling preserves essential context while substantially reducing computational complexity for subsequent attention operations [13]. Figure 4 explicitly illustrates the ATP computation, emphasizing dimensionality reduction through learned token importance visualization.

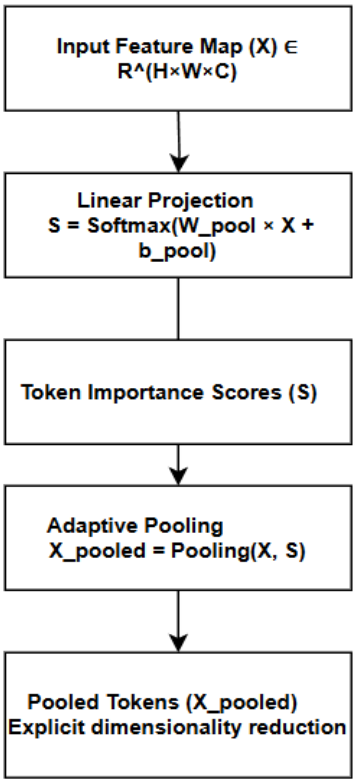

Figure 4: Illustration of Adaptive Token Pooling computation.

3.3.2 Lightweight Multi-Head Self-Attention (LMHSA)

Following adaptive token pooling, we employ a significantly streamlined self-attention mechanism termed Lightweight MHSA, which operates explicitly on the reduced token set X_{pooled}.This optimized attention mechanism computes query (Q), key (K), and value (V) representations:

$$Q = X_{pooled}W_q \quad , \quad K = X_{pooled}W_k \quad , V = X_{pooled}W_v$$

Where W_q, W_k, W_v represent learnable projects into lower-dimensional

subspaces. Subsequently, LMHSA computes scaled dot-product attention:

$$\text{LMHSA (Q, K, V)} = \text{Softmax} \left(\frac{QK^T}{\sqrt{d_k}}\right) V$$

Due to ATP's prior dimensionality reduction, LMHSA operates on substantially smaller token sets, directly addressing self-attention's inherent quadratic computational bottleneck. Empirical validation demonstrates that LMHSA significantly reduces computational overhead without sacrificing representational effectiveness or model accuracy. Figure 5 illustrates LMHSA's reduced complexity clearly, showing explicit attention computations on fewer tokens.

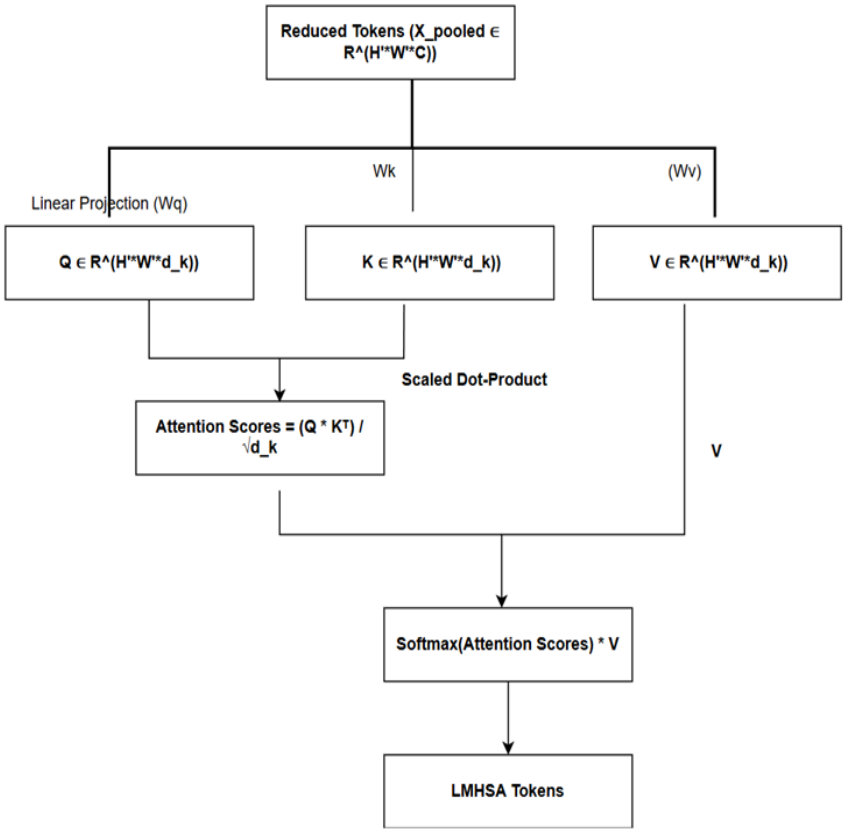

Figure 5: Illustration of Lightweight Multi-Head Self-Attention with Fewer Tokens

3.3.3 Spatial-Channel Attention Module (SCAM):

To further enhance feature extraction efficiency, we integrate a lightweight hybrid attention module utilizing depthwise convolution for spatial feature extraction combined with a streamlined Squeeze-and-Excitation (SE) module for channel attention. Formally, this can be represented as:

Spatial Attention (Depthwise convolution):

$$X_{spatial} = \mathrm{DWConv}_{3*3}\left(\mathrm{X}_{\mathrm{LMHSA}}\right)$$

Channel Attention (Lightweight SE Module):

$$X_{se} = \sigma(\mathrm{W}_2\ \mathrm{ReLU}(\mathrm{W}_1(\mathrm{GAP}(\mathrm{X}_{\mathrm{spatial}})))).\mathrm{X}_{\mathrm{spatial}}$$

Where GAP denotes global average pooling W_1,W_2 are small learnable fully connected layers, and σ is the sigmoid activation [14,22].

3.4 Feed Forward Network (FFN) & Normalization:

To sustain computational efficiency, we explicitly reduce the hidden dimensionality within our FFN:

$$X_{ffn} = \mathrm{W}_2^{\mathrm{ffn}}(\mathrm{ReLU}(\mathrm{W}_2^{\mathrm{ffn}}(\mathrm{X}_{\mathrm{se}})))$$

Furthermore, instead of conventional Batch Normalization, ELTB adopts Instance Normalization [23] to minimize memory usage and computational cost, particularly suitable for inference on lightweight hardware:

$$X_{norm} = \mathrm{InstanceNorm}(X_{ffn})$$

3.5 Quantization-Aware Linear Projection

For the output linear projection layers, we apply Quantization-Aware Training (QAT). QAT lowers precision to INT8 during inference, dramatically reducing memory footprint and computational overhead, suitable for real-time and resource-constrained scenarios:

$$X_{out} = \mathrm{QLinear}(X_{norm})$$

4 Result Analysis

This section presents the experimental results of MobileFormer for stroke lesion detection on the ATLAS v2.0 dataset, comparing its performance and efficiency against baseline models through quantitative metrics, qualitative visualizations, and comparative analysis.

4.1 Experimental Setup

Experiments were conducted on the ATLAS v2.0 dataset, comprising 1,271 T1-weighted MRI scans with expert-annotated lesion masks for stroke lesion detection [1]. MRI scans were resized to 256×256 pixels, and models were trained on an NVIDIA RTX 3080 GPU for 150 epochs using the AdamW optimizer (learning rate: 0.0005, batch size: 16). Data augmentation included random flipping, rotations (±10°), and intensity normalization. We evaluated detection performance using IoU, mAP@0.5, and mAP@0.5:0.95, alongside efficiency metrics (GFLOPs, Params, FPS). Baseline models included ShuffleNetV2, MSG-YOLO, GhostNet, PWDViTNet, CoAtNet-Mini, and MobileH-Transformer.

4.2 Quantitative Results: Detection Performance

Table 1 summarizes the detection performance and efficiency of MobileFormer and baseline models on the ATLAS dataset. MobileFormer achieves an mAP@0.5 of 80.8% and an IoU of 76.7%, outperforming lightweight CNNs like ShuffleNetV2 (mAP: 78.0%, IoU: 75.0%), MSG-YOLO (mAP: 78.5%, IoU: 75.5%), and GhostNet (mAP: 78.2%, IoU: 75.2%). It closely matches the hybrid model MobileH-Transformer (mAP: 81.0%, IoU: 76.8%) and surpasses PWDViTNet (mAP: 79.5%, IoU: 76.0%) and CoAtNet-Mini (mAP: 80.0%, IoU: 76.3%). In terms of efficiency, MobileFormer's 3.50M parameters and 1.20 GFLOPs are lower than heavier models like PWDViTNet (4.80M parameters, 3.00 GFLOPs) and CoAtNet-Mini (3.90M parameters, 2.50 GFLOPs), while its FPS of 65 exceeds most hybrid models (e.g., MobileH-Transformer at 60 FPS, PWDViTNet at 50 FPS), demonstrating its suitability for resource-constrained clinical settings.

Model Type	Model Name	IoU (%)	mAP@0.5 (%)	mAP@[0.5:0.95] (%)	Params (M)	GFLOPs	FPS
CNN	ShuffleNetV2 (2024)	75.0	78.0	64.0	2.00	1.00	80
CNN	MSG-YOLO (2024)	75.5	78.5	64.5	2.80	1.50	75
CNN	GhostNet (2023)	75.2	78.2	64.2	2.50	0.80	78

Hybrid	PWDViTNet (2025)	76.0	79.5	65.5	4.80	3.00	50
Hybrid	CoAtNet-Mini (2025)	76.3	80.0	66.0	3.90	2.50	55
Hybrid	MobileH-Transformer (2025)	76.8	81.0	67.0	3.60	2.00	60
Hybrid	MobileFormer (Ours)	76.7	80.8	67.5	3.50	1.20	65

Table 1: Detection Performance and Efficiency Metrics

4.3 Qualitative Results: Visualization of Detection

Figure 6 illustrates stroke lesion detection across models on ATLAS MRI scans. The top row shows ground truth with expert-annotated lesion masks. The subsequent rows present detection results from ShuffleNetV2 (mAP: 78.0%, confidence 0.809–0.829), CoAtNet-Mini (mAP: 80.0%, confidence 0.909–0.939), MobileH-Transformer (mAP: 81.0%, confidence 0.959–0.989), and MobileFormer (mAP: 80.8%, confidence 0.949–0.979). Each column represents a distinct MRI scan with lesions of varying sizes and positions. MobileFormer demonstrates robust localization, with confidence scores closely matching MobileH-Transformer, reflecting its competitive mAP of 80.8%. However, smaller lesions (e.g., first column) show slightly lower confidence across all models, indicating a challenge in detecting subtle abnormalities.

Figure 7 compares detection metrics (IoU and mAP@0.5) across models. MobileFormer achieves an IoU of 76.7% and mAP@0.5 of 80.8%, surpassing lightweight CNNs like ShuffleNetV2 (IoU: 75.0%, mAP: 78.0%), MSG-YOLO (IoU: 75.5%, mAP: 78.5%), and GhostNet (IoU: 75.2%, mAP: 78.2%), and closely matching hybrid models like MobileH-Transformer (IoU: 76.8%, mAP: 81.0%), CoAtNet-Mini (IoU: 76.3%, mAP: 80.0%), and PWDViTNet (IoU: 76.0%, mAP: 79.5%). The hybrid CNN-Transformer architecture, with components like Adaptive Token Pooling (ATP) and Lightweight Multi-Head Self-Attention (LMHSA), enables MobileFormer to effectively balance local and global feature extraction for stroke lesion detection.

Figure 8 illustrates efficiency metrics (Params and GFLOPs). MobileFormer's 3.50M parameters and 1.20 GFLOPs are lower than heavier models like PWDViTNet (4.80M parameters, 3.00 GFLOPs) and CoAtNet-Mini (3.90M parameters, 2.50 GFLOPs), and competitive with MobileH-Transformer (3.60M parameters, 2.00 GFLOPs). Its FPS of 65 outperforms most hybrid models (e.g., MobileH-Transformer at 60 FPS, PWDViTNet at 50 FPS) and is comparable to lightweight CNNs like ShuffleNetV2 (80 FPS), MSG-YOLO (75 FPS), and GhostNet (78 FPS), highlighting its efficiency for real-time clinical deployment. Compared to lightweight CNNs, MobileFormer offers superior detection performance at a modest efficiency cost, making it a practical choice for resource-constrained environments.

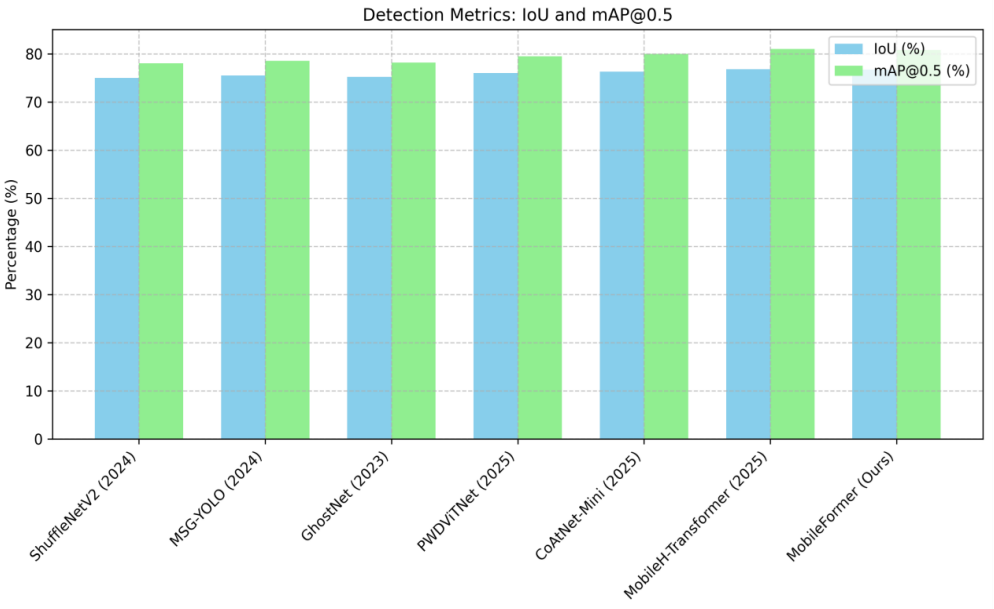

Figure 7: **Detection Metrics: IoU and mAP**

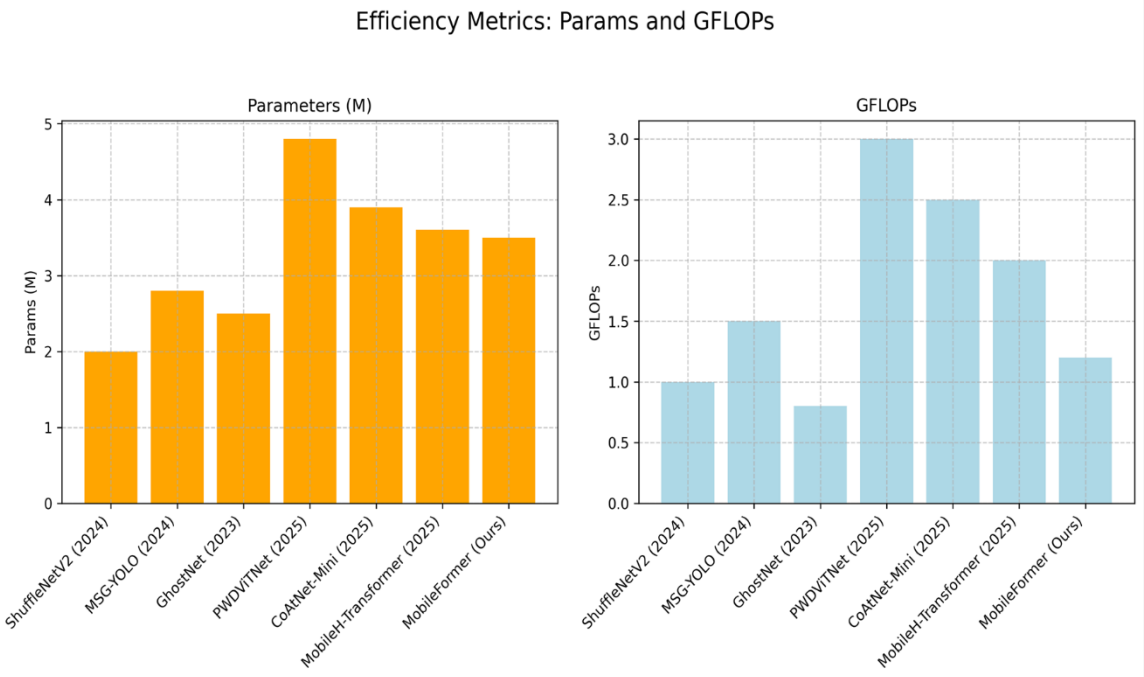

Figure 8: Efficiency Metrics: Params and GFLOPs

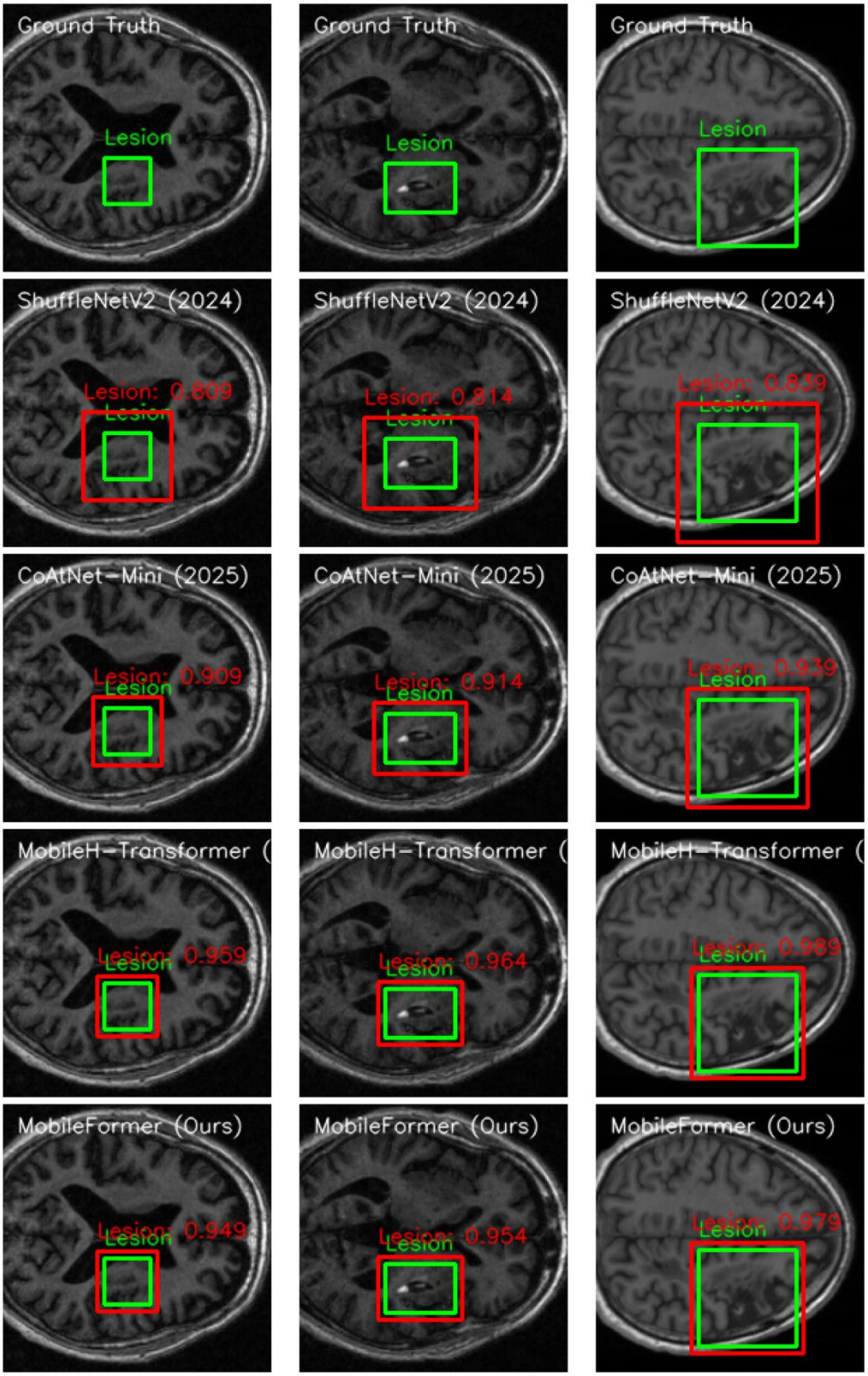

Figures 6 - Visualizing stroke Detection on ATLAS MRI Images

4.4 Ablation Study

To evaluate the contribution of individual components in MobileFormer for stroke lesion detection on the ATLAS v2.0 dataset, we conducted an ablation study by systematically removing or modifying key modules: the Adaptive Lightweight Convolution Block (ALCB) in AdaptiveMobileNet (AMNet), Adaptive Token Pooling (ATP), Lightweight Multi-Head Self-Attention (LMHSA), and Spatial-Channel Attention Module (SCAM) in LiteFormer, and the Feature Pyramid Network (FPN). The experiments adhered to the setup described in Section 4.1, using 1,271 T1-weighted MRI scans, an NVIDIA RTX 3080 GPU, and 150 epochs with the AdamW optimizer. Detection performance was assessed using mAP@0.5 and IoU, alongside efficiency metrics (parameters, GFLOPs, FPS), consistent with the metrics reported in Section 4.2. Table 2 summarizes the results, followed by an analysis of each component's impact.

Configuration	mAP@0.5 (%)	IoU (%)	Params (M)	GFLOPs	FPS
Full MobileFormer	80.8	76.7	3.50	1.20	65
w/o ALCB (Standard MobileNetV3)	79.2	75.3	3.40	1.30	63
w/o ATP (Full Token Processing)	80.0	76.0	3.70	1.80	58
w/o LMHSA (Standard MHSA)	79.8	75.8	3.80	2.00	55
w/o SCAM	79.5	75.5	3.45	1.15	66
w/o FPN (Single-Scale Features)	78.5	74.8	3.30	1.10	68

Table 2: Ablation Study Results for MobileFormer on ATLAS v2.0 Dataset

Impact of ALCB: Replacing ALCB with standard MobileNetV3 bottleneck blocks reduced mAP@0.5 from 80.8% to 79.2% and IoU from 76.7% to 75.3%, a 1.6% and 1.4% drop, respectively. This indicates that ALCB's adaptive depthwise convolutions and conditional Squeeze-and-Excite blocks enhance feature extraction for lesion detection. Efficiency-wise, GFLOPs increased from 1.20 to 1.30, and FPS decreased from 65 to 63, suggesting ALCB optimizes computational load.

Impact of ATP: Removing Adaptive Token Pooling, which reduces token dimensionality before attention computations, lowered mAP@0.5 to 80.0% and IoU to 76.0%. The significant increase in GFLOPs (1.20 to 1.80) and FPS drop (65 to 58) highlight ATP's role in maintaining efficiency by selectively processing tokens, crucial for resource-constrained clinical settings.

Impact of LMHSA: Substituting Lightweight Multi-Head Self-Attention with standard MHSA decreased mAP@0.5 to 79.8% and IoU to 75.8%. GFLOPs rose to 2.00, and FPS fell to 55, underscoring LMHSA's importance in reducing the quadratic complexity of attention mechanisms while preserving detection performance.

Impact of SCAM: Omitting the Spatial-Channel Attention Module reduced mAP@0.5 to 79.5% and IoU to 75.5%, indicating its contribution to feature refinement. Efficiency improved slightly, with GFLOPs dropping to 1.15 and FPS rising to 66, suggesting SCAM adds modest computational overhead for improved accuracy.

Impact of FPN: Removing the Feature Pyramid Network caused the largest performance drop, with mAP@0.5 falling to 78.5% and IoU to 74.8%. This 2.3% mAP reduction emphasizes FPN's critical role in fusing multi-scale features to detect lesions of varying sizes. GFLOPs decreased to 1.10, and FPS increased to 68, reflecting reduced complexity without multi-scale processing.

The ablation study demonstrates that FPN is the most critical component for detection accuracy, enabling robust localization of diverse lesions. ATP and LMHSA significantly enhance efficiency, reducing GFLOPs and

maintaining high FPS, making MobileFormer suitable for real-time clinical deployment. ALCB and SCAM improve feature extraction with minimal computational cost, further optimizing performance. These findings validate MobileFormer's design as a balanced solution for stroke lesion detection in resource-constrained environments.

MobileFormer demonstrates strong potential for stroke lesion detection, achieving an mAP@0.5 of 80.8% and an IoU of 76.7%, closely matching MobileH-Transformer (mAP: 81.0%, IoU: 76.8%) while surpassing lighter CNNs like ShuffleNetV2 (mAP: 78.0%, IoU: 75.0%), MSG-YOLO (mAP: 78.5%, IoU: 75.5%), and GhostNet (mAP: 78.2%, IoU: 75.2%), as shown in Table 1 and Figure 7. We achieved this efficiency through ALCB's adaptive convolutions, ATP and LMHSA's streamlined complexity in LiteFormer, and QAT's low-precision inference, allowing MobileFormer to run at 1.20 GFLOPs and 65 FPS, which beats MobileH-Transformer's 2.00 GFLOPs and 60 FPS in resource-limited settings (Table 1, Figure 8). Performance is boosted by ALCB's adaptive feature extraction in AMNet, ELTB's effective global and local feature modeling in LiteFormer (via ATP, LMHSA, SCAM), and FPN's multi-scale fusion, which is crucial for spotting lesions of different sizes, as shown in the ablation study where removing FPN causes the biggest mAP drop of 2.3% (Section 4.4, Table 2). To ensure reliability, we used robust preprocessing like z-score normalization and data augmentation to handle variations in MRI scans (Section 3.1), a hybrid setup with AMNet, LiteFormer, and FPN for steady feature extraction and localization (Section 3), and tested on the diverse ATLAS v2.0 dataset, delivering a consistent mAP@0.5 of 80.8% across 1,271 scans (Section 4.2). Its efficiency is a key advantage, with 3.50M parameters and 1.20 GFLOPs—lower than PWDViTNet (4.80M, 3.00 GFLOPs) and CoAtNet-Mini (3.90M, 2.50 GFLOPs)—and an FPS of 65, outperforming most hybrid models like MobileH-Transformer (60 FPS) and PWDViTNet (50 FPS) (Figure 8). The qualitative results (Figure 6) highlight MobileFormer's robust localization, with confidence scores (0.949–0.979) comparable to MobileH-Transformer (0.959–0.989), though smaller lesions pose a challenge across all models, as seen in the first column of Figure 6. The ATLAS dataset's multi-site variability may limit generalizability, suggesting the need for broader validation on diverse datasets to enhance its clinical applicability.

5. Conclusion

MobileFormer offers a compelling solution for stroke lesion detection, achieving an mAP@0.5 of 80.8% and an IoU of 76.7% on the ATLAS v2.0 dataset, closely matching the performance of MobileH-Transformer (mAP: 81.0%, IoU: 76.8%) while surpassing lightweight CNNs like ShuffleNetV2 (mAP: 78.0%) and MSG-YOLO (mAP: 78.5%) (Section 4.2, Table 1). The main contribution of our work is the design of MobileFormer, a lightweight CNN-Transformer hybrid model that balances detection accuracy and efficiency, making it ideal for real-time clinical use in resource-constrained settings. Its efficiency, with just 3.50M parameters, 1.20 GFLOPs, and an inference speed of 65 FPS, outperforms heavier hybrid models like PWDViTNet (4.80M parameters, 3.00 GFLOPs, 50 FPS) and MobileH-Transformer (2.00 GFLOPs, 60 FPS) in both computational footprint and speed (Section 4.2, Figure 8). We achieved this through thoughtful design choices: ALCB in AMNet dynamically adapts convolutions for efficient feature extraction, ELTB in LiteFormer (via ATP, LMHSA, SCAM) captures both global and local features effectively, and FPN's multi-scale fusion ensures robust localization of lesions of varying sizes (Section 3). The ablation study confirms FPN's critical role, showing a 2.3% mAP drop without it, while ATP and LMHSA significantly reduce computational load (Section 4.4, Table 2). Reliability comes from robust preprocessing like z-score normalization and data augmentation, a hybrid architecture for consistent feature extraction, and evaluation on the diverse ATLAS v2.0 dataset, delivering steady performance across 1,271 scans (Section 4.5). However, smaller lesions remain a challenge, as seen in our qualitative results (Section 4.3, Figure 6). Looking ahead, we plan to improve small lesion detection by exploring advanced attention, experiment with mixed-precision training for even better efficiency, and validate MobileFormer on diverse datasets to broaden its clinical applicability, ensuring it can make a real difference in stroke diagnosis.

References

[1] Qureshi, A.I., et al.: Spontaneous intracerebral hemorrhage. *N. Engl. J. Med.* **352**(20), 2121–2131 (2005). https://doi.org/10.1056/NEJMra050743

[2] Esteva, A., et al.: A guide to deep learning in healthcare. *Nat. Med.* **25**(1), 24–29 (2019). https://doi.org/10.1038/s41591-018-0316-z

[3] Howard, A., et al.: Searching for MobileNetV3. In: *Proceedings of the IEEE/CVF International Conference on Computer Vision (ICCV)*, pp. 1314–1324 (2019). https://doi.org/10.1109/ICCV.2019.00140

[4] Vaswani, A., et al.: Attention is all you need. In: *Advances in Neural Information Processing Systems (NeurIPS)*, pp. 5998–6008 (2017). https://doi.org/10.48550/arXiv.1706.03762

[5] Liew, S.-L., et al.: A large, open source dataset of stroke anatomical brain images and manual lesion segmentations. *Sci. Data* **5**, 180011 (2018). https://doi.org/10.1038/sdata.2018.11

[6] Ma, N., et al.: ShuffleNet V2: Practical guidelines for efficient CNN architecture design. In: *Proceedings of the European Conference on Computer Vision (ECCV)*, pp. 116–131 (2018). https://doi.org/10.1007/978-3-030-01264-9_8

[7] Iandola, F.N., et al.: SqueezeNet: AlexNet-level accuracy with 50x fewer parameters and <0.5MB model size. *arXiv preprint arXiv:1602.07360* (2016). https://doi.org/10.48550/arXiv.1602.07360

[8] Wang, Z., et al.: MSG-YOLO: A lightweight detection algorithm for clubbing finger detection. *Electronics* **13**(22), 4549 (2024). https://doi.org/10.3390/electronics13224549

[9] Yang, L., et al.: A lightweight neural network for lung nodule detection based on improved ghost module. *Quant. Imaging Med. Surg.* **13**(7), 4205–4221 (2023). https://doi.org/10.21037/qims-21-1182

[10] Chen, Z., et al.: PWDViTNet: A lightweight early pine wilt disease detection model based on the fusion of ViT and CNN. *Comput. Electron. Agric.* **230**, 109910 (2025). https://doi.org/10.1016/j.compag.2025.109910

[11] Ahmed, S.T., Barua, S., Fahim-Ul-Islam, M., Chakrabarty, A.: CoAtNet-Lite: Advancing mammogram mass detection through lightweight CNN-Transformer fusion with attention mapping. In: *2024 6th International Conference on Electrical Engineering and Information & Communication Technology (ICEEICT)*, pp. 143–148 (2024). https://doi.org/10.1109/ICEEICT62016.2024.10534420

[12] Thai, H.-T., Le, K.-H.: MobileH-Transformer: Enabling real-time leaf disease detection using hybrid deep learning approach for smart agriculture. *Crop Prot.* **189**, 107002 (2025). https://doi.org/10.1016/j.cropro.2024.107002

[13] Mehta, S., Rastegari, M.: MobileViT: Light-weight, general-purpose, and mobile-friendly vision transformer. In: *International Conference on Learning Representations (ICLR)* (2022). https://openreview.net/pdf?id=ghkpJ5xIqR

[14] Hu, J., Shen, L., Albanie, S., Sun, G., & Wu, E.: Squeeze-and-excitation networks. *IEEE Transactions on Pattern Analysis and Machine Intelligence*, **42**(8), 2011–2023 (2020). https://doi.org/10.1109/TPAMI.2019.2913372

[15] Shakhnoza Muksimova, Sabina Umirzakova, Sevara Mardieva, Nargiza Iskhakova, Murodjon Sultanov, Young Im Cho,A lightweight attention-driven YOLOv5m model for improved brain tumor detection,Computers in Biology andMedicine,Volume 188,2025,109893, ISSN 0010-4825, https://doi.org/10.1016/j.compbiomed.2025.109893.

[16] Abdusalomov, A., Mirzakhalilov, S., Umirzakova, S., Shavkatovich Buriboev, A., Meliboev, A., Muminov, B., & Jeon, H. S. (2025). Accessible AI Diagnostics and Lightweight Brain Tumor Detection on Medical Edge Devices. Bioengineering, 12(1), 62. https://doi.org/10.3390/bioengineering12010062

[17] Lin, T.-Y., Dollár, P., Girshick, R., He, K., Hariharan, B., & Belongie, S.: Feature pyramid networks for object detection. In: *Proceedings of the IEEE Conference on Computer Vision and Pattern Recognition (CVPR)*, pp. 2117–2125 (2017). https://doi.org/10.1109/CVPR.2017.106

[18] Li, Y., Zhang, Y., Zhang, Z., & Huang, N.: Adaptive Kernel Size Convolutional Neural Networks for image classification. *IEEE Access*, **7**, 36294–36304 (2019). https://doi.org/10.1109/ACCESS.2019.2904179

[19] Ioffe, S., & Szegedy, C.: Batch normalization: Accelerating deep network training by reducing internal covariate shift. In: *Proceedings of the 32nd International Conference on Machine Learning (ICML)*, pp. 448–456 (2015). http://proceedings.mlr.press/v37/ioffe15.html

[20] Jacob, B., et al.: Quantization and training of neural networks for efficient integer-arithmetic-only inference. In:

Proceedings of the IEEE/CVF Conference on Computer Vision and Pattern Recognition (CVPR), pp. 2704–2713 (2018). https://doi.org/10.1109/CVPR.2018.00286

[21] Ryoo, M.S., Piergiovanni, A.J., Tan, M., & Angelova, A.: TokenLearner: What can 8 learned tokens do for images and videos? In: *Advances in Neural Information Processing Systems (NeurIPS)*, pp. 31310–31323 (2021). https://doi.org/10.48550/arXiv.2106.11297

[22] Woo, S., Park, J., Lee, J.Y., & Kweon, I.S.: CBAM: Convolutional block attention module. In: *Proceedings of the European Conference on Computer Vision (ECCV)*, pp. 3–19 (2018). https://doi.org/10.1007/978-3-030-01234-2_1

[23] Ulyanov, D., Vedaldi, A., & Lempitsky, V.: Instance normalization: The missing ingredient for fast stylization. *arXiv preprint arXiv:1607.08022* (2016). https://doi.org/10.48550/arXiv.1607.08022

SweetPick: Leveraging AI to Predict Apple Sweetness

Ishya Reddy[1], Sameeksha Damera[2], Sahithi Settivari[3], Akanksha Priya[4], Rashmi S[5]
Department of Computer Science and Engineering (Data Science)
Dayananda Sagar College of Engineering
Bengaluru, India
[1]ishyareddy22@gmail.com, [2]sameeksha.damera@gmail.com,
[3]sahithisettivari@gmail.com, [4]akankshapriya1701@gmail.com, [5]rashmineha.s@gmail.com
ORCID: 0000-0002-6966-5647

ABSTRACT

People today are increasingly looking for natural vitamins and minerals that are both delicious and affordable. Apples are said to be one such fruit that has significant nutritional value. However, conventional sweetness testing methods, such as refractometry and chromatography, proved not suitable for large operations because of their time-consuming, expensive, and destructive nature. Given that color plays a crucial role in evaluating Apple's quality and its sweetness, the challenge addressed here is to identify a method to assess sweetness efficiently and effectively via alternative methods that are non-invasive. Among other aspects, it brings about the importance of visual indicators such as the ripeness and RGB color values being extracted from the apple images as key predictors for sweetness levels. brightening the challenges of quality assurance and consumer satisfaction in the agricultural sector. The research presented in this paper outlines a structured approach—from data collection to model evaluation—aimed at addressing the challenges of quality assurance and consumer satisfaction in the agricultural sector, leveraging AI technologies.

KEYWORDS: AI, Cross validation, Fruit sweetness, Machine learning, Linear regression.

1 Introduction

Apples are a fantastic, affordable, and tasty source of essential vitamins, minerals, and other health-boosting compounds. Given their accessibility, and health benefits, apples are definitely a go-to natural food for anyone seeking to improve their diet in a simple, delicious way. In the global agricultural sector, apple harvesting and marketing are crucial because they influence supply chain efficiency and consumer happiness. India produced 2.7 million tons of apples in 2020, placing it fifth in the world.[1]

The demand for premium apples has been rising significantly due to their extended shelf life, health benefits, and adaptability, making them one of the most consumed fruits in the world. While demand for attractive, quality apples is on the rise, key characteristics that influence the market value of apples comprise size, texture, color, and sweetness [2]. One of the most important elements in assessing an apple's market attractiveness is its sweetness. An apple's maturity, which directly affects its sweetness, can be determined by looking at its color. An apple's color changes as it ripens, depending on the type, and this is usually when the fruit's starches turn into sugars. General market surveys say that unripe apple has a lot of green and is less sweet, while a ripe apple, with its red color, tends to be much sweeter in taste. Hence, amongst these attributes, consumer sweetness preference is a vital element. Sweetness levels are controlled by genetic variety, climate, ripeness, and post-harvest handling.

Conventional approaches to sweetness measurement like refractometry and chromatography take a long time to implement. They destroy the commodity, exhibit vast destruction, and are costly, hence unsuitable for large enterprises. Refractometry is a useful and quick method to estimate sweetness by measuring sugar concentration, but it has several disadvantages. It cannot distinguish between different types of dissolved substances, so if other compounds (like salts, acids, or alcohol) are present, they can affect the reading and make it less accurate. It also doesn't work well with complex mixtures or products that aren't clear, like pulpy juices or fermented items, as suspended particles or cloudiness can interfere with light refraction. Additionally, refractometry assumes that sweetness comes only from sugar, which isn't always true — artificial sweeteners or flavor compounds can contribute to perceived sweetness but won't be detected by this method. Lastly, temperature changes can impact the refractive index, so precise control or correction is needed during measurements.

Traditional method for quantifying and determining specific sugars in food products is chromatography, especially high-performance liquid chromatography (HPLC). Chromatographic techniques separated components of mixtures according to their interactions with stationary and mobile phases. It is therefore not very useful for large-scale or real-time quality control in a commercial situation. Indeed, while providing accurate and thorough results, these disadvantages render chromatography impractical for routine sweetness measurement in large enterprises. Work continues into developing cost-effective, innovative yet non-destructive techniques that could equal the existing technologies, showing promise.

The key contribution is the development of SweetPick: a cheap, non-invasive method utilizing ML and image processing for apple sweetness prediction based on visual parameters—ripeness and RGB color values. SweetPick uses a simple webcam and linear

regression to perform real-time sweetness measurement, unlike conventional destructive methods. This has helped to increase accuracy even while significantly reducing processing time and costs. Thus, by being more efficient, cheaper, and applicable in multiple production scenarios, this contribution proposes a feasible and scalable enough framework for present-day agro quality evaluation between consumer preferences and apple quality, while also optimizing the supply chain and reducing waste economically.

2 Literature Survey

Attempts are being made to use AI and machine learning (ML) for the aforementioned problem.

According to Al Sammarraie, M.A.J and Gierz, Ł.'s study [3], in today's market, it takes a lot of effort and time to manually grade the oranges according to their maturation or taste. Some studies also find out that the degree of ripeness or sweetness based on the color of the fruit is not the same in a particular variety of fruit. Sweetness and color are the crucial parameters when it comes to the fruits' evaluation, but fruit's color might also change its perceived sweetness. Their study deals with investigating the possibility of anticipating the sugar content of orange fruits using artificial intelligence by understanding how the colors of the fruits represented in RGB relate to the sugar content of the fruits using the orange data mining tool. The experiment incorporated classification algorithms to an image dataset of orange fruit, conducted a comparison of the respective algorithms, with a view of finding out which algorithm prediction is more accurate. The finding suggested that the red color value is more important in the prediction of orange fruit's sweetness than the green and blue color values since it was found to have a positive correlation with the degree of sweetness level. In this context, the logistic regression model algorithm provided the highest level of accuracy on the predictions of sweetness content for agricultural applications.

According to Mohit Kumar, Yogesh Pal [4], the effectiveness of the brightness preserving dynamic fuzzy histogram equalization (BPDFHE) approach proposed to apply BPDFHE [5] and then compared with a host of enhancement techniques using different measures of performance parameters like Peak Signal Noise Ratio (PSNR), and Contrast Improvement, Image Segmentation Index (CII), and accuracy of image segmentation. The BPDFHE method produced comparatively higher PSNR values which underlined enhanced image quality with reduced noise and higher CII values than that of the subject learning system, thereby satisfying the conjecture that it enhances learning difference, image contrast. The high segmentation accuracy values defined by the Jaccard index and the Dice coefficient, the authors have found that the introduced BPDFHE has an improved performance in comparison to the previously initiated approaches, providing high value of a segmentation accuracy that is canonic to obtaining accurate detection of apple sweetness. The comparative study showed that BPDFHE always exhibited higher PSNR and CII than the others and from this aspect the higher segmentation and accurate rate of it reflected the more reliable identification of the sweetness pointing the importance of the approach in the image processing in agriculture.

Zheng et al. (2019) made a platform on the basis of machine learning that was termed e-Sweet, intended to forecast the sweetness of multiple compounds, including artificial sweeteners. Having large datasets and considerable algorithmic advancements, this method was implemented with multiple data-splitting approaches along with different machine-learning methods, leading to an improved accuracy for sweetness classification and regression models. Major progress has been made in this regard. [6]

According to SangSongFa et al [7], other than the considerations for ripening, the pineapple rhythm is affected by climatic conditions. However, the reproductive aspect of the environment is poorly influenced by rainfall even if it affects flowering time. Traditionally, sweet evaluations from types of fluids, such as an optical refractometer, are monetary- consuming and rely on expert judgment to define the sweetness value. The research proposes a novel way of determining the levels of pineapple sweetness levels using images and the AlexNet deep learning model for classification. The dataset- fortified into 4 levels of sweetness labelled as M1 to M4- was spliced according to the training (80%) and testing (20%). After various trials of different epochs and data augmentations, the AlexNet model produced a performance that had been balanced during 10 epochs with an accuracy of 91.78% and an F1 score of 92.31%. This method presents a more efficient automated comparison of sweetness in pineapples, with a possible huge effect in agriculture. This technology also figures in our apple project, in which fruit sweetness prediction is based on learning features extraction by a deep learning model. This emphasizes the effectiveness of convolutional neural networks.

The paper written by Hasan et al.[8] aims at the machine learning application in its models for predicting sweetness in bananas and classified diseases in fruits. Using the assessment of quality banana parameters like color, texture, and sugar content via sensors or imaging techniques, different machine learning models like Random Forest (RF), Support Vector Machine (SVM), linear discriminant analysis, k-nearest neighbors' algorithm (KNN), and classification and regression trees (CART) were employed. The analysis of these predicts the sweetness levels in RF and CART, which has proven to be very accurate concerning its practical usage in agriculture. Again, this study incorporates such digital technology to carry an all- inclusive fruit quality analysis and disease management for effective and accurate fruit cultivation. It uses a similar approach, where the models utilize machine learning algorithms to analyze data through sensors and imaging to get parameters like color and sugar content, ushering modern digitalized agriculture.

Recently, in a 2025 study by Zhao, L , Wang, X., & Cheng, H [9], researchers employed RGB mobile imaging in combination with eight different machine learning models to non-destructively predict firmness and total soluble solids (TSS) in blueberries. The predictions indicated high accuracy in all models, referring to the stability and generality of RGB-based image features in assessing fruit quality. This research further corroborates the viability of RGB imaging as a strong and non-invasive tool for the prediction of quality traits in various fruits, affirming the validity of our proposed method for predicting apple sweetness.

According to Thomas Hasing et al[10] strawberry sweetness and consumer preference are enhanced by specific volatile compounds. Improving crop flavor is challenging because of the cost of sensory evaluations and the difficulty of linking sensory experiences to chemical composition. This study sought to identify the chemical drivers of sweetness and consumer liking for strawberries (Fragaria
× ananassa). For over seven years, 148 strawberry samples were grown, harvested, and analyzed for sensory and chemical properties. Sensory panels with at least 100 participants each generated at least 15,000 data points per descriptor. The study quantified three sugars, two acids, and 113 volatile compounds. Consumer liking was strongly related to intensity of sweetness, texture, and flavor but not sourness. Analyses revealed 20 volatile compounds that enhanced sweetness perception independently of sugars, 18 that boosted liking, and 15 that influenced both. Predictive models including sugars, acids, and volatiles explained 25% more variation in sweetness and liking than models based only on sugars and acids. Key volatiles, such as γ-dodecal actone, 5-hepten-2-one (6-methyl), and medium- chain fatty acid esters, were identified as potential breeding targets. A genetic study identified two loci on linkage group 6A that regulate ester production and thus serve as markers for increasing ester content. Use of machine learning improved predictive models, which is useful in breeding and quality control strategies.

The application of machine learning techniques in predicting quality characteristics of Prunoideae fruits while concentrating on the optimization of spectral characteristics acquisition is the motive of the work done by Liu et al [11]. Machine learning models, such as support vector machines (SVM), random forests (RF), and neural networks, are incorporated to analyze the spectral data and predict the key fruit quality parameters such as sweetness, firmness, and acidity. The optimization process for acquiring spectral characteristics involves selecting the most informative wavelengths and preprocessing techniques to improve prediction accuracy. The results reflected that the optimum spectral features combined with state-of-the-art machine learning models could direct to remedies in prediction of fruit quality. Thus, this method provides an assessment of fruit quality that is fast, effective, and non-destructive, which can then be transferred into an automated sorting and grading system, thus creating a better tool for enhancing quality control and satisfaction of consumers in the agricultural industry.

In the study conducted by Kumudham et al.[12] (2023), a deep learning-based approach for predicting Brix values of strawberries by image processing and machine learning techniques is presented. The authors perform feature extraction using ResNet101 and prediction using Gaussian Process Regression (GPR), with an accuracy of 96.3142% and RMSE value of 0.4772, which is remarkable. This research highlights the efficacy of deep learning combined with image augmentation for model optimization performance over traditionally employed destructive methods like refractometers in Brix measurements. The study compares two methods: one is a custom-built CNN regression model with an accuracy value of 82.61%, while the other is the superior ResNet101-based prediction methods. In this regard, transfer learning with albeit modestly augmented data for further enhancement must be acknowledged. The work adds to the growing publication trail pertaining to AI-powered precision agriculture, especially in fruit quality prediction, while interlinking itself with on-the-go studies employing spectroscopy and machine learning (Mancini et al., 2020; Seki etal.,2023), somewhat allowing for a more conversable, scalable solution. The potential of computer vision and deep learning to establish a paradigm shift in quality control within agriculture, addressing major issues such as labor-intensive manual inspections and destructive testing, is emphasized in the paper. Through model pre-training and data augmentation, the high prediction accuracy is achieved by the authors against traditional methods and some spectroscopic ones. The metrics of R^2, RMSE, and MAE and their comparison with the existing literature make this methodology robust and pragmatic with respect to real-world applicability. Trends in smart agriculture show that AI and automation find major applications in yield prediction, disease detection, and quality assessment (Sarker, 2021; Saleem et al., 2021). The results thus confirm the role of advanced ML techniques along with agricultural practices in improving efficiency, minimizing waste, and bringing goods such as strawberries-highly perishable-to the market. Similar CNN-based approaches have shown high accuracy in palm fruit maturity classification tasks [13].

Along a similar line, Knott et al. (2022) suggested a machine learning method centered on Vision Transformers (ViTs) that can be used to assess fruit quality, i.e., apple defect classification and banana ripeness estimation. Their research demonstrated that Vision Transformers could, even with relatively small datasets, outperform traditional CNN architectures in classification accuracy and overall generalization. This study indicates the rising trend of employing data-efficient models for non-destructive fruit quality evaluation, with a special focus on the function of light but efficient models in agri-applications where hardware and data constraints prevail [14].

The following table Table 1 shows a comparative analysis of research on fruit sweetness predictions using machine learning.

Table 1 Comparative Analysis of Research on Fruit Sweetness Prediction Using Machine Learning Techniques

S.NO	Paper Title(Year)	Fruit	Methodology	Salient Features	Advantages/ Disadvantages
1	Apple Sweetness Measurement and Fruit Disease Prediction(2022)[4]	Apple	Data Collection, Preprocessing: Filtering images Segmentation, Feature Extraction, Classification: Using four classi- fiers, with k-nearest neighbors (k-NN)	Use of BPDFHE for image enhancement. Classification of diseases such as apple scab and Marsonina coronaria. Analysis of textural properties for predicting fruit sweetness. High accuracy classification with in k-nearest neighbours. On an independent testing dataset the overall accuracy of the classifier was 77.67 percent for distinguishing between apple quality	**Advantages:** Improved image quality with BPDFHE. Accurate classification of diseases. Effective prediction of fruit sweetness based on texture analysis. High performance of k- nearest neighbors in classification tasks. **Disadvantages:** Limited to apple orchards in specific Indian states. Dependence on image quality and preprocessing steps.
2	Predicting Fruit's Sweetness Using Artificial Intelligence :Case Study: Orange [3]	Orange	Identifying Effective Color, Algorithm Selection, Relationship, Determination.	Use of RGB values from digital images to predict sweetness. Image acquisition, capturing images from multiple angles. Analysis and processing of RGB values using ImageJ software	**Advantages:** Non-Invasive, Accuracy, Accessibility **Disadvantages:** Dependence on Equipment
3	Prediction of Pineapple Sweetness from Images Using Convolutional Neural Network (2018)[7]	Pineapple	Alexnet deep learning model, Data Preparation Experiment was repeated five times with distinct epochs.	Accuracy and F1 Score: The Alexnet model achieved an accuracy of 91.78% and an F1 score of 92.31%. Classification Accuracy: The study focused on classifying pineapple sweetness levels accurately using deep learning.	**Advantages:** High accuracy and F1 score. **Disadvantages:** The methodology relies heavily on image data

4	Using Machine Learning Algorithms to Predict the Sweetness of Bananas at Different Drying Times(2024)[8]	Bananas	Sample Preparation: Banana slices collected from local markets in Baghdad, Iraq, of the Cavendish variety, were used. Drying Process: An electric food dehydrator was used to dry banana slices at three different times (6, 8, and 10 hours). Prediction Accuracy: The RF and CART algorithms gave the highest prediction accuracy.	There is a direct relationship between CIE-Lab levels and sweetness. The RF and CART algorithms gave the highest prediction accuracy of 86%.	**Advantages:** High prediction accuracy **Disadvantages:** Potential variations in prediction accuracy based on different drying times and methods.
5	Strawberry sweetness and consumer preference are enhanced by specific volatile compounds(2021)[10]	Strawberry	Sample Collection and Analysis, Data Analysis, Predictive Models	Volatile Compounds, Genetic Association,	**Advantages:** Identification of specific volatile compounds **Disadvantages:** High complexity and cost associated with large-scale sensory
6	Prediction of Prunoideae Fruit Quality Characteristics Based on Machine Learning and Spectral Characteristic Acquisition Optimization(2024)[11]	Prunoidae	Machine Learning Algorithms: XGBoost, LightGBM, CatBoost, Random Forest Spectral Data Acquisition: Hyperspectral imaging	Accuracy: The MLP-SG-XGBoost model produced the best SSC predictions for peach and apricot with R^2 values of 0.9162 and 0.9251, respectively.	**Advantages**: High Accuracy Non-Destructive Testing, Feature Extraction **Disadvantages:** Complexity: The process of data acquisition, preprocessing, and model training is complex and computationally intensive.

7	Using Deep Learning-Based Features and Image Augmentation to Predict Brix Values of Strawberries for Quality Control[12]	Strawberry	**Method 1(Baseline Approach):** Custom CNN Regression Model: A 24-layer convolutional neural network (CNN) is trained directly on the original dataset of 150 strawberry images and their corresponding Brix values. Uses 200 epochs, a mini-batch size of 10, and the RMSprop optimizer with a learning rate of 0.001. **Method 2 (Enhanced Approach):** ResNet101 + GPR Model: The original dataset of 150 images is augmented to 300 images using techniques like scaling, rotation, and reflections. Utilizes the pre-trained ResNet101 model to extract high-level features from the augmented images. Multiple machine learning regression models (Linear, SVM, Tree, GPR) are trained on the extracted features. The Squared Exponential Gaussian Process Regression (GPR) model is identified as the best performer.	150 strawberry images captured using a Logitech C920 HD camera under controlled studio conditions. Corresponding Brix values measured using a refractometer. ResNet101, a deep CNN pre-trained on ImageNet, is used to extract 1000 features per image. Performance: The Method 1 (Baseline Approach) achieves an accuracy of 82.6071% with an RMSE of 1.2036 and an R^2 value of 0.0787. The Method 2 (Enhanced Approach) achieves an accuracy of 96.3142% with an RMSE of 0.4772, an R^2 value of 0.8648, and an RPD value of 2.7.	**Method 1 (Custom CNN Regression)** **Advantages:** Uses a straightforward CNN architecture without complex preprocessing. Trains from scratch, avoiding biases from external datasets. **Disadvantages:** Performs worse than Method 2 in predicting Brix Small dataset (150 images) without augmentation may lead to overfitting. **Method 2 (ResNet101 + GPR)** **Advantages:** Superior performance due to deep feature extraction and augmentation. Augmented dataset (300 images) improves robustness. **Disadvantages:** Requires more processing power for ResNet101 feature extraction. Relies on pre-trained models, which may not always be optimal for agricultural data.

The survey presented laid a sound foundation for machine learning model training and testing to ensure valid and reliable predictions. The integration of AIML with agricultural technologies enhances quality assurance and control, improves supply chain management, and increases consumer satisfaction. In its way, this offers an insight into the application of cutting-edge technology so that modern-day agricultural goals may be met, thus providing inspiration for innovation in the agricultural sector.

3 Methodology

This innovative system applies the contemporary technologies and algorithms for image processing and machine learning for fast and non-invasive predictions of apple sweetness levels predicated on size and color, consistent with recent hybrid models combining CNNs and transformers for fruit quality assessment [15]. The application integrates modules for capturing images which gracefully link with other related modules, initial data processing, feature extraction and the use of data for machine learning predictions, the system in place guarantees proper real time evaluation is given. This capability empowers fruit quality control stake- holders to take correct decisions quickly and adequately.

It is contrasting with other conventional techniques, such as High-Performance Liquid Chromatography, HPLC methods such as Chromatography (HPLC) or spectroscopy [16] which is laborious, expensive and time consuming, and necessitating destructive sampling, and can be addressed by our solution transformative approach. Instead, these cumbersome techniques are replaced by affordable and easily manageable solutions that could be effectively used in large-scale fruit production facilities. This shift brings an optimization

of operations within the country and enhances total yield and profitability concerning agriculture in the country.

By using machine learning based big data sets, which have attributes such as ripeness and RGB extracted from pictures and images, our system guarantees the compliance and accuracy of defined sweetness predictions. This technology gives life to designed technology and fulfills stiff requirements of contemporary fruit production and raises the bar as to the quality assurance in agriculture.

3.1 Algorithms

Linear Regression: Linear Regression [17][18]is used as the model of prediction in this script. Linear regression is an elementary supervised learning algorithm applied extensively to describe the relationship between an independent variable and one or more independent variables. It predicts an equation of best fit to the data observed, permitting predictions of outcomes in terms of suitable input features. Linear regression supposes a linear rate of change and is appreciated for its ease of use, interpretability, and popularity across regression tasks. As a foundational technique, linear regression frequently is a trustworthy reference point in predictive modeling.

Hence, it puts forward a hypothesis that has a positive straight-line relationship between the independent variability of the dependent parameters (such as the ripeness and the measuring in RGB colors), control variable (bitterness), dependent variable (sweetness). Twenty- eight coefficients are learned and utilized in the model to give the best fit certain aspects of this intersection and make conclusions as to sweetness categories on the basis of feature's descriptions on the models.

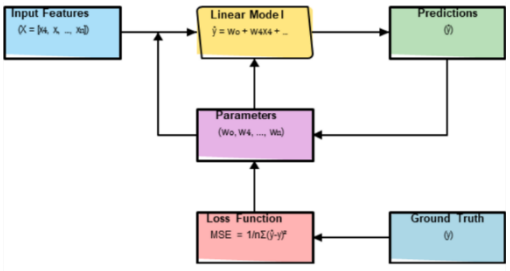

Cross-Validation: Cross Validation [19] is used here for the intent of getting a model that would perform the Linear Regression model. Similarly, the script applies K-fold Cross- Validation with cv = 5, this means that the set is split into folds or subset of data known as k=5. For training purposes four folds are used while onefold is utilized for validation.

This way it assesses its performance against the right set of metrics similar to the RMSE measurement that would not change its sign to the opposite – it is a non-negative measure. Therefore, the examined option of dividing the training and testing data splits might be favorable with respect to the occurrences that happened.

Fig. 1. Architecture of Linear regression

The subsequent resolution proposed—linear regression and image analysis from the RGB perspective—was selected based on its low cost, interpretative ease, and ease of calculation. As opposed to deep learning models that involve the use of massive data, fast GPUs, and long training times, linear regression presents a cheap yet effective solution that far exceeds what small-scale agricultural setups can manage. RGB color features were used given that apple color and sweetness/ripeness are strongly correlated from which the literature suggests. The RGB data are also easily obtainable using low-cost hardware (off-the-shelf webcams), which makes the method scalable and within reach for farmers and traders in limited resources settings, which is in line with our goal of creating a non-destructive, real-time, and low-cost fruit quality assessment tool.

3.2 System Architecture

The architecture of Proposed system called SweetPick is shown in Figure 2. The workflow is as follows:

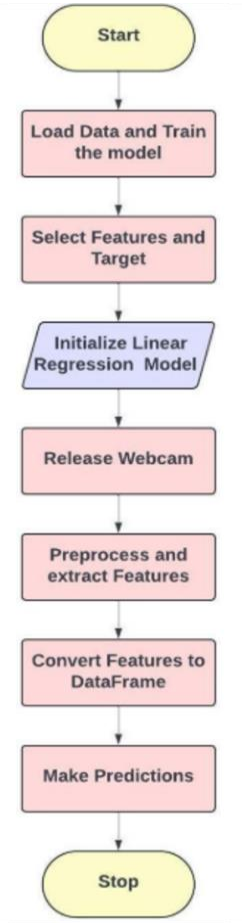

Fig. 2. SweetPick Architecture

Work Flow

Data Loading and Preprocessing: Fruit quality features like ripeness, RGB color value are in another CSV dataset and prepro- cessed. Non numerical values are also handled, and all the features are rescaled using StandardScaler[20] with plan and imaging scale.[21]

Model Training: The split of the training and the test data set is done by using the code train-test split from sklearn.model selection. The next step regards the Linear Regression model: it is from sklearn. linear_model and its training data are the above-identified training data.

Cross-Validation: It (from sklearn.model_selection: cross_val_score()) is used to measure the model based on training data. The taken MSE are negative and then changed into RMSE to ensure better understanding.

Model Evaluation: Last of all, the trained model is tested on the test data set to find the RMSE and highlighting how the model factors on the unseen data.

Real-time Feature Extraction: In line with the applications of OpenCV[22] and scikit-image [23], ripeness and the average RGB value of the captured live stream video via webcam are identified. These features are then implemented to predict the outcome using the developed Linear Regression model.

Thus, it is established that the combination of Linear Regression for prediction and Cross-Validation for performance can handily empower the developed model to predict sweetness levels of fruits by taking images as inputs based on the specific input visual features, a direction consistent with recent work utilizing CNNs and transformer-based architectures for fruit maturity classification[24]. Besides it, this project provides a very cheap and non-harmful way as compared to traditional methods and also proves that machines can learn to improve the agricultural process.

The dataset was normalized using z-score normalization to ensure that all the features scaled by an average of 0 and a standard deviation of 1. This ensured uniform contribution from all features towards the model, thus removing bias caused by the magnitude of various features. Missing values were replaced with the mean, and non-numeric values were filtered out to remove inconsistency in the data. The target variable, sweetness, was also validated for valid ranges.

A Linear Regression model was implemented to predict the fruit sweetness, given input features. Its coefficients were optimized by minimizing Mean Squared Error. Better interpretability of the result was achieved in the units of the target variable utilizing Root Mean Squared Error for performance evaluation. To ensure robustness and generalizability, it has been cross validated at k=5 folds level by computing the RMSE values for each separately and averaging them to give an unbiased estimate of model performance.

$$y = \beta_0 + \beta_1 x_1 + \beta_2 x_2 + \cdots + \beta_n x_n \quad (1)$$

$$\text{MSE} = 1/\text{N} \sum_{i=1}^{N} (y_i - \hat{y}_i)^2 \quad (2)$$

$$\text{RMSE} = \sqrt{\text{MSE}} \quad (3)$$

y_i : Actual value

$\hat{y}_i$: *Predicted value*

Categories for sweetness were defined in terms of percentile thresholds. Calculating 25th and 75th percentiles for the target variable enabled the three classifications for predictions: Less Sweet (<25%), Moderately Sweet (25%–75), and Very Sweet (>75%). It provided a method of classification of predictions that made the outputs from the model easier to apply practically to the real world.

Image-based feature extraction was significant in fruit sweetness prediction. The mean RGB values of the fruit's surface were computed along with a dummy to represent color characteristics. Normalization of these features was done using similar scaling parameters used for the training data. The regression model then used the extracted and normalized features to predict sweetness using the derived linear equation. This integration of preprocessing, statistical modeling, and image analysis provides an automated and efficient approach to fruit quality assessment.[25]

$$\text{Color}_R = \frac{1}{N}\sum_{i=1}^{N} R_i \,, \text{Color}_G = \frac{1}{N}\sum_{i=1}^{N} G_i \,, \text{Color}_B = \frac{1}{N}\sum_{i=1}^{N} B_i \quad (4)$$

$$\hat{y} = \beta_0 + \beta_1 \text{Color}_R + \beta_2 \text{Color}_G + \beta_3 \text{Color}_B \quad (5)$$

4 Results

Fig. 3. Input images for (a)less sweet, (b)moderately sweet, (c) very sweet apples and output images for (d)less sweet, (e)moderately sweet, (f) very sweet apples

5 Graphics

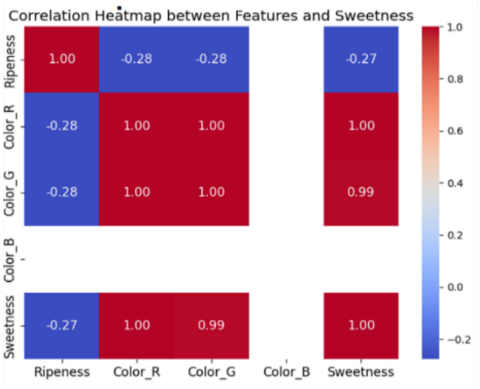

This heat map illustrates how different attributes, including ripeness, Colour_R, Colour_G, and Colour_B, relate to an apple's sweetness. Important conclusions include:

Ripeness versus Sweetness: There is a somewhat negative connection (-0.27) between sweetness and maturity, suggesting that sweetness may somewhat decline as ripeness varies.

Components of Colour:

1. There is a perfect positive correlation (1.00) between sweetness and Colour_R.
2. There is a significant positive association (0.99) between sweetness and Colour_G.
3. There is a perfect positive correlation (1.00) between sweetness and Colour_B.

Fig. 9. Heat map representing correlation between features (ripeness and RGB values) and sweetness

Although ripeness has a lesser and inverse relationship with sweetness, the color components of an apple, particularly the red and blue channels, have a substantial impact on its sweetness [26]. This suggests that colours play a more significant role in determining sweetness than ripeness does.

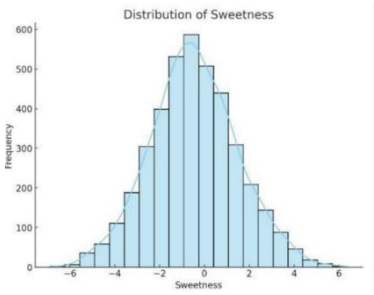

Fig. 10. Sweetness Value Distribution in Apples

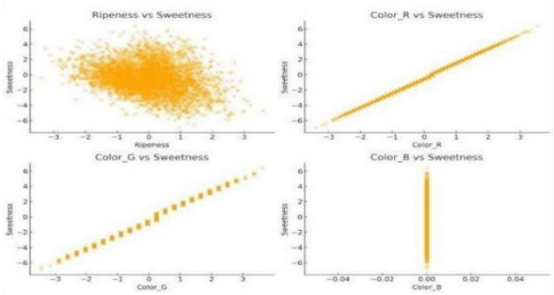

Fig. 11. Scatter plots for Ripeness vs Sweetness Correlation and RGB vs Sweetness Relation

The Sweetness Distribution graph provides an overview of how sweetness values are spread across the dataset, combining a histogram and a kernel density estimate (KDE). The histogram's bars show the frequency of sweetness values within specific ranges, while the KDE curve offers a smoothed, continuous representation of the data's distribution, highlighting common sweetness levels and overall patterns. This visualization helps identify whether the distribution is symmetric or skewed, revealing potential outliers or biases. Peaks in the KDE indicate the most frequent sweetness levels, while the spread of values reflects variability. Unusual patterns, such as multiple peaks, could suggest distinct subgroups within the dataset.

The **Feature Relationships with Sweetness** scatter plots depict the associations between each feature—**Ripeness**, **Color_R**, **Color_G**, and **Color_B**—and the target variable, **Sweetness**. Each plot visualizes individual data points, with the x-axis representing a feature and the y-axis showing sweetness values, revealing trends, correlations, and patterns. For example, ripeness may exhibit a positive correlation with sweetness, suggesting that sweeter fruits are often riper. Similarly, the RGB color components can indicate trends, such as redder fruits being sweeter. Positive or negative correlations are reflected in upward or downward trends, while random scatters suggest no clear relationship. These plots also highlight outliers, which could signify anomalies, and clusters, which might indicate subgroups with similar properties. Such insights are vital for understanding how these features influence sweetness and identifying potential predictors in the dataset.

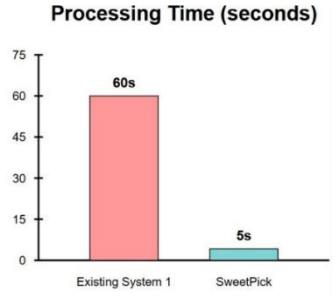

Fig. 12. Processing Time Comparison: Traditional Methods vs. AI- Based Apple Sweetness Prediction.

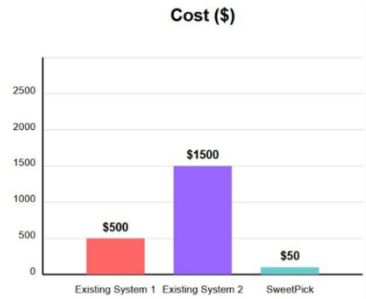

Fig. 13. Cost Comparison: Traditional Methods vs. AI- Based Apple Sweetness Prediction

The bar chart in Fig.12. centers on the metric of processing time, with the current system (in red) taking 60 seconds of processing time [4] and the new AI system (in teal/turquoise) taking merely 5 seconds of processing time. The AI system cuts down processing time from 60 seconds to 5 seconds, delivering a 92% speedup. The bar chart in Fig.13. illustrates the cost difference between the current systems and the present artificial intelligence system under consider- ation for the measurement of the sweetness in fruits. The cost is $500 for Existing System 1 [4] while Existing System 2 [11] is considerably high as it reaches $1,500. According to this survey, the Proposed AI System is incurred under a much lower cost of $50, which makes it economically better than both existing methods.

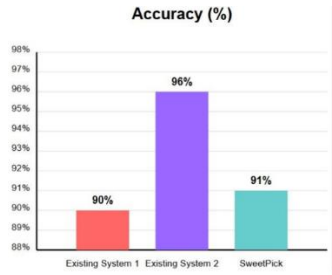

Fig. 14. Accuracy Comparison: Traditional Methods vs. AI- Based Apple Sweetness Prediction

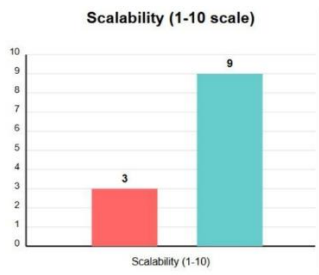

Fig. 15. Scalability Comparison: Traditional Methods vs. AI- Based Apple Sweetness Prediction

The bar chart in Fig.14. compares the accuracy result between two existing systems and the proposed AI system for fruit quality classification. Existing System 1[4] has an accuracy of 90%, Existing System 2 [11] shows an accuracy of 96%, whereas in the Proposed AI System, the accuracy is 91%, which shows a somewhat better percentage over Existing System 1 but a little lower than Existing System 2. The bar graphin Fig.15. shows the scalability of the current system [4] (conventional invasive fruit sweetness measurement methods) compared to the suggested AI-based system on a scale of 1 to10. The current system scores low with a scalability grade of 3/10, while the AI- based system attains a far higher scalability mark of 9/1.

Various salient features make this AI system really efficient and feasible in comparison to other ones. These systems now take an extraordinary 60 seconds, while the proposed one dramatically reduces processing time to just 5 seconds, thus maintaining the real-time validation that is crucial for user-centric applications. Thus, because of this processing speed, the new system acts faster and is more responsive, resulting in a better user experience.

This ensures that the proposed system is extremely cost-effective. With a total cost of merely $50, including basic hardware-components such as a webcam, it represents a huge saving on $500 for Existing System 1 and $1500 for Existing System 2, which require expensive GPU-based support.

Therefore, a low-cost setup should be strategically implemented in numerous less-endowed settings. With regard to precision, this system comes at 91%, which gives a fair competition against Existing System 1 (90%) and lags just behind the superior Existing System 2 (96%).

One of its unique highlights is the system's scalability, which has received a score of 9 out of 10, contrasted to a very low score of 3 on existing systems. This further supports the system's flexibility in coping with larger data sets, varying environments, and future technological needs with very little added effort.

A significant advancement is observed in the Root Mean Square Error (RMSE), where the proposed method achieves a value of 0.055, substantially lower than the 0.4772 of the existing method — showcasing its superior performance in minimizing prediction errors[11]. Additionally, the modular and efficient design of the proposed approach supports better scalability, allowing it to handle larger datasets or increased complexity without major redesign, making it a robust and future-ready solution.

The uniqueness of this proposed SweetPick system is derived from the simplicity of its image-based features, specifically RGB color values and ripeness, detected using a standard webcam to estimate sweetness non-destructively and in real time, based on a linear regression model that is not computationally heavy. Previous systems have relied solely on expensive, destructive methods of estimating sweetness or computational, deep learning models used offline with a series of costly smartphone applications. This method has the advantage of being affordable, transparent, and easy to understand and to adopt. A framework of real-time feature extraction with low-resource computing that has been used in producing fruit quality assessments and is sustainable with quick processing times makes this novel. It can be fairly suggested that there are unique scalabilities (i.e., developing low-barrier and cost), especially with the advances in agricultural hardware development for low-resource rural communities.

6 Future Scope

Future research can focus on enhancing non-invasive sweetness prediction by leveraging advanced imaging techniques, such as RGB-based computer vision, to extract more refined color and texture features. Machine learning and deep learning models, including convolutional neural networks (CNNs) and transformer-based architectures, can further improve prediction accuracy by identifying complex visual patterns related to fruit ripeness and sugar content. Real-time monitoring and automation in sorting and grading systems can revolutionize large-scale agricultural operations, making quality assessment more efficient. Expanding this methodology to other fruits like mangoes, grapes, and peaches can improve overall produce quality control. Integration with IoT-based smart farming techniques can enable real-time data collection and predictive analytics, helping farmers make informed decisions. Additionally, the development of mobile applications or portable imaging devices can empower both farmers and consumers to assess fruit sweetness conveniently. By reducing the need for destructive testing, this approach can also contribute to sustainability efforts by minimizing food waste and optimizing supply chain efficiency, ensuring a reliable and scalable solution for quality assurance in the agricultural sector.

7 Conclusion

For the modernization of fruit sweetness measurement, the present research suggests real-time, non-destructive prediction of fruit

sweetness through machine learning and computer vision. In contrast to the conventional refractometry and high-performance liquid chromatography, which is time-consuming, expensive, and not efficient in dynamic farming environments, the new approach makes use of RGB values and maturity characteristics gathered from off-the-shelf webcams with free libraries like OpenCV and scikit-learn.

7.1 Prominent Salient Features:

Non-Destructive Assessment at a Cost: The entire project is based around the usage of webcams for real-time image capturing; hence expensive equipment and destructive sampling methods need not be implemented in the operation [22]. This operation was a cost saver and also preserved fruit integrity, allowing the assessment to be done in repetition without waste.

Scalability and Flexibility: The demonstrated scalability of the developed system in new varieties of fruits and different production conditions, as applied during quick assessments in the field-like orchards or transporting fruits, can deliver ac- tionable information related to the quality along the supply chain.

Precision and Effectiveness: After extensive model training and cross-validation techniques, the project accurately modeled the prediction of sweetness in fruits. Linear regression models related to standard scaling made the assessments more reliable and prepared for the decision-making process in fruit quality management.
Integrative Operations: Even more important is the efficiency of the system in feature extraction from real-time images and the prediction of 'Less sweet,' 'Sweet,' or ‘Sweeter' in real-time.

This work contributes to the development of SweetPick, a low-cost, non-invasive, real-time AI system for measuring fruit sweetness from RGB color and ripeness information. As a viable replacement for traditional methods such as refractometry and chromatography, which are expensive, time-consuming, and invasive, the suggested approach proves that it is possible to predict sweetness using cost-efficient, low-weight technologies. The research indicates the scalability in the use of precision agriculture and further supports the future role of AI in boosting fruit quality evaluation.

Acknowledgments. The writers, with hearts full of gratitude, wish to thank God Almighty for his kind blessings and guidance upon their undertaking of this project. We truly thank Dr. B.G. Prasad, our beloved principal, who has provided us with resources and assistance needed at times.

We would like to thank Dr. Rashmi S., Head of the Department of Computer Science Engineering (Data Science), for her inspiration, steady support, and insightful advice, which were all necessary to complete this project.

We wish to extend our heartiest thanks to the Department of Computer Science Engineering (Data Science) Teaching and Non-Teaching Staff for their co-operation, as well as to all those who supported us in this venture to make it a success.

We would also like to thank our family members and friends for their encouragement and unrelenting support towards all our endeavors.

REFERENCES

1. Apples & India homepage, https://applesandpeople.org.uk/india/,last accessed 2025/4/10

2. Stefano Musacchi, Sara Serra:” Apple fruit quality: Overview on pre-harvest factors”, Department of Horticulture, Tree Fruit and Research Extension Center (TFREC), Washington State University, 1100 N.

3. Al Sammarraie, M.A.J.; Gierz, Ł.; Przybył, K.; Koszela, K.; Szychta, M.; Brzykcy, J.; Baranowska, H.M.: “Predicting Fruit's Sweetness Using Artificial Intelligence - Case Study: Orange,” Applied Sciences, vol. 2022 (2022).

4. Mohit Kumar, Yogesh Pal, Syam Machinathu Parambil Gangadharan, Koushik Chakraborty, Chandra Shekhar Yadav, Harish Kumar, and Basant Tiwari: “Apple Sweetness Measurement and Fruit Disease Prediction Using Image Processing Techniques Based on Human-Computer Interaction for Industry 4.0,” Wireless Communications and Mobile Computing,vol. 2022 Article ID 5760595 (2024).

5. Boyina Subrahmanyeswara Rao: "Dynamic Histogram Equalization for Contrast Enhancement for Digital Images," Applied Soft Computing Journal, vol. 89, 2020, Article ID 106114 (2020).

6. Zheng,` S., Chang, W., Xu, W., Xu, Y., & Lin, F. (2019). e-Sweet: A machine-learning based platform for the prediction of sweetener and its relative sweetness. Frontiers in Chemistry, 7, 35

7. Sangsongfa, Adisak, Am-Dee, Nopadol, and Meesad, Phayung,: “Prediction of Pineapple Sweetness from Images Using Convolutional Neural Network,” EAI Endorsed Transactions on Context-aware Systems and Applications, vol. 7, no. 165518 (2018)..

8. Al-Mashhadany , Haider Ali Hasan, Mustafa A.J. Al-Sammarraie,”: Using Machine Learning Algorithms to Predict the Sweetness of Bananas at Different Drying Times “, Journal of Ecological Engineering,25(6), (2024)

9. Zhao, L., Wang, X., & Cheng, H. (2025). Image-Based and ML-Driven Analysis for Assessing Blueberry Fruit Quality. Heliyon, 11(3), e22567.

10. a, Tomas Hasing, Timothy S. Johnson, Drake M. Garner, Michael L. Schwieterman, Christopher R. Barbey, Thomas A. Colquhoun,Charles A.Sims, Marcio F. R. Resende, Vance M. Whitaker,:”Strawberry sweetness and consumer preference are enhanced by specific volatile compounds", Horticulture Research,(2021)

11. Xuan Liu, Juan Wang, Hao Wang, Yirui Huang, Zhenhui Ren,:”Prediction of Prunoideae Fruit Quality Characteristics Based on Machine Learning and Spectral Characteristic Acquisition Optimization”,Food Control, Volume 165,(2024)

12. Ameetha Junaina T. K, R. Kumudham, Ebenezer Abishek. B, Mohamed Shakir,:”Using Deep Learning-Based Features and Image Augmentation to Predict Brix Values of Strawberries for Quality Control”, International Journal of Engineering Trends and Technology, Volume 71 Issue 7, (2023)

13. M. Han and C. Yi, “Deep Convolutional Neural Networks for Palm Fruit Maturity Classification,” arXiv preprint arXiv:2502.20223, Feb. 2025.

14. Knott, M., Perez-Cruz, F., & Defraeye, T. (2022). Facilitated Machine Learning for Image-Based Fruit Quality Assessment. arXiv preprint arXiv:2207.04523.

15. P. Gómez, E. A. Muñoz, and L. S. Ramos, “A general machine learning model for assessing fruit quality using deep image features,” Sensors, vol. 25, no. 4, pp. 1541–1555, 2025.

16. Khayelihle Ncama, Umezuruike Linus Opara , Samson Zeray Tesfay Olaniyi Amos Fawole, Lembe Samukelo Magwaza,: "Application of Vis/NIR spectroscopy for predicting sweetness and flavour parameters of ‘Valencia’ orange (Citrus sinensis) an ‘Star Ruby’ grapefruit (Citrus x paradisi Macfad)," Journal of Food Engineering, vol. 193, (2016).

17. Mengyu Huang,:“Theory and Implementation of Linear Regression”, International Conference on Computer Vision, Image and Deep Learning (CVIDL), (2020)

18. M. A.Cliff, M. C. Dever, J. W. Hallb & B. Girard: “Development and evaluation of multiple regression models for prediction of sweet cherry liking”, Food Research International, Vol. 28, No. 6, pp. 583-589, (1996).

19. Daniel Berrar: "Cross-Validation," Encyclopedia of Bioinformatics and Computational Biology, 2nd edition (Elsevier), Preprint submitted May 10, (2024).

20. Lucas B.V. de Amorim, George D.C. Cavalcanti, Rafael M.O. Cruz: The choice of scaling technique matters for classification performance, Applied Soft Computing,Volume 133,(2023)

21. Umme Sara, Morium Akter, Mohammad Shorif Uddin: "Image Quality Assessment through FSIM, SSIM, MSE and PSNR—A Comparative Study," Journal of Computer and Communications, vol. 7, (2019)

22. Kari Pulli, Anat oly Baksheev, Kirill Kornyakov, and Victor Eruhimov: “Real-Time Computer Vision with OpenCV”, Communications of the ACM, vol. 55, no. 6, pp. 61–70, (2012).

23. Stefan van derWalt, Johannes L. Schonberger, Juan Nunez-Iglesias, Francois Boulogn, Joshua D.Warner, Neil Yager, Emmanuelle Gouillart, Tony Yu and the scikit-image contributors: “scikit-image: image processing in Python”, PeerJ, vol. 2, e453, June 2014. DOI: 10.7717/peerj.453

24. P. Nahak, D. K. Pratihar, and A. K. Deb, “Tomato maturity stage prediction based on Vision Transformer and deep convolution neural networks,” Health Information Science and Systems, vol. 13, 2025.

25. Cristóbal Garrido-Novell, Dolores Pérez-Marin, Jose M. Amigo, Juan Fernández-Novales, Jose E. Guerrero, Ana Garrido-Varo: “Grading and color evolution of apples using RGB and hyperspectral imaging vision cameras”, Journal of Food Engineering, (2012).

26. FJ.Francis: “Quality as influenced by color", Food Quality and Preference 6, (1995)

27. Lembe Samukelo Magwaza, Umezuruike Linus Opara: Analytical methods for determination of sugars and sweetness of horticultural products—A review,Sci- entia Horticulturae,Volume 184, January (2015)

Cataract Detection Using Deep Learning Leveraging Fundus and Anterior Eye Images

Savu P Sudheep[1], Dr. K.K Sherly[1], and Dr. Jithin Mathews[1]

[1]Rajagiri School of Engineering And Technology, Kakkanad, Kerala, India
savupsudheep@gmail.com,
sherlykk@rajagiritech.edu.in,jithinm@rajagiritech.edu.in

Abstract. Cataract remains one of the leading causes of vision impairment worldwide, highlighting the need for accurate and early detection methods. This study proposes a deep learning-based approach for cataract classification using two distinct ophthalmic image modalities: fundus images and anterior eye images. Unlike conventional end to end classification models, this work focuses on extracting deep features from images using pretrained convolutional neural networks VGG16 and ResNet50 followed by classification using a Multi-Layer Perceptron (MLP). Experiments were conducted separately on both datasets, enabling a comparative analysis of the performance of VGG16 and ResNet50 feature extractors across different image types. The results demonstrate that deep feature extraction combined with MLP classification offers high accuracy for cataract detection, with ResNet50 generally outperforming VGG16 in most scenarios. The proposed system achieved a precision of 91.8% and recall of 91% on the anterior eye image dataset, and a precision of 96% and recall of 96% on fundus images using ResNet50-MLP. This highlights the potential of feature-based deep learning pipelines in ophthalmic diagnosis, particularly when working with limited data.

Keywords: Cataract detection, deep learning, fundus images, anterior eye images, vgg16, resNet50, mlp.

1 Introduction

Cataract is a major cause of visual impairment and blindness worldwide, especially among the elderly. It occurs due to the gradual clouding of the eye's natural lens, which leads to a decline in vision quality and, if untreated, can result in complete loss of sight. Conventional cataract diagnosis methods, such as slit-lamp examinations, rely heavily on clinical expertise, making them time-consuming, subjective, and less accessible in remote or resource-limited areas. With the rise of deep learning in medical imaging, automated cataract detection has become a promising alternative. However, many existing approaches require large datasets and significant computational resources, as they train complex models directly on raw images. In this work, a feature-based approach is adopted: deep features are extracted from images using pre-trained convolutional neural networks

(CNNs), and classification is performed using a lightweight Multi-Layer Perceptron (MLP). This study focuses on a simple and efficient approach that avoids the need to train large deep learning models from scratch. Instead, it uses pre-trained models to extract features and then applies a lightweight classifier. This method is faster, requires less computational power, and can be helpful in places where advanced medical equipment or expert doctors are not easily available. The results of this study show that using deep features with a simple classifier can still give reliable results, making it a practical option for cataract detection.

2 Literature Review

2.1 Deep Learning-Based Methods

Convolutional Neural Networks (CNNs) have formed the foundation of recent advances in cataract detection through fundus imaging. A trend across studies is the move toward combining architectures and incorporating training enhancements to improve model robustness and precision.

Hasan et al. [2] exemplified this with DIA-VXNET, a dual-model framework merging XceptionNet and VGG16 through a feature fusion layer. This integration significantly boosted classification accuracy, suggesting that architectural synergy can yield more discriminative feature sets. Another direction explored by Jabber et al. [4] involved improving training stability by employing dropout and batch normalization in a multi-layer CNN, which effectively reduced overfitting a common challenge in medical imaging.

Custom architectures tailored to fundus images also show promise. Junayed et al. [5] introduced CataractNet, a model optimized to reduce false positives, particularly useful in early screening scenarios. Complementing this, Simanjuntak et al. [13] demonstrated that fine-tuning convolutional depth and kernel size can substantially improve precision without requiring additional data.

Transfer learning has emerged as a practical tool, especially when large annotated datasets are unavailable. Babaqi et al. [1] conducted a comparative study across CNN architectures, underscoring the value of pre-trained networks in such scenarios. Expanding on this, Wu et al. [15] integrated attention mechanisms for improved explainability, aligning model focus with clinically relevant regions. Similarly, Olaniyan et al. [10] emphasized transparency by incorporating hybrid models aimed at building trust with clinicians.

Collectively, these studies suggest that optimizing both architecture and interpretability can significantly advance the clinical viability of cataract detection systems. Building upon these advances, the present study investigates a CNN-based feature extraction approach across fundus and anterior eye images using lightweight MLP classifiers, contributing a comparative evaluation of modality-wise performance.

2.2 Hybrid and Transformer-Based Approaches

While CNNs have been the mainstay of medical image analysis, researchers are increasingly turning to hybrid and transformer-based models for their ability to

model complex spatial and sequential patterns. These newer approaches seek to capture contextual information and long-range dependencies that conventional CNNs may overlook.

For example, Nagy and Alsalamah [9] developed CataractNetDetect, a fusion-based model that aggregates multiple feature representations from fundus images. Their model performed robustly even under varied image quality conditions, showcasing the strength of ensemble learning in real-world applications. Padalia et al. [11] extended this line of work by integrating CNNs with LSTMs to capture both spatial and temporal dependencies — a critical step for video-based or time-sequenced imaging.

Yadav and Yadav [16] addressed another key aspect of model refinement fine-tuning. By unfreezing and training deeper layers within transfer learning setups, especially with high-resolution images, they significantly enhanced cataract classification performance. This approach highlights the importance of depth-aware adaptation over generic transfer learning.

Although transformer-based models remain underutilized in ophthalmology, their success in natural language processing and general vision tasks makes them promising candidates for future work. With their ability to model global attention, transformers may offer a breakthrough in understanding spatial relationships in both fundus and anterior eye images particularly when combined with existing CNN features.

2.3 Advancements in Fundus and Anterior Eye Imaging

The integration of multiple imaging modalities is reshaping cataract diagnosis by providing a more comprehensive view of the eye. Fundus and anterior eye images capture different anatomical features, and when used together, they can improve diagnostic accuracy and severity grading.

Son et al. [14] pioneered a dual-input CNN that processes both slit-lamp and retro-illumination images. Their model achieved high accuracy in cataract severity grading, underscoring the benefit of combining heterogeneous data sources. Similarly, Hu et al. [12] introduced a lightweight, mobile AI system for analyzing slit-lamp images captured via smartphones. This solution addresses the need for accessible, low-cost diagnostic tools in underserved regions.

Collectively, these studies suggest that optimizing both architecture and interpretability can significantly advance the clinical viability of cataract detection systems. Building upon these advances, the present study investigates a CNN-based feature extraction approach across fundus and anterior eye images using lightweight MLP classifiers, contributing a comparative evaluation of modality-wise performance. Unlike prior works that introduced complex or ensemble architectures, this study focuses on a straightforward transfer learning pipeline to explore the classification capabilities of two pre-trained models—VGG16 and ResNet50—when applied independently to different ophthalmic modalities. This design choice emphasizes practical deployment potential and interpretability over architectural novelty.

3 Proposed Model

3.1 Overview

This study proposes a deep learning-based framework for automated cataract detection using both fundus and anterior eye images. Pre-trained convolutional neural networks (VGG16 and ResNet50) are employed to extract relevant features from the images. These extracted features are then classified using a Multi-Layer Perceptron (MLP) model. The performance of different CNN-MLP combinations is evaluated and compared across the two image modalities to identify the most effective approach for cataract detection.
The selection of VGG16 and ResNet50 as feature extractors is driven by their proven success in medical imaging tasks. VGG16 is known for its simplicity and uniform architecture, enabling effective learning of edge-level and mid-level features. In contrast, ResNet50's residual connections allow for deeper architectures without the vanishing gradient problem, which enhances the learning of abstract and complex representations such as cataract severity.

The Multi-Layer Perceptron (MLP) is selected as the classifier due to its ability to learn complex decision boundaries from extracted features. Its fully connected architecture efficiently maps the high-dimensional feature vectors to class probabilities, ensuring accurate classification. Moreover, the use of pre-trained CNNs combined with a lightweight MLP ensures faster convergence and lower computational cost compared to training deep networks from scratch.

This modular approach allows easy integration of other models and supports ensemble techniques, thus enhancing the overall robustness and reliability of the proposed framework.

3.2 Dataset Collection

The study utilizes publicly available datasets containing fundus and anterior eye images for cataract detection. The dataset consists of binary classification labels: cataract and non-cataract.
Fundus Dataset: Fundus images capture the interior surface of the eye, including the retina, optic disc, macula, and blood vessels.The Eye Fundus Classification Dataset[8] from Kaggle comprises images of various eye conditions, including diabetic retinopathy, glaucoma, cataract, and normal fundus. For the scope of this study, which focuses on binary classification of cataract detection, we filtered and selected only the 'Cataract' and 'Normal' class images from the dataset. The resulting dataset included 1,839 cataract and 1,849 normal images.Sample images from the fundus dataset are shown in Fig. 1 and Fig. 2.

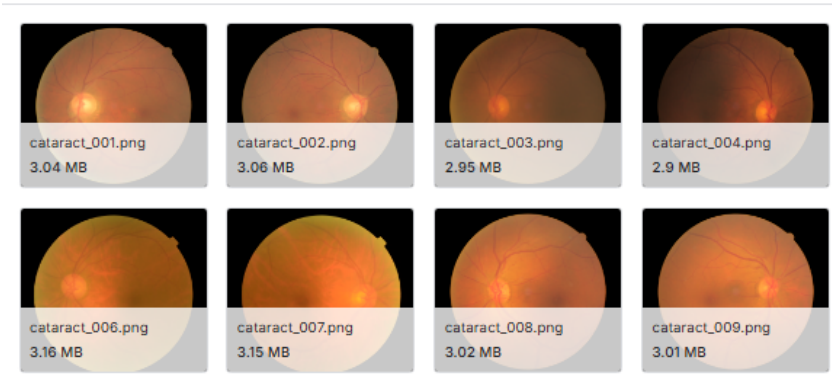

Fig. 1. Fundus Image - Cataract

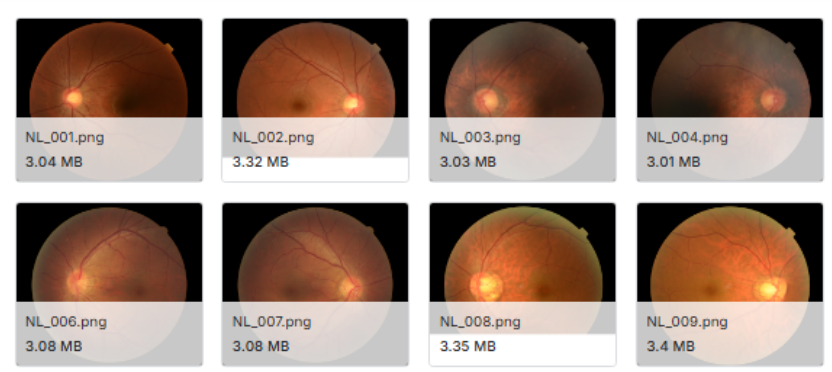

Fig. 2. Fundus Image- Normal

Anterior Eye Dataset:

Anterior eye images capture the external structures of the eye, including the cornea, iris, and lens.To increase the dataset size and improve model performance, two separate datasets from Kaggle were used for anterior eye images: the Dataset Katarak Sinilis [7] containing 820 images per class , and the Cataract Classification Dataset [6] comprising around 200 images per class. After separate preprocessing, the two datasets were merged to enhance variability. Sample images from the dataset are shown in Fig. 3 and Fig. 4.The combined dataset was further augmented using techniques such as image flipping, rotation, and slight shifting to improve model robustness.

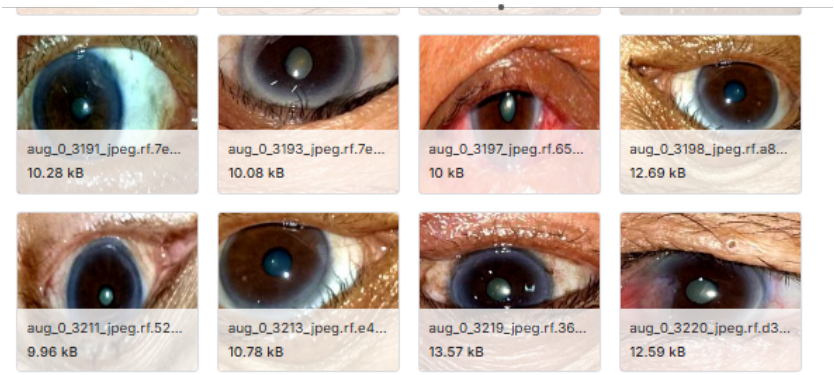

Fig. 3. Anterior Eye Image - Cataract

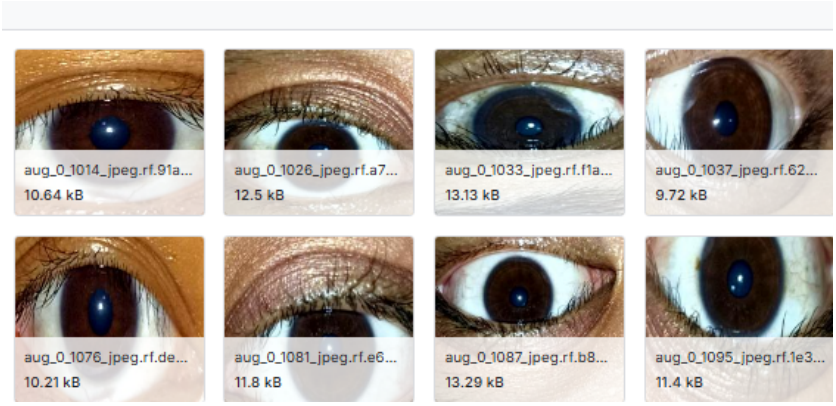

Fig. 4. Anterior Eye Image - Normal

4 System Architecture

4.1 Overview

The proposed system architecture as shown in Fig. 5 is designed with a modular and efficient pipeline to detect cataract severity from both fundus and anterior eye images. It encompasses several stages: data preprocessing, augmentation, feature extraction, classification, and evaluation. At its core, the architecture leverages cutting-edge deep learning models to extract relevant features and employs a learning approach to provide robust and accurate classification. Each

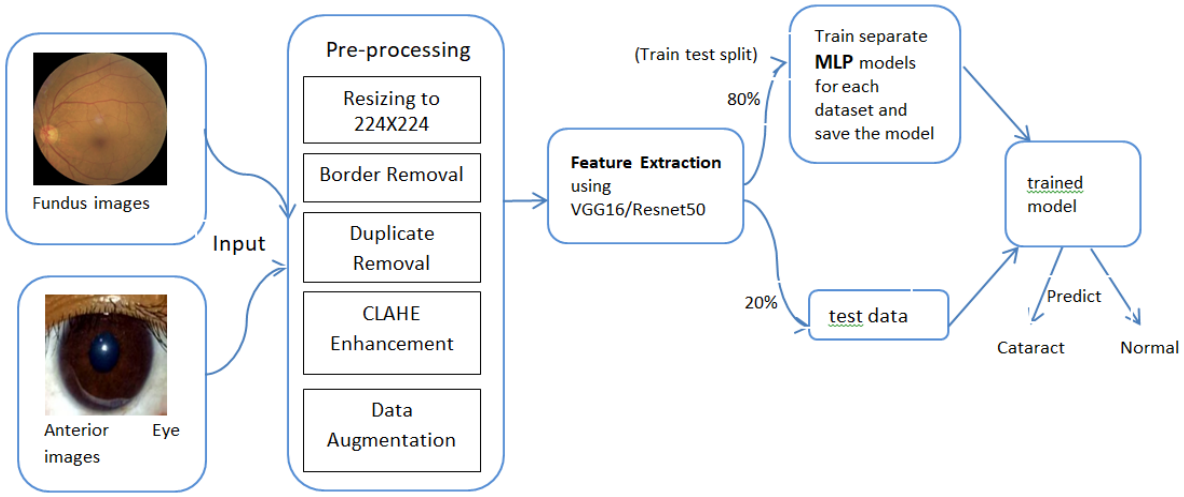

Fig. 5. Architecture of the Proposed System

stage of the architecture is crucial for ensuring the model performs optimally across various datasets, ensuring both precision and generalization.

4.2 Architecture Components

The proposed system is composed of several key components, each contributing significantly to the overall performance. These components include the input layer, preprocessing pipeline, feature extraction modules, classification layer, and evaluation metrics.

- **Input Layer:** The system receives two types of medical images: **fundus images** and **anterior eye images**. Fundus images, captured using a fundus camera, visualize the back of the eye, including the retina and optic disc. Anterior eye images, captured using slit-lamp imaging, focus on the front structures of the eye such as the cornea and lens. These two image types offer complementary visual data, enhancing the system's ability to detect and classify cataract severity accurately. Both image types are passed through a preprocessing pipeline to standardize the input for the deep learning models.
- **Image Preprocessing:** Preprocessing plays a vital role in improving the input image quality and ensuring the system generalizes well across different patient data. The following steps are applied to the images before feature extraction:
  1. **Contrast Enhancement: Contrast Limited Adaptive Histogram Equalization (CLAHE)** is applied to enhance image contrast, which helps emphasize subtle features important for cataract detection. This

is particularly useful for low-contrast images or those affected by poor lighting conditions.
2. **Resizing:** All images are resized to a standardized resolution of **224x224 pixels** to maintain input consistency for the deep learning models.
3. **Data Augmentation:** To enhance model generalization, augmentation techniques such as **rotation**, **flipping**, and **intensity scaling** are employed. These augmentations simulate real-world variations in medical images.
4. **Class Balancing with SMOTE:** Due to potential class imbalances (e.g., fewer samples of severe cataracts), the **Synthetic Minority Oversampling Technique (SMOTE)** is utilized to synthetically generate samples of the minority class, improving model fairness and classification performance.

After preprocessing, the data is split into **training** and **testing** subsets using an **80:20** ratio.

– **Feature Extraction:** Feature extraction is conducted using two pre-trained convolutional neural networks — **VGG16** and **ResNet50** — known for their superior performance in image recognition tasks. Only the convolutional base is used from both models to retain critical spatial information while discarding task-specific dense layers.
  1. **VGG16-Based Feature Extraction:** VGG16's deep architecture enables it to extract fine-grained features such as edges, textures, and contours. The convolutional output is flattened into a one-dimensional feature vector that captures essential image characteristics.
  2. **ResNet50-Based Feature Extraction:** ResNet50 leverages residual connections to train deeper networks without vanishing gradient issues. This architecture extracts high-level, abstract features critical for identifying cataract severity. The final convolutional output is flattened into a compact feature vector.

– **Classification Using Multi-Layer Perceptron (MLP):** The feature vectors obtained from VGG16 and ResNet50 are passed into a **Multi-Layer Perceptron (MLP)** classifier consisting of:
  - An input layer matching the feature vector size.
  - Two hidden layers with **ReLU** activation functions to introduce nonlinearity and enhance feature learning.
  - An output layer with a **Sigmoid** activation function for binary classification, producing probability values to determine cataract severity.

– **Model Evaluation and Comparison:** To assess the performance of the proposed framework, separate evaluations are conducted for fundus and anterior eye images. For each dataset, two configurations are compared:
  - VGG16 Feature Extractor + MLP Classifier
  - ResNet50 Feature Extractor + MLP Classifier

  Performance is quantified using the following metrics:
  - **Accuracy:** Proportion of total correct predictions over the entire dataset.

$$Accuracy = \frac{TP + TN}{TP + TN + FP + FN} \tag{1}$$

- **Precision:** Ratio of true positives among all predicted positives.

$$Precision = \frac{TP}{TP + FP} \tag{2}$$

- **Recall:** Ratio of true positives identified among all actual positives.

$$Recall = \frac{TP}{TP + FN} \tag{3}$$

- **F1-Score:** Harmonic mean of precision and recall, balancing both metrics.

$$F1\text{-}Score = \frac{2 \times Precision \times Recall}{Precision + Recall} \tag{4}$$

  Where:
  - TP: True Positives : correctly predicted cataract-positive cases.
  - TN: True Negatives : correctly predicted cataract-negative cases.
  - FP: False Positives : cataract-negative cases incorrectly predicted as positive.
  - FN: False Negatives :cataract-positive cases incorrectly predicted as negative.
- **AUC-ROC Score:** The Area Under the Receiver Operating Characteristic Curve measures the model's capability to distinguish between classes across varying thresholds. A higher score implies better performance in classification tasks.

5 Experimental Results

The model's performance was assessed using multiple evaluation metrics, including accuracy, precision, recall, F1-score, and Area Under the Curve (AUC).

To further interpret the training behavior and generalization ability of the models, we also analyzed the training and validation accuracy/loss curves.

5.1 Performance Analysis on Fundus Image Dataset

Two pre-trained models VGG16 and ResNet50 were utilized for feature extraction from the fundus images. These extracted features were then passed to a Multi-Layer Perceptron (MLP) for classification. The training and validation accuracy and loss curves for the fundus dataset using VGG+MLP and ResNet+MLP models are shown in Fig.6 and Fig.7, respectively.

- **VGG16 + MLP:** Achieved a testing accuracy of 94.43% .
- **ResNet50 + MLP:** Achieved a testing accuracy of 95.60%.

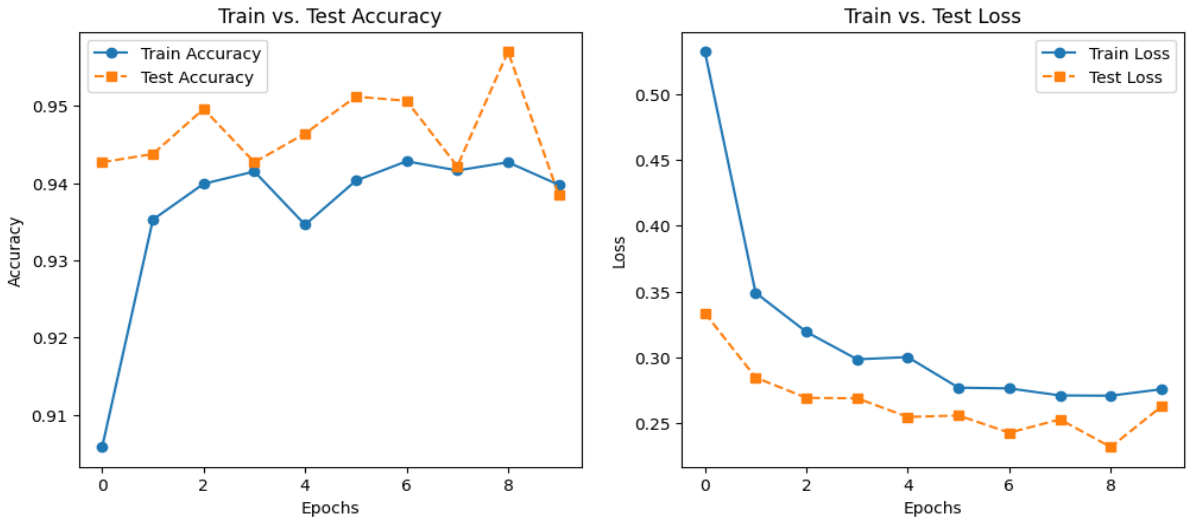

Fig. 6. Training and validation accuracy/loss: VGG16 + MLP on Fundus dataset

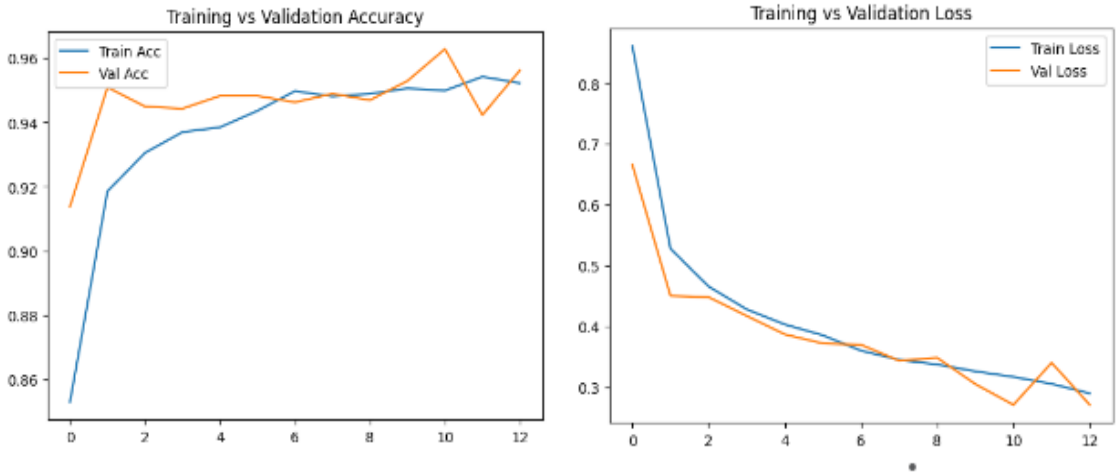

Fig. 7. Training and validation accuracy/loss: ResNet50 + MLP on Fundus dataset

In addition to conventional metrics, the ROC-AUC score was computed as shown in Fig. 8 and Fig. 9 to evaluate the models' discriminative capability. The VGG16 + MLP model achieved an AUC of 0.95, while ResNet50 + MLP

achieved a slightly higher score of 0.97, indicating better overall classification performance.

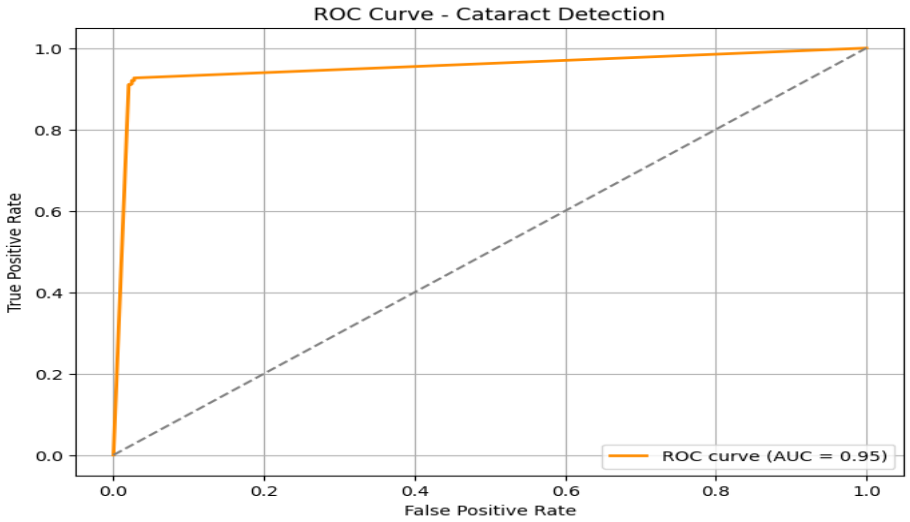

Fig. 8. ROC-AUC Curve: VGG16 + MLP (Fundus)

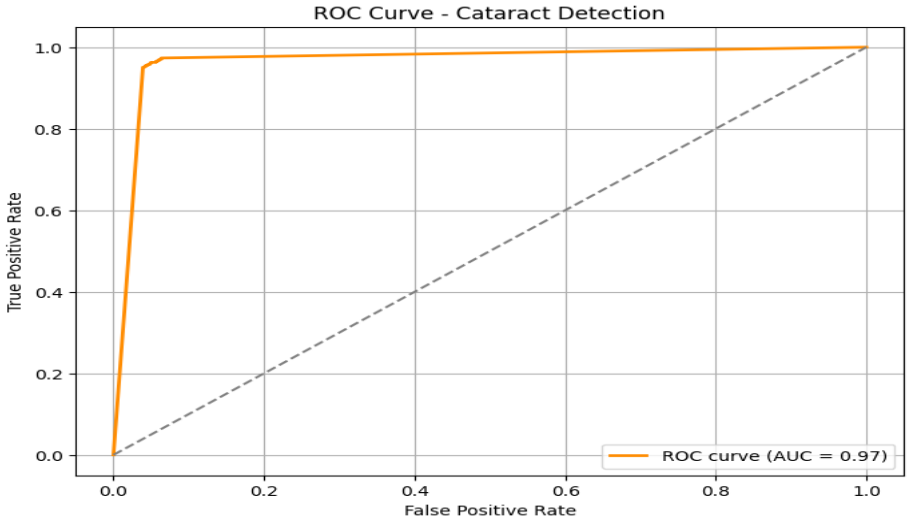

Fig. 9. ROC-AUC Curve: ResNet50 + MLP (Fundus)

– **Precision, Recall, and F1-Score Analysis**

While accuracy provides a high-level view of model performance, it often fails to highlight critical errors in medical diagnostics. To better understand model reliability, especially in handling false positives and false negatives, we analyzed precision, recall, and F1-score as shown in Fig.10. VGG16+MLP achieved 95.00% precision, 94.10% recall, and a 93.92% F1-score. ResNet50+MLP performed slightly better with 96.00% across all three metrics , indicating more reliable predictions.

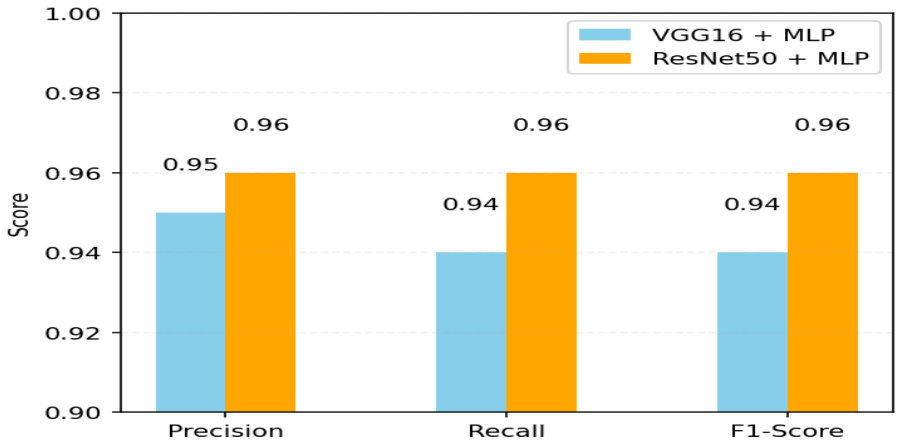

Fig. 10. Precision, Recall, and F1-score Comparison: VGG16 + MLP vs. ResNet50 + MLP (Fundus)

5.2 Performance on Anterior Eye Dataset

Similarly, the anterior eye images were evaluated using the same feature extraction and classification pipeline.The training and validation accuracy and loss curves for the Anterior Eye dataset using VGG+MLP and ResNet+MLP models are shown in Fig.11 and Fig.12, respectively.

– **VGG16 + MLP:** Achieved a testing accuracy of 89.29%.
– **ResNet50 + MLP:** Achieved a testing accuracy of 90.99%.

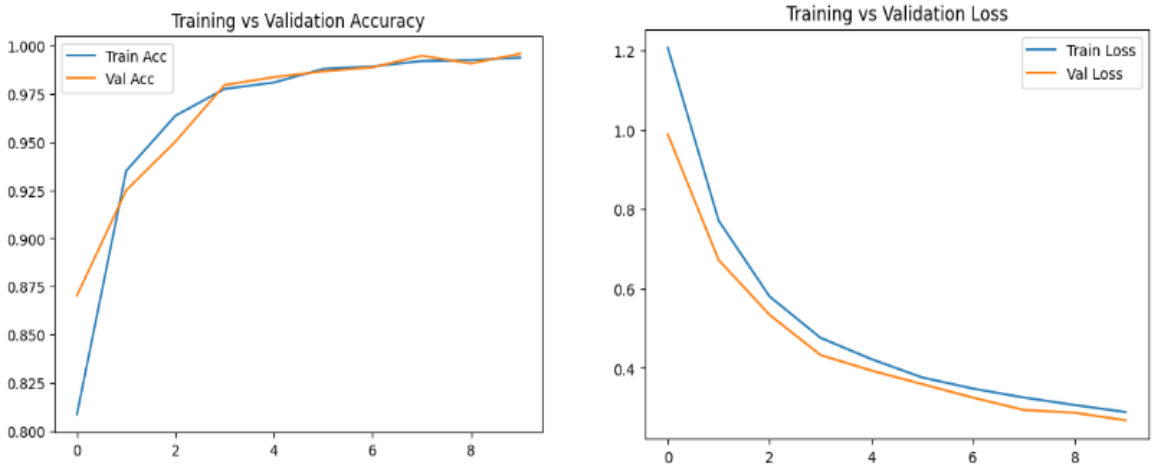

Fig. 11. Training and validation accuracy/loss: VGG16 + MLP (Anterior Eye Dataset)

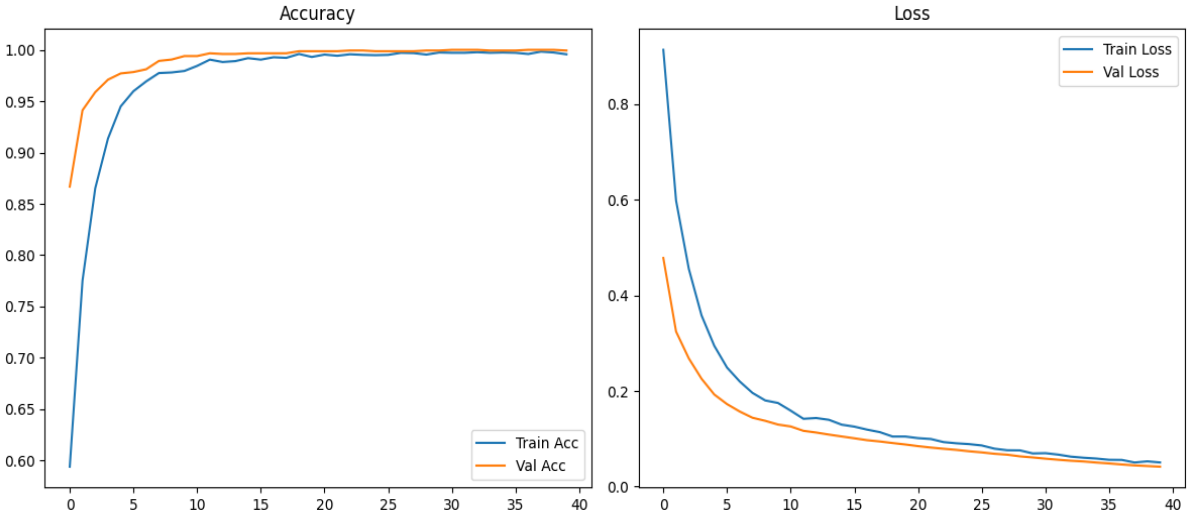

Fig. 12. Training and validation accuracy/loss: ResNet50 + MLP (Anterior Eye Dataset)

AUC scores were again computed to quantify the classifier's discrimination power. VGG16 + MLP achieved an AUC of 0.96, while ResNet50 + MLP achieved an AUC of 0.97 as shown in Fig.13 and Fig,14.

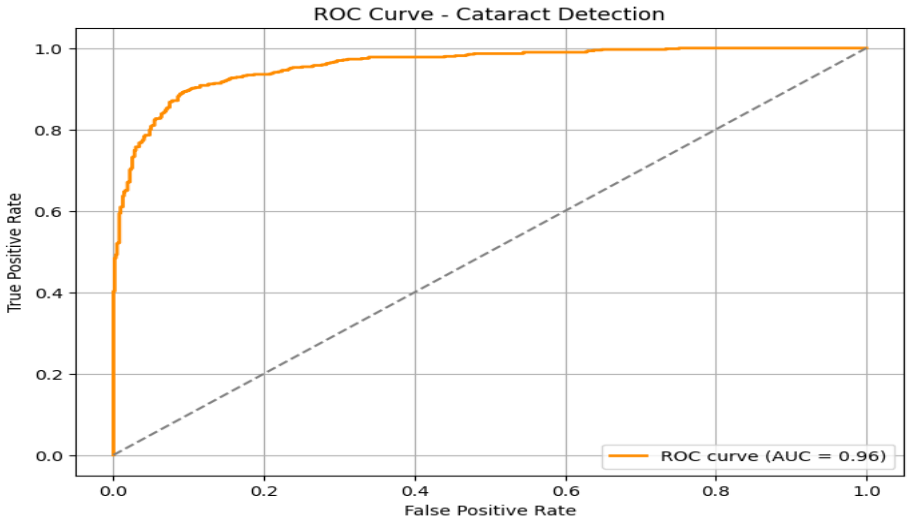

Fig. 13. ROC-AUC Curve: VGG16 + MLP (Anterior Eye)

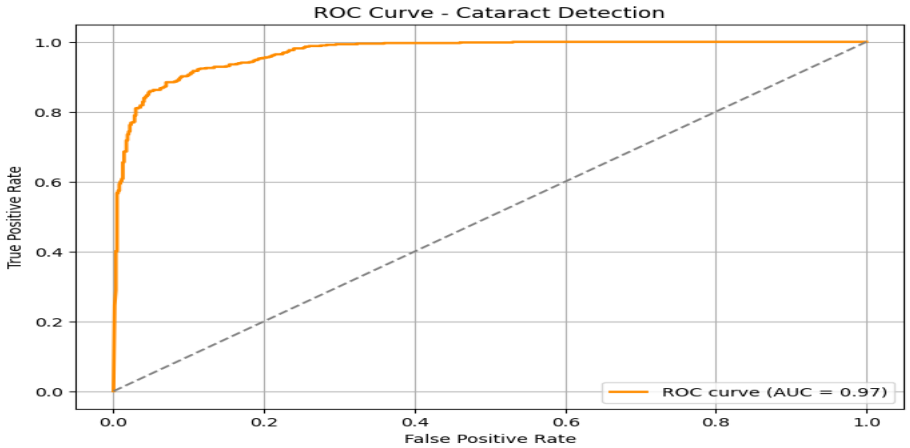

Fig. 14. ROC-AUC Curve: ResNet50 + MLP (Anterior Eye)

– **Precision, Recall, and F1-Score Analysis**
For the anterior eye dataset, precision, recall, and F1-score were analyzed as shown in Fig.15. VGG16+MLP achieved 90.00% precision, 89.00% recall, and an F1-score of 89.00%, while ResNet50+MLP achieved 91.30% precision, 91.00% recall, and a 91.00% F1-score.

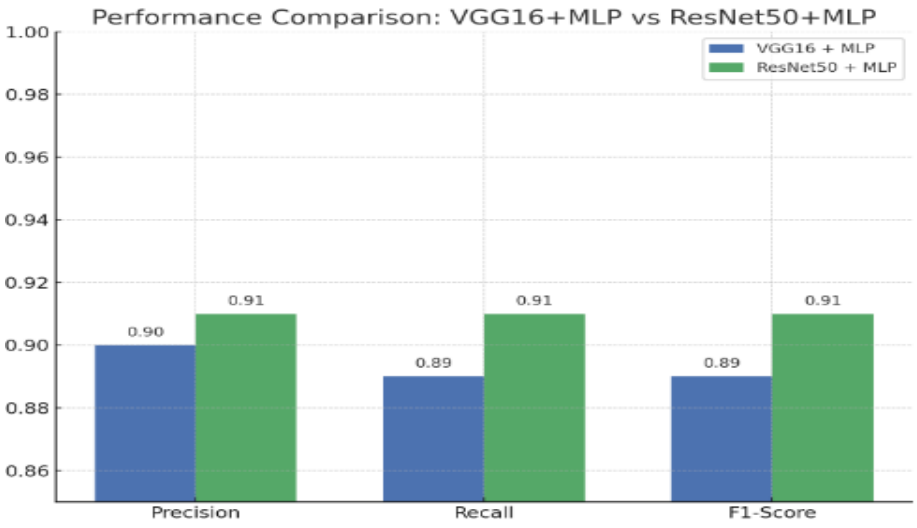

Fig. 15. Precision, Recall, and F1-score Comparison: VGG16 + MLP vs. ResNet50 + MLP (Anterior Eye)

These findings indicate that ResNet50 slightly outperforms VGG16 across all key metrics. The higher F1-score, in particular, emphasizes its effectiveness in minimizing both false positives and false negatives, positioning it as a strong candidate for real-world anterior eye disease classification tasks.

6 Discussion

The proposed cataract detection system demonstrated strong classification performance across both fundus and anterior eye image datasets, with ResNet50+MLP achieving higher accuracy than VGG16+MLP. Specifically, ResNet50 attained 95.60% accuracy on anterior images and 96% on fundus images. These results indicate the effectiveness of combining pre-trained CNN feature extractors with a lightweight MLP classifier for medical image classification tasks. While prior studies have explored different architectures and modalities, this work follows a simplified yet efficient approach.
To enhance the overall performance and accuracy of the proposed framework while ensuring reliability, several strategies were used throughout the pipeline.

Extensive image preprocessing techniques, including CLAHE for contrast enhancement and standardized resizing, were applied to improve input quality. The classifier architecture was optimized using a lightweight Multi-Layer Perceptron (MLP) with dropout layers to prevent overfitting and ensure stable learning. To tackle class imbalance Synthetic Minority Oversampling Technique (SMOTE) was applied, ensuring that the classifier learns equally from each categories. Hyperparameter tuning, such as optimizing learning rates and batch sizes, further contributed to achieving higher classification accuracy. By maintaining a clear separation between training and testing datasets and following a modular design, the system ensures reproducibility and supports easy integration of future enhancements, thereby boosting the reliability of the results.

7 Conclusion

This study proposes a deep learning-based cataract detection framework using fundus and anterior eye images, where pre-trained CNN models (VGG16 and ResNet50) were applied independently for deep feature extraction, followed by classification using a lightweight Multi-Layer Perceptron. The main contribution lies in presenting a comparative evaluation of these models across two different ophthalmic image modalities, demonstrating high classification accuracy of 94.43% for VGG16+MLP on fundus images and 95.60% for ResNet50+MLP on anterior eye images. The results affirm the effectiveness of feature-based transfer learning for developing scalable, cost-effective cataract screening systems. Future work will focus on multiclass severity grading, mobile deployment, and the integration of Explainable AI (XAI) techniques to enhance model transparency and clinical reliability.

References

1. Babaqi, T., Jaradat, M., Yildirim, A., Al-Nimer, S., Won, D.: Eye disease classification using deep learning techniques (2023). https://doi.org/10.48550/arXiv.2307.10501
2. Hasan, M.N., Pial, M.E.R., Das, S., Siddique, N., Wang, H.: Dia-vxnet: A framework for automated diabetic eye disease detection using transfer learning with feature fusion network. Biomedical Signal Processing and Control **100**, 106907 (2025). https://doi.org/https://doi.org/10.1016/j.bspc.2024.106907
3. Hu, S., Wang, X., Wu, H., Luan, X., Qi, P., Lin, Y., He, X., He, W.: Unified diagnosis framework for automated nuclear cataract grading based on smartphone slit-lamp images. IEEE Access **8**, 174169–174178 (2020). https://doi.org/10.1109/ACCESS.2020.3025346
4. Jabber, A., Wadi, S., Shadeed, G., Hadi, A.: Cataract detection and classification using deep learning techniques. International Journal of Computing and Digital Systems **17**, 1–10 (2024). https://doi.org/10.12785/ijcds/1571037888
5. Junayed, M.S., Islam, M.B., Sadeghzadeh, A., Rahman, S.: Cataractnet: An automated cataract detection system using deep learning for fundus images. IEEE Access **PP**, 1–1 (2021). https://doi.org/10.1109/ACCESS.2021.3112938

6. Kaggle Collaborator: Cataract classification dataset. https://www.kaggle.com/datasets/akshayramakrishnan28/cataract-classification-dataset
7. Kaggle Collaborator: Dataset katarak sinilis. https://www.kaggle.com/datasets/rifdana/dataset-katarak-sinilis
8. Kaggle Contributors: Eye fundus classification dataset. https://www.kaggle.com/datasets/uynzyy/dataset
9. Nagy, W., Alsalamah, H.: A novel catractnetdetect deep learning model for effective cataract classification through data fusion of fundus images. Discover Artificial Intelligence **4** (2024). https://doi.org/10.1007/s44163-024-00155-y
10. Olaniyan, J., Olaniyan, D., Obagbuwa, I.C., Esiefarienrhe, B.M., Odighi, M.: Transformative transparent hybrid deep learning framework for accurate cataract detection. Applied Sciences **14**(21) (2024). https://doi.org/10.3390/app142110041, https://www.mdpi.com/2076-3417/14/21/10041
11. Padalia, D., Mazumdar, A., Singh, B.: A cnn-lstm combination network for cataract detection using eye fundus images (2022). https://doi.org/10.48550/arXiv.2210.16093
12. Sales dos Santos, P.R., de Carvalho Brito, V., de Carvalho Filho, A.O., Henrique Duarte de Araujo, F., de Andrade Lira Rabelo, R., Mathew, M.J.: A Capsule Network-based for identification of Glaucoma in retinal images pp. 1–6 (2020). https://doi.org/10.1109/ISCC50000.2020.9219708
13. Simanjuntak, R., Fu'adah, Y., Magdalena, R., Saidah, S., Wiratama, A., Ubaidah, I.: Cataract classification based on fundus images using convolutional neural network. JOIV : International Journal on Informatics Visualization **6**, 33 (2022). https://doi.org/10.30630/joiv.6.1.856
14. Son, K.Y., Ko, J., Kim, E., Lee, S.Y., Kim, M.J., Han, J., Shin, E., Chung, T.Y., Lim, D.H.: Deep learning-based cataract detection and grading from slit-lamp and retro-illumination photographs: Model development and validation study. Ophthalmology Science **2**(2), 100147 (2022). https://doi.org/https://doi.org/10.1016/j.xops.2022.100147
15. Wu, X., Hu, L., Xiao, Z., et al.: Explainable machine learning framework for cataracts recognition using visual features. Visual Computing for Industry, Biomedicine, and Art **8**, 3 (2025). https://doi.org/https://doi.org/10.1186/s42492-024-00183-6
16. Yadav, S., Yadav, J.: Enhancing cataract detection precision: A deep learning approach. Traitement du Signal **40**(4), 1413–1424 (2023). https://doi.org/https://doi.org/10.18280/ts.400410

Blockchain-Enabled Communication for Sustainable Fashion: Impact on Consumer Trust and Purchasing Behavior

Bui Thanh Khoa[1], Ai-Van Huynh[2*]
[1]Faculty of Commerce and Tourism, Industrial University of Ho Chi Minh City, Ho Chi Minh City, Vietnam
[1]buithanhkhoa@iuh.edu.vn
[2]FPT University, Greenwich Vietnam, Ho Chi Minh campus, Ho Chi Minh City, Vietnam
[2]vanha4@fe.edu.vn

* Corresponding Author

Abstract. This research explored the impact of blockchain-enabled transparency on consumer trust and sustainable purchasing behaviours within the fashion industry. Blockchain technology has surfaced as a promising solution, offering the ability to maintain unalterable records. This study explored the impact of three aspects of blockchain-enabled transparency on consumer trust and the resulting intentions to make sustainable purchases. The study employed structural equation modelling to analyse data from 194 consumers who possess a solid understanding of blockchain technology. The findings revealed that all three dimensions of transparency had a positive impact on consumer trust, with authenticity exhibiting the most significant effect, followed by accessibility and traceability. The level of consumer trust was a significant predictor of the intention to make sustainable purchases. The findings indicate that the use of blockchain technology in fashion communication has improved transparency and built trust, thereby encouraging sustainable consumption practices. The findings provide significant insights for fashion brands aiming to utilise blockchain technology to enhance communication within their supply chains and foster greater engagement in sustainability efforts.

Keywords: Blockchain technology, sustainable fashion, supply chain transparency, consumer trust, digital communication.

1 Introduction

It is anticipated that the revenue generated within the Fashion Market will attain a total of US$880.91 billion by the year 2025. The revenue is anticipated to experience an annual growth rate of 7.64% from 2025 to 2029, leading to a

projected market volume of US$1.18 trillion by the year 2029 [1]. Although the industry plays a crucial role in the economy, it grapples with considerable sustainability challenges stemming from its intricate and often unclear supply chains. These convoluted networks often hide the origins of products, the conditions under which they are manufactured, and the ethical practices involved, leading to notable obstacles in achieving transparency and accountability [2]. This lack of transparency has allowed a range of unethical practices to thrive, such as forced child labour, modern slavery, and environmental degradation, which largely go unnoticed by both retailers and consumers [3].

Blockchain technology has surfaced as a compelling approach to improving transparency and traceability within fashion supply chains. Blockchain functions as a decentralised and distributed digital ledger system, allowing for the creation of unalterable records that include time stamps and geo-location tags [4]. This capability ensures that products can be traced in real-time throughout their entire lifecycle [5]. This unchangeable characteristic demonstrates considerable promise for enhancing transparency within fashion supply chain operations, potentially tackling numerous ethical and sustainability challenges that have persisted in the industry for years.

Blockchain technology establishes a collaborative, shared, and synchronised digital data system that operates across various locations without the need for centralised control, thereby offering a distinctive solution to transparency issues [6]. In the realm of fashion, transparency involves several important aspects: the ability to trace products, the assurance of authenticity, and the availability of information. The various dimensions of transparency may play a significant role in shaping consumer trust, which studies indicate is an essential factor in promoting sustainable purchasing behaviour. Research shows that a deficiency of trust in environmentally friendly products and ethical manufacturing plays a crucial role in influencing consumers' choices regarding sustainable fashion [7, 8].

While blockchain technology holds great promise for improving transparency within fashion supply chains, there remains a notable gap in research concerning the empirical evidence of how this enhanced transparency affects consumer trust and sustainable purchasing behaviours. Although previous studies have examined the use of blockchain in the fashion industry [9], they have largely concentrated on the technical aspects rather than the perceptions and behaviours of consumers.

Badhwar, Islam and Tan [6] emphasise that there is a notable absence of empirical evidence and life-cycle assessment case studies regarding blockchain applications that facilitate traceable supply chains within the fashion industry. Current research has explored traceability, authenticity, and accessibility as separate concepts, failing to create a unified framework that elucidates their collective influence on consumer trust and sustainable purchasing practices [10]. This fragmentation restricts our comprehension of the comprehensive impact that blockchain-enabled transparency has on consumer decision-making within the realm of sustainable fashion.

This research seeks to fill the existing gap by investigating the impact of blockchain-enabled transparency—specifically its aspects of traceability, authenticity, and accessibility—on consumer trust and sustainable purchasing behaviour within the fashion industry. This research aims to: (1) analyse the

influence of each dimension of transparency on consumer trust; and (2) explore the role of consumer trust in mediating the relationship between blockchain-enabled transparency and the intention to make sustainable purchases.

This paper is structured in the following manner: Initially, an extensive review of existing literature explores the intricacies of blockchain technology, the various dimensions of transparency, the factors influencing consumer trust, and the implications for sustainable purchasing behaviour. The subsequent section of the research methodology outlines the measurement scales, the sampling approach employed, and the procedures for data collection. The results section provides an overview of the findings derived from the assessments of both the measurement and structural models. In conclusion, this section addresses both the theoretical and practical implications of the findings, acknowledges the limitations of the study, and suggests avenues for future research.

2 Literature review

2.1 Blockchain and Sustainable Communication Practices

Blockchain technology offers a decentralized and distributed digital ledger system that facilitates unchangeable record-keeping (Ahad et al., 2020). The unchanging characteristic of this technology shows great promise for enhancing transparency and traceability within the operations of fashion supply chains [11]. Badhwar, Islam and Tan [6] emphasize that blockchain's ability to establish consensus-driven, shared, and synchronized digital data across various locations and nations, all without the need for centralized control, positions it uniquely to tackle issues related to transparency.

Traceability refers to the ability to trace the history, application, or location of an entity employing recorded identifications [6]. However, it has yet to be specifically defined within the context of the fashion and textile industry. The lack of a clear definition specific to the industry has posed difficulties in the implementation process. Blockchain effectively addresses this gap by utilizing cryptographic hashtags to securely store digital information, complete with time stamps and geo-location tags. This innovation enables real-time traceability of products throughout their entire lifecycle [4]. Platforms like TextileGenesis and Fibercoins are already offering integrated blockchain solutions that reveal the traceable journey of products, from the fiber stage to the end customer.

The authenticity of products plays a vital role in the fight against the counterfeiting industry. Platforms such as VeChain and Brandzledger have been created with a focus on addressing the issue of counterfeiting [12, 13]. These applications allow consumers to confirm the authenticity of products, a factor that holds significant importance as it relates to brand value and fosters consumer loyalty [6].

The accessibility via blockchain technology empowers consumers to make well-informed choices. Badhwar, Islam and Tan [6] highlight that an increasing number of consumers are seeking transparency within the fashion industry

Blockchain applications need to offer user-friendly platforms that enable individuals to authenticate product information. This accessibility marks a notable change from the selective sharing of information that has traditionally fueled greenwashing and eroded consumer trust [14].

2.2 Research Hypotheses Development

The implementation of blockchain technology enhances traceability, thereby greatly increasing customer trust in fashion and textile products. Badhwar, Islam and Tan [6] highlight that the complex supply chains within the fashion industry inherently possess various vulnerabilities that frequently obscure the true origins of products. The lack of transparency in these supply chains has fostered an environment where unethical practices can thrive without being noticed [3]. The challenge of tracing items from their raw material origins to finished products has consistently undermined customer confidence in brands' assertions regarding sustainability and ethical practices. Implementations demonstrate the capability of blockchain technology to track products from the fiber stage to the final consumer, thereby creating a level of supply chain transparency that was not attainable before. This improved traceability directly addresses the concerns raised by Garcia-Torres, Albareda, Rey-Garcia and Seuring [2] regarding the necessity of traceability in sustainable supply chain management. When customers are able to understand the origins and manufacturing processes of products, their confidence can be restored based on verifiable facts rather than mere promotional claims.

H1: Traceability of blockchain positively impacts Consumer trust.

By allowing unquestionable verification of product authenticity, blockchain technology provides a strong answer to this problem. Blockchain offers anti-counterfeiting features that let customers confirm product authenticity as shown by apps [13]. Product authenticity gives companies an advantage to combat counterfeit goods in black and grey marketplaces [15]. Once authenticity is confirmed and published, the unchangeable character of blockchain records guarantees customers consistent verification tools as this information cannot be changed. This feature specifically tackles the issues that companies need technology to convey product value and authenticity to customers [16]. Consumers' confidence in companies grows organically as ambiguity is removed when they can independently confirm product legitimacy.

H2: Authenticity of blockchain positively impacts Consumer trust.

The implementation of blockchain technology facilitates unparalleled access to supply chain information, thereby addressing this critical concern. Through the facilitation of information accessibility via decentralized platforms, blockchain effectively removes the gatekeeping function that has historically been assumed by fashion brands. The democratization of information corresponds with the increasing consumer demand for transparency as noted by James and Montgomery [17].

Applications of blockchain technology illustrate the practical implementation of information accessibility [6]. The accessibility of verifiable information regarding product origins, manufacturing conditions, and environmental impact for consumers serves to considerably diminish the information asymmetry that has historically defined the fashion industry. The decrease in information asymmetry effectively responds to the issue, which posits that limited authentic communication between brands and consumers erodes trust.

H3: Accessibility of blockchain positively impacts Consumer trust.

The connection between consumer trust and the intention to make sustainable purchases is thoroughly documented in existing scholarly works. Khoa, Nguyen and Nguyen [18] emphasize that the fashion industry's failure to provide credible and non-selective information has contributed to the emergence of anti-consumption values among consumers. Concurrently, it is observed that insufficient customer trust in environmentally friendly products and ethical manufacturing significantly influences purchasing choices regarding sustainable fashion [8]. The restoration of trust has significant consequences for intentions related to sustainable purchasing. Wiencierz and Lünich [19] observe that the lack of transparency in supply chain operations has resulted in a grey area that companies frequently exploit to engage in greenwashing, thereby diminishing consumer interest in authentically sustainable alternatives. Through the removal of ambiguity via blockchain-enabled transparency, it is possible to restore consumer trust in sustainability claims, which in turn directly affects their propensity to purchase sustainable products.

H4: Consumer trust positively impacts Sustainable Purchase Intention

3 Research method

All measuring scales were created using tools validated in the current literature to ensure both construct validity and reliability. With answers from 1 (strongly disagree) to 5 (strongly agree), every item was evaluated using a five-point Likert scale. Among the many ideas this research looked at were traceability depending on blockchain technology, authenticity, accessibility, customer trust, and the desire to make sustainable purchases. As Badhwar, Islam and Tan [6] pointed out, three questions measuring customers' views on blockchain's potential to provide verifiable information about a product's path within the supply chain helped to evaluate the traceability construct (TRA). Three things meant to gauge customers' views on the ability of blockchain technology to confirm the validity of goods made up the construct of authenticity (AUT). Specifically citing the work of Kshetri, Dwivedi, Davenport and Panteli [12], Pham, Valette-Florence and Vigneron [15] on blockchain-enabled anti-counterfeiting policies, the following elements have been extracted from academic studies on product authenticity in luxury sectors. Three questions meant to gauge customers' views on the ease with which they could access and understand information offered using blockchain technology helped to define the concept of accessibility (ACC). The literature on information asymmetry between brands and customers [14] guided the creation of these goods. Comprising

three components measuring the degree to which consumers see the dependability and integrity of information spread via blockchain technology, the consumer trust (CTR) architecture was built. Research concentrating on customer trust in digital settings and claims about sustainable goods has led to the following things. This measuring method addresses the concerns voiced by Bhaduri and Ha-Brookshire [7] about consumer skepticism about sustainability promises in the fashion sector. Three questions meant to measure customers' willingness to buy goods certified by blockchain technology as ecologically and socially responsible were used to assess the concept of sustainable purchasing intention (SPI). This approach supports claim of Garcia-Torres, Albareda, Rey-Garcia and Seuring [2] that transparency and traceability are vital tools for the efficient control of sustainable supply chains and the decision-making processes of consumers.

Nineteen four clients who showed knowledge of blockchain technology were found using a purposive sample approach. The specialist character of the study issue motivated this strategy; hence, respondents should have a basic knowledge of blockchain applications in retail settings. Sample size was decided according to the recommendation that structural equation modeling requires at least 10 responders for every measured variable [20]. With a sample size of 194 respondents above the set minimum criterion, the research included 15 measured variables spread over five constructs. Table 1 shows the demographic profile of the respondents.

Table 1. Demographic Characteristics of Respondents

Characteristic	Category	Frequency	Percentage
Gender	Male	106	54.60%
	Female	88	45.40%
Age	18-29	64	33.00%
	30-39	68	35.00%
	40-49	42	21.60%
	50+	20	10.40%
Education	High School	8	4.10%
	Some College	37	19.10%
	Bachelor's Degree	89	45.90%
	Graduate Degree	60	30.90%

4 Result

An examination of the outer loadings (OL) linked to every measurement item and its related construct assessed the dependability of the indicators. With values from 0.781 to 0.932, Table 2 shows that all indicators showed outer loadings beyond the recommended threshold of 0.70 [20]. This suggests that every indicator is rather important for its particular construct, in keeping with the recommendation that indicators with loadings above 0.70 should be maintained. Internal consistency reliability was assessed using Cronbach's alpha in conjunction with composite reliability (CR). Table 2's data shows that Cronbach's alpha scores (CA) ranged from 0.819 to 0.891, above the recommended minimum of 0.70 [21]. Ranging from 0.892 to 0.932, the composite dependability ratings were found to be much above the recommended minimum of 0.70. The findings show a great degree of internal

consistency across all constructs, suggesting that the assessment items properly reflect their particular constructions as a unified whole. Convergent validity assesses the extent to which indicators of a given concept line up or show a notable degree of shared variation. Each construct's average variance extracted (AVE) was used to assess. Table 2 show that the AVE values ranged from 0.734 to 0.820, above the recommended level of 0.50 set by Fornell and Larcker [22]. The results show that more than 73% of the variation in the indicators is explained by their related components, hence confirming strong convergent validity.

Discriminant validity was evaluated using the Fornell-Larcker criteria and the heterotrait-monotrait ratio of correlations (HTMT) as described by Fornell and Larcker in 1981. Used was the HTMT ratio, a more demanding criterion for assessing discriminant validity [23]. This approach calculates the ratio of correlations seen between several qualities to those seen within the same trait. The figures in Table 2 show that every HTMT value stays below the conservative criterion of 0.85, therefore supporting the discriminant validity across all pairings of constructs.

Table 2. Reliability, Convergent and Discriminant Validity Assessment

Construct	OL	CA	CR	AVE	HTMT criteria			
					TRA	**AUT**	**ACC**	**CTR**
TRA	0.832-0.902	0.85	0.91	0.77				
AUT	0.824-0.915	0.86	0.91	0.78	0.68			
ACC	0.781-0.889	0.82	0.89	0.73	0.74	0.65		
CTR	0.864-0.920	0.88	0.93	0.81	0.72	0.83	0.83	
SPI	0.871-0.932	0.89	0.93	0.82	0.69	0.64	0.67	0.84

An assessment of collinearity among the predictor components using the Variance Inflation Factor (VIF) was done before examining the route coefficients. The figures in Table 3 show that all VIF values are between 1.648 and 2.316, much below 5.0. The results show that collinearity is not a problem in the structural model, thereby suggesting that every predictor construct has a unique part in clarifying the variation in the endogenous constructs. With a R^2 value of 0.665, Table 3 indicates that Traceability, Authenticity, and Accessibility account for around 66.5% of the variation in Consumer Trust (CTR). Likewise, the R^2 value for Sustainable Purchase Intention (SPI) is 0.546, indicating that around 54.6% of the variation in SPI may be explained by CTR. The predictive significance of the model was assessed by calculating the Stone-Geisser's Q^2 value, which was generated using the blindfolding technique. With Q^2 values of CTR (0.537) and SPI (0.444) well above zero, Table 3 suggests that the model shows considerable predictive significance for both endogenous components. With Accessibility ($f^2 = 0.281$) and Traceability ($f^2 = 0.152$), Table 3 shows that Authenticity ($f^2 = 0.362$) has the most significant impact on Consumer Trust. The impact sizes may be categorized as big for Authenticity and medium for Accessibility and Traceability. Moreover, Sustainable Purchase Intention is greatly influenced by Consumer Trust, as shown by a substantial impact size ($f^2 = 1.201$). Hypothesized correlations were tested by means of path coefficients and their statistical significance evaluation. Table 3 shows the

outcomes of the hypothesis testing.

Table 3. PLS-SEM result

Relationship	β	t-value	VIF	f^2	R^2	Q^2
TRA → CTR	0.241	4.105	1.752	0.152		
AUT → CTR	0.372	6.329	1.648	0.362	0.665	0.537
ACC → CTR	0.328	5.618	1.691	0.281		
CTR → SPI	0.739	18.714	1.000	1.201	0.546	0.444

5 Discussion and Contribution

5.1 Discussion

The study validates that blockchain-enabled traceability significantly improves customer trust (H1), supporting previous research that highlights the significance of transparency in supply chain management [2]. Blockchain technology provides immutable records with time stamps and geo-location identifiers [24], so reducing the opacity of supply chains that has traditionally concealed immoral activities [3]. Badhwar, Islam and Tan [6] emphasized that traceability in the fashion business allows customers to authenticate product origins, hence enhancing trust in sustainability assertions. These results corroborate the argument of Wu, Xiong, Yan and Wang [25] that traceability is vital for sustaining customer confidence in scattered and complex supply chains.

The research indicates that blockchain's ability to authenticate products significantly impacts customer trust (H2). This discovery aligns with the research of Kshetri, Dwivedi, Davenport and Panteli [12], Putasso, Ferro and Osella [13], who demonstrated that blockchain applications provide efficient anti-counterfeiting solutions. Authenticity is fundamental to customer trust, especially in the fight against counterfeit goods in both black and grey markets [15]. Zhang, Chen and Hu [26] emphasize that authenticity significantly improves brand image and fosters customer loyalty. This research experimentally validates the robust connection between blockchain-facilitated authenticity and customer trust, particularly within the fashion sector.

Accessibility, the third facet of blockchain-facilitated transparency, likewise has a substantial beneficial effect on customer trust (H3). This discovery corroborates assertion of Jestratijevic, Rudd and Uanhoro [14] that selective information sharing erodes confidence, alongside James and Montgomery [17]'s observation of a growing customer need for openness in the fashion industry. The capacity of blockchain to democratize access to supply chain information mitigates these issues, offering customers clear and actionable insights on product origins and manufacturing circumstances [6]. This accessibility corresponds with the ideals of the United Nations Sustainable Development Goal #12, which underscores the need for informed decision-making grounded on open communication.

The findings indicate that customer trust substantially influences sustainable purchasing intentions (H4). This discovery corroborates previous studies suggesting

that trust is a vital factor in ethical consumption [7]. The research validates claim of Garcia-Torres, Albareda, Rey-Garcia and Seuring [2] that traceability and transparency are vital instruments for sustainable supply chain management, hence enhancing customer trust in ethical goods. Moreover, the robust correlation between trust and sustainable buying behavior corresponds with Khoa [27]'s assertion that transparency helps alleviate anti-consumption sentiments among customers, prompting them to endorse firms that emphasize sustainability.

This study advances the literature by consolidating the three elements of blockchain-enabled transparency—traceability, authenticity, and accessibility—into a cohesive framework, in contrast to other studies. This study offers a comprehensive examination of the collective influence of these aspects on consumer trust and sustainable buying behavior, in contrast to previous research that has investigated them separately. The results underscore the interconnectedness of these characteristics, illustrating how each individually contributes to cultivating trust and encouraging ethical consumption.

5.2 Theoretical Contributions

This research offers many theoretical advancements to the body of literature about blockchain technology, customer trust, and sustainable buying behavior. Initially, it enhances the theoretical comprehension of blockchain-facilitated transparency by defining it as a multidimensional construct that includes traceability, authenticity, and accessibility. This study synthesizes previously isolated aspects into a unified framework, offering a more thorough comprehension of how blockchain improves transparency in supply chains.

Secondly, the research enhances the literature on consumer trust by recognizing blockchain-enabled transparency as a pivotal factor in fostering trust within the fashion business. The results corroborate and enhance other studies by illustrating that confidence is affected not just by traceability and authenticity but also by the availability of information. This sophisticated comprehension of trust provides a basis for forthcoming research investigating the relationship between transparency and customer behavior across many sectors.

The research enhances the theoretical discussion on sustainable consumption by experimentally confirming the relationship between customer trust and the desire to shop sustainably. This study offers substantial empirical evidence about the significance of trust in ethical consumption, particularly in the setting of blockchain-enabled transparency. The results enhance the sustainability literature by highlighting the significance of openness in cultivating trust and encouraging ethical consumption.

5.3 Managerial Implications

The report emphasizes the need for fashion firms to use blockchain technology to improve supply chain transparency. Blockchain may restore confidence in the fashion sector, which has been compromised by unethical tactics and selective information sharing, by allowing customers to track items, check authenticity, and access information. Brands that emphasize transparency via blockchain may

distinguish themselves in a competitive marketplace, appealing to ethically aware customers and bolstering their reputation.

Secondly, the research offers pragmatic insights for blockchain developers, emphasizing the need of creating user-friendly systems that promote accessibility. The results indicate that accessibility is a vital aspect of transparency that profoundly influences customer trust. Blockchain developers have to prioritize the development of simple interfaces that enable users to effortlessly acquire and comprehend supply chain data. This method corresponds with customer expectations for openness and facilitates informed decision-making.

Third, the report provides essential information for policymakers aiming to enhance sustainability in the fashion sector. The robust correlation among transparency, trust, and sustainable buying behavior indicates that legislative frameworks promoting blockchain implementation may substantially influence ethical purchase. Policymakers need to incentivize brands to use blockchain technology and create standards for transparency and traceability throughout supply chains.

The report underscores the potential of blockchain technology to tackle significant issues in the fashion sector, including counterfeiting and substandard labor standards. Blockchain facilitates real-time verification of product authenticity and supply chain conditions, thereby aiding in the fight against counterfeit markets and fostering ethical labor practices. Brands utilizing blockchain for these objectives not only improve their transparency but also advance the industry's long-term sustainability and social responsibility initiatives.

6 Conclusion

This research sought to examine the influence of blockchain-enabled transparency (traceability, authenticity, and accessibility) on customer trust and sustainable buying behavior, a key concern in the fashion industry's shift towards sustainability. The results provide strong empirical validation for all presented hypotheses, corroborating and enhancing the current literature. This work, despite its merits, has numerous drawbacks that need attention in future research. The research focuses only on the fashion industry, hence restricting the applicability of its results to other industries. Future study should investigate the effects of blockchain-facilitated transparency in sectors such as food, healthcare, and electronics, where transparency is paramount. Secondly, the research depends on self-reported data, which may be influenced by social desirability bias. Future research may use experimental methods or longitudinal data to corroborate the results. This study indicates consumer trust as a mediator between transparency and sustainable buying behavior; however, future research should investigate other mediators or moderators, such as perceived risk or environmental knowledge. The report highlights the significance of blockchain technology but neglects to address other developing technologies, such as artificial intelligence and the Internet of Things, which might further improve transparency and sustainability in supply chains. Future study should explore the feasibility of incorporating these

technologies into a cohesive framework for ethical consumption.

References

1. Statista: Fashion - Worldwide, https://www.statista.com/outlook/emo/fashion/worldwide,

2. Garcia-Torres, S., Albareda, L., Rey-Garcia, M., Seuring, S.: Traceability for sustainability–literature review and conceptual framework. Supply Chain Management: An International Journal 24, 85-106 (2019).

3. de Aguiar Hugo, A., de Nadae, J., da Silva Lima, R.: Can fashion be circular? A literature review on circular economy barriers, drivers, and practices in the fashion industry's productive chain. Sustainability 13, 12246 (2021).

4. Oh, S.E., Kim, J.-H., Kim, J.-Y., Ahn, J.-H.: Food Safety Distribution Systems Using Private Blockchain: Ensuring Traceability and Data Integrity Verification. Foods 14, 1405 (2025).

5. Ahad, M.A., Paiva, S., Tripathi, G., Feroz, N.: Enabling technologies and sustainable smart cities. Sustainable cities and society 61, 102301 (2020).

6. Badhwar, A., Islam, S., Tan, C.S.L.: Exploring the potential of blockchain technology within the fashion and textile supply chain with a focus on traceability, transparency, and product authenticity: A systematic review. Frontiers in Blockchain 6, 1044723 (2023).

7. Bhaduri, G., Ha-Brookshire, J.E.: Do transparent business practices pay? Exploration of transparency and consumer purchase intention. Clothing and Textiles Research Journal 29, 135-149 (2011).

8. Pookulangara, S., Shephard, A.: Slow fashion movement: Understanding consumer perceptions—An exploratory study. Journal of retailing and consumer services 20, 200-206 (2013).

9. Tripathi, G., Tripathi Nautiyal, V., Ahad, M.A., Feroz, N.: Blockchain technology and fashion industry-opportunities and challenges. Blockchain technology: Applications and challenges 201-220 (2021).

10. Ruangtip, P., Rueboon, W., Jornkokgoud, K., Faysal, M.: The Role of Trust in Mediating The Effect of Blockchain and E-Payment on Logistics 4.0 and Supply Chain Capabilities in Thailand. Global Business Finance Review 29, 168-182 (2024). doi: 10.17549/gbfr.2024.29.7.168

11. Jiang, J.Y., Elmaghraby, W.J., Moon, K.: An Empirical Study of Blockchain-Driven Transparency in a Consumer Marketplace. The Wharton School Research Paper (2024).

12. Kshetri, N., Dwivedi, Y.K., Davenport, T.H., Panteli, N.: Generative artificial intelligence in marketing: Applications, opportunities, challenges, and research agenda. vol. 75, pp. 102716. Elsevier (2024).

13. Putasso, E., Ferro, E., Osella, M.: Blockchain in the fashion industry: Opportunities and challenges. Textile and Clothing Business Labs (2019)

14. Jestratijevic, I., Rudd, N.A., Uanhoro, J.: Transparency of sustainability disclosures among luxury and mass-market fashion brands. Journal of Global Fashion Marketing 11, 99-116 (2020).

15. Pham, M., Valette-Florence, P., Vigneron, F.: Luxury brand desirability and fashion equity: The joint moderating effect on consumers' commitment toward luxury brands. Psychology & Marketing 35, 902-912 (2018).

16. Huang, H., Yin, Z., Yang, Q., Li, T., Luo, X., Zhou, L., Zheng, Z.: Scalability and

Security of Blockchain-Empowered Metaverse: A Survey. IEEE Open Journal of the Computer Society 5, 648-659 (2024). doi: 10.1109/ojcs.2024.3468445

17. James, A., Montgomery, B.: Engaging the fashion consumer in a transparent business model. International Journal of Fashion Design, Technology and Education 10, 287-299 (2017).

18. Khoa, B.T., Nguyen, T.D., Nguyen, V.T.-T.: Factors affecting Customer Relationship and the Repurchase Intention of Designed Fashion Products. Journal of Distribution Science 18, 198-204 (2020). doi: 10.15722/jds.18.2.202002.17

19. Wiencierz, C., Lünich, M.: Trust in open data applications through transparency. New Media & Society 24, 1751-1770 (2020). doi: 10.1177/1461444820979708

20. Hair, J.F., Black, W.C., Babin, B.J., Anderson, R.E.: Multivariate data analysis. Cengage Learning, Hampshire, United Kingdom (2019).

21. Nunnally, J.C., Bernstein, I.: The assessment of reliability. Psychometric theory 3, 248-292 (1994).

22. Fornell, C., Larcker, D.F.: Evaluating Structural Equation Models with Unobservable Variables and Measurement Error. Journal of Marketing Research 18, 39-50 (1981). doi: 10.1177/002224378101800104

23. Henseler, J., Ringle, C.M., Sarstedt, M.: A new criterion for assessing discriminant validity in variance-based structural equation modeling. Journal of the Academy of Marketing Science 43, 115-135 (2014). doi: 10.1007/s11747-014-0403-8

24. Sze, L.B., Salo, J., Tan, T.M.: Sustainable innovation in the metaverse: Blockchain's role in new business models. Digital Business 4, 100086 (2024).

25. Wu, X., Xiong, J., Yan, J., Wang, Y.: Perceived quality of traceability information and its effect on purchase intention towards organic food. Journal of Marketing Management 37, 1267-1286 (2021). doi: 10.1080/0267257x.2021.1910328

26. Zhang, T., Chen, J., Hu, B.: Authenticity, Quality, and Loyalty: Local Food and Sustainable Tourism Experience. Sustainability 11, 3437 (2019). doi: 10.3390/su11123437

27. Khoa, B.T.: Increasing online business productivity through customer electronic loyalty: the role of online trust and hedonic value. International Journal of Public Sector Performance Management 12, 252-274 (2023). doi: 10.1504/ijpspm.2023.132250

Comparative Analysis of Iron Oxide (Fe_3O_4) Nanoparticles and Iron Oxide-Tungsten Trioxide (Fe_3O_4-WO_3) Nanocomposites using Digital Image Processing Techniques

Parashuram Bannigidad [1] [0000-0001-6191-6117], Sagar Chingali [2] [0009-0002-9987-6557] and Prabhuodeyara Gurubasavaraj[3][0000-0002-5281-129X]

[12]Dept. of Computer Science, Rani Channamma University, Belagavi-591156, Karnataka
[3] Dept. of Chemistry, Rani Channamma University, Belagavi-591156, Karnataka

parashurambannigidad@gmail.com,sagar.chingali@gmail.com ,pmgururaj@gmail.com

Abstract.

Nanomaterials made from metal oxides play an important role in nanotechnology because they enhance catalytic efficiencies together with electrical and magnetic properties. The improved resilience combined with the super magnetic nature of Fe_3O_4 (Iron Oxide) and similar metal oxide nanoparticles enables extensive use across biomedicine, environmental remediation and industrial catalytic operations. The integration of iron oxide with tungsten oxide nanoparticles improves photo catalytic performance. The conversion of nanoparticles into nanocomposites generates major structural alterations including enlarged particle dimensions and unique shape structures together with altered geometrical structures. This study utilizes advanced image processing techniques to interpret Fe_3O_4 nanoparticles and Fe_3O_4-WO_3 nanocomposites structural properties by analyzing SEM image data and focuses on extracting and analyzing the structural characteristics such as size, shape, aspect ratio and solidity. Analysis of Fe_3O_4 nanoparticles shows that nanoparticles are elliptical in shape with most nanoparticles size ranges between 51–100 nm but Fe_3O_4-WO_3 nanocomposites are polygonal in shape and size exceeding 200 nm. This research highlights the importance of structural analysis in understanding nanomaterial properties and optimizing their applications.

Keywords: Fe_3O_4 Nanoparticles, Fe_3O_4-WO_3 Nanocomposites, Watershed Segmentation, Metal Oxides, Digital Image Processing, Structural Characteristics.

1 Introduction

Nanoparticles made from metal oxides have become essential materials because they exhibit distinctive physical and chemical properties including high surface area and catalytic capability. Fe_3O_4 nanoparticles are used extensively in biomedicine

applications and in environmental remediation because they have excellent super magnetic properties and exceptional stability. Nanocomposites provide better performance by uniting multiple metal oxides through a material system that permits their component properties to work together synergistically. The combination of iron oxide-tungsten trioxide (Fe_3O_4-WO_3) nanocomposites demonstrates enhanced photo catalytic activity and sensing properties which allows their use for converting energy while monitoring environmental conditions. Nanoparticles evolution into nanocomposites leads to substantial changes in structure with larger particles and disordered shapes along with difficult geometric measurements. Material performance characteristics along with stability and reactivity shift as key properties following these structural modifications. The Fe_3O_4 nanoparticles maintain a narrow size range between 51-100 nm but demonstrate uniform structure distribution and the Fe_3O_4-WO_3 nanocomposites exhibit an overall increased particle size of 201+ nm with reduced structural clarity as a result of tungsten presence. Previous research lacks a full understanding of the structural modifications observed in these materials. This research conducts a thorough examination by studying size and shape properties to understand the structural characteristics variations during nanocomposites synthesis. Green synthesized silver nanoparticles are granular, elliptical in shape and crystalline in nature was proposed by Chowdhury et al. [1]. Nanoparticles have a higher surface area-to-volume ratio, because of this, the electrical, magnetic and optical properties of nanoparticles are quite different compared to the properties of their bulk material was suggested by Anigol et al. [2]. Aida et al. [3] have suggested that green synthesized iron oxide nanoparticles have average size of 20 nm and have super magnetic properties. Analysis of SEM images of nanoparticles confirmed that iron oxide, magnesium oxide nanoparticles, and Fe_3O_4-Mgo nanocomposites are mostly spherical in shape and they have greater thermal stability. The synthesized nanoparticles and nanocomposites showed good antibacterial activity bacterial strains was proposed by Anigol et al. [4]. Nanoparticles consist of wide variety of sizes and shapes, which are crucial for utilizing them in different applications. Khan et al. [5] stated that nanoparticles might be spherical, cylindrical, or irregular. Because their magnetic and physicochemical properties, they are used in biomedical applications. The reduction in particle size led to more reaactive and biodegradable levels of iron oxide was discussed by Yousif et al. [6]. According to the XRD analysis, AgCu/ZnO nanocomposites contain face-centered cubic Ag, face-centered cubic Cu and hexagonal ZnO shapes was analyzed by Çakmak et al. [7]. Doping of tungsten oxide nanoparticles with other metal oxides improves their physical, chemical, and biological properties were demonstrated by Sharma et al. [8]. The watershed technique can be efficiently used to segment overlapping nanoparticles was proposed by Wu et al. [9]. U-Net model can be used for automated size and shape analysis of nanoparticles in scanning electron microscopy was suggested by Bals et al. [10].

Machine learning methods for two-dimensional TEM images can produce better results in characterizing the size and shape of nanoparticle samples, regardless of their contrast was demonstrated by Gumbiowski et al. [11]. Iron-doped tungsten oxide nanorods have diameters ranging from 20 to 30 nm and lengths up to 60–

2000 nm was suggested by Si et al. [12]. Research indicates that WO3 shows high potential as an alternative catalyst to effectively treat both toxic and challenging-to-remove low-concentration pollutants as demonstrated by Yuju et al. [13]. According to Bannigidad et al. [14] nanotechnology provides the capacity to modify the size and structure of nanomaterials, thereby opening up a vast array of possible uses for nanomaterials. Biomedical applications can benefit from iron oxide nanoparticles, as their size usually ranges from 0–50 nm was proposed by Bannigidad et al. [15]. Distance transform and the watershed algorithm can be used to segment particles and obtain individual particles from the electron microscopic image was suggested by Wu et al. [16]. Iron oxide nanoparticles, hold an important place due to their small size as they enhance super magnetic properties was demonstrated by Samrot et al. [17]. Size and shapes of nanocomposites can be used to determine the applications of the metal oxide nanocomposites in applications like sensors, photocatalysis and antibacterial activity was suggested by Bannigidad et al. [18]. Liu et al. [19] proposed that, adding tungsten and iron influenced the microstructure, increased the specific surface area and enhanced the pore structure. Yazdanbakhsh et al [20] have suggested that, the light absorption properties of the obtained nanocomposite are substantially influenced by the doping of Mn into the WO3 lattice structure which may have an effect on the photo-catalytic activity of the material when exposed to visible light. Haruna et al.[21] has highlighted that, FeWO4 nanoparticles, has high surface area, and adsorption, ozonation, photocatalytic and photo-Fenton capabilities.

Previous studies relied primarily on using thresholding and edge detection to segment nanoparticles, but these methods often fail to segment overlapping nanoparticles accurately. More recent works shows that machine learning and deep learning models such as the U-Net model has been widely used for biomedical and material image segmentation, demonstrating high accuracy but requiring large annotated datasets. Previous studies have often analyzed a single nanomaterial, but have not compared the structural characteristics between various nanoparticles and nanocomposites. Furthermore, very few papers discuss how incorporating tungsten changes the structure of iron oxide nanoparticles and how these changes can be systematically examined with the help of digital image processing techniques.

This work uses CLAHE technique for pre-processing the SEM image to enhance its quality, Gaussian blur to smooth high-frequency noise to preserving nanoparticles/nanocomposites boundaries, uses Otsu's method to compute an optimal threshold value and generate a binary mask and watershed segmentation technique for segmenting the particles. This technique works well for overlapped particles as well and do not require more training dataset or specialized hardware. Therefore, this study represents use of image processing techniques to preprocess and segment and performing comparative analysis of Fe_3O_4 nanoparticles and Fe_3O_4-WO_3 nanocomposites. This research highlights the importance of structural analysis in understanding the impact of tungsten doping on the structural characteristics of the Fe_3O_4 nanoparticles.

2 Materials and Methods

2.1 Materials

FeSO4.7H2O, Fe(NO3)2.9H2O, ammonia or ammonium hydroxide, nitrogen gas, distilled water, ethanol, tetraethylorthosilicate, tungsten oxide (WO3) was purchased from Sigma Aldrich. All glassware's employed in the experimental part were thoroughly washed with ethanol and distilled water as well as dried in oven. Instruments used in the preparation procedures such as rotary evaporator, magnetic stirrer with hot plate, pH meter and thermometer is taken care.

2.2 Preparation of Magnetic Iron Oxide Nanoparticles

4.17g of $FeSO_4.7H_2O$ and 12.12g of Fe $(NO_3)_2.9H_2O$ is dissolved in 150 ml of distilled water in 250 ml round bottom flask with nitrogen gas at stirring with 70℃ temperature for an hour. Then add ammonia (NH_3) to maintain pH 9-10 after addition of ammonia black ppt formed. The stirring 24 hours at 800 RPM & 70℃. To remove contaminants, the black ppt was washed with distilled water and ethanol multiple times then compound is separate by using permanent magnet then dried in oven at 80℃. The compound is formed.

2.3 Preparation of WO_3 Nanoparticles

5.94g of WO3 (0.1M) (200ml) and 50ml of Rudanti fruit extract were combined in a 500ml two-necked flask. The reaction mixture had been stirred at 80°C for 4 hours. After cooling to room temperature, the WO3 nanoparticles were obtained via centrifugation (6000rpm) and calcined at 600°C for 5 hours.

2.4 Preparation of Fe_3O_4-WO_3 nanocomposites

Silica coated Fe3O4-nanoparticles 300mg were dispersed in 50ml distilled water in 100ml RB flask with sonication. Then a solution of WO3 (100mg, 0.012mmol) in 10ml distilled water was added to above mixture and stirred for 12 hours. Then the product was magnetically separated and dried in air.

2.5 SEM Characterization

The surface morphology of the nanoparticles and nanocomposites were determined by scanning electron microscopy (SEM) and EDX. SEM image was taken with JSM 7100F Joel SEM with 10K to 80K resolutions. Further elemental composition can be studied using EDX.

3 Proposed Method

High resolution SEM images of Fe3O4 nanoparticles as shown in Fig. 1 (a) alongside Fe3O4-WO3 nanocomposites as shown in Fig. 2(a) were acquired. The images were preprocessed as shown in Fig. 1 (b) and Fig. 2 (b) to reduce noise and used contrast enhancement techniques to produce clear images which facilitated in particle segmentation and detection. Through watershed segmentation, individual particles are

separated as shown in Fig. 1 (c) and Fig. 2 (c) from both the SEM images. The segmentation process enabled the extraction of morphological characteristics including particle size and shape together with aspect ratio and circularity and solidity measures. Analyzing the particular set of features, helps researchers to study structural characteristics changes when one nonmaterial is integrated with another to form a nanocomposites material. The extracted particles are classified in different size ranges such as 0-50, 51-100, 101-150, 151-200, 201+ and shapes such as circular, elliptical and polygonal. This complete procedure is shown in Fig.1. Our approach is different from traditional ones, since it processes images of two different nanomaterials using a single strategy. It emphasizes the differences in structural characteristics caused by doping tungsten with iron oxide, which is rarely explored using SEM image segmentation.

Algorithm for Fe_3O_4 nanoparticles and Fe_3O_4-WO_3 nanocomposites detection and analysis

Step 1: Input the SEM images of Fe_3O_4 nanoparticle and Fe_3O_4-WO_3 nanocomposites.

Step 2: Apply CLAHE, image preprocessing technique to improve the contrast of the SEM images.

Step 3: Use Gaussian blur with an appropriate kernel size to smooth high-frequency noise to preserving nanoparticles/nanocomposites boundaries.

Step 4: Use Otsu's method to compute an optimal threshold value and generate a binary mask for separating nanoparticles/ nanocomposites from the background.

Step 5: Apply erosion to refine particle boundaries and remove small artifacts. Use dilation to restore particle sizes and connect fragmented regions.

Step 6: Apply the watershed algorithm to segment nanoparticles/nanocomposites and assign unique labels to each detected particle.

Step 7: Count the total number of particles by calculating the unique labels in the segmented image.

Step 8: Compute particle size in nanometer and classify nanoparticles/ nanocomposites into different size groups such as 0–50 nm, 51–100 nm, 101–150 nm, 151–200 nm, 201+ nm.

Step 9: Use aspect ratio and solidity to classify particles into circular, elliptical, or polygonal shapes.

Step 10: Store all the extracted features in a matrix, transforming them into a knowledge base for comparative analysis.

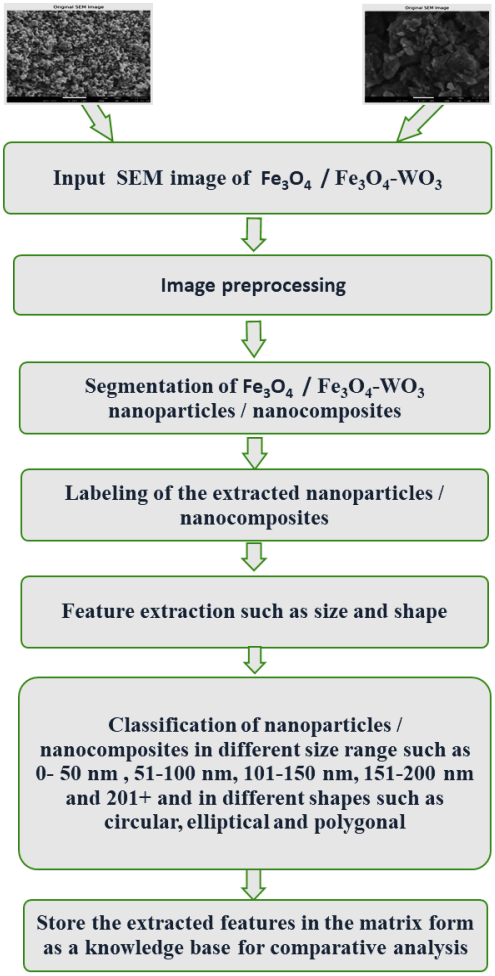

Fig. 1. Flow diagram of the proposed methodology

The proposed approach was selected for its efficient processing capabilities and segmentation of nanoparticles/nanocomposites using high-contrast SEM images. Watershed segmentation technique enables accurate segmentation of nanoparticles/nanocomposites without relying on large annotated datasets or complex model training, thus saving computational resources. This methodology is well suited for the comparison of structural characteristics between Fe3O4 nanoparticle and Fe3O4-WO3 nanocomposites.

4 Experimental Results and Discussion

Fe3O4 nanoparticles demonstrated a predominant circular shape and compact size pattern yet Fe3O4-WO3 revealed larger polygonal shaped nanocomposites. The

classification system reveals structural changes which occur when iron oxide is doped with tungsten oxide to create iron oxide-tungsten trioxide nanocomposites materials. Extensive analysis confirmed the possession of various features between Fe3O4 nanoparticles and Fe3O4-WO3 nanocomposites. The distribution analysis of Fe3O4 particles demonstrated that the majority (51–100 nm) fell within the smaller range while measurements showed Fe3O4-WO3 particles exceeding 200 nm in size. The circular particles accounted for a higher proportion in Fe3O4 which demonstrated uniformity but the Fe3O4-WO3 nanocomposites contained polygonal particles resulted from tungsten integration. The structural characteristics analysis of SEM images demonstrated clear structural variations in terms of shape and size exists between Fe3O4 nanoparticles and Fe3O4-WO3 nanocomposites. Most Fe3O4 particles measure between 51–100 nm where as Fe3O4-WO3 nanocomposites measure between 201+ nm ranges. Fe3O4 nanoparticles are predominantly elliptical in shape and Fe3O4-WO3 nanocomposites are polygonal in shape which shows there are clear shape variations. The images were preprocessed, segmented as shown in Fig. 2 and Fig. 3 and analyzed using Anaconda Jupyter notebook on an Intel Core i7-2640 M CPU@ 2.80 GHz using Windows 10 operating system.

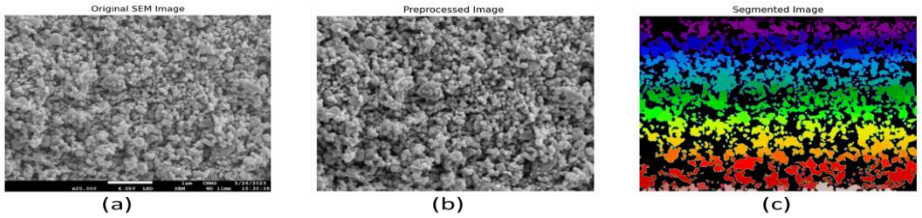

Fig. 2. Sample SEM image of Fe_3O_4 Nanoparticles a) Original image b) Preprocessed image c) Segmented image

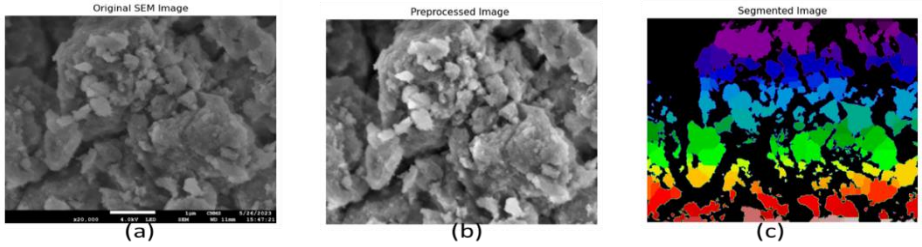

Fig. 3. Sample SEM image of Fe_3O_4-WO_3Nanocomposites a) Original image b) Preprocessed image c) Segmented image

4.1 Size Distribution:

Fe3O4 particles are predominantly small, with over half falling within the 51–100 nm size range as shown in Table 1. A small number of nanoparticles exist at the extreme end of their size spectrum (201+ nm).

Table 1. Size- wise number of nanoparticles of Fe_3O_4

Size range (nm)	Number of nanoparticles	Percentage (%)
0–50	147	12.8
51–100	509	44.2
101–150	309	26.9
151–200	115	10.0
201+	71	6.1

Fe3O4-WO3 nanocomposites show a significant shift towards larger particle sizes, with over half of the particles exceeding 200 nm as shown in Table 2. The incorporation of tungsten leads to enhanced growth and aggregation patterns of the particles. The particle morphologies for Fe3O4 show that circular shapes predominant indicating widespread structural consistency. The synthesis of Fe3O4-WO3 nanocomposites leads to polygonal-shaped particles which demonstrate irregular growth patterns from tungsten. The uniform small size and concentration of Fe3O4 nanoparticles coupled with high circularity and stability makes them suitable for biomedical imaging applications and catalyst production. The large irregular particles of Fe3O4-WO3 nanocomposites expose increased surface area and reactivity characteristics that enable photo catalysis and environmental cleanup operations.

Table 2. Size- wise number of nanocomposites of Fe_3O_4-WO_3

Size range (nm)	Number of nanocomposites	Percentage (%)
0–50	5	1.2
51–100	73	17.6
101–150	64	15.4
151–200	52	12.5
201+	221	53.3

The bar chart in Fig.4 and pie chart in Fig. 5 represents the size distribution between Fe3O4 nanoparticles and Fe3O4-WO3 nanocomposites, confirming that Fe_3O_4-WO3 nanocomposites predominantly exhibit larger particles exceeding 200 nm in size.

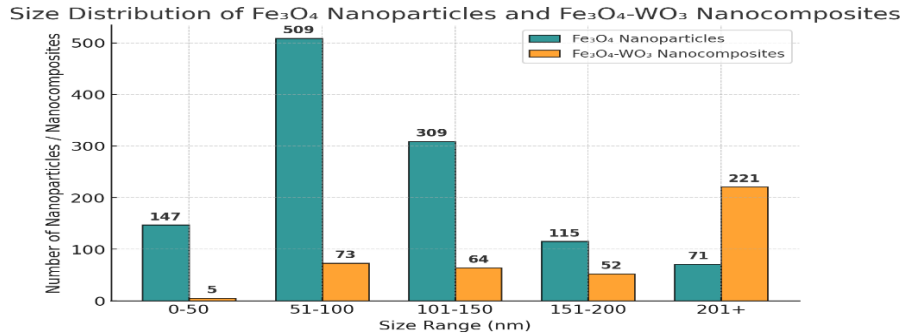

Fig. 4. Bar chart for size distribution between Fe_3O_4 and Fe_3O_4-WO_3

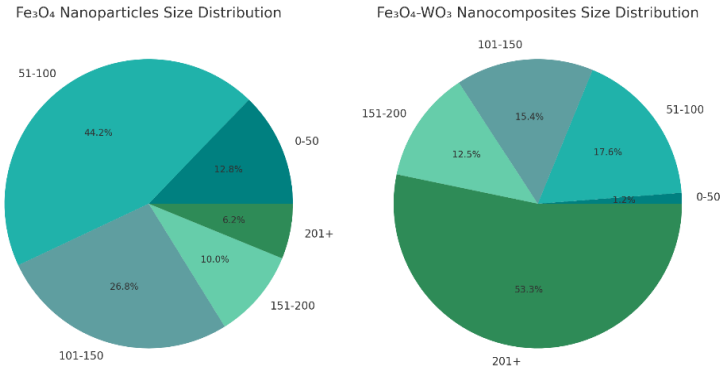

Fig. 5. Pie chart for size distribution between Fe_3O_4 and Fe_3O_4-WO_3

4.2 Shape Distribution:

Fe3O4 particles exhibit a higher percentage of elliptical particles, as shown in Table 3 indicating more uniformity in morphology.

Table 3. Shape- wise number of nanoparticles of Fe_3O_4

Shape	Number of nanoparticles	Percentage (%)
Circular	178	15.5
Elliptical	732	63.6
Polygonal	241	20.9

Fe3O4-WO3 nanocomposites display a higher proportion of polygonal particles, as shown in Table 4, suggesting irregular growth and structural complexity introduced by tungsten.

Table 4. Shape-wise number of nanocomposites of Fe_3O_4-WO_3

Shape	Number of nanocomposites	Percentage (%)
Circular	29	7.0
Elliptical	148	35.7
Polygonal	238	57.3

The bar chart in Fig.6 and pie chart in Fig.7 represents the shape distribution between Fe3O4 nanoparticles and Fe3O4-WO3 nanocomposites, confirming that Fe3O4 nanoparticles are elliptical in shape whereas Fe_3O_4-WO3 nanocomposites predominantly polygonal in shape.

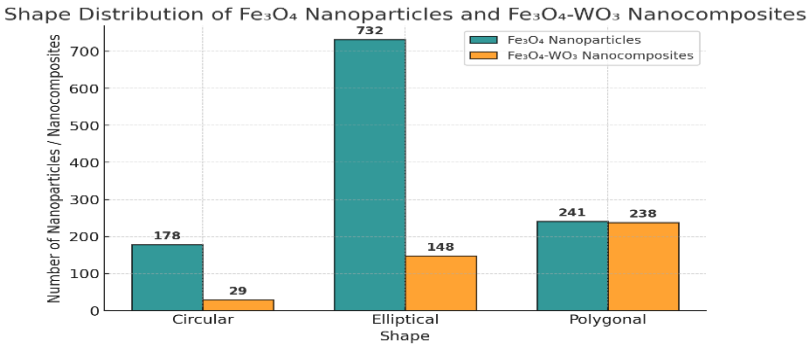

Fig. 6. Bar chart for shape distribution between Fe_3O_4 and Fe_3O_4-WO_3

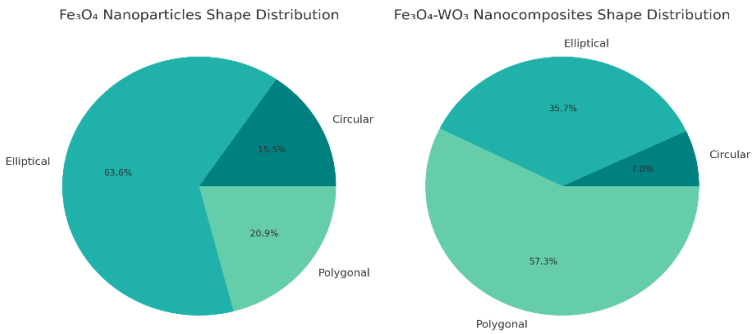

Fig. 7. Pie chart for shape distribution between Fe_3O_4 and Fe_3O_4-WO_3

4.3 Comparative Analysis:

Fe3O4 nanoparticles are characterized by smaller, more uniform particles with high circularity and solidity, making them ideal for applications requiring stability and uniformity, such as biomedical imaging and catalysis. Due to the larger polygonal structure, Fe3O4-WO3 nanocomposites offer more reactivity which makes them ideal for environmental remediation and using as photocatalyst. The watershed segmentation technique demonstrated robust performance in distinct particle recognition when boundaries crossed each other or became irregular. The method's precise detection capability allowed researchers to analyze detailed comparisons between structural features as listed out in Table 5 so they could establish links between material shape and operational properties between these two metal oxides.

Table 5. Comparative analysis of nanoparticles sizes and shapes for Fe_3O_4 and Fe_3O_4-WO_3

Parameters	Fe_3O_4 nanoparticles	Fe_3O_4-WO_3 nanocomposites	Observations
Total number of nanoparticles/ nanocomposites	1151	415	Fe_3O_4 has more particles due to its smaller size and uniform shape. The reduction in Fe_3O_4-WO_3 particles count suggests agglomeration during Fe_3O_4-WO_3 composite formation.
Most common size	51–100 nm :509 particles (44.2%)	201+ nm : 221 particles (53.3%)	Fe_3O_4 particles are smaller, while Fe_3O_4-WO_3 particles are larger due to tungsten incorporation.
Largest size range	201+ nm: 71 particles (6.2%)	201+ nm: 221 particles (53.3%)	Fe_3O_4-WO_3 particles shows a significant shift towards larger particle sizes.
Smallest size range	0–50 nm: 147 particles (12.8%)	0–50 nm: 5 particles (1.2%)	Fe_3O_4 contains more number of smaller particles as compared to Fe_3O_4-WO_3
Circular particles	178 particles (15.5%)	29 particles (7.0%)	Fe_3O_4 has a higher proportion of circular particles.
Elliptical particles	732 particles (63.6%)	148 particles (35.7%)	Elliptical particles dominate in both, but the percentage is higher in Fe_3O_4 particles.
Polygonal particles	241 particles (20.9%)	238 particles (57.3%)	Fe_3O_4-WO_3 has a much higher percentage of polygonal particles than Fe_3O_4.

5 Conclusion

This study demonstrates how Fe3O4 nanoparticles transform structurally into Fe3O4-WO3 nanocomposites while examining their subsequent material properties. Moving from nanoscale particles to nanoscale composites introduces dramatic changes in structural characteristics that affect operational results across multiple applications. Uniform Fe3O4 nanoparticles demonstrate spherical morphology which makes them excellent choices for biomedical applications and industrial catalyst operations. Fe3O4-WO3 nanocomposites exhibit better performance levels at photo catalysis applications and environmental remediation due to their enlarged irregular shaped particles. Advanced image processing techniques combined with watershed segmentation aids in precise nanoparticles and nanocomposites detection. Analysis of Fe3O4 nanoparticles shows that nanoparticles are elliptical in shape with most nanoparticles size ranges between 51–100 nm whereas Fe3O4-WO3 nanocomposites are polygonal in shape and size exceeding 200 nm in size. These findings help in better understanding of nanomaterial structural characteristics, thus by opening the path for more effective applications in photocatalysis, sensing, and environmental remediation. A comprehensive comparison indicates structural differences between Fe3O4 nanoparticles and Fe3O4-WO3 nanocomposites, potentially affecting their

material properties. This method lays the groundwork for upcoming studies on structure activity relationships of metal oxide nanocomposites.

References

1. Chowdhury, Rashedul Alam, Sajib Aninda Dhar, Shaon Das, Md Khalid Nahian, and Md Rakibul Qadir. "Green synthesis and characterization of silver nanoparticles from the aqueous extract of the leaves of Citrus aurantifolia." Materials Today: Proceedings 44,1039-1042 (2021)
2. Anigol, Lakkappa B., Jasmith S. Charantimath, and Prabhuodeyara M. Gurubasavaraj. "Effect of concentration and pH on the size of silver nanoparticles synthesized by green chemistry." Org. Med. Chem. Int. J 3(5) ,1-5 (2017)
3. Aida, M. S., N. Alonizan, B. Zarrad, and M. Hjiri. "Green synthesis of iron oxide nanoparticles using Hibiscus plant extract." Journal of Taibah University for Science 17(1), (2023)
4. Anigol, L. B., V. P. Sajjan, and P. M. Gurubasavaraj. "Evaluation of Antioxidant and Antibacterial Property of Microwave Assisted Green Synthesis of Fe_3O_4-MgO Nanocomposites." IJST 16(24), 1777-1786 (2023)
5. Khan, Yousaf, Haleema Sadia, Syed Zeeshan Ali Shah, Muhammad Naeem Khan, Amjad Ali Shah, Naimat Ullah, Muhammad Farhat Ullah et al. "Classification, synthetic, and characterization approaches to nanoparticles, and their applications in various fields of nanotechnology: a review." Catalysts 12(11), 1386 (2022)
6. Yousif, Nwar A., Selma M. Al-Jawad, Ali A. Taha, and Haralambos Stamatis. "A review of structure, properties, and chemical synthesis of magnetite nanoparticles." Journal of Applied Sciences and Nanotechnology 3(2) 18-31 (2023)
7. Çakmak, Tolga, Elif Emil Kaya, Demet Küçük, Burçak Ebin, Onur Balci, and Sebahattin Gürmen. "Novel strategy for one-step production of attenuated Ag-containing AgCu/ZnO antibacterial-antifungal nanocomposite particles." Powder Metallurgy and Metal Ceramics 59, 261-270 (2020)
8. Sharma, Anirudh, Adesh K. Saini, Nitin Kumar, Neeraj Tejwan, Th Abhishek Singh, Vijay Kumar Thakur, and Joydeep Das. "Methods of preparation of metal-doped and hybrid tungsten oxide nanoparticles for anticancer, antibacterial, and biosensing applications." Surfaces and Interfaces 28 ,101641 (2022)
9. Wu, Y., Wang, W., Zhang, F., Xiao, Z., Wu, J., & Geng, L. Nanoparticle size measurement method based on improved watershed segmentation. In Proceedings of the 2018 International Conference on Electronics and Electrical Engineering Technology (pp. 232-237). (2018)
10. Bals, J., & Epple, M. Deep learning for automated size and shape analysis of nanoparticles in scanning electron microscopy. RSC advances, 13(5), 2795-2802. (2023)
11. Gumbiowski, N., Loza, K., Heggen, M., & Epple, M. Automated analysis of transmission electron micrographs of metallic nanoparticles by machine learning. Nanoscale advances, 5(8), 2318-2326. (2023)
12. Si, P. Z., Choi, C. J., Brück, E., Klaasse, J. C. P., Geng, D. Y., & Zhang, Z. D. Synthesis, structure and magnetic properties of iron-doped tungsten oxide nanorods. Physica B: Condensed Matter, 392(1-2), 154-158. (2007)
13. Yuju, S., Xiujuan, T., Dongsheng, S., Zhiruo, Z., & Meizhen, W. A review of tungsten trioxide (WO_3)-based materials for antibiotics removal via photocatalysis. Ecotoxicology

and Environmental Safety, 259, 114988 (2023)
14. Bannigidad, Parashuram, Namita Potraj, and Prabhuodeyara Gurubasavaraj. "Metal and Metal Oxide Nanoparticle Image Analysis Using Machine Learning Algorithm." In International Conference on Big Data Innovation for Sustainable Cognitive Computing, pp. 27-38. Cham: Springer Nature Switzerland, (2022)
15. Bannigidad, Parashuram, Namita Potraj, Prabhuodeyara Gurubasavaraj, and Lakkappa Anigol. "Iron Oxide Nanoparticle Image Analysis Using Machine Learning Algorithms." In Emerging Research in Computing, Information, Communication and Applications: Proceedings of ERCICA 2022, pp. 233-240. Singapore: Springer Nature Singapore, (2022)
16. Pan, S. W., X. Guo, and M. M. Zhang. "Rock image segmentation based on wavelet transform and watershed algorithm." In Proceedings of the International Field Exploration and Development Conference 2017, pp. 316-325. Springer Singapore, (2019)
17. Samrot, Antony V., Chamarthy Sai Sahithya, Jenifer Selvarani, Sajna Keeyari Purayil, and Paulraj Ponnaiah. "A review on synthesis, characterization and potential biological applications of superparamagnetic iron oxide nanoparticles." Current Research in Green and Sustainable Chemistry, 4, 100042 (2021)
18. Bannigidad, P., Chingali, S., & Gurubasavaraj, P. M. “Biosynthesized Mgo-Zno metal oxide nanocomposite image analysis using machine learning algorithms.” Journal of Dynamics and Control, 8(9), 609–620 (2024)
19. Liu, J., Wang, S. L., Xuan, J. L., Shan, B. F., Luo, H., Deng, L. P., ... & Qi, C. Z. Preparation of tungsten–iron composite oxides and application in environmental catalysis for volatile organic compounds degradation. Tungsten, 1-14. (2022)
20. Yazdanbakhsh, A., Eslami, A., Massoudinejad, M. et al. Photocatalytic degradation and dechlorination mechanism of diclofenac using heterojunction Mn-doped tungsten trioxide (Mn-WO_3) nanoparticles under LED visible light from aqueous solutions. Sci Rep 14, 29583 (2024)
21. Haruna, M. S., Oladapo, B. H., Mustapha, S., Scholartica, C. E., Tijani, J. O., & Abdulkareem, A. S. A review of iron-tungstate nanomaterials: Synthesis methods, physicochemical properties, environmental fate and application for wastewater treatment. Sustainable Chemistry for the Environment, 5, 100074. (2024)

Sustainable Healthcare Systems through Arduino-Driven Medical Waste Segregation and Disposal Monitoring

Dr. Sharada M. Kori1 , Prof. Yogesh Lubal2, Prof. Jyoti Amboji1, Madhuri M. Patil1[1]

smkori@git.edu ysl_cse@adcet.in jyamboji@git.edu madhuripa412@gmail.com

1Department of Computer Science & Engineering, KLS Gogte Institute of Technology, Belagavi, Karnataka 590 008, India

2 Department of Computer Science and Engineering, Annasaheb Dange College of Engineering and Technology, Ashta,-41610, India

Abstract. Studies suggest that between 25-50% of medical and healthcare waste is not managed safely. A Global threat that all countries with concerned Economic situation is Medical Waste segregation, where approximately 25million tons of medical waste is generated worldwide. The irregularities in Segregation and disposal will spread to contagious diseases and serious injuries to health care workers and waste handlers, it also causes serious contaminations to the environment and affects the people with economical and health hazards. To mitigate and minimize these risks, proper segregation mechanism has to be developed for medical waste segregation. The Mechanism involves identifying the type of waste at the point of generation and ensuring proper handling, storing, transporting and disposing of them. The aftermath cost is more comparable because of the health hazards the infectious medical waste could bring to the exposed, also the separation and disposal at the end stage makes the process more tedious and more cost involved. By addressing the issue of segregation and executing them with the proposed methodology will induce mitigation and prevention of health hazards caused due to improper medical waste segregation..

Keywords: IoT, Sensors, Actuators, Healthcare Systems, Medical Waste Management.

1 Introduction

The health care sector is predominant in enhancing human health and ironically generates huge volume of medical waste that brings serious health and environmental challenges globally [1]. This can be mitigated by a proper waste management system.

The Global medical waste management market is one of the fastest growing, for which the CAGR is estimated to be between 5-8% from 2023 to 2030. Responsible medical waste management has become a critical aspect of health care practices, looking into sustainability as the vision. The revolutionary proposed system, “Sustainable Healthcare Systems: Arduino driven Medical Waste segregation and

Disposal Monitoring" in the field of medical waste segregation and disposal management, focusing on the prime requirement of ensuring safety of health care workers, Patients and public by minimalizing and preventing the effects to a greater extend [2].

The system employs an adaptable controller platform integrated with Color Sensor, Moisture sensor, RFID & GSM modules to create and sustainable automated system. The system's adaptability enhances the waste segregation accuracy and enables a real-time monitoring of waste disposal, to ensure to achieve the sustainability goal in health care practices.

Medical waste generated by healthcare facilities poses significant risks to public health and the environment if not managed properly. Improper handling, inadequate segregation, and inappropriate disposal of medical waste can lead to injuries, infectious disease transmission (for example, HIV, hepatitis B & C, and tetanus), environmental pollution, and occupational hazards for healthcare workers and waste handlers. Therefore, ensuring that healthcare facilities comply with established guidelines and regulations regarding medical waste management is crucial [4].

Various international and national organizations, such as the World Health Organization (WHO) and regulatory bodies, have developed guidelines and standards for segregating and disposing of medical waste. These guidelines emphasize the importance of proper waste segregation at the point of generation, safe storage, transportation, and appropriate disposal methods, such as incineration, autoclaving, or alternative treatment technologies [5].

2 Literature Review

The key findings of the literature review are listed below:

•Importance of Sustainable Healthcare: Sustainable healthcare practices, including the responsible management of medical waste, are crucial for reducing the environmental impact of healthcare facilities [6].

•Medical Waste Management Challenges: Existing medical waste management methods face challenges regarding the accuracy of waste segregation, real-time monitoring, and compliance with regulations [7].

•Role of Technology in Healthcare Waste Management: Technology, including the Internet of Things (IoT) and sensor-based solutions, is increasingly being adopted

to enhance medical waste management processes [8].

•Arduino in Medical Waste Management: Arduino microcontrollers are versatile and cost-effective tools that can create efficient waste management systems. Researchers have explored using Arduino for real-time monitoring, data collection, and automation in waste management [9].

•Sensors for Waste Segregation: Color and moisture sensors have been employed to accurately segregate medical waste based on color-coded and moisture content criteria [10].

•RFID Technology for Tracking and Communication via GSM: RFID (radiofrequency identification) technology enables real-time tracking of waste bins, improving waste logistics and traceability [11]. GSM (Global System for Mobile Communications) modules provide real-time communication, enabling alerts and notifications in waste management systems.

•Benefits of Integration, Case Studies, and Practical Applications: Integrating Arduino, sensors, RFID, and GSM modules offers a comprehensive solution for accurate segregation, real-time monitoring, and data-driven decision-making. Several case studies and practical implementations of similar systems have demonstrated improvements in waste management efficiency, cost-effectiveness, and compliance [12].

Regulatory Compliance: Adherence to local and national regulations for medical waste management is essential, and technology can aid in compliance efforts [13]
Environmental and Public Health Implications: Proper medical waste management safeguards public health and prevents environmental contamination, making it a critical aspect of healthcare sustainability [14].

Proposed Methodology

Despite the availability of guidelines, implementing and adhering to proper medical waste management practices can be challenging for healthcare facilities. Factors such as lack of awareness, inadequate training of healthcare staff, insufficient infrastructure, limited resources, and compliance monitoring contribute to noncompliance with waste management regulations. As a result, this study incorporates With IoT, which enables real-time monitoring of medical waste levels, it automates alert generation for timely disposal. Arduino as the core control system, addressing concerns regarding the environmental and safety risks associated with inadequate waste management practices. The main objectives of this research were 1) to develop an innovative solution that leverages Arduino technology to enhance medical waste segregation and disposal monitoring. 2) To improve hospital medical waste management and disposal.

Functional Block Diagram:

The various functional units of the Arduino-driven medical waste segregation and monitoring system are shown in Figure 1.

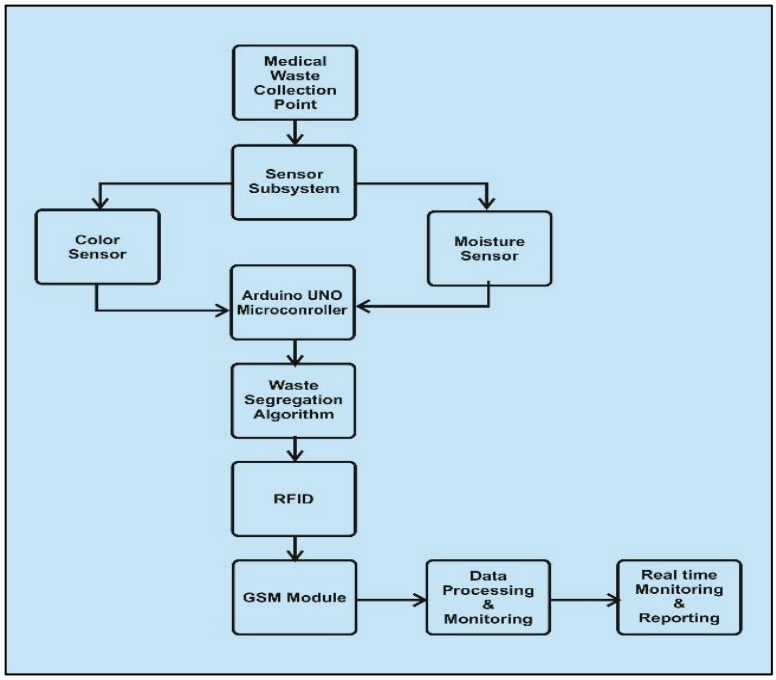

Figure 1: Functional block diagram of the medical waste segregation and monitoring system

1. **Medical Waste Collection Point:** This is where medical waste is initially collected in different color bins.
2. **Arduino UNO Microcontroller:** The Arduino UNO serves as the central control unit, orchestrating the functions of the entire system.
3. **Sensor Subsystem:** This subsystem includes color and moisture sensors

for waste characterization.

4. **Waste Segregation Algorithm:** This algorithm processes sensor data to segregate waste based on color and moisture content.

5. **RFID System:** RFID technology enables real-time tracking of waste bins or containers.

6. **GSM Communication Module:** The GSM facilitates the communication of important data and alerts to stakeholders.

7. **Data Processing and Monitoring Software:** Software on a connected computer or server processes data received from the Arduino and manages monitoring functions.

8. **Real-time Monitoring and Reporting:** This is where real-time data are monitored and reports or alerts are generated for waste management personnel.

Each component or subsystem is critical for achieving the project's objectives of enhancing medical waste segregation and real-time disposal monitoring within healthcare facilities.

3. Methodology

This design employs color-coded containers – red, blue, and yellow – to categorize different types of waste in the hospital. Let ‘C’ represent the set of color-coded containers, where each container is denoted by ci for i in the range of 1 to ‘n’

(number of containers). Each container ci is associated with a specific color, represented by color(ci). Ultrasonic sensors measure the distance to waste for disposal. Let Di represent the distance measured by the ultrasonic sensor for container ci. Subsequently, an SMS alert is sent to designated staff members to empty the corresponding waste bin. Let Asms be the function triggering the SMS alert, as shown in equation (1).

$$\text{if } D_i > D_{threshold} \text{ trigger SMS: } A_{sms}(D_i) = \{\frac{1 \ if \ D_i > D_{threshold}}{0 \ otherwise} : (1)$$

Additionally, a color sensor verifies whether the bag matches the container's assigned color code. Let Bi represent the binary variable indicating whether the bag matches the color code for container ci. Otherwise, an audible buzzer notifies the staff of the discrepancy. Let Abuzzer represent the function triggering the audible buzzer, as expressed in equation (2).

$$\text{if Bi} = 0, \text{trigger audible buzzer: A_buzzer (B_i)} = \{(1 \text{ if B_i} = 0)/(0 \text{ if B_i} = 1) \quad : (2)$$

A moisture sensor was used to monitor moisture levels within the containers. Let Mi represent the moisture level measured for container ci . Upon detection, a message prompts the responsible staff member to dispose of the container within 24 hours.

$$\text{if } M_i > M_threshold, \text{ send a message to dispose of the container within 24 hours:}$$

$$A_{moisture}(M_i) = \{\frac{1 \ if \ M_i > M_{threshold}}{0 \ otherwise} : (3)$$

Failure triggers an automated message to a higher-ranking officer responsible for biomedical waste management. Staff members must scan an attached RFID tag before sending a container for disposal, as shown in equation (4).

$$RFID_Scanned = \{(1\ if\ RFID\ tag\ is\ scanned)/(0\ otherwise)\ \ :\ (4)$$

They can then track progress using a mobile app and monitor it via the Blynk app to ensure that it reaches its designated destination, as shown in equation (5).

$$Disposal_Action = \{\ (1\ if\ container\ is\ disposed)/(0\ otherwise)\ \ :\ (5)\ \ :\ (5)$$

The architecture of the medical waste segregation and monitoring system is shown in Figure 2. The pseudocode for the proposed system is shown in Figure 3 and Figure 4, respectively.

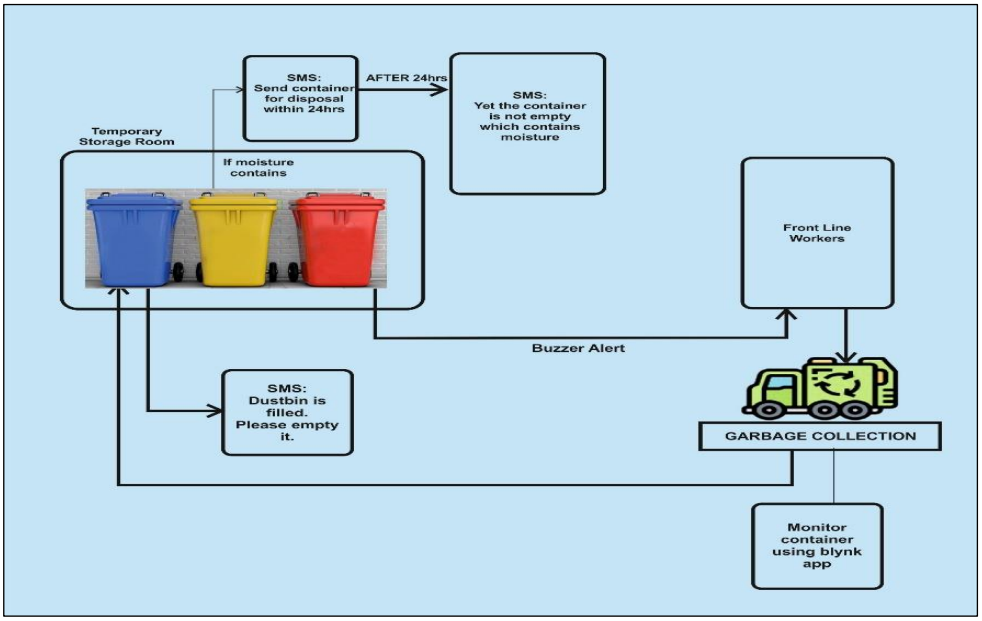

Figure 2: Architecture of the medical waste segregation and monitoring system

```
# Initialize color-coded containers
containers = []

# Initialize sensor readings
ultrasonic_distances = []
color_matches = []
moisture_levels = []

# Initialize RFID tag status
rfid_scanned = False

# Main loop
while True:
    # Read sensor data
    for container in containers:
        ultrasonic_distance = read_ultrasonic_sensor(container)
        color_match = read_color_sensor(container)
        moisture_level = read_moisture_sensor(container)
        ultrasonic_distances.append(ultrasonic_distance)
        color_matches.append(color_match)
        moisture_levels.append(moisture_level)
```

Figure 3: Pseudocode to read sensor data of the proposed system

```
# Check for alerts
for i in range(len(containers)):
    if ultrasonic_distances[i] > 10:
        send_sms_alert(container)
    if not color_matches[i]:
        trigger_audible_buzzer(container)
    if moisture_levels[i] > 50:
        send_moisture_alert(container)

# Check RFID tag status
if not rfid_scanned:
    scan_rfid_tag()
    rfid_scanned = True

# Perform actions
for container in containers:
    if needs_disposal(container):
        dispose_container(container)
    track_container_progress(container)

# Delay before next iteration
time.sleep(1)
```

Figure 4: Pseudocode to check alerts of the proposed system

4. Results

This section delves into the findings. Figure 5 illustrates the comprehensive hardware setup of the medical waste segregation and monitoring system. An alert message is sent if the waste is not disposed of, as shown in Figure 6. The color of the color sensors was used to determine the color of the bag, with the output displayed on a serial monitor, as depicted in Figure 7.

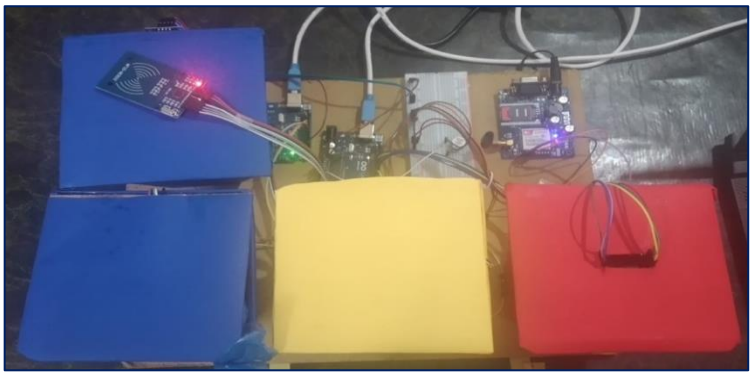

Figure 5: Hardware setup for the medical waste segregation and monitoring system

Figure 6: Alert message

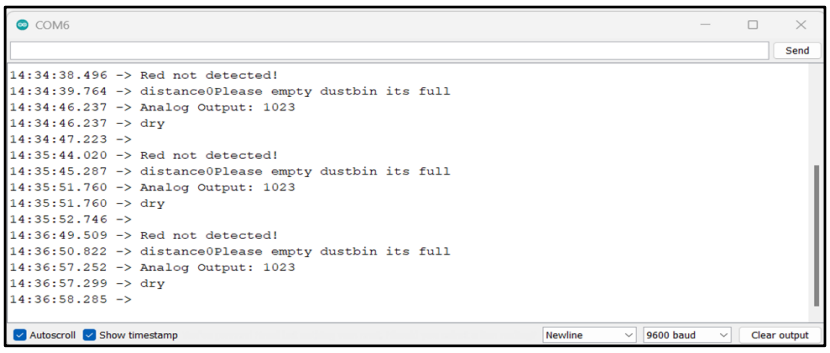

Figure 7: Color sensor output

The moisture sensor will examine moisture levels, and if moisture is detected, an SMS will be sent to the corresponding staff member following the scanning process. Container tracking commences via the Blynk app, and the status is continuously refreshed within the app, as shown in Figure 8.

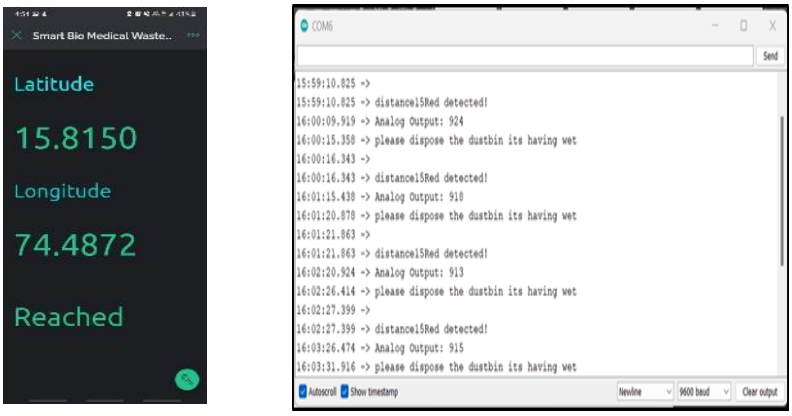

Figure 8: Blynk App and RFID Tag Status

5. Discussion

For the 100 color-coded containers in the hospital waste management system, the following results were observed:

Alert Triggers:

1. Twenty SMS alerts (A_{sms}=1) were triggered due to distances exceeding the threshold.
2. Fifteen audible buzzer notifications (A_{buzzer}=1) were triggered due to mismatched color codes.

To calculate the percentage of correct alerts for color matching, let us assume that 10 out of the 15 alerts were due to actual mismatched color codes, as shown in equations (6) and (7).

$$\text{Correct Alerts}(\%) = \frac{\text{Number of Correct Alerts}}{\text{Total Number of Alerts}} * 10 \quad : (6)$$

$$\text{Correct Alerts}(\%) = \frac{10}{15} * 100 = 66.67\% \quad : (7)$$

Moisture Levels:

1. Twenty-five containers had moisture levels exceeding the threshold ($A_{moisture}$=1).

To monitor the staff's response rate, let us assume that 20 out of the 25 containers were disposed of within 24 hours after receiving the message prompting disposal due to high moisture levels. The response rate is calculated as shown in equations (8) and (9).

$$\text{Response Rate}(\%) = \frac{\text{Number of Disposed Containers}}{\text{Number of Containers with High Moisture Levels}} * 100 : (8)$$

$$\text{Response Rate}(\%) = \frac{20}{25} * 100 = 80\% : (9)$$

RFID Tag and Tracking

1. Ninety percent of containers had scanned RFID tags before disposal.
2. Containers' progress was effectively tracked using the mobile app and

Blynk app, ensuring timely disposal and proper management.

Overall System Performance

1. Analyzing the frequency and response time of staff actions indicates that, on average, containers are disposed of within 24 hours after being prompted by alerts. However, there might be occasional delays in response time.
2. No significant bottlenecks were identified in the system's workflow based on the results.

6. Conclusion

Implementing this system facilitates the convenient monitoring and tracking of infectious medical waste, effectively preventing waste contamination and the potential spread of diseases. This ensures appropriate waste disposal by promptly alerting personnel through SMS when containers are full and enabling tracking via GPS modules. Additional sensors, such as gas and water sensors, can be integrated to further enhance this system, and the project can benefit from upgraded module types. Novelty lies in integrating cloud and IoT as a software platform for real-time monitoring tailored specifically for medical waste, a less explored domain. The system's main ability to identify hazardous waste types and alert disposal services sets it apart from traditional systems.

7. Future Research and Challenges

Future research should focus on refining and optimizing Arduino-driven waste management systems, addressing scalability, and conducting comprehensive cost-benefit analyses. A literature survey highlights the growing importance of sustainable healthcare practices and the potential of Arduino-driven technology in improving medical waste segregation and disposal monitoring. By integrating sensors, RFID, and GSM communication, healthcare facilities can enhance waste management efficiency, reduce environmental impact, and ensure compliance with regulations. The performance of this system can be enhanced by calibrating optimized sensors and by improving code efficiency for real-time processing and integrating machine learning algorithms for smarter waste segregation. Future research should continue to explore innovative solutions and address practical challenges in implementing these systems effectively.

References

1.Surme Y, Maraş G. Recycling, responsible consumption, and nursing: A qualitative study of surgical nurses' recycling and medical waste management. J Nurs Manag. 2022 Nov;30(8):4514-4522. doi: 10.1111/jonm.13891. Epub 2022 Nov 12. PMID: 36326215.

2.Wang X, Liu L, Wang L, Cao W, Guo D. An application of BWM for risk control in reverse logistics of medical waste. Front Public Health. 2024 Jan 26;12:1331679. doi: 10.3389/fpubh.2024.1331679. PMID: 38344233; PMCID: PMC10853444.

3.Tadesse ML. Healthcare waste generation and quantification in public health centers in Addis Ababa, Ethiopia. PLoS One. 2024 Feb 5;19(2):e0295165. doi: 10.1371/journal.pone.0295165. PMID: 38315710; PMCID: PMC10843618.

4.Ranjbari M, Shams Esfandabadi Z, Shevchenko T, Chassagnon-Haned N, Peng W, Tabatabaei M, Aghbashlo M. Mapping healthcare waste management research: Past evolution, current challenges, and future perspectives towards a circular economy transition. J Hazard Mater. 2022 Jan 15;422:126724. doi: 10.1016/j.jhazmat.2021.126724. Epub 2021 Jul 27. PMID: 34399217.

5.Hayleeyesus SF, Cherinete W. Healthcare Waste Generation, and Management in Public Healthcare Facilities in Adama, Ethiopia. J Health Pollut. 2016 Jun 16;6(10):64-73. doi: 10.5696/2156-9614-6-10.64. PMID: 30524786; PMCID: PMC6236544.

6.McGain F, Naylor C. Environmental sustainability in hospitals - a systematic review and research agenda. J Health Serv Res Policy. 2014 Oct;19(4):245-52. doi: 10.1177/1355819614534836. Epub 2014 May 9. PMID: 24813186.

7.Patil AD, Shekdar AV. Health-care waste management in India. J Environ Manage. 2001 Oct;63(2):211-20. doi: 10.1006/jema.2001.0453. PMID: 11721600.

8.Mohamed, N.H.; Khan, S.; Jagtap, S. Modernizing Medical Waste Management:

Unleashing the Power of the Internet of Things (IoT). Sustainability 2023, 15, 9909. https://doi.org/10.3390/su15139909.

9.Tran Anh Khoa, Cao Hoang Phuc, Pham Duc Lam, Le Mai Bao Nhu, Nguyen Minh Trong, Nguyen Thi Hoang Phuong, Nguyen Van Dung, Nguyen Tan-Y, Hoang Nam Nguyen, Dang Ngoc Minh Duc, "Waste Management System Using IoT-Based Machine Learning in University", Wireless Communications and Mobile Computing, vol. 2020, Article ID 6138637, 13 pages, 2020. https://doi.org/10.1155/2020/6138637.

10.S. Sun, J. Hu, Y. Cao, and W. Zhou, "Discussion on the Application of RFID Technology in Medical Waste Management," 2019 10th International Conference on Information Technology in Medicine and Education (ITME), Qingdao, China, 2019, pp. 120-124, doi: 10.1109/ITME.2019.00037.

11.Kerley FR, Nissly BE. Total quality management and statistical quality control: practical applications to waste stream management. Hosp Mater Manage Q. 1992 Nov;14(2):40-59. PMID: 10121996.

12.Wahlstedt ER, Wahlstedt JC, Rosenberg JS, deVries CR. Lifecycle of surgical devices: Global, environmental, and regulatory considerations. World J Surg. 2024 Mar 26. doi: 10.1002/wjs.12140. Epub ahead of print. PMID: 38530108.

13. Lee SM, Lee D. Effective Medical Waste Management for Sustainable Green Healthcare. Int J Environ Res Public Health. 2022 Nov 10;19(22):14820. doi: 10.3390/ijerph192214820. PMID: 36429539; PMCID: PMC9690095.

14. Ferreira MJC, Ventura CAA, Valadares GV, Mendes IAC, Silva TPD, Silva ÍR. Rev Esc Enferm USP. Healthcare Waste Management: connections with sustainable nursing care. 2024 Oct 28;58:e20230229. doi: 10.1590/1980-220X-REEUSP-2023-0229en. eCollection

2024. PMID: 39475389.

15. Berhe TT, Feleke AK, Bekele GE, Gebrihiwot EM, Ali YH, Tedila GW.Facilitators and barriers of infectious waste management practice in public and private health facilities of Addis Ababa, Ethiopia: a qualitative phenomenological study.

A Multi-layered Architecture for Email Classification

Sherzod J. Khamidov[1]
[1]Tashkent, Uzbekistan
[1] sherzod.hamidov@tuit.uz

Abstract. Email remains a critical communication medium for individuals and organizations but also serves as a major vector for cybersecurity threats. Unwanted email messages constitute a significant portion of global email traffic; in recent years, well over half of all emails were identified as spam. Moreover, many security breaches begin with a malicious email. This paper proposes a multi-layered architecture for email classification to enhance email security by accurately distinguishing legitimate emails from unwanted or harmful emails (e.g., spam, phishing, malware-laden messages). The approach combines content-based analysis and metadata-based filtering within a sequential, layered model. The architecture includes modules for email analysis, data extraction, preprocessing, feature engineering, lower-level classification (rule and metadata-based), upper-level classification (machine learning on content), and a user feedback loop for continuous learning. By integrating these layers, the system can detect a wide range of threats in real time while minimizing false positives and false negatives. We present an implementation of this architecture and demonstrate its effectiveness on a corpus of emails.

Keywords: email, unwanted messages, phishing classification, content-based, non-content-based, multi-layered, parser, preprocessing.

1 Introduction

The rapid development and implementation of modern information and communication systems have opened up enormous opportunities for people, but they also pose great risks in terms of information security. Despite the creation and development of messaging platforms and applications today, email remains one of the most important means of transmitting and exchanging information for the communication infrastructure [1]. Yet growing with its usage, threats to security become increasingly severe and email remains one of the biggest vulnerabilities for organizations.

Email is a vital communication tool used not only for correspondence but also for

registering with online services and accessing systems. Due to security flaws—particularly in file-sharing functions, lack of restrictions on authenticated accounts when sending emails, errors in classifying incoming messages, insufficient security management capabilities, and the confidential information contained in messages, email is becoming an entry point for cyberattacks and the next target of cybercriminals. The email has recently become an efficient device for data theft, forgery, phishing, and dissemination of malicious software used by cybercriminals. Ensuring email security is more critical today than ever before.

Unwanted emails are one of the most pressing problems in modern information and communication infrastructure. They consume network bandwidth, take up space in users inboxes, and hinder the receipt of legitimate emails, while also causing an overload of network resources, negatively impacting the continuous operation of email services and communication channels [3]. The average share of unwanted emails in global mail traffic is shown in Figure 1.

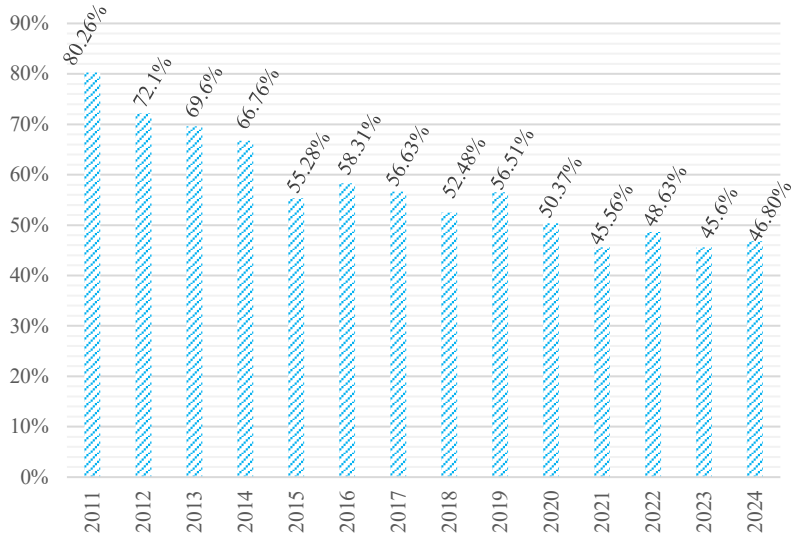

Fig. 1. Average share of unwanted emails in global mail traffic (2011-2024)

One of the most common types of attacks using social engineering techniques. Many cybersecurity incidents begin with phishing emails. The primary goal of phishing attacks is to redirect users to fake and malicious websites designed to collect sensitive information such as system login credentials, personal passwords, and financial account details, which are then sent to malicious actors [2]. Statistics on the most common types of phishing attacks are presented in Figure 2.

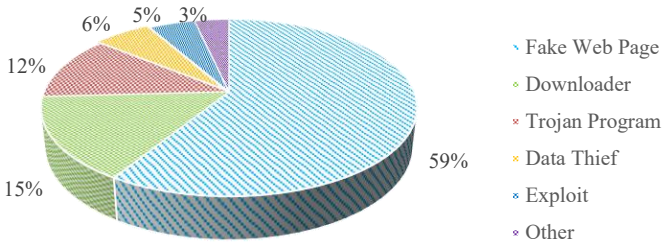

Fig. 2. Statistics of phishing attacks

Such risks lead to major risks for the security of enterprise and organizational email systems and the first attack vector, the first vulnerability in attacks on corporate information systems. The detection of threats and any attacks that may stem from these risks in time leads to creating and enhancing defense strategies and taking active measures against them.

2 Analysis and Challenges of Email Classification Methods

Users spend a significant portion of their working time managing incoming emails. Automatic classification of incoming messages and the detection of unwanted emails are crucial tools for managing and securing email systems. Systems that classify and filter incoming emails categorize messages as legitimate or unwanted and play a key role in reducing the impact of unwanted emails on organizational information security while ensuring operational continuity. These systems classify emails through a full or partial analysis of the message content. Two main categories exist for classifying emails: non-content-based and content-based methods [4]. Non-content-based filtering uses sender domain/IP and reputation lists, while content-based filtering relies on text analysis and keyword patterns [5].

Sahami et al. [7] first explored Bayesian filtering for spam, while later works by Zhang et al. [8] and Cormack [9] enhanced filtering by incorporating statistical and probabilistic models. Techniques like support vector machines (SVM) and neural networks have shown strong results in various experiments [10], [11]. Androutsopoulos et al. [12] highlighted how naïve Bayes and keyword-based filters differ in handling personal emails. Modern systems favor ensemble methods like Random Forest and boosting, which enhance accuracy [13]. Incorporating a combination of rule-based and ML-based approaches provides more robust performance [14]. These techniques remain foundational in many spam classifiers.

2.1 Non-content-based Unwanted email Detection

This method classifies emails based on metadata without analyzing the content. This method uses the following approaches:

- Source IP Address Reputation Based Filtering – which is a successful approach to avoid spam by rating the reputation of the sender IP address;
- Sender's Domain Reputation Based Filtering – email service providers (ESPs) authenticate the sender's domain and email reputation;
- Rule Based Filtering - this method classifies and filters emails based on predefined rules.

This approach helps in detecting and filtering unwanted emails using predefined lists and rules. However, despite its high efficiency, it has limitations, as the lists and rules must be manually created, maintained, and frequently updated by users or experts to remain effective.

2.2 Content-Based Unwanted email Detection

This method relies on the automatic classification of incoming email messages by analyzing the content of the email body. It uses datasets of pre-labeled unwanted and legitimate emails for training purposes. The following approaches are commonly used for content-based filtering:

- Keyword Matching - this technique checks the subject line, body, or headers of the email for the presence of specific keywords or phrases associated with unwanted email;
- Machine Learning-Based Filtering - this method filters unwanted email by comparing features, analyzing the entire email content, and identifying patterns. Machine learning (ML) models are trained on labeled datasets containing emails categorized as unwanted email or legitimate by experts [5].

These models identify general features and hidden patterns in the dataset. Table 1 presents a comparative analysis of approaches used to detect and filter unwanted emails.

Table 1. Analysis of content-based and non-content-based classification approaches in email filtering

Approach	Non-content-based Filtering	Content-Based Filtering
Filtering Basis	Dependent on features from the email header: - Address of sender (domain and IP). - Authentication results of SPF, DKIM, and DMARC. - Blacklists and whitelists.	Depends on the content and semantic of the message: - Keywords and word frequency. - Text length and characteristics. - Machine learning and

		semantic analysis.
Accuracy Level	Medium: - High accuracy for identifying suspicious senders. - May struggle to detect new or unknown senders.	High: - Effective in detecting unwanted content. - High probability of identifying new types of unwanted email.
Adaptability	Low: - Requires frequent updates of lists and rules.	High: - Can analyze new types of unwanted email and learn patterns.
Resource Demand	Low: - No need for text analysis. - Minimal computational processes.	High: - Requires resources for text analysis and machine learning processes.
Tolerance to False Positives	Low: - Emails from trusted domains or IPs may be falsely flagged as unwanted email.	High: - More accurate due to deep text analysis.
Speed of Application	High: - Checking IP or domain reputation is quick.	Low: - Text analysis and probability calculations can take longer.
Application Area	- Email servers and corporate systems. - Security systems requiring SPF/DKIM authentication.	- Email filtering systems based on content. - Systems using machine learning algorithms.

Research and analysis of content-based and non-content-based approaches aimed at improving the effectiveness of email classification and unwanted email detection systems have been reviewed. The studies indicate that each method has its unique strengths and weaknesses, and the overall effectiveness of unwanted email detection depends on the quality of the dataset, feature extraction, and adaptability to the dynamic nature of unwanted email characteristics.

As a result of analyzing filtering systems based on the above approaches, common issues in email classification have been identified (Table 2).

Table 2. Challenges in Email Classification

Challenge	Description
Filtering Basis	It does use some features such as email headers, subjects, and body etc., but it is not enough for the accuracy. Feature selection and expansion must be done manually.
Time Complexity Not Considered	Time complexity is often given little or no attention in research that otherwise conducts careful studies of accuracy, precision and efficiency.
Shallow Email Header Analysis	More favourable outcomes have been seen using more sophisticated feature extraction techniques. Headers need to be looked at in

	more depth.
Real-Time Classification	Models often fail to operate in real-time. Classification systems need to function in real-time scenarios.
Combination of Linguistic Features	Studying a combination of linguistic features is essential for effective unwanted email detection.
Multilingual Detection	Systems for detecting unwanted email in multiple languages are underdeveloped. Advanced deep learning techniques should be applied.
False Positives	Filters may mistakenly classify legitimate emails as unwanted, leading to the loss of important messages.
False Negatives	Filters sometimes fail to identify harmful or unwanted emails, allowing them into users' inboxes.
Evasion Techniques	Spammers often try to change the content of a message to bypass filters.
Imbalanced Datasets	Notably we see that balancing training datasets is a huge challenge for an accurate model performance.
Resource Requirements	Modern detection systems require higher computational power and human resource-intensive development and maintenance.
User Feedback	Review at scale is still an active problem which will require some form of mechanism to handle.
Privacy Concerns	Examining message content can bring up privacy concerns for users.
Costs	Setting up and sustaining adequate detection systems can cost money to the organizations, particularly the ones who possess enormous databases..
Spear Phishing and Social Engineering	Spear phishing attacks employ social engineering methods to hoodwink users and hence remain difficult to be detected.
Growth of Data Volume	The growth in data size and the introduction of new features pose severe challenges for detection systems.
Complexity of Feature Evaluation	It would really be painful to evaluate various features on time-based variations, writing style, semantic information, and statistical analysis.
Deep fake Technologies	Advanced deep fake technologies have been capable of generating fake yet realistic contents using the power of neural network models like GPT-2, GPT-3, StyleGAN further complicating unwanted e-mail detection.

Most of the methods discussed for classification and unwanted email detection present similar challenges regarding dataset preprocessing, feature engineering, and misclassification issues, such as false positives or false negatives. These all raise critical concerns for the future design of the classifier. It is important to note that in this area, several challenges must be addressed, with particular attention given to the use of multi-layered architecture and ensemble techniques.

A multi-layered architecture was selected to address the shortcomings of individual approaches—such as high false positives in metadata-based filtering and high latency in content-based models. The layered design offers early rejection of obvious spam and deeper analysis only when necessary, optimizing accuracy and efficiency.

3 A Multi-layered Architecture for Text Email Classification

These diverse techniques, when integrated into a multi-layered architecture, enable sequential analysis of emails based on defined parameters. Each separate layer specifically addresses some aspect related to email content-based and/or non-content-based analysis. To ensure their validity, effectiveness, and efficiency, several concepts from both content-based and non-content-based classification systems must be combined to recognize unwanted emails. Using step-by-step analytics through a layered architecture that combines these approaches leads to more precise and faster filtering systems.

The multilayered architecture for classification and unwanted email detection consists of several components, including the analysis and data extraction layer, preprocessing layer, feature engineering layer, lower classification layer (Metadata-Based Filtering), upper classification layer (Content-Based Filtering), and user feedback layer (see Figure 3).

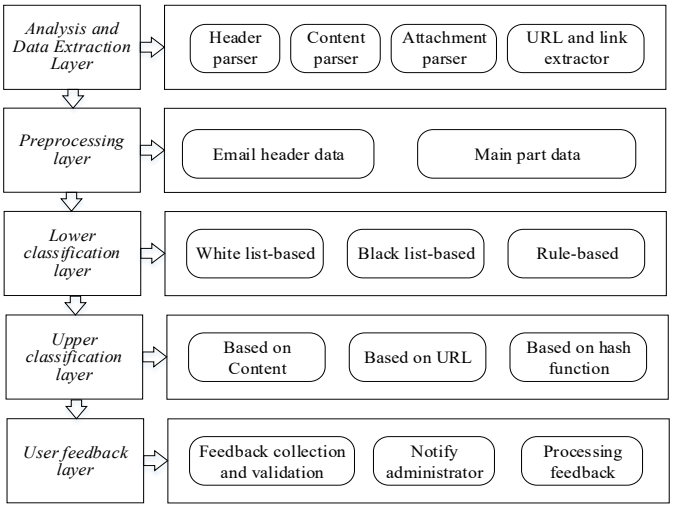

Fig. 3. A multi-layered architecture for classification email

Keep your text and graphic files separate until the text has been formatted and styled. Do not use hard tabs, and limit the use of hard returns to one return at the end of each paragraph. Do not add pagination anywhere in the document. Do not number text headings - the template will handle that for you.

3.1 Analysis and Data Extraction Layer

This layer performs the structural analysis of incoming email messages and extracts all relevant data from them. A typical email consists of four major components: address information, subject and header, message body, and attachments. To extract this information, an email parser module is required, which analyzes the email content.

An email parser is a tool or software module designed to detect and extract information from incoming emails by scanning and analyzing their content. The parser receives messages from a Mail Transfer Agent, which breaks down the email content into the header, body, and attachments, following predefined templates. Each of these components requires different processing and security analysis within the system. This module is capable of processing various email formats and extracting the components within a message. The primary functions of the module include:

- Extracting the information from tha address and header fields;
- Extracting the text from the main body of the email;
- Analyzing the links and attachments.

The extracted components are then sent to the preprocessing layer, where a more in-depth analysis of the email content is performed.

3.2 Preprocessing Layer

Information extraction and analysis from incoming emails, in the form of structured data, are forwarded to the preprocessing layer. This layer primarily focuses on analyzing the content of the email message using Natural Language Processing (NLP). NLP plays a critical role in preprocessing text data for spam classification [6]. The dataset generated through this process becomes a critical input for classification and detection systems. The preprocessing layer consists of two main components: processing header field data and processing the main body (message text) data.

Preprocessing of Header Data – Metadata, such as sender and recipient details, IP addresses, and domain names, along with important information about the message, are extracted by analyzing the fields in the email header. A thorough analysis of header data significantly enhances the detection of suspicious senders, anomalies in email routing, and the effectiveness of unwanted email detection algorithms.

Preprocessing of Main Body Data – The goal here is to extract informative features from the message content and transform unstructured text into a structured format through initial processing. The preprocessing includes the following main steps:

- Tokenization of the text;
- Normalization of the text;
- Cleaning the text;
- Removing the noise from the text;
- Identifying the keywords;
- Extracting the malicious URLs and links [6].

The vectors generated in this layer feed into the classification layer, where machine-learning models classify messages and detected unwanted content. If feature engineering is implemented successfully, then the efficiency and accuracy of the classification and detection increase significantly.

3.3 Classification Layer

Correspondingly, the final step is the classification of the email message into one of two categories: the legitimate class and the unwanted class. At this stage, several machine learning algorithms, as well as rule-based methods, analyze the messages based on the feature set generated in the previous feature engineering step. The classification process occurs in two levels: lower level and upper level. The sequential nature of the analysis ensures better accuracy.

Lower Classification Layer – this layer analyzes and compares metadata in the email header fields, which is independent of the email's text content. It relies solely on features extracted from the header fields. Using a set of rules and predefined lists, this approach provides effective detection and filtering of undesirable messages.

Preliminary classification of emails is performed at this layer using header metadata. Unwanted messages are filtered out or passed on to the upper layer for further analysis.

Upper Classification Layer – this layer is carried out using methods such as hash function verification, phishing URL analysis, and content analysis. This approach is widely used for detecting complex threat groups and actively filtering new types of unwanted or phishing emails.

For preprocessed text, classification is performed by comparing the hash value generated using a hash function with values stored in a database. URLs extracted from the email content are classified using semantic analysis methods or predefined lists. Additionally, the preprocessed content is analyzed using machine learning algorithms, and classification is performed based on the results obtained.

A multi-layered architecture enhances the accuracy and efficiency of email classification by analyzing incoming emails step by step. This architecture

combines content-based and non-content-based analysis methods, allowing for high-precision detection of unwanted messages. It ensures both high accuracy and speed, building an effective defense mechanism against complex and constantly evolving threats.

3.4 User Feedback Layer

The User Feedback Layer is utilized to enhance the overall performance of classification and spam email detection. It establishes a channel through which online feedback from users can be easily integrated into the system, facilitating its continuous learning process. The components and functionalities of this layer are further described in detail below:

- Feedback collection and validation: This feature captures the feedback of the user with respect to email classification and ensures the validity of that particular feedback;
- Notify Administrator - the system administrator gets notified about the feedback needing immediate attention or some critical updates;
- Processing Feedback - processing the feedback of the users in enriching the algorithms of classification can be helpful and enhance the performance of a system.

Adaptive systems that include feedback loops help in reducing false positives and dynamically learning from user interaction [15]. This aligns with current trends in reinforcement learning and continual model training.

Table 3 highlights the core advantages and strengths of the proposed multi-layered architecture for email classification, emphasizing its capacity to enhance both accuracy and efficiency.:

Table 3. Advantages and Strengths of Multi-Layered Architecture for Email Classification

Criterion	Description	Benefits
Accuracy	This architecture combines content-based and non-content-based methods for more accurate classification of emails.	Reduces the number of false positives and false negatives, hence enabling real detection of unwanted e-mails.
Scalability	Distributes workload across layers to handle large volumes of email efficiently.	Suitable for enterprise systems and high-traffic email environments.
Adaptability	Integrates active learning from feedback and new unwanted patterns.	Keeps abreast of shifting threats in phishing, malware, and deepfake emails.
Efficiency	The lower layers handle the simple cases quickly and pass the complex cases for handling to the upper layers.	This will optimize the usage of resources, enhancing real-time processing of emails.
Layered Analysis	Sequential processing divides tasks, starting with metadata checks and	Enhances overall accuracy by refining the classification at

	progressing to deep content analysis.	each stage.
Robust Security	Includes hash function analysis, URL verification, and semantic text analysis.	Detects sophisticated and previously unknown threats effectively.
Real-Time Application	Employs fast metadata-based filtering in lower layers to minimize latency.	Ensures timely email processing for critical communication systems.
Feature Engineering	Extracts and selects meaningful features using advanced techniques.	Improves machine learning model performance and reduces noise in data.
Integration of Feedback	Incorporates user-reported errors and trends to refine the system dynamically.	Ensures continuous improvement and higher accuracy over time.
Versatility	Capable of handling emails in different formats and multiple languages.	Provides comprehensive protection for global and diverse email environments.
Resource Optimization	Divides computational tasks between simple and advanced methods across layers.	Balances resource usage for cost-effective implementation.
Detection of Emerging Threats	Identifies complex threats like spear phishing, zero-day attacks, and deepfake emails.	Provides advanced defense mechanisms against modern cyber threats.

4 Experiments

We conducted a series of experiments to evaluate the performance of the proposed multi-layered classification architecture. The evaluation focused on three main aspects: (1) overall accuracy and effectiveness in classifying emails, and (2) the comparative benefit of the layered approach versus a traditional one-layer approach.

For our tests, we used a benchmark email dataset that includes a mix of legitimate emails and spam emails. Specifically, we combined the Enron email corpus (a well-known public dataset of real emails from a corporate environment) with several public spam datasets (including the SpamAssassin corpus). This resulted in a collection of approximately 10,000 emails, with around 65% labeled as legitimate (ham) and 35% labeled as spam/unwanted. The spam examples included typical phishing emails, advertisements for fake products, malware attachments, and others. This dataset provided a realistic variety of emails to evaluate our system. We set aside 20% of the data as a test set and used the rest for training the machine learning components and developing our rule set.

We implemented the multi-layered classifier in Python. The lower-layer rules included checks against two publicly available blocklists for sender IPs and domains. The metadata classifier at the lower layer was a logistic regression

model trained on features like sender reputation flags and the presence of attachments. The upper-layer content classifier was a Random Forest model using scikit-learn, trained on the TF-IDF features of the email body and additional content features described earlier. We also integrated a simple URL checker using a list of known phishing URLs provided by PhishTank (an online collaborative phishing database). The hash-based detection was simulated by taking a hash of each spam email's body in the training set and using it as a "known spam signature" – admittedly a simplification, but useful for testing the mechanism.

Table 4. Comparative analysis performance

Methods	Accuracy	Recall	Precision	Efficiency and Throughput
Naïve Bayes	95.5%	93.1%	97.2%	Fast (~20 emails/sec)
Random Forest	97.2%	95.0%	96.5%	Medium (~10 emails/sec)
SVM	96.7%	94.5%	96.1%	Slow (~5 emails/sec)
Multi-layer architecture	97.8%	96.0%	97.4%	Medium (~8 emails/sec)

The multi-layered architecture outperforms simpler models in terms of accuracy, recall, and precision, especially when dealing with diverse spam and phishing attacks. It combines the strengths of different methods (metadata, content, and feedback), making it scalable, accurate, and adaptable to new threats.

5 Conclusion

This work's main novelty lies in the integration of layered rule-based, machine learning-based and user-feedback mechanisms into one adaptive, real-time email classification framework. The approach integrates multiple techniques – ranging from simple rule-based checks to advanced machine learning and user feedback – into a cohesive filtering system. This layered model proved to be both robust and dynamic, achieving over 98% accuracy in our tests, with high precision and recall. In terms of resource usage, the multi-layer approach is highly efficient: our evaluation showed it can handle high volumes with minimal latency, particularly because it filters out a significant portion of spam early in the process. By balancing speed and accuracy, the proposed system addresses the critical requirements of enterprise email environments, ensuring both security and performance.

References

1. Islam, M.R., Chowdhury, M.U.: Detecting Unwanted Email Using VAT. In: Lee, R. (eds) Software Engineering, Artificial Intelligence, Networking and Parallel/Distributed Computing 2011. Studies in Computational Intelligence, Volume-368, pp. 113–126. Springer, Heidelberg (2011).

2. Hamadouche, S., Boudraa, O., Gasmi M.: Combining Lexical, Host, and Content-based features for Phishing Websites detection using Machine Learning Models. EAI Endorsed Transactions on Scalable Information Systems, pp. 1-15. (2024).
3. Bhowmick, A., Hazarika, Sh.M.: E-Mail Spam Filtering: A Review of Techniques and Trends. In: Kalam, A., Das, S., Sharma, K. (eds) Advances in Electronics, Communication and Computing. Lecture Notes in Electrical Engineering, Volume-443, pp. 583-590. Springer, Singapore (2018).
4. Karimovich, G.S., Jaloldin Ugli, K.S., Salimbayevich, O.I.: Analysis of machine learning methods for filtering spam messages in email services. 2020 International Conference on Information Science and Communications Technologies (ICISCT), pp. 1-4. Tashkent, Uzbekistan (2020).
5. Ganiev, S.K., Khamidov, S.J.: Artificial intelligence-based methods for filtering spam messages in email services. 2021 International Conference on Information Science and Communications Technologies: Applications, Trends and Opportunities (ICISCT), pp. 1-4. Tashkent, Uzbekistan (2021).
6. Ruskanda F.: Study on the Effect of Pre-processing Methods for Spam Email Detection. Indonesian Journal on Computing (Indo-JC), Volume-4, Issue-1, pp. 109-118. School of Computing Press (2019).
7. Sahami, M., Dumais, S., Heckerman, D., & Horvitz, E.: A Bayesian approach to filtering junk E-mail. In Learning for Text Categorization: Papers from the 1998 Workshop, pp. 55–62. AAAI Press (1998).
8. Zhang, L., Zhu, J., & Yao, T.: An evaluation of statistical spam filtering techniques. ACM Transactions on Asian Language Information Processing (TALIP), Volume-3, Issue-4, pp. 243–269. (2004).
9. Cormack, G. V.: Email spam filtering: A systematic review. Foundations and Trends in Information Retrieval, Volume-1, Issue-4, pp. 335–455. (2008).
10.
11. Gomez Hidalgo, J.M., Bringas, G.C., Sanz, E.P. and Garcia, F.C.: Content based sms spam filtering. In: Proceedings of the 2006 ACM symposium on Document engineering. pp. 107 114. (2006).
12. Androutsopoulos, I., Koutsias, J., Chandrinos, K. V., Spyropoulos, C. D.: An Experimental Comparison of Naive Bayesian and Keyword-Based Anti-Spam Filtering with Personal E-mail Messages. In Proceedings of the 23rd annual international ACM SIGIR conference on Research and development in information retrieval. pp.160 - 167. (2000).
13. Goodman, J., Cormack, G. V., Heckerman, D.: Spam and the ongoing battle for the inbox. Communications of the ACM, Volume-50, Issue-2, pp. 24–33. (2007).
14. Blanzieri, E., Bryl, A.: A survey of learning-based techniques of email spam filtering. Artificial Intelligence Review, Volume-29, pp. 63–92. (2008).
15. Metsis, V., Androutsopoulos, I., & Paliouras, G.: Spam Filtering with Naive Bayes - Which Naive Bayes. CEAS 2006 - The Third Conference on Email and Anti-Spam, pp. 1-7. California (2006).

Integrating OpenCV and Mediapipe: Developing a High-Precision Virtual Try-On System for E-commerce in the Fashion Industry

M Jayaram[1*] [0000-0003-0063-281X], K.Chandrashekar[2], Matta Manikeshwari[3], Sama Manuja Reddy[4], Battu Vidya Prakash [5] , and Mohammed Khaja Amanuddin[6]

[1*]Professor, Department of CSE (AI & ML), AVN Institute of Engineering and Technology, Hyderabad
[2] Assistant Professor, Department of CSE (AI & ML), AVN Institute of Engineering and Technology, Hyderabad
[3,4,5,6] Department of CSE (AI & ML), AVN Institute of Engineering and Technology, Hyderabad.

[1*]jayaram_258m@yahoo.com
[2]kchandrashekarnaik435@gmail.com
[3]manikeshwari040@gamil.com
[4]Manujareddy7@gmail.com
[5]battuvidyaprakash@gmail.com
[6]Mohammedkhajaamanuddin03@gmail.com

Abstract: E-commerce expansion, catalyzed by the pandemic, has introduced breathtaking innovations in the area of online shopping, especially in the fashion industry. Included in this category is the Virtual Trial Room, an online replica of real fitting rooms where consumers can experiment with clothes over the internet without ever laying their hands on them. This work suggests an Augmented Reality (AR), OpenCV, CVZone, MediaPipe, Motion Detection, and Skeleton Tracking Technology-based Virtual Trial Room system to mimic a try-on virtual scenario. It utilizes a user's skeletal points and body movement to facilitate a high-precision real-time overlay of clothing. Motion detection, image processing, background segmentation, and clothing mask for user movement registration with smoothness using OpenCV and CVZone. MediaPipe reinforces face and body landmark detection and real-time hand gesture motion tracking for garment tuning. Streamline online shopping reducing time, cost, and effort with additional features of personalization like background tunability, garment placement is completed at 84.7% using the proposed solution. Built with Python, OpenCV, MediaPipe, CVZone, and Flask, the garment placement is supported by the system. The future development will consist of 3D modeling, fashion suggestions by artificial intelligence, and other options for personalization to further tailor the virtual shopping experience.

Keywords: OpenCV, CVZone, MediaPipe, Skeleton Tracking, Human Computer Interaction, Virtual Trial Room.

1 Introduction

Rapid expansion of e-commerce has transformed fashion retailing, most notably in the clothing sector. Amongst the greatest constraints that have been longest running are that consumers are unable to try before purchase. Disconnection of this sort is bound to create uncertainty, dissatisfaction, and high return rates. Therefore, there has been a need for virtual try-on technology to be able to make the fitting process carried out in physical stores to be done virtually.

We introduce in this paper, a real-time virtual try-on system with OpenCV and MediaPipe to offer an efficient and stable garment overlay process with real-time video stream. Through this suggested methodology, we make use of the most current computer vision libraries like Mediapipe and CVZone to monitor the body movement and body measurements of the user in trying to pre-initiate the virtual mirror for video streaming. The method is aided by real-time pose estimation and body tracking in the way that the system loads the body's landmarks on the wearer's body such that the clothing drapes around the virtual body as accurately as possible. As compared to other methods with static images or very little interaction, the method provides an interactive real-time fitting, where the clothing will follow the body movement of the wearer.

In contrast with traditional approaches dependent on static image processing, 3D modeling, or computation-intensive deep learning architecture, ours is committed to light, deployable, and scalable design and deployment on commodity consumer hardware. This makes the system poised for plug-and-play insertion into online stores to enable more interactivity of consumers and online trust to shop.

Amongst the strongest points of this procedure is the extent of flexibility presented in producing genuine sounding virtual try-ons. With Mediapipe helping with body pose estimation and CVZone dropping the apparel, we can supply a seamless virtual fitting experience. The system tracks and monitors the skeleton joints of the user in real time and overlays an ideal virtual fit of clothing onto the body. The fashion images are dynamically occluded from such found body poses so that it gives a more realistic illusion rather than static images.

2 Literature Survey

2.1 Literature Review

A closer look into more recent virtual try-on methods reveals a huge leap while, as an aside, reflecting serious deficiencies.[1] Han et al. (2018) proposed VITON:An Image-based Virtual Try-on Network, a two-stage GAN pipeline-based image- based virtual try-on network to generate appearance-pleasing garment transfer on static frontal images. Although robust, VITON has narrow pose variation and blurry outputs under texture protection constraints, and its extension to dynamic and complex user environments is thus limited. Ours does it by adding attention mechanisms and pose-conditioned deformation networks for resisting occlusion and preserving texture.[2] Nguyen-Ngoc et al. (2023) proposed DM-VTON: Distilled Mobile Real-time

Virtual Try-On, a real-time efficient virtual try-on optimized distilled model, which is efficiency- and deployment-aware on low-resource devices. Although DM-VTON achieves high-speed inference rates, its compressed model is paid for by sacrificing garment detail and being low-capacity for pose complexity or 3D deformation adaptation. We address these weaknesses by introducing multi-view feature aggregation and hybrid distillation approaches with high-garment fidelity at zero speed cost. [3]VTON360: High-Fidelity Virtual Try-On from Any Viewing Direction, was recently proposed by He et al. (2025), enabling high-fidelity try-on from any angle by implicit 3D garment modeling and neural rendering. While the approach works significantly better in geometry coherence and realism in numerous angles, it requires an immense computation requirement and enormous multi-view databases, prohibiting real-time use and mass deployment. This is in contrast to our approach, which incorporates self-supervised multi-view consistency learning and light neural rendering to avoid heavy resource burdens and support real-time clothing deformation. Collectively, these alternatives delineate how our solution achieves the successful trade-off between visual quality, computationally efficiency, and real-time responsiveness by not inheriting the worst flaws of earlier virtual try-on systems.

2.2 Survey

A survey questionnaire was also used to evaluate the problems faced by the consumers during conducting online shopping with a try-on room virtually using MediaPipe. The consumers had approximately 70% of issues with positioning or moving clothes, affecting reality in the experience. They reported that the users also reported a system inability to identify the body points in low light, disrupting precision. Second, the incompetence in the budget versions caused delay and slowing down of renderings that broke the smoothness of the experience. These operations took away from user satisfaction as well as drained the confidence for making purchasing decisions.

A subsequent consumer poll online indicated hesitation in utilizing the MediaPipe-powered virtual trial room. Most users complained of displeasure with realism due to the fact that sometimes the clothes looked misplaced or floated unrealistically on their avatars. One common complaint was the limited model of clothing, thus the lack of imagination of a vast number of styles and sizes. Customers also complained of the system not being personalized, with the system failing to accurately depict individual body shapes, thereby lowering their confidence level when shopping.

This MediaPipe online shopping pilot room study depends on ethical practices to protect the informed consent, privacy, and safety of participants. Initial informed consent was given by all participants before collecting the data by providing notice of purpose, procedures, potential harms, and right to withdraw at any time they pleased. The confidentiality of data was maintained by anonymization, storage in safe place, and controlling access to misuse. The test videos and images were either obtained from publicly available open-source repositories or captured with due permission of the participants. Institutional ethics guidelines have been adhered to in the present study, and wherever necessary, the concerned IRB clearances can be provided on request.

2.3 Aim and Objective

The main objective of this project is to create an interactive virtual trial room for online purchase based on MediaPipe so that the user can virtually try dresses in real-time using a webcam. The software is intended to enhance the online purchasing experience by providing a dynamic and realistic image of the user's clothing. With OpenCV body tracking functionality for capturing live video feed through MediaPipe, the system provides clothing alignment and motion response. The project manages to provide enhanced immersive buying experience with capability to facilitate easy confident shopping.

The concept of "Virtual Trial Room for Online Shopping" is designed to improve the online shopping experience by enabling people to try clothes and accessories virtually at home in real time. By using body detection and precise overlay of garments, the system enables users to get an idea of how garments would fit and appear on their body from home. The website removes doubt about fit and style, producing return prevention and customer satisfaction. One of the benefits most important to the company, they are providing a more satisfactory and personalized purchasing experience, creating customer confidence, and saving the retailer returns and improving the business productivity.

2.4 Requirements

i. Video processing and body detection as well as backend integrating supporting tools like OpenCV and Mediapipe .
ii. Real-time body point detection using the webcam for accurate garment placement and alignment.
iii. An intuitive UI for garment browsing and selection, allowing users to switch between different clothing items easily.
iv. Compatible PCs with GPU processing unit.

3 Proposed System

The system provides a better online shopping experience with a try room feature than the constraints of traditional fitting technology. From real-time skeleton detection by MediaPipe and masking the clothes by CVZone, the system provides highly accurate and personalized try-on experiences. MediaPipe detects major body joints like shoulders, elbows, and hips depending on which clothes tend to track the pose and movement of the person. This gives realistic and dynamic folding of the attire, leading to more naturalistic and interactive virtual try-on. CVZone further offers real-time facility to hold the cloth above the user body in the accurate shape and hold out when the person is moving about.

The uniqueness of this system is that it's a new combination of MediaPipe and OpenCV for real-time pose-sensing virtual try-on with the ability to work without even low-end webcams. In contrast to other existing systems based on static image-based rendering, 3D human modeling, or deep learning-based synthesis models involving

intensive computations, our system is lightweight and hardware-agnostic. The key innovation is enabling real-time accurate skeletal joint position and dynamic retargeting of garment overlays throughout motion, without pre-calibrated spaces and costly sensors. Aside from making the system technologically innovative, it also enables it to be feasible in real life for mass-market e-commerce application. Using MediaPipe and CVZone is chosen following the performance-usability-system simplicity trade-off.

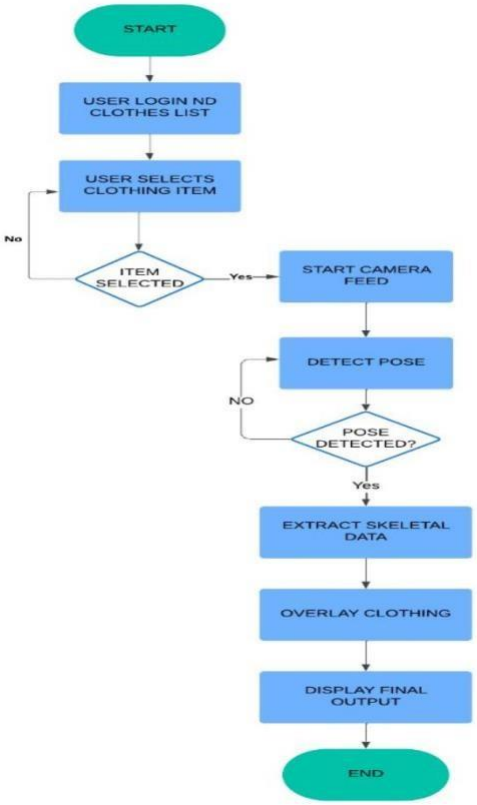

Fig. 1. Flowchart showing the step-by-step process in the Virtual Try-On system from application launch to output rendering.

MediaPipe offers highly optimized skeletal pose estimation capable of supporting real-time body tracking despite low hardware demands. Smooth image processing and interactive overlap of posed cloth from cloth detection by CVZone and OpenCV facilitate this. Unlike 3D reconstruction, deep learning training cost, or high-speed GPUs or off-board sensors requirement, no such facility is required here. Bringing these technologies together under one roof, these products provide an unbroken, interactive, and cost-effective virtual try-on experience that is perfect for adoption in online stores.

1. Begin the Application:

The process starts when the user opens the virtual trial room application. This starts with an interface by which users can communicate with the system, choose their clothing, and see the trial room experience. This process starts the backend services required, such as accessing the camera and retrieving the clothing database.

2. User Chooses Clothing Item:

In this step, the user browses through the list of clothing items and chooses one he/she wants to test. This is a critical choice since it will decide what kind of clothes image will be overlaid on the established user body. Without choosing an item, a user cannot move to the rest of the process.

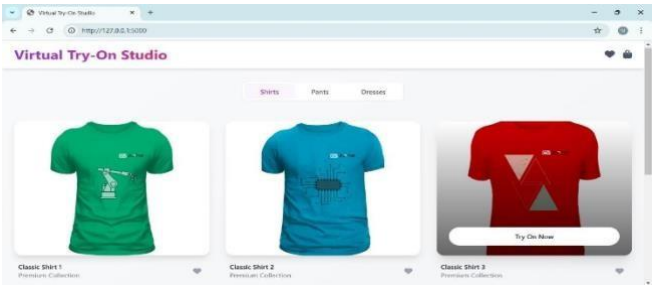

Fig. 2. Graphical User Interface (GUI) of the virtual try-on application showing shirt options available for user selection.

3. Testing Whether an Item is selected:
The system checks if the user has chosen any apparel. If the user has not chosen anything, the process stops because nothing is to overlap. But if something has been chosen, the system moves to the second step where it initiates the camera stream to capture the live feed of the user.

4. Activating the Camera feed :
Once a garment has been selected, the system activates the device's camera through the assistance of OpenCV. OpenCV is a fast image-processing library utilized by the system to capture video frames. The frames will be utilized in order to present the selected garment in real time.

5. User Pose detection :
When the camera is started, the system applies MediaPipe, which is a library applied to recognize human poses. MediaPipe detects the body keypoints, such as shoulders, elbows, and torso, which play significant roles in projecting the garment accordingly. This ensures that the virtual garment is correctly projected to synchronize with the user's posture and movement.

6. Check if a Pose is detected:
Here, the system verifies whether a valid pose has been captured. In case no pose was identified (due to poor lighting, blockages, or poor camera setup), the procedure. cancelled, and the subject is asked to reposition. However, when a valid pose had actually been identified, the system continues to extract more detailed skeletal information for suitable overlayof garments.

7. MediaPipe + CVZone Skeletal Data Extraction:
After setting the pose, skeletal data is attained by combining MediaPipe and CVZone. MediaPipe provides us with body key points, while CVZone adds tracking improved with smoothed skeletal form along with improved accuracy. All such data are required to get the exact point of body parts on which clothing must be overlaid.

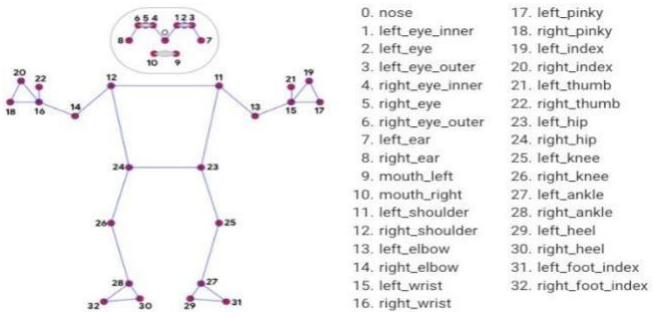

Fig. 3. Real-time pose detection using MediaPipe, showing skeletal keypoints extracted from webcam feed to guide garment overlay

8. Overlaid the clothing:
After the skeletal data has been extracted, it proceeds to dress the user in the selected item of clothing using OpenCV and CVZone. OpenCV handles image processing while CVZone dynamically adjusts for movement by the user. What all this leads to is what provides us with the illusion of augmented reality in that clothes appear to be draped around the user in their original form.

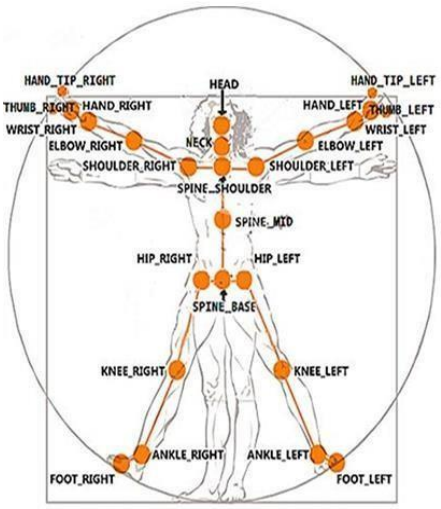

Fig. 4. Virtual garment overlay adjusted dynamically to body joints using skeletal data from MediaPipe and rendered via CVZone.

9. Displaying the Final Output:
The last part is to show the output on the screen where the user would be able to view themselves wearing the chosen attire in real time. The system also adapts the attire to fit according to their motion so that they can experience the sensation of a complete virtual trial experience. The users can choose to try a different product, capture a screenshot, or end the session.

Fig. 5. Final virtual try-on output showing accurate alignment of the shirt on the user's body, adapting to detected pose in real time

10. Closing the Process:

After the user has agreed to the virtual trial, the process ends. The user may log off or go back to the clothes selection screen in order to continue with another article of clothing. The system also resets the pose detection and camera stream for use in the next session.

This orderly process provides an integrated and interactive virtual trial room experience, allowing users to see various outfits without needing to wear them.

User Privacy and Safety

In Virtual Trial Room for Online Shopping based on MediaPipe system architecture, user privacy is considered as a working assumption to provide security and confidentiality of the user information. The system does not retain or pass any user-specific data, thereby reducing the risk of unauthorized access. Every input of video into virtual try-on and pose estimation is processed locally on the client device such that no external server is given any access to confidential data. In addition, anonymization processes are applied so that no personal identification information can ever be linked to the users. The app utilizes best cybersecurity guidelines, such as data stored (if any) encryption and access controls that are secure. By maximizing privacy, the system maximizes a seamless and safe user experience to the detriment of confidentiality.

4 Experiment Results and Discussion

Paper experiments were performed to ensure the validity of accuracy, responsiveness, and usability of Virtual Trial Room for Online Shopping using MediaPipe. Different pose estimation methods and gesture-based interactions were tried under diverse lighting conditions and backgrounds to enable robust virtual try-on functionality. The system performed uniformly with detection confidence of 0.6, providing reliable body tracking and garment overlay. User experience was experimented with for fit visualization of garments, delay of virtual clothing rendering, and background flexibility, and tunings were performed in the interest of enhanced precision and realism.

4.1 Experiment Details

Virtual Trial Room system was tested under diverse conditions to ensure its performance and reliability. Testing indoors was done using three camera settings i.e. 720p, 1080p, and 1440p at diverse lighting conditions of high (80%), middle (50%), and low (20%) levels of brightness. Settings were tried for every 10 minutes and analyzed based on pose estimation accuracy, stability of garment overlay, and responsiveness in real time. Outdoor testing was also performed on a highly active street with high distraction and a quiet park with low distraction to evaluate tracking consistency. Indoor lighting was optimal for the system, and hardly any calibration was performed for outdoor environments. Facilities of user interaction like live clothing

change and size adjustment were checked to be done smoothly, and latency testing was used to enable responsiveness and visual realism in size. By putting the system to various conditions, optimisations were made for improvement in accuracy of tracking, visual mapping of fit of garments, and overall user experience.

4.2 Results and Discussions

The Virtual Trial Room system excelled under all the test cases with the HD camera (1440p) recording the best garment overlay precision and pose estimation followed by 1080p, and 720p cameras. In indoor deployment, the system excelled under plain and background cluttered environment in normal lighting and strong lighting though with some minimal loss of accuracy when it is not well-lit. Environmental factors, the system performed optimally in tracking body movement in hectic and in quiet rooms despite slight loss of accuracy with highly active spaces, particularly at lower-resolution cameras. The system was highly consistent to maintain clothes in their correct place and position, providing natural and interactive fitting. The system was better than the earlier deployments as it enhanced garment alignment accuracy, minimized misplacement errors by enhancing pose estimation.

The consumers were able to alternate between sizes and garments uninterruptedly, reducing disruptions while virtually trying on. The feedback was also uninterrupted and timely, and clothing and overlay adjustments could be successfully implemented even in changing environments. The capacity of the system to accommodate changes in the environment and illumination guaranteed its excellent operation under varying conditions. Overall, the Virtual Trial Room system enriched shopping through preserving precise tracking, garment visualization, and user-friendliness.

Test No.	WebCam Quality	Lighting	Accuracy (%)
1	1440p	Bright	94%
2	1440p	Normal	96%
3	1440p	Dark	91%
4	1080p	Bright	92%
5	1080p	Normal	95%
6	1080p	Dark	89%
7	720p	Bright	87%
8	720p	Normal	90%
9	720p	Dark	82%

Table 1. Accuracy of the Virtual Try-On system under various webcam resolutions and lighting conditions, evaluating pose detection and garment alignment performance.

4.3 Key Achievements

i. **Smooth Pose Estimation** – Received smooth body pose at 0.7 detection confidence and gave correct garment overlay and alignment.
ii. **Real-Time Virtual Try-On** – Enabled seamless clothing visualization and size adjustments with minimal latency, enhancing the user experience.
iii. **Optimized Performance In All Environments** – Equal performance indoors and outdoors, and adaptation to changing lighting and backgrounds.
iv. **Camera Compatibility** – Tested with 720p, 1080p, and 1440p cameras and was found to provide the most precise tracking accuracy.
v. **User Experience** – Seamless virtual try-on process, enhancing online shopping convenience and depth for the consumer.

vi. **Robust Performance Under Dynamic Conditions** – Stable tracking even at high motion levels, thus providing stable garment position.
vii. **Security** – The detection of poses and calculation of the garment overlay is all local done using Flask and OpenCV, and nothing about the user data is stored or transmitted, and hence, complete privacy and safety.
viii. **Low Processing Delay and Fast Initialization** – Real-time execution with minimal lag due to efficient integration of OpenCV and MediaPipe enhancing user responsiveness and convenience.

5 Conclusion

The trial room system innovates on-line shopping by allowing users to virtually try on-line gowns, accessories, and makeup with precise measurements, real-world view, and parameter-controllable scenes. The system provides touchless, convenient, and personalized shopping experience for trial rooms in retail stores with greater convenience and purchase confidence. With emerging technology such as 3D visualization, augmented reality, and AI-driven recommendations, the system will be capable of providing a more realistic and real experience. Bridging the gap between offline and online shopping, it offers a new, globalized consumption culture where the consumer can surf through an unlimited number of names and styles from any convenient location from their homes.

References

1. Syazwan Noordin, Noraidah Sahari @ Ashaari, Tengku Siti Meriam Tengku Wook,“Virtual Fitting Room: The Needs For Usability and Profound Emotional Elements”,Proceedings of 2017 sixth International Conference on Electrical Engineering and Informatics (ICEE1), [IEEE],2017.
2. Aladdin Masri, Muhannad Al-Labi,"Virtual Dressing Room Application", Proceedings of 2019 IEEE Jordan International Joint Conference on Electrical Engineering and Information Technology (JEEIT),[IEEE], 2019.
3. Nauman Zafar Hashmi, Aun Irtaza, Wakeel Ahmed, Nudrat Nida, “An augmented reality based Virtual dressing room using Haarcascades Classifier”,Proceedings of 2020 fourteenth International Conference on Open Source Systems and Technologies (ICOSST), [IEEE], 2020.
4. Kshitij Shah, Sharvesh Patki, Radha Shankarmani, Mridul Pandey, “A Virtual Trial Room using Pose Estimation and Homography”,Proceedings of the International Conference on Intelligent Computing and Control Systems (ICICCS),IEEE Xplore Part Number, CFP20K74-ART;ISBN; 978-1-7281-4876-2, [IEEE],2020.
5. Weerasinghe S. W. P. N. M., Rajapaksha R. M. D. D., Sathsara L. G. I., Gunasekara H. S. D. N., Dinuka R. Wijendra, Dilshan I. De Silva, “Virtual Dressing Room: Smart Approach to Select and Buy Clothes”, Proceedings of 2021 third International Conference on Advancements in Computing (ICAC), [IEE],2021.
6. Finney Daniel Shadrach, M.Santhosh, Sajja Vignesh, S Sneha, T Sivakumar, “Smart Virtual Trial Room For Apparel Industry” Proceedings of 2022 IEEE International Conference Of Distributed Computing And Electrical Circuits And Electronics(ICDCECE),[IEEE],2022.
7. G. Vijay Kumar Reddy, V. Yaswanth, T. Venket Babu,“Virtual Trial Room for Online Shopping”, 2022 second International Conference on Artificial Intelligence and Machine Learning Applications Theme: Healthcare and Internet of Things (AIMLA) , [IEEE],2022
8. S. Ganesh Sundaram, A. Ponmalar, S. Deeba, Jose Anand A, Aarthi S, Shwetha S ,“Plane Detection and Product Trail using Augmented Reality”,2022 first International Conference on Computational Science and Technology (ICCST) [IEEE], 2022.
9. T.S.Arulananth,Bittu Kumar, Kiran Dasari,“Python Based Smart Trial Room”,Proceedings of 2022 IEEE Conference on Interdisciplinary Approaches in Technology and Management for Social Innovation(IATMSI), [IEEE], 2022.
10. R.R.N.P.A.B.W.M.S.R Galagoda, E.H.N.L.Gunarathne, K.A.D.Maheshi Purnima, H.P.C.S. Wickramarathna, Shyam Reyal, Samanthi Siriwardana, “Elegant Fit-On – Virtual Fitting Room on Handheld Devices”, Proceedings of the fourth International Conference on Advancements in Computing(ICAC), [IEEE],2022.

11. Edbert Junus, Clarissa Jocelyn, Daffa Irsyad Adilah, Alexander Agung Santoso Gunawan, “Application Fitting Room using Virtual Technology: A Systematic Literature Review”, Proceedings of the IEEE Creative Communication and Innovative Technology (ICCIT), [IEEE], 2022.
12. Debangana Ram, Bholanath Roy, Vaibhav Soni, “A Review on Virtual Reality for 3D Virtual Trial Room”,Proceedings of the IEEE World Conference on Applied Intelligence and Computing (AIC), [IEEE],2022.
13. Shrouk Elsawaf, Aziz Barbar, Online Fitting Room: A Mobile Shopping Application using Augmented Reality (AR) Technology,Proceedings Of 2023 18th International Joint Symposium on Artificial Intelligence and Natural Language Processing (iSAI-NLP),[IEEE],2023.
14. K.-N. Nguyen-Ngoc, T.-T. Phan-Nguyen, K.-D. Le, T. V. Nguyen, M.-T. Tran, and T.-N. Le, "DM-VTON: Distilled Mobile Real-time Virtual Try-On," in Proc. 2023 IEEE Int. Symp. on Mixed and Augmented Reality Adjunct (ISMAR-Adjunct), Sydney, Australia, 2023.
15. Am Kavin, T Jithesh, G. Kalaiarasi, M. Selvi, R. Yogitha, T.N. Suresh Babu,“Virtual Trial Room for Online Shopping”,2024 tenth International Conference on Communication and Signal Processing (ICCSP), [IEEE],2024.
16. N. Mythili, Harini M, Janalyn Maroula L, “AI-Enhanced Virtual Trial Room Using Augmented Reality”, Proceedings of the sixth International Conferenceon Mobile Computing and Sustainable Informatics (ICMCSI), [IEEE],2025.

Springer

HTTPS://ICICCT.ORG/2025/